



I
N
A
P

I
M
W
A

M
W
D

11th ICARD | IMWA | MWD

Volume II

**Christian Wolkersdorfer | Lotta Sartz
Anne Weber | Jo Burgess | Gilles Tremblay**



RISK TO OPPORTUNITY

Volume 2

in memoriam _____

Paul Younger

Philip Hobbs

Peter Gunther

RISK TO OPPORTUNITY

Volume 2

Proceedings of the
11th ICARD | IMWA | MWD Conference –
“Risk to Opportunity”

10 – 14 September 2018

Pretoria, South Africa

Editors

Christian Wolkersdorfer

Lotta Sartz

Anne Weber

Jo Burgess

Gilles Tremblay



11th International Conference on Acid Rock Drainage (2018: Pretoria, South Africa)
International Mine Water Association
WISA Mine Water Division

Risk to Opportunity
2018, Pretoria, South Africa
Tshwane University of Technology (TUT)

ISBN 978-0-620-80650-3 (2 Volumes)
© INAP | IMWA | WISA MWD 2018

Editors

Christian Wolkersdorfer, Lotta Sartz, Anne Weber, Jo Burgess, Gilles Tremblay

Cover Design

Karoline Wolkersdorfer, Christian Wolkersdorfer

Layout and Typesetting

Jigsaw Graphic Design

Cover Photograph

Christian Wolkersdorfer – Mine Water discharging from an abandoned mine shaft (18 Wince) in the Westrand.

Papers with the © sign have been peer reviewed. All abstracts were initially reviewed by 2 – 3 experts of the International Scientific Committee.

Printed in South Africa on certified paper

www.INAP.com.au
www.IMWA.info
www.WISA-MWD.org

Organizers

International Network of Acid Prevention



International Mine Water Association



WISA Mine Water Division



International Scientific Committee (ISC)

Teresa Albuquerque, Portugal	Duk-min Kim, South Korea
Bert Allard, Sweden	Robert Lawrence Kleinmann, United States
John George Annandale, South Africa	Frans Knops, Netherlands
Margarida Horta Antunes, Portugal	Ulla Lassi, Finland
Mona Arnold, Finland	Tim Lilley, United Kingdom
Thitiphan Assawincharoenkij, Thailand	Zaibin Liu, China
Tim Aubel, Germany	Jorge Loredó, Spain
Mattias Bäckström, Sweden	Simon Antony Lorentz, South Africa
Jeff Bain, Canada	Paul Joel Lourens, South Africa
M Dolores Basallote, Spain	Mark Lund, Australia
Melanie Lise Blanchette, Australia	Maria Mamelkina, Finland
Rob Howell, United Kingdom	Malibongwe Shadrach Manono, South Africa
Charlotte Barbara Braungardt, United Kingdom	Thirumurugan Marimuthu, India
Jo Burgess, South Africa	Vhahangwele Masindi, South Africa
Juan Cepriá, Spain	Matthew P. McGann, Peru
Hana Kirsten Christenson, New Zealand	Thomas Metschies, Germany
Henk Coetzee, South Africa	Philip Graeme Morgan, United Kingdom
Jacob Grant Croall, United States	Jacek Motyka, Poland
Gareth Digges La Touche, United Kingdom	Ritva Muhlbauer, South Africa
Enrico Dinelli, Italy	Victor A. Munoz Saavedra, Canada
Kajetan d'Obyrn, Poland	Kevin Myers, United States
Catherine Joanna Edward, South Africa	John William Neale, South Africa
Scott Effner, United States	Carmen Mihaela Neculita, Canada
Nils Eriksson, Sweden	Michael Paul, Germany
Nuria Fernandez Castro, Brazil	Steven Richard Pearce, United Kingdom
Linda Ann Figueroa, United States	Daniele Pedretti, Finland
Michael Moore Gabora, United States	Jaakko Olavi Pellinen, Finland
Marwan Ghanem, Palestinian Territories	Nadine Piatak, United States
Cleber Jose Baldoni Gomes, Brazil	James Pope, New Zealand
Bashan Govender, South Africa	Ana Claudia Queiroz Ladeira, Brazil
Ros Green, Australia	Marja-Liisa Räisänen, Finland
Antti Häkkinen, Finland	Nad'a Rapantova, Czech Republic
Robert S Hedin, United States	Carlos Ruiz Cánovas, Spain
Kari Heiskanen, Finland	Liudmila Rybnikova, Russia
Amy L Hudson, United States	Lotta Sartz, Sweden
Andrew Kinnon Hughes, United Kingdom	Christopher James Satterley, United Kingdom
Andrei Ivanets, Belarus	Ralph Schöpke, Germany
Ryan Thomas Jakubowski, United States	Martin Schultze, Germany
Ewa Janson, Poland	Robert R Seal, United States
Tommi Johansson, Finland	Maria Sinche-Gonzalez, Finland
Andrew Clifford Johnstone, South Africa	Alison Sinclair, Australia
Margarete Maria Kalin, Switzerland	Sarah Jane Wolfe Skinner, South Africa
Päivi M. Kauppila, Finland	Mariette Smart, South Africa
Anu Kettunen, Finland	Frank Stapelfeldt, Brazil
Muhammad Kamran Khalid, Finland	Wanghua Sui, China
Elena Khayrulina, Russia	Piia Katariina Suvio, Canada

International Scientific Committee (ISC) continued

Jouni Torssonen, Finland

Gilles Tremblay, Canada

Sari Annikki Tuomikoski, Finland

Wilfried Uhlmann, Germany

Robert Paul van Hille, South Africa

Danie Vermeulen, South Africa

Ian Watson, United Kingdom

Anne Weber, Germany

Walter Weinig, United States

Helena Wessman-Jääskeläinen, Finland

Roderick David Williams, United States

Christian Wolkersdorfer, Finland

Peter Woods, Austria

Zhenguo Xing, China

Jorge Zafrá, Peru

Local Organizing Committee (LOC)

Champion

Richard Garner

Co-Chairs

Christian Wolkersdorfer

IMWA President

Gilles Tremblay

INAP Technical Director

Jo Burgess

Water Research Commission

Members

Henk Coetzee

Council of Geoscience

Lester Goldman

Water Institute of Southern Africa

Bashan Govender

Department of Water and Sanitation

Philip Hobbs†

CSIR

Stephinah Mudau

Chamber of Mines

Blanché Postma

Clean Stream Environmental Consultants

Lotta Sartz

IMWA General Secretary

Jaco Seaman

Water Institute of Southern Africa

Chris Swartz

Chris Swartz Water Utilisation Engineers

John Waterhouse

IMWA Past President

Administration

Zicki Joubert

Tshwane University of Technology (TUT)

Danielle Henn

Conference Consultancy South Africa (Pty) Ltd





Welcome to South Africa!

We, the organisers and the champion of the 11th ICARD, IMWA, INAP and WISA welcome you with a warm Sawubona to Pretoria, South Africa. This is the first ICARD held in South Africa, IMWA returns for a third time and, for the Mine Water Division it is the homeland of WISA's Mine Water Division. We are proud to combine our efforts: instead of having three different conferences in one year, we can offer delegates one mine water conference of the highest calibre, with nearly 350 experts from all around the world.

As you will see from browsing through the programme, the majority of the papers will deal with mitigation, remediation, and responsible mine water management. This falls beautifully within the chosen theme of our conference, which is "Risk to Opportunity". What does that mean? It means that we need to see the risks that are involved in managing or mitigating mine water, and specifically that acid rock/mine drainage must be considered an opportunity. It is an opportunity to learn from each other and to plan for the future. This, exactly, is what this year's conference aims to be: a platform for exchanging ideas and experience from mining operations to remediation of abandoned mine sites in various climatic and cultural conditions.

When in South Africa, one must not forget to speak about transformation. The papers presented by our colleagues clearly show that transformation is an integral part of the work that our community is doing. A lot of students and young professionals are coming from previously disadvantaged communities to present their work, resulting in an increase the number of well-educated local students. Gender equality is another goal, and the fact that nearly one third of the registered delegates are female clearly shows progress to encourage young female students to join the mining environmental community.

Mining is seen as environmentally and ecologically unfriendly. This is primarily caused by examples of unethical mining and the past negative track record of the mining industry. Yet the situation has changed globally with most mining companies now seeing themselves as responsible for the sustainable use of earth resources. Though mining *per sé* cannot be sustainable, the entire production process from exploration to exploitation to closure can be. This combined conference shall therefore be the first "Green" Conference in ICARD's history. This means that carbon offsetting will be achieved by planting an adequate number of trees to compensate for the conference's carbon footprint. In addition, similar to the IMWA 2010 in Sydney, Nova Scotia, Canada, the conference shall avoid plastic containers wherever possible, and the amount of garbage produced shall be kept to the unavoidable minimum. Each item produced and used during the conference shall be from a "Green" perspective. Please help us to keep this conference as green as possible by avoiding waste wherever possible and use the glass bottles provided to get your water from the dispensers.

We hope that you will have a successful conference and we are looking forward to seeing you over the next several days.

Richard Garner, Jo Burgess, Gilles Tremblay, Christian Wolkersdorfer

— Volume 1 — Topics 1-8

— 1 Mining for Closure —

Dent, Julia; Williams, Martin; Draba, Bakary Bespoke Field Columns to Assess Hexavalent Chromium Risk for Refinement of Mine Closure Plans	3
Devoy, Cora Ann; Wrong, Linda Ann; Collins, Kevin; Mathur, Shilika Former Galmoy Mines Tailings Restoration Project	9
Green, Ros; Lee, Steven; Kleiber, Chris; Terrusi, Lisa; Glasson, Kate Strategies for Managing Chemically Reactive Mineral Waste at Rio Tinto Iron Ore Mines	17
Landers, Matt; Maddocks, Greg; Forbes, Amanda; Nucifora, Candice; Jones, Jason; Mandaran, Kristian; Wilson, Ward; Stephen, Newman Mount Isa Mines Rehabilitation Materials Sampling and Analysis Program for Closure Planning	21
Lemière, Bruno; Jacob, Jérôme; Bellenfant, Gaël Geology, Genetic Processes and their Consequences on Environmental Impacts at the Abandoned W Mine of Engualès, Aveyron, France	27
Lund, Mark Andrew; Blanchette, Melanie Lise; Harkin, Colm Seasonal River Flow-through as a Pit Lake Closure Strategy: Is it a Sustainable Option in a Drying Climate?	34
Martin, Nicholas D.; Gabora, Michael M. Modeling Complex Mine Water Closure Challenges using a Coupled FEFLOW-GoldSim Model	41
Mokhahlane, Lehlohonolo Determination of Acid Rock Drainage from Underground Coal Gasification at a Pilot Plant in Majuba	47
Nepomuceno, Alessandro Managing ARD in a Gold Mine in the Vicinity of Paracatu Town, MG State, Brazil	52
Nigéus, Susanne Pia Teresia; Maurice, Christian Monitoring a Field Application of Green Liquor Dregs, a Paper Mill Residue, in a Sealing Layer on Top of Mine Waste	57
Salmon, David Anthony Managing Uncertainty in Planning Opencast Coal Mine Final Void Closure and Relinquishment	64
Wang, Changshen Facing challenges of closure boom of Permo-Carboniferous underground coalmines in North China: a medium-size hydrogeochemical simulation experiment	70





Xu, Zhimin; Sun, Yajun; Zhang, Mengfei The Safety Management of Adjacent Coalmines after Mine Closure- A Case Study of a Closed Coalmine in Xuzhou Mining District, China	74
Jewiss, Carrie Sara; Pope, James; Craw, Dave The Influence of Rainfall on the Characteristics of Historic Acid Mine Drainage on the Denniston Plateau, New Zealand	80
<hr/> — 2 Water Treatment Processes in Perspective — <hr/>	
Aubel, Tim; Kober, Eugen; Janneck, Eberhard; Rolle, Jessica Use Of Ceramic Nanofiltration Membranes With High Specific Surfaces For The Processing Of Bio-Leachate And The Treatment Of Saline Mine Water	83
Bannister, Alyson; Brabham, Peter; Jones, Tim; Bowell, Rob Performance and Review of Passive Minewater Treatment Sites, Pelenna Valley, Wales	84
Bowell, Rob Assessment of Scordite Precipitation from Mine Waters	91
Broemme, Katrin; Trinh, Viet Quoc; Greassidis, Sandra; Stolpe, Harro Material flow analysis for spatiotemporal mine water management in Hon Gai, Vietnam	97
Cukrowska, Ewa Maria; Ochieng, Levi; Tutu, Hlanganani; Chimuka, Luke Speciation Analysis of Colloidal Silica in Acidic Conditions	103
Deng, Jinxun; Xu, Ying; Cheng, Hong; Li, Jianhua; Zhou, Genmao; Zhang, Chong Experimental Study of Removal of Organic Matters from Alkaline Uranium Leaching Solution with Ultrafiltration	109
du Preez, Kerri; Gericke, Mariekie; Maharajh, Dheepak The Impact of Sulphide Concentration on Microbial Activity in a Biological Sulphate Reduction Process	114
Forbes, Emma; Trumm, Dave; Bell, David; Pope, James Comparison of Diversion Well Substrates for the Treatment of Acid Mine Drainage, Bellvue Mine, West Coast, New Zealand	116
Gault, Andrew; Harrington, Jim; Robertson, Cameron; Simair, Monique; Friesen, Vanessa Pilot Study of In Situ Biological Treatment at the Silver King Mine, Keno Hill, Yukon	121
Hamai, Takaya; Sato, Yuki; Kojima, Kazuhiro; Masaki, Yusei; Hayashi, Kentaro; Sowanaka, Masahiro; Masuda, Nobuyuki; Kobayashi, Mikio; Sakata, Takeshi Pilot Scale Tests of Compact (Short Retention Time) Passive Treatment Process for Acid Mine Drainage Using Agri-Waste in Japan	128
Hammond, Andrew Michael; Drummond, Ashton Blake A Critical Review On The Performance of the Gypsum Precipitation Reactors on HIPRO® AMD Plants At EWRP, OWRP and MWRP	133





Marais, Tynan Steven; Huddy, Robert John; van Hille, Robert Paul; Harrison, Susan Therese Largier	
The Effect of Temperature on the Kinetics of Sulphate Reduction and Sulphide Oxidation in an Integrated Semi-Passive Bioprocess for Remediating Acid Rock Drainage	140
Mashalane, Tlou Betty; Novhe, Ntshengedzeni Obed; Yibas, Bisrat; Coetzee, Henk; Wolkersdorfer, Christian	
Metal Removal from Mine Water Using Passive Treatment Technologies (Anaerobic and Aerobic) in the Ermelo Coalfields, Mpumalanga, South Africa	146
Nairn, Robert W.; Shepherd, Nicholas L.; Danehy, Timothy; Neely, Cody	
Aeration via Renewable Energies Improves Passive Treatment System Performance	151
Nappa, Marja; Kiipula, Kaisa; Kyllönen, Hanna; Kaartinen, Tommi; Pajarre, Risto; Kangas, Petteri	
Valorisation Of Effluent From Metal Recovery Plant	157
Neale, John William; Gericke, Mariekie; Mühlbauer, Ritva	
On-Site Pilot-Scale Demonstration of a Low-Cost Biological Process for the Treatment of High-Sulphate Mine Waters	164
Novhe, Ntshengedzeni Obed; Yibas, Bisrat; Coetzee, Henk; Atanasova, Maria; Mashalane, Tlou Betty; Vadapalli, Viswanath Ravi Kumar; Wolkersdorfer, Christian	
Geochemistry and Mineralogy of Precipitates Formed During Passive Treatment of Acid Mine Drainage in Ermelo Coalfield, South Africa	171
Oyewo, Opeyemi Alice; Wolkersdorfer, Christian; Onyango, Maurice S.; Amos, Adeniyi	
The Performance of Nano-sized Banana Peels in the Removal of Vanadium from mine water	177
Petschel, Brendan Emil; Drummond, Ashton	
A Review of Brine Treatment Technologies for MIW Treatment Plants	182
Ramakuela, Mashudu; Adeniyi, Amos; Onyango, Maurice Stephen; Mbaya, Richard; Oyewo, Opeyemi	
Performance Evaluation of Orange Peels as Anti-Scaling Agent for Pretreatment of Water	188
Schabronath, Christoph Alexander	
A novel sampling technique using a sediment collector (SECO) to collect particles from suspended matter in mine water with regard to long term monitoring	193
Totsche, Oliver; Lucke, Beate; Benthous, Friedrich-Carl	
In-Lake Neutralization Of Mine Lakes – 15 Years Of Continuous Development	199
Trumm, Dave; Christenson, Hannah; Pope, James; Watson, Kerry; Mason, Kathy; Squire, Russel; McDonald, Grant; Mazzetti, Anne	
Treatment of High Mn Concentrations at Waihi Gold Mine, New Zealand by Two Methods: A Limestone Leaching Bed and a Slag Leaching Bed	204
Ulbricht, Antje; Bilek, Felix; Brömme, Katrin	
Development of a Technical Concept of Spatial and Temporal Coordinated Mine Water Recycling Exemplified by a Mining Area with Urban Influence	210





Naidoo, Roxanne; du Preez, Kerri; Govender-Ragubeer, Yageshni Are We Making Progress in the Treatment of Acid Mine Drainage?	215
Villa Gomez, Denys; Hofmann, Harald; Zhang, Chenming; Williams, David; Gomes, Patrick Botsch Cellette Assessing Biotic and Abiotic Conditions for Understanding Bioleaching Processes in Tailings	221
<hr/> 3 Produced Water <hr/>	
Robertson, Alan McLeod; Maddocks, Greg Arthur; Kelly, Ben; Sheppard, Ian Application of a Coal Seam Gas Waste Product as part of the Rehabilitation Program for a Copper Heap Leach Operation	231
<hr/> 4 Saline and Neutral Mine Water <hr/>	
Annandale, John George; du Plessis, H Meiring; Tanner, Phil D; Burgess, Jo Suitability of mine water for irrigation: a risk based, site-specific DSS	239
Ben Ali, Houssem Eddine; Neculita, Carmen Mihaela; Molson, John W.; Maqsoud, Abdelkadir; Zagury, Gérald J. Performance of Passive Systems for Mine Drainage Treatment at High Salinity and Low Temperature	245
Herrell, Michael Keith; Vandenberg, Jerry; Faithful, John; Hayward, April; Novy, Lukas Long-term Water Management of Saline Groundwater at the Ekati Diamond Mine	252
Nkansah-Boadu, Frank; Hatam, Ido; Taylor, Jon; Baldwin, Susan Bio-reduction of Selenium Oxyanions in the Presence of Nitrate in Neutral pH Coal Mining Influenced Water	258
<hr/> 5 Electrochemical Treatment Options <hr/>	
Mamelkina, Maria A.; Tuunila, Ritva; Sillanpää, Mika; Häkkinen, Antti; Cotillas, Salvador; Lacasa, Engracia; Rodrigo, Manuel A. Continuous Electrocoagulation Process For Treatment Of Mining Waters	267
<hr/> 6 Acceptability of Processed Mine Water <hr/>	
Hammond, Andrew Michael; Drummond, Ashton Blake Producing High Quality Drinking Water from Mine Impacted Water At High Plant Recoveries Using Reverse Osmosis Membranes	275
Hudson, Carla Achieving Sustainable Mine Closure Through the Use of Mine Water	282
Mukwena, Tafadzwa; Van Der Walt, Jeremia Jesaja Lonmin Integrated Water Resource Management System	283





Satterley, Christopher James; Thorn, Peter; Davies, Susan; Cox, Nick Potential for Co-treatment of Mine Water and Waste Water in Waste Water Treatment Works	288
Vaezihir, Abdorreza; Safari, Fatemeh; Javani, Hossein; Mazaheri, Nader The Efficiency of Open Lime-Zeolite Channel System in Treatment of Acid Mine Drainage (AMD) Released from Sungun Copper Mine	295

— 7 Prediction

Barnes, Samantha; Martindale, Richard Lifetime Assessment of an Operating Tailings Facility through Modelling of the Unsettled Tailings Layer	303
Becker, Megan; Charikinya, Edson; Ntlhabane, Sithembiso; Voigt, Marcelene; Broadhurst, Jennifer; Harrison, Susan TL; Bradshaw, Dee An Integrated Mineralogy-based Modelling Framework For The Simultaneous Assessment Of Plant Operational Parameters With Acid Rock Drainage Potential Of Tailings	309
Bowell, Rob; Sapsford, Devin Geochemical assessment of Metal/Metalloid release by contrasting laboratory methods; The importance of secondary minerals	315
Declercq, Julien; De Los Hoyos, Camilo; Griffith, Ruth; Bowell, Rob The Challenges of Predictive Numerical Calculation within Hypersaline Brines: Examples from Lithium Brines	321
Digges La Touche, Gareth; Brookes, Freddy Ecohydrology in Mine Water Studies	328
Fosso-Kankeu, Elvis; Redelinghuys, Johannes Bacterial Ecology of Biofilms Sustaining Pollution by Acid Mine Drainage Near Mining Areas in Mpumalanga Province – South Africa	332
Garrick, Hollie; Digges La Touche, Gareth; Maksimainen, Tomi; Girard, Romain; Hayes, Eoghan Probabilistic Simulation of Snowmelt and Runoff at Mine Sites in Cold Climates	339
Guseva, Olga; Opitz, Alexander K. B.; Broadhurst, Jennifer L.; Harrison, Susan T. L.; Bradshaw, Dee J.; Becker, Megan Fe-Sulfide Liberation and Association as a Proxy for the Interpretation of Acid Rock Drainage (ARD) Test Results	345
Hällström, Lina; Alakangas, Lena; Martinsson, Olof Metal Release from Acidic and Near-Neutral pH-Conditions in Historical W, CU and F Skarn Tailings at Yxsjöberg, Sweden	351
Harck, Terry Richard Making Your Results Stick - Using General Likelihood Uncertainty Estimation (GLUE) In Water Quality Prediction From Coal Discard	357





Hudson, Amy L; Harley, Andrew; Richardson, Doc Combining Predictive Modeling and a Full-Scale Analog to Reduce Uncertainty	363
Caldwell, Robert John; Irwin, Robert A Kinetic Investigation of Siderite Oxidation during Laboratory Neutralization Potential Determinations	369
Jagert, Felix; Hahn, Florian; Ignacy, Roman; Bussmann, Gregor; Bracke, Rolf Mine Water Of Abandoned Coal Mines For Geothermal Heat Storage: Hydrogeochemical Modeling And Predictions	375
Kollias, Konstantinos; Mylona, Evangelia; Adam, Katerina; Papassiopi, Nymphodora; Xenidis, Anthimos Assessment of Silica Coating as a Technique for the Control of Acid Generation from Pyritic Tailings	381
Lahdenperä, Esko; Koiranen, Tuomas Effects of Variable Feeds in Wastewater Plants by Means of Process Simulation	387
Lusunzi, Rudzani; Gumbo, Jabulani Ray; Yibas, Bisrat; Obed, Novhe Acid Base Accounting (ABA) Of Mine Tailings For The Potential Of Acid Mine Drainage In The Sabie-Pilgrim's Rest Goldfields, South Africa	392
Makaula, Didi Xhanti; Huddy, Robert; Fagan-Endres, Marijke; Harrison, Sue A Flow-Through Biokinetic Test For Characterizing Acid Rock Drainage (ARD) Potential: Investigating Metabolic Activity On Pyrite-Bearing Waste Rock Surfaces In An Unsaturated Ore Bed	399
Maksimovich, Nikolai; Pyankov, Sergey; Khmurchik, Vadim; Berezina, Olga; Demenev, Artem; Sedinin, Alexey Coal Basins and the Environment	406
Metschies, Thomas; van Berk, Wolfgang; Jenk, Ulf; Paul, Michael Predicting Natural Attenuation for Flooding of an Isl-Uranium Mine – Potentials and Limitations	411
Moyo, Annah; Amaral Filho, Juarez; Broadhurst, Jennifer Lee Characterising the Environmental Risks of Coal Preparation Wastes: A Study of Fine Coal Slurry Waste and Discard from South African Collieries	417
Opitz, Alexander; Broadhurst, Jennifer; Harrison, Susan; Bradshaw, Dee; Becker, Megan Understanding Mineralogy As A Tool For Acid Rock Drainage Characterisation	424
Pope, James; Christenson, Hannah; Gordon, Kerry; Nigel, Newman; Trumm, Dave Wall Wash Samples to Predict AMD Longevity at Coal Mines in New Zealand	430
Puhlovich, Alan Anton Model Simulations of the Layered Development of Waste Rock Stockpiles, Progressive Moisture Changes and Potential Seepage Generation in a Low Rainfall Environment: Case Study of an Australian Mine Development	436
Roetting, Tobias S; Dent, Julia; Reyes, Rene Life-of-mine Water Management And Treatment Strategies	442





Salmon, Ursula; Marton, Richard; O’Kane, Michael Evolving Kinetic Testing Methods to Incorporate Key Dynamic Waste Rock Dump Parameters	447
Santos, Renata; Vila, Maria Cristina; Fernandes, António; Guimarães, Sara; Ferreira, Diana; Fiúza, António Contribution of Data Analysis for the Environmental Study of Post-closure Coal Ash Landfill	452
Steinepreis, Mark David; Blowes, David W; Amos, Richard T; Stastna, Marek; Wilson, Gordon Ward Temporal Variability and Gas Transport Rates in Waste Rock	458
Sui, Wanghua; Yang, Binbin; Liu, Jiawei Qualitative and Quantitative Decision-Making Model to Determine the Size of Safety Pillars for Mining under Sand Aquifers	465
Van Tol, Johan; Lorentz, Simon The Application of Hydropedology Surveys to Quantify Near-Surface Impacts from Mining Waste	471
van Zyl, Albertus Johannes; Naicker, Koovila; Barnard, Philip Risk-based Modelling of Soil Cover for Rehabilitation Planning of Coal Discard Facility in South Africa to Achieve Groundwater Quality Criteria	476
Vilela, Fernando; Lima, Geraldo; Macniks, Jéssica; Ferreira, Juliene; Le Petit, Mark Evaluation and Comparison of Kinetic Tests Performed with the Humidity Cell, Column and Funnel Methods and Proposition of a Model with the Disposition Way	481
Wilson, David; Amos, Richard T.; Blowes, David W.; Langman, Jeff B.; Smith, Leslie; Sego, David C. Diavik Waste Rock Project: A Mechanistic Approach To The Prediction Of The Geochemical Evolution Of Sulfidic Waste Rock	487
Zanetti, Caroline Sant’Ana; Vasconcelos, Flavio de Moraes; Sousa, Rayssa Garcia; Silva, Marco Antonio A new approach To Validate A Mixing Zone Study Of A Gold Mine Effluent	493

— 8 Mitigation —

de los Hoyos, Camilo Raul; Marrero, Diego Alejandro; Sitjá y Balbastro, Juan Martín; Declercq, Julien; Bowell, Robert John Remediation Options For Wind-remobilised Pb-Zn Old Tailings: An Example From An 80-year Pb-Zn-Ag Mine in NW-Argentina	501
Goodman, William Mario; Van Dyk, Deon; Grobler, Nico; Osborne, Antony Water Ingress Mitigation Programs for Underground Mines: Hydrogeological and Rock Mechanical Demands on Grout Properties	507
Holland, Martin; Witthüser, Kai Thorsten Horizontal Scavenger Borehole System For Plume Containment	512





Jensen, Soren Ross; Clark, Cal; Noel, Marie-Christine; Foster, Jennifer Mine Design for In-Situ Control of Selenium and Nitrate	518
King, Karen Nicole; Lottreaux, Gareth Yanfolila Gold Mine Open Pit Slope Depressurisation, Mali	524
Larsen, Morten Birch; Jia, Yu; Joensen, Sigga Use of Residues Generated from Construction and Fish Industries to Remediate Mine Drainage in Greenland	529
McDonald, Johann; Lorentz, Simon Vermiculite Covers on Mining Wastes in a Semi-Arid Environment in South Africa	535
Mjonono, Donald; Harrison, Sue; Kotsiopoulos, Athanasios Development Of Co-Disposal Methods For Fine Coal Waste and Coal Discards To Facilitate The Prevention Of Acid Mine Drainage	541
Morton, Kym Lesley The WIN-WIN Solution To The Clean-up Of Mine Residue - An Innovative And Cost Effective Method To Reduce Acid Drainage From Mine Residue	548
Ntholi, Thakane; de Wit, Maarten Passive Underground Mine-water Purification System (PUMPS) : A conceptual geo-engineering model designed for the treatment and management of acid mine water in the Witwatersrand gold mines, South Africa	553
Pouliot, Sandra; Bussière, Bruno; Dagenais, Anne-Marie; Wilson, Ward; Letourneau, Yanick Evaluation of the Use of Paste Rock as Cover Material in Mine Reclamation	559
Stander, Helene-Marie; Harrison, Susan TL; Broadhurst, Jennifer L Re-purposing Acid Generating Fine Coal Waste: An Assessment And Analysis Of Opportunities	565



9 Geochemistry Hidrogeology

- Christenson, Hana; Pope, James; Craw, Dave; Johns, Justin; Newman, Nigel; Trumm, Dave**
Characterisation of As Geochemistry in Mine Tailings from a Mesothermal Gold Deposit 573
- Crozier, Trevor; Paszkowski, Dawn; Parent, Genevieve; Cook, Diana; Mann, Vanessa; Mendoza, Carl; Provost, Heather; Martin, Alan J.; Helsen, Jordi; Bain, Jeff; Blowes, David; Gaspar, Christopher; Russell, James**
Permeable Reactive Barrier Feasibility Assessment at Goldcorp's Red Lake Gold Mines: Hydrogeological, Geochemical and Geotechnical Design Considerations 579
- Digges La Touche, Gareth; Balding, Barry; Keenan, Brian; Digges La Touche, Susan**
Sinkhole Development on Mine Flooding 585
- Chimhanda, Wadzanai; Duthe, Diana Mary; Kawali, Liisa**
Unraveling the convoluted marbles of a Namibian Gold Mine 591
- Gałuszka, Agnieszka; Migaszewski, Zdzisław Maksymilian**
Extremely High Levels of Trace Elements in Aerial Parts of Plants Naturally Growing in the Wiśniówka Acid Mine Drainage Area (South-Central Poland) 598
- Gautama, Rudy Sayoga; Kusuma, Ginting Jalu; Pujiantoro, Eko; Wisnugroho, Pajar Hariadi**
On The Spatial Variation of Rock Geochemical Characteristics in Coal Mining: Case Bukit Asam Coal Mine in South Sumatra, Indonesia 604
- Gautama, Rudy Sayoga; Perkins, William; Bird, Graham; Adjie, Wisjnoe; Moore, Oliver; Kusuma, Ginting Jalu; Badhurahman, Abie**
Acid Mine Drainage in a Tropical Environment: A Case Study from Bukit Coal Mine Site in South Sumatra, Indonesia 611
- Hamberg, Roger; Maurice, Christian; Alakangas, Lena**
Cementation Of Cyanidation Tailings – Effects On The Release of As, Cu, Ni And Zn 617
- Helsen, Jordi; Martin, Alan J.; Crozier, Trevor; Parent, Genevieve; Mann, Vanessa; Mendoza, Carl; Gaspar, Christopher; Russell, James**
Permeable Reactive Barrier Feasibility Assessment at Goldcorp's Red Lake Gold Mines: Validation of Seepage Flow Paths through Tracer Testwork 623
- Johnson, Raymond H.; Tigar, Aaron; Morris, Sarah; Campbell, Sam; Tafoya, Kara; Bush, Richard; Frazier, William**
Column Tests and Multilevel Well Geochemistry to Explain Contaminant Plume Persistence Issues Downgradient of a Former Uranium Mill Site 629
- Kassahun, Andrea; Paul, Michael**
Mine Water Tracer Substances for Biogeochemical Processes in Flooded Uranium Mines 635
- Keller, Jason Mathew; Banuelos, Jaime; Bunting, Lindsey; Milczarek, Mike; Lattin, Daniel; Moore, Scott; Zhan, Guosheng**
Monitoring of Waste Rock Dump Surface Water Drainage and Channel Infiltration 641





Kennedy, Lizel; Johnstone, Andrew Clifford An Investigation of the Water Quality of Four Coal Mine Pit Lakes in South Africa	647
Komulainen, Jere Johannes; Vaittinen, Tiina; Picken, Päivi; Heikkinen, Eero Hydrogeological Bedrock Characterisation Based on Posiva Flow Log Measurement Data	654
Love, David; Bezuidenhout, Nico; Lupankwa, Keretia Understanding Acid Rock Drainage in the West African Shield	660
Martin, Alan J.; Helsen, Jordi; Crozier, Trevor; Parent, Genevieve; Paszkowski, Dawn; Mendoza, Carl; Provost, Heather; Gaspar, Christopher; Russell, James Permeable Reactive Barrier Feasibility Assessment at Goldcorp's Red Lake Gold Mines: Delineation of Groundwater Flow Paths and Contaminant Behaviour	666
Migaszewski, Zdzisław Maksymilian; Gałuszka, Agnieszka Geologic and Mineralogic Implications for Element and Isotope Signatures in the Wiśniówka Acid Mine Drainage Waters (South-Central Poland)	672
Mpetle, Matsatsi; Johnstone, Andrew The Water Balance of South African Coal Mine Pit Lakes	679
Naicker, Koovila; Van Zyl, Albert; Barnard, Philip Prediction of Seepage Quality from Coal Discard Facility in a Semi-Arid Climate	685
Nicholson, Ronald Vincent; Shaw, Sean; Barabash, Sarah; Stirling, Jim Evaluation of Acid Rock Drainage Potential in a Retrospective Study 25 Years after Mine Closure: Acid Base Accounting Statistics are Not Sufficient	692
Ochieng, Levi Determination of the Rate of Release of Nitrates from Waste Rock, Tailings and Kimberlitic Materials under Site Conditions – A Case Study	699
Papini, Gerry; Gossen, Jake; Pierce, Ben Consideration of Metal-Attenuation in Groundwater Quality Prediction	705
Puhlovich, Alan Anton Critical Importance of Conceptual Model Development When Assessing Mine Impacts on Groundwater Dependent Ecosystems: Case Study of an Australian Mine Development	711
Robertson, Lindsay Anne; Durocher, Jennifer Lee; Usher, Brent Laboratory Simulated Tailings Drain Seepage Columns: Flooded and Free-Draining Conditions	717
Salifu, Musah; Alakangas, Lena; Martinsson, Olof; Billström, Kjell; Ingri, Johan; Dold, Bernhard Sr/Ca and $^{87}\text{Sr}/^{86}\text{Sr}$: A Tracer For Geochemical Process In Mine Wastes	723
Sidenko, Nikolay V. Nitrogen Leaching From Explosives Into Mine Water Of An Underground Mine	729
Skinner, Sarah Jane Wolfe Platinum Tailings Review – A comparison of the water quality in the tailings dam to the surrounding groundwater	733





Sun, Yajun; Xu, Zhimin; Cui, Siyuan; Gao, Shang The Formation Mechanism of High Salinity Groundwater in Arid Area and Its Influence on Coalmines – A Case Study of a Coalmine in Xinjiang, China	738
Szczepiński, Jacek Groundwater Flow Model in the Area of the Extensive Open Pits Lignite Mining Activities	744
Valente, Teresa Maria; Pamplona, Jorge Monitoring of a Public Water Supply System: A Case of Groundwater and Surface Water Contamination by Acid Rock Drainage	751
Van Aardt, Joanne Michelle; Howell, Robert; Bérubé, Kelly; Jones, Tim; Lusambo, Victor Geochemical and Bioreactivity Assessment of Future Mining Operations at Mutanga Uranium Project, Southern Province, Zambia	757
Woloshyn, Kai Skyler; Gault, Andrew G Long Term Effectiveness of an Adit Plug – Passive Treatment for Adit Discharge in a Northern Climate	763
Wyatt, Lee M; Watson, Ian A; Moorhouse, Arabella ML Adaptive Mine Water Treatment: Modelling To Long-term Management	769
Zielke-Olivier, Josepha Simone Doris Renate; Vermeulen, Danie An Integrated Approach To Evaluate The Hydrogeological Setting Around A Water-filled Quarry In A Mining Environment	775
Åhlgrén, Kristina; Sjöberg, Viktor; Bäckström, Mattias Leaching of U, V, Ni and Mo from Alum Shale Waste as a Function of Redox and pH - Suggestion for a Leaching method	782

10 Catchment Management

Boland, Martin Paul; Yohannes, Rezene; White, Jamie; Benghiat, Phil; Daley, Stuart Integrated Numerical Model Development For Sustainable Management Of Mine Water In A Semi Arid Environment	791
Burke, Jacqueline The Influence of Water Use Licences on Mine Water Management	797
Coetzee, Henk Reconstructing Historical Mine Water Management Practices for a Portion of the East Rand Gold Field, South Africa Using Long-Term Map and Image Time Series	803
David, Katarina; Timms, Wendy; Baker, Andy; McGeeney, Dayna Water Sources to Support Swamp Ecosystems near Underground Mining Development	808
Dong, Shuning; Liu, Zaibin Coal Mine Water Hazard Accurate Detection and Efficient Control Technology	815
Harrison, Susan Therese Largier; Slatter-Christie, Kerry; Broadhurst, Jennifer L Integrating Competing Water Needs of Mining and Mineral Processing with the Environment, Community and Economic Activity in a Mining-dominated Catchment	820





Jarvis, Adam; Davis, Jane; Orme, Patrick; Potter, Hugh; Gandy, Catherine Evaluating Metal Behaviour And Mine Water Treatment Benefits In Abandoned Mine Catchments With Variable Pollutant Load Inputs	826
Laubrich, Jan; Rosemann, Robert Water Management at the Former Uranium Production Tailings Pond Helmsdorf	833
Long, Chazanne; De Wit, Maarten; Coetzee, Henk Hydrochemical Characterisation Of Mine Drainage Discharging Into The UNESCO Fossil Hominid Site Of South Africa	838
Onnis, Patrizia; Byrne, Patrick; Hudson-Edwards, Karen A.; Stott, Tim; Hunt, Christopher Source Apportionment of Trace Metals Over a Range of Stream Flows Using a Multi- method Tracer Approach	843
Shepherd, Nicholas Lee; Nairn, Robert W. The Effects of <i>Castor canadensis</i> (North American Beaver) Colonization on a Mine Drainage Impacted Stream	849

11 Economics of Mine Water

Banga, Chantal Mbala; Wolkersdorfer, Christian; Klingelhöfer, Heinz Eckart Implementing Sustainability Management Accounting Techniques for the Effective Management of Acid Rock Drainage	859
Dingley, Karen Assessing and Mitigating Risk to Mining – Can we “Future Proof” the Industry?	865
Do, Hao Hong; Trinh, Viet Quoc; Frör, Oliver To Invest Or Not To Invest? – A Valuation Of Public Benefits From Mine Water Treatment In Ha Long, Vietnam	871
Kluza, Anna; Evans, Lee Practical Applications of Groundwater Modelling for Dewatering Management in Open Pit and Underground Mining, Didipio, Philippines.	878
Verger, Robert Paul; Steyn, Jarmi; Labuschagne, Pieter; Schmidt, Roxane; Fourie, Johan; Pretorius, Freek Viability Of Converting A South African Coal Mining Pit Lake System Into A Water Storage Facility	884

12 Mine Water By Products

Gomez-Arias, Alba; Castillo, Julio; Welman-Purchase, Megan; Maleke, Maleke; van Heerden, Esta; Vermeulen, Danie Neutralization of Acid Drainage and Concentration of Rare Earth Elements Using Carbonatites; Results from a Bench Scale Experiment	893
Janneck, Eberhard; Glombitza, Franz; Aubel, Tim; Schönherr, Petra; Palitzsch, Wolfram; Killenberg, Arvid; Schubert, Volker; Weber, Lutz Utilization Of Iron Ochre – Making Auxiliary Water Treatment Materials From Mine Water Treatment Waste	899





Maree, Johannes Philippus; Mtombeni, Tabani; Ramothole, Phalakwane; Letjiane, Leny Treatment Of Copper Leachate For The Recovery Of Valuable Products	904
Muedi, Khathutshelo Lilith; Brink, Hendrik Gideon; Masindi, Vhahangwele; Maree, Johannes Philippus Recovery and Synthesis of Al^{3+}/Fe^{3+} Polycationic-Nanocomposites from Acid Mine Drainage Treatment Process and their Respective Application in the Removal of Arsenic and Chromium Ions from Polluted Water Resources	911
Sukati, Bonokwakhe Hezekiel; Annandale, John George; deJager, Pieter Christiaan; Tanner, Phil Can Phosphate Be Used To Improve The Hazardous Status Of High Density Sludge And Transform It Into A Usable Product?	916
Takaluoma, Esther; Pikkarainen, Tuomo; Kemppainen, Kimmo Adsorption And Desorption Of Metals Onto Reusable Adsorbent	923
Van der Walt, Mias; Van Der Merwe, Hayley Water Reuse In The Mining Industry – A Resource, Financial And Socio-Economic Imperative.	929
Vasconcelos, Flavio Morais; Zanetti, Caroline Sant'Ana; Soares, Adriano Marcio Colloids and its Influence in the Water Quality Diagnosis of Tailings Dam	934
Villa Gomez, Denys; Liu, Yun; Vaughan, James; Marcellin, Esteban; Wyman, Valentina; Serrano, Antonio; Southam, Gordon Microbial-mediated Ni and Co recovery from mine tailings	940

— 13 Best Practice Guidelines —

Parbhakar-Fox, Anita; Fox, Nathan; Ferguson, Tony; Hill, Roger; Maynard, Ben Dissection of the NAG pH Test: Tracking Efficacy Through Examining Reaction Products	949
Puell, Jorge; Lazaro, Paloma Solution Collection System For a ROM Leach Dump: Design Criteria to Meet Best Available Control Guidelines	956
Tremblay, Gilles International Network for Acid Prevention (INAP)	962

— 14 Piloting of the Waste Discharge Systems —

Aubé, Bernard; Lamares, Moacir; Lone Sang, Stéphan Pilot Optimisation of Sulphate Precipitation in the High-Density Sludge process	971
Franzsen, Sebastian; Bonner, Ricky; Germishuizen, Charne Estimation of Nanofiltration Solute Rejection in Reverse Osmosis Concentrate Treatment Processes	977
Aubé, Bernard; Lamares, Moacir; Lone Sang, Stéphan A Pilot Comparison of Sulphate Removal Technologies at Neves-Corvo	983





__ 15 Funding Models for Mine Water

- Drummond, Ashton Blake; Hammond, Andrew Michael**
Regional Mine Water Treatment Plant – Tolled Treatment Financial Analysis and Viability 993

__ 16 Mine Water Hydraulics

- Bai, Haibo; Li, Hao; Ma, Dan; Du, Bin**
Occurrence of Coal Seam as Main Aquifer 1001
- Gebrekristos, Robel; Trusler, Graham**
Groundwater Modelling in Support of Post-Closure Acid Mine Drainage and Treatment Planning – Case Study 1005
- Mahomed, Ismail; Kessopersadh, Colleen; Alipour, Mahmoud**
Furthering The Conceptual Groundwater Model For The Sarcheshmeh Copper Pit, Iran 1011
- Morton, Kym Lesley**
The Anatomy And Circulation Of Mine Water In Carbonatite Mines, Specifically Diamond Mines 1017
- Wolkersdorfer, Christian; von Hünefeld-Mugova, Elke**
Flow measurement using the salt dilution method at the mine water influenced Tweelopiespruit, Witwatersrand, South Africa 1024

__ 17 New Technologies

- Brown, Adrian**
Passive Metal Mining and Mine Water Treatment Using Crushed Concrete 1029
- Castendyk, Devin; Hill, Bryce; Filiatreault, Pierre; Straight, Brian; Alangari, Abdullah; Cote, Patrick; Leishman, William**
Experiences with Autonomous Sampling of Pit Lakes in North America using Drone Aircraft and Drone Boats 1036
- Chiodza, Godknows Kudzai; Harrison, Sue; Fagan-Endres, Marijke**
Desulphurisation Of Fine Coal Waste Tailings Using Algal Lipids. 1042
- Frau, Ilaria; Wylie, Steve; Byrne, Patrick; Cullen, Jeff; Korostynska, Olga; Mason, Alex**
New Sensing System Based on Electromagnetic Waves and Functionalised EM Sensors for Continuous Monitoring of Zn in Freshwater 1049
- Grewar, Tamsyn**
Reuse Of Treated Mine-Impacted Water As A Potential Resource For Accelerated Carbon Sequestration 1056
- Hahn, Florian; Ignacy, Roman; Busmann, Gregor; Jagert, Felix; Bracke, Rolf; Seidel, Torsten**
Reutilization Of Mine Water As A Heat Storage Medium In Abandoned Mines 1057





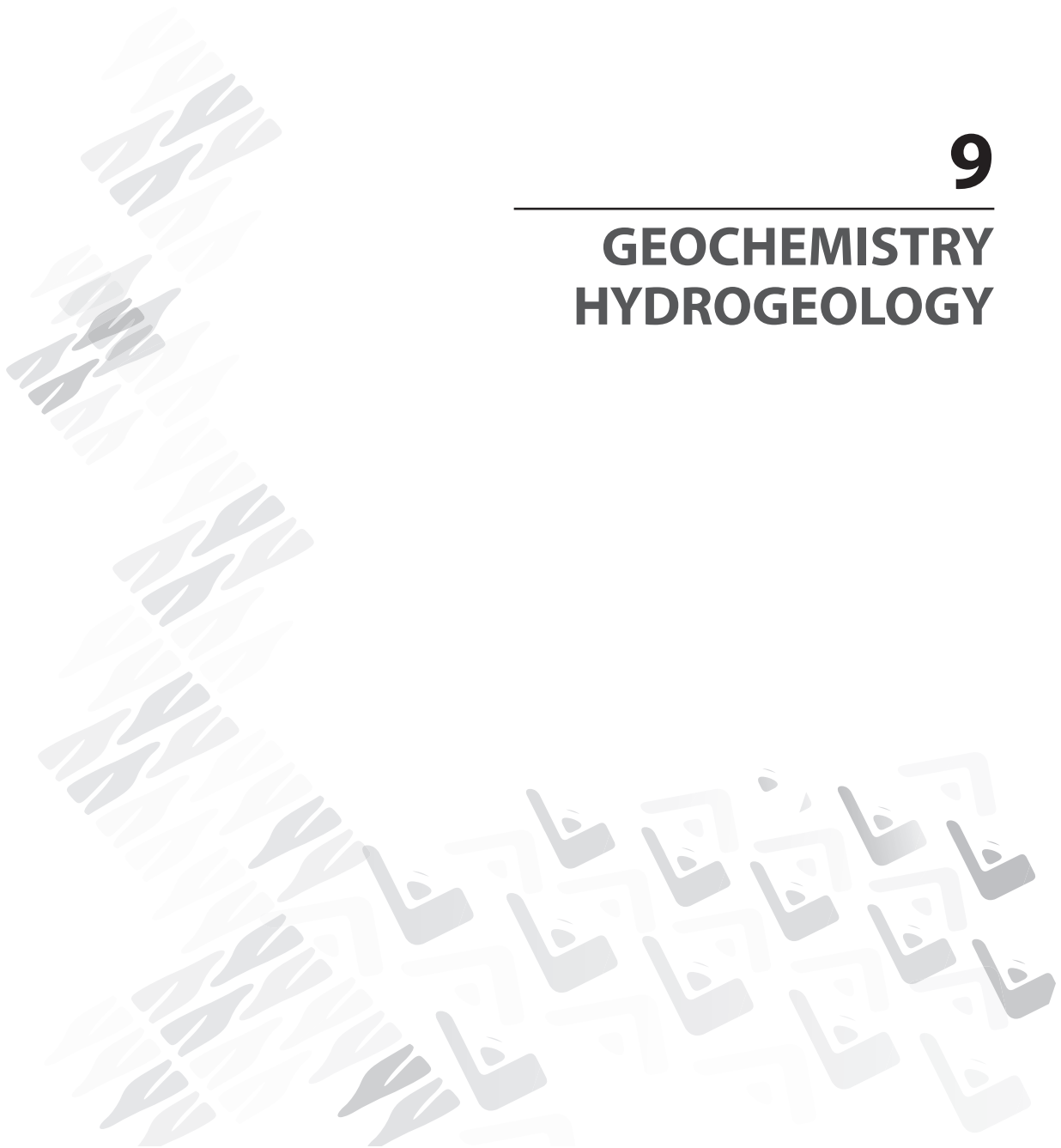
Herrell, Michael Keith; Kristina, Skeries; Vandenberg, Jerry; Faithful, John; Hayward, April; Novy, Lukas Influence of Probability Distribution Function Sampling Frequency on Stochastic Water Quality Model Predictions	1063
Hessler, Tomas; Huddy, Robert; Harrison, Susan T.L The Preferential Localisation of SRB in an Acetate Supplemented Up-Flow Anaerobic Packed Bed Reactor	1069
Jackson, Laura Marie; Parbhakar-Fox, Anita; Fox, Nathan; Cooke, David R; Harris, Anthony; Savinova, Ekaterina Integrating Hyperspectral Analysis And Mineral Chemistry for Geoenvironmental Prediction	1075
Johnson, Brent C.; Rohal, Pamela A.; Eary, L.E. {Ted} Coupling PHREEQC with GoldSim for a More Dynamic Water Modeling Experience	1081
Mabuka, Thabo; Govender-Opitz, Elaine; Harrison, Susan T.L. Recovery of Value from an Electronic Waste Stream using a Biological Matrix	1087
Man, Malcolm; Sparrow, Ben; Low, Megan A Cradle to Grave Treatment Solution for Mine Waters	1093
Masindi, Vhahangwele; Shingwenyana, Rhulani Reclamation, Recovery and the Synthesis of Valuable Minerals from Acid Mine Drainage Treatment Process	1099
Milczarek, Michael; Keller, Jason; Hendrickx, Jan; Partey, Frederick; Geddis, Michael High Resolution Estimates of Tailings Facility Evaporation Using Landsat Data	1105
Mosai, Alseno Kagiso; Kotze, Izak; Chimuka, Luke; Cukrowska, Ewa; Tutu, Hlanganani The Recovery Of Pt(IV) From Aqueous Solutions By APDEMS-functionalised Zeolite	1111
Ruhland, Grit What Art Can Tell About Modified Environmental Systems	1117
Sartz, Lotta; Sädbom, Stefan; Bäckström, Mattias Remediation of Historic Waste Rock by Injection of Green Liquor Dregs – Results From a Field Scale Trial, Gladhammar, Southern Sweden	1124
Sibanda, Lesley Kudakwashe; Broadhurst, Jennifer Exploring An Alternative Approach To Mine Waste Management In The South African Gold Sector	1130
Williams, Martin; Pinana, Eduardo; Opara, Ola; Adams, Jack Electrobiological Reduction for Low Level Selenium Removal from Mine Water and Reverse Osmosis Brine	1136

— Lagniappe —

Author Index	xxxix
Keyword Index	xxxvii



**GEOCHEMISTRY
HYDROGEOLOGY**



Characterisation of arsenic geochemistry in mine tailings from a mesothermal gold deposit

H. Christenson¹, J. Pope¹, D. Craw², J. Johns³, N. Newman¹, D. Trumm¹

¹CRL Energy Ltd, 97 Nazareth Ave, Christchurch, New Zealand,

²Geology Department, University of Otago, 360 Leith Street, Dunedin, New Zealand,

³Oceana Gold Ltd, Macraes, Otago 9483, New Zealand

Abstract

Macraes mine was opened in 1989, and extracts mesothermal gold from a shearing zone in the Otago schist. The gold occurs in pyrite and arsenopyrite, which comprise 1 % of the ore. In September 2015 an 80 m core was drilled through the northern end of the Mixed Tailings Facility (MTF) that received flotation and sulfide concentrate tailings from 1990 to 2014. Adaptations to ore processing occurred over this period, including the introduction of pressure oxidation in 1999.

Preliminary study of the core has involved characterisation of a section at 44 m depth, and a section at 77 m depth. The shallower sample has brown tailings, indicative of iron oxide minerals produced during pressure oxidation. The deep sample is grey, similar to the original colour of the schist. The tailings porewater at both depths contains 2 ppm As. Arsenic in the tailings is associated predominantly with iron oxide minerals at 44 m depth, and with sulfide minerals at 77 m depth. A sequential extraction showed promise as a way to investigate mineral associations in the MTF, and preliminary geochemical modelling suggests that sorption equilibria are a key process in determining As concentrations in pore water of the tailings facility.

Introduction

The Macraes mine extracts mesothermal gold from a mineralised shear zone in the Otago Schist (Figure 1). The ore typically has 1 % pyrite and arsenopyrite which contain encapsulated gold, in the order of 1.6 grams per tonne (Milham and Craw 2009). The mine was opened in 1989, and has undergone several changes to the ore processing regimes over its lifetime (Figure 2). This has led to variations in the chemistry and composition of the mine wastes over this time.

Ore processing at the site uses a combination of physical and chemical processes to extract gold. The ore is crushed and ground to sand and the sulfide rich fraction is concentrated using froth flotation. The gangue is deposited into the Mixed Tailings Facility (MTF), while the concentrate is further milled to $15 \pm 10 \mu\text{m}$ prior to oxidation and gold extraction. The gold is extracted from the sulfide fraction by carbon-in-pulp cyanidation (Craw et al. 1999). When the mine opened in 1989 this extraction was performed directly on the

sulfide concentrate, without the oxidation step. Between 1989 and 1993, the arsenopyrite-bearing concentrate tailings were stored in a separate facility to the flotation tailings (Craw et al. 1999), however from 1993 onwards the concentrate tailings were also sent to the MTF.

In order to maximise gold extraction, a pressure oxidation plant was commissioned in 1999 which treated the sulfide concentrate prior to cyanidation (Craw 2003). The concentrate is roasted in an oxygen rich autoclave (225°C , 3800 kPa O_2) for 1 hour which causes nearly complete oxidation of the sulfides (Craw 2006). The oxidation process generates sulfuric acid, which is managed via limestone addition to maintain a solution pH between 1 and 2. The principal wastes formed in the pressure oxidation plant are calcium sulfate (as anhydrite and/or gypsum), jarosite, iron (oxyhydr)oxide (as hematite or ferrihydrite), and amorphous iron arsenate. The discharge from the pressure oxidation plant is treated by carbon-in-pulp cyanidation and then deposited in the MTF with the flotation tailings. Be-



tween 1999 and 2000, the concentrate tailings collected between 1989-1993 were reprocessed through the oxidation plant and sent to the MTF. In 2007, the plant also started processing concentrate from the Globe mine near Reefton, which has 4% stibnite in addition to pyrite and arsenopyrite (Milham and Craw, 2009).

Arsenic is an environmentally relevant element that is present in the MTF at Macraes mine. Consent conditions for Macraes set As limits and monitoring requirements for the mine and associated facilities. Seepage from the tailings is captured in a dedicated drainage system and returned to the processing plant as part of the process water circuit. Release of As from the MTF is an environmental risk, the magnitude of which is dependent on the geochemistry of the tailings and the in situ processes occurring in the impoundment. The changes in ore processing over the lifetime of Macraes mine has altered the geochemistry of the As bearing phases in the tailings. Characterisation of the tailings and processes controlling As mobility will help to inform management practices required into the future. In 2015, a core was taken through 80 m of the MTF. This paper tests a sequential extraction to investigate the as-

sociation of As with minerals in tailings from two sections of the core that have undergone different gold extraction processes.

Methods

The core was extracted from the MTF in September 2015, and was cut into sections, wrapped in cling film, and frozen. The frozen sections were stored at -18°C prior to analysis. Two core depths were selected for provisional study; one at 77 m depth near the base of the core, and one at 44 m depth. Ten-centimetre subsamples were cut from the frozen sections with a saw, and thawed in a nitrogen atmosphere in a glove box. A plastic knife was used to remove sample that had been in contact with the metal saw. The 10 cm sub-sample was homogenised by mixing, and then placed into 50 mL centrifuge tubes. The tubes were centrifuged for 16 hours and pore water that pooled on top was collected. The pH of the pore water was measured with a calibrated pH meter. Subsamples of the pore water were then diluted with degassed distilled water prior to analysis.

Arsenic speciation in the pore waters was measured using the spectrophotomet-

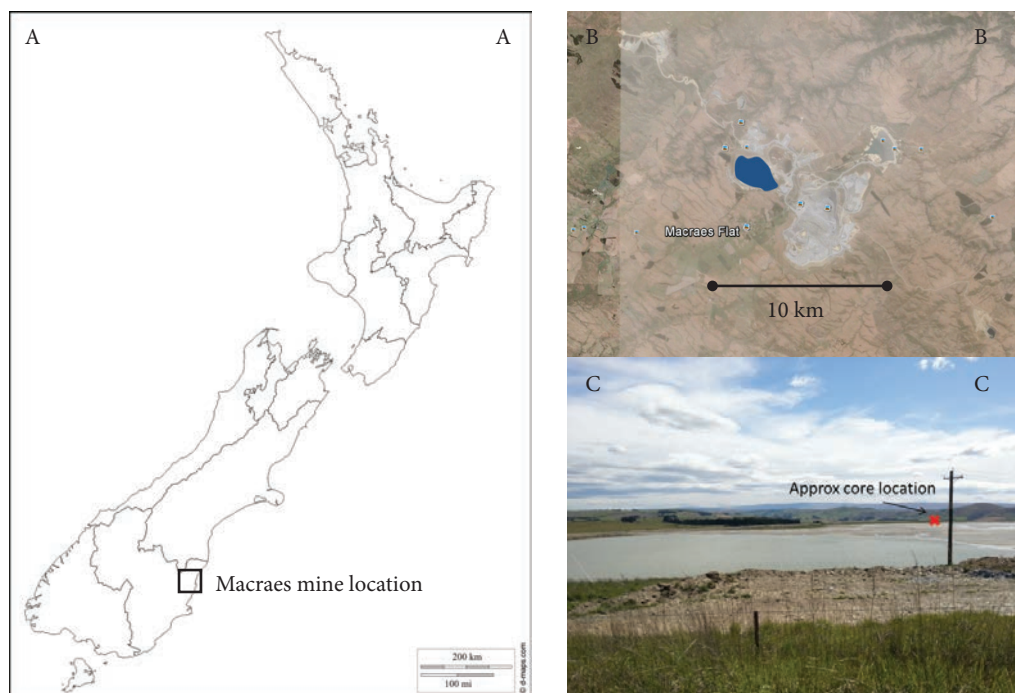


Figure 1. The location of the Macraes mine (A), tailings dam (B, blue shading) and core site (C) in Otago. Images A and B adapted from d-maps and Google Earth respectively.



ric method of Johnson and Pilson (1972). This method takes advantage of the reactivity of arsenate and phosphate with molybdenum blue complexes, and manipulates arsenic oxidation state to determine the arsenate and arsenite concentrations by difference.

The phase associations of arsenic in the tailings were investigated using sequential extraction techniques. These techniques use increasingly aggressive chemical reagents to target dissolution of mineral groups in undried solid samples depending on their re-

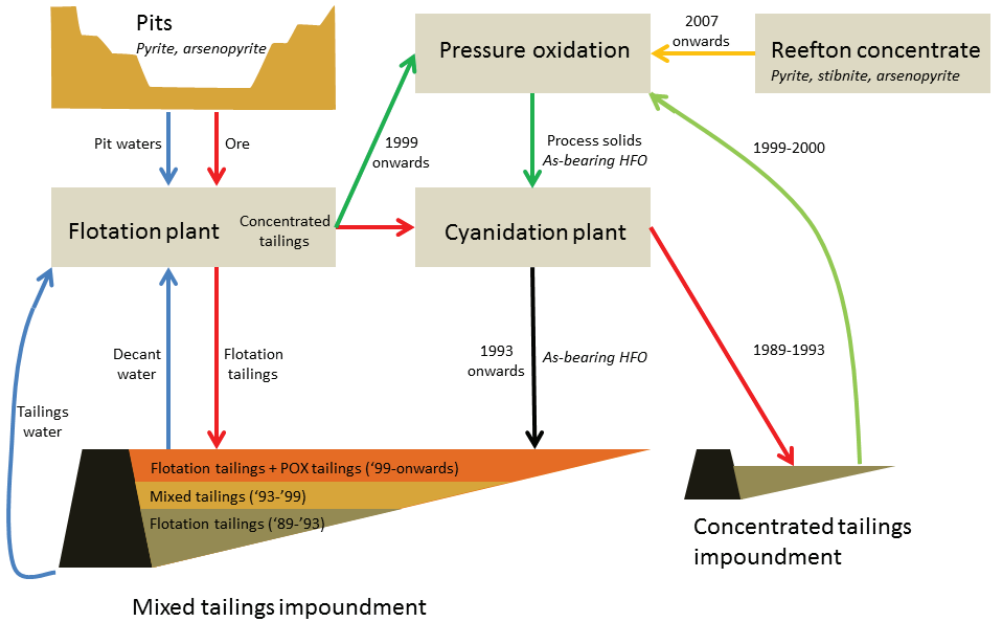


Figure 2. Processing systems at Macraes mine, modified from Milham and Craw (2009).

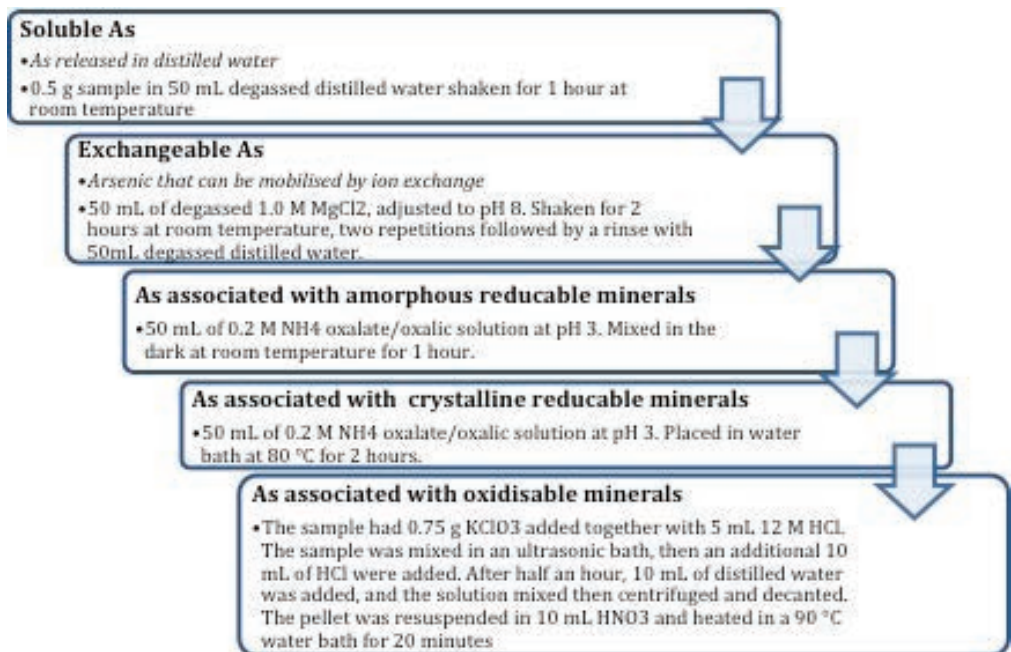


Figure 3. A summary of the sequential extraction from Nieva et al. (2016).



activity. This results in operationally defined fractions that are intended to represent elemental relationships with particular mineral constituents of the tailings. In this study an extraction scheme used by Nieva et al. (2016) was adapted to target arsenic associated with soluble, exchangeable, amorphous and crystalline oxides, and sulfide phases (Figure 3). After each extraction step the sample was centrifuged for 15 minutes and the supernatant filtered and collected for analyses. The next reagent was added to the remaining solid in the centrifuge tube. In addition, an extraction was performed in aqua regia to determine the total concentration of arsenic present in the tailings. A certified reference material (CRM-RTS 3a from Canmet Mining) comprised of sulfide ore mill tailings, was extracted alongside the tailings extracts. The pore water, sequential extraction and aqua regia extracts were analysed for Al, As, Fe, Mn, P, S and Sb by ICP-MS and for chloride and sulfate by ion chromatography methods at an accredited laboratory.

Geochemical modelling was performed using Visual MINTEQ (Gustafsson, 2009), with the default comp_2008.vdb, thermos.vdb and type6.vdb databases for component, aqueous species and solubility thermodynamic data. Bicarbonate was not analysed due to insufficient sample volume, and so a calculated concentration to balance ions in solution was used for modelling. Sorption to iron oxides was modelled using the diffuse layer model (DLM) with the “HFO (Dzombak and Morel)” and “Goethite (Weng et al)” models in Visual MINTEQ.

Results

The tailings from 77 m depth in the MTF were grey, with a clay-like texture (Figure 4). The grey colouring is similar to that of the schist that is visible around the Macraes area. A few millilitres of pore water were able to be extracted from the tailings, and the pore water pH was 8.58. Unfortunately, the volume was too small to allow for speciation analyses to be performed, however ICP-MS revealed 2 mg/L of arsenic is present in the pore water. The tailings from 44 m depth were brown in colour (Fig. 4.), and had some coarser material mixed in with the clay-like textured material. A greater volume of pore water was able to be extract-

ed from the 44 m tailings. Pore water pH was 8.14, and the 2 mg/L of arsenic present was speciated entirely as As V. Provisional modelling indicated that at both depths the tailings were saturated with respect to aluminium hydroxide phases, and that the tailings at 44 m depth were close to saturation with respect to gypsum and anhydrite.

The sequential extraction results show markedly different As chemistry in the tailings at the two depths (Figure 5). At 77 m depth, arsenic was predominantly associated with sulfide minerals, and at 44 m depth, arsenic was predominantly associated with reducible metal oxide minerals. There were higher concentrations of soluble and exchangeable As in the tailings from 77 m depth. In the CRM and the 44 m depth tailings sample, the sum of the sequential extraction concentrations was very similar to the concentration from the aqua regia digest. The 77 m sample had significantly lower concentrations extracted with aqua regia than in the sequential extraction. The CRM sample had 99% recovery of As, indicating good extraction by both the sequential extraction and aqua regia methods.

Iron in the tailings was predominantly in an oxidised form. The mineral forms were not identified, but in the deep tailings a greater proportion of Fe was mobilised in the extraction phase targeting amorphous metal oxides. In the shallow tailings more than twice as much iron was present in a crystalline rather than amorphous iron oxide form. There was more sulfide associated iron in the deep tailings from 77 m than the shallow tailings at 44 m, however some sulfide associated iron persisted in the shallow sample. Iron in the CRM was 88 % recoverable in aqua regia.



Figure 4. Subsamples of tailings from 77 m depth (grey, above) and 44 m depth (brown, below) showing the colour difference between the samples.



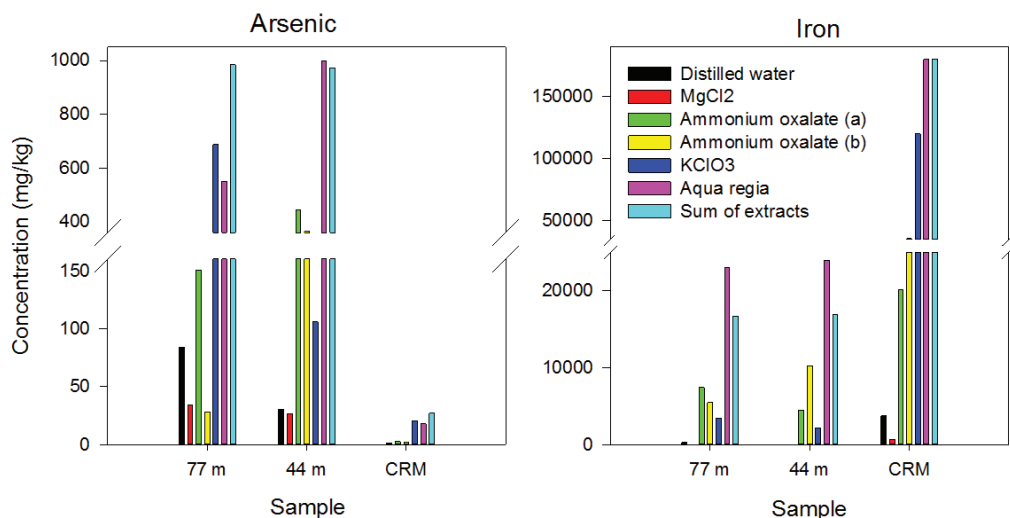


Figure 5. Concentrations of As and Fe dissolved in each step of the sequential extraction process, together with the sum of concentrations, and the concentration dissolved in aqua regia.

Discussion

The concentration of arsenic in both the pore water of the tailings, and the tailings themselves was similar at the 44 m and 77 m sample depths. However, the phase associations of arsenic in the tailings were distinct. Arsenic in the ore occurs predominantly in pyrite and as arsenopyrite, and it is apparent the changes in gold extraction practises used at the mine have altered the distribution of arsenic between the operationally defined mineral fractions in the tailings.

Preliminary modelling of pore waters showed no arsenic minerals close to saturation at either depth, and so it seems likely sorption equilibria may be more important for determining pore water As concentrations than solubility equilibria. It was interesting however that despite identical As concentrations in the pore water, the soluble and exchangeable As fractions in the tailings was substantially larger in the 77 m depth tailings. This is likely a result of greater solubility of the As containing minerals at depth. For instance arsenopyrite is more soluble than iron arsenate. Other possible reasons may include pH and arsenic speciation. The 77 m depth pore water sample was not analysed for As III/V speciation, however if there was a proportion of As present as As III, it may be more easily mobilised by the earlier extractions than As V due to its typically lower affinity for iron ox-

ide surfaces at pH \approx 8. The pore water pH was 8.58 at 77 m depth, compared to 8.14 at 44 m.

If adsorption equilibria are a primary control on As mobility, comprehensive modelling of the pore water solutions and the adsorbing phases may improve understanding on the processes controlling pore water As concentrations in the system. This will be performed as this project progresses. As part of this further assessment methods such as those employed by Keon et al. (2001), using a phosphate solution to competitively desorb As from iron oxides may be employed. This will allow some distinction to be made between adsorbed versus co-precipitated As species, which may have different mobilities.

At 44 m depth 83% of the arsenic present was soluble in ammonium oxalate extractions, with 45 % soluble at room temperature and 38 % soluble at 80°C. At the Giant mine in Canada, milled concentrate showed a similar distribution of As association to those observed in the tailings at Macraes mine. Prior to roasting, As was principally associated with sulfide minerals in the mill product, while the roasted product had As predominantly associated with amorphous metal oxides (Walker et al. 2015). The arsenic distribution is contrasting to that of the iron itself, which had a greater proportion present in crystalline forms in the pressure-oxidation tailings at Macraes mine. These results are



consistent with papers interpreting mineralogy of pressure oxidation tailings from Macraes, which contain amorphous iron arsenate, jarosite, amorphous iron oxy-hydroxide and hematite (Craw 2003; Craw 2006). At 77 m depth, 70% of the arsenic present was associated with sulfide minerals. It seems little alteration of the As containing minerals in the ore occurred during processing. A small proportion of sulfide bound As persists in the pressure oxidation tailings from 44 m as well, which may be due to incomplete oxidation of the sulfide concentrate, and/or incomplete removal of the sulfide fraction during flotation.

The sequential extraction technique showed some interesting and coherent results, however other results indicate some further method development will be required. The aqua regia extraction targets most non-silicate phases. In the 77 m depth tailings sample, the sum of extracted As was 984 mg/kg As as opposed to 550 mg/kg As by aqua regia extraction. The values extracted by sequential extraction and aqua regia were within a few percent of each other for the 44 m and CRM samples, and equated to 99% recovery of As in the CRM. Subsample heterogeneity may be responsible for the difference in these results. Going forward there will be greater repetition of samples to ensure the capabilities of the method are well understood.

Conclusions

The As chemistry in the MTF at Macraes mine is influenced by gold extraction techniques. Tailings that were directly extracted have As predominantly associated with sulfide minerals, whereas tailings that have undergone pressure oxidation have As associated largely with metal oxides. The solid tailings contain close to 1000 mg/kg of As, and pore water concentrations are 2 mg/L at both tailings depths. It is likely that sorption equilibria are important in regulating As concentrations in the tailings.

Continuing study of the core will characterise pore water and tailings chemistry throughout the length of the core, and geochemical modelling will be applied to assess the processes controlling pore water arsenic concentrations.

Acknowledgements

This research is funded by the New Zealand Ministry of Business, Innovation and Employment under contract FRST CRLE1403 – Mine Environment Life Cycle Guide. We acknowledge OceanaGold and staff for provision of the core samples.

References

- Craw, D. (2003). “Geochemical changes in mine tailings during a transition to pressure-oxidation process discharge, Macraes Mine, New Zealand.” *Journal of Geochemical Exploration* 80(1): 81-94.
- Craw, D. (2006). “Pressure-oxidation autoclave as an analogue for acid-sulphate alteration in epithermal systems.” *Miner Deposita* 41: 357-368.
- Craw, D., D. Chappell, M. Nelson and M. Walrond (1999). “Consolidation and incipient oxidation of alkaline arsenopyrite-bearing mine tailings, Macraes Mine, New Zealand.” *Applied geochemistry* 14(4): 485-498.
- Johnson, D. L. and M. E. Q. Pilson (1972). “Spectrophotometric Determination of Arsenite, Arsenate, and Phosphate in Natural Waters.” *Analytica Chimica Acta* 58(1972): 288 - 299.
- Keon, N., C. Swartz, D. Brabander, C. Harvey and H. Hemond (2001). “Validation of an arsenic sequential extraction method for evaluating mobility in sediments.” *Environmental Science & Technology* 35(13): 2778-2784.
- Milham, L. A. and D. Craw (2009). “Antimony mobilization through two contrasting gold ore processing systems, New Zealand.” *Mine Water and the Environment* 28: 136-145.
- Nieva, N., L. Borgnino, F. Locati and M. García (2016). “Mineralogical control on arsenic release during sediment-water interaction in abandoned mine wastes from the Argentina Puna.” *Science of the Total Environment* 550: 1141-1151.
- Walker, S., H. Jamieson, A. Lanzirrotti, G. Hall and R. Peterson (2015). “The effect of ore roasting on arsenic oxidation state and solid phase speciation in gold mine tailings.” *Geochemistry: Exploration, Environment, Analysis* 15(4): 273-291.





Permeable Reactive Barrier Feasibility Assessment at Goldcorp's Red Lake Gold Mines: Hydrogeological, Geochemical and Geotechnical Design Considerations[©]

T. Crozier¹, D. Paszkowski¹, G. Parent¹, D. Cook¹, V. Mann¹, C. Mendoza¹,
H. Provost¹, A.J. Martin², J. Helsen², J. Bain³, D.W. Blowes³, C. Gaspar⁴, J. Russell⁴

¹BGC Engineering Inc., 980 Howe St, Vancouver, Canada

²Lorax Environmental Services Ltd., 2289 Burrard St., Vancouver, Canada

³University of Waterloo, Waterloo, Ontario

⁴Goldcorp Red Lake Gold Mines, Balmertown, Canada

Abstract

Goldcorp is assessing the feasibility of using permeable reactive barriers (PRBs) to intercept and treat tailings-derived seepage in a discontinuously confined sand and gravel aquifer down-gradient from the Campbell Complex Tailings Management Area (Ontario, Canada). Uncertainty in hydrogeological, geochemical and geotechnical site conditions, and PRB matrix properties was managed using an iterative design process informed by staged site investigations, field-scale tracer migration studies, advanced hydrogeological and geotechnical laboratory testing, numerical groundwater flow modeling, and evaluation of removal rates for parameters of primary concern (As, Co, Fe) in laboratory-based geochemical flow-through column studies.

Keywords: PRB design, bioremediation, hydraulic residence time, iron, arsenic, cobalt

Introduction

Goldcorp is assessing the feasibility of using PRBs (Blowes et al. 2000) to intercept and treat groundwater affected by seepage from the Red Lake Gold Mines Campbell Complex Tailings Management Area (TMA). This paper, which presents hydrogeological, geochemical and geotechnical considerations driving PRB design, represents the third in a series of three papers relating to PRB feasibility at the Campbell Complex. The other two papers, presented as part of these proceedings, describe the groundwater plume distribution and contaminant behaviour (Martin et al., 2018), and present the results of tracer testwork designed to confirm contamination flowpaths (Helsen et al., 2018).

The Campbell Complex is located 7 km northeast of the Town of Red Lake in north-western Ontario and has been the site of gold-ore mining and milling operations since 1949. Tailings have been discharged to the current TMA since 1983. A portion of the water that accumulates in the TMA infiltrates into the subsurface and travels along the “Red Lake

Flow Path,” a groundwater flow path that discharges to ditches draining a golf course (GC ditches), which in turn feed a downstream wetland and lake (Martin et al. 2018).

Seepage flows show tailings-related signatures reflecting mill process waters (SO₄, Cl, NH₃, CN, Cd, Co, Cu, Ni and Zn) and remobilization from tailings solids (Fe and As). As, Co and Fe represent the parameters of primary concern (POPCs) given exceedances of their site-specific groundwater targets in the TMA pond source water and down-gradient plume. Secondary target parameters include SO₄, NO₃, NO₂, Cd, Cu, Ni and Zn. Pilot study results indicated that primary and secondary parameters were amenable to treatment with a common PRB design (Bain and Blowes, 2005).

Assessments completed in support of feasibility design for the PRB include: 1) detailed site characterization of the physical and chemical hydrogeology (Martin et al. 2018); 2) advanced laboratory-based testwork to evaluate geotechnical and hydrogeologic properties of the aquifer and the PRB reactive



matrix materials; 3) *in situ* tracer testwork to evaluate contaminant migration pathways (Helsen et al. 2018); 4) predictive numerical groundwater flow modeling; and, 5) evaluation of removal rates for POPCs in laboratory-based geochemical flow-through column studies.

Overview of Proposed PRB Design

Site investigations since 1990 have delineated a 200 m wide plume at the downstream toe of the West Dam of the TMA (Martin *et al.* 2018). Staged implementation of the PRB is proposed to optimize design and construction methods prior to placing the PRB across the full plume width. Initial emplacement of the PRB would be a 30 m long segment oriented parallel to the downstream toe of the West Dam and perpendicular to groundwater flow (Figure 1). Based on preliminary design results, the PRB width would be designed to achieve a hydraulic residence time (HRT) of 4 to 7 days. To maximize remedial benefit, it would be located to intercept the highest hydraulic conductivity (K) zones of the aquifer, which also exhibit the highest concentrations

of POPCs. Results from a tracer migration study (Helsen et al. 2018) confirmed the selected location would treat TMA-affected groundwater that discharges to the downstream receiving environment.

The PRB would be placed to intersect the sand and gravel aquifer from competent bedrock (17 to 20 m below ground surface) to a nominal depth of 5 m below grade. A soil-cement-bentonite surface seal would serve as backfill from the top of the reactive matrix materials to ground surface. Seal and matrix materials were designed to equal or surpass strength and density characteristics of the native materials.

PRB design followed typical engineering work flow: 1) pilot study to demonstrate treatment efficacy; 2) preliminary design to identify preferred construction methodologies and inform subsequent investigation and study; and, 3) feasibility level design. The feasibility study focused on improving cost evaluations and assessing geotechnical, hydrogeological and geochemical design considerations identified during preliminary stages (Table 1).

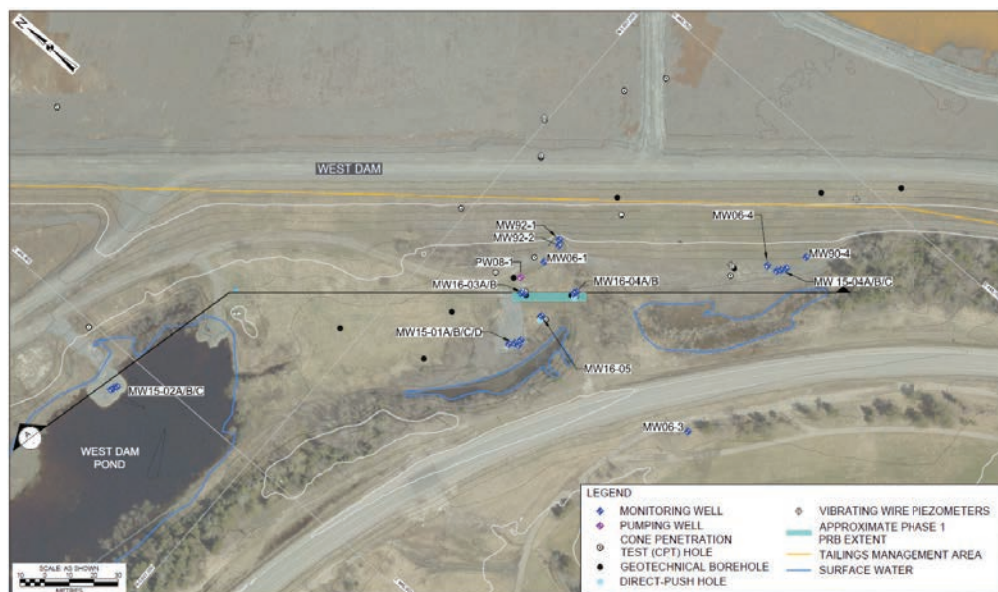


Figure 1. Location of proposed PRB, downstream toe of West Dam of the Campbell Complex TMA.



Geotechnical Design Considerations

Geotechnical challenges related to PRB design included emplacement at the toe of an upstream, compacted clay core, zoned-earth-fill embankment (West Dam) and soft glacio-lacustrine silts and clays confining an artesian, fining-upwards, glaciofluvial sand and gravel aquifer. Interpretation of cone penetration test (CPT) results also indicated the presence of potentially liquefiable sands and silts within the footprint of the proposed PRB.

Prior to CPT liquefaction screening, preliminary design of the PRB considered a 30 m long, 18 m deep, up to 3 m wide reactive matrix emplaced using a biopolymer- or guar-slurry-supported trenching method. 2-D limit equilibrium analyses were conducted to evaluate stability of the adjacent West Dam and Hwy 125, including required trench setback distances. Trench stability analyses, including 3-D limit equilibrium, were also

conducted to assess slurry head and trench panel requirements to prevent trench collapse during construction. However, to mitigate the potential for static liquefaction, secant-pile-type construction was considered as a preferred alternative to trenching, with overlapping large-diameter holes and temporary casing using caissons. This method permits additional flexibility and tooling to be used in the event boulders are encountered at the aquifer-bedrock interface during construction (Table 1).

Piping or clogging of the PRB were also considered; anticipated hydraulic head gradients from predictive numerical modeling, combined with continuous erosion filter (CEF) tests, indicated that piping failure is unlikely. The secant-pile construction method further reduces this risk as the overlapping of bores minimizes potential for through-going seams of segregated PRB materials.

Table 1. *Geotechnical, Hydrogeological and Geochemical Design Considerations for a PRB on the Red Lake Flow Path, Campbell Complex TMA, Ontario, Canada.*

Category	Risk/Consideration	Design Approach/Mitigation
Geotechnical		
Local stability of trench	Trench collapse	2-D then 3-D limit equilibrium stability analyses
TMA West Dam & HWY 125 stability	Slope failure	2-D limit equilibrium stability analyses
	Soft foundation soils	Advanced laboratory testing
	Static Liquefaction	Critical-state soil mechanics analyses
Piping failure	PRB clogging	Filter relationships screening
	Ground loss	Continuous erosion filter (CEF) tests
	Plume bypass	Construction contingency
Hydrogeological		
Aquifer hydraulic properties	Heterogeneity	“Point-” and “Aquifer-scale” testing for K, S
	Anisotropy	3-D numerical groundwater flow modeling
PRB materials	Properties not quantified	“High” and “Average” value design scenarios
	Segregation when placed	Advanced laboratory testing
Hydraulic head gradients	Seasonal variation	Continuous monitoring + consistent survey
	Measurement accuracy	High and Average condition design scenarios
Plume bypass	Poor initial location	<i>In situ</i> tracer study (Helsen <i>et al.</i> 2018)
	Bypass around PRB	3-D numerical groundwater flow modeling
Geochemical		
POPCs	Treatability	Pilot study results assessed by flow-through column study (Martin <i>et al.</i> 2018)
Products of reaction	Harmful concentrations	Literature review
Reaction rates	HRT	Monitoring trigger response action plan
PRB matrix composition	Cost of ZVI	Flow-through column study
		Flow-through column study evaluated ZVI composition of 10% and 25% by volume
Other		
TMA dam raise	Higher head gradient	3-D numerical groundwater flow modeling
TMA closure	Lower head gradient	3-D numerical groundwater flow modeling

1. K – hydraulic conductivity; S – storage properties; HRT – hydraulic residence time; ZVI – zero valent iron



Hydrogeological Design Considerations

Hydrogeological considerations for the design are associated with heterogeneity and anisotropy in hydraulic properties of the aquifer (Martin *et al.* 2018) and the unquantified hydraulic properties of the PRB materials. Seasonal variation in hydraulic head gradients, the magnitude of the gradients and the accuracy of groundwater levels also introduce uncertainty. Horizontal hydraulic conductivity (K_H) of the sand and gravel aquifer near the Phase 1 PRB ranges from 1×10^7 m/s to 3×10^3 m/s (Figure 2) and spans 5 to 6 orders of magnitude in the till unit at depth (Martin *et al.* 2018). Aquifer effective porosity (n_{eff}) ranges from 0.2 to 0.4 while horizontal hydraulic head gradients (i_H) in the PRB area range from 0.01 to 0.001 with an average of 0.007 (Martin *et al.* 2018).

A custom-built large laboratory flow-through cell (0.6 m wide \times 0.6 m high \times 1.20 m long) and large permeameter test cells (0.30 m dia. accommodating lengths of 0.10 and 0.30 m) were used to evaluate hydrogeologic parameters for proposed PRB materials. K_H was 3×10^{-3} and 6×10^{-3} m/s with an anisotropy ratio (K_H/K_V) of 5 to 10.

The potential for hydraulic bypass of the plume around or under the PRB, as well as “short-circuiting” through the PRB at locations where higher K aquifer materials are present was evaluated using a 3-dimensional (3-D) numerical groundwater flow model (MODFLOW-SURFACT model developed in Groundwater Vistas, ESI 2011). The model was calibrated to steady-state hydraulic heads, average discharge rates to the GC ditches, and a 3-day pumping test completed in PW08-01 (Figure 1). The PRB was implemented in the model as a 1.2 m wide zone with lengths from 30 to 200 m to evaluate HRT, bypass potential, changes in flow to the GC ditches and hydraulic head changes under the TMA. Effects from increasing the TMA pond level (i.e., TMA dam raise) and post-closure conditions (i.e., no operating pond) were also simulated.

Key findings from the groundwater flow model include: 1) HRT in the PRB is largely controlled by K_H and i_H of the aquifer surrounding the treatment zone, provided K of the PRB is greater than K of the aquifer; 2) K of the PRB matrix should lie in the range from 10^{-6} to 10^{-3} m/s to avoid elevated heads beneath the West Dam of the TMA; 3) HRT

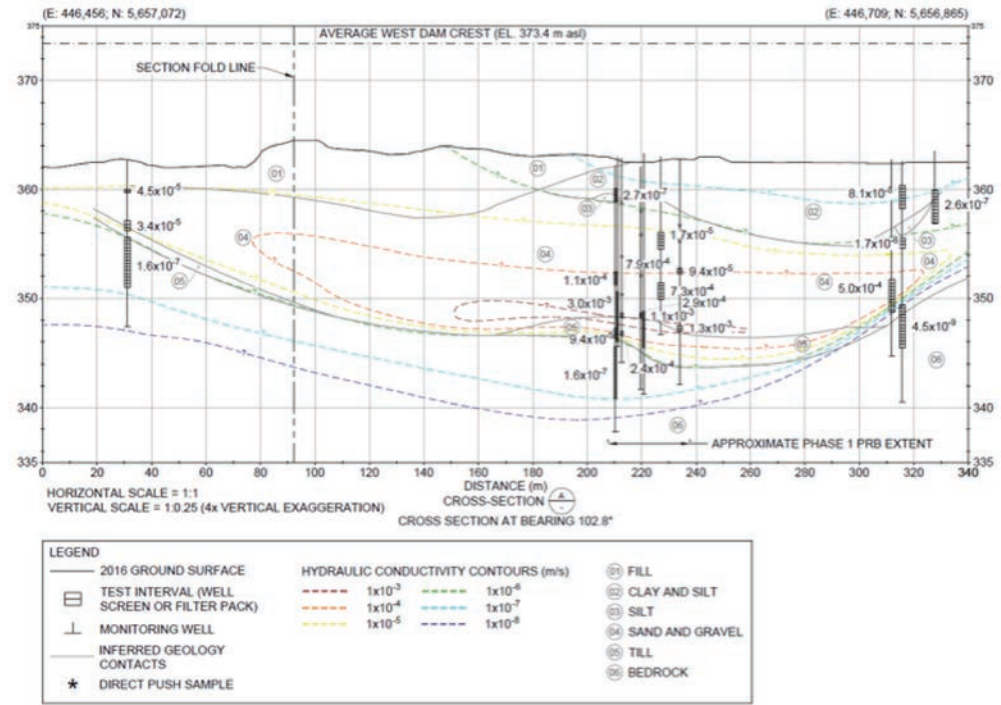


Figure 2 – Cross-section A showing geologic materials and interpreted K horizons along the PRB



Table 2. HRTs, hydrogeologic properties and calculated PRB design widths required to treat As, Fe and Co for High and Average design scenarios during Operations and Post-Closure.

Parameter	High Case		Average Case	
	Operations	Post-Closure	Operations	Post-Closure
HRT (days)^(1,2,3)				
As		1.9		0.75
Fe		11		7.1
Co	16	24	34	14
Hydrogeologic Properties (units as shown)				
K ⁽⁴⁾		3x10 ⁻³ m/s		5x10 ⁻⁴ m/s
n _{eff} ⁽⁵⁾		0.35		0.40
iH ⁽⁶⁾	0.003	0.0015	0.002	0.001
Required PRB treatment widths (m)				
As	4	2	.2	0.1
Fe	24	12	2	0.8
Co	13	27	8	2

1. High Operations scenario influent concentrations were set to maximum As, Co and Fe values recorded between 2006 and 2016 at monitoring wells immediately up-gradient (MW92-1, MW92-2, and MW06-1) and within the footprint (MW16 03A/B and MW16-04A/B) of the Phase 1 PRB (Figure 1). Average Operations scenario influent concentrations were set to highest 50th percentile As, Co and Fe values observed in the same wells over the same period.
2. As and Fe concentrations for the High and Average Post-Closure scenarios were assumed to remain unchanged since As and Fe are generated through the reductive dissolution of Fe-oxide phases in the tailings, and this process is anticipated to continue over decadal time scales.
3. The primary source of Co is mill effluent, and therefore Co concentrations are expected to decline at closure. Data from site wells were examined to establish High (0.1 mg/L) and Average (0.06 mg/L) Post-Closure influent values.
4. K for High Operations and Post-Closure scenarios is based on the highest values measured in the aquifer. K for Average Operations and Post-Closure scenarios is the geometric mean of test results from wells MW15-01B, MW16 03A/B, MW16 05, MW06-1, MW92-1, MW16-04B, MW06-4 screened inside the 10⁻⁵ m/s K contour (Figure 2).
5. n_{eff} of *in situ* PRB materials could not be evaluated by laboratory testwork; best estimates were based on total porosities of the individual PRB materials, experience and literature.
6. iH assigned to High Operations scenario was set to 0.003 to reflect the high end of the range measured in wells nearest to Phase 1 (0.001 to 0.004) during the period from August 2016 to April 2017; iH for the Average Operations scenario was set to 0.002, the average over the same period. iH for Post-Closure scenarios was set to 50% of Operations values based on groundwater flow modeling results.

in the range of 4 to 7 days for a 1.2 m wide PRB are unlikely adjacent to the most conductive zones of the plume during operating conditions; and, 4) under post-closure conditions, hydraulic head gradients decline such that targeted HRTs may be realized.

Geochemical Design Considerations

Flow-through column experiments using TMA-affected groundwater from the Red Lake Flow Path indicated a reactive matrix composed of 25% zero valent iron (ZVI), 30% organic materials and 45% sand and fine gravel (by volume) could achieve remedial targets for As, but not for Co or Fe (data not shown). Removal rates for Co were lower than anticipated, likely because non-labile Co complexes were present (Martin *et al.* 2018). Additionally,

calculation of Fe removal rates from column studies were confounded by early-time release of dissolved Fe associated with reductive dissolution of ZVI corrosion products.

Performance of the PRB was evaluated by considering the HRT required to reduce concentrations of POPCs to acceptable levels (defined by site-specific targets). HRT was calculated as the quotient of the difference between influent POPC concentration and the target post-treatment concentration divided by mass removal rates derived from the geochemical flow-through column studies (data not shown). To account for temperature difference between laboratory columns (23°C) and aquifer groundwater (6°C) a factor of 3.0 was applied to derive a temperature-scaled HRT (Benner *et al.* 2002).



PRB treatment widths (W_{PRB}) required to achieve targeted post-treatment concentrations were calculated as the product of HRT for each of the POPCs and average linear groundwater velocity, calculated as $(K_H i_H) / n_{eff}$. Sources of uncertainty in hydrogeological and geochemical design variables were accounted for by considering four design scenarios (Table 2): a High case and an Average case for each of Operations and Post-Closure conditions.

Required treatment widths to achieve target remediation values for As, Co and Fe are shown in Table 2. HRTs and treatment widths for As (0.1 to 4 m) for all design scenarios are considered practical from the perspectives of construction methodology and working space. In contrast, HRTs and treatment widths required to treat Fe for the High Operations scenario (24 m) and High Post-Closure scenario (12 m) are considered impractical. However, HRTs and treatment widths for the Average Operations and Post-Closure scenarios are within practical ranges (HRT of 7 days, treatment widths of 0.8 to 2 m). HRTs and treatment widths required to support the removal of Co to concentrations less than the target values are impractical for all but the Average Post-Closure scenario.

Conclusions

Geotechnical concerns related to using a bio-polymer- or guar-slurry-supported trenching method were managed by changing to a secant-pile-type construction method. Evaluation of HRTs and PRB treatment widths for the four design scenarios considered indicated that design and installation of the PRB will treat As but is not practical for full treatment of all POPCs. In particular, design of the PRB to treat current Co concentrations is not recommended given the uncertainty in treatment efficiency (owing to the prevalence of non-labile complexes generated during ore processing) and the likelihood that Co concentrations will decline once operations cease. Design of the PRB to treat Fe for the High Operations scenario is also not recommended due to the treatment width required and uncertainty in treatment efficacy.

Design of the PRB to treat Fe concentrations for the High Post-Closure scenario (i.e., treatment width of 12 m) as part of a long-

term passive closure strategy may have merit. A lower bound on the design treatment width of 2 m was recommended to address Fe concentrations for the Average Operations scenario. This minimum treatment width would also reduce As concentrations for the High Post-Closure scenario to less than the target concentration.

The work completed emphasizes the critical need for robust characterization, detailed understanding of physical and chemical aspects of the flow system, and a phased design approach.

Acknowledgements

Goldcorp Canada is acknowledged for allowing the presentation of the data and discussion herein.

References

- Bain J., and Blowes D. 2005. Third Year Progress Report - An In-Situ Treatment System for the Remediation of Arsenic Bearing Tailings Water at Campbell Mine. Report prepared for Placer Dome Technical Services Ltd. and Campbell Mine Ltd., January 2005.
- Benner S.G., Blowes D.W., Ptacek C.J., Mayer K.U. (2002) Rates of sulfate reduction and metal sulfide precipitation in a permeable reactive barrier. *Appl. Geochem.* 17, 301-320.
- Blowes D.W., Ptacek C., Benner S.G., McRae C.W.T., Bennett T.A., Puls R.W. (2000) Treatment of inorganic contaminants using permeable reactive barriers. *J Contam Hydrol* 45: 123-137.
- Environmental Simulations Inc. [ESI] (2011). *Groundwater Vistas*, V. 6.52, Build 14. Reinholds, PA., U.S.A.
- Helsen J., Martin A.J., Crozier T., Parent G., Mann V., Gaspar C., Russell J. (2018) Permeable Reactive Barrier Feasibility Assessment at Goldcorp's Red Lake Gold Mines: Validation of Seepage Flow Paths through Tracer Testwork. 11th International Conference on Acid Rock Drainage, Pretoria, South Africa, September 10-14, 2018.
- Martin A.J., Helsen J., Crozier T., Parent G., Paszkowski D., Mendoza C., Provost H., Gaspar C., Russell J. (2018) Permeable Reactive Barrier Feasibility Assessment at Goldcorp's Red Lake Gold Mines: Delineation of Groundwater Flow Paths and Contaminant Behaviour, 11th International Conference on Acid Rock Drainage, Pretoria, South Africa, September 10-14, 2018.





Sinkhole development on mine flooding[©]

Gareth Digges La Touche¹, Barry Balding², Brian Keenan², Susan Digges La Touche³

¹*Golder, 20 Eastbourne Terrace, London, W2 6LG, United Kingdom, gdltouche@golder.com*

²*Town Centre House, Dublin Road, Naas, Co. Kildare, W91 TD0P, Ireland*

³*Golder, 20 Eastbourne Terrace, London, W2 6LG, United Kingdom*

Abstract

The development of dropout dolines during large scale dewatering operations is a well known and well understood phenomenon. Dropout dolines form due to soil collapse into an underlying void over bedrock fissures, typically in limestone, dolomite or gypsum rocks. During the rapid dewatering of calcareous strata dropout dolines have been known to develop and are a known risk during dewatering operations, when groundwater levels are rapidly reduced in the overlying overburden, resulting in high vertical groundwater flow gradients and changes in in-situ stress conditions.

This paper presents an atypical case of the development of a dropout doline during mine flooding. Dropout dolines typically form rapidly, in a matter of minutes, collapsing into a void that has evolved over a considerably longer timeframe. The case reported in this paper is associated with a former metalliferous mining operation in Ireland where the orebody is situated within a Carboniferous dolomitic limestone host rock. Dolomitisation and mineralisation occurred during the early Carboniferous and karst development took place during the Tertiary when groundwater levels were lower and humid climate conditions allowed active karst formation. The karst features subsequently became infilled with weathered rock and sediments during the Quaternary.

The presence of karst (palaeo) was known prior to mining and a number of features were identified. No doline development was observed during mine development and operation, although dewatering was undertaken to facilitate development. Following the cessation of mining, dewatering operations ceased and groundwater levels recovered to pre-mining levels. The dropout doline is believed to have developed immediately following the recovery of groundwater levels.

In this paper the chain of causation will be explored and the remedial solution that was implemented to facilitate the continuation of the original land use will be described. The paper will conclude by identifying the risk factors that should be considered during future similar mine closure operations.

Keywords: karst, sinkhole, doline, closure.

Introduction

Limestone terrains are often known for the presence and development of karst landforms, through the dissolution of rock and the development of a well-connected underground drainage network. These landforms may be covered by allogenic sediments such as glacial till or by residual soils. A common hazard in karst terrains is the potential for the overlying soils to be transported into an underlying bedrock opening so that a void migrates pro-

gressively upwards by progressive collapse to form a dropout doline (Waltham et al 2010). In February 2014 a sinkhole or dropout doline appeared after a night over heavy rain in a field above the worked out mine. The doline was elliptical in plan, measuring ca. 13m along its long axis, ca. 8 m along its short axis and ca. 7 m in depth (Figure 1). The sinkhole was steep-sided with no bedrock visible in its walls or base, both of which were composed of sandy glacial till.





Figure 1 Sinkhole a few days after development.

Geology

The area is underlain by a sequence of partially dolomitised Lower Carboniferous limestones which was subject to extensive, but episodic, karstification during the Tertiary Period, 65.5 – 2.6 million years ago (Drew & Jones 2000 and Coxon & McCarron 2009). During the early Tertiary a karstic drainage system developed in the area, with water movement concentrated along predominantly north-northwest to south-southeast and north to south trending strike slip faults. At this location, a north-northwest to south-southeast trending fault zone, known as “The Main Fissure”, was mapped underground. This sub-vertical feature pinches and swells over very short distances both along the dip and strike, with weathered areas up to 8 m wide being recorded. It is of note that the Main Fissure is situated below the doline (Figure 2) and the long axis of the doline aligns with the trend of the fissure. In contrast to the north-northwest to south-southeast and north to south trending

features the east to west trending faults tend to be tight and there has been minimal water movement along these structures and hence an absence of karst development.

By the mid-Tertiary karstification had reached a depth of at least 40m in the Gal-moy area and solution dolines had developed in which organic clays accumulated (Coxon & McCarron, 2009). Evidence from underground mapping indicates that karstification had developed to ca 90 m depth in some areas. During the Quaternary the climate oscillated between cold (glacial) and warm (interglacial) stages, however by the start of the Holocene, about 12,000 years ago, the area was ice free and the voids in the limestone that had formed in the Tertiary had become clogged with sediment and there was no longer any active groundwater circulation. In this area the limestone is covered by approximately 5 m of sandy glacial sediments with a well-developed clay matrix, known locally as Boulder Clay.



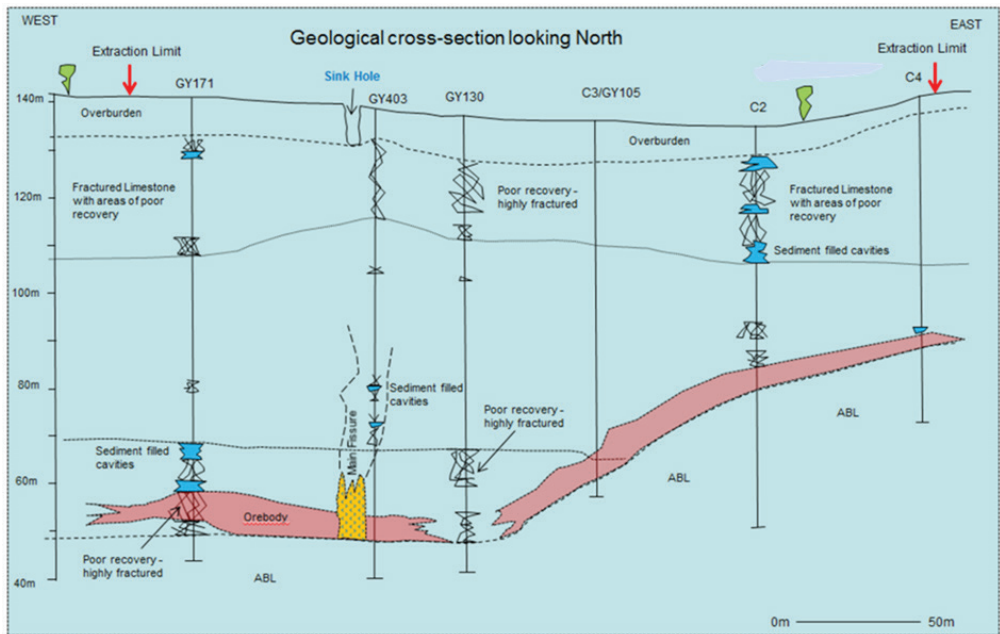


Figure 2 Relationship between the mine workings and the sinkhole.

Groundwater Regime

The Galmoy mining district occurs within a tightly-bounded block of Carboniferous Waulsortian dolomitised limestone (the “Galmoy Block”). All of the orebodies occur close to the southern end of the Galmoy Block, in close proximity to the east to west trending G Zone Fault Zone. During mine dewatering, the boundaries of the block acted to localise the area of drawdown, which was very well defined around the mine area. Groundwater recharge to the Galmoy Block is mostly derived from infiltration of precipitation and local runoff. Most of the block has a natural recharge of between 200 and 350 mm/year.

Dewatering, and underground mining, commenced at Galmoy in the middle of 1995. Mining continued until 2012 and dewatering ceased in 2013. The recovery of groundwater levels was rapid and the water-table had recovered to pre-mining conditions by March 2014.

Potential Mechanism of Doline Formation

Closed depressions, commonly referred to as sinkholes or dolines, are the commonest landform in karst areas. There are six broad types of sinkhole, which are described in

Waltham et al (2010) and in all cases focussed vertical groundwater movement and bedrock dissolution are essential precursors to their formation.

In solution sinkholes there is dissolutional lowering of the bedrock surface with drainage focussed on a central fissure or fissures. Environmental change may lead to solution sinkholes being filled with sediment and buried sinkholes are common in Ireland. The formation of collapse sinkholes requires focussed dissolution of bedrock at depth leading to the growth of a void in the roof which ultimately fails. Cap-rock sinkholes are a special type in which the collapse propagates upwards through non-limestone cover rocks. There are two types of subsidence sinkhole, dropout and suffosion, which have a common origin. A fracture in the bedrock is enlarged by dissolution until it reaches a size sufficient for turbulent flow and the transport of sediment. Where the superficial deposits overlying the bedrock are non-cohesive, they gradually slump into the enlarged fissure forming a broadly conical suffosion sinkhole. Where the superficial deposits are cohesive the basal sediment is washed into the bedrock fissure forming a void that grows upwards from the bedrock-overburden interface to form



an arch. The arch grows until a threshold is reached where it is no longer able to support the overburden and then collapses to form a dropout sinkhole with near-vertical sides.

It is considered that the sinkhole at Galmoy is a dropout doline formed due to a combination of the following factors.

- The presence of a palaeokarstic void system, the Main Fissure, which had been filled with sediment;
- Lowering of the local water-table by dewatering and intersection of the Main Fissure in the mine which together allowed the flow-path down the fissure to be re-activated. Groundwater flowed down the fissure towards the mine, taking with it some of the fissure sediment fill and opening void space within the fissure. The process was enhanced by concentration of surface drainage at the location of the Main Fissure due to a depression in the rockhead (the solid rock surface under the overburden) along the Main Fissure and an up gradient catchment associated with the Main Fissure;
- The development of open voids within the glacial till due to washout of material through fractures (i.e. palaeokarst features) in the bedrock associated with the Main Fissure; and
- Exceptional rainfall over the preceding period and infiltration, coupled with the spreading of agricultural water on the field sometime in the 24 hour period before the sinkhole appeared, which increased the weight of the overburden and acted as the trigger for collapse into the void which formed the sinkhole.

Scoping calculations of the potential for collapse of a soil voussoir arch based on the range of likely soil properties (density, thickness, cohesion, friction angle, void radius and groundwater flow velocity) at the site were undertaken using the method published by He et al (2003). The conditions were found to be consistent with a marginal stability condition, i.e. consistent with the potential for the formation of a dropout doline.

The timing for the development and formation of the doline may be considered in four stages as illustrated on Figure 3):

A. Development of palaeokarst (65.5 million

to 12,000 years ago): Evidence from mid-Tertiary organic clays in buried sinkholes in the area indicates that there was an active karst at this time and it is considered likely that groundwater was circulating through the Main Fissure. There may have been subsequent periods of active karstification but by 12,000 years ago all the voids in the limestone that had formed in the Tertiary had become clogged with sediment and there was no longer any active groundwater circulation through them;

B. Pre-mining (12,000 to 20 years ago): During the Holocene there was slow groundwater flow at shallow depth through immature fissures some of which are likely to have been slightly enlarged by dissolution to form channels and conduits. The water-table would have been similar to that which it has recovered to following cessation of dewatering with very low hydraulic gradients and consequent low groundwater velocities which would have been insufficient to entrain and transport sediment. Hence, no void could have formed in the overburden at this stage;

C. During Mining: During the mining stage dewatering had the effect of lowering of the water-table and increasing the water velocity (especially during periods of recharge) giving rise to a greater washout potential. The higher velocity water flows in the Main Fissure accelerated the removal of sediment and water through this route and it is likely that voids formed in the Main Fissure allowing sediment to be moved down from the overburden and development of a void at the base of the overburden; and

D. February 2014: Upon cessation of mine related dewatering the water-table began to return to its original pre-mining stage level. Importantly, as water was no longer being removed from the mine, active circulation of groundwater ceased and the rainfall recharge gradually filled up all of the voids with a consequent steady rise in the water-table. Observations of turbid water in some wells for a short period suggests that there may have been a final phase of sediment mobilisation as the water-table approached pre-mining levels and groundwater started to flow through



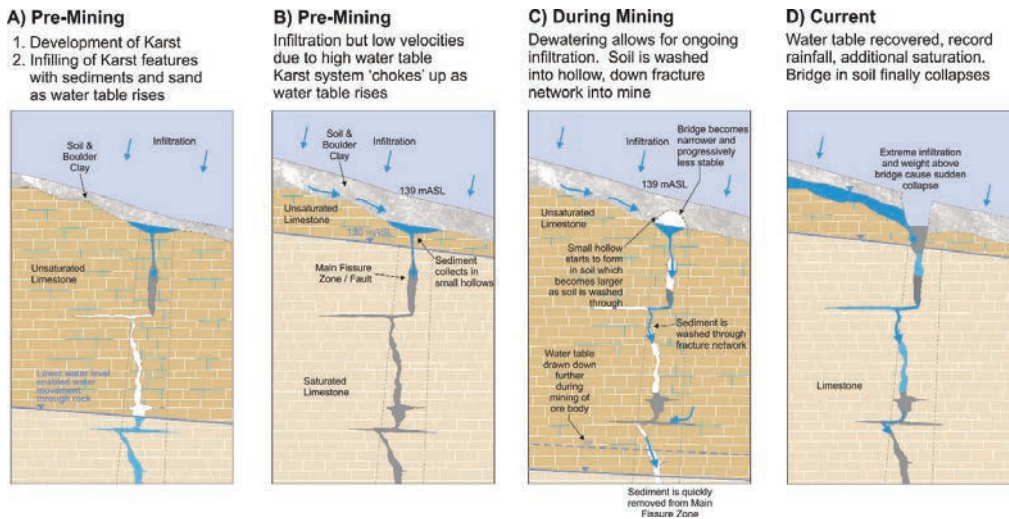


Figure 3 Sinkhole formation mechanism.

pre-mining paths. It is likely that the void within the overburden had grown to a size whereby the arch was close to the instability threshold. The period of heavy rain, possibly assisted by application of water to the field, increased the weight of the overburden to such an extent that the unstable arch collapsed suddenly, giving rise to a 'dropout sinkhole'.

Remediation

To remediate the sinkhole and allow the return of the field to agricultural use, a permeable plug was recommended to conserve the drainage pathway and to help alleviate the formation of further sinkholes in the vicinity. This was achieved (Figure 4) through the use of a simple bridging mechanism (≈ 1 m diameter boulders), over the throats between the limestone pinnacles which were exposed through excavation; the lower section comprising a permeable rip rap and ballast plug encapsulated in a geotextile. The upper section of repair entails compacted layers of rock fill/glacial till and a final capping layer of appropriate subsoil and topsoil to rehabilitate the agricultural surface.

Conclusion

The sinkhole that occurred at Galmoy can be classified as being a dropout sinkhole, most

likely occurring as a result of: water infiltration into the underlying Main Fissure due to the bedrock depression above it and lowering of the water-table by mine dewatering; the washout of the sediments within the fissure zone into the mine workings; the formation of a void and voussoir arch at the base of the overburden material as the sediments were washed through; and, heavy rainfall immediately prior to the collapse that acted as the trigger for the collapse of the arch in the overburden above the void.

The particular combination of features in this instance, comprising the Main Fissure developed by enhanced weathering along a dominant north-northwest trending structure which facilitated an increased depth of karst development, created a subsurface geomorphology which concentrated flow towards and through the Main Fissure in the vicinity of the sinkhole prior to the system being choked. The Main Fissure is a unique feature within the mine and so comparable conditions are unlikely to occur elsewhere in the vicinity of the mine. This provides a unique set of circumstances that coincide at this particular location and which are not (to our knowledge) repeated elsewhere in the vicinity of the mine. It is considered that the potential of future sinkhole development in this area will remain at historical background levels.



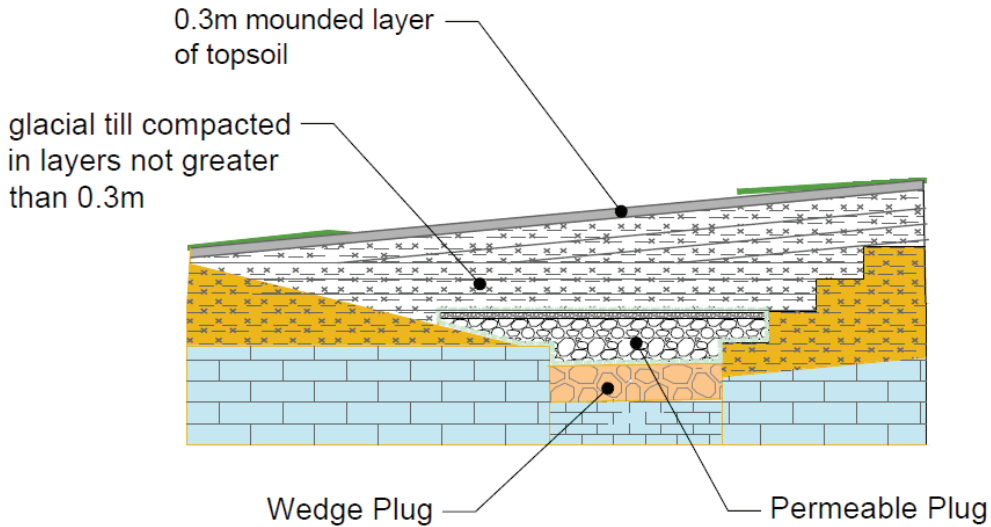


Figure 4 Implemented approach to sinkhole remediation.

References

- Coxon P, McCarron S (2009) Cenozoic: Tertiary and Quaternary (until 11,700 years before 2000), In: Holland, C. H. and Sanders, I. S. (eds.), The Geology of Ireland. 2nd Edition. Edinburgh: Dunedin Academic Press, 355 – 396
- Drew DP, Jones GL (2000) Post-Carboniferous, pre-Quaternary karstification in Ireland. Proc. Geol. Assn., 111: 345-353
- He K, Liu C, Wang S (2003) Karst collapse related to over-pumping and a criterion for its stability. Environmental Geology, 43: 720-724
- Waltham T, Bell F, Culshaw M (2010) Sinkholes and Subsidence. Karst and Cavernous Rocks in Engineering and Construction. Praxis Publishing Ltd, 382 pp



Unravelling the Convolted Marbles of a Namibian Gold Mine

W. Chimhanda¹, D.M. Duthe¹, L Kawali²

¹*Itasca Africa (Pty) Ltd, P. O. Box 3918, Rivonia 2128, South Africa; dduthe@itasca-africa.com, wchimhanda@itasca-africa.com*

²*B2Gold Namibia (Pty) Ltd, PO Box 80363, Olympia, Windhoek, lkawali@b2gold.com*

Abstract

Otjikoto Gold Mine is located in the arid northern part of Namibia in the Okonguarrie schists and marbles of the Damara Orogeny and 70 km to the SW of Kombat underground copper mine that suffered serious flooding in 2005. The over folded synclines and anticlines have resulted in a complex hydrogeological environment that required an extensive geochemical and hydrogeological field programme to understand the zones of recharge, storage and risks in terms of groundwater ingress to the open pit mining operations.

Hydrochemical and isotope fingerprinting (stable isotopes and tritium), has shown that a source of the groundwater ingress to the mine, (located in the low permeability schists and albitites of the Okonguarrie Formation) is the Karibib Marbles, an important regional aquifer, supplying the nearby towns. North-south fault structures have provided hydraulic connection to the limbs of the Karibib anticline transecting the intermediate Ghaub diamictite and aquitard, resulting in recharge to zones with enhanced storage capacity along the fold axes and albitised contacts of the Okonguarrie Formation marble stringers. The conceptual hydrogeological model includes a complex interlayering due to allogenic and autogenic recharge of the marbles, clearly distinguishable from the hydrochemistry and piezometric responses to testing of a prototype dewatering borehole with linear flow.

To quantify the ingress rates and evaluate pore pressures behind the heterogeneous and anisotropic pit high walls, a numerical flow model was developed to simulate the complexities of the conceptual hydrogeological model. Predictive simulations indicate groundwater ingress rates to the pit can be reduced significantly by targeting the marble structures and dewatering the confined aquifer, which also acts as an underdrain to depressurizing the overlying less permeable schists.

The combined collection of geochemical and hydrogeological data was used to unravel the sources and recharge mechanisms of ingress to the pits and to quantify the potential for acid rock drainage following closure of the mine.

Introduction

A gold mine is located in the arid northern part of Namibia in the Okonguarrie schists and marbles of the Damara Orogeny and 70 km to the SW of Kombat underground copper mine that suffered serious flooding in 2005. The over folded synclines and anticlines have resulted in a complex hydrogeological environment that required an extensive geochemical and hydrogeological field programme to understand the zones of recharge, storage and risks in terms of groundwater ingress to the open pit mining operations.

Hydrochemical and isotope fingerprinting (stable isotopes and tritium), has shown that a

source of the groundwater ingress to the mine, (located in the low permeability schists and albitites of the Okonguarri Formation) is the Karibib Marbles, an important regional aquifer, supplying the nearby towns. North-south fault structures have provided hydraulic connection to the limbs of the Karibib anticline transecting the intermediate Ghaub diamictite and aquitard, resulting in recharge to zones with enhanced storage capacity along the fold axes and albitised contacts of the Okonguarrie Formation marble stringers. The conceptual hydrogeological model includes a complex interlayering due to allogenic and autogenic recharge of the marbles, clearly distinguish-



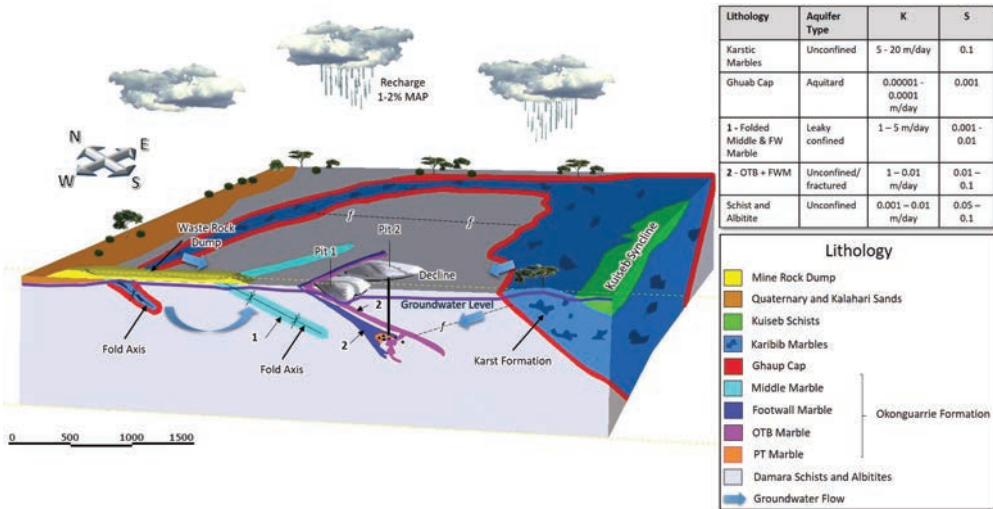


Figure 1 Conceptual hydrogeological model

able from the hydrochemistry and piezometric responses to testing of a prototype dewatering borehole with linear flow.

Conceptual Hydrogeologic Model

Figure 1 shows the conceptual hydrogeological model of the mine area. Regional geological information, mine geological model and lithological models provided by the mine were used to develop a Leapfrog regional model, which is the basis of the conceptual and numerical groundwater model.

The outcropping Karibib Marble forms the topographical highs and has higher groundwater potential due to the recharge from rainfall via the karsts and sinkholes. This is the major aquifer that is used regionally by surrounding farmers. The Ghaub Cap at the base of the Karibib Marbles is considered an aquitard restricting groundwater flow from the Karibib Marbles resulting in the differential piezometric head between the marbles and the Okonguarri Formation.

Although the schists and albitites of the Okonguarri Formation have lower permeability, there is hydraulic connection via faults and structures to the surrounding Karibib Marbles, resulting in the localised development of water bearing zones, particularly associated with the fold hinges of the marbles of the Middle Okonguarri Formation (OTB, Middle (OTJ) Marble and FW Marble) as supported by aquifer testing results. In reality,

although the marble bands are conceptualised as discrete units separated by albitite, according to the geological logs, there are several stringers and lenses of marble in the entire marble package (OTB, FWM including the intermediate albitite) which is generally 60 m in thickness, increasing in the south to > 100 m. The hydraulic connectivity between the marble bands could therefore be significant, particularly in fault zones or major joints.

There is also direct but lesser recharge of the unconfined OTB and FW marble bands through the overlying calcretes and schists, resulting in a similar water type but showing increased ion exchange, older in signature and being more depleted in deuterium (more negative $\delta 2H$) due to the longer flow path through the calcretes. The recharge for this arid area occurs following >1:5 Year events as intense precipitation and consecutive rainfall days, when rainfall exceeds evaporation. Infiltration to the groundwater table can occur through the sinkholes and cavities in the outcropping Karibib Marbles as well as, to the lesser extent, through the calcrete. An estimate of recharge to groundwater as 20% during years with higher rainfall (>700 mm/annum) results in a rise in the water table, that slowly dissipates until the next extreme rainfall period. However, for modelling purposes, this is considered the cumulative rainfall over a 10 year period (following a 1:10 year rainfall event and the remaining years recharge



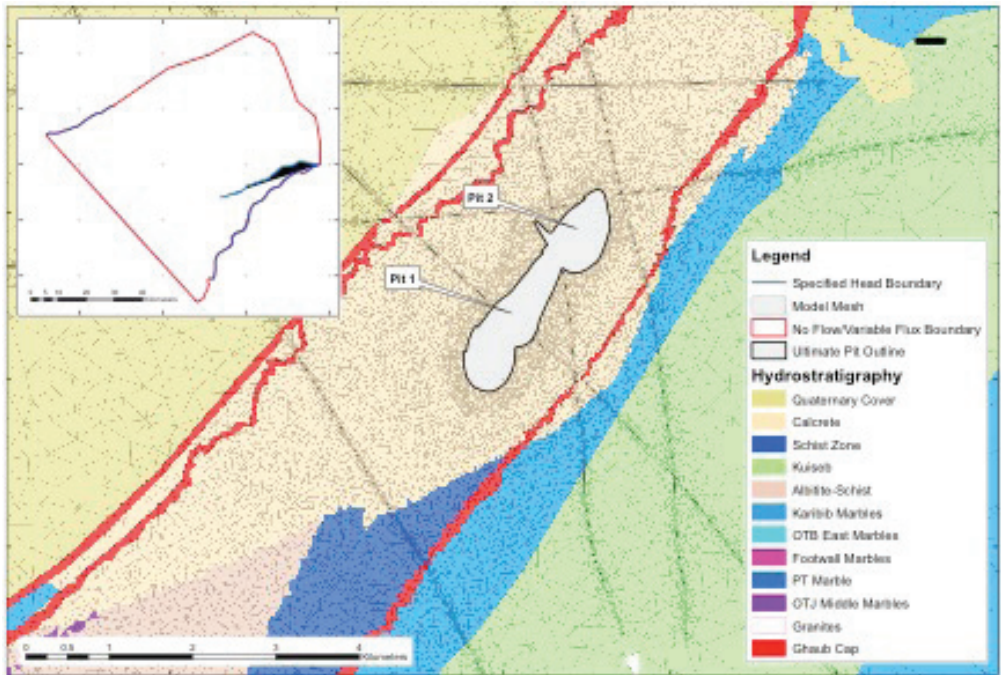


Figure 2 Plan View Showing Discretization and Hydrostratigraphy with pits

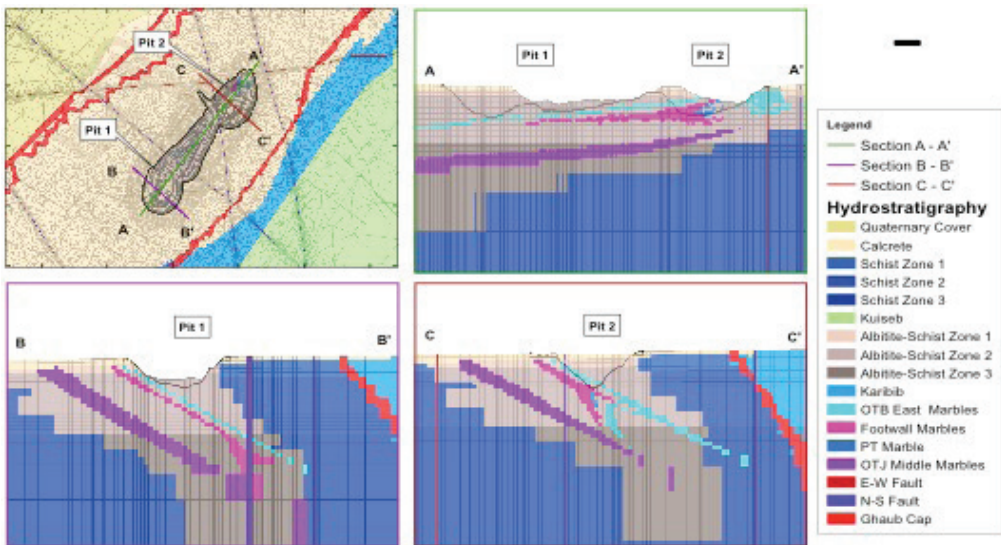


Figure 3 Section View Showing Discretization and Hydrostratigraphy with pits

is considered negligible) and the simulated annual recharge estimate is therefore 2 % of the MAR in the Karibib Marbles (with karstic landform) and less for the diffuse allogenic recharge lower permeability Okonguarrie Formations overlain by calcrete (<1%).

Numerical Groundwater Model

The 3-D numerical groundwater flow model was constructed based on the conceptual hydrogeological model using the finite element code MINEDW version 3.04 (Azrag et al., 1998). The numerical groundwater model



domain is shown in Figure 2 as well as the model boundaries.

For the steady-state simulation, the south-eastern and part of the north-western model boundary were assigned as specified heads with the hydraulic head set equal to the topographical elevation and coincide with the main rivers that drain into the Ugab Catchment to the west and the Upper Omatoko Basin to the north-east. The model domain is quite large in order to include the Karibib Marbles which is the main water supply aquifer in the region. Therefore in the absence of any other significant hydrological features the remaining boundaries were set at an arbitrary distance of approximately 30 km from the mine. These were assigned as no flow boundaries during steady state. For the transient simulations, the no flow boundaries were changed to variable-flux boundary conditions.

The bottom boundary of the model is defined as a no-flow boundary at the somewhat arbitrary elevation of 300 mamsl, about 1000 m below base of the Pit 1 and Pit 2 (1260 and 1355 mamsl respectively) so that the boundary would have no influence on the predictive simulations of the model. The upper model boundary of the groundwater flow system is the phreatic surface, which is calculated by the model.

Model Grid and Discretization

The model mesh is finely discretised in the mine footprint area comprising of the pits to enable better numerical resolution and to represent the hydrostratigraphic units in detail as shown in Figure 3. The horizontal dimensions of the elements in mine footprint area are approximately 20 to 30 m. The model mesh was vertically discretised into approximately 15 m thick layers over the vertical pit extent to adequately represents the significant hydrostratigraphic units while still maintaining numerical efficiency and to enable a refined determination of the seepage faces.

In the mesh, the primary hydraulic properties (i.e., the hydraulic conductivity, specific storage, and specific yield) are assigned to the elements representing the various hydrostratigraphic units, and the model-calculated heads and flows are associated with the nodes. During simulation of mining, the finite-element grid within the pit is “collapsed”

to represent the changing configuration of the pit. The hydraulic properties of the collapsed elements are changed as necessary to maintain the original “hydrostratigraphy” of the pit area.

Simulation of Open Pits

Using a model time step of one month, the elevation of the pit bottom was assumed to change every month during the period of simulation, the 10-year Life of Mine (LoM) up to December 2023. The monthly configuration of the pit was linearly interpolated between the original ground surface and the planned yearly pit configuration.

Using this methodology, excavation of the pit with time was simulated in the model with nodes within the pit being assigned time-variable elevations using the collapsing grid capability of *MINEDW*. A node representing the pit sides or bottom, a special type of drain node, produces water if the model-calculated groundwater level at the node is higher than the specified elevation of the node. If the calculated groundwater level is lower, the drain node is simply dry. *MINEDW* thereby enables a very realistic simulation of the pit configuration and inflow conditions. In each time step of the numerical simulation, the elevations of all of the drain nodes are specified and changed as necessary to replicate the mine plan.

The stress releases to the rock and disturbance to the rock due to excavation results in the rock beneath the pit benches to be more permeable than the in-situ rock. The disturbed rock is referred to as the zone of relaxation (ZOR). The thickness of the ZOR could be as thick as several hundred meters. *MINEDW* is able to simulate the development of the ZOR according to the mining schedule by increasing the K value of the ZOR along the depth as time-variant conductivity. Simulations of the development of the ZOR according to the mining schedule are important in the prediction of pore-pressure distribution within the slope. The ZOR was simulated for the pits as 1/3 of the pit depth as time-variant conductivity.

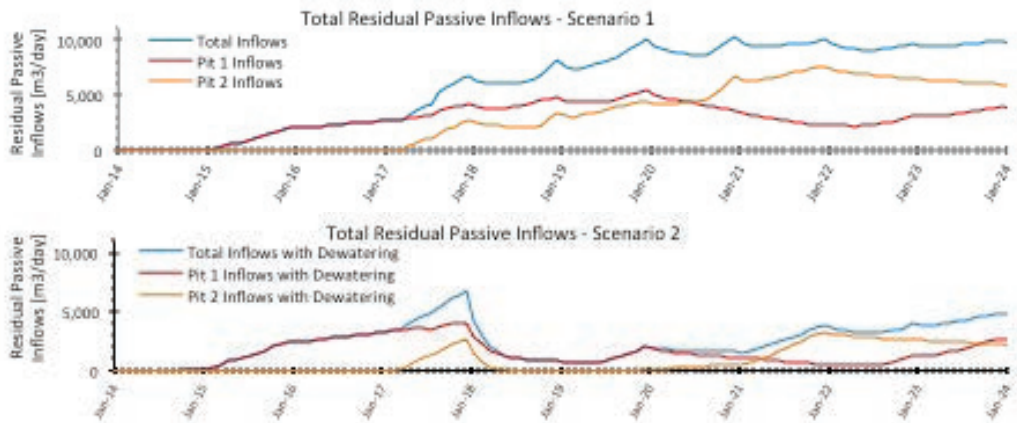
Simulation of Hydrogeology

The hydraulic parameters of importance in investigating groundwater flow are hydroau-



Table 1. Summary of the Scenarios for Predictive Simulation

Scenario	Description
1	Predictive simulations with pits and current water supply holes
2	Predictive simulations with pits, current water supply holes with dewatering from the following holes: PB1(200m ³ /hr); PB2(80m ³ /hr); PB3(70m ³ /hr); PB4(2m ³ /hr); and PB5(80 m ³ /hr).

*Figure 4 Predicted Residual Passive Inflows Scenario 1 and 2*

lic conductivity, specific storage and specific yield. These parameters control the ease with which groundwater can move through the subsurface and how much water can be released from the system, thus are important to estimate inflows into the pits, propagation of drawdown and ability to depressurise. The primary hydraulic parameters are assigned to the elements representing the various hydro-stratigraphic units, and the model-calculated water levels and flows are associated with the nodes. The simulated hydraulic properties of the various units in the model, after steady state and transient calibration, are within the range of the values determined from the packer testing and test pumping and included in the conceptual model (Figure 1).

Predictive Simulations

The predictive simulations were conducted to quantify the ingress rates and evaluate pore pressures behind the heterogeneous and anisotropic pit high walls, as well as simulate the complexities represented in the conceptual hydrogeological model. Predictive simulations indicate groundwater ingress rates to the pits can be reduced significantly by targeting the marble structures and dewatering

the confined aquifer, which also acts as an underdrain to depressurizing the overlying less permeable schists. Therefore the primary target zones for dewatering are the folded marble which are the largest contributor of groundwater to the pits.

For the purpose of the simulations, the proposed dewatering boreholes were planned to start pumping in 2018. The scenarios simulated are summarised in Table 1 where the first scenario represents the status quo at the mine and scenario 2 incorporates the proposed dewatering with the average pumping rates determined from pump testing data analysis.

Predicted Residual Passive Inflows

The predicted residual passive inflows (RPI) into the pits are shown in Figure 4 for Scenarios 1 and 2.

The predictive simulations for Scenario 1 shows that RPI into Pit 1 is predicted to increase steadily to a maximum of $\approx 5\,530$ m³/day in December 2019. Thereafter the inflows are expected to reduce to $\approx 2\,000$ m³/day as Pit 2 deepens and then increase steadily to $\approx 3\,900$ m³/day at the end of the 10year LOM. Proposed dewatering, Scenario 2, will re-



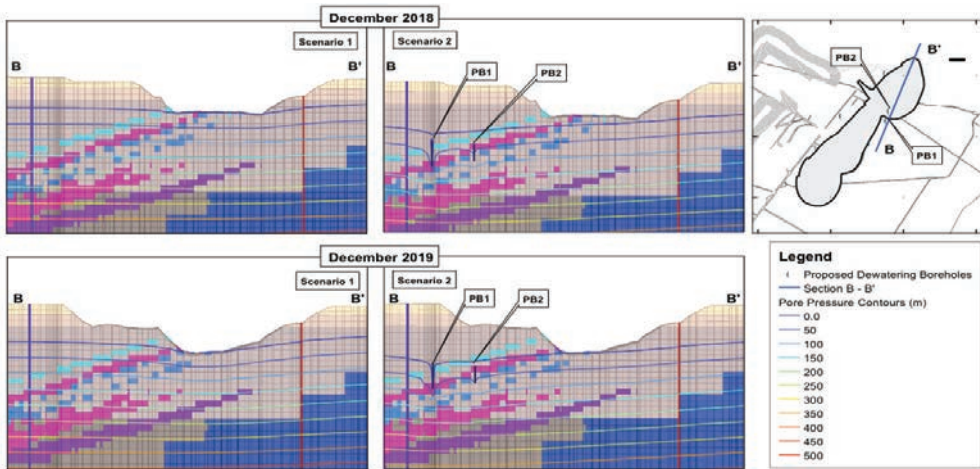


Figure 5 Section through Pit 2, PB1 and PB2 Showing Phreatic Surface and Pore Pressure – 2018 and 2019

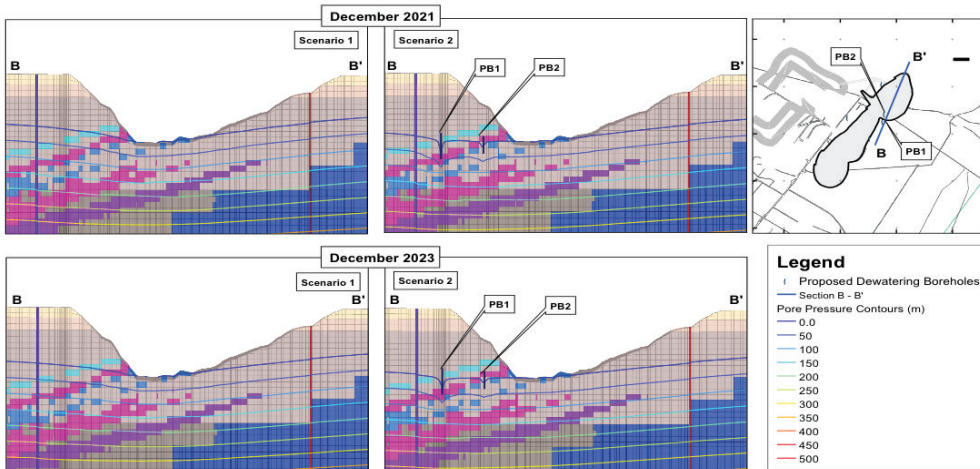


Figure 6 Section through Pit 2, PB1 and PB2 Showing Phreatic Surface and Pore Pressure – 2021 and 2023

sult in a decrease in RPI to a maximum of $\approx 4\,000\text{ m}^3/\text{day}$ as the boreholes come on line. Thereafter the inflows are expected to reduce to $\approx 200\text{ m}^3/\text{day}$ as Pit 2 deepens and then increase steadily to $\approx 2\,000\text{ m}^3/\text{day}$ at the end of the 10year LOM as the dewatering boreholes become less effective to dewater the deeper portions of the pit.

The predictive simulations for Scenario 1 shows that RPI into Pit 2 is predicted to increase steadily to a maximum of $\approx 7\,600\text{ m}^3/\text{day}$ as the pit expand and deepens. Thereafter the inflows are expected to steadily decrease to $\approx 5\,800\text{ m}^3/\text{day}$ as operations ceases in Pit 2 until the end of the 10-year LOM. Proposed dewatering, Scenario 2, will result in a de-

crease in RPI to a maximum of $\approx 2\,600\text{ m}^3/\text{day}$ as the boreholes come on line. Thereafter there will be no inflows until 2021 where inflows are expected to increase steadily to $\approx 2\,500\text{ m}^3/\text{day}$ at the end of the 10year LOM as the dewatering boreholes become less effective to dewater the deeper portions of the pit.

Phreatic Surface and Pore pressure

The phreatic surface and distribution of pore pressures for Scenario 1 and 2 are shown in Figure 5 and 6 for a section across Pit2, the PB1 and PB2 for December 2018, 2019, 2021 and 2023. The results of the simulations show that active dewatering (Scenario 2) will result in significantly lowering of the



phreatic surface using proposed dewatering boreholes. The proposed boreholes are able to reduce the residual passive inflows into the pit and depressurize the pit walls. The phreatic surface will be drawn down fully in the deepest section of the pit or to below pit bottom for both pits during operation therefore there is no indication there will be build-up of pore pressures. The reduction of pore pressures is attributed to the continued depressurisation from the targeted marbles. However, localised and transient pore pressure build up could occur in response to recharge events.

Conclusions

The proposed dewatering strategy of targeting the marble structures and dewatering the confined aquifer, which also acts as an underdrain to depressurizing the overlying less permeable schists will result in a decrease of inflows into the pits. However as the dewatering boreholes become less effective to dewater the deeper portions of the pit residual passive inflows into the pits. The results of the simulations show that active dewatering will result in significantly lowering of the phreatic surface using proposed dewatering boreholes as well as depressurize the pit walls indicating that there will be no build-up of pore pressures. However, localised and transient pore pressure build up could occur in response to extreme recharge events.

A phased approach will be required to meet the operational dewatering target as the dewatering plan is optimized through predictive simulations and model update. The numerical modeling results through calibration, suggest that the spatial variation of hydraulic parameters, anisotropy and geological com-

plexity still requires further refinement as the project advances.

The predictive simulations are therefore considered a first order approximation based on the data available and assumptions made. Improvements to the model predictions can be realized by updating the model as the understanding of the spatial variation of hydraulic parameters and/or geological complexity is acquired as the project advances.

Acknowledgements

The authors thank the Mine for allowing us to use the data from their operation for this publication for ICARD | IMWA | MWD 2018.

References

- Azrag, E.A., Ugorets, V.I., and Atkinson, L.C., Use of a finite element code to model complex mine water problems: Proceedings of symposium on mine water and environmental impacts, vol. 1, International Mine Water Association (Johannesburg, September 1998)
- Beale G; J Read. 2013. Guidelines for Evaluating Water in Pit Slope Stability. CSIRO, pp 600
- Beyer M, M Gaj, P Koeniger, J Hamutoko, S Uugulu, H Wanke, C Lohe, T Himmelsbach and M Billib (20014) Deuterium labelling of soil water movement in the Cuvelai-Etoshia Basin, Namibia Geophysical Research Abstracts Vol. 16, EGU2014-4012-2, 2014
- Külls C. (2000) Groundwater of the North-Western Kalahari, Namibia – Estimation of Recharge and Quantification of the Flow Systems. Doctorate Thesis submitted at the Julius-Maximilian University of Würzburg.
- Read J and P Stacey (2009) Guidelines for Open Pit Design, CSIRO Publishing pp 495



Extremely high levels of trace elements in aerial parts of plants naturally growing in the Wiśniówka acid mine drainage area (south-central Poland)

Agnieszka Gałuszka, Zdzisław M. Migaszewski

Geochemistry and the Environment Div., Institute of Chemistry, Jan Kochanowski University, 15G Świętokrzyska St, 25-406 Kielce, Poland, aggie@ujk.edu.pl, zmig@ujk.edu.pl

Abstract

Above-ground parts of vascular plant species (39 samples) and mosses (5 samples) growing in the Wiśniówka acid mine drainage area (south-central Poland) were collected in the summer of 2015-2017. All samples were analyzed for 10 trace elements (As, Cd, Co, Cr, Cu, Mn, Ni, Pb, U, Zn) and rare earth elements (REE) using the ICP-MS technique. Results of analyses showed that As, Cd, Cr, Ni, U and REE were heavily enriched in plant samples compared with their natural concentrations in plant material. Moss samples showed the highest element bioaccumulation regardless of the sampling period and the species examined.

Keywords: vascular plants, moss, acid mine drainage, trace elements, rare earth elements

Introduction

Acid mine drainage (AMD) areas are not favorable habitats for plants because the soil shows low pH, excess of bioavailable phytotoxic metal ions and decreased nutrient levels (Simate and Ndlovu 2014). For most of the plant species optimal soil pH is within the range of 6-8 (Läuchli and Grattan 2017). Acidic soil (pH<5.5) causes increased uptake of phytotoxic metal ions such as Al^{3+} and Mn^{2+} by plants. At the low soil pH, essential nutrients including Ca, Mg, N, P and K are leached and may become deficient in plants. However, there are plant species tolerant to these harsh environmental conditions. They belong to specific ecotypes showing evolutionary adaptation to metal toxicity (Batty 2005). These plant species are often studied for their use in phytoremediation of mining areas (Favas et al. 2014; Fernández et al. 2017).

Comparison of metal levels in the above-ground organs of plant species native to the mining areas is important for selection of species useful for soil remediation or extraction of metals from ashed plant biomass (Gałuszka et al. 2015). Natural and constructed wetlands have been used for AMD remediation since the 1980s (Johnson and Hallberg 2002).

Some authors have argued that the role of plants in passive treatment of AMD is of minor importance (Nyquist and Greger 2009). Nevertheless, the accumulation of metals in plant biomass has attracted an increased interest in terms of its use in phytoremediation and phytomining technologies (Abreu et al. 2008; Robinson et al. 2009; Wang et al. 2017).

In this study nineteen species of the most abundant plants growing in the acid mine drainage area in south-central Poland were compared with the reference plant (Markert 1992) for their trace element concentrations. Plant samples were collected from sites with a different impact of AMD on the plant growth substrate (mine tailings, mine spoil, soil and acidic pools). The aim of this study was to select the species showing the highest bioaccumulation potential for their possible use in phytoremediation and phytomining.

Methods

The study area covers the western part of the Holy Cross Mountains (HCM), within a dismembered Wiśniówka massif (elevation of 457 m above sea level) built of Upper Cambrian rock formations composed of quartzites, quartzitic sandstones and mudstones alternating with clayey-silty shales with py-



rite and goethite-hematite mineralization zones that predominate in the Podwiśniówka quarry located in the easternmost part of the Wiśniówka mining area (Migaszewski et al. 2016). The abundance of microcrystalline pyrite exposed to weathering conditions caused a wide occurrence of AMD in the former pits, ditches and ephemeral pools. Some of AMD samples collected from ditches near the tailings pile show one of the highest concentrations of As (370 mg/L) and REE (6.29 mg/L) worldwide (Migaszewski et al. 2016).

For the purpose of this study 44 plant samples were collected from nine sites (A–I) in the Wiśniówka mining area (south-central Poland) (fig. 1). Additionally, three samples of AMD waters were collected from sites B (ditch near siding track), F (ditch near mine office building) and I (Podwiśniówka acid pit lake). These sites are the most influenced by pyrite oxidation and AMD generation. Water samples were filtered in situ using 0.45 µm pore-sized PTFE syringe filters.

The number of sampled plant species corresponded to their abundance in the study area. Samples were collected during three vegetation seasons. The following species were collected during this study (site and >1 sample numbers in parentheses):

- in 2015, *Juncus effusus* (sites A–D; 5 samples), *Tussilago farfara* (site B),
- in 2016, *J. effusus* (sites A, B, C, D, H, I; 10 samples), *T. farfara* (sites B, E, F, G, I; 5 samples), *Matricaria chamomilla* (sites B and G; 2 samples), *Typha angustifolia* (site A), *Salix alba* (site D), *Pleurozium schreberi* (site F), *Drepanocladus aduncus* (site F),
- in 2017, *Pteridium aquilinum* (site F; 2 samples), *Betula pendula* (site F), *Salix cinerea* (site F), *Sorbus aucuparia* (site F), *Populus tremula* (site F), *Vaccinium myrtillus* (site F), *Pinus sylvestris* (site F), *Frangula alnus* (site F), *J. effusus* (site F), *Quercus petraea* (site F), *Chamaenerion angustifolium* (site F), *Oxalis acetosella* (site F), *T. farfara* (site F), *D. aduncus* (site F), *Mnium affine* (site F), *P. schreberi* (site F).

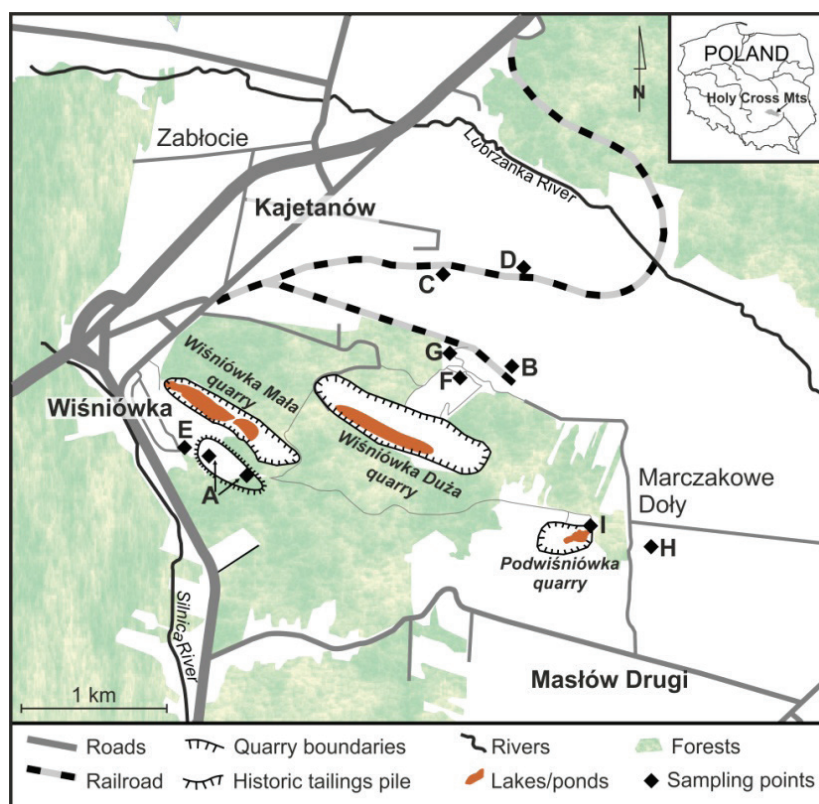


Figure 1 Location of study area and sampling sites A–I.



After transporting the samples to the Environmental Analytical Laboratory of the Institute of Chemistry, Jan Kochanowski University in Kielce on the day of sampling, plant samples were carefully washed and air-dried. After drying, the samples were ground and digested in a closed microwave system using $\text{HNO}_3/\text{H}_2\text{O}_2$ solution. Trace elements were determined by the ICP-MS technique (quadruple instrument, model Elan DRCII, Perkin-Elmer). Accuracy of measurements was checked using two plant certified reference materials, NIST-1573a Tomato leaves and NIST-1575a Pine needles and two water reference materials NIST 1643e (trace elements in water) and PPREE (standard reference water sample for REE determinations).

Results

Table 1 shows element concentration ranges and mean values in plant samples calculated for each year. There is a high variability in element concentrations, which results from

the site-specific environmental conditions and inter-species differences in element accumulation. The lowest mean element concentrations (except for Cd and Cu) were found during the first year when only six samples of vascular plants were collected. In every year of study, Mn and Zn showed the highest mean concentrations whereas U the lowest ones in all the samples examined.

Comparison of these results with typical concentrations of elements in plant material ('a reference plant' according to Markert 1992) indicates that all samples are enriched in As. The mean concentrations of the other elements are usually higher than those in a reference plant.

The results of analysis of acid mine drainage water samples are shown in table 2. In samples from sites B, F and I arsenic is the most abundant trace element, but its highest level was recorded at site F. This sample also revealed the highest contents of other trace elements, except for Cu and Pb.

Table 1. Element concentration ranges and mean values in samples collected during 2015-2017 compared with those in a reference plant (Markert 1992).

mg/kg	2017 (n=17)		2016 (n=21)		2015 (n=6)		Reference plant
	range	mean	range	mean	range	mean	
As	0.610-11.2	3.41	0.238-22.8	3.29	0.435-2.38	1.22	0.1
Cd	0.027-1.04	0.330	0.015-1.46	0.480	0.194-1.26	0.518	0.05
Co	0.1-5.83	1.24	0.039-4.46	1.03	0.055-0.659	0.334	0.2
Cr	0.5-90.1	13.5	0.710-84.5	9.91	1.23-12.6	3.65	1.5
Cu	1.99-11.7	5.83	3.58-19.7	10.5	4.01-8.68	5.91	10
Mn	26.0-3313	969	48.0-1735	427	81.6-478	281	200
Ni	1.60-33.5	8.44	1.95-44.2	10.9	0.913-6.60	2.45	1.5
Pb	0.290-4.90	1.27	0.038-4.53	0.574	0.130-3.41	0.854	1
U	0.002-0.218	0.051	0.001-0.287	0.038	0.001-0.125	0.031	0.01
Zn	8.80-165	53.0	12.2-159	56.6	19.4-53.4	36.9	50
ΣREE	0.360-26.5	4.85	0.006-28.1	4.48	0.095-4.17	1.48	1.13

Table 2. Element concentrations in AMD water samples collected from sites B, F and I.

mg/L	Site B	Site F	Site I
As	30.4	34.6	19.2
Cd	0.003	0.058	0.003
Co	0.910	4.71	1.55
Cr	1.06	2.26	0.892
Cu	4.53	6.37	7.64
Mn	12.4	122	1.16
Ni	1.32	6.02	1.73
Pb	0.004	0.002	0.003
U	0.117	0.464	0.147
Zn	0.647	6.19	0.142
ΣREE	2.42	17.6	0.932



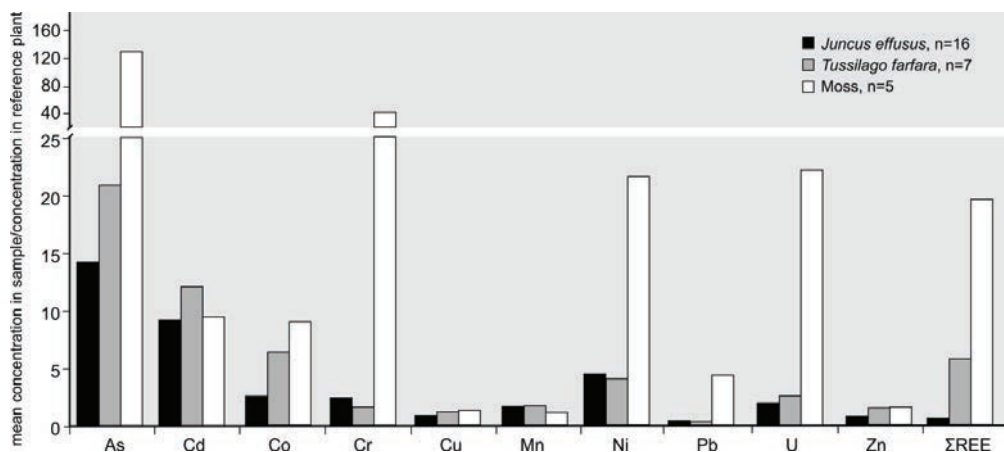


Figure 2 Mean element concentrations in samples of *J. effusus*, *T. farfara* and mixed-moss species divided by element concentrations in the reference plant.

Discussion

Comparison of the obtained results with those derived from other studies of trace elements in plant samples collected at AMD-impacted sites (Stoltz and Greger 2002; Anawar et al. 2011; Liao et al. 2016) shows that the element concentration levels are similar, except for lower content of Pb in plants of the Wiśniówka area. The periodically waterlogged plants exhibit strongly enhanced accumulation capabilities compared to those growing at sites only slightly influenced by AMD waters. The moss samples exhibited the highest concentrations of the determined elements of all the plant samples examined. Their enrichment in trace elements, especially in As, Cr, Ni, U and REE, was much higher than in the vascular plants. The moss samples showed Cr concentrations in the range of 39.9–90.1 mg/kg, which was far above 5.2 mg/kg considered as a toxic level of this element in plant leaves (Shanker et al. 2005). Mosses lack roots and they take up elements through an ion-exchange process, mostly from wet deposition (Onianwa 2001). These plants are considered to be good bioindicators of different classes of pollutants. Vascular plants take up elements mostly from soil, and their leaves are protected by a cuticle that restricts direct absorption of ions from water. This is the reason why the higher levels of trace elements are expected to occur in the moss samples examined. Comparison of the mean element concentrations in the moss species, *J. effusus*

and *T. farfara* normalized to their content in the reference plant is shown in fig. 2.

Mosses are often found in acidic habitats (Sevink et al. 2015). They seem to be well-adapted to high metal ion concentrations in acidic water and are able to accumulate elements in their tissues (Gough et al. 2006). All of the moss samples were collected at site F, which was seasonally waterlogged by seeps that drain a nearby tailings pile. A simple diffusion of ions available for mosses in AMD water caused a substantial enrichment of the samples in trace elements.

Distribution patterns of REE vary among different species of plants at the same location and even among the same species. Of the REE concentrations, La, Ce and Nd contents were the highest in all plant samples. Maximum concentrations of REE were found in samples collected at the sites where AMD is generated (sites B, F and I). Of all the plant samples examined, the mosses and one sample of vascular plant (*T. farfara*) were extremely enriched in REE (16.5–28.1 mg/kg), whereas the other samples showed REE concentrations in the range of 0.006–3.75 mg/kg. The REE patterns of the moss samples normalized to North American Shale Composite (NASC) show almost identical trends with positive anomalies of Nd, Sm, Eu, and Gd (fig. 3). These patterns are different from that of the acidic water collected at site F, that displays a shift toward Tb and Gd positive anomalies with distinct enrichments in heavy REE (Gd–Lu; HREEN-ASC/LREENASC = 1.86).



Accumulation of REE in moss samples is of the highest practical importance for possible recovery of these critical elements from AMD. Mosses show high metal adsorption/desorption capacities. Usefulness of biosorption of Nd by lyophilized biomass of moss species *Physcomitrella patens* has already been confirmed in a laboratory experiment by Heilmann et al. (2015). Our study reports for the first time high REE accumulative properties of living moss species growing in natural conditions.

High concentrations of REE in moss samples show a potential for using these plants for REE recovery either by phytomining (after ashing of the plants to produce bio-ore) or via direct leaching (desorption of REE from moss tissues and their recovery from aqueous solution). Ashing of the fern *Dicranopteris dichotoma*, which is a REE hyperaccumulator, increased its total REE concentrations from 2032 mg/kg to 1.6% (Liu et al. 2017). However, plant ashes contain amorphous phases that stabilize REE and prevent them from leaching. Thus, direct extraction could be more effective in REE recovery. Mosses, despite their lower REE accumulation potential compared with REE hyperaccumulators, seem to be attractive biosorbents because they absorb REE by a simple proton exchange (Heilmann et al. 2015) and show high desorption capabilities for metal ions (Grimm et al. 2008). Recovery of REE from mosses by direct leaching seems to be easier than from vascular plants.

Conclusions

In the study of plants naturally growing in the Wiśniówka AMD area, high bioaccumulation of As, Cr, Ni, U and REE has been shown by three terrestrial moss species: *Pleurozium schreberi*, *Drepanocladus aduncus* and *Mnium affine*. The results of this study support the use of moss biomass for AMD treatment and REE recovery. However, further studies are needed to determine direct leaching of REE from moss tissues.

Acknowledgements

This study was supported by the National Science Center, a research grant no. 2015/17/B/ST10/02119.

References

- Abreu MM, Tavares MT, Batista MJ (2008) Potential use of *Erica andevalensis* and *Erica australis* in phytoremediation of sulphide mine environments: São Domingos, Portugal. *J Geochem Explor* 96(2-3):210–222, doi:10.1016/j.gexplo.2007.04.007
- Anawar HM, Freitas MC, Canha N, Santa Regina I (2011) Arsenic, antimony, and other trace element contamination in a mine tailings affected area and uptake by tolerant plant species. *Environ Geochem Health* 33(4):353–362, doi:10.1007/s10653-011-9378-2
- Batty LC (2005) The potential importance of mine sites for biodiversity. *Mine Water Environ* 24(2), 101–103, doi:10.1007/s10230-005-0076-0

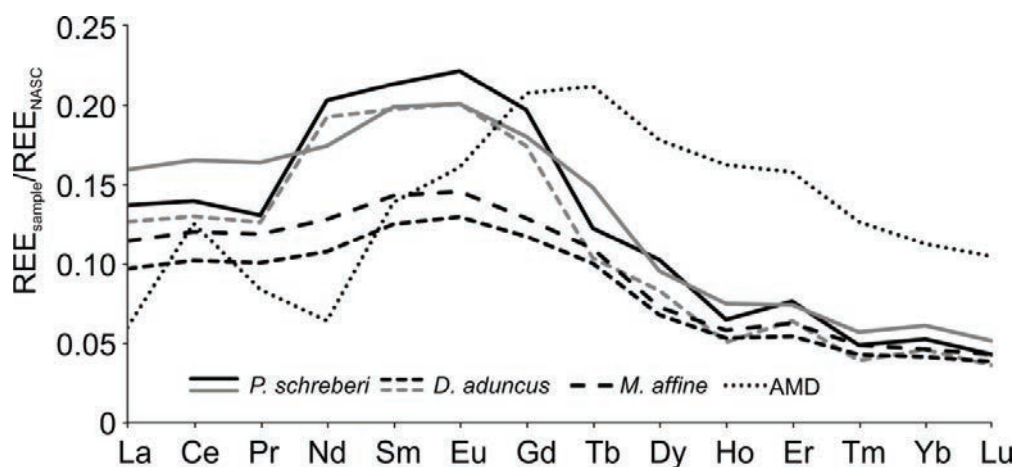


Figure 3 NASC-normalized REE patterns in moss samples and AMD water sample collected at site F.



- Favas PJC, Pratas J, Varun M, D'Souza R, Paul MS (2014) Phytoremediation of soils contaminated with metals and metalloids at mining areas: potential of native flora. In: Hernandez-Soriano MC (Ed), *Environmental Risk Assessment of Soil Contamination*, InTech, Rijeka, Croatia, p 485–517, doi:10.5772/57469
- Fernández S, Poschenrieder C, Marcenò C, Gallego JR, Jiménez-Gómez D, Bueno A, Afif E (2017) Phytoremediation capability of native plant species living on Pb-Zn and Hg-As mining wastes in the Cantabrian range, north of Spain. *J Geochem Explor* 174:10–20, doi:10.1016/j.jgeoxplo.2016.05.015
- Gałuszka A, Krzciuk K, Migaszwski ZM (2015) A new two-step screening method for prospecting of trace element accumulating plants. *Int J Environ Sci Te* 12(10):3071–3078, doi:10.1007/s13762-014-0719-4
- Gough LP, Eppinger RG, Briggs PH, Giles S (2006) Biogeochemical characterization of an undisturbed highly acidic, metal-rich bryophyte habitat, east-central Alaska, USA. *Arc Antarct Alp Res* 38(4):522–529, doi:10.1657/1523-0430(2006)38[522:BCOAHU]2.0.CO;2
- Grimm A, Zanzi R, Björnborn E, Cukierman AL (2008) Comparison of different types of biomasses for copper biosorption. *Bioresource Technol* 99(7):2559–2565, doi: 10.1016/j.biortech.2007.04.036
- Heilmann M, Jurkowski W, Buchholz R, Brueck T, Becker AM (2015) Biosorption of neodymium by selected photoautotrophic and heterotrophic species. *J Chem Eng Process Technol* 6(4):241, doi: 10.4172/2157-7048.1000241
- Johnson DB, Hallberg KB (2002) Pitfalls of passive mine water treatment. *Rev Environ Sci Bio* 1(4):335–343, doi: 10.1023/A:1023219300286
- Läuchli A, Grattan SR (2017) Plant stress under non-optimal soil pH. In: Shabala S (Ed), *Plant Stress Physiology*, 2nd Edition, CABI, Boston, MA, p 201–216
- Liao J, Wen Z, Ru X, Chen J, Wu H, Wei C (2016) Distribution and migration of heavy metals in soil and crops affected by acid mine drainage: public health implications in Guangdong Province, China. *Ecotox Environ Safe* 124:460–469, doi:10.1016/j.ecoenv.2015.11.023
- Liu C, Yuan M, Liu WS, Guo MN, Huot H, Tang YT, Laubie B, Simonnot MO, Morel JL, Qiu RL (2017) Element case studies: rare earth elements. In: Van der Ent A, Echevarria G, Baker AJM, Morel J-L (Eds), *Agromining: extracting unconventional resources from plants*, Mineral Resource Reviews series, Springer Nature, Cham, Switzerland, p 297–308
- Markert B (1992) Establishing of ‘Reference Plant’ for inorganic characterization of different plant species by chemical fingerprinting. *Water Air Soil Poll* 64(3):533–538, doi:10.1007/BF00483363
- Migaszwski ZM, Gałuszka A, Dołęgowska S (2016) Rare earth and trace element signatures for assessing an impact of rock mining and processing on the environment: Wiśniówka case study, south-central Poland. *Environ Sci Pollut Res* 23(24):24943–24959, doi:10.1007/s11356-016-7713-y
- Nyquist J, Greger M (2009) A field study of constructed wetlands for preventing and treating acid mine drainage. *Ecol Eng* 35(5):630–642, doi:10.1016/j.ecoleng.2008.10.018
- Onianwa PC (2001) Monitoring atmospheric metal pollution: a review of the use of mosses as indicators. *Environ Monit Assess* 71(1):13–50, doi:10.1023/A:1011660727479
- Robinson BH, Bañuelos G, Conesa HM, Evangelou MW, Schulin R (2009) The phytomanagement of trace elements in soil. *Crit Rev Plant Sci* 28(4):240–266, doi:10.1080/07352680903035424
- Sevink J, Verstraten JM, Kooijman AM, Loayza-Muro RA, Hoitinga L, Palomino EJ, Jansen B (2015) Rare moss-built microterraces in a high-altitude, acid mine drainage-polluted stream (Cordillera Negra, Peru). *Water Air Soil Poll* 226(6):201, doi: 10.1007/s11270-015-2390-x
- Shanker AK, Cervantes C, Loza-Tavera H, Avudainayagam S (2005) Chromium toxicity in plants. *Environ Int* 31(5):739–753, doi: 10.1016/j.envint.2005.02.003
- Simate GS, Ndlovu S (2014) Acid mine drainage: Challenges and opportunities. *J Environ Chem Eng* 2(3):1785–1803, doi:10.1016/j.jece.2014.07.021
- Stoltz E, Greger M (2002) Accumulation properties of As, Cd, Cu, Pb and Zn by four wetland plant species growing on submerged mine tailings. *Environ Exp Bot* 47(3):271–280, doi:10.1016/S0098-8472(02)00002-3
- Wang L, Ji B, Hu Y, Liu R, Sun W (2017) A review on in situ phytoremediation of mine tailings. *Chemosphere* 184:594–600, doi:10.1016/j.chemosphere.2017.06.025



On The Spatial Variation of Geochemical Rock Characteristics in Coal Mining: Case Bukit Asam Coal Mine in South Sumatra, Indonesia

Rudy Sayoga Gautama¹, Ginting Jalu Kusuma¹, Eko Pujiantoro²,
Pajar Hariadi Wisnugroho²

¹Department of Mining Engineering, Faculty of Mining & Petroleum Engineering, Institut Teknologi Bandung, Jl Ganesha 10, Bandung 40132, Indonesia

²PT Bukit Asam, Jl Parigi, Tanjung Enim 31716, Indonesia

Abstract

Bukit Asam Coal Mine, consisting three mining blocks, namely Muara Tiga Besar (MTB), Air Laya (TAL), and Banko Barat (BB) is one of the important coal mine in Indonesia. Having high rainfall, mine water management in Bukit Asam Mine is quite challenging and most of the pits have acid mine drainage problem. Mining pits in all mining blocks are excavating the same coal seams which also means the same interburden or lithology. The mine water in the three mining blocks is showing different quality. In general, mine water in the pit sump in BB has pH of 2.92-3.06, whilst in TAL pH 4.10-4.12 as well as in MTB pH 4.41-6.57. To understand the spatial characteristics of overburden and interburden, rock characterization programs have been conducted which included sampling campaign followed by laboratory tests, both static and kinetic test. Rock samples representing different lithology and mining blocks were collected from cores of 31 drill holes.

The results indicate that there were a variety of geochemical characteristic in each mining blocks, both vertically and laterally. Vertical variety relates to the difference in lithology whereas the lateral characteristic variation also exists on some specific interburden samples from the same lithology. Analysis on the quality of leachate water from laboratory column leach tests were comparable with the quality of mine water taken from the pit sump.

Keywords: AMD in coal mine, rock geochemical characterization, spatial variability

Introduction

Indonesia is the world 5th coal producer and one of the world's largest coal exporters with 27.7% of export on a tonnage basis (IEA, 2017). The main coal basins are South Sumatra Basin in the island of Sumatra and Kutai & Barito Basins in Kalimantan.

Bukit Asam Mine is located in South Sumatra coal basin. It is operated by a state-owned company named PT Bukit Asam (or PTBA). Coal mining activity in this area began in 1919 during Dutch colonial period. Bukit Asam Mine covers an area of approximately 100 km² and is one of the important coal producers in Indonesia. As high as 18.7 million tons of coal have been excavated in 2016 from several open pits operating in three mining blocks, namely Muara Tiga Be-

sar (MTB, in the west), Air Laya (TAL, in the middle), and Banko Barat (BB, in the east). Mine pits in all mining blocks are excavating the same coal seams, namely A1, A2, B1, B2 and C seams and the coal quality is heavily influenced by intrusion activity as indicated by the existence of three intrusive bodies in this area. Having high rainfall, mine water management in Bukit Asam Mine is quite challenging and most of the pits have acid mine drainage problem.

Monitoring of water quality from mine pit sumps indicated the acid drainage in most of the pits. Less acid with pH of from 4.49 to 6.57 has been measured in MTB and there is a trend that to the east (Banko pit 1) the mine drainage becomes more acid except Banko Barat Pit 3 (see figure 1).



We conducted study to analyse the geochemical characteristics of coal seam interburden from different mine blocks since the pit sump water quality depends on the rock geochemical characteristics in the respective pits. Rock samples had been collected from 31 core drills representing different lithology from the three mining blocks.

Geological Setting and Mining Activities

Regional geology

The South Sumatra coal basin is one of the most important coal mining regions in Indonesia (Thomas, 2005). This basin is tectonically active and the coal in some parts has been affected by igneous activity (Belkin, 2009) as shown in Figure 2. South Sumatra Basin is a back-arc basin, which was formed during east-west extension which took place during pre-Tertiary and early Tertiary (de Coster, 1974).

The stratigraphy of South Sumatra Basin is summarized in Gafoer (1986). There are 5 formations in PTBA mine areas, i.e. Aluvial Deposit (Qa) consists of sand, silt and clay; Volcanic Deposit Dempo (Qhvd) consist of andesitic volcanic breccia, lava and tuff; Andesite (Qpva) consist of igneous rock of andesitic rock in the joint of dykes; Air Benakat Formation (Tma) consist of alteration of

claystone, siltstone and shale., mostly calcareous and carbonaceous.; and Muara Enim Formation (Tmfm) consists of tuffaceous claystone, siltstone and sandstone with coal intercalation. The coal bearing Muara Enim Formation consists of tuffaceous claystone, siltstone and sandstone with coal intercalation as shown in figure 3.

Shell Mijnbouw (1976) divided the Muara Enim Formation into two parts (members), known as the lower MPa (Middle Palembang 'a') and the upper MPb (Middle Palembang 'b'). Both members have been subdivided again into M1 – M4 Both MPa and MPb contain about eight coal seams. It is estimated that the maximum net coal thickness is about 140 m. Some economically valuable coal seams are those from the upper part of MPa (Mangus, Suban and Petai). In Tanjung Enim, the Mangus, Suban and Petai coal seams each split into two seams, namely Upper (A1) and Lower (A2) Mangus seams, Upper (B1) and Lower (B2) Suban seams and Upper (C1) and Lower (C2) Petai seams. The coal-bearing strata were subjected to at least one period of folding and faulting, and later to invasion by plug-like masses of andesite (Amijaya, 2006).

Those three coal seams, Manggus (A1 & A2), Suban (B) and Petai (C), are found and mined in all mining blocks (MTB, TAL and BB). Single B seam is found in MTB and in TAL and BB Suban seam splits into B1 and B2 seams.

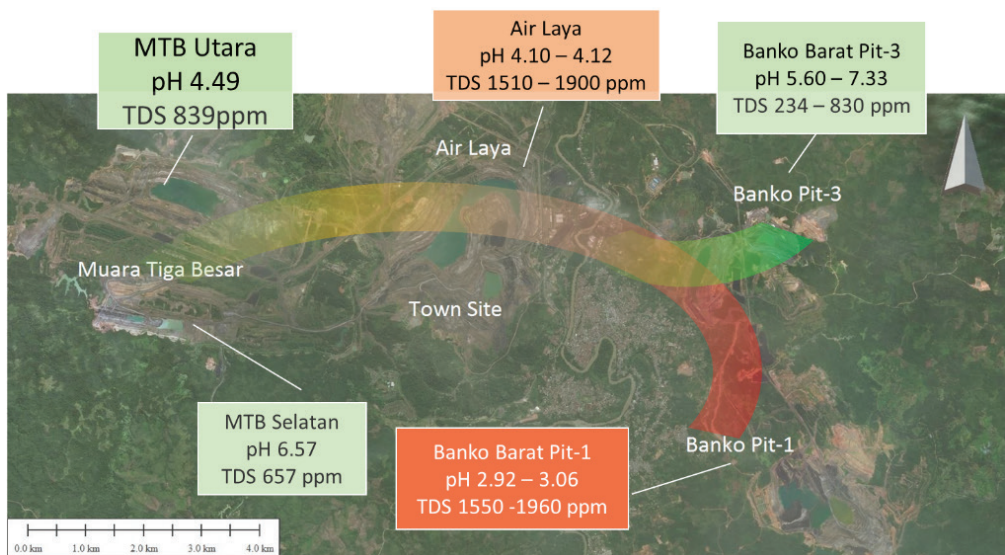


Figure 1 Mine Sump Water Quality



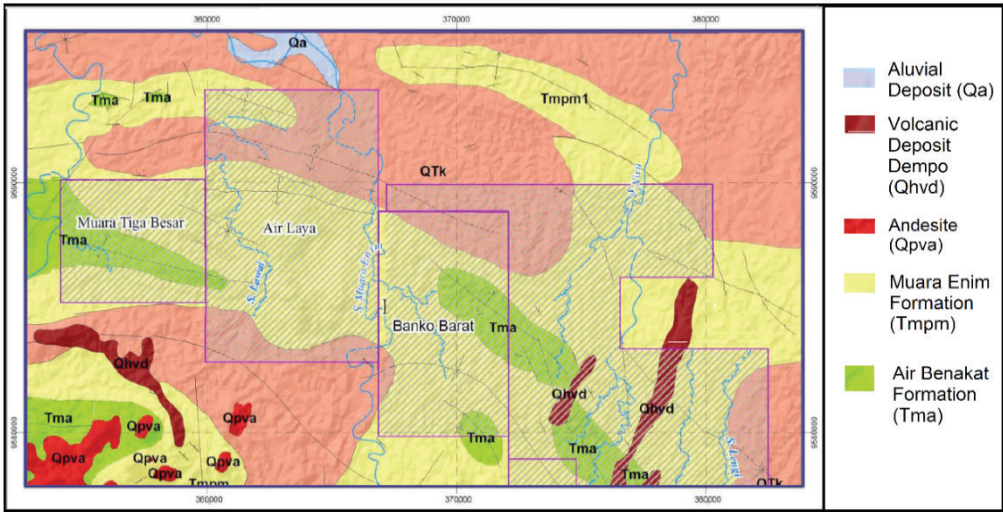


Figure 2 Geological Map of PTBA (Modified from Gafoer,1986).

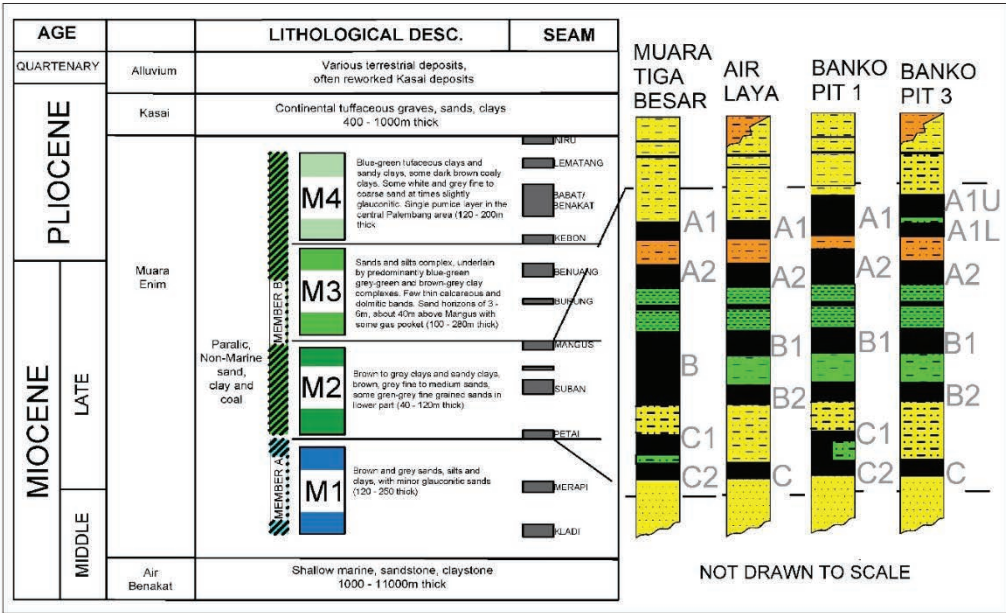


Figure 3 Regional Stratigraphy of Muara Enim Formation (Modified from Gafoer,1986)

Coal seams in PTBA intercalated with sedimentary rock layer (interburden) named based on their location relative to coal seam (e.g. Interburden A1-A2 for layer between coal seam A1 and coal seam A2). Thickness of stratigraphic layers and coal seams are varying for each mine areas and resumed in Table 1.

Mining activities

Surface mining system is implemented to mine the coal using a conventional truck and shovel method. A bucket wheel excavator is also operating in one of the pit in Muara Tiga Besar. From the mining front the ROM coal is hauled with dump trucks to the ROM stockpile then conveyed to the train loading



Table 1. Thickness of stratigraphic layers (in meter)

Stratigraphic Layer	Lithology	Mining Blocks		
		MTB	TAL	BB
Coal A1		6.80 – 10.00	6.50 – 10.00	6.50 – 9.00
Interburden A1-A2	Tuffaceous Sandstone	1.74 – 2.70	6.85 – 17.30	12.3 – 19.50
Coal A2		9.80 – 14.75	5.00 – 12.90	7.50 – 11.50
Interburden A2-B1/B	Claystone, sandstone layer	10.90 – 35.12	29.30 – 42.20	12.10 – 38.10
Coal B1	Claystone, siltstone layer		8.00 – 12.00	9.10 – 14.10
Interburden B1-B2	Sandstone with siltstone,	Coal B	3.06	24.90 – 57.10
Coal B2	claystone	15.30 – 20.00	3.00 – 5.00	4.35 – 5.55
Interburden B2-C		42.00 – 44.70	34.76 – 45.78	33.10 – 82.74
Coal C		0.80 – 2.75	6.00 – 10.00	11.00 – 11.30

Table 2. Static Test Result

Stratigraphic Layer / Mine Area (%)	TS	ANC	NAPP	pH Paste	NAG pH	NAG pH 4,5	NAG pH 7	
	(%)	(kg H2SO4/ ton)	(s.u.)	(s.u.)	(kg H2SO4/ ton)			
IB A1-A2	MTB	0.23 ± 0.41	4.32 ± 5.96	2.64 ± 8.70	5.46 ± 1.74	4.35 ± 1.19	4.54 ± 8.52	12.07 ± 12.86
	TAL	0.07 ± 0.10	10.81 ± 9.10	-8.8 ± 10.26	8.84 ± 1.25	6.36 ± 1.36	1.99 ± 5.61	5.35 ± 11.27
	BB	0.24 ± 0.30	11.90 ± 8.64	-4.41 ± 13.69	7.61 ± 1.42	5.01 ± 1.76	7.41 ± 15.66	16.03 ± 24.68
IB A2-B1/B	MTB	0.95 ± 0.48	11.13 ± 5.97	17.88 ± 18.49	6.31 ± 1.09	2.96 ± 0.52	21.37 ± 14.41	38.85 ± 20.96
	TAL	0.42 ± 0.23	15.14 ± 11.60	-2.34 ± 16.11	5.51 ± 1.29	2.83 ± 0.71	41.84 ± 30.12	65.73 ± 43.69
	BB	0.80 ± 0.62	14.99 ± 11.16	9.59 ± 24.68	6.06 ± 1.80	3.23 ± 0.98	23.26 ± 27.51	-42.70 ± 37.93
IB B1-B2	MTB	-	-	-	-	-	-	-
	TAL	0.74	11.84	10.83	3.81	2.45	41.58	83.97
	BB	0.92 ± 0.81	13.45 ± 8.66	14.66 ± 25.78	5.38 ± 1.00	3.14 ± 0.85	25.10 ± 24.47	44.52 ± 34.61
IB B2-C	MTB	0.89 ± 0.77	12.19 ± 6.23	14.92 ± 25.74	5.29 ± 0.74	2.97 ± 0.30	19.87 ± 22.72	33.98 ± 30.42
	TAL	0.35 ± 0.19	13.38 ± 7.12	-2.52 ± 10.14	5.18 ± 0.85	2.76 ± 0.36	27.67 ± 20.74	48.25 ± 28.14
	BB	0.96 ± 0.67	14.34 ± 23.80	15.56 ± 36.03	5.29 ± 1.48	3.10 ± 0.75	22.25 ± 24.24	38.05 ± 30.53

Note: All data reported in mean ± standard deviation. TS=total Sulphur, MPA= Maximum Potential Acidity, ANC=Acid Neutralizing Capacity, NAPP=Net Acid Producing Potential, NAG=Net Acid Generating; IB=Interburden, MTB=Muaa Tiga Besar, TAL=Air Laya; BB=Banko Barat

station (TLS) for further transportation to the ports using railway.

Geochemical Characterization

Rock geochemical characterization has been conducted on samples collected from cores of 31 drill holes representing three mining blocks. Rock geochemical characterization based on AMIRA (2002) is conducted by performing static test consisting of paste pH (1:2), Net-Acid Generation Test, Total Sulphur and Acid Neutralizing Capacity Test. Statistic of static test is shown in Table 2.

Laboratory-scale kinetic test using Free Draining Column Leach Test method for selected samples was also performed to verify the static test results. Result of static test (NAPP and NAG pH value) and pH range of kinetic

test is shown on Table 3. The kinetic test result shows that IB A1-A2 layer yields circumneutral-alkalic pH leachate ranging from 6.72 to 9.20, whilst IB B1-B2 produces acidic leachate ranging from 2.75 to 4.15. IB A2-B1 and IB B2-C yields various pH leachates.

Discussion

Vertical variation of geochemical characteristic on each mine area

Stratigraphically, MTB mine is consisting of IB A1-A2, IB A2-B and IB B-C layer. Whereas, TAL mine and BB mine are consisting of IB A1-A2, IB A2-B1, IB B1-B2 and IB B2-C layer. In MTB mine, IB A1-A2 layer is classified as NAF (Non-Acid Forming) since it has NAPP value of 2.64 ± 8.70 kg H₂SO₄/ton,



Table 3. Static Test (NAPP and NAG pH) and Kinetic test result for Selected Samples

Stratigraphic Layer / Mine Area NAPP (kg H2SO4/ton		Static Test		
		NAG pH (s.u.)	Kinetic test leachate pH (s.u.)	
IB A1-A2	MTB	1.89	5.45	6.72 – 8.02
	TAL	-96.32	7.72	8.05 – 7.87
	BB	-9.71	3.29	9.20 – 8.10
	MTB	16.26	2.64	3.95 – 6.20
IB A2-B1/B	TAL	35.85 - 38.25	2.56 - 3.16	4.34 – 3.83
	BB	9.12 - 36.57	3.21 - 3.62	2.10 – 8.40
	MTB	-	-	-
	TAL	43.06	6.55	2.75 – 4.15
IB B1-B2	BB	23.86	2.93	2.80 – 4.10
	MTB	0.43	6.66	7.02 – 8.20
	TAL	17.44 - 22.05	2.88 - 3.54	2.89 – 7.10
	BB	13.16 - 19.97	2.24 - 2.42	2.10 – 6.80

NAG pH value of 4.35 ± 1.19 and kinetic test leachate pH values ranges 6.72 to 8.02. The IB A2-B layer is classified mainly as PAF (Potentially Acid Forming) with NAPP value of 17.88 ± 18.49 kg H₂SO₄/ton, NAG pH value of 2.96 ± 0.52 and kinetic test leachates pH values ranges 3.95 – 6.20. The lower IB B-C with NAPP value of 14.92 ± 25.74 kg H₂SO₄/ton, NAG pH value of 2.97 ± 0.30 is classified mainly as (low) PAF since it has kinetic test leachates pH values ranges 7.02 – 8.20.

The IB A1-A2 layer in TAL mine is classified as NAF with NAPP value of -8.8 ± 10.26 kg H₂SO₄/ton, NAG pH value of 6.36 ± 1.36 and kinetic test leachate pH values from 8.05 – 7.87. Layer IB A2-B is classified mainly as PAF with NAPP value of -2.34 ± 16.11 kg H₂SO₄/ton, NAG pH value of 2.83 ± 0.71 and kinetic test leachates pH values ranges 4.34 – 3.83. Layer IB B1-B2 is classified mainly as PAF with NAPP value of 10.83 kg H₂SO₄/ton, NAG pH value of 2.45 and kinetic test leach-

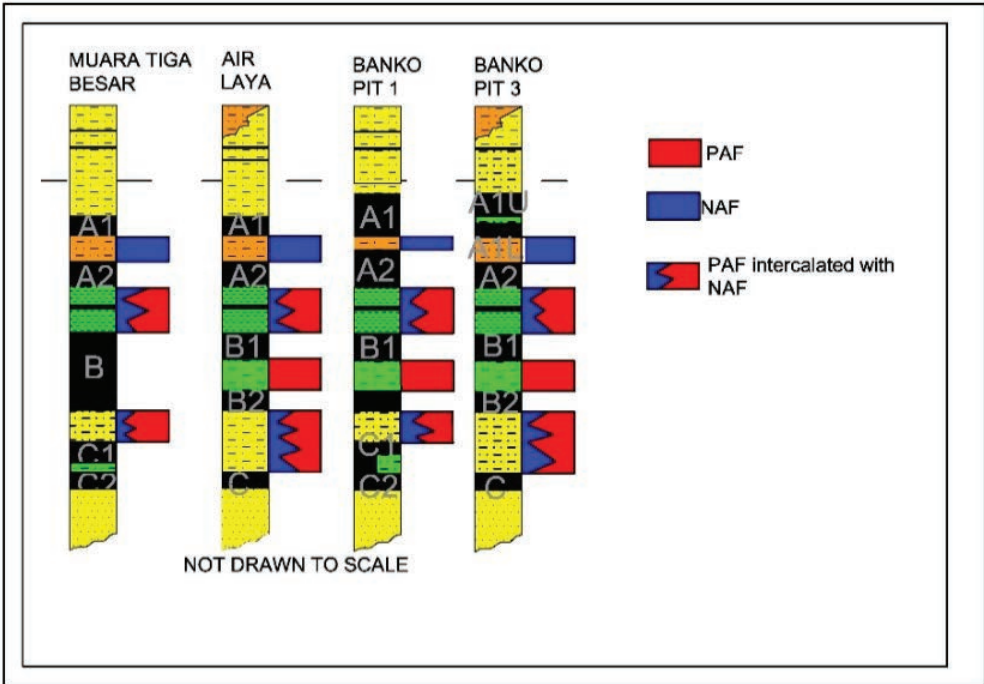


Figure 4 Geochemical Classification based on Stratigraphic Layers



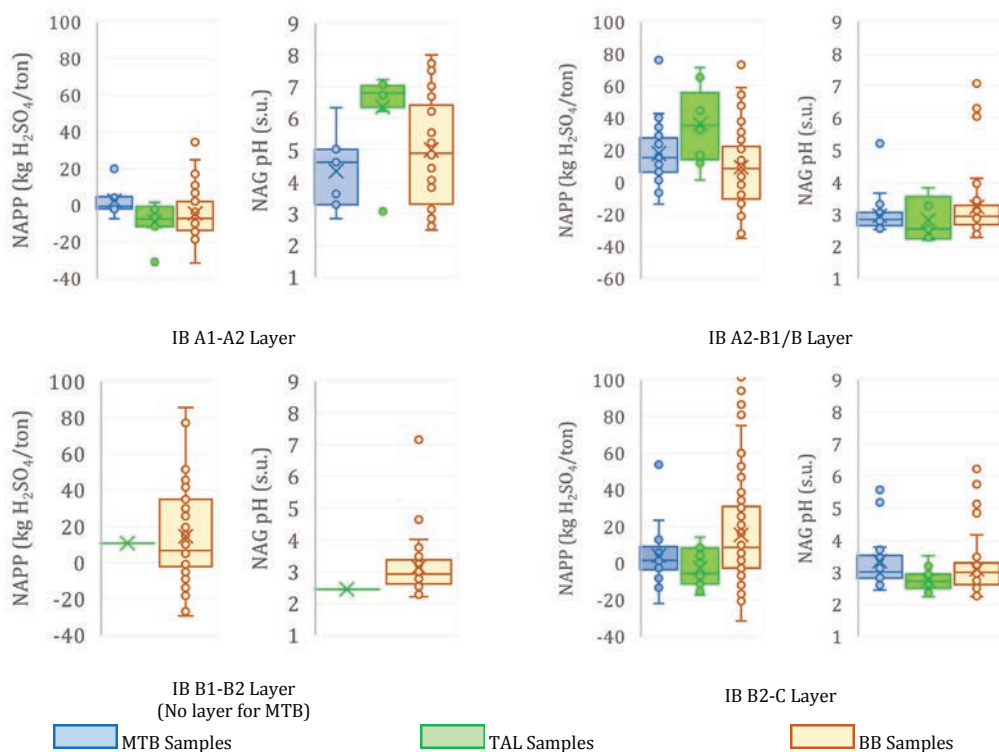


Figure 5 Boxplots of Static Test Result for each stratigraphic layer

ates pH values ranges 2.75 – 4.15. Layer B2-C is classified mainly as PAF with NAPP value of -2.52 ± 10.14 kg $\text{H}_2\text{SO}_4/\text{ton}$, NAG pH value of 2.76 ± 0.36 and kinetic test leachates pH values ranges 2.89 – 7.10.

Similar with TAL mine, in BB mine IB A1-A2 layer classified as NAF with NAPP value of -4.41 ± 13.69 kg $\text{H}_2\text{SO}_4/\text{ton}$, NAG pH value of 5.01 ± 1.76 and kinetic test leachate pH values ranges 9.20 – 8.10. The following layer of IB A2-B is classified mainly as PAF with NAPP value of 9.59 ± 24.68 kg $\text{H}_2\text{SO}_4/\text{ton}$, NAG pH value of 3.23 ± 0.98 and kinetic test leachates pH values ranges 2.10 – 8.40. Layer IB B1-B2 is classified mainly as PAF with NAPP value of 14.66 ± 25.78 kg $\text{H}_2\text{SO}_4/\text{ton}$, NAG pH value of 2.45 and kinetic test leachates pH values of 3.14 ± 0.85 . Layer B2-C is classified mainly as PAF with NAPP value of 15.56 ± 36.03 kg $\text{H}_2\text{SO}_4/\text{ton}$, NAG pH value of 3.10 ± 0.75 and kinetic test leachates pH values ranges 2.10 – 6.80.

It can be concluded that vertical stratigraphical variation is evident as follows: IB A1-A2 classified as NAF, IB A2-B1 classified

as PAF intercalated with NAF, IB B1-B2 classified as PAF, B2-C classified as PAF intercalated with NAF, as shown in figure 4.

Lateral variation of geochemical characterization

Lateral variation of geochemical characteristics is proven by comparing the same stratigraphic layer of three mine blocks as shown in Figure 5. It is found that there are variations of geochemical characteristics of some stratigraphic layers along MTB to TAL and BB as indicated from the results of static and kinetic tests particularly NAPP and NAG values. In all mine blocks IB A1-A2 is classified as NAF whereas IB A2-B1/B and IB B2-C are classified as PAF. Difference in geochemical characteristics exist among the PAF layer. The NAG pH value of IB A2-B1/B layer and IB B2-C layer at TAL mine and BB pit 1 tend to be lower than at MTB and BB-3 mine. This lateral variation of geochemical characterization is possibly explained by geological setting of mine areas. It seems that quarternary andesitic intrusions in the south and under-



neath of TAL affected the coal and IB layers in TAL mine. In BB, there is significant difference between pit 1 in the south and pit 3 in the north. The PAF characteristic in BB pit 1 is similar to TAL mine while BB pit 3 is dominated by NAF material. Refer to the case in TAL, it seems that there exist the sub-surface influence of andesitic intrusion activity as indicated in the southeast of BB in the geological map.

Conclusions

Vertical or stratigraphical variation of geochemical characterization is evident by comparing static and kinetic test results for each mine areas. It is concluded that IB A1-A2 is classified as NAF, IB A2-B1 is classified as PAF intercalated with NAF, IB B1-B2 is classified as PAF, and B2-C is classified as PAF intercalated with NAF,

Lateral variation of geochemical is evident due to quarternary andesitic intrusion. IB A1-A2 classified as NAF in all mine areas. IB A2-B yields more acid in TAL mine, compare to BB and MTB based on NAPP and NAG pH values. IB B1-B2 is classified as PAF in TAL and BB and IB B2-C is classified as PAF and yields more acid in BB mines compare to BB and MTB. Lateral variation shows elevated acidity from MTB to BB, except BB Pit 3 Timur due to its distant location to the intrusion bodies.

Acknowledgements

The authors thank PT Bukit Asam Indonesia for assistance and helping during water and rock sampling and the permission for this publication

References

- Amijaya, D. H. (2005). Paleoenvironmental, paleoecological and thermal metamorphism implications on the organic petrography and organic geochemistry of tertiary Tanjung Enim coal, South Sumatra Basin, Indonesia. Aachen, Techn. Hochsch., Diss., 2005 (Nicht für den Austausch).
- AMIRA. 2002. ARD Test Handbook. Project P387A. Prediction and Kinetic Control of Acid Mine Drainage, AMIRA International Limited, Melbourne, Australia.
- Belkin, H. E., Tewalt, S. J., Hower, J. C., Stucker, J. D., & O'Keefe, J. M. K. (2009). Geochemistry and petrology of selected coal samples from Sumatra, Kalimantan, Sulawesi, and Papua, Indonesia. *International Journal of Coal Geology*, 77(3-4), 260-268.
- De Coster, G. L. (1974), The Geology of the Central and South Sumatra Basin, *Proceedings of 3rd Annual Convention IPA*, June 1974, Jakarta.
- International Energy Agency (2017), *Coal Information Overview* (2017 Edition)
- Gafoer, S., Cobrie, T., & Purnomo, J. (1986). Geological Map of the Lahat Quadrangle, South Sumatra, scale 1: 250.000. Geological Research and Development Centre, Bandung.
- Shell Mijnbouw N.V. (1976). Geological study of the Bukit Asam coal mines, Jakarta, 18 pp. (unpublished)
- Thomas, L.P. (2005). Fuel resources: coal. In: Barber, A.J., Crow, M.J., Milsom, J.S. (Eds.), *Sumatra: Geology, Resources and Tectonic Evolution*, *Memoirs No. 31*, Geological Society, London (2005), pp. 142-146



Acid Mine Drainage in a Tropical Environment: A Case Study from the Tanjung Enim Coal Mine Site in South Sumatra, Indonesia

Rudy Gautama Sayoga¹, William Perkins², Graham Bird³, Wisjnoe Adije¹,
Oliver Moore^{2,4}, Ginting Jalu Kusuma¹, Abie Badhurahman¹

¹*Bandung Institute of Technology, Faculty of Mining and Petroleum Engineering, Jl. Ganesha 10, Bandung 40132, Indonesia*

²*Aberystwyth University, Department of Geography and Earth Sciences, Aberystwyth, SY23 3DD, UK*

³*School of Environment, Natural Resources and Geography, Bangor University, Bangor, Gwynedd, SY23 2UW, 4UK Scientific Analysis Laboratories Ltd, 69 Hadfield St, Stretford, Manchester M16 9FE*

Abstract

Indonesia is one of the world's most important coal producers and exporters. The state owned mining company (PT Bukit Asam or PTBA) operates an open pit coal mine at Tanjung Enim in South Sumatra; extracting Miocene/Pliocene coal from a back arc basin which has been influenced by igneous activity. Mining takes place in 3 separate pits called Air Laya, Muara Tiga Besar Utara (MTBU) and Banko Barat. These pits each contain pit lakes which are filled, predominantly, by rainwater. This region has a tropical climate. Field and laboratory measurements reveal that the pit lakes vary from acidic (pH 2.6) to circum-neutral (pH 6.6) and this is reflected in the chemistry of the waters. The waters are calcium, magnesium sulfate dominated but show elevated Al, Fe and Mn (26.7, 60.2 and 21.3 mg/L respectively) in the most acidic examples. The mine waters also show variation in trace elements linked to the acidity. Treatment of the mine waters is performed using a range of passive to semi-passive methods which include lime addition (up to 1800 t a⁻¹), settling lagoons and reed/floating plant beds. During the wet season the peak flow from the largest pit to one of the treatment systems is 875 L h⁻¹. Chemical stratigraphy of the overburden/interburden rocks reveals differences in the leachable trace elements which can be linked to the potential acid formation.

Keywords: Indonesia | South Sumatra | AMD|Coal mine water | Water treatment

Introduction

Indonesia is the world's 5th largest producer and its second highest exporter of coal (BP 2017). The estimated value of coal exports from Indonesia in 2016 was more than 18 billion US dollars. Coal mining is concentrated on the islands of Kalimantan and Sumatra. Here we describe the hydrochemistry of mine drainage at the Tanjung Enim mine site in south Sumatra; the largest open pit coal mine in Sumatra. This site lies approximately 165 km from the city of Palembang. PT Bukit Asam (PTBA), a state-owned mining company, operates the mine, at Tanjung Enim. The mine is located within the South Sumatra Basin; an extensional basin which lies to the east of the active volcanic arc in South Sumatra.

This basin was formed in a back-arc setting during the pre-early Tertiary Period (Daly et al. 1987). At the mine site, the rocks belong to the Muara Enim Formation (MEF), which consists of mudstones, siltstones, sandstones, and coal beds that were deposited during the Late Miocene to Early Pliocene Periods. Amijaya and Littke (2006) interpret this as a shallow marine to non-marine sequence linked to a tropical deltaic system. Later deformation has given rise to set of NW-SE to E-W trending folds which develop local dips of between 5° and 30°. During the Late Tertiary and Early Quaternary Periods the area was subjected to igneous intrusions, of an andesitic composition, that caused local thermal metamorphism, resulting in an increase in the grade of some of the coals.



There are three coal seams at the Tanjung Enim site, which are, from oldest to youngest, the Petai, Suban and Mangus seams. Locally these are known as the C (Petai), the B2 and B1 (Suban) and the A2 and A1 (Mangus). These seams range in thickness: the C seam is between 7 and 10 m; the B2 seam is between 4 and 5 m; the B1 seam is between 8 and 12.3 m; the A2 is between 9 and 12.8 m and the A1 is between 6.5 and 10 m. Previous work by Gautama (1994) and Gautama and Hartaji (2004) has shown that acid mine drainage is an important issue at the Tanjung Enim mine. Gautama and Hartaji (2004) demonstrated that the source of the AMD is predominantly from the overburden and inter-seam rocks (interburden) and they were able to differentiate between potentially acid forming (PAF) and non-acid forming (NAF) rocks by the application of both static and kinetic testing procedures.

The mine site is bisected by the Enim River with two open pits (Air Laya and Muara Tiga Besar [MTBU]) to the west and Banko Barat to the east (Fig. 1). PT Bukit Asam has a total mining licence for 66,414 ha at Tanjung Enim and in 2017 the three open pits had a combined area of 15,421 ha; the individual areas being: MTBU 3300 ha; Air Laya 7621 ha and Banko Barat 4500 ha (PTBA 2017). It is informative to note that the three mine pits remove coal from all of the seams from C to A1 and thus there is no difference between the coals extracted from the individual open pits.

South Sumatra has a tropical climate, which shows only a limited change in temperature throughout the year. At Tanjung Enim the annual mean temperature is 26.6 \pm 0.4 $^{\circ}$ C with a maximum of 31.8 $^{\circ}$ C. The rainfall at the mine site is seasonal with the wettest months being December and January (with typical rainfall totals of 378 and 395 mm, respectively) and the driest months being June, July and August (with typical rainfall totals of 137, 110 and 130 mm, respectively) – these data are sourced from Climate-Data.org. The rainfall is the greatest source of water at the mine site since there is limited groundwater infiltration to the open pits. The tropical climate combined with the seasonal and stormy nature of the rainfall, makes the treatment of mine water challenging. Mine

water is pumped from the open pits up to a maximum rate of 875 m³ h⁻¹ and treated in a variety of passive/semi-passive treatment systems (which are described below) before being discharged into the local river. The mine is governed by the Decree of the Minister of the Environment Nr. 113 year 2003 on Effluent Environmental Standard for Coal Mining Activities. This states that discharges must not exceed: pH 6-9; TSS 400 mg/L; Fe (total) 7 mg/L; Mn (total) 4 mg/L. Prior to this study there was only limited data on the chemical composition of the water from the mine site, driven by the requirements of the Decree, and limited information regarding the temporal variability in water chemistry. In addition, this study considers the implications of the nature and variability of mine water chemistry on treatment approaches.

Methods

A series of water samples were collected at the mine site between October 2015 and February 2018 so that both ‘dry season’ and ‘wet season’ data were available. In addition to the sets of discrete sampling operations, in July of 2016 a time series of field measurements was made at the outlet from one of the passive treatment systems at the site (see logging site Fig. 1), in order to better understand the short-term variability in the chemistry of waters subjected to treatment. This set of data was collected every 10 minutes from 15:45 on 22nd July to 12:05 on 24th July (total time of 43 hours and 20 minutes). This time series was able to collect data through a rainstorm event at 21:24 on 22nd July. Water chemistry was recorded by an Aquaread AP-800 multi-probe/datalogger and flow stage by In-Situ Inc. Rugged Troll 100 water level logger with an additional barometric pressure logger. The sampling sites are shown on Figure 1 together with a set of unified sample location names/numbers. Samples were collected from the pit lakes, as close as possible to the floating pumping pontoons and also from the inlet and outlet of the different treatment systems. As far as possible the ‘outlet’ sampling points in this study correspond with points used by PTBA for their routine discharge monitoring.

In the field the pH, oxidation-reduction potential, temperature and some conductivi-



ty measurements of the waters was monitored using portable (Hanna) meters and probes. Discharge data was also measured/estimated at each site and calibrated using staging points where possible. Water samples were filtered in the field using a hand-held syringe system and 47 mm diameter 0.45µm cellulose nitrate membrane filter. Samples for cation analysis were acidified in the field whilst those for anion analysis were not. Chemical analyses were conducted in the laboratories at Aberystwyth University and the Laboratory of Hydrogeology & Hydrochemistry, Bandung Institute of Technology. Major cations were determined using atomic absorption spectrophotometry using multi-element synthetic calibration standards, minor and trace elements were determined by ICP-MS and anions were determined by ion chromatography

Results

Field measurements of the water in the open cast pits of the three mine areas reveal a distinct and consistent variation in the pH of the waters, with those samples from Air Laya and MTBU having a higher pH than the two pit lakes of Banko Barat (pit 1 and pit 3). The pH values were typically 6.3 (Air Laya), 4.1 (MTBU), 2.8 (Banko Barat pit 1) and 3.1 (Banko Barat pit 3). The field observations show that the pit lake at Banko Barat (especially pit 1) has a red colouration which is distinct from the other pit lakes. Throughout this study the pH values have remained fairly constant even when comparing ‘wet’ and ‘dry’ season results. The typical range of the pit lake surface pH is included in Table 1. This is somewhat surprising since the pit lakes represent rainfall collected in the pit bottom rather than the influx of groundwater; which is known to be a limited influence at this site. It might be expected that during the wet season dilution by rainwater would affect the pH of the pit lakes but this is not the case. Field measurements of ORP were also collected during the 2016 dry season sampling and these data show a range from 85 mV for the Air Laya pit to 483 mV for the Banko Barat pit 3. These data can be used to plot the position of each water sample on an Eh-pH diagram for iron species; adjusted to the measured water temperature of $\approx 32^{\circ}\text{C}$. These data show that the pit lake waters are close to the boundary between Fe^{2+} in solu-

tion and iron oxy-hydroxide precipitates and this could be buffering the pH/ORP within the mine waters.

The time series for water monitored at a treatment pond outlet shows a diurnal variation in temperature of $\approx 5^{\circ}\text{C}$ with the lowest temperature recorded at $\approx 07:00$ (27.3°C) and the highest temperature recorded at 16:30 (32.6°C). This change is not reflected in the ORP or DO data which only show minor fluctuations through the 43 hour period. The storm event produced a marked change in the discharge and an accompanying increase in the turbidity of the water (from a baseline of ≈ 10 NTU to a peak of ≈ 130 NTU before the readings stabilised at ≈ 50 NTU for the remainder of the time period). The changes in the water quality are the result of increased run-off from the coal stockpile because the pumps that deliver water from the Air Laya pit were turned off at the time of the data collection. The changes in water chemistry following the storm event also highlight the challenge posed by these events in the management and treatment of mine waters.

Laboratory measurements on the water samples have been used to characterise these mine waters for the first time. The major elements in the waters shows that they are dominated by calcium and magnesium sulfate as shown by the data in Table 1. Analysis of the waters collected during the dry season in 2016 confirms that these waters are saturated or close to saturated with anhydrite and gypsum. In addition to the major elements the mine waters have elevated levels of aluminium, iron and manganese (highest values of 26.7, 60.2 and 21.3 mg/L respectively in the waters of the Banko Barat pit 1).

The waters show differences that reflect the pH and Eh conditions illustrating the increased solubility of elements in more acidic waters. There is a number of elements which are a cause for concern because they exceed the environmental legislation in Indonesia (Fe and Mn). Furthermore there are elements which are potentially toxicity to the local aquatic environment (Al being one of the more important). Most of these elements are found at their highest concentration in the waters from Banko Barat pit 1 with intermediate concentrations in MTBU and Banko Barat pit 3 waters and the lowest concentrations in Air Laya



Table 1. Major element composition of mine waters from the 4 pit lakes (Air Laya, MTBU, Banko Barat (BB))– data for July 2016 (all results in mg/L).

Site name	Na	K	Ca	Mg	pH range	SO ₄
Air Laya	200	15.4	134	45.8	5.8-5.9	936
MTBU	83.6	12.5	129	54.5	3.5-4.2	1000
BB pit 1	135	15.4	200	126	2.6-2.9	2010
BB pit 3	37.6	9.0	110	58.3	3.1-3.9	868

Table 2. Trace element composition of mine waters from the 4 pit lakes (Air Laya, MTBU, Banko Barat (BB))– data for July 2016* (dry season) and December 2107** (wet season). All results in ug/L except Mn and Fe in mg/L.

Site	Al	Mn	Fe	Co	Ni	Sr	Ba	ΣREE	Th	U
Air Laya*	14	5.0	0.03	38	46	954	47	1	n.d	n.d
MTBU*	1360	7.73	2.5	89	106	1040	47	52	0.2	0.8
BB pit 1*	7730	21.3	60.2	273	338	1680	38	1250	5.5	3.6
BB pit 3*	2143	7.65	9.5	96	117	577	49	107	1.9	2
Air Laya**	111	6.1	0.1	45	52	900	40	6.1	0.7	0.5
MTBU**	1120	6.81	0.28	77	84	913	50	43	0.1	0.3
BB pit 1**	8950	11.1	21.2	199	261	943	51	261	8.5	5.5
BB pit 3**	3450	7.45	3.76	138	179	585	59	130	1.2	2.4

waters. This can be illustrated by considering a selection of trace elements with data presented in Table 2 for both the dry and wet seasons.

The data for Air Laya shows relatively low concentrations of all of the trace elements when compared to the other sites; which is consistent with the circum-neutral pH of this pit lake. The high Fe and Mn content of Banko Barat pit 1 is also reflected in the high Al, other first row transition metals, Sr, total REE and Th and U. It seems reasonable to suggest that many of the elements are elevated because of the acidic nature of these waters but that there is also a lithological/mineralogical control on the chemistry that reflects the spatial distribution of the extraction pits. This is best illustrated by comparing the waters from MTBU and Banko Barat pit 3. These two waters have similar pH values and also similar major element concentrations but the two vary in their total REE and Th and U concentrations; suggesting a source for these trace elements that is spatially controlled and generally higher in the Banko Barat area than the MTBU area. Equally the source of Sr and Ba favours the sites to the west (Air Laya and MTBU). Gautama et al. (this volume) have investigated the link between the potential acid formation of the

overburden/interburden at the Tanjung Enim site and their data shows that trace elements are not homogeneously distributed through the different horizons. Vanadium and Mo, as an example of trace elements commonly associated with coal-bearing rocks, show their highest concentrations in the interburden between the A1 and A2 seams whereas Sr shows a peak in concentration in the same horizon followed by a general decrease in the deeper interburden rocks. Nickel and Cr show a general increase in concentration with depth whereas Ce and U are highest in the middle of the sequence.

All of the pit lakes exceed the permissible concentration for Mn but only the Banko Barat pits exceed the limits for Fe. These waters require treatment before they can be discharged into the local river.

Each of the mining areas has at least one passive/semi-active water treatment system. These range from settlement lagoons, which generally have some lime addition at the inlet, to a complex treatment system involving reed beds and floating plant-based adsorbers. PTBA uses around 1800 tonnes of lime per year which is added to the more acidic waters prior to the treatment cells. During this study samples were collected at the inlet and outlet



Table 3. Major element composition of mine waters treated in the Air Laya/Stockpile treatment system data for July 2016 (all chemical results in mg/L).

Site name	pH	Eh(mv)	K	Mn	Fe	SO ₄
Inlet water	6.13	220	30.3	0.69	0.52	106
Intermediate 1	6.02	62	5.59	0.66	0.58	191
Intermediate 2	6.45	64	4.92	0.65	n.d.	204

of some of the treatment systems to gauge the efficiency of Fe and Mn removal. The treatment system employing reed beds to treat the water from the Air Laya pit as well as water draining from one of the main coal stockpiles at the site was considered in more detail, with samples collected from intermediate stages as well as the inlet and outlet. This scheme covers an area of approximately 62,000 m² and consists of a series of 12 ponds which are, in order: 3 settlement ponds; 4 typha reed beds with floating ferns (*Typha sp.* and *Salvania natans*); 3 ponds with floating vetiver plants for metal removal (*Viveria zizanoides*) and 2 ponds with common water hyacinth (*Eichhornia crassipes*). In the study four sites were selected which covered both the inlet and outlet of passive treatment beds as well as two intermediate sample points; one at the inlet to the middle typha bed and one at the inlet to the first floating vetiver lagoon. The results from 2015 show that the treatment system removes Al and Fe to below the limit of detection and the Mn from 24.5 mg/L to 0.1 mg/L. When the system was studied in detail in 2016 the concentration of elements in the input water was lower because the only water being treated was draining from the coal stockpile. In 2016 the intermediate samples showed that Fe was removed but Mn remained constant (at ≈650 µg/L) until the final outlet sample. The same sample set showed that K was depleted by a factor of 6 because it is an important nutrient whereas Ca, Mg and Sr all increased from the dissolution of added lime. Results for the 2016 study of this treatment system are shown in Table 3.

Dry season data for the MTBU treatment cells show that these work to remove Fe (2.5 to 0.2 mg/L) but have little effect on the Mn (6.6 to 5.8 mg/L) which reflects the difficulty in removing Mn by settlement lagoons or pH adjustment alone. This mine water would not comply with the Indonesian Government Decree of 2003.

Conclusions

We have reported new data for the Tanjung Enim open pit coal mine waters for the first time. We have shown that much of the mine water at the Tanjung Enim site has elevated concentrations of Fe and Mn which exceed the permissible discharge limits for Indonesian coal mines. There are, in addition, other potentially harmful elements present in the mine waters that are not routinely analysed such as Al. There are only limited seasonal effects at this site with some dilution demonstrated in the wet season data. There is a spatial difference in the pit lake chemistry that cannot be easily linked to the coal being extracted from the different mine pits and must, therefore, be related to the distribution of potential acid formation in the interburden across the area.

Acknowledgements

The authors thank the British Council for the Global Innovation Initiative (GII) funding which facilitated this collaborative project between institutions in the UK, USA and Indonesia. The authors also thank the PTBA staff at Tanjung Enim for hosting the visitors and accompanying the team on sampling trips around the site.

References

- Amijaya H, Littke R (2005) Microfacies and depositional environment of Tertiary Tanjung Enim low rank coal, South Sumatra basin, Indonesia. *Int J Coal Geology* 61:197-221, doi: 10.1016/j.coal.2004.07.004
- BP Statistical Review of World Energy June 2017 (2017) – 66th edition
- Daly MC, Hooper BGD, Smith, DG (1987) Tertiary plate tectonics and basin evolution in Indonesia. *Proceedings of the 6th Regional Congress on Geology, Mineral and Hydrocarbon Resources of Southeast Asia (GEOSEA VI)*, Jakarta, 1-28



Gautama RS (1994) Acid water problem in Bukit Asam Coal Mine, South Sumatra, Indonesia. *Int Mine Water Association Proceedings* 1:533-542

Gautama RS, Kusuma GJ, Pujiantoro E, Wisnugroho PH (2018) On The Spatial Variation of Rock Geochemical Characteristics in Coal Mining: Case Bukit Asam Coal Mine in South Sumatra, Indonesia. *This volume*.

Gautama RS, Hartaji S (2004) Improving the accuracy of geochemical rock modelling for acid rock drainage prevention in coal mine. *Mine Water Environ* 23(1):100-104

PTBA Annual Company report (2017) PT Bukit Asam Tbk. Jakarta

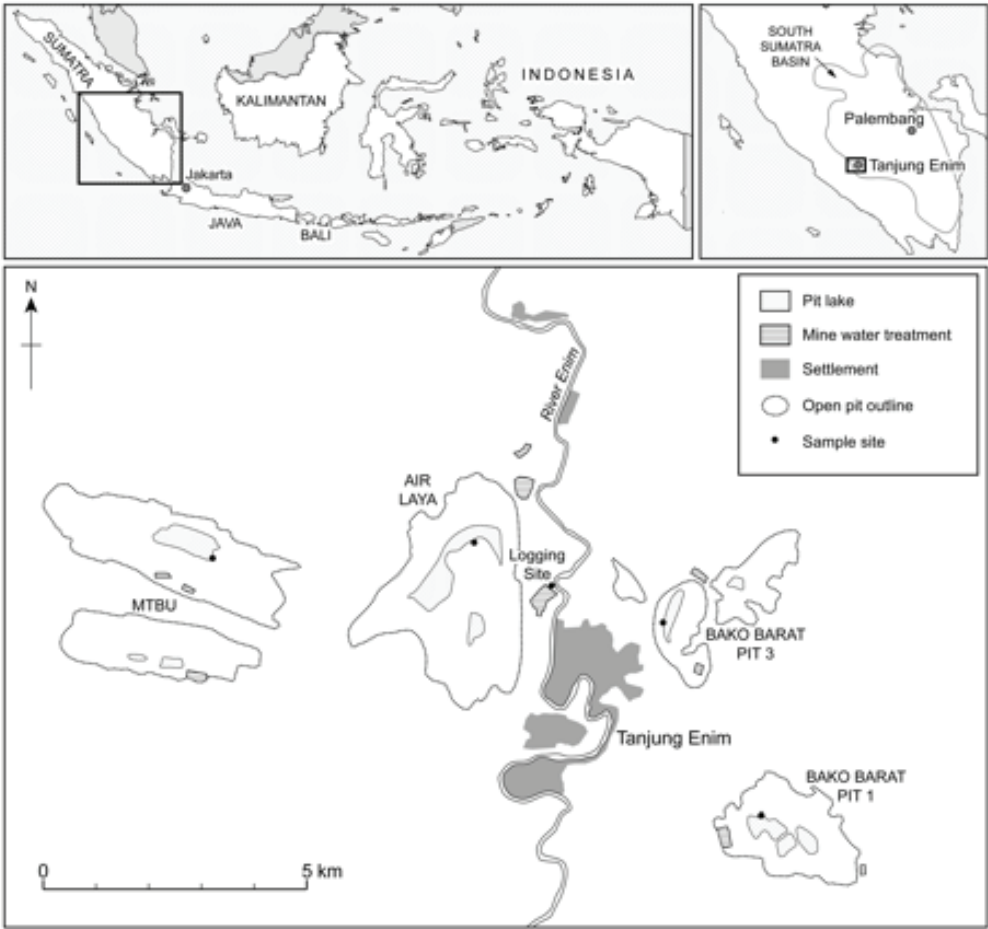


Figure 1 Study location map showing the position of the south Sumatra basin and the area of the mine (top left) and a detailed map of the Tanjung Enim site with the individual mine pits indicated, the pit lakes and the key sampling locations shown.



Cementation of cyanidation tailings – Effects on the release of As, Cu, Ni and Zn[®]

Roger Hamberg, Lena Alakangas, Christian Maurice,

*Luleå University of Technology, Division of Geosciences and Environmental Engineering, 971 87
Luleå, Sweden, roger.hamberg@ltu.se*

Abstract

Maintaining saturated conditions in two cemented paste backfill (CPB)-mixtures (1-3 wt.% of binders) based on cyanidation tailings was vital for reducing the pyrrhotite oxidation rate and the release of Cu, Ni and Zn. The opposite was true for As, that desorbed from Fe-precipitates and formed soluble Ca-arsenates. Flooding of CPB-fillings could be a long-term process, where unsaturated zones can form within CPB-masses. At this stage, leachates from CPBs (1 wt. %), became acidic, causing As-release to decrease but the opposite for Cu. In CPBs (3wt. %), As-release was unaltered but the Zn-release increased as binder-related Zn-phases dissolved in alkaline conditions.

Keywords: Tailings management, cement, trace metal leaching

Introduction

Cyanide-leaching is used when gold occurs as inclusions in sulfide minerals that might contain As, Cu, Ni and Zn. However, it is a common fact that mining processes are never 100 % effective and remnants of gold and sulfide minerals are always present in the cyanidation tailings (CT). So, effects of the sulfide oxidation or the oxidation itself must be obstructed to ensure the stability of As, Cu, Ni and Zn. Therefore, before further managing CT, it is critical to understand how the cyanide leaching process could affect the mobility of Cu, Ni, As and Zn. One way of managing CT is the use of a method called Cemented paste backfill (CPB). In CPB, low proportions (3-7 wt. %) of cementitious binders are mixed with CT to form a saturated, monolithic mass. CPB aims to reduce oxygen availability and the sulfide oxidation rate. Belie et al. (1996) suggested that a strength loss within a cement-stabilized material could cause the leachability of metals to increase. In a CPB-material, the formation of Calcium-Silicate-Hydrates (C-S-H) is the main contributor to the mechanical strength. Sulphates from the sulfide oxidation may react with the C-S-H, forming ettringite and gypsum (a sulphate attack), and cause a strength loss within the CPB. In some underground workings, strength of the CT-CPB-material

is of less concern, but aims to enhance trace metals stability still exist. At completely saturated conditions in the CPB-materials, sulfide oxidation is obstructed and sulfates mainly supposed to be pre-oxidized products (Benzazoua et al. 2004). In field conditions, extended time periods are expected for the groundwater table to rise and flood the CPB-materials. During that period of time, local desaturation in the CPB-monoliths is possible and this could increase the sulphide oxidation rate (Ouellet et al. 2006). It is therefore important to investigate the geochemical stability of As, Cu, Ni and Zn in CPB materials where unsaturated areas are present. For this reason, it is important to study: (1) how the cyanide leaching process and an associated water treatment affect the mobility of Cu, As, Ni and Zn in tailings, (2) how the use of a low-strength CPB affect leaching of As, Cu, Ni and Zn, (3) how does the establishment of unsaturated zones within low-strength CPB mixtures affect leaching of As, Cu, Ni and Zn?

Materials and Methods

Prior to cyanide leaching, an oxidation step is added to liberate the gold occurring as inclusions in arsenopyrite/pyrrhotite. In the oxidation step and the cyanide leaching process, pH is raised to 10-11 while oxygen is added. In an subsequent water treatment process, H₂O₂, CuSO₄ and lime (pH of 10) was added in or-



der to detoxify residual cyanides. To immobilize the metal(oid)s, $\text{Fe}_2(\text{SO}_4)_3$ is then added until the pH of the cyanidation tailings (CT) slurries was reduced to 7-8.5 before deposition in the tailings dams, in accordance with legal guidelines. Binders used in CPBs were: Portland cement (CE) and biofuel fly ash (FA). Elemental compositions of ore, CT, CE and FA are presented in table 1. FA is classified as a class C fly ash according to (ASTM C618-05) as the content of $\text{SiO}_2 + \text{Al}_2\text{O}_3 + \text{Fe}_2\text{O}_3$ is approx. 60 wt. %. XRD and SEM-EDS revealed that pyrrhotite (1 wt. %) and arsenopyrite (0.1 wt. %) are the main Fe- and As-sulphide minerals. Arsenopyrite grains have iron-oxide-rims that could sequester arsenates. CT was considered to be acid-generating with a NNP of -60.8 kg CaCO_3 /tonne, 20 % of CT have a particle size of less than 19.5 μm .

Speciation-solubility calculations were performed with the geochemical code PHREEQC. Element concentrations, redox-potential (Eh), and pH in leachates from the TLT and WCT were used.

Preparation of CT-CPB-mixtures

CPB-Mixtures were selected to have a strength of 200 kPa with a minimal proportion of binders. CPB-mixtures (CE and CE-FA) are based on CT; and consist of CE (1 wt.% of cement) and CE-FA (2 wt. % of cement, 1 wt. % of FA). CPB-mixtures of CE and CE-FA were cured for 31 days or 446 days, hereafter named CE31, CE446, CE-FA31 and CE-FA446. CE31 and CE-FA31 were kept in humid (85 % humidity), room tempered, dark conditions until the 31th day. CE446 and CE-FA446 were kept in dark, room temperatured conditions (approx. 50 % humidity) un-

til the 446th day to facilitate the formation of unsaturated zones within the monoliths.

Sequential extraction test

Fractionation of Ca, S, Ni Zn, Cr and Cu was assessed using the modified sequential extraction scheme described by Dold (2003). CT, CE446 and CE-FA446 was used and extracted with five different solutions in succession. Overall details about the extraction procedure are presented in Hamberg et al., (2016).

Flooded monoliths – Tank leaching test (TLT)

TLT were conducted with CT, CE-FA31, CE-FA446, CE31 and CE446. Duplicate CPB-samples were removed from the bottles after 31 or 446 days. Granular CT and CE 446 (disintegrated) were placed in paper filter bags with 0.45 μm pores inside nylon sample holders. Water was exchanged and analyzed after 0.25, 1, 2.25, 4, 9, 16, 36 and 64 days. Results were expressed in mg/m^2 .

Weathering cell test

CT, CE31 and CE-FA31 (crushed) and approximately 70 g of the resulting material was placed on a paper filter in a Büchner-type funnel. Duplicate samples were then subjected to weekly cycles involving one day of leaching, three days of ambient air exposure, another day of leaching and finally two days of air exposure. The test was conducted over a period of 32 cycles (217 days). During cycles 13 - 18, 1M HCl was added to simulate the degeneration of cementitious phases within the CPB-materials.

Table 1. Elemental composition and Paste-pH of Ore, CT, Fly ash and Cement

	Unit	Ore	CT	Fly ash	Cement
As	mg/kg TS	4703 ± 781	1070 ± 30	124 ± 5	10.2 ± 0.2
Cu	" "	82.0 ± 12.1	147 ± 7	136 ± 10	86.2 ± 2.9
Ni	" "	126 ± 12	63.8 ± 2.1	114 ± 9	63.8 ± 1.3
Zn	" "	10.6 ± 1.5	25.0 ± 0.42	374 ± 10	149 ± 3
Paste-pH	-	N.D	5.03 ± 0.25	13.2 ± 0.6	12.7 ± 0.3



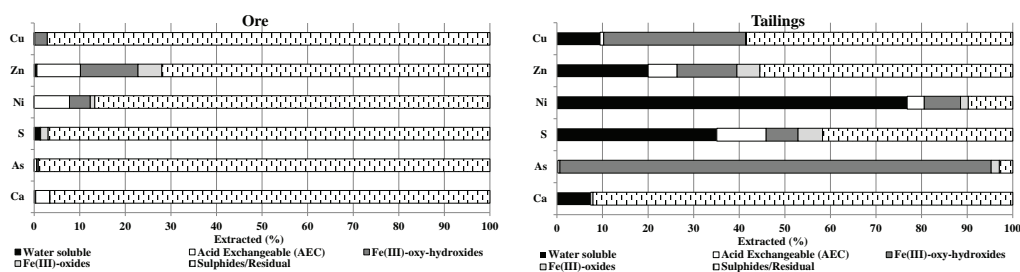


Fig. 1. Fractionation of Cu, Zn, Ni, S, As and Ca in CT and Ore.

pH-dependent leaching test

Duplicate samples from the outermost areas of CE-FA446 and CE446 were crushed into a pulverized material that was exposed to three HNO_3 concentrations. The pH ranged from 8 to ≈ 2.7 corresponding to the normal pH of CE446, CE-FA446 and CT, respectively.

Results and Discussion

A significant difference in fractionation is the higher proportion of water-soluble Cu, S, Ni and Zn in the CT compared to that in ore. Sulfides in the ore oxidized during the cyanidation process. Major proportions of sulfide-associated As and Cu was then re-sented as Arseniosiderite or in Cu- and As-bearing Fe-precipitates, mainly associated with amorphous Fe-precipitates in the water treatment process. These phases are stable at oxidizing environment at a pH of 4-8. Of Cu, Zn and Ni, Cu is most extensively removed from solution by adsorption onto ferrihydrite (Dzombak and Morell, 1990). In CT, this would explain why a larger proportion of Cu, compared to Zn and Ni, is associated with the Fe(III) oxy-hydroxide-fraction (Fig. 1). To ensure immobility of As, Cu, Ni and Zn in the further management of CT, maintaining neutral, oxidized conditions, is therefore of major importance.

Ferrihydrite in CT dissolved throughout the whole TLT, but Cu and As release was still low, even though pH decreased below 3.5 at the end of the TLT (Fig. 9). Diffusion in CT could have been hindered by the appearance of a Fe crust that are common in mine

waste dumps cementing the pores and reducing metal release. Instead, a release of Cu, Ni, and Zn in CT was mainly governed by water soluble phases while an As-release was less abundant and governed by As(III)-species. In CE31 and CE-FA31, high water saturation levels were maintained to reduce the sulfide oxidation rate. But the evolution of pH (10-8) and Si, suggested that a sulfide oxidation has occurred to some extent, dissolving the cementitious phases. During the curing period, water-soluble species of Cu and Ni precipitated as hydroxides, and/or adsorbed onto Fe precipitates and C-S-H surfaces that were stable throughout the TLT releasing very small amounts of Ni and Cu. A Zn release from CE31 and CE-FA31 was amphoteric while greatest when $\text{pH} > 8$ and < 10 and about ten-fold higher than the release of Ni and Cu (but still lower than from CT). A release of Zn can also originate from the binders themselves. According to Lou et al. (2011) the Zn release from a class C fly ash (as in CE-FA31) is due to the dissolution of calcium aluminosilicate glass more soluble under alkaline conditions than acidic. The release of As was up to 18 times higher from CE31 and CE-FA31 compared to CT and greatest as the pH decreased from 10 (11) to 8 (Fig. 2). Alkaline conditions in CT-CPB leachates caused desorption of As(V) from the As-bearing Fe precipitates, while adsorption of As(V) is largely ineffective at $\text{pH} \approx 10$. As(V) released could then re-adsorb onto C-S-H-surfaces or form Ca arsenates, which dissolves readily as the pH drops below 10 (Benzaazoua et al. 2004).



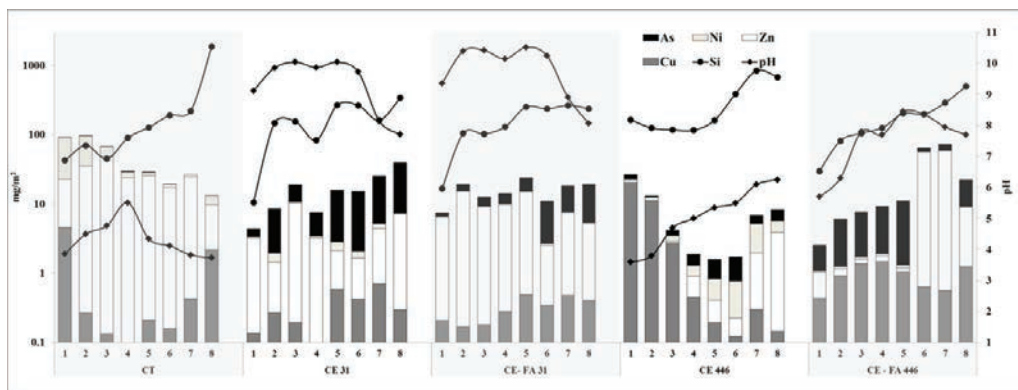


Fig. 2. Evolution of pH, Ferrihydrite, As, Cu, Ni, Si and Zn (in mg/m²) in CT, CE31, CE-FA31, CE446 and CE-FA446 during the TLT.

The establishment of unsaturated zones within the CT-CPB mixtures promoted sulfide oxidation and acidic conditions in the TLT leachates. During the formation of the CT-CPBs, the water-soluble fractions of Cu, Ni and Zn in the CT seemed to have been redistributed to less recalcitrant phases (AEC-fraction) (Fig. 3). The evolution of pH in the CT-CPB leachates during TLT suggested that a strength-loss has occurred, as the cementitious phases are highly soluble at pHs lower than 9. In CE446, a majority of the Cu release occurred as the Cu-bearing Fe precipitates dissolved and was greater than from CT, even though the water-soluble fraction of Cu was less for CE446 (Figs. 1, 3).

The Cu-fraction released under neutral conditions is higher compared to Zn and Ni (Fig. 4). As pH is lowered, this fraction can re-adsorb onto Fe-precipitates. These newly-formed Cu-Fe precipitates are, however, less stable in acidic conditions than those originally formed (Munk et al., 2002). This, in turn, probably resulted in a more abundant release of Cu from CE446 during the TLT than from CT. The amount of Zn released from CE-FA446 was twice that from CE-FA31, but more than a 10-fold higher compared to that in CE446 (Fig. 2). The evolution of pH and Zn could be explained with the variance of Zn species, and the water migration in the CT-CPB mixtures. However, less Zn was released from CE-FA31 compared to CE-FA446, despite the higher pH (in which Zn-bearing calcium aluminosilicate glass is more soluble) in the CE-FA31 leachates (Fig. 2). This might be

due to increased water transport through the unsaturated CE-FA446 mixture. Ni release was low, irrespective of the water saturation level in the CT-CPBs. As the water saturation levels decreased, As release from CE-FA mixtures increased while the opposite was true for CE mixtures. Cementitious As-phases still existed for CE-FA446, releasing more As, while in CE446, the As release seems to have been governed mostly by As(III) species that are less attached to oxide surfaces.

During the WCT, the Ni-release exhibited a typical water-soluble-behaviour while most abundant initially and thereafter steeply decreased and diminished towards the end (Fig. 5). Towards the end, the molar ratios of Fe/S in CT leachates increased to ≈ 0.8 , indicative of pyrrhotite oxidation occurring at a higher rate (Fig. 5). As pH was lowered to < 4 , As- and Cu-release increased due to the destabilization of ferrihydrite and a more extensive sulfide oxidation. At this stage, Zn release was not pH-related, Fe release or the dissolution of ferrihydrite (Fig. 5). Instead, Zn release probably originated from Zn impurities in pyrrhotite. WCT:s was carried out using crushed CT-CPB-mixtures in an oxidized environment. Therefore, cementitious phases dissolved at a higher rate in the WCT compared to that in TLT (Fig. 5), followed by a rapid decrease in pH (from pH 11 or 10 to pH 8). In the CT-CPB-mixtures, the Ni-, Cu- and Zn-release were substantially lowered compared to that in CT. The opposite was true for the As-release (2-4 times greater) (Fig. 5). In the TLT-leachates, pH was main-



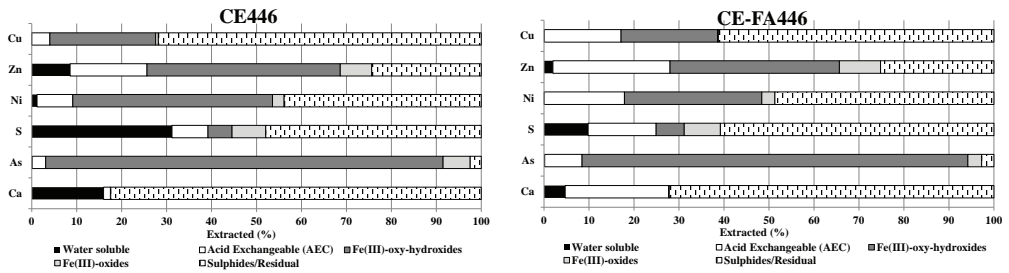


Fig. 3. Fractionation of Cu, Zn, Ni, S, As and Ca in CE446 and CE-FA446.

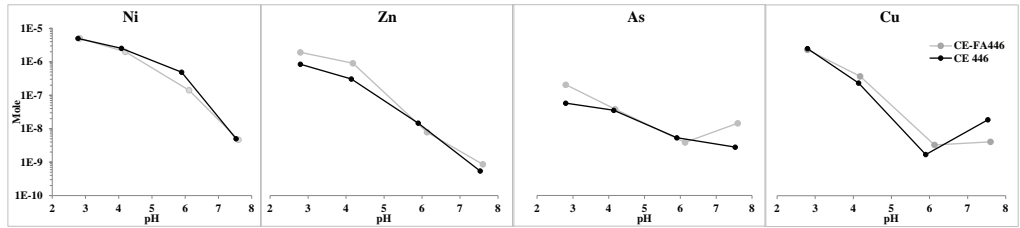


Fig. 4. Evolution of As, Cu, Ni and Zn in CE446 and CE-FA446, during the pH-dependent leaching test

tained at alkaline levels for a prolonged period compared to that in WCT due to a lower reactivity at water saturated conditions. This probably caused more As, Cu, Ni and Zn to desorb from Fe precipitates in the CT-CPB:s during the TLT compared to that in WCT. As acid was added to stimulate dissolution of the cementitious phases, the release of As, Ni, Cu and Zn increased in conjunction with Fe, and was more abundant from CE31 compared to CE-FA31 (Fig. 5). Large proportions of these

elements were associated with amorphous Fe precipitates (Fig. 3).

This might explain a greater, Fe-related release of As, Cu, Ni and Zn from CE31 compared to CE-FA31, while the pH was slightly lower in CE31 leachates (Fig. 5). In the CT-CPB mixtures, Cu release seemed less affected by accelerated weathering, compared to Ni and Zn. That is because Cu being readily adsorbed to Fe precipitates at a pH of 4, whereas Ni and Zn remains in solution (Dzombak and Morel 1990).

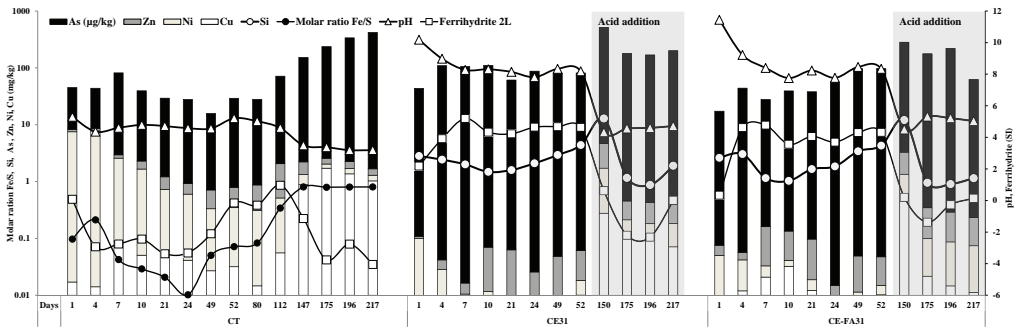


Fig. 5. Evolution of pH, Fe/S-molar ratio, Ferrihydrite, As, Cu, Ni, Si and Zn in CT, CE31 and CE-FA31 (acid addition on days 70-150) during the WCT.



Conclusions

In this study, CT used in the CPBs originates from a cyanide leaching process used to extract gold from inclusions in arsenopyrite and pyrrhotite. A significant proportion of sulfides oxidized during cyanidation, an addition of Fe-oxides seemed to have been insufficient to adsorb all the dissolved sulfide-related Cu, Zn and Ni. A significant proportion of Cu, Zn and Ni in the tailings were, therefore, water-soluble and could dissolve in mildly acidic conditions. A major proportion of As were associated with amorphous Fe-precipitates. Pyrrhotite and arsenopyrite still occurred in the tailings to a small extent, governing the acid generation and some of the As release. Managing the CT by a low strength CT-CPB-application decreased leaching of Ni and Zn. In water saturated conditions, the release of As was low from granular CT, in despite of acidic conditions, due to the formation of an enclosing Fe-oxide crust. In CT-CPB-mixtures, low amounts of Cu, Ni and Zn were released, due to desorption and dissolution of cementitious species. The dissolution of cementitious As-phases or Ca-arsenates caused the As-release to be a 10-18-fold higher in CT-CPB:s compared to that from CT. As the water saturation levels decreased within the CT-CPB mixtures, sulfide oxidation progressed more extensively and the release of Cu, Ni, and Zn increased from all of the CT-CPB mixtures. However, the Zn and Ni release was still lower compared to CT. In CE mixtures, Cu release increased and became greater compared to CT, due to a substantial proportion of acid-intolerant phases susceptible to remobilization in acidic conditions. Arsenic leaching increased compared to that from CT, regardless of binder proportion and water saturation level.

Acknowledgements

This work was supported by the Ramböll Sverige AB, Ramböll Foundation, SUSMIN – Tools for sustainable gold mining in EU, and the Center of Advanced Mining and Metallurgy (CAMM) at Luleå University of Technology.

References

- Belie ND, Verselder HJ, Blaere BD, Nieuwenburg DK, Verschoore R, (1996). Influence of the cement-type on the resistance of concrete to feed acids. *Cem Concr Res.*, 26 (1996), pp. 1717-1725.
- Benzaazoua M, Fall M, Belem T, (2004). A contribution to understanding the hardening process of cemented pastefill. *Miner Eng* 17 (2), 141–152. doi:10.1016/j.mineng.2003.10.022.
- Dold B, (2003). Speciation of the most soluble phases in a sequential extraction procedure adapted for geochemical studies of copper sulfide mine waste. *J Geochem Explor* 80 (1), 55–68.
- Dzombak DA, Morel FMM, (1990). *Surface Complexation Modelling: Hydrous Ferric Oxide*. John Wiley and Sons, Toronto, Canada.
- Li XD, Poon CS, Sun H, Lo IMC, Kirk, D, (2001). Heavy metal speciation and leaching behaviors in cement based solidified/stabilized waste materials. *J. Hazard Mater.* 82 (3), 215–230. doi:10.1016/S0304-3894(00)00360-5.
- Luo Y, Giammar DE, Huhmann BL, Catalano JG, (2011). Speciation of selenium, arsenic, and zinc in class C fly ash. *Energ Fuel.* 25(7), 2980-2987. 10.1021/ef2005496
- Munk L, Faure G, Pride DE, Bigham JM, (2002). Sorption of trace metals to an aluminum precipitate in a stream receiving acid rock-drainage, Snake River, Summit County, Colorado. *Appl Geochem* 17, 421–430.
- Ouellet S, Bussière B, Mbonimpa M, Benzaazoua M, Aubertin M, (2006). Reactivity and mineralogical evolution of an underground mine sulphidic cemented paste backfill. *Miner Eng.* 19(5), 407–419. doi:10.1016/j.mineng.2005.10.006.





Permeable Reactive Barrier Feasibility Assessment at Goldcorp's Red Lake Gold Mines: Validation of Seepage Flow Paths through Tracer Testwork[©]

Jordi Helsen¹, Alan Martin¹, Trevor Crozier², Genevieve Parent², Vanessa Mann², Carl Mendoza², Christopher Gaspar³, James Russell³

¹*Lorax Environmental Services Ltd., 2289 Burrard St., Vancouver, BC, Canada, V6J 3H9,
jordi.helsen@lorax.ca*

²*BGC Engineering Inc., Suite 500, 980 Howe St., Vancouver, BC, Canada V6Z 0C8*

³*Goldcorp Red Lake Gold Mines, 15 Mine Road, Bag 2000, Balmertown, Ontario, Canada, P0V 1C0*

Abstract

A critical design element in support of a permeable reactive barrier (PRB) feasibility assessment was to maximize the likelihood that the PRB location will intercept seepage pathways that connect a tailings management area (TMA) to downstream surface water receptors. A tracer test was conducted to better define the hydraulic connection between the TMA and downstream receptors through the injection of fluorescent dye tracers into groundwater wells screened in the sand and gravel aquifer, which is interpreted to be the principal conduit for TMA-related seepage. Results confirmed a hydraulic connection between the proposed PRB location and downstream receptors.

Keywords: hydraulic connection, uranine, rhodamine, PTSA, fluorometer

Introduction

The Campbell Complex (Goldcorp's Red Lake Gold Mines) is located in Balmertown, 7 km northeast of the Town of Red Lake in northwestern Ontario, and has been the site of gold-ore mining and milling operations since 1949. Tailings have been discharged to the current tailings management area (TMA) since 1983. A portion of the water that accumulates in the TMA infiltrates into the sub-surface and travels along groundwater flow paths (designated as "Red Lake Flow Path") that discharge to ditches draining a Golf Course (GC), which in turn feed a downstream wetland and lake. Groundwater along this flow path carries mine-related parameters associated with mill process waters (SO_4 , Cl, NH_3 , CN, Cd, Co, Cu, Ni and Zn) and remobilization from tailings solids (Fe and As).

Goldcorp is assessing the feasibility of using PRBs (Blowes et al., 2000) to intercept and treat TMA-derived seepage to mitigate groundwater degradation and minimize the potential for adverse effects to downstream aquatic receptors. This paper, which describes

the results of tracer testwork designed to confirm contaminant pathways, represents the second of a series of three papers relating to PRB feasibility at the Campbell Complex. The other two papers, also presented as part of these proceedings, describe TMA plume distribution and contaminant behaviour (Martin et al., 2018) as well as hydrogeological, geochemical and geotechnical considerations driving PRB design (Crozier et al., 2018).

A key objective of the Phase I PRB (PRB; Crozier et al., 2018) placement is to intercept the seepage pathway that connects the TMA to downstream surface water receptors. To investigate the hydraulic connection between the proposed PRB location and the downstream GC ditch system, tracer testwork was conducted. This involved the injection of fluorescent dyes in key monitoring wells situated within the core of the groundwater plume to be intercepted by the PRB, and monitoring within the downstream ditch network. An improved understanding of the TMA-seepage pathway has relevance to PRB siting, design and performance evaluation.



Methods

Tracer testwork included laboratory and field components: 1) fluorometer configuration and calibration; 2) establishment of fluorometer measurement responses and potential cross-fluorescence effects; 3) tracer injection; and 4) tracer monitoring. Tracer test methods were coordinated by Lorax Environmental, while all on-site lab and field work was conducted by Red Lake Gold Mines.

Fluorescent Dye Tracers

Three fluorescent dye tracers were used in the tracer testwork: 1) Rhodamine WT (rhodamine); 2) Uranine K Liquid (uranine); and 3) 1,3,6,8-Pyrenetetrasulfonic Acid Tetrasodium Salt (PTSA). Tracer selection was based on tracer properties (e.g. availability, affordability and low detection limits), in addition to the sensitivity and availability of fluorometer sensors.

Fluorometer Configuration and Calibration

Fluorescence measurements were collected using a submersible fluorometer (Turner Designs C3) equipped with three optical sensors (rhodamine, uranine, PTSA), rechargeable battery pack and mechanical wiper. All three fluorometer sensors were calibrated prior to field deployment and initiation of the tracer test (i.e. tracer injection).

Fluorometer sensors were calibrated in direct concentration mode with temperature compensation for rhodamine (temperature compensation was not available for uranine or PTSA). A series of tracer standard solutions was prepared by diluting the fluorescent dyes (21.7% rhodamine, 39.5% uranine, and 10% PTSA) with site water collected at GC DITCH (Figure 1). These standard solutions were used to calibrate all three fluorometer sensors and to establish sensor responses

throughout their linear measurement range. Tracer standard solution concentrations ranged from approximately 0.05 to 520 ppb (Table 1). The fluorometer was calibrated by conducting a 1-point calibration of each sensor using tracer standards of approximately 50 ppb (53.9 ppb rhodamine, 49.1 ppb uranine, 49.7 ppb PTSA). Once calibrated, the linear response range was established for all three tracers to determine how fluorometer response may be affected by site water chemistry (i.e. GC DITCH water).

Rhodamine, uranine and PTSA all have unique fluorescing wave lengths that are not expected to interfere with each other under laboratory conditions (when measured with the submersible fluorometer). However, since all three tracers were injected into the same aquifer, lab-based experiments were conducted to assess the potential for cross-fluorescence effects in site waters, over a range of concentrations. Cross-fluorescence testing was conducted by measuring fluorescence of two site water samples containing all three tracers at concentrations of approximately 0.5 ppb and 430 to 470 ppb.

Tracer Injection

Rhodamine, uranine and PTSA were injected into the sand and gravel aquifer (the interpreted principal conduit for seepage of TMA-affected waters) in late August 2016. Tracer injection was conducted at four existing monitoring wells, located up gradient (MW06-1), down gradient (MW15-01B), and within the footprint (MW16-03B, MW16 04B) of the proposed PRB (Figure 1). A single tracer was injected into each well, with uranine injected into two wells (Table 2). A cross-section showing hydrostratigraphy and well locations along the Red Lake Flow Path is provided in Martin et al. (2018), the first of three papers relating to PRB feasibility at the Campbell Complex.

Table 1. Tracer Standard Solutions.

Tracer Dye	Undiluted Concentration (Weight %)	Standard Solution Concentrations (ppb)
Rhodamine	21.7	0.054, 0.54, 5.4, 53.9, 516.2
Uranine	39.5	0.049, 0.49, 4.9, 49.1, 470.2
PTSA	10	0.50, 5.0, 49.7, 476.1



Tracer dyes were injected with a portable peristaltic pump (Masterflex E/S) equipped with dedicated silicone pump-head tubing (3/8" × 1/4") connected to HDPE tubing (1/4" × 0.17") in each well. Undiluted tracer dye was injected into each well by pumping uniformly across the entire screened interval in a single motion, commencing at the bottom and ending at the top of the well screen. Injection volumes were based on tracer dye concentrations, 2-dimensional (2-D) transport calculations, and the detection limits and linear response ranges of the fluorometer sensors. Injection rates ranged from 0.4 to 1.0 L/min.

Hydraulic conductivity measurements at the four injection wells range over slightly more than one order of magnitude (Table 2). Hydraulic conductivity is highest at rhodamine injection well MW06-1 and lowest at PTSA injection well MW15-01B.

Predicted arrival times for the three tracers in the GC ditch network were estimated to range between 87 and 1400 days after injection, based on 2-D transport calculations (results not shown). The predicted arrival times for peak rhodamine, uranine and PTSA concentrations in the GC ditch were 87 days (≈2.9 months), 94 and 120 days (≈3.1 and 3.9 months), and 1400 days (≈3.8 years), respectively, assuming a transport distance of 220 m between the injection wells and monitoring point in GC ditch.

Tracer Monitoring

Tracer monitoring was conducted with the fluorometer through a combination of automated, hourly in-situ measurements, and periodic, manual ex-situ measurements (ranging in frequency from three times a week to bi-monthly). Automated monitoring was conducted at GC DITCH (approximately

Table 2. Tracer Injection Summary.

Well	Screen Length (m)	Hydraulic Conductivity (m/s)	Injection Date	Tracer	Concentration (Weight %)	Volume (L)
MW15-01B	0.92	9.4×10^{-5}	24-Aug-16	PTSA	10	6.1
MW06-1	2.90	1.1×10^{-3}	25-Aug-16	Rhodamine	21.7	6.0
MW16-03B	0.46	8×10^{-4}	25-Aug-16	Uranine	39.5	1.5
MW16-04B	0.46	1×10^{-3}	29-Aug-16	Uranine	39.5	1.2

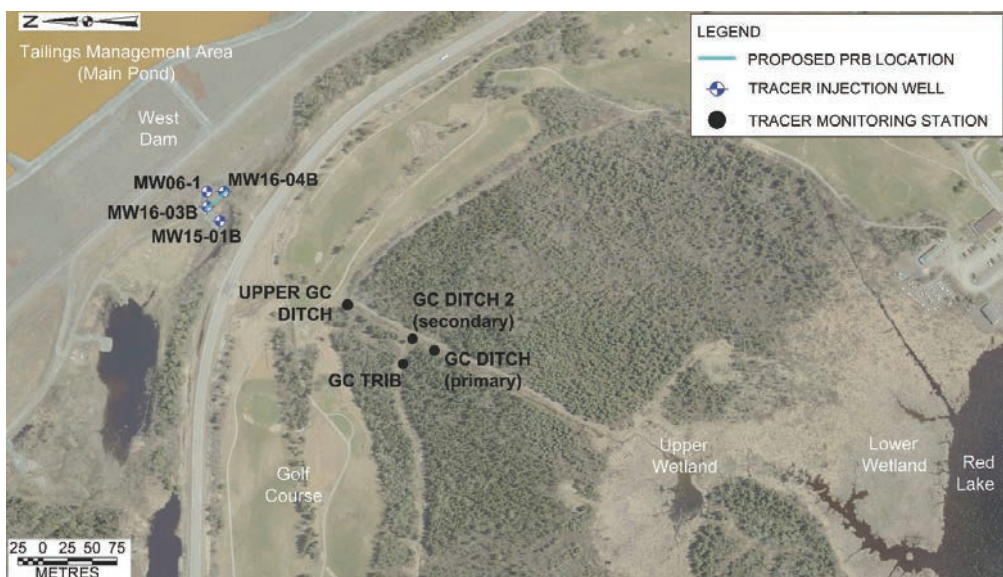


Figure 1 Tracer Test Study Area.



10 m downstream of the junction with the tributary ditch; (Figure 1)) between August 22 and November 11, 2016, at which time the fluorometer was removed from GC DITCH due to freezing temperatures and ice formation. Manual monitoring was conducted thereafter until the end of testing on March 17, 2017. Manual monitoring consisted of the collection of water samples from GC DITCH, GC TRIB and UPPER GC DITCH (Figure 1), and subsequent tracer measurements in the laboratory. Tracer measurements in the lab were collected on a time interval of every second for several minutes. Most manual monitoring at GC DITCH was completed at the primary station (GC DITCH), except for two measurements that were collected at the secondary station GC DITCH 2 on December 12 and 14, 2016 due to snow and ice which prevented sampling at the primary station (Figure 1).

Turbidity was measured in surface water samples collected from UPPER GC DITCH, GC TRIB, GC DITCH and GC DITCH 2 during fluorometer calibration and tracer monitoring, because high turbidity has the potential to interfere with tracer measurements. Turbidity measurements were collected using a portable turbidimeter (Hach 2100Q).

Results and Discussion

Fluorometer Response and Cross-Fluorescence Measurements

The fluorometer showed linear responses to tracer concentrations in the following ranges: 5 to 520 ppb for rhodamine, 0.05 to 470 ppb for uranine, and 0.5 to 480 ppb for PTSA. Cross-fluorescence was greater at low concentrations. Relative percent difference (RPDs) values between measured and reference standard solutions ranged from 136 to 200% for the low-concentration mixed-tracer solution (0.5 ppb). In contrast, RPD values ranged between 25 and 34% for the high-concentration mixed-tracer solution (430 to 470 ppb).

Rhodamine was not detected in the low-concentration mixed-tracer solution (0.5 ppb), consistent with the rhodamine response measurements. Uranine and PTSA showed strong interference signatures at low concentrations. This is consistent with low uranine

levels being detected (0 to 2.8 ppb) while establishing rhodamine and PTSA response measurements, as well as low PTSA levels being detected (0 to 5.5 ppb) while establishing uranine and rhodamine sensor responses.

Based on fluorometer response testing, the lower limits of reliable measurement for the three tracers were estimated to be 5 ppb for rhodamine, 3 ppb for uranine, and 6 ppb for PTSA. Cross-fluorescence effects were expected to result in overestimated uranine and PTSA readings at low concentrations (≈ 0.5 ppb).

Tracer Monitoring Results

Automated and manual monitoring results for the GC ditch system for rhodamine and uranine are presented in Figure 2; PTSA results are not shown since it was only detected on three occasions at levels below the limit of reliable measurement. Daily precipitation measured at the Environment Canada Red Lake meteorological station is also shown for reference.

Rhodamine was first detected during manual monitoring at GC DITCH and GC TRIB in early December 2016. However, initial rhodamine levels were low at GC DITCH (0.5 to 0.7 ppb) and GC TRIB (0.5 to 0.7 ppb). Rhodamine levels subsequently decreased rapidly to below detection by mid December 2016 (Figure 2).

Uranine levels at GC DITCH fluctuated within background levels (0 to 3 ppb) during automated monitoring and increased in December 2016 (during manual monitoring), peaking at 6.0 ppb in GC DITCH (December 20) and 6.9 ppb in UPPER GC DITCH (December 29). Uranine levels decreased slowly thereafter, throughout January and February, before levelling off in March 2017 (Figure 2).

Uranine was detected at GC TRIB during manual monitoring; however, in contrast to the temporal trends observed at UPPER GC DITCH and GC DITCH (i.e. rise and fall of concentrations), uranine levels largely remained within previously detected levels during automated monitoring at GC DITCH and below the limit of reliable measurement.

Turbidity levels in UPPER GC DITCH, GC DITCH, GC DITCH 2 and GC TRIB water samples were generally below 20 nephelometric turbidity units (NTU). Turbidity lev-



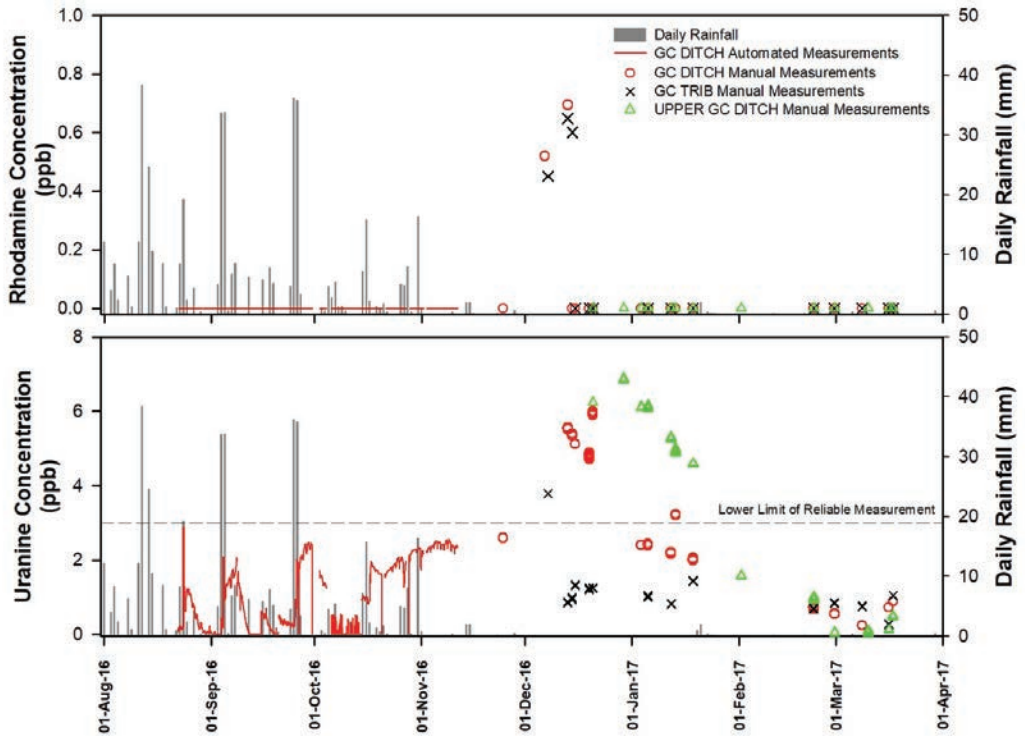


Figure 2 Rhodamine (top) and uranine (bottom) concentrations in the GC Ditch system.

els occasionally spiked up to 140 NTU due to difficulties with sampling through snow and ice and/or low flows. The magnitude of turbidity is not predicted to have had a significant bearing on tracer measurements.

Overall, uranine tracer signatures measured in UPPER GC DITCH and GC DITCH provide evidence of a groundwater connection between the proposed PRB location and GC ditch. This conclusion is based on: 1) uranine concentrations that were at least twice the lower limit of reliable detection; 2) peak concentrations more than twice background levels; and 3) temporal trends characterized by a rise and fall of uranine concentrations typical of dispersion resulting from transport of an instantaneous slug injection through a groundwater flow system. Cross-fluorescence effects are not believed to be significant in the observed uranine concentration ranges. Uranine detected at GC TRIB was characterized by relatively stable concentrations that fluctuated within the range of background levels and remained below the limit of reliable measurement. These observations suggest that the groundwater flow path at the proposed PRB

location is not strongly connected to the GC tributary ditch or that uranine concentrations had decreased to the extent that they were not measurable above background.

Uranine concentrations measured at GC DITCH peaked on December 20, 2016, approximately 3.7 months after tracer injection at MW16-04B and 3.8 months after injection at MW16-03B. These observed arrival times are close to the predicted arrival times of approximately 3.1 and 3.9 months for injections at MW16-04B and MW16 03B, respectively, lending further confidence to the detection of a tracer signature in the ditch network.

Although rhodamine was detected at GC DITCH and GC TRIB, its tracer signature did not yield conclusive evidence. This relates to detected concentrations that were low and close to lower limits of detection. As such, it is not possible to discern whether rhodamine concentrations measured at GC DITCH and GC TRIB were representative of an actual tracer signature or noise. It should be noted, however, that the period of possible rhodamine detection coincided with the predicted arrival time, lending some confidence to the



possibility of a positive signature in the ditch system, particularly in light of the arrival of uranine.

PTSA was not detected in the GC ditch system. However, this result does not disprove a connection of the groundwater flow path between injection well MW15-01B and the downstream GC ditch system. Specifically, the lower hydraulic conductivity at MW15 01B ($K = 9.4 \times 10^{-5}$ m/s) would result in significantly longer travel times for PTSA in comparison with the other injection wells. Transport calculations used in the design of the tracer test suggest that tracer monitoring was suspended well before the predicted arrival time of peak PTSA concentrations in the GC ditch system (≈ 3.8 years).

Conclusions

The salient conclusions of the tracer study can be summarized as follows:

- Tracer calibration and response results for site waters suggest that the use of rhodamine, uranine and PTSA can provide accurate and reproducible results over a wide range of tracer concentrations.
- Uranine tracer signatures measured at UPPER GC DITCH and GC DITCH provided confirmatory evidence of a hydraulic connection between the proposed PRB location and the GC ditch. These data suggest that PRB installation at the proposed location will have a direct influence on water chemistry in the ditch/wetland system.
- The arrival of uranine at UPPER GC DITCH and GC DITCH agreed well with predicted arrival times, illustrating that the understanding of the physical hydrogeology of the site is fairly robust.
- Uranine detected at GC TRIB was characterized by relatively stable concentrations that fluctuated within the range of background levels and remained below the lower limit of reliable measurement. This is indicative of a weak or non-existent connection between the proposed PRB and the GC tributary ditch;

- Rhodamine was detected in GC DITCH and GC TRIB; however, due to the low magnitude of tracer measurements, no definitive conclusions could be drawn.
- The absence of detectable PTSA concentrations in the GC ditch system does not discount the conclusion of a hydraulic connection between the injection well (MW15-01B) and the downstream GC ditch system. Specifically, the lack of a PTSA signature can be linked to the lower hydraulic conductivity at MW15-01B, which would result in significantly longer travel times for the tracer.

Acknowledgements

Goldcorp Canada is acknowledged for allowing presentation of the data and discussion herein. The authors thank two anonymous reviewers whose input greatly improved the quality of the manuscript. Thanks is also given to Chris Bourque for testing/configuring the fluorometer, Tyler Provencal for carrying out manual tracer monitoring, and Greg Morris for figure preparation.

References

- Blowes DW, Ptacek C, Benner SG, McRae CWT., Bennett TA, Puls RW (2000) Treatment of inorganic contaminants using permeable reactive barriers. *J Contam Hydrol* 45: 123-137.
- Crozier TW, Paszkowski D, Parent G, Cook D, Mann V, Mendoza C, Provost H, Martin AJ, Helsen J, Bain J, Blowes DW, Gaspar C, Russell J (2018) Permeable Reactive Barrier Feasibility Assessment at Goldcorp's Red Lake Gold Mines: Hydrogeological, Geochemical and Geotechnical Design Considerations, 11th International Conference on Acid Rock Drainage, Pretoria, South Africa, September 10-14, 2018.
- Martin AJ, Helsen J, Crozier T, Parent G, Paszkowski D, Mendoza C, Provost H, Gaspar C, Russell J (2018) Permeable Reactive Barrier Feasibility Assessment at Goldcorp's Red Lake Gold Mines: Delineation of Groundwater Flow Paths and Contaminant Behaviour, 11th International Conference on Acid Rock Drainage, Pretoria, South Africa, September 10-14, 2018.





Column Tests and Multilevel Well Geochemistry to Explain Contaminant Plume Persistence Issues Downgradient of a Former Uranium Mill Site

Raymond H. Johnson¹, Aaron Tigar¹, Sarah Morris¹, Sam Campbell¹, Kara Tafoya²,
Richard Bush³, William Frazier³

¹Navarro Research and Engineering, Inc., Contractor to the U.S. Department of Energy Office of
Legacy Management, Grand Junction, Colorado, USA 81503, ray.johnson@lm.doe.gov

²LMATA Government Services LLC, Subcontractor to Navarro Research and Engineering, Inc., Grand
Junction, Colorado, USA 81503

³U.S. Department of Energy Office of Legacy Management, Grand Junction, Colorado, USA 81503

Abstract

At a former uranium mill site in Riverton, Wyoming, USA, legacy mill tailings were moved to a nearby disposal cell. However, groundwater below and downgradient of the former tailings impoundment had already been contaminated. The compliance strategy is 100-year natural flushing, but the downgradient movement of plume contaminants has stalled near the groundwater discharge point. To better understand why this is occurring, core samples of alluvium were collected for analyses of solid-phase uranium concentrations and laboratory column testing. Multilevel wells were completed in the same core holes and monitored for almost 2.5 years. The resulting data indicate that a silt layer provides a storage mechanism for uranium, sulfate, and chloride. Uranium is more concentrated in the silt layer over the uranium plume. This stored uranium can later be released during flooding or high recharge events and creates a persistent uranium plume.

Keywords: uranium, Riverton, plume persistence, secondary contaminants

Introduction

Milling activities at a former uranium mill site near Riverton, Wyoming, USA, processed uranium ore from 1958 to 1963. Uranium mill tailings were removed and surface reclamation was completed by the U.S. Department of Energy (DOE) in 1989. However, shallow groundwater beneath and downgradient of the site is still contaminated with greater than 2 mg/L uranium. Detailed groundwater sampling was completed in 2012 (DOE 2013) using direct-push, temporary, piezometer sampling to create a detailed map of the uranium plume (fig. 1). Other contaminants are relatively coincident with the uranium plume, with some offsets for different contaminants (DOE 2016).

Groundwater modeling predicted that natural flushing of the groundwater aquifer to a nearby river would achieve compliance

with applicable groundwater protection standards by the year 2097 (DOE 1998). Initial data from 1989 to 2009 indicated that overall, contaminant concentrations below the former mill site and downgradient of it were declining steadily. However, local flooding in 2010 mobilized stored contaminants in the downgradient floodplain and resulted in an increase in groundwater contaminant concentrations, including uranium (fig. 2). Thus, we define plume persistence as contaminant concentrations that remain at concentrations higher than originally predicted due to previously unrecognized contaminant sources. These stored contaminants or persistent secondary contaminant sources were not considered in the original conceptual site model and groundwater modeling predictions with natural flushing (Dam et al. 2015).



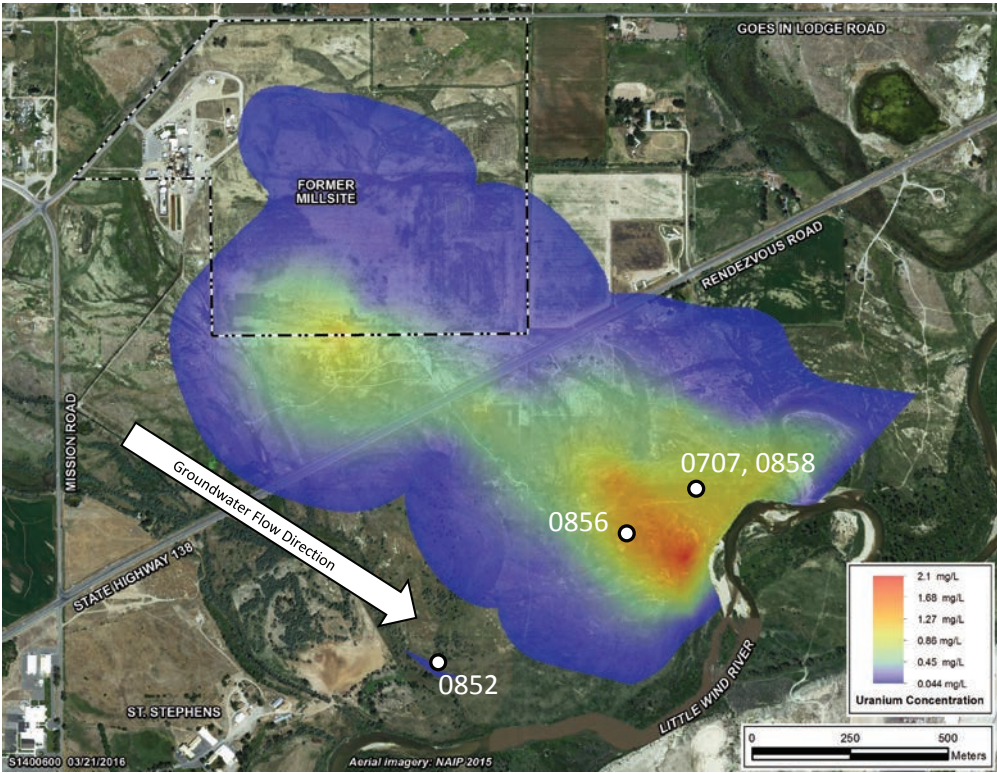


Figure 1 Uranium plume at the Riverton site in 2012 with key sample locations (red is higher concentration).

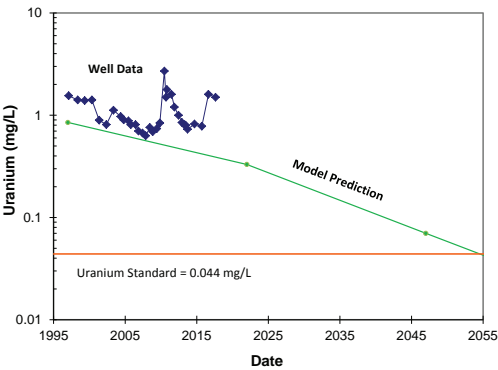


Figure 2 Model predictions (DOE 1998) compared to measured uranium concentrations for well 0707 (see location in fig. 1).

The zone with higher uranium concentrations near the Little Wind River (fig. 1) was a focus area for solid-phase sampling in 2015 (DOE 2016) to determine the concentrations and locations of secondary contaminant sources. This work identified two main materials with higher uranium concentrations,

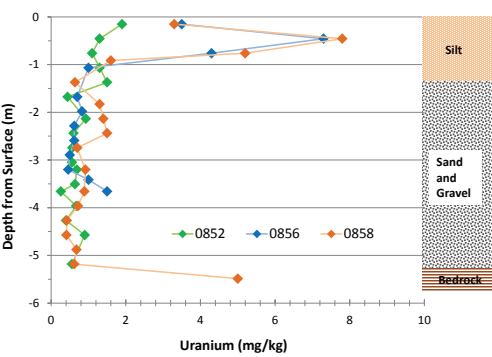


Figure 3 Solid-phase uranium data for locations 0852, 0856, and 0858 with generalized stratigraphy (see fig. 1 for locations).

which are a silt layer from approximately 0 to 1.5 m below ground surface and an organic-rich zone at approximately 1.5 to 2.5 m below the ground surface (DOE 2016; Johnson et al. 2016). The general stratigraphy with solid-phase uranium concentrations within (0856 and 0858) and outside (0852) of the contami-



nant plume is shown in Figure 3. In general, the uppermost stratigraphic layer is 1.5 m of silt that remains unsaturated most of the year but can become saturated during spring runoff due to flooding or higher water-table conditions. The silt is underlain by about 4 m of sand and gravel, and the organic-rich zones are discontinuous silty layers (old river bank sediments) within the sand and gravel. The Wind River Formation is below the sand and gravel aquifer at about 5.5 m below ground surface and forms a semi-confining layer. While the organic-rich zone is an additional control on contaminant transport, this paper focuses on the release of contaminants from the silt zone. Column tests were performed on material from the silt layer and the underlying sand and gravel. These column results are compared to multilevel groundwater samples collected over almost 2.5 years at the same locations that the sediment for the column tests was collected.

Methods

Column tests were completed in 5.1 cm × 45.7 cm Plexiglas tubing packed with air-dried, <2 mm size sediment in 5.1 cm lifts, with tamping between lifts, until the column was filled with ≈22.9 cm of solid material. The solids were topped with a fabric filter and then with ≈6.4 cm of 5 mm clean glass beads to prevent material movement during column filling. A tube was placed at the top filter (top of the column) and attached to a 60 mL syringe to obtain the effluent pore fluid for analyses. The influent water was added to the column at the rate of ≈3 mL/min from the bottom. Each column was allowed to equilibrate for 24 ± 2 hours before another pore volume of influent was put through the column, and the effluent water was collected for analyses each day. The influent water for the columns was deionized water with 0.001 M HCl (provides 31 mg/L of chloride), unless otherwise noted. The small amount of acid was added to represent the slightly acidic conditions produced by soil gas carbon dioxide in the subsurface. Sample analyses were completed using ion chromatography (IC) and inductively coupled plasma mass spectrometry (ICP-MS) techniques.

Sediment core was collected using a sonic

drilling rig with well installations completed in the same core hole. Multilevel well installations were completed using continuous multichannel tubing (CMT) that was cut in the field based on the geology to provide three sampling ports with depth. The CMT was attached to a traditional plastic well riser pipe with a bottom screen (0.3 m) to provide a fourth groundwater sampling interval. Water sampling was done using a peristaltic pump, and water analyses were completed using IC and ICP-MS techniques.

Column Test Results

Column test results are shown below for location 0852 silt (fig. 4), which is a location outside of the uranium plume and for location 0858 silt (fig. 5), which is within the uranium plume (fig. 1). Data from 0852 show that the release of uranium, sulfate, and chloride from the silt can occur in areas outside of the uranium plume and that uranium can be released above the maximum concentration limit of 44 µg/L. Likewise, the location 0858 silt layer also releases uranium, sulfate, and chloride, but with much higher uranium concentrations. The solid-phase data from the silt over the plume (fig. 3) indicate higher uranium concentrations, which are subsequently released in column flushing. In both columns, chloride flushes within the first pore volume whereas uranium and sulfate are released more slowly. In the 0858 silt column (fig. 5), 12 pore volumes are required to reach the uranium standard of 44 µg/L and 6 pore volumes are required to reach the sulfate secondary standard of 250 mg/L.

A column test of the sand and gravel aquifer material with background groundwater as the influent was also completed (fig. 6). These data show limited retention of uranium on the main aquifer material, similar to the flushing of sulfate and chloride (fig. 6). Both uranium and sulfate are flushed to below standards in less than 3 pore volumes after accounting for constituent release as a difference from the influent concentration.



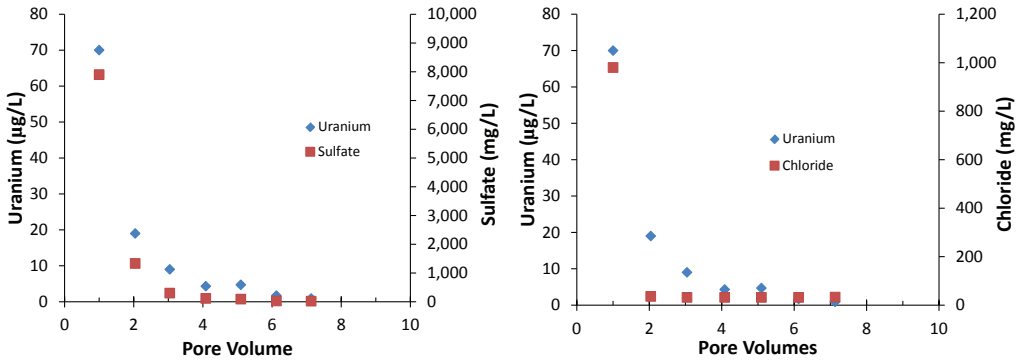


Figure 4 Column test: Effluent data from silt material at location 0852 collected 0.3–0.76 m below ground

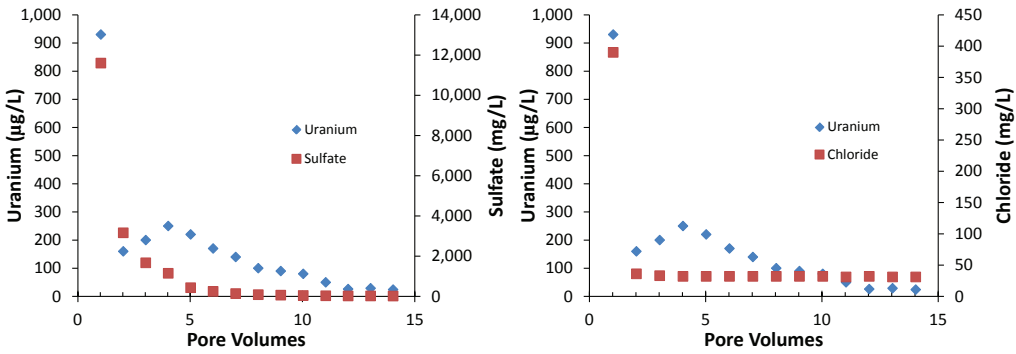


Figure 5 Column test: Effluent data from silt material at location 0858 collected 0–0.76 m below ground surface.

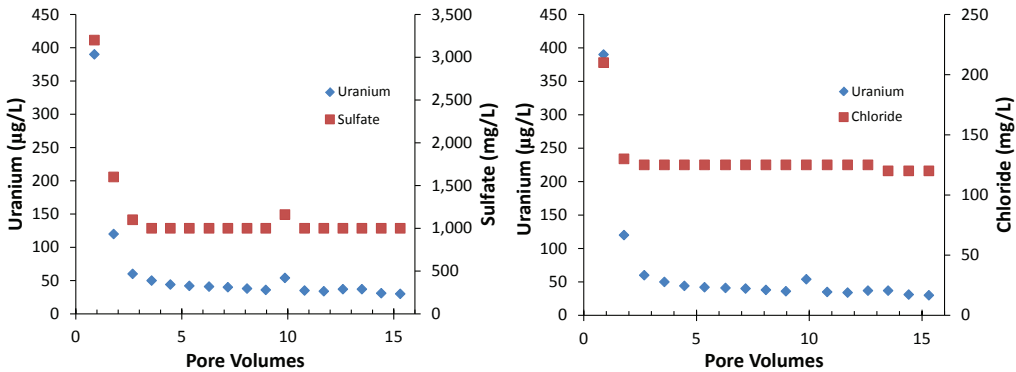


Figure 6 Column test: Effluent data from sand and gravel material at location 0858 (note that influent solution was background groundwater that had 28 µg/L uranium, 1,000 mg/L sulfate, and 125 mg/L chloride).

The column for the location 0858 silt has an additional geochemical control on the release of uranium based on the concentration curve reaching a secondary peak at 4 pore volumes. On the basis of a preliminary data

evaluation, this appears to be due to changes in calcite solubility, which then influences uranium mobility. Geochemical modeling and detailed interpretations of the column data are still ongoing.



Multilevel Groundwater Sampling Results

Multilevel groundwater sampling has been ongoing at locations 0852 and 0858 for almost 2.5 years. Both locations show significant spikes in uranium concentrations in May of 2016 (figs. 7 and 8), especially at the shallower sampling ports. The solid line in Figures 7 and 8 indicates a large flooding event on May 8, 2016, due to heavy rainfall locally and upstream. Similarly, a dashed line in Figures 7 and 8 indicates another large rain event on March 31, 2017, which caused minor flooding. Additional flooding occurred from June 9 through 19, 2017 during runoff from mountain snow melt. Sulfate and chloride trends (not presented) are similar to the uranium results. The post-flooding (May 2016) sulfate concentration increases at 0852-1 and 0858-1 relative to 0852-4 and 0858-4 are similar at 5,200 and 5,400 mg/L, respectively, and chloride increases are 660 and 280

mg/L, respectively. The same comparisons for uranium increases are 120 and 2,520 $\mu\text{g/L}$, respectively (figs. 7 and 8). The April 2017 concentrations changes were more subtle. In May 2016, post-flood constituent increases start at the top of the aquifer, until mixing throughout the aquifer occurs with time (figs. 7 and 8). Over time, these increased concentrations decline as less contaminated groundwater from upgradient flushes through the sand and gravel aquifer.

Conclusions

Solid-phase data (fig. 3) indicate retention of uranium in the silt material over the uranium plume (fig. 1) that can contribute uranium to the underlying sand and gravel aquifer (figs. 7 and 8). Column tests provide uranium release concentrations (figs. 4 and 5) that are similar to those seen in the field (figs. 7 and 8). Column flushing of the silt took 12 pore volumes to get uranium concentrations below standards. A location outside the contaminant

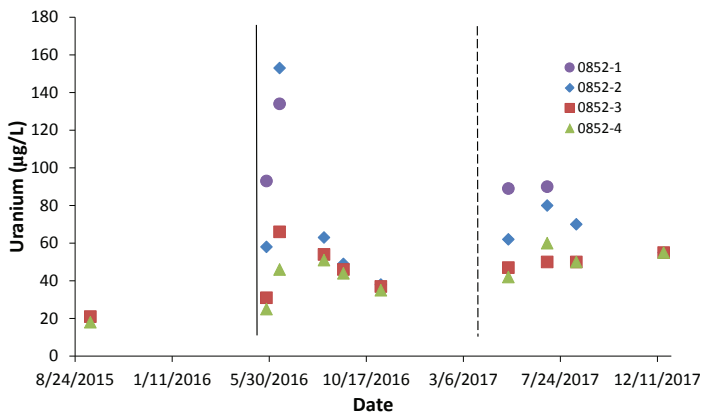


Figure 7 Multilevel groundwater data at location 0852 (outside of the plume). Solid line indicates flooding on May 8, 2015, and dashed line indicates flooding on March 31, 2017. Sample depths for levels 0858-1, -2, -3, and -4 are 1.6, 3.0, 3.7, and 4.4 m, respectively.

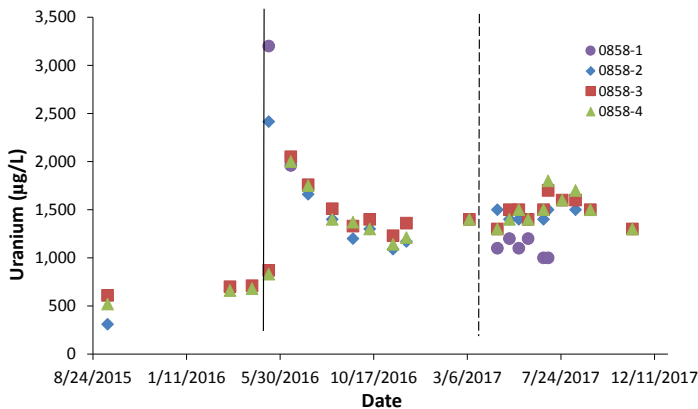


Figure 8 Multilevel groundwater data at location 0858 (within the plume). Solid line indicates flooding on May 8, 2015, and dashed line indicates flooding on March 31, 2017. Sample depths for levels 0858-1, -2, -3, and -4 are 1.1, 2.4, 3.9, and 5.3 m, respectively.



plume (0852) indicates that the release of uranium, sulfate, and chloride after flooding or high recharge events is a naturally occurring process. The sulfate and chloride release concentrations at the location outside of the contaminant (0852) are similar or even greater than from the location within the uranium plume. However, the data within the uranium plume (0858) indicate that the uranium release here is much greater than the uranium release at the location outside of the plume (0852). These results indicate that the silt layer provides a storage mechanism for uranium that creates a plume persistence issue. This storage and release keeps the uranium plume from declining near the Little Wind River and delays natural flushing beyond initial expectations.

The original conceptual model of natural flushing in the sand and gravel aquifer is still valid when looking at contaminant transport within the sand and gravel only. However, the continued inputs of uranium and other contaminants from the silt layer were not considered in the original conceptual model (Dam et al. 2015). As a result, the silt material coupled with flooding or high recharge events creates uranium concentration spikes after these events (figs. 2, 7, and 8). This leads to a new conceptual model that helps explain the plume persistence issues at the site.

Acknowledgements

Funding for this work was provided by the U.S. Department of Energy Office of Legacy Management. The authors thank St. Ste-

phen's Mission in Riverton, Wyoming, and the Northern Arapaho and Eastern Shoshone Tribes for continued access to the site for field activities and sampling. We also thank the U.S. Geological Survey office in Riverton, Wyoming, for providing local personnel to assist with groundwater sampling.

References

- Dam WL, Campbell S, Johnson RH, Looney BB, Denham ME, Eddy-Dilek, CA, Babits SJ (2015) Refining the site conceptual model at a former uranium mill site in Riverton, Wyoming, USA, *Environ Earth Sci*, DOI 10.1007/s12665-015-4706-y, 74(10), 7255–7265
- DOE (1998) Final Site Observational Work Plan for the UMTRA Project Site at Riverton, Wyoming, Report No. U0013801. U.S. Department of Energy, Albuquerque, New Mexico, USA
- DOE (2013) 2012 Enhanced Characterization and Monitoring Report, Riverton, Wyoming, Report No. LMS/RVT/S09799. U.S. Department of Energy, Grand Junction, Colorado, USA
- DOE (2016) 2015 Advanced Site Investigation and Monitoring Report, Riverton, Wyoming, Processing Site, Report No. LMS/RVT/S14148. U.S. Department of Energy, Grand Junction, Colorado, USA
- Johnson RH, Dam WL, Campbell S, Noël V, Bone SE, Bargar, JR, Dayvault J (2016) Persistent Secondary Contaminant Sources at a Former Uranium Mill Site, Riverton, Wyoming, USA. In: Drebenstedt C & Paul M: IMWA 2016 Mining Meets Water Conflicts and Solutions, Freiberg/Germany (TU Bergakademie Freiberg) 398–404



Mine Water Tracer Substances for Biogeochemical Processes in Flooded Uranium Mines

Andrea Kassahun¹, Nils Hoth², Michael Paul¹

¹WISMUT GmbH, Jagdschänkenstraße 29, 09117 Chemnitz, Germany, a.kassahun@wismut.de

²University of Mining and Technology Freiberg, Dept. of Mining and Special Construction Engineering, Zeunerstraße 1A, 09596 Freiberg, Germany

Abstract

Analysis of redox-sensitive ions, dissolved gases, sulphate isotopes, arsenic species, organic compounds and microbial DNA in four flooded uranium mines revealed the presence of highly diverse and metabolizing microbial communities comprising different species of bacterial, archaeal and fungal domains. Microbial sulphate reduction and methanogenesis were evident from both chemical and microbial analysis. A whole suite of other microbial metabolic activities was deduced from the presence of certain pollutant species, organic compounds and established metabolic pathways of the analysed microbial community. Biochemical processes are relevant for the water quality of the investigated mines.

Keywords: mine water microbial community, microbial metabolism, mine water quality

Introduction

After East German uranium industry was decommissioned in 1990, an unprecedented close-out and remediation programme was launched immediately thereafter. The programme is run by Wismut GmbH, a governmentally owned remediation enterprise. In 1990, the operation of five underground uranium mines was stopped. Mine flooding started between 1992 and 2001 and was completed more than one decade ago, except for one mine. Mine water concentrations of uranium, arsenic, 226-radium, metals and salts exceed regulatory discharge limits and require active water treatment. According to current estimates, water treatment is expected to continue beyond 2040. Within the first decade of flooding, dilution of dissolved pollutant inventory has been the determining process for mine water quality. As flooding proceeds, concentration curves of several pollutants deviate from an ideal exponential decline behavior. Site specific, both rapid pollutant concentration declines and permanent stable pollutant concentration levels were observed in different mine waters. Biogeochemical reactions within the flooded uranium mines might be involved in these effects. For example, microbial uranium reduction can cause rapid drops in uranium concentrations.

Likewise, stable pollutant concentrations can relate to microbial pollutant mobilization from primary and secondary minerals within the flooded mines. In order to identify the relevance of biogeochemical processes for mine water quality and to deduce consequences for water treatment operations, Wismut's flooded uranium mines were analysed for microbial mine water tracer substances.

Methods

Mine water sampling was performed in several sampling campaigns during 2013 – 2017. Four mines were sampled at least twice. Two mines are characterized by iron rich mine water with acid to slightly acidic pH (Königsstein mine and Ronneburg mine), while mine water from the two other mines are poor in iron, rich in arsenic and of neutral pH (Pöhla mine and Schlema mine).

Since microbial mine water tracer substances are sensitive to aeration, special effort was made to realize fast on-site measurement and sample conservation procedures. On-site measurements included probe measurements (pH, redox potential) and photometric measurements for ferrous and sulphide ions. For sample conservation, on-site filtration and chemical stabilization, quick-freezing using dry ice, and filling of deaerated sampling containers



Table 1. Parameter selection, sample conservation and analytical methods.

Parameter	Sample conservation	Analytical method
pH, redox potential	Sample conservation Analysis immediate after sampling	pH / redox measuring apparatus multi 9430; pH probe Sentix 980, redox probe Sentix ORP 900 (WTW) Spectrophotometer photoLab 6600 UV-VIS (WTW);
Ferrous iron, Sulphide ions	Analysis immediate after sampling	Spectroquant test kits for ferrous iron (1 – 5 mg/L) and sulphide (0.02 – 1.5 mg/L) analysis (Merck)
Dissolved gases (CO ₂ , CH ₄ , H ₂ , O ₂)	Filling of deaerated sampling containers	GC-TCD after gas phase equilibration (GFI Groundwater Consulting Institute Dresden)
³⁴ S, ¹⁸ O sulphate isotopes	Zinc acetate -stabilization	ES/IRMS and TC/EA after barium sulphate precipitation (Helmholtz Centre for Environmental Research, Halle)
Arsenic species (arsenite, arsenate, monomethyl arsonate, dimethyl arsenate, thioarsenates)	Membrane filtration (0.2 µm), EDTA stabilization and quick-freezing	IC- / HPLC-ICP-MS (GFI Groundwater Consulting Institute Dresden; sub-contractors University of Bayreuth and Medical Laboratory Bremen)
Carbohydrates	Quick-freezing	Spectrophotometric analysis after phenol-sulfuric acid reaction (GFI Groundwater Consulting Institute Dresden)
Trace organic compound screening	Filling of air tight sampling containers	GC-MS after ethyl acetate extraction / MSTFA derivatization; NIST data base identification (GFI Groundwater Consulting Institute Dresden)
Microbial DNA	Membrane filtration (sterile) or ethanol stabilization in sterile sampling containers	DNA fragment Next-Gen sequencing after extraction, amplification and purification; BLAST analysis and classification (contract analysis Blue Biolabs GmbH, Berlin)

were used. Table 1 contains the parameters selected to trace microbial processes in mine water with reference to sample conservation, analytical methods, and contracted labs.

Results and discussion

For overall water quality characterization of the four mines, table 2 shows selected average solute concentrations of the respective mine effluents entering the water treatment plants (average over last five years; Wismut database). Mine water microbial tracer contents are given in table 3. They were analysed at the monitoring points used for routine sampling. Isotopic analysis was performed for Ronneburg mine water only. Therefore, another three mine water monitoring points were sampled additionally. Data are shown in table 4. Table 5 contains results of qualitative screening analysis for mine water trace organic compounds. Table 6 summarizes prevailing bacteria, archaea and fungi in the mines identified from DNA analysis of the sampled mine water.

Provided that oxidation of the mined and accessory minerals (e.g. uraninite, sulphides, arsenides) during mining operation generated the primary pollutant source, oxidized geochemical conditions are expected for

the polluted mine water. When mine flooding proceeds beyond first flush, both chemical and microbial reactions might consume oxidizing solutes, cause drops in overall redox potentials and change water speciation. Redox potential data in table 2 and 3 indicate oxidized geochemical conditions for Königstein but oxygen depletion for all other mines. Ferrous dominates the iron speciation in all mines. Besides for Königstein, sulphide ions and dissolved methane were detected in all mine waters. Both solutes trace microbial sulphate reduction and methanogenesis, respectively. Consequentially, sulphate reducers (*Desulfurivibrio* spp.) and methanogens (*Methanoregula*, *Methanomassiliicoccaceae*, *Methanobacterium*) were identified in the microbial population of the three mines (see table 6).

Results of isotopic analysis at dissolved sulphate in Ronneburg provide further evidence for microbial sulphate reduction (see table 4). Microbial sulphate reduction enriches both ³⁴S and ¹⁸O isotopes in the remaining dissolved sulphate (Knöller 2004). Figure 1 illustrates a proportional increase in heavy S and O isotopes corresponding to a decrease in sulphate concentration of Ronneburg mine water from different monitoring wells.



Table 2. Average solute concentrations (2013 - 2017) of mine effluents.

Mine site	Königstein (well A & B)	Ronneburg (well 2)	Schlema	Pöhla (mine drainage collector)
pH / E _H [mV]	3 / 640	6.4 / 170	7.1 / 120	7.1 / 84
EC [mS/cm]	2.5	4.4	1.7	0.5
HCO ₃ [mg/L]	<5	360	580	330
SO ₄ [mg/L]	1,100	2,750	500	<2
Ca [mg/L]	270	465	150	48
Mg [mg/L]	23	420	98	16
Fe [mg/L]	75	165	4.3	4.7
U [mg/L]	10	0.75	1.4	0.013
As [µg/L]	38	204	1,450	1,900

Table 3. Microbial tracer substance concentrations in sampled uranium mine effluents (mean values).

Mine site	Königstein	Ronneburg Probe readings	Schlema	Pöhla
pH / E _H [mV]	3 / 650	6.6 / 130	7.3 / 185	7.3 / 110
Photometric on-site measurements				
Fe ^{II} [mg/L]	35	170	3.7	5
total Fe [mg/L]	45	184	4.3	4.6
S ²⁻ [µg/L]	< 20	25	38	120
Dissolved gases				
O ₂ [mg/L]	5	0.4	1.4	0.2
CO ₂ [mg/L]	55	125	66	26
CH ₄ [mg/L]	< LD	0.2	0.3	4
H ₂ [mg/L]	< LD	0.3	< LD	< LD
Arsenic species				
total As [µg/L] (WISMUT database)	43	150	1,570	1,850
As (III) [µg/L]	22.4	0.4	806	1,132
As (V) [µg/L]	4.9	0.3	21	57
Monomethylarsonic acid MMA, [µg/L]	< LD	0.2	< LD	< LD
Arsenobetain [µg/L]	0.3	0.1	< LD	< LD
Thioarsenates (Mono-, Di-, Trithio- arsenate)	< LD	< LD	1 – 2 % of total As	1 – 2 % of total As
not identified As species [µg/L] (Fe-/ DOM-As-colloids)	15.4	149	727 - 743	637 - 661
Dissolved organic carbon				
DOC [mg/L]	1	2.2	3	3
Carbohydrates [mg/L]	n.a.	<0.5 – 2.9	6.9	7.7

Results of arsenic species analysis (table 3) also point to microbial processes. While the speciation predominance of arsenite might be explained by arsenolite dissolution, the existence of organoarsenic compounds (Königstein and Ronneburg) and thioarsenates (Schlema and Pöhla) is exclusively related to microbial metabolism. Methylation

is a well-known microbial strategy for arsenic detoxication (Bentley 2002) and highly mobile thioarsenates were shown to form under sulphate reducing conditions (Burton 2013). Despite the application of sophisticated analytical methods, a considerable arsenic fraction could not be identified (probably Fe- or DOM-As-colloids). Dissolved organic car-



Table 4. Isotopic signatures of sulphate in Ronneburg mine water.

Monitoring point	Inflow WTP	Mine water monitoring wells		
	Well 2	e-1292	e-1303	e-1328
Isotopic signature				
$\delta^{34}\text{SO}_4\text{S}$ [‰ VCDT]	2.0	8.9	10.7	2.4
$\delta^{18}\text{SO}_4\text{O}$ [‰ VSMOW]	1.6	6.2	9.6	-0.2
Water quality parameter (date of isotopic analysis)				
pH	6.5	8.6	7.4	6.7
SO_4 [mg/L]	2,750	487	91	741

Table 5. Trace organic compounds in sampled uranium mine effluents.

Mine site	Königstein	Ronneburg	Schlema	Pöhla
Carboxylic acids (qualitative screening)				
Benzoic acid	detected		detected	detected
Butanoic acid			detected	
Succinic acid	detected	detected	detected	detected
3,4-Dihydroxy-butanoic acid	detected		detected	detected
2-Hydroxyglutaric acid				detected
Lactic acid	detected			
Glyceric acid	detected		detected	detected
Glycolic acid	detected			
Miscellaneous organics (qualitative screening)				
Isosaccharinic acid lactone			detected	detected
Tetrahydroxyhexanoic acid lactone				detected
Phenol derivatives			detected	detected
Pyridine derivatives			detected	
Alkanes		detected	detected	

bon in mine water traces microbial activity insofar as individual substances are microbial substrates and / or metabolites. Table 3 shows surprisingly high concentrations of carbohydrates, which are known to be produced as extracellular polymeric substances (EPS) by e.g. autotrophic iron oxidizing bacteria (Johnson 2014). Fungal metabolites might constitute another source of carbohydrates. Table 6 discloses a great diversity of fungi detected in the mine water, most of them known as soil fungi related to leaf and wood decay (e.g. *Cadophora* spp., *Patinella* spp.). The existence and role of fungal communities in waterlogged, oxygen deficient environments was under debate for long. Within the last decade, it has been recognized e.g. in marine habitats, sulfidic hydrothermal spring systems, anaerobic groundwater and acid mine water environments (Brad 2008), (Luo 2005),

(Amaral Zettler 2002). The detection of fungal DNA, carbohydrates and further fungal metabolites as well as cellulose degradation products like organic acids, phenol derivatives and isosaccharinic acid lactones (see table 5) suggests fungal activity in the flooded mines. By supplying biodegradable organic carbon, fungal mine timber decay might even be the important driver of other biogeochemical processes in flooded mines.

As evident from table 6, the flooded mines contain diverse bacterial and archaeal communities as well. Autotrophic sulphur (*Sulfuricurvum* spp. at Schlema and Pöhla, *Acidithiobacillus* spp. at Königstein) and iron oxidizers (*Galionella* spp., *Sideroxydans* spp. at Ronneburg) are the most abundant bacteria, some of them able of using nitrate for anaerobic oxidation. Nitrifying bacteria (*Nitrospira* spp., *Candidatus Nitrotoga*), an-



Table 6. Mine water microbial biocenosis.

Königstein mine	Ronneburg mine	Schlema mine	Pöhla mine
Bacterial DNA			
Acidithiobacillus spp.	Galionella sp.	Sulfuricurvum spp.	Sulfuricurvum spp.
Sulfuriferula spp.	Sideroxydans spp.	Sulfurimonas spp.	Sulfurovum spp.
Bacteriovoracaceae	Candidatus Nitrotoga	Thiobacillus spp.	Synthropus spp.
Xanthomonadales	Nitrospira spp.	Desulfurivibrio spp.	Nitrospira spp.
Leptospirillum spp.	Sulfuricurvum spp.	Galionella sp.	Desulfurivibrio spp.
Halanaerobiales	Desulfurivibrio spp.	Nitrospira spp.	Sulfuritalea spp.
Archaeal DNA			
Candidatus Nitrosotalea	Crenarchaeota MCG [pGrfC26]	Crenarchaeota MCG [pGrfC26] & [B10]	Methanosarcinales [Candidatus]
Thermoplasma spp.	Parvarchaeota [WCHD3-30]	Parvarchaeota [WCHD3-30]	Methanoperedens]
	Thermoplasmata [BSLdp215]	Thermoplasmata [DHVEG-1]	Candidatus Nitrosopumilus
	Methanomassiliicoc-caceae	Methanomassiliicoc-caceae	Methanoregula
	Methanosarcinales [ANME-2d]	Methanosarcinales [ANME-2d]	Methanobacterium
Fungal DNA			
Cladosporium spp.	uncultured soil fungus	Acremonium spp.	Patinella spp.
Cadophora spp.	uncultured Pseudeurotium	Exophiala spp.	Acremonium spp.
Boothiomycetes spp.	uncultured Glomeromycota	Patinella spp.	uncultured fungi
Articulospora spp.	Saccharomycetales	uncultured fungi	Exophiala spp.
Rhizophydium spp.		Cladosporium spp.	Cladosporium spp.
		Mycosparella spp.	Mortierella spp.
			Aspergillus spp.

aerobic fermenting bacteria (*Synthropus* spp., *Halanaerobiales*), sulphate and iron reducers (*Desulfurivibrio* spp., *Xanthomonadaceae*) and a wide diversity of archaea involved in methane and nitrogen cycling (*Methanosarcinales*, *Methanomassiliicoccaceae*, *Methanoregula*, *Methanobacterium*, *Candidatus Nitrosopumilus*) add to the highly diverse microbial community in the flooded mines. In total, around 100 bacterial and half as much fungal and archaeal species were detected in each mine. Complex interactions of the individual microbial species as known for biofilm communities is highly probable. For example, heterotrophic bacteria can metabolize fungal

cellulose degradation products and provide substrates like organic acids, alcohols, hydrogen and carbon dioxide for e.g. sulphate reducing bacteria, which can live in syntrophy to anaerobic methanotrophic archaea by extracellular electron transfer too. Likewise, nitrate based sulphur oxidation might relay on nitrification of ammonium which in turn is produced by wood degrading fungi and nitrogen fixing methanogenic archaea. Organic matter, nitrogen and electron cycling are yet unknown but most relevant to understand biogeochemical processes and their effects on pollutant mobility in flooded uranium mines.



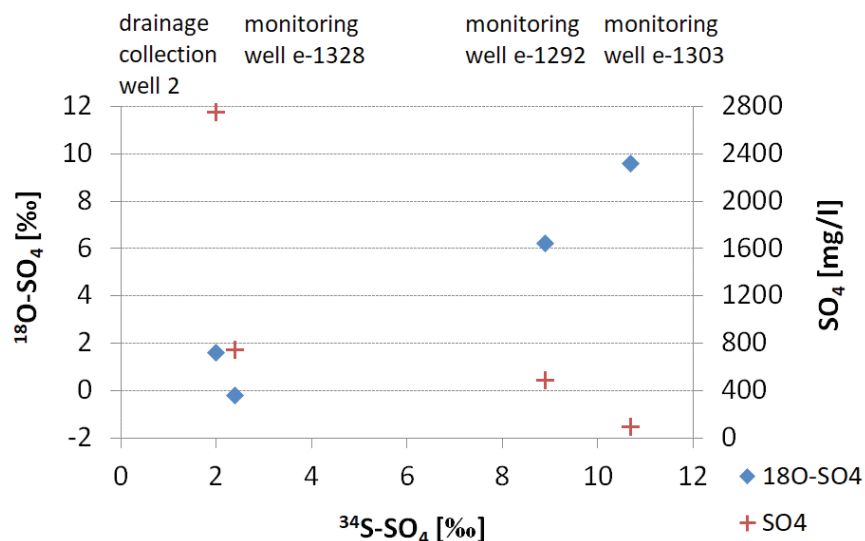


Figure 1 Ronneburg mine water: ^{34}S - and ^{18}O -Isotopes and SO_4 concentrations.

Conclusions

Analysis of redox sensitive ions, dissolved gases, sulphate isotopes, arsenic species, organic compounds and microbial DNA in four flooded uranium mines revealed the presence of highly diverse and metabolizing microbial communities comprising species of different genera of bacterial, archaeal and fungal domains. Their interplay in organic matter, nitrogen and electron cycling is of high relevance for mine water speciation and pollutant mobility. For example, the identified iron and sulphate reducers are capable of uranium reduction, which can lead to in-situ uranium immobilization and uranium concentration decline as observed in Pöhla mine. On the other hand, anaerobic microbial oxidation of arsenic containing primary sulphides by e.g. identified sulphur oxidizing microbes and complexation of dissolved arsenic by microbial metabolites might cause constantly high arsenic levels in mine waters as is also observed in Pöhla and Schlema. Further investigation of the metabolic interplay of identified microbial communities and its effects on pollutant speciation can help to reveal mine water quality trends and to develop innovative mine water treatment technologies.

References

- Amaral Zettler L.A., Gomez F., Zettler E., Keenen B.G., Amils R., Sogin M.L. (2002) Eukaryotic diversity in Spain's River of Fire, *Nature* 417:137
- Bentley R., Chasteen T. G. (2002) Microbial methylation of metalloids: Arsenic, antimony, and bismuth. *Microbiol. Mol. Biol. Rev.* 66:250–271
- Brad T., Braster M., van Breukelen B.M. (2008) Eukaryotic Diversity in an Anaerobic Aquifer Polluted with Landfill Leachate. *Appl. Environ. Microbiol.* 74:3959–3968
- Burton E.D., Johnston S.G., Planer-Friedrich B. (2013) Coupling of arsenic mobility to sulfur transformations during microbial sulfate reduction in the presence and absence of humic acid. *Chem Geol* 343:12–24
- Johnson D.B., Hallberg K.B., Hedrich S. (2014) Uncovering a Microbial Enigma: Isolation and Characterization of the Streamer-Generating, Iron-Oxidizing, Acidophilic Bacterium “*Ferroplasma myxofaciens*”. *Appl. Environ. Microbiol.* 8:672–680
- Knöller K, Fauville A, Mayer B, Strauch G, Frieze K, Veizer J. (2004) Sulfur cycling in an acidic mining lake and its vicinity in Lusatia, Germany. *Chem Geol* 204:303–323
- Luo Q., Krumholz L.R., Najar F.Z., Peacock A.D., Roe B.A., White D.C., Elshahedi M.S. (2005) Diversity of the Microeukaryotic Community in Sulfide-Rich Zodletone Spring (Oklahoma). *Appl. Environ. Microbiol.* 71:6175–6184





Monitoring of waste rock dump surface water drainage and channel infiltration

Jason Keller¹, Jaime Banuelos², Lindsey Bunting², Mike Milczarek², Robert Rice², Daniel Lattin³,

¹*GeoSystems Analysis, Inc., Hood River, OR, USA*

²*GeoSystems Analysis, Inc., Tucson, AZ, USA*

³*Homestake Mining Company, Lower Lake, CA, USA*

⁴*Barrick Gold Corporation, Salt Lake City, UT, USA*

Abstract

A series of low-cost, high-resolution game cameras (flow-imagery) and resistance sensors (inundation sensors) were installed in unlined drainage channels at a reclaimed waste rock dump (WRD) to determine the distribution, duration and estimated infiltration of surface water into the channel areas. Estimated drainage channel infiltration from the flow-imagery and inundation sensor data was 3.6 percent of the estimated WRD seepage collection volume during the same monitoring time period. The flow-imagery and inundation sensor monitoring results provided a clear indication that most of the water entering the WRD seepage collection pond is from a source other than drainage channel infiltration.

Keywords: Infiltration, Seepage, Flow-imagery, Inundation, Monitoring

Introduction

Surface water flow over unlined drainage channels can be a primary source of net infiltration into closed waste rock dump (WRD) facilities in semi-arid regions (Flint and Flint, 2007; Scanlon et al., 1999; Zhan et al., 2014). Thus, understanding the contribution of net infiltration into unlined drainage channels to a WRD water budget is important to prioritize closure design efforts to minimize seepage from closed WRD facilities.

A relatively inexpensive and efficient method to quantify drainage channel flow characteristics and infiltration is the use of low-cost, high-resolution game cameras to monitor surface water depth and event duration (flow-imagery). Low cost resistance sensors can also be installed to detect the onset and duration of surface inundation (the beginning and end of a flow event) and provide a high-resolution complement to flow-imagery.

To determine the distribution, duration and estimated infiltration of surface water in unlined drainage channel areas, a series of game cameras and inundation sensors were installed at different locations at a closed and

reclaimed WRD. The site is located in a temperate Mediterranean climate that receives approximately 800 mm/yr of precipitation, which mostly occurs between the months of December to March. Annual average minimum and maximum temperature is 8 °C and 22 °C, respectively.

Methods

In February 2015, five inundation monitoring stations were installed along western and southern portions of a bench on a closed WRD. Stations were located in areas known to collect and pond surface water runoff. Three stations were located on the western portion of the WRD bench (W1, W2, W3) and two stations on the southern portion of the bench (S1 and S2). Each station included one game camera, two staff gauges to estimate the water ponding depth from the flow-imagery, and four resistance sensors equally spaced across the monitoring area. The total length of each monitoring location ranged from 49 m to 100 m.

Game cameras (Reconyx Hyperfire, WI, USA) were fastened to t-posts and programmed to take a photograph every fifteen minutes (Figure 1). Two staff gages were in-



stalled at each location; one at 4.6 m and a second at 9.1 m from the camera. Reflective tape was placed across the gages at 15 cm intervals to provide added visibility for images taken at night. Pin flags were placed at 1.5 m intervals laterally from each staff gage, perpendicular to the field of view and towards the channel edges to allow for visual estimation of lateral water extent during inundation events.

Resistance sensors (GSA, AZ, USA) were installed at the low point in the drainage channels and connected to an EM50 datalogger (Decagon, WA, USA). These sensors function by measuring the resistance between two stainless steel probes exposed above the soil surface (Figure 1). Dataloggers were pro-

grammed to record sensor readings every five minutes.

Results

The study period extended from March 1, 2015 to March 31, 2016. Mine site monthly precipitation rates for the monitoring period, along with historical mean monthly precipitation, are presented in Figure 2. Total precipitation for the monitoring record was 56.9 cm, compared to a historic mean of 77.2 cm for the same 13-month period. Precipitation during the study period generally followed historic precipitation trends, however, cumulative annual precipitation at the beginning of the monitoring period (late winter, 2015)



Figure 1 A) Inundation sensor, B) camera installed on t-post for flow-imagery monitoring, C) sample flow-imagery image, including flagging.



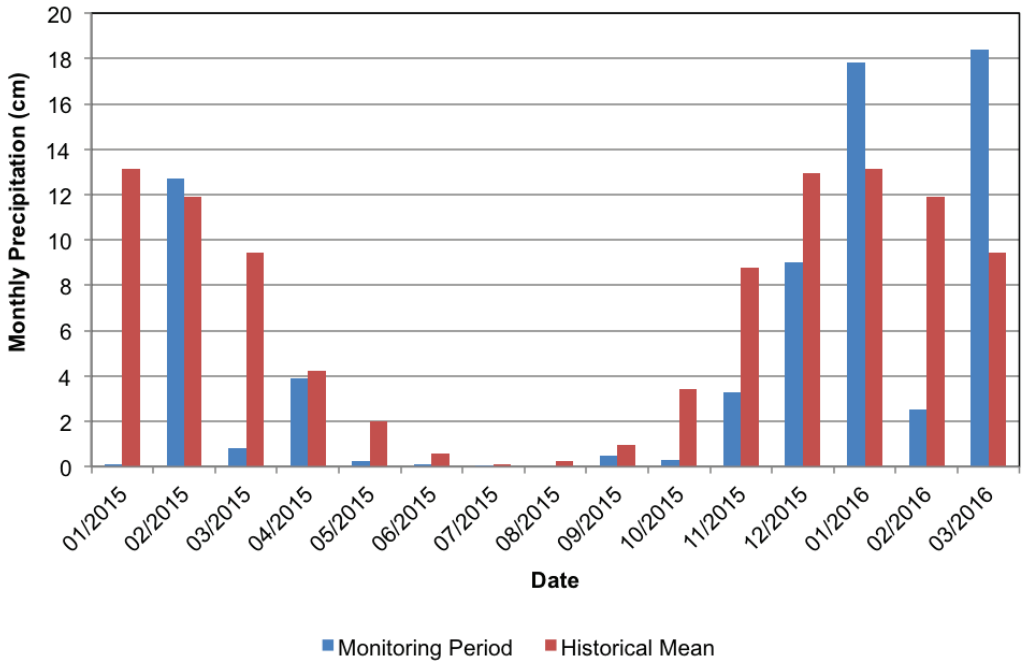


Figure 2 Mean monthly precipitation for the monitoring period and historical average (November 1954 to March 2016)

was far below average with a total precipitation of 13.6 cm compared to a historic mean of 34.5 cm. A precipitation total of 47.7 cm was measured from December 2015 through March 2016, approximately equal to the historic precipitation average of 47.4 cm for this four-month period.

Flow-imagery photos over each inundation event were analyzed to determine the hourly inundation area and depth of inundation within the field of view of the camera. Resistance sensor response was then analyzed to estimate the inundation area length, total inundation area, and inundation start and end times. The width of the inundation area observed in the photo was assumed to exist over the entire length of the inundation area.

Figure 3 presents an example of a flow-image during an inundation event at the S1 monitoring location and the change in water depth from the start to the end of inundation. Over the monitoring period, observed inundation water levels were generally below 15 cm, with the highest water level observed being 41 cm.

Resistance sensors recorded less than -50 ohms under dry conditions (no inundation)

and greater than -50 ohms when inundated with water. Figure 4A shows an example of an inundation event at the S1 monitoring location as indicated by a sharp decrease in resistance for the duration of inundation; Figure 4B presents an example of the estimated inundation area over the same time period. The inundation area was observed to increase with increasing precipitation. After precipitation stopped, individual inundation sensors responded depending on location. Sensors S1-1 and S1-4 were furthest from the center of the inundation area and were first to record less than -50 ohms as the precipitation event ceased and the inundation area decreased. The two middle sensors (S1-2 and S1-3) measured inundation for longer.

Inundation periods were observed between December 2015 and March 2016, coinciding with the months of increased precipitation. Inundation duration ranged from 2 hours to 645 hours and a maximum wetted area over all five stations of approximately 1,170 m² was observed.

Flow-imagery photos were analyzed for each inundation event to determine the rate of change in water depth to estimate the infil-



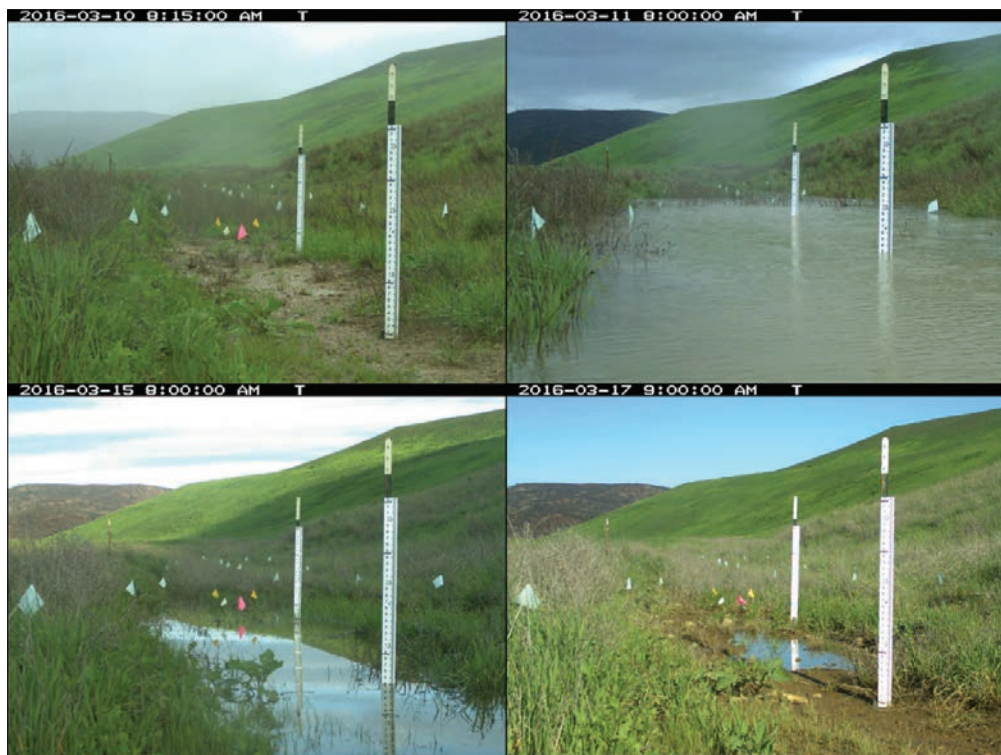


Figure 3 Inundation event from March 10, 2016 08:00 to March 17, 2016 09:00

tration rates of for each area. Infiltration rates were calculated by dividing the change in water depth by the duration of infiltration. Table 1 presents the geometric mean calculated infiltration rates for each station. Geometric mean infiltration rates calculated from the inundation events ranged from 6.8×10^{-6} cm/sec to 7.7×10^{-5} cm/sec.

Hourly infiltration volumes resulting from each inundation event at each station were calculated by multiplying the infiltration rate by the estimated hourly inundation area. Hourly infiltration volumes were then summed over each inundation event to estimate the total volume of infiltration. Table 2 presents the monthly total estimated infiltration volumes for each station and for all monitoring stations combined. The total estimated infiltrated volume over the period of monitoring was 396 m^3 . Dividing the estimated infiltrated volume by the total drainage channel monitored area ($1,407 \text{ m}^2$), equates to 0.3 m^3 of infiltration per 1 m^2 .

To estimate the infiltration volumes for all drainage channels on the WRD, the monthly

infiltration volume per area of drainage channel (Table 2) was multiplied by the estimated drainage channel area on all WRD benches. The actual area that inundates on other drainage channel areas was not known but was assumed to be 25 percent of the total drainage channel area based on the area known to become inundated within the monitored drainage channel area.

Estimated total WRD infiltration volumes are presented in Table 3. The total estimated WRD drainage channel infiltration volume for the monitoring period was $2,200 \text{ m}^3$. Estimated drainage channel infiltration volumes were compared to actual WRD seepage collection volumes for the time period of December 2015 to March 2016. WRD seepage collection volumes follow monthly precipitation and infiltration trends, and, therefore, monthly seepage collection volumes were assumed to include drainage channel infiltration volumes for similar months (i.e. no time lag). Through December 2015 through March 2016, the total estimated WRD drainage channel infiltration volume ranged from



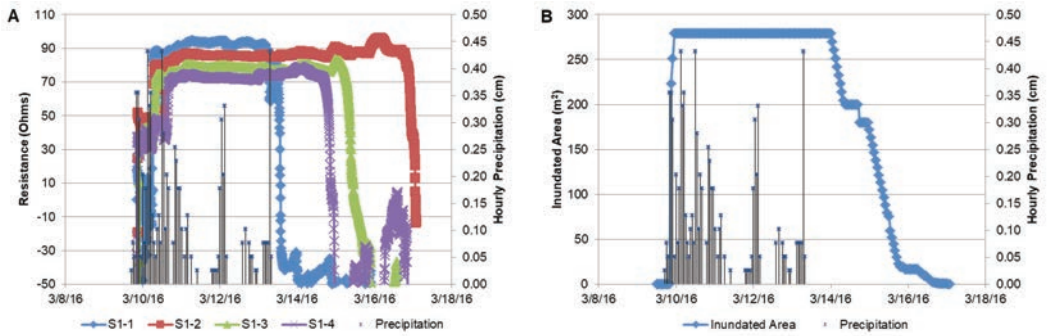


Figure 4 A) Measured resistance and precipitation, and B) estimated inundated area and precipitation from March 10, 2016 08:00 to March 17, 2016 09:00

Table 1. Geometric mean calculated infiltration rate

Station	Geometric Mean Infiltration Rate (cm/s)
W1	1.2E-05
W2	1.1E-05
W3	6.8E-06
S1	7.7E-05
S2	2.5E-05

Table 2. Estimated station infiltration volume

Month	Station					Monthly Total	
	S1	S2	W1	W2	W3	m³	(m³/m² Drainage Channel) ¹
	m³					m³	
12/2015	0	0	0	0	1	1	0.0
01/2016	78	25	17	32	11	163	0.1
02/2016	0	0	0	0	0	1	0.0
03/2016	117	41	36	22	16	232	0.2
Total	194	67	52	55	28	396	0.3

¹Total monitoring station surface area: 1,407 m²

Table 3. WRD seepage collection volumes and estimated bench drainage channel infiltration volumes

Month	Seepage Collection Volumes		Drainage Channel Infiltration Volumes
	m³	m³	Percent of Total Seepage Collection Volume
12/2015	9,600	0	0.0
01/2016	14,300	900	6.3
02/2016	11,500	0	0.0
03/2016	26,500	1,300	4.9
Total	61,900	2,200	3.6



less than 0.1 percent to 6.3 percent of the total seepage collection volume and averaged 3.6 percent of the seepage collection volume. Even if 100% of the drainage channel area inundated, only 14.4% of the seepage could be attributed to channel infiltration. These results indicate that most water entering the WRD seepage collection pond is from a source other than drainage channel infiltration.

Conclusions

Low-cost, high-resolution game cameras to monitor surface water depth and event duration in conjunction with resistance sensors to detect the duration of surface inundation offer a relatively inexpensive and efficient method to quantify surface water flow in ephemeral channels and estimate infiltration. Based on flow-imagery and resistance sensor data, drainage channel infiltration volumes were estimated to be 3.6 percent of the WRD seepage collection volume during the same monitoring time period. These results provide a clear indication that most of the water entering the WRD seepage collection pond is from a source other than drainage channel infiltration.

Acknowledgements

The authors thank staff and management at Homestake Mining Company and Barrick Gold Corporation for their support of this

project and for permitting the presentation of this work. Special thanks to Homestake Mining Company support staff for maintaining equipment and downloading data.

References

- Flint AL, Flint LE (2007) Application of the basin characterization model to estimate in-place recharge and runoff potential in the basin and range carbonate-rock aquifer system, White Pine County, Nevada, and adjacent areas in Nevada and Utah. USGS Scientific Investigation Report 2007–5099, Washington DC, USA
- Scanlon BR, Langford RP, Goldsmith RS (1999) Relationship between geomorphic settings and unsaturated flow in an arid setting. *Water Resour Res* 35:983–999
- Zhan G, Keller J, Milczarek M, Giraudo J (2014) 11 years of evapotranspiration cover performance at the AA leach pad at Barrick Goldstrike Mines. *Mine Water Environ* 33(3):195–205, doi:10.1007/s10230-014-0268-6





An Investigation of the Water Quality of Four Coal Mine Pit Lakes in South Africa[©]

Lizel Kennedy¹, Andrew Johnstone²

¹University of the Free State, 205 Nelson Mandela Dr, Park West, Bloemfontein, 9301,

kennedylizel@yahoo.co.za

²GCS (Pty) Ltd, 63 Wessel Road, Rivonia, Johannesburg, South Africa, 2128,

andrewj@gcs-sa.biz

Abstract

Extensive opencast mining in the South African coal fields dating from the 1870's had left numerous pit lakes of various age and sizes. These pit lakes pose risks to the environment in terms of discharge and release of contaminated water into the surrounding water resources. A study of the water quality of four existing end-pit lakes in the Mpumalanga, Waterberg and KZN coal basins has been undertaken, with the aim of establishing the physical structure and hydrochemistry of typical coal mine pit lakes found in South Africa. Current results of this Water Research Commission funded project show that the water chemistry varied markedly between coal fields, while it was found that thermal stratification occurred as a function of the depth of the pit lake. Shared chemical characteristics of the pit lakes included slightly alkaline pH, EC between 120-500 and low trace metal concentrations, indicating the mature nature of these lakes. The lakes are very well vegetated with significant algal biomass and water plants.

Keywords: Pit lakes, physiochemical parameters, water quality, phytoplankton

Introduction

According to De Lange et al. (2018) approximately 6000 abandoned or ownerless mines exist in South Africa. Pit lakes are water bodies that formed in the final voids of opencast mines and were generally left unrehabilitated, as they were in operation prior to the introduction of environmental legislation in South Africa (De Lange et al. 2018). Hence, most of these lakes are ownerless, with only a crude estimate of their exact number (De Lange et al. 2018). Furthermore, in South Africa, pit lakes are commonly associated with coal mines, especially in the Mpumalanga and KZN coal fields, which host the majority of mineable coal in the country and are associated with the phenomenon of acid mine drainage (AMD) (Hancox and Götz 2014). Subsequently, preconception of poor water quality, in terms of acidic pH, high TDS and elevated heavy metals exists regarding pit lakes, with related liability and costly remediation. However, in certain cases, as pit lakes age, they can achieve neutral pH without any special remediation measures, even if the water quality

started out as acidic. This phenomenon was demonstrated by Lake Nenkersdorf and Lake Bergwitz in Germany, which turned neutral within 5 and 25 years, respectively (Jordan and Weder 1995).

In opencast areas, much of the ground-water influx is dependent on the state of post mining rehabilitation. A hydraulic link exists whereby rainfall infiltrates into the spoil and then into the final void. The final pit lake is essentially a product of the receiving water quality over the duration of flooding. Nevertheless, current research of mine water in South Africa lacks detailed investigations of pit lakes. Several factors influence the final water quality of a pit lake, such as geology, hydrology, climate, pit shape, water balance, physical and chemical limnology, lake geochemistry, and sediment biogeochemical processes and wall rock reactivity (Castendyk et al 2015). The study presented in this paper aims to fill the current gap by presenting the physiochemical profiles of temperature (T), electrical conductivity (EC), dissolved oxygen (DO), redox potential (ORP) and pH, water



chemistry and phytoplankton composition of four end pit lakes (age 8 to 17 years) measured during field investigations conducted between November 2016 to November 2017. The end purpose of the study was to evaluate the evolution and current status of the water quality, in terms of their hydro- geochemistry and biological quality.

Description of Study Sites

The selected study areas are situated in the Waterberg coal basin (WB pit lake), Mpumalanga (KC pit lakes) and KZN coal fields (RK pit lake) of the Karoo Supergroup, east of 26°E, South Africa, shown in Figure 1. The coal, mainly low-grade sub-bituminous to mid-bituminous, occurs in the Vryheid formation in the Ecca Group of the Main Karoo Basin, where coal seams are contained in a 70 m thick succession of alternating bands of coal and sedimentary formations. In the northern sub-basins, the coal is contained in the Grooteveld formation and Vryheid formation, with a stratigraphic thickness of 120

m (Hancox and Götz 2014). Pyrite (FeS_2) is a dominant sulphide mineral present in South African coal, but many studies have also shown an abundance of acid buffering minerals, such as calcite (CaCO_3), occurring with the coal seams. Consequently, mine waters are not necessarily acidic, but often high in dissolved salts (Usher, 2003).

The WB pit lake showed the highest probability to have a monimolimnion based on its high relative depth. The other three pit lakes were linear and shallow with small relative depths. Table 1 gives a summary of the physical characteristics of the four pit lakes.

Methods

Physiochemical Parameter Profiles

Physiochemical profiles of the pit lakes were obtained: the decisions of sampling methodology were based on the structure of the profiles. Profiling was conducted on three occasions for every pit lake during November 2016 to November 2017, where profiles were obtained in at least two locations in every pit

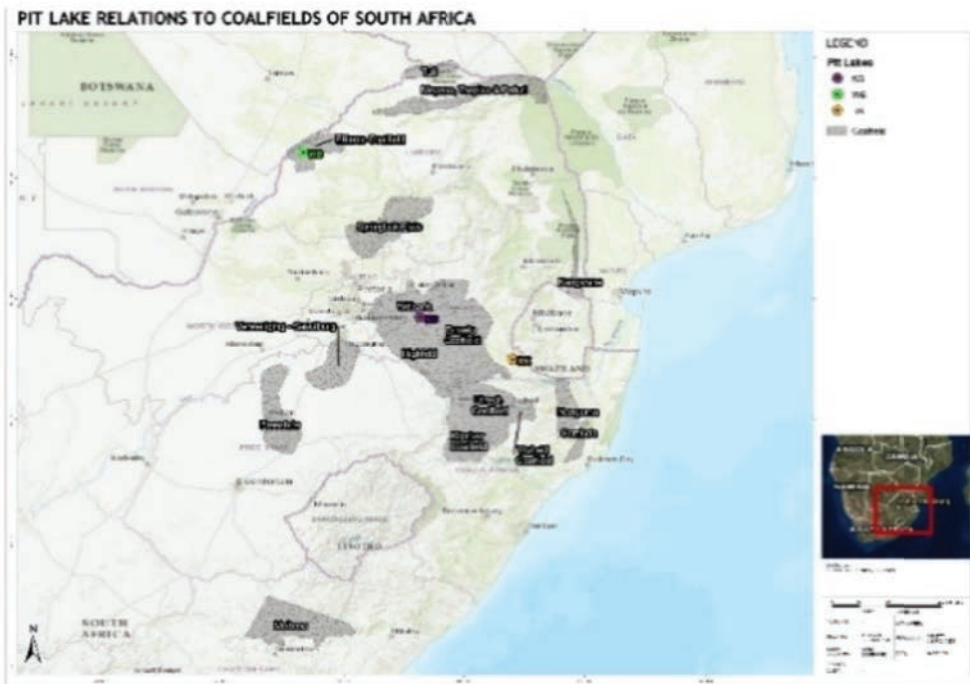


Figure 1 Study area locations in the Main Karoo basin (Mpumalanga coal fields- KC (a) and KC (b) and KZN coal fields - RK) and Northern sub-basins (Waterberg coal basin- WB pitlake) (Modified after Snyman, 1998).



Table 1. Physical characteristics of the pit lakes, their mining history, age and relative depth (O/C = Opencast; U/G = Underground).

Pit lake	Method of Mining	Mining history	Age of pit lake (years)	Max sat. depth (m)	Max surface area (m ²)	Max volume (m ³)	Relative depth (%)*
WB	O/C bulk	08/2009-	8	70	18 241	487082	46
KC (a)	excavation	05/2010	16	6.8	180 130	393 225	1.4
KC (b)	O/C strip, roll over	1996 –2002		12	51 230	249 694	4.7
RK	O/C, U/G bord & pillar	1999-2006	17	12	12 968	367 124	9.3

*Relative depth ($z_{\text{relative}}\%$), which is the ratio of maximum depth (z_{max}) to lake surface area (A_{surface}) (Castendyk et al 2015), as per $z_{\text{relative}}(\%) = (50 \times z_{\text{max}} \times \sqrt{n}) / \sqrt{A_{\text{surface}}}$.

lake to establish lateral homogeneity of the water. Accordingly, physiochemical profiles obtained at the deepest location in each pit lake were used for sampling depth determinations. The field measurements of T, DO, EC, pH and ORP were conducted in vertical profiles using a calibrated EXO1 multiparameter probe (YSI Incorporated, Yellow Springs Instruments). A reading was taken at 0.3 m depth intervals, and allowing 5 seconds response time for equilibration of the DO sensor with the water, in order to obtain the most accurate readings possible.

Water Sampling and Analysis

Sampling and analysis proceeded for water chemistry, chlorophyll-a concentration and phytoplankton communities. Based on important changes observed in the profiles, with specific attention to sharp changes in T, EC and ORP, water sampling was conducted at specific depths in the pit lakes. A purging pump connected to the appropriate length of hose and a power source was used to conduct the sampling. Collectively, 101 samples were analysed for inorganic chemistry and a further 10 for chlorophyll-a and phytoplankton for the four pit lakes during the study period. The following sets of samples were collected at each decided depth in the pit lakes during every sampling event: (1) a 1 L unfiltered, unacidified sample for alkalinity (determined by titration in the laboratory) and major anions (Ion Chromatography) (2) a 1 L sample, filtered (0.45 µm MCEO syringe filters) and acidified to pH<2 with conc. HNO_3 , for dissolved metal concentrations (ICP-OES) (3)

2L unfiltered, unacidified sample for chlorophyll-a concentrations where the sample depth was based on changes in DO and T in the profiles (4) a 100 ml sample for phytoplankton taken at same depth as chlorophyll-a and preserved with 1%. Additionally, groundwater samples were collected from monitoring boreholes on the respective sites, by purging the borehole and bailing. All samples were kept at 4°C and transported to their respective laboratories within 24 h.

Results and Discussion

All four pit lakes were holomictic during the study period. Holomictic pit lakes are typically well mixed and consist of an epilimnion and hypolimnion, separated by a zone of rapidly decreasing temperature, the metalimnion. The aforementioned was observed clearly in the deep WB pit lake (Figure 2), which displayed stratification of T and DO during the summer months, and a homogenous EC with depth. During the winter turn-over in WB, the EC remained at 180 mS/m, the T cooled to a uniform 18°C and the whole water column became oxygen-saturated (8mg/L). For the shallower KC (a&b) and RK pit lakes (Figure 3 and Figure 4), weak thermal stratification was observed during the summer, which was subject to wind action, with uniform EC. Lower DO concentrations were detected in the KC(a) pit lake. KC(a) also showed a reduced layer at the bottom, with corresponding decrease in pH and increased EC at the same depth. Even though the RK pit lake is the oldest of the lakes, it had the lowest EC, indicating lower overall mineralisation.



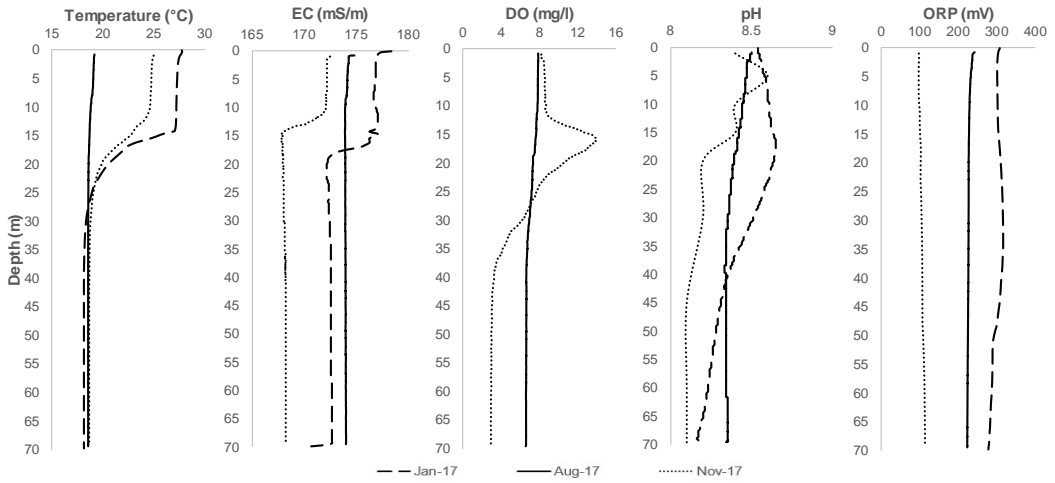


Figure 2 Profiles of T, EC, DO, pH and ORP for WB pit lake showing a thermocline at 13-16 m and an oxygen maximum at approximately 15 -16 m.

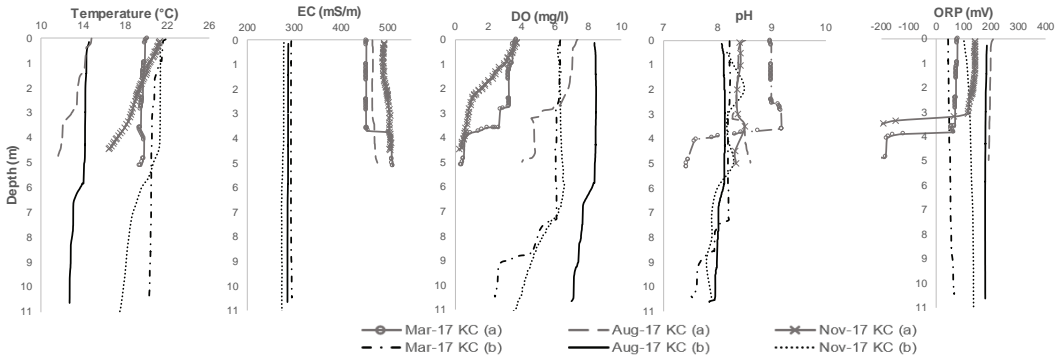


Figure 3 Profiles of T, EC, DO, pH and ORP for KC (a) and KC (b) pit lakes during the March, August and November 2017 surveys.

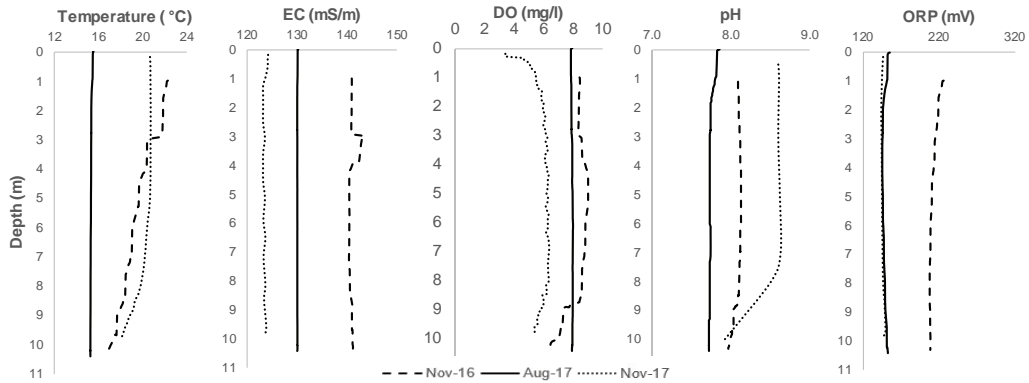


Figure 4 Profiles of T, EC, DO, pH and ORP for RK pit lake, showing a thermocline at 3 m in November 2016.

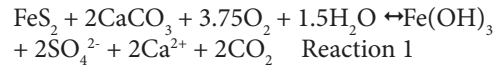


Water Chemistry

A Piper diagram (Piper 1944) was used to characterise the hydrogeochemical facies of the coal mine pit lakes and groundwater samples. The diagram (Figure 5) indicated that the pit lake waters may be classified as Na-Cl, Na-SO₄ and Ca-SO₄ facies types for WB, KC and RK, respectively. The groundwater from the studied regions which filled the pit lakes, classified as Na-Cl, Na-HCO₃ and Ca-HCO₃ types for the WB, KC and RK sites, respectively.

A general trend of pit lake water evolving towards permanent hardness, typically plotting in block B of the Piper diagram, was observed for the pit lakes of KC and RK. Hard water and high salt concentrations are typical of South African coal mine waters (Usher 2003). Geologically, the aquifers of the Karoo Supergroup consist of weathered regolith overlaying layers of siltstones, sandstones, carbonaceous shale and coal of the Ecca Group. These formations mainly contain in-

ert minerals, together with mainly calcite (rather than dolomite) and accessory pyrite. Natural buffering of AMD by the surrounding or co-disposed rock therefore releases SO₄ and Ca (and Mg) into the water according to Reaction 1, which gives rise to hardness (Gomo 2017).



At the RK site, the contribution of the mine groundwater rising through old underground workings and leaching sulfide oxidation products to the pit lake, was visible in the high SO₄ concentrations relative to that of the surrounding aquifer. The KC pit lakes displayed dominance of both Na and Ca, with SO₄. Here, the pit lake water was influenced by groundwater flowing through, and interacting with the heterogeneous spoil materials in the backfill, adding SO₄ to the water by leaching pyrite oxidation products.

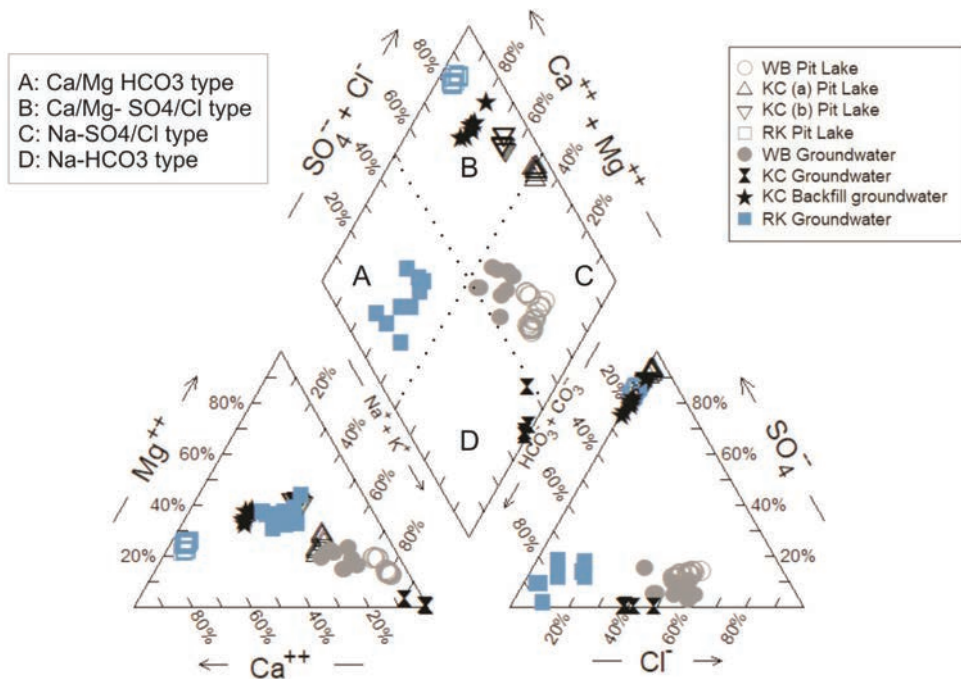


Figure 5 Piper diagram showing the plotting from all the coal mine pit lakes and groundwater samples.



Furthermore, the natural aquifer at KC was classified as Na-HCO₃ type, where the origin of high HCO₃ could be due to coalification processes, as explained by Usher (2003), and the Na enrichment explained by reactions of cation exchange of Ca and Mg in favour of Na taking place in exchange sites of clay minerals. The pit lake water of WB evolved towards higher Na concentrations, and had Na/Na+Cl (in meq/L) ratios of >0.5, which, according to Hounslow (1995) indicates the process of albite weathering or ion exchange. At the high pH and oxidative ORP conditions encountered in the WB, KC and RK pit lakes, Fe and Mn were expected to be present in low concentrations. Fe and Mn are typically removed from the solute load by adsorption on Fe oxyhydroxides and precipitation. Higher relative Mn concentrations in the water can be explained by the stability of Mn over a wider range of pH and redox potential, as well as the slower oxidation of Mn relative to that of Fe (Denimal et al 2005).

Table 2 shows the arithmetic mean and standard deviation values for dissolved components, as well as pH and EC for all the samples taken during all the seasons at all depths in the pit lakes. Moreover, water in the

pit lakes were compared to groundwater data from the studied sites (Table 2). Major differences between groundwater and pit lake compositions were found for Ca, Mg, Na HCO₃, SO₄ and Cl concentrations.

Phytoplankton

Freshwater organisms, especially phytoplankton, have been found to reflect changes in environmental conditions and as such, biota found in polluted waters are different than those found in non-polluted waters (Wetzel, 2001). Furthermore, pit lakes pose unique habitats to organisms where conditions, such as light availability, nutrient levels and pH are especially stressful, hence the diversity of organisms are expected to be lower than in natural environments. In the studied pit lakes, total phosphorous (TP) and inorganic nitrogen were both limiting factors, with concentrations of less than 250 µg/L TP and 100-115 µg/L inorganic nitrogen for KC and RK pit lakes, classifying them as oligotrophic to mesotrophic (Wetzel 2001). WB pit lake showed a higher load of inorganic nitrogen, mostly due to NO₃-N (267 µg/L) but also classified as oligo-mesotrophic according to Wetzel (2001). The average chlorophyll-a concen-

Table 2. Arithmetic mean and standard deviation values of the water components concentration (mg/L), pH and electrical conductivity (mS/m) from studied coal mine pit lakes and groundwater in the same study sites.

	Ca	Mg	Na	K	Fetotal	Mn	HCO3	Cl	SO ₄	pH	EC
WB pit lake											
Mean(n=24)	24.8	30.8	306.9	20.1	<0.05	<0.01	363	319.2	100.4	8.4	185
SD	2.2	4.6	30.8	3.1	-	-	38	14.1	6.8	0.17	5.9
KC pit lakes											
Mean(n=38)	213	185.8	423.8	28.3	0.09	0.22	220	36	2108	8.1	360
SD	55.5	82.7	175.8	8	0.2	0.33	38	12	752.3	0.3	90.4
RK pit lake											
Mean(n=17)	219.6	45.5	18	5.5	<0.05	0.017	141	2.6	607.7	7.8	137
SD	13.7	4.2	1	0.3	-	0.013	12	0.3	25.9	0.13	4.5
WB GW											
Mean(n=10)	77	32	218	29.7	<0.05	0.22	437	307	37	7.15	168
SD	4	2	42.8	8.5	-	0.09	12	55.6	1.5	0.35	15.5
KC GW											
Mean (n=4)	2.3	0.87	357.6	4.8	0.06	<0.01	516	200	1.4	8.4	156
SD	0.3	0.16	36.7	1.2	0.07	-	72	18.4	1.3	0.41	32
KC backfill											
Mean (n=8)	399.7	182.2	202.2	29.3	0.04	2.13	538	22.6	1639	7.3	329
SD	23	33.1	10.8	1.5	0.01	0.4	165	3.8	166.2	0.2	12
RK GW											
Mean(n=10)	7	4.7	6.6	2.6	0.4	<0.01	35	4.5	5.4	7.4	9.2
SD	1.9	0.8	1.4	0.4	0.5	-	12	1	2.4	0.12	2.6

GW Groundwater, SD Standard Deviation, Mean Arithmetic



trations were 6 µg/L, 12 µg/L and 5 µg/L for WB, KC and RK, respectively. Many freshwater pollution algae were analysed in the pit lakes and identified up to genus level. Overall, Chlorophyta and Cryptophyta dominated the pit lake waters, with *Ankistrodesmus*, *Chlorella*, *Cryptomonas* and *Chlamydomonas* being present in the highest cell volumes. These phytoplankton species have been found in other South African freshwater impoundments, such as the studies conducted on the Loskop dam in the Olifantsriver Catchment. The specific role and relevance of the phytoplankton in the presented pit lakes will be investigated in a future paper.

Conclusions

Waters from the studied coal mine pit lakes showed high content of dissolved elements and circum-neutral to alkaline pH. A comparison between the groundwater and coal mine pit lake waters indicated that the respective mining processes and connectivity to underground workings or rehabilitated backfill may have played a notable role in the evolution of the final pit lake water qualities of the RK and KC pit lakes. The stand-alone WB pit lake showed water qualities much closer to that of the natural surrounding aquifer. All the pit lakes showed holomictic circulation patterns which did not seem to impact on the chemical signatures of the pit lakes. From a water quality point of view, the research so far, indicates that intentional flooding of a final void in a coal mine area looks like a viable solution for mine closure.

Acknowledgements

The authors would like to express gratitude towards the Water Research Commission,

South Africa, for provision of funding for the project.

References

- Castendyk DN, Eary LE, Balistrieri LS (2015) Modelling and management of pit lake water chemistry: Theory. Applied Geochemistry 57: 267-288, doi: 10.1016/j.apgeochem.2014.09.004.
- De Lange WJ, Genthe B, Hill L, Oberholser PJ (2018) Towards a rapid assessment protocol for identifying pit lakes worthy of restoration. Journal of Environmental Management 206: 949-961, doi: 10.1016/j.jenvman.2017.11.084.
- Gomo M (2017) Conceptual hydrogeochemical characteristics of a calcite and dolomite acid mine drainage neutralised circumneutral groundwater system. Water Science. doi: 10.1016/j.wsj.2018.05.004.
- Hancox PJ and Götz AE (2014) A Review article: South Africa's Coal fields - A 2014 perspective. International Journal of Coal Geology 132 170-254, doi: 10.1016/j.coal.2014.06.019.
- Hounslow AW (1995) Water quality data: Analysis and interpretation. New York: Lewis Publishers.
- Jordan H, Weder HJ (1995) Hydrogeologie-Grundlagen und Methoden. F. Enke Verlag, Stuttgart.
- Snyman CP (1998) Coal. In: Wilson M.G.C. and Anhaeusser C.R. (Eds), The Mineral Resources of South Africa, sixth ed, Handbook 16, Council for Geoscience, Pretoria.
- Usher BH (2003) The development and evaluation of hydrogeochemical prediction techniques for South African coal mines. PhD Thesis, University of the Free State, South Africa.
- Wetzel RG (2001) Limnology: Lake and River Ecosystems, third ed. Academic Press, San Diego, California, 1006 pp.



Hydrogeological Bedrock Characterisation Based on Posiva Flow Log Measurement Data

Jere Komulainen¹, Tiina Vaittinen², Päivi Picken³, Eero Heikkinen²

¹Pöyry Finland Oy, Jaakonkatu 3, 01620 Vantaa, Finland, jere.komulainen@poyry.com

²Pöyry Finland Oy, Jaakonkatu 3, 01620 Vantaa, Finland

³Pöyry Finland Oy, Koskikatu 27 B, 96100 Rovaniemi, Finland

Abstract

The hydrogeological characterisation of soil and bedrock at a mining site is needed for both planning dewatering and for environmental risk assessment in mining projects. The required level of detail is dependent on both the project's development phase and site-specific requirements. This also requires a flexible investigation approach.

The Posiva Flow Log (PFL) is a measurement method which has been developed based on the high requirements needed for spent nuclear fuel repository studies. Nevertheless, the PFL method is very flexible and the measurement speed vs. measurement accuracy can be adjusted even during a measurement. Therefore, PFL utilization was also introduced in the mining industry. This paper summarizes how the PFL method can support bedrock characterisation.

Keywords: Posiva Flow Log, PFL, hydrogeology, bedrock characterisation, borehole

Introduction

Water management planning is one of the most critical tasks in the mining industry and requires a good understanding of the site hydrogeology. Hydrogeological studies start with site conceptualisation. This includes a description of the relevant water bodies and catchment areas, the topography, position of the bedrock surface, bedrock characteristics, known fractured zones, soil layers, information on the groundwater table, climate data and a draft of the planned operations. The first conceptualization enables planning the hydrological and hydrogeological field measurement campaigns. Field measurements are needed for gaining representative input data for assessments and modelling work. Field data is also used for reviewing and updating the conceptualization.

The first hydrogeological field testing campaigns should take place well in advance during the early mining project development stages. Mines also expand, and complementary hydrogeological measurement and hydrogeological model updates are also needed by operating mines. Furthermore, complementing the data during the mine's operational time allows further model calibration.

Conceptualization and field data are used further in the generation of a numerical hydrogeological model. Numerical hydrogeological modelling is used for estimating the water quantities leaking into the underground workings or open pits. Modelling is also used for understanding how mine dewatering affects the groundwater table in the surroundings. The need to understand the mine site hydrogeology is not limited to the mine operational time: to a reasonable extent, also post-closure groundwater flows must be understood. The risks of contamination transport via groundwater may increase after mine closure. After pits or underground workings are filled with water, groundwater no longer flows into the mine – it flows away from the mine, and its extent depends on the site-specific circumstances.

In addition to flow data, hydrogeological field campaigns can also provide information on electrical conductivity, redox potential measurements, pH and chemical substances. Sometimes also isotope samples are taken. This data can help to understand groundwater regime and contact with surface water bodies. Water quality data, for example information on salinity, is also needed for water management planning.



Requirements for groundwater field measurement data include its representativeness, (correct and adjustable) accuracy and suitability as input data for the modelling work. Also, effective ways to collect both physical and chemical field data are increasingly needed for generating better input data for both water management planning and environmental impact assessments. To serve these objectives, utilization of Posiva Flow Log (PFL) measurements in mining environments was initially started. The following chapters summarize some benefits of the method and suitable utilization situations based on experience.

Posiva Flow Log (PFL) measurement methods

In crystalline bedrock most of the groundwater movement occurs in fractures. Therefore, a definition of fractures and their properties is highly important. A common solution to collecting actual water conductivity data is through water flow measurements in boreholes drilled into the bedrock. There are a large range of flow measurement techniques. At one end of the range are pumping tests in which the entire borehole is treated as one source. At the other end of the range are very detailed double packer measurements, in which individual fractures can be studied separately isolating them from rest of the borehole. The cost and required time to conduct measurements varies, and selecting a suitable measurement method requires an understanding of the different measurement techniques. Additionally, understanding the measurement conditions at the study area affects the reasonable usage of the measurement data.

Posiva Flow Log (PFL) devices have been developed for use in boreholes drilled into crystalline bedrock in which the borehole walls are smooth and the collapse of the borehole is not likely. This ensures that rubber disks isolating the target borehole section do

not leak and the flow from a specific borehole section is guided through the flow sensor. Fractures and fractured zones in a borehole naturally cause rubber disks to leak but this is not a problem when the length of a fractured zone along a borehole is shorter than length of the measurement section used, and as long as the measurement interval is short enough. The measurement section length can be tens of meters. Figure 1 shows a PFL tool that is lowered into a borehole.

In any measuring approach, it is very important to know if the measuring affects the measured quantity and how. The existence of groundwater in bedrock fractures and pores can be estimated based on geophysical studies without drilling holes into the bedrock, but an estimation of flow rates in fractures requires steering the actual flow through a flow sensor. Drilling a borehole into the bedrock definitely affects the ground water flow conditions and this has to be taken into account in the modelling. Before drilling a borehole, water flows along fractures and there are usually no large pressure gradients along a fracture. After a borehole has been drilled, the water flow along a fracture is affected by the borehole and large pressure gradients are possible in fractures close to borehole.

After borehole has been drilled, the ground water flow between the borehole and fractures stabilises to a certain level. Alternatively, if flow rates in pumped conditions are needed, the borehole is pumped and flow stabilisation is allowed. These are the flows that can be measured but should not be affected by the measurement device. This is valid for measurement methods that require steady state conditions and the duration of the entire measurement is kept short by maintaining a steady state throughout the entire measurement. If steady state flow condition cannot be maintained while the measurement device is placed into a fracture, some stabilisation time is required at each measurement position to achieve a steady state.



Figure 1. PFL tool with 0.5 m long measurement section. Yellow rubber disks isolate the measurement section.



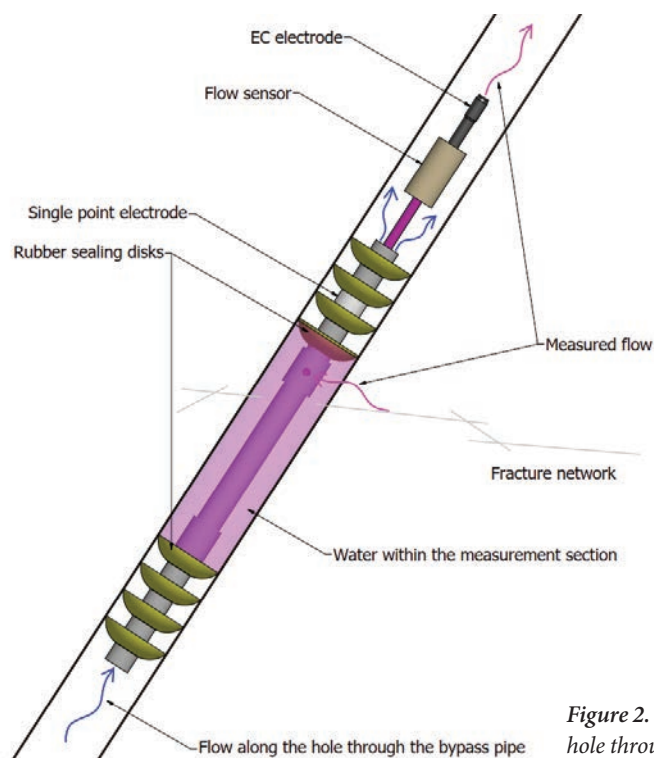


Figure 2. Flow from the bedrock into a borehole through the flow sensor in a PFL probe.

The PFL measurement method has been designed so that it does not affect the water flow from the fracture or the flow in a borehole. Figure 2 illustrates how the flow from a bedrock fracture is guided through the flow sensor in a PFL probe and how the flow in a borehole is steered past the probe. The two flow paths through the PFL measurement tool have been designed so that the flow in the borehole can be quite large, up to 100 L/min, and it does not cause friction that would prevent the water flow in the borehole or cause a pressure difference over the probe. The flow channel from the measurement section over the flow sensor and electrical conductivity electrode is smaller to enable very accurate measurement, and therefore large flows can be affected by the probe. Based on experimentation, flows smaller than 5 l/min through a flow sensor do not result in large flow changes.

One of the key features of the PFL method is the adjustable section length and measurement interval. These two elements determine how accurately an individual fracture's flows are measured and localised in a borehole.

A short section length helps to identify and measure individual fractures' flows: if only one fracture is within the measurement section the measured flow comes from the individual fracture. On the other hand, a short measurement section length and interval increase the measurement time and the possibility of rubber disk leakages in fractured borehole sections.

An example of a measurement that has been conducted with two measurement section lengths is presented in Figure 3. Theoretically, all four fractures can be found and flow rates can be determined based on both measurements, but the spatial accuracy is lower when a longer measurement interval is used. All fractures between consecutive measurement points are treated as one fracture. A longer measurement section length also increases uncertainty in the definition of the flow rate. In this example, the flow rates of fractures at depths of 41.5 m and 44.8 m can be measured directly, but determination of flow rates for fractures at depths of 42.6 m and 43.8 m requires observing changes in the flow curve when a 2 m section length is used.



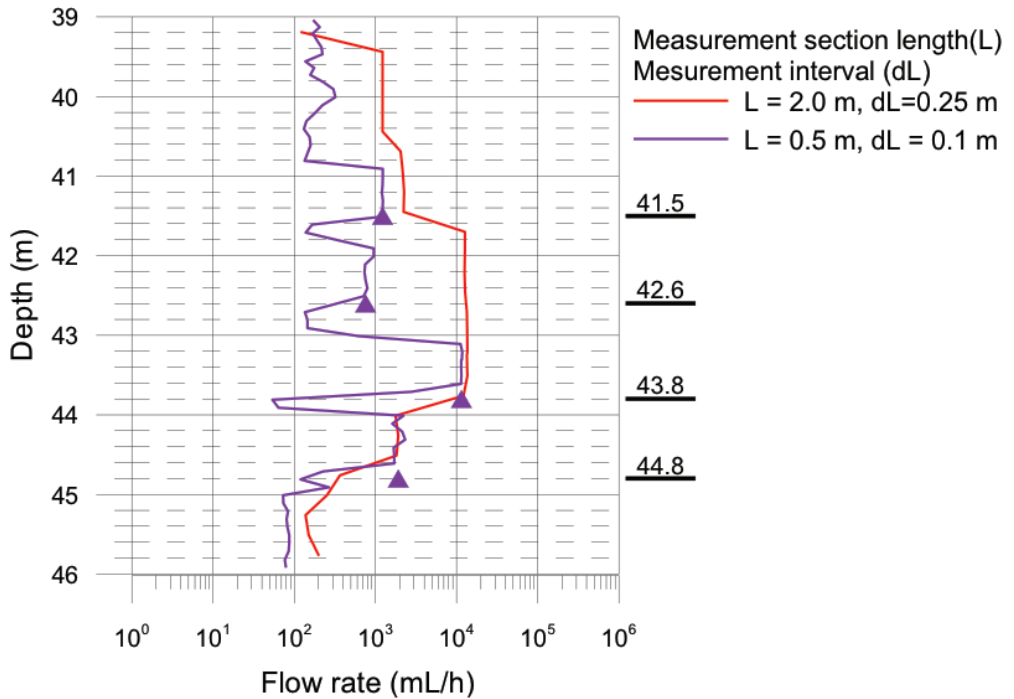


Figure 3. Fracture flows measured with 0.5 m and 2 m measurement section lengths.

When a 0.5 m section length is used, all fracture flows can be measured separately.

In addition to measuring groundwater flows a PFL tool can be equipped with a water sample container to take samples of the water coming from the fracture. The water samples can be taken from fractures without mixing the water with the borehole water. Water sample container can be closed at a fracture and the water pressure can be maintained until the water sample is released from the container in a laboratory.

Monitoring

Once an initial site-specific survey has been performed and construction of underground workings begins, a hydrogeological monitoring programme should be determined. The programme needs to be specified depending on the hydrogeological conditions, assessed effects on groundwater pressure and water table, and possible risk of contamination transport. Typically, hydrogeological monitoring covers both the groundwater table in the soil layer and pressure in the bedrock. Groundwater sampling and analysis are an essential part of conventional monitoring programmes.

Hydrogeological monitoring can be composed of both automatic measurements, which provide continuous time series information on short-term changes, and measurement campaigns. Different kinds of PFL-measurements are suitable for monitoring campaigns, e.g., when information on flow, pressure, or groundwater composition at varying depths are needed.

Parameters for numerical modelling

One modelling parameter that is obtained from PFL measurements is the specific capacity of the fractures ($Q/\Delta h$). This parameter is obtained by measuring fracture flows in two different pressure conditions. Usually, the first measurement run is conducted in non-pumped conditions where the flow rates are usually small. The second measurement run is conducted while the borehole water level is lowered by pumping water out of the borehole. The water level in the borehole is kept stable before and during flow logging in order to maintain steady state conditions. Another way to obtain the specific capacity is to conduct only one measurement run while the water level is lowered and to assume that the flow



rates in the non-pumped conditions are equal to zero. This is reasonable if the flow rates are assumed to be small in non-pumped conditions. If the studied area is flat and there are no underground facilities, large flows under non-pumped conditions should not occur. This is also a matter of accuracy for which the specific capacity needs to be defined. If only a rough estimation is needed, the flow rate in non-pumped conditions can be disregarded and Q can be the flow rate in pumped conditions. For modelling purposes, the specific capacity is usually converted to transmissivity by assuming the flow geometry for the flow coming from the bedrock into the borehole and using Thiem's equation (Marcily 1986). In addition to the transmissivity, the hydraulic head of a fracture can be determined based on flow measurements under two different pressure conditions. This is done assuming a linear dependency between the fracture flow and the borehole pressure and extrapolating a pressure that corresponds to a zero flow rate. Theoretically the calculated pressure should be equal to measured value when the fracture is isolated by double packer. PFL probe can be modified by replacing rubber disks by double packer to measure pressure while fracture flow is zero. This setup is suitable only for measuring individual fractures.

Fractures that can be detected by PFL measurements have to be connected to a water source either directly or through a fracture network. Fractures crossing a borehole can have large transmissivities but if they are not connected to a water source or there is small transmissivity in the fracture network between a borehole and water source large transmissivities will not be detected. This has to be taken into account while using the measurement data in modelling.

Modelling methods

PFL results can be used in hydrogeological models. These models can be parametrised from the hydraulic conductivity data obtained from the PFL measurements. Especially important parameters include the fracture locations and fracture transmissivities. Different models have different requirements for the input data. For example, for the Discrete Fracture Network (DFN) model, accurate fracture locations are beneficial, but if

the model is constructed from cubic blocks the block size determines how accurately the fracture locations are required. The PFL measurement method can be adapted to different requirements.

The Discrete Fracture Network (DFN) model represents that ground water flows mainly occur in fractures in crystalline bedrock (Hartley 2013a). The model assumes that the ground water flows are constrained by the fracture walls and there is no flow between fractures if the fractures do not intersect. The model can be calibrated and tested by simulating actual measurements taken with a PFL device.

The PFL measurement data is a key resource for DFN modelling as individual fracture locations can be determined to a high degree of accuracy and connected to fractures determined from core samples. This makes it possible to assign hydraulic properties for individual fractures. With other measurement methods individual fractures cannot be assigned to single fractures identified from core sample as the hydraulic properties are determined for borehole sections - not for individual fractures. In those cases, either the hydraulic data has to be divided for multiple fractures, or the fractures have to be lumped together for the assignment of hydraulic properties.

The Continuous Porous Media (CPM) model assumes that over a specified volume in crystalline bedrock the ground water flows can be presented homogeneously (Hartley 2013b). Typically, the hydraulic properties of each hydrostratigraphic volume are specified using available measurement data. Another approach is to divide the bedrock into blocks and specify the hydrogeological properties of the blocks. The advantage to this approach is that the location of the measured values can be taken into account more accurately.

Hydraulic interference tests

After a general hydrogeological bedrock characterisation has been made, some specific structures might require more detailed studies. Especially structures that do not fit into a model that assumes a homogeneous porous media might need special attention. Hydraulic interference tests can be performed by causing temporary interference to



a hydrogeological structure or by monitoring changes caused by excavations or similar activities.

A conventional approach to measuring and evaluating changes in hydrogeological structures crossing boreholes is to install multipacker pressure monitoring systems into the boreholes. For small scale testing, this might be a simple and cost effective method, but if the number of observed fractures or borehole sections is large, there are better solutions. Also, if the fractures are close to each other and need to be treated separately, using packers to isolate fractures might not work due to packer dimensions. With the PFL measurement method, flow changes caused by interference can be evaluated for individual fractures. A basic configuration of the test is to measure the fracture flows before interference is initiated, to obtain reference values - and during the interference, to evaluate possible changes in fracture flow rates.

The magnitude of the interference affects the ability to detect flow changes. Therefore, detailed planning is essential. Causing interference in a surface borehole is usually done by isolating a borehole section from the rest of the borehole and changing the pressure by pumping water out of the test section. Theoretically this works well, but depending on fracture properties and other technical details, achieving large pressure changes might be challenging. Causing interference in a borehole that has been drilled from underground workings makes the pumping out of the borehole easier. In a subsurface borehole, isolating a borehole section and letting the water flow out of a section while the rest of the borehole is closed can be considered the same as pumping in a surface borehole.

During both PFL measurements, the entire borehole should be under same the pressure conditions (same water level). Therefore, if a flow change caused by interference is large, the flow change can affect the water level in the borehole and in that way affect the flow rates at other fractures which are not di-

rectly connected to the interfered structure. These two kinds of affects can be separated if the specific transmissivities of the fractures are known and the flow change caused by water level changes can be subtracted from the flow rate.

In a mining environment, there are usually multiple events that can cause changes to fracture flow rates. Therefore, it is beneficial to keep the duration of the test short so that the changes caused by the intended interference can be detected. Another way to make sure that observed flow change has been caused by an intended interference is to position the PFL probe at a fracture and change the interference. This requires more time per fracture than measuring flow rates systematically, but it is an efficient addition to the observation of steady state changes.

Summary

PFL measurements are a useful way to provide hydrogeological data for mine operations throughout the lifecycle of a mine. Conceptualization before operations begin, dewatering during the production phase and post closure monitoring, all require knowledge about water flows in the bedrock. Modelling of the bedrock properties should be done systematically throughout the lifecycle of a mine taking into account the requirements of the different phases.

References

- Marcily G (1986) Quantitive Hydrogeology, Groundwater Hydrology for Engineers. Academic Press, Inc., London.
- Hartley L, Roberts, D (2013a) Summary of discrete fracture network modelling as applied to hydrogeology of the Forsmark and Laxemar sites. SKB R-12-04, Svensk Kärnbränslehantering AB.
- Hartley L, Hoek J, Swan D, Appleyard P, Baxter S, Roberts D, Simpson T (2013b) Hydrogeological Modelling for Assessment of Radionuclide Release Scenarios for the Repository System 2012. Eurajoki, Finland, Posiva Oy, Working Report 2012-42.



Understanding Acid Rock Drainage Risk in the West African Shield

David Love¹, Nico Bezuidenhout², Keretia Lupankwa¹

¹Golder, P O Box 6001 Halfway House, 1685, South Africa, dalove@golder.com

²Golder, 6925 Century Avenue, Suite #100, Mississauga, Ontario, L5N 7K2, Canada

Abstract

The Birimian and Tarkwaian rocks of the Paleoproterozoic West African Shield host some of the most important gold reserves in the world, deposited during successive hydrothermal sulphide alteration events, which were channelled by shear zones and thrusts during the regional Eburnean tectono-thermal deformation event. The hydrothermal fluids were auriferous and sulphide-rich, resulting in two distinct types of mineralisation: (1) Gold-bearing quartz and quartz-ankerite veins, occurring in NNE-SSW trending shear zones or thrust folds, usually in Birimian metasediments, with associated sulphides deposited on the fragmented wall rock. (2) Disseminated gold-bearing pyrite and arsenopyrite, occurring in halos within the same shear zones or thrust folds as the quartz veins.

The sulphidic nature of the gold deposits lead to a high risk of acid rock drainage (ARD). The environmental geochemistry of fourteen mines and deposits in the West African Shield was studied, using a combination of techniques. Weathering profiling, using a model initially developed by Senes, was used to divide rock and saprolite into three weathering zones, distinguishable in borehole core. Mineralogical profiles were used to characterise rock units by the relative abundance of macroscopic sulphide and carbonate minerals. Conventional acid base accounting was also done to provide quantitative acid generation and neutralisation potential. Combined logs were then prepared from these three profiles, showing the geochemical behaviour of the different rock units.

The results of the study show two key drivers of acid rock drainage risk: firstly, the degree of weathering: the Oxide Zone, from which both the acid-generating sulphide minerals and the acid-neutralising carbonate minerals have been largely leached, is non-acid generating. The Transitional Zone, from which the carbonate minerals have been largely leached but the sulphide minerals remain is almost always acid generating. The Fresh Zone, from which neither sulphides nor carbonates have been leached is uncertain and the second key driver of acid rock drainage risk applies: the abundance of acid neutralising carbonate minerals, which varies significantly from deposit to deposit – being at least partially controlled by the host rock mineralogy.

Since the two key drivers relate to the weathering zone classification and the host rock lithological units, this translates to readily-defined blocks and tonnages, giving the opportunity for separation of mine waters of different qualities and the selective handling of waste rock. Given the repeatability of this approach, it is suggested that it can be applied in principle across the West African Shield.

Keywords: Acid rock drainage, West Africa, gold, weathering, sulphide

Introduction

The Birimian and Tarkwaian rocks of the Paleoproterozoic West African Shield host some of the most important gold reserves in the world, deposited during successive hydrothermal sulphide alteration events, which

were channelled by shear zones and thrusts during the regional Eburnean tectono-thermal deformation event. The hydrothermal fluids were auriferous and sulphide-rich, resulting in two distinct types of mineralisation: (1) Gold-bearing quartz and quartz-an-



kerite veins, occurring in NNE-SSW trending shear zones or thrust folds, usually in Birimian metasediments, with associated sulphides deposited on the fragmented wall rock. (2) Disseminated gold-bearing pyrite and arsenopyrite, occurring in halos within the same shear zones or thrust folds as the quartz veins. The sulphidic nature of the gold deposits lead to a high risk of acid rock drainage (ARD).

Methods

The environmental geochemistry of fourteen mines and deposits in the West African Shield was studied, using a combination of techniques. Weathering profiling, using a model initially developed by SENES, was used to divide rock and saprolite into three weathering zones, distinguishable in borehole core. Mineralogical profiles were used to characterise rock units by the relative abundance of macroscopic sulphide and carbonate minerals. Conventional acid base accounting was also done to provide quantitative acid generation and neutralisation potential. Combined logs were then prepared from these three profiles, showing the geochemical behaviour of the different rock units.

Case Studies

Introduction

The West African Precambrian Shield is a tectonic province dominated by two Lower Proterozoic volcano/sedimentary sequences that are important for the occurrence of gold mesothermal mineralization, the Birimian Supergroup and the Tarkwaian Group (Figure 1).

The Birimian, a dominantly marine turbidite series, is composed largely of phyllites, schists, meta-greywackes and, in places, is inter-bedded with meta-volcanic rocks including lavas, and volcanoclastic rocks (Hammond and Tabata, 1997). Non-conformably overlying the Birimian are the continental clastics of the Tarkwaian Group (Oberthür et al., 1997). These clastics were derived from the weathering of Birimian rocks and granitic batholiths (Dampare et al., 2005). The Birimian and Tarkwaian were subjected to regional deformation in the 2.0-2.2 Ga Eburnean orogeny, resulting in major thrusts and shear zones (Blenkinsop et al., 1994; Oberthür et

al., 1997). Birimian rocks are intensely folded (mostly isoclinal) and faulted, whereas the Tarkwaian units display a more broad-scale folding and less tectonic disturbance. Both the Birimian and Tarkwaian display greenschist regional metamorphism, and the mafic dykes have been carbonate-altered (Mumin et al., 1994).

Shear Zone Gold Deposits

The majority of the gold deposits studied (11/14) are hosted on northeast-southwest trending shear zones (Allibone et al., 2002). These shear zones form the boundary between the volcano-sedimentary Birimian belts and the Tarkwaian sedimentary basins. They are a few metres to hundreds of metres wide and display different styles of deformation, probably related to varying competencies of the different rock units. The shear zones are frequently intruded by granitoids and less frequently by mafic (dolerite) to ultramafic dykes.

The hydrothermal gold occurs in quartz-carbonate veins, with large pyrite crystals, minor arsenopyrite at some sites, minor to accessory chalcopyrite and accessory pyrrhotite, galena and sphalerite. The carbonates in the veins are mainly dolomite and ankerite. Beyond the veins, gold-bearing pyrite and arsenopyrite crystals occur disseminated in halos around the shear zone.

Thrust Fold and Placer Gold Deposits

The Banket series of the Tarkwaian Group host the remaining deposits (3/14). The Bankets comprise quartz pebble conglomerates of the Tarkwaian Group, and carry detrital gold, magnetite and haematite (Oberthür et al., 1997). They were formed as alluvial fan deposits with braided stream channels reworking the fans. The braided rivers concentrated gold particles within the coarse, high-energy channel conglomerates. The sediments were ultimately derived from the erosion of Birimian rocks. The Eburnean orogeny resulted in major thrust folds (Blenkinsop et al., 1994), which have folded the Banket series in mainly north-south trending, northwards plunging synclines and anticlines, with the reefs often thickened in the fold noses.

The Bankets are dominated by oxide and silicate minerals, with few sulphides present.



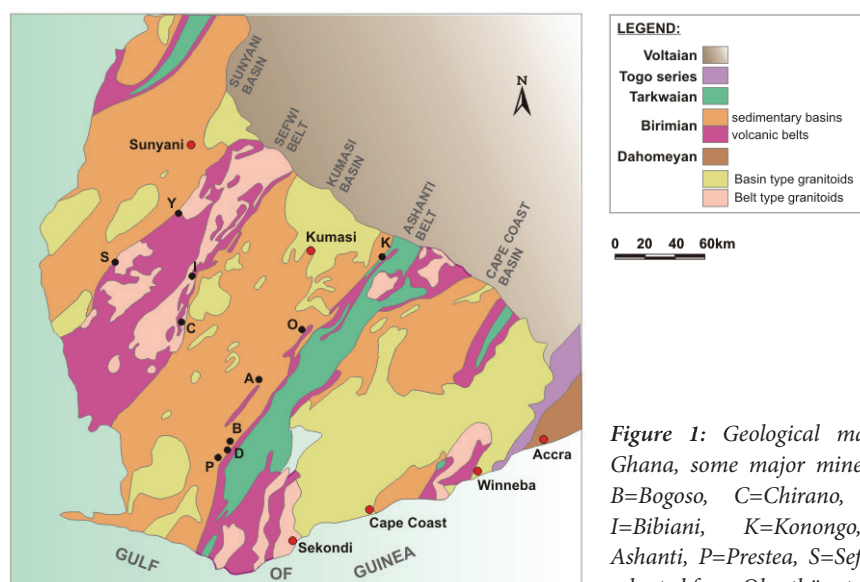


Figure 1: Geological map of Western Ghana, some major mines: A=Ayanfuri, B=Bogoso, C=Chirano, D= Dumasi, I=Bibiani, K=Konongo, O=Obuasi-Ashanti, P=Prestea, S=Sefwi, Y=Yameo), adapted from Oberthür et al. (1997)

The same applies to the thrust folds, where sulphides have been removed by silicification during folding.

Geochemical Model

Weathering zones

SENES (1999) proposed a weathering model for the environmental mineralogy of a Ghanaian gold deposit, and this has proved quite robust and have been adapted through observations from other sites over the years:

- The upper oxide zone comprises a 40 to 200 m thick heavily weathered zone, comprising an uppermost layer of either clay or laterite, and a thick saprolite layer. Typically, all carbonate and sulphide minerals have been leached from both zones. The rocks are heavily oxidised, with frequent iron oxide alteration, and is typically non-acid generating, due to the absence of both sulphide minerals and carbonate minerals. Where the uppermost layer is laterite, a mottled zone often forms at the base of the laterite, where metals and semimetals leached out of the laterite are concentrated. This can lead to quite high concentrations, but the elements are typically in oxide form and with low solubility.
- The transition facies is 5 to 20 m thick weathered rock, from which carbonate minerals have been removed by dissolu-

tion weathering. Sulphide minerals are still present and unoxidised. This is typically acid-generating, due to the presence of sulphide minerals and absence of carbonate minerals.

- Below the transition facies is the fresh facies, where both sulphide and carbonate minerals have not been oxidised and leached out. This may be acid-generating or not, depending upon the balance between sulphide minerals and carbonate minerals.

This model is summarised in Figure 2.

Acid base accounting

Putting together the acid base accounting data for the fourteen deposits, by comparing the sulphur content of the rock materials (which shows the potential to generate acid) and the neutralisation potential ratio (which shows the balance between acid-generating minerals and acid-neutralising minerals) showed a number of trends – Figure 3.

The oxide rocks are almost entirely non-acid generating, largely due to the absence of sulphide minerals. The fresh rocks have variable sulphide content, often quite high, but over half of such materials have sufficient acid-neutralising material (mainly carbonates) to balance the acid generation. Much, but not all, of the transition material, is acid-generating,



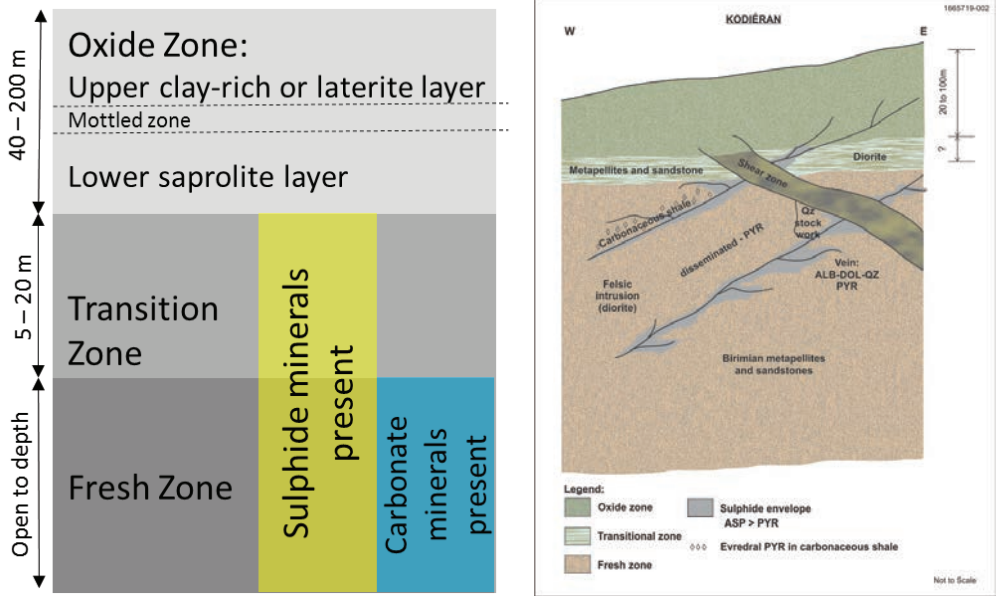


Figure 2: Summary of the weathering and acid rock drainage generation model of West African gold deposits: (left) conceptual overview, (right) example showing shear zone and mineralogy

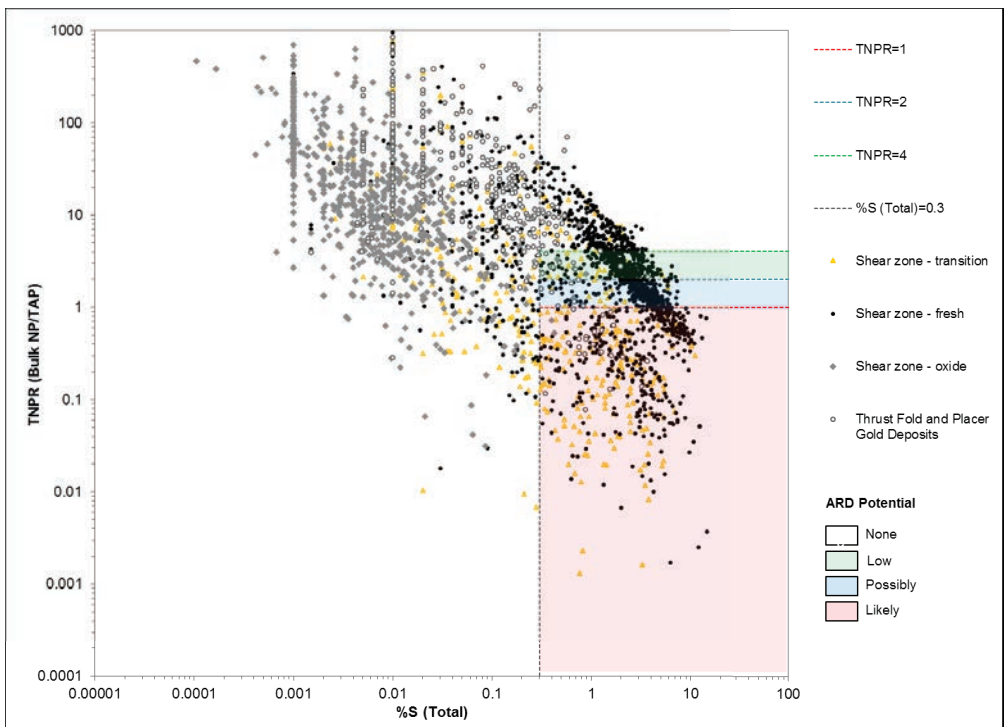


Figure 3: Acid rock drainage generation potential of West African gold deposits, classification from Price et al. (1997) and Soregaroli and Lawrence (1997)



with moderate to high sulphide content which is not balanced by neutralising minerals.

The thrust fold and placer deposits, being dominated by silicate mineralogy, are mainly non-acid generating.

Combined logs

An example of a combined log is shown in Figure 4. The preponderance of acid-generating material in the transition zone is clear. In Figure 5, at a second site, it can be seen that the acid-generating material occurs mainly within a specific depth band.

Discussion

The results of the study show two key drivers of acid rock drainage risk: firstly, the degree of weathering: the Oxide Zone, from which both the acid-generating sulphide minerals and the acid-neutralising carbonate minerals have been largely leached, is non-acid generating. The Transitional Zone, from which the

carbonate minerals have been largely leached but the sulphide minerals remain is almost always acid generating. The Fresh Zone, from which neither sulphides nor carbonates have been leached is uncertain and the second key driver of acid rock drainage risk applies: the abundance of acid neutralising carbonate minerals, which varies significantly from deposit to deposit – being at least partially controlled by the host rock mineralogy.

Conclusions

Since the two key drivers relate to the weathering zone classification and the host rock lithological units, this translates to readily-defined blocks and tonnages, giving the opportunity for separation of mine waters of different qualities and the selective handling of waste rock. Given the repeatability of this approach, it is suggested that it can be applied in principle across the West African Shield.

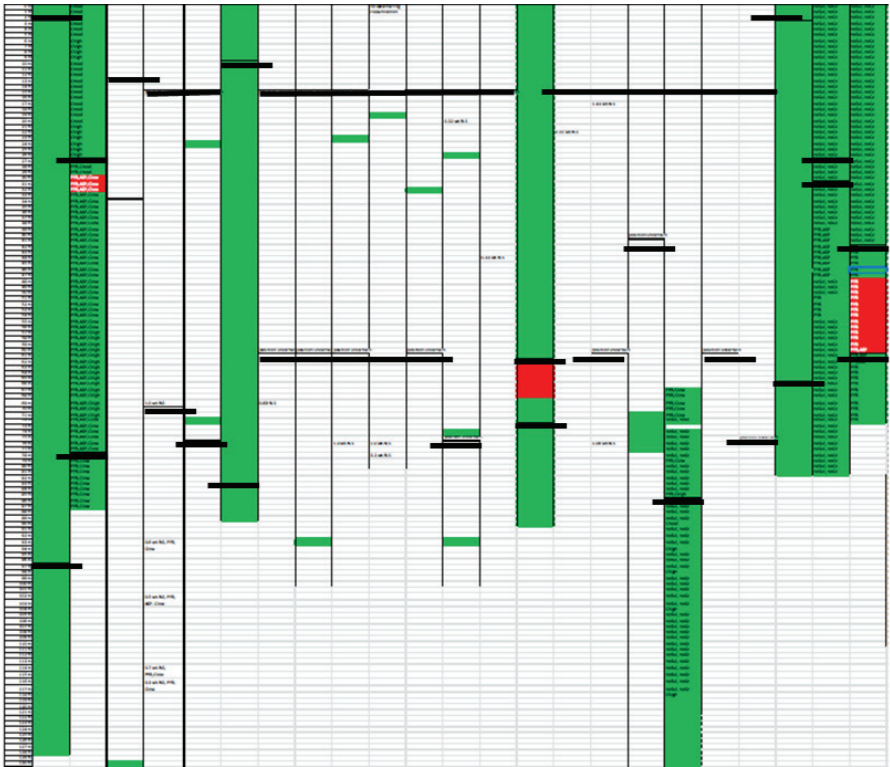


Figure 4: Example of twenty-three combined logs for a site, with observations arranged by depth (y-axis), thick black lines showing top and bottom of transition zone, red for acid-generating material and green for non-acid generating material



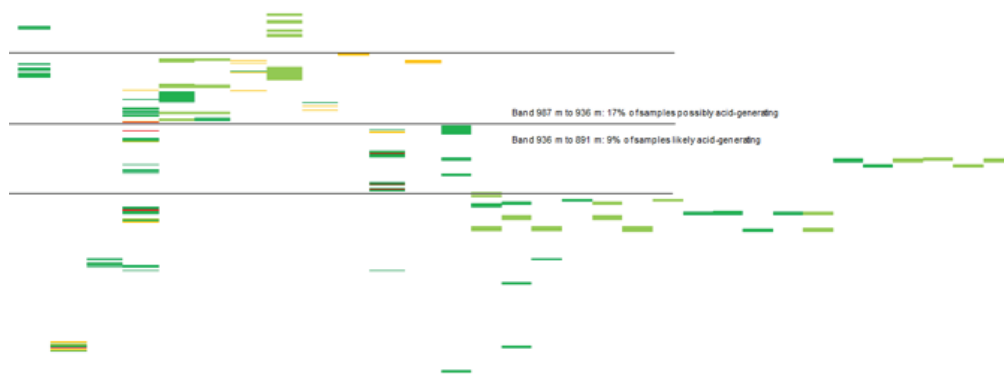


Figure 5: Example of thirty-one combined logs for a site, showing the occurrence of acid-generating material in a band, thick black lines showing top and bottom of transition zone, red for acid-generating material and green for non-acid generating material

Acknowledgements

The authors thank Abosso Goldfields Ltd, Golden Star Bogoso/Prestea Ltd, Golden Star Resources Ltd, Goldfields Ghana Ltd, Kinross Chirano Goldfields Ltd, Newmont Goldfields Ghana Ltd and Societe de Minies de Madiana S.A. Guinea.

References

- Allibone A, Teasdale J, Cameron G, Etheridge M, Uttley P, Soboh A, Appiah-Kubi J, Adamu A, Arthur R, Mampmhey J, Odoo B, Zuta J, Tsikata A, Pataye F, Famiyeh S, Lamb E (2002). Timing and structural controls on gold mineralisation at the Bogoso Gold Mine, Ghana, West Africa. *Economic Geology*, 97: 949-969.
- Blenkinsop T, Schmidt Mumm A, Kumi R, Sangmor S (1994). Structural geology of the Ashanti gold mine. *Metallogenesis of selected gold deposits in Africa*. *Geologisches Jahrbuch D*, 100: 131-153.
- Dampare S, Shibata T, Asiedu D, Osae S (2005). Major element geochemistry of Proterozoic Prince's Town granitoid from the southern Ashanti volcanic belt, Ghana. *Earth Science Reports*, 12: 15-30.
- Hammond NQ, Tabata H (1997). Characteristics of ore minerals associated with gold at the Prestea mine, Ghana. *Mineralogical Magazine*, 61: 879-894.
- Manu J, Asiedu DK, Anani CY (2012). Geochemistry of Birimian phyllites from the Obuasi and Prestea Mines, Southwestern Ghana: Implications for provenance and source-area weathering. *International Journal of Basic and Applied Sciences*, 2: 12-19.
- Mumin AH, Fleet ME, Chrysosoulis SL (1994). Gold mineralization in As-rich mesothermal gold ores of the Bogoso-Prestea mining district of the Ashanti Gold Belt, Ghana: remobilization of "invisible" gold. *Mineralium Deposita*, 29: 445-460.
- Oberthür T, Weiser T, Amanor JA, Chrysosoulis SL (1997). Mineralogical setting and distribution of gold in quartz veins and sulphide ores of the Ashanti mine and other deposits in the Ashanti belt of Ghana: genetic implications. *Mineralium Deposita*, 32: 2-15.
- Price WA, Morin K, Hutt N (1997). Guidelines for prediction of acid rock drainage and metal leaching for mines in British Columbia: Part II. Recommended procedures for static and kinetic tests. In: *Proceedings of the Fourth International Conference on Acid Rock Drainage*. Vancouver, B.C. Canada, 1: 15-30.
- SENES (1999). *Acid Rock Drainage Assessment for Bogoso Gold Mine, Ghana*. SENES Consultants Limited, 211pp.
- Soregaroli BA, Lawrence RW (1997). *Waste Rock Characterization at Dublin Gulch: A Case Study*. *Proceedings of the Fourth International Conference on Acid Rock Drainage*, Vancouver, B.C. Canada, p631-645.



Permeable Reactive Barrier Feasibility Assessment at Goldcorp's Red Lake Gold Mines: Delineation of Groundwater Flow Paths and Contaminant Behaviour ©

A.J. Martin¹, J. Helsen¹, T. Crozier², G. Parent², D. Paszkowski², C. Mendoza²,
H. Provost², C. Gaspar³, and J. Russell³

¹Lorax Environmental Services Ltd., 2289 Burrard St., Vancouver, Canada

²BGC Engineering Inc., 980 Howe St, Vancouver, Canada

³Goldcorp Red Lake Gold Mines, Balmertown, Canada

Abstract

At the Campbell Complex (Ontario, Canada), Goldcorp is assessing the feasibility of using permeable reactive barriers (PRBs) to intercept and treat tailings-related seepage, with As, Co and Fe representing the primary parameters of concern. Based on the distribution of hydraulic conductivity and geochemical species, most of the seepage is inferred to flow through a discontinuously confined sand and gravel aquifer. Arsenic shows a strong degree of attenuation in groundwater. In contrast, Co exhibits strongly conservative behaviour that can be linked to the presence of non-labile complexes. Dissolved Fe shows variable behaviour that is likely linked to variations in redox conditions. Implications for PRB design are discussed.

Keywords: Groundwater remediation, arsenic, cobalt, iron

Introduction

The Campbell Complex (Goldcorp's Red Lake Gold Mines) is located in Balmertown, 7 km northeast of the Town of Red Lake in northwestern Ontario, and has been the site of gold-ore mining and milling operations since 1949. Tailings have been discharged to the current tailings management area (TMA) since 1983. Mineral processing wastes within the TMA consist of: 1) flotation tailings (1983-present); 2) calcine tailings produced through roasting of sulfide concentrates (pre-1991); and 3) autoclave wastes generated through pressure oxidation and neutralization of sulfide concentrates (1991-present).

A portion of the water that accumulates in the TMA infiltrates into the subsurface and travels along groundwater flow paths that discharge to ditches draining a golf course, which in turn feed a downstream wetland and lake (pathway designated as "Red Lake Flow Path") (Figure 1). Seepage flows show tailings-related signatures related to mill process waters (SO₄, Cl, NH₃, CN, Cd, Co, Cu, Ni

and Zn) and remobilization from tailings solids (Fe and As). As, Co and Fe represent the primary parameters of concern in groundwater given the magnitude of concentrations in relation to site-specific groundwater targets. Seepage waters are characterized by circum-neutral to slightly basic pH (7 < pH < 8.5).

To reduce the degradation of the aquifer and minimize the potential for adverse effects to aquatic receptors in the downstream wetland and lake, Goldcorp is assessing the feasibility of using PRBs (Blowes et al., 2000) to intercept and treat TMA-derived seepage. This paper, which describes TMA plume distribution and contaminant behaviour, represents the first of a series of three papers relating to PRB feasibility at the Campbell Complex. The other two papers, also presented as part of these proceedings, describe the results of tracer testwork designed to confirm contaminant pathways (Helsen et al., 2018) as well as hydrogeological, geochemical and geotechnical considerations driving PRB design (Crozier et al., 2018).



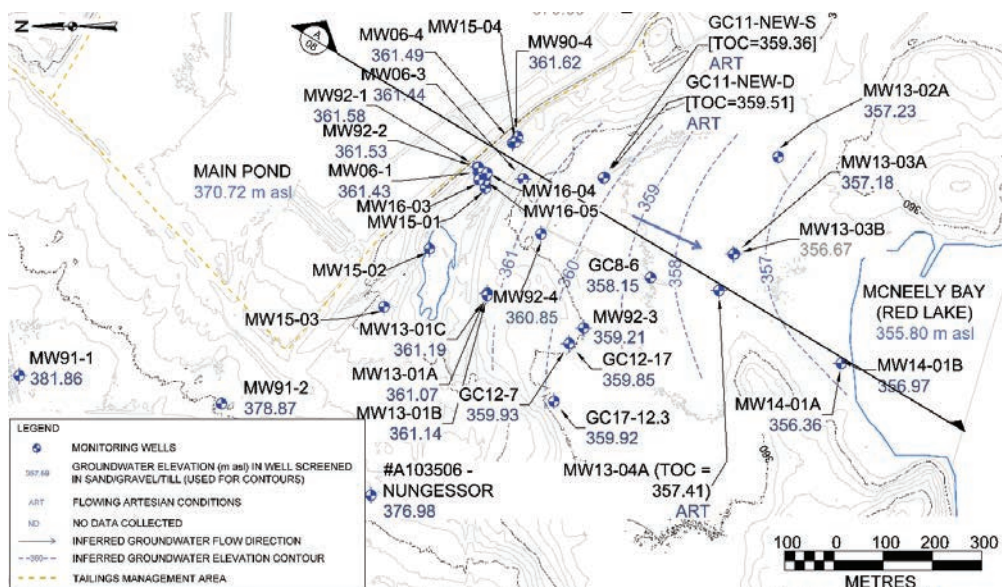


Figure 1 Inferred groundwater elevation contours along Red Lake Flow Path. Locations of monitoring wells, plume flow direction, and Cross Section A indicated (May 2017 water levels shown).

Results and Discussion

Physical Hydrogeology

The physical hydrogeologic conditions along the Red Lake Flow Path have been evaluated in detail since 1990 through the installation, hydraulic conductivity (K) testing and monitoring of multiple monitoring wells. The current program includes the collection of water levels and water samples from wells that span multiple locations and depths along the Red Lake Flow Path (Figure 1).

The hydrostratigraphy of the Red Lake Flow Path can be broadly described as a leaky sand and gravel aquifer, overlain by a discontinuous confining clay and clayey-silt, underlain by a discontinuous sandy to gravelly till, and confined at depth by bedrock (Figure 2). Hydraulic conductivities (K) and thicknesses of the various units are presented in Table 1. K values were determined through slug testing. Recharge enters the groundwater system from two main source areas: 1) the TMA Main Pond, either through the peat and silt layers or through stratigraphic windows in these layers inferred by others (e.g., Ross 1998); and 2) from infiltration of precipitation, snowmelt, and runoff downgradient of the Main Pond. Based on the distribution of measured hydraulic conductivities and geo-

chemical species, most of the TMA seepage is inferred to flow through the sand and gravel, and, to a lesser extent, the till.

Water elevations of the Main Pond (≈ 370 m asl) and McNeely Bay (Red Lake) (≈ 356 m asl) act as gradient controls on the Red Lake flow path. The horizontal hydraulic gradient within the sand and gravel aquifer ranges between 0.001 and 0.01 (average of 0.007), with groundwater flow directed southwest, from the TMA towards Red lake. Groundwater levels in monitoring wells completed along the Red Lake Flow Path fluctuate seasonally by approximately 0.1 m to 2.5 m.

Chemical Hydrogeology

The distribution of the TMA-related plume was evaluated through the generation of 2-D contour maps (Figure 3). These were generated by hand using data collected between August and December, 2016. At locations where nested wells were installed in two or more stratigraphic units (e.g., sand+gravel, clay+silt, etc.), the highest concentration at a given site was selected for contouring. Tracers of TMA seepage (Cl and SO_4) show maximum concentrations in deeper portions of the sand and gravel aquifer and till zones. Elevated concentrations of Cl and SO_4 are evident at



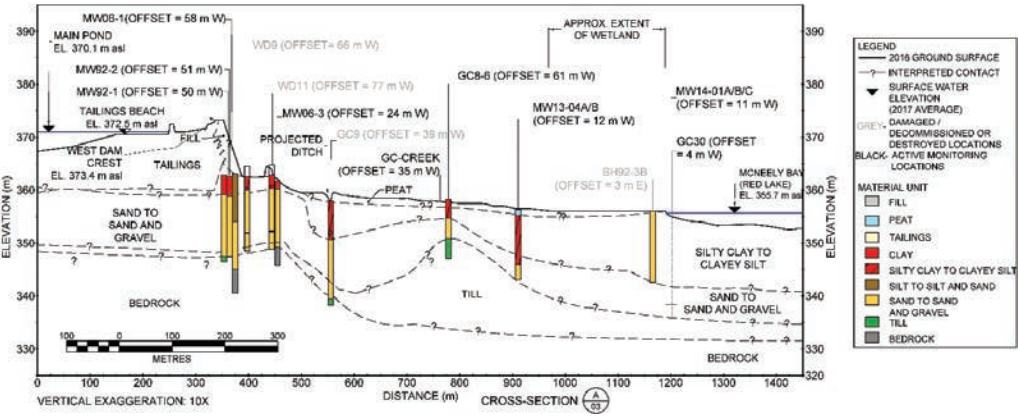


Figure 2 Stratigraphic Cross Section A along Red Lake Flow Path (as shown in Figure 1)

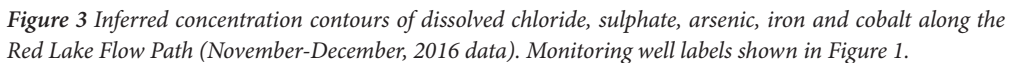
Table 1. Stratigraphy and hydraulic parameters of the groundwater system along Red Lake Flow Path.

Stratigraphic Unit	Location and Description	Thickness (m)	Hydraulic Conductivity (K) (m/s)
Peat	Peat interpreted to be present in undisturbed areas along the Red Lake Flow Path	0 to 1	1×10^{-5}
[Glacio-Lacustrine] Clay and Silt	Mainly low- to high-plastic clay with some low/non-plastic silt intervals, particularly encountered at the base of the deposit, and less frequently at the top of the deposit.	3 to 5	1×10^{-8} to 5×10^{-7}
[Glacial Outwash] Sand and gravel	Overall fining-upwards sequence, grading from a well-graded sand and/or gravel at depth to a silty and poorly sorted sand, in some places interbedded with silt, in the upper portion of the deposit.	8 to 11	1×10^{-7} to 3×10^{-3}
[Glacial] Till	Mainly sands of varying coarseness, gravel, cobbles and occasional boulders, within a matrix of fine silts and sands.	2 to 3	1×10^{-8} to 1×10^{-4}
Bedrock	Moderately weathered to fresh mafic volcanic. Undulating, and present at depths between 16 and 19 m below ground surface	Not Applicable	5×10^{-9} to 2×10^{-7}

the most downstream monitoring wells, illustrating that the influence of the TMA seepage plume extends to Red Lake (Figure 3). At the most downstream well (MW14-01A), the 2017 concentration of chloride (181 mg/L) is 35% of the concentration observed in the Main Pond of the TMA (2017 median = 518 mg/L), reflecting some dilution of the Main Pond signature. Using chloride as an indicator of plume distribution, the cross-sectional area of the plume along the West Dam alignment extends for over 200 m in width, and a depth defined by the thickness of the sand-gravel aquifer (9-15 m).

Based on comparison to site-specific groundwater targets, As, Co and Fe represent the primary parameters of concern for groundwater management along the Red Lake Flow Path. Secondary parameters of concern include SO_4 , Cd, Cu, Ni, Zn and NH_3 , given the elevated concentrations of these parameters in the Main Pond. All the primary and secondary parameters of concern listed (except for NH_3) are amenable to PRB treatment using a common design (USEPA 2005). The main source of tailings-derived Fe originates from the reductive dissolution of Fe(III)-oxide tailings materials in suboxic





The reductive dissolution of As-bearing Fe oxides is the principle source of As within tailings materials, as described by McCreadie et al. (1996) and Martin et al. (2002). Along the West Dam in wells screened in the sand and gravel aquifer (e.g., MW92-1), there is clear evidence of As enrichment (1 to 2 mg/L) (Figure 3). In contrast, further downgradient

at MW06-3 (≈ 150 m downgradient of the West Dam), dissolved As concentrations are low and within background ranges (0.005 to 0.015 mg/L). Overall, the low As values at the intermediate and downstream portions of the plume indicate that As is strongly attenuated along the groundwater flow path within close proximity to the West Dam. Attenuation mechanisms may include: 1) precipitation as secondary sulfides in zones of SO_4 reduction in upgradient portions of the plume that migrate through peat; 2) adsorption to clay minerals; 3) sorption of As with Fe oxides in aerobic zones. Of these, the precipitation of secondary As-sulfides is supported by the occurrence of As removal from solution in zones of sulfate reduction (the latter inferred by measurements of dissolved H_2S and $\delta 34\text{S}$) (McCreadie et al. 1996).

In contrast to Fe and As, the bulk of the Co in TMA seepage originates from mill process waters that are discharged to the Main Pond (Figure 1). Within the conductive sand and gravel aquifer in proximity to the West Dam (e.g., MW92-1), concentrations range from 0.10 to 0.20 mg/L (Figure 3). Downgradient of the West Dam, dissolved Co concentrations show a progressive decline to values of approximately 0.06 mg/L at MW14-01A (at Red Lake). However, the persistence of elevated Co concentrations along the Red Lake Flow Path all the way to Red Lake indicate that Co is behaving in a more conservative manner than As.

Cobalt Speciation

To further the understanding of Co behaviour along the Red Lake Flow Path, and to provide information in support of closure planning, Co speciation analysis was conducted on groundwater samples collected between the TMA and Red Lake. Speciation analysis was conducted using diffusive gradients in thin films (DGT) (methods described in Davison and Zhang, 1994). DGT is a diffusion-based method that measures free Co ions (Co^{2+}) and kinetically-labile Co complexes which exhibit dissociation kinetics within the timeframe of their transport

through a diffusive gel layer (on the order of minutes), thus providing a proxy for the labile metal fraction (Martin and Goldblatt, 2007). The method excludes particles, colloids and strongly-bound complexes.

The results for groundwater samples collected along the Red Lake Flow Path show that the vast proportion ($\approx 90\%$) of Co in the groundwater system is present as non-labile Co complexes (Figure 4). These speciation results can explain the conservative nature of Co behaviour within the groundwater/surface water system, as well as poor removal of Co observed in PRB lab column experiments (data not shown).

The specific nature of the Co complexes present along the Red Lake Flow Path cannot be ascertained with the available data. Possible species may include Co-cyanide complexes and/or Co-organic complexes (associated with the addition of carbon-based flotation reagents used in ore processing). The strong positive correlation of dissolved Co with T-CN ($r^2=0.95$) may indicate the importance of Co-CN complexes (Figure 4).

Conclusions

Overall, robust delineation of seepage flow paths and contaminant behaviour is critical to the design of groundwater remediation measures. In this regard, multiple studies were required to define the hydrostratigraphy, unit thicknesses, spatial variability in K, hydraulic gradients, groundwater velocities, contaminants of concern and contaminant behaviour. This field-based information, combined with lab-scale testwork, formed the basis for PRB design with regards to location, dimensions, hydraulic retention time, and reactive matrix (as presented in Crozier et al., 2018).

Acknowledgements

Goldcorp Canada is acknowledged for allowing the presentation of the data and discussion herein. The authors also thank two anonymous reviewers whose input greatly improved the quality of the manuscript. Thanks is also given to G. Morris (Lorax) for figure preparation.



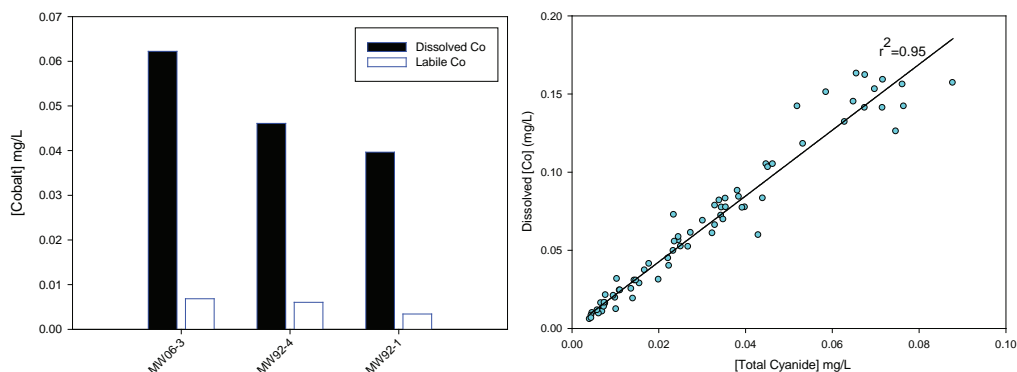


Figure 4 (Left) Concentrations of dissolved Co and labile Co (as determined by diffusive gradients in thin films) for samples at various monitoring wells along the Red Lake Flow Path (2017 data). (Right) Regression plot showing dissolved Co versus total cyanide (2017 data for groundwater wells and surface waters along Red Lake Flow Path).

References

- Blowes DW, Ptacek C, Benner SG, McRae CWT, Bennett TA, Puls RW (2000) Treatment of inorganic contaminants using permeable reactive barriers. *J Contam Hydrol* 45: 123-137.
- Crozier TW, Paszkowski D, Parent G, Cook D, Mann V, Mendoza C, Provost H, Martin AJ, Helsen J, Bain J, Blowes DW, Gaspar C, Russell J (2018) Permeable Reactive Barrier Feasibility Assessment at Goldcorp's Red Lake Gold Mines: Hydrogeological, Geochemical and Geotechnical Design Considerations, 11th International Conference on Acid Rock Drainage, Pretoria, South Africa, September 10-14, 2018.
- Davison W, Zhang H (1994). In situ speciation measurements of trace components in natural waters using thin-film gels. *Nature* 367:545-548.
- Helsen J, Martin AJ, Crozier T, Parent G, Mann V, Gaspar C., Russell J (2018) Permeable Reactive Barrier Feasibility Assessment at Goldcorp's Red Lake Gold Mines: Validation of Seepage Flow Paths through Tracer Testwork., 11th International Conference on Acid Rock Drainage, Pretoria, South Africa, September 10-14, 2018.
- Martin AJ, Pedersen TF (2002) Seasonal and interannual mobility of arsenic in a lake impacted by metal-mining. *Env Sci Tech* 36:1516-1523.
- Martin AJ, Goldblatt R. (2007). Speciation, behaviour and bioavailability of copper downstream of a mine-impacted lake. *Environ Toxicol Chem* 26: 2594-2603.
- McCreadie H, Blowes DW, Ptacek C, Jambor JL (2000) Influence of reduction reactions and solid-phase composition on porewater concentrations of arsenic. *Env Sci Tech* 34:3159-3166.
- Ross C (1998) A Hydrogeological and Geochemical Study of a Gold Mine Tailings-Derived Plume, Campbell Mine, Balmertown Ontario. M.Sc. Thesis, University of Waterloo.
- USEPA (2005). Permeable Reactive Barriers for Inorganic and Radionuclide Contamination. Prepared by K. Bronstein for the U.S. Environmental Protection Agency, August, 2005.



Geologic and mineralogical implications for element and isotope signatures in the Wiśniówka acid mine drainage waters (south-central Poland)

Zdzisław M. Migaszewski, Agnieszka Gałuszka

Jan Kochanowski University in Kielce, 15G Świętokrzyska St, 25-406 Kielce, Poland;

e-mail: zmig@ujk.edu.pl, aggie@ujk.edu.pl

Abstract

Hydrogeochemistry of Wiśniówka AMD area (south-central Poland) correlates with geology and mineralogy of Upper Cambrian (Furongian) quartzite-shale rock series. The lowermost part of this geologic section contains enormous amounts of pyrite, which is unusual in sedimentary rock mining. Moreover, this pyrite shows specific mineralogical characteristics (predominance of microscopic grains, framboids, As-banded microtextures) and negative sulfur isotope signatures. Another feature is a lack of effective-buffering minerals except for less reactive clay minerals. Additionally, the shale interbeds are commonly enriched with REE-rich aluminophosphate/phosphate minerals. Specific element and isotope signatures of rocks and waters were used to solve different geologic and environmental issues.

Keywords: pyrite, REE minerals, element signatures, stable sulfur isotopes

Introduction

Mineral and rock mining operations leave waste rock, tailings piles, settling ponds, tailings pools/seeps, acid pit ponds and lakes that may severely impact the environment. Of different active and abandoned mining areas, AMD sites are among the most hazardous ones jeopardizing different environmental compartments and human health (e.g. Plumlee 1999; Simón et al. 2001; Nordstrom 2011; Plumlee, Morman 2011; Kossoff et al. 2014; Brown et al. 2017). The main natural process of concern is the oxidation of pyrite and occasionally other Fe-bearing sulfide minerals leading to generation of sulfuric acid and various ochreous precipitates combined with a release of deleterious metal(loid)s. Pyrite is a ubiquitous mineral in massive sulfide ore and coal deposits (e.g. Plumlee 1999; Alpers et al. 2003) or mineralized rock formations (Reichenbach 1993; Migaszewski et al. 2016, 2018ab).

The element composition of AMD water bodies correlates with the local/regional geologic setting and mineral composition. However, the original element concentration patterns undergo changes as a result of geochemical processes commonly induced and

catalyzed by microbial activity. The knowledge of different geologic, mineralogical and geochemical aspects provides both critical information on potential AMD hazards and proxies for reconstruction of paleoenvironmental conditions. The principal objective of this and previous studies (e.g. Migaszewski et al. 2009, 2014, 2016, 2018ab) was to elucidate variations in concentration patterns of metal(loid)s and rare earth elements (REE; La through Lu) in AMD waters and stable sulfur isotope ratios in pyrite and dissolved sulfates of the Wiśniówka mining area in the context of lithologic and mineralogical characterization of regional Upper Cambrian rock series.

Study area

The Wiśniówka AMD area is located within the western part of the Cambrian Main Range (Holy Cross Mountains), about 5 km north of the provincial capital city of Kielce (south-central Poland). The Main Range lies in the immediate proximity of the nearly parallel Holy Cross Fault (HC Thrust) that separates two tectonic units (terrane)s: the Łysogóry Block from the Małopolska Block (fig. 1A). The study area includes the Upper Cambrian (Furongian) section composed of alternating



quartzite/quartzitic sandstone and clayey-silty shale beds, locally with thin bentonite and tuffite layers. Tectonic setting is very complex, which is evidenced by the presence of numerous folds, slices and faults offsetting the original rock bedding (Żylińska et al. 2006 and references therein). This geologic complexity is the cause of dismembered topography of the Wiśniówka massif. In contrast to the remaining regional Cambrian formations, this site is highlighted by the occurrence of two pyrite mineralization zones of different age: the oldest (lowermost Upper Cambrian) cropping out in the Podwiśniówka quarry and the youngest (middle Upper Cambrian) exposed in the Wiśniówka Duża quarry (Migaszewski et al. 2016, 2018ab).

The principal raw material is quartzite/quartzitic sandstone that has been extracted for manufacturing of crushed aggregates. The over century lasting strip mining has left numerous tailings piles and acid water bodies of diverse geochemistry. Complex studies have been conducted in this mining area for a decade. These encompassed different aspects of mineralogy, isotope geochemistry and hydrogeochemistry in abandoned quarries and historic mine waste heaps (e.g. Migaszewski et al. 2009, 2016, 2018ab). The situation has

worsened after quarrying for quartzite in the Podwiśniówka stone pit during 2013–2014. As a result of quartzite extraction a broad pyrite mineralization zone was exposed. The lowest mining bench was filled up with acid water forming a new lake (fig. 1B). In addition, to make it worse, the mine wastes were piled over a vast mining area giving rise to formation of strongly acidic seeps and pools. Another, although less dramatic threat to the environment, was posed by deeper quartzite extraction in the Wiśniówka Duża quarry. As a result of this 2017-mining operation a lake formed reaching 4 ha in area (fig. 1C). This situation gave us an opportunity to begin a new study of AMD waters and rocks employing advanced geochemical and mineralogical methods.

Methods

Fieldwork included collection of 40 rock samples from the Podwiśniówka and Wiśniówka Duża outcrops and additionally water samples from the neighboring AMD lakes. The latter were sampled in 8 series during 2016–2017. For the purpose of this study, fieldwork also included direct measurements of pH, electric conductivity (EC) and temperature (T) of water, using a manual micro-processor pH/Eh-meter SP300 and EC-meter

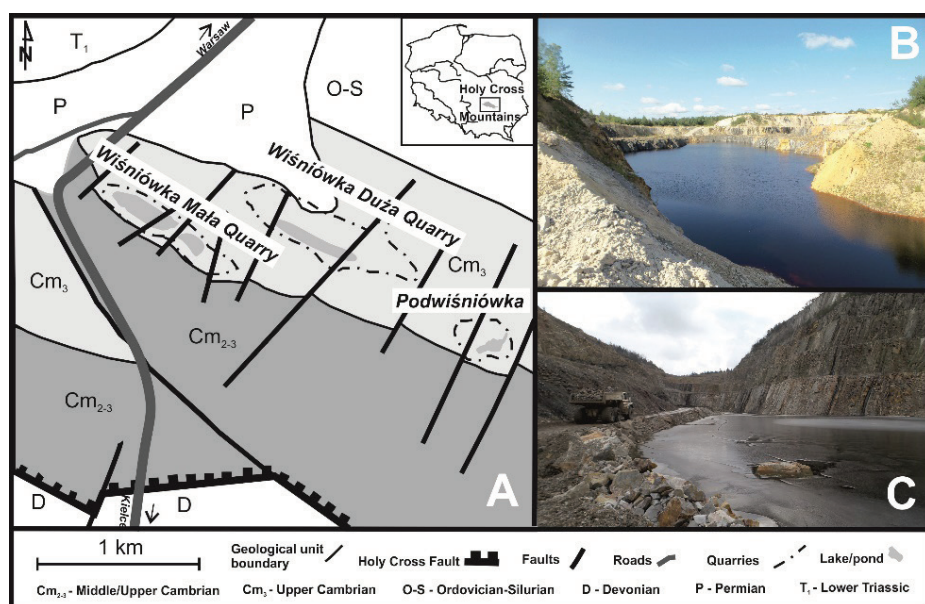


Figure 1 (A) Geologic sketch map of Wiśniówka mining area (Żylińska et al. 2006 modified by the authors) with a view of (B) Podwiśniówka and (C) Wiśniówka Duża acid pit lakes.



SC300 (both Slandi, Poland). Besides, concentrations of dissolved SO_4^{2-} and PO_4^{3-} were determined using a field spectrophotometer LF-300 (Slandi, Poland).

Trace element determinations in rocks and waters were made using an inductively coupled plasma-mass spectrometer (ICP-MS; model ELAN DRC II, Perkin Elmer). The stable S isotope determination in pyrite and dissolved sulfates was performed off-line on a dual inlet and triple collector isotope ratio modified mass spectrometer MI-1305 equipped with modified inlet and detection systems on SO_2 gas. The isotope analysis was performed at the Mass Spectrometry Laboratory, Maria Curie-Skłodowska University in Lublin (Poland).

The principal objective of petrographic and mineralogical examinations was to find mineral phases responsible for geochemistry of nearby AMD water bodies. These included optical microscopy (Leica M205 A and Nikon LV 100 Pol), scanning electron microscopy combined with energy dispersion spectrometry (SEM-EDS; model LEO 1430, Carl Zeiss

Jena) and electron microprobe (EMP; model Cameca SX-100). The SEM-EDS and EMP studies were performed at the Microanalysis Laboratory, Polish Geological Institute-National Research Institute in Warsaw.

Mineralogy and geochemistry of bedrock

Most of the Podwiśniówka beds comprise enormous amounts of pyrite which is a predominant sulfide mineral in the study area. The other sulfides (e.g. galena, sphalerite, chalcopyrite, chalcocite, tetrahedrite) are extremely scarce forming tiny endomorphs several micrometers across. Pyrite usually occurs in the form of microscopic grains and framboids averaging 0.00X–0.X mm in diameter (fig. 2A). Most of the Podwiśniówka pyrite grains show a zonal microtexture composed of alternating As-rich (up to 8.2%) and As-depleted bands (fig. 2B). Another distinctive feature of the Wiśniówka bedrock is a lack of effective acid-buffering gangue and rock-forming minerals except for low-buffering

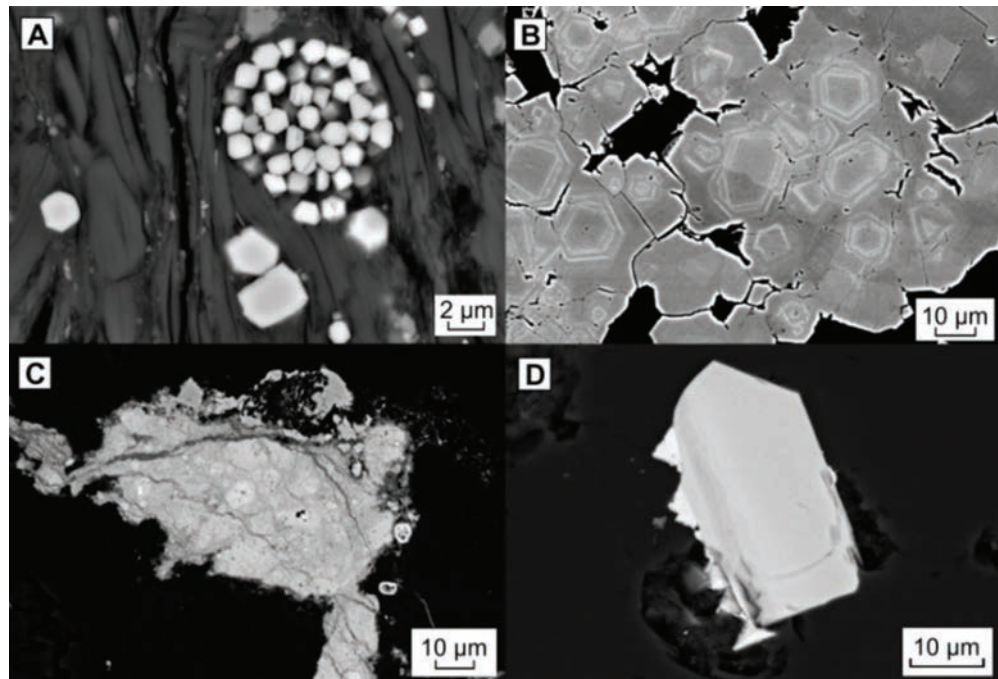


Figure 2 Back-scattered SEM images of: (A) pyrite framboid, (B) alternating bands of As-rich (light gray) and As-depleted (gray) pyrite, (C) LREE-rich goyazite crystals ($\text{SrAl}_3[(\text{PO}_4)_2(\text{OH})_6]$, white) within REE-depleted goyazite matrix (gray), (D) HREE-rich xenotime pyramidal crystals (YPO_4) growing on detrital zircon (ZrSiO_4).



clay minerals (illite, smectite, mixed-layered illite-smectite, kaolinite/nacrite and subordinate chlorite). Nonetheless, these minerals are a source of high contents of Al in the waters examined. Both clayey-silty shales and subordinate quartzites also contain REE-rich aluminophosphate and phosphate minerals (fig. 2C, D) that undergo dissolution by pyrite oxidation products releasing different ions into acid water bodies.

As opposed to Wiśniówka Duża, the Podwiśniówka beds are highlighted by distinctly higher contents of As, Cu, Cr, Ni and Co (Table 1). In both sites arsenic predominates in quartzites/sandstones whereas the other elements, especially REE, in clayey-silty shales. It is interesting to compare North American Shale Composite (NASC)-normalized REE contents. Both quartzites and clayey-silty shales show an abundance

of light REE (LREE; La through Eu) over heavy REE (HREE; Gd through Lu) which is evidenced by the LREE/HREENASC ratio of 1.44–1.45 (Wiśniówka Duża) to 1.78–1.80 (Podwiśniówka) (fig. 3A).

Metal(loid)s and REE in AMD waters

The pH of Podwiśniówka acid pit lake was stable varying from 2.4 to 2.6. The EC was in the range of 2862 to 4920 $\mu\text{S}/\text{cm}$ whereas concentrations of SO_4^{2-} and PO_4^{3-} varied from 2510 to 6000 mg/L and from 2.37 to 10.0 mg/L. In contrast, the Wiśniówka Duża acid pit lake revealed the pH in the range of 3.0 to 3.7, the EC 379 to 2172 $\mu\text{S}/\text{cm}$ and distinctly lower concentrations of SO_4^{2-} (135–1440 mg/L) and PO_4^{3-} (<0.01–0.455 mg/L). The highest pH and the lowest EC values and SO_4^{2-} , PO_4^{3-} and trace element concentrations were noted in March of 2017 during the large influx of melt-

Table 1. Mean values and concentration ranges of selected elements in major rock lithotypes of Podwiśniówka and Wiśniówka Duża quarries.

Localization/rocks	As	Co	Cr	Cu	Ni	ΣREE
	mg/kg (ppm)					
Podwiśniówka quarry1)						
Clayey-silty shales (n = 13)	965±853 (128–2888)	11.2±8.29 (<1–25)	139±57.8 (51–286)	128±192 (14–635)	24.2±12.6 (6–53)	291±78 (131–457)
Quartzites/sandstones (n = 13)	2135±2369 (48–6363)	5.81±8.20 (<1–29)	40,8±13.2 (23–78)	22.1±15.9 (6–66)	13.0±20.2 (1–76)	109±58.4 (39.4–265)
Wiśniówka Duża quarry2)						
Clayey-silty shales (n = 9)	20±9.64 (7–32)	1±1.21 (<1–4)	101.7±15.9 (87–135)	18.8±10.5 (7–36)	8.89±2.70 (6–15)	203±38.7 (155–271)
Quartzites/sandstones (n = 5)	190±297 (3–696)	1.3±1.2 (<1–3)	34.2±14.8 (22–59)	17.2±7.09 (11–29)	5.60±5.22 (1–14)	94.3±26.6 (61–126)

¹owermost Upper Cambrian lithostratigraphic series

²middle Upper Cambrian lithostratigraphic series

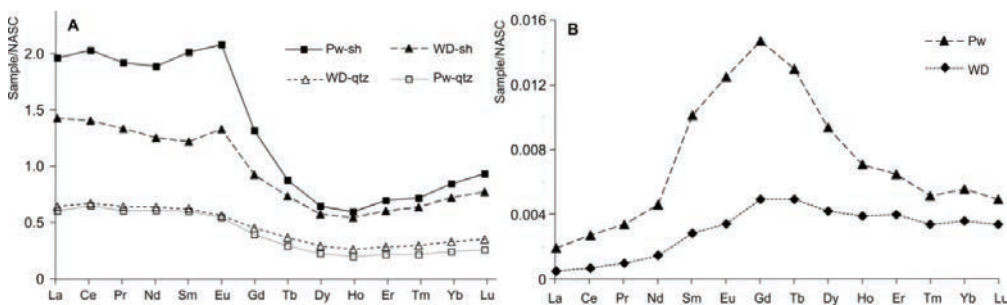


Figure 3 NASC-normalized mean REE concentration patterns of: (A) Podwiśniówka and Wiśniówka Duża clayey-silty shales (Pw-sh, WD-sh) and quartzites (Pw-qtz, WD-qtz) vs. (B) Podwiśniówka (Pw) and Wiśniówka Duża (WD) acid pit lakes.



and rainwaters into these water bodies (fig. 4).

The Podwiśniówka acid pit lake is also highlighted by the presence of REE, whose concentrations vary from 0.36 to 0.93 mg/L. These levels are higher than in the Wiśniówka Duża acid pit lake (0.04–0.35 mg/L) presumably due to larger amounts of reactive products of pyrite oxidation that come into contact with REE-rich rocks. It is interesting to note that the NASC-normalized REE concentrations patterns in these two water bodies show different shapes. The Podwiśniówka shale-normalized profile is characterized by the predominance of medium REE whereas that of Wiśniówka Duża shows enrichment in heavy REE (fig. 3B).

Sulfur isotope signatures

The mean $\delta^{34}\text{S}$ values of Wiśniówka pyrite are $-24.0 \pm 3.1\text{‰}$ (Podwiśniówka) and $-17.4 \pm 7.2\text{‰}$ (Wiśniówka Duża). These differences are also reflected in the $\delta^{34}\text{S}$ of dissolved sulfates amounting to $-15.3 \pm 1.0\text{‰}$ (Podwiśniówka) and $-10.0 \pm 1.7\text{‰}$ (Wiśniówka Duża) (Migaszewski et al., 2018a). These negative sulfur isotope signatures are also unusual in sedimentary pyrites of the regional Cambri-

an lithostratigraphic section and in dissolved sulfates of local springs, streams and rivers, for instance in Holy Cross Mountains National Park located approx. 15 km east of the study area, the $\delta^{34}\text{S}\text{-FeS}_2$ values are positive with a mean of $8.7 \pm 1.0\text{‰}$ and $6.2 \pm 4.6\text{‰}$, respectively (Michalik, Migaszewski 2012). The same positive values have been found in most farmer's wells and unpolluted rivers of the Wiśniówka neighboring area.

Application of geochemical tracers

Different trace element and NASC-normalized REE profiles of Podwiśniówka (As>Cu>Co≈Ni>Cr and roof-shaped MREE) and Wiśniówka Duża (Cu and step-shaped HREE) were used to localize “hot spots” and provenance of exposed or unexposed deleterious mine waste material (Migaszewski et al. 2016, 2018ab). These tracers were also applied to: (i) pinpoint unexposed pyrite assemblages within faulted zones during mining operations, (ii) identify perched aquifers that recharge farmer's wells (Migaszewski et al. 2014), and (iii) determine the extent of uncontrolled acid spills into streams and rivers. In all these cases water samples were collected from

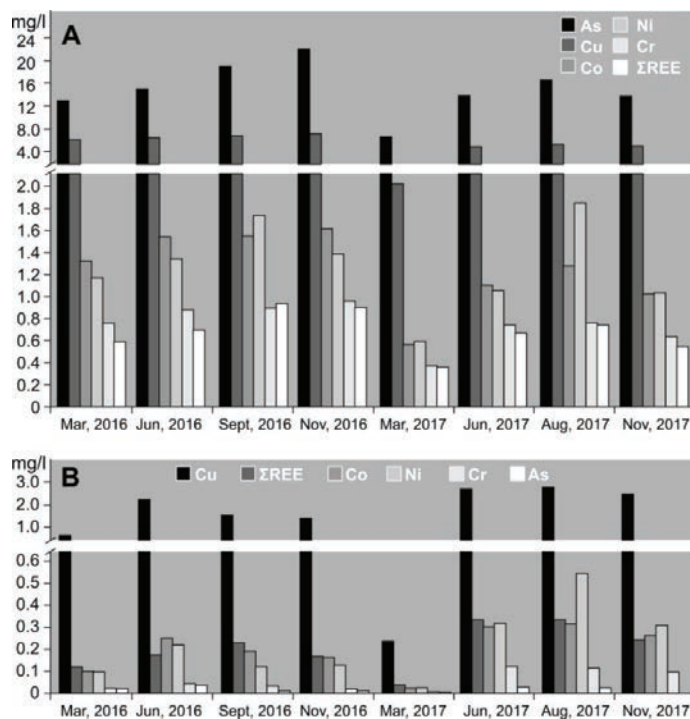


Figure 4 Concentrations of As, Cu, Co, Ni, Cr and REE in (A) Podwiśniówka and (B) Wiśniówka Duża acid pit lakes during 2016–2017.



pools, streams and wells for determining pH and trace element and REE concentrations.

The same objectives were achieved using sulfur isotope signatures despite the fact that this method is more expensive and time-consuming compared to element/REE tracers. However, some uncontrolled spills or discharges into streams and rivers give rise to an appearance of negative sulfur isotope signatures even in the absence of characteristic yellow-orange coloring (Migaszewski et al. 2018a). This is induced by different behavior of cations and anions in the environment. The former are easily adsorbed by natural colloids as opposed to anions. The negative sulfur isotope ratios will enable us to reconstruct Wiśniówka Late Cambrian euxenic-anoxic paleoenvironment. This may cast new light on the Cambrian history of the Holy Cross Mountains inlier located close to the Trans-European Suture Zone (TESZ) that separates the Precambrian East European Craton from the Paleozoic Platform of Central Europe.

Conclusions

The present and previous studies have indicated that geochemistry of Wiśniówka AMD waters reflects different mineralogy and geochemistry of two pyrite mineralization zones enhanced by geochemical interactions that occur in the rock-water-colloid systems. These and other features along with negative sulfur isotope signatures enabled us to evaluate an impact of AMD waters on the adjacent environment, establish the provenance of tailings pile material and acid tailings pools, and provide information for mining operations in a tectonically-affected area.

Acknowledgements

This study was supported by the National Science Center, a research grant #2015/17/B/ST10/02119.

References

- Alpers CN, Nordstrom DK, Spitzley J (2003) Extreme Acid Mine Drainage from a Pyritic Massive Sulfide Deposit: The Iron Mountain End-Member. In: Environmental Aspects of Mine Wastes. Jambor J, Blowes DL, Ritchie AIM (Eds). Mineral Assoc Canada Short Course Series 31, 407–430
- Brown GE, Hochella Jr MF, Calas G (2017) Improving Mitigation of the Long-Term Legacy of Mining Activities: Nano- and Molecular-Level Concepts and Methods. *Elements* 13(5):325–330, doi: 10.2138/gselements.13.5.325
- Kossoff D, Dubbin WE, Alfredsson M, Edwards SJ, Macklin MG, Hudson-Edwards KA (2014) Mine tailings dams: characteristics, failures, environmental impacts. *Appl Geochem* 51:229–245, doi: 10.1016/j.apgeochem.2014.09.010
- Michalik A, Migaszewski ZM (2012) Stable sulfur and oxygen isotope ratios of the Świętokrzyski National Park spring waters generated by natural and anthropogenic factors (south-central Poland). *Appl Geochem* 27:1123–1132, doi:10.1016/j.apgeochem.2012.02.025
- Migaszewski ZM, Gałuszka A, Dołęgowska S (2016) Rare earth and trace element signatures for assessing an impact of rock mining and processing on the environment: Wiśniówka case study. *Environ Sci Pollut R* 23:24943–24959, doi:10.1007/s11356-016-7713-y
- Migaszewski ZM, Gałuszka A, Dołęgowska S (2018a) Stable isotope geochemistry of acid mine drainage from the Wiśniówka area (south-central Poland). *Appl Geochem* 95:45–56, doi.org/10.1016/j.apgeochem.2018.05.015
- Migaszewski ZM, Gałuszka A, Dołęgowska S (2018b) Arsenic in the Wiśniówka acid mine drainage area (south-central Poland) – mineralogy, hydrogeochemistry, remediation. *Chem Geol* 493:491–503, doi.org/10.1016/j.chemgeo.2018.06.027
- Migaszewski ZM, Gałuszka A, Migaszewski A (2014). The study of rare earth elements in farmer's well waters of the Podwiśniówka acid mine drainage area (south-central Poland). *Environ Monit Assess* 186:1609–1622, doi: 10.1007/s10661-013-3478-7
- Migaszewski ZM, Gałuszka A, Hałas S, Dąbek J, Dołęgowska S, Budzyk I, Starnawska E, Michalik A (2009) Chemical and isotopic variations in the Wiśniówka Mała mine pit water, Holy Cross Mountains (South-Central Poland). *Environ Geol* 57:29–40, DOI 10.1007/s00254-008-1279-z
- Nordstrom DK (2011) Mine Waters: Acidic to Circumneutral. *Elements* 7(6):393–398, doi: 1811-5209/11/0007-0393\$2.50 DOI: 10.2113/gselements.7.6.393
- Plumlee GS (1999) The Environmental Geology



- of Mineral Deposits. In: Plumlee GS, Logsdon MJ (Eds). *The Environmental Geochemistry of Mineral Deposits, Part A. Processes, Techniques, and Health Issues*. Soc Econ Geologists Rev in Econ Geol 6A, p 71—116
- Plumlee GS, Morman S (2011) Mine Wastes and Human Health. *Elements* 7(6):399–404, doi: 1811-5209/11/0007-0399\$2.50 DOI: 10.2113/gselements.7.6.399
- Reichenbach I. (1993) Black shale as an environmental hazard; a review of black shales in Canada. *Geol Surv of Canada. Open-File 2697*, p 1–62
- Simón M, Martín F, Ortiz I, García I, Fernández J, Fernández E, Dorronsoro C, Aguilar J (2001) Soil pollution by oxidation of tailings from toxic spill of a pyrite mine. *Sci Total Environ* 279:63—74, doi: 10.1016/S0048-9697(01)00726-4
- Żylińska A, Szczepanik Z, Salwa S (2006) Cambrian of the Holy Cross Mountains, Poland: biostratigraphy of the Wiśniówka Hill succession. *Acta Geol Pol* 56(4):443—461





The Water Balance of South African Coal Mines Pit Lakes[©]

Matsatsi Mpetle¹, Andrew Johnstone²

¹*University of the Free State, 205 Nelson Mandela Dr, Park West, Bloemfontein, 9301,
matsatsimpetle@gmail.com*

²*GCS Water and Environmental (Pty) Ltd, 63 Wessel Road, Rivonia, 2128, South Africa,
andrewj@gcs-sa.biz*

Abstract

Pit lakes form in open cast mines which extend below the groundwater level, after dewatering stops. Groundwater levels are disturbed during mining and associated dewatering operations. The information presented in this paper serves to determine if pit lakes are an environmentally stable/ viable solution for South African coal mines after closure.

Pit lake water balances to approximate the final water volume and rest water elevation were constructed with the use of a Goldsim program. Two case studies of South African Coal Mine Pit Lakes will be discussed;

- The first study area is a standalone pit lake located in the Waterberg Coalfield and no backfilled has been used in attempt to close the final void; and
- The second study area consists of a series of 7 pit lake (of which only 4 are investigated for this study) associated with a single mining operation and is located in the Highveld Coalfield. Some portions of the mine have been rehabilitated.

Both study areas are located in climatic settings where average annual rainfall exceeds mean annual evaporation. Pit lake water balance modelling demonstrates that both study areas operate as terminal sinks, with the great evaporation potential keeping the pit lake water levels below discharge points. Climate plays an important role in understanding the key drivers of the pit lake water balance and therefore extreme weather conditions to address the effects of wet and dry scenarios were applied to the models to determine if the pit lakes would result in mine water discharge during wet weather events.

The net losses or gains of the pit lakes were determined from stage curves which were based on the bathymetric survey of each pit lake. While the accuracy of the water balances is dependent in the accuracy of the input parameters, a limitation to the water balance modelling is gaps in the data. Water balance modelling is applied to determine the behaviour of the coal mine pit lakes under investigation and their potential for mine water overflow.

Keywords: Pit Lakes, Water Balance, Closure Option

Introduction

A water balance model is described as an accounting for the volume of water flow rate from all probable sources (Gholamnejad, 2008). The final pit lake volume is influenced by a range of factors such as rainfall, evaporation, hydrogeology and the pit geometry. Water balance models are generally based on the law of conservation of mass which states that whatever water enters the storage should equal to the water stored or released from

storage. In its simplest form, the equation may be written as:

$$\text{Inflow} = \text{Outflow} \pm \Delta \text{Storage}$$

The aim of the present study is to develop water balance models for South African Coal pit lakes, to increase understanding of the pit lake hydrology before concluding whether or not pit lakes are an environmentally suitable method for South African open pit coal mines. Depending on the components of the pit lake



water balance, it may take several years before equilibrium state is reached (ÜNSAL, 2013). Calculations are conducted to determine the behaviour of the pit lakes over a predictive period of 20 years (2018-2038).

Pit lakes in semi-arid climatic settings are usually classified as ‘flow-through’ or ‘terminal sinks’ (McCullough et al., 2013). Once mining stops, groundwater levels rebound and together with rainfall and runoff, contribute to fill the final void. Terminal sinks may form in arid environments where the potential evaporation is higher than the mean precipitation and the pit lake water elevation is below the surrounding pre-mining groundwater level (Niccoli, 2009). If the pit lake water level reaches the pre-mining groundwater elevation and water is released into the aquifer as groundwater seepage, the pit lake is classified as a ‘flow-through’ (McCullough et al., 2013).

Figure 1 shows the locations of the areas under investigation. Each study area demonstrates unique hydrogeological conditions and therefore, conceptual models were constructed separately.

Methods

Climatic data for input were obtained from Water Resources of South Africa database (WRC, 2015). Aquifer parameters were ob-

tained by means of constant drawdown test, which involved the abstraction of a measured volume of water from a borehole whilst the water levels are recorded. Pump test data was analysed using the Jacob-Cooper solution.

Runoff coefficients suggested by (Hodgson and Krantz, 1998) were applied to the runoff calculations using the equation provided by (Castendyk, 2009) which is as follows:

$$Q = CIA$$

Where Q is the runoff inflow volume, C is the runoff coefficient, I is the total precipitation and A is the area over which runoff occurs.

(Marinelli and Niccoli, 2000) provides a set of analytical equations for groundwater inflow to a cylindrical pit (used to estimate flow to Pit Lake A), as follows:

$$Q_1 = W\pi(r_0^2 - r_p^2)$$

Where Q_1 is the inflow from the pit walls, W is the recharge flux, r_0 is the radius of influence, and r_p is the radius of the pit lake.

Groundwater inflow through the pit bottom is given by the equation:

$$Q_2 = 4 \times r_p \times (K_{h2}/m_2) \times (h_0 - d); m_2 = (K_{h2}/K_{v2})^{1/2}$$

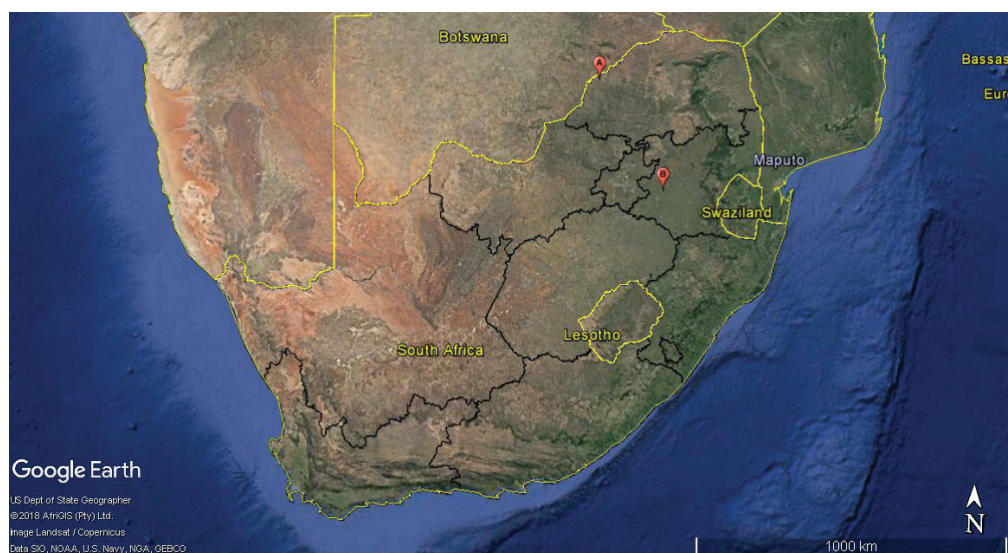


Figure 1 Locality map of study areas



Where r_p is the radius of the pit lake, K_{h2} and $Kv2$ are the hydraulic conductivity for the materials below the confining layer, h_0 is the pre-mining groundwater level and d is the pit lake depth.

The Dupuit-Forchheimer analytical equation given below was used to estimate groundwater inflow to Pit Lake B:

$$Q_g = \pi K (h_0^2 - h_w^2) / \ln (r_0 / r_w)$$

Where K is hydraulic conductivity (m/d), h_0 is the pre-mining groundwater level (m), h_w is the depth of the pit lake (m), r_0 is the radius of influence (m) and r_w is the radius of the pit lake (m).

(Singh and Atkins, 1985) suggests the usage of an equation given by (Mansur and Kaufman, 1962) to calculate the radius of a rectangular open pit:

$$r = (2/\pi) \times (Y.W)^{1/2}$$

Where Y is the length of the open pit, W is the width of the open pit and r is the equivalent radius of the mine. This equation is applied to Pit Lake B to account for the irregular shape.

The conceptual models were constructed from all available information, including borehole logs, to graphically illustrate the hydrogeological factors affecting the open pits. Water balance models were developed with the use of Goldsim Academic version to account for the volume of water in the pit lakes and to predict future pit lake water levels and volumes over wet and dry scenarios.

Models were run under probabilistic simulations using the Monte Carlo approach

with 50 realizations. Rainfall was modelled as a stochastic element, assuming a gamma distribution. This simulation approach was used with intend to account for uncertainty and incorporate variability (McPhail, 2005).

Case Study 1

Pit Lake A is situated in the Waterberg Coalfield of South Africa, and formed as a result of bulk sample excavation. The total volume of the pit lake is approximately 101 99 00 m³. Mining started in 2009 and ended in 2010, after which the final void filled with water. Main facilities of the mine consists of the open pit of approximately 90 m depth, with a waste rock storage area located southwest of the open pit. Groundwater flow is towards the Limpopo River, in a north easterly direction. The area experiences mean annual precipitation of 438 mm and an average potential evaporation of 1950 mm/a. The Waterberg Coalfield is classified as an arid climate area. Topography of the area is naturally undulating, dipping gently towards the Limpopo River. Geological setting of the area consists of the complete Karoo Supergroup succession with coal-bearing zones present in the Vryheid and Grooteegeluk Formations of the Ecca Group.

Figure 2 illustrates the components of the water balance model take into consideration during calculation. The topography of the area is fairly flat and therefore runoff is minimal. Runoff from in-pit slopes is however, expected to affect the water balance as the slopes are more compacted compared to the topsoil.

Pit in-filling time series data which has been monitored from the time of closure was

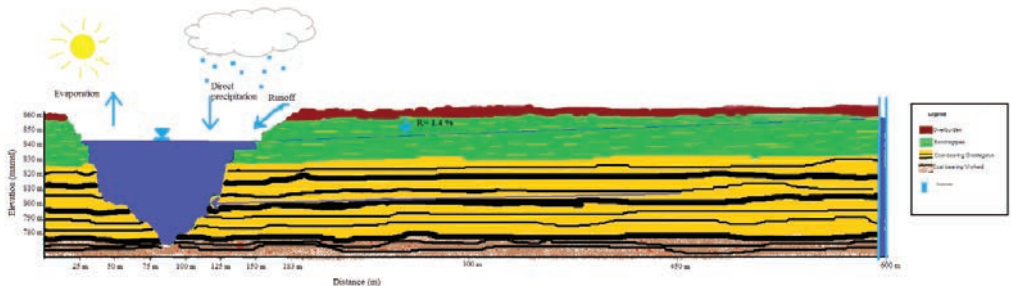


Figure 2 Pit Lake A Conceptual Model



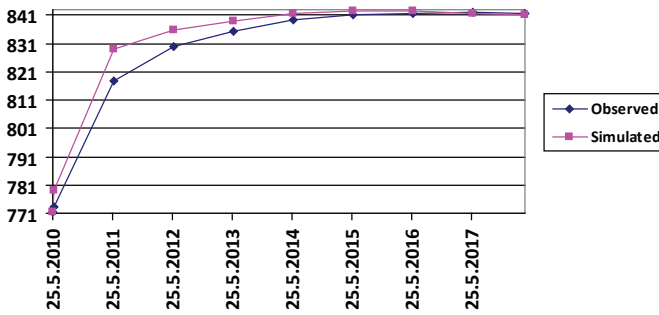


Figure 3 Simulated vs. Observed pit lake water levels

Table 1. Water balance summary for Pit Lake A

Runoff (m ³)	Rainfall (m ³)	Groundwater Inflow (m ³)	Evaporation (m ³)	Volume of water in pit lake (m ³)	Percentage Filled (%)
14066	58896	644384	218087	499259	49

used to calibrate the model and Figure 3 compares the simulated pit lake elevation results determined using the most probable scenario and the observed pit lake elevation. A 98% correlation exists between the simulated and observed results.

Table 1 below is a summary of the cumulative volumes of water which has contributed to the current balance of water in the pit lake. Groundwater accounts for 90% of the total volume contribution. Rainfall and Runoff account for 8% and 2% respectively.

Wet case scenario shows that the volume of water in the pit lake could reach 549 580 m³ at an elevation of 844 mamsl, while the dry case scenario shows that the volume of water in the pit lake could reach 455 577 m³ at an elevation of 838.5 mamsl.

Case Study 2

Pit Lake B is situated in the Highveld Coal-field of the Mpumalanga Province of South Africa. Seven pit lakes are present at this site which is partially backfilled and rehabilitated. Two streams are within the vicinity of the mining area, serving as the lowest elevations for surface drainage. Geologically, the study area is underlain by a thin sequence of Dwyka and Middle Ecca strata lying on an undulating floor composed of felsites, granites and diabase associated with the Bushveld Complex (Buchan et al., 1980). The coal bearing zone is approximately 70 m thick with five coal seams. Mean annual precipitation value

for the catchment is 671 mm and average annual evaporation is 1600 mm.

Figure 4 demonstrates the conceptual model for the Kriel site where material has been backfilled into the open pit in an attempt to close the void. However, the pit lakes remained as final voids after backfilling. Areas near the streams where not mined, these areas are represented by the undisturbed Karoo strata as illustrated. Information regarding the undisturbed geology were obtained from borehole geological logs.

Final pit lake voids are of varying sizes and ages. Properties of the pit lakes were determined from analyses bathymetric surveys. Points at which mine water will overflow to the surface were modelled using the digital elevation model of the mine area surface and pit lake bathymetries. Global Mapper version 13 was used to simulate water level elevations to the points where overflow would occur.

No in-pit filling data were available for Pit Lake B, however, simulated results were compared to LiDAR elevation data which was only recorded from 2013. Table 3 shows is a summary of the cumulative volumes of water which have contributed to the current balance of water in the pit lakes.

The rest water elevation of the pit lakes at the time of reporting was 1536 mamsl, which is also assumed to be the water elevation in the backfilled material. Extreme wet weather conditions could potentially cause the pit lakes to overflow.



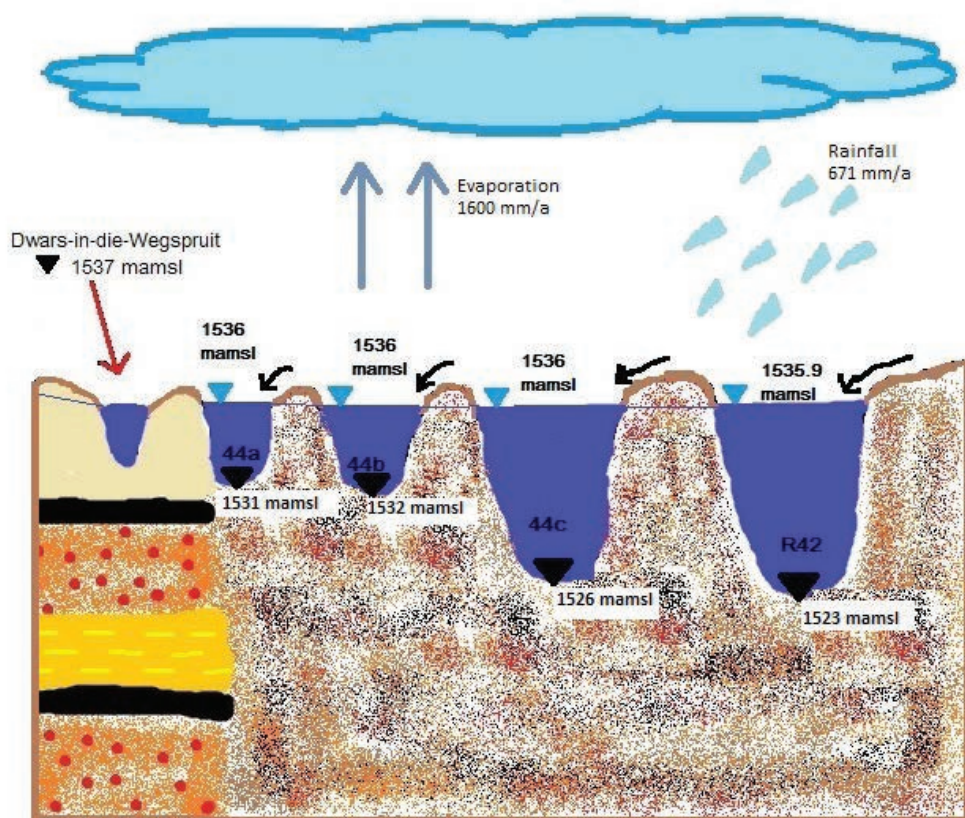


Figure 4 Pit Lake B Conceptual Model

Table 2. Geometrical properties of the pit lakes

Pit Name	Age (years)	Depth (m)	Total Volume (m3)	Point of Overflow(mamsl)
44a	13	6	424932	1537
44b	13	5.4	96687	1537
44c	13	10.5	202428	1537
R42	13	13.1	356489	1537

Table 3. Water balance summary for Pit Lake B

Pit Name	Groundwater Inflow (m³)	Rainfall (m³)	Runoff (m³)	Outflow (m³)	Volume achieved (m³)	Percentage filled
44a	1108000	1100000	245795	2198000	255713	60
44b	222846	344601	187817	687884	67379	70
44c	250828	236866	146460	472094	162060	80
R42	564644	400940	86477	724813	327268	92



Conclusions

The pit lakes may be classified as terminal sinks due to the resultant negative balance. Pit Lake B would require management for water level elevations to avoid the risk of overflow. It is unlikely that Pit Lake A will overflow.

(Westcott and Watson, 2007) suggests the evaluation of features such as geology, bathymetry and water balance before deciding on a closure option. Pit Lake A may be considered for recreational (i.e. boating and diving) due to its great depth. Pit Lake B is shallow in depth, and easily accessible. An advantage for livestock to access water without any major engineering work required. There is a potential for farm fishing as fish have been identified at both sites.

For the improvement of results, it is recommended that measurement of site specific data such as rainfall and evaporation; and daily pit lake water levels be monitored especially for Pit Lake B. Based on the analysis of available data and constructed models, the hydrogeological systems of the pit lakes under investigation are expected to remain terminal sinks.

Acknowledgements

The authors wish to thank the Water Research Commission for funding the project and Anglo American Inyosi Coal: Kriel Colliery and Sasol Mafutha where the studies were conducted.

References

BUCHAN, I. F., BAARS, L. F. & NORTHCOTE, C. S. 1980. Opencast coal mining at Kriel Colliery. *Journal of the Southern African Institute of Mining and Metallurgy*, 80, 46-55.

CASTENDYK, D. 2009. Predictive Modeling of the Physical Limnology of Future Pit Lakes. In: CASTENDYK D., E. T. (ed.) *Mine Pit Lakes Characteristics, Predictive Modeling and Sustainability*. Society for Mining, Metallurgy and Exploration.

GHOLAMNEJAD, J. 2008. Evaluation of pit lake formation in choghart iron mine of Iran by us-

ing simulation approach. *Journal Of International Environmental Application And Science*, 8, 57-65.

HODGSON, F. D. I. & KRANTZ, R. 1998. Investigation into groundwater quality deterioration in the Olifants River catchment above the Loskop Dam with specialised investigation in the Witbank Dam sub-catchment, Water Research Commission.

MANSUR, C. & KAUFMAN, R. 1962. Dewatering. *Foundation engineering*, 303.

MARINELLI, F. & NICCOLI, W. L. 2000. Simple analytical equations for estimating ground water inflow to a mine pit. *Groundwater*, 38, 311-314.

MCCULLOUGH, C. D., MARCHAND, G. & UNSELD, J. 2013. Mine closure of pit lakes as terminal sinks: best available practice when options are limited? *Mine Water and the Environment*, 32, 302-313.

MCPHAIL, G. 2005. Getting the Water Balance Right. *Tailings & Paste Management Decommissioning*. Australian Centre for Geomechanics.

NICCOLI, W. L. 2009. Hydrologic characteristics and classifications of pit lakes. In: CASTENDYK D., E. T. (ed.) *Mine Pit Lakes: Characteristics, predictive modeling, and sustainability*. Littleton: SME Inc.

SINGH, R. & ATKINS, A. 1985. Application of idealised analytical techniques for prediction of mine water inflow. *Mining science and technology*, 2, 131-138.

ÜNSAL, B. 2013. Assessment of Open Pit Eastern Requirements and Pit Lake Formation for Kişladağ Gold Mine, Uşak-Turkey. Doctor of Philosophy in Geological Engineering, Middle East Technical University.

WESTCOTT, F. & WATSON, L. 2007. End Pit Lakes Technical Guidance Document. Clearwater Environmental Consultants Inc.

WRC 2015. Water Resources of South Africa. Pretoria: Water Research Commission. <http://www.waterresourceswr2012.co.za> accessed (31/07/2017)



Prediction of seepage quality from coal discard material in an semi-arid climate

Koovila Naicker¹, Philip Barnard¹, Albert van Zyl²

¹Golder Associates Africa (Pty) Ltd., P.O. Box 6001, Halfway House, 1685, Midrand, South Africa, knaicker@golder.co.za; pbarnard@golder.co.za

²Terrasim CC, Suite 87, Private Bag X8, Elarduspark, 0047, South Africa, avanzyl@terrasim.co.za

Abstract

In the prediction of seepage chemistry an important aspect is the upscaling of the results of laboratory scale kinetic test work to equilibrium conditions typical of full-scale mine site components.

Geochemical characterisation was conducted on coal discard waste material as part of a cover design options analysis. Humidity cell results were up-scaled by modelled gravimetric moisture to predict interstitial/pore water TDS concentrations range. The up-scaled seepage quality ranges were evaluated for solubility controls in PHREEQC. The study formed part of an integrated source-pathway-receptor modelling for single and dual-layer store and release covers to mitigate contaminated seepage entering the groundwater.

Keywords: coal discard, humidity cell, source-term, source-pathway-receptor modelling

Introduction

Alternative cover design options with the least potential for groundwater contamination and post-closure risk was investigated in terms of the requirements of the National Environmental Management: Waste Amendment Act - NEMWAA, 2014 (Act No. 26 of 2014) and regulations GN R.634 to 636 for management of mining residues. The investigation involved a source-pathway-receptor (SPR) approach to quantify relationships between the sources of contamination (Discard Dump) and (potential) receptors of contamination by considering relevant pathways and processes. Integration from unsaturated flow modelling, geochemistry and groundwater specialist studies demonstrated the environmental impacts from selected cover designs. The cover design options included a geo-synthetic cover and soil cover with varying thickness. Thick soil covers over coal discard facilities in arid and semi-arid regions are considered a cost-effective store and release covers that are cost-effective to mitigate the impacts of acidic to saline seepage entering the receiving groundwater environment.

The paper presents the geochemistry component of the risk-based SPR model-

ling. The receiving groundwater, of low background quality, was defined as the receptor in the modelling study. The coal mine is situated on the Waterberg coalfield near Lephalale in the Northern Province of South Africa. The regional geology in the area is characterised by the igneous and sedimentary rocks of the Karoo Supergroup, comprising from surface of the Stormberg Group, Beaufort Group, Ecca Group and the Dwyka group forming the basement. The coalfield is fault-bounded and forms a graben structure.

Average summer and winter minimum and maximum temperatures range from 11–40°C and 0–28°C respectively. Mean Annual Potential Evaporation (FAO Penman-Monteith (1992) equivalent) of 1710 mm/yr for the study area exceeds Mean Annual Precipitation (MAP) of 430 mm/yr. Rainfall is highly seasonal with 95% of annual rainfall occurring during the rainy season from October till April. According to INAP (2009), this climate is suitable for a store and release cover.

Approach and Methodology

The methodology followed for the geochemistry assessment is consistent with the series Best Practice Guidelines (BPG) for Water Re-



source Protection in the South African Mining Industry - G4 Impact Prediction (DWAf 2008) and Global Acid Rock Drainage - GARD Guide (INAP, 2012). The methodology applied included:

Review: Previous discard material static and kinetic characterisation and onsite soil availability reviewed, to develop fieldwork and sampling plan and cover designs options.

Fieldwork and Sampling: In-situ permeabilities (soil and discard material) determined, and fresh and oxidised discard samples collected from test pits (≈ 3.5 m in depth) on ramps and centre of the dump. The samples were submitted for geochemical static and kinetic characterisation to SANAS-accredited laboratories. Static testwork included; mineralogy by XRD; total elemental analysis by four acid digestion; Acid Base Accounting (ABA); sulphur speciation; Net Acid Generation (NAG); Distilled water leach at 1:20 solid: liquid ratio and analysis of the leachate; Particle size analysis; and humidity cells for kinetic testing; and soil moisture contents.

Geochemical and Unsaturated modelling: Average oxygen consumption in the 50m coal discard dump calculated in 1D Oxygen diffusion model. Modelling of moisture variation within the discard profile as a function of climate, water retention and in situ permeabilities completed in SVFLUX software (SoilVision Systems). Modelled moisture time series used to upscale weekly kinetic data to derive interstitial/pore water (seepage) qualities ranges. PHREEQC Interactive (Parkhurst and Appelo, 1999) was used to identify solu-

bility controls on the average, 10th and 90th percentile seepage qualities.

Log triangular distribution of seepage TDS concentration used as input in ConSim model (Golder, 2005) and ChemFlux finite element unsaturated contaminant transport model (SoilVision Systems 2016) to simulate TDS loads at the base of the facility and vadose zone pathway. Monitoring time series data from historic boreholes immediately surrounding the facility was used to validate model results. Unsaturated pathway modelling integration for thick single- and dual-layer store and release covers constructed with onsite soils is presented in Van Zyl et.al (2018).

Impact Assessment: Solute transport model (MODFLOW software) demonstrated the potential risks to the downstream groundwater receptor for cover design options by modelling dispersion, and dilution of TDS loads in surrounding areas from the coal discard dump.

Results

Field programme

Table 1 provides coal discard and interburden samples (27) collected from the mine that report to the coal discard facility.

In-field permeability measurements with a Guelph permeameter were completed on 3 sites on coal discard dump and potential soil cover materials identified onsite. The saturated hydraulic conductivities (K_{sat}) for the coal discard was measured as 5.90×10^{-3} - 2.52×10^{-2} cm/s or 5.0 to 21.5 m/day. The K_{sat} is very high due to the high coarse fragments (>4.75 mm) contents of ≈ 63 -81%.

Table 1. Discard Materials Collected (2006- 2016)

Material Type/Source	Discard Age	Date	Sample ID	No.samples
Discard facility	Partially weathered (1 yr)	2006	Discard_comp	3
Discard facility-NE,	Historic, weathered test pits (≈ 10 yrs)	2016	Discard_1300, Raffu ramp	2
Northern ramp	Partially weathered-fresh	2007,	Kidney_discard	2
Discard stockpile	(≈ 2 mon)	2016		8
Wash Plant	Fresh discard	2006	GG1, GG2,GG4,GG5	4
		2016	GG2, GG8, GG1 GG4/5	3
Interburden	Fresh blasted material	2006	Bench 7A,8,10	3
		2007	Bench 7A,8,10	2
		2016	Bench 8&10	



Analytical programme

Characterisation of the discard material involved: moisture content determination; particle size distribution analyses; Acid base accounting (ABA) with sulphur speciation, Mineralogical analyses (XRF and XRD); Distilled water shake flask test and kinetic tests by humidity cell method

Analytical results

Sulphur speciation results for selected samples indicated that sulphide S is the dominant sulphur form in the coal discard materials

collected from the Plant and discard facility. Acidic-circum-neutral Paste pH results indicate the presence of dissolving carbonates to buffer acid generation from sulphide minerals in the short-term. Mineralogical compositions for the discard samples indicated calcite $\approx 1\text{-}2\%$, dolomite $\approx 1\text{-}2\%$ and pyrite $\approx 1\text{-}3\%$.

ABA results (Figure 2) indicated that majority coal discard sample (with exception of 1 fresh plant discard) have low Nett Potential Ratio or NPR (ratio of Neutralising Potential - NP and Acid Potential - AP) < 2 . The coal discard sample classified as Potentially Acid Generation (PAG) according to Price.

Table 2. Sulphur Speciation for selected coal discard samples

Sample	Paste pH	Total C	Total S	Sulphide S	Sulphate S	S other
Kidney_discard	7.7	16	1.8	1.6	0.024	0.086
Discard_1300	3.6	13	1.3	0.32	0.50	0.44
Raffu_ramp	5.5	13	1.1	0.28	0.47	0.30
Plant_GG2	7.7	12	2.3	2.1	0.010	0.18
Plant_GG8	7.4	34	3.3	2.9	0.004	0.36
Plant_GG1	7.6	11	2.6	2.5	0.009	0.051
Plant_GG45	6.9	34	6.4	6.4	0.007	0.023
GG1_HC1	na	na	3.4	3.0	0.005	0.45
GG2_HC2	na	na	1.7	1.5	0.013	0.22
GG4/5_HC3	na	na	8.1	6.7	0.013	1.46
Bench 8 -HC4	na	na	6.4	5.2	0.015	1.18
Bench 10-HC5	na	na	0.07	0.02	0.01	0.04

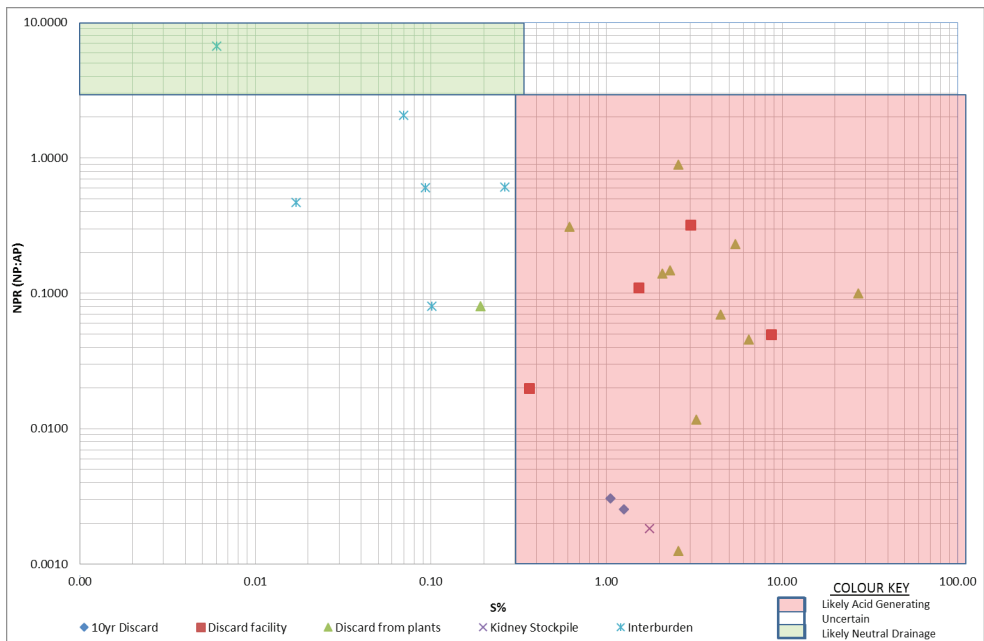


Figure 1 Total S vs NPR for coal discard material



Kinetic Results

Selected kinetic results for the coal discard material were assumed representative of coal discard facility. The highest TDS rate (2 700 mg/kg/week) was recorded for Plant 4&5 that handles coal with Tot S > 6%. The results for

Plant 4&5 was included since it contributes < 25% of the total volume of discard material reporting to facility. Material balance for discard volumes from each plant was not made available for the study (Figure 2 and 3).

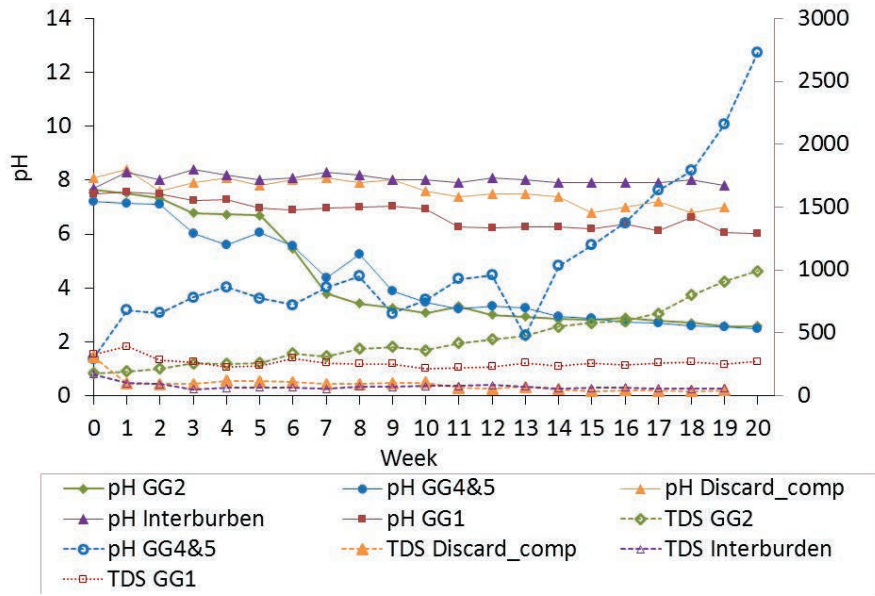


Figure 2: Kinetic results for coal discard material pH and TDS rate vs time

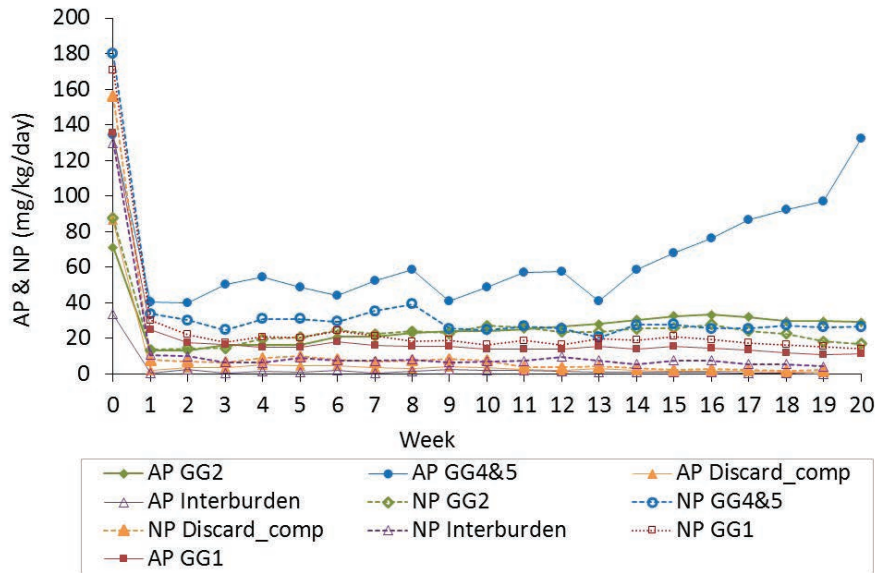


Figure 3 Kinetic results for coal discard material - Acid Potential and Neutralisation Potential (NP) vs time



Modelling Results

Oxygen diffusion

Oxygen is a rate-limiting factor in geochemical processes in discard materials. Indicative diffusion rates and oxygen concentrations at depth within the discard materials were calculated Fick's law. Atmospheric oxygen was predicted to be available at depth of the coal discard facility (50m). Table 3 presents the primary oxidation rate from humidity cells and from oxygen diffusion modelling.

Moisture content

One dimensional flow profiles (0-5m and 5-50m) were used to model the moisture

conditions and saturation within the coal discard facility. The assumption is made that the simulated moisture and flow through the one dimensional flow profiles are spatially representative of the flows that would occur at the various sections. The predicted distribution in gravimetric water/moisture content or for an uncovered discard is shown in Figure 4. The moisture contents (Table 4) was predicted from precipitation, rainfall distribution and climate conditions, material hydraulic properties of three (3) discard samples and the effect of moisture retention of the discard profile.

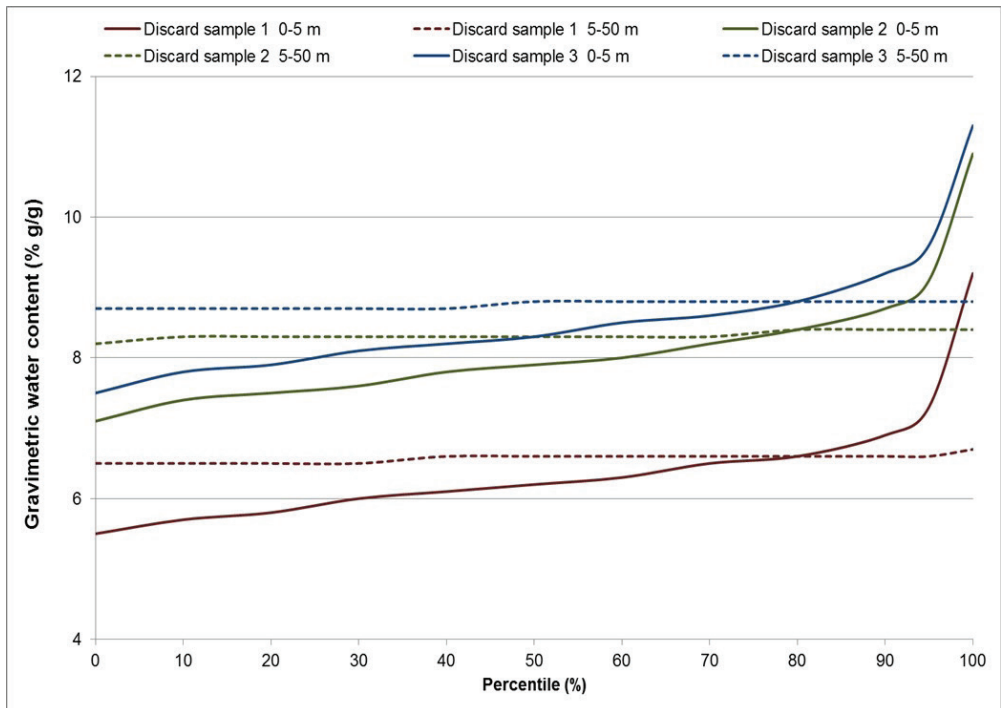


Figure 4. Predicted discard moisture conditions

Table 3. Predicted oxygen diffusion rates

	Primary Oxidation Rates			
	Units	Min	Ave	Max
Oxygen flux at waste interface	KgO ₂ /m ² /s	1.78E-08	2.50E-08	3.00E-08
Calculated pyrite oxidation rate	gFeS ₂ /t/week	1.2	1.6	2.0
Humidity cell rates for pyrite oxidation	gFeS ₂ /t/week	215	428	313
Number of times slower than humidity cell rates		185	261	313



Table 4. Moisture Modelling Results

	Discard 1	Discard 2	Discard 3
Laboratory measurements	5.7	7.4	7.8
Predicted moisture	6.5	7.5	8.9

The modelled moisture content time series was applied to upscale weekly humidity cell (liquid: solid ratio of 2:1) results as representative of coal discard interstitial pore solution over time. Geochemical solubility controls were assessed on the 10th, average and 90th percentile up-scaled pore qualities for each humidity cell in PHREEQC Interactive (USGS, 2017).

Table 5 provides the predicted seepage quality (selected parameters) from the coal discard facility under oxidising conditions and in equilibrium with air (O₂ and CO₂). Selection of pyrite as an equilibrium phase switches the redox to slightly reducing condi-

tions. The elevated magnesium and sulphate concentrations is due to pyrite oxidation; and subsequent dolomite buffering. Minerals predicted to control the dissolved concentrations (sulphate, calcium, chromium, manganese, iron, aluminium and barium) in the seepage were; gypsum, Cr(OH)₃(am), rhodochrosite, goethite, diaspore, and barite and dolomite.

A log-triangular distribution for TDS seepage from the coal discard (Table 5) was applied in the ConSim model for various cover options to simulate flow to the unsaturated zone and immediate groundwater environment (after dilution into the receiving groundwater).

Table 5. Summary of PHREEQC modelling (selected parameters) for coal discard seepage

Parameter	90 th Percentile	Average	10 th Percentile
pH	4.59	7.83	8.02
pE*	0.3-11	-3.6-8.0	-3.9-8.0
Alkalinity	<1	47	59
Cl	21	10	2.2
S(6)	8 292	2 535	342
TDS (by Sum)	10 781	3 387	517
F	5.5	2.8	0.27
Na	53	30	6.0
K	67	34	6.2
Ca	446	541	111
Mg	1 691	191	18
Al	4.6	0.00035	0.00048
Fe	152	0.12	0.028
Mn	24	2.1	0.20
Cr	0.0080	0.00023	0.00014
Cu	0.068	0.067	0.0033
Si	14	6.9	0.17
Zn	15	0.44	0.15



Conclusions

Lower moisture retention and saturation predicted in the uncovered discard material resulted poor seepage quality due to high rate of oxygen diffusion and higher oxidation rates. Source-pathway-receptor modelling, based on site specific conditions and cover configurations demonstrated potential long-term impacts from a thick evaporative covers and geosynthetic liner. The overall study approach demonstrated that the required groundwater quality criteria can be met with the alternative (cost-effective) cover design.

References

- Golder Associates (2007). LandSim Version 2.5.17. Golder Associates UK Ltd.
- Golder (2005). Contamination Impact on Groundwater: Simulation by Monte Carlo Method. UK Environment Agency R&D Publication 132.
- INAP (2014). The International Network for Acid Prevention. Gobar Acid Rock Drainage Guide (GARD Guide), <http://www.gardguide.com>
- SoilVision Systems (2016). SVFlux and Chem-Flux Saturated / Unsaturated Finite Element 1D/2D/3D Seepage Modelling Software. SoilVision Systems Ltd., Saskatoon, Canada.
- PHREEQC Interactive, USGS Version 3.312.12
- Van Zyl A, Naicker K and Barnard P (2018). P Risk-based Modelling of Soil Cover for Rehabilitation Planning of Coal Discard Facility in South Africa to Achieve Groundwater Quality Criteria, IMWA conference proceedings.



Evaluation of Acid Rock Drainage Potential in a Retrospective Study 25 Years after Mine Closure: Acid Base Accounting Statistics are Not Sufficient

R.V. (Ron) Nicholson¹, Sean Shaw², Sarah Barabash¹ and John Lundagan³

¹*EcoMetrix Incorporated, 6800 Campobello Road, Mississauga, Ontario Canada, rnicholson@ecometrix.ca, sbarabash@ecometrix.ca,*

²*Ministry of Energy and Mines, British Columbia, Canada, Sean.Shaw@gov.bc.ca,*

³*ArcelorMittal Dofasco, john.lundrigan@arcelormittal.com*

Abstract

Waste rock at a former iron mine with 70 million tonnes of rock distributed in 15 discrete deposits was evaluated for acid generating characteristics. Two of the 15 deposits exhibited acidic drainage while all others remained neutral 25 to 40 years after deposition. The carbonate neutralization potential (Carb-NP) exceeded the acid potential (AP) in all deposits and only 10% of the samples represented potentially acid generating (PAG) material. The acid drainage from the 2 deposits could not be readily explained by average ABA characteristics. Differences in spatial distributions of sulphide and carbonate minerals in piles can explain differences in neutral and acidic conditions.

Keywords: ICARD, IMWA, MWD 2018, acid base accounting, iron mine, closure, acid drainage, carbonate neutralization potential

Introduction

The former Sherman Mine, located in Ontario, Canada, exploited iron oxide from a banded iron formation operated from 1968 to 1990. Reclamation of the site occurred between 1990 and 1995. Five open pits (North, South, East, West and Turtle) produced about 70 Mt of mine rock stored in 15 discrete rock deposits.

The iron deposits primarily consisted of magnetic iron oxide (magnetite) and carbonate minerals with sulphide minerals, primarily pyrite (FeS₂) and marcasite (FeS₂) that occurred in carbonaceous bands adjacent the ore in the South and East pits. Most mine rock was typically deposited adjacent to the pits. Prior to 1977, some sulphide rock was used for roadbed construction and some was deposited in rock piles. Rock that was identified after 1977 as high sulphide and potentially acid generating from the South and East Pits was segregated and deposited within saturated tailings.

Two of 15 rock deposits exhibited acidic drainage. All others had neutral drainage 25 to 40 years after deposition. One area that exhibited acidic drainage represented a pile

of mine rock from the early mining of the South Pit. The other area represented a road embankment (East Embankment) that was constructed from South Pit mine rock early in the operation. While the acid drainage reports to an on-site lake, the acid and metals are assimilated in the receiving environment and the water meets stringent regulatory requirements for the protection of aquatic life prior to leaving the former mine site.

This study focused on the sampling of the rock piles and contact waters from the individual piles and deposits to assess the characteristics that could be used to understand the differences between the piles that produced acidic drainage and those that produced neutral drainage. The rock was assessed for acid base accounting (ABA) characteristics and the porewaters evaluated for chemical constituents related to sulphide oxidation and neutralization reactions.

Methods

As part of an investigation of acid generation at the mine site in 2014, over 500 individual mine rock samples were collected from the 15 mine rock deposits. These samples were re-



covered. More than 200 rock samples, from 48 boreholes and 42 test pits, were submitted for ABA analysis and 58 test pit samples were subjected shake flask extraction (SFE) tests to assess porewater concentrations. The porewater concentrations were calculated from the soluble masses of constituents from the SFE divided by the measured water contents of the rock samples. The number of rock samples collected from each individual deposit was approximately proportional the rock mass in each pile relative to the total rock on site. Mineralogy was assessed quantitatively on selected sample using the QEM Scan method.

Acid Base Accounting Results for all Rock Samples

Carbonate minerals within the mine rock from the West and North pits were primarily composed of calcite and dolomite, with siderite and ankerite making up a substantial portion of the carbonates in the rock from the South, East and Turtle pits. Overall, carbonate contents ranged from 0.06% to 18% CO_3 with a geometric mean value of 2.2% CO_3 (50 kg- CaCO_3 /tonne). The acid base accounting (ABA) characterisation included carbonate analysis on all samples and modified Sobek test (Lawrence and Wang, 1996) with siderite correction (Skousen et al., 1997).

Comparison between the modified Sobek and siderite corrected NP values showed excellent agreement (Figure 1). The calculated carbonate neutralisation potential (Carb-NP) and the Sobek-NP results gave a strong correlation coefficient ($R^2 = 0.98$) with slightly smaller Carb-NP values than Sobek-NP values below levels of 100 kg CaCO_3 /t (Figure 1). The Carb-NP values were considered to represent the “effective” NP and were therefore used to calculate the NP/AP ratios (NPR) in order to classify samples for the potential to generate acid or not (Price, 2009).

The mine rock contains sulphide minerals, mainly pyrite, with sulphide-sulphur contents ranging from 0.01% to 5% S and a geometric mean value of 0.24% S. About 50% of the samples contained less than 0.1% S. The sulphide-sulphur content represents approximately 88% of the total sulphur in the mine rock, and 12% of the total sulphur is present as sulphate, which is consistent with weathering for three decades or more.

The geometric mean Carb-NPR values for all mine rock was 9.5, suggesting that all rock combined should represent non-PAG material. About 10% of the 210 samples had Carb-NPR values less than 1, representing PAG rock and 83% had Carb-NPR values greater than 2, representing non-PAG rock (Figure 2).

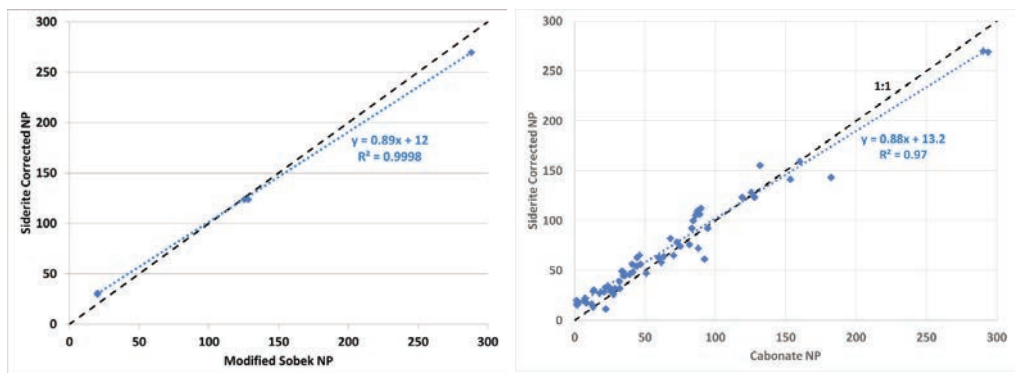


Figure 1. Siderite corrected NP compared to modified Sobek NP (left) and carbonate NP (right).



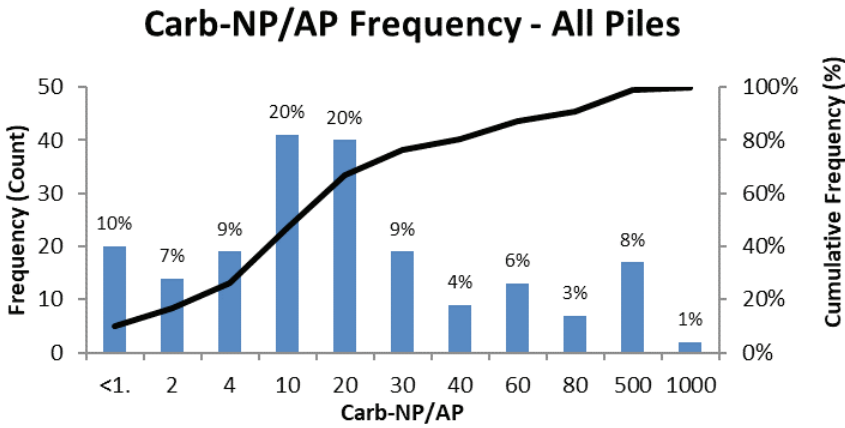


Figure 2: A frequency distribution plot of Carb-NPR for all rock samples.

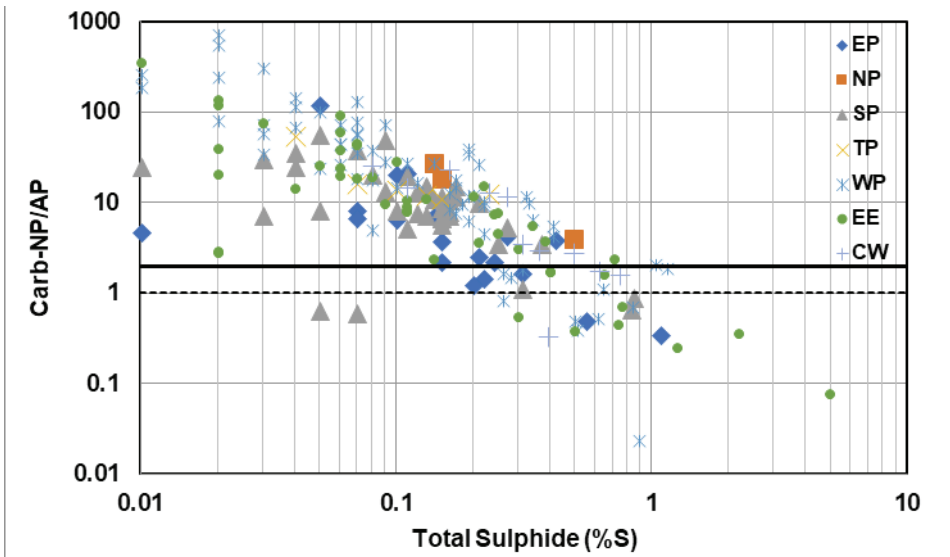


Figure 3. Carb-NP in relation to sulphide content for samples from the individual pits.

Acid Base Accounting Results from Individual Piles

The results for the various piles, including those from the East Pit (EP), North Pit (NP), South Pit (SP), Turtle Pit (TP), West Pit (WP), the East Embankment (EE) and Causeway (CW) were examined separately. The Carb-NPR and sulphide sulphur results in Figure 3 show that rock samples from all pits have similar ranges of values and all but the North Pit and Turtle pit have samples with NPR values less than 1. The three highest sulphide contents were in samples from the East Embankment.

Assuming that the neutralization potential is effective and that it will maintain neutral pH conditions when consuming acid, a sample with a Carb-NPR of greater than two will be considered non-PAG. A sample with a Carb-NPR less than one will be classified as PAG and a sample with a Carb-NPR between one and two will be classified as uncertain. The statistics for the Carb-NPR values for rock from the individual piles and/or pits are summarized in Table 1. The results show that only 20 of the 210 samples had Carb-NPR values less than one and would be considered as PAG. The percentage of samples



representing PAG material in individual piles or pits range from 0 to 15%. The two rock deposits exhibiting acidic drainage, the East Embankment and South Pit-northeast (SP-NE) are highlighted with 15% and 8% of the samples, respectively, having Carb-NPR values less than one. About 6% of the samples had Carb-NPR values between one and two and represent an uncertain classification. The remaining 81% of the samples represent non-PAG material.

The geometric mean value for Carb-NPR values of the individual rock units range from 2.1 to 14 with an overall geometric mean of 9.5, suggesting statistically that the rock piles overall should represent non-PAG material. The two rock piles exhibiting acidic drainage had geometric mean Carb-NPR values of eight, similar to the overall geometric mean of 9.5. Many of the rock units had 10th percentile Carb-NPR values less than one with an overall 10th percentile of 0.8, consistent with 10% of the overall samples having Carb-NPR values less than one.

The frequency distributions for sulphide-sulphur and Carb-NP for all rock samples were similar among all deposits. However, t-test results show that the mean Carb-NP values are significantly different ($p < 0.01$) between the East embankment and all other rock samples and F-test results indicate that the variances in sulphide and Carb-NP are significantly different ($p < 0.001$) for the East embankment samples compared to all others. Nonetheless, these statistically significant differences do not provide a strong indication of the potential for acid generation.

Porewater Chemistry from Individual Piles

The results of the shake flask extractions (SFE) were used to estimate the concentrations of products of sulphide oxidation and acid neutralization in the porewaters of the waste rock pile. All SFE rinse waters had neutral pH with values greater than or equal to six. A plot of calcium plus magnesium with sulphate is shown in Figure 4. In theory, the neutralization of the acid by the dissolution of carbonate minerals should result in a slope between one and two depending on whether one or two moles of calcium-magnesium carbonate solids dissolved to neutralize the two moles of acid produced with one mole of sulphate.

The calcium plus magnesium to sulphate molar ratios vary with the concentrations of sulphate in the porewaters as shown in Figure 4. At sulphate concentrations greater than about 1000 mg/L, the calcium plus magnesium to sulphate ratio is consistently equal to one and the calcium concentration is likely controlled by precipitation of gypsum ($\text{CaSO}_4 \cdot 2\text{H}_2\text{O}$) and this reaction likely plays a role in the control of the calcium plus magnesium to sulphate ratios. At sulphate concentrations between 100 and 1,000 mg/L, the average calcium plus magnesium to sulphate ratio is equal to about two. A ratio of two agrees with the theoretical upper bound value for dissolution of calcium-magnesium carbonate minerals by acid in an open system. This suggests that an NP/AP ratio of two is appropriate to classify non-PAG materials in these waste rock piles. At sulphate concentra-

Table 1. Summary of Carb-NPR values from individual pits and piles. Piles with acid drainage are highlighted.

Mine Rock Stockpile	Number of Samples	Geometric Mean	10th Percentile	90th Percentile	# of Samples Carb-NPR < 1.0	% of Samples Carb-NPR < 1.0	# of Samples Carb-NPR < 2.0, >1.0	% of Samples Carb-NPR < 2.0, >1.0
Causeway	12	5	0.7	26	1	8%	2	17%
East Embankment	47	8	0.5	68	7	15%	3	6%
EP	19	2.1	0.5	7	2	11%	3	16%
NP	3	13	7	26	0	0%	0	0%
SP-NE	24	8	1.7	36	2	8%	0	0%
SP-SW	19	11	3.0	32	2	11%	0	0%
TP	15	14	4	81	0	0%	0	0%
WP	71	14	0.7	143	6	8%	5	7%
All	210	9.5	0.8	75	20	10%	13	6%



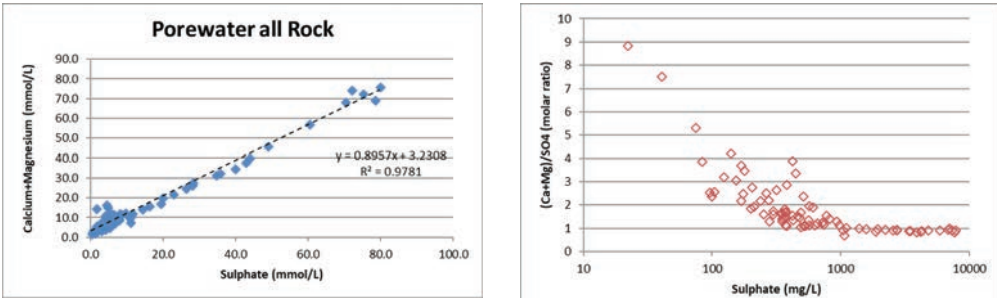


Figure 4. Calcium plus magnesium concentrations (left) and calcium plus magnesium to sulphate molar ratios (right) variations with sulphate concentrations.

Table 2. Geometric mean concentrations of calcium, magnesium and sulphate concentrations and average calcium plus magnesium to sulphate molar ratios in porewaters from individual pits and piles. Piles with acid drainage are highlighted.

Mine Rock Stockpile	Number of Samples	Ca (mg/L)	Mg (mg/L)	SO4 (mg/L)	Average (Ca+Mg)/SO4 molar ratio
East Embankment	16	491	136	1391	1.6
EP	9	140	124	503	1.9
NP	2	176	42	446	1.3
SP-NE	9	229	76	515	2.5
SP-SW	7	251	62	554	1.6
TP	10	163	77	448	2.9
WP	29	183	70	466	1.9
All	82	220	85	557	2.0

tions of less than 100 mg/L, the calcium plus magnesium to sulphate ratios increase well above two suggesting that carbonate mineral dissolution is not controlled by acid produced by sulphide oxidation in the few samples with the lower sulphate concentrations.

The calcium, magnesium and sulphate concentrations in the porewaters in the East Embankment, that generates acid drainage, were typically two times greater than those from the other piles and pits (Table 2) and the calcium and sulphate values appear to be near gypsum solubility. The porewater concentrations in the other acid generating pile (SP-NE) do not appear to be different than those from the other non-acid generating piles.

The average calcium plus magnesium to sulphate ratios for individual piles range between 1.3 and 2.9 with an overall average of 2.0 (Table 2). There are no evident differences in the ratios between the acid generating and neutral drainage piles.

The depletion rates for sulphide and carbonate solids in the piles were estimated from concentrations in porewater samples adjusted to loading rates (Table 3). The porewater concentrations in samples collected from the top 5 m of the various rock piles were converted to a loading rates assuming a one-year residence time. Sulphide depletion rates were based on geometric mean sulphate loadings and carbonate depletion rates were based on geometric mean calcium plus magnesium loadings. Depletion times were then calculated from the geometric mean sulphide and carbonate contents, assuming 50% of the total sulphide and total carbonates were available for reaction measured values.

The sulphide depletion times for the individual rock piles ranged from 6 to 40 years from the date of sampling in 2014. The carbonate depletion times ranged from 44 two 800 years. The carbonate depletion times in the acid generating piles (EE and SP-NE) were in the low end of the range but estimated



to be many decades into the future and other neutral drainage piles had similar depletion times.

Discussion

The results of this investigation have shown through many lines of evidence regarding the ABA characteristics of the waste rock materials that, on average, the rock at this former iron mine is non-PAG. This raises important questions. How does acid generation occur in a rock pile with excess carbonate neutralization potential? And, how do we avoid this risk in studies that are intended to predict future behaviour of waste rock for proposed mines?

A modelling study by Pedretti et al. (2017) addressed the generation of acidity in the rock piles as a function of different spatial distributions of acid generating and acid neutralizing minerals within the pile. The authors demonstrated that rock piles with the same overall NPR could produce either neutral or acidic drainage as a result of different distributions of sulphide and carbonate solids. In addition, the study showed that there may be high probabilities of producing acidic drainage in rock piles with average NPR values of two, a value that would typically be used to characterize rock as non-PAG. In a mixed pile containing PAG and non-PAG rock, maintaining a low probability of generating acid in the future may require an average NPR as high as 10

or greater. These results highlight the risks of using simple averages for acid base accounting to predict the acid generating potential of waste rock piles containing mixtures of PAG and non-PAG materials.

To date, strategies such as layering and encapsulating PAG materials with non-PAG materials in rock piles to mitigate acid generation have not been encouraging. Segregation of PAG from non-PAG rock for special management of the high-risk materials may be necessary to reduce the cost risks associated with potentially acidic drainage in mixed piles.

Conclusions

On average, the rock at the former Sherman mine had adequate neutralization potential to consume all potential acid produced by sulphide mineral oxidation. All piles had geometric mean Carb-NPR values that ranged from 2.1 to 14 and statistically would be classified as non-PAG piles. There were no obvious ABA characteristics that differentiated the acid generating pile from those with neutral drainage. No discernible differences were noted in the porewater chemistries between piles that were acid generating and those that had neutral drainage. The differences between the production of acid drainage in two piles and neutral pH drainages in the other 13 deposits were attributed to differing distributions of sulphide and carbonate minerals as suggested if a modelling

Table 3. Geometric mean sulphide and carbonate contents and calculated depletion times of rock in individual piles in 2014. Piles with acid drainage are highlighted.

Pile	Sulphide Sulphur %S	Carbonate %CaCO ₃	Sulphide Depletion Time (a)	Carbonate Depletion Time (a)
EE	0.13	3.3	6	61
EP-N	0.21	1.9	34	98
EP-NE	0.23	1.2	24	44
NP-N	0.22	8.7	29	464
SP-NE	0.11	2.6	12	98
SP-SW	0.14	3.6	15	141
TP-E	0.08	2.9	6	87
TP-N	0.14	5.1	6	132
TP-NE	0.09	5.6	39	503
WP-N	0.21	5.1	14	151
WP-NE	0.24	4.6	20	155
WP-S	0.09	7.7	14	404
WP-SE	0.12	2.5	14	103
WP-SW	0.05	9.7	15	806



investigation by Pedrettia et al. (2017). Mixing PAG and non-PAG rock with overall NPR values of greater than 2 does not guarantee neutral drainage. However, the risk of acid generation is likely low for the piles that have geometric mean NPR values greater than 10. Segregation of PAG rock for special management, when it represents smaller proportions of the total mine rock inventory, may represent a low risk alternative to mitigate acid generation.

Acknowledgements

The authors wish to thank ArcelorMittal Dofasco for supporting this work and the publication of this paper.

References

- Lawrence, R.W. and Wang, Y. (1996) Determination of neutralization potential for acid rock drainage prediction, MEND report 1.16.3, Mine Environment Neutral Drainage (MEND), Ottawa, ON, 149 p.
- Pedrettia, Daniele., K. Ulrich Mayer and Roger D. Beckie (2017) Stochastic multicomponent reactive transport analysis of low quality drainage release from waste rock piles: Controls of the spatial distribution of acid generating and neutralizing minerals, *J. Contam. Hydrol.*, 201: 30-38.
- Price, W.A. (1997) Draft guidelines and recommended methods for the prediction of metal leaching and acid rock drainage at minesites in British Columbia, British Columbia Ministry of Employment and Investment, Energy and Metals Division.
- Price, W.A. (2009) Prediction manual for drainage chemistry from sulphidic geologic materials, Canadian MEND report 1.20.1, Natural Resources Canada.
- Skousen, J.G., Renton, J., Brown, H., Evans, P., Leavitt, B., Brady, K., Cohen, L. and Ziemkiewicz, P. (1997) Neutralization potential of overburden samples containing siderite, *Journal of Environmental Quality*, Vol. 26(3), pp. 673–681.



Determination of the Rate of Release of Nitrates from Waste Rock, Tailings and Kimberlite in Field Conditions – A Case Study

Levi Ochieng, Björn Schröder

SRK Consulting, 265 Oxford Road, Illovo, Johannesburg, 2196, South Africa

Abstract

This paper presents a case study on the determination of the release rate of nitrates from waste rock, tailings and kimberlite using field kinetic tests (FKT). The FKT cells were monitored over a period of 3 years. The results of the study discussed in this paper include particle size distribution, mineralogy, percentages of leached nitrates, trends in leached nitrates (seasonal variability) and nitrates leaching rates. Geogenic nitrogen, also detected in basalt and kimberlite, is also discussed in this paper. The purpose of the study was to inform the development of a sustainable nitrates management plan.

Keywords: Field kinetic tests, nitrates, kimberlite, tailings, waste rock

Introduction

Nitrates are readily soluble in water and in this context constitute the aqueous phases of materials containing ammonium nitrate from explosives. However, establishing a direct link between blasting residues and nitrates entering the water system is extremely difficult to achieve. This is mainly because of the complexity of the deportment of nitrogen species following a blast, microbial activity that metabolises nitrate and ammonia and the lack of techniques to “fingerprint” nitrogen in residues to the nitrogen in explosives. The study used FKT monitored over a period of 3 years to establish the sources of elevated levels of nitrates in surface water at a mine and to determine the rate of release of nitrates from waste rock, tailings and kimberlite. The purpose of the study was to inform the development of a sustainable nitrates management plan for the mine.

The study site was characterised by extreme winter conditions with temperatures ranging between -15°C and 10°C. Maximum temperatures average 23°C in summer with a mean annual rainfall of 750 mm. Snowfalls are frequent and common between May and September.

Methods

The study established discrete FKT cells of blasted and unblasted waste rock, kimberlite and tailings. The cells were made of 1m³

polyvinyl chloride (PVC) barrels loaded with approximately 3.5 tonnes of test material. The cells were leached with rainwater from direct precipitation. The leachates were collected in 1.5L sample bottles and overflow from the sample bottles collected in 5L buckets.

The data collected during sampling included the date of sampling, volume of leachate collected in the sample bottles and buckets, temperature, pH, electrical conductivity and nitrate concentrations in the leachates.

Geochemical analysis undertaken on sub samples of the test materials included particle size distribution, mineralogical analysis by X-ray diffraction and batch leach test. Geogenic nitrogen in drill core samples of basalt (waste rock) and kimberlite were analysed using automated (Metrohm) Ion Chromatography.

Results and Discussion

Particles size distribution

Blasted waste rock consisted of 62% gravel, 24% sand, 12% silt and 2% clay. Blasted kimberlite was 84% gravel and 16% sand. Tailings was 88% sand and 12% gravel. Blasted waste rock was characterised by a finer particle fraction relative to the rest.

Particle size distribution is expected to have a significant influence on nitrate leaching rates in the materials. The nitrates in the materials occur mainly as mixed salts within the friable matrix (clay, silt and sand) and on the surfaces of the gravels following blasting.



Mineralogy

Silicate minerals, mainly plagioclase, smectite and diopside, dominated the waste rock, kimberlite and tailings mineralogy, Table 1. Calcite was present in kimberlite and tailings. X-ray diffraction did not identify any nitrogen bearing minerals.

pH of leachates

An increase in pH from neutral to alkaline occurred in the leachate from all the materials over time, Figure 1, except UBWR sample that appears to be going acidic in the December 2017 data. The increase in pH is attributed to the dissolution and weathering

of calcite, diopside and aluminosilicates that contributed to the overall neutralisation potential in the leachates.

Nitrogen species

The dominant nitrogen species leached from the materials was nitrate. The concentrations of nitrite (<0.1 mg/kg N) and ammonium (0.4 – 5.6 mg/kg N) were substantially lower than the concentrations of nitrate (0.4 – 26 mg/kg N) in the leachates. Ammonium will convert to nitrite, and nitrate under oxidising conditions, such as aeration or excavation, while nitrate will convert to ammonium under reducing circumstances.

Table 1. Mineralogical composition of waste rock, kimberlite and tailings.

Mineral Group	Mineral Name	Formula	BWR	UBWR	UBWRN	KMB	Tailings
Dissolving	Calcite	CaCO ₃				1.3	3.0
Fast weathering	Diopside	CaMgSi ₂ O ₆	23	24	26	21	16
Intermediate	Biotite	K(Mg,Fe) ₃ ((OH) ₂ AlSi ₃ O ₁₀)				8.1	14
weathering	Chlorite	(Mg,Fe) ₅ Al(AlSi ₃ O ₁₀)(OH) ₈	5.3	5.2	4.1	8.8	15
	Enstatite	MgSiO ₃	2.1	5.3	8.2		
	Heulandite	CaAl ₂ Si ₇ O ₁₈ (H ₂ O) ₆	1.8	2.2	2.3		
	Natrolite	Na ₂ Al ₂ (Si ₃ O ₁₀)(H ₂ O) ₂				1.1	
	Scolecite	CaAl ₂ Si ₃ O ₁₀ (H ₂ O) ₃				1.9	
	Stilbite	NaCa ₂ Al ₃ Si ₃ O ₃₆ ·14H ₂ O	4.9	5.1	2.8		
Slow weathering	Kaolinite	Al ₂ Si ₂ O ₅ (OH) ₄				2.9	5.7
	Plagioclase	(Na,Ca)(Si,Al) ₄ O ₈	43	32	34	9.5	3.1
	Smectite	CaMg ₂ AlSi ₄ (OH) ₂ ·H ₂ O	19	16	22	45	43
Very slow weathering	Muscovite	KAl ₂ (AlSi ₃ O ₁₀)(OH) ₂	1.8				

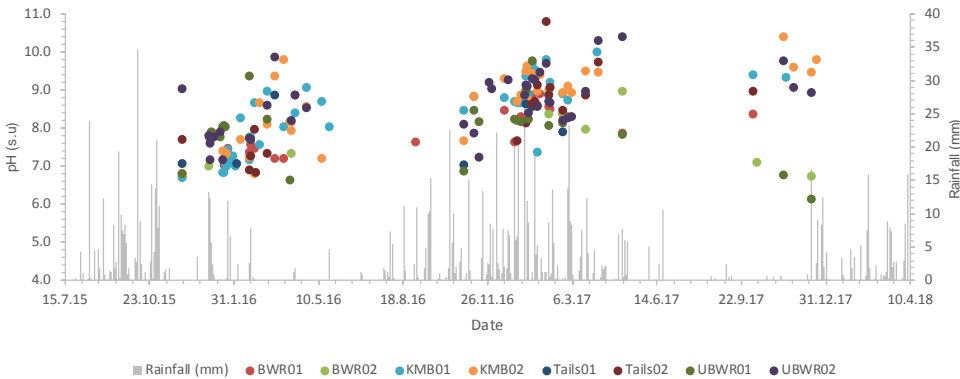


Figure 1 Graph showing change in pH over time for blasted waste rock (BWR), kimberlite (KMB), tailings (Tails) and unblasted waste rock (UBWR).



Table 3. *Percentage of nitrates leached from the leachable content in the materials.*

Description of test materials	FKT Cell	Total leached NO ₃ as N from bulk leaching (mg/kg)	Total leached NO ₃ as N from FKT (mg/kg)	Percentage of leached NO ₃ as N (%)
Blasted waste rock	BWR01	26	2.5	9.6
	BWR02		0.96	3.7
Blasted Kimberlite	KMB01	5.6	3.9	69
	KMB02		1.8	32
Tailings	Tails01	5.6	0.02	0.35
	Tails02		0.62	11
Un-blasted waste rock	UBWR01	0.4	0.049	12
	UBWR02		0.084	21

Percentages of leached nitrates

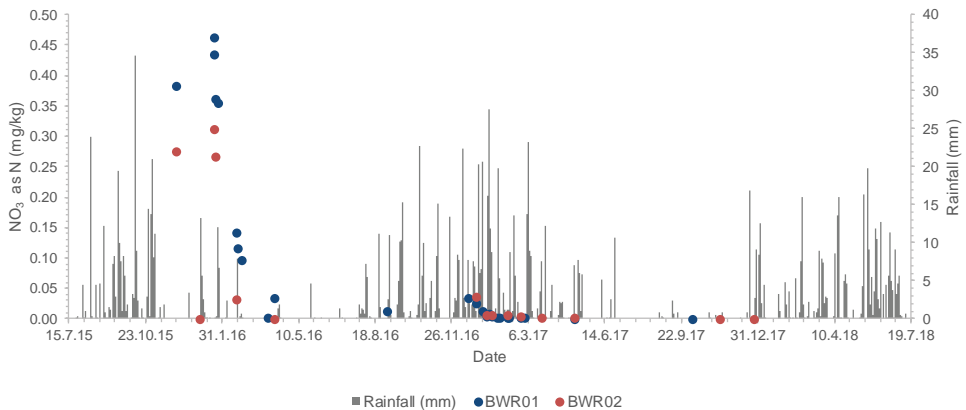
Kimberlite leached out the highest percentage of nitrates, 32-69%, of its leachable nitrate content, Table 3. Blasted waste rock leached out 3.7-9.6% while unblasted waste rock leached out 12-21%. The difference in particle size distribution accounted for the variability in the blasted and unblasted waste rock leaching rates. The unblasted waste rock had a higher gravel and sand content (88-93% gravel and 7-12% sand) relative to the blasted waste rock (62% gravel, 24% sand). The tailings leached 0.35- 9.4% of its leachable nitrate content.

Figure 2 to Figure 5 show the trends in leached nitrates from 2015 to 2017. The high-

est concentrations of leached nitrates occurred in the first rainy season in summer, October 2015 to April 2016. The leached concentrations dropped steadily in the subsequent rainy seasons, with little or no nitrates recorded in the leachates by the third year of leaching.

The trends showed that nitrates leached from the waste rock, kimberlite and tailings during summer from October to April. Insufficient to no leachates emanated from the materials during winter from May to September due to frozen conditions and lack of rainfall.

In reality, as deposition continues with the addition of more materials on the dumps and stockpiles, a continuous source of nitrates is maintained rather than depleted.

**Figure 2.** *Graph showing change in nitrate concentration in leachate from blasted waste rock (BWR).*

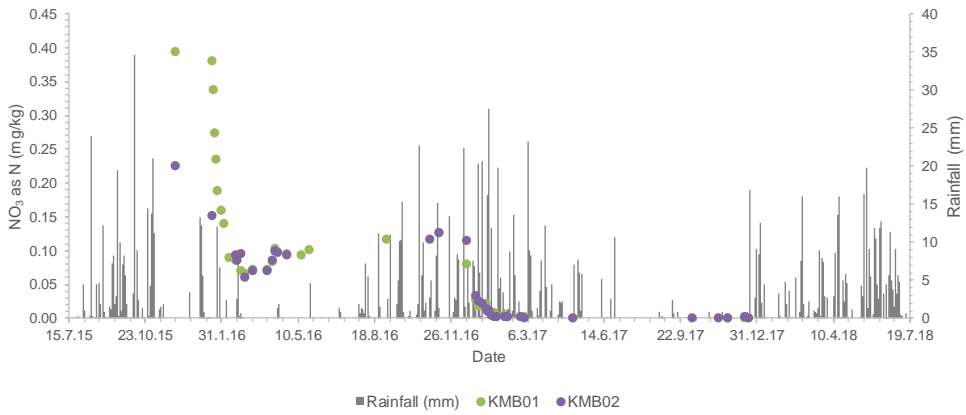


Figure 3 Graph showing change in nitrate concentrations in leachate from Kimberlite (KMB).

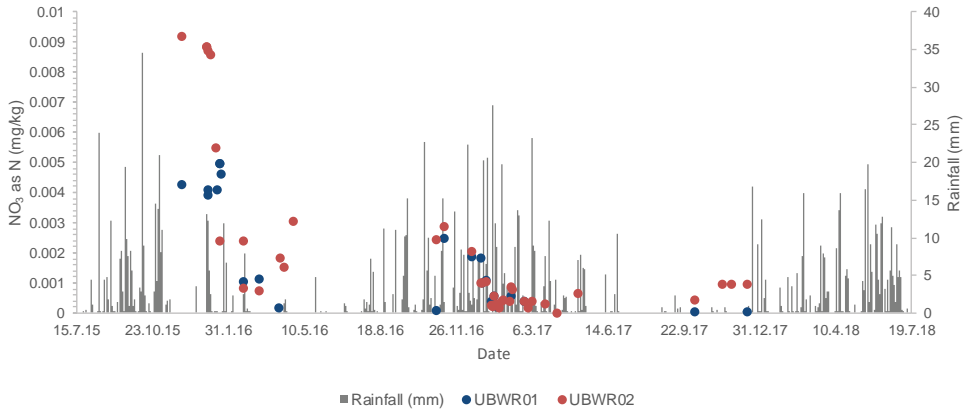


Figure 4 Graph showing change in nitrate concentrations in leachate from unblasted waste rock (UBWR).

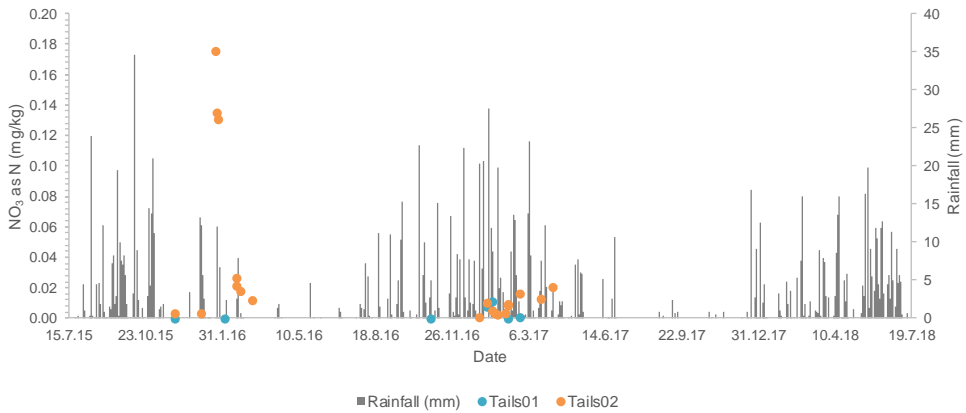


Figure 5 Graph showing change in nitrate concentrations from leachate from tailings (Tails).



Nitrate leaching rates

Blasted kimberlite (0.0002-0.024 mg/kg/day N) and waste rock (0.0001-0.019 mg/kg/day N) had high nitrate leaching rates relative to the tailings (0.0002-0.008 mg/kg/day N) and unblasted waste rock (0.0001-0.0024 mg/kg/day N), Table 2.

The study established the nitrate leaching rates to be as follows in decreasing order:

Blasted kimberlite > blasted waste rock > tailings > unblasted waste rock

The nitrate leaching rates of the waste rock, kimberlite and tailings were related to the particle size distribution in the materials rather than to the material types. Particle size distribution influences the size and distribution of the voids within the materials, which serve as pathways and storage spaces for fluids and gases contained in and moving through the material. The nitrates in the materials occur mainly as mixed salts within the friable matrix and on the surfaces of the larger particle fractions following blasting.

In reality, while the tailings nitrate leaching rates may be representative of the actual tailings conditions, the waste rock and kimberlite nitrate-leaching rate may be slightly lower than the actual waste rock dump and kimberlite stockpile because the actual dumps/stockpiles are characterised by a larger particle size fractions than the test materials.

Geogenic nitrogen

Various studies indicate that geogenic nitrogen contributes to ecosystem nitrogen saturation (more nitrogen available than required by biota), which leads to nitrogen leaching and elevated concentrations of nitrate in surface and groundwater (Dahlgren 1994, Holloway et al 2002). Release of nitrogen through weathering occurs at ecologically significant rates, with nitrogen release rates ranging from 10-20 mol N cm² s⁻¹ corresponding to nitrogen fluxes of 4-37 kg N ha⁻¹ yr⁻¹ (Holloway et al., 1999).

This study detected geogenic nitrate nitrogen of a range of 0.09 – 1.3 mg/L N in the leachate from un-weathered basalt and kimberlite. However, the quantified concentrations of the geogenic nitrates in un-blasted basalt and kimberlite were significantly low (> 5 times lower) relative to the quantified concentrations in the blasted basalt and kimberlite. Although insignificant relative to the explosives source, geogenic nitrogen occurs in the basalt and kimberlite and contribute to the nitrate loadings into the system.

Conclusions

The study established the nitrate leaching rates, associated with the particle size distribution, to be as follows in decreasing order:

Blasted kimberlite > blasted waste rock > tailings > un-blasted waste rock

Table 2. Nitrate leaching rates from the FKT cells.

Description of test material	FKT Cell	NO3 leaching rates (mg/kg/day)	
		Min	Max
Blasted waste rock	BWR01	0.0001	0.019
	BWR02	0.0001	0.018
Blasted Kimberlite	KMB01	0.0002	0.023
	KMB02	0.0002	0.024
Tailings	Tails01	0.0003	0.008
	Tails02	0.0002	0.008
Unblasted waste rock	UBWR01	0.0001	0.0024
	UBWR02	0.0001	0.0024



The study recommended nitrate reduction at source through improved handling, storage and blasting practices. The study also recommended that the stockpiling of kimberlite ore over an extended period, especially during the summer rains, should be minimised.

The predominant nitrogen species leached from the cells was nitrate. Although the concentrations of leached ammonium and nitrites were substantially lower than leached nitrates, ammonium will convert to nitrite, and nitrate under oxidising conditions, while nitrate will convert to ammonium under reducing circumstances. Therefore, all the nitrogen species are monitored in surface and groundwater.

Although insignificant relative to the nitrates from explosives, geogenic nitrogen contribute to the overall nitrate loading into the surface water system from the basalt and kimberlite.

Acknowledgements

The authors thank SRK Consulting South Africa for providing the opportunity and support for the writing of this paper. James Lake, Jo Daneel, Leone Ramatekoa and Mamosa Mohapi provided input and critical comments on the paper.

References

- Dahlgren RA (1994) Soil acidification and nitrogen saturation from weathering of ammonium-bearing rock. *Nature* 368:838-841, doi:10.1038/368838a0
- Holloway JM, Dahlgren RA (1999) Geologic nitrogen in terrestrial biogeochemical cycling. *Geology* 27(6):567-570, doi: 10.1130/0091-7613(1999)027<0567:GNITBC>2.3.CO;2
- Holloway JM, Dahlgren RA (2002) Nitrogen in rock: occurrences and biogeochemical implications. *Global Biogeochemical Cycles* 16(4):1118, doi:10.1029/2002GB001862



The role of metal-attenuation in groundwater quality prediction

G. Papini, P. Geo¹, J. Gossen, P. Eng¹, B. Pierce²

¹*Hemmera, an Ausenco company, Burnaby, British Columbia, gpapaini@hemmera.com*

²*Gibraltar Mines Limited*

Abstract

In this study we used PHREEQC to model metal attenuation in groundwater at a mine in central British Columbia. The results of the study were used to estimate metal loadings from groundwater in a site-wide water quality model. The focus was metal mobility in alluvial material downgradient of a pit lake and inactive heap-leach pile. The study included analysis of aquifer mineralogy and the model was calibrated using the mine's environmental monitoring database. The data were used to predict possible future concentrations at model prediction nodes (receptor) when loadings were combined with numerical groundwater model flow predictions.

Keywords: geochemical modelling, heap-leach, raffinate, pit lake, breakthrough curve

Objective

Previous water quality models have used rock dump and tailings seepage quality as the groundwater source term without consideration of metal attenuation. When applied in catchment-based, mass-balance models, these conservative source terms are thought to over estimate the groundwater loadings to surface water. This can lead to unrealistic predictions of potential environment effects and instill a sense of urgency for groundwater recovery and treatment. Our aim has been to incorporate metal attenuation considerations so that less conservative metal loadings from groundwater can be applied in site-wide water quality modelling.

Introduction

The mine has operated since the early 1970s and in 2013 increased mill throughput from 55 ktpd to 85 ktpd. Parts of several dumps were heap leached from 2007 to 2015. The pregnant leach solution was collected in ponds at the base of the leach facilities and pumped to the solvent extraction and electrowinning plant. Although underlain by naturally-occurring low permeability materials, seepage through the base of the heap-leached rock piles and collection ponds is thought to constitute the primary contaminant source to groundwater.

Important metal attenuation processes at mining sites include pH buffering and acid

neutralization; adsorption at the mineral-water interface; mineral precipitation and dilution / dispersion (Wilkin 2007). Previous model predictions considered only dilution/dispersion because of uncertainty quantifying the long-term stability of other processes. Field studies and column tests have shown that mineral assemblages present in tailings piles, underlying aquifers, and receiving waters play a pivotal role in controlling pH (Blowes and Ptacek 1994). Mineral phases important in buffering pH are calcite/siderite, iron and aluminium hydroxides and aluminosilicates.

Oxidation of iron sulphides in mine wastes results in the release of iron, sulphate, acidity and metals to solution. High aluminium and silica concentrations can occur from weathering of aluminosilicate minerals at low pH. Oxidation and hydrolysis reactions can subsequently lead to the precipitation of a wide array of hydroxide, sulfate and/or hydroxy-sulphate minerals depending on the geochemical and biogeochemical conditions (Nordstrom and Aplers 1999). These secondary minerals play important roles in attenuating contaminants from mine effluents. Examples of secondary minerals formed from acid mine waters that sorb or co-precipitate metals include hydrous ferric oxides (HFO); gibbsite (aluminium hydroxide); goethite (iron oxyhydroxide) and schwertmannite (hydroxy-sulphate).



Site Setting

The mine catchments vary in elevation from approximately 1,260 metres above sea level (masl) in the east to a lake and wetland-filled valley in the west at elevation around 830 masl. The flow path considered in this study is from a pit lake elevation at approximately 896 masl over approximately 500 m to a creek. The mean annual precipitation is 524 mm/year with about one quarter occurring as snow. Creek flows are seasonal (2 – 200 L/s) and higher in spring because of snow melt. Temperatures are below freezing from November through March when much of the precipitation falls as snow. Mean monthly temperatures vary from -12°C to 17°C.

The deposit host rocks are late Triassic to Early Jurassic intrusive granites. The deposits are classified according to structural system, and referred to as porphyry ores, and shear zone ores. The southerly dip of the mineral zones is offset by a series of northerly trending, generally steeply west dipping faults. The area has been intensely glaciated and most of the bedrock is covered by lodgement till, accompanied in places by ablation moraine and glaciofluvial deposits.

Older pits are used to store process water, including spent raffinate from the heap leach piles. Groundwater flow from these pit lakes and surrounding waste rock areas is predominantly through bedrock but also through glaciofluvial deposits downgradient of the waste rock dumps and within alluvial deposits west of the mining area. Shallow bedrock in the mining areas appears to have elevated hydraulic conductivity (1E-06 m/s to 5E-07 m/s) in comparison to undisturbed areas. The average hydraulic conductivity measured in glaciofluvial materials is

4E-06 m/s; however, there is a two to three order-of-magnitude difference in hydraulic between silty-clay till and the glaciofluvial sand and gravel.

Low pH seeps are observed at or near the base of the dumps. The seeps are seen to daylight where there is a change in slope or outcrop of low-permeability till. The seep flows are largely diverted to the mine's water management system. However, deeper flow systems and re-infiltration of seep water may bypass the collection ditches; although evidence for this is not conclusive.

Mineralogical Investigation

Sampling locations were selected as close to the toes of waste rock dumps that could be accessed by a drilling rig. Continuous soil samples were collected using a Sonic drill and submitted for total element (Sodium Peroxide Fusion, ICP-OES/MS & Eltra) and mineralogical analyses (XRD). Epoxy grain mounts were analysed using QEMSCAN Particle Map Analysis (PMA) at 3.0 µm pixel resolution to provide modal mineralogy combined with SEM-EDS to investigate the deportment of Cu, Fe and Mn. QEMSCAN is a definitive quantitative method based on a combination of Energy Dispersive Spectrometric (EDS) and Backscatter Energy (BSE) properties of the sample. Groundwater and seep samples were submitted for analysis of major and minor cations and anions, total and dissolved metals (ICPMS), pH and conductivity.

The mineralogical results from QEMSCAN improved the resolution of the ‘amorphous materials’ reported from XRD analysis. The soil mineralogy is comprised predominantly of quartz (52%) and feldspar (33%) with minor epidote (4%), Fe,Mg-silicates (3.8%), muscovite (2.9%) and chlorite (1.4%); and trace HFO (1%), garnet (0.2%), and CuOx/hydrox (0.01%). Approximately 3% was comprised of ‘others’, which are low BSE materials (possibly amorphous) that may comprise sulphides, carbonates, oxy-hydroxides and clays. MnOx/hydrox were generally absent or occurred in very low abundance. Al-hydroxides were not detected but may be present as amorphous phases. Carbonate minerals were not explicitly identified; however, total inorganic carbon analyses using the Elemental method indicated from 0.1% – 0.7 wt%. Carbonates (up to 6% calcite and 12% ankerite-dolomite) are present in waste rock samples collected as part of ML/ARD monitoring (SRK 2016).

Geochemical Modelling

Contaminant transport modeling was conducted using PHREEQC to simulate advective and dispersive groundwater flow; aqueous complexation; mineral dissolution and precipitation along a groundwater flow path; and adsorption and desorption on/off mineral surfaces. PHREEQC calculates one-



dimensional transport using a series of equal volume cells with specified groundwater composition and primary mineralogy. Secondary mineral phases are specified that can precipitate if they reach saturation. Each cell also has a defined surface which specifies the concentration of adsorbent minerals such as HFO. Contaminant transport through bedrock was not modeled because it has a lesser role in metal attenuation and is difficult to model.

Water quality from the pit lake was used as the source term (solution zero) and invariant over the model run of 105 years to predict potential post-closure groundwater quality. The initial mineral and groundwater composition along the flow path was based on unimpacted conditions. Important minerals considered to control Cu concentrations included calcite; copper carbonate; copper molybdenate; goethite and hydrous ferric oxide (HFO). PHREEQC separates HFO into strong binding sites (Hfo_s) and weak binding sites (Hfo_w). Dzombak and Morel (1990) determined that HFO has 0.2 mol Hfo_w sites/mol-HFO and 0.005 mol Hfo_s sites/mol-HFO.

Multiple simulations were completed by varying the input parameters to assess range in the results and sensitive parameters. Model calibration was carried out by comparing model results to analytical results from down-gradient monitoring wells to identify the best fit for multiple parameters. A good fit in both the monitoring results matching the predicted results as well as the input parameters matching field measured parameters (e.g. carbonates and HFO) provided confidence that the best fitting simulation could be used to predict concentrations at the prediction nodes. The breakthrough curve (Figure 1) shows pH, sulphate and metal concentrations (mg/L) over a 105-year period at a prediction

node considered to be the receiving environment.

Results

The model indicates that pH will drop in several incremental steps from around pH 7.6 to pH 6.68 at the receptor over the modelled period. Sulphate increases to approximately 1,500 mg/L early in the modelled period. Copper and Zn increase but stabilize at 0.12 mg/L and 0.0018 mg/L respectively after 12 years. Cobalt increases to 0.34 mg/L after about 25 years and Cd to 0.017 mg/L after about 75 years. (Figure 1).

Table 1 shows that Solution zero pH is buffered in the aquifer to pH 7.49 at the end of mining (2021) and at pH 6.68, 100 years post-closure (2121). All the metals are attenuated several orders of magnitude (up to four orders of magnitude for Cu) at the end of mining; however, Co and Cd breakthrough in the post-closure because of loss of attenuation in the aquifer.

A spatial profile for dissolved metals, pH and sulphate (Figure 2) shows dissolved concentrations along the flow path in 2121. After 105 years, the pH near the source is approximately 3.9 creating conditions conducive to alunite and $CuMoO_4$ precipitation. At this pH, HFO reacts to form goethite and mineral precipitation appears to attenuate molybdenum concentrations.

Where calcite is present, pH remains buffered at approximately 6.7. Adsorption of cadmium, cobalt, copper and zinc onto HFO is an important attenuation mechanism at this pH. Early precipitation of goethite along the flow path is expected to provide adsorptive sites for dissolved metals.

Once calcite has depleted, the pH drops to approximately 4.9. Under these conditions, goethite stops precipitating and mala-

Table 1. Average solution zero (mg/L) and predicted concentration at prediction node

Parameter	Solution zero	2021	2121
pH	4.42	7.49	6.68
Cu	355	0.0002	0.002
Co	0.31	0.00	0.33
Cd	0.011	0.000	0.017
Zn	2.4Cd	0.006	0.120
SO4	1,520	100-1,000 ¹	1,480

¹Sulphate curve range based on breakthrough in Figure 1



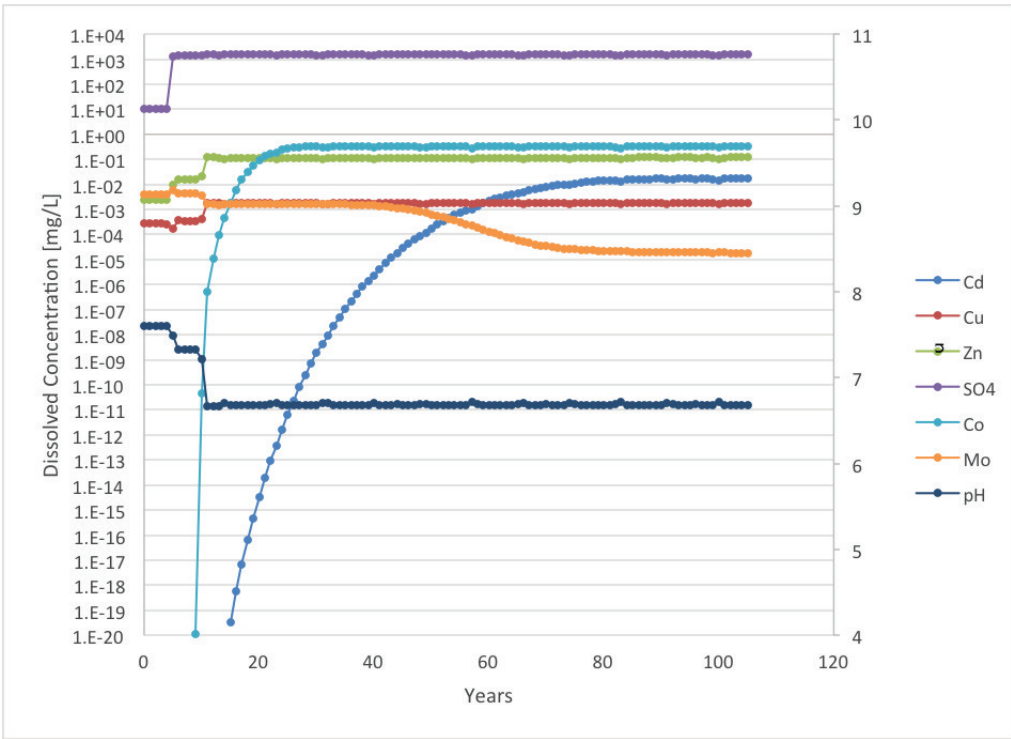


Figure 1 Breakthrough curve at prediction node approximately 500 m from source (CaCO_3 0.4%; HFO 0.02%; v - 100 m/y).

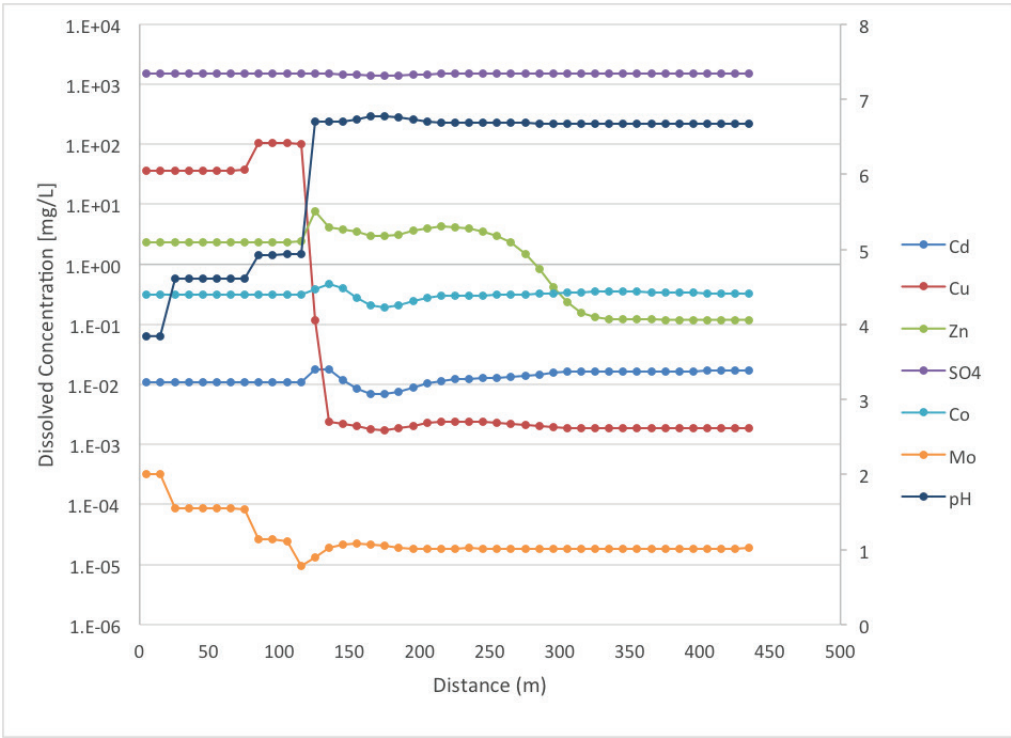


Figure 2 Post Closure (2121) concentrations (mg/L) along flow path (CaCO_3 0.4%; HFO 0.02%; v - 100 m/y).



chite and cupricferrite precipitate. Low pH favors copper adsorption onto HFO surfaces whereas these conditions are less favorable for cadmium, cobalt and zinc adsorption. Adsorption of cadmium and cobalt appears to be less favorable where pH is buffered to circumneutral values (Figure 2).

Conclusions

Geochemical modelling was carried out to simulate metal attenuation along the groundwater flow path with the objective of constraining groundwater metal loadings to surface water. The results indicate that although metal attenuation is significant, it is unstable where calcite is depleted in the aquifer. The groundwater velocity may overestimate the timing of the breakthrough curves; monitoring results suggest a slower rate of change

than predicted in the breakthrough curves.

Metal precipitation and adsorption on HFO is important in attenuating metals along the flow path, however, the depletion of calcite and ensuing reduction in pH can result in metal desorption from HFO sites and metal breakthrough at the receptor. Cobalt and Cd do not appear to attenuate to the extent of Cu and Zn and breakthrough occurs post closure.

This study is a preliminary attempt to understand the geochemical processes along this groundwater flow path. Ongoing characterization and calibration of the model coupled with frequent water quality monitoring will improve confidence in the metal loading predictions. Better understanding of carbonate distribution in the overburden aquifer would better constrain the model.

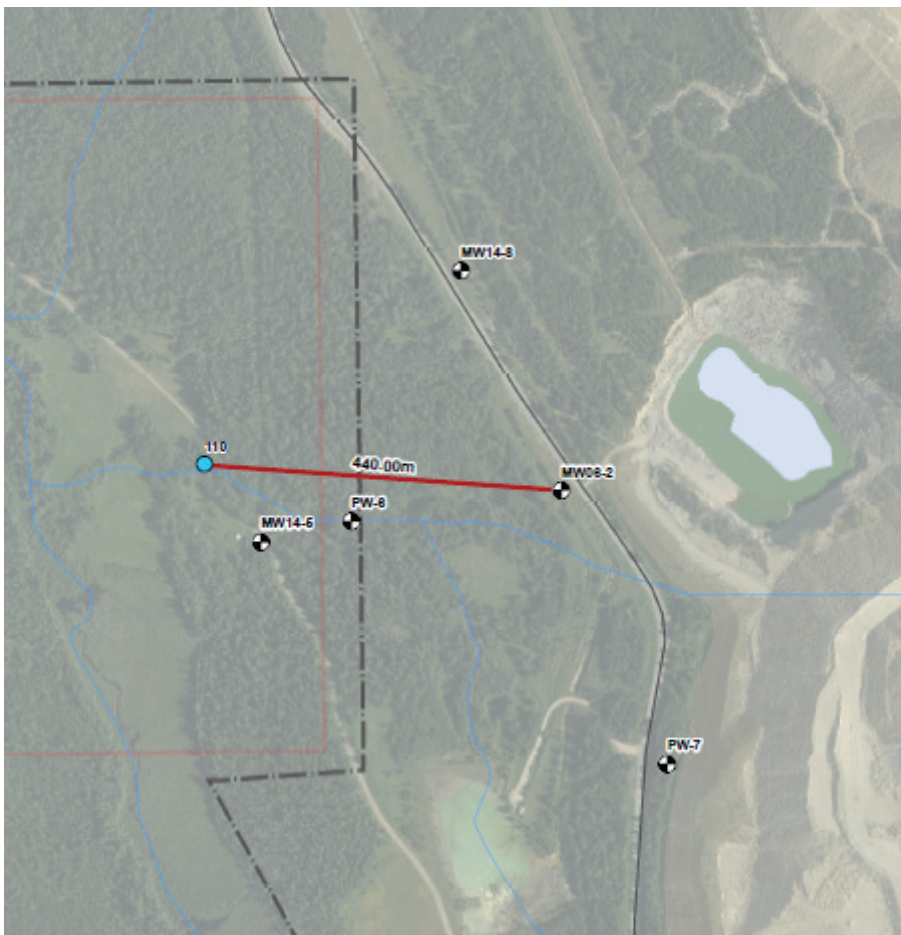


Figure 3 Pit lake, monitoring wells and prediction node



References

- Blowes DW, Ptacek CJ (1994) Acid-neutralization mechanisms in inactive mine tailings. In DW Blowes and JL Jambor, Eds. The environmental geochemistry of sulphide mine wastes, p.;271-292. Mineral Association of Canada, Waterloo.
- Dzombak DA, Morel FMM (1990) Surface Complexation modelling: hydrous ferric oxide. Wiley, New York.
- Nordstrom DK, Alpers CN (1999) Geochemistry of acid mine waters. In: G.S. Plumlee and MJ Logsdon Eds. The Environmental Geochemistry of Mineral Deposits, 6A, p.133-160. Society of Economic Geologists, Littleton.
- SRK (2016) Metal leaching and acid rock drainage characterization and drainage program. 2015 annual report prepared for Taseko Gibraltar Mines Ltd.
- Wilkin RT (2007) Metal Attenuation Processes at Mining Sites – Ground Water Issue. United States Environmental Protection Agency. EPA/600/R-07/092. September 2007.



Critical importance of conceptual model development when assessing mine impacts on groundwater dependent ecosystems: case study of an Australian mine development

Alan Anton Puhlovich

Golder Associates Pty Ltd, 1 Havelock Street West Perth Western Australia 6005 Australia

Abstract

Changes to groundwater conditions were assessed in the context of proposed open cut mining potentially impacting local groundwater dependent ecosystems (GDEs). Assessment of baseline groundwater conditions and reviews of published information on local GDEs and ecological studies were used to assess the nature of groundwater dependence of local GDEs. A revised conceptual model of GDEs found that key flora/fauna communities were more likely to be influenced by rainfall infiltration to the unsaturated zone in basement rocks (unaffected by mining) and recharge – discharge processes of nearby palaeochannel aquifers than those groundwater systems directly influenced by mining.

Keywords: hydrogeology, mine dewatering, impacts, groundwater dependent ecosystems

Introduction

SIMEC Mining is currently considering developing a new, hematite iron ore (open cut) mine at Iron Sultan, located at Camel Hills ("Site"), approximately 45 km west of the town of Whyalla in South Australia, Australia (Figure 1). A hydrogeological assessment was undertaken to evaluate potential changes to groundwater conditions as a result of the proposed mine.

The scope of the assessment comprised drilling investigations, well installations, field permeability testing, water quality sampling and analyses and assessment of other available data.

Site Setting

The Site is located in the Gawler Ranges district and to the west of the Iron Baron Mining Area (IBMA) (Figure 1) and within an arid to semi-arid climate, with potential evaporation substantially higher than rainfall (average rainfall and "Class A" pan evaporation are around 270 and 2,550/annum, respectively). The Site is located on the western flank of the regionally extensive, north-south trending Middleback Ranges (approximate elevation of 350 m Australian Height Datum, mAHD). A series of inter-connected salt lakes and playas, lie to the west of the Site (approximate elevation of 180-200 mAHD). The District is

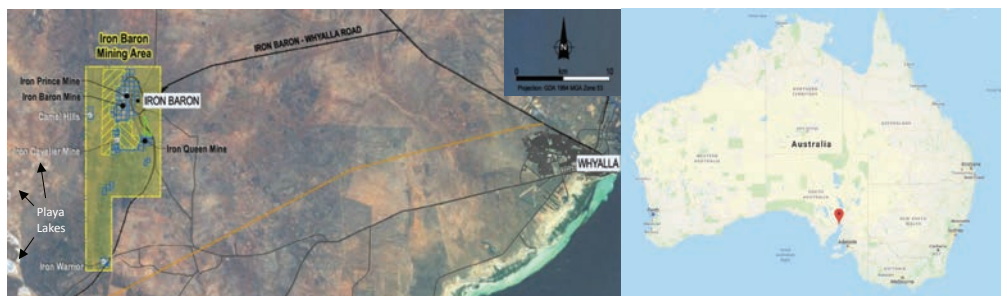


Figure 1 Site Location (adapted from information provided by SIMEC Mining)



characterised by three major physiographic units, “Sand Dunes & Flats”, “Plains” and “Hills & Rises” (DEWNR, 2013). A number of GDEs have also been mapped at a regional level. Surface water runoff is to the west, with flows in creeks between the salt lakes / playas typically ephemeral.

Regional Geology and Hydrogeology

The Site is situated in the Gawler Craton, a stable crystalline basement province containing Archaean to Mesoproterozoic rocks with thin overlying sediments of Neoproterozoic to Quaternary age overlying the basement rock (Rudd, 1094; Drexel et al., 1993). The key units in the region belong to the Middleback Subgroup and comprise a basal dolomite unit overlain by two iron formations that are separated by a schist unit of clastic origin. The depositional environment is interpreted to have been a shallow sea with a north-south trending shoreline with periods of shoreline progradation and marine transgression (Roache, 1996). The Kimban Orogeny has resulted in formation of broad, open folds and major north to northeast-trending mylonitic shear zones. The Kalinjala Mylonite Zone is a major north-south linear zone of intense ductile deformation extending the length of the eastern Eyre Peninsula (Roache, 1996). This depositional and orogenic environment has resulted in the formation of the steeply dipping, north-south trending Middleback Ranges.

The regional hydrogeology is characterised by unconfined/confined, fractured rock hydrogeological units of the Middleback Ranges underlying unconfined aquifers in surficial Tertiary and Quaternary sediments located in lower areas of the landscape. The fractured rock units are saline to brackish with low yields. Groundwater of potable quality is mostly found in Quaternary limestone and Tertiary sand aquifers along the south and west coasts (Berens et al., 2011).

Although groundwater recharge rates to the fractured rock units are not well understood, recharge is thought to mostly occur where basement rocks outcrop or sub-crop at or near the Ranges (Berens et al., 2011). Recharge to fractured rock groundwater sys-

tems in this setting is considered to be irregular and localised (Berens et al., 2011).

Initial Conceptual Model

Prior to the undertaking of field (hydrogeology) investigations, an initial hydrogeological (conceptual) model was developed to describe groundwater conditions, with a focus on likely groundwater recharge – discharge processes.

Groundwater recharge occurs along the ranges, with groundwater flows from these areas to the west. Hydraulic gradients are a subdued reflection of the topographic gradients. Groundwater discharges to the salt lakes / playas and supports their presence. Vegetation in the salt lakes / playa areas rely on groundwater sourced from groundwater recharging in the ranges.

Hydrogeology Investigations

The key stratigraphic units of interest are the Katunga Dolomite, Lower Middleback Formation and Cook Gap Schist of the Middleback Subgroup, which together with steeply dipping banded iron formations (BIFs), comprise the north-south trending main ridge of the Middleback Ranges (Parker and Flint, 2012). Granitic basement and dolerite is commonly encountered on both sides of Camel Hills, with dolerite and amphibolite intrusions found as cross-cutting structures. Schist / quartzite units are observed along the eastern side of the hills (Parker and Flint, 2012). The results of site mapping indicate that a north-south striking limonite-goethite orebody exists and is bound by the BIFs (east), granitoid rocks (west) and fault structures to the north and south (Figure 3). Quaternary-age scree deposits overlie the bedrock to the west of the Site. Fractured rock aquifers are present at depth, with the groundwater system low yielding and saline-hypersaline quality. Recharge occurs along the ranges to the east of the deposit, with groundwater discharging to the west towards the salt lakes / playas (Figure 1).

Baseline hydrogeological investigations were undertaken to characterise site groundwater conditions and define, by way of reviews of published information on local GDEs and ecological studies, the nature of groundwa-



ter dependence of GDEs at and downstream of the deposit. Hydraulic conductivities of the orebody rocks (CHMW02 & 05) were measured to range between 2.7 to 3.5×10^{-3} m/s, whereas the east and west wall rocks (CHMW01, 3 & 4) have measured hydraulic conductivities that range from 2.1×10^{-7} to 8.9×10^{-6} m/s. Groundwater within the orebody rocks typically have lower Chloride concentrations (78 to 96 mg/L, CHMW02 & 05) than that found in groundwater in wall rocks (275 to 750 mg/L, CHMW01 & 3), suggesting higher rate of groundwater movement along the north-south orebody.

The orebody rocks are interpreted to form a “strip aquifer”; mining below the water table is likely to cause preferential flows and draw-downs beyond the pit to be greater along strike of the orebody. Groundwater levels across the site, measured at the time of site investigations range between 150.0 and 150.5 mAHd and in-

dicate a westerly hydraulic gradient reflecting topographic gradients (Figure 2).

Revised Conceptual Model

The initial conceptual model has been revised in light of further analysis of site hydrogeological and other data. Key focus of this revision was the interpretation of likely interactions between groundwater conditions and GDEs. Regional scale mapping of GDEs (NWC, 2012) was utilised, with two key GDE types identified locally: 1. GDEs that rely on subsurface presence of groundwater (vegetation), 2. GDEs that rely on surface expression of groundwater (rivers, wetlands, springs) (Figure 3). This revision of the conceptual model proposes a subdivision of upland, mid-catchment and lowland groundwater sub-catchments, corresponding with the three major physiographic units, Sand Dunes & Flats, Plains and Hills & Rises (Figure 4).

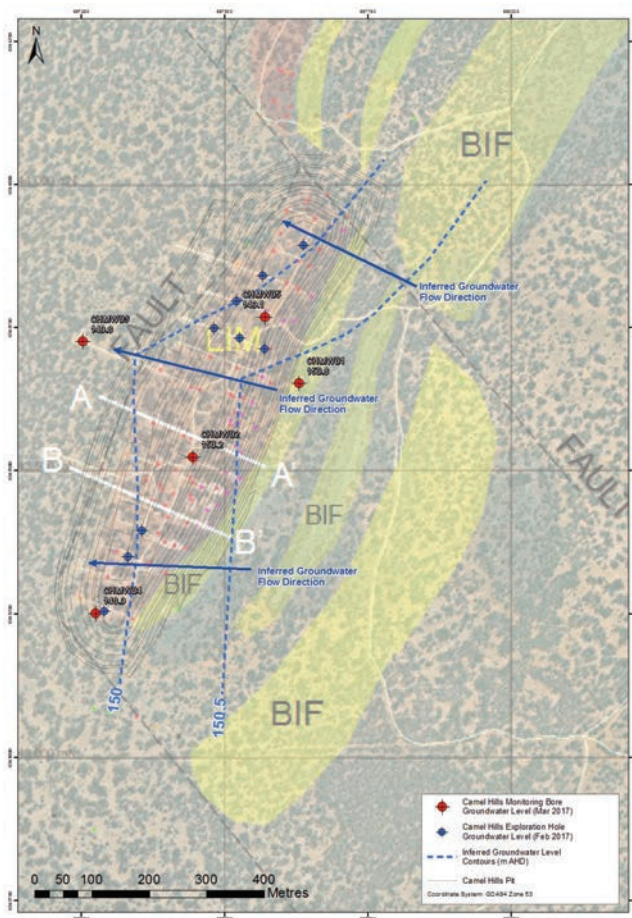


Figure 2 Site Geology, Groundwater Levels and Flow Directions



Upland Area

Groundwater recharge rates are highest in the Upland Area (“Hills & Rises”), primarily due to the presence of outcropping bedrock units (i.e. fractured BIFs, Quartzites). The results of site investigations indicate that local hydrogeological units are strongly anisotropic, with east-west hydraulic conductivities orders-of-magnitude lower than north-south hydraulic conductivities. This is due to the depositional and orogenic environment resulting in north-south striking rocks. Estimates of net groundwater recharge have been made using the CSIRO groundwater recharge-discharge calculation method (Leaney et al., 2011) and available groundwater quality data. Specific inputs included annual rainfall, annual rainfall chloride flux, groundwater chloride concentration, soil clay content, soil type, and vegetation type. Net groundwater recharge rates are estimated to range from 0.3 to 6.1 mm/year (or about 0.1 to 2.3 % of average annual rainfall).

Key terrestrial vegetation species in this area include Hummock grassland (*Triodia irritans*), Gilja (*Eucalyptus brachycalyx*) Red Mallee (*Eucalyptus oleosa*) (EBS 2015) (Brandle, 2010). These are deep rooted plant species, particularly the *Triodia* species which is very deep-rooted. Given that historic depths

to groundwater (at IBMA) are reported to range from 40.46 to 122.22 m below ground level (Jacobs, 2017), it is expected that these species tap small pockets within faulted / fractured rocks that are highly weathered and contain infiltrated waters. These pockets are seasonally replenished by direct infiltration of rainfall. It is interpreted that for this reason mapping data show vegetation density in this area to be low and GDEs mapping data (Figure 4) suggest that there is a “*low potential for groundwater interaction*”.

Mid-Catchment Area

Groundwater recharge rates are likely to be substantially lower than in the Upland Area (“Plains”) due to the presence of above-water table Quaternary scree deposits, which mostly lie above the water table and minimise downward percolation of infiltrated waters. Estimated baseflow rates to the Lowland Area to the west, based on measured hydraulic conductivities and gradients are very low, estimated to be just 90 m³/day/1 km section. This calculation assumes a notional 20 m aquifer thickness contributes to groundwater discharges to stream / drainage lines between salt lakes and playas to the west in the Lowland Area. The mapped data indicate a “*high potential for groundwater interaction*” with

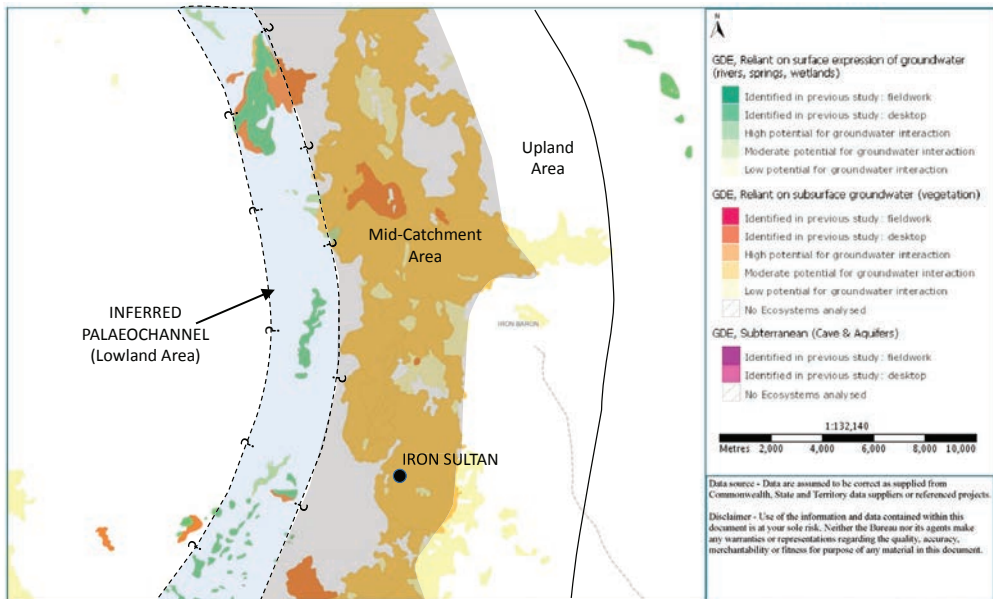


Figure 3 Mapped GDEs (adapted from NWC, 2012)



vegetation density higher than in the Upland Area and more dependent on groundwater. It is interpreted here that the presence of scree deposits and greater degree and depth of weathering provide a larger and more uniform storage of rainfall infiltration, above the water table, supporting this higher vegetation density.

Lowland Area

The Lowland Area (“Sand Dunes & Flats”) is characterised by saltmarsh, sand dunes and plains. Small watercourses, such as Salt Creek located to the south of the study area, drain surface runoff between (and to) the salt lakes / playas. While there are no known stream-flow gauging data for any of these local watercourses, anecdotal evidence indicates that these watercourses are ephemeral and only flow periodically during the months of February to March, when high intensity storms (e.g. related to ex-tropical cyclones in the summer months) are at their greatest (Mining Plus, 2015); Jacobs, 2017).

It is interpreted that a palaeovalley exists along an indicative alignment as illustrated in Figure 3, based on the locations of mapped GDEs as well as regional palaeovalley mapping undertaken by Bell et al. (2012). It is expected it has a much higher storage capacity and hydraulic conductivity than adjacent and more extensive weathered and fractured basement aquifers. The cross-sectional area and properties of the aquifers in the palaeovalley aquifers are unknown but expected to be similar to the Gawler-Eucla palaeovalley “demonstration site” (Magee, 2009).

Conceptually, it is considered that given the likely low permeabilities of basement rock, and ephemeral nature of flows to high intensity rainfall events along and to the palaeovalley, that groundwater is not a significant contributor to surface water flows. However, groundwater heads at the palaeovalley are probably strongly controlled by heads in the adjacent basement rock. Groundwater discharge rates to the salt lakes / playas, and related drainage lines, are likely at around the same rates of evaporation, resulting in surface precipitation of salt at the surface.

Key vegetation in the saltmarsh and drainage areas includes (*Eucalyptus Oleosa*

ssp oleosa) (*Eucalyptus gracilis*) (*Lomandra effusa*) (*Geijera linearifolia*) (*Triodia scariosa ssp scariosa*) (Bebbington 2011) Sandhill Wattle (*Acacia ligulata*), Lignum (*Muehlenbeckia cunninghamii*) and Samphire (*Tecticornia indica*), while in the sand dune and plain areas there are Black Oak (*Casuarina Pauper*), Cypress Pine (*Callitris glaucophylla*), Mallee pine (*Callitris preissii*) and Boonaree (*Heterodendrum oleaefolium*) (Brandle, 2010). The underlined species are deep rooted (BGSa, 2018) and do not source saline groundwater. It is inferred that these plant species draw groundwater from shallow aquifers within palaeochannel sediments and sediments in other drainage lines. These aquifers are periodically recharged during periods of high stream flow (seepage losses) and infiltration of runoff from adjacent areas (Figure 4).

Conclusions

The results of the study have led to modification of the conceptual model in that the vegetation communities are more likely to rely on direct rainfall infiltration to the unsaturated zone and/or shallow ephemeral aquifers within drainage / palaeovalley-related sediments rather than discharge of deeper, regional groundwater. Specifically, the study has found that local areas along the creek line where deeper-rooted vegetation are noted are more likely to be tapping into small zones where local recharge of groundwater occurs and collects in fresh water “pockets”, above the regional, saline water table. Salt lake and salt marsh surface features present in the salt lake / playas reflect zones of groundwater discharge and salt accumulation, primarily in areas where shallow clays are present in the near-surface. The study highlights the critical importance of understanding GDEs, the nature of their occurrence and their connections with local and regional groundwater systems.

Acknowledgements

The author thanks SIMEC Mining (Jennifer Gerard and Chris Smyth) for supporting the preparation of this paper and presentation of company information and Jennifer Lallier, Aidan Moyse and Wade Dodson for their technical assistance.



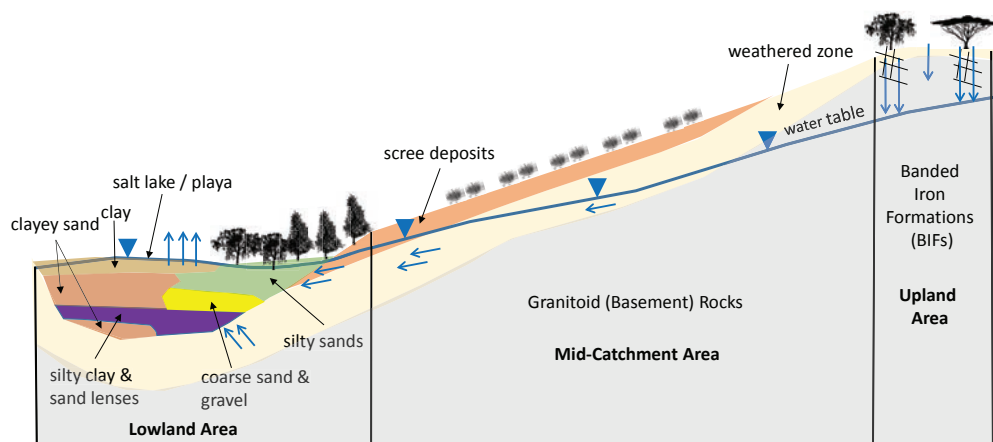


Figure 4 Revised Conceptual Model

References

- Bell, J.G., Kilgour, P.L., English, P.M., Woodgate, M.F., Lewis, S.J. and Wischusen, J.D.H. (compilers), 2012, WASANT Palaeovalley Map – Distribution of Palaeovalleys in Arid and Semi-arid WA-SA-NT (First Edition), scale 1:4 500 500. Geoscience Australia Thematic Map (Geocat No. 73980).
- Berens, V., Alcoe, D. and Watt E., 2011, Non-prescribed Groundwater Resources Assessment – Eyre Peninsula Natural Resources Management Region, Phase 1 – Literature and Data Review, DFW Technical Report 2011/16, Government of South Australia, through Department for Water, Adelaide.
- Botanic Gardens of South Australia (2018): Plant Selector (<http://plantselector.botanicgardens.sa.gov.au>)
- Brandle, R. (2010) A Biological Survey of the Eyre Peninsula, SA. Dept. for Environment and Heritage, SA.
- Department of Environment, Water and Natural Resources (2013), Gawler Ranges District Profile – Characteristics and Challenges.
- Drexel, J.F., Preiss W.V. and Parker, A.J., (1993), The Geological Survey of South Australia. Vol. 1, The Precambrian. South Australia. Geological Survey. Bulletin, 54.
- Ecological Australia (2017), Surface Water Assessment – Iron Baron Mining Area. Report prepared for Arrium Mining. September 2017.
- Jacobs (2017), Iron Baron Hydrogeological Impact Assessment, Assessment of Revisions to Tailings Deposition and Dewatering. Report to Simec Mining. 15 September 2017.
- Leaney, F., Crosbie, R., O'Grady, A., Jolly, I., Gow, L., Davies, P., Wilford, J. and Kilgour, P., 2011, Recharge and discharge estimation in data poor areas: Scientific reference guide, CSIRO. 61 pp.
- Magee, J.W., 2009, Palaeovalley Groundwater Resources in Arid and Semi-Arid Australia – A Literature Review. Geoscience Australia Record 2009/03. 224 pp.
- Mining Plus Pty Ltd. (2015), Cavalier, Empress and Baroness High Level Hydrological Review. Report prepared for Arrium Mining Limited.
- National Water Commission (2012), Atlas of Groundwater Dependent Ecosystems (GDE Atlas) Phase 2. Task 5 Report: Identifying and Mapping GDEs.
- Parker, A.J. and Flint, R.B., 2012, Middleback 1:100,000 Scale Geological Map, South Australian Department for Manufacturing, Innovation, Trade, resources and Energy, Adelaide.
- Roache, 1996. The geology, timing of mineralisation, and genesis of the Menninnie Dam Zn-Pb-Ag deposit, Eyre Peninsula, South Australia. PhD Thesis. December 1996.
- Rudd, E.A., 1940, The Geology and Ore Reserves of the Middleback Ranges, South Australia. 26/2/40 1940.





Laboratory Simulated Tailings Drain Seepage Columns: Flooded and Free-Draining Conditions

Lindsay Robertson¹, Jennifer Durocher², Brent Usher³

¹*Klohn Crippen Berger Ltd., Associate, Sr. Geochemist 101-1361 Paris St. Sudbury, ON, P3E 3B6, lrobertson@klohn.com, jdurocher@klohn.com*

²*Klohn Crippen Berger Ltd, Associate, Sr. Hydrogeochemist, Level 5 – 43 Peel St, Brisbane, QLD 4101 busher@klohn.com*

Abstract

The weathering and oxidation of sulphides in tailings disposal areas can contribute significant concentrations of metal(loid)s, and sulphate to the tailings pore water and dam drainage systems. Elevated concentrations lead to the formation and accumulation of secondary minerals in key drainage features, resulting in a change in physical dam fill characteristics.

Test columns were designed to understand the formation of secondary minerals in underdrainage systems under open and flooded conditions. Both test columns resulted in secondary mineral accumulation and results indicate the chemical composition of the tailings and pore water, and availability of oxidants in the drainage system play a role in the formation of secondary minerals.

Keywords: secondary mineral precipitates, laboratory columns, tailings, ARD/ML

Introduction

The oxidation and subsequent dissolution of sulfide minerals in tailings storage facilities (TSFs) results in the release and mobilization of metals, metal(loid)s, sulphate, and acidity, to the tailings surface and pore waters. These processes are commonly known as acid rock drainage (ARD) and metal leaching (ML). Reviews of sulphide oxidation, the formation of acid mine drainage and the mobilization of metal(oid)s are given by, Lindsay et al (2015), Alpers (1999), Blowes (2003) and Lottermoser (2007); among many others.

When ML/ARD is present, the concentrations of Fe and sulphate (among others) within the pore water can reach supersaturation with respect to secondary minerals and form precipitates. Physical changes to the tailings and dam materials, due to the dissolution of primary tailings grains and precipitate accumulation can compromise the physical stability of tailings dams by changing the material permeability and possibly increasing the phreatic surface within the structural shell of the dam. The objective of this assessment was to evaluate the difference in seepage compo-

sition (as it relates to secondary mineral precipitates) from a free flowing (or open drain system) and a flooded (less oxic) drain type to support the design of future tailings dam buttress drains. The sites evaluated in this study consist of legacy tailings dams containing moderately sulphidic tailings (2% to 10% pyrite and pyrrhotite) in Canada.

Methods

Column Testing

Several methods of investigation were employed to meet the overall objective including a field water quality monitoring program, solid-phase and static geochemical leachate testing on tailings materials, and a laboratory column experiment. The laboratory column program was designed to assess the accumulation of precipitates in granular materials under controlled laboratory conditions. The columns simulate the set up of two dam buttress drain designs; a simulated “oxic” free-draining and “anoxic” flooded drain. The experimental set up and analysis program are described further below. A schematic of the test columns is presented in fig. 1.



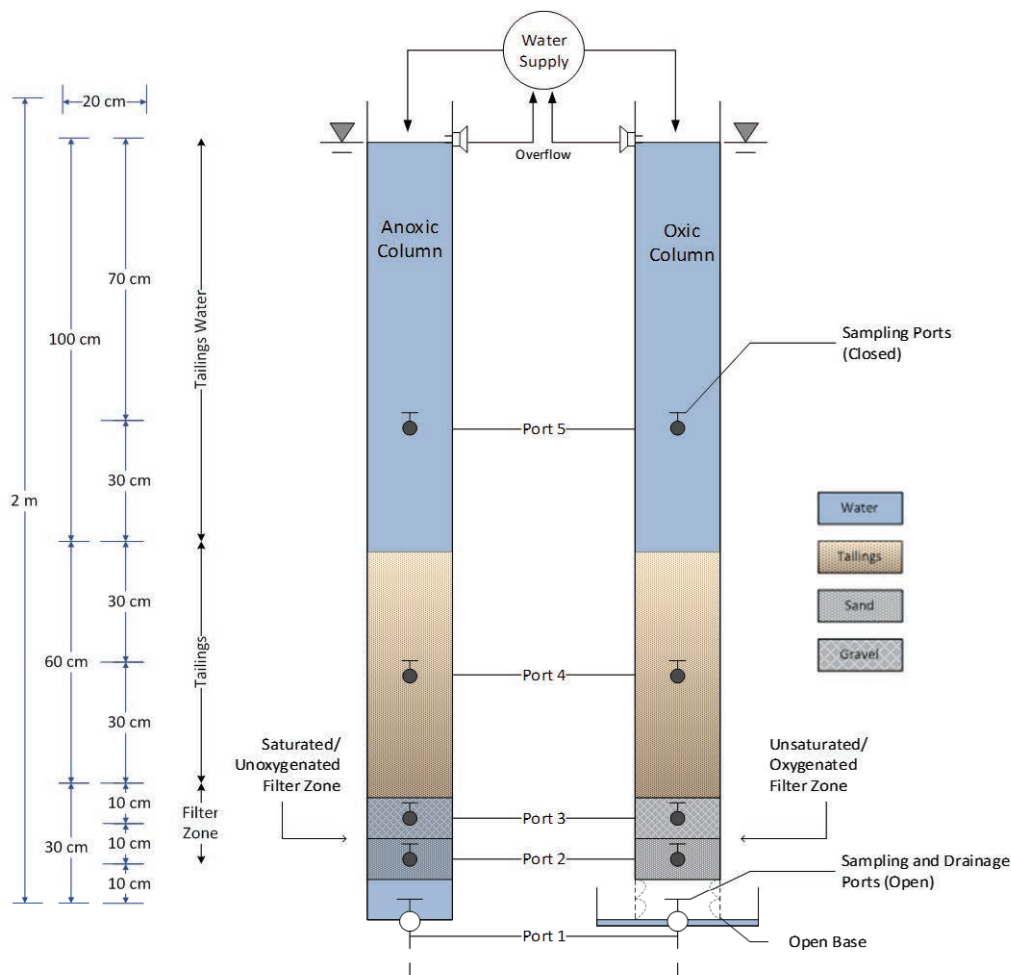


Figure 1 Column Test Schematic.

Flow through the columns and the residence time of pore waters was controlled by the permeability of the materials. The tailings ($K_{\text{sat}} \approx 2 \times 10^{-6}$ m/s), filter sands ($K_{\text{sat}} \approx 1 \times 10^{-4}$ m/s), and filter gravel ($K_{\text{sat}} \approx 1 \times 10^{-2}$ m/s) were excavated from the tailings area, and sourced from local stockpiles, respectively. The tailings were mixed before being split and placed in the columns. Tailings were subaqueously deposited, allowed to settle, and the supernatant was removed. Tailings pond water was filled above the tailings layer and a constant head was maintained by sustaining a constant feed of water and an overflow drain. The top of the test column was open to air and water from the overlying water column was allowed to percolate through each of the layers and drain freely through the bottom of

each column. Flow rate through the columns was approximately 6 L/day.

The upper (Port 5) and lower (Port 1) ports, representing the overlying water and base, respectively, were sampled weekly from both columns and select parameters were measured immediately [pH, redox potential (Eh), temperature (T), electrical conductivity (EC), and dissolved oxygen (DO)]. These parameters were measured every five weeks in the other ports. Pore water was collected every five weeks for laboratory analysis of pH, Eh, T, DO, acidity, alkalinity, chloride, bromide, nitrate (as N), nitrite (as N), sulphate, phosphate, hardness (as CaCO_3), total Fe^{2+} , total Fe^{3+} , dissolved metal(loid)s, and total metal(loid)s. The columns operated for 55 weeks.



Field Testing

Field monitoring of tailings pond water, tailings pore water from sampled monitoring wells, freely flowing embankment drain pore water, embankment drain pipes, freely flowing embankment seepage emergence points, and downstream (DS) seepage collection ponds has occurred for various dam and drain configurations, including a flooded toe drain, and open drain conditions (fig. 2).

Select parameters were measured immediately (pH, Eh, T, EC, and DO) and laboratory analysis of the parameter suite described for the column testing was conducted at an accredited laboratory within recommended test hold times.

Results

Tailings Pond and Pore Water

Tailings pond water quality, is assumed to be at equilibrium with the atmosphere and is represented generally by low pH (<5.0), moderate to high Eh (200 mV to 400 mV), and relatively low dissolved and total iron concentrations. Similar characteristics are observed in the column testing, though total iron concentrations are observed to be lower in the column testing. Tailings pore water characteristics are significantly different from the tailings pond water, with sulphide oxidation and secondary mineral dissolution processes resulting in changes in pH, Eh, and metal concentrations (Durocher et al, 2017) (tab. 1).

The pond water, in both columns and on site, has a much lower total iron and sulphate concentrations compared to the tailings pore water. This is due to changes in equilibrium conditions between the pond and tailings and the availability of iron from oxidized and partially oxidized tailings. The total iron concentrations in the field are significantly higher than the column testing due to a lower Eh allowing more Fe^{2+} to remain in solution.

Tailings Drain and Seepage Water

Significant differences are observed between the flooded and free draining systems in the columns and field conditions within the drain water (Port 2 and Port 3). The flooded drain was observed to be more effective at keeping iron in solution than the free draining column (fig. 3).

The testing indicates that the operational conditions of the columns are sufficiently different to result in different water quality. The pH (fig. 4) and Eh (fig. 5) in the drain layers of the columns were similar, however the flooded column maintained higher total iron concentrations in the drain for longer. A decrease in total and dissolved iron was also observed in the flooded column from the tailings pore water to the base indicating a mass loss through precipitate formation at times during the testing. Precipitates were observed forming at the top and bottom of the sand layers and in the gravel layers in both columns.

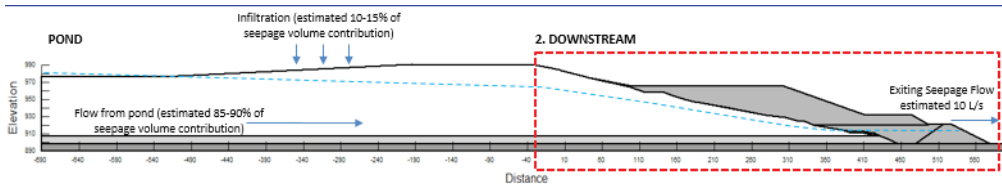


Figure 2 Field Monitoring Location Schematic.

Table 1. Average Results for Tailings Pond and Pore Water

Parameter	Port 5 – Flooded	Port 5 – Free Draining	Tailings Pond Field Results	Port 4 – Flooded	Port 4 – Free Draining	Tailings Pore Water Field Results
pH (units)	3.7	3.7	3.4	4.4	4.4	5.7
Eh (mV)	279	288	329	201	178	55
SO ₄ (mg/L)	979	981	947	1206	1163	4875
T-Fe (mg/L)	0.45	0.17	1.4	39	32	1767
D-Fe (mg/L)	0.20	0.13	1.0	35	30	1542



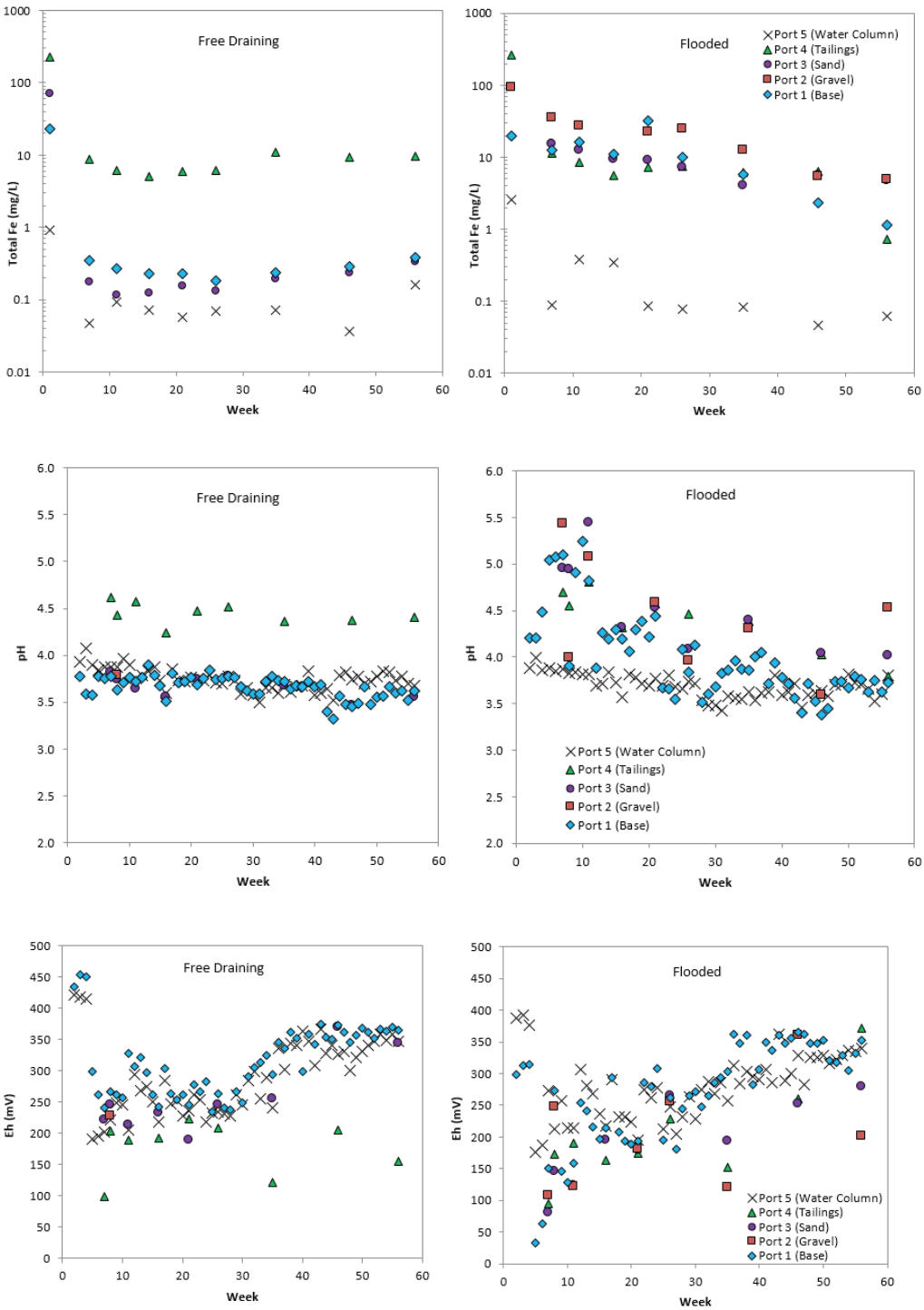


Figure 5 Eh over Time (Both Columns).



Water quality measured at the base of the columns at the start of testing were significantly different between columns between set-up and operation (flooded and free draining), however, over the test period, the pH and Eh at the base of the columns became similar as new pond water percolated through the columns (fig. 4 and fig. 5). These changes in pH and Eh, also resulted in changes to the dissolved and total iron concentrations at the base of the flooded column, with a decrease in total iron from 20 mg/L to 1 mg/L and dissolved iron from 13 mg/L to 0.3 mg/L. Total iron concentrations in the free-draining column were steady over the test period (fig. 3).

The drain and seepage water observed in the field exhibited similar trends to the column testing between the tailings porewater and seepage emergence points (tab. 2). The total and dissolved iron concentrations in the free draining dam are much lower than the flooded drain due to the age and operation of the facility behind the dam. In the field, the flooded drain system exhibited a larger decrease in both total and dissolved iron outside the drain more immediately than the free draining system where the change in total and dissolved iron concentrations are observed largely within the dam drain.

The flooded drain system does not achieve anoxic conditions (under field or laboratory conditions), with Eh values reported between 33 mV and 350 mV in the columns and between 156 mV and 450 mV in the field. The flooded system does however result in less oxidic conditions overall than the free draining system. The DO ranges from 4.4 mg/L to 9.0 mg/L in the columns and 4.2 mg/L to 11.1 mg/L in the field (DO is greater than 9 when T is less than 10°C). This was also observed by (Awoh *et al*, 2014) with a similar size column

set-up. Their findings indicate that the oxygen contained within the overlying water is replenished in the tailings pore water leading to mildly oxidic conditions. This mechanism is important when evaluating the continued oxidation of sulphides, and changes to equilibrium conditions in the pore water.

Saturation Indices and Mineral Precipitation

The geochemical software PHREEQC_i was used to understand aqueous speciation, saturation and potential geochemical reactions in the column pore waters. This geochemical modelling was compared with field observations and mineralogical testing for the different drain configurations.

The saturation index (SI) for various iron minerals including those previously observed in SEM investigations were predicted for pore waters using PHREEQC_i (WATEQ4f). Results indicate the average pore water in both columns is supersaturated with respect to many mineral phases including Goethite ($\alpha\text{FeO}(\text{OH})$), Hematite (Fe_2O_3), Jarosite ($\text{KFe}_3(\text{SO}_4)_2(\text{OH})_6$), Maghemite ($\gamma\text{Fe}_2\text{O}_3$), Ferrihydrite ($\text{Fe}_{10}\text{O}_{14}(\text{OH})_2$), and Melanterite ($\text{FeSO}_4 \cdot 7(\text{H}_2\text{O})$). While direct precipitation of many of these phases are not expected under the conditions in the pore waters, these minerals have been observed as secondary coatings as a result of ageing and crystallization of ferric sulphates and hydroxides like Schewertmannite ($\text{Fe}_{16}\text{O}_{16}(\text{OH})_{12}(\text{SO}_4)_2$) and Ferrihydrite.

Precipitates were observed in both columns throughout the testing. This was also observed in the field investigations, however the field accumulation of precipitates in the free-flowing drain system were significantly higher than the accumulation in the flooded

Table 2. Average Results for Dam Drain and Seepage Water

Parameter	Tailings Pore Water - Flooded	Dam Drain - Flooded	Seepage - Flooded	Tailings Pore Water - Free Draining	Dam Drain - Free Draining	Seepage - Free Draining
pH (units)	6.4	5.2	4.9	5.6	6.3	3.8
Eh (mV)	37	140	193	52	101	287
SO ₄ (mg/L)	6138	3978	3315	3100	1280	1432
T-Fe (mg/L)	1540	1242	687	80	31	35
D-Fe (mg/L)	1085	1010	681	35	1	25



drain. Field observations and testing of precipitates show good correlation with predicted minerals including iron oxy-hydroxides, iron oxy-sulphates, and sulphate minerals.

Summary

In the free draining system, as water moves through the tailings, total and dissolved iron, sulphate, and other parameters increase due to oxidation and dissolution of sulphides and secondary minerals. Equilibrium conditions in the tailings pore water (low Eh) allow for total and dissolved iron concentrations to remain high in the pore water. When tailings pore water moves through the drain, equilibrium conditions change, and the increased availability of oxidants (both O₂ and Fe³⁺) and increased Eh cause aqueous Fe²⁺ in porewater to oxidize and form secondary Fe³⁺ oxy-hydroxides and/or sulphates along the emerging seepage pathway.

In the flooded system, the tailings pore water characteristics are similar to the free draining system until seepage reaches the flooded drain. In the flooded drain, the availability of oxidants (and change in Eh) is limited. The equilibrium conditions change, but the reaction processes responsible for the formation of secondary minerals are also limited, resulting in sustained total and dissolved iron concentrations in solution.

Conclusions

The objective of the column testing was to obtain a better understanding of the geochemical reactions occurring in simulated drain conditions under a controlled laboratory setting. The columns were designed to assess the differences between the free-draining and flooded drain types and whether the flooded drain provided a significant improvement in reducing precipitate accumulation and geochemical changes within the system.

Based on the work performed to-date, pore waters in both columns were elevated in iron and sulphate concentrations. The reduction in concentration of total and dissolved iron observed between the tailings pore water and drain effluent in the free draining column

indicates that more iron is lost to secondary mineral precipitation in the free draining column than the flooded column. However, visual observations indicate that the small loss of iron between the tailings pore water and seepage in the flooded system is also resulting in precipitate formation. These laboratory observations compliment the field observations including changes in water quality and observed precipitate accumulation in the dam drains. Additional work is ongoing to assess the rate of precipitate accumulation and to further quantify the effectiveness of the flooded drain on reducing precipitate accumulation.

Acknowledgements

The authors thank the project team involved in the work for their contributions to the experimental design and test methods.

References

- Alpers Boorman, R.S., and Watson, D.M. 1976. “Chemical processes in abandoned sulphide tailings dumps and environmental implications for North Eastern New Brunswick”. Canadian Inst. Min. Bulletin., Vol 69, pp. 86-96.
- Awoh, A.S., Mbonimpa, M., Bussiere, B., Plante, B., and Bouzahzah, H. 2014. “Laboratory study of highly pyritic tailings submerged beneath a water cover under various hydrodynamic conditions.” Mine Water Environ, Vol 43, pp. 241-255.
- Blowes, D. W., Ptacek, C. J., Jambor, J. L. and Weisener, C. G. 2003. “The geochemistry of acid mine drainage”. 9.05. In Treatise on Geochemistry, Ed. Sherwood, B., Holland, H.D., and Lollar K.K.T Vol. 9. pp. 149-204
- Durocher, J.L., Robertson, L.A., and Usher, B.H. 2017. “Sulphide oxidation in TSFs and its influence on long term dam stability”. Paper presented at Tailings and Mine Waste, Banff, AB.
- Lindsay, M.B.J., Moncur, M.C., Bain, J.G., Jambor, J.L., Ptacek, C.J., and Blowes, D.W. 2015. “Geochemical and mineralogical aspects of sulphide mine tailings”. Applied Geochemistry, Vol 57, pp. 157-177.
- Lottermoser, B.G., 2007., Sulfidic Mine Wastes. In Mine Wastes-Characterization, Treatment, Environmental Impacts., Second Ed. Springer.



Sr/Ca and $^{87}\text{Sr}/^{86}\text{Sr}$: A tracer for geochemical processes in mine wastes.

Musah Salifu¹, Kjell Billström², Olof Martinsson¹, Johan Ingri¹, Bernhard Dold¹,
Lena Alakangas¹

¹*Division of Geosciences and Environmental Engineering, Department of Civil, Environmental and Natural Resources Engineering, Luleå University of Technology, 97187, Luleå, Sweden.*

²*Department of Geological Sciences, Swedish Museum of Natural History, Frescativägen 40, Box 50007, 104 05 Stockholm, Sweden.*

Abstract

Understanding geochemical processes in mining environments are essential to waste management decisions including remediation. In an attempt to understand geochemical processes, chemical data have mostly been used but these have often led to inaccurate conclusions. Therefore, in this work $^{87}\text{Sr}/^{86}\text{Sr}$, Sr/Ca and other elemental ratios (Ca/K and Rb/Sr) in leachates were employed to constrain the geochemical processes in an abandoned tungsten (W) tailings in Yxsjöberg, South-Central Sweden. The results of this study indicate that coupling chemical ratios with $^{87}\text{Sr}/^{86}\text{Sr}$ ratios offer better insights in discriminating between different geochemical processes in mine wastes.

Keywords: Acid Mine Drainage, Yxsjöberg, Skarn tailings, Sr isotopes, Silicate weathering.

Introduction

Negative effects of acid mine drainage (AMD) generated from sulphide oxidation and other acid generating sources have resulted in environmental considerations gaining prominence in the assessment of the economic feasibility of mine projects (Azcue 2012). The roles of buffering minerals in neutralizing acidity are therefore critical in mine environments. In typical mine settings, carbonates, silicates and (oxy)-hydroxides play major roles in acid neutralization (e.g. Jurjovec et al. 2002).

Strontium (Sr) and calcium (Ca) are geochemically similar in terms of ionic radius and ionic charge (Marcus and Kertes 1968) and can substitute for each other in mineral lattices such as in carbonates and some silicates. This allows the use of Sr as a proxy for Ca in many studies (e.g. Pett-Ridge et al. 2009; Tipper et al. 2006). Rubidium (Rb) on the other hand, is geochemically similar to potassium (K) and substitutes for K in K-bearing mineral lattices. ^{87}Rb undergoes radioactive β^- decay to produce stable ^{87}Sr . As a consequence, K-bearing minerals (e.g. biotite, K-feldspar, muscovite) are high in $^{87}\text{Sr}/^{86}\text{Sr}$ ratios (Faure 1986; Clow et al. 1997). In addition, $^{87}\text{Sr}/^{86}\text{Sr}$ ratios have the advan-

tage of not being fractionated by low temperature geochemical processes such as mineral precipitation (Capo et al. 1998).

Considering that the acid neutralizing minerals are either enriched in Rb and K or Sr and Ca, then their dissolution should release variable $^{87}\text{Sr}/^{86}\text{Sr}$ ratios into leachates, since they have distinct $^{87}\text{Sr}/^{86}\text{Sr}$ ratios. In this study, $^{87}\text{Sr}/^{86}\text{Sr}$ and Sr/Ca as well as other chemical ratios (Ca/K and Rb/Sr) and concentrations in leachates, tailings and minerals have been used to trace geochemical processes including acid-neutralization that have occurred within mineralogically-complex historical tungsten (W)- skarn deposit in Yxsjöberg, South Central Sweden.

Methods

Tailings were collected by percussion drilling from the Yxsjöberg W-skarn deposit. The drill core extends to a depth of 6m and is subdivided into 18 subsamples. Minerals including K-feldspar, garnet, plagioclase, amphibole, pyroxene, calcite, scheelite, fluorite and helvine were separated from diamond drill cores belonging to the orebodies from which the tailings originated. *Batch leaching tests* were performed on tailings with a 1:10 solid (tailings) to liquid (MilliQ water) ratio fol-



lowing the procedure outlined in the Swedish standard institute's compliance test for granular wastes and sludges (SS-EN 12457-2:2003).

Sr isotope compositions of whole-rock tailings, individual minerals and leachates were analyzed using multicollector inductively-coupled plasma mass spectrometry (MC-ICP-MS). *Chemical compositions* of seventy (70) elements in leachates were carried out by inductively coupled plasma-sector field mass spectrometry (ICP-SFMS). All analyses (chemical compositions and isotopes) were carried out at ALS Scandinavia AB, Luleå, Sweden. *Mineralogical studies* of the tailings profiles were carried out using optical microscopy, X-ray diffraction (XRD) (PANalytical Empyrean) and Raman spectroscopy (Bruker).

Results and Discussions

Mineralogical and isotopic characterization of tailings

Minerals identified in the tailings include amphibole, pyroxene, biotite, plagioclase,

K-feldspar, garnet, calcite, fluorite, hematite, helvine, muscovite, Fe-(oxy)hydroxides, magnetite, scheelite and gypsum.

The distribution of Sr isotope ($^{87}\text{Sr}/^{86}\text{Sr}$) ratios in the tailings profile is shown in figure 1. The tailings have been categorized into four zones namely; upper oxidized zone (UOZ), lower oxidized zone (LOZ), upper unoxidized zone (UUZ) and lower unoxidized zone (LUZ) based on pH, chemical data and colour. The oxidized zones (upper and lower) are characterized by low pH, ranging from 3.6 to 4.5 whereas the unoxidized zones (upper and lower) have pH values between 5.3 and 7.9. The oxidized zones recorded radiogenic signatures (0.8479 -1.2664) compared to the less radiogenic ratios (0.8329- 1.0679) in the underlying unoxidized zones.

$^{87}\text{Sr}/^{86}\text{Sr}$ ratios in minerals

The average $^{87}\text{Sr}/^{86}\text{Sr}$ ratio of the minerals is shown in table 1. All minerals analyzed for $^{87}\text{Sr}/^{86}\text{Sr}$ are present in the tailings. Scheelite recorded the lowest $^{87}\text{Sr}/^{86}\text{Sr}$ values of 0.7085 whilst K-feldspar recorded the highest ratio of 2.3984.

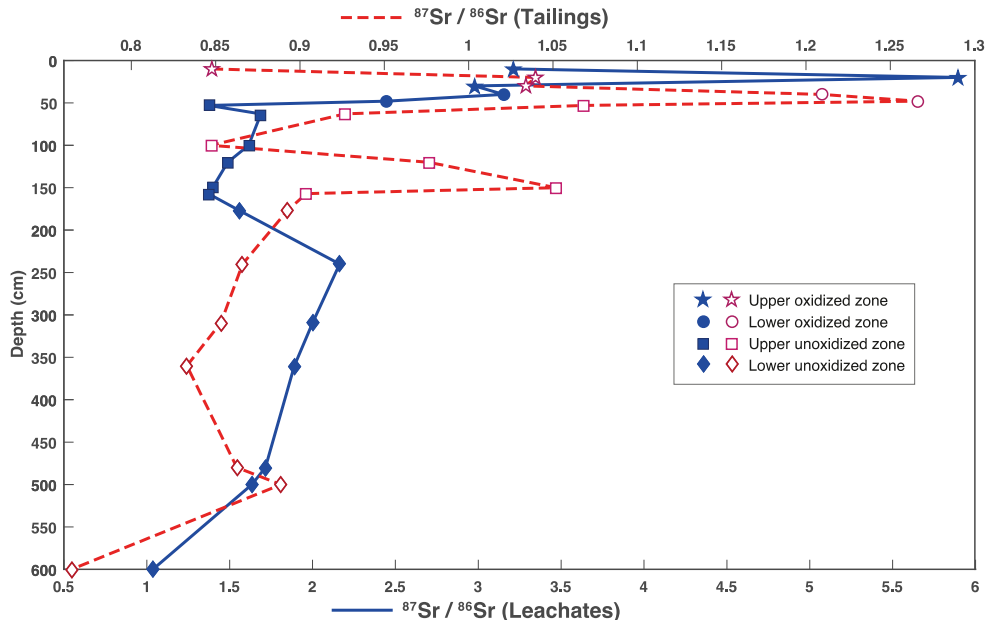


Figure 1: Sr isotopes ratios ($^{87}\text{Sr}/^{86}\text{Sr}$) in leachates (—) and tailings (---) from Yxsjöberg mine site, Sweden. The $^{87}\text{Sr}/^{86}\text{Sr}$ signatures at 600 cm depths represents a mixture of tailings and till and have been neglected in this study.



Table 1. Average $^{87}\text{Sr}/^{86}\text{Sr}$ ratios in minerals.

Mineral	Amp (n=4)	Px (n=2)	Grt (n=2)	Hel (n=2)	Plag (n=2)	Kfs (n=1)	Cal (n=1)	Fl (n=2)	Sch (n=2)
$^{87}\text{Sr}/^{86}\text{Sr}$	0.8124	0.7270	0.8107	1.2010	0.7114	2.3984	0.7163	0.7086	0.7085

n= number of minerals analyzed. Am= amphibole; Px= pyroxene; Grt= garnet; Hel=helvine; Pl=plagioclase; Kfs= K-feldspar; Cal=calcite; Fl= fluoride, Sch= scheelite

Table 2. Chemical composition of leachates from the Yxsjöberg W-tailings deposit, Sweden.

Description	Depth(cm)	pH	Ca (mg/L)	K (mg/L)	Rb (ug/L)	Sr (ug/L)	SO ₄ ²⁻ (ug/L)
UOZ	10	4.5	6	5	33	1.6	16
UOZ	20	4.4	9	8	94	1.5	29
UOZ	30	3.9	16	9	179	2.3	60
LOZ	40	3.7	214	13	434	15	593
LOZ	48	3.6	441	25	645	39	1106
UUZ	49	5.3	127	5	121	18	257
UUZ	63	6.3	62	4	82	10	84
UUZ	100	7.3	211	7	135	23	469
UUZ	120	6.7	615	12	255	54	1369
UUZ	150	6.8	590	11	221	56	1322
UUZ	157	6.9	525	11	199	48	1205
LUZ	177	7.2	65	12	91	11	150
LUZ	240	7.4	56	7	100	7	130
LUZ	309	7.6	41	7	75	6	92
LUZ	360	7.9	27	6	54	5	60
LUZ	480	7.7	38	5	59	6	90
LUZ	500	7.6	86	8	102	16	201
LUZ ^a	600	7.3	251	10	147	64	576

^a mixture of tailings and till. UOZ= upper oxidized zone, LOZ= lower oxidized zone, UUZ= upper unoxidized zone, LUZ= lower unoxidized zone.

Chemical and isotopic composition of the leachates

The chemical composition of the leachates is presented in table 2. Ca concentrations ranged from 6 - 441 mg/L in the oxidized zones and 27 - 615 mg/L in the unoxidized zones. For K, the concentrations ranged from 5 - 25 mg/L in the oxidized zones whilst the unoxidized zones had values between 4 and 12 mg/L. The highest concentrations of Rb were registered in the oxidized zones (33 - 645 µg/L) compared to the unoxidized zones (54 - 255 µg/L). In contrast to the trend of Rb, the unoxidized zones had the highest Sr and sulfate (SO₄²⁻) concentrations.

The Sr isotopes ratios ($^{87}\text{Sr}/^{86}\text{Sr}$) in the oxidized zones were more radiogenic relative to the unoxidized zones. The $^{87}\text{Sr}/^{86}\text{Sr}$ ratios ranged from 2.4448- 5.8755 in the oxidized zones whilst the unoxidized zones had $^{87}\text{Sr}/^{86}\text{Sr}$ ratios ranging between 1.3712 and 2.1634 (Figure 1).

Geochemical processes

The leachates in the upper oxidized zone showed very radiogenic $^{87}\text{Sr}/^{86}\text{Sr}$ ratios ranging from 2.9776 to 5.8755. This feature points towards weathering of biotite, K-feldspar and muscovite which are the only known radiogenic minerals identified in this zone. The decomposition of Rb-rich minerals such as biotite, K-feldspar and muscovite could result in $^{87}\text{Sr}/^{86}\text{Sr}$ enrichment in pore water with a resultant depletion in the residual weathered material (Blum et al. 1993; Bullen et al. 1997; Blum and Erel 1997). This is consistent with the observations in figure 1 where the leachates showed high $^{87}\text{Sr}/^{86}\text{Sr}$ ratios whereas the tailings revealed low $^{87}\text{Sr}/^{86}\text{Sr}$ ratios. In addition, since biotite, K-feldspar and muscovite are Rb-K rich or Sr-Ca poor, a leachate primarily controlled by the dissolution of these minerals should result in high Rb/Sr and low Ca/K ratios. Furthermore, although these minerals (biotite, K-feldspar, muscovite) are considered



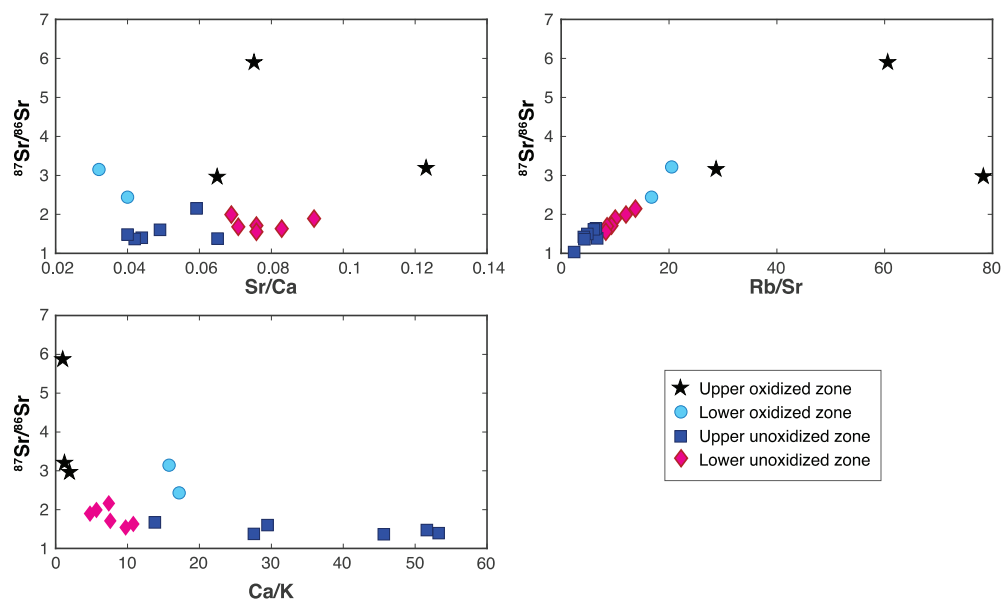


Figure 2: Sr/Ca, Rb/Sr and Ca/K ratios in leachates from the Yxsjöberg W-tailings deposit, Sweden. Ratios are in molar units.

Sr-Ca poor, their weathering will elevate Sr/Ca ratios in leachates since they have negligible Ca relative to Sr. Leachates in the upper oxidized zone shows relatively high Sr/Ca and Rb/Sr ratios but a low Ca/K ratio (figure 2). This indicates that the leachates are controlled by the dissolution of K-Rb bearing minerals.

Trends of Sr/Ca, Rb/Sr and Ca/K ratios in the leachates in the lower oxidized zone are in contrast to the upper oxidized zone although the $^{87}\text{Sr}/^{86}\text{Sr}$ ratios are still radiogenic (figures 1 & 2). Reduction in Sr/Ca and Rb/Sr ratios and corresponding increment in Ca/K ratio in this zone suggest additional dissolution of Ca-bearing minerals. Considering the prevailing pH conditions (pH= 3.6-3.7), the dissolution of amphibole, plagioclase and fluorite could be favoured (Schott et al. 1981; Brantley et al. 1998; Wong et al. 2003). In addition, a positive trend between Ca and SO_4^{2-} (figure 3) suggests that gypsum dissolution is also a possible mechanism controlling the decreased Sr/Ca and increased Ca/K ratios.

Less radiogenic $^{87}\text{Sr}/^{86}\text{Sr}$ ratios (1.3712-1.6884) were recorded in leachates of the

upper unoxidized zone relative to the overlying oxidized zones (figure 1). These $^{87}\text{Sr}/^{86}\text{Sr}$ ratios do not directly reflect the signature of any of the minerals analyzed. In addition, the Sr/Ca and Ca/K ratios display similar trends to that of the lower oxidized zone (figure 2). This zone also shows positive anomalies of Ca and SO_4^{2-} (figure 3) as observed in the lower oxidized zone. Since $^{87}\text{Sr}/^{86}\text{Sr}$ ratios are not affected by dilution, this could indicate the dissolution of gypsum.

In the lower unoxidized zone, the $^{87}\text{Sr}/^{86}\text{Sr}$ ratios are more radiogenic (1.6341-2.1634) than the overlying upper unoxidized zone. These increased $^{87}\text{Sr}/^{86}\text{Sr}$ ratios correspond to a Sr/Ca ratio similar to the upper oxidized zone (figure 2). Furthermore, the Ca/K ratios are “sandwiched” between that of the upper and lower oxidized zones but skewed towards the upper oxidized zone. This suggests the influence of a radiogenic source particularly K-bearing minerals. Sr losses from biotite and K-feldspar have been reported to be rapid (Clow et al. 1997) and as such the radiogenic Sr could be attributed to these minerals.



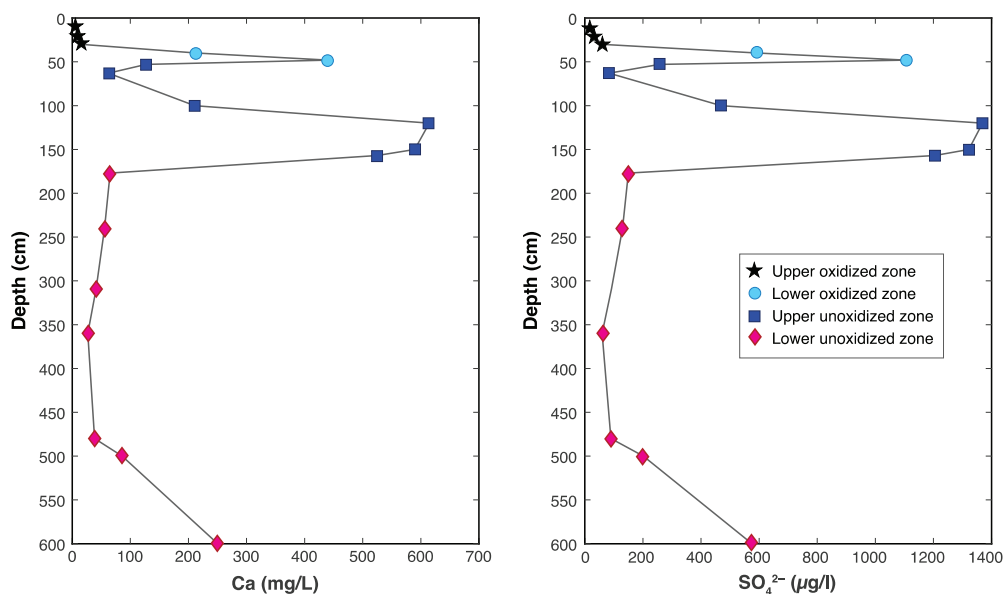


Figure 3: Ca and SO_4^{2-} distribution in leachates from the Yxsjöberg W-tailings deposit, Sweden.

Conclusions

The $^{87}\text{Sr}/^{86}\text{Sr}$ ratios and chemical ratios (Ca/K, Sr/Ca and Rb/Sr) in leachates shows variations in the four main zones of the tailings namely; upper oxidized, lower oxidized, upper unoxidized and lower unoxidized zones. These variations are reflections of the different geochemical processes occurring in the tailings. Radiogenic $^{87}\text{Sr}/^{86}\text{Sr}$ ratios recorded in the oxidized zones suggests the weathering of biotite, K-feldspar and muscovite. High Ca/K and low Sr/Ca ratios in the lower oxidized zone indicates dissolution of Ca-bearing minerals including gypsum. Similarity between Sr/Ca and Ca/K ratios as well as correlation between Ca and SO_4^{2-} in the upper unoxidized zone to that of the lower oxidized zone points to gypsum dissolution. In the lower unoxidized zone, Sr/Ca ratios and Ca/K depicts that of the upper oxidized zone with an increased $^{87}\text{Sr}/^{86}\text{Sr}$ ratio which is attributed to biotite and K-feldspar.

Acknowledgements

This research was funded by European Union's Interreg Nord project; Min North (Grant number: 20200531) with support from the Center of Advanced Mining and Metallurgy (CAMM2). We are grateful to

Dr. Thomas Aiglsperger for his assistance in mineralogy and Milan Vnuk for his help in preparing the figures.

References

- Azcue JM (2012) Environmental impacts of mining activities: Emphasis on mitigation and remedial measures Springer Science and Business Media.
- Blum JD, Erel Y (1997) Rb/Sr isotope systematics of a granitic soil chronosequence: The importance of biotite weathering. *Geochimica et Cosmochimica Acta*, 61(15), 3193-3204.
- Blum JD, Erel Y, Brown K (1993) $^{87}\text{Sr}/^{86}\text{Sr}$ ratios of Sierra Nevada stream waters: Implications for relative mineral weathering rates. *Geochimica et Cosmochimica Acta*, 57(21-22), 5019-5025.
- Brantley S, Chesley J, Stillings L (1998) Isotopic ratios and release rates of strontium measured from weathering feldspars. *Geochimica et Cosmochimica Acta*, 62(9), 1493-1500
- Bullen T, White A, Blum A, Harden J, Schulz M (1997) Chemical weathering of a soil chronosequence on granitoid alluvium: II. Mineralogic and isotopic constraints on the behaviour of strontium. *Geochimica et Cosmochimica Acta*, 61(2), 291-306.
- Capo RC, Stewart BW, Chadwick OA (1998) Strontium isotopes as tracers of ecosystem pro-



- cesses: Theory and methods. *Geoderma*, 82(1), 197-225.
- Clow DW, Mast MA, Bullen TD, Turk JT (1997) Strontium 87/strontium 86 as a tracer of mineral weathering reactions and calcium sources in an alpine/subalpine watershed, Loch Vale, Colorado. *Water Resources Research*, 33(6), 1335-1351.
- Faure G (1986) *Principles of Isotope geology*.
- Jurjovec J, Ptacek CJ, Blowes DW (2002) Acid neutralization mechanisms and metal release in mine tailings: A laboratory column experiment. *Geochimica et Cosmochimica Acta*, 66(9), 1511-1523.
- Marcus Y, Kertes AS (1968) *Ion exchange and solvent extraction of metal complexes*. Wiley Interscience, New York, 1046 pp.
- Pett-Ridge JC, Derry LA, Barrows JK (2009) Ca/Sr and $^{87}\text{Sr}/^{86}\text{Sr}$ ratios as tracers of Ca and Sr cycling in the Rio Icos watershed, Luquillo mountains, Puerto Rico. *Chemical Geology*, 267(1-2), 32-45.
- Schott J, Berner RA, Sjöberg EL (1981) Mechanism of pyroxene and amphibole weathering—I. experimental studies of iron-free minerals. *Geochimica et Cosmochimica Acta*, 45(11), 2123-2135.
- Svensk Standard (2003) Characterization of waste-leaching-compliance test for leaching of granular waste materials and sludges. SS-EN 12457-2. Swedish Standard Institute.
- Tipper ET, Bickle MJ, Galy A, West AJ, Pomiès C, Chapman HJ (2006) The short term climatic sensitivity of carbonate and silicate weathering fluxes: Insight from seasonal variations in river chemistry. *Geochimica et Cosmochimica Acta*, 70(11), 2737-2754.
- Wong M, Fung K, Carr H (2003) Aluminium and fluoride contents of tea, with emphasis on brick tea and their health implications. *Toxicology Letters*, 137(1), 111-120.





Nitrogen leaching from explosives into mine water of an underground mine. ©

Nikolay Sidenko

Stantec Consulting Ltd. 500 - 311 Portage Ave, Winnipeg, Manitoba, Canada

Abstract

Ammonium nitrate is a major reagent of mining explosives. It is relatively soluble and is leached out from undetonated explosives into mine water. The fraction and speciation of nitrogen leached into mine water are important factors controlling the chemistry of mine water discharge. This paper investigates factors affecting the fraction of leached nitrogen and nitrogen speciation in an underground mine operating in Northern Manitoba, Canada. These factors include rate of explosive use, type of explosive and dewatering flow rate. The study is based on records of explosive use and on monitoring of quantity and quality of mine water and for four years.

Results of this study shows that on average, 16.5% of the mass of nitrogen used in explosives was leached to mine water during monitoring period. The study did not show difference between ammonium nitrate/fuel oil (ANFO) and emulsion in leaching rates of nitrogen. Increase in mine inflow rates overtime does not result in higher nitrogen leaching rates, but it may be causing a declining time-trend of nitrogen concentrations in mine water. In mine water, the major nitrogen species are nitrate (55% of total N) and ammonia (42% of total N) with a minor amount of nitrite (2.1% of total N). This speciation is close to the original nitrogen distribution in the ammonium nitrate indicating a limited reactivity of nitrogen species after the blasting and dissolution of explosives.

This paper compares results of this study to literature data and provides useful quantitative data for predictions of water quality and environmental protection planning.

Keywords: nitrogen, ammonia, nitrate, mine water, underground

Introduction

Ammonium nitrate is a major reagent of mining explosives. It is relatively soluble and is leached out from explosives into mine water. The fraction and speciation of nitrogen leached into mine water are important factors controlling the chemistry of discharges and the receiving water bodies (Frandsen et al 2008). This paper presents a case study of nitrogen leaching from an underground mine operating in Northern Manitoba, Canada. The mine owners of mine prefer to keep the name of the project anonymous, replacing mine name with X in the references.

Geology and Hydrogeology

The deposit is volcanic massive sulphide (VMS) type and is located in the Precambrian metavolcanics covered with Ordovician sedimentary rocks and overburden. The Precambrian rocks underlying the Ordovician cover

include a section of deeply weathered rocks which varies in thickness from 5 to 25 metres (Bailes 2010). Most of the orebody is located between 100 and 300 m below the ground. The ore is primary mined for copper with gold and silver being secondary economic metals.

Hydrogeological testing conducted indicated that there is high hydraulic conductivity of shallow rock extending up to 23 m deep from the surface. Half of hydraulic conductivity values estimated were between 10^{-5} m/s and 10^{-6} m/s (Golder 2011). This is consistent with poor consolidation of Ordovician sedimentary and weathered Precambrian metavolcanics rocks. Below 42 m, the Precambrian rock and ore have lower hydraulic conductivities, ranging between 10^{-7} m/s and 10^{-8} m/s. Grouting of mine workings has helped to reduce groundwater inflow from the shallow rock to the mine.



Methods

This study is based on records of explosive use and on monitoring of quantity and quality of mine water and for four years (2014–2017). Records of the mass and type of explosives used were available on daily basis for first 1.5 years and as monthly averages afterwards. The explosives contained 65% (by mass) of ammonium nitrate on average, which is equivalent to 24 % (by mass) of nitrogen. This information allowed for the calculation of the rate of ammonium nitrate and nitrogen used by mine (R_U , kg/day).

The leaching rates for nitrogen (R_L , kg/day) were calculated by multiplying outflow rate from the mine (Q , m³/day) by concentration of nitrogen species (C , mg of N/L) and divided by conversion volume factor (1000 liters to m³). Outflow rates were calculated by the mine operators from flowmeter readings recorded with approximately a weekly interval. Mine water samples were taken weekly during the first year and biweekly thereafter. Samples were kept at $\approx 4^\circ\text{C}$ and shipped to a certified laboratory (ALS, Winnipeg) within the required hold times and tested for ammonia, nitrite and nitrate nitrogen. Concentrations of nitrogen in these species were added to calculate the concentrations of total nitrogen in mine water for each day of sampling. For the days without flow or concentration records, the last recorded value was assumed until the next flow record or sampling event occur, respectively. Daily values were averaged for each month and the percentage of nitrogen lost (NLOST, %) in a given month was calculated as $N_{\text{LOST}} = R_L/R_U \times 100\%$.

Results and Discussion

Between 2014 and 2018, the powder factor ranged between 0.64 kg and 0.66 kg of explosive per tonne of material blasted, with approximately 600 kilo tonnes mined each year. Average monthly leaching rates ranged between 13.7 kg N/day and 65.4 kg N/day with a mean value of 39.7 kg of N/day (fig. 1a). Average monthly leaching rates do not show a statistically significant correlation with monthly use of explosives indicating that there are other factors affecting nitrogen leaching to mine water.

The monthly percentage of leached nitrogen (NLOST) ranged from 4.7% to 32.2%, averaging at 16.5% of mass nitrogen used in explosives. Similar range of nitrogen loss (12%–28%) was estimated for the development of the underground mine (Moring and Hutt 2008). The case studies of open pit coal mines in British Columbia, show lower average percentages of leached nitrogen (up to 5%) than in this study (Ferguson and Leask 1988).

The major explosive type was emulsion (82%), with small amounts of ammonium nitrate/fuel oil–(ANFO) (18%). A limited percentage of ANFO ($\approx 3\%$) was used in the first 1.5 years and increased thereafter (to $\approx 29\%$, fig. 1a). Revey's (1996) laboratory tests showed that ANFO has higher dissolution rates than emulsion. The data from our field study do not support this observation because there is no statistically significant correlation between use of ANFO and nitrogen leaching rates. Also, mean nitrogen leaching rates in first 1.5 years (40 kg N/day) and in the remaining monitoring period (39 kg N/day) are similar.

The major groundwater inflow to the mine is expected from shallow bedrock showing high hydraulic conductivity values. Mine outflow ranged from 341 to 957 m³/day on monthly basis, averaging at 632 m³/day. The mean annual outflow increased from ≈ 510 m³/day in 2014 to 760 m³/day in 2017. Pronounced increase in outflow was observed in spring months, between March and June followed by stabilization or slight decline (fig. 1b). The linear regression for outflow show long-term increasing trend, while the trend for nitrogen leaching rate show no significant change. The disagreement between these long-term trends indicate that increase in mine inflow/outflows does not seem to affect leaching rates.

Average monthly nitrogen concentrations in mine water range from 26.7 mg N/L to 114.8 mg N/L with mean value of 64.4 mg N/L. Long-term regression for nitrogen concentrations show a declining trend, which can be attributed to an increase in outflow volume resulting in dilution mine water (fig. 1c).



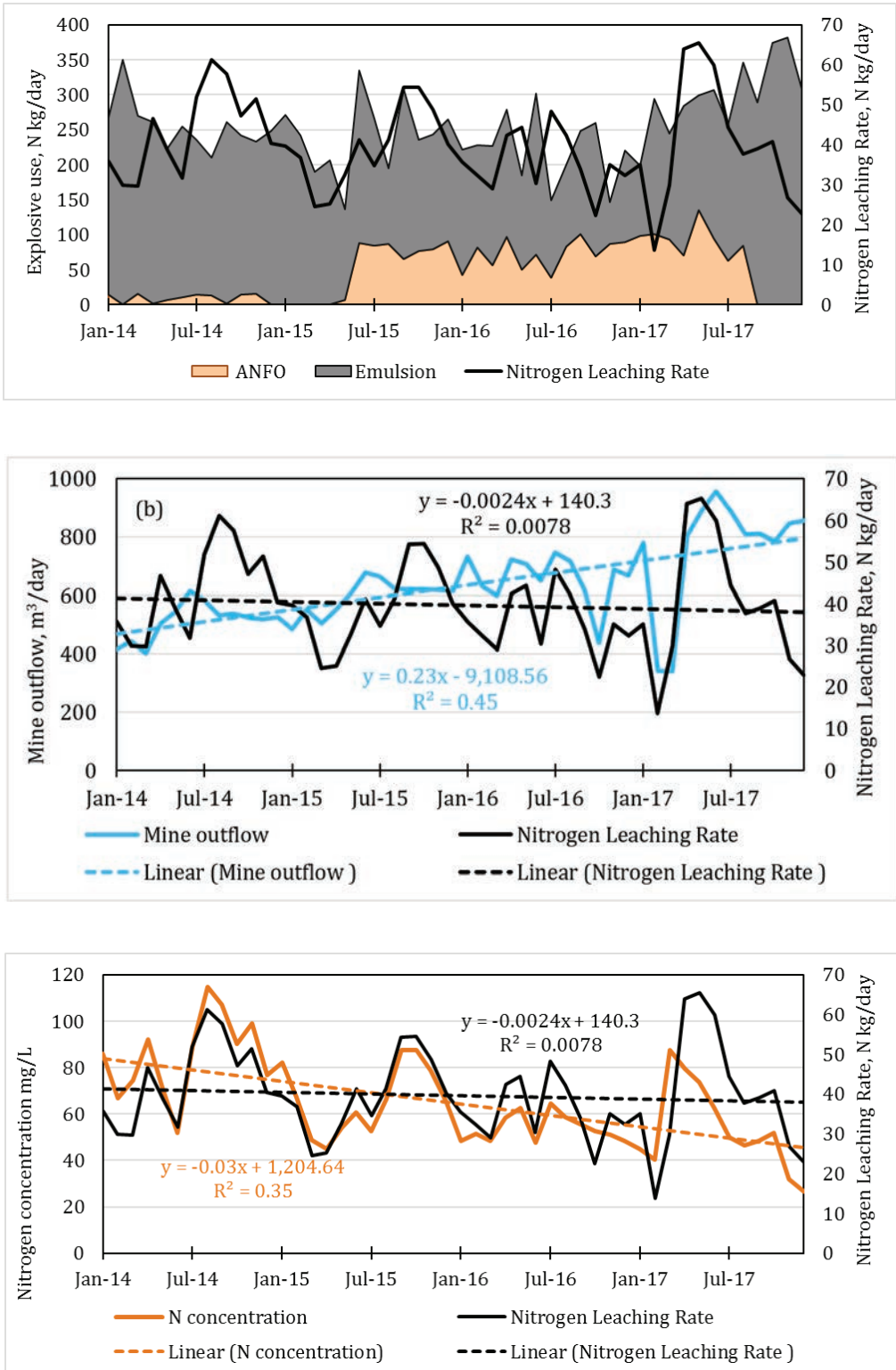


Figure 1. Time trends for mean monthly leaching rates and a) type and of rate explosive use, b) mine outflow and c) nitrogen concentration in mine water.



In mine water, the major nitrogen species are nitrate (55% of total N) and ammonia (42% of total N) with minor contribution of nitrite (2.1% of total N). This speciation is close to the original nitrogen distribution in the ammonium nitrate indicating a limited reactivity of nitrogen species after the blasting and dissolution of explosives. Similar distribution of nitrogen species was found in discharge from the underground mine by Morin and Hutt (2008).

Conclusions

The findings of this study can be summarized as follows:

- On average 16.5% of mass nitrogen used in explosives was lost to mine water during monitoring period.
- The study did not show a difference in leaching rates of nitrogen between ANFO and emulsion.
- Increase in mine inflow rates overtime does not result in higher nitrogen leaching rates, but it may result in declining trend of nitrogen concentrations in mine water
- Nitrogen speciation in mine water is close to the original nitrogen distribution in the ammonium nitrate indicating a limited reactivity of nitrogen species after blasting and dissolution of explosives.

The paper also provides useful numerical data for predictions of water quality and environmental protection planning.

Acknowledgements

The authors thank mine owners and operators for providing data. This research was financially supported by a Greenlight grant through the Creativity & Innovation program at Stantec.

References

- Bailes AH (2010) Geological setting of the X deposit and relationship to the Tower zone. Unpublished report.
- Ferguson KD, Leask SM (1988) The Export of Nutrients from Surface Coal Mines, Environment Canada Regional Program Report 87-12, 127 pp.
- Frandsen S, Widerlund A, Hebert RB, Ohlander B (2008) Nitrogen effluents from mine sites in the northern Sweden – environmental effects and removal of nitrogen in recipients. Proceedings of 8th ICARD Conference. Skelleftea, Sweden.
- Golder (2011) 2011 hydrogeological investigations X project. Unpublished report.
- Revey, GF (1996) Practical methods to control explosives losses and reduce ammonia and nitrate levels in minewater. Mining Engineering (July): 61-64.
- Morin KA, Hutt NM (2009) Mine-water leaching of nitrogen species from explosive residues. Proceedings of GeoHalifax2009 Conference: p 1549-1553.





Platinum Tailings Review - A comparison of the water quality in the tailings dam to the surrounding groundwater

Sarah Jane Wolfe Skinner

SRK Consulting, South Africa

Abstract

There are a number of platinum mines in South Africa that exploit platinum group minerals (PGMs) within the Rustenburg Layered Suite of the Bushveld Igneous Complex (BIC). The platinum tailings generated following processing of the ore is disposed of in tailings storage facilities (TSF) and, whilst not acid generating, comprise elevated salts which could leach to the groundwater.

A preliminary comparison of the PGM TSF leachate quality to that of the surrounding groundwater quality was carried out for selected sites. The nitrate concentrations are comparatively higher in the TSFs leachate than in the surrounding groundwater suggesting that nitrates are possibly lost/assimilated within the TSF.

Keywords: Nitrate, Tailings dams, Platinum

Introduction

Platinum group minerals (PGMs) (platinum, palladium, rhodium, iridium, osmium and ruthenium) in South Africa are extracted from the UG2 and/or Merensky Reef (MR) located within the Rustenburg Layered Suite of the Bushveld Igneous Complex (BIC). The BIC covers an area of over 450 km (east to west) and over 200 km (north to south) in the northern part of South Africa extending into Botswana. There are more than twenty mines that exploit PGM's across South Africa, (refer to Figure 1 below).

Although the UG2 and/or MR tailings material is non-acid generating; it comprises elevated salts and nitrogenous compounds derived from the explosives used during blasting and the chemicals utilised for the processing of the ore which can leach to the groundwater, (Bosman, 2009). A simplified flow sheet of a platinum processing plant is provided after Haggard et.al 2015.

Many of the areas in which the platinum mines are located are water stressed and the communities, particularly in the northern limb and eastern limbs, rely on groundwater to satisfy their domestic needs and to support subsistence crops and livestock. Nitrate concentrations of greater than 20 mg/L as N are a common occurrence in groundwater in the Northern and North-West Provinces of

South Africa and baseline nitrate levels can typically vary from <0.1 to over 80 mg/L as N, (Tredoux et.al 2009, E Martinelli and Associates 1999, SRK 2001, Barnard, 2000). The leachate of contamination from the TSF can therefore result in further (localised) deterioration of the groundwater quality to concentrations which are significantly higher than the South African National Standard (SANS 241, 2015) for nitrate of 11 mg/L, (SANS 241- 2015).

Methods

The baseline water quality for the general area was referenced from historical records which pre-date the TSFs, information sourced from the National Groundwater Archive and/or from boreholes located up-gradient of the facilities. The nitrate and ammonia concentrations reported in the National Groundwater Archive (accessed May 2018) provide an indication of the variability of the data where:

- Nitrate concentrations are reported as between <1 to over 125 mg/L as N in boreholes located on the eastern limb and <1 to over 140 mg/L as N in boreholes located on the western limb whilst
- Ammonia concentrations are reported as between <0.1 mg/L as N and 6 mg/L as N in boreholes on the eastern limb and 13 mg/L as N for boreholes on the western limb.



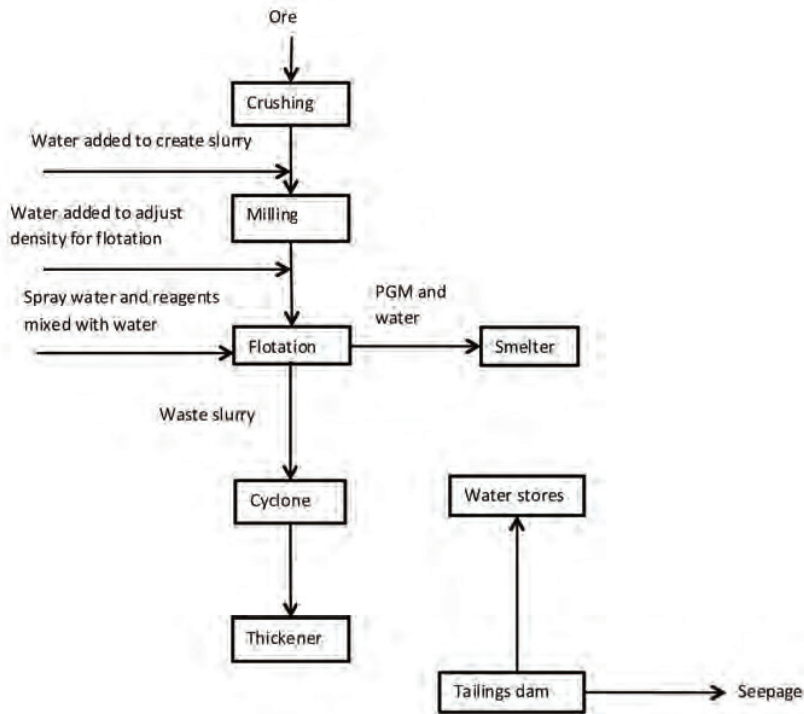


Figure 1 Simplified water flow sheet for a platinum processing plant, after Haggard, 2015

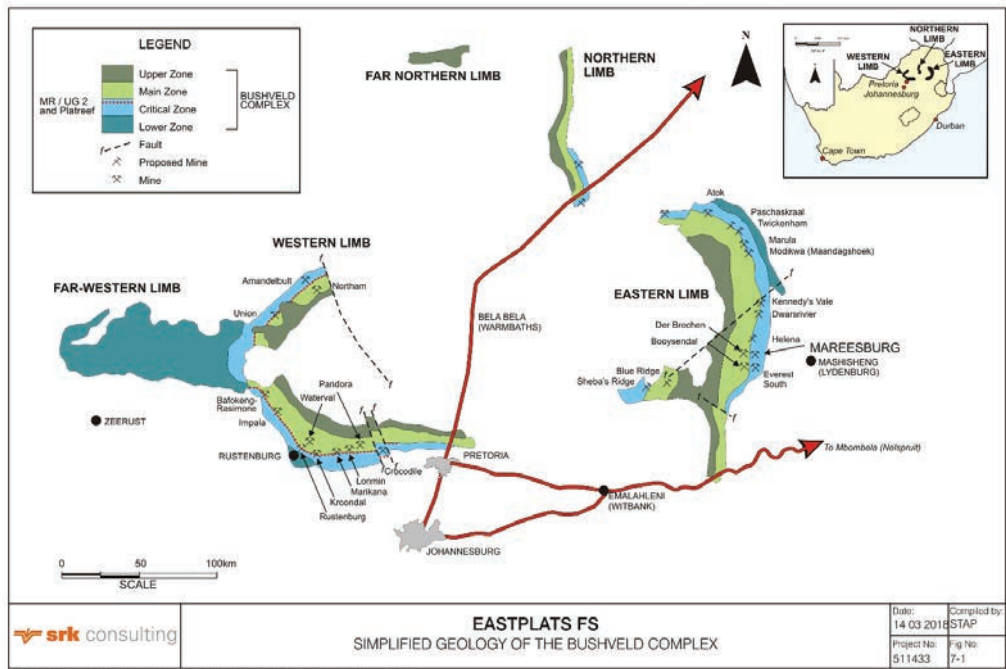


Figure 2 Simplified geology of the Bushveld Igneous Complex, SRK Consulting



This variability is also observed on a local scale, where groundwater quality varies significantly across the mine areas. This is probably due to the heterogeneity of the aquifers where the transmissivity of the aquifer is governed by the fracturing (orientation, spacing, connectivity etc.) present in the underlying lithologies.

Despite the data variance, it is possible to obtain an indication of the correlation between the tailings leachate concentrations (as in the penstock and/or return water dams) and the surrounding groundwater. The graphs below (Figures 3, 4 and 5) present a summary of the information collated as part of this study:

- Ambient groundwater quality for boreholes (as discussed above) where the median data is provided,
- Median and 95th percentile of time series data (where available) for the tailings leachate concentration. If only one data set was available, this was included as the 95th percentile and indicated as such on the sample ID
- The groundwater quality for boreholes within the vicinity of the TSF (indicated as affected boreholes) is represented by the 95th percentile.

The SANS 241-2015 drinking water quality standard is provided for comparison to the nitrate (11 mg/L as N) and TDS (1200 mg/L). If TDS was not reported, it was estimated from the result for electrical conductivity (EC).

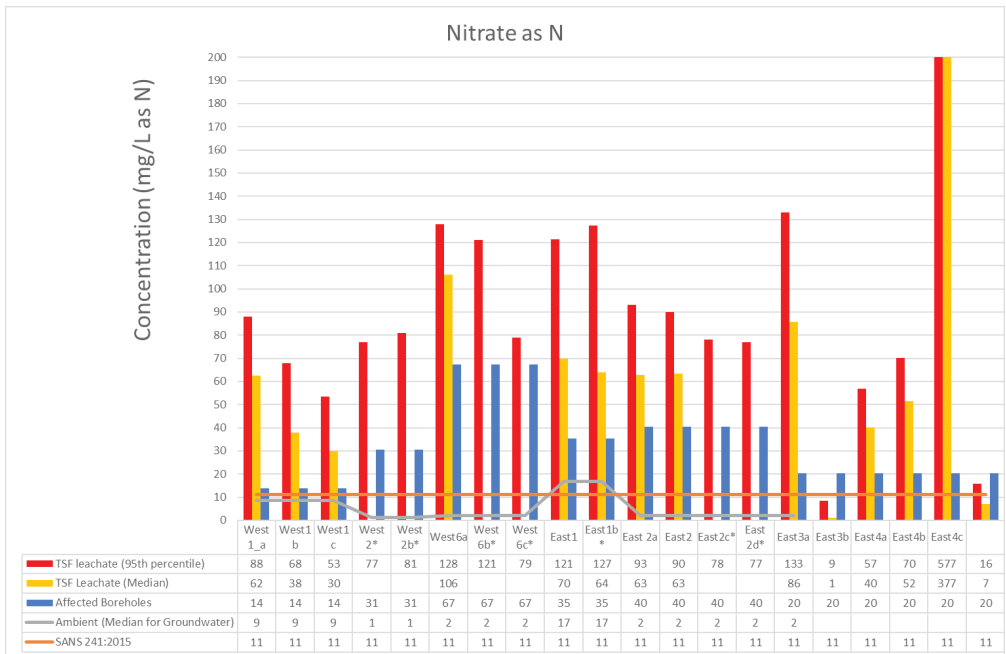


Figure 3 Nitrate concentrations in the TSF leachate as compared to groundwater quality for selected mines in the Western and Eastern Limb of the BIC.



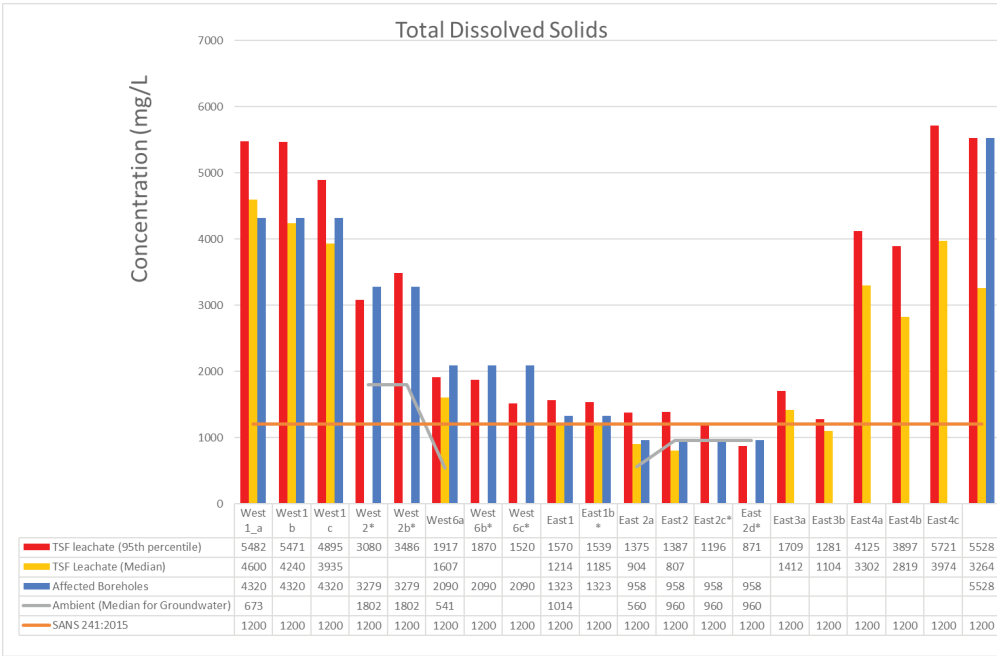


Figure 4 Total Dissolved Solids (TDS) concentrations in the TSF leachate as compared to groundwater quality for selected mines in the Western and Eastern Limb of the BIC.

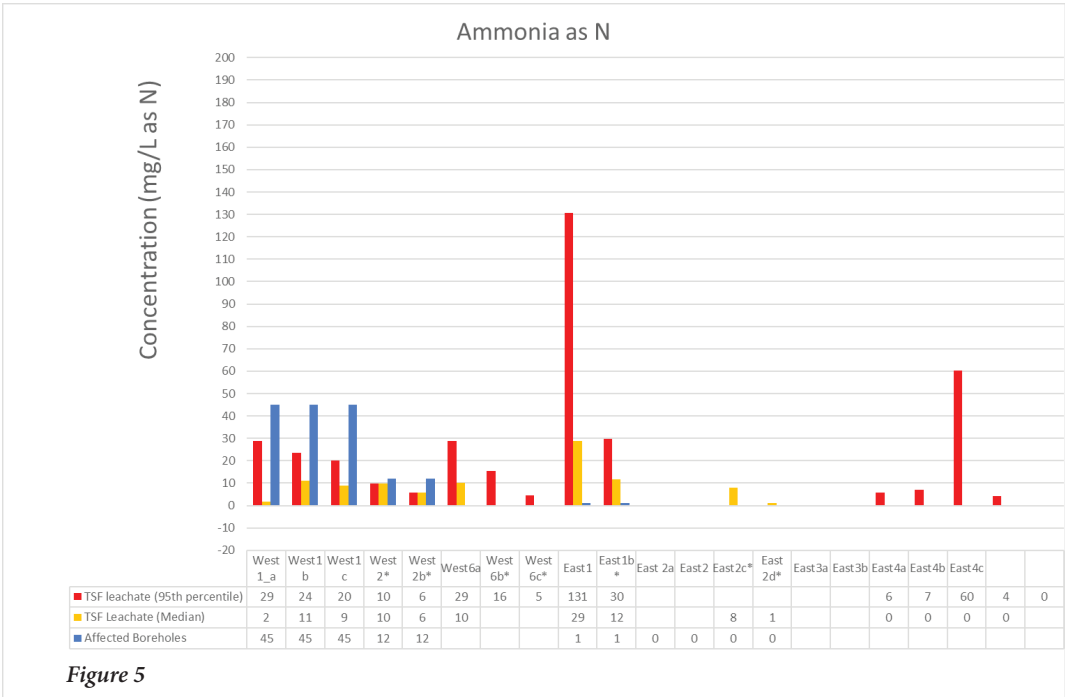


Figure 5



Conclusion

Ammonia is often excluded from the monitoring analyses. As observed in Figure 4 above, ammonia should be included in the assessment. Higher concentrations were observed in the groundwater quality within the Western limb boreholes but this should be confirmed by expanding the study area and including ammonia in the monitoring program.

Nitrate concentrations in the datasets reported are generally lower in the groundwater samples than the tailings leachate. Conversely, the TDS reported in the boreholes is generally within a similar range to that reported in the groundwater.

Since nitrate is highly soluble and mobile in groundwater; the concentrations could be expected to be higher than are observed in this investigation. This preliminary comparison of the PGM TSF leachate quality to surrounding groundwater quality could imply that nitrogen is possibly being lost/assimilated within either the TSF, the soil matrix or within the aquifer itself.

This data suggests that further investigation is merited into whether there are naturally occurring processes within or underlying the TSF which could mitigate the potential for leaching/contamination of the groundwater. This information can then be used in the design and/or management of the TSF to reduce the impact of the TSF's to groundwater. It is noted, however, that this assessment doesn't include other leachables that could leach from the TSF.

Further interrogation would be necessary to confirm these findings and should include for example, an analysis of the sodium and chloride variance, whether aerobic or anaerobic conditions exist in or under the TSF, the age, design and operation of each TSF, rain events, chemicals used in the TSF slurry, type of tailings (UG2 versus Merensky or a mix-

ture with slag or brine), vegetation on the TSF soil characteristics below the TSF, flow drivers, hydrogeology and hydrochemistry.

Acknowledgements

The author would like to thank Jacky Burke, Angelika Möhr and Albert Carow for their assistance in sourcing and collating the information used for this assessment.

References

- Barnard, H (2000) An explanation of the 1:500 000 General Hydrogeological Map Johannesburg 2526, Department of Water Affairs and Forestry.
- Bosman, C. (2009) “The hidden dragon: Nitrate Pollution from open-pit mines – A case study from the Limpopo Province, South Africa. International Mine Water Conference Proceedings. 19-23 October 2009. 849-857
- E Martinelli and Associates (1999) Report on Hydrogeology and Groundwater resources of Winmarshoek 250KT compiled for Trojan Platinum (Pty) Ltd Report 839.
- Haggard, E.L, Sheridan, C.M., and Harding, K.G (2015) “Quantification of water usage at a South African platinum processing plant” Water SA Vol. 41 No. 2 WISA 2014 Special Edition 2015
- Department of Water and Sanitation (2018). National Groundwater Archive. Data access in May 2018.
- South African Bureau of Standards (2011), SANS 241 Drinking water quality standard
- Tredoux, G. (1993) “A preliminary investigation of the nitrate content of groundwater and limitation of the nitrate input,” report to the Water Research Commission by the Groundwater programme division of Water Technology CSIR, Stellenbosch, WRC Report No. 368/1/93
- Tredoux, G. and du Plessis, H.M. (1993) “The Groundwater nitrate hazard,” paper presented at the proceedings of the Third Biennial Conference, May 1993, the Water Institute of Southern Africa.



The Formation Mechanism of High Salinity Groundwater in Arid Area and Its Influence on Coalmines—A Case Study of a Coalmine in Xinjiang, China

Yajun Sun, Zhimin Xu, Siyuan CUI, Shang Gao

*School of Resources and Geosciences, China University of Mining and Technology,
Xuzhou 221116, China*

Abstract

The Turpan-Hami basin in western China's Xinjiang Province is a typical arid region, where there is no surface water and almost no meteoric precipitation. However, in this basin, abundant groundwater exists in Dananhu mining area, and the maximum mine water inflow is over 3000 m³/h. It has a great influence on the safety production of the coalmine, and has also produced a large amount of the drainage costs. In order to find out why there is so much water in such arid areas, based on field investigation and monitoring, this paper studies the recharge source, the geological environment and the cyclic condition of the groundwater, as well as its influence on coal mining in this extremely arid area. The research finds that, firstly, the groundwater in this study area is macroscopically recharged by the Tianshan Mountains' snowmelt water through piedmont alluvial-pluvial fan in the way of underground runoff. Secondly, present in the high potassium, sodium contained and high porosity Jurassic aquifer, the groundwater characterizes is very high salinity and the Total Dissolved Solids (TDS) is up to 17 g/L under the strong evaporation and concentration effects. In addition, along the groundwater pathway from Tianshan Mountains' recharge source to the Dananhu mining area (about 150 km), the TDS increases from 0 g/L to 40 g/L gradually. This indicates that the groundwater cycle condition becomes worse constantly, and this can also be influenced by the local hydrogeological boundary and tectonic conditions. To conclude, the results of the paper highlight that, on the one hand, the abundant groundwater, recharged from the faraway Tianshan Mountains' snowmelt, significantly influences the mining safety of the coalmines; on the other hand, high salinity groundwater reflects that, the groundwater circulation is turning worse because of the boundary condition in the mining area, and these provide cogent basis for the program development of the mine drainage strategies.

Keywords: snowmelt, underground runoff, mine water inflow, mine drainage

Introduction

Western China has abundant coal reserves and a fragile ecological environment. It is a typical arid area. (Zhang et al. 2015) There is no surface water, and almost no atmospheric precipitation. In recent years, with the shift in the center of coal mining in China and the increasing intensity and scale of coal mining in the west, specific hydrogeological problems, such as highly saline groundwater, the closed mining conditions, and the large amount of mine water inflow, are constantly emerging. For example, the mine water inflow in the

Ehuobulake Coalmine reaches more than 1,850 m³/h (Zheng et al. 2013), which seriously threatens the coalmine safety.

In view of these problems, Chinese scholars (Li et al. 2013; Li et al. 2016a,b; Xu et al. 2018) have mostly studied the formation and evolution of high salinity groundwater in the arid areas by means of field investigations, hydrochemical data analysis, and isotopic tracing. For example, Li and Hao (1999) studied the pattern of groundwater formation and evolution in the inland basin of Northwest China by analyzing the sampled water chem-



istry data and systematically expounded the formation and evolution law of the underground salt water. Lei et al. (2016) studied the obvious stratification in the chemical characteristics of the underground water in the Ningxia area of China. Water infiltration and evaporation have an obvious influence on the water quality of the regional groundwater; Ren and Yan (1999) analyzed the chemical characteristics and formation mechanisms of groundwater in the plain area of the Dalate Banner, Inner Mongolia, China. The authors focused on the spatial distribution characteristics and formation mechanisms of the chemical components of the phreatic and confined water. The results showed that the quality of the phreatic water was influenced by concentration and filtration mechanisms. In general, due to the climatic drought in western China, groundwater is subject to evaporation during runoff, and the groundwater chemistry gradually changes along the percolation path. In the discharge area, leaching, concentration, decarbonation, and desulphidation may occur along the seepage path. The water chemistry is generally a reflection of the higher salinity of sodium sulfate, sodium chloride, and sodium chloride of the water.

This paper takes the Dananhu mining area, which is located in the Turpan-Hami basin in the eastern Xinjiang Province, as an example, to study the source, environment, and cycling conditions of groundwater and the impact on the regional coalmines under extreme drought conditions.

Hydrogeological Setting of the Study Area

The Dananhu mining area is located in the Dananhu Township, Hami City, Xinjiang, China (Figure 1), and is part of the Dananhu Depression of the Turpan-Hami basin. The basin and the surrounding mountainous system have different hydrogeological systems (Tan, 2002). From a macroscopic point of view, the climate in the study area is extremely dry and reflects the overall characteristics of the Gobi Desert. There is no surface water and the average annual rainfall is less than 50 mm, but the evaporation exceeds 3,000 mm. The large amount of snowmelt water, stemming from the eastern Tianshan Mountains in the northern part of the study area, is the only source of recharge water in the region.

Overall, the hydrological and geological conditions of the study area are characteristi-

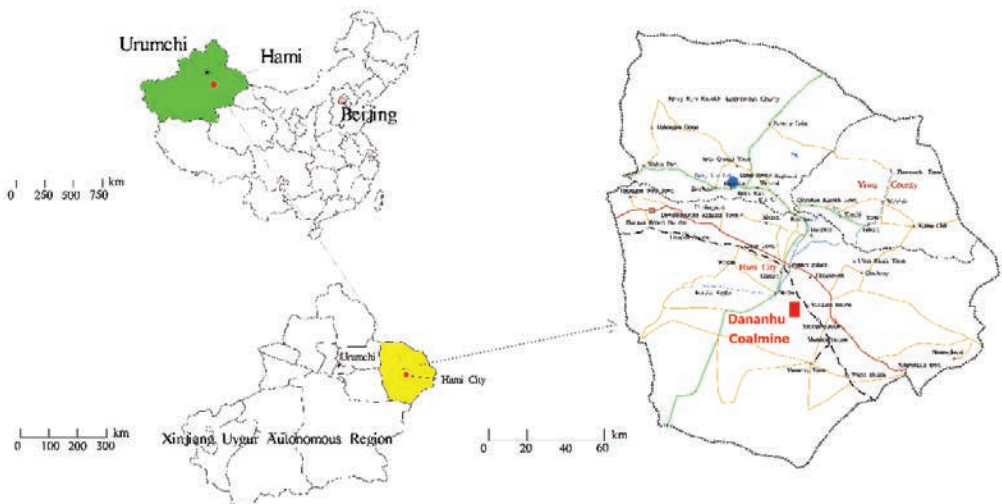


Figure 1 Location of the Dananhu NO. 5 Coalmine.



cally thought of as closed: the southern and western parts of the study area are bound by the Jueluotage Uplift, characterized by a large area of igneous dew that has a good water insulation ability; the north boundary is the Sha'er Lake Uplift, which is also composed of igneous rocks. A supply gap exists in the middle, but the groundwater level in the northern area of the Sha'er Lake Uplift decreased, and, as such, recharge of the region is not currently possible. It has been determined that the Sha'er Lake Uplift is an impervious boundary; there is no natural impervious boundary in the east. Therefore, there is potential for groundwater recharge. It is assumed that the snowmelt from the Tianshan Mountains reaches the edge of the Dananhu Depression in a north to south direction and then enters the depression from east to west along the gap, recharging the groundwater in the mining area (Figure 2).

Research Methods

A survey route was planned and executed according to the hydrogeological structure characteristics and macro-recharge conditions of the flood plain in front of the Tianshan Mountains (as shown in Figure 3). During the field survey and investigation, several surface and phreatic water samples are collected on the way from the Tianshan

Mountains to the eastern edge of the Dananhu Depression. When entering the Dananhu Depression, samples could only be collected from the confined water in the coalmines. Three mine water samples were collected from the confined water and four samples from phreatic and surface water.

Results and Discussion

High salinity mine water formation

Groundwater salinity characteristics
On the basis of the analysis of regional macro-recharge water sources and hydrogeological boundary conditions in the study area, groundwater recharge routes in the mining area were identified on the basis of changes in salinity of the collected water samples along the survey route.

Table 1 outlines the variation in salinity between the water samples. The results indicate that the salinity of the snowmelt from the Tianshan Mountains was 287 mg/L, representing the regional supply source. With increasing distance along the groundwater runoff path from the mountains, the phreatic groundwater was recharged by snowmelt water, and the salinity of the groundwater increased to 660 mg/L. This occurs when the snowmelt water flows along the Tianshan Mountains to the east edge of the Dananhu Depression. When the water reached the

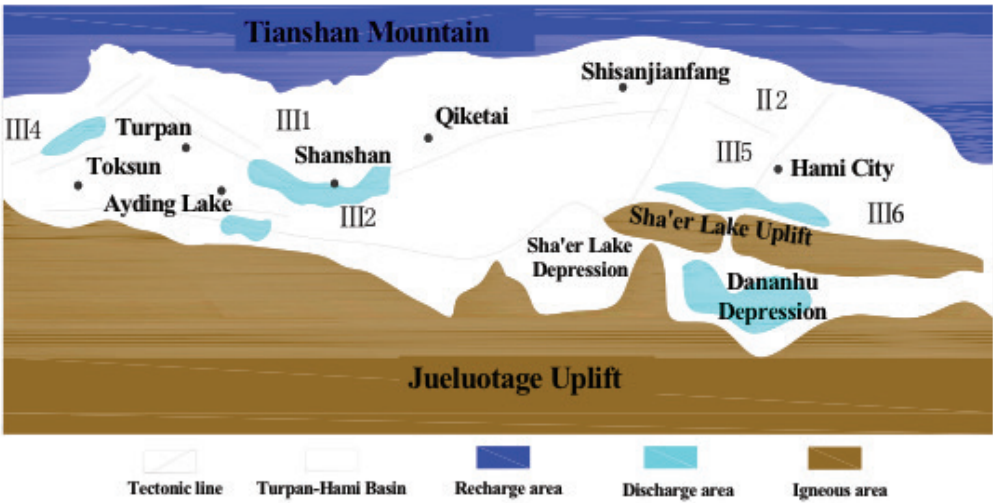


Figure 2 Hydrogeological of the study area.



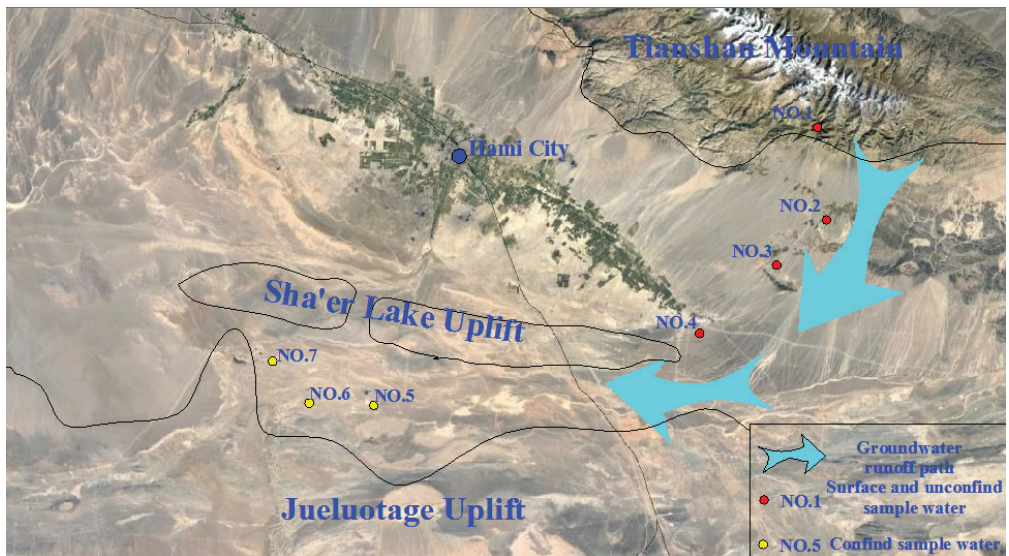


Figure 3 Map of the survey road.

depression, the salinity of the groundwater increased sharply from the east to the west because of concentration due to the intense evaporation. At depth in the Dananhu Depression, the salinity in the Dananhu No. 5 Coalmine was 17,670 mg/L and up to 40,000 mg/L at the most western end of the depression in the Goushen NO. 1 Coalmine. When combining the observations of the western, northern, and southern hydrogeological boundaries, it was concluded that the snowmelt from the Tianshan Mountains supplies groundwater to the study area through long-distance subsurface runoff. However, because of the changing regional hydrogeological conditions and poor recharge conditions, mainly caused by evaporation losses typical of recharge steaming style, the groundwater along the path is characterized by a gradual increase in the salinity from east to west and the formation of highly saline conditions in the mining area.

Groundwater chemical ion characteristics

Because of the gradual deterioration in the circulation conditions during the recharge of mine water from the snowmelt, combined with the closed boundary conditions of the Dananhu Depression, some water samples were collected along the route to determine the mine water environment (Table 2).

According to the analysis of water quality evolution, in the process of remotely replenishing mine water from the snowmelt from the Tianshan Mountains, the ion concentration increases as the recharge distance increases. The proportion of K^+ , Na^+ , and Cl^- with high solubility increased continuously along the flow path, whereas the proportion of weakly soluble Ca^{2+} and Mg^{2+} and acidic SO_4^{2-} and HCO_3^- decreased. Finally, the main cations present in the Dananhu NO. 5 Coalmine are K^+ and Na^+ , and the main anion is Cl^- , forming $Cl \cdot SO_4 \cdot Na$ water. These results indicate that after the submergence of snowmelt water into the groundwater, evaporation due to the climatic drought is the main excretion method. Cations that have low solubility of salts in the water, such as Ca^{2+} and Mg^{2+} , precipitated first, followed by highly soluble K^+ and Na^+ . At the same time, due to the closed circulation conditions of the recharge process, the groundwater flow is slow allowing for SO_4^{2-} and HCO_3^- in the groundwater to produce “desulfurization” and “decarburization” and the proportion of them slowly decrease. This indicates that the underground water system in the mining area exhibits evaporative excretion, closed conditions, and poor fluidity in the environment.



Table 1. Groundwater salinity test results in the study area.

NO.	Sampling point	Water types	Salinity (mg/L)
1	Uradai Reservoir	Snowmelt water	287
2	Santoul Village	Phreatic aquifer	298
3	Qincheng Reservoir	Surface water	293
4	Zhongmei NO. 10 Coalmine	Phreatic aquifer	660
5	Zhongdiantou Coalmine	Confined aquifer	14000
6	Dananhu No. 5 Coalmine	Confined aquifer	17670
7	Guoshen No. 1 Coalmine	Confined aquifer	40000

Table 2. Summary of groundwater quality.

NO.	Sample point	The main ion content (mg/L)					
		K ⁺ Na ⁺	Ca ²⁺	Mg ²⁺	Cl ⁻	SO ₄ ²⁻	HCO ₃ ⁻
1	Uradai Reservoir	27.32	48.68	12.83	10.21	110.31	127.04
2	Santoul Village	9.36	63.49	20.54	13.61	75.73	201.3
3	Qincheng Reservoir	18.81	52.91	19.25	23.79	83.14	161.28
4	Zhongmei NO. 10 Coalmine	206.24	11.84	1.80	129.23	256.84	0
6	Dananhu NO. 5 Coalmine	4203.25	859.78	322.74	6940.85	2604.60	134.06

Impact on the mine water inflow

During the mining process, the water inflow rate in the Dananhu NO. 5 Coalmine exceeds 3,000 m³/h, which increases the threat of mine water hazards and has a great impact on coalmine safety, but the highly saline and the Cl⁻•SO₄²⁻•Na type ions characteristics of the mine water indicate that the groundwater recharge is minimal, and evaporation is the main excretion method. So, it can thus be inferred that the abundant underground water in the coalmine is dominated by static reserves. Therefore, during the mining process, the water inflow from aquifers in the vicinity of the coal-bearing strata can be treated with hydrophobic pressure reduction or pre-drainage.

Conclusions

(1) The intensity and scope of coal mining in the western part of China are gradually increasing. New hydrogeological problems are constantly emerging. The formation of mine water in the region have been identified, and their environment is of great significance for safety of coalmine production. Therefore, an effective method is needed to solve this problem.

- (2) In this study, water samples were collected during field surveys. Combined with regional macro-hydrogeological boundary conditions, the groundwater recharge route was determined starting from the snowmelt from the Tianshan Mountains that remotely recharges the mining area from north to south and then from east to west. Affected by evaporation and concentration along the way, the snowmelt from the Tianshan Mountains becomes highly saline under the closed environment of the groundwater system in the mining area, which is rich in potassium and sodium salts.
- (3) The results of the study have identified the formation process of mine water,,Therefore, it provides the basis for targeted mine safety and the prevention and control of mine water hazards. This also provides guidance and reference for mine water hazards with similar conditions.

Acknowledgements

This research was financially supported by The National Basic Research Program of



China (No.2013CB227901), the National Key Research and Development Program of China (No.2017YFC0804101) and the National Natural Science Foundation of China (No. 41502282). The authors thank the editors and reviewers for their constructive suggestions.

Reference

- Lei D, Wang W, Zhou L et. al. (2016) The formation of shallow fresh groundwater in the north of Yanchi county, Ningxia, China: main influencing factors and mechanism[J]. *Environ Earth Sci* 75: 461-474.
- Li P, Qian H, Wu J et. al.(2013) Major ion chemistry of shallow groundwater in the Dongsheng coalfield, Ordos basin, China. *Mine Water Environ* 32(3): 195-206
- Li P, Wu J, Qian H (2016a) Preliminary assessment of hydraulic connectivity between river water and shallow groundwater and estimation of their transfer rate during dry season in the Shidi River, China. *Environ Earth Sci* 75(2):99
- Li P, Wu J, Qian H et. al. (2016b) Hydrogeochemical characterization of groundwater in and around a wastewater irrigated forest in the southeastern edge of the Tengger Desert, northwest China. *Expos Health* 8(3):331-348
- Li W, Hao A. (1999) Groundwater formation and evolution model of the inland arid basin in northwest China and its significance[J]. *Hydrogeology and Engineering Geology* 04:30-34.
- Miao X, Wang A, Sun Y, et al. (2009) Research on basic theory of mining with water resources protection and its application to arid and semi-arid mining areas[J]. *Chinese Journal of Rock Mechanics and Engineering* 28(2):217-227.
- Ren Z, Yan J. (1999) Analysis of groundwater hydrochemical characteristics and formation mechanism in plain area of Dalate Banner, Inner Mongolia[J]. *Coal Geology of China* 11(3):30-34.
- Tan H. (2002) Study of hydrogeological conditions in Turpan-Hami basin[J]. *Uranium Geology* 18(2):97-103.
- Xu,Z Sun Y, Gao S et al. (2018) Groundwater Source Discrimination and Proportion Determination of Mine Inflow Using Ion Analyses: A Case Study from the Longmen Coal Mine, Henan Province, China[J].*Mine Water and the Environment*, <https://doi.org/10.1007/s10230-018-0512-6>
- Zhang D, Liu H, Fan G, et al. (2015) Connotation and prospection on scientific mining of large Xinjiang coal base[J].*Journal of Mining Safety Engineering* 32(1):1-6.
- Zheng B, Wu J. (2013) Analysis of Mine Water Filling Factors in Ehuobulake Coal Mine[J].*Coal Science and Technology* 3:65-67.



Groundwater Flow Model in the Area of the Extensive Open Pits Lignite Mining Activities

Jacek Szczepiński

"Poltegor-Institute" Institute of Opencast Mining, Wrocław, Poland, jacek.szczepinski@igo.wroc.pl

Abstract

Due to completion of lignite production in the Konin Lignite Area, the opportunity for a new open pit construction is considered. In the vicinity of the new potential mining area, there are two open pits still in operation and a post-mining reservoir, which is under the process of flooding. The dewatering of these pits results in change of hydrodynamic conditions in the area, which will influence the mine water inflow into the new open pit and its environmental impact. All these phenomena were simulated in a transient groundwater flow model, in which the new open pit as well as neighboring open pits are simulated.

Keywords: open pit, lignite, groundwater modeling

Introduction

Due to completion of lignite production in the Konin Lignite Area located in the central part of Poland, the opportunity for a new open pit construction is considered. The „Mąkoszyn - Grochowska” deposit with geological reserves of 80 MT and lignite production capacity of 3.5 MT/year is an option. Outside of the potential mining area, there are still two open pits in operation - „Tomisławice” open pit (5 km away) and „Drzewce” open pit (21 km away) - as well as „Lubstów” post mining void (11 km away), which is under the process of flooding (Fig. 1). As a result, the modeling study for the new open pit has been performed which take into consideration the changeable hydrodynamic conditions in the area influenced by dewatering of the neighboring pits as well as process of flooding the post-mining reservoirs.

Site description and hydrology

The lignite deposit „Mąkoszyn-Grochowska” is located in the area of Greater Lake District (Kondracki 2000). It occurs in the Notec river valley with many lakes and wetlands. The ordinates of the land are from 90 to 110 m a.s.l. Outside of the river valley an upland areas grow up to 160 m a.s.l. and they are cut by erosive glacial gutters. A very significant element of hydrology of this region are lakes (Brdowskie, Głuszyńskie, Lubotyńskie,

Modzerowskie), mainly groove and post-glacial ones. The average annual precipitation amounts to approximately 550 mm/y and the land evaporation is 500 – 520 mm/y (Ziętkowiak 2003). Through the northern part of the deposit the first-order watershed runs, separating the Odra and Vistula basins (Fig. 1). The average groundwater flow from this area accounts from 0.9 l/s/km² (Graf 2003) for Vistula basin in the north, to 2.19 l/s/km² for Odra basin in the south (Orszynowicz, Wierzbicka 1970).

Geological and hydrogeological conditions

The region of the deposit lies in the northern part of the basin called niecka mogileńsko-łódzka, which roof is formed by upper Cretaceous sediments. Taking into account the dewatering conditions, two hydrogeology complexes have been determined within this area: Quaternary complex and Neogen – Paleogen- Cretaceous complex. The hydrogeological conditions in these areas are characterized by four aquifers – two over and two below the lignite seam (Fig. 2). The first aquifer (Quaternary) of free water table consists of the sands and gravels just below the terrain surface. Its thickness is from 1 to 20 m and average permeability of 0.000174 m/s, but sometimes in old buried valleys it reaches thickness of 40 m and permeability



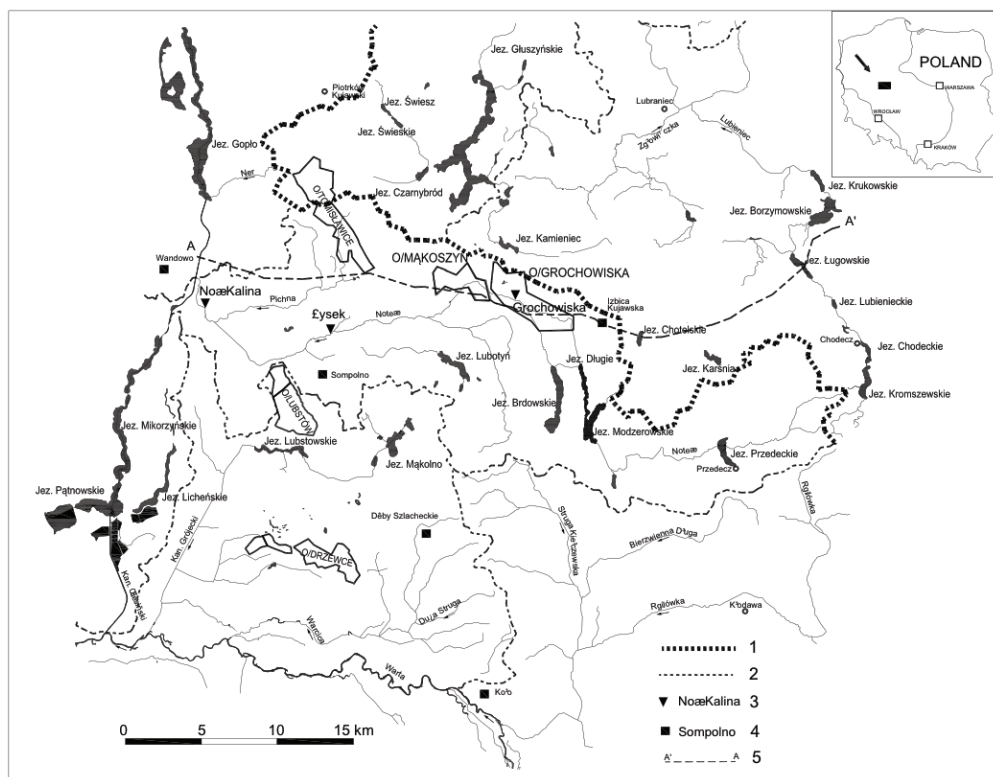


Figure 1 Hydrographic map of the „Mąkoszyn – Grochowska” lignite deposit area (modified from Stachy ed., 1987). Explanations: 1- first order watershed, 2-other watersheds, 3-hydrometric station, 4-precipitation station, 5-hydrogeological

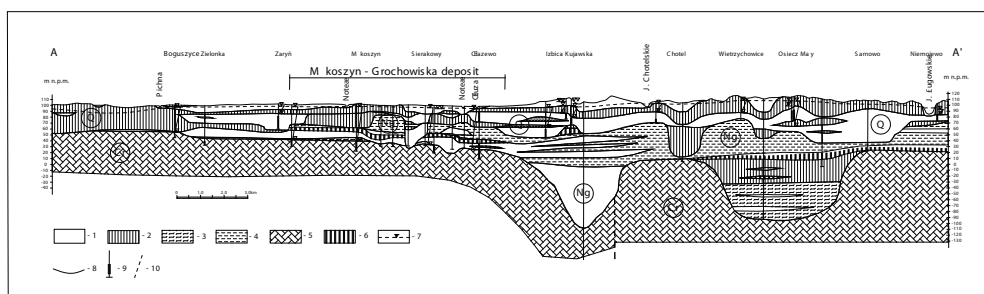


Figure 2 Hydrogeological cross-section (Szczepinski Straburzyńska-Janiszewska, 2011). Explanations: 1-fine sands, 2-glacial tills, 3-silts, 4-clays, 5-marls and dolomites, 6-lignite, 7-Neogene-Paleogene-Mesozoic aquifer piezometric surface, 8-stratigraphic boundary, 9-screeded intervals, 10-faults.

of 0.000578 m/s. The second aquifer (Quaternary) is located in sandy layers and lenses within clays with thickness 10 - 20 m and permeability varies from 0.000058 to 0.00029 m/s. The third aquifer (Neogene-Paleogene) is located in the fine widespread Neogene and reduced Paleogene sands underlying the lig-

nite seam. Its thickness varies from 10 to 60 m and permeability from 0.000012 to 0.00017 m/s. The fourth aquifer occurs in the fissured Cretaceous marls and limestones underlying Neogene - Paleogene sands, with permeability coefficient from 0.000034 to 0.00035 m/s. The specific yield of aquifers varies from 0.06

to 0.203 and storativity varies from 0.00015 to 0.002.

Groundwater in the Quaternary aquifers are under unconfined and semi-confined conditions and Neogene-Paleogene and Cretaceous aquifers occurs under confined conditions. Slight isolation and sometimes its lack between the Cretaceous and Neogene-Paleogene lignite underlying aquifer, enable hydraulic contacts between these aquifers, which is provided by the similar water table level and the low variability of chemical composition.

The recharge areas are the moraine uplands occurring to the south and east of the deposit. The Quaternary water-table aquifer is recharged by infiltration of precipitation and the lower aquifers are recharged by leakage of water from the Quaternary aquifers or directly through the hydrogeological windows. The Quaternary water table is from 120-140 m a.s.l. in the recharge areas up to about 90 -100 m a.s.l. in the area of the deposit. The groundwater level in the Neogene - Paleogene - Cretaceous complex is few meters lower than in the overburden aquifer and stabilize from 120 m a.s.l. to 100 m a.s.l. in the deposit area. In natural conditions groundwater was discharged by rivers and many lakes. Currently, as a result of the "Drzewce", "Tomisławice" and "Lubstów" opencasts dewatering, they become the center of groundwater discharge for all aquifers in the western part of the area.

Mine dewatering

Lignite production in the "Mąkoszyn-Grochowska" deposit is planned to be carried out in the years 2026-2044. The opening of the deposit is foreseen in the western part of the "Mąkoszyn Field" and the lignite production will progress to the south-east direction towards the "Grochowska Field". It is assumed to start construction of the drainage system from 2022. It is expected that groundwater will be lowered by pumping wells to the depth of 30 – 60 m and the cone of depression will be developed in the Quaternary and Neogene-Paleogene sands as well as in the Cretaceous marls and dolomites. Currently, the groundwater level in the neighboring "Drzewce", "Tomisławice" and "Lubstów" open

pits is lowered to 30 - 80 m. Water from the drainage system will be discharged through a network of pipelines, ditches and canals to Notec river. After the ending of lignite production, the post-mining reservoir located in the south-eastern part of the "Grochowska Field" will be flooded.

Groundwater flow model

A 3-dimensional finite difference model has been used based on MODFLOW code (McDonald and Harbaugh 1988) in conjunction with the MODFLOW-Surfact (Version 3) code. The modeling has been undertaken using the Groundwater Vistas (Version 5.36) software package (ESI 2006). The conceptual model for the area was based on investigations undertaken by the Geological Institute and mining company. A three-dimensional numerical model has been developed, which covers an area of 1293 km². The model is discretized with a uniform 250 m by 250 m grid, which gives a grid mesh of 181 rows and 155 columns. The model was divided into five vertical layers - three aquifers and two aquitards. The aquifers represent: 1. the upper Quaternary water table porous aquifer, 2. the lower Quaternary porous aquifer, 3. the Neogene-Paleogene-Cretaceous porous - interstice aquifer which includes interconnected the sands and marls and mudstones. Between the aquifers, there are two layers represented by aquitards comprised of clays and silts.

The south and east external boundaries were determined by the rivers and lakes and the north boundary of the model was located far outside of the potential range of the cone of depression. Depends on types of hydrogeological interactions these boundaries are represented by 1. $H = \text{const}$. 2. $Q = 0$ and 3. $Q = f(H)$ boundary conditions. The west boundary of the model was located on to the east side of the "Tomisławice", "Drzewce" and "Lubstów" open pits. The dewatering operations as well as the process of flooding the post mining open pits were modeled by progressive assignment of Modflow the Time-Variant Specified Head cells $H = f(t)$ to active mining areas in accordance with the respective project mine plans and/or modelling studies performed for these open pits before.



Municipal wells located in the model were represented by boundary condition $Q = \text{const.}$ and rivers and lakes inside of the model area were simulated using Modflow's River cells $Q = f(H)$ with streambed conductance from 0.001 to 5 m/d. The dewatering operation of the “Mąkoszyn-Grochowiska” was modeled by progressive assignment of Modflow the Time-Variant Specified Head cells $H = f(t)$ in accordance with the mine plan. The effective infiltration $Q = \text{const.}$, varies over the area and depends on the lithology of the land. It differs from 4.6 to 15.3% of average annual precipitation. To ensure appropriate representation of the change of effective infiltration during the groundwater table fluctuation, the recharge and evaporation packages were used for modelling studies.

At the first stage of model calculation, the groundwater flow model for quasi-natural conditions was performed at the end of 2008, i.e. before the starts the “Tomisławice” and “Mąkoszyn-Grochowiska” pits dewatering and just before the flooding of the “Lubstów” post-mining water reservoir. The model was calibrated for steady-state condition (Fig. 3). The heads from steady-state runs were used as initial conditions for the transient simulation for the period from 2008 to 2009, in which the model was verified, taking into account dewatering of the “Tomisławice” and “Drzewce” pits, as well as flooding the “Lubstów” post mining reservoir. The model calibration and verification has been based on the available water level data recorded in wells and piezometers located in all aquifers.

In the next stage the predictive simulation was carried out for the period from 2010 to 2021, to determine the hydrodynamic conditions in the area of the “Mąkoszyn-Grochowiska” deposit just before the dewatering of this pit.

In each 5 year stress periods covering the time span from 2010 to 2021, the boundary conditions simulating the “Tomisławice” and “Drzewce” deposits dewatering and the “Lubstów” post-mining reservoir flooding were assigned. The heads from 2021 were used as initial conditions for transient simulation of “Mąkoszyn-Grochowiska” dewatering process in years 2021 – 2044. It was assumed that the dewatering of this open pit be simulated in four stress periods: 2022-2029, 2030-2034, 2035-2039 and 2040-2044 by progressive assignment of Modflow the Time-Variant Specified Head cells $H = f(t)$ in accordance with the mine plan. Its range has been limited by the area of dewatering wells. Due to the hydraulic contacts between all the aquifers, the Neogene-Paleogene-Cretaceous aquifer was assumed as the basic one from the dewatering point of view.

Results and discussion

The results of calibration and verification were evaluated taking into account the adjustment of the measured and simulated heads and groundwater flow as well as the simulated mine water inflow into the neighboring pits to the field measured inflow.

The results for steady state conditions indicate effective infiltration of 1.83 l/s/km². The recharge from precipitation amounts to 11.0 % for layer I, 6.2 % for layer II and 1.0 % for layer III of the average precipitation for this area (0.55 m/y) (table 1). Layer I, which is almost totally recharge from precipitation is discharged to rivers, lakes and open pits dewatering system of “Drzewce” and Lubstów” (43.5 %), while 56.5% of the groundwater percolate to lower layers. Discharge out of the model area represent mainly the drainage by open pits located in the western part of the area (Fig 4).

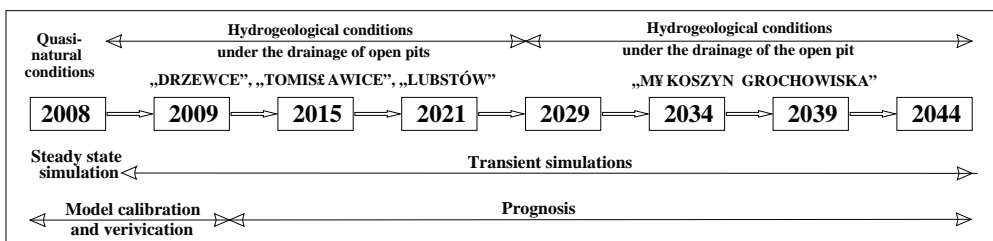


Figure 3. Stages of the model solution for “Mąkoszyn-Grochowiska” open pit.



Table 1. Groundwater balance at the „Mąkoszyn-Grochowska” region in quasi-steady state conditions at 2008, [m³/min].

Layer	Recharge from precipitation	Discharge out of the model area	Leakage from overlying layer	Discharge to rivers and lakes (external boundary conditions)	Intake wells
I	142.0	15.1	–	46.7	–
II	–	24.4	80.2	37.8	3.5
III	–	3.7	14.5	–	10.8

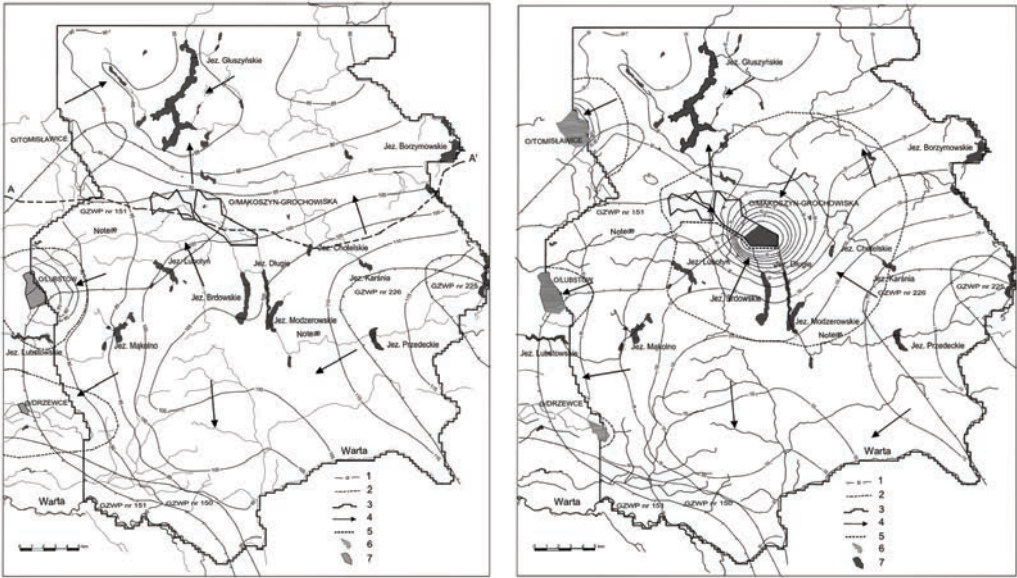


Figure 4 Map of of hydroisohypses of the Neogene-Paleogene-Mesozoic aquifer a) in quasi-natural conditions, 2008 y, b) in hydrodynamic conditions for 2044 y., computer model prediction. Explanation: 1-piezometric surface of Neogene-Paleogene-Mesozoic aquifer, 2-range of the cone of depression, 3-model boundary, 4-groundwater flow direction, 5-hydrogeological cross-section, 6-mine drainage area, 6-pit lakes

Table 2. Groundwater balance at the „Mąkoszyn-Grochowska” region, before dewatering operations at 2021, [m³/min].

Layer	Recharge from precipitation	Discharge out of the model area	Leakage from overlying layer	Discharge to rivers and lakes (external boundary conditions)	Intake wells	Recharge from static resources
I	157.6	14.8	–	43.9	–	3.4
II	–	23.7	102.3	31.6	3.5	0.1
III	–	33.4	43.6	–	10.7	0.6

The groundwater balance at the "Mąkoszyn-Grochowska" region, just before starting of dewatering operations at 2021 indicates that discharge to rivers and lakes will decrease, while the leakage from layer I increases due to moving the dewatering system in the "Drzewce" pit toward western boundary and starting dewatering operation in the "Tomisławice" open pit.

As a consequence, the mine water inflow from layer III increases (Table 2).

The groundwater balance at the end of lignite production in the "Mąkoszyn-Grochowska" pits at 2044 shows further decrease of discharge to rivers and lakes



Table 2. Groundwater balance at the „Mąkoszyn-Grochowiska” region, before dewatering operations at 2021, [m³/min].

Layer	Recharge from precipitation	Discharge out of the model area	Leakage from overlying layer	Discharge to rivers and lakes (external boundary conditions)	Intake wells	Recharge from static resources
I	157.6	14.8	–	43.9	–	3.4
II	–	23.7	102.3	31.6	3.5	0.1
III	–	33.4	43.6	–	10.7	0.6

Table 3. Groundwater balance at the „Mąkoszyn-Grochowiska” region at the end of dewatering operations at 2044, [m³/min].

Layer	Recharge from precipitation	Discharge out of the model area	Leakage from overlying layer	Discharge to rivers and lakes (external boundary conditions)	Intake wells	Recharge from static resources
I	166.8	22.4	–	40.6	–	4.4
II	–	21.2	108.2	25.9	3.5	0.1
III	–	48.9	57.8	–	10.7	1.8

* including groundwater inflow to dewatering system of „Mąkoszyn-Grochowiska” open pit

and greater leakage from layer I to lower layers (Table 3). It is due to dewatering of "Mąkoszyn-Grochowiska" pit and the process of flooding "Drzewce", "Lubstów" and "Tomisławice" post mining voids (Fig. 4).

The results of the modelling study for mining conditions (2022 – 2044) indicate that during the "Makoszyn – Grochowiska" dewatering system operation groundwater mine water inflow into the proposed open pit mine will reach from 40 to 60 m³/min. Due to the lowering of groundwater table the average effective infiltration in the area of cone of depression will account for 3.18 l/s/km² and reach 18.6% of the average precipitation ratio. The cone of depression will develop in all directions, covering Notec river and its tributaries as well as nearby lakes. The total area covered by the upper Quaternary aquifer will reach 130 km², and by the Paleogene-Neogene-Mesozoic aquifer 390 km² (Szczepiński 2011).

The modelling studies performed in the area with many open pits require taking into consideration not only the pit being under the study but also other pits, which dewatering or flooding may influence on the study area. Because dewatering is a process variable in time and space, the models must be solved in transient simulation and in each stress period it is necessary to update boundary con-

ditions representing the dewatering systems of all pits in the modeled area.

References

- Anderson M.P., Woessner W.W., 1992, Applied Groundwater Modeling, Groundwater Flow and Advective Transport. Academic Press Inc., San Diego–New York–Boston.
- Czyż J., Jagodziński Z., 2008 – "Mąkoszyn – Grochowiska" deposit exploitation project. KWB Konin S.A., Kleczew, (not published). (in polish)
- Fiszer J., Derkowska-Sitarz M., 2010 Forecast of development of depression cone and water inflows to brown coal mine Konin including designed open pits Tomisławice and Ościslów. Biul. Państw. Inst. Geol., 442: 37-41. (in polish)
- Graf R., 2003 – Comment on the hydrographic map of Poland. 1: 50 000, Sompolno sheet, UAM w Poznaniu (in polish)
- Kondracki J., 2000 – The Regional Geography of Poland. PWN, Warszawa. (in polish)
- McDonald M.G., Harbaugh A.W., 1988, A Modular Three-Dimensional Finite Difference Ground-Water Flow Model. Techn. of Water-Resources Investigations of the U.S. Geol. Surv. Book 6, Chapt. A1, Washington.
- Orszynowicz J., Wierzbicka B., 1970 – The share of groundwater in the Odra river basin and the rivers of West Pomerania. Zakład Badania Odplywu IMGW, Warszawa. (in polish)
- Stachy J. ed., 1987 – The Hydrological Atlas of Po-



- land, IMGW. Wyd. Geol. Warszawa. (in polish)
- Szczepiński J., 2013 Numerical modeling in hydrogeological studies to assess the impact of open pit mines on the environment. Wyd. Geoinż., Górni. Geol. PWr p.200 (in polish)
- Szczepiński J. Straburzevska-Janiszewska B., Prediction of the depression cone range for lignite open pit Mąkoszyn-Grochowiska KWB "Konin" S.A., 2011 Biul. Państw. Inst. Geol., 445: 671-684. (in polish)
- Ziętkowiak Z., 2003 – Comment on the hydrographic map of Poland. 1 : 50 000, Izbica Kujawska sheet, UAM w Poznaniu (in polish)



Monitoring of a public water supply system: A case of groundwater contamination by acid rock drainage[©]

Teresa Valente¹, Jorge Pamplona¹

¹*Institute of Earth Sciences, University of Minho, Campus de Gualtar, 4710-057 Braga, Portugal, teresav@dct.uminho.pt*

Abstract

The present study shows hydrochemistry of shallow groundwater from two wells planned to supply public fountains in the north of Portugal. One of the wells suffers higher impact by acid rock drainage due to mineral-water interaction in a host lithology richer in sulfides. Dissolution of sulfate efflorescences, infiltration and recharge, structural faults, and high porosity of the terrain control the evolution trends of water chemistry. The study concludes by noting the strong contamination, including by toxic elements (Al, Mn, Cd), making impossible to use the water for public supply as planned.

Keywords: ARD, volcanogenic affinity rocks, public supply

Introduction

The exposition of sulfide-rich rocks to weathering conditions results in acidic contamination, which often occurs as a consequence of the exploitation of coal and metals sulfide-rich mines. The leachates drained from waste dumps, piles and other mining structures result in acid mine drainage (AMD), creating one of the most problematic types of aquatic contamination worldwide. This acidic contamination may also develop under natural conditions, and in these cases the process takes the denomination of Acid Rock Drainage (ARD). When the geology is propitious to the appearance of ARD, the same effects that of AMD are expected to occur. So, the pH of runoff water is usually below 4 and newly formed minerals are commonly developed.

One of the most typical and problematic contexts of ARD arises from the rock excavation for constructions. For example, exposition of road cuts presents the appropriate conditions for the process, directly revealed by the presence of secondary minerals, as well as acid contamination of surface runoff. However, ARD may occur in other kind of scenarios, being only necessary appropriate conditions for sulfides oxidation as in the present case.

Sometimes water supply systems for small populations are implemented without the

proper geological study. Moreover, excavation and terrain moving in the presence of sulfide-rich lithologies may result in development of ARD. In these conditions, ARD may affect the quality of the environment, namely by limiting the potential uses of water. The present study is focused on one of these cases, located in the north of Portugal, in which ARD compromises the usefulness of groundwater planned for public supply. The main objectives are (i) to describe the hydrochemical properties of shallow groundwater, assessing its quality as drinking water; (ii) to evaluate the seasonal response of the wells and respective water chemistry; (iii) to model the mineral-water interactions responsible for water properties in the sulfide-rich lithology.

Site description

The study site (Serro) is located in the north of Portugal; it is in one the rainiest regions of the country with average annual precipitation in the range of 1600-2000 mm. Figure 1 shows location and geological setting. The sector is located in the neighbouring of Serra de Arga (Dem, Caminha, NW Portugal) and it is mostly constituted by metamorphic rocks highly deformed, bounded by tectonic contacts belonging to the Arga Unit (Lower Allochthon). This unit is characterized by mil-



limetric alternations of metapsammities and phyllites with abundant disseminated sulfides. It may contain intercalations of quartz-phyllites and volcanic to volcanoclastic rocks of different chemistry (Meireles et al., 2014). Surrounding this unit there is a monotonous sequence of metamorphic biotite micaschists (Meireles et al., 2014).

Two wells for obtaining water were installed in this site (SRn and SRs, in figure 1-B). A small reservoir receives and mixes the water from the two wells, which was then sent to the distribution network planned to supply some residences and a local system of public fountains. The dismantling and topographical regularization of the terrain for the installation of these wells promoted the exposure of the sulfide-rich rocks to weathering.

From this works also resulted a small waste dump and some preferential channels for surface runoff (Oliveira et al., 2010). Before excavation, ferruginous colours were already observed on the exposed rocks as features of sulfide oxidation. Figure 2 illustrates the rock fragments that compose the waste dump and that are widespread in the area, reflecting the dominant lithologies.

The area shows evident manifestations of ARD, such as secondary minerals covering rock fragments (Figure 2 - right) and the typical ochre colours of the surface drainage (Figure 3 - left). Oliveira (2011) identified the salt efflorescences that cover rock fragments, revealing the dominance of Fe and Al-Mg-Ca sulfates.

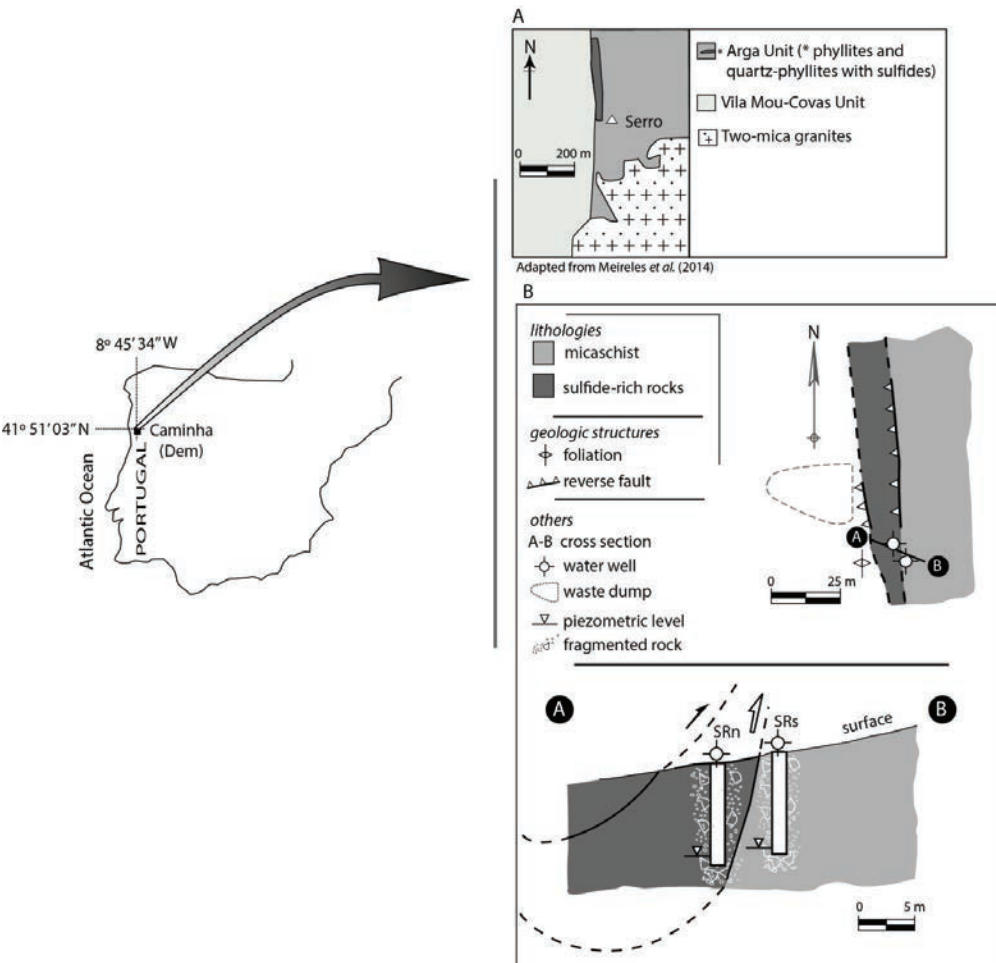


Figure 1 Location and geology of the study area. SRn and SRs represent the two wells.



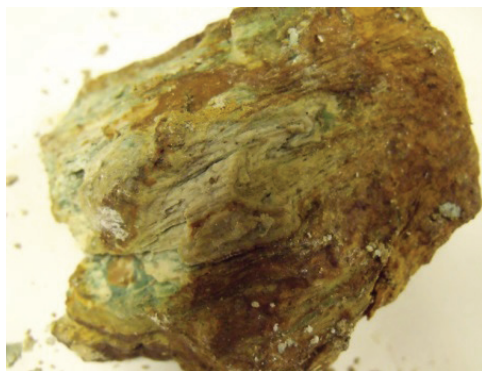


Figure 2 Images of rocks with volcanic affinity that typically have banded dissemination of sulfides (left); often covered by Fe-Al salt efflorescences (right).

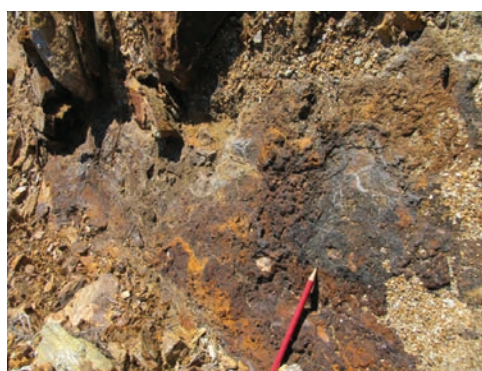


Figure 3 – Image of the ochre products in the study area. Crustification of surface drainage channels (left); Deposition of fluffy precipitates in the pipes, associated with the long term passage of the water (right).

Methods

The water wells were submitted to monitoring during 12 months for in situ parameters (pH, electric conductivity (EC), and temperature), anions, like sulfate, acidity, and alkalinity. Metals and arsenic were analysed in dry conditions (at the end of summer, September), before the first rains. Anions were obtained by ion chromatography, while acidity and alkalinity were determined by volumetric determination. Inductively coupled plasma mass spectrometry was used for metals and arsenic. Ochre products deposited in the pipes (Figure 3 – right) were also analysed by X-ray powder diffraction (XRD) (Philips PW 1710, APD), using CuK α radiation.

Results and discussion

The study performed by Oliveira et al (2010) pointed out, for the first time, the occurrence

of ARD in the Serro site. This previous work indicated low pH (2.53) and high concentrations of acidity, sulfate and metals for the runoff water. Also, Oliveira (2011) presented preliminary results about the acid nature of the water supplied by the public system of fountains located in the village of Dem-Caminha (Figure 1).

Figure 4 shows the individual behaviour of the two wells, based on the results obtained for an entire year of monitoring. Seasonal trends of pH and EC (Figure 4-a) suggest higher stability for SRs (see figure 1-B for location). The influence of ARD is clear for SRn, with average values of pH and EC of 3.76 and 433 μ S/cm, respectively. In accordance with this ARD conditions, the ochre product deposited in the pipe of SRn was identified as a mixture of schwertmannite and goethite, minerals typically found in AMD environments (e.g., Bigham et al., 1996, 1998; Dold, 2003).



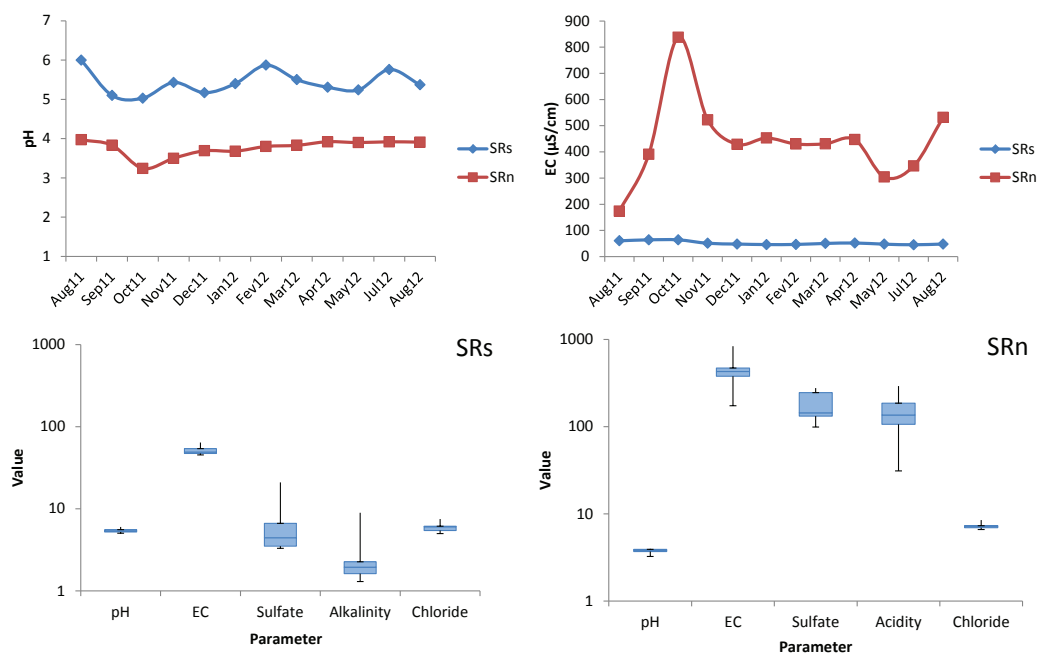


Figure 4 Water properties. a) Seasonal behaviour of pH and Electric conductivity (EC); b) Box plots for SRs and SRn. Sulfate and chloride are expressed in mg/L; acidity and alkalinity are expressed in mg/L CaCO₃.

The worst conditions were detected in October, in the sequence of the first rain episode. This effect, plainly observed for EC, has been extensively referred in AMD scenarios, associated with salt efflorescences that are able to retain sulfates and metals during dry season (Alpers et al., 1994; Valente et al., 2013; Viers et al., 2018). Their dissolution by the first rains generates contaminant solutions, explaining the high EC. Figure 4-b confirms the strong ARD conditions for SRn, which behaves as acid sulfate water. On the contrary, SRs has alkalinity (although low values) and the sulfate signature is not so evident. Here chloride has similar expression (6-7 mg/L).

The metallic signature of groundwater in dry conditions is presented in figure 5, highlighting the distinctive chemistry of both wells. SRn has higher concentration for all elements, except the As, which presents the same low value for both wells (0.15 μg/L). Among the metals, Mn and Zn occur with relevant expression, reaching in SRn 2.4 and 1.8 mg/L, respectively. Concentrations in this well infringe the standards set by the European framework for water quality for most of the metals. The Al also deserves to be highlighted, since it surpasses the standard, even in SRs.

The different chemistry can be explained by the location of the two wells. Although both suffer the influence of sulfides, SRn is right in the middle of rocks with abundant sulfide disseminations, while SRs is hosted in the micascists (Figure 1).

Major ion composition of the water depends on the host rocks composition and dissolution rates of minerals. Water-rock interaction causes the dissolution of sulfides, like pyrite and sphalerite (equation 1) and precipitation of secondary minerals, namely in fractured zones. Due to the low depth of the wells, the shallow groundwater is young and exposed to supply of metals and sulfate from surface acidic leachates, mainly under salt dissolution conditions. Equation 2 expresses this liberation process for halotrichite, one of the common secondary minerals at this site (Oliveira et al., 2010). The abundant chlorite and other Al-silicates also dissolve under these acidic conditions, releasing the highly toxic Al (equation 3). Thus, the high porosity of the terrain, enhanced by the mobilization and fragmentation facilitate the infiltration of these leachates. Furthermore, structural faults contribute to contamination by ARD.



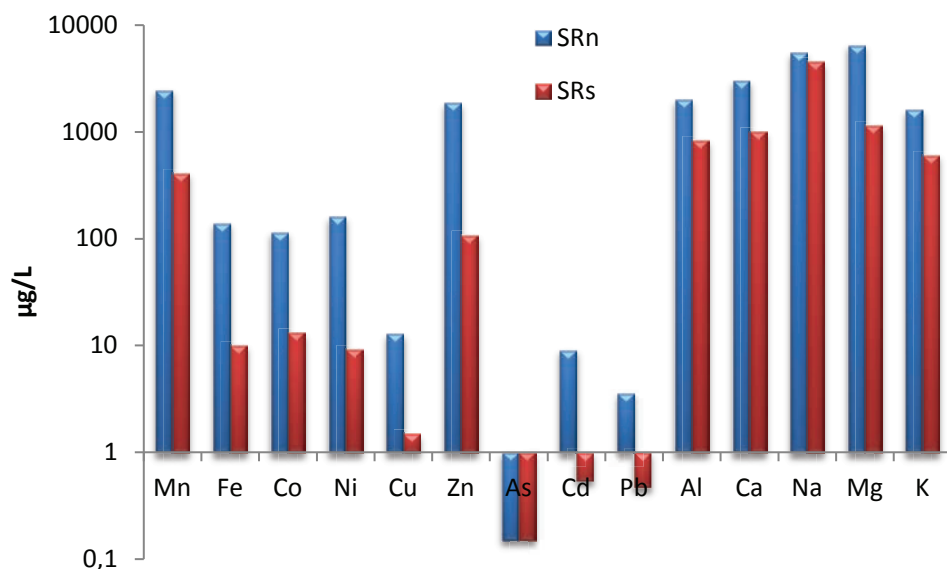
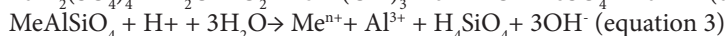
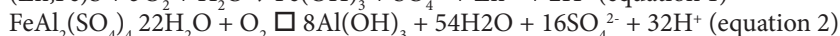
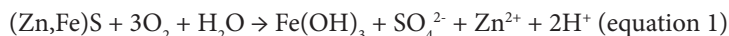


Figure 5 Metals and As concentrations for SRn and SRs. Data from a sampling campaign performed in September (dry conditions).



Conclusion

The obtained results indicated the presence of acid sulfate water, which emerged with high contents of toxic elements. The ochre product that forms on the borehole tap was identified as schwertmannite mixed with goethite, in accordance with the pH and sulfate values. The pH value, aluminium, zinc, and manganese contents are some of the most problematic parameters. Specifically, manganese concentrations are about 50 times higher than the limit allowed by the Portuguese legal framework. The water properties are directly controlled by seasonal variations, mainly promoted by rainfall and dissolution of secondary sulfates. Structural faults and high porosity of the terrain promote infiltration and recharge of these solutions, enhancing acidity and metal contents of the groundwater.

As a result of the presented monitoring procedure, the water supply system is now closed, avoiding the risk to the population. Nevertheless, mineralogical and physico-chemical indicators of ARD persist. The presence of sulfide-rich rock fragments at the

surface together with fractures contributes to maintenance of water contamination.

Acknowledgements

Financial support was provided by the national budget of the Portuguese Republic through FCT — under the project PEst-OE/CTE/UI0697/2011.

References

- Alpers C.N., Blowes D.W., Nordstrom D.K., Jambor J.L. (1994) Secondary minerals and acid mine-water chemistry. In: Jambor, J.L., Blowes, D.W. (Eds.), Short Course Handbook on Environmental Geochemistry of Sulfide Mine-wastes. Mineral Assoc. Can., p. 247–270.
- Bigham J.M., Schwertmann U., Traina S.J., Winland R.L., Wolf, M. (1996) Schwertmannite and the chemical modeling of iron in acid sulfate waters. *Geochim. Cosmochim. Acta* 60: 2111–2121.
- Dold B. (2003) Dissolution kinetics of Schwertmannite and Ferrihydrite in oxidized mine samples and their detection by differential X-ray diffraction (DXRD). *Appl. Geochem.* 18: 1531–1540.



- Meireles C, Pamplona J, Castro P. (2014) Lito e tectono-estratigrafia da Unidade do Minho Central e Ocidental: uma proposta de reclassificação. *Comum. Serv. Geol.*, 101: 269-273. [abstract in English].
- Oliveira J., Valente T., Leal Gomes C. (2010) Environmental geochemistry and mineralogy of acid rock drainage related with Silurian lithologies at Serro (Caminha, N Portugal). *E-Terra, Geosciences on-line Journal, Geotic*, vol. 9 (14). <http://e-terra.geopor.pt>, ISSN 1645-0388.
- Oliveira L. (2011) Fenómenos de contaminação metálica associados à evolução supergénica de paragéneses sulfuretadas em formações do Silúrico (Caminha, N de Portugal). Master thesis in “Ordenamento e Valorização de Recursos Geológicos”, Universidade do Minho. [Abstract in English].
- Pereira, coord. (1989) *Carta Geológica de Portugal*, Folha 1, escala 1:200.000; *Serv. Geol. Portugal*, Lisboa.
- Valente T., Grande J.A., de La Torre M.L., Santiesteban M., Ceón J.C. (2013) Mineralogy and environmental relevance of AMD-precipitates from the Tharsis mines, Iberian pyrite Belt (SW, Spain). *Appl. Geochem.* 39: 11-25.
- Viers, J., Grande J.A., Zouiten C., Freydier R., Masbou J., Valente T., de la Torre, M., Destrienneville C., Pokrovsky O. (2018)- Are Cu isotopes a useful tool to trace metal sources and processes in acid mine drainage (AMD) context? *Chemosphere* 193: 1071-1079





Geochemical and Bioreactivity Assessment of Future Mining Operations at Mutanga Uranium Project, Southern Province, Zambia

Joanne van Aardt¹, Robert Howell², Kelly Bérubé³, Tim Jones¹ and Victor Lusambo⁴

¹*Department of Earth Sciences, Cardiff University, Cardiff, Wales*

²*SRK Consulting, Cardiff, Wales*

³*School of Biosciences, Cardiff University, Cardiff, Wales*

⁴*GoviEx Limited, Lusaka, Zambia*

Abstract

Current concerns over global warming and fossil fuel impacts have led to an increasing demand for low CO₂ producing forms of energy, including nuclear power, resulting in increased uranium exploration activity. However, concern exists for the release of radionuclides and associated metals from such mining and therefore require continuous monitoring and adaptive management.

Low grade ore, waste rock and surface samples were collected from the Mutanga Project, a prospective uranium mine in the southern province of Zambia. Currently there are no mining activities but it is proposed that open-pit mining be initiated at two sites along with acid heap leaching and development of waste rock facilities on small seasonal feeder streams running into Lake Kariba.

Analytical techniques in accordance with appropriate British and Analytical Standards were used in this study, such as X-ray fluorescence (XRF), X-ray diffraction (XRD) and Inductively Coupled Plasma-Mass Spectrometry (ICP-MS). Leachate tests were employed to assess the geochemical properties and mobility of target metals, focusing on vanadium, titanium, lead and uranium. The potential bioreactivity of airborne mineral mine dust was evaluated using a Plasmid Scission Assay (PSA), where the ability of mineral particulate matter to generate Reactive Oxygen Species (ROS) and damage plasmid DNA, over a dilution range was assessed.

The results from the 22 samples indicated very low levels of target metals were mobilised within the leachates, while the additional dilution influence from Lake Kariba would mitigate any potential impacts. The PSA analysis indicates fine dust particles could be ingested and potentially cause DNA damage, due to the high crystalline silica content within these samples. A noticeable dose effect was observed. In order to mitigate this risk, dust suppression in the mining and process facilities is recommended along with personal dust protection for mine personal involved in extraction process.

Keywords: uranium mine, mobility, bioreactivity, target metals

Introduction

The current world energy system in unsustainable, with respect to fossil fuel supply (Dittmar, 2012). Uranium provides a means of alternative fuel (nuclear energy) which is essential when faced with the current global warming issues, due to the low carbon emissions of this fuel source. Nuclear energy generates 14% of the world energy sector, with the current global demand for uranium being approximately 67000 tonnes per year. The

world's current measured U-resources (5.9 million tonnes) is estimated to last about 90 years, representing a higher level of assured resources in comparison for most other minerals.

Uranium is mined similarly to other metals by techniques such as open pit, underground mining and in-situ leaching (ISL). Activity surrounding the Mutanga Uranium project is focused on extracting mineable economic orebodies from the deposits, with



the intention of mining 18.8 million tonnes of U-ore. The favoured treatment method for U-extraction is an operational method of acid heap leaching. Heap leaching occurs with low-grade deposits, where the broken ore is stacked on an impermeable surface and irrigated with an acidic solution for a period, after which the pregnant liquor is collected and treated to recover the U. This ore will be processed into uranium oxide concentrates (U_3O_8), commonly known as “Yellow Cake” and shipped to the International market for use in nuclear energy generation. Currently the project area has no known environmental liabilities as mechanised mining activities have yet to take place.

The process of extracting metals from underground ore deposits tends to generate large amounts of waste, as the metal ore of value is only a small fraction of the material being mined. This resulting waste has a large impact on the environment, as it may result in air pollution, ground deformation, water and ground contamination and water resource depletion.

This paper reviews the impact of extracting and dumping uranium mine waste rock on seasonal feeder streams, and the risks of this process on the surrounding communities and Kariba Dam in the southern province of Zambia. This involves assessing the geochemistry of the specific area, and the leaching potential and mobility of target metals focussing on uranium (U), lead (Pb), titanium (Ti) and vanadium (V), as well as determining the bioreactivity and toxicity of rock samples on receptor DNA. It is important to understand the toxicity of a material or compound by examining the degree of reactivity with regards to biological mechanisms or within physiological conditions. The bioreactivity has been assessed using particulate matter (PM), the ability of this matter to produce reactive oxygen species (ROS) and the interaction of these ROS with DNA.

Mineralisation On-Site

The initial identification of uranium (U) mineralisation in the Siavonga District occurred in 1957, with further exploration activities revealing the bulk uranium mineral resources are made up of three main deposits, Mutanga,

Dibwe and Dibwe East, with additional smaller deposits also discovered. The Mutanga ore is a Sandstone-type deposit, which formed in permeable sandstone aquifers, below the water table at low temperatures. In these settings, oxidising groundwater flowing into the aquifer from the surface carries aqueous uranyl U^{6+} complexes which have been leached from the overlying strata, deeper into the system. When this water encounters sulphides, organic matter or hydrocarbons, the aqueous uranyl is reduced and insoluble U^{4+} is precipitate. The majority of the U found at Mutanga is contained within Uranium-Calcite-Potassium minerals of Autunite and minor Meta-Autunite, with approximately 2% of the U-bearing mineralisation comprised of brannerite and coffinite.

The uranium is sourced from surrounding Proterozoic gneisses and plutonic basement rocks, where post lithification groundwater table variations caused these U^{4+} minerals to be dissolved and transported in solution and redeposited in specific reducing environments in clay-rich zones, along fractures within siltstones and sandstones of the EGF (Anderson et al, 2017). Mineralisation takes place either by dissemination, fracture controls or mud-replacement. Disseminated U_3O_8 occurs as interstitial crystals of varied sizes within sandstones, conglomerates and mud- layers, balls and flakes. Sulphides such as pyrite forming beside U_3O_8 may be indicative of transitional zones where groundwater has moved through the lithology.

Methods

Samples were collected from the site for chemical analysis and were chosen based on their in-situ U concentrations to target low-grade ore (100-200ppm) and waste rock samples from different depths. Surface samples were collected from each deposit location and were chosen based on strategic positioning of the future waste rock dump at Mutanga and the leach pad at Dibwe, both from the Escarpment Grit Formation.

Several tests were carried out in accordance with relevant standards to determine the geochemical properties of the samples, including X-Ray Florescence (XRF), from which samples of chemical interest (i.e. high



U and Pb) were selected for further testing. These samples were then analysed using leachate tests, Inductively Coupled Plasma Mass Spectrometry (ICP-MS) and X-Ray Differentiation (XRD).

To assess the bioreactivity of the samples, an invitro Plasma Scission Assay (PSA) was conducted on all surface samples, and selected core samples. This provided an indication of the quantity of target metals contained within these samples, and the effect these metals have on a plasmid DNA molecule.

Results

Each sample contained a silicon content of between 25 to 30%, with very small amounts of target metals, with rubidium and strontium being most abundant (up to 196.29ppm). Significant levels of titanium were observed in comparison to other target metals, with a wide weight percentage range within samples, from as low as 1% to 16%. The low-grade ore samples appear to have a smaller Ti content within their location, with the Mutanga more Ti-rich than Dibwe.

The lead content was very low, with trace amounts located across all samples. The Pb trend remains rather consistent, with a higher content observed at Dibwe compared to Mutanga (see Figure 1 below). There does not appear to be any relationship between the Pb and U content. Of the 22 samples collected, only four samples showed any trace of uranium, which were three of the six low grade ore samples along with a Dibwe waste rock

footwall sample, where the U content is the highest obtained, at 47.63ppm.

Leaching Rates and Mobility

The target metal content leaching out of the samples is significantly low, with the most abundant elements leached out being titanium (average of 5.25ppm), potassium, silicon and aluminium. Only trace elements of vanadium, lead and uranium were recorded (average of 1.9ppb, 10.1ppb and 59.8ppb respectively). The initial compositional values were analysed against the quantities of each element found within the leachates, to provide an indication of how mobile each element is in neutral pH water.

The elements all have very low mobility rates as seen in Figure 2. The mobility averages for both vanadium and lead are slightly lower in comparison to the titanium and uranium rates. The uranium mobility average seems to be higher due to the rate of approximately 1% from a Dibwe waste rock footwall sample, while the remaining values are minor.

Mineralogy

The bulk of each sample is composed of quartz (SiO_2), a potassium-rich alkali feldspar, microcline (KAlSi_3O_8) and the clay mineral, kaolinite ($\text{Al}_2\text{Si}_2\text{O}_5(\text{OH})_4$). None of the components observed are linked to minerals closely associated with uranium minerals.

The low-grade ore samples show a wider range of quartz compositions, with Dibwe having much lower quantities than Mutanga.

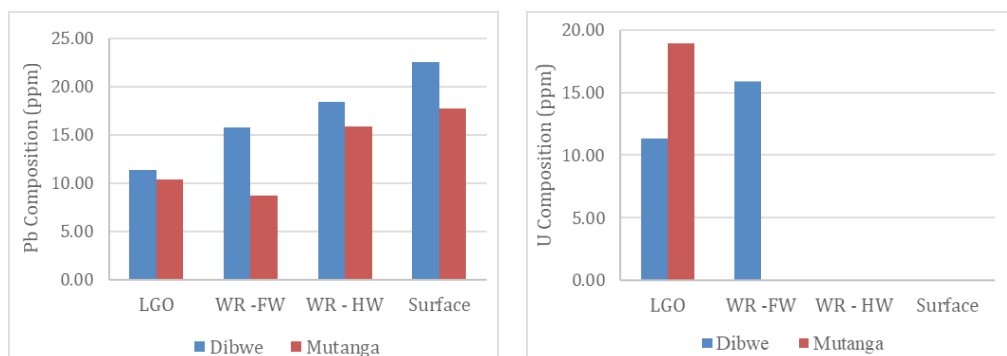


Figure 1. Lead and uranium content found in the low-grade ore (LGO), waste rock footwall (WR-FW) and hanging wall (WR-HW) and surface samples collected from the Dibwe and Mutanga site



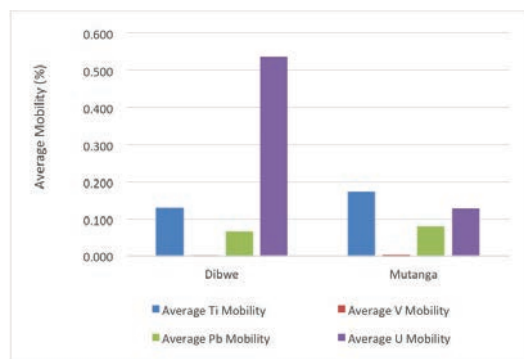


Figure 2. Mobility rates of titanium, vanadium, lead and uranium across the Dibwe and Mutanga regions

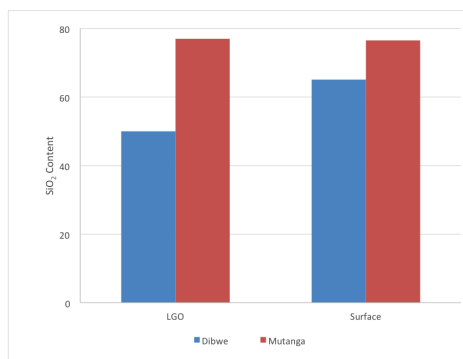


Figure 3. SiO₂ content found within low-grade ore (LGO) and surface samples from Dibwe and Mutanga

After quartz, these samples are dominated by feldspar minerals, comprised of microcline and albite. Smaller amounts of clay minerals are also observed here, in the form of kaolinite and montmorillonite. The waste rock samples appear to have a more diverse range of minerals, with quartz, feldspar and clay minerals, as well as small amounts of siderite and opal. The SiO₂ trend shows the samples of Mutanga have a higher quartz content compared to those from Dibwe (Figure 3). The lowest quartz content is seen in a Dibwe low grade ore sample (50%) and waste rock hanging wall sample (57%), compared to the lowest SiO₂ content of 70% from Mutanga in both a low-grade ore and waste rock dumping surface

Bioreactivity

The impacts of the sample PM on plasmid DNA was observed at concentrations between 50 to 1000µg/ml to determine whether any bioreactivity has a dose-dependent response range. A general trend of increasing DNA damage with increasing concentration can be observed, indicating a dose effect, whereby the more concentrated the sample, the higher the observed DNA damage. The average percentage of damaged DNA across all samples is 27%, indicating overall moderate damage being done to the DNA. The oxidative potential of the PM collected from the Mutanga Project was examined using the PSA and TD20 (toxic dose causing 20% damage) values, which were calculated using linear regression. These results reinforce

the trends above, showing a general minor increase in plasmid damage with increasing concentration. There is a clear correlation between the target metal content and the TD20 concentration, where samples with a higher target metal content showed a lower concentration needed to damage 20% of the DNA within the plasmid and are therefore more toxic to DNA. The relationship between the silicon content and the TD20 shows a similar trend to the one above, where the higher the silicon content within the sample, the lower the concentration of the sample needed to damage 20% of the plasmid DNA.

Discussion

The samples showed very small amounts of trace metals, such as vanadium, rubidium, strontium, lead, thorium and uranium, while the amount of titanium was slightly more significant in comparison. These low levels across the samples are however well below any significant thresholds, and therefore do not pose a significant health risk to the surrounding environment.

The observed average value for vanadium from the site was safely below the threshold value of 130ppm, however some of the samples displayed significantly higher readings. An important example of this is seen at the Dibwe surface site, where the observed V content was 100ppm higher than the threshold value. This may therefore be an important component to consider when dealing with dust control within this area.



Table 1. Threshold vales of Ti, V, Pb and U compared to average observed vales of these elements within the Mutanga site

	Threshold Values	Average Observed Values
Titanium	1000-10000ppm ¹	4249ppm
Vanadium	Soil threshold: 130ppm ^{2,3}	77ppm
		Dibwe surface samples: 230ppm
Lead	20-150ppm ⁴	14ppm
Uranium	23ppm (residential); 300 (industrial) ⁵	6ppm

¹Aubert & Pinta, 1977; ²Gummow et al. 2005; ³Sabbioni et al. 1996, ⁴Beyer, 1990, ⁵Canadian Council, 2007

Previous testing on the site has shown the acid-producing potential of the rock surrounding the uranium ore, and therefore should be noted. Siderite has the potential to act as a neutralising mineral, and therefore the presence of it on site suggests the possibility for the waste rock to provide local neutralisation to any acidification occurring in ground or surface water due to pyrite oxidation, only where oxygen is absent from the system (Younger, 2004). The mobility factors of titanium, vanadium, lead and uranium are very low (0.00 – 0.33%), therefore confirming that these target metals will not readily enter the surrounding environment. Ti and Pb generally tend to be immobile or have lower mobility rates compared to other metals in sedimentary environments (Gabler, 1997), and as the pH of the groundwater increases between its range of 6.5 and 9.5 the Pb mobility decreases. The low mobility rates of V and U may be caused by either unfavourable pH levels or redox conditions (Gabler, 1997).

Once these target metals are mobilised within a water source, and enter Kariba, they are diluted even further. Lake Kariba holds an incredibly large volume of water of approximately $185 \times 109\text{m}^3$ at maximum retention level. This provides a further target metal buffer, as the small concentrations of Ti, V, Pb, U and other metals reaching this lake experience a large-scale dilution factor, thereby reducing the target metal concentrations even further.

Results from the PSA testing showed a relatively moderate average of 27% DNA damage across all samples. Substantially more damage was done to plasmid DNA from surface sample in comparison to core samples, which may likely be due to the higher silicon content contained within the surface. This means that without any cellular protection,

supercoiled DNA exposed to these surface samples could become linearized (no relaxed DNA was observed). These particles initiated oxidative destruction in a dose-dependent way, where DNA subjected to higher concentrations of each sample showed more damage in four of the six samples.

The target metal and TD20 relationship showed that the higher the metal content, the lower the concentration of the sample needed to destroy 20% of the DNA, and therefore provides evidence that target metals can be linked to DNA destruction. However, the target metal content within these samples was too low to be the primary cause of this plasmid damage, indicating other factors being responsible for this DNA damage. Therefore, the silicon content was considered as an influential factor, as known studies have showed a link between the inhalation of crystalline silica dust and cell damage, resulting in serious lung disease (Greaves, 2000; Chanda-Kapata *et al.*, 2016). When comparing the Si content from the XRF and the TD20 values, a similar trend to the target metals was seen, where higher Si contents meant lower TD20 values, and therefore higher toxicity. This was taken further, and the silicon dioxide (SiO_2) relationship was studied. This trend showed a similar inverse relationship, providing evidence that SiO_2 has an effect on DNA damage and therefore toxicity. Overall it can be assumed that potential DNA damage can be done on the plasmid DNA, from exposure to the particulate matter from these samples, partly a result of the significant silicon dioxide content. This is likely to be the cause of most of the damage, however other elements or factors may be acting in simultaneously to damage the DNA and would therefore need to be considered.



Conclusion

The target metal content of the low-grade ore, waste rock and surface samples of Mutanga Uranium Project are too low to have a significant influence on the surrounding community. This therefore suggests the mining process and resultant dumping of mine waste rock onto seasonal feeder streams will not cause the leaching and mobility of significant quantities of these target metals into the environment. Due to the dose-dependent relationship observed, these risks are further reduced by the large dilution influence of Lake Kariba. The moderate levels of DNA damage observed is most likely the result of the silicon content within these samples, due to the low target metal content established. Previous case studies conducted on the influence of silicon dioxide on human receptors have shown a link between fibrosis and related respiratory and lung diseases, and therefore monitoring and duct control measures should be implemented to reduce exposure to SiO_2 of workers on site.

Acknowledgements

The authors thank GoviEx Ltd for granting access to their site and supplying necessary samples for this study, SRK for providing the necessary contacts which made the project possible, as well as Cardiff University for providing the required resources and equipment, and the staff for their assistance with project guidance and laboratory work.

References

- Anderson, M. B., Stirling, C. H., Weyer, A. (2017). Uranium Isotope Fractionation. *Reviews in Mineralogy and Geochemistry*. 82, pp.799-850.
- Aubert, H., Pinta, M. (1977). Trace Elements in Soils. *Developments in Soil Science*. Vol. 7.
- Beyer, W.N. (1990) Evaluating Soil Contaminants. U.S Fish and Wildlife Service. Biological Report. 90(2): 25pp.
- Canadian Council of Ministers of the Environment. (2007). Canadian Soil Quality Guidelines for the Protection of Environmental and Human Health. In: Canadian Environmental Quality Guidelines, 1999.
- Chanda-Kapata, P., Osei-Afriyie, D., Mwansa, C., Kapata, N. (2016). Tuberculosis in the Mines of Zambia: A Case for Intervention. *Asian Pacific Journal of Tropical Biomedicine*. 6(9): 803-807.
- Dittmar, M. (2012). Nuclear Energy: Status and Future Limitations. *Energy*. 37: 35-40.
- Greaves, I.A. (2000). Not-So-Simple Silicosis: A Case for Public Health Action. *American Journal of Industrial Medicine*. 37: 245-251.
- Gummow, B., Botha, C.J., Noordhuizen, J.P.T.J., Heesterbeek, J.A.P. (2005). The Public Health Implications of Farming Cattle in Areas with High Background Concentrations of Vanadium. *Preventive Veterinary Medicine*. 72: 281-290.
- Sabbioni, E., Kueera, J., Pietra, R., Vesterberg, O. (1996). A Critical Review on Normal Concentrations of Vanadium in Human Blood, Serum and Urine. *The Science of the Total Environment*. 118: 49-58.
- Younger, P.L. (2004). Environmental Impacts of Coal Mining and Associated Wastes: A Geochemical Perspective. *Special Publications*. 236: 169-209.





Long Term Effectiveness of an Adit Plug – Passive Treatment for Adit Discharge in a Northern Climate

Kai Skyler Woloshyn¹, Andrew G. Gault²

¹*Alexco Environmental Group Inc., #3- 151 Industrial Road Whitehorse, Yukon, Canada, kwoloshyn@alexcoresource.com*

²*Alexco Environmental Group Inc., #400 - 8 King Street East, Toronto, Ontario, Canada, agault@alexcoresource.com*

Abstract

Low-cost, long-term passive treatment to improve water quality from flowing adits is desirable, particularly in remote, cold-climate locations where active treatment is not practicable. This paper assesses the effectiveness of the installation an adit plug and other reclamation work at the Tom lead-zinc-silver exploration site located in remote eastern Yukon, Canada.

The Tom adit plug is a good example of a low maintenance, and cost-effective closure strategy particularly in northern Canada that has been able to stabilize acid rock drainage and metal leaching from a flowing adit, which is meeting its closure objectives and licenced discharge standards.

Keywords: adit plug, water quality prediction, acid rock drainage, passive treatment

Introduction

The Tom Property is located in the remote Macmillan Pass area, near the Yukon-Northwest Territories border, Canada. Between 1970 and 1982, 3,523 m of underground development was done via an adit located at 1,440 masl (Abermin Corporation, 1986). Approximately 52,000 m³ of waste rock and ore from the underground development was stockpiled on the slopes adjacent to the adit. When the underground workings were extended, significant inflows of water eventually resulted in a shut-down in 1982. Exploration activities ended at the Tom property in the early 1990s and, between 1992 and 1994, the Tom adit was covered with granular fill and drainage pipes were installed to permit the water from the underground workings to drain to surface. In 1994, a notification from the federal government that the property had been reclaimed to satisfactory conditions was received.

In the spring of 1999, a routine inspection by government inspectors found that the adit backfill had been breached by water from the adit. It was hypothesized that the drainage pipe through the backfill in the adit had frozen and the hydraulic head that had developed behind the frozen face eventually

overcame the resistance of the backfill and washed it out. At the time, the adit discharge was noted to have degraded since the adit breach and did not meet regulatory standards at that time.

In order to address these issues, and in consultation with regulators, a surface and underground reclamation program was developed and implemented between 2000 and 2010. As part of comprehensive reclamation measures, an adit plug was installed as a long-term passive treatment solution to improve the adit discharge quality by reducing the oxidation of sulphide minerals, resulting in decreased acidity, zinc and other metal concentrations. This type of passive treatment was selected as the preferred option in consultation with local regulators and in consideration of several factors, including the remote northern location of the site, seasonal access, and lack of power source.

This paper presents the results from the first seven years of the adit plug's performance. Water quality predictions are compared with the post-adit results for the flushing, short and long term phases. Implications for ongoing closure and reclamation planning are discussed.



Site Conditions

The Tom deposit is a Sedex type lead-zinc-silver deposit that is hosted within the Lower Earn Group (Devonian). The Group contains the Itsi Member (sandstone, siltstone and shale), Tom Sequence (shale and chert), and Macmillan Pass Member (chert pebble conglomerate) (Abbot, 1983). Static geochemical testing on approximately 39 samples indicate that all the units tested in the region have the potential for acid generation and metal leaching. The sedimentary rocks contain sulphide minerals including pyrite, sphalerite and galena.

Naturally-elevated metals in the undeveloped surrounding area's surface waters have been well-documented in studies completed during the past 40 years. This includes over seventeen years of monitoring and studies for the purposes of characterizing anthropogenic and natural metal loading observed in the Upper South Macmillan River watershed, including Sekie Creek #2 (Figure 1). Background water quality in Sekie Creek #2 is influenced by natural acid rock drainage (ARD) and metal leaching, with the loadings contributing the majority of zinc to the receiving environment, the South Macmillan River. Investigations and studies show the Tom adit's contribution to metal loading at downstream locations is insignificant, including those with known fisheries presence (Garter Lee, 2008).

Tom Property Reclamation Plan

From 2000-2009, baseline data collection, reclamation planning, and the necessary regulatory project support and approvals to implement the reclamation plan were completed. Figure 1 shows the main reclamation program features. The reclamation plan was implemented in 2009 and completed in 2010, including:

- Installing the Tom adit plug;
- Constructing a bypass raise including shotcreting the downstream raise;
- Installing covers for the waste rock pile and the sludge pond; and
- Installing a lined discharge channel.

The adit plug construction was completed on August 28, 2010. Between August 28 and September 13, 2010 (16 days), controlled

re-flooding of the underground workings ($\approx 18,000 \text{ m}^3$) was conducted, with discharge resuming from the adit once the water level reached 24 m above the adit floor (September 13, 2010). During the previous 16-day construction period, flow from the adit had ceased and weekly monitoring was conducted in Sekie Creek2, showed that the adit water discharge was not a significant loading source to the receiving environment. Since construction, the hydrostatic pressure (water level) behind the plug has been continuously monitored by a vibrating wire piezometer and has remained stable at approximately 24 m above the adit floor. Upon completion of this work, the adit discharge was effectively isolated from the waste rock and directed along a high density polyethylene (HDPE) lined channel.

Post-Adit Plug Water Quality Predictions

As part of the environmental assessment and regulatory applications to support the reclamation work, post-adit plug water quality was predicted for three different post-adit plug phases: flushing, short term and long term (Table 1). Due to a number of environmental variables, the different phases were not initially defined with fixed time periods, but were determined through monitoring of the adit discharge. The flushing phase was anticipated to last approximately one year, the short term phase was anticipated to last 1-5 years, and the long term phase was expected to start thereafter. These three phases were developed to replicate the expected adit discharge transition from oxygen-rich to oxygen-reduced conditions and their anticipated metal concentrations. The adit water quality predictions for the three different phases were conducted using three different data sets (static geochemical testing, historical adit water quality, and background water quality).

Table 1 summarizes the results of static geochemical testing for seven rock samples collected in 2007 from the adit wall for parameters that have effluent quality standards in the adit discharge. These samples are characterized by total sulphur ranging from 1.08 to 4.63% and all with a neutralization potential ratio (NPR) of less than one. Shake flask tests were conducted on the seven rock samples using adit water to predict the wa-



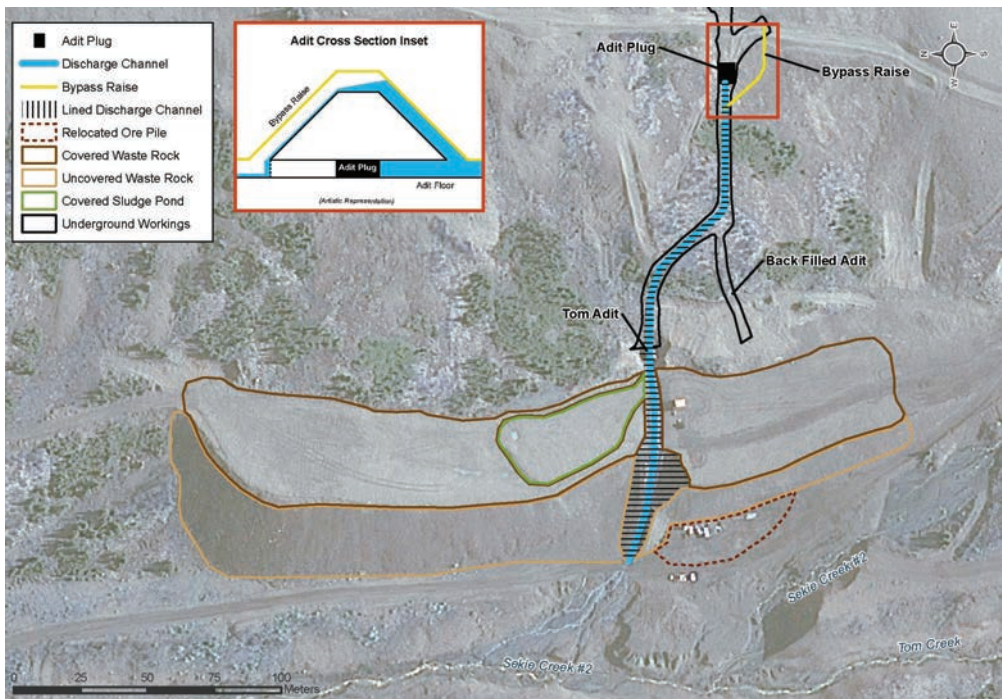


Figure 1 Tom property reclamation plan features layout

ter quality during the flushing phase. Table 1 presents the maximum concentrations observed from the shake flask tests that were incorporated into the flushing phase water quality predictions.

The short-term adit water quality was predicted using the 75th percentile from the pre-adit plug discharge covering a 10 year data set consisting of 40 sampling events. The long-term phase was predicted using the 95th percentile of the 11 background stations that are upstream of the Tom adit and workings or in adjacent undeveloped watersheds from 2000 to 2017 (67 events).

Additionally, several underground investigations were undertaken to better understand the mass balance of the adit discharge from the east zone, west zone and flooded decline. The east and west zone were characterized by pH 3 water with elevated metals, including total zinc greater than 30 mg/L, whereas the flooded decline water quality had a pH of 6.25 and total zinc concentration of 15 mg/L. A summary of the decline water quality is presented in Table 2.

Results

The Tom adit discharge water quality (W5) summary statistics for 45 sampling events from September 13, 2010 to September 6, 2017 are presented in Table 2. Overall, the post-adit plug discharge water quality has shown improvements in comparison to the pre-adit plug period of April 4, 2000 to August 25, 2010.

pH

The post-adit plug discharge pH improved, rising from the median pre-adit plug pH of 3.3 to a post-adit plug pH ranging from 3.9 to 4.9. The less acidic pH currently observed is likely a by-product of the flooded underground workings and the decrease in oxidation of the adit wall rock. The post-adit plug adit water pH results are stable between pH 4.0 and 4.5 and are less acidic than all the predicted phases, as well as the pH measured at all stations that are representative of naturally-occurring surface water in Sekie Creek #2.

Table 1. Summary of Tom adit water quality post-adit plug installation as predicted from tests on rock samples collected in 2007

Parameter	Unit	Flushing	Short Term	Long Term
Physical Parameters				
Field pH	pH	3.10	3.4	3.52
Specific Conductance (field)	µS/cm	5124	1825	2106
Acidity	mg/L CaCO ₃	2800	893	1614
Sulphate	mg/L	3200	1100	1568
Metals				
Total Copper	mg/L	2.12	0.0995	1.78
Total Iron	mg/L	858	218	240
Total Lead	mg/L	0.0663	0.117	0.070
Total Nickel	mg/L	2.78	1.56	3.13
Total Zinc	mg/L	31.4	25.9	29.1
Dissolved Arsenic	mg/L	0.429	0.029	0.043

Table 2. Summary statistics for Tom adit (W5), flooded decline (DC) and background stations

	Field pH pH unit	Specific Conduc- tance µs/ cm	Sulphate mg/L	Total Iron mg/L	Total Lead mg/L	Total Nickel mg/L	Total Zinc mg/L	Dissolved Arsenic mg/L
W5 – Tom Discharge Pre-Adit Plug, April 4, 2000 to August 25, 2010								
number of observations	24	26	37	40	40	40	40	39
Minimum	2.80	1215	155	80.0	0.085	0.698	10.5	0.0114
Median	3.33	1586	1000	190	0.108	1.37	24.3	0.0246
Maximum	3.90	2004	1530	269	0.128	2.31	30.1	0.0360
95 th Percentile	3.73	1920	1412	248	0.126	2.05	28.7	0.0331
W5 – Tom Discharge Post-Adit Plug, September 13, 2010 to September 6, 2017								
number of observations	42	43	45	45	45	45	45	45
Minimum	3.88	1325	730	109	0.064	0.85	16.7	0.001
Median	4.31	1622	1190	280	0.172	1.54	22	0.086
Maximum	4.89	2024	1440	331	0.295	2.05	29	0.135
95 th Percentile	4.60	1900	1360	320	0.214	1.90	25.8	0.100
DC - Flooded Tom Decline Discharge Pre-Adit Plug, July 2008 to June 2010								
number of observations	7	7	7	7	7	7	7	7
Minimum	6.15	1036	585	107	0.0003	0.535	12.6	0.0056
Median	6.25	1211	640	132	0.00045	0.63	14.5	0.0127
Maximum	6.57	1270	662	140	0.00079	0.71	17.7	0.0171
95 th Percentile	6.54	1259	658	139	0.00076	0.71	17.3	0.0167
Background Stations, 2000 to 2017								
number of observations	277	277	273	277	277	277	277	277
Minimum	2.60	55	11	0.09	0.00005	0.011	0.07	0.0001
Median	3.03	1110	569	56.5	0.02	1.01	5.74	0.0038
Maximum	4.43	3820	3970	542	0.10	6.27	61.3	0.0995
95 th Percentile	3.52	2106	1568	240	0.070	3.13	29.1	0.0429



Copper

The post-adit plug copper concentrations are considered to be stable and are below the long-term prediction and Effluent Quality Standard. The first sample collected on September 13th, 2010, had an initial elevated total copper concentration of 1.86 mg/L, attributable to elevated suspended solids. The total copper concentrations during the post-adit plug period showed an initial increasing trend until June 2013, when a maximum of 0.414 mg/L was observed followed by a decreasing trend and has stabilised below 0.250 mg/L.

Lead

The total lead concentrations observed to date are all below the effluent quality standard of 0.4 mg/L, but greater than the long term prediction (0.07 mg/L). The post-adit plug total lead concentrations have ranged from 0.064 to 0.295 mg/L for the 45 monitoring events post-adit plug installation. Since the installation of the adit plug, total lead concentrations steadily declined to 0.15 mg/L until late summer 2017. Total lead concentrations approximately doubled in July 2017 from 0.152 mg/L to 0.289 mg/L in August and 0.295 mg/L in September 2017, which are the maximum concentrations observed to date.

Zinc

The total zinc concentrations in samples collected during the post-adit plug period have been less than predicted and are below the total zinc concentrations observed pre-adit plug installation. Total zinc concentrations in adit water samples collected during this post-plug period have ranged from 16.7 to 29.0 mg/L, with all of the 45 samples containing total zinc at concentrations below the long-term prediction (29.1 mg/L). There was an observable decreasing trend in the total zinc concentrations since 2010, with the lowest historical total zinc concentration measured in June 2017 (17.9 mg/L). All total zinc concentrations were below the effluent quality standard since it became in effect April 29, 2016.

Arsenic

Dissolved arsenic concentrations have been discussed rather than total as the regulatory standard is for dissolved arsenic. The dissolved arsenic concentrations (0.0009 to 0.135 mg/L) observed during all the post-adit plug monitoring events were well below the dissolved arsenic EQS of 1.0 mg/L. Concentrations have been below the flushing prediction of 0.443 mg/L, although slightly above the predicted short term and long term predictions. The dissolved arsenic concentrations show a stabilized trend.

Nickel

Post-adit plug total nickel concentrations in adit waters were below pre-adit plug nickel concentrations observed in 2009 and 2010 as well as the effluent quality standard of 2.1 mg/L, although there is more variation in the results. Total nickel concentrations (0.848 to 2.05 mg/L) for all post-adit plug monitoring events were below the flushing and long term predictions, while 21 of 45 samples were above the short term prediction. The most recent total nickel concentration of 1.59 mg/L is slightly above the short term prediction of 1.56 mg/L.

Flow Rates

The adit discharge pre-adit plug was characterized by a median flow of 9.9 L/s and the post-adit plug discharge was characterized by a median flow of 12.1 L/s. The slight increase in the median flow level during the post-plug period is attributed to the increased accuracy of flow measurements resulting from the development of the lined discharge channel.

Discussion

The predicted Tom adit discharge water quality recorded during the period following the adit plug installation, using static geochemical tests and background water quality, has been a reasonably effective approach in predicting the flushing phase and long term adit water quality for the first seven years. Utilizing the 75th percentile for the pre-adit plug concentrations was concluded to not be an appropriate tool in determining the short



term post-adit plug concentrations and a higher percentile or different method would be recommended for future projects.

The data resulting from the shake flask tests on adit water and adit wall rock for determination of flushing-phase water quality indicates that this was a generally effective method to establish conservative water quality predictions for the Tom adit discharge. Testing of the leachability of iron hydroxide sludge that coats the adit floor and discharge area with adit water was determined to be a supporting factor to assist in the development of the post-adit plug water quality predictions, but based on the concentrations observed to date, the approaches used are recommended in predicting the flushing phase concentrations for sites of similar nature.

Due to the naturally-elevated metal concentrations in regional background waters of Sekie Creek #2 and the South Macmillan River, resulting from local natural ARD and metal leaching, the data suggests that the most effective and most applicable long-term site specific water quality objectives for the Tom adit discharge would be best developed using statistical analysis from background water quality.

Although concentrations of total lead and dissolved arsenic are slightly higher in the post-adit plug water quality when compared to the pre-adit plug median concentrations, the concentrations show a stabilization of these parameters and are lower than the effluent quality standards. Total zinc post-adit plug discharge concentrations have shown a decreasing trend and are below the pre-adit plug zinc concentrations observed in 2009 and 2010. The adit plug has resulted in lower oxidation reduction potential from 450 mv to between 250 to 300 mv. If the change in oxidation reduction potential in the adit discharge further reduces, the long term adit discharge is anticipated to improve the water quality as shown in Table 2.

Conclusion

The first seven years of Tom adit discharge data have been within the predicted water quality for the flushing phase with the exception of total lead, which has stabilized at concentrations less than the applicable regulatory standard. Future water quality predictions for flushing phases from an adit plug built as a passive treatment system are recommended to incorporate static geochemical testing including shake flask tests using all adit wall rock units intercepted by the underground workings with adit water. The adit discharge has been generally within the long term phase water quality predictions with variations in the trend shown by total lead and dissolved arsenic. Utilising the background method to establish long term predictions is therefore concluded to be appropriate.

Additional monitoring will be completed in 2018 to 2020 to further assess the water quality trends identified from the first seven years of post-adit plug monitoring. The analytical results for work conducted to date will be used to develop, in association with regulatory guidance, the final closure plan for the Tom property. The adit plug at the Tom property has demonstrated its effectiveness and appropriateness as a long term passive treatment solution for a remote exploration site location, demonstrating clear improvements in pH and alkalinity, and the stabilization/decrease of regulated metal concentrations, including zinc, in the adit discharge.

References

- Abbot, 1983, Geology Macmillan Fold Belts, Exploration and Geology Services Division, DI-AND
- Abermin Corporation (1986) Tom/Jason Feasibility Study (Private company document)
- Gartner Lee Limited, Project Proposal for an Installation of an Adit Plug and Associated Workings at the Tom Valley Property, 2008





Adaptive mine water treatment: modelling to long-term management

Lee Malcolm Wyatt, Arabella Mary Louise Moorhouse, Ian Andrew Watson

*Coal Authority, 200 Lichfield Lane, Mansfield, Nottinghamshire, NG18 4RG, United Kingdom
leewyatt@coal.gov.uk*

Abstract

Following the closure of coal mines in the UK, and since its inception in 1994, the Coal Authority manages mine waters in the coalfields of Great Britain. Often the mine water is controlled and treated to either prevent new discharges occurring, or to remediate existing pollution. This paper describes how changes in mine water quality and differences to predicted scenarios result in an adaptive long-term approach to mine water treatment. It gives two case study examples of how mine water treatment schemes have, and continue to adapt to, changes in mine water and the development of new technologies.

Keywords: Mine water, adaptive treatment, long-term management, coal mining

Introduction

Mine water chemistry from abandoned mines in the UK is of variable quality. In most areas, multiple mines and seams form a complex mining system, which can contain mine waters with different chemical characteristics. In contrast to other countries, the mine water in the UK is predominantly net-alkaline or circum-neutral, with iron concentrations ranging from <1mg/L to >200mg/L. The geology and the depths of the mine workings also results in variable salinity throughout the UK, with chloride concentrations ranging between <20mg/L and >20,000mg/L.

In some instances, predictions of mine water quality have been required prior to designing and building treatment schemes. Generally the predictions of chemistry are based on first-flush phenomena and sulfur content of the coal (e.g. Younger, 2000 and Banks, 2004). Over time, however, mine water quality often changes, and this can result in a reappraisal of the most appropriate and cost beneficial treatment methodology.

In addition to mine water quality changing naturally over time, underground changes in mining systems can also result in abrupt changes to the mine water chemistry and/or quantity. For example, a collapse of a roadway may not only result in a diversion of the flow pathways in the mine system, but may also allow mine waters with differing water chemis-

try to mix, thereby changing the characteristic of the mine water. Such instances are rare, but the impacts can suddenly manifest at a treatment scheme and can necessitate prompt action, with the possibility of leading to a permanent change in water treatment.

Since 1994, the Coal Authority has amended a number of treatment systems to reflect changes in mine water quality and quantity. This paper presents two examples of how treatment schemes have been impacted by changes to the mine water occurring naturally over time.

Case study 1: Blenkinsopp (multiple changes to treatment)

Blenkinsopp is the collective name for a small group of mines (total area of 5km²) located in Northumberland (northeast England), south of Hadrian's Wall World Heritage Site. The mines solely worked the Little Limestone coal seam and were abandoned in 2002. Following abandonment of the mines, it was predicted that iron-rich mine water would discharge via the shaft and former treatment ponds to the nearby river, the Tipalt Burn (flows to the River South Tyne 3km to the east) by April 2005 (Younger, 2003). Predictions of the mine water chemistry were also undertaken by Younger (2003 and 2004) to assess the initial quality of the mine water and how this could change over time.



Initial Predictions

Initial predictions of the mine water quality (Younger, 2003 and 2004) were made using a combination of: previous pumped data; water chemistry data collected within the mine (during operation); geological data (e.g. information on the local geology and sulfur content within the coal); the type of mining employed in the area; and comparisons with other similar coal mines located in the region. Based on a review of this information, Younger (2003 and 2004), predicated that the initial (first flush) of mine water would likely be net-acidic ($\text{pH} \approx 3.5$), with an iron concentration in the region of 300mg/L, reducing to ≈ 100 mg/L (with an increase in $\text{pH} \approx 6$) after a few weeks following decant.

It was expected that the first flush mine water would be net-acidic, due to pyrite content in strata overlying the coal seam. The majority of the first flush mine water was predicted to be sourced from the older, upper pillar and stall workings. The presence of limestone goaf above the later, deeper longwall workings was predicted to provide sufficient buffering capacity to generate net-alkaline mine water. Over time, and following rebound, this net-alkaline water would mix with the net-acidic waters, eventually neutralising the acidity to allow a net-alkaline mine water to reach surface. Using the behaviour of water recovery at geologically similar nearby mines as a proxy, the long-term discharge was therefore expected to become net-alkaline with an iron concentration in the region of 14mg/L. The estimated timeframes given for this improvement in water quality was predicted to take between 7 and 11 years.

In addition to water chemistry predictions, future flow rates were also estimated for Blenkinsopp by Younger (2003 and 2004). It was estimated that flow rates would be in the order of 21L/s, with some seasonal variation (18L/s in the summer and 24L/s in the winter). These predications were made using a number of factors including: observed makes of water (from the Smallburn Shaft, main sump pumps and Wrytree dip pump); pumping quantities during mining; loss of head-dependant flows; and comparisons with other similar coal mines located in the area.

Observed Conditions

Pumping eventually commenced on 18th January 2005, at a flow rate of 14L/s, later reduced to 10L/s. Predictions made by Younger and Thorn (2006), suggested that overflow of the mine water would have occurred in March 2005 had pumping not started; which was very close to the date predicted by Younger (2003 and 2004). The actual mean pumped flow rate from 2010 to 2018 has been 25L/s. This is similar to the predictions made in 2003, with the minor difference likely due to the water being pumped water in contrast to the predicted gravity overflow conditions. Thus, the predictions made in 2003, for rebound and flow rate, can be regarded as accurate.

Conversely, the same cannot be said for predictions of chemistry, which transpired to be more challenging than expected. While the pH of the water was slightly less acidic to that predicted (the modal average over the first year of pumping was $\text{pH} 4.5$), the initial iron concentrations were $>1,000\text{mg/L}$, over three times higher than the expected 300mg/L. With the majority of the iron being present in the ferrous form (typically 98%), the passive treatment scheme was inadequate to treat the mine water to meet the required design limit of 5mg/L, despite the initially low flow rate. Consequently, an active High Density Sludge (HDS) plant, using sodium hydroxide (25%) had to be installed at the site; this remained operational until 2008 due to sustained elevated ($>200\text{mg/L}$) iron concentrations.

In 2003, it was predicted that the mine water quality would improve over time (iron concentrations in the region of 14 to 30mg/L), with an estimated timeframe of 7 to 11 years. After 13 years of operation however, the iron concentrations remain higher than the estimates. Since the start of 2017, total iron concentrations generally range between 70 – 100mg/L, with ferrous iron continuing to account for the greater proportion (97%) of the iron in the mine water. The alkalinity of the mine water has improved however, with a mean concentration of 180mg/L (expressed as CaCO_3) recorded since 2017, combined with a circum-neutral pH ranging between 6.0 and 6.5. Although this decrease in iron



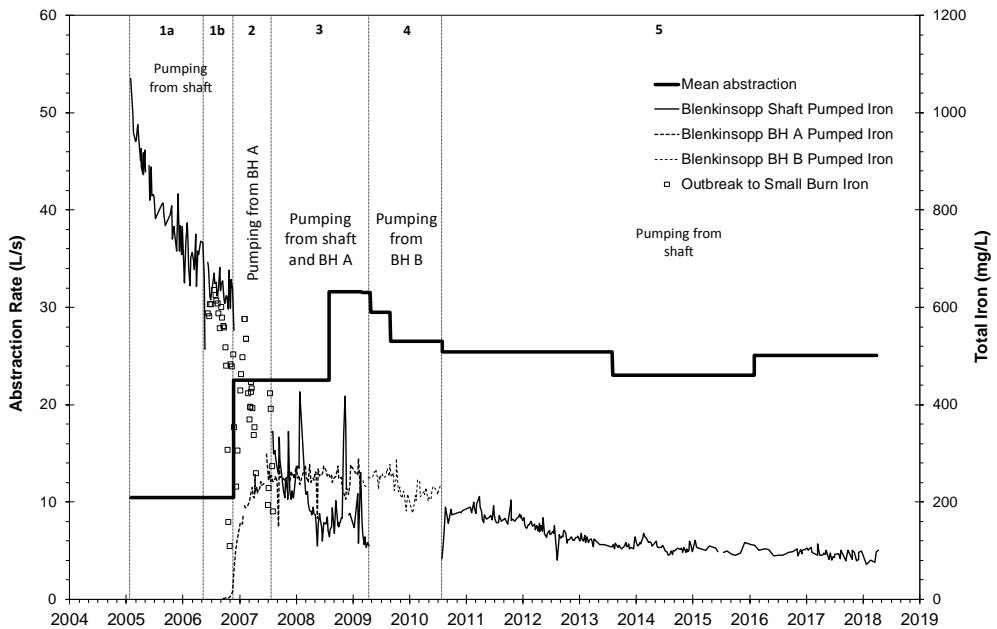


Figure 1 Trends in iron and pumping at Blenkinsopp from 2004 to 2018

and increase alkalinity has been more gradual than expected, it has allowed the treatment of the mine water to evolve over time as a result. The trends in iron concentrations and changes in pumping are shown in Fig. 1.

Following the decommissioning of the HDS plant in 2008 (when iron concentrations were generally $<200\text{mg/L}$), semi-passive treatment was used. An overview of the changes to the treatment methodology is shown below. The greatest change has been in recent years however, with the cessation of chemical dosing in 2015. This has resulted in the scheme operating passively for this first time since commissioning in 2005, whilst continuing to comply with its environmental permit (5mg/L total iron and 2mg/L dissolved iron).

An overview of the various changes to have taken place at Blenkinsopp in terms of both the pumping arrangement and treatment of the mine water treatment are as follows:

- 2005 to 2008: Temporary HDS plant, with addition of sodium hydroxide (25%).
- 2006: Pumping borehole (BHA) constructed and operational.
- 2008: Mine water treated semi-passively using the initial scheme, which comprised: Newton aerator; mixing channel,

settlement ponds and aerobic wetland augmented with chemical dosing using sodium hydroxide (25%) added in to the mixing channel.

- 2009: Pumping borehole (BHB) constructed and operational.
- 2011: Ochre sludge drying bed added to the scheme.
- 2012: Temporary aeration cascade added after Newton aerator, new longer dosing channel added, with ongoing chemical dosing using sodium hydroxide (25%).
- 2014: New conventional stepped aeration cascade replaced the Newton aerator and temporary cascade.
- 2015: Cessation of chemical dosing, and use of passive treatment.

In summary, when comparing the predictions made for Blenkinsopp, with reality, the following conclusions can be made:

- estimated date of potential uncontrolled discharge was accurate.
- predicted flow rates for a gravity discharge are only fractionally lower than the abstraction rate typically employed in 2018.
- net-acidic nature of the first flush of mine water was predicted.



- modelled mine water chemistry under-estimated the iron-concentration by a factor of 3, resulting in requirement for a temporary HDS plant.
- longevity of the iron concentration was under-estimated by a factor of between 2 and 5, requiring longer-term use of chemical dosing.
- initial treatment required use of HDS plant and not the intended passive treatment
- quantities of chemicals used decreased and ceased, and passive treatment was enhanced, but on a much longer timescale than anticipated.

Case study 2: Horden (active to passive treatment)

Horden is located in County Durham (north-east England) on the Durham Heritage Coast; mining in the area ceased in 1992. It forms part of a complex mining block (area of >165km²), which contains numerous interconnected collieries that worked multiple seams, and includes exposed and concealed Coal Measures; in addition to some offshore workings. Mine water is pumped at Horden in conjunction with the nearby Dawdon active treatment plant, located in the same mining block, to prevent pollution of a regionally important drinking water aquifer (the Raisby Formation [Magnesian Limestone]) in the overlying Permian strata.

After mining and pumping in the area ceased in 1990's, it was identified in the early 2000's, that there was a threat to the aquifer from the rising mine water. In order to provide time to investigate and confirm longer-term pumping strategies to protect this regionally important water supply, pumping was initially resumed at Horden in 2003; this slowed the rate of the rising mine water in the area. As a result of the mine water quality and short timeframe available to deploy an alternative system, the initial treatment at Horden was a temporary HDS plant, to remove the iron. Active treatment was initially chosen for this site due to the reliability of the technology, its versatility in treating a range in iron concentrations, expected during first flush, and salinity conditions, and its ability to comply with a discharge permit of

10mg/L total iron. Following the construction of a permanent active treatment plant at Dawdon, which controls the water levels in the northern area of the mining block, the active treatment system at Horden was replaced by a more sustainable passive system; this became operational in 2011. A reduction in abstraction flow rates at Horden (due to pumping at Dawdon from 2009), with reductions in iron (<150 to ≈75mg/L by 2010) and chloride concentrations (≈30,000 to <15,000mg/L), enabled a passive treatment system to be built. Today, the passive system is treating ≈60mg/L of iron to comply with a revised (as of 2015) loading based permit of 173kg/day; this scheme discharges directly to the North Sea via an outfall pipe. A challenge to the use of conventional passive treatment methods at Horden however, is the elevated salinity of the mine water. These conditions therefore required modelling before a passive scheme could be constructed, to ascertain if the mine water salinity would be acceptable for conventional polishing wetlands.

Initial Predictions

Analysis of shaft samples and pumping data collected during mining, showed high chloride concentrations (>20,000mg/L) were likely in the mine water at Horden. Geochemical modelling was therefore undertaken using the methods described in Waterchem (2007). The modelled results predicted that chloride concentrations at Horden would initially rise from <5,000mg/L, to typical values ranging between 25,000 and 45,000mg/L; taking between 2 and 15 years to reach a peak. Following this, it was predicted that the chloride concentrations would decrease and reach concentrations between 15,000 and 25,000mg/L after a period of 25 to 30 years.

During the feasibility stages of the Horden and Dawdon long-term treatment options, the tolerance to chloride for the various types of reeds typically used in wetlands (e.g. *Phragmites australis* or Common reed) was tested. Initial estimates for an upper limit of 5000mg/L chloride were given for the reeds; although this was later revised to 10,000mg/L. Information presented in Batty (2003) quotes concentrations of up to 20,000mg/L for *P. australis* and *Typha latifolia* (Reed-mace), but suggests that normal growth for *P. australis*



is up to 10,000mg/L. Both these species are commonly used for mine water treatment in the UK, with *P. australis* used at Horden.

Observed Conditions

Chloride data collected throughout the operation of the active and passive treatment schemes, in addition with pumping information, are shown on Fig. 2. In line with the predictions from the modelling, Fig. 2 shows that the peak in chloride concentration ($\approx 30,000\text{mg/L}$) occurred in 2008, after four years of pumping. This timescale is on the shorter end of the estimate, but still falls within the timescales of 2 – 25 years suggested by the model. Furthermore, the peak chloride concentration also fell within the mid-range of concentrations predicted by the model. Following the peak concentration, a gradual decrease in chloride concentrations was observed, to approximately 17,000mg/L. A further stepped decrease in chloride concentrations occurred in 2009, when abstraction rates at Horden were reduced as the Dawdon active plant came online. Since 2009, the chloride concentration at Horden has varied between 5,000 and 15,000mg/L. This variation is influenced by changes in the pumping rate at Horden.

Based on the modelled and observed chloride concentrations recorded at Horden (Fig. 2), during the operation of the active treatment system, it was concluded that the mine water could be treated passively by aeration cascade; settlement lagoons; and aerobic reed bed wetlands. However, it would be necessary to maintain the chloride concentrations, ideally below 10,000mg/L to protect the reeds in the wetlands. The mine water in this region is stratified, with hyper-saline waters being present at depth. If abstraction rates at Horden exceed 50L/s, there is a risk that the hyper-saline waters are extracted at the site. Consequently, pumping at Horden is limited to $\approx 50\text{L/s}$. As can be seen in Fig.2, the abstraction rate at Horden is operating near to this level, which at times results in waters $>10,000\text{mg/L}$ chloride being treated by the scheme. The total amount of water required to be pumped in the mining block to protect the aquifer is 100 to 150L/s. Hence, there is a need to pump the additional flows at the active Dawdon plant.

In summary, when comparing the predictions made for Horden with reality, the following conclusions can be made:

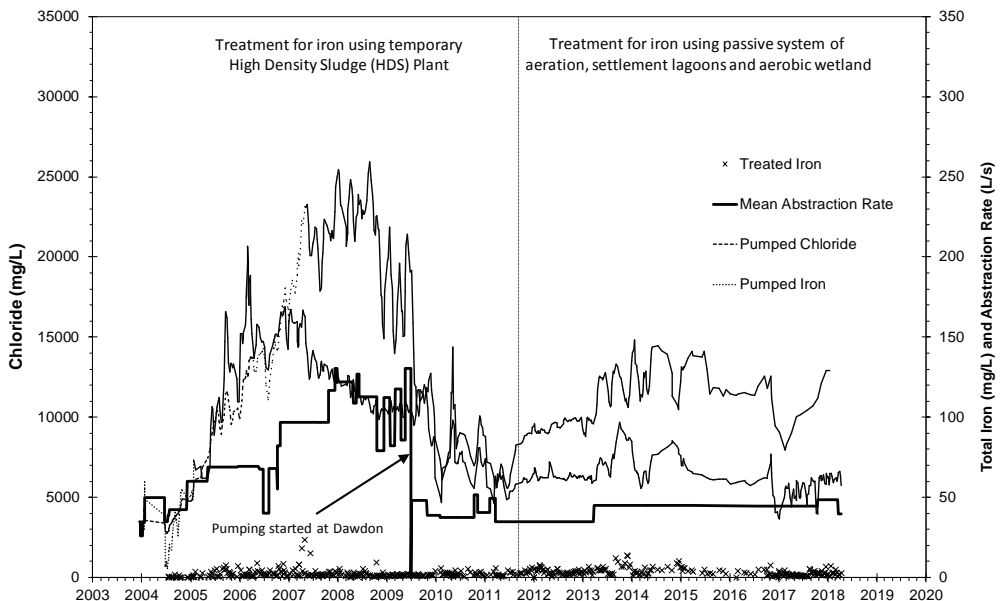


Figure 2 Trends in iron, chloride and pumping at Horden from 2003 to 2018



- long-term plan was to abstract and treat mine water at both Horden and Dawdon
- initial treatment required a temporary HDS plant to remove iron from the saline water
- long-term modelled chloride concentrations ($>20,000\text{mg/L}$) were greater than those observed, and the timescales to achieve these lower concentrations was shorter (5 years instead of >20 years)
- observed peak chloride concentration fell within the suggested range and was attained within the timescales predicted
- modelling showed chloride concentration at Horden would eventually reduce to levels close to those acceptable for passive treatment technology
- active treatment switched to passive treatment in 2011, although the reeds do struggle with the higher chloride concentrations
- strict controls of pumping between Horden and Dawdon are needed to reduce chloride and iron loading at Horden

Summary

Prediction of mine water quality and flow rates has proven difficult within complex mine systems in the UK. Modelling of chemistry and mine water flows can provide a high level overview of water quality (e.g. high-iron, low-iron, high-salinity). However, extra information from pumping tests and long-term monitoring is required to assess more accurately how the mine water changes under different conditions, and also how mine water treatment needs to be adapted to these changes. Furthermore, developments in mine water treatment technologies also need to be considered when assessing the potential for evolution of a mine water treatment scheme. For long-term mine water management, all these aspects need to be considered holistically, and where possible, it is advantageous

if any future potential changes to treatment are accommodated at, or in, an existing treatment scheme.

References

- Banks D (2004) Geochemical processes controlling minewater pollution. In Proceedings of the 2nd IMAGE-TRAIN Advanced Study Course. Groundwater management in mining areas, p 17–44
- Batty LC (2003) Effect of salinity on the growth of wetland macrophytes. Prepared for the Coal Authority
- Waterchem (2007) Optimization of mine water discharge by monitoring and modelling of geochemical processes and development of measures to protect aquifer and active mining areas from mine water contamination (Waterchem). Research Fund for Coal and Steel RFC-CR-03006, Technical report no.7
- Younger PL (2000) Predicting temporal changes in iron concentrations in groundwaters flowing from abandoned deep mines: a first approximation. *J. of Contaminant Hydrology* 44: 47–69
- Younger PL (2003) Report on mine water rebound and likely post-rebound water quality at Blenkinsopp Colliery, Northumberland. Prepared for WS Atkins Consultants Ltd on behalf of the Coal Authority.
- Younger PL (2004) Acidic leachate, limestone goaf: hydrogeochemical observations and predictions for remediation planning at Blenkinsopp Colliery, Northumberland (UK). In Young RN and Thomas HR (Eds) *Geoenvironmental engineering – Integrated management of groundwater and contaminated land*. Proceedings of the 4th conference of the Geotechnical Association, 28–30 June 2004, pp 367–374
- Younger PL, Thorn P (2006) Predictions and reality: Generation of strongly net-acidic mine waters through flooding of underground coal mine workings with limestone roof strata, Blenkinsopp Colliery (Northumberland, UK). 7th ICARD March 26–30, 2006, pp2542–2557



An integrated approach to evaluate the hydrogeological setting around a water-filled quarry in a mining environment

Josepha S.D.R. Zielke-Olivier, Danie Vermeulen

University of the Free State, Institute for Groundwater Studies, 205 Nelson Mandela Drive, Park West, 9301 Bloemfontein, South Africa, josephazielke@gmail.com, vermeulend@ufs.ac.za

Abstract

An integrated approach was employed using electrical resistivity tomography, aquifer tests, hydrochemistry and isotopes data to evaluate the geohydrological setting and pollution distribution around a water-filled quarry. A discard dump upstream from the quarry was identified as the main source of pollutants. Pollutants were transported along a fault system and a hydraulic zone at 20 m depth and concentrated in the quarry. Overflow from the quarry led to a rapid distribution of pollutants along the surface. This study indicated that the combination of analytical tools was efficient in identifying pollution sources and flow paths into and subsequently from the quarry.

Keywords: Hydraulic zone, fault system, discard dump, hydrochemistry

Introduction

Mining and industrial activities alter the Earth's sub-surface leading to changes in the natural surface- and groundwater flow paths and hydraulic conductivities of disturbed ground. In addition, mine water seepage from discard dumps often affect the water quality of the surrounding environment (Morin and Hutt 2001). Poor water quality was detected in a water-filled quarry at an industrial and mining complex in the north-eastern section of the Karoo Basin, Mpumalanga, South Africa. Locally, the area is dominated by the Permian Vryheid Formation of the Ecca Group, containing upward-coarsening cycles of siltstone, mudstone, immature sandstone and carbonaceous shale (Johnson et al. 2006). Several faults were mapped in the area, which form part of a larger graben structure with a displacement of approximately 22 m (pers. com. Vermeulen 2015). Two aquifer types control the geohydrological setting and were classified as the upper weathered and a deeper fractured Ecca aquifer (Grobelaar 2001), with an average yield of 0.6 L/s and 0.2 L/s, respectively (King 2003). Although these aquifers are relatively low yielding, bedding planes and secondary structures such as fractures and faults could form preferential flow and transport paths for contaminants from mining activities into the quarry.

A continuous hydrocensus at the study site indicated that the quarry had high sulfate concentrations resulting in an elevated electrical conductivity (EC), exceeding the water use license requirements of 90 mS/m and a TDS of 585 mg/L of the industrial complex. The quarry was mined for dolerite in the production of gravel during the construction of a railway line. It is underlain by a fault system and located in a graben north of an active discard dump for coal fines. Previous research in the area highlighted that seepage from the discard dump in the south had leaked into the groundwater and that the graben functioned as a highly conductive zone contributing to the spreading of contaminants towards the quarry (pers. com. Vermeulen 2015). As a mitigating measure, a cut-off trench was constructed around the discard dump which improved the groundwater quality immediately surrounding the trenched area. However, the water chemistry of the quarry did not improve over time. Therefore, it was recommended to re-evaluate the hydrogeological setting around the quarry to identify the sulfate source leading to elevated EC and TDS values.

This study aimed to identify the groundwater flow direction within the graben and potential flow paths for contaminants into and from the water-filled quarry. An integrated approach was utilized by applying electri-



cal resistivity tomography, groundwater levels, aquifer tests, water chemistry and isotope analyses. The objectives were to determine the source of high EC and sulfate concentration found in the quarry and surroundings, and to evaluate the distribution of mine water seepage along the mapped fault system.

Methods

Electrical resistivity tomography (ERT)

Electrical resistivity tomography measures the apparent resistivity of geological units by inducing an electrical current into the sub-surface via electrodes. The apparent resistivity is then obtained as the product of a measured resistance from the ground and a geometric factor for a given electrode array (Reynolds 2011). Since different lithologies are more or less resistive to an induced electrical current, changes in the geology and groundwater occurrences can be detected. A Terrameter ABEM SAS 1000 with a Lund Imaging System and a Wenner array was utilized to measure the apparent resistivity of the sub-surface. A grid with 13 traverses was surveyed

around the quarry to identify low resistivity areas indicative of possible groundwater flow paths (Fig. 1). A unit electrode spacing of 2.5 m was chosen based on a) the need to record data with a high spatial resolution and b) the physical limitations on the lengths of the electrode arrays posed by the surface infrastructure, quarries and wetlands. The measured data was modelled with the software RES2D-INV (Loke and Barker 1996) and interpolated with the Krigging method to generate a horizontal visualization of the ERT model.

Aquifer tests

Slug tests were employed to estimate an initial yield of the borehole to assess its viability for a pumping test. In addition, a slug test provides a first indication of the aquifer transmissivity, considering 90% recovery of the static water level (van Tonder and Vermeulen 2005). All slug tests were interpreted with the FC program for Aquifer Test Analysis (van Tonder et al. 2013). To evaluate the slug test data, the harmonic mean was calculated to alleviate the impact of large outliers.

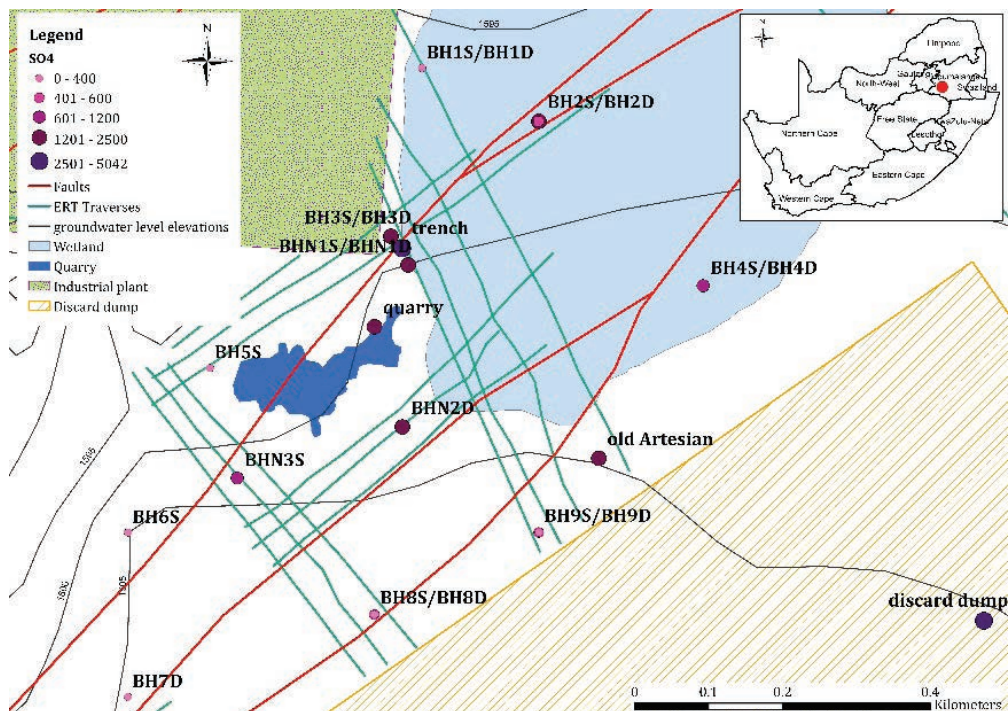


Figure 1 Schematic map of the study site indicating geophysical survey traverses and sample locations with proportional sulfate concentrations.



Constant rate pumping tests were conducted over a minimum time of eight hours to determine the aquifer parameters. Prior to each pumping test, a calibration test was performed by pumping the borehole at three different rates of the pump capacity and evaluating the recovery of the static water level to more than 90%, to obtain an appropriate pumping rate (van Tonder *et al.* 2001a). Each pumping test was executed according to the procedure described in the pumping manual for fractured rock aquifers by van Tonder *et al.* (2001a) and interpreted based on the basic flow characteristic (FC) method. This method applies derivative fitting of drawdowns and includes boundary information as well as the Gaussian error propagation analysis to estimate the sustainable yield of a borehole (van Tonder *et al.* 2001b).

Water sampling for chemical and isotope analysis

Water samples were collected with a metal flow-through bailer and stored in pre-rinsed plastic bottles for chemical analyses and in glass bottles for isotope analyses. An Inductive Coupled Plasma/Optical Emission Spectrometry was used to determine the elemental concentrations of the samples by the Institute for Groundwater Studies (IGS) laboratory. A Los Gatos Research (LGR) Liquid Water Isotope Analyser was employed by the iThemba laboratory to determine the stable isotope composition of δD and $\delta^{18}O$. These delta values were expressed as per mil deviation relative to a known standard, standard mean ocean water (SMOW).

Geophysical investigation

Three general resistivity zones were identified in the ERT model around the water-filled quarry: A zone of low resistivity below 13 Ωm , an intermediate resistivity zone ranging from 16 to 142 Ωm and a zone of high resistivity above 212 Ωm . A high resistivity zone ($>470 \Omega m$) north of the quarry suggested the presence of a dolerite sill (Fig. 2B, C and D) and was confirmed by geological logs obtained during previous construction in the area. A wetland north-east of the quarry correlates with low resistivity values due to saturated material (Fig. 2B). This saturated zone extends partially to a depth of approximately

20 mbgl (Fig. D). Another low resistivity zone was identified at the contact between the dolerite sill and the country rock north of the quarry and along the northern fault extending to the saturated zone of the wetland (Fig. 2B). These low resistivity zones could either indicate the presence of clay-rich material or saturated material. This together with the fractured zone and the fault could represent groundwater flow paths from the quarry into the shallow weathered aquifer feeding into the wetland. South-west of the quarry, an additional zone of low resistivity was modelled, which is intersected by the northern fault. Drilling of an analytical borehole, BHN3S (Fig. 1), into this zone showed that the area was backfilled with coarse ash, dolerite and other building material with a groundwater level at 4.22 mbgl.

In the south-east of the model section, the geology showed high resistivity values eluding to the presence of a dolerite sill, confirmed by subsequent drilling (BH8D, Fig. 1). Similar results were found at a depth of approximately 12 mbgl, except for an additional low resistivity zone that was visible along the middle fault, south-east of the quarry (Fig 2C). At an approximate depth of 19.7 mbgl, the low resistivity zone along the middle fault was more pronounced and extended to the south-east of the southern fault (Fig. 2D). This zone borders the active section of the discard dump and could indicate that mine water seeps into the underlying strata along these faults. The low resistivity zones together with the groundwater level elevations support the presence of flow paths from the discard dump to the quarry and from the quarry into the wetland along the northern fault and dolerite contact zone.

Aquifer testing

A slug test investigation provided an initial estimate of the fracture (T_{early}) and matrix transmissivity (T_{late}) as well as the hydraulic conductivity (K) of the fracture. The average T_{early} and T_{late} in the graben was 2 m^2/d and 0.17 m^2/d , respectively. In the fault zone, the average T_{early} was one order of magnitude higher and the average T_{late} two orders of magnitude higher compared to the graben. The average hydraulic conductivity of the fracture was estimated at 12.04 m/d. Borehole



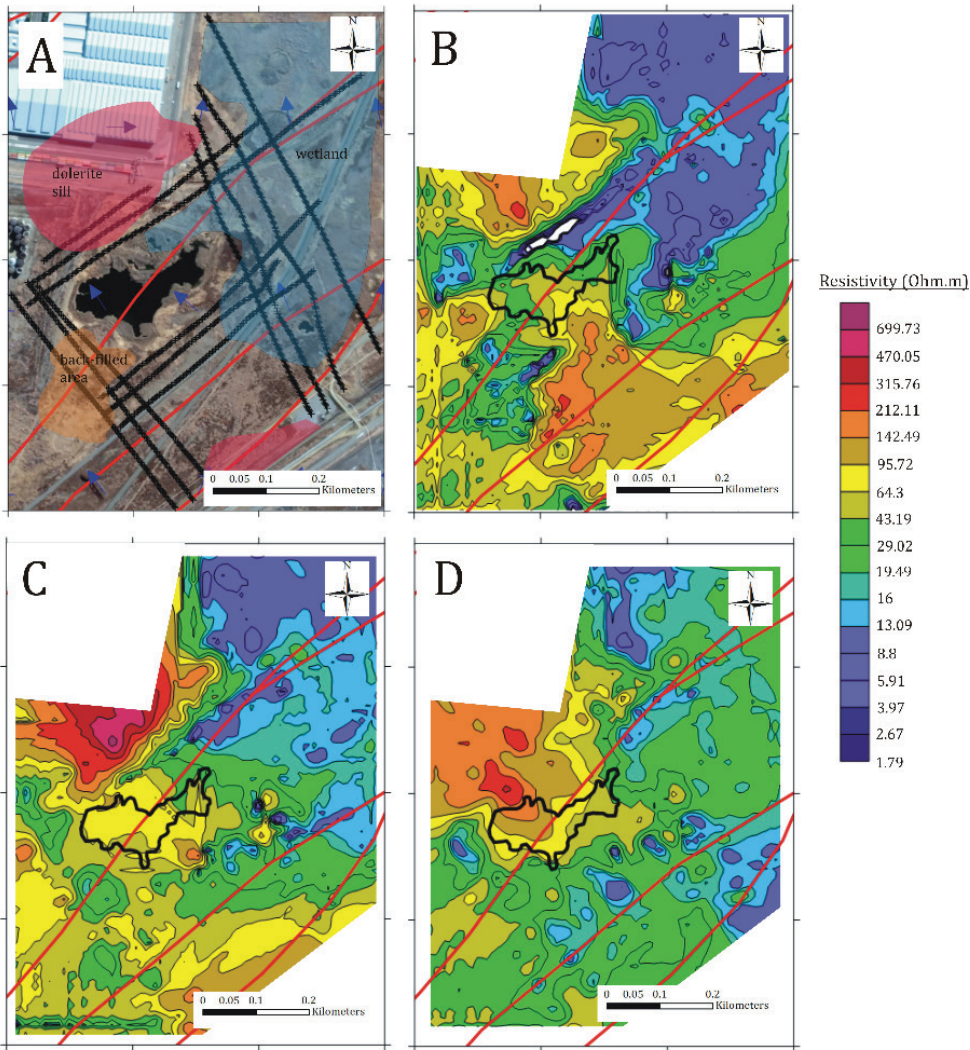


Figure 2 Resistivity interpretation: A) satellite image with resistivity profiles and groundwater flow direction (Google Earth pro 2018); B) resistivity distribution at a depth of 6.22 m; C) 12 m; and D) 19.7 m below surface; mapped faults are indicated in red.

BHN3S was drilled into the back-filled area and had an elevated T_{early} of $1760.07 \text{ m}^2/\text{d}$, T_{late} of $6.23 \text{ m}^2/\text{d}$ and an estimated K-value of 8800.37 m/d of the fracture. This was also the only borehole deemed viable to conduct a pumping test. Based on the basic FC method, borehole BHN3S had a T_{early} and T_{late} of $29.28 \text{ m}^2/\text{d}$ and $27.9 \text{ m}^2/\text{d}$, respectively which relates to the unconsolidated material of the back-filled area.

Hydrochemistry and isotope study

A water type distribution in form of stiff diagrams and EC values indicated an area with high EC ($>370 \text{ mS/m}$) values from the discard dump to north of the quarry (Fig. 3). The slurry pond of the discard dump contained mine water characterized by SO_4 , Na and K. Groundwater samples north of the discard dump to north of the quarry and water from the quarry itself contained predominantly



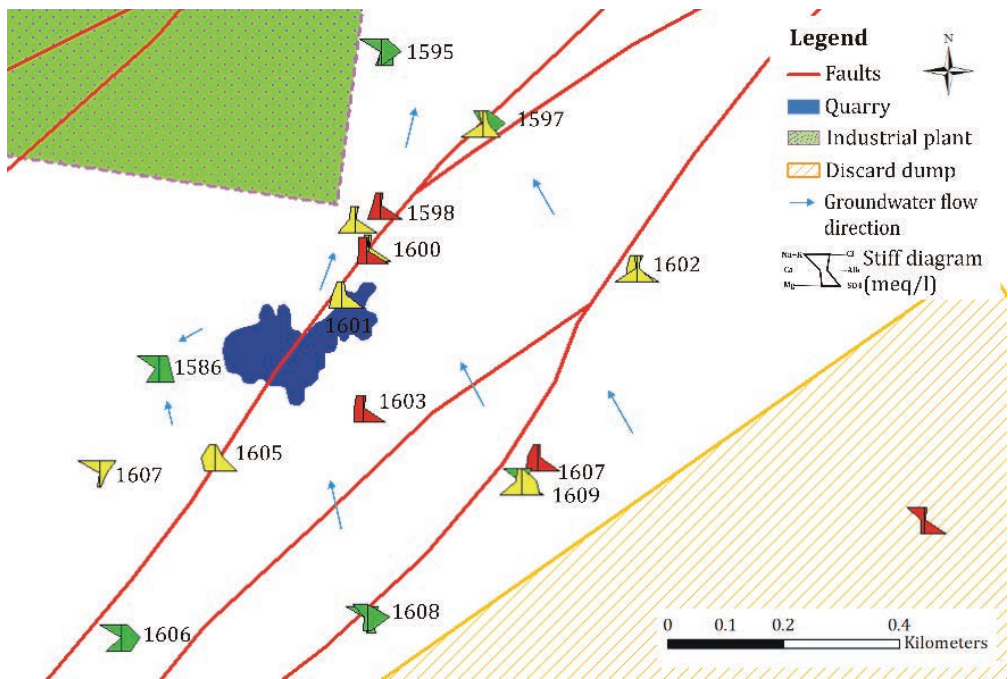


Figure 3 Water type distribution with means of Stiff diagrams, water level elevations (m) and colour coded EC values according to SA drinking water standards (mS/m): green < 150, yellow < 370 and red > 370.

SO₄ and Mg. This area with high EC values and same groundwater chemistry correlates with the low resistivity zone identified during the ERT survey and supports the presence of flow zones from and into the quarry (Fig 2). In addition, the groundwater flow direction points towards the north with elevated hydraulic heads in the boreholes adjacent to the discard dump.

West of the quarry, the groundwater was dominated by Mg, Na and K. Further north, boreholes were unpolluted and more alkaline in nature, characterized by Mg, HCO₃, Na and K. Analytical borehole BHN3S contained elevated Ca, Mg and SO₄ concentrations which were likely to have originated from the back-filled material. Based on the local groundwater flow direction and pumping test results, a connection exists between the back-filled area with a high transmissivity and the quarry.

A surface- and groundwater isotope analysis around the quarry demonstrated that most groundwater samples plotted along the global meteoric water line (GMWL) defined by Craig (1961) (Fig. 4). This indicates that the groundwater is mainly of meteoric origin.

In comparison, boreholes BHN1D, BHN1S, BHN2D, BH3D, BH3S and BH4S deviated from the GMWL and local meteoric water line (LMWL) as they were more isotopically enriched than the other groundwater samples. An enrichment was caused by secondary evaporation during rainfall, seasonal variations in precipitation and mixing of surface- and groundwater (Clark and Fritz 1997) such as seepage from the isotopically more enriched quarry. The surface water samples form a different group being isotopically enriched due to an extended evaporation period. Furthermore, the same grouping supports the conjecture that the quarry and trench receive seepage from the discard dump upstream, taking the groundwater chemistry, flow directions and conductive zones, identified in the ERT, into consideration.

Discussion and conclusion

An analysis of the groundwater flow directions, chemistry and isotope study together with the ERT model suggests that seepage from the quarry feeds into a wetland to the north-east. A link between the quarry and saturated zone of the wetland was identified



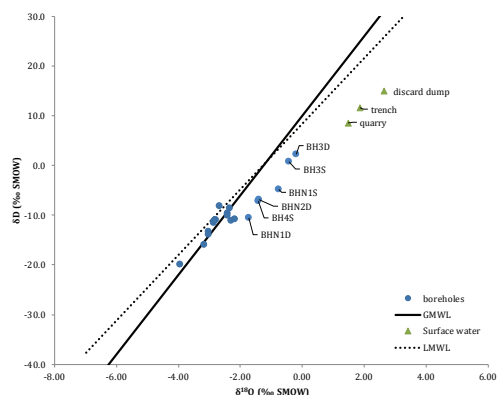


Figure 4 $\delta^2\text{H}$ and $\delta^{18}\text{O}$ relative to standard mean ocean water (SMOW) of surface- and groundwater samples collected around the quarry compared to the global (GMWL) and local meteoric water line (LMWL).

along a contact zone between a dolerite sill and country rock in the shallow weathered aquifer as well as through the fault system (Fig. 2). These observations are further supported by the local groundwater flow directions and chemistry SO_4 and Mg dominated groundwater compared to unpolluted boreholes characterised by Mg, HCO_3 , Na and K groundwater in the northern section of the study area. Additionally, continuous surface overflow from the quarry contributes to elevated sulfate concentrations measured in the trench and wetland downstream of the quarry.

Furthermore, this investigation indicated that the quarry and wetland receive mine water from the discard dump via a hydraulic zone along the southern faults at an approximate depth of 20 mbgl. This hydraulic zone was identified by low resistivity values in the ERT model (Fig. 2D) and confirmed with a down-the-hole profile of borehole BH4D, displaying an increase in EC and a drop in pH at an approximate depth of 19 mbgl. Sulfate and Mg dominated groundwater in the hydraulic zone and water sampled from the quarry and trench downstream, support the presence of a conduit between the discard dump, the quarry and the adjacent wetland. Next to the discard dump, borehole BH9D displayed an elevated piezometric head and transmissivity compared to other boreholes, suggesting a connection with the discard dump. A high skin value obtained during the pumping test

indicated that a piezometric head was caused by the elevated water table in the adjacent discard dump (pers. com. Vermeulen 2015). In addition, groundwater levels of the monitoring boreholes in the study area showed a flow direction from the discard dump towards the north which forms a topographic low at a bordering river.

A connection between the back-filled area west of the quarry and the quarry itself was confirmed by means of low resistivity values and a pumping test. The pumping test displayed high transmissivity values for both the fracture and matrix and a fast recovery of the static water level of the borehole. Overall, the pumping tests in the area highlighted that the groundwater flow occurs rather along a zone and not along a single fracture based on similar Tearly and Tlate values for fracture and matrix, respectively according to the FC method. This study showed that a combination of analytical methods including ERT, aquifer tests, groundwater flow directions, hydrochemistry and isotope data was sufficient in identifying groundwater flow paths into and from a water-filled quarry and detecting pollution sources.

Although the active section of the discard dump is lined and a cut-off trench was constructed around the facility to prevent mine water seepage from reaching the surface- and groundwater, this study found that these measures were insufficient. It is recommended to construct a numerical flow model to determine the salt load contribution of the discard dump into the system and to evaluate at which depth the present trench would be effective in intercepting the seepage from the dump. Water treatment options for the quarry should be assessed and surface overflow should be prevented by implementing a pumping system.

Acknowledgements

The authors thank all the students from the Institute for Groundwater Studies (IGS) who assisted during the field work of this project.

References

- Clark I, Fritz P (1997) Environmental Isotopes in Hydrogeology. CRC Press, USA, 328 pp
- Craig H (1961) Isotopic variations in meteoric waters. Science 133: 1702–1703



- Grobbelaar R (2001) The Long-Term Impact of Interminable Flow from Collieries in the Mpumalanga Coalfields. Master Thesis, Univ of the Free State, 136 pp (unpublished)
- King GM (2003) An Explanation of the 1:500 000 General Hydrogeological Map: Vryheid 2730. Department of Water Affairs and Forestry, Pretoria, 41 pp
- Loke MH, Barker RD (1996) Rapid least-squares inversion of apparent resistivity pseudosection by a Quasi-Newton method. *Geophysical Prospecting* 44: 131–152
- Morin KA, Hutt NM (2001) Environmental Geochemistry of Minesite Drainage: Practical Theory and Case Studies. MDAG Publishing, Vancouver, British Columbia, 333 pp
- Reynolds JM (2011) An Introduction to Applied and Environmental Geophysics. 2nd ed. Wiley-Blackwell, West Sussex, UK, 696 pp
- van Tonder G, Bardenhagen I, Riemann K, van Bosch J, Dzanga P, Xu Y (2001a) Manual on pumping test analysis in fractured-rock aquifers. Institute for Groundwater Studies, Univ of the Free State, 129 pp
- van Tonder GJ, Botha JF, Chiang W-H, Kunstmann H, Xu Y (2001b) Estimation of the sustainable yields of boreholes in fractured rock formations. *Journal of Hydrology* 241: 70–90
- van Tonder G, de Lange F, Gomo M (2013) FC program for Aquifer Test Analysis. Institute for Groundwater Studies, Univ of the Free State, South Africa
- van Tonder GJ, Vermeulen PD (2005) The Application of Slug Tests in Fractured Rock Formations. *Water SA* Volume 31, 2April 2005, ISBN 0378-4738
- Vermeulen PD (2015) Personal communication, Institute for Groundwater Studies, Univ of the Free State, South Africa



Leaching of U, V, Ni and Mo from Alum Shale Waste as a Function of Redox and pH – Suggestion for a Leaching method ©

Kristina Åhlgren, Viktor Sjöberg, Mattias Bäckström

Man-Technology-Environment Research Centre, Örebro University, Fakultetsgatan 1, 701 82 Örebro, Sweden, kristina.ahlgren@oru.se, viktor.sjoberg@oru.se, mattias.backstrom@oru.se

Abstract

Alum shale residues in the form of fines and ash were leached at different pH and redox conditions. Total concentrations and mineral analysis indicate loss of some elements in burned shale, and redistribution of others. Uranium and nickel were shown to be more leachable from fines than from ashes. Decreased pH favoured leaching of Ni, U and V, whereas increased pH resulted in increased leaching of molybdenum. Redox conditions affected leaching of Mo and V, but not U and Ni. Thus the method can be used as an estimate for leaching at different redox and pH conditions.

Keywords: Kvarntorp, alum shale, leaching, uranium, vanadium

Introduction

Alum shale in the Kvarntorp area, Sweden (figure 1), was used for oil production during 1942-1966. There is still untouched alum shale in the area, as well as remains from the production in the form of both burned shale (shale ash) and crushed but otherwise unprocessed shale (fines). The shale contains pyrite and forms acid rock drainage (ARD). It is of interest to increase the knowledge of the behaviour of the shale and the shale residues due to the risk of leaching of elements such as nickel and uranium. Examining only the total metal concentration will not necessarily provide information about the potential impact on the environment or metals available for leaching. The aim of this study is to gain increased information about the leaching behaviour of the material and to test the influence of pH and Eh on the leachability of elements.

Methods

Solid samples of both fines and two types of shale ash were collected and leaching was performed under laboratory conditions. The material was sieved and the fraction <2 mm was used in all tests. Manipulation of pH was done by addition of hydrochloric acid or sodium hydroxide, so that a pH range from 3 to at least 9.5 was obtained. Eh was varied by



Figure 1 Kvarntorp is located about 200 km to the west of Stockholm, Sweden.



addition of hydrogen peroxide or hydroxyl ammonium chloride. The redox experiments were not adjusted with respect to pH which implies that their pH was ruled by the redox reactions. For all materials a liquid to solid ratio of 10 was used and all samples were shaken intermittently. After 1, 7 and 28 days, pH (Metrohm 6.0257.000 with temperature compensation), electrical conductivity (Radiometer CDC836T-6, with temperature compensation), redox potential (Thermo Scientific REDOX/ORP 9678BNWP) and element concentrations were measured. For element analysis 100 µl was pipetted from the samples after centrifugation and diluted 100 times before analysis with ICP-MS (Agilent 7500cx).

Samples for total concentrations were sent to MS Analytical (Vancouver). Total concentrations were determined after alkaline fusion, aqua regia or four acid digestions followed by ICP-MS or ICP-AES. The materials were also examined by quantitative phase analysis by XRD.

Results and discussion

Total concentrations and mineral composition

Analysis of total concentrations shows that the fines have higher concentrations of uranium and nickel, but lower concentrations of vanadium and molybdenum than the shale ash (see table 1).

In the fines the sulfur content reached 7.9 % while the ashes contain 3.2 and 0.54 % sulfur respectively. The loss of some elements and redistribution of others due to the burn-

ing process is also reflected in the mineral differences between the fines and the ashes. As can be seen in table 2, no pyrite is present in the ashes and iron is instead found in goethite and hematite.

For the leaching tests in this study, measurements of pH and redox potential for the reference samples indicate that oxygen diffusion through the test tubes is not expected to influence the results to any greater extent, since no variation between day 1, 7 and 28 was observed.

Uranium

Highest concentrations of uranium (up to 9 500 µg/L) were found in leachates from fines. Even when considering the amount of uranium leached compared to the total content in the material, more uranium was leached from the fines than from the ashes (table 3). According to Armands (1972) the leachability of uranium in shale heated to 600°C or more is decreased, which is in line with the results of this study.

At low pH the leaching of uranium increased from both the fines and the shale ashes, while manipulation of the redox potential through the addition of hydroxyl ammonium chloride or hydrogen peroxide did not show any impact that could be distinguished from the accompanied pH change (figure 2). For fines, a pH above 4 gave lower aqueous concentrations than in leachates consisting of only deionized water. This indicates that pyrite weathering may enhance the leaching of uranium from the fines. For the ashes low

Table 1. Total concentrations for U, V, Ni, Mo and S in the different materials.

Sample	U, mg/kg	V, mg/kg	Ni, mg/kg	Mo, mg/kg	S, %
Fines	240	420	180	130	7.9
Shale ash (A)	200	660	51	210	3.2
Shale ash (B)	160	750	42	160	0.54

Table 2. Mineral wt. %

Sample	goethite	hematite	jarosite	gypsum	k-feldspar	pyrite	quartz	Illite/ musc
Fines	-	-	-	13	15.5	12.1	29.8	16.7
Shale ash (A)	5.9	11.2	4.6	19.2	18.2	-	34.2	6.0
Shale ash (B)	8.9	17.5	3.3	1.4	22.5	-	42.8	3.6



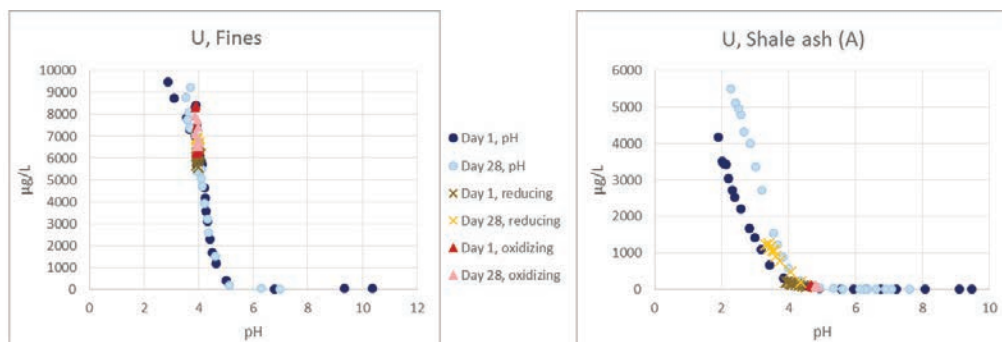


Figure 2 Leaching of uranium was increased with decreased pH for fines and ashes. Manipulation of the redox potential did not show any impact on leaching that could be distinguished from pH effects caused by redox-reactions.

concentrations of uranium were obtained unless the pH was below 4, which is below the natural pH for both ashes.

Vanadium

Accumulation of vanadium in sediments is favoured by good supply of vanadium from circulating seawater, slow sedimentation rate and a stratified partially anoxic water column (Breit and Wanty 1991). Organic materials can reduce V(V) to V(IV) but a stronger reducing agent, such as H_2S is needed for reduction of V(IV) to V(III) which is the least soluble redox state (Wanty and Goldhaber 1992). In alum shale it is believed that a series of reduction, adsorption and complexation reactions between V(V) and dissolved or particulate organic matter immobilized vanadium (Schovsbo 2001). Wright et al. (2014) also suggest that V(III) co-precipitation with Fe-oxides is a possible removal mechanism for vanadium under anoxic conditions.

For vanadium higher concentrations were found in the leachates from the ashes than from the fines (figure 3). Both pH and redox potential affected the leaching of vanadium and for the fines it was observed that the vanadium concentration increased with increased amount of hydroxyl ammonium chloride. This increase declined somewhat after day 1 and after 28 days, the difference from the control samples was small and rather indicated lower concentrations in the samples with added hydroxyl ammonium chloride than in those with only deionized water. For the ashes, increased amount of hydroxyl

ammonium chloride resulted in higher concentration of vanadium in the leachate, but contrary to the fines, these concentrations increased with time. Also higher amount of hydrogen peroxide added, resulted in increased V concentrations in the leachates for the ashes, but these concentrations decreased with time. For the fines, hydrogen peroxide did not increase the concentration of vanadium in the leachates. Both pH below 4 and above 9 increased the leaching. Even though there are different outcomes for the leaching efficiency, vanadium turned out to be not very leachable by the treatments in this test and in no sample more than 6 % was leached (table 3). The behaviour of vanadium indicates that vanadium is incorporated as vanadium(III) in iron(III) phases. Those are either dissolved during reducing conditions or oxidation of vanadium(III) increases its solubility. However the limited solubility of vanadium(III) and the poor attack of hydrogen peroxide on vanadium(III) in ordered iron(III) oxides limits the overall leaching of vanadium.

Nickel

As for uranium, the highest concentrations of nickel was found in leachates from fines, up to 8 000 µg/L corresponding to 43 % being leached (table 4). For nickel it has been suggested that in alum shale it is not concentrated in the pyrite as otherwise is the case for marine black shales (Armands 1972 and references therein) but probably bound organically. Lavergren (2008) suggests that nickel have a large abundance in sulfides more easily



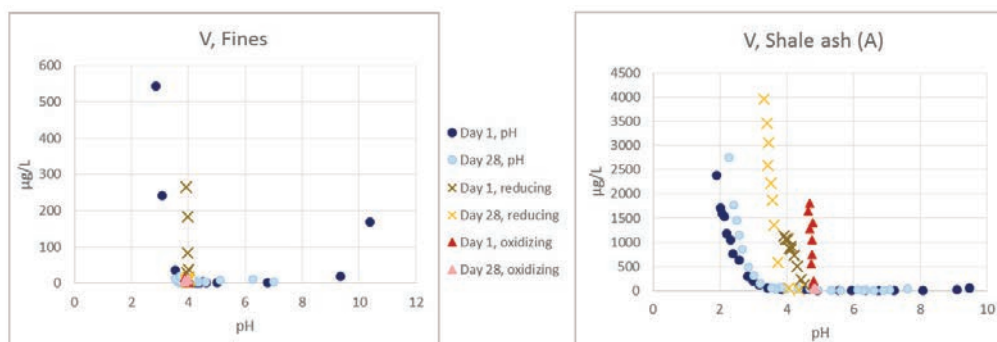


Figure 3 Leaching of vanadium was favoured by low pH, but also by high pH to some extent. The pH in the redox potential manipulated samples was controlled by redox reactions and were not pH manipulated. For shale ash both reducing and oxidizing conditions resulted in increased leaching that can be distinguished from the pH change.

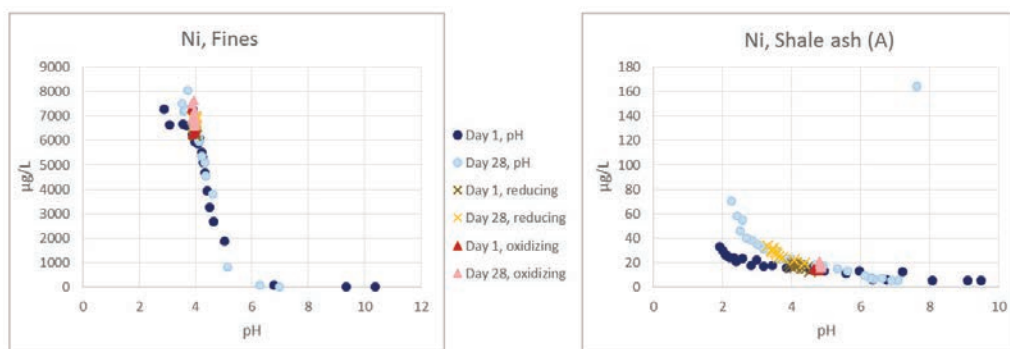


Figure 4 Leaching of nickel was favoured by low pH and showed no impact from manipulation of the redox potential.

oxidized than pyrite in e.g. the alum shale in Degerhamn, Öland. Schovsbo (2001) holds it for likely that nickel was immobilized within the sulfate reduction zone during shale formation. Whether present in pyrite or bound organically, nickel is expected to be affected by heating, either due to oxidation of pyrite or due to oxidation of organic phases. Higher total concentrations of nickel is found in fines than in the ashes. Nickel showed increased leaching by decreased pH but manipulation of the redox potential shows no impact that could be distinguished from the pH effect (figure 4). As the fines generate quite low pH, 35 % of the nickel was leached already with only deionized water.

Molybdenum

As for vanadium, higher concentrations of molybdenum were found in leachates from ashes than from fines. Studies of euxinic sediments have shown that molybdenum is not expected to mainly be found in molybdenite, but in other Mo(V)-S compound(s) (Dahl et al. 2013). Chappaz et al. (2014) argue that pyrite is not the primary host for Mo in euxinic sediments, but that there is a strong correlation between Mo and TOC that remains to be resolved. In this study, leaching of molybdenum increased with higher pH, both for the fines and the two ashes (figure 5). The fines did not show any impact from redox manipulation on molybdenum concentrations while



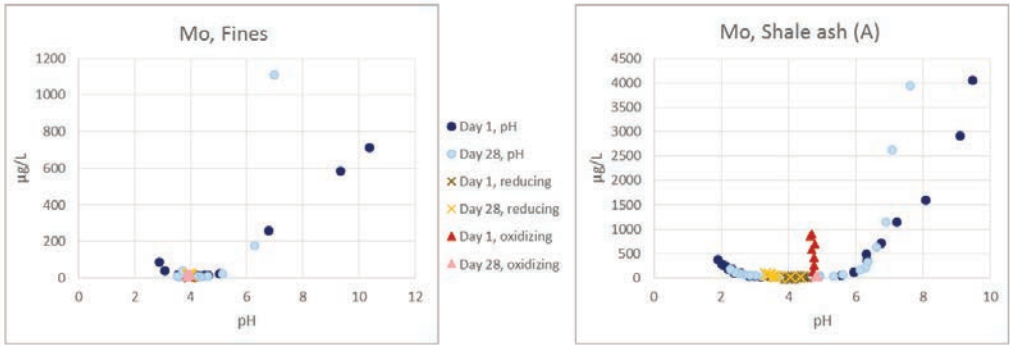


Figure 5 Leaching of molybdenum increased by increasing pH for both fines and ashes. For one of the ashes (A) also oxidizing conditions enhanced leaching that could be distinguished from pH changes, while ash B did not show any impact from redox potential manipulation (B is not included in the figure).

Table 3. Percentage of uranium and vanadium leached from fines and shale ash in deionized water (D.I.), and the range for the percentage leached in manipulated samples (pH or redox).

Uranium		% leached	pH
Fines	D.I.	24	4
	Range	0.04-38	
Ash (A)	D.I.	0.23	4.82
	Range	0.002-26.5	
Ash (B)	D.I.	0.09	7
	Range	0.01-6.5	

Vanadium		% leached	pH
Fines	D.I.	0.02	4
	Range	0.003-1.2	
Ash (A)	D.I.	0.03	4.82
	Range	0.0065-5.7	
Ash (B)	D.I.	0.04	7
	Range	0.02-3.6	

Table 4. Percentage of nickel and molybdenum leached from fines and shale ash in deionized water (D.I.), and the range for the percentage leached in manipulated samples (pH or redox).

Nickel		% leached	pH
Fines	D.I.	35	4
	Range	0.1- 43	
Ash (A)	D.I.	0.27	4.82
	Range	0.1-3.1	
Ash (B)	D.I.	0.098	7
	Range	0.03-6.6	

Molybdenum		% leached	pH
Fines	D.I.	0.09	4
	Range	0.03-8.0	
Ash (A)	D.I.	0.12	4.82
	Range	0.04-19	
Ash (B)	D.I.	0.53	7
	Range	0.06-30	

one of the ashes did. Added hydrogen peroxide resulted in increased leaching of molybdenum day 1 and 7, while the concentrations were back on the pH curve on day 28, i.e. did no longer show any increase.

Conclusions

Both fines and ashes showed increased leaching of uranium, vanadium and nickel at low pH, while leaching was increased for molyb-

denum at increased pH. The fines still contain pyrite and generate leachates with low pH which enhances further weathering and leaching of uranium and nickel, but not that much of vanadium. For the ashes, weathering with only deionized water added was not very important, whereas forced pH changes in some cases resulted in an increase of elements in the leachates. Nevertheless, even with forced decrease of pH, the ashes did not



reach the same release of uranium and nickel as the fines (nor in percentage leached nor in concentration). The impact that the shale residues have on the environment is dependent on the distribution of the varying types of waste and possible buffering materials (such as lime waste). Two ashes were analysed and even though they distinguish from the fines in the same way, they also display some mutual differences. This reflects the heterogeneity of the material, possibly both original differences in the shale and differences that emanate from inequalities in the treatment during the oil production process (e.g. different types of ovens).

The new method works as a fairly good estimate for leachate composition due to changes in pH and redox potential. It does not require any sequential leaching which makes it possible to also include time as a parameter.

Acknowledgements

The municipality of Kumla is acknowledged for giving access to the Kvarntorp area and permission to collect samples.

References

- Armands G (1972) Geochemical studies of uranium, molybdenum and vanadium in a Swedish alum shale. *Stockh Contrib Geol* 27:1-148, Acta Univ. Stockholmensis
- Breit GN, Wanty RB (1991) Vanadium accumulation in carbonaceous rocks: A review of geochemical controls during deposition and diagenesis. *Chemical Geology* 91:83-97.
- Chappaz A, Lyons TW, Gregory DD, Reinhard CT, Gill BC, Li C, Large RR (2014) Does pyrite act as an important host for molybdenum in modern and ancient euxinic sediments? *Geochimica et Cosmochimica Acta* 126:112-122.
- Dahl TW, Chappaz A, Fitts JP, Lyons TW (2013) Molybdenum reduction in a sulfidic lake: Evidence from X-ray absorption fine-structure spectroscopy for the Mo paleoproxy. *Geochimica et Cosmochimica Acta* 103:213-231.
- Lavergren U (2008) Metal dispersion from natural and processed black shale. School of Pure and Applied Natural Sciences, Faculty of Natural Sciences and Engineering, University of Kalmar, Sweden. Dissertations series no 57. PhD-thesis.
- Schovsbo NH (2001) Why barren intervals? A taphonomic case study of the Scandinavian Alum Shale and its fauna. *Lethaia* 34:271-285.
- Wanty RB, Goldhaber MB (1992) Thermodynamics and kinetics of reactions involving vanadium in natural systems: Accumulation of vanadium in sedimentary rocks. *Geochimica et Cosmochimica Acta* 56:1471-1483.
- Wright MT, Stollenwerk KG, Belitz K (2014) Assessing the solubility controls on vanadium in groundwater, northeastern San Joaquin Valley, CA. *Applied Geochemistry* 48:41-52.



10

CATCHMENT MANAGEMENT



Numerical model development for sustainable management of mine water in a semi-arid environment

Martin Boland¹, Rezene Yohannes², Jamie White³, Phil Benghiat¹, Stuart Daley⁴

¹Piteau Associates UK, Canon Court West, Abbey Lawn, Shrewsbury, Shropshire, SY2 5DE, UK, mboland@piteau.com

²Bisha Mining Share Company, 61 Mariam Gimby, Asmara, Eritrea. ryohannes@bishamining.com

³Environmental Consultant to Bisha Mining Share Company jamiwhite@iprimus.com.au

⁴WSP, The Pump House, Cotton Hill, Shrewsbury, Shropshire, SY1 2DP, UK, stuart.daley@wsp.com

Abstract

Bisha Mine is located in an arid to semi-arid area of Western Eritrea. The site lies within the Mogoraib River Basin, an ephemeral tributary of the Gash-Barka, one of Eritrea's five major river systems. Water for the mine site is principally derived from a wellfield aligned along the Mogoraib River, with the boreholes drawing water from both the alluvial gravels and the underlying fractured bedrock. This aquifer system also provides water for the local Bisha community as well as baseflow to the regionally important Barka River located 12km downstream of the site.

Sustainable water management is key to both continued operation of the site and for other groundwater dependent users/systems in the area. Water levels show both seasonal trends related to surface water flow during the wet season (July – September) superimposed on longer term trends related to groundwater abstraction.

In order to determine how to best sustainably manage water at the site, both during operations and in closure, a linked regional groundwater/site water balance model was developed using the MODFLOW/MT3D/GOLDSIM codes. Quantifying recharge in this climatic environment presented one of the most significant technical challenges for the study in terms of both baseline data collection and analysis of environmental data.

Groundwater modelling was used to optimise wellfield design and operation in order to minimise groundwater level drawdown. It was recommended that future boreholes should be drilled deeper to focus abstraction on the underlying fractured bedrock, and that abstraction rates should ideally be reduced and distributed across the wellfield to improve the sustainability of the operation.

Keywords: Semi arid environment, groundwater recharge, groundwater flow modelling

Introduction

Water scarcity is frequently identified as one of the key concerns for mining companies. Mining projects require water at almost every stage of the process, however a large proportion of these projects are located in water-stressed regions of the world such as Africa, Australia and Latin America. The International Council on Mining and Metals (ICMM), in its position document on water stewardship (ICMM 2017), stated that mining projects were encountering increasing levels of social conflict related to water, while the financial cost associated with water related infrastructure accounted for up to 10% of the mining industries capital expenditure.

The criticality of water availability is now reflected in the strategic planning of all major mining companies. The Anglo American (AA) CEO, Mark Cutifani, in his 2017 keynote presentation to the Mining Indaba in South Africa stated that “approximately 80% of our operations across the world are in water-stressed areas. This is why we are working towards building the water-less mine”, while it was AA's aim to “eliminate, the use of freshly drawn water from our mining processes”.

These issues with respect to water availability are at their most extreme in the semi arid to arid regions of the world. At the same time quantification of water resource availability in this type of hydrological environ-



ment provides a number of specific challenges, including measurement of highly localised rainfall events and determination of how this rainfall translates to recharge of the groundwater aquifer. These technical requirements need to be properly understood in order to both design an appropriate environmental data collection programme required to underpin the resource evaluation, and to ensure the proper application of analytical approaches to evaluating groundwater sustainability.

This paper presents the results of a comprehensive study undertaken by the Bisha Mining Share Company (BMSC) at its Bisha Mine in Eritrea, in which it evaluated the data and analytical tools available to the project to underpin sustainable management of its water resources in a challenging semi arid environment.

Background

The Bisha Mine, which has been operating since 2010, is located in an arid to semi-arid area of Western Eritrea. The site lies within the Mogoraib River Basin, an ephemeral tributary of the Gash-Barka, one of Eritrea's five major river systems. Since the end of 2010, raw water supply for mine operations has been primarily derived from a wellfield aligned along the Mogoraib River. This aquifer system also provides water for the local Mogoraib communities as well as baseflow to the regionally important Barka River located 12km downstream of the site.

Water supply from the Mogoraib wellfield has been augmented with pumping from a second smaller wellfield in the alluvial deposits of the Freketet, a tributary of the Mogoraib, and from periodic pumping of the closed Harena pit and its associated dewatering boreholes.

As part of effectively managing its water supply BMSC commissioned a comprehensive review of their hydrological monitoring network/data, and the development of both Modflow and GoldSim numerical models, which would support them in the operational management/optimisation of water use, and allow predictive simulation of future impacts of water abstraction. The studies were also used as the basis for identifying any addition-

al environmental data requirements needed to improve sustainable water management in this semi arid environment.

Rainfall

Rainfall has been measured intermittently since 1999 at six locations within the Bisha project area. Measured annual rainfall ranges between 111 mm/yr (2002) and 411 mm/yr (2007). However annual rainfall is observed to differ significantly between rain gauge records across the project area (e.g. in 2005, 146.5 mm was recorded at the Camp rain gauge compared to 220 mm recorded at the Italian Station rain gauge, which are approximately 8km apart). Where rainfall differences between rain gauges are consistent each year, the discrepancy can potentially be attributed to the type of rain gauge being used. However inconsistent annual rainfall differences are likely to be a function of the localized nature of rainfall across the Bisha Project area. For example, in 2012 the Camp weather station recorded nearly 40 mm more rain than the gauge located at the Tailings Management Facility (TMF) weather station which is 2km away. In 2013 this trend was reversed with ~50 mm more rainfall was recorded at the TMF weather station.

The daily rainfall record also reflects the localized nature of rainfall across the Bisha Project area, with significant rainfall recorded at one of the project rain gauges not being detected at the other, or different magnitudes of rain being recorded on the same day (e.g. 26th August 2015, 31 mm at the TMF WS and 74 mm at the Village WS).

This disparity between the magnitude and duration of rain on an annual basis indicates that annual rainfall statistics, a fundamental input parameter to water resource sustainability assessment, must be used with caution when considering site hydrology. Thus a very wet year may not mean a very hydrologically active year, as high rainfall may have occurred over a short period of time e.g. in 2011 when ~26% of the annual rainfall occurred on a single day (2011 annual rainfall was 235 mm of which 61.3 mm occurred on 23rd July). This in turn will strongly influence the percentage of rainfall which may become groundwater recharge.



River stage and flow data

Hydrological data has been collected manually at five locations across the project site in order to assess both surface water management requirements at the Bisha Mine site, and to determine the potential for surface water to provide a mine water supply source. Stage-discharge relationships were determined for each monitoring station based on the estimates of flow and the associated river stage. These data have been further analysed to try and quantify runoff coefficients for each of the gauging station catchments. Derived coefficients ranged between 0.01 and 0.71 with the majority falling between 0.01 to 0.3 [Coefficients were derived for the Shatera gauging station which exceeded 1 (suggesting more runoff was generated than rainfall) however these have been excluded from the data set]. The huge range of derived run-off coefficients indicates the difficulty in relating spot rainfall measurements to rapid flood flow generated in this type of environment. Wheater and Brown (1989) presented an analysis of a 597 km² subcatchment of the wadi Yiba in Saudi Arabia, where runoff coefficients derived using data from 5 rain gauges within the catchment varied from 0.059 to 0.79 (similar in range to those derived for Bisha), with the greatest runoff volume being associated with the smallest measured rainfall event, suggesting that even this relatively high

density of rain gauges was not sufficient to capture the rainfall events which were giving rise to specific events at the flow gauging stations. Their conclusion was that application of rainfall depth-area-frequency relationships in this type of climate, beyond the area of storm coverage, was difficult due to the limited spatial area of storm rainfall events, the complex channel routing within wadi systems, and the impact of transmission losses, where runoff flow dissipates through infiltration into the wadi bed.

Significant flow has been observed in the Mogoraib during a period when no rainfall was recorded at the project rain gauges. Additionally no flow was measured in the Freketet or Shatera Rivers at the same time, indicating that rain falling in the upper reaches of the Mogoraib catchment, and outside the project area, was responsible for this observed flow. Entire river flow events are also observed on a sub-daily time period. Water levels have been observed at the Upper Mogoraib gauging station to have increased from 0 m, peaking at 2.96 m before receding back to 0 m over a 21 hr period. In addition, a stage as high as 1.57 m has been observed over a period of 9 hours between zero flow conditions. This indicates that monitoring of rainfall and flow data on a sub-daily frequency is required in order to accurately de-

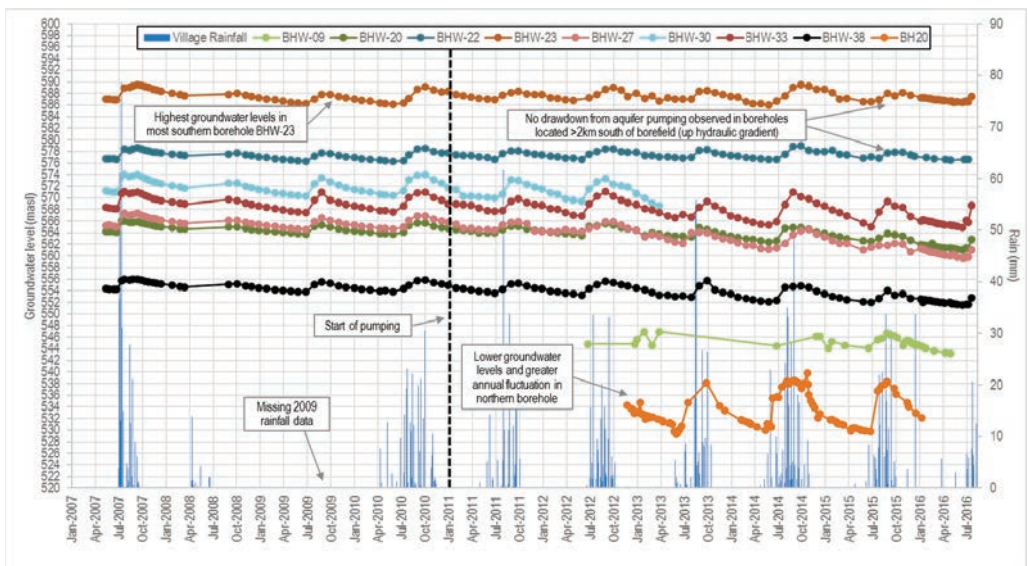


Figure 1 Groundwater levels in selected boreholes along the Mogoraib River



fine rainfall-runoff processes for this type of project area.

Mogoraib Aquifer

Groundwater levels have been recorded in the Mogoraib aquifer boreholes since June 2004. A plot of selected groundwater levels, together with rainfall data from the Camp(Village) rain gauge, is presented in Figure 1. Groundwater levels follow a seasonal trend consisting of rapid increase as a result of wet season recharge from ephemeral flow in the Mogoraib River followed by natural recession through the dry season.

Boreholes with thicker layers of high storage alluvium (such as BHW-22 and BHW-18) show subdued response to the early rainfall events as the field capacity of the unsaturated sediments takes time to be reached. Once the field capacity is reached, the individual responses become more noticeable and show larger changes in water level. Boreholes in areas of very thin to no alluvium which penetrate directly in to the low storage transition zone, show much greater changes in groundwater level.

Rainfall-runoff conceptual model

The hydrology of the Bisha project area is typical of arid and semi-arid climates. River flow is generated from highly localized, high-intensity short-duration convective rainfall events that generally occur during a distinct wet season. Annual evaporation is recorded to be far in excess of recorded rainfall. Sparse vegetation, clay rich soils and soil crusting limits infiltration rates. Water generated from rainfall events is therefore dissipated as sheet run-off or lost via evaporation. In parts of the catchment sheet run-off is concentrated by topography and delivered to the river systems, which are otherwise dry as they receive little to no baseflow. Rainfall is therefore the primary hydrological input to river flow. Studies have also shown that there is potential for sheet run-off to decrease following a wet year due to enhanced vegetation cover (Wheater 2010).

The sporadic, high-intensity short-duration rainfall events lead to sub-daily hydrograph responses with steeply rising and falling limbs. Stream flow is not continuous with individual rainfall events generating peak river flow with short lag times (potentially

sub-hourly) before quickly dissipating back to zero. Flow in the larger catchments, such as the Mogoraib River, may result from many unrelated localized storms occurring away from the project area. Conversely smaller catchments (e.g. Freketet) only flow after very local rainfall events and will not receive run-off from storms of limited spatial extent. Studies have shown that river flows in these environments often move down channels as a “flood wave”, as rainfall events are localized, short duration and intense and short, while the river catchments are extremely responsive. This type of flow dominates in the Mogoraib River and explains the large differences in flow recorded at the Upper and Lower Mogoraib stations, as manual measurement of stage/flow may not have been at a high enough frequency to capture the flood wave, and related flow may not have been measured simultaneously at both stations.

Surface water - groundwater interactions

As distributed infiltration of rainfall through catchment soils is limited due to soil crusting and high evaporation rates, channel bed infiltration will be the dominant process of groundwater recharge in the project area. Recharge will occur as flood flows lose volume to bed infiltration during downstream propagation. This conceptualization is supported by monitored groundwater levels which show seasonal fluctuations close to river channels and almost no response away from areas of drainage.

Recharge to groundwater underlying river channels will be a function of the time in which the river is flowing. Two dimensional numerical experiments in similar environments have shown that “infiltration opportunity time” (duration and spatial extent of surface wetting) is more important than high flow stage in controlling infiltration to groundwater. Thus antecedent moisture conditions are a key control on unsaturated zone flow with the expectation that higher moisture contents within the unsaturated zone will increase infiltration rates. Moisture content will increase with longer periods of river flow. Maximum groundwater recharge will occur from frequent river flow events of large areal extent, and therefore “hydrologically active” years may be more important than “wet years”.



Conventional hydrological modelling approach

The conventional approach to quantifying recharge to the Mogoraib aquifer would be to determine the relationship between rainfall and run-off and then to establish the relationship between the resulting stream flow and recharge. However, as has been outlined in the preceding sections, accurately modelling these processes in semi-arid and arid climates is complicated given the challenges in recording both the necessary rainfall and flow data. These challenges include:

- Highly localized rainfall events: Flow may be generated in project rivers from rainfall events that are not accurately recorded at project rain gauges. A study at Walnut Gulch in Arizona which has a similar climate and wet season indicated that a rainfall correlation of $r^2=0.9$ between rain gauges would require a gauge spacing of 300 – 500 m apart (i.e. at distances further than this, recorded rainfall at each station becomes less likely to reflect the same rainfall event).
- Frequency flow/stage measurements: Flow rates in the Bisha environment can vary significantly on a sub-hourly time period and therefore a dataset collected on a longer frequency than this will not accurately reflect river conditions.
- Dynamic channel morphology: Each flow event has the potential to significantly change the channel morphology at each gauging station. This means that derived stage-discharge relationships may not remain valid over time, as the relationship can change, even between successive flow events. Therefore flow records calculated from stage are likely to be inaccurate and may result in large difference between two calculations of river flow.
- Inaccuracy of flow measurement: High flows are challenging to measure accurately and will likely be inaccurate where estimates have been made using channel cross sectional areas and Manning's n.

Given the uncertainty in the rainfall and flow data, conventional methods of rainfall-runoff assessment are not considered applicable, as reflected in previous calculations of run-off

coefficients for site ranging from 0.01 to 0.71 (and in excess of 1 at the Shatera rain gauge).

Quantification of groundwater recharge from water level data

In order to define an initial groundwater recharge rate as the basis for numerical flow modelling a recharge volume was calculated based upon selected wells along the Mogoraib River using:

- the increase in water level in the alluvium occurring during wet season periods of recharge;
- an estimated alluvial aquifer storage of 6%. This value was estimated based on an analysis of groundwater level decrease against measured pumping rates;
- the rate of groundwater recession at different groundwater elevations based on recorded dry season rates of recession.

The estimated annual recharge rates are presented in Table 1.

The best recharge record available is for BHW-39 where a good correlation has been identified between groundwater recharge and daily rainfall events over 3.5 mm at the Camp (Village) WS. The strength of the correlation however decreases if the threshold rainfall event for inclusion in the analysis is increased or decreased (Figure 2), while the derived relationship does not show a linear increase between recharge and wet days from a zero value. This suggests that recharge from initial flow events is less than recharge occurring from subsequent events (e.g. recharge from 15 wet days is roughly double the recharge from 10 wet days), an observation that is consistent with the conceptualisation that increased recharge occurs as a result of increased unsaturated zone moisture content.

Mogoraib aquifer abstraction sustainability assessment

A two layer Modflow groundwater flow model was developed to look at the long term sustainable yield from the Mogoraib aquifer system. The first layer corresponds to the Mogoraib and Freketet alluvial aquifers, while the second layer represents the underlying bedrock. Although the conceptual model suggested that recharge in the study area largely reflected seasonal flood water which



Table 1. Preliminary estimates of groundwater recharge (mm)

	BHW39	BHW32	BHW24	BHW33	Average
2007	280	275		372	309
2008	129	111	114	84	110
2009	157	154	147	297	189
2010	289	276	226	405	299
2011	167	152	131	213	166
2012	255	259		384	299
2013	237	153		235	208
2014	313			373	343

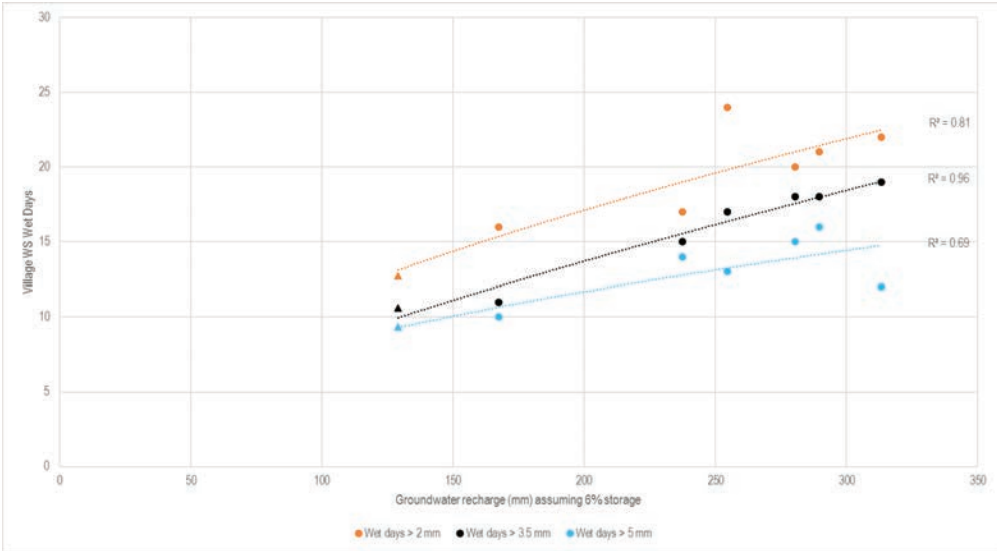


Figure 2 Estimated wet season groundwater recharge as a function “wet day” rainfall magnitude

infiltrates through the bed of ephemeral river channels, with little infiltration of distributed rainfall, an initial groundwater model with no distributed recharge could not be calibrated to observed groundwater levels. Therefore an initial starting point of 0.7% of MAP was used, indicating that recharge probably does occur away from the wadiis, in response to local ponding of water from intense rainfall events and/or the occurrence of concentrated flow due to localized steep topography e.g. the toe of hillsides. This represented an important conclusion in terms of “harvesting” runoff for water supply.

The groundwater model predicted that the alluvial aquifer unit alone does not receive sufficient recharge to supply all water demand, and that groundwater flow from the underlying fractured bedrock is required to sustain the required water supply. The drought simu-

lations showed that the increased drawdown would reduce the efficiency of the pumps and therefore the achievable yield. In order to maximize the water that is recoverable, additional boreholes should be drilled so that individual well abstraction rates can be reduced whilst still meeting required volumes under groundwater stress conditions.

References

- International Council on Mining and Metals (2017) Position statement on water stewardship
- Wheater (2010) Hydrological processes, groundwater recharge and surface water/groundwater interactions in arid and semi-arid areas. Groundwater modelling in arid and semi-arid areas. International Hydrology Series p 5-20
- Wheater and Brown (1989) Limitations of design hydrographs in arid areas. Proceedings of the 2nd British Hydrological Society Symposium p 49-56





The influence of licence conditions on mine water management

Jacky Burke

SRK Consulting, PO Box 55291, Northlands, 2116, South Africa

Abstract

Mines in South Africa are required to obtain a Water Use Licence (WUL) and must undertake compliance audits to assess the extent to which compliance to the WUL is being achieved. Over time it has become clear that mining operations vary in taking ownership of the issued WUL and putting measures in place for achieving compliance. This variation impacts on meeting the objectives of a WUL, namely to protect the Water Resource but without limiting the economic benefit of the mining operation. A Licence Implementation Plan is proposed to incorporate the WUL into the day to day mining operations.

Keywords: Department of Water and Sanitation (DWS), Licence Implementation Plan (LIP), Water Use Licence (WUL), Water Use Licence Application (WULA)

Introduction

Mining operations in South Africa are required to obtain a Water Use Licence (WUL) in terms of the National Water Act, Act 36 of 1998 (Act) before any Section 21 water use activities may commence. Water uses that require authorisation in terms of Section 21 of the Act are presented in Table 1 below. Mines in operation prior to the promulgation of the Act have been required to obtain a WUL for the existing operations in order to continue mining. WULs are issued by the National Department of Water and Sanitation (DWS) based on information provided in a Water Use Licence Application (WULA). WULA content has been informed by various guidelines but was standardised in March 2017 with promulgation of the WULA regulations (Government Notice R267, Government Gazette 40713, 24 March 2017), which should facilitate the WULA review process. Inclusion of a 300-day WULA time frame in Regulation R267 aligns WULAs with the Environmental Impact Assessment (EIA) and Environmental Management Plan (EMP) processes required for environmental authorisation of mines. Alignment of the WULA and EIA/EMP processes is schematically presented in Figure 1.

Each WUL issued contains the following:

- A general set of conditions applied to all issued WULs;

- Site specific conditions based on the information provided in the WULA, outcomes of any engagement between the applicant and DWS during the WULA review process and the DWS management objectives for the catchment within which the mine falls;
- Quality and quantity limits for the authorised Section 21 water uses. Water quality limits may also apply for the surface and groundwater resources in the mine area.

An on-line WULA submission system, known as the Electronic Water Use Licence Application and Authorisation System or e-WULAAS, was launched in several catchments in 2017 to support the 300-day process and follows the three phases in Figure 1 below. Objectives of the e-WULAAS are two-fold (DWS, 2017):

- Firstly to provide an online portal to DWS clients to register and subsequently submit their water uses alongside the current paper based system.
- Secondly the system will provide an internal web based interface for the authorisation staff to manage, coordinate, track and finalise the authorisation processes of registered water uses culminating in the issuing of a WUL.

The system is being further developed based on user feedback towards continual improvement



Table 1. Section 21 water uses

Section 21	Description of use	Comment
(a)	Taking water from a water resource	Any reuse of water authorised under Section 21(j) will also trigger Section 21(a) water use
(b)	Storing water	Applies to clean/raw water storage
(c)	Impeding or diverting the flow of water in a watercourse	Mining activities within 100 m or 100 year floodline of a watercourse or within 500 m of a wetland also trigger this use
(d)	Engaging in a stream flow reduction activity	
(e)	Engaging in a controlled activity (e.g. irrigation with water containing waste and recharging an aquifer)	Only use of land for afforestation currently applies
(f)	Discharging waste or water containing waste into a water resource through a pipe, canal, sewer or other conduit	In the context of mining irrigation with water containing waste and recharging an aquifer will trigger this use Reuse optimisation has to be demonstrated before this use will be approved for mining
(g)	Disposing of waste in a manner which may detrimentally impact on a water resource	Applies to storage of dirty water, disposal of mine residues and run of mine or other stockpiles that may have the potential to pollute water Does not typically apply to mining
(h)	Disposing in any manner of water which contains waste from, or which has been heated in, any industrial or power generation process	
(i)	Altering the bed, banks, course or characteristics of a watercourse	Section 21(c) water uses also trigger Section 21(i) water use as does undermining of a watercourse (mining within 100 m vertical depth of a watercourse)
	Removing, discharging or disposing of water found underground for the continuation of an activity or for the safety of persons	Dewatering of open pit and underground workings
(j)	Using water for recreational purposes	May apply to water bodies on mine property used for fishing, boating or other recreational purposes
(k)		

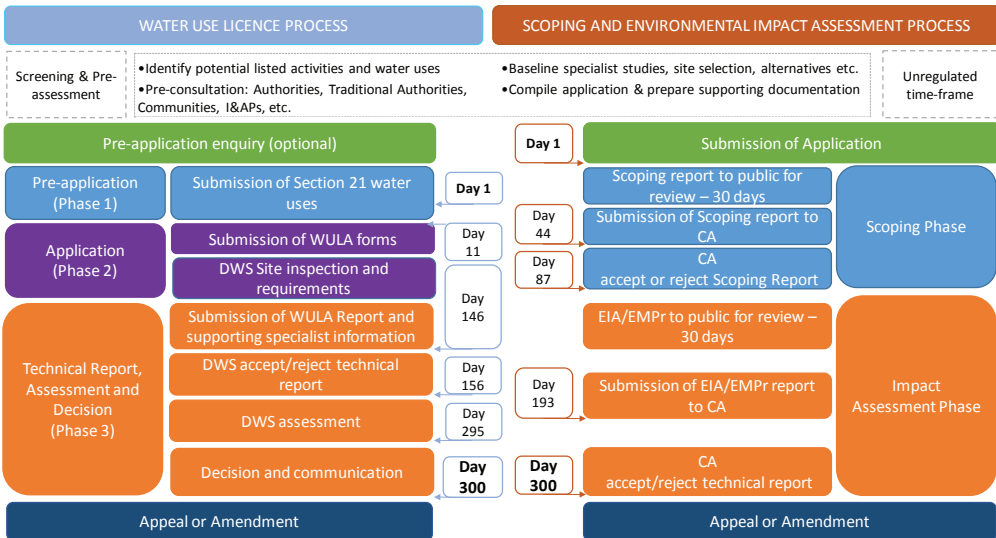


Figure 1: Alignment of the 300-day WULA and EIA/EMP processes

that will facilitate role out to the catchments not yet geared up for online submissions.

Currently the biggest challenge for WULA approval is limited resources within the DWS to adhere to the regulated time frames. A related challenge is having adequate specialist information in the initial application to demonstrate to DWS that impacts on the water resource and the communities that rely on

this water will be appropriately minimised and managed. As WULAs may be initiated at pre-feasibility or feasibility stage to allow sufficient time for approval prior to project implementation, limited project information may be available to inform the studies.

Over almost two decades of mines applying for and operating under WULs it has become clear that mining operations vary in the



extent to which ownership of the issued WUL is taken and measures are put in place to comply to the WUL and WULA commitments. WULA commitments become legally binding once the WUL is issued, as WULs typically have one or more conditions requiring that the authorised water uses are carried out in accordance with the ‘Report’, the ‘Report’ being the WULA and all supporting documentation as defined at the start of the WUL.

How a WULA may influence WUL conditions, what influences implementation of the WUL and how development of a Licence Implementation Plan (LIP) can facilitate incorporation of the WUL into the day to day mine operations is discussed.

How a WULA may influence WUL conditions

With each new WUL that is issued, additions to the suite of general conditions and site specific conditions that have been based on the WULA content are evident. In instances where the WULA related condition may have been taken out of context or misinterpreted by DWS, this can lead to errors or technical issues in the WUL that pose a regulatory risk to the licensee. For examples, a Rock Engineering report may cover the full extent of the mining area where undermining may occur and include pillar and stope specifications for all levels. If the WUL stipulates incorrect details for the undermining area, the implication may be that no mining or only limited mining can occur in that area. As an amendment application to rectify the error may take some time this could delay mining with serious economic implications. In the case of vegetation of clean water diversions, the hydraulic forces along steep sections of the diversion may render the establishment of vegetation not feasible with only a hard engineering approach viable (concrete, gabions etc.) to protect against erosion and sustain the diversion’s integrity.

To minimise the risk of impractical and unrealistic WUL conditions based on the specialist report findings and recommendations included in the WULA, the following approach to developing a WULA is proposed: developing a WULA is proposed:

- **Combined specialist site assessments** as far as this is practical and/or as a minimum pre- and post site work integration sessions that

include the respective specialists, project engineers, designers, project manager and site geologist. The key specialists in this regard are the geohydrologist, hydrologist, aquatic specialist, heritage specialist/archaeologist and possibly also a hydropedologist if mine dewatering or any other mine activity has the potential to impact on river baseflow.

- **An integration workshop** with the applicable specialists and project manager at draft report stage to optimised structuring of the reports to minimise the potential for information being taken out of context for inclusion in WUL conditions, alignment of findings and recommendations and where considered applicable, preparation of appropriate motivation(s) for proposed alternative to anticipated WUL conditions – mostly related to Section 21(c) and (i) conditions. For example, hydrological motivation for sections of a clean water diversion that need hard engineering instead of the DWS preferred vegetation.

As the WUL applicant has control over the detail provided in the WULA, it is important when preparing a WULA to ensure high quality specialist input and that all information included in the WULA is clear and concise with all specialist recommendations and management commitments practical, reasonable and achievable. Should DWS deem that the submitted information is inadequate, additional specialist work including amendments to designs may be required for the WULA to be approved.

What influences implementation of the WUL

Over time there has been a greater emphasis of WUL conditions on resource quality which encompasses the following (DWS, 2016):

- quantity: assurance of instream flow;
- quality: physical, chemical and biological;
- instream and riparian habitat;
- aquatic biota.

In order to fully comply with the resource quality related conditions in a WUL mines are required to extend managing water and water containing waste generated and consumed on site to managing the riparian zone and underlying aquifers, and all influences



Table 2. Factors that can influence WUL implementation and compliance

Factor	Influence
WUL Conditions	<p>Negative:</p> <ul style="list-style-type: none"> • Extent to which the conditions are applicable and appropriate for the operation including conditions with errors. • Extent to which the conditions are achievable within the stipulated time frames and available budgets. • Conditions that are ambiguous or unclear and require clarification. <p>Positive:</p> <ul style="list-style-type: none"> • Opportunity to improve on operational awareness and efficiencies. • Benchmarks against which the operation can assess its performance.
Resources	<ul style="list-style-type: none"> • The extent to which personnel delegated with implementing the WUL have familiarized themselves with, and made others aware of the WUL requirements • Support provided by fellow colleagues and management in developing and implementing improvements in water management measures. • Availability of an appropriate WUL implementation budget with priority on actions needed to address non-compliant audit findings and avoid further non-compliant findings in future audits.
DWS relations	A positive relationship with, and support from DWS.

on these as stipulated in the WUL. Factors that can influence implementation of and thus compliance to the WUL are presented in Table 2. Managing these factors can be facilitated through a formalised Licence Implementation Plan (LIP) discussed in the next section.

Licence Implementation Plan

Development of a LIP provides an approach for improving the manner in which WULs are incorporated into the day to day running of operations thus facilitating compliance to the WUL. A LIP can assist with audits especially those conducted by the DWS Compliance and Enforcement officials as documentation and compliance records back dating to when the WUL was first issued may be requested during the audit. A lot of unnecessary time can be wasted in sourcing this information if an effective LIP is not in place.

The LIP can range from a simple Excel file to an interactive web-based system. A schematic representation of a LIP is presented in Figure 2. The main steps in developing a LIP are as follows:

- Convert the WUL to an Excel format.
- Categorise the WUL conditions to facilitate implementation and auditing. Proposed categories are as follows:
 1. **Document needed** as proof of compliance e.g. meter calibration certificate;

2. **Site assessment required** to verify compliance e.g. adequate bunding in place;
 3. **Timeline applies**, mostly related to required submissions to DWS e.g. quarterly monitoring data, annual audit reports etc.
 4. **To note** i.e. not auditable/not yet applicable, but important to be aware of e.g. timeline is in the future or Section 21 water use has not yet been initiated;
 5. **Amendment needed** – it is important to review the WUL details for correctness and engage with DWS to amend any errors.
- For **Category 1** items develop a list of supporting documentation required, remembering to include reference to the WUL Condition number. Collate what is available and develop a schedule for obtaining outstanding documentation and routinely required documentation e.g. annual water balance updates. Set up appropriate folders and registers for storage and record keeping, respectively. Where the document may require appointment of a service provider to undertake a particular study e.g., update of a groundwater model, this will need to be scheduled and budgeted for well in advance of the stipulated deadline.



- For **Category 2** items develop a list of activities, equipment, facilities or any other materials that may be required to give effect to the site requirements. Prioritise the requirements based on current level of non-compliance, risk of ongoing non-compliance, costs, time required for implementation and any other factors that may apply. Once prioritised, develop a schedule for implementation, apply for budget and put the necessary measures in place to adhere to the schedule.
- Most **Category 3** items will have a link to Category 1 and/or Category 2 Items. Develop a schedule of required submissions and actions, and a system of reminders to ensure deadlines are met. The mine is required to notify DWS if a deadline cannot be met and submit an extension request. An amendment application may be required for unreasonable timelines or align timelines for routine data submissions

sions especially where the DWS offices are located far from the site and DWS insists on hard copy submissions.

- In order to align the various actions and ensure a cost-effective approach is factored into the LIP, actions can be grouped into sub-categories with categories that will apply to most mining WULs provided in the LIP Schematic in Figure 2.
- Formalise the above in a documented LIP Procedure that is allocated a company document number and approved by management. Review and revise the LIP Procedure as required to keep it current.

To ensure the LIP is effectively implemented the following will be required:

- Development of a program for ongoing training and awareness on the WUL conditions and supporting LIP. Linking this into existing programs will be most effective. Where significant behavioural

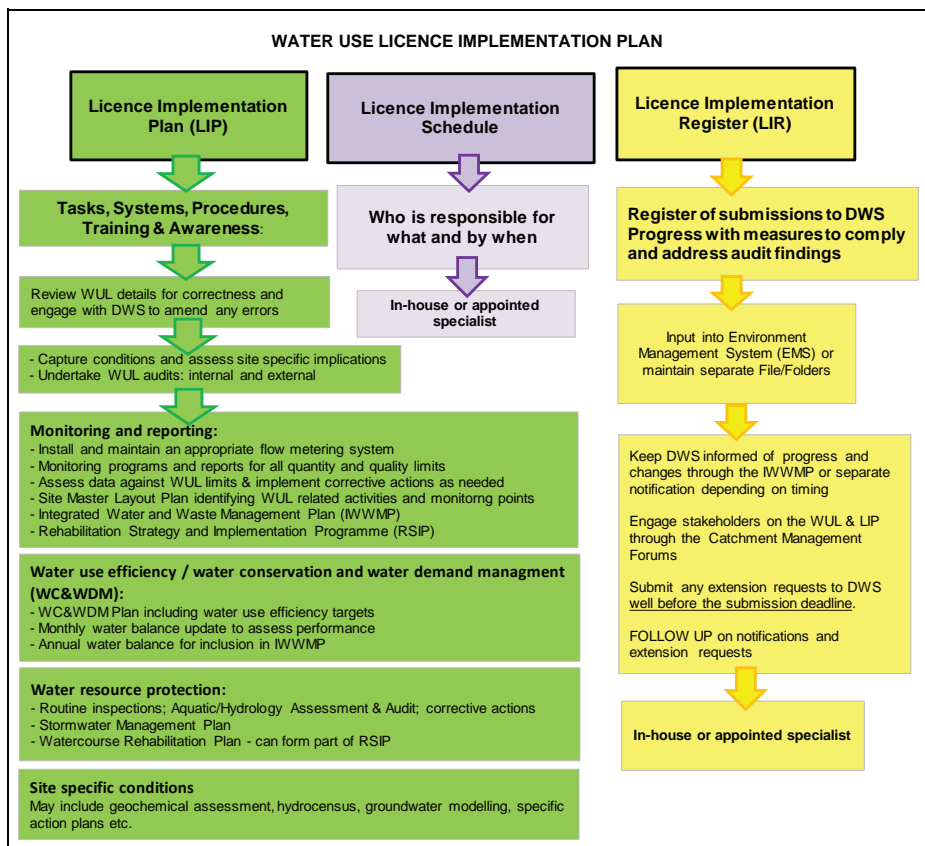


Figure 2: Licence Implementation Plan



changes are needed to give effect to the LIP in order to comply to the WUL, it is important for all personnel to understand what changes are needed, why these changes are needed and how these change will benefit the water resources. A key example is changeover from wet to dry cleaning or use of process water instead of potable water wherever possible.

- Allocate tasks and timelines for implementation and compliance. An interactive on-line system that caters for scheduled reminders and tracking progress will facilitate this process. Extension of the existing Environment Management System, that everyone should be familiar with, to cater for this step, rather than development of a new system is recommended.
- Review and report on progress at the routine management meetings. This is a critical step to maintain management buy-in to ongoing WUL compliance.
- Develop and maintain a Licence Implementation Register that can generate records of submissions to DWS and progress reports on all actions, especially corrective actions to address audit findings and recommendations.
- Maintain records of all DWS engagements and notifications in the WUL folders as these will be important to provide to DWS Compliance and Enforcement officials when they conduct WUL compliance audits on site.

Conclusion

Awareness of WUL conditions and how these can be influenced by the WULA and in turn can influence water management practices on mine sites is important to optimise protection of water resources and maximise the socio-economic benefits of the mining operation. A suitable LIP is required to facilitate WUL compliance and requires to be supported by adequate resources, an implementation schedule and implementation register that will provide the required records for compliance audits.

References

- Department of Water and Sanitation (2017) User Manual: Water Use Applicant e-WULAAS Electronic Water Use Application and Authorisation System, Document Version 1.0. Draft Compiled by IEMSYS CC, Final Completed by: DWS
- Department of Water and Sanitation (2016) One-Day Training Presentation: National Water Act, 1998 (Act No. 36 of 1998) S21(c) & (i) Water Use Authorisation. Pretoria Available from: <http://www.dwa.gov.za/Documents/Section21/> [Accessed 26 April 2018]
- Republic of South Africa (1998) National Water Act, Act 36 of 1998. Government Gazette No. 19182. Pretoria
- Republic of South Africa (2017) Regulations regarding the procedural requirements for water use licence applications and appeals. Government Notice R267, Government Gazette 40713. Pretoria





Reconstructing Historical Mine Water Management Practices for a Portion of the East Rand Gold Field, South Africa Using Long-Term Map and Image Time Series

Henk Coetzee

Council for Geoscience, Private Bag X112, Pretoria, South Africa henkc@geoscience.org.za

Abstract

Gold and uranium have been extracted from the conglomerates of the Witwatersrand since the late 19th Century. The development of the mining industry, its related industries and the economic development which followed transformed the open farmland which had existed before mining into a highly urbanised and industrialised area, with a population of over 10 million people. While underground gold mining continues from rocks of the Witwatersrand Supergroup to the east, west and south of Johannesburg, formal mining ceased in the original three goldfields, the West Rand, Central Rand and East Rand, when the last mine stopped dewatering in 2010. Water inflows have been a challenge to mining since the early days, but in recent years, the rising water levels and consequent risk of pollution has received considerable attention. Historical and modern spatial data, covering more than a century of mining has been compiled and used to investigate the hydrological evolution of a portion of the East Rand Goldfield, to unravel the engineering measures which were used to better manage water in the mining areas and to develop recommendations for improved water management in the future.

Keywords: time series, spatial data, mine hydrology, Witwatersrand, East Rand

Introduction

History of gold mining in the Witwatersrand

Gold was discovered in South Africa's Witwatersrand – the area centred around what is now the cities of Johannesburg, Ekurhuleni and Mogale City – in 1886. Mines developed rapidly along the strike of the outcropping Witwatersrand Supergroup conglomerates, with three main goldfields, the West Rand, Central Rand and East Rand, developing, separated by geological features referred to as the Witpoortjie Gap and Boksburg Gap, respectively. Ultimately, these three goldfields would extend along more than 100km along strike, accessing the outcropping Witwatersrand rocks in all three goldfields as well as the sub-outcrops below younger cover rocks in parts of the East Rand goldfield.

These three goldfields, along with other areas where the Witwatersrand strata are mined to the west, south west and east of the original mining areas, have produced approximately half of all the gold ever mined (Gold Wage Negotiations 2015). Figure 1 shows

the contribution of different gold producing areas to world production in 1930, with the Transvaal contribution coming largely from the Witwatersrand. Multiple gold- and uranium-bearing conglomerate layers made up the total resource in these areas.

Due to practical considerations such as ventilation, access to remote areas of the workings, pumping of water and safety considerations, the mines within each goldfield are all interconnected at depth. This facilitated mining while all mines were operational, but led to problems when mines started to close. Mine closure was generally not managed with consideration of all impacts, in particular the potential of water entering one mine to flood neighbouring mines. Because of this, as underground mines started to close, the water levels within the closed mines would rise to the level of interconnection with an adjacent mine and then start to flow to that mine, increasing the volume which the remaining mines needed to pump. Over time, the burden of pumping became too onerous for the remaining mines, hastening their eventual closures.



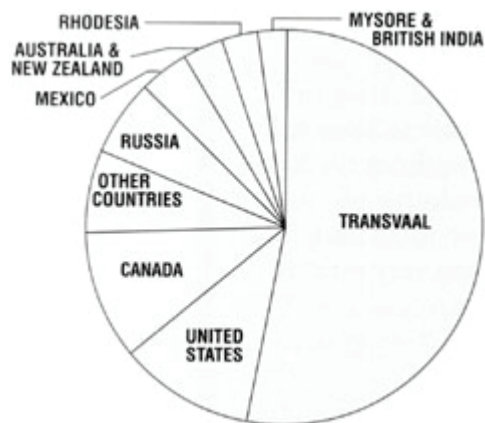


Figure 1 World gold production in 1930 (Potenza et al. 1996)



Figure 2 Steeply dipping stope in an early Witwatersrand underground mining operation (Ball 2015)

In 2010 the pumps at the Grootvlei Mine in South Africa's East Rand gold field were switched off, allowing the interconnected mine workings of the gold field to flood. This necessitated the construction, by the South African State, of expensive pump-and-treat infrastructure to maintain a safe water level in the underground workings and reduce the impact of the discharge of mine water to the surface water environment. In parallel to this process, efforts are underway to reduce the seepage of surface water to the underground mines to limit the cost of pumping and treating mine water.

Spatial development around the Witwatersrand mines

From the outcrops, the conglomerate layers dip to the south, with very steep dips in some areas (Fig 2). This necessitated development to great depths, with the mines becoming the deepest in the world by the early 20th century, and led to a pattern of development, with urban development to the north of the outcrop, extending along the mining belt to the west and east from Johannesburg. A subsidence-prone zone to the south of the outcrop has been left largely undeveloped, with the exception of some tailings storage facilities in this area. To the south of this zone, additional urban development, including the southern suburbs of Johannesburg and the township Soweto developed.

The Witwatersrand (meaning “ridge of white waters” in Afrikaans) refers to the ridge defined by quartzite layers which lie stratigraphically below the gold-bearing conglomerates.

This ridge acts as a continental watershed, with the main drainage direction to the south, crossing the mining belt to the south. In parts of Johannesburg, an east-west drainage direction is also present.

Mine water management in the Witwatersrand

Water inflows have been an ongoing problem in the Witwatersrand's gold mines, back to the earliest days of mining. Scott (1995) reports that acid mine drainage was well known as early as 1903, with many later references to the problem (e.g. Hocking 1986). Scott (1995) also describes the construction of canals to carry surface water over the undermined zone, thereby reducing the ingress of water to the underground workings, in at least two locations in the Central Rand. The issue of acid mine drainage in the Witwatersrand rose to prominence around the time that the last mines were closing and the prevention of ingress was highlighted in a report to a high-level government committee appointed to address this issue (Coetzee et al. 2011). This report recommended the installation of pump-and-treat systems to maintain environmentally safe water levels in the underground workings while, inter-alia, developing and implementing measures to reduce ingress to the underground mine workings.

In addition to pumping water from the workings, the early miners developed extensive surface infrastructure to carry water over their shallow workings, reducing the volume



to be pumped. Unfortunately, many of the detailed records related to this infrastructure are no longer accessible, although the remains to these structures can be identified in the field in some areas.

Time series analysis

Time series analysis is commonly carried out on spatial data sets. This may be quantitative, using measured or calculated quantities such as reflectance, vegetation indices etc. For this study, a qualitative approach has been followed due to the length of time over which changes need to be detected – more than 100 years – and the variety of spatial data available.

Study area: the East Rand outcrop zone

Background studies on mine water ingress (Esterhuysen et al. 2008) have identified a zone in the northern part of the East Rand Goldfield where the gold-bearing Witwatersrand strata outcrop (Fig 3 a) and were mined from the surface to considerable depth.

Analysis of historical spatial information

A collection of spatial information has been assembled, which has been used to attempt to reconstruct a hydrological history of the area. This includes geological and topographic maps, aerial photographs, satellite images and underground mine plans. A limited set of maps is presented (Figs 3, 4 and 5). Within this area, a number of areas of surface water accumulation have been identified, which were canalised during the period of active mining (Fig 3 b and Fig 4a).

An important feature in this area is an old clay quarry, where brick clay was mined from the younger Karoo Supergroup cover (showing in grey on Fig 3 a). On the 1939 topographic map (Fig 3 b), this is marked as Steenmakery (Afrikaans for brickworks) (in the eastern portion of the map, south of the railway line). The Main Reef sub-outcrops here below the Karoo cover and was mined via an incline shaft. By 1953 (Fig 4 a), an un-vegetated area is seen at this point, while con-

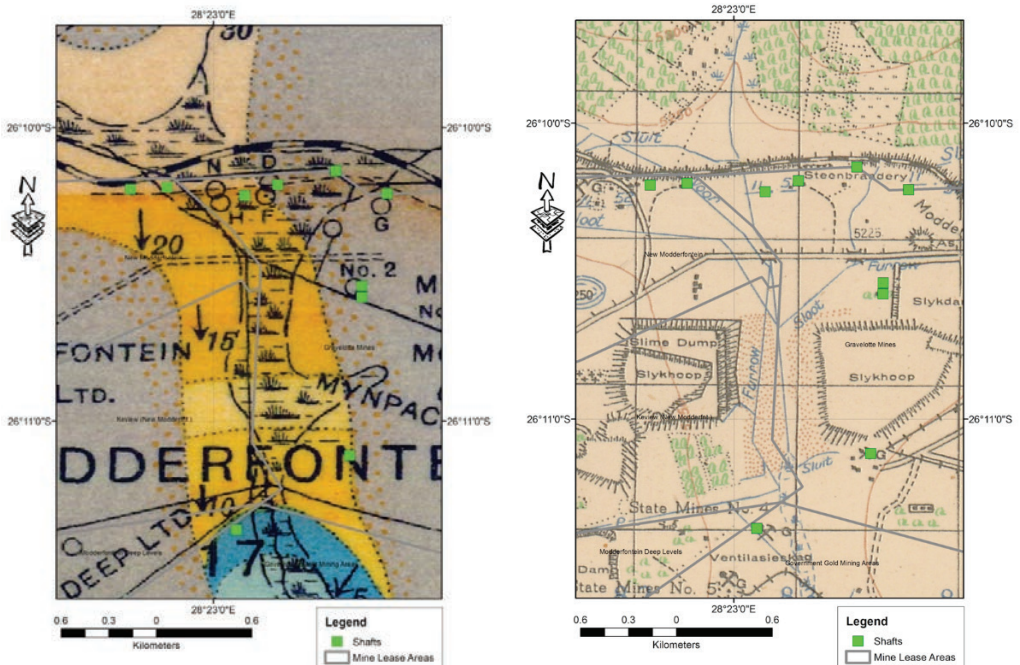


Figure 3 a. Geological map from 1916 (Mellor 1916), showing an area of wetland development, perpendicular to the strike of the Witwatersrand strata (orange colour with the Main Reef showing by a dashed line immediately south of the railway). **b.** Extract from a topographic map of the same area in 1939, showing the development of canals, conveying water across the mining area (south of the Main Reef outcrop). Identified mine shafts shown as green blocks.



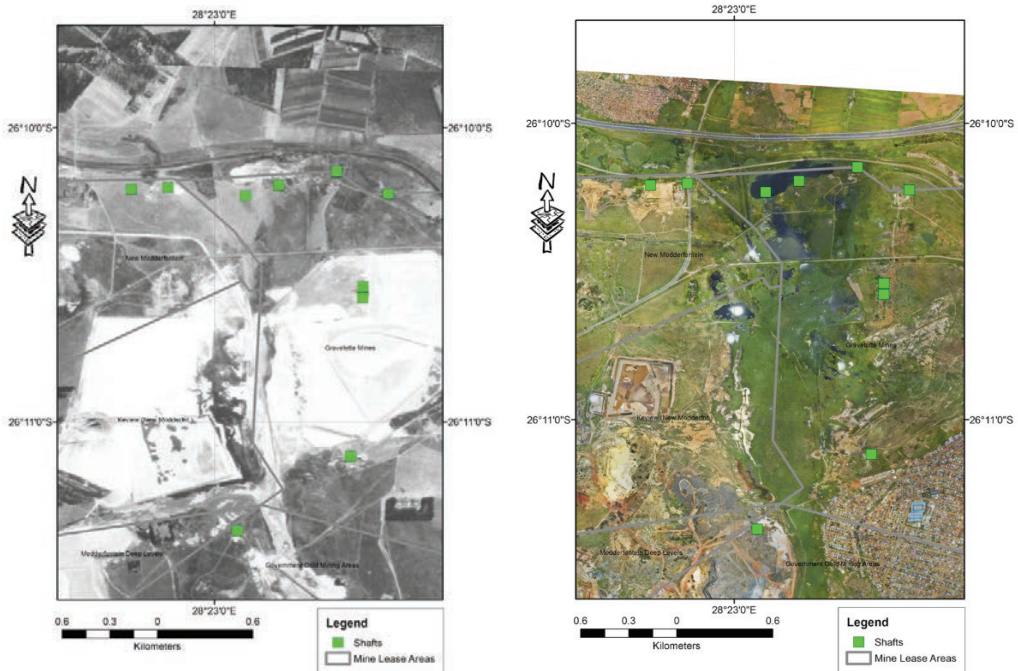


Figure 4 a. Aerial photograph of the study area from 1953. b. Colour aerial photograph from 2016.

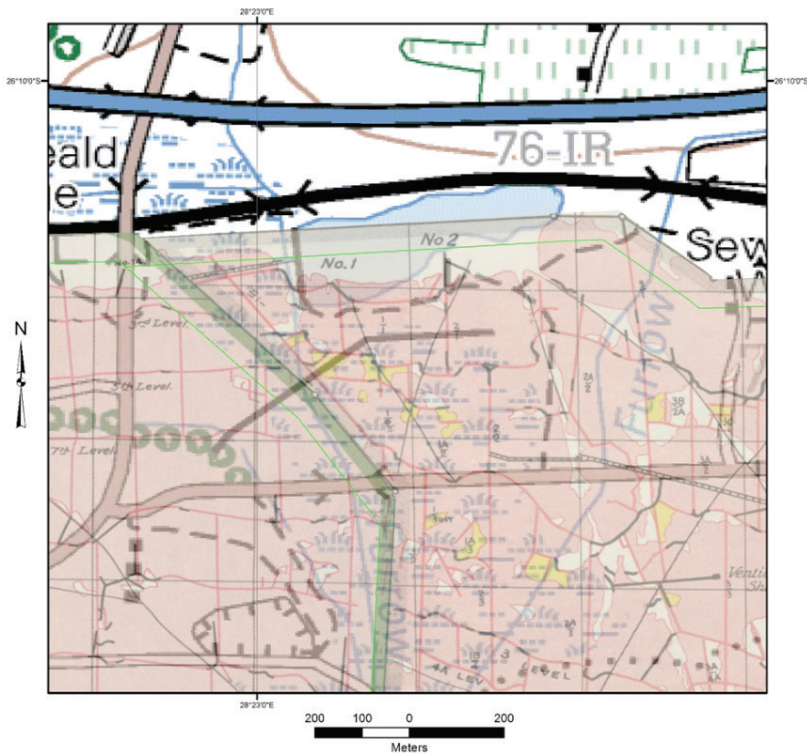


Figure 5 The flooded clay quarry at Modderbee, from a topographic map from 2010, with a plan of underground mine workings (mined out areas in pink). Note the positions of two shafts (shown as No.1 and No.2, relative to the flooded area).



temporary topographic maps show this as a quarry. Now, with underground gold mining having ceased in this area, and the clay quarry having closed, the quarry is flooded, while the canals have degraded to the point where the undermined zone is now covered by shallow lakes and wetlands (Fig 4 b and Fig 5).

This analysis can then be incorporated with other information, such as additional water inputs from upstream urban areas and sewage treatment (approximately 28,000 m³ is discharged into the area daily by two sewage treatment plants (ERWAT 2018) upstream), topographic information which could assist in hydrological modeling, the locations of known mining features, anecdotal information regarding historical water intrusions related to flooding (Scott 1995, pers. comm. H Trouw, GoldOne) etc.

Discussion

Over more than a century, mining transformed the landscape from what Mellor (1917) described as follows:

“The country possesses many natural attractions. For the greater part of the year it is thickly covered with grass, while even in the face of the rocky escarpments of the north slopes of the Rand, is diversified by numerous evergreen shrubs and trees.”

Today, Johannesburg and the surrounding towns are an industrial and residential metropolitan area with a population of more than 10 million people. This has led to substantial increases in the amount of run-off and discharged water entering the surface water environment, particularly as most of the water used in the domestic and industrial sectors is sourced from outside the local catchments, but discharged into local streams and rivers after use and treatment. This increased volume of surface water is believed to contribute to the ingress of water to the underground mine workings.

Conclusion

A spatial time-series dating back to 1916, comprising geological maps, topographic maps, aerial photographs, satellite images and mine plans was assembled with the ob-

jective of unravelling the history of mine water management structures constructed over the past century. This has allowed the reconstruction of historical surface hydrology as the cities and towns in the area grew, showed how mining developed and how surface water was diverted away from undermined areas and how, as mines closed, this infrastructure fell into disrepair. Understanding the historical measures used to reduce water ingress to the underground mines while they were still operating, it has been possible to recommend the reconstruction of some infrastructure to limit the costs of water management in this area in the future.

References

- Ball P (2015) Hard Rock Mining in South Africa - The Cornish Connection. <http://www.theheritageportal.co.za/article/hard-rock-mining-south-africa-cornish-connection>. Accessed 14 May 2018
- Coetzee H, Hobbs PJ, Burgess JE, et al (2011) Mine Water Management in the Witwatersrand Gold Fields With Special Emphasis on Acid Mine Drainage. Inter-Ministerial-Committee on Acid Mine Drainage, Pretoria
- ERWAT (2018) Plants. In: Plants. <http://www.erwat.co.za/plants>. Accessed 14 May 2018
- Esterhuysen S, van Tonder DM, Coetzee H, Mafanya T (2008) Draft regional closure strategy for the East Rand Gold Field. Council for Geoscience, Pretoria
- Gold Wage Negotiations (2015) South African gold, today and tomorrow. Johannesburg, South Africa
- Hocking A (1986) Randfontein Estates: The first hundred years. Hollards, Bethulie
- Mellor ET (1916) Geological Map of the Witwatersrand Gold Field
- Mellor ET (1917) The geology of the Witwatersrand: An explanation of the Geological Map of the Witwatersrand Gold Field. Union of South Africa, Department of Mines and Industries, Geological Survey, Pretoria
- Potenza E, Versfeld R, Delius PNSM, Snaddon C (1996) All That Glitters: an Integrated Approach to South African History. Maskew Miller Longman
- Scott R (1995) Flooding of Central and East Rand Gold Mines; An investigation into controls over the inflow rate, water quality and the predicted impacts of flooded mines, Water Research Commission, Pretoria



Hydrogeochemical characterisation of swamps near underground mining development

¹David, K., ²Timms, W., ³Baker, A. and ⁴McGeeney, D.

^{1,3}UNSW, School of Minerals and Energy Resources Engineering, Sydney, Australia

²School of Engineering, Deakin University, Melbourne, Australia;

³Connected Waters Initiative Research Centre, UNSW Australia

⁴Australian Museum, Sydney, Australia

Abstract

Underground mining developments in many areas have little influence on surface waters and ecosystems, however, there are considerable risks in some locations due to ground movement and subsidence. Many swamps are mapped in the proximity of underground coal mines on the Newnes Plateau, Eastern Australia. These swamp ecosystems depend on wet and moist conditions, however there is concern that effects of mining may reduce groundwater flow and contribute to drying of swamps.

We collected water and organic matter samples from three swamps near longwall panels prior to their extraction to complement baseline studies of the swamps. We use the geochemistry of water samples along with carbon and nitrogen stable isotopes ($\delta^{13}\text{C}$ and $\delta^{15}\text{N}$) of organic matter to provide information on the functioning of this ecosystem.

Results of $\delta^{13}\text{C}$ and $\delta^{15}\text{N}$ indicated that microbial activity is highest from surface to 60 cm depth, decreasing with depth and confirms organic matter sources. Hydrogeochemistry indicates that rainfall quickly reaches groundwater and that its residence time is relatively short. Natural seasonal trends in geochemistry indicate dissolution of plagioclase and mobilisation of Mg and no change in naturally occurring trace metal concentrations.

Keywords: stable isotopes, hydrogeochemistry, swamps, longwall mining

Introduction

Underground mining developments in many areas have little influence on surface waters and ecosystems, however, there are considerable risks for these natural assets in some locations due to ground movement and subsidence. Upland swamps in the Sydney region are elongated narrow features which occur high in the landscape at the headwaters of the creeks (above 600 mAHD) (Fig. 1). The swamps provide a moist environment for a number of protected and endangered flora and fauna species, and also contribute to stream flow and water quality (Fryirs et al 2014, Cowley et al 2016, Hose et al 2014). However, several swamps have been degraded due to urban development, forest plantations, recreational activity and longwall mining (Young, 2017). Variable climate and wildfire are also threats to these swamp ecosystems that are protected by government regulation.

Information on the influence of subsidence on ecology and its response to changes in the shallow groundwater and surface water balance are currently limited (CoA, 2014), so additional studies and monitoring of the swamps are in progress.

Before potential changes related to mining can be considered, it is important to understand the behaviour of swamps in the natural conditions along with their temporal variations. These include changes in the water regime, water quality, and groundwater. Both lithology and topography play an important role in the control of the swamp morphology and its spatial extent (McHugh, 2012). Recently published literature has considerably improved the understanding of the swamps by investigating their morphology and ecosystems. For example, Fryirs et al (2014) propose the swamp model where the swamps comprise the mineral rich sand and loam deposits,



which reflect the mineral–sand trapping and accumulation on the floor of the valley. Cowley et al (2016) identifies contemporary sands unit, which underlay the peat, with low water holding capacity and low organic content such that it impedes the water flow. Hose et al (2014) discussed drainage from the swamp indicating that the hillslopes and marginal zones drain more quickly than the main swamp axis. They conclude that the changes in vegetation types spatially and over time are directly related to groundwater levels which influence moisture in the overlying peat.

This paper aims to characterise the hydro-geochemistry of several swamps, to complement other baseline studies and monitoring prior to potential effects of subsidence by longwall mining. The paper focuses on hydrogeochemical data and stable isotopes of carbon, nitrogen, oxygen and hydrogen to

provide information on organic matter and water within the swamps.

Methods

Fieldwork to collect water, sediment and organic matter samples occurred during relatively dry (May 2016) and wet (October 2016) period, and also during May 2017. The water and groundwater samples for major ion analysis and stable isotopes were collected from temporary hand augered holes located in three swamps: GG, CC and GGSW. Each narrow auger hole was refilled with the materials sourced from each hole immediately following sampling. Sediment samples for pore water analysis were collected from augered holes. Organic matter was collected from both the augered holes and from the swamp surface and side of the swamp. The location of the samples is shown on Fig. 1, along with

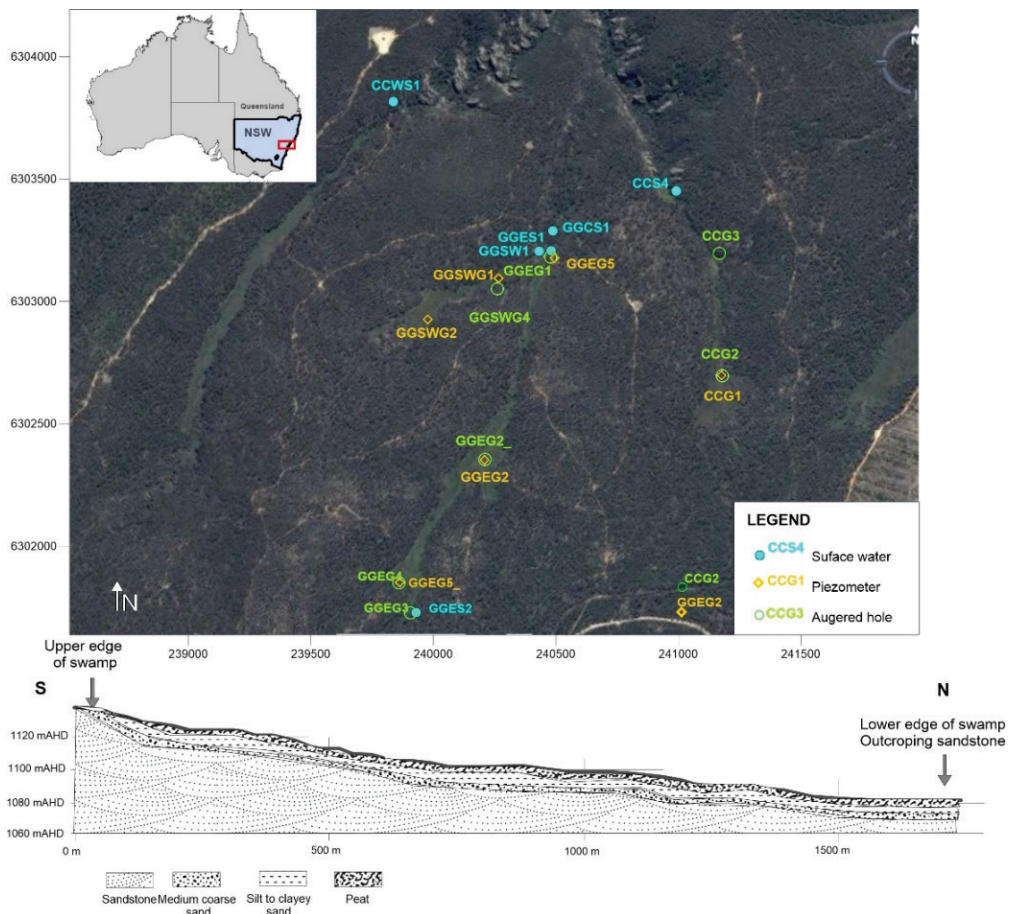


Figure 1 Map with sample locations and typical stratigraphic cross section



the typical cross section based on the augered holes along three transects.

Groundwater was sampled directly from augered holes, field parameters were measured immediately (pH, EC, DO, temperature) and samples field filtered (0.45 micron) for major ions analysis. Groundwater from existing piezometers (CCG1, GGEG2, GGEG5x, GGEG5 and GGSWG1) was sampled by bailing three volumes and then the same procedure was followed as for the augered holes. Surface water samples were collected at the downgradient end of the swamp and at one upgradient location (GGEG2) where this was possible. Major ion water samples (n=18) were analysed for chloride and sulphate by ISPMS and calcium, potassium, magnesium, sodium, silica and sulphur by inductively coupled plasma-optical emission spectroscopy (ICP-OES) at the UNSW Mark Wainwright Analytical Centre. Selected elements and trace metals were analysed by ISPMS.

Carbon and nitrogen stable isotope ratios on organic matter was analysed by Flash 2000 elemental analyser coupled to Delta V Advantage IRMS (mass spectrometer) at the UNSW Mark Wainwright Analytical Centre. Samples (n=37) were prepared by drying, grinding by mortar and pestle, weighing the samples and preparing in tin capsules, typically 0.5 mg in weight. Given that the signal for carbon was too high and for nitrogen too low, the samples size was adjusted to around 0.2 mg for carbon and over 1 mg for nitrogen. Two standards (USGS40 and USGS41) were included in the analysis after every tenth sample. The isotope ratios were reported as the relative ‰ difference between sample and conventional standards (Vienna Pee Dee Belemnite (VPDB) for carbon and atmospheric nitrogen (Air-N₂) for nitrogen isotopes). Measurements were to an instrument precision of approximately 0.2‰ for $\delta^{15}\text{N}$ and $\delta^{13}\text{C}$. The sampling error was assessed as a difference between the duplicate samples of the same organic matter sampled at the same depth. These differences were larger than the instrument precision, with the median difference 0.13 ‰ for $\delta^{15}\text{N}$ (n=14) and 0.68 ‰ for $\delta^{13}\text{C}$ (n=34).

Pore water samples for stable isotopes were collected, preserved and prepared based on Wassenaar and Hendry (2008) method.

Sediment samples were collected every 10-20 cm with depth. The pore water samples were analysed for $\delta^2\text{H}$ and $\delta^{18}\text{O}$ in the UNSW laboratory using a LGR water vapour analyser (WVIA RMT-EP). Three LGR standards and SMOW were used for calibration.

Results and discussion

Water chemistry

The chemistry for groundwater samples (n=12) was typical of a natural uncontaminated environment, with low salinity (23.7-190.4 $\mu\text{S}/\text{cm}$) and relatively low concentrations of dissolved oxygen (DO) (0.8 to 7.2 mg/L, and the mean of 3.5 mg/L). The highest DO value was possibly affected by pumping and purging of a 10-m deep piezometer GGEG5, installed in the Hawkesbury Sandstone (HBSS) on the side of the swamp. Surface water samples (n=6) were more oxidised as expected from 8.6 to 9.1 mg/L, and had low electric conductivity (EC) of 4.5 to 21.8 $\mu\text{S}/\text{cm}$. pH was acidic ranging from 3.9 to 6.0 for groundwater samples and pH 3.7 to 4.8 for surface waters. These results reflect the organic content of swamp sediments and decomposition.

Although, the groundwater was fresh, the major ion composition for GG, GGSW and CC swamps indicates domination by sodium-chloride (Na-Cl), followed by lesser contribution from calcium (Ca) and sulphate (SO_4) (Fig. 2) during May and October 2016. These periods include both dry and wet weather conditions, respectively. Bicarbonate (HCO_3) was calculated assuming cation balance equilibrium, with overall HCO_3 concentration low except for several groundwater samples. Groundwater samples have increased Ca concentration compared to surface water samples resulting from plagioclase dissolution. Plagioclase along with quartz is the main constituent of sandstone. Samples collected in May 2017 (average rainfall conditions) have same anion but different cation composition, with abundance of magnesium (Mg) in both surface and groundwater, and reduction in Na. Mg is highly mobile element, and can occur in sandstone due to weathering of aluminosilicates containing Mg. It needs to be noted that sampling in May 2017 occurred after substantial rainfall event (20 mm) which



resulted in mobilisation of Mg. However, there were no changes in naturally occurring element concentrations (Al, As, Mn, Zn, Sr, Ba) with $p > 0.05$ (T-test for means) therefore no mobilisation in groundwater occurred as a result of rainfall event (with all concentrations above the level of reporting).

Stable carbon and nitrogen isotopes in organic matter

The results showed large variability in the isotopic composition: $\delta^{15}\text{N}$ ranged from -0.1 to 11.85 ‰ (average 4.7‰, standard deviation 3.1‰, $n=35$) (Fig 3a) while $\delta^{13}\text{C}$ ranged from -25.3 to 33‰ ($n=31$) where highest value

sample is the outlier possibly an error in measurement. The range of $\delta^{15}\text{N}$ is consistent with values from literature for pristine groundwaters (Heaton, 1986). $\delta^{13}\text{C}$ occurs in a much narrower range with an average of -27.8‰ and standard deviation 1.64‰. It is observed that the samples follow an enrichment trend in $\delta^{15}\text{N}$ with depth (from 0 to 12‰), which is followed by uniform trend towards the base of the swamp sediments at 120 cm depth. The reason for depleted values in the upper horizons can be explained by higher microbial activity compared to deeper horizons but also by presence of past fire events (Schmidt and Stewart, 2003).

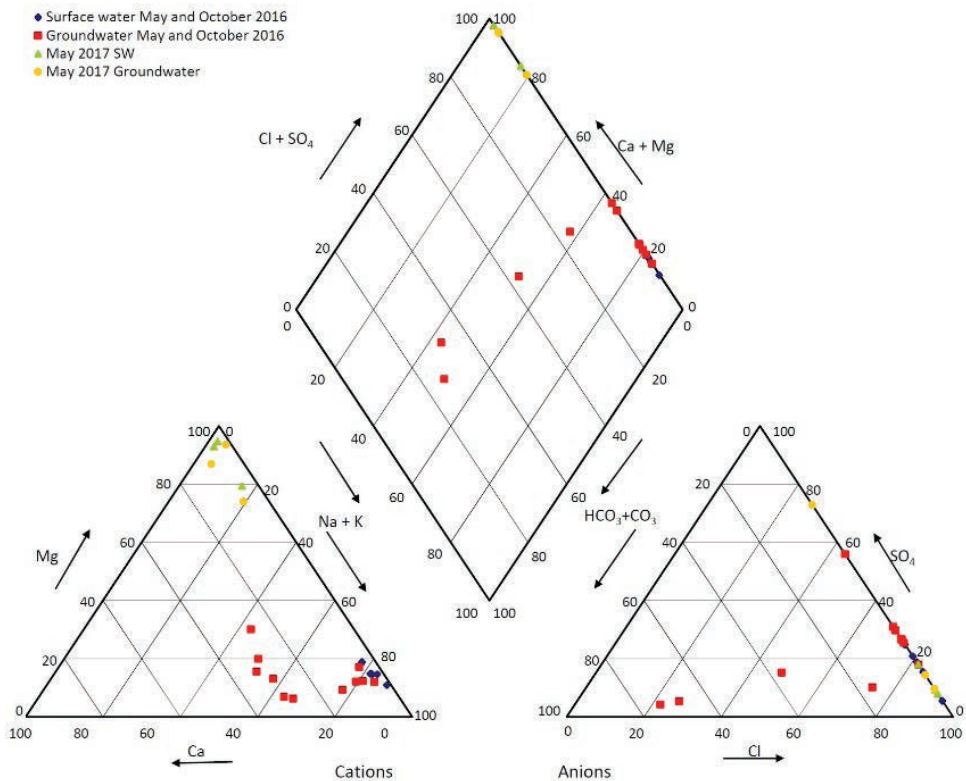


Figure 2 Percent cation (a) and anion (b) in groundwater samples from CC, GGSW and GG and surface water draining those swamps, samples include all sampling periods.

Table 1. Difference between swamps based on $\delta^{13}\text{C}$ and $\delta^{15}\text{N}$ (P-value is significance level derived from one-way ANOVA test).

Swamp	CCG	GGEG	GGSW	p-value
$\delta^{15}\text{N}$ mean (SD)	4.26 (3.07)	5.61(3.54)	4.43(1.42)	0.49
$\delta^{13}\text{C}$ mean (SD)	-27.568(1.66)	-28.119(1.75)	-27.522(1.15)	0.58



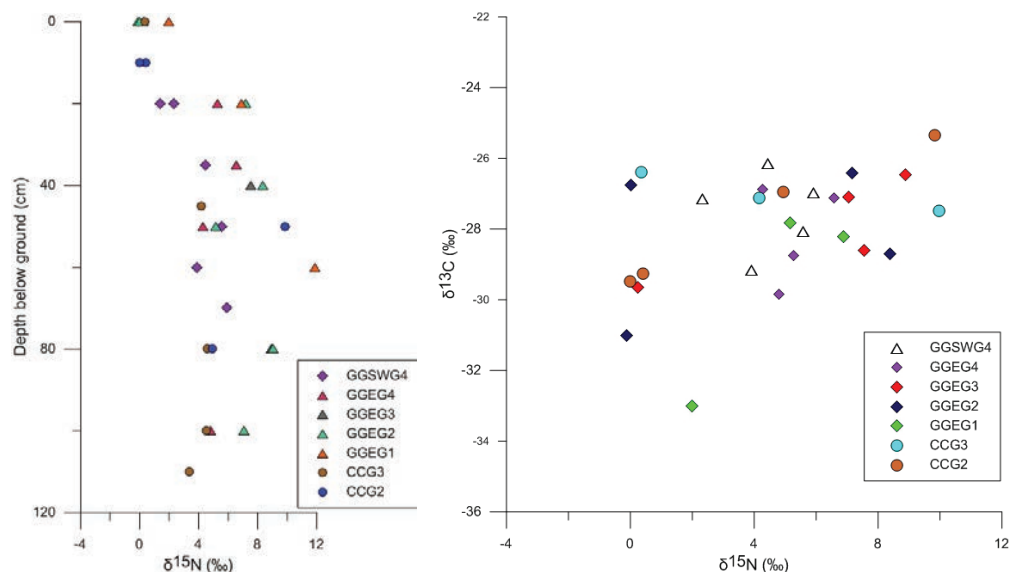


Figure 3 Plot of $\delta^{15}\text{N}$ with depth for GG, GGSW and CC swamps and nitrate values in surface and ground-water during dry (May 2016) and wet weather (October 2016) (a) and $\delta^{13}\text{C}$ and $\delta^{15}\text{N}$ of organic matter samples in swamp sediments from CC, GG and GGSW swamps, separated based on individual swamps (b)

To investigate further this change in $\delta^{15}\text{N}$ with depth, a dual isotope plot of carbon versus nitrogen isotope is presented to determine if a discrete domain exists and define the source of material for the swamp (Fig. 3b). The results are compared to typical isotopic values from literature (Deegan and Garritt, 1997) which confirms that the swamps are typical of terrestrial environments. Depleted $\delta^{13}\text{C}$ values (around -29‰) occur in a narrow range and indicate landscape dominated by woody vegetation (Fry, 2006). The $\delta^{13}\text{C}$ values of organic samples from these swamps thus suggests sources influenced by woody vegetation, such as *Boronia* shrubs within the swamp. Although these isotopes show variability within each of the swamps, neither $\delta^{13}\text{C}$ or $\delta^{15}\text{N}$ were found to be considerably different between three swamps ($p > 0.05$) (Table 1).

Stable oxygen and deuterium isotopes in waters

Preliminary results of stable oxygen and deuterium isotopes indicate that all surface,

pore water and groundwaters were similar to rainfall, with some samples enriched due to evaporation. The local meteoric water line (LMWL) and weighted rainfall average shown in Fig. 4 is from Lithgow rainfall data ($\delta^2\text{H} = 7.99\delta^{18}\text{O} + 16.6$; Hughes and Crawford, 2013).

Pore water samples from GG and CC swamps collected in May 2016 after long dry period, plot below the LMWL indicating an evaporation trend (slope of 4.2 for CC and 4.6 for GG swamp). If the regression lines are extended for both swamps to LMWL, they fall within the rainfall range for Lithgow. Pore water samples collected in October 2016 after a relatively cool and wet period plot mainly along the LMWL, with samples from May 2017 (average rainfall conditions) plotting along and above the LMWL. These results from the wetter period reflect the rainfall signature as observed from mean weighted rainfall average. Additional more detailed work will quantify the relative importance of rainfall and shallow groundwater flow to the swamp water balance (David et al, 2018 in review).



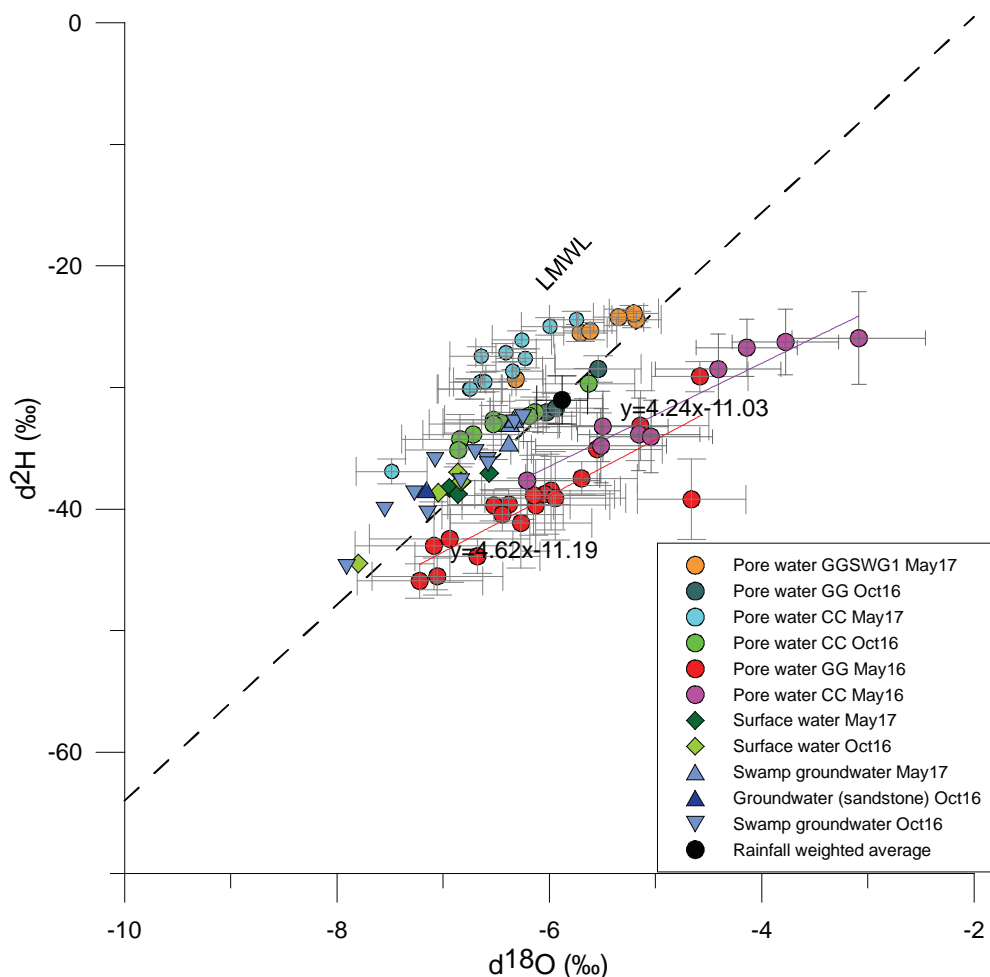


Figure 4 Isotopic composition of pore water, groundwater and surface water samples in three swamps

Conclusion

Multiple investigation techniques have provided some important insights into the sources of organic material and water to the swamp, and hydrogeochemistry of the swamp in the natural condition. Depleted $\delta^{15}\text{N}$ indicates microbial activity in the upper peat and soil horizons, while $\delta^{13}\text{C}$ results point to terrestrial swamp environments with woody vegetation. Slightly higher groundwater EC compared to surface water, and slightly elevated calcium compared to surface water is indicative of short residence time within the swamp. Rainfall recharge changes the cation composition of natural groundwaters, however mobilisation of naturally occurring trace metals was not observed. Recharge to the swamp sediments is sourced from rainfall

during wet periods, with evaporative losses during dry periods. Further detailed studies will quantify the relative importance of rainwater and groundwater in relation to peat and sediment within the swamp, and to the overall water balance during varying hydrological conditions.

Acknowledgements

The authors would like to acknowledge the support of Centre for Water Initiative, School of Biological and Earth Sciences and Bioanalytical Mass Spectrometry Facility at UNSW Australia. Funding for IRMS equipment was provided by Australian Research Council LIEFF grant LE130100069. We thank Russell Pickford for assistance and guidance with sample analysis, and T. McMillan for assis-



tance with sample collection. Field work and sample analysis was funded independently by UNSW.

References

- Commonwealth of Australia (COA) (2014) Temperate Highland Peat Swamps on Sandstone: ecological characteristics, sensitivities to change, and monitoring and reporting techniques, Knowledge report, prepared by Jacobs SKM for the Department of the Environment, Commonwealth of Australia.
- Deegan LA, Garritt RH (1997) Evidence for spatial variability in estuarine food webs. *Marine Ecology Progress Series* 147: 31-47.
- Cowley KL, Fryirs KA, Hose GC (2016) Identifying key sedimentary indicators of geomorphic structure and function of upland swamps in the Blue Mountains for use in condition assessment and monitoring. *Catena* 147: 564-577.
- David K, Timms W, Hughes CE, Crawford J, McGeeney D. (2018): Application of pore water stable isotope method to characterise a wetland system, *Hydrol. Earth Syst. Sci. Discuss.*, <https://doi.org/10.5194/hess-2018-237>, in review.
- Fry, B. 2006 *Stable isotope ecology*, Springer, LA, pp 317.
- Fryirs K, Freidman B, Williams R, Jacobsen G. (2014). Peatlands in eastern Australia? Sedimentology and age structure of temperate highland peat swamps on sandstone (THPSS) in the Southern Highlands and Blue Mountains of NSW, Australia. *Holocene* 24(11): 1527-1538.
- Hose GC, Bailey J, Stumpp C, Fryirs K. (2014) Groundwater depth and topography correlate with vegetation structure of an upland peat swamp, Budderoo Plateau, NSW, Australia. *Ecohydrology* 7(5): 1392-1402.
- Hughes CE, Crawford J (2013) Spatial and temporal variation in precipitation isotopes in the Sydney Basin, Australia, *Journal of Hydrology* 489; 42-55.
- McHugh, EA (2014) The geology of the shrub swamps within Angus Place, Springvale and the Springvale mine extension project areas, Appendix 18, Centennial coal Springvale extension SSD5594 Application.
- Schmidt S, Stewart G R (2003) Delta N-15 values of tropical savanna and monsoon forest species reflect root specialisation and soil nitrogen status. *Oecologia*, 134(4), 569-577.
- Wassenaar LI, Hendry M J, Chostner VL, Lis GP (2008) High resolution pore water $\delta^2\text{H}$ and $\delta^{16}\text{O}$ measurements by H_2O (liquid) - H_2O (vapour) equilibration laser spectroscopy. *Environmental Science and Technology*, 42(24), 9262-9267.
- Young, A. R.M. 2017. Upland swamps in the Sydney region. Thirroul, NSW. Dr Ann Young



Coal mine water hazard accurate detection and efficient control technology based on comprehensive drilling methods[©]

Shuning Dong, Liu Zaibin, Wang Hao, Chai Rui1

*Xi'an Research Institute of China Coal Technology and Engineering Group, Xi'an, 710077, Shaanxi, China
Shaanxi Key Laboratory of Coal Mine Water Hazard Prevention and Control Technology, Xi'an,
710077, Shaanxi, China*

Abstract

In order to prevent and relieve coal mine water hazards in China, mine water accurate detection and efficient control techniques were studied based on applications of multiple drilling methods. Surface directional drilling was applied in deep buried areas to cover main detection and governance region. Radial jet drilling technique was applied to control shallow area, marginal region and directional drilling blind area. In areas with no ground drilling condition, underground drilling technique was applied. Accurate detection method was developed by analyzing multi source data obtained through different drilling methods. Study showed that faults can be identified by directional drilling logging data and radial jetting process data. To enhance control efficiency, non-blind borehole layout method was studied by using different kind of drilling methods comprehensively.

Keywords: directional drilling, radial jet drilling, accurate detection, efficient control

Introduction

Water hazards in coal mines mean the phenomena that surface and underground water enters suddenly into a mine during construction and production. Water hazard in coal mines is related to factors such as geological tectonics, mining activities, geo-stress and hydraulic features of groundwater. As shallow coal resources in North China have become depleted, mining depth has gradually increased in recent years (Dong, 2007). Since Ordovician limestone comprise confined karst aquifers, and are characterized by extremely high water pressure, water leaking out of them is a huge threat. Deep mining flooding disasters in the past have led to considerable property losses and personal injuries. Water conducting channels such as faults are difficult to detect in advance using vertical boreholes despite the application of conventional fault detection methods. It is therefore of critical importance to detect water conducting channels for controlling groundwater hazard efficiently.

At present, water hazard prevention and control technology is developing towards regional, accurate and efficient control. Core part of mine water accurate and efficient con-

trol technologies is the integral drilling technology including surface directional drilling, surface radial jet drilling and underground long distance directional drilling. Comprehensive drilling technology extend data sources and can provide large amount multi source data which can be used as a basis for detecting faults and other structures. This paper is mainly about how to analyse different kind of drilling data and how to use multiple drilling technologies more efficiently.

Comprehensive drilling technologies

Surface directional drilling

Surface directional drilling is the major drilling approach for surface regional governance engineering, surface horizontal branch drilling means the drilling technology that a vertical borehole is drilled from the surface, turns into a horizontal well at definite angle in a target horizon. For surface horizontal directional drilling, multiple branch boreholes are drilled from a main surface borehole to control the range of grouting reconstruction in target aquifer, achieving the objective of regional grouting reconstruction, as shown in figure 1. After entering into the target layer, borehole extends horizontally or nearly



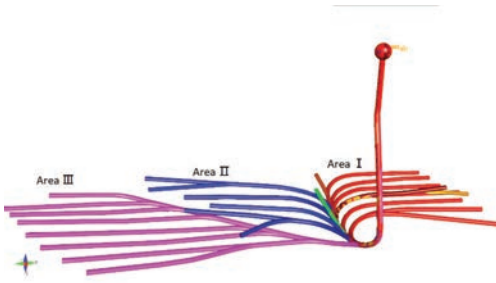


Fig.1 Subarea layout of directional boreholes

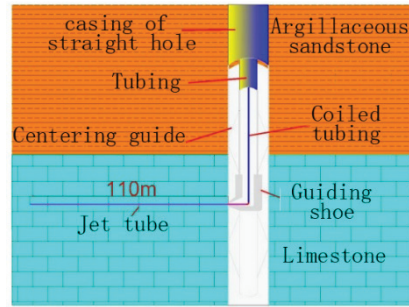


Fig.2 Schematic radial jet process

horizontally along the target layer, detects efficiently the development situation of karst, structure and fractures in the target layer within the scope of drilling, broadening the control range of the borehole, improving the groutability and the effect of reconstruction and reinforcement.

Surface radial jetting

Hole-forming technology with radial jet uses the principle of high pressure hydraulic cutting, relies on simultaneously forward and successively jetted high pressure water to form hole, as shown in figure 2. The jet of high pressure water cuts forward and break the surrounding rocks, provides backward power for the jet nozzle and the tube to move forward. The maximum jet pressure is up to 137MPa, the aperture of jet hole is 25~75mm, the maximum hole depth until now is 110m. In the same well multiple horizontal boreholes can be drilled in radial direction at the same stratum or different horizons.

Before drilling a radial borehole, a straight hole should be drilled firstly by using an ordinary rotary drilling rig, after the borehole enters into Ordovician limestone, the borehole is washed and drilling is ended to observe the static water level. Then pump in test is conducted to measure the specific water adsorption rate of the injected interval, suitable grouting materials and formula are selected to start grouting, after the technical grouting standards are achieved, the borehole is cleaned to start drilling of radial jet perforation. In principle, each radial perforation is completed in one time, later drilling and

grouting are completed successively according to the sequence of perforation-forming by jet and grouting.

Underground directional drilling

The technology combining underground directional drilling and high pressure grouting can also be achieved, as shown in figure 3. An underground directional borehole consists of a casing interval, a rotary deflecting interval, a directional deflecting interval and a steady inclined interval (Li, 2013). A directional drilling technology with a positive displacement motor is used to conduct directional deflecting and steady inclined drilling, the borehole trajectory is measured in real time and controlled accurately so that the borehole extends at long distance in a targeted layer of grouting, when necessary, branch holes are drilled to increase the exposure range of an aquifer by borehole.

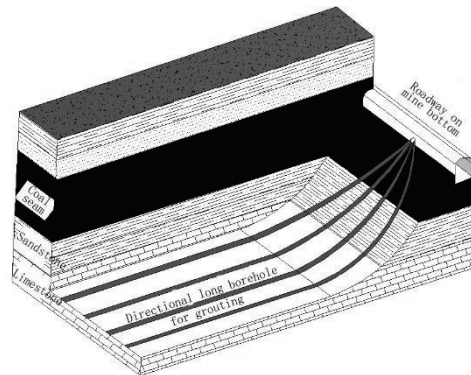


Fig.3 Schematic of underground directional boreholes



Accurate detection from multisource data

Fault identification based on directional borehole logs

The principle of natural gamma-ray logging while drilling (LWD) relies on the natural radioactivity of a formation and its standard unit of measurement is defined by the American Petroleum Institute (API). Natural gamma-ray parameters are used to precisely identify the characteristics of a formation in combination with geometric parameters of borehole trajectory and geological data. Thus, a higher logging value therefore implies a larger intensity of rock radioactivity (Fletcher, 2008). Figure 4 shows data series of natural gamma-ray LWD at four directional boreholes (S4, S5, S6, S7) of a regional control project at Xingdong coal mine in Hebei province.

In order to extract the implicit information of the fault in the natural gamma-ray LWD, we use the time-frequency analysis and Short Time Fourier transform. Time-frequency analysis can transform the GR data curve into time domain and frequency domain to explain, and it will highlight the change of the curve reflecting the fault information in these domains (Lu, 2013). Through this method, the results show that using Hamming window function and selecting 127 samples of window function we can calculate the amplitude and spectrum of the resistivity curves, which can greatly improve the ability of distinguishing fault zone.

Compared with the conventional method, the recognition rate of fault is increased by time-frequency analysis. When there is fault in the layer, the GR data will show an anomaly with respect to the bedrock. Thus, fault zones

can be identified by the natural gamma-ray LWD in parallel directional holes. Combining geological data, all three high amplitudes can be inferred under the impact of the same fault, and are connected as line of fault trend on the flat surface, fault 1. The time-frequency analysis presented above shows that because the amplitude of the S5 hole is very high, between 2,673 m and 2,800 m, this is likely a fault point named Fault point. The distribution of faults on this plane is shown in figure 5.

Fault detection by jetting process data

It usually needs three boreholes to determine the occurrence and location of a fault. A fault can be exposed in a single vertical borehole by multiple jetting boreholes then the occurrence and location can be determined. Jetting hole should be constructed after drawing the projection profile in the area where the fault may exist. Jetting pressure should be selected according to different lithology. Fault point can be determined according to jetting phenomenon such as coiled tubing jump, tubing flabby, speed slow down or the change of proper jetting pressure. Three-point method can be used to determine fault occurrence and position based the determination of multi fault points, as shown in figure 6.

Borehole layout method for efficient controlling

Boreholes drilled by different kind of drilling methods provide grouting channels to control mine water. Usually a single drilling method is difficult to control the whole mining area comprehensively, thus, comprehensive drilling technologies should be combined under specific construction conditions. Borehole layout is constrained by various conditions

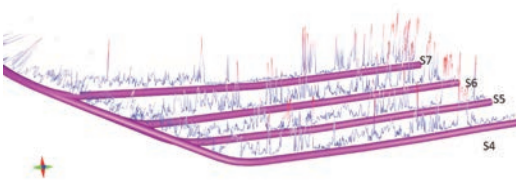


Fig.4 GR data at four boreholes in 3D space

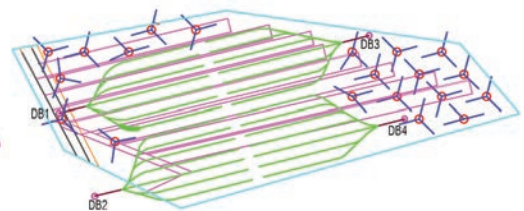


Fig.7 Borehole layout for efficient controlling



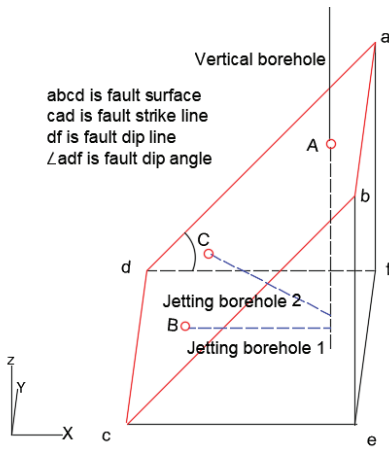


Fig.6 Fault detection based on radial jetting

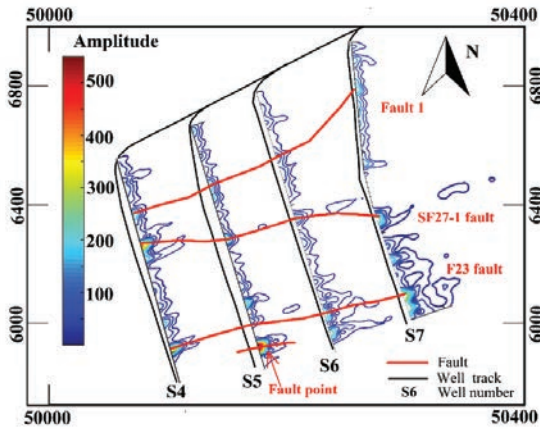


Fig.5 Fault zones delineation based on four holes based on GR

such as ground condition, mining plan and target layer characteristics. To enhance control efficiency, surface directional drilling and radial jet drilling methods were applied at a regional control area with water inrush coefficient larger than 0.1MPa/m of Dongpang coal mine at Hebei Province, as shown in figure 7. The regional control area is an irregular triangle and the grouting layer buried depth is from 420m to 640m. Surface directional drilling boreholes control the main scope while radial jet boreholes control shallow, edge and corner areas which is blind area of directional drilling.

Conclusions

Surface directional drilling technology is mature, has high drilling efficiency, less surface orifices, hole-forming by surface radial jet does not have requirement for the depth of straight hole, radial hole enters directly into formations, does not need a radius of turning circle, surface hole opening position does not have blind area, borehole layout is flexible. Underground radial drilling technology is not limited by ground conditions but by the distribution of workings.

Coordination of different drilling approaches can form control technology without blind area. Surface directional drilling engineering is arranged in areas of deeper burial depth. Shallow parts, corners and blind area of directional drilling are controlled by radial

jet holes, the areas that surface drilling can't cover are controlled by underground drilling so as to achieve the complete coverage of the whole controlled region.

In addition of normal detection methods, fault identification methods based on directional borehole logs and radial jetting process were put forward. Integral comprehensive drilling technology and accurate detection methods can achieve efficient control in areas with water hazards.

Acknowledgements

This paper is supported by the Project Sponsored by the National Key Research and Development Program of China (2017YFC0804100).

References

- Amara K A, Pan H, Ma H, et al. (2017) Use of spectral gamma ray as a lithology guide for fault rocks: A case study from the Wenchuan Earthquake Fault Scientific Drilling project Borehole 4 (WFSD-4). Applied Radiation & Isotopes, 128, 75-85.
- Dong S, Hu W (2007) Basic features and major influencing factors of water hazards in China's coal mines. Coal Geology & Exploration, 05: 34-38.
- Dong S, Liu Q (2009) Study on relative agluclide existed in mid-Ordovician limestone top in North China coal field. Journal of China Coal Society 34(3), 289-292.



- Fletcher P, Jamieson A M, Harry R (2008) Recognition of Milankovitch cycles in the stratigraphic record: application of the CWT and the FFT to well-log data. *International Journal of Mining Science and Technology*, 18(4), 594-598.
- Jin D, Liu Y, Liu Z, et al. (2013) New progress in research on prevention and control technology of serious water inrush disasters in coal mines. *Coal Science and Technology*, 01: 25-29.
- Li Q, Shi Z, Fang J (2013) Directional drilling technology and equipment for in-advance grouting consolidation of seam floor. *Metal Mines*, 2013, 47(9): 126–131.
- Liu Z, Jin D (2013) Research on failure law of surrounding rocks during mining lower seam group in North China coalfields. *Coal Science and Technology*, 2013 (07):24-27, 31.
- Lu W, Li F (2013) Seismic spectral decomposition using deconvolutive short-time Fourier transform spectrogram. *Geophysics*, 78(2), V43-V51.
- Zhou, B, Hatherly, P, & Sun, W (2017). Enhancing the detection of small coal structures by seismic diffraction imaging. *International Journal of Coal Geology*, 178.



Integrating competing water needs of mining and mineral processing with the environment, community and economic activity in a mining-dominated catchment

Susan T. L. Harrison^{1,2}, Kerry Slatter-Christie^{1,3}, Jennifer Broadhurst¹

¹*Future Water Research Institute, University of Cape Town, South Africa*

²*Centre for Bioprocess Engineering Research, Department of Chemical Engineering, University of Cape Town, South Africa. sue.harrison@uct.ac.za*

³*Kalao Solutions, Johannesburg, South Africa.*

Abstract

The mining sector is facing increasing regulatory and social pressures to demonstrate efficient use of water resources on both a local and catchment scale. This paper presents an integrated approach to mine water use and management, and highlights the need to consider the role of secondary water resources, fit-for-purpose water use and the essential requirement to monitor water quality, as well as quantity, in such integrated systems. It aims to provide a basis on which to identify key knowledge gaps that need to be addressed to move towards a new paradigm of water management in 'mining' catchments in increasingly water scarce environments.

Keywords: water catchment areas, flotation, water quality, water management

Introduction

Water is considered the top long-term global risk by the World Economic Forum (2016). With increasing global and local water requirements, demand now outstrips supply. To ensure ongoing development and stable economic futures, three approaches are key regards water: firstly, more efficient use of water, thereby reducing demand; secondly, mobilising new water resources, other than surface and ground water sources; and thirdly, integrating water demand and supply across competing needs within a region. In this paper, we explore the potential and value of an integrated approach using, as a scenario, the activities within a catchment serving mines and mining communities in a water-scarce developing world context.

In developing regions, a mine site forms a nucleus, drawing in migrants with its potential for jobs, wealth creation and development. Its arrival is super-imposed on an existing system of livelihood and economic activity, resulting in competing needs and shifting priorities. Considering this in the context of water, competing needs and trade-offs develop rapidly between the stakeholders. Within the regional scenario, a range of sub-systems within the region interact. These

sub-systems include (i) the 'livelihood water needs' of local communities, (ii) those associated with community economic activity (including small scale agriculture), (iii) water requirements of the mine and mineral processing facility (process water), (iv) water use by the commercial agricultural sector and, (v) water uses of the towns in the catchment area, including the industrial sector.

Owing to the associated wealth and opportunity brought to a region by a new mine, it has typically taken centre stage with regards to management of water resources in the catchment (fig.1). Increasingly, through the system of water use licences, introduced as a national government intervention (South Africa) with the aim to achieve effective water management, a more integrated positioning has been developing. Very effectively, the need to obtain a social licence to operate, places water management as central to the mining operation's success. The mine now needs to show its social responsibility towards water use, not only in terms of reducing the use of potable water and improving water reuse / recycling, but also in trying to ensure that the local communities around the mine have access to potable water.



This paper discusses a changing framework of water use, identifies potential new water sources and investigates the potential for integrated water use, as well as identifying the extended knowledge required to achieve this. Knowledge of all stakeholders' water requirements, including “fit-for-use” water, is of major importance in developing new paradigms for water use which should, in turn, ensure that the water demands of all users within a catchment are met. By working with the entire catchment and understanding the catchment's water balance, it is more likely that the water demands of the catchment can be met, underpinning economic development and the achievement of acceptable quality of life in water-scarce communities.

Integrated use of mine water across catchments

Figure 2 introduces the evolution in thinking towards integrated water management across all stakeholders within the catchment, rather than independent consideration as an internal company-specific problem. Figure 2 shows that the water rights for the mine and its operations are firmly embedded in the integrated framework, as is the need to address

water requirements across the catchment, particularly those of growing communities in the surrounding region.

Reduction of abstraction of fresh water is essential to reduce the water footprint of the mine, to avoid perceptions of water competition, to protect the environment and natural ecosystems and to win and protect the social licence to operate. Water supply may be drawn from numerous sources. Historically, abstraction from ground and surface water reserves were the most common. This was followed by transportation of water from adjoining catchments. Increasingly the ‘used water’ category is of interest for water supply. This serves two important functions. Firstly, focus on the quality of ‘used water’ is an important step in mitigating its pollution potential. Secondly, the treatment of used water to ‘fit for purpose’ positions it as a potential supply, thereby reducing abstraction or increasing supply or both. Traditionally such ‘used’ water has been considered within the mine's boundaries e.g. ash dam and return water from tailings storage facilities, as part of the water recycle from process. An integrated water management approach considering water sources, used water and water

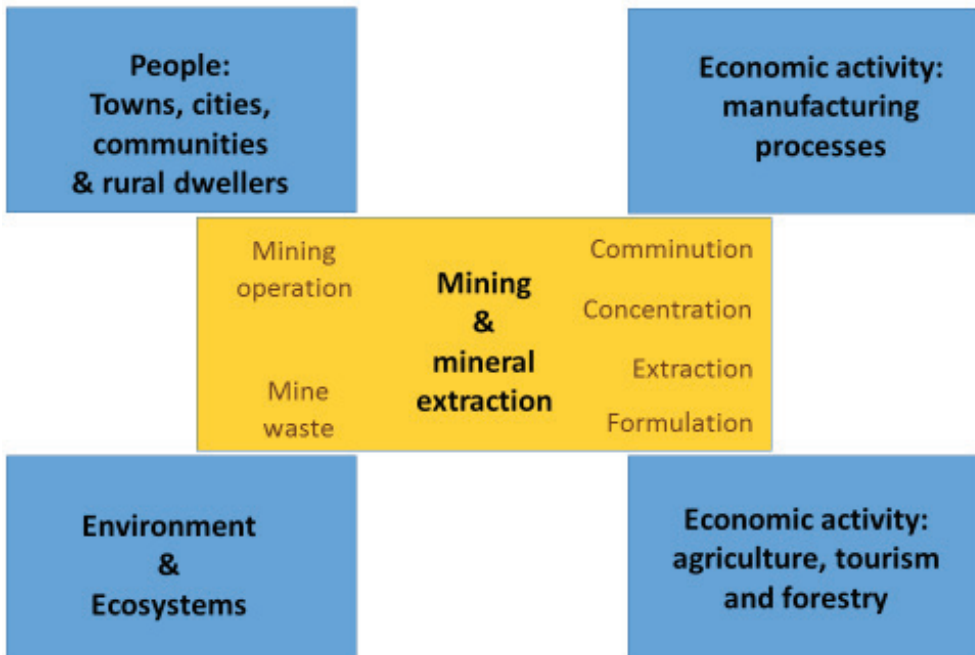


Figure 1 Activities competing for water use in catchments housing mining operations



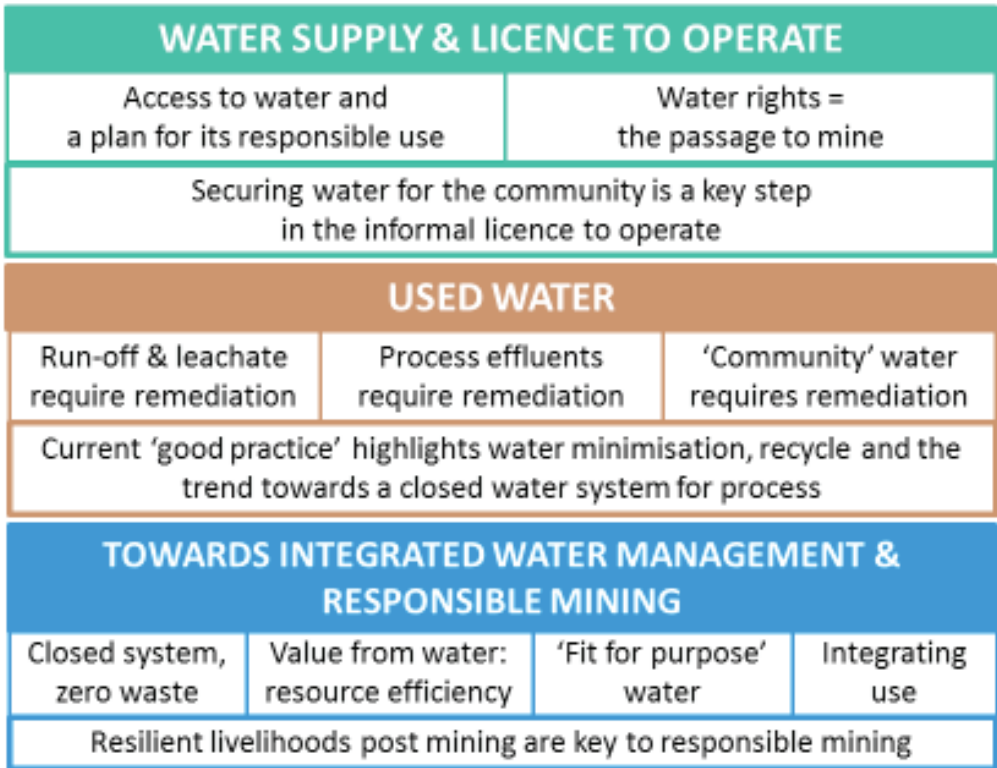


Figure 2 Progression in approaches to integrated water management between mine, community and activities within the catchment

demand across the whole catchment, giving cognisance to transport distances, allows for improved allocation of fit for purpose water with minimal additional treatment. Such re-visioning of water management is developing rapidly in mining operations. For example, in South Africa some mining companies are contributing to the provision of clean water in water-stressed areas through the establishment collaborative partnerships with government and civil society. In the Mpumalanga coalfields of South Africa, acid mine drainage is treated in a water reclamation plant, supplying in excess of 30ml/day potable water to the local municipality (Gunther et al. 2006) , whilst the recently established Mine Water Coordinating Body (MWCB) aims to promote effective mine water management and re-use specifically through cross-sectoral and multi-stakeholder engagement and innovation. These approaches can lead to establishing trust and enhancing company reputation, ultimately reducing the risk of conflict and

improving water security, and contributing to the social licence to operate.

Re-visioning water use in mining operations

Over the past 10 years, mining companies have focussed on water as a key enabler and thereby a key risk to their operation. Water impacts a mine’s operation both directly and indirectly; the risk of water scarcity and water quality are direct impacts, while indirect impacts are the potential of open water systems to contribute to pollution and environmental challenges, and the perceived competition for water having potential to threaten the social licence to operate. Increasingly mine sites are working towards a reduced water footprint, through reducing the footprint of fresh water, by increasing the amount of water recycle / reuse (closing water circuits) and by assessing the potential for dry processing.

As an example, the developments in water sources for flotation may be considered.



Substantial research has been focussed on the impact of water quality on flotation as the mineral pulp processed through this concentration step comprises some 80 – 85% water (Levay et al. 2001). Water forms a key transporter and processing medium in the metallurgical plants. Increasingly this water is sourced from diverse sources, including *worked water* from the plant: such as recycle water from the thickeners, filters, de-watering units, internal recycle water from the float cells, and return water from tailings storage facilities (Muzenda 2010, Liu et al. 2013). Raw water includes water not previously used on plants such as borehole or ground water of varying quality, pit water, surface water, potable water, process water from surrounding industrial activities and treated sewage effluent (Liu et al. 2013). While traditionally, only raw water not previously used in any process was brought into the minerals processing operation as make-up water. Now, effluent water or treated effluents such as process water from surrounding industrial activities and treated sewage effluent are being utilised as make-up water to the process.

The quality of water is influenced by dissolved solutes such as detergents, organic carbon, hydrocarbons, metal ions, residual flotation reagents, dissolved oxygen, suspended solids and pH. Such components impact flotation through impacting hydrophilicity and hydrophobicity, metal exchange, pH, slurry viscosity, and froth stability, which in turn affect reagent usage and pH thereby impacting recovery, grade and mass pull (Muzenda 2010, Corin et al. 2011, Manono et al. 2013). While fresh water is typically acknowledged to yield the best performance, a consistent water supply facilitates development of a successful flotation protocol with good performance. The most challenging is a water supply of variable quality and quantity (Liu et al. 2013). Increasingly it is recognised that, by using separate reservoirs for differing water sources (separated wastewaters rather than directly mixing all waste streams), variability can be overcome to some degree by appropriate dilution, mixing and blending, provided water monitoring is available to inform the blending. Most importantly, the prior-year practice of mixing all waste streams as re-

ceived, which simplifies the core process, is increasingly recognised as poor practice where water re-use is desired.

An example of use of blended ‘fit for purpose’ water sources for flotation is at Mogalakwena Platinum Mine, (Anglo American) in Limpopo, South Africa. Here treated sewage effluent, return water from tailings storage facilities and plant recycle water are blended to the required quality, thereby freeing piped potable water for community and other uses. Similarly, the new Ivanhoe platinum mine in the same area will utilise treated sewage effluent as process water. A benefit of using the treated sewage effluent is the investment of the mining houses in the upgrading of the sewage treatment works of nearby towns in order that they are able to supply the required volume at the required quality.

The ongoing challenge of meeting conflicting water needs is further demonstrated by Anglo American Platinum’s recent commitment (March 2018) to deliver 3.5 million litres per day to communities in 42 villages surrounding Mogalakwena Mine in the Greater Mapela Region. This water will be produced from boreholes that will be sunk in the area. Anglo American Platinum has also committed to reducing fresh water abstraction by 50% in water scarce regions such as Limpopo (Mining Weekly 2018).

Similarly, in Peru, the Freeport-McMoran Inc.-owned Cerro Verde copper mine secured water for its major extension by constructing a wastewater treatment plant to treat 85% of the sewage produced from the 1 million people living in Arequipa; this sewage water was previously discharged to the Rio Chili river. The treated water equates to $1.8 \text{ m}^3 \text{ s}^{-1}$ and provides adequately for the plant extension, while also releasing clean water to the river, thereby aiding downstream agriculture (Fraser 2017). The cost and technical challenges of this project were substantial but this initiative of the mining company secured its own water needs, ensured health and safety through sanitation, re-vitalised the river and aided agricultural security by offsetting competition for water between farmers and the mine (Fraser 2017).

While acknowledging the great developments in knowledge of the impact of water



quality on flotation over the past 10 years, Liu et al. (2013) highlighted the gaps in our knowledge base that constrain the use of, or performance with, non-conventional water sources in flotation. The impact of abiotic solutes on flotation has been broadly studied, however understanding the effect of biotic components remains very limited. Similar challenges are found in other extraction units e.g. leaching or bioleaching. Further, potential water sources for flotation and other aspects of mine operation are typically assessed starting with internal water sources. External ‘fit for purpose’ sources, rather than pristine sources, may provide great opportunities across an entire water system, with the added benefit of freeing up pristine water for other uses and eliminating or reducing release of low quality water streams to the environment. Typically the flotation process is adjusted to accommodate the water quality; equally, the water quality could be adjusted to accommodate its final use. Water quality monitoring has the potential to provide insight into what happens if water quality is varied. Monitor-

ing may also allow for a seasonal change in reagent regime as water quality may be impacted by seasonal changes. Increasingly, it is recommended that water issues are addressed as part of the risk assessment.

Water quality as a key player

Requirements of water of differing quality based on its final use is well documented. In Table 1, this is clearly illustrated, showing the potential to select or blend to obtain appropriate sources matching application. The same is true for operations within the metallurgical processing train; however, these remain to be defined with equal clarity and will vary as a function of unit operation, active agents used, mineral ore processes etc.

Site-specific information is required for rigorous application of the approach while process specific information will provide a framework within which to identify key variables for consideration. Work is currently being performed at an Anglo American Platinum operation to understand which compo-

Table 1. Water quality requirements depend on application. Orange shading demonstrates the most stringent requirement. Concentrations are given as mg/l unless otherwise specified. For surface water and ground water, letters identify the application that defines specification of these guidelines (IRMA 2016).

Metal	Human health drinking water a	Water to Irrigate b	Aqua-culture water c (FW/ Mar.)	Aquatic organisms in fresh water d	Recrea-tion water	Surface water	Ground water
Aluminium	100	5000	30	55		30 ^c	100 ^a
Antimony	6		50 / 30			6 ^a	6 ^a
Arsenic	10	100		24	50	10 ^a	10 ^a
Cadmium	5	10			5	X ^c	5 ^a
Chromium (tot)	50	100	[20 as Cr(VI)]		50	50 ^a	50 ^a
Copper	1000	200				^d	200 ^b
Iron	300	5000	10 / 10	300	300	10 ^c	300 ^a
Manganese	50	200	10 / 10	1700	100	10 ^c	50 ^a
Nickel	20	200	100/100		100	^d	20 ^a
Uranium (U ²³⁸)	20 (1)	100 (0.2)		15		15 ^d (1 ^b)	20 ^a (1 ^a)
Alkalinity			20-100				
Chlorine	5	1	2	3	1	2 ^c	1 ^b
Chloride	250	100		120	400	100 ^b	100 ^b
CN (µg/l)	200		5 / 5	5	100	5 ^d	0.2 ^a
H2S			1 / 1	2	50	1 ^c	
NO3	10	100	50 / 100	13	10	10 ^a	10 ^a
NO2	1	10	0.1/ 0.1	0.6	1	0.1 ^c	1 ^a
pH	6.5-8.5	6.5-8.4	6.5-9.0	6.5-9.0	6.5-8.5	6.5-8.4 ⁺	6.5-8.5 ^b
SO4	500	1000			400	400 ^e	500 ^a
TSS		30	40 / 10	15	30	15 ^d	
TDS	500	1000			1000	500 ^a	500 ^a



nents of treated sewage water have negative or positive impacts on flotation.

Once these impacts are understood better blending techniques will be used such that as little as possible high quality water needs to be used, without compromising plant performance. In this case water monitoring is essential – particularly of the source water, as the blend may need to change if the source water quality improves or becomes worse.

Conclusions and key gaps for ongoing study

This study highlights the needs for and benefits of an integrated and holistic approach to water management within catchments in general, but specifically those home to mining operations. Through the use of an external frame of reference from the mine, which is both a water user and a (waste)water generator, a range of pristine and used water sources are available. By treatment to ‘fit for purpose’ for the needed task and optimised allocation to task, abstraction of pristine water sources can be reduced or, where scarce, retained for key uses such as human consumption.

The use of ‘fit for purpose’ water supply requires rigorous understanding of the impacts of components of the water stream, including minor components, on the process or activity, requiring such knowledge bases to be expanded and shared across activities such as agriculture, aquaculture, minerals processing, wastewater treatment, industrial sectors, and the local ecosystems amongst others. Our research will be extended to address the gaps identified towards developing this rigorous understanding.

Finally, by using circular economy and industrial ecology approaches, as appropriate, to water management, the integrated impact must be considered, especially that on ecosystems.

Acknowledgements

The funding of the DST and NRF, South Africa through the SARChI Chair in Bioprocess Engineering is gratefully acknowledged.

References

- Corin KC, Reddy A, Miyen L, Wiese JG, Harris PJ 2011. The effect of ionic strength on plant water on valuable mineral and gangue recovery in a platinum bearing ore from the Merensky reef. *Minerals Engineering* 24: 131-137
- Fraser J 2017. Peru water project: Cerro Verde case study – mining-community partnerships to advance progress on sustainable development goal 6 (Access to clean water and sanitation). Canadian International Resources and Development Institute (CIRDI) Report 2017-002
- Günther P, Mey W, van Niekerk A 2006. A sustainable mine water treatment initiative to provide potable water for a South African city: a public-private partnership. Paper presented at the Water in Mining Conference, Brisbane, QLD, November, 14-16
- IRMA 2016. IRMA standard for responsible mining IRMA-STD-001. www.responsiblemining.net
- Levay WM, Smart R, Skinner G 2001. The impact of water quality on flotation performance. *J.SAIMM* 101: 69-75
- Liu W, Moran CJ, Vink S 2013. A review of the effect of water quality on flotation. *Minerals Engineering* 53:91-100. [Doi.org/10.1016/j.mineng.2013.07.011](https://doi.org/10.1016/j.mineng.2013.07.011)
- Manano MS, Corin KC, Wiese JJ 2013. The effect of ionic strength of plant water on foam stability: a 2-phase flotation study. *Minerals Engineering* 40: 42-47
- Muzenda E 2010. Investigation into the effect of water quality on flotation performance. *World Academy of Science, Engineering and Technology* 45: 237-241
- World Economic Forum 2016. Mapping mining to the Sustainable Development Goals: an atlas. http://www3.weforum.org/docs/IP/2016/IU/Mapping_Mining_SDGs_An_Atlas.pdf (downloaded May 2018)



Evaluating metal behaviour and mine water treatment benefits in abandoned mine catchments with variable pollutant load inputs

Adam P Jarvis¹, Jane E Davis¹, Patrick HA Orme¹, Hugh AB Potter² and Catherine J Gandy¹

¹*School of Engineering, Newcastle University, Newcastle upon Tyne, UK. NE1 7RU, adam.jarvis@newcastle.ac.uk*

²*Environment Agency, Horizon House, Bristol, UK, BS1 5AH*

Abstract

The results of three synoptic survey investigations of the importance of diffuse mining pollution are reported. The three watersheds range in size from 10 – 3 000 km². In all three of them diffuse pollution – from a combination of groundwater inputs, waste rock runoff and sediment remobilisation – becomes increasingly important at higher river flow-rates. Whilst point source remediation is predicted to result in substantial improvements in downstream water quality during low flow conditions, at higher flows reductions in downstream metal concentrations may be less than 30%.

Introduction

Abandoned metal mines are a major source of freshwater pollution in the UK. In excess of half of the entire mass flux of zinc and cadmium to the streams and rivers of England and Wales arise from abandoned metal mines (Mayes et al., 2010), with less than half coming from all other sources of pollution combined. Consequently there is an ongoing programme of UK government investment in designing and building treatment systems to lower the burden of metals entering freshwaters in abandoned metal mine districts. In most cases the treatment initiatives are targeted at point sources of pollution i.e. from abandoned mine entrances, since it is comparatively straightforward to (a) characterise such discharges in terms of flow-rate and water quality and (b) engineer a structure to capture such discharges and direct them into a treatment system.

However, there is a growing body of evidence that point source pollution is not the only cause of degradation of downstream water bodies (e.g. Mighanetara et al., 2009). Diffuse sources of mine water pollution – such as arise due to surface runoff from mine waste rock, direct inputs of groundwater to surface waters, and remobilisation of metals from riverine sediments – may be a variably important source of pollution. The measurement,

interception and treatment of such sources of pollution is far more challenging than equivalent interventions for point source pollution. Properly quantifying diffuse source pollution is important though, as without such understanding it is not possible to calculate the true benefits of – potentially costly – point source pollution remediation schemes in the same watersheds. Ultimately, as more and more point source treatment systems are installed, remediation of diffuse pollution sources will become the limiting factor to further improvements in river water quality in mined watersheds.

Over the last 5 – 10 years we have undertaken long-term synoptic monitoring in contrasting abandoned mine watersheds to fully characterise the nature and extent of diffuse mining pollution, and therefore to understand the benefits of point source remediation. Particular challenges in executing such monitoring programmes are (a) accurately measuring flow-rate and (b) monitoring across the full range of hydrological conditions and (c) monitoring in sufficient locations to derive the importance of diffuse pollution sources during any single set of hydrological conditions. Here we report on the results of those monitoring programmes and the implications of the work.



Study areas

Three mining-impacted rivers were the focus of the investigation:

- 1) The Coledale Beck is an upland river in the English Lake District National Park (Cumbria), with a watershed area of approximately 10 km². At an elevation of 280 m above sea level (a.s.l) is the abandoned Force Crag lead / zinc / barytes mine (54°35'00"N 3°14'23"W), which was finally abandoned in 1991. In addition to a major point source of mine water pollution, and several smaller ones, there are extensive areas of waste rock which are obvious candidate sources of diffuse pollution. The Coledale Beck drops steeply, from an elevation of 550 m to 100 m above sea level over a horizontal distance of 4 km. Further details on the geology and mining in the area can be found in Postlethwaite (1913).
- 2) The River Nent is also in Cumbria, and it too is an upland river. It is a tributary of the River Tyne, which drains east to the North Sea. The River Nent watershed lies in the upper reaches of the River Tyne system, and has an area of approximately 100 km². The watershed was extensively mined for lead and zinc. There are four major point source discharges to the River Nent, two in the vicinity of the village of Nenthead (450 m a.s.l; 54°47'09"N 2°20'30"W), and the other two some 2 km downstream. Upstream of these point discharges there are extensive tracts of exposed waste rock.
- 3) The River Tyne is one of the largest river systems in northern England, with a watershed area of nearly 3 000 km². It has two main branches: the River North Tyne and River South Tyne (the River Nent is a tributary of the latter), which meet 2 km upstream of the town of Hexham, at 54°59'19"N 2°07'50"W. Within the watershed of the River South Tyne is the North Pennine orefield, which was one of the most productive mining areas (for Pb and Zn) in the UK during the 18th and 19th centuries. The Environment Agency (England and Wales) has flow gauging facilities at several locations down the

length of the River Tyne, which were critical during this investigation.

Location maps are not shown here for reasons of space. However, the results reported below are exclusively comparing the metal flux of an individual point source, or sum of point sources, compared to metal flux at an in-stream location (usually downstream), across hydrological conditions. It is the comparison between point source flux and in-stream flux that is key, rather than the exact locations of the various points.

Methods

The key to deriving the importance of diffuse pollution sources is the synchronous measurement of flow-rate and water quality of both point sources and in-stream locations. In-stream locations includes both upstream and downstream of the point sources, and upstream and downstream of suspected / potential diffuse sources. In order to be able to compare metal flux (mass per unit time) at different locations sampling at all locations had to be undertaken within a single day, and whilst hydrological conditions were constant. To understand the importance of diffuse pollution under different hydrological conditions it was necessary to sample on different days when hydrological conditions were different. In order to capture as wide range of hydrological conditions as possible monitoring was undertaken over at least a period of 12 months.

On the Coledale Beck one Environment Agency flow gauging structure was available for use. This was located immediately downstream of the Force Crag mine site, and therefore was used routinely. Sharp-crested V-notch weirs have been installed on many of the smaller streams and discharges in the watershed. At other locations on the river salt gulp dilution gauging was undertaken periodically to measure flow-rates at key locations. In brief, field methods involved injection of up to 7 kg of lab-grade NaCl into the river, with downstream semi-continuous conductivity logged using a YSI ProPlus conductivity meter. 2 × 1 L river water samples, and 2 × 25 mL salt solution samples, were collected for the subsequent calibration re-



quired for flow calculation (Hersch, 1998). On the River Nent there are no flow gauging structures, and therefore salt gulp dilution gauging was used for determining flow at all locations. On the River Tyne use was made of flow gauging infrastructure installed and operated by the Environment Agency (England and Wales). In particular, use was made of two gauges on the River South Tyne, at Featherstone and Haydon Bridge, and a third on the River Tyne at Bywell.

Water samples were collected simultaneous to flow measurement. Samples were collected in 30 mL plastic vials, with those for subsequent metals analysis acidified with lab-grade concentrated nitric acid. Samples for filtered metals analysis were filtered through a 0.45 µm cellulose nitrate filter. pH, conductivity and temperature were measured on site using a pre-calibrated Myron L 6P Ultrameter. Total alkalinity was determined at the time of sample collection using a Hach Digital Titrator with 1.6N sulphuric acid or 0.16N sulphuric acid with a Bromcresol-Green Methyl-Red indicator. Analysis of total and filtered metals was subsequently undertaken using a Varian Vista-MPX ICP-OES or Agilent 770 Series ICP-MS, as appropriate for the metal concentration.

Blanks and standards were used throughout and triplicate samples analysed periodically. Anion analysis was conducted using a Dionex DX320 ion chromatograph.

Results and Discussion

Coledale Beck: There is a single major point source of pollution from the Force Crag mine to the Coledale Beck (referred to as Level 1). It is a groundwater discharge from the abandoned underground workings, and consequently has a rather consistent flow-rate, as indicated on Figure 1. It also has a consistent Zn flux, varying from 2.9 to 4.3 kg/d. During low flow conditions this point source of pollution accounts for the majority of the Zn in the Coledale Beck downstream of the mine site (Site ID #4; Figure 1). However, as flow-rate in the Beck increases the Zn flux in the river increases sharply also, and these increases are not accounted for by the Level 1 point source (flow of the Coledale Beck during monitoring event 5, on Figure 1, was 390 L/s). Under the highest flow conditions monitored during this work Zn flux in the Coledale Beck reached 13.9 kg/d, with the Level 1 point source representing only 26% of this total (3.65 kg/d).

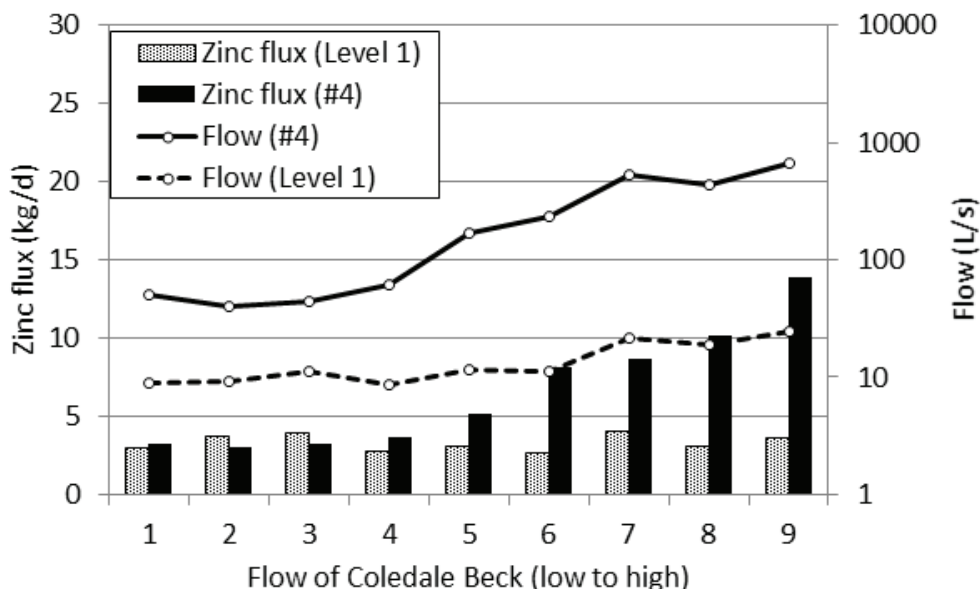


Figure 1 Zinc flux of the major point source (Level 1) of pollution to the Coledale Beck and the Coledale Beck itself (site ID #4), as a function of flow-rate in the Beck (Flow on monitoring event 1 was 111 L/s and on monitoring event 9 it was 1487 L/s).



From these data it is possible to calculate the improvements in water quality arising from treatment of the major point source of pollution, Level 1. Under low flow conditions in the Coledale Beck more a substantial reduction in Zn concentration in the Beck should be feasible (over 90% reduction). However, as flow-rate in the Beck increases, and diffuse pollution sources such as waste rock runoff and groundwater inputs increase in importance, the benefits of treatment diminish; at the highest flow rates point source treatment is predicted to result in Zn concentration reductions in the river of less than 20%.

River Nent: There are four major point source mine water discharges to the upper River Nent: Rampgill, Capelcleugh, Haggs and Croft. The Haggs and Capelcleugh discharges are the most important point sources of pollution to the River Nent in terms of Zn pollution (the Haggs flux is shown on Figure 2). The Capelcleugh discharge is the most important source of Cd and Ni, and the Haggs discharge is the second most important. Point mine water discharges are of limited signifi-

cance as sources of Pb pollution to the River Nent.

For the range of flow conditions monitored during this investigation the point sources of mine water pollution were responsible for between 37% (at higher flow conditions) and 85% (at lowest flow conditions) of the filtered Zn flux of the River Nent downstream (Zn is predominantly present in its filtered form; Figure 2). The Haggs and Capelcleugh discharges are the most important contributors of Zn (and Cd and Ni); the Haggs discharge accounted for between 14% (at higher flow conditions) and 33% (at lowest flow conditions) of the Zn flux of the River Nent during this investigation, and equivalent figures for the Capelcleugh discharge were 14% and 34% for higher and lower flow conditions respectively (Figure 2). Mass balance calculations suggest that treatment of either of these discharges (to remove 90% of the Zn) would lower Zn concentrations in the River Nent by between approximately 15 – 30%. Equivalent calculations for the Rampgill and Croft discharges suggest that Zn concentrations in the River Nent would be lowered by

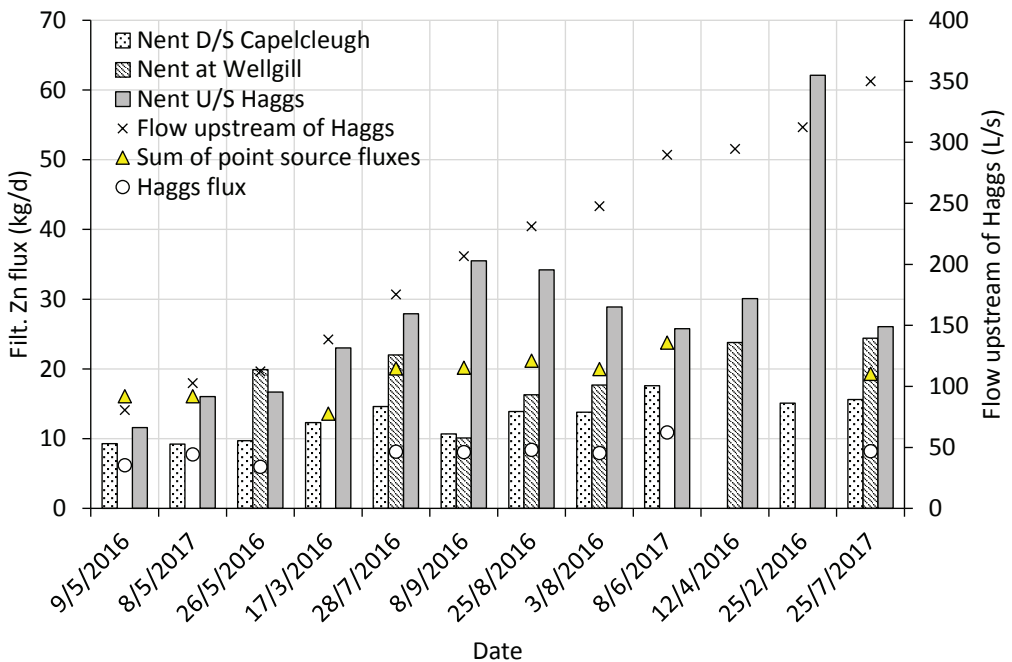


Figure 2 Filtered zinc ($< 0.45 \mu\text{m}$) flux of point sources and in-stream locations on the River Nent, as a function of flow-rate in the river



no more than 10% and 5% respectively. These figures are likely to be best case scenario. This is because the flow conditions in the River Nent during the investigation were not particularly high; at higher River Nent flow-rates the benefits of point source treatment are likely to be less, due to the increasing importance of diffuse source pollution during such hydrological conditions.

Even under the relatively low flow conditions during this investigation diffuse metals pollution has been shown to be significant in the River Nent catchment. As has been found elsewhere, diffuse pollution becomes more important at higher flows. It is difficult to be certain, but it appears as though direct inputs of polluted groundwater may be the most important source of diffuse metals pollution in the study reach of the River Nent.

River Tyne: The Zn flux from the River Nent (above) discharges to the River Tyne. For the data presented here, at its highest the flux from the River Nent is a little over 60 kg Zn/d (Figure 2). However, even though the River Nent is the most important source of metals to the River Tyne, the zinc flux from it is minor

compared to that in the lower reaches of the River Tyne, which at the highest flows recorded exceed 15 000 kg/d (Figure 3). What is notable from Figure 3 is that above a flow-rate of around 300 L/s particulate Zn (i.e. associated with suspended sediment) begins to dominate the total flux of metal. Metal-polluted waste rock and sediments are distributed throughout the River Tyne catchment, in the river itself, in river bank materials, and on floodplains. Although filtered Zn concentrations increase somewhat as flows increase, the very highest fluxes are a consequence of resuspension and transport of the finer, metal-polluted, sediments in the lower-lying reaches of this mature river. This is in contrast to the Coledale Beck and River Nent, in which the Zn flux is dominated by filterable metal in all but the very highest flow conditions (not recorded here). This point is shown in Figure 4, which shows that on all but one occasion ($n = 17$) more than 90% of Zn was present in its filterable ($< 0.45 \mu\text{m}$) form. Thus, the form of the diffuse Zn in the lower lying River Tyne contrasts with its form in the more juvenile, up-land rivers which have far less fine particulate matter (silts and sands).

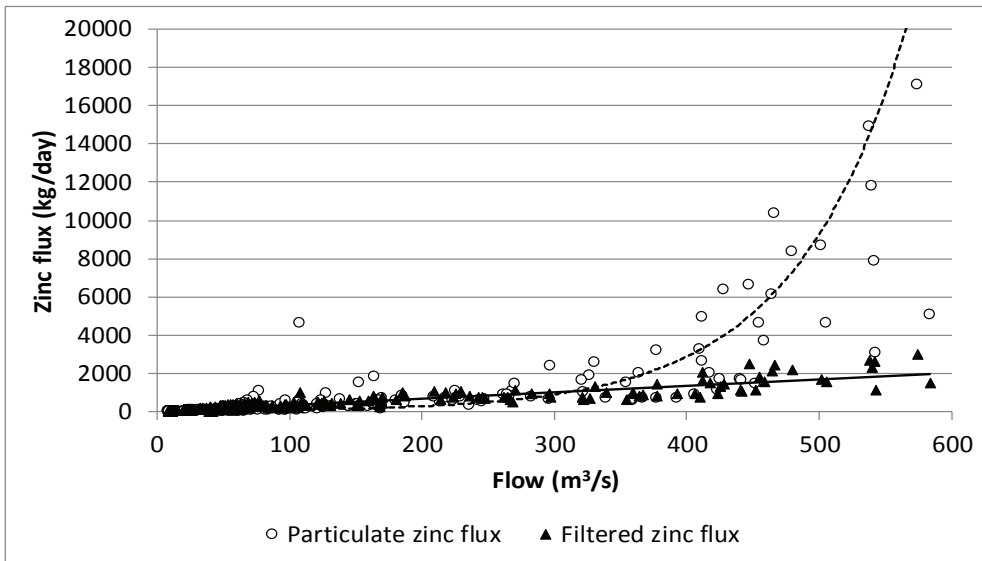


Figure 3 Particulate and filtered zinc flux in the River Tyne under varying hydrological conditions



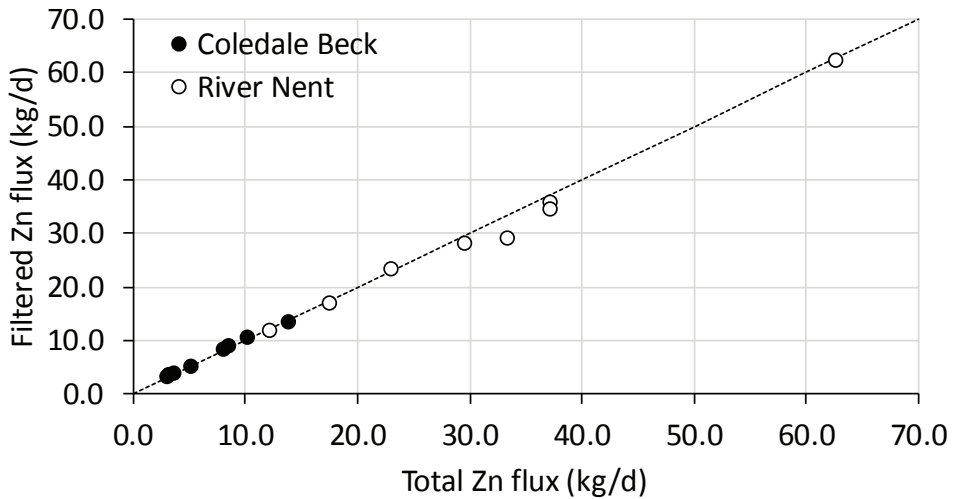


Figure 4 Total and filtered zinc concentrations in the Coledale Beck and River Nent, Cumbria, illustrating that zinc is primarily present in filterable ($< 0.45 \mu\text{m}$) form

Data in Figures 3 and 4 suggest that point source remedial interventions in the River Nent are unlikely to result in any substantive reduction of Zn flux in the lower reaches of the River Tyne. However, two points need to be borne in mind:

- 1) Zn in point sources of pollution on the River Nent may be held in transient storage in finer sediments downstream (in the River Tyne), and therefore effectively act as a diffuse source when they are remobilised during higher flow events i.e. contribute to the particulate Zn flux shown in Figure 4.
- 2) Monitoring exercises such as those described here fail to quantify metal flux transported as bed load (via traction and saltation), which may become important sources of pollutants in the water column following erosion.

Therefore remedial interventions for point sources of pollution may in fact result in somewhat greater benefits than implied by Figures 3 and 4 alone.

Conclusions

The results of investigations of the importance of diffuse abandoned mine pollution in three contrasting watersheds are considered. In the upland catchments of the Coledale Beck and River Nent point source pollution is key to in-stream metal flux at low flow conditions.

However, at higher river flows diffuse pollution sources become increasingly important. Under such conditions diffuse sources, such as groundwater inputs and waste rock runoff, start to dominate metal flux. Consequently the potential benefits of point source remediation diminish substantially under such hydrological conditions. In the large, lower-lying, River Tyne catchment (downstream from the River Nent) very high zinc fluxes are evident at higher flows. In contrast to the upland river systems, here it is particulate zinc that is a key contributor to the absolute flux, which in essence reflects the long term impacts of widespread historic mining pollution. As point source pollution remediation initiatives become more widespread in the UK, diffuse sources of abandoned metal mine pollution will increasingly become the limiting factor to further improvements in water quality.

Acknowledgements

The work reported here has been funded by a variety of organisations, including the UK Government Department for Food and Rural Affairs (Defra), Environment Agency (England & Wales), Port of Tyne, Newcastle City Council and the UK Coal Authority. We are indebted to the national Trust, owner of the Force Crag mine, for allowing access and providing background information (Mr John Malley in particular). The views expressed are those of the authors and not necessarily the



Environment Agency, or any other organisation mentioned herein.

References

Herschy, R.W. (1998) *Hydrometry: Principles and Practices* (2nd Edition). Wiley: Chichester, England.

Mayes, WM, Potter, HAB, Jarvis, AP (2010) Inventory of aquatic contaminant flux arising from histor-

ical metal mining in England and Wales. *Science of the Total Environment*, 408(17), 3576 - 3583.

Mighanetara, K, Braungardt, CB, Rieuwerts, JS, Azizi, F (2009) Contaminant fluxes from point and diffuse sources from abandoned mines in the River Tamar catchment, UK. *Journal of Geochemical Exploration*, 100(2-3), 116 - 124.

Postlethwaite, J (1913) *Mines and Mining in the Lake District*. W. H. Moses & Sons Ltd: Whitehaven, UK.



Water management at the former uranium production tailings pond Helmsdorf

J. Laubrich¹, R. Rosemann¹, J. Meyer², A. Kassahun²

Wismut GmbH, ¹water treatment systems Ronneburg, ²water management division, Chemnitz

Abstract

Remediation of the tailings pond Helmsdorf, the second largest tailings management facility (TMF) from former East German uranium production, is a major project of Wismut GmbH. The remediation strategy consists in dry stabilization, soil covering and dams reshaping for long-term stability. It allows free discharge of surface water and seepage water collection for treatment. Water management has played a key role for the progress of remediation right from the beginning.

In 1995 a newly-built water treatment plant (WTP) started running to clean up the pond and seepage water prior to its discharge (main contaminants: As, U, Ra-226). During operation of the WTP, the technology has been modified several times for different reasons: changes in water quality and pollutant speciation, economic reasons, adaption to changes in water catchment. All of these modifications and measures for maintenance had to be managed while water treatment was running continuously.

To prepare for a future long-term water treatment focusing on seepage cleanup only, several treatment technologies were examined. The site specific performance of the most favourable technology – ion exchange in combination with adsorption – was tested in a pilot plant. In addition, hydrological estimations were made to evaluate the amount of contaminated seepage water after final coverage. On this basis, a new WTP is currently planned. Water treatment will be performed by that new WTP from 2020 onwards.

Keywords: TMF, uranium, arsenic, radium, water treatment, operational technology modifications

Introduction

Remediation of the tailings pond Helmsdorf, the second largest tailings management facility (TMF) from former East German uranium production, is a major project of Wismut GmbH.

The Helmsdorf tailings management facility was established by the damming of two valley locations. It was operated from 1958 to the shut-down of ore processing in 1989. Some data on the starting conditions of remediation are given in table 1.

The remediation strategy is:

Removal of pond water, followed by interim covering, dewatering, contouring and final covering of the tailings; vegetating for erosion protection and afforestation of covered tailings areas.

Water management has played a key role

for the progress of remediation right from the beginning.

Its task was to create the conditions for further cover of tailings and avoid the outflow of seepage water from the dams into natural water bodies. In our understanding, water management consists of

- catchment of contaminated water,
- water treatment and
- discharge of uncontaminated water to receiving waters.

The three key aspects of water management are interconnected and influenced by the remediation process. The focus of this paper is on water treatment and its operational modification.

Water drainage and treatment causes about 22% of the overall operational site remediation cost of ~130 million €.



Table 1. starting conditions for water management and remediation

Tailings area	ha	200
Water cover	ha	116
Volume supernatant water (pond water)	Mm ³	5
Maximum tailings thickness	m	55
Maximum water depth	m	14
Pond water concentration of U	mg/L	6.5
Pond water concentration of As	mg/L	120
Pond water concentration of Ra-226	mBq/L	800
Pond water concentration of SO ₄	g/L	6
Pond water concentration CO ₃ /HCO ₃	g/L	5
Pond water pH		9

Water treatment during remediation

Two different technologies have been used since starting water treatment. From 1995 until 2003, ion exchange in combination with flotation was applied. Since the reconstruction of the WTP in 2003, lime precipitation has been used. (see figure 1). Until now, nearly 26 million m³ of contaminated water were treated (50 % cleaned up by ion exchange/flotation and 50 % by advanced lime precipitation).

The following aspects required operational modifications in the water treatment process:

- Changes in water quality by natural processes
- Increasing turbidity of the contaminated water
- Changes in water drainage regime
- Cost optimizations
- Progress in site remediation

Changes in water quality

The pond water was characterized by very low nutrient concentrations except for phosphate. Nevertheless, the C:N:P ratios resulted in the occasional growth of algae in the summer periods. The elevated summer concentrations of algae strongly affected ion exchange in the water treatment. It led to coatings on the exchange resin and resin washing had to be performed more frequently. The lime precipitation technology is much more robust in this respect. However, high algae concentrations lead to a rise in chemical oxygen demand (COD), which is a regulatory monitoring value as well. Experiments with special activated carbon and the addition of oxidation agents did not show any effect on COD. In this case,

we were successful in reaching an arrangement with our national authorities allowing for higher discharge limits (30 → 80 mg/l).

Algae growth moreover led to the formation of a layer of dead organic material with a thickness of maximum 1 m on the tailings pond surface. Thereby a reduction zone developed in deeper pond zones and arsenate ions were reduced to arsenite ions. The remaining arsenic effluent concentrations after treatment were in accordance with regulatory limits but, nevertheless, led to higher fish toxicity in the receiving waters. Therefore, a simple air oxidation step was added. After 2004, aeration was replaced by pre-oxidation in the stripping columns.

Changes in water drainage regime

The pond water concentrations were reduced stepwise by rainfall dilution whereas the seepage concentrations stayed on a higher level. Since the year 2012, the former pond water was eliminated nearly completely. Only the deepest point of the tailings pond got regularly refilled after heavier rainfalls. To ensure an ongoing remediation in the central (deepest) area of the tailings pond, a separate storage and homogenization pool (SHP) was built (volume 40,000 m³). By pumping the pond water to the storage pool, the deepest areas of the pond could be kept dry without reaching the capacity limits of the WTP.

The seepage water generally showed a higher concentration than the pond water body or the water in the storage pool. With a decreasing inflow of uncontaminated waters to the pond / pool, the characteristics of surface and seepage waters were converging. Especially in dry periods the concentrations



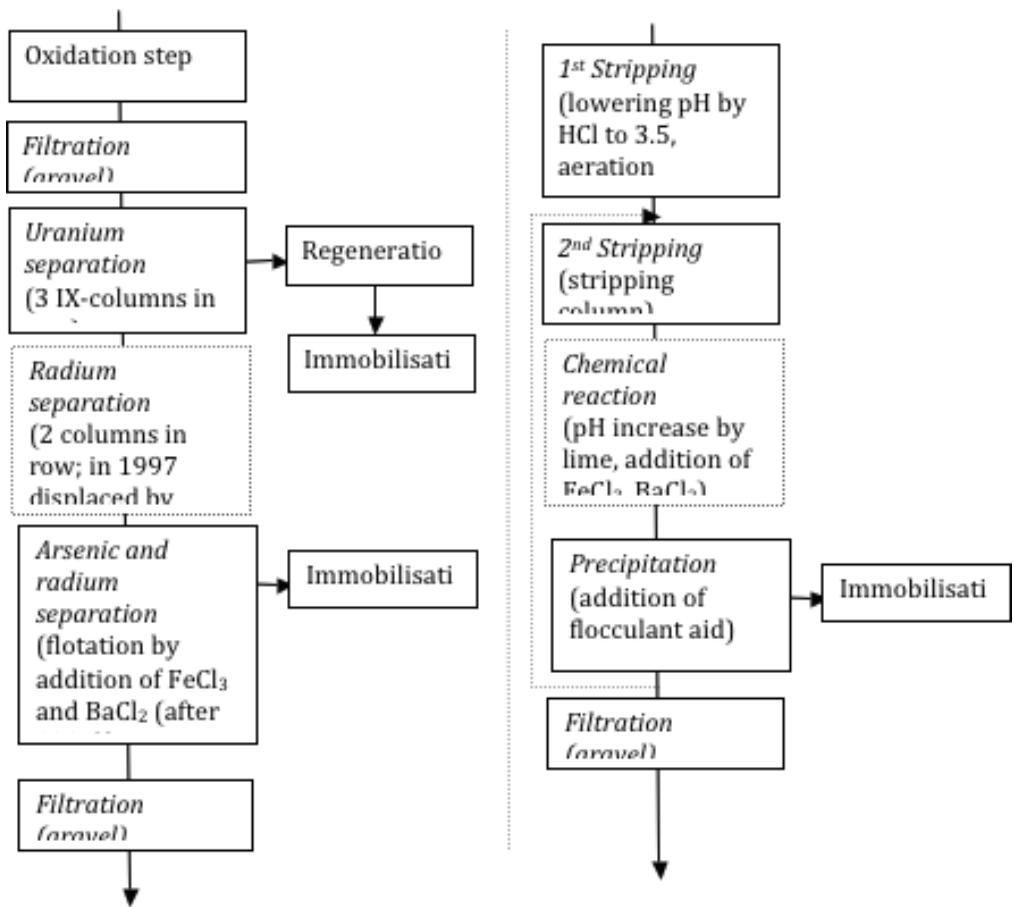


Figure 1 Technological schemes of water treatment at Helmsdorf site (left: 1995 -2003, right: 2003 – now)

in the SHP rose continuously. These elevated pollutant concentrations did not allow to operate the WTP at its maximum capacity. Recirculation of treated water became necessary in order to stabilise the separation of uranium. About 50 % – 60 % of the treated water had to be recirculated. The maximum throughput dropped to 60 m³/h.

To prevent calcination in parts of the pipeline system, anti-scaling agents are applied. Prior to the addition of the anti-scaling agent, possible effects of these chemicals on the water treatment process were checked in lab studies.

Turbidity

To enforce subaquatic consolidation in the tailings, the tailings pond bottom was covered with dump material, which was dropped

from ships. The dumping of the gravel-like material led to an increase in turbidity in the pond water. This was critical to the ion exchange operation. The exchange columns were blocked by the suspended particles, leading to the necessity of weekly resin washing.

The wash-out of soil from the tailings cover after heavy rainfall can cause problems in the lime precipitation technology as well. In most cases, the sedimentation in the SHP was enough to settle the suspended solids. But in some rare cases, the fine soil particles almost led to an overloading of the sedimentation basin in the water treatment plant. The only possible and fast reaction was the reduction of the throughput. In the long term, the fast grassing of the final tailings cover is the best choice.



Remediation process

As shown in figure 3, the maximum water treatment capacity was never used. To expect 100 % use of capacity is obviously not realistic. Experience from other treatment plants shows that 90 – 95 % of the maximum capacity is reachable. During the first operation period (1995 – 2003), the mentioned problems (algae, turbidity, other technical problems) led to the insufficient use of the capacity. From 2004 – 2010, the throughput was limited by radiation protection regulations. The area of uncovered tailings (distance between the water line of the pond water and areas covered with geotextiles only) was not allowed to be wider than 15 m in order to prevent dust abrasion. After decreasing the water level, the free tailings sludge had to be consolidated for several weeks until it became passable.

Cost optimizations

The first WTP consisted of two separate lines for residue immobilisation (one for arsenic and radium residues and one for uranium containing residues). The two different immobilisation lines were cost intensive. With the decision, that a further use of the uranium immobilisation product will not be feasible, the purpose of its separate immobilisation got lost. Facing the technical problems and in order to reduce the water treatment costs, the WTP was reconstructed in 2003. The technology was changed to lime precipitation.

After finishing of the pond water in 2012, the treatment capacity of 200 m³/h was no longer necessary. Instead of operating the plant continuously with a low throughput, campaign operation was established after 2012. With some technical improvements it became possible to work in campaigns in

winter, too. At the moment the plant operates one week and pauses for two weeks. Nevertheless, the oversized plant works quite uneconomically at the moment.

Long-term water treatment

Water treatment will be needed for at least 30 years after finishing the tailings remediation. Seepage waters from the dams will be the main sources of contaminated water. Effects linked to the pond water body (like increased turbidity or algae growth) will not occur anymore.

The first investigations in a long-term treatment technology started in 2006. At that time, the application of biological processes was seen as a favourable technology. However, experiments on uranium removal by bacteria or algae characeen showed insufficient results at the Helmsdorf site. Similar experiments and a long-term test of a wetland on other Wismut remediation sites failed as well. Therefore, wetlands and biological driven processes were excluded from further considerations on long-term water treatment in Helmsdorf. Both lime precipitation and the combination of ion exchange and adsorption technology were pointed out in a first feasibility study on long-term treatment at the site. Cost calculations for these two technologies showed economic benefits for a centralized treatment. On the basis of these first evaluations a pilot plant was built to test the combination of ion exchange and adsorbent technology on site. Results of complementary lab experiments on retention mechanisms [kassahun] were used to optimize the pilot experiments and significantly improved the resins uranium load capacity.



Figure 2 Tailings pond Helmsdorf in 1991 (left) and 2014 (right)



Table 2. Cost drivers of two different possible technologies for long term water treatment

Test #	Test pH	Advanced lime precipitation	ion exchange/adsorption technology
Chemicals	HCl	1491 t/a	419 t/a
	CaO	42 t/a	-
	FeCl ₃	111 t/a	-
	BaCl ₂	3 t/a	-
	cement	94 t/a	60 t/a
	Adsorbents	-	165 t/a
Power consumption		602 MWh	398 MWh
operators		5 h/d	1,5 h/d
Number of Technical devices (pumps, stirrers)		55	29

On the basis of long lasting monitoring data on seepage water quantity and quality predictions on further water treatment needs were made. Feasibility evaluation of the selected treatment technologies included auxiliary aspects like

- waste management
- use of different adsorbents and resin types (availability, supplier independence)
- influence of anti-scaling agents

By a seven years period of pilot plant testing, the stability of the ion exchange / adsorption technology was proven. The pilot plant data were used as input for further technical planning. Another effect was that personnel training on a new technology were performed by the pilot plant operation. Based on the convincing results, costs for a period of 30 years were calculated and compared to lime precipitation costs. There is a cost advantage for the ion exchange/adsorption technology. At least for the specific situation at Helmsdorf site the ion exchange/adsorption technology is linked to lower risks than the lime precipitation technology (increasing prices for chemicals, power consumption and technical failures). Table 2 compares different cost drivers of the two technologies.

On this basis, a new ion exchange / adsorption technology WTP is currently at the planning stage. The new WTP will operate from 2020 onwards. Unlike the existing WTP, the new plant will be remote-controlled from a WTP which is about 30 km away.

Acknowledgements

The site remediation activities are part of the Wismut mining and environmental rehabilitation project. It is financed by the Federal Government of Germany. The project's success is based on the work of many colleagues, external contractors and local authorities.. We wish to thank all those who contributed with their excellent expertise and cooperation.

References

- [kassahun] KASSAHUN, A., LAUBRICH, J., PAUL, M. (2016): Feasibility study on seepage water treatment at a uranium TMF site by ion exchange and ferric hydroxide adsorption, in: DREBENSTEDT, C., PAUL, M. (EDS.): IMWA 2016 – Mining Meets Water – Conflicts and Solutions, TU Bergakademie Freiberg, 858 (www.imwa.info)



Hydrochemical characterisation of mine drainage discharging into the UNESCO Fossil Hominid Site of South Africa

Chazanne Long^{1,2}, Maarten de Wit², Henk Coetzee³

¹Sci-Ba, 601 Salga House, 5 Waterkant Street, Cape Town, 8000, South Africa, chazanne@sci-ba.co.za

²AEON, Faculty of Science, Nelson Mandela University, 6031, South Africa

³Council for Geoscience, 280 Pretoria Street, Silverton, Pretoria, 0184, South Africa

Abstract

Mine drainage affects waters locally and regionally and can have far reaching environmental and economic impacts. Therefore, it is important to be able to quantify the changes in hydrochemistry and to be able to measure the extent of the impacts of mine waters to be able to assess when mitigation steps need to be taken, and to decide on the best methods of mitigation and remediation based on scientific baseline studies.

We present findings from a study area that extends from the West Rand Goldfield of the Witwatersrand, South Africa, to Hartbeespoort Dam in the North and that encloses protected national spaces, including the internationally recognised UNESCO site known as the Fossil Hominid Site of South Africa (FHSa), locally referred to as the Cradle of Humankind World Heritage Site (COH WHS).

The research results highlight a need for further investigations to provide realistic solutions that can be implemented to mitigate potential negative outcomes that mine drainage discharges have on the environment and economy, in-line with national and global legislation to preserve and protect world heritage areas. The findings have implications for mine water legislation and monitoring in areas of active and historic mining, and for water resource management, in particular where UNESCO sites are located.

Keywords: ICARD, IMWA, Hydrochemistry, mine water, acid mine drainage, gold mining, West Rand, Witwatersrand, Crocodile River, Cradle of Humankind World Heritage Site, Fossil Hominid Site of South Africa, UNESCO.

Introduction

Mine waters exhibit a range of pH and dissolved solutes, where waters with pH less than 6 are referred to as acid mine drainage (AMD), and waters with pH greater than 6 are classified as saline drainage (SD) or neutral mine drainage (NMD) depending on the concentration of dissolved solutes (Ficklin et al., 1992; Verburg et al., 2009).

Gold mining in the Witwatersrand Goldfield started in 1886 and over 130 years of mining history, more than 150 mining companies have mined gold from the Witwatersrand Goldfield (McCarthy, 2006, 2010). The Witwatersrand collectively hosts the world's largest gold deposits and gold mining across the Witwatersrand has shaped the South African economy (McCarthy, 2010; Durand, 2012). Gold mining has also left many mine shafts and tunnels across the

Witwatersrand exposed to air and water so that oxidation and secondary mineralisation along the wall rock has been allowed develop over many decades. Although there is not connectivity between the various Goldfields of the Witwatersrand, there is connectivity within a single Witwatersrand Goldfield (e.g. the West Rand Goldfield). Gold ore deposits in the West Rand Goldfield were the first to become uneconomic to mine and the mining companies in this goldfield ceased underground mining operations and groundwater pumping in 1998. The mine void space was allowed to completely flood, and as the groundwater levels rebounded, reactions between the water with primary sulfide and secondary minerals in the presence of air formed an acidic mine drainage, that has been permitted to reach the ground surface in 2002 (Hobbs and Cobbing, 2007).



it was reported that the Tweelopie Spruit had been transformed from a non-perennial to a perennial river (Hobbs and Cobbing, 2007). The acidic mine drainage has continued to discharge into the Tweelopie Spruit for a further five years, as observed during this study in 2011-2012.

Water resources and water quality are important economic and social drivers necessary to sustain and develop the economy, and meet the supply demands for residential, health, environmental and cultural uses of a population (Price, 2003; Hobbs and Cobbing, 2007; McCarthy, 2010).

Increased solute loads in surface waters, coupled with increased precipitation of ‘yellow boy’, or ochre, downstream from the mines presents environmental consequences that modify channel stability, channel width and bank morphology. This affects the ecosystems and agricultural land use immediately adjacent to the river e.g. cultivation of crops, water abstraction and recreational activities (Goudie and Viles, 2016). River bed armouring from the precipitation of ‘yellow boy’ may influence infiltration rates and aquifer recharge downstream of mines (Goudie and Viles, 2016).

The UNESCO site known as the Fossil Hominid Site of South Africa (FHSaSA) is locally referred to as the Cradle of Humankind World Heritage Site (COH WHS), is located approximately 10 km north east of the West Rand Goldfield (Figure 1). Only one of the four mine properties that make up the West Rand Goldfield drains northward, while the other three collectively drain south westward into the Vaal River catchment. All mine drainage received by the downstream UNESCO site is therefore contributed from Randfontein Estates mine property only.

The UNESCO site is a globally important cultural heritage area that hosts some of the oldest discovered hominid fossils and is a major contributor to our understanding of the evolution of modern hominids over the past 3.5 million years. The COH WHS hosts many fossiliferous sites, including the famous Sterkfontein caves where “Mr Ples” was discovered (Hobbs and Cobbing, 2007; Unesco, 2015; Maropeng - Official Visitor Centre, 2018; Tawane and Thackeray, 2018).

This study characterises the West Rand mine drainage to define the chemistry of the mine drainage and to determine the extent of the hydrochemical interaction within the UNESCO cultural site and beyond.

Methodology

36 locations were sampled, collected quarterly for an annual cycle during 2011/2012. Physical parameters pH, EC and temperature were recorded in the field, and samples were analysed by IC and q-ICP-MS techniques.

Median values were used to determine the hydrochemistry of surface waters across the sub-catchment draining the West Rand, using two available mine discharge classification schemes, namely the Global Acid Rock Drainage Guide (Verburg et al., 2009) and the deposit-based classification developed by the USGS (Ficklin et al., 1992; Plumlee et al., 1999). This is the first time this type of quantitative and comparative study has been performed in South Africa.

Data are described and compared with other published datasets. Surface waters are classified according to existing classification systems for mine waters, followed by the characterisation of a ‘West Rand highly metalliferous AMD signature’ (WR AMD) and a ‘baseline signature’ for the study area. The quantity of acid and metals in mine waters are presented here.

To identify and characterise the baseline signature for river water in the study area, data for each sample collected for the baseline rivers for the duration of the sampling period were plotted on GARD sulfate vs pH and Ficklin Σ Metals vs pH. Based on these figures, there exists a cluster of rivers with hydrochemistry defined with a pH greater than 6.2, sulfate concentrations less than 50 mg/L and Σ Metals < 201 μ g/L. This cluster defines the baseline hydrochemistry signature for the study area during the sampling period.

Results and Discussion

Binary mixing curves were calculated between the average baseline and the ‘WR AMD’ signature (the first water sample taken outside of the Randfontein Estates Mine Property). This allows quantification of the WR AMD component at various points downstream of the point source to be quantified (Fig 2).



Trends associated with precipitation between Randfontein Estates Mine Property and the exit of the Tweeloeie Spruit from the Krugersdorp Game Reserve plots sub-parallel to the binary mixing curve, whereas CA07 and downstream of this location within the COH WHS plot away from the mixing curve. This indicates that a more complex set of processes is occurring within the COH WHS other than mixing of two end-member compositions. The mine drainage component at CA19 is quantified at ~75% which confirms that only a small reduction in the AMD signature occurs between Randfontein Estates Mine Property and the entry into the COH WHS (a length of 10.4 km). Yet there exists only an ~10% mine drainage signature at CA07 (adjacent to the Sterkfontein Caves), which is offset to the mixing curve. This indicates that within the first 2.2 km of entry into the COH WHS there is a ~65% decrease in the AMD signature.

The mine drainage signature is observable between sampling position CA09 and CA24 (a maximum distance of 54.2 km from source) according to the sulfate concentrations which are persistent (Figure 2), whereas the mine drainage signature is observable until CA07 (12.6 km from source) according to Σ Metals (Figure 2).

Conclusions

The results of this work with the use of these classifications shows that the mine drainage generated from the WR AMD can be described as an acidic (pH = 3.19 to 3.36), highly metalliferous (Σ Metals = 2564 to 3141 $\mu\text{g/L}$) mine drainage, and with (SO_4^{2-} = 3217 to 3532 mg/L). This mine drainage has been allowed to discharge continuously into the environment for the past sixteen years following the flooding of mine voids in the West Rand Goldfield. The results confirm that the WR AMD signature is traceable through the

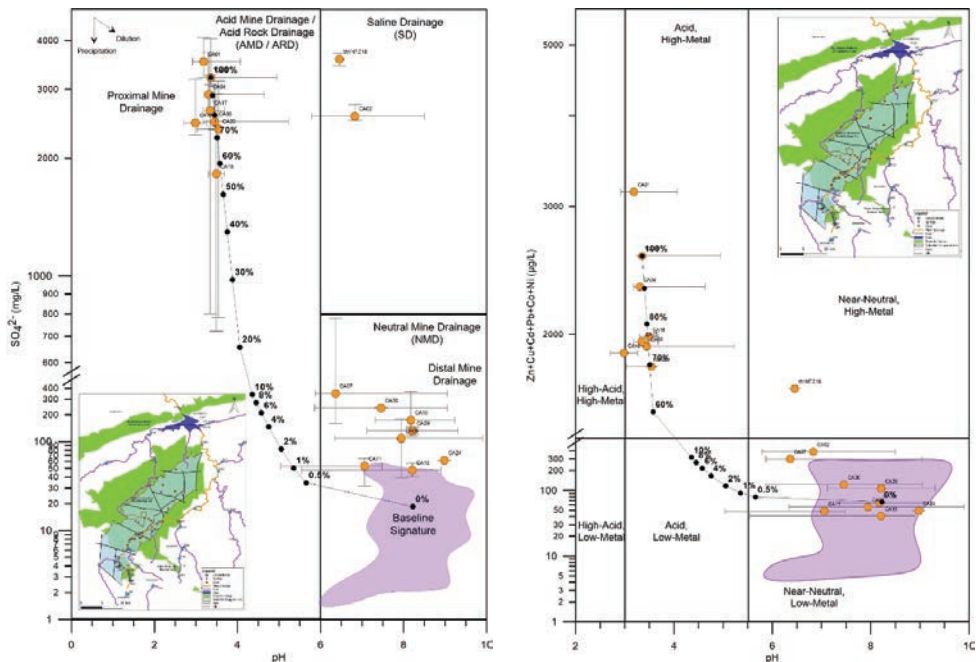


Figure 2: 2a (GARD Classification showing SO_4^{2-} vs pH load evolution of the main tributary from its source in the West Rand to the outlet with Hartbeespoort Dam, map shown in inset. Binary mixing curve superimposed between the AMD point source (CA03) and an average baseline signature composition, see map shown in inset.) 2b (Ficklin Classification showing Σ Metals vs pH load evolution of the main tributary from its source in the West Rand to the outlet with Hartbeespoort Dam, map shown in inset. Binary mixing curve superimposed between the AMD point source (CA03) and an average baseline signature composition, see map shown in inset.)



COH WHS with a maximum of up to 54 km (based on sulphate that persistently remains in the dissolved phase) downstream of the Randfontein Estate Mine Property, which is the sole source of mine discharge to the area. In addition to the surficial contamination, there is evidence of groundwater – surface water interactions within the karstic terrain of the UNESCO FHSa mostly from recorded evidence of previously non-perennial rivers becoming perennial rivers.

The findings highlight the need for mitigation of WR AMD discharge into the environment and appropriate remediation to be performed along the affected river courses. On-going monitoring and further research is needed to determine the possible consequences that the WR AMD discharge has on the environment and on yet undiscovered fossils within the cave systems of the karstic UNESCO cultural site. Research is needed to provide realistic solutions that can be implemented to mitigate potential negative outcomes identified and that are in-line with national and global legislation to preserve and protect this world heritage area.

Acknowledgements

The authors thank AEON for providing funding, and Council for Geoscience for access to their chemical laboratory facilities. This is AEON contribution number 176 and Iphakade 187.

References

- Durand, J. F. (2012) ‘The impact of gold mining on the Witwatersrand on the rivers and karst system of Gauteng and North West Province, South Africa,’ *Journal of African Earth Sciences*, 68, pp. 24–43. doi: 10.1016/j.jafrearsci.2012.03.013.
- Ficklin, W. H. et al. (1992) ‘Geochemical classification of mine drainages and natural drainages in mineralized areas,’ *Proceedings of the 7th International Symposium on Water–Rock Interaction*, pp. 381–384.
- Goudie, A. S. and Viles, H. A. (2016) *Geomorphology in the Anthropocene*. Cambridge: Cambridge University Press. doi: 10.1017/CBO9781316498910.
- Hobbs, P. J. and Cobbing, J. (2007) *A Hydrogeological Assessment of Acid Mine Drainage Impacts in the West Rand Basin, Gauteng Province, Assessment*. Pretoria: Centre for Scientific and Industrial Research (CSIR). doi: Report no. CSIR/NRE/WR/ER/2007/0097/C. CSIR/THRIP.
- Maropeng - Official Visitor Centre (2018) Explore the Sterkfontein Caves. Available at: <http://www.maropeng.co.za/content/page/explore-the-caves> (Accessed: 27 December 2017).
- McCarthy, T. S. (2006) ‘The Witwatersrand Supergroup’, in Johnson, M. R., Anhaeusser, C. R., and Thomas, R. J. (eds) *The Geology of South Africa*. Pretoria Johannesburg: Council for Geoscience Geological Society of South Africa, pp. 155–186.
- McCarthy, T. S. (2010) *The decanting of acid mine water in the Gauteng city-region: Analysis, prognosis and solutions*. 1st edn. Johannesburg: Gauteng City-Region Observatory.
- Plumlee, G. S. et al. (1999) ‘Geologic controls on the composition of natural waters and mine waters draining diverse mineral-deposit types’, in *The environmental geology of mineral deposits*. 1st edn. Denver: Society of Economic geologists, pp. 373–432.
- Price, W. A. (2003) ‘Challenges posed by metal leaching and acid rock drainage, and approaches used to address them’, *Environmental Aspects of Mine Wastes*, 31, pp. 1–10.
- Tawane, G. M. and Thackeray, J. F. (2018) ‘The cranium of Sts 5 (“Mrs Ples”) in relation to sexual dimorphism of *Australopithecus Africanus*’, *South African Journal of Science*, 114(1–2), pp. 12–19. doi: 10.17159/sajs.2018/a0249.
- Unesco.org (2015) Fossil Hominid Sites of South Africa. Available at: <http://whc.unesco.org/en/list/915> (Accessed: 1 December 2017).
- Verburg, R. et al. (2009) ‘The global acid rock drainage guide (GARD Guide)’, *Mine Water and the Environment*, 28(4), pp. 305–310. doi: 10.1007/s10230-009-0078-4.



Source Apportionment of Trace Metals Over a Range of Stream Flows Using a Multi-method Tracer Approach

Patrizia Onnis¹, Patrick Byrne¹, Karen A. Hudson-Edwards², Tim Stott¹, Christopher Hunt¹

¹*Liverpool John Moores University, Natural Science and Psychology, Liverpool L3 3AF, UK*

²*Environment & Sustainability Institute and Camborne School of Mines and, University of Exeter, Penryn, TR10 9DF, UK*

Abstract

Pollution from abandoned mines is a major cause of environmental legislation failure. Remediation of mining-impacted river catchments must be underpinned by detailed and catchment-scale data that includes loading assessments over a range of stream-flow. In this study, a constant injection tracer coupled with synoptic sampling allowed quantification of main Zn sources along a polluted UK river. Downstream of the mine workings, Zn load changes were measured under a range of flows. Our data highlight the variability of Zn dispersion in response to different streamflows. We emphasise the necessity of using a multi-tracer approach for assessing spatial and temporal metal distribution.

Keywords: multi tracer approach, metal mine waste, contaminated catchment, trace metals, hydrological variations

Introduction

Identifying and quantifying sources of mine waste in river catchments is confounded by the extensive nature of historical mining operations that have generally resulted in multiple potential sources of mine pollution across a catchment that can vary in importance as a function of hydro-meteorological conditions (Cánovas et al. 2010). The tracer injection and synoptic sampling approach, developed by the U.S. Geological Survey (Kimball et al. 2002), provided a framework to develop spatially detailed assessments of pollutant concentrations and loads to enable effective remediation. However, changes in loads and sources can occur especially during rainfall-runoff events and this is particularly problematic in temperate climates like the UK (Jarvis and Mayes 2012, Byrne et al. 2013). Here, we propose a development of this approach that provides a means to supplement spatial variation with temporal variability by integrating the tracer results with slug load estimations. The specific aim of this work was to develop a low cost and effective methodology for capturing metal load variation and to provide better advice for long-lasting remediation strategies.

Study Area and Methods

Wemyss and Graig Goch mines (central Wales, UK) were exploited for Zn and Pb sulfide ores until the beginning of the 20th century. Numerous potential point and diffuse sources of contamination are present in this catchment that cause downstream water quality to be classified as 'poor' by the European Union Water Framework Directive standards, due to their elevated Pb, Zn and Cu concentrations. These mines are drained by Nant Cwmnewyddion (fig.1) which flows eastwards into the Afton Ystwyth. Drainage from Frongoch mine emerges into the Nant Cwmnewyddion via the Frongoch Adit (F.A. in fig.1) and represents a major point source of metal contamination. Potential diffuse sources are present as waste heaps at various locations along the Nant Cwmnewyddion.

Assessment of spatial load variations

Metal loadings were established at 24 sites along a 2 km reach of the upper catchment using the tracer injection and synoptic sampling approach (Runkel et al. 2013). The major advantages of this approach over traditional methods (e.g. the velocity-area approach) for streamflow and metal loading estimation are



improved accuracy and spatial coverage, and the potential to use the synoptic data for pre-mining water quality modelling and remediation modelling (Byrne et al. 2017). In July 2016 a solution of sodium bromide, with bromide (Br) concentration of 69 g/l, was injected into Nant Cwmnewyddion above the mine workings at an average rate of 195 ml/min for 31 hrs. No rain occurred during the tracer injection time. Synoptic sampling was undertaken when Br plateau concentrations were reached and proceeded from downstream to upstream. Samples were collected at stream sites and all visible inflows. Distances along the river are hereafter indicated as metric distances from the tracer injection site. Streamflow was calculated at each synoptic site by dividing the product of injection parameters (injectate discharge and Br concentration) by the sample site Br concentration (Kimball et al. 2002). Zn metal loads were calculated as the product of streamflow and Zn concentration. Source apportionment of Zn mass was conducted by comparing total Zn loads to cumulative Zn loads. Results of this experiment are referred as “flow 2” results throughout the text.

Zn load and streamflow variations

Three sites, upstream Wemyss Mine (W.M., 56 m), downstream Frongoch adit (F.A., 880 m) and Graig Goch Mine (G.G., 1645 m) were monitored during different weather conditions. Water samples were collected and in situ parameters (pH, EC and T) measured. At the most downstream site streamflow was measured through slug injection of sodium chloride, a rapid technique for discharge estimation described by Moore (2005). The monitoring samplings occurred twice and the two observed flows are hereafter called “flow 1” and “flow 3”. Flow 1 sampling followed a few days of warm and dry weather; on the other hand flow 3 monitoring was undertaken under a storm event. The product of Zn concentration and streamflow data of flow 1 and flow 3 generate Zn load values for comparison between these two events and, furthermore, with flow 2 data.

Samples for Zn analysis were passed through 0.45 µm filters, acidified (2% nitric acid) and measured by Inductively Coupled Plasma Mass Spectroscopy. Samples for Br analysis were passed through 0.2 µm filters and measured by Ion Chromatography.

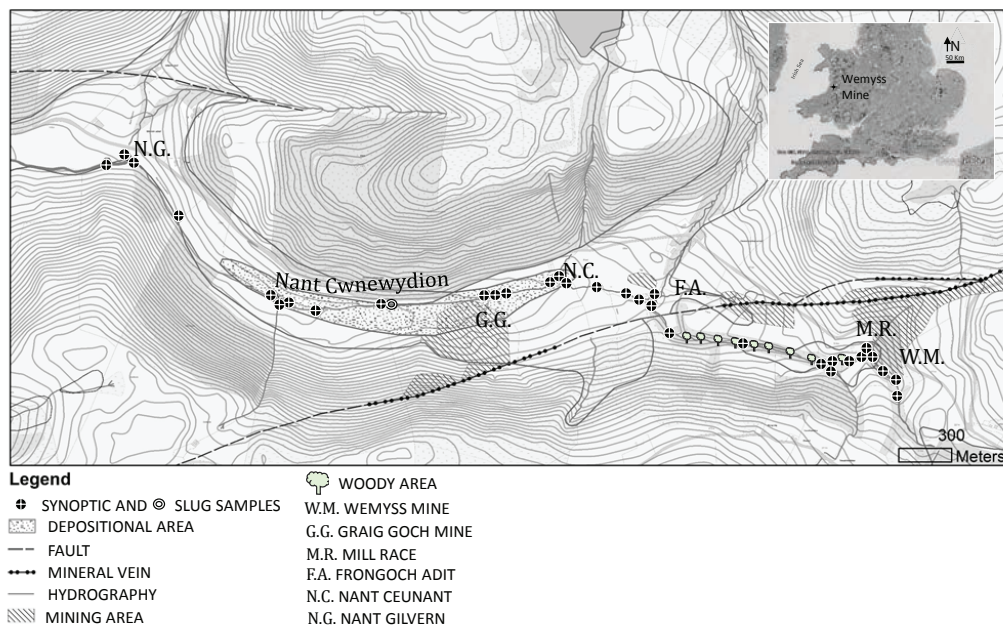


Figure 1 Map of the study site showing geographical location, synoptic sampling sites along Nant Cwmnewyddion and main features (refer to the legend for the keys). Map created using EDINA Digimap Ordnance Survey Service (2018).



Results and discussion

Stream water chemistry

Nant Cwmnewyddion has a pH of 6 ± 0.3 , it is less acid in the headwaters and more acid at the downstream site. No important pH variations were observed during the different stream flows. Zn concentrations at Graig Goch Mine (G.G., 1645 m) are reported in table 1 for the three streamflow estimates. All of the reported Zn concentration values exceed the environmental quality Zn thresholds of $8 - 50 \mu\text{g/l}$ indicated by the UKTAG (2012).

Assessment of Zn spatial load variations

In this section data from flow 2 are discussed in order to quantify Zn sources at Nant Cwmnewyddion study reach. Along the river, flow 2 streamflow estimates (fig.2) show the influ-

ence of three main inflows Frongoch Adit (F.A.), Nant Ceunant (N.C.) and Nant Gilvern (N.G.). A gradual streamflow increase is also notable in the reach from 1314 m to 1961 m which is not directly related to any observed inflows. In figure 3.a, Zn concentration shows an articulate pattern with steep increases after Mill Race (M.R.) and Frongoch Adit (F.A.). Metal loading data indicate substantial variation along the study reach river with the major source of Zn identified as a point source input from the Frongoch Adit (F.A.). Frongoch Adit, with 3.91 mg/l Zn concentration, contributes 57% to the total Zn load and is responsible for an increase in Zn concentration (from 1.06 to 2.89 mg/l) and load (from 42 to 250 mg/s) between site 847 m and site 880 m . Furthermore, figure 3.a indicates a rise in

Table 1. Downstream Graig Goch Mine (1645 m) data: discharge (Q), dissolved Zn concentration (mg/l) and load (mg/s).

Streamflow	Technique	Site (m)	Date	Weather	Q (l/s)	Zn (mg/l)	Zn (mg/s)
Flow 1	Slug	1645	09/06/2016	Dry	32	3.43	110
Flow 2	Tracer	1645	01/08/2016	Dry	146	1.95	285
Flow 3	Slug	1645	16/06/2016	Stormy	645	2.30	1484

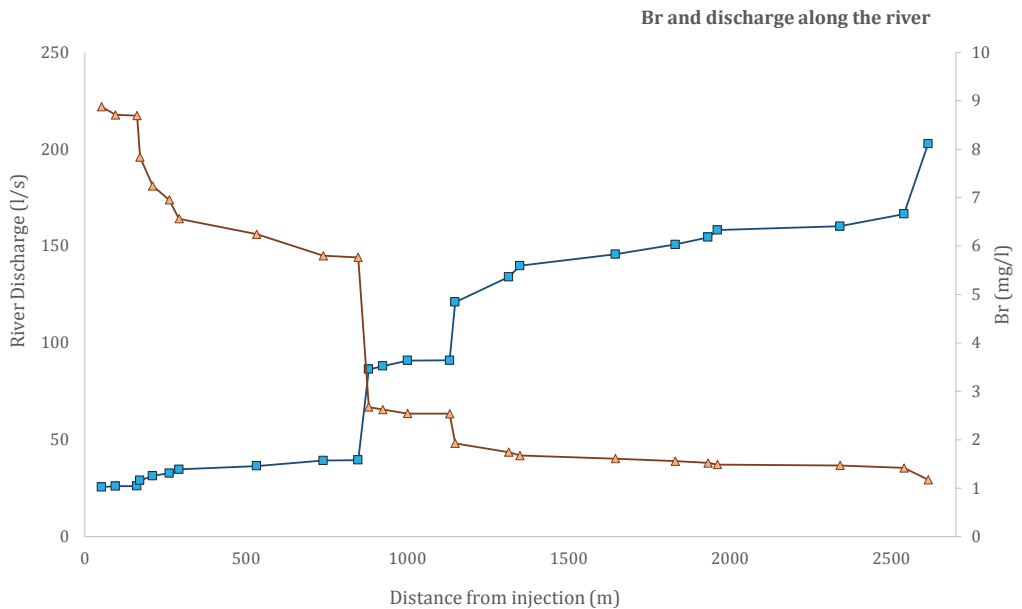


Figure 2 Br river concentration (triangles) during long tracer injection and river discharge (squares) changes along Nant Cwmnewyddion.



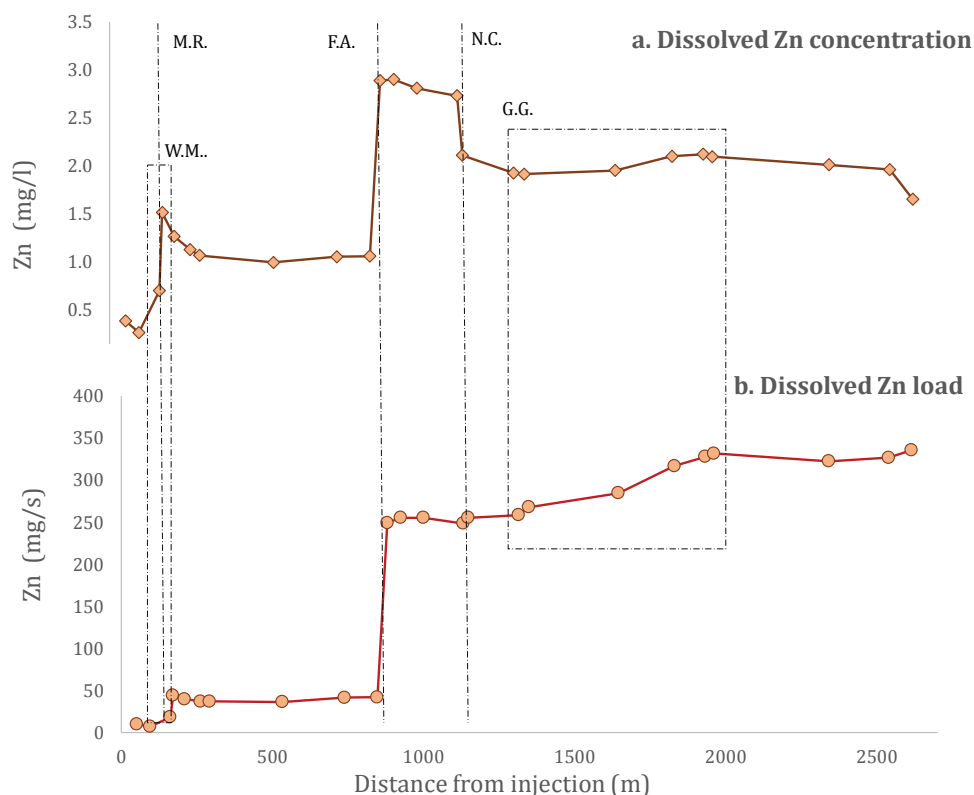


Figure 3 Dissolved Zn concentration (a.) and load (b.) along Nant Cwmnewyddion. Inflow positions are indicated by capital letters (M.R. Mill Race, F.A. Frongoch Adit, N.C. Nant Ceunant,) and mine areas by W.M. (Wemyss Mine) and G.G. (Graig Goch Mine).

Zn concentration from 0.70 to 1.52 mg/l from 162 m to 171 m, downstream of Mill Race (M.R.). However, it should be noted that this river runs alongside unconsolidated mine waste (Wemyss Mine) which is dominated by lateral seepages draining into the main river; the previous segment of river (95 to 162 m) contributes c. the 3% to the total Zn load (fig.4); the river reach from 95 m to 171 m is likely subject to a diffusive Zn source. In this segment, a total of 37 mg/s of Zn was gained, equivalent to 10% of the cumulative Zn load. A third area of metal sources can be identified from 1314 m to 1961 m, with Zn concentration rise from 1.93 mg/l to 2.10 mg/l and load increases from 259 to 332 mg/s. In this segment, Graig Goch mine waste dominated the left bank and a series of small pipes were seen to contribute a small discharge into Nant Cwmnewyddion water. Their Zn concentration increased constantly from down- to up-

stream (0.57 to 4.46 mg/l). Generally, Graig Goch Mine contributes 20% to the total cumulative load (fig.4). Summarising, three main sources are identified as contributing to the cumulative total load, Frongoch adit with 57%, Graig Goch Mine with 20% and Wemyss mine with 10% (fig.4).

Zn load and streamflow variations

At 1645 m site (downstream G.G.) streamflow estimates (tab.1) show a temporal variability of streamflow values with flow 1 (32 l/s) lower than flow 3 (645 l/s) and flow 2 falling between them (146 l/s). Zn load values (tab.1) indicate a clear proportional increase of load related to streamflow values: 110 mg/s at flow 1, 285 mg/s at flow 2 and 1484 mg/s at flow 3. These results suggest Zn dispersion responds to streamflow variations. Although flow 3 diffuse sources accounted for 30 % of the total Zn load, our data suggest that dif-



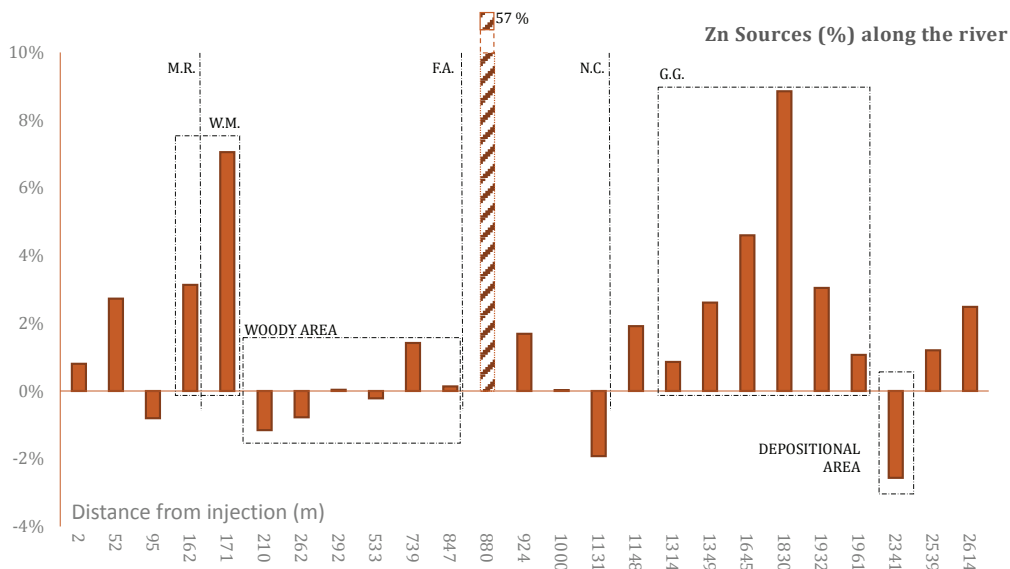


Figure 4. Dissolved Zn sources and attenuation processes along the river reach. The dashed rectangular, representing the F.A. contribution, has been cut and value reported on top (57%). Inflow positions are indicated by capital letters (M.R. Mill Race, F.A. Frongoch Adit, N.C. Nant Ceunant,) and mine areas by W.M. (Wemyss Mine) and G.G. (Graig Goch Mine).

fuse sources may increase in importance during higher flow conditions and rainfall-runoff events. Between 880 m and 1645 m (downstream F.A. and G.G.) differences in Zn concentration are captured in the different sampling time. The lowest, -0.39 mg/l measured during the higher flow, flow 3, indicates that the water from overland flows is carrying Zn mass with it and the dilution effect is less obvious compared to lower flow conditions, flow 1, when a variation of -1.24 mg/l was estimated. During flow 2 an average situation was observed with a variation of -0.94 mg/l of Zn in the same river segment.

Possible processes leading to an increase of diffusive pollution during high streamflow conditions, as flow 3, are mainly dissolution and washing of efflorescent salts (Cánovas et al. 2010). At the mine heaps and river channel, alternating wet - dry soil conditions may have promoted the oxidation of Zn-bearing minerals and oversaturated pore and interstitial water or pools allowed the precipitation of secondary minerals and efflorescence salts (Hudson-Edwards et al. 1999, Lynch et al. 2016). During our lower flow sampling, flow 1, efflorescent salts were noticed at different heights on the riverbank. In addition,

Palumbo-Roe et al. (2013) recorded the presence of sphalerite (ZnS) at Wemyss and Graig Goch mine waste heaps. Furthermore, no difference between dissolved and total Zn have been measured, therefore Zn is most likely to come from the dissolution processes rather than colloidal suspension processes. In conclusion, dissolution of oxidised sphalerite and Zn-bearing fluorescence may be the cause of the diffuse contamination, the dispersion of which can be accentuated during high flow conditions or storm events by the rapid movement of the water in the channel and overland flow (Byrne et al. 2013).

Conclusion

The purpose of this study was to identify spatial and temporal variations in Zn load in a mining impacted river. Using a tracer injection and synoptic sampling approach sources at different river stages were identified: Frongoch Adit (57% of Zn); Wemyss Mine (10% of Zn) and Graig Goch Mine (20% of Zn). The latter two sources were diffuse in nature and possibly a result of hidden seepages and oxidation-dissolution of Zn-bearing minerals. Slug injections, conducted downstream of the mine workings at different times and



river stages, captured the proportional response of Zn load to streamflow values. These data, in association with observed concentration changes, indicate that diffuse sources are likely to be more impacting during high flow conditions. This theory needs to be supported by a streamflow and Zn load database. More streamflow measurements have been undertaken along Nant Cwmnewyddion and a further tracer injection has been planned for summer 2018 at the same river reach.

In conclusion, these results highlight the benefit of using a tracer injection for source apportionment in impacted river catchments and the necessity to integrate it with over-time load monitoring to understand variability over different hydrological conditions.

Acknowledgements

The authors gratefully thank Liverpool John Moores University for funding PO Ph.D. scholarship allowing this research to be undertaken. University College London and the University of Manchester are gratefully acknowledged for providing chemical analysis. The authors would like to thank the Natural Resources of Wales and Ilaria Frau for their valued assistance.

References

- Byrne P, Reid I, Wood PJ (2013) Stormflow hydrochemistry of a river draining an abandoned metal mine: the Afon Twymyn, central Wales. *Environ Monit Assess* (2013) 185:2817–2832
- Byrne P, Runkel RL, Walton-Day K (2017) Synoptic sampling and principal components analysis to identify sources of water and metals to an acid mine drainage stream. *Environ Sci Pollut Res* DOI 10.1007/s11356-017-9038-x
- Cánovas CR, Olías M, Nieto JR, Galván L (2010) Wash-out processes of evaporitic sulfate salts in the Tinto River: hydrogeochemical evolution and environmental impact. *Appl Geochem* 25: 288–301
- Hudson-Edwards KA, Schell C, Macklin MG (1999) Mineralogy and geochemistry of alluvium contaminated by metal mining in the Rio Tinto area, southwest Spain. *Applied Geochemistry*, 14, 1015–1030
- Jarvis AP, Mayes WM (2012). Prioritisation of abandoned non-coal mine impacts on the environment. Environment Agency Science Report SC030136/R12, Bristol: Environment Agency
- Kimball BA, Runkel RL, Walton-Day K, Bencala KE (2002) Assessment of metal loads in watersheds affected by acid mine drainage by using tracer injection and synoptic sampling: Cement Creek, Colorado, USA. *Appl Geochem* 17:1183–1207. doi:10.1016/S0883 2927(02)00017-3
- Lynch SFL, Batty LC, Byrne P (2016) Critical control of flooding and draining sequences on the environmental risk of Zn-contaminated riverbank sediments *J Soils Sediments* DOI 10.1007/s11368-016-1646-4
- Moore RD (2004) Introduction to Salt, Dilution Gauging for Streamflow Measurement: Part 1. *Streamline Watershed Management Bulletin* Winter 2003/04 Vol.7/No.4, p 20-23.
- Palumbo-Roe B, Wragg J, Cave M, Wagner D (2013). Effect of weathering product assemblages on Pb bioaccessibility in mine waste: implications for risk management. *Environ Sci Pollut Res Int.* 2013 Nov;20(11):7699-7710. doi: 10.1007/s11356-013-1515-2
- Runkel RL, Walton-Day K, Kimball BA, Verplanck PL, Nimick DA (2013) Estimating instream constituent loads using replicate synoptic sampling, Peru Creek, Colorado. *Journal of Hydrology* 489: 26–41
- UKTAG (2012) Updated Recommendations on Environmental Standards River Basin Management (2015-21)



The Effects of *Castor canadensis* (North American Beaver) Colonization on a Mine Drainage Impacted Stream

Nicholas L. Shepherd, Robert W. Nairn

202 W. Boyd St. Room 334, Norman, OK, USA, 73019

Abstract

Net alkaline mine drainage began discharging in 1979 and negatively impacted the aquatic and terrestrial biota near a 1.6 km reach of an unnamed tributary (UT) to Tar Creek, located in the Oklahoma, USA portion of the abandoned Tri-State Lead-Zinc Mining District. By 2015, *Castor canadensis* (North American Beaver) had colonized UT, transforming the stream into a series of impoundments created by beaver dams. The increased surface area and retention time provided by the impoundments reduced Fe and Cd aqueous concentrations by over 60%. However, the precipitated metals resulted in elevated Cd, Fe, Pb, and Zn concentrations in stream sediments.

Keywords: *Castor canadensis*, Beaver, Ecosystem Engineer, Tar Creek

Introduction

This paper investigated the hydrological and chemical impacts of *Castor canadensis* (North American Beaver) colonization on a first-order stream, contaminated with net alkaline mine drainage (MD). The stream is located within the Tar Creek Superfund Site, the Oklahoma, USA portion of the Tri-State Lead-Zinc Mining District (TSMD). The TSMD was in operation from the mid-19th century until the 1970s and produced approximately two million tons of lead and nine million tons of zinc (ODEQ, 2006). During mining, large pumps were used to dewater the mines. However, when operations ceased, groundwater recharged, filling the voids, and discharging metal-laden water under artesian pressure into receiving streams in 1979.

The study site was one of these receiving streams, an unnamed tributary (UT) to Tar Creek. The study reach of UT is approximately 1.6 km and receives two primary sources of MD. UT and the contributing sources of water are regularly monitored for water quality by The Center for Restoration of Ecosystems and Watersheds (CREW). The first source is the Southeast Commerce (SEC) discharge, located at the start of the study reach and contributing approximately 375 L/min containing 133 mg/L Fe, 9.7 mg/L Zn, 63 µg/L Pb, and 31 µg/L Cd. The second discharge, located 0.5 km downstream, is the Mayer

Ranch site. In 2008, the Mayer Ranch Passive Treatment System (MRPTS) was constructed to treat 600 L/min of MD. The system has approximate effluent metals concentrations of 0.65 mg/L Fe, 0.46 mg/L Zn, with Cd and Pb below practical quantitation limits (PQL). Therefore, the raw MD in UT from the SEC discharge is diluted after the MRPTS effluent enters the stream (Figure 1)

Beaver are known as ecosystem engineers, which are organisms with the potential to significantly modify their surroundings (Naiman et al., 1986). The construction of beaver dams has been shown to improve water quality, reduce peak flows due to storm events, and increase storage capacity in streams through the creation of wetlands (Naiman et al., 1986; Snodgrass and Meffe, 1998; Hardisky, 2011; and Puttock et al., 2017). However, the impacts of beaver on MD impacted streams has not been studied. Beaver activity was noticeable on UT in 2014. By 2015, beaver had converted the study reach of UT into a series of beaver impoundments. This study investigated four aspects of *Castor canadensis* colonization on UT: (1) retention of metals in UT due to beaver impoundments, (2) metals contamination and leachability of sediments (3) potential for metal mobilization during dam destruction and (4) hydrologic and habitat alterations due to the presence of dams using tracer studies and rapid habitat assessments.



Methods

Large beaver dams on UT that impounded water above bankfull and maintained a change in elevation head on opposite sides of the dam were identified and sampled to address retention of metals due to beaver impoundments and consequent metals accumulation in stream sediments (Figure 1). In addition, an existing man-made low water crossing (LWC) was sampled because it also met the above criteria. Water and sediment samples were collected at the inflow and outflow of each impoundment. Inflow was defined as the location where water levels began to exceed bankfull. Outflow samples were collected in the pooled water immediately be-

fore each dam. If distinct layers of sediment were present, two samples were collected. The water and sediment samples were analyzed for total metals using hot nitric acid digestion and subsequent ICP-OES analysis (USEPA Methods 3015 and 6010). Sediment samples with the greatest metals concentrations were then analyzed for leachability using USEPA method 1311 for toxicity characteristic leaching procedure (TCLP). Three sampling events took place from August 2016 to January 2017. Due to inconsistencies with beaver activity, not every dam was present at each sampling event. If a dam was absent, that location was not sampled for that event. Sediment samples were analyzed for statistical significance using a paired, one-tailed T-Test.

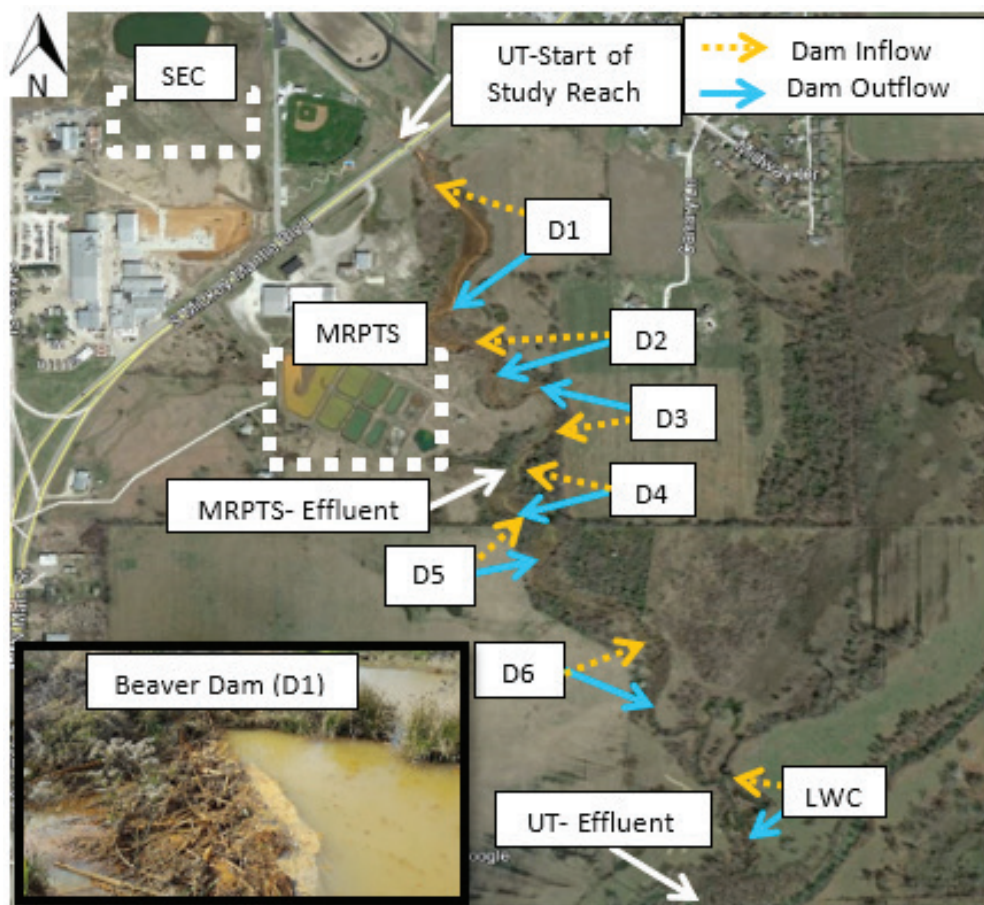


Figure 1 Beaver dam locations along UT in Commerce, OK, USA with arrows indicating inflow and outflow of each impoundment from beaver dam construction (Google Earth, 2017). Example of a beaver dam (D1) shown in the bottom left corner. Abbreviations: Southeast Commerce site (SEC), unnamed tributary (UT), Mayer Ranch Passive Treatment System (MRPTS), low water crossing (LWC), beaver dams (D#).



Next, metal remobilization due to beaver dam failure was evaluated. Starting at the most downstream dam (D6), every beaver dam was sequentially destroyed, using hand tools, to an elevation consistent with the streambed. Water samples for total metals analysis were collected at the location of the destroyed dam. Samples were collected 5, 35, and 65 minutes after dam removal. Five months later, the most upstream dam (D1), nearest the SEC discharge, was destroyed again and sampled every 30 minutes for six hours using an autosampler with flow determined by an acoustic Doppler current profiler.

To investigate hydrologic and habitat alterations caused by beaver colonization, two rapid habitat assessments, based on the USEPA's *Rapid Bioassessment Protocols for Use in Wadable Rivers and Streams*, were conducted over a one-month period. The first took place with all beaver dams intact and the second was conducted after dams were removed for the metal remobilization study. Multiparameter datasondes equipped with rhodamine sensors were deployed at the midpoint (near D2 Out) and the end of the UT study reach, collecting data every 30 minutes for six hours. Rhodamine was injected at the start of study reach UT with and without beaver dams.

Results and Discussion

Table 1 shows mean metals concentrations of the three sampling events in and out of each beaver dam. The most upstream dams, nearest the SEC discharge, had greater initial

metals concentrations and showed greater Fe removal rates than downstream dams that were influenced by the dilution of treated MD downstream of the MRPTS effluent. Only three dams (D1, D4, and LWC) had samples collected for all three events, therefore only these dams were used for statistical analyses using a paired, one-tailed T-test. D1 showed significant decreases in Cd, Fe, Pb, and Zn ($p < 0.05$), while dams downstream of MRPTS (D4 and LWC) did not show statistically significant decreases in metals concentrations ($p > 0.05$). The beaver impoundments resembled a series of oxidation wetlands due to increased surface area and retention time, allowing Fe to precipitate and settle as iron oxyhydroxides. The decrease in Cd was likely the result of sorption to the precipitated Fe, which has been documented in the MRPTS oxidation pond, resulting in nearly identical Fe and Cd removal trends (Nairn et al., 2009). Oxidation ponds are often designed to remove $20 \text{ g Fe m}^{-2} \text{ day}^{-1}$, by comparison, the Fe removal rate at D1 had a calculated average of $4.12 \text{ g Fe m}^{-2} \text{ day}^{-1}$. Utilizing the flow-rate of 375 L/min , D1 removed approximately 12 kg Fe per day.

Pb showed minimal changes in concentration after D1. In passive treatment, Pb is removed via vertical flow bioreactors that promote bacterial sulfate reduction in an anoxic environment (Nairn et al., 2009). The reducing environment necessary to remove Pb was likely not present in the beaver impoundments, which is supported by the small changes in the Pb concentrations (Table 1).

Table 1. Total aqueous metals concentrations (mg/L) in and out of beaver impounded water in a MD impacted tributary to Tar Creek located in Oklahoma, USA

Site	Cd		Fe		Pb		Zn	
	In	Out	In	Out	In	Out	In	Out
D1	0.012	0.004	45.03	22.40	0.048	0.036	6.37	4.77
D2	0.003	0.002	4.99	11.55	0.033	0.033	4.81	3.87
D3	0.002	0.002	10.24	8.45	0.034	0.031	3.97	3.93
D4			3.78	3.36	0.032	0.029	2.72	2.32
D5			4.90	3.58	0.036	0.034	2.06	1.98
D6			0.49	0.49	0.034	0.026		
LWC			0.65	0.39	0.028	0.025	1.78	1.80



All sediment samples had at least one metal that exceeded the probable effects concentrations (PEC) specific to the Tar Creek Superfund Site (Ingersoll et al. 2009; Table 2). Cd, Pb, and Zn concentrations were 7, 3, and 4.5 times the PEC, respectively, and five sediment samples contained greater than 20% Fe. Most of the sediment samples collected at the outflow of dams had clear stratification (D4, D5, and D6), attributed to sedimentation occurring near the dam. Cd and Fe concentrations were significantly greater in the surface layer of sediment compared to the bottom layer ($p=0.018$ and $p=0.020$, respectively). The inflow sediment samples had significantly lower Fe and Zn concentrations when compared to the surface layers of the outflow sediments ($p=0.023$ and $p=0.049$, respectively). The greater concentrations of metals at the surface layer of the dam outflow compared to both the inflow and bottom layer of the outflow sediment samples were attributed to the precipitated metals settling near the base of the beaver dam.

Seven sediment samples were selected for TCLP analysis. None of the samples had Pb concentrations that exceeded the Resource Conservation and Recovery Act (RCRA) standard of 5.0 mg/L, while only a single site, D4 In, exceeded the Cd RCRA standard of 1.0 mg/L, containing 1.08 mg/L. The remaining six samples showed an average of 0.2 mg/L Cd, therefore further sampling should be conducted to confirm the Cd concentration at D4.

The removal of each beaver dam using hand tools created a flushing event, releasing a pulse of water that suspended precipitated metals. Table 3 shows the metals concentrations collected at 5-, 35-, and 65-minute intervals after each dam was destroyed. These data showed increasing concentrations of Fe over the one-hour time interval at all dams, with Cd following the same trend at D1. Zn and Pb did not produce consistent trends over time at each dam, suggesting Pb and Zn are not as readily mobilized compared to Fe and Cd.

Utilizing data from the rapid habitat assessments, the estimated volume of water stored by each beaver dam was calculated and used to determine the mass of metals mobilized at each dam (Table 3). Since D1 is the most upstream dam, nearest the SEC discharge, it had the highest initial concentrations of metals, resulting in the greatest mass of mobilized metals. At D1, Fe contributed 98% of the mobilized mass of metals of the four metals presented in Table 3. Using the Fe removal rate for D1 of 12 kg Fe per day, D1 mobilized 4.5 days of retained Fe after dam removal.

The sequential dam removal event confirmed that metal remobilization may occur, but it did not indicate how long the concentrations may remain elevated. A six-hour sampling event conducted at D1 was designed to investigate the duration of the elevated metals concentrations. The experiment

Table 2. Sediment metals concentrations (mg/kg) at varying depths (cm) in and out of beaver impounded water in a MD impacted tributary to Tar Creek located in Oklahoma, USA

Site	Depth	As	Cd	Fe	Pb	Zn
PEC			11.1		150	2,083
D1 In	0-60	8.17	75.4	204,000	500	9,240
D1 Out	0-50	39.9	88.6	167,000	377	10,300
D4 In	0-20	11.9	146	122,000	522	10,600
D4 Out	25-35	7.21	11.6	19,900	1,360	1,460
D4 Out	0-25	57.2	70.2	228,000	477	9,400
D5 In	0-45	5.3	8.38	14,000	28.8	863
D5 Out	20-50	10.1	21.7	51,000	419	2,500
D5 Out	0-20	53.8	137	266,000	384	21,400
D6 In	0-15	5.44	20.3	26,100	628	22,400
D6 Out	7-30	18.6	120	149,000	626	14,700
D6 Out	0-7	18.5	234	252,000	538	13,000
LWC In	0-30	4.08	21.2	9,560	192	2,930
LWC Out	0-45	23.8	93.2	221,000	360	13,500



Table 3. Total aqueous metals concentrations collected at 5-, 35-, and 65-minute intervals after each dam was removed and calculated mean mass of metals mobilized based on volume of water released at each dam in a MD impacted tributary to Tar Creek located in Oklahoma, USA

Dam #	Volume	Time	Cd	Fe	Pb	Zn	Cd	Fe	Pb	Zn
	(m ³)	(min)	Aqueous Concentration (mg/L)				Mass of Metals Mobilized (g)			
D1	1315	5	0.004	22.7	0.037	4.55	9.16	55,300	54.7	4,580
		35	0.007	43	0.039	3.83				
		65	0.010	60.4	0.049	3.23				
D4	296	5	<PQL*	1.04	0.029	0.211		513	9.38	94
		35	<PQL*	1.75	0.032	0.356				
		65	<PQL*	2.41	0.035	0.519				
D5	503	5	<PQL*	0.763	0.031	0.102		580	14.1	44.8
		35	0.001	0.785	0.025	0.074				
		65	<PQL*	1.91	0.028	0.092				
D6	96	5	<PQL*	0.75	0.032	0.106		75.5	2.89	8.85
		35	<PQL*	0.599	0.03	0.09				
		65	<PQL*	1	0.028	0.079				

was originally designed for twelve hours of sampling, but water levels were too low to collect water samples after six hours. The first sample after the dam was removed had elevated metals concentrations attributed to the initial disturbance of precipitated metals. After one hour, Pb and Zn showed no change in concentrations over time (Figure 2). From the sixty-minute sample to the 270-minute sample, an increasing trend in Fe and Cd concentrations was shown (Figure 2). In contrast, velocity demonstrated a decreasing trend for the first two hours, starting at three meters per second and falling below the detection limit of the instrument after two hours. The decreasing velocity over time while Fe and Cd concentrations increased suggest the initial pulse is the driving force that suspends the metals, and the six-hour sampling period is an insufficient amount of time for the metals to resettle. Iron sludge settling rates can vary between 0.2 cm/min and 1.9 cm/min, noting that any disturbance has the potential to decrease the rate (Dempsey and Jeon, 2001; Dietz and Dempsey, 2002). The dam removal in this study was performed using hand tools, it is hypothesized that in the event the dams fail due to storm events, the mass of metals mobilized will increase due to the greater velocities and disturbance associated with a storm event capable of destroying the beaver dams.

The rapid habitat assessment conducted with and without beaver dams that the presence of beaver dams resulted in overall greater habitat scores, 140 points with dams and 128 points without dams, but there was no significant difference between the categories of the classification system. The notable difference between the two habitat assessments was the greater mean width of water with dams, 7.7 m, compared to 3.3 meters without dams. From the habitat assessment parameters, the total volume of water stored by the beaver dams was approximately 2,500 m³. The volume was verified using stream gauge stations on Tar Creek upstream and downstream of the UT confluence. The spike in the downstream hydrograph following dam removal was subtracted from the base flow to find the volume of water released. The second method resulted in a stored volume of approximately 3,200 m³.

The rhodamine study found the presence of beaver dams increased the retention time of UT by 23%. Most of the excess retention time occurred on the downstream half of the study reach (Table 4). Since this study was conducted in a MD impacted stream, sorption of rhodamine to Fe was problematic and caused low recoveries, 9% with dams and 24% without dams. Similar studies conducted on non-MD impacted streams reported up to 89% rhodamine recovery (Jin et al., 2009).



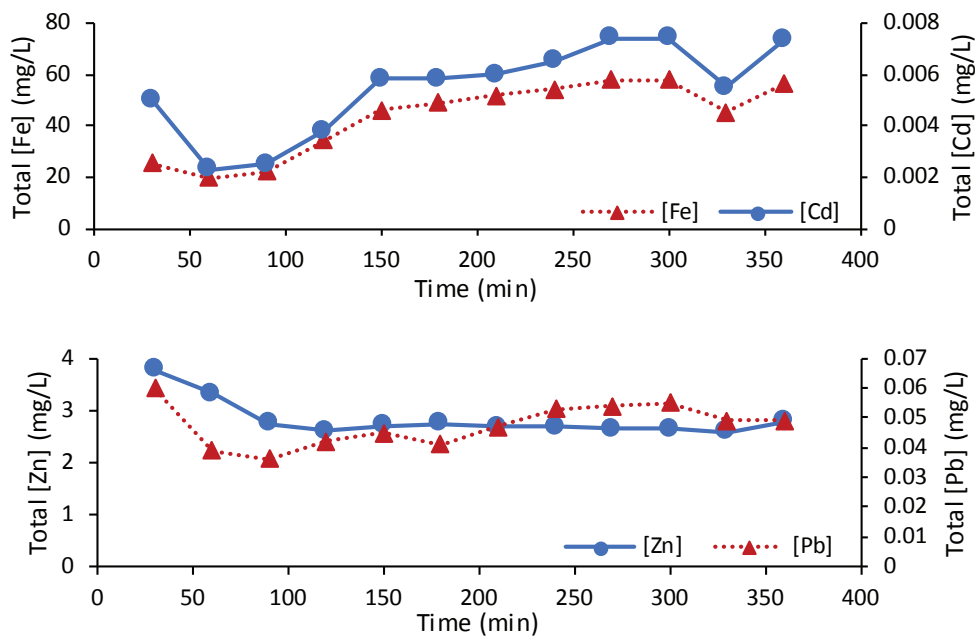


Figure 2 Total aqueous metals concentration collected every 30 minutes for six hours after D1 beaver dam removal in a MD impacted tributary to Tar Creek located in Oklahoma, USA

Table 4. Conservative tracer studies using rhodamine using two sensors located at the midpoint and end of a MD impacted tributary to Tar Creek located in Oklahoma, USA conducted with and without beaver dams

Parameter	With Dams		Without Dams	
	Midpoint	End	Midpoint	End
Recovery (%)	8.61	9.15	28.47	23.50
Total time until pulse passes (hrs.)	79.0	242.5	113.5	177.0
Mean retention time (hrs. after injection)	48.0	155.0	52.2	126.0
Dispersion coefficient (m2/s)	0.14	20.87	1.61	5.13
Dead volume per bulk volume	53.2	36.6	-162.3	-84.8
Index of short circuiting	-0.21	0.85	0.46	0.27

There were also environmental factors that influenced the results. An inescapable issue when working with beaver was their ability to rapidly reconstruct dams. A pressure sensor in UT recorded continuously increasing water depths associated with beaver reconstructing a dam starting four hours after being destroyed. The immediate reconstruction of dams likely caused an increased retention time because the stream did not remain free of beaver dams.

Conclusions

Beaver colonization on a net alkaline mine drainage impacted stream was shown to

decrease metals concentrations via the construction of beaver dams, causing large impoundments with greater surface area and increased retention time. The precipitated metals caused elevated stream sediment concentrations, with the greatest concentrations occurring in the surface layer of sediment nearest the dams. In the event of beaver dam failure, whether caused by man or storm events, a portion of the retained oxidized metals will be mobilized downstream. Overall, beaver are ecosystem engineers providing valuable services by not only improving water quality of a MD impacted stream, but also by establishing wetlands which promote

biodiversity and flood attenuation by increasing storage capacity of the stream (Snodgrass and Meffe, 1998; Hardisky, 2011; and Puttock et al., 2017).

Acknowledgements

This project was funded by the Oklahoma Department of Environmental Quality (Agreement PO 2929019163 SRA FY15-ORA4-14) and the Grand River Dam Authority (Agreements GRDA 060910 and GRDA08272015). Support for this study was provided by members of the Center for Restoration of Ecosystems and Watersheds (CREW).

References

- Dietz JM, Dempsey BA (2002) Innovative Treatment of Alkaline Mine Drainage Using Recirculated Iron Oxides in a Complete Mix Reactor. Proceedings, 2002 National Meeting of the American Society of Mining and Reclamation, Lexington, KY, June 9-13
- Dempsey BA, Jeon B (2001) Characteristics of Sludge Produced from Passive Treatment of Mine Drainage. *Geochemistry: Exploration, Environment, Analysis*, 1: 89–94
- Hardisky T (2011) Beaver Management in Pennsylvania. Pennsylvania Game Commission
- Ingersoll CG, Ivey CD, Brumbaugh WG, Besser JM, Kemble NE (2009) Toxicity Assessment of Sediments from the Grand Lake O' The Cherokees with the Amphipod *Hyaella azteca*. U.S. Fish and Wildlife Service
- Jin L, Siegel DI, Lautz KL, Otz MH (2009) Transient Storage and Downstream Solute Transport in Nested Stream Reaches Affected by Beaver Dams. *Journal of Hydrological Processes* 23:2438–2449
- Naiman RJ, Melillo JM, Hobbie JE (1986) Ecosystem Alteration of Boreal Forest Streams by Beaver (*Castor Canadensis*). *Journal of Ecology* 67(5):1254–1269
- Nairn RW, Beisel T, Thomas RC, LaBar JA, Strevett KA, Fuller D, Stronsnider WH, Andrews WJ, Bays J, Knox RC (2009) Challenges in Design and Construction of a Large Multi-Cell Passive Treatment System for Ferruginous Lead-Zinc Mine Waters. Proceedings, 2009 National Meeting of the American Society of Mining and Reclamation, Billings, MT, Revitalizing the Environment: Proven Solutions and Innovative Approaches May 30 – June 5
- Oklahoma Department of Environmental Quality (ODEQ) (2006) Oklahoma Plan for Tar Creek. ODEQ
- Puttock A, Graham HA, Cunliffe AM, Elliot M, Brazier RE (2017) Eurasian Beaver Activity Increases Water Storage, Attenuates Flow and Mitigates Diffuse Pollution from Intensively-Managed Grasslands. *Science of the Total Environment* 576:430–443
- Snodgrass JW, Meffe GK (1998) Influence of Beavers on Stream Fish Assemblages: Effects of Pond Age and Watershed Position. *Ecological Society of America* 79:928–942



**ECONOMICS OF
MINE WATER**





Sustainability Management Accounting Techniques for Acid Rock Drainage Management: A Literature Review

Chantal Mbala Banga¹, Heinz Eckart Klingelhöfer¹, Christian Wolkersdorfer^{2,3}

¹*Tshwane University of Technology (TUT), Department of Managerial Accounting and Finance, Private Bag X680, Pretoria 0001, South Africa, chantalbangamba@gmail.com, KlingelhoferHE@tut.ac.za*

²*Lappeenranta University of Technology, Laboratory of Green Chemistry, Sammonkatu 12, 50130 Mikkeli, Finland, christian@wolkersdorfer.info*

³*South African Research Chair for Acid Mine Drainage Treatment, Tshwane University of Technology (TUT), Private Bag X680, Pretoria 0001, South Africa*

Abstract

Acid rock drainage (ARD) is a sustainability problem in the mining industry, which requires considerable efforts for its management. This paper addresses the environmental, social and economic issues associated with ARD prevention and assessment. Although hydrological and mineralogical tools have been generally used in these two managerial parts of ARD, Sustainability Management Accounting Tools (SMATs) as instruments useful in providing sustainability information have never been implemented. Therefore, various SMATs are presented for effective management of ARD prevention and assessment. Moreover, the findings propose ways that these may help to solve problems in a sustainable manner.

Keywords: Acid rock drainage, prevention, assessment, sustainability management accounting tools

Introduction

Acid rock drainage (ARD) and acid mine drainage (AMD) are major environmental problems occurring during and after mining activities (de Almeida et al. 2015: 353, Wolkersdorfer 2008) and might pollute land or local ground and surface water (Fan et al. 2017). This leads to water quality problems, scarce water resources and menace to aquatic animals (Dyanty 2014). Above all, it may pose a threat to human health (Betrie 2014). Therefore, two sustainability elements, namely environment and community are main concerns of ARD. While ARD management focuses on the minimization of environmental influences (Frostad 1999, Wolkersdorfer 2008), costs remain a main challenge and economic incentives can be important for decision-making (Fan et al. 2017, Kazadi Mbamba et al. 2012: 13). Hence, both environmental impacts and financial benefits are substantial elements of ARD management (Nleya et al. 2016). However, sustainability has been poorly perceived in ARD management. Furthermore, its components, includ-

ing environmental, social and economic aspects, are often taken only separately into account. Developing effective ARD management strategies is therefore a challenge, since these strategies should be aligned with ARD risks (Parbhakar-Fox et al. 2014: 11). In line to these strategies, various models and methods have been used as ARD tools to provide geological, hydrogeological and mineralogical information (Parbhakar-Fox and Lottermoser 2015, Becker et al. 2015: 33). However, although ARD is naturally associated with sustainability issues, sustainability models and methods have never been developed and implemented, besides sustainable rehabilitation as a focus of Anawar (2015). Nevertheless, such tools could be helpful in providing environmental, social and economic information and they could be flanked by employing Sustainability Management Accounting (SMA). SMA can be understood according to Arroyo (2012: 287–288) and Maas et al. (2016:241) as the generation/collection, analysis and use of monetary and non-monetary sustainability information in order to achieve





and communicate organisational, environmental, social, and economic performance, i.e. a sustainable organisation.

This paper aims to determine, by means of a literature review, the extent to which sustainability is considered in ARD management and to show how Sustainability Management Accounting (SMA) could help in this area. Therefore, it discusses sustainability management accounting techniques that are able to support the delivery of sustainability information associated with ARD prevention and assessment. Problems associated with the integration of sustainability into ARD are investigated in order to identify appropriate sustainability management accounting tools (SMATs) that could be used for the effectiveness of its management in general and particularly of its prevention and assessment.

Literature Review

Sustainability Issues in Acid Rock Drainage Management and Possible Anchor Points for Sustainable Management Accounting

This section reviews the environmental, social and economic problems associated with ARD prevention and assessment. Environmental issues have been the concern of some recent studies conducted in ARD prevention and assessment. For instance, Abrosimova et al. (2015) evaluated two combinations of test protocols to refine the predictive accuracy of the acid potential. Their findings showed that the most ecologically dangerous species predominated in the drainage solutions, and the co-precipitation with goethite and hematite had a positive effect on the environment. Therefore, as already acknowledged by Jasch (2003), there appears to be a need to identify such environmental influences physically and monetarily. In a like fashion, Betrie et al. (2015, 2016) offered a methodology for assessing ecological risks through probability bounds. They found the existence of a high probability of ecological risk caused by metals transported into a nearby lake, requiring the implementation of probability estimation techniques. Regrettably, the probabilistic risk analysis method implemented by Saha et al. (2017) was found to be difficult since the input parameters failed to be remediated as fixed-point values. Hence, this may require

the use of appropriate tools. However, Zmijewski (1984) already asserted that the lack of using appropriate estimation techniques leads to biased parameters in the study on methodological issues associated with the estimation of Financial Distress Prediction Models. These parameters include: oversampling falling within choice-based sample biases and the “complete data” falling into sample selection biases. Hence, there is a need of good probability estimation techniques that could provide reasonable probability information. Further, Jeen et al. (2014) evaluated the mixtures of amendments for treatment of acid rock drainage. While the cost of reactive material was low, long-term maintenance costs were required. Nevertheless, the implementation of organizational decision making often pays only little attention on regular maintenance costs (Fryling 2010). Thus, it would be useful to have an estimation maintenance costs technique.

Both environmental and economic problems have been addressed by Nuzzio et al. (2011) through the assessment of techniques used to differentiate and identify water samples from different ARD sources. They believe that this will economically control ecological changes and remediation efforts. Therefore, it will be necessary to develop monetary techniques for controlling environmental development as e.g. explored by Darnall and Edwards (2006). Furthermore, Alakangas et al. (2013: 7908) used mixtures of methods as a neutralization fashion of preventing ARD. They found that economic and logistical factors could be the limitation to supplementary neutralizing materials. Logistics costs are countless and considerably unstable which has led to them being estimated as high (Engblom et al. 2012). Therefore, there appears to be a need of identifying such costs for material acquisition. Moreover, environmental problems were also presented by a high potential of pH leachates, requiring the identification of adequate information addressing them in the context of ARD prevention. Further, Mäkitalo et al. (2014) applied the green liquor dregs for preventing ARD formation and mitigating its negative effects including environmental deterioration and high maintenance costs which required the reduc-





tion of such expenses (Kokubu and Kitada 2015). To assess the environmental and human toxicity, Life Cycle Assessment was used by Broadhurst et al. (2015) to evaluate the broader environmental consequences of the pre-disposal treatment. Although the process revealed substantial reduction in the effects of ARD on human toxicity and eco-toxicity to the environment, some effects, such as more carbon consumption, fossil fuel depletion, terrestrial acidification higher emissions of carbon dioxide, sulfur dioxide and xanthate to the environment, were remarkable. Hence, the authors recommend the environmental benefits capture of improved resources. Therefore, techniques should be able to provide information about the state of the present and the future of an environment and the community as well as about the benefits of its management, even though, from the operational level, not all environmental issues can be addressed (Papaspypopoulos et al. 2012).

Finally, the environmental, social and economic problems associated with the use of mine technology for the minimization of acid formation were revealed by Kefeni et al. (2017). This included alternative solutions for the environmental problems caused by AMD, the reduction of environmental pollution, an employment rate increase and the establishment of cost treatment and benefits. This requires the use of sustainability tools.

Sustainability Management Accounting Techniques (SMAT)

SMATs reviewed in this paper include: Environmental Management Accounting, EMA (Jasch & Lavicka 2006: 1214, 1226; Sands et al. 2016: 135), which encompasses both the monetary and the physical aspects (Burritt et al. 2002: 39, 48f). Also, the link between EMA and Environmental Reporting is useful in disclosing ecological information merely for industry activities associated with environmental impacts (Sulaiman and Mokhtar 2012: 85, 97). EMA metrics for internal decision-making include both: physical metrics for material and energy consumption, flows, and final disposal, and monetarized metrics for costs, savings, and revenues related to activities with a potential environmental impact (Jasch 2003). Cost-Volume-Profit Analysis

provide probability information in supporting decision-making under uncertainty, and Risk Heat Maps focus on the internal control of the likelihood and the impact of physical asset risk by representing the resulting qualitative and quantitative evaluations of the probability of risk occurrence and providing visual information about the risk assessment process (CGMA 2016). Cost-Benefit Analyses provide information for prioritizing the measurement and effectiveness of disaster risk management (Mechler 2016). In addition to this, Petcharat and Mula (2009: 56) applied the Activity-Based-Costing method, in which environmental and social cost information is delivered to support internal decision-making. Similarly, Rodríguez-Olalla and Avilés-Palacios (2017: 1, 7, 10, 13f) suggested the incorporation of an Activity-Based Sustainability model for the delivery of information supporting all activities involved in the business process. Moreover, van Heeren (2001: 1, 2, 12) implemented the Balanced Business Scorecard and in a similar fashion, Sands et al. (2016: 134–135) the Sustainability Balanced Scorecard for the measurement of sustainability performance. Environmental performance indicators summarise environmental data into relevant information enabling the control, target setting, outlining performance improvements, benchmarking and reporting (Jasch 2009), while Risk Management Accounting can be useful in identifying, assessing, treating, monitoring risks and evaluating its effectiveness (Soin and Collier 2013). Multi-Criteria Decision Analysis and Costs Probability distributions can be used for prediction and decision making purposes.

Learnings from Literature: SMATs for ARD

Above, we revealed firstly, environmental issues and secondly, three groups of concurrent sustainability problems associated with ADR prevention and assessment such as environmental and economic, environmental and social as well as social and environmental, social and economic. Applying SMATs as presented earlier, allows responding to these concerns as follows:

Environmental solutions: In order to facilitate the identification of environmental impacts





as addressed by Abrosimova et al. (2015), Environmental Performance Assessment may be combined with Management Accounting Control to assess positive environmental impacts and collect environmental information for the management and maintenance of these impacts. The Activity-Based Sustainability model may be useful in supporting all activities involved in the identification of environmental impacts, while the Sustainability Balanced Scorecard can enable the measurement of environmental impacts and their benefits. Besides this, it also provides Environmental Performance Indicators that can be used for future performance improvement. Environmental Reporting can be used to report the actual state of the mine site environment. Moreover, Multi-Criteria Decision Analysis allows for future decisions about measures, strategies formulation and costs involved in maintaining these positive impacts. In relation with the issue raised by Betrie et al. (2015, 2016), both, Cost-Volume-Profit Analysis and Risk Heat Map allow assisting the assessment of ecological risk. The former technique provides reasonable probability information to support decision-making under uncertainty as well as information on the future volume of activities related to of the environmental risk assessment as well as the estimated costs and future benefits of such activities. The later tool quantitatively and qualitatively assesses the risk and its impacts. Costs Probability distributions can be used for the prognosis of environmental risks caused e.g. by metals transported into a nearby lake, estimated costs, probable effects and possible decision-making purposes. Furthermore, these profanities have to be analyzed. Risk Management Accounting can control all processes of risks management including identification, assessment and treatment of potential dangers of the mine site. In order to solve the problem associated with long-term maintenance costs for ARD assessment, as revealed in the study of Jeen et al. (2014), Environmental Management Accounting can provide satisfactory information about all current and future costs associated with the maintenance of the mine site. This can help in determining costs at a low rate. In the same way, these techniques will assist in providing

information on the environment in terms of maintenance reduction costs problems as addressed by Mäkitalo et al. (2014), likewise to overcome the economic, logistical factors and material acquisition that could be the limitation to ARD prevention (Alakangas et al. 2013: 7908).

Environmental and Economic Solutions: In response to Nuzzio et al. (2011), Environmental Cost Management is suggested for the monitoring of current and future costs associated with the effects of ecological changes and of remediation efforts respectively to ARD assessment. Accordingly, this will develop the benefits of ARD assessment.

Environmental and Social Solutions: For the case described by Broadhurst et al. (2015), information may be available within the Environmental Management Accounting tool; in particular, its physical component can be used to prevent and assess physical environmental damages through relevant information.

Environmental Social and Economic Solutions: Activity-Based Costing and Activity-Based Sustainability can be simultaneously used to deal with the problem mentioned by Kefeni et al. (2017). While the first method deals with environmental and social cost information, the second one supports all activities involved in the process of ARD impact assessment. Thus, together they can effectively support the internal decision-making. Above these, management accounting tools allow for the provision of sustainability information (Matambele, 2014: VI) through the collection of information related to sustainability problems, effects, impacts, assessment, reparation and costs.

Conclusions

Our results show that ARD prevention and assessment firstly face environmental problems and secondly simultaneous environmental and economic, environmental and social as well as environmental social and economic issues. This confirms that sustainability is a fundamental concern for ARD management. Since SMA allows for monitoring, evaluating managing and communicating sustainability issues, this paper suggested various SMATs with the potential of solving the mentioned



problems. The findings support the view that SMATS could be indeed helpful and suitable for the effectiveness of ARD prevention and assessment.

References

- Abrosimova N, Gaskova O, Loshkareva A, Edelev A, Bortnikova S (2015) Assessment of the acid mine drainage potential of waste rocks at the Ak-Sug porphyry Cu–Mo deposit. *J Geochem Explor* 157:1–14
- Alakangas L, Andersson E, Mueller S (2013) Neutralization/prevention of acid rock drainage using mixtures of alkaline by-products and sulfidic mine wastes. *Environ Sci Pollut Res* 20:7907–7916.
- Anawar HMD (2015) Sustainable rehabilitation of mining waste and acid mine drainage using geochemistry, mine type, mineralogy, texture, ore extraction and climate knowledge. *J Environ. Manage* 158:111–121
- Arroyo P (2012) Management Accounting Change and Sustainability: An Institutional Approach. *J Account Organ Change* 8(3):286–309
- Becker M, Dyantyi N, Broadhurst JL, Harrison STL, Franzidis JP (2015) A mineralogical approach to evaluating laboratory scale acid rock drainage characterization tests. *Miner Eng* 80:33–36
- Betrie GD (2014) Risk management of acid rock drainage under uncertainty. PhD Thesis. University of British Columbia
- Betrie GD, Sadiq R, Morin KA, Tesfamariam S (2015) Ecological risk assessment of acid rock drainage under uncertainty: The fugacity approach. *Environ Technol Innovation* 4:240–247
- Betrie GD, Sadiq R, Nichol C, Morin KA, Tesfamariam, S (2016) Environmental risk assessment of acid rock drainage under uncertainty: The probability bounds and PHREEQC approach. *J Hazard Mater* 301:187–196
- Broadhurst JL, Kunene MC, von Blottnitz H, Franzidis JP (2015) Life cycle Assessment of the desulfurisation flotation process to prevent acid rock drainage: a base metal case study. *Min Eng* 76:126–134
- Burritt R, Hahn T, Schaltegger S (2002) Towards a comprehensive framework for environmental management accounting: link between business actors and environmental management accounting tools. *Aust Account Rev* 12(2):39–50.
- Darnall N, Edwards D (2006) Predicting the cost of environmental management system adoption: the role of capabilities, resources and ownership structure. *Strategic Manage J* 27: 301–320
- de Almeida RP, Leite ADL, Soares AB (2015) Reduction of acid rock drainage using steel slag in cover systems over sulfide rock waste piles. *Waste Manage Res* 33(4):353–362
- Dyantyi N (2014) Application of mineralogy in the interpretation of laboratory scale acid rock drainage (ARD) prediction tests: A Gold Case Study. MSc Thesis. University of Cape Town
- Engblom J, Solakivi TB, Oyli JT, Ojala L (2012) Multiple-method analysis of logistics costs. *Intern J Prod Econ* 137:29–35
- D'Onza G, Greco G, Allegrini M (2016) Full cost accounting in the analysis of separated waste collection efficiency: A methodological proposal. *J. Environ. Manage* 167:59–65
- Fan R, Short MD, Zeng SJ, Qian G, Li J, Schumann RC, Kawashima N, Smart RS, Andrea R, Gerson AR (2017) The formation of silicate-stabilized passivating layers on pyrite for reduced acid rock drainage. *Eng. Sci. Technol* 51:11317–11325
- Frostad S (1999) Prediction of acid rock drainage red mountain project. BSc thesis. University of British Columbia
- Fryling M (2010) Estimating the impact of enterprise resource planning project management decisions on post-implementation maintenance costs: a case study using simulation modeling. *Enterp Inf Syst* 4(4): 391–421
- Jasch C, Lavicka J (2006) Pilot Project on sustainability management accounting with the styrian automobile cluster. *J Cleaner Prod* 14:1214–1227
- Jeen SW, Bain JG, Blowes DW (2014) Evaluation of mixtures of peat, zero-valent iron and alkalinity amendments for treatment of acid rock drainage. *Appl Geochem* 43:66–79
- Jozsa PG, Schippers A, Cosma N, N. Sasaran N, Kovacs ZM, Jelea M, Vlichnea AM, Sand W (1999) A large-scale experiment for safe-guarding mine waste and preventing acid rock drainage. *Proc Metall* 9: 749–758
- Kazadi Mbamba C, Harrison STL, Franzidis JP, Broadhurst JL (2012) Mitigating acid rock drainage risks while recovering low-sulfur coal from ultrafine colliery wastes using froth flotation. *Min Eng* 29:13–21





- Kefeni KK, Msagati TAM, Mamba BB (2017) Acid mine drainage: prevention, treatment options, and resource recovery: A review. *J Cleaner Prod* 151(10):475–493
- Kokubu K, Kitada H (2015) Material flow cost accounting and existing management perspectives. *J Cleaner Prod* 108:1279–1288
- Mäkitalo M, Maurice C, Jia Y, Öhländer B (2014) Characterization of green liquor dregs, potentially useful for prevention of the formation of acid rock drainage. *Minerals* 4(2):330–344
- Maas K, Schaltegger S, Crutzen N (2016) Reprint of Advancing the Integration of Corporate Sustainability Measurement, Management and Reporting. *J Cleaner Prod* 136:1–4.
- Matambele K (2014) Management accounting tools providing sustainability information for decision-making and its influence on financial performance. MPhil thesis. University of South Africa
- Mechler R (2016) Reviewing estimates of the economic efficiency of disaster risk management: opportunities and limitations of using risk-based cost-benefit analysis. *Nat Hazard* 81:2121–2147
- Nuzzio DB, Zettler ER, Aguilera A, Amaral-Zettler LA (2011) A direct in situ fingerprinting method for acid rock drainage using voltammetric techniques with a single renewable gold micro-electrode. *Sci Total Environ* 409:1984–1989
- Parbhakar-Fox AK, Edraki M, Hardie K, Kadletz O, Hall T (2014) Identification of acid rock drainage sources through mesotextural classification at abandoned mines of Croydon, Australia: implications for the rehabilitation of waste rock repositories. *J Geochem Expl* 137:11–28
- Parbhakar-Fox A, Lottermoser BG (2015) A critical review of acid rock drainage prediction methods and practices. *Min Eng* 82:107–124
- Petcharat N, Mula JP (2009) Identifying system characteristics for development of a sustainability management accounting information system: towards a conceptual design for the manufacturing industry. Fourth international conference on cooperation and promotion of information resources in science and technology, IEEE, Beijing, China, 56–64, doi:10.1109/COINFO.2009.19
- Papaspyropoulos KG, Blioumis V, Christodoulou A.S, Birtsas PK, Skordas K.E (2012) Challenges in implementing environmental management accounting tools: the case of a nonprofit forestry organization. *J Cleaner Prod* 29–30: 132–143
- Rodríguez-Olalla A, Avilés-Palacios C (2017) Integrating sustainability in organisations: An activity-based sustainability model. *Sustainability* 2017(9):1072, doi:10.3390/su9061072
- Saha N, Rahman MS b, Ahmed MB, Zhou JL, Ngo HH, Wenshan Guo W (2017) Industrial metal pollution in water and probabilistic assessment of human health risk. *J Environ Manage* 185:70–78
- Sands J, Lee KH, Fonseka KBM (2016) Advancing sustainability management accounting in the Asia Pacific region. *Account Res J* 29(2):134–136, doi:10.1108/ARJ-03-2016-0035
- Stewart W (2005) Development of acid rock drainage prediction methodologies for coal mine wastes. PhD Thesis. University of South Australia
- Sulaiman M, Mokhtar N (2012) Ensuring sustainability: a preliminary study of environmental management accounting in Malaysia. *Int J Bus Manage Sci* 5(2): 85–102
- van Heeren A (1998) Management Accounting for sustainable development – A chain related case study between Costa Rica and the Netherlands. Paper presented at the Seventh International Conference of Greening of Industry Network, Rom:1–13 (online). <https://pdfs.semanticscholar.org/34a7/62095c59171056a9fcab0b4500a607913a02.pdf> Accessed 2018-06-07
- Wolkersdorfer C (2008) Water Management at Abandoned Flooded Underground Mines – Fundamentals, Tracer Tests, Modelling, Water Treatment. Springer, Heidelberg
- Zmijewski ME (1984) Methodological Issues Related to the Estimation of Financial Distress Prediction Models. *J Account Res* 22:59–82, doi:10.2307/2490859





Assessing and Mitigating Risk to Mining - Can we “Future Proof” the Industry?

Karen Dingley

WSP Ltd, karen.dingley@wsp.com

Abstract

Mining operators throughout the world, and those looking to invest in mining, are exposed to **risk** on a daily basis. Analysts reflect on the “top 10 risks to mining” on an annual basis, and generally these are consistent year on year, albeit the order influenced by immediate political and/or economic forces. Realistically however, how many of these really are tangible risks that could (and should) hamper an appetite for investment? Can the industry navigate its way through inevitable **uncertainty** that comes with global macro-economic change, political will (or lack thereof), and predicted longer term changes to our **climate**?

This paper considers the potential risks to the mining industry, with a specific focus upon Africa. We reflect upon the **appetite** that we see for accepting risk across the junior, mid-tier and major operator base, and international investors. We consider the options for sensibly mitigating risk, and we look into the **future** to gauge how the industry might improve not only its own resilience to change, but at the same time protect the communities, the customers, and the environment that is directly impacted by mining.

Introduction

Risk is an inherent trait of operating in the mining industry, from establishing the financial and legal framework for constructing the mine, to the inherent safety hazards that exist for our staff working on the ground.

Whilst the somewhat fatalistic approach to mine safety has certainly now largely gone, we have seen that the industry’s approach to appraising and mitigating risk has not fundamentally changed throughout our journey with the mining industry over the last 60 years. As engineers, we like to think that we are working with an exact science. This is not strictly true however – we are as susceptible to the cycle of trial and error as anyone.

In early 2016 I was called to Brazil as a lead engineer to support in the restoration of over 100km of river and protection of communities downstream of a major tailings reservoir. Nineteen (19) people were killed when the dam catastrophically failed. Relatively soon after the failure, discussions were being held about the restoration of the reservoir to enable production to re-commence - but the communities that had survived the breach were still living and working downstream.

Check dams were being constructed downstream to capture residual tailings following a rainfall event – but it was not rainfall that caused the failure, it was liquefaction. Had any lessons been learned at all?

The mining world did respond with immediacy to the failure, with many operators implementing audits of their tailings facilities. When you consider the ultimate cause of the breach in Brazil, it is clear that it was not simply the physical manifestation of the reservoir that was the root cause of the problem. Effective governance, knowledge management, clear responsibilities – all of these directly contributed to the collapse. Arguably these will not be captured by an audit of the tailings dam.

More fundamentally however, what will be the longer term implications for the mining world? In light of the fact that 19 lives were lost, thousands of people permanently lost their homes, hundreds of kilometres of a relatively pristine river system was significantly damaged – is there any case whatsoever for us to re-construct the tailings reservoir at the same location? Can we really engineer out all risk?



Conversely, a major contributor to the failure was the construction of upstream raises on the dam. It would appear that the Brazilian regulatory system is very unlikely to ever permit an upstream raise ever again in light of the disaster, and many governments have muted that they may follow suit. Is this an appropriate response? What would be the impact on the mining industry if such a dictate was introduced more widely?

As engineers we can exercise the benefit of hindsight and point to the state of the tailings on which the raise was being constructed in Brazil. Hindsight provides excellent 20-20 vision, and indeed we all know the importance of firm foundations for any structure, with or without an engineering degree.

And consider the injuries and deaths that occur in mining accidents around the world. These were generally all avoidable accidents, and the technology was in place in each circumstance to prevent these events from occurring. Do we therefore as the mining industry ultimately define risk in such a way that we accept that accidents will happen? And how do we define an “accident” if we can, in most circumstances, and again with the benefit of hindsight, explain why it occurred and that it should never have happened?

Top 10 Risks to Mining, Today & Into the Future

A comparison between the top ten risks identified by the mining industry during the height of the boom in 2011/2, and in our current, more cautious situation, flags some unsurprising differences. The availability of both skilled and unskilled labour during 2011/2 was a key concern. When speaking to those that were involved in the mining industry at that time and are no longer, arguably their primary risk now will be the availability of a secure job.

Nevertheless, there are far more consistencies than differences in this comparison. Global macro-economic forces, government interactions, the availability of water and power – all continue to heavily influence the success (or otherwise) of a mining venture.

Looking into the future, how do we foresee these may change? How might they influence our appetite for risk? Or the way in

which we develop, operate and close mines, so as to mitigate these risks?

Current projections in relation to the way in which we live indicate that by 2050, as an example:

1. Prosthetics could get so advanced in the next 10 years they could give people new skills;
2. Self-driving vehicles could be ubiquitous in the next 10 years;
3. 3D-printing could be used to construct more houses in 20 years;
4. We could rely entirely on renewable energy by the year 2050.

(source: Ian Pearson, Futurist)

This would suggest that the demand for metals will continue well into the future, though arguably with a demonstrable shift away from bulk commodities. So mining is here to stay.

The UK Ministry of Defence has stipulated the following as their prediction of the state of play in Sub-Saharan Africa in 2045:

1. Sub-Saharan Africa will almost certainly remain a region of significant political and economic differences by 2045, but overall the region's economy should grow.
2. Governance in the region is likely to improve and the current trend towards representative government is likely to continue, although this will probably be resisted by some authoritarian regimes, possibly leading to violence.
3. The risk of state-on-state conflict is likely to reduce but will almost certainly remain a concern. The African Union's ability to deal with crises is likely to improve, but it will probably still require international assistance for more demanding situations.
4. Climate change is likely to have a severe impact on some parts of sub-Saharan Africa, with agriculture particularly badly affected.

Once again, this would suggest consistency in risk trends that we have seen in the recent boom bust cycle will inevitably continue into the future. The availability of water and energy will continue to be a challenge, whilst demand for them will increase. Governments will change, and uncertainty in security, regulation, and appetite to encourage international investment will remain. It is interesting to



therefore reflect on how industry navigates risk today, and whether there may be questions to ask in relation to the need for change looking ahead.

Appetite for Risk Today & Future Proofing the Industry

The Market

No industry exists without a customer base, and indeed the market has been one of the key risks to global mining in recent years. The only true certainty in the many analyses and predictions that underpin the market media is that uncertainty is inherent.

The management teams of majors are replaced, and mining juniors come and go, in response to changing market conditions that many feel should have been predicted. Was it really feasible for the changes that have occurred over the last 5 years to have been accurately foreseen however? Or is it more reasonable to expect organisations to exercise a degree of foresight that commodity prices do inevitably fluctuate, and hence exercise sensible limits on their unit cost of production, so as to protect their assets when prices begin to fall? Reflecting back on the rate with which money was being spent during the recent boom, one must question how much restraint was being shown in anticipation of a cooling of the market.

It is also recognised however that shareholders demand optimal profits. So where does the responsibility ultimately sit? The public call for CEO scalps is rapid when profits fall, yet the demand to optimise return while the market is strong will inevitably be the key measure of corporate success.

It has been increasingly evident that the recent boom also led to a rapid over supply in commodities. It is broadly accepted that a drop in key currencies, aligned with a dramatic fall in the price of oil, resulted in a favourable tail wind that enabled mines to continue operation when arguably they were no longer viable. This simply resulted in further flooding of the market, and finger pointing as commodities continued to slide as supply rapidly out-stripped demand.

We have unsurprisingly seen a rapid increase in the demand for closure support in recent years. Interestingly however, we are

also seeing a number of the mines being prepared for closure being given a last reprieve, in response to fluctuations in commodity prices. This has been particularly evident in copper, nickel, and iron ore (for example), where mines are being temporarily placed into care and maintenance, only to be rapidly re-started as the price point climbs back into the black.

Considering market risk therefore, what is a reasonable expectation? Is it one of flexibility, i.e. to be able to respond to the inevitable market fluctuations in an uncertain world? Should we be designing mines that can be “switched on and off”, varying production (or closing it down temporarily altogether) to meet market needs?

Indeed, is there a potential argument for market regulation to control the supply of ore to the marketplace? With OPEC representing a working example of what can be achieved when producers exercise ultimate control over what will be supplied to the markets, are there lessons that can be taken (and improved upon) to develop a working model for mining?

Considering regulatory frameworks, it is evident that there is an appetite for a legislative response to perceived inequity in mining practices across the globe. The European Union is introducing legislation that will come into force from 2020 under which manufacturers will need to ensure that their supply chain is demonstrably free of “conflict minerals”.

Currently the commodities affected are relatively few in number, however awareness is increasing in relation to the impact that western consumerism is having on working conditions in the developing world. The term “modern slavery” is becoming more and more actively used, and governments are responding proactively (if slowly) in an effort to identify and protect against it, both in their own countries and abroad.

Funding

Securing funding for the development of a mine has become more and more challenging in recent years. Interestingly, the availability of money is not necessarily a constraint. Indeed investors have considerable funds and the appetite to invest remains strong.



Ultimately however, the appetite for risk has diminished, particularly where financing the junior space. Investors today are not looking for a quick return. They are seeking a longer term commitment that will involve taking the mine into operation, reflecting a tangible change in the management expertise required to progress a junior mining venture. For those that are willing to see it through, the financial backing is there.

It is evident however that there is a tangible shift away from the desire to seek “international funding”, in light of the increasing appetite for investment from China. Securing money from the western markets brings with it a requirement to satisfy international standards, and the cost and time implications that come with this. Generally however, the national legislative frameworks throughout Africa are robust, embracing the core intent of the international standards.

In our experience, whether the additional time and money invested ultimately alters the rigour with which the environment and the community is considered and protected through the design, construction and operation of the mine, fundamentally comes down to the integrity of the author and the operator. As we know is the case with many of our clients, we apply our global experience and expertise in all of the work that we do. Ultimately therefore, our recommendations for consultation, mitigation, and design will meet international best practice irrespective of the regulatory framework within which we are working.

There is a debate at play therefore as to whether organisations that choose to proceed with funding that avoids the need for formal compliance with international standards are taking “short cuts”. In doing so, they are perceived to be accepting an increased level of risk, and indeed imposing this on the environment in which they work.

We would argue that, in many circumstances, the integrity of the operator and their appointed engineers will inherently mean that the ultimate outcome will fundamentally be the same. As a result, the saving in time and money that will be achieved should not automatically be dismissed as an irresponsible approach that is fraught with risk. Instead, this

should reflect (under most circumstances) a considered decision, and a commitment to progressing the investment within the community in which the mine will be operating.

Energy & Water

Energy and water have been identified as key risks to the mining industry, and indeed to the world in general, for many years. Security of supply is absolutely fundamental to the running of any operation, and competition for diminishing resources can be fierce. This is set within a backdrop of a rising global conscience in relation to the protection of the environment, both today and into the future.

Energy (Power)

The availability of secure energy to fuel heavy industry is very limited, particularly on the African continent. This is a function of both geography, and limited available government investment in both capital spend and maintenance. When money is invested, not surprisingly there is a general consensus that this should be focussed towards enabling communities rather than industry, which holds relative wealth.

The result has for many years been a reliance on diesel fuelled generators – well tested, easily installed, and relatively straightforward to maintain. The competition for fuel is significant however, and many of us will have experienced the frustration of attempting secure a priority delivery in an environment that could, at times, be best described as rationing. And whilst the unit price of fuel to those in Europe will appear reasonable, the reality is that the cost in Africa is significant, reflecting a substantial proportion of the overall cost at any stage of the mining life cycle.

We have been working with investors and governments throughout the African continent (and globally), for many decades to develop long term sustainable power supply solutions. We have seen technology evolve, and the definition of “sustainable” change over time, lurching between social, environmental, financial, and longevity connotations. What is very evident however is that what we refer to as “renewable” solutions in the West are in fact now eminently workable solutions



for industry. Far from the small turbine installed on the corner of the mine office to power the lights, harnessing and storing solar power for the full time operation of a mine camp is now tried, tested and cheap. Needless to say, this also substantially contributes to the environmental credentials of the mine.

Water

Water is also a very precious resource. It is also, at times, a damaging and disruptive waste product. Interestingly we often see water being considered at a relatively late stage in the planning of a mine, and yet without a secure water supply throughout the year, a mine simply cannot operate. There is generally an underlying perception that water can always be sourced by some means, irrespective of the topography and geology, and crucially irrespective of the existing demands that are already in place on the finite available reserves. This can often lead to a substantial unanticipated hike in capital and operating costs to bring water to and from the site. Water is a heavy commodity to move, and an energy intensive commodity to treat.

Water can also be extremely problematic if not catered for in the early planning of infrastructure throughout the site, no matter how arid the environment. Many of the most extensive retrospective drainage and erosion control measures that we have had to develop for mining clients are situated in the desert regions of North Africa and the Middle East. The effective sizing and placement of water storage facilities and drainage systems is a cheap and easy exercise when carried out at an early stage. This also allows informed decision making as to the investment that is wanted in relation to space and cost, against the likelihood of operational downtime and asset damage due to flooding. When this is carried out reactively, typically it will be in response to the magnitude of the event that triggered the problem.

Inevitably adopting a reactive approach following a significant rainfall event will also mean that uncontrolled flooding has occurred, mobilising material from the mine site and washing it into downstream environments. At best this is often significant base loads of silt, sand and mud. Generally howev-

er there will also be contaminants mobilised that have the potential to cause harm. Mining operators will very rarely allow this to happen knowingly, but one occurrence will typically draw the attention of the community and the regulators, bringing with it considerable scrutiny, criticism, and often hefty fines. It is a scenario best, and very easily (and cheaply) avoided.

Permitting & Taxation

The risks and uncertainties associated with permitting and taxation is consistently flagged within the top ten to the mining industry, particularly when looking to develop and operate on the African continent.

From a permitting perspective, national legislation is generally very robust as alluded to earlier, and largely commensurate with international standards in most circumstances. The difficulty rests typically in the capacity and capability of the respective ministries to implement the legislation effectively. This can lead to a subjective application of legislative requirements that imposes greater restrictions on some operators than are required of others. This can include those that are seeking international funding, and therefore self-impose stringent criteria that must be met.

Ultimately however, our experience is once again that generally that there is a tacit intent from all parties to operate with integrity throughout the permitting process. Mining companies, irrespective of their size, typically hold a concerted commitment to their Corporate Social Responsibility credentials. In doing so, there is an inherent desire to comply with legislation, to operate without compromising the natural environment, and to support the local communities within which they are situated.

Indeed the corporate commitment to the communities within which the mines are being developed by international ventures is generally unquestionable. We see honest investment into education, medical support, upskilling and employment, and improving community infrastructure on a daily basis. The financial return is clearly a key priority, however this comes with a genuine desire to materially leave a positive legacy behind.



The payment of taxes and royalties is tacitly interlinked to this commitment, ensuring that a usually not insignificant proportion of the wealth generated remains in the country. The equitable application of this wealth is critical however, and this responsibility lies with the government departments that are the recipients of this money. Unfortunately it is evident that the money does not always reach the communities that are directly impacted by the mining, and/or in greatest need. This can undermine trust, particularly where criticism is then levelled at the mining company for not demonstrating material local investment.

Certainty in relation to the taxes that will be levied can also represent a key risk, and it is incumbent on governments to demonstrate consistency in the long-term if they are to encourage international investment in industry and infrastructure.

Closing Comments

So how do we “future proof” the industry against risk? Some risks are relatively straightforward, for example energy and water. These can be scientifically appraised, and whilst as engineers we are yet to create rain, we can enable informed decision making. And we do have practical cost-effective alternatives to “de-risk”, both today and into the future, through the implementation of alternative technologies. This simply requires early engagement by the mines.

Nevertheless, the question of re-defining best practice, or perhaps introducing greater self-regulation within the industry, does remain. Is there a need to factor greater flexibility into our mines in the future, so that

they can be readily turned on and off to meet fluctuating market demands? Is there a responsibility for miners to diversify so that shareholder returns are protected during a downturn? Is there a need to introduce industry best practice that will pre-empt emerging legislation in relation to “modern slavery” and the sourcing of minerals?

Inevitably there are risks that ultimately cannot be mitigated against, and the government framework within which we operate will always be the gift of the host country. An effective and thorough due diligence process, and a steadfast commitment to act with integrity throughout the life of mine, is all that can be done to address this.

Irrespective of these risks however, the appetite to invest in mining in Africa remains strong. It is a continent with considerable untapped resources, and an extraordinary capacity for great things. We have had the privilege of working and living in Africa for many years, and we never cease to be amazed at the resourcefulness and resilience that we experience every day.

The risks that are inherent within mining will inevitably remain, and some will come and go as we continue through boom and bust commodity cycles. The industry is inherently a robust one however, and one that operates with a conscience. Lessons are learned with the benefit of hindsight, and time will tell whether these are applied should commodity prices soar to giddy heights once again in years to come. Either way, mining will continue to be a very important industry to Africa, and absolutely fundamental to global progress.





To Invest Or Not To Invest? – A Valuation Of Mine Water Recirculation Comprising Private And Public Benefits In Ha Long, Vietnam ©

Hao Hong Do¹, Viet Quoc Trinh², Oliver Frör¹

¹*Institute of Environmental Sciences, Department of Environmental Economics, University of Koblenz-Landau, Fortstraße 7, D-76829 Landau, Germany, hao_do@uni-landau.de*

²*Institute of Environmental Engineering and Ecology, Faculty of Civil and Environmental Engineering, Ruhr-University Bochum, Universitätsstraße 150, D-44780 Bochum, Germany*

Abstract

Whilst pursuing profitable targets in business, environmental protection and conservation activities by mining companies are hardly pursued. This study aims to reveal the feasibility to gain benefits while investing in water treatment to recycle and reutilize mine water and achieve an efficient and environmentally benign water management in the Ha Long coal mining region in Vietnam. A cost-benefit and payback period analysis are conducted to provide a framework for the investment decision. Furthermore, a survey based on contingent valuation is adopted to estimate the willingness to pay for clean rivers in urban areas nearby the mining operations.

Key words: cost-benefit analysis, contingent valuation, ecosystem services, mine water, developing country

Introduction

Water resources are becoming increasingly scarce, albeit its essential role for human life. It has been one of the most widely overused and polluted natural commodities on our planet. Besides, coal mining causes not only severe pollution of surface and groundwater but also hazards to the surrounding nature and ecosystem. Nonetheless, available literature concerning economic concepts of the solutions of these mine water-related issues is mainly about the economic efficiency of a technological application within the private investment of mining companies (Haibin & Zhenling 2010; Dharmappa et al. 2000); the potential effects to society are rarely considered thoroughly. Thus, this paper attempts to identify and associate the positive welfare gained from an efficient mine water management in two ways: the mining company on the one hand and society on the other hand, or in other words, the internal and external benefits. First, it provides a cost-benefit analysis of the investment in water treatment plants for recirculation and reuse within the coal mining industry in Vietnam. Thence, it employs an economic valuation of the external

benefits of such an investment in improving the river aquatic environment, hence the ecosystem, in the vicinity of the hard coal mining region in Ha Long peninsula, Vietnam.

In Vietnam, the coal mining industry has experienced a long history of 178 years. It is located mostly in the northern regions of the country. In 1994 the Prime Minister enacted the establishment of Vietnam national coal and mineral industries holding corporation limited (Vinacomin), with one hundred percent of the charter capital coming from the State. Contributing the largest portion to the economic structure of Quang Ninh province, the hard coal mining industry proves to be an important sector. Whilst Ha Long Bay has been a UNESCO world natural heritage site twice, coal exploitation comprises nearly 50 percent of the city's total economy (Vietnam Institute for Urban and Rural Planning 2013), severely adding to the pollution of this tourism city – the centre of the province with rapid economic development. Although the mining companies have continuously enhanced equipment for purification of mine water, the vulnerability still remains in the current system. Each day, mining activities



in Ha Long release about 95,000 cubic meters of mine water. By 2016, 51 percent of mine water volume was not properly treated but directly discharged into the environment, causing pollution for adjacent rivers. On account of the scarcity of this natural resource and the economic growth, Ha Long is forecast to be in a shortage of freshwater at 28,000 cubic meters per day by 2030. For the above reasons, the WaterMiner project, funded by the German Federal Ministry of Education and Research (BMBF), focuses on improving the efficiency and effectiveness of mine water management within Ha Long peninsula through the material flow analysis (Brömme et al. 2018), the technical concepts (Ulbricht et al. 2018), and the economic concepts. The remaining structure of the paper is as follows: the next section presents the cost-benefit analysis of mine water recirculation and reuse for an individual mining company; the following section analyses the social benefits by a non-market valuation technique; finally, the paper discusses and concludes.

Estimation of internal benefits – an investment cost analysis

Nui Beo Coal joint stock company, a subsidiary of Vinacomin which we use as a case study, exploits both open-pit and underground mining, of which the latter consumes extensively more water during operation than the former. The implementation of underground mining since 2017 has led to a sudden tremendous demand for clean water. Currently, the provision of clean water relies upon the water company of the province (Quawaco), meanwhile, a vast amount

of mine water is discharged into the environment after partial treatment. With the expansion of coal mining, the gap between demand and supply of acceptable water quality for different use purposes is increasing and thus raises awareness for the potential of recycling and reusing mine water.

For that reason, this study focuses on the approach of recirculation and reuse of mine water. Mine water treatment in all coal mines is managed by Vinacomin environment company, to which each subsidiary mining company pays fees for the services. The mine water treatment plant in Nui Beo company reaches the capacity of 1,200 cubic meters per hour, generating output water satisfying the national standard for industrial wastewater. This water is reused for such as coal selecting, dust control, road washing, machine washing whilst water with higher quality for domestic use needs further treatment. Thence, a newly supplementary water treatment station advances the treated mine water to the water qualifying the national standard.

Mine water from the underground pit is less likely to depend on the season and is thus more stable in volume than the open-pit mining. 200 litres per day is the average amount of needed water per worker for regular operation such as washing work clothes and equipment, bathing after work and cooking. Currently, the total number of workers of the company is 1500 persons projected to be doubled by 2025. In reality, the amount of consumed water is higher than the projected amount due to the currently low consciousness of saving water of workers. From this circumstance, a flexible treatment capacity is

Table 1 Quantity and costs of water supply for domestic use.

Pos.		Amount/day (m ³)	Amount/year (m ³)	Unit cost (VND/m ³)	Cost/year (VND)
1	Produced water	400	146,000	6,618	966,228,000
2	Water bought from clean water supplier				2,204,600,000
	The first 200 m ³ /day	200	73,000	12,500	912,500,000
	The next 200 m ³ /day	200	73,000	17,700	1,292,100,000
3	Variable cost saving				1,238,372,000
4	Initial investment				6,885,333,146



necessary. Altogether, after thorough consideration, an investment into an automatically supplementary water treatment system with a capacity of 400 m³/day is plausible to recirculate mine water for domestic use.

In the economic and technical report of water treatment plant for domestic use (VITE-Vinacomin 2016), the list of supplementary treatment costs includes (i) chemical ingredients: pH balancing, nano iron(0), NaClO, (ii) electricity, (iii) labour, (iv) maintenance, which are transformed into 3,120; 2,680; 808; and 10 VND per cubic meter, respectively. In summary, the unit cost yields 6,618 VND (US\$ 0.292/m³). The supplementary plant locates in the adjacent area of the existing one to acquire the advantage in water delivery. Table 1 exhibits the cost-benefit analysis of an investment in a supplementary water treatment facility. Benefits stem from the monetary saving from further treatment and recirculation of water instead of buying from external suppliers.

Based on the results of table 1, the net present value (NPV) is calculated towards 2030 under the current plan of coal mining in this company. The NPV of an investment in 2017 at about 6.885 billion VND (pos. 4) following with about plus 1.238 billion VND saved annually cash flows (pos. 3) in a duration of 13 years yields about 5.291 billion VND, given that the discount rate is proposed by the State Bank of Vietnam (2017) at 4.25% (The use of a discount rate in this analysis depends on the expected price changes of purchased water. If we expect a price change in the range of the assumed discount rate, the rate should be ignored. Conversely, if price changes are expected to be very low, the discount rate should be used.). Another technique to evaluate the economic feasibility of the supplementary water treatment is the payback period, which is estimated at 5.56 years, whereas the discounted payback period using the same discount rate as in NPV extends to 6.48 years. Since the underground mining of Nui Beo is projected to continuously function for a long time, at least beyond 2030, the positive profit for the investor is unambiguous by comparison.

Estimation of external benefits - a contingent valuation study

Method

Ecosystem services typically represent non-market goods since they are provided free of charge by nature. Usually, property rights to them are not assigned, therefore, they cannot be included in the market mechanism. As mentioned above, investments into water recirculation and reuse require more advanced water treatment technology so that water discharged into the rivers will be much cleaner and will allow those downstream river ecosystems to provide better services to society. In this paper, we aim at valuing these external benefits by the non-market valuation technique contingent valuation which has become one of the standard methods for the economic assessment of ecosystem services. However, it has only rarely been applied in Vietnam and so far not at all in the context of mine water.

It is standard technique in environmental economics to use contingent valuation (CV) and choice experiments (CE) as stated preference methods for valuing non-market ecosystem services. In these methods, a representative survey is used to establish a hypothetical market and describe scenarios of an environmental improvement for which respondents can then state their personal willingness to pay (WTP). CE is employed to measure marginal values of various independent ecosystem service changes, whereas CV is used for directly measuring the value of a fixed combination of such ecosystem service changes. Which of the two methods to adopt follows from the specific research purpose.

Mine water pumped from open-pit and underground mines is not the only concern of the WaterMiner project. Further focus is placed on the management of surface water runoff which is contaminated by very much impurities such as coal, coal sludge, coal gangue, rock, and soil. While upgrading the collection and treatment of mine water and surface runoff, the positive spill-over effects on the adjacent ecosystem of discharging rivers are noticeable. These ecosystem services



are classified as public goods by reason of the naturally non-excludable and non-rivalrous characteristics. The first aim of the study was to assess the overall value of the generated environmental public goods in a pilot survey serving as initial steps to understand the research object. To this end, the CV method was employed. Subsequently, the implicit WTP, thus the utility, of the households towards the entirely non-market improvement in the currently polluted river is uncovered by their stated preference. The second aim of the study was to determine the budget constraint of the residents in such a hypothetical market experiment. This led to the adoption of a double-bounded dichotomous choice elicitation question format. After the first closed-ended question about WTP, the follow-up bid is contingent upon the initial response. I.e., the second bid would be higher or lower whether the first answer is ‘yes’ or ‘no’, respectively. There are four possible pairs of outcome: (i) yes-yes, (ii) yes-no, (iii) no-yes, and (iv) no-no. Then, the estimation of results relies on the Maximum likelihood approach laid out by Hanemann et al. (1991). The influence of bids on the probability of willingness to contribute is tested using probit models.

To investigate the value of these environmental changes, a pilot survey of 30 door-to-door in-person interviews was implemented in November 2017 with households living along and nearby Lo Phong river. Before this survey, several expert interviews to understand the locality, current environmental problems, future plans, and appropriate payment amounts have been conducted with the regional authorities from DONRE, DOC, Quawaco, heads of residential quarters, members of Farmers Union and inhabitants of relevance. Further, in the WaterMiner project, environmental economists worked closely with ecologists, engineers, and specialists from Vinacomin.

The Lo Phong river is 7.11 km long, located in the Ha Phong ward. On the one hand, the Lo Phong river receives water from two large surface mines, namely Ha Tu and Tan Lap. Besides, it had played a role as a transferring channel for mine water pumped from the Ha Tu mining workshop to the treatment plant only until 2017 when a pipeline

system was constructed instead. Mine water discharged in the river has not always been totally collected to be treated in the treatment station. Typically, a huge amount of surface water from mining workshops containing an abundance of coal, rock, and soil runs directly to the river in the rainy season. On the other hand, municipal wastewater from adjacent residential areas flows directly to the Lo Phong river. Eventually, the river is highly polluted, which triggers various environmental threats, harms the riparian vegetation and leads to health-related risks (Hendryx and Ahern 2009). Altogether, the concerns regarding polluted water caused by acid mine water, coal sludge and municipal wastewater as well as water flow disturbance triggered by rock, soil, and solid waste and risk of flood in the rainy season have become quite strong.

According to the contingent valuation technique and the NOAA Panel guidelines (Arrow et al. 1993), a questionnaire was designed with four parts: (i) an introduction of the WaterMiner project and the survey, (ii) questions about the connection of the river and its ecosystem services with participants’ livelihood used as a warm-up, (iii) attitudinal questions, scenario description and the WTP elicitation question and (iv) socio-demographic questions. To obtain the constraint in monetary contributions, two bids were raised regarding the monthly WTP in a three-year period. The first bid was fixed at 40,000VND (US\$ 1.8), then the second bid depended on the answer to the first question. If the answer was ‘yes’, the follow-up bid increased to 50,000VND (US\$ 2.2); otherwise, in case it was ‘no’, the follow-up bid decreased to 25,000VND (US\$ 1.1). The response rate was 100%.

Data description and regression results

On average, the participants’ age is 48.9, of which 58.6% are female. A majority of them have lived there for a long period; the mean is 28 years, which implies that they have witnessed considerable changes of the river and its ecosystem services over time. High school or vocational training is the average education level. The mean income of the participants is quite low, ranging between 2 and 5 million VND/month (US\$ 88–US\$ 220/month). Un-



der the circumstances of living on the outskirts of Ha Long and the reference from the classification of income tax in Vietnam, the participants' income is categorized into 5 levels. The attitudinal questions follow a five-level Likert scale. The mean participant assesses their own awareness of environmental protection to be fairly good. Plus, they feel fairly confident that other inhabitants would be willing to pay as well.

Table 2 reports the summary regression results of 5 models: double-bounded regression, interval regression, ordered probit, probit with pooled data, and probit in panel data. To control over heteroscedasticity in standard errors, the Huber-White procedure is applied in all regressions except model 1. Regardless of numerous attitudinal and socio-demographic questions in the enquiry, all regressions involve only regressors that significantly explain the probability and amount of WTP and produce higher log-likelihood values to mitigate consuming the degrees of freedom of the models. Income, gender and personal self-awareness of environmental protection significantly affect the WTP of inhabitants in the vicinity of Lo Phong river in the same direction across 5 models. The dependent variables in model 1 and 2 are bid values offered to respondents. The former uses

a command developed by López-Feldman (2012) and the latter is based on the interval regression command with controlling over heteroscedasticity in Stata. In respect of the 4 possible outcomes mentioned above, the true utilities of respondents fall into 4 ranges: [0; 25,000], [25,000; 40,000], [40,000; 50,000], and [50,000; +∞]. Outcomes indicate no divergence in coefficients between these two models. If the respondent's income increases to the next level, *ceteris paribus*, the monthly WTP will increase statistically significantly by 20,040 VND. Instead of ranging the respondents' WTP into intervals, the dependent variable is coded into 4 corresponding orders: 1, 2, 3, 4. Model 3 illustrates results of an ordered probit model as expected. An upgrade in income level reduces significantly the probability of refusing the project, in the meantime raising significantly the probability of supporting the project at the highest bid. Overall, the estimated mean WTP is 44,256 VND/month, being statistically significant at 0.1% with the 95% confident interval [38,409; 50,103].

To capture the cost effect on the probability of support for the project, probit models are employed. The individual responses to three bid-levels are transformed into the binary variable with 1 implying in favour and

Table 2 Regression results.

Variable	Model 1 <i>Double-bounded</i>	Model 2 <i>Interval reg.</i>	Model 3 <i>Ordered probit</i>	Model 4 <i>Probit</i>	Model 5 <i>xtProbit</i>
	Coeff. (s.e)	Coeff. (s.e)	Coeff. (s.e)	ME (s.e)	ME (s.e)
Income	20.04*** (4.864)	20.04*** (5.429)	1.663*** (0.390)	0.659*** (0.123)	0.613*** (0.134)
Gender (M=0, F=1)	16.51*** (6.063)	16.51** (6.760)	1.356*** (0.504)	0.506*** (0.147)	0.474*** (0.166)
Self-awareness	-6.934** (3.464)	-6.934* (4.088)	-0.566* (0.318)	-0.206** (0.099)	-0.203** (0.098)
Bid level				-0.025*** (0.005)	-0.025*** (0.005)
Constant	17.74 (12.48)	17.74 (16.423)	- -	- -	- -
Log-likelihood	-29.19	-29.19	-28.93	-	-
Wald Chi-square	18.12***	14.20***	19.65***	49.14***	46.27***
McFadden R2	-	-	0.286	0.456	-

*** Significant at least at 1% level; ** Significant at least at 5% level; * Significant at least at 10% level.



0 implying opposition. The number of observations is thus artificially augmented to 90. Under this arrangement of the data set, it is essential to control on cluster-robust standard errors. Specifically, model 4 is a pooled probit model with the cluster effect on individual meaning 30 clusters. Model 5 uses the panel data format on the basis of probit regression with the heteroscedasticity-robust and the population-averaged effect. Since the estimation in panel data accounts for the dependence over time, or bid in this case, the potential efficiency increases. For better interpretation, table 2 demonstrates outcomes of model 4 and 5 in marginal effects (ME), which are consistent with results of three previous regressions. Higher income people are significantly more likely to say ‘yes’ to the offer than the counterparts with lower income. Females are significantly more willing to contribute than males. In contrast, people considering themselves having a higher awareness of environmental protection are less likely to support the project than the counterparts. Notably, as the bid increases by 1000 VND, *ceteris paribus*, the probability of support decreases statistically significantly by 2.5%.

Discussion and conclusions

Facing the increasing demand for water and the shortage of water supply in the future in Ha Long in general and in the mining company in particular, the water treatment technology for domestic water use in Nui Beo partly solves the problem. Additionally, it offers the company the considerable autonomy in water provision for its regular operations, which brings various merits and not just economic advantages. As demonstrated using the example of Nui Beo coal mining company, the investment in a treatment station with a capacity of 400 m³/day involves a 5.56-year payback period or 6.48-year after discounting. Moreover, the NPV indicator lasting in 13 years shows a positive number at about 5.291 billion VND. Considering the long-term mining activity of the company, an investment is clearly preferable.

From the survey results, detrimental impacts on the ecosystem of Lo Phong river primarily triggered by mine water and municipal wastewater lead to the high willingness

of inhabitants along the river to financially support the project to generate ecosystem services. As expected, the budget constraint is significantly of crucial importance in the WTP of respondents. Likewise, the monetary amount of bids significantly affects the support of the program in an adverse direction. Females and those with lower self-awareness of environmental protection are more likely to be in favour of the project. Perhaps people who are more willing to pay for the environmental improvement regard it as a means to compensate for their not-yet well environmental consciousness. Remarkably, the ratio of the mean monthly contribution to the average income of the participants is rather large, about 1%-2%, albeit at a low absolute value (US\$ 1.95) compared to the WTP in developed countries.

Altogether, this study reveals that not only internal benefits for the mining company itself but also the external benefits spilling over to society as a whole are the notable rewards of an efficient and effective management of mine water for recycling and reuse. The measurement methods bring transferable and applicable prospects to other mining companies in Vietnam and in other developing countries with similar features. Notwithstanding, the recycling possibility of mine water to direct drinking water is not covered in the paper. Because the study relies solely on monetary values, it lacks the resolution to cope with the limit of stating positive values due to households’ budget constraints. In poor nations, typically in rural or suburban regions, household income is extremely low so that people can hardly afford any monthly extra expense. Regardless of the significant WTP in terms of money from this study, further research with new approaches to capture the comprehensive WTP, hence the social benefits, of the very low-income group is needed and expected to shed new light on valuing those external benefits.

Acknowledgements

The authors wish to thank the German Federal Ministry of Education and Research (BMBF) for funding this project. The authors are thankful for the coordination with the colleagues from WaterMiner and Vinacom.



References

- Arrow K, Solow R, Portney PR, et al (1993) Report of the NOAA Panel on Contingent Valuation. *Fed Regist* 58:4601–4614. doi: 10.1258/095646202760029804
- Brömme K, Trinh VQ, Greassidis S, Stolpe H (2018) Material flow analysis for spatiotemporal mine water management in Hon Gai, Vietnam. In: *Proceedings 2018 of the International Mine Water Association Congress IMWA*. Pretoria, South Africa
- Dharmappa H., Wingrove K, Sivakumar M, Singh R (2000) Wastewater and stormwater minimisation in a coal mine. *J Clean Prod* 8:23–34. doi: 10.1016/S0959-6526(99)00309-1
- Haibin L, Zhenling L (2010) Recycling utilization patterns of coal mining waste in China. *Resour Conserv Recycl* 54:1331–1340. doi: 10.1016/j.resconrec.2010.05.005
- Hanemann M, Loomis J, Kanninen B (1991) Statistical Efficiency of Double-Bounded Dichotomous Choice Contingent Valuation. *Am J Agric Econ* 73:1255–1263. doi: 10.2307/1242453
- Hendryx M, Ahern MM (2009) Mortality in Appalachian coal mining regions: the value of statistical life lost. *Public Health Rep* 124:541–550. doi: 10.1177/003335490912400411
- López-Feldman A (2012) Introduction to Contingent Valuation Using Stata. MPRA. doi: 10.1258/095646202760029804
- The State Bank of Vietnam (2017) Decision No.1424/QĐ-NHNN
- Ulbricht A, Bilek F, Brömme K (2018) Development of a technical concept of spatial and temporal coordinated mine water recycling exemplified by a mining area with urban influence. In: *Proceedings 2018 of the International Mine Water Association Congress IMWA*. Pretoria, South Africa
- Vietnam Institute for Urban and Rural Planning (2013) Adjustments of Masterplan for Ha Long city – Quang Ninh province to 2030, vision towards 2050 [*in Vietnamese*]
- VITE-Vinacomin (2016) The economic and technical report of water treatment plant for domestic use [*in Vietnamese*]



Practical Applications of Groundwater Modelling for Dewatering Management in Open Pit and Underground Mining, Didipio, Philippines ©

Anna Kluza¹ and Lee Evans²

¹*OceanaGold Philippines Inc., Didipio Operations, 2nd Floor, Carlos J. Valdes Building, 108 Aguirre Street Legaspi Village, 1229 Makati City, Philippines, Anna.Kluza@oceanagold.com*

²*GHD 2 Salamanca Square, Hobart, Tasmania, 7000, Australia*

Abstract

Groundwater modelling has been used to inform dewatering management decisions at the Didipio mine. The modelling approach benefited from the scale and pace of mining, particularly the rapid vertical development of the open cut mine. In addition to this, ongoing data collection and hydrogeological involvement allowing refinement and validation, has resulted in a tool that can be practically applied to the mining geometry and schedule to predict the relative differences between mining and dewatering approaches. High groundwater inflows have been successfully predicted in advance of mining, providing justification to adequately resource the dewatering efforts required for successful mining.

Keywords: Groundwater modelling, dewatering management, predictions, open pit, underground

Introduction

The OceanaGold Philippines Inc. (OGPI), Didipio project is located in Nueva Vizcaya Province, on the island of Luzon in the Philippines (fig. 1). Didipio is a high grade porphyry copper-gold open pit and underground mine. Production is in the range of 150,000 – 160,000 oz gold and 18,000 – 19,000 t copper per year with an estimated mine life to 2032 (OceanaGold 2018).

The regional geology comprises late Oligocene volcanic, volcanoclastic, intrusive and sedimentary rocks overlying a basement complex of pre-Cenozoic age tonalite and schist (Griffiths et al. 2014). The Didipio deposit is hosted within the Didipio Stock, which is in turn part of the larger Didipio Igneous Complex (Griffiths et al. 2014). The deposit has been identified as an alkalic copper-gold porphyry system that includes at least four intrusive igneous phases (Wolfe and Cooke 2011).

The project entered construction in 2011, mining commenced in August 2012 and commercial production was declared in April 2013. Mining of the open cut was completed in May 2017. The open pit extends 220 m below its access, which lies in a valley at approx-

imately 670 m above sea level at the foot the Mamparang Mountains, which locally peak at 987 m above sea level. The development of the underground mine commenced in March 2015 and extends 450 m below the open pit. Beyond the mine area, the area is populated and/or cleared for farming with adjacent areas heavily forested, particularly in the elevated mountainous terrain (fig. 1). The area receives a high rainfall with an average of 3.4 m based on the last 10 years of data (Medidas and Kluza 2016). High runoff results in large flows in the Dinauan, Surong, and Didipio rivers (Figure 1).

Pre-mining Hydrogeology at Didipio

Initial hydrogeological assessments (Dames and Moore 1995) included packer tests resulting in 16 estimates of hydraulic conductivity as well as pumping and flow recession tests resulting in 29 estimates of transmissivity. A significant baseline hydrogeological dataset is documented in Coffey (1998a and 1998b) including: temporal hydrographs for groundwater levels at 9 locations (13 bores) and flows in 8 artesian drill holes over time; 68 drawdown and recovery test hydrographs



including data for a 33 day pumping test; groundwater bore logs; 72 estimates of hydraulic conductivity; and 27 estimates of storage. RDCL (2008) conducted packer tests

resulting in 8 estimates of hydraulic conductivity. With these data as background, MWES (2011) produced a groundwater flow model for mine dewatering and site water supply.

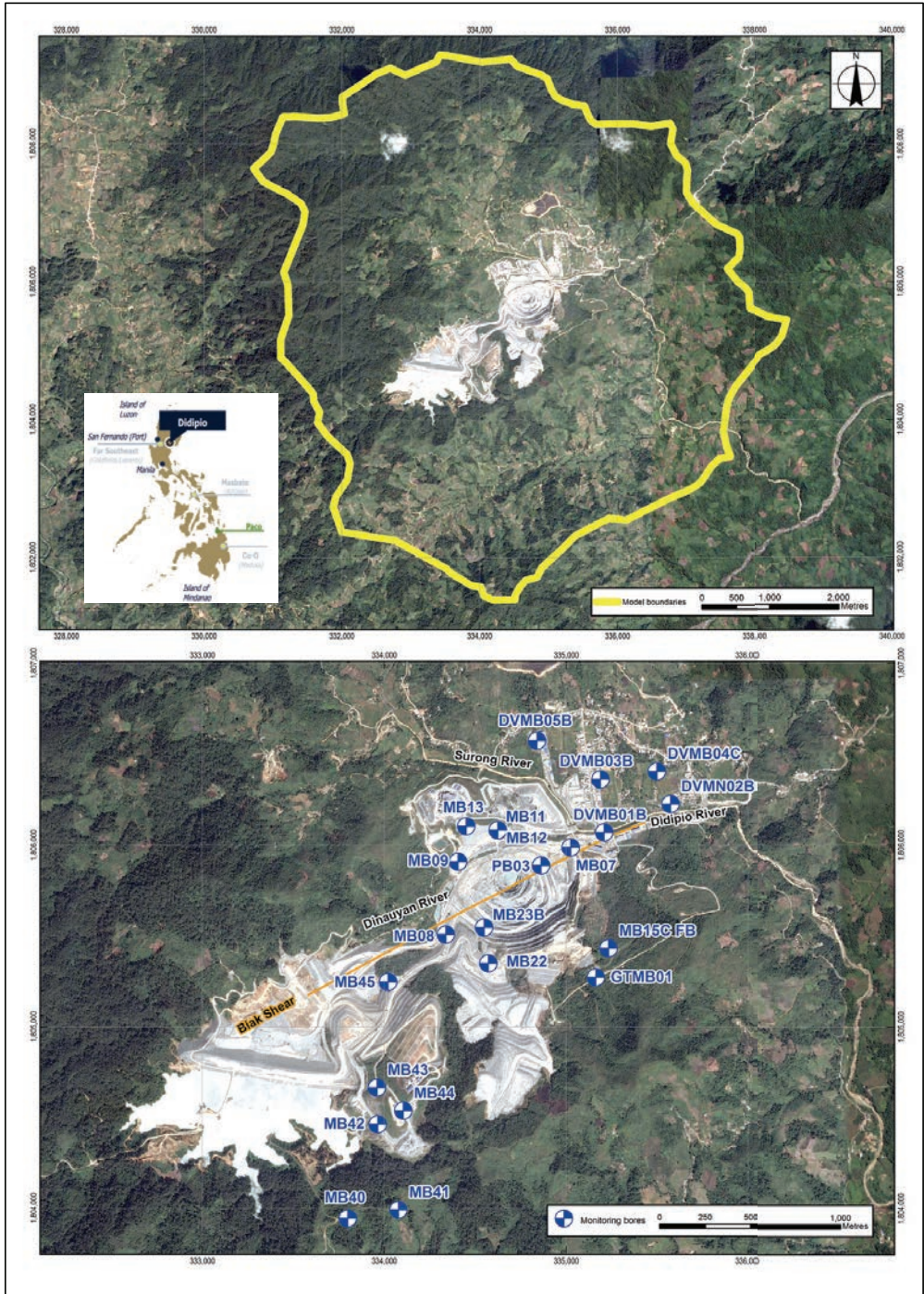


Figure 1 Location map, groundwater model boundary, monitoring bore locations and local rivers



The above works established the conceptual hydrogeological model of a highly hydraulically conductive regional scale fault zone (the Biak Shear), in a relatively low hydraulically conductive basement.

Optimisation study: Didipio Mine Hydrogeology and Groundwater Model (2012-2014)

GHD has been involved in hydrogeology during the mining stages at Didipio, initially as part of an optimisation study documented in Griffiths et al. (2014). The hydrogeological work of this study involved the following phases:

- Phase 1 Site Hydrogeological Assessment (December 2013)

With all groundwater monitoring bores destroyed in the period between 1999 and 2013, the first phase of the contemporary works oversaw the drilling of new groundwater monitoring bores, as well as the initiation of open pit and bore pumping data collection by OGPI site staff.

- Phase 2 Hydrogeological Modelling For Open Pit Mining (2014)

With an acceptable calibrated model resulting in reasonable predictions of mine water inflows, defensible results about the relative benefits of different dewatering approaches were demonstrated and informed management decisions were then able to be made based on the model results. At that stage this included demonstration of the relative benefits of perimeter bores, in-pit bores and sump pumping in this unique hydrogeological setting. Thus, OGPI focussed its open pit dewatering resources on in-pit sump pumping approach.

- Phase 3 Hydrogeological Modelling For Underground Mining (2014)

The initial GHD groundwater model predicted the underground inflows at rates at 450 L/s. At this stage the confidence in the model was limited due to the lack of hydrogeological data in the underground mining area, and that the calibration of the model was primarily based on a single 33 day pumping test stress.

- Phase 4 Validation and Calibration Hydrogeological Modelling (2014)

The influence (stress) of the open pit mining on the groundwater regime provided a local but rapid drawdown at a scale that could be replicated in the groundwater model, improving the level of confidence in the model in a relatively short time frame. This presented an opportunity to validate the model with the outcomes demonstrating that the groundwater models predicted groundwater inflows were inline with the measured open pit inflows.

Key to models design were accurate monthly pit shells provided by OGPI, which provided the dominant model stress when applied to model as drain elevations changing over time. The study also demonstrated the value of both groundwater monitoring infrastructure and well co-ordinated and prolonged data collection by OGPI site staff.

- Phase 5 Final Mine Design Hydrogeological Modelling (2014)

Phase 5 took the validated and recalibrated groundwater model and produced predictive inflow simulations for numerous mine designs and schedules as part of the optimisation study. The final mine design and schedule from the Didipio Optimisation Study was then incorporated into the groundwater flow model. Over the underground mining life, the modelled flows rise sharply with the vertical advancement of the decline and peak at approximately 450 L/s. Whilst key hydrogeological data remained sparse at depth, the mine geometry and schedule were able to be incorporated into the model at a higher degree of fidelity increasing the confidence in the model outputs. This work increased the confidence for OGPI to design and procure infrastructure at the scale of the predicted dewatering requirement.

Continued groundwater data collection (water levels and in-pit sump pumping) coupled with collecting data from the early underground development was recommended. These data were expected to provide validation and recalibration opportunities for the hydrogeological model, to further increase confidence in predictive flows and aid in the



decisions associated with the detailed design of underground dewatering infrastructure.

Recent Groundwater Modelling at Didipio

Since the initial optimisation study work (2015 onwards), GHD has remained involved with the site, providing a combination of hydrogeological advice, ongoing groundwater modelling support and training for on-site staff. Additional works undertaken by OGPI has involved modelling different mining approaches and schedules (both underground and open pit); the relative benefits of different underground and open pit dewatering strategies; increasing the layering to allow analysis of flows by both time and by mine pit and underground level.

In 2017, GHD and OGPI collaborated again on a second major stage of validation and calibration of the groundwater model. The recent work benefited from: continued regular monitoring of pumping and water level data by OGPI site staff; an increased dataset of hydraulic conductivity interpretations within the orebody and surround country rock ($n=158$) from slug and packer; and an external review of the groundwater modelling works to date (Dodson 2017).

- Current Didipio groundwater model inputs

The Didipio groundwater model is constructed in the Groundwater Modelling System (GMS) interface and uses MODFLOW NWT. The model is divided into 30 vertical layers that allow the underground mine geometry and schedule to be inputted in detail using linear drains. Transient TINs of the mine pit at a monthly resolution provide drain elevation inputs. The WELLS package is used to model existing extraction bores and the RIV package represents the rivers. General heads are applied only on the Biak Shear, otherwise no flow boundaries are applied to surface topographical divides (fig.1). Recharge is applied at 10% of rainfall which also corresponds to OGPIs chloride mass balance calculations.

The latest work comprised of: increasing the model boundaries to a distance beyond the influence of the mine dewatering (backed by the external review recommendation) to a model grid of 7.5 by 7.5 km (fig. 1) with

a base cell size at 15 m, and simplifying the complexity of the model (reducing from 17 geological and hydraulic parameters (fig. 2) to 3 key hydrogeological units, namely hard rock, Biak shear and oxidised/alluvial material) whilst not increasing model residuals in the observation bore network (fig. 1). This enabled the application of hydraulic conductivity properties at approximately the geometric mean of the large testing dataset of 0.33 m/day (applied as 0.5 and 1 m/day) for the Biak Shear and 0.026 m/day (applied as 0.03 m/day) for all hard rocks. All cells are convertible from confined to unconfined with specific yield assigned at 0.01 for the Biak Shear; and storativity values assigned at 0.00005 and 0.000001 (1/m) for the Biak Shear and hard rocks respectively.

- Current Didipio groundwater model outputs

With the open cut now finished, the primary objective for the groundwater model is to predict underground inflows. The model is capable of replicating observed underground inflows (fig 3.) with a scaled root mean squared (RMS) residual of 11% for underground flows. The modelled peak inflows range from approximately 450 to 475 L/s. This gives increased confidence in the model predictions going forward, however, it has always been recognised that the groundwater flow model is not designed for, nor capable of predicting mine inrush conditions and these need to be considered separately.

Despite the inflow calibration success, overall the groundwater model currently is not calibrating as well for groundwater levels (based on standard scaled RMS measures, although this is significantly improved if pit and underground induced and observed levels are included in the statistics). It is assumed that this is in part due to the complexities in the overlying oxidised/alluvial material, which appears to have little impact on mine inflows, but do impact shallow groundwater levels. Some bores, however, in key areas adjacent to the mine, are calibrating very well (i.e. MB23B on fig. 1) especially considering the very large drawdowns observed. Improved calibration of groundwater levels represents an area for improvement and would be required if the groundwater flow model was intended to be



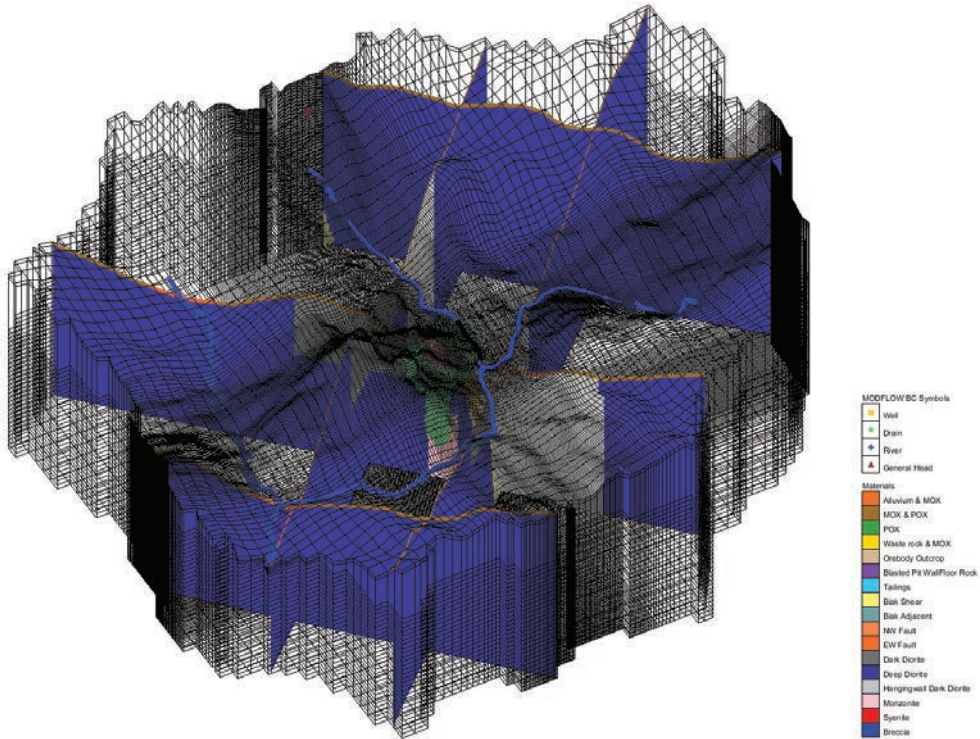


Figure 2 3D representations of the Didipio groundwater model looking west at a dip of 45 degrees

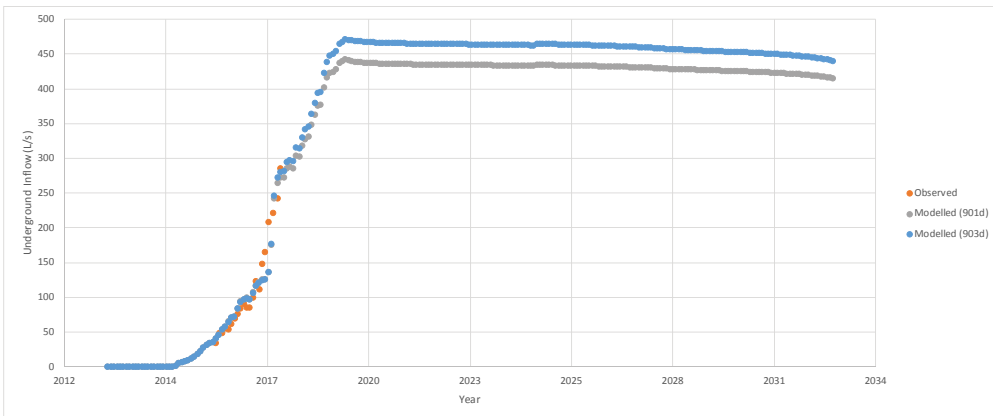


Figure 3 Observed vs modelled underground inflows and predicted inflows

used for alternate uses, i.e. for the accurate consideration of the aquifer drawdown from an environmental perspective.

Summary and Conclusions

Groundwater modelling for mine dewatering management is an important tool to aid management decisions to ensure that dewatering approaches are appropriately sized, funded

and implemented. This paper presents the groundwater modelling journey undertaken at the Didipio mine.

Mining progressed at fast pace and the resultant influence on the groundwater regime provided a local but rapid drawdown at a scale that was able to be replicated with the groundwater models and at a pace that enabled a higher degree of confidence to



be obtained from the models in a relatively short time frame. Installation of groundwater monitoring infrastructure and ongoing groundwater level and pumping monitoring acted as a thorough calibration dataset. This allowed the dewatering drawdown associated with the open pit mine development, which was an order of magnitude greater than that from bore pumping alone, to be included as a known stress in the model. Thus pumping and open pit mining were the inputs to the model as stresses and the subsequent model level and flow results were able to be compared with the monitored groundwater levels and mine pumping.

With a model resulting in reasonable predictions of mine water inflows, defensible results about the relative benefits of different dewatering approaches were demonstrated and informed management decisions were then able to be made based on the model results. This includes for example: the relative benefits of perimeter bores, in-pit bores and sump pumping in this hydrogeological setting; the scale of the predicted dewatering required based on different mining approaches and schedules (both underground and open pit); and the relative benefits of different underground dewatering strategies.

Likewise, the relatively large scale of the predicted dewatering rates, and their rapid and ongoing validation, for both the underground and open pit mine, provides the ongoing justification for funding: appropriately engineered dewatering systems; recruiting and retaining appropriately skilled staff and resources relative to the scale and importance of the dewatering task; ongoing assessment of performance and refinement of the groundwater model; and continued use of the groundwater modelling to aid management decisions.

Acknowledgements

The authors thank GHD and OGPI respectively. In addition the authors would like to thank Wade Dodson for his review of the modelling and valued input.

References

- Coffey (1998a) ‘Didipio Copper-Gold Project, Analysis of Hydrogeological Field Data – Mine Dewatering Study’, Coffey Partners International Pty Ltd, Report G413/5-CM for Climax Mining Ltd, May 1998
- Coffey (1998b) ‘Didipio Copper-Gold Project, Hydrogeological Assessment Stage II, Analyses of Additional Field Groundwater Study’, Coffey Partners International Pty Ltd, Report G63001/1- AW for Climax Mining Ltd, 21 September 1998
- Dodson W (2017) Didipio Copper Gold Mine, Luzon, 2017 Groundwater Model Review, Golder Associates Report No. 1783322-001-R-Rev, November, 2017
- Dames and Moore (1995), ‘Climax Mining Limited, Didipio Gold-Copper Project, Didipio Feasibility Study, Report on Groundwater and Dewatering Aspects Revision 3
- Griffiths S, Holmes M, Moore J (2014) NI 43-101 Technical Report for the Didipio Gold / Copper Operation Luzon Island, Philippines S0037-REP-020-0 October 2014
- Medidas CT, Kluz AT (2016) Mine Surface Water Management: Didipio Mine Case Study GEOCON 2016: Mineral and Energy Resources Development in New Era of Change
- MWES (2011) Groundwater Flow Model Mine Dewatering & Site Water Supply Didipio Gold-Copper Project June 2011
- OceanaGold (2018) <https://www.oceanagold.com/our-business/philippines/didipio-mine/GPI>
- RDCL (2008) Geotechnical Assessment of the Proposed Didipio Open Pit, Didipio Gold-Copper Project, OceanaGold Philippines Inc
- Redden R (2012), Didipio – Learning the lessons, adapting and getting ready for production, in Proceedings of Project Evaluation Conference, Melbourne, Victoria, May 2012
- Wolfe RC, Cooke DR (2011) Geology of the Didipio Region and Genesis of the Dinkidi Alkaline Porphyry Cu-Au Deposit and Related Pegmatites, Northern Luzon, Philippines. *Economic Geology*, 106:1280-1286



Viability of converting a South African Coal Mining Pit Lake System into a Water Storage Facility

Robert Paul Verger¹, Jarmi Steyn², Johan Fourie³, Pieter Labuschagne⁴, Roxane Schmidt⁵, Henri Botha⁶, Freek Pretorius⁷

¹GCS Water and Environmental Consultants (Pty) Ltd, 63 Wessel Road, Woodmead, Johannesburg, Gauteng, RSA, robertv@gcs-sa.biz

²Tendele Coal Mining, 37 Peter Place, Lyme Park, Bryanston, Johannesburg, 2021, South Africa Jarmi@somkhele.co.za

³Geostratum Consult (Pty) Ltd, P.O. Box 793, Park South 1910, South Africa johan@geostratum.co.za

⁴GCS Water and Environmental Consultants (Pty) Ltd, 63 Wessel Road, Woodmead, Johannesburg, Gauteng, RSA, pieterl@gcs-sa.biz

⁵GCS Water and Environmental Consultants (Pty) Ltd, 63 Wessel Road, Woodmead, Johannesburg, Gauteng, RSA, roxanes@gcs-sa.biz

⁶GCS Water and Environmental Consultants (Pty) Ltd, 63 Wessel Road, Woodmead, Johannesburg, Gauteng, RSA, henrib@gcs-sa.biz

⁷Inqubeko Consulting Engineers, 12 Wildebees Street, Empangeni, KwaZulu-Natal, RSA, freek@inqubeko.co.za

Abstract

Coal opencast pit-lake water in South Africa is not normally used for drinking water, because of poor water quality. A multi-disciplinary team investigated the viability of pumping water from an adjacent river system into neighbouring opencast voids to create an artificial pit-lake storage system that could provide water for human consumption. This paper summarises results of an ongoing investigation that involved determining water availability in the local river, supplementing inflows into the pit lake, and an assessment of likely water qualities in the pit-lake. Results are promising, as this initiative will both increase the reliability of water supply to the local community and save costs in closing the mine.

Keywords: coal mining, dynamic water balance, geochemistry, pit lake, water supply

Introduction

South Africa is largely a semi-arid country where water is very scarce. During droughts there is little water available in river and streams for long periods of time. The Constitution of South Africa states that everyone has the right to have access to sufficient water and requires that reasonable legislative and other measures be taken to provide sufficient potable water to communities. A local municipality located near the Somkhele Anthracite Mine (Somkhele) in the KwaZulu-Natal Province experiences serious water shortages. Only 69% of people in this municipality have access to potable water (Mtubatuba Local Municipality 2017). When surplus water is available in the nearby Mfolozi River, there is potential to store water in mined-out open pit voids, creating a pit-lake storage system and later

treat the water for human consumption at a neighbouring Water Treatment Plant (WTP).

The proposed pit lake storage system would consist of 3 linked pits: North Pit 1, North Pit 2 and South Pit. Pumping of water from the Mfolozi River towards either the South Pit or the North Pit 1 is proposed. This pit lake system can function as a balancing dam, which provides water during drought periods. Rapid flooding of the pit lake system and a constant fresh water intake from the Mfolozi River will inhibit oxidation of remaining sulphide mineralisation and maintain good water qualities in the pit lake system.

Methods

Water availability in the proposed North Pit 1, North Pit 2 and South Pit-lake system with added water pumped from the Mfolozi



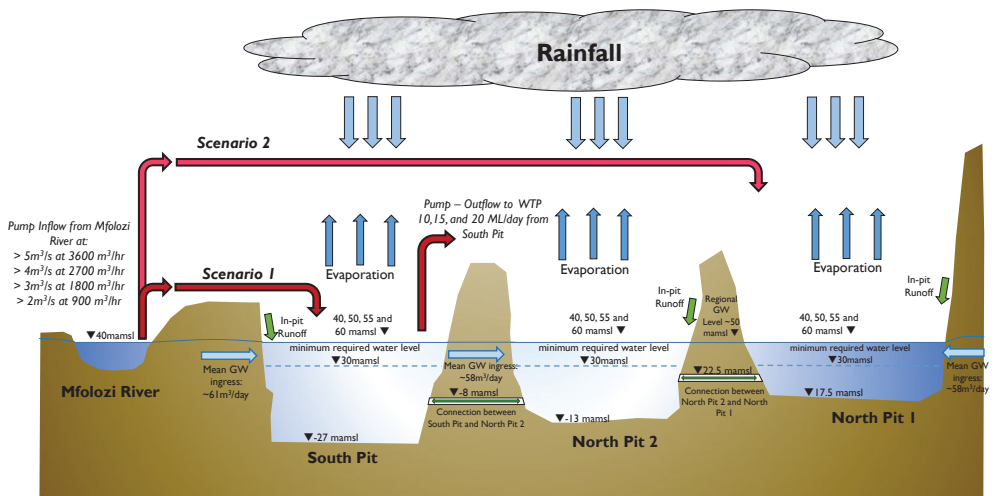


Figure 1 Conceptual Layout of Pit-lake System.

River was simulated. A probabilistic pit-lake water balance model was set up using Gold-Sim® software. Two (2) pumping scenarios, as depicted in Figure 1 were investigated:

- Scenario 1: water is pumped from the Mfolozi River straight into the South Pit; and
- Scenario 2: water is pumped from the Mfolozi River straight into the North Pit 1.

In addition to pumping scenarios, different Full Supply Level (FSL) operating levels (namely 60 metres above mean sea level (mamsl), 55 mamsl, 50 mamsl and a conservative level of 40 mamsl) in the pit lakes were investigated, together with different levels of water supply (10 ML/d, 15 ML/d and 20ML/d) to a Water Treatment Plant (WTP) .

A Reserve Ecological Water Requirement (EWR) was subtracted from the simulated actual river flow to determine available flow at Somkhele. Available water was further divided into normal and surplus flow, where normal flow (for each month of the year) is defined as flow that is exceeded in 70% of years and surplus flow is any excess above normal flow. A portion of surplus flow, especially flood peaks, in the Mfolozi River is abstracted into the pit lake storage system, in a manner that stabilises river flow and improves water availability to all downstream users. The proposed pit lake system acts as a balancing dam that abstracts only surplus

flow above 17 ML/d (>2 m³/s) and will only improve the hydrological situation during lows flows. During low flows the pit lake system will not abstract water from the river, but water will still be supplied to the WTP that serves the local community. The benefits of this balancing dam include meeting a portion of the (existing) Basic Human Need (BHN) requirements.

Measured river flow data of Mfolozi River from the Department of Water and Sanitation (DWS) gauging stations W2H005 and W2H006 (1960-2016) were obtained and proportionally extended for the downstream catchment, up to Somkhele, using simulated natural runoff records from Water Resources of South Africa, 2012 Study (WR2012 database) (Bailey and Pitman 2015).

Other input data obtained, included a sufficiently long daily rainfall record from the South African Weather Service (SAWS) for rainfall station 0339352_W (Kangela). Evaporation data were obtained from the WR2012 database (Bailey and Pitman 2015) and converted to lake evaporation. Parameters of a daily stochastic rainfall model were determined by using the methodology of Boughton (1999). Groundwater inflow into the pit-lake was simulated using methods described by Marinelli and Niccoli (2000). A topographical survey of the opencast mine pits was used to determine potential storage capacities of the pit lake system (Fig.2).



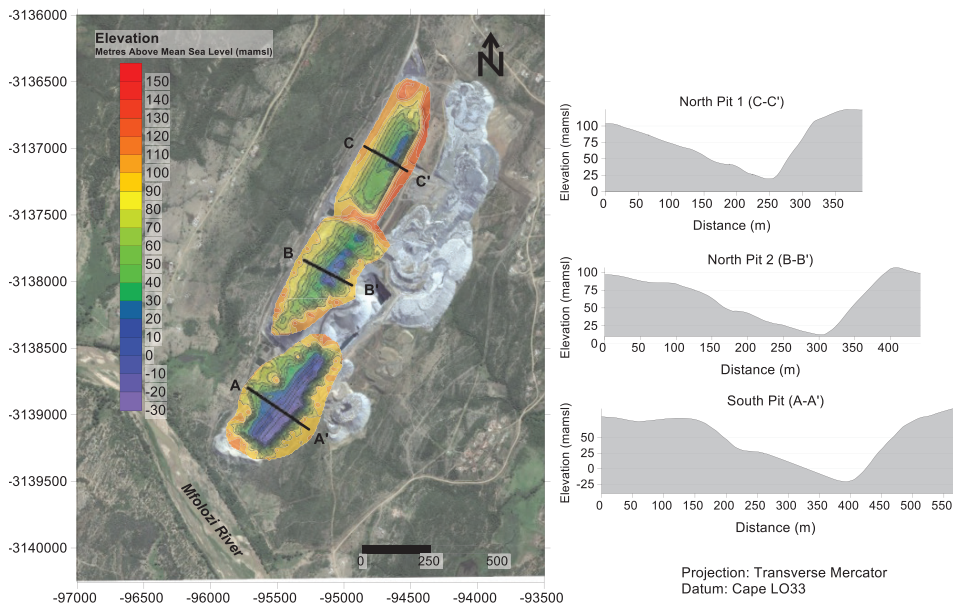


Figure 2 Topography of opencast mine pits (with profiles).

Water quality modelling estimated water quality in the various Somkhele opencast pits. A total of 25 rock samples from the existing opencast pits and borehole core samples were collected for geochemical testing. One (1) river sand sample was taken from the Mfolozi River bed. Test methods for the geochemical study are listed in Table 1.

A conceptual model was developed, which included typical processes that control acid-mine drainage generation. Geochemical

modelling provided estimates of water quality for the pit lake system. Interaction between the mineral-, water- and the gas phases was modelled using the Geochemist's Workbench Professional®.

Water Resource Availability

Likely available flow at Somkhele for 96 years is displayed (Fig. 3) and was simulated at 600 million m³/year with the Normal Wet Weather Flow (NWWF) equalling 670 mil-

Table 1 Description of test methods.

Test procedure	Expected outcome	Method
Acid-base accounting (ABA) (25 samples)	To indicate the long-term potential for AMD assuming all acid is generated by pyrite.	Modified Sobek (Lawrence and Wang 1997)
Net-acid generating (NAG) (25 samples)	To indicate the net potential for AMD after oxidation with hydrogen peroxide.	ASTM E1915-13 (2013)
X-ray diffraction (9 samples)	Minor to dominant minerals present in rocks.	-
X-ray fluorescence (8 samples)	Major oxides and trace elements present in rocks.	ASTM D4326-13 (2013)
Reagent water leach, 9 samples	To determine chemicals of concern that may potentially leach from samples.	Based on AS 4439.3 (1999) with additional ICP and UV-VIS analyses.
Peroxide Leach (3 samples)	To determine chemicals of concern that may potentially leach from the sample after oxidation by peroxide.	Based on ASTM E1915-13 (2013) with additional ICP and UV-VIS analyses on leachate.



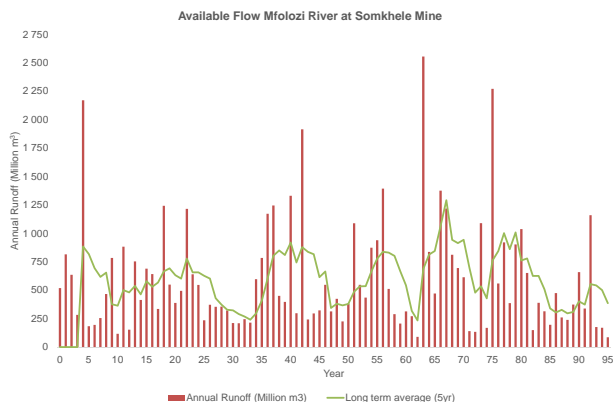


Figure 3 Timeline of the 96-years flow availability of the Mfolozi River at Somkhele.

lion m³/year and the Normal Dry Weather Flow (NDWF) equalling 300 million m³/year. Monthly available flow at the Mfolozi River after releasing the EWR is, on average, 424 million m³/year.

Water levels simulated at 55 mamsl FSL for scenario 1 and scenario 2 in North Pit 1 and South Pit are presented (Fig. 4). It takes approximately 1 year to fill the pit lake system for both scenarios with no pumping to the WTP. Probabilities of water levels dropping below 40 mamsl is approximately 1:236 years for scenario 1 and 1:260 years for scenario 2. Low and very low risks of interruptions to 20 ML/d water supply to the WTP (water level <30 mamsl) were also simulated at FSL water levels of 50mamsl (1:166 years), 55mamsl (1:625 years) and 60 mamsl (>1:1 000 years).

A lower risk of exposing pit walls to oxidation suggests that pit water quality of the pits will be marginally better if water is pumped to North Pit 1 (scenario 2). Although water levels occasionally dropped below 40 mamsl, a sufficiently reliable supply of water (at 20 ML/d) to the WTP is achieved if target FSL water levels are maintained at 50, 55 and 60 mamsl.

Water Quality

Main lithologies are shale and sandstone and are mostly comprised of quartz and muscovite as major minerals with kaolinite, plagioclase and microcline as minor minerals. Small amounts of pyrite are present that can generate acid mine drainage, but carbonates present will provide some neutralising potential.

Water samples were collected from the sumps at the bottom of the operational open-cast pits. The pH was neutral in all samples (>pH 7.7). EC was elevated above the South African National Standards (SANS) drinking water standard (>170 mS/m). Marginally to highly elevated anions included Na, SO₄, N, Cl, ammonia (as N) and F. Pb (0.016 mg/L) and Mn (1.59 mg/L) were erratically elevated in some samples. The river sand sample has a very low sulphide %S (below detection) and also have a very low neutralisation potential. It is expected that river sand samples have no potential to generate acidic drainage.

Due to large pumped volumes, the pit lake system will be a flow-through pit lake with no stratification taking place. A pit lake system designed with final pit water FSL between 40 and 60 mamsl, will leave most of the pit walls exposed to oxidation, especially in the North Pit 1 and North Pit 2. Run-off from the exposed pit walls/floor will have an increased TDS due to the oxidation of sulphides. In the long-term runoff into the pits will not acidify as more than 70% of waste rock has adequate neutralising potential. Neutralising minerals may only be partially exposed and run-off will initially drop to about pH 6 for about 20 years for the best case and about 40 years for the intermediate scenario. As a worst case, for wall rocks with a high pyrite content, the pH will drop to about pH 5 for about 10 years and then recover to pH 6 until year 70. In all cases the pH will recover over the long-term to >pH 8.



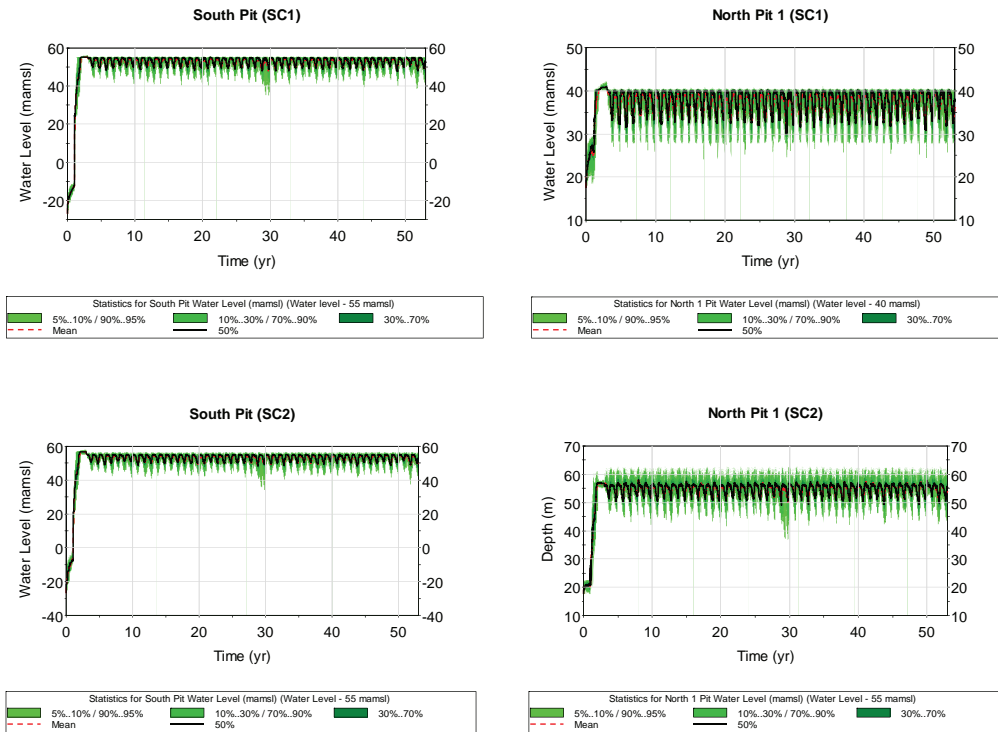


Figure 4 Simulated pit lake water levels at 55 mamsl and pumping at 20 ML/d to the WTP for scenario 1 (top) and scenario 2 (bottom).

Sulphate will become the dominant anion in pit runoff due to sulphide oxidation and secondary sulphate mineral dissolution. Sulphate initially reaches concentrations of up to 2 200 mg/L in run-off, which corresponds with currently observed water qualities in North Pit 2. As the secondary minerals in the wall rock deplete, sulphate concentrations in run-off will first reduce to 1 000 mg/L before decreasing further to about 350 mg/L.

Pit water will remain circum-neutral with pH above pH 6.5 and metal concentrations below 1 mg/L for scenario 1. A higher pump rate and a higher pit FSL have a positive effect on pit water quality. South Pit water will initially have a high TDS as pumped river water encounters the floor material (1 800 mg/L) (Fig. 5). Pit water quality will, however, improve significantly within 5 - 10 years owing to large volumes pumped from the river and reaches a pseudo-steady state after this time (with a TDS of 300-450 mg/L at 10 years and 260-330 mg/L at 100 years). After closure,

North Pit 2 water quality will reach a pseudo-steady state within 30-40 years (TDS of 510-1000 mg/L at 10 years and 320-580 mg/L at 100 years). North Pit 1 water quality will reach a pseudo-steady state within 30-40 years (with a TDS of 940-1800 mg/L at 10 years and 470-870 mg/L at 100 years).

Water quality effects are less pronounced in scenario 2 (Fig. 5), because of inflow of river water in North Pit 1 and high resultant flow between the pits dominates the pit water quality. North Pit 1 water quality will improve significantly within 1 - 3 years (due to the large volume of river water pumped towards the pit) and the TDS will reach a pseudo-steady state after this time (\approx 260-340 mg/L at 10 years and \approx 240-280 mg/L at 100 years). The North Pit 2 water quality will improve significantly within 1 - 3 years (due to the large inflow of relatively clean water from North Pit 1) and the TDS will reach a pseudo-steady state after this time (\approx 280-420 mg/L at 10 years and \approx 250-310 mg/L at 100



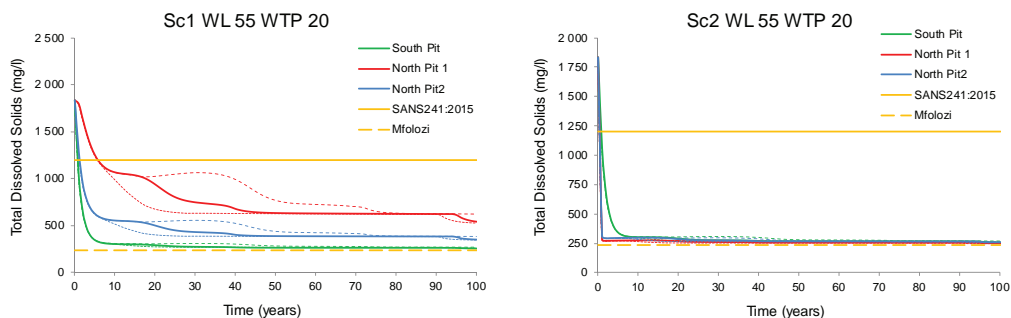


Figure 5 Change in pit water quality over model time at 55 mamsl FSL for scenario 1 (left) and scenario 2 (right) for a 20ML WTP. The solid line presents the intermediate case and the upper and lower dashed lines the worst and best case.

years). South Pit water quality will improve significantly within 5 - 10 years (due to the large inflow of relatively clean water from North Pit 2) and the TDS will reach a pseudo-steady state after this time (≈ 290 - 460 mg/L at 10 years and ≈ 250 - 340 mg/L at 100 years). South Pit will have a slightly higher TDS than the other pits because it is situated furthest downgradient.

Summary Conclusion

This investigation indicated that water supplied from the pit lake system will be a more reliable alternative than supplying water directly from the Mfolozi River. The local river cannot reliably supply drinking water directly to the WTP, whereas a pit-lake system can function as a balancing dam of up to 11.7 Mm^3 (at 55mamsl FSL), which provides water during drought periods. Water quality will still be within the drinking water limits based on worst-case assumption of the impact of the pit walls on water quality for all scenarios. The nearby WTP could be upgraded to meet current shortfalls in supply to meet local domestic water demands.

Ongoing investigation include the selection of an abstraction site and selection need to be made based on accessibility to the site, river bed stability and confirmation on whether expected pump rates could be obtained. Additional pump testing on the Mfolozi River bed is recommended in order to confirm whether the water quality in the river bed will not deteriorate over time. Mfolozi River flow and the pit water levels

should be monitored on a monthly basis. Further test work should also include kinetic leach testing on selected wall rocks in order to better estimate the expected impact of the material on drainage water quality. Also the geochemical model should be updated over the life of the project in order to calibrate and validate its results with the actual site conditions.

Acknowledgements

The authors thank Somkhele Anthracite Mine for allowing and approving the submission of this work and paper to be presented at the 2018 IMWA conference in Pretoria. In addition, thanks to reviewers of this paper and to all who contributed to the results of this study.

References

- AS4439.3-1997 (1997) Wastes, sediments and contaminated Soils Part 3: Preparation of leachates - bottle leaching procedure. Standards Australia. Sydney
- ASTM E1915-13 (2013) Standard test methods for analysis of metal bearing ores and related materials for carbon, sulfur and acid-base characteristics. ASTM. West Conshohocken, PA
- ASTM D4326-13 (2013) Standard test method for major and minor elements in coal and coke ash by X-Ray fluorescence. ASTM. West Conshohocken, PA
- Bailey AK, Pitman WV (2016) Water Resources of South Africa, 2012 Study. Study of the Water Research Commission. WRC Project No. K5/2143/1. August 2016




- Boughton W (1999) A daily rainfall generating model for water yield and flood studies. CRC for Catchment Hydrology, Report 99/9
- Lawrence W, Wang Y (1997) Determination of neutralization potential in the prediction of acid rock drainage. In Proc. 4th International conference on Acid rock Drainage (IcArD). Vancouver, Canada, pp. 451-464
- Marinelli F, Niccoli WL (2000) Simple analytical equations for estimating ground water inflow to a mine pit. *Ground Water* 38 (2), 311-314
- Mtubatuba Local Municipality (2017) Integrated Development Plan (IDP) for Mtubatuba Local Municipality. Draft Report: 2017/2018 TO 2021/22. March 2017





12

**MINE WATER BY
PRODUCTS**



Neutralization of Acid Drainage and Concentration of Rare Earth Elements Using Carbonatites – Results from a Bench Scale Experiment

Alba Gómez-Arias^{1,2,3}, Julio Castillo², Megan Welman-Purchase⁴, Maleke Maleke², Esta van Heerden², Danie Vermeulen¹

¹*Institute for Groundwater Studies, University of the Free State, Nelson Mandela Drive, 9301 Bloemfontein, South Africa. vermeulend@ufs.ac.za, gomezarias@ufs.ac.za*

²*Microbial, Biochemical and Food Biotechnology, University of the Free State, Nelson Mandela Drive, 9301 Bloemfontein, South Africa. castillohernandezj@ufs.ac.za malekem@ufs.ac.za esta@iwatersolutions.co.za*

³*Department of Earth Science, University of Huelva, El Carmen S/N 21071 Huelva, Spain.*

⁴*Department of Geology, University of the Free State, Nelson Mandela Drive, 9301 Bloemfontein, South Africa. PurchaseMD@ufs.ac.za*

Abstract

Remediation of acid mine and industrial drainages has high costs involved due to the infrastructure, consumables and disposal of the waste produced by current water treatments. This study provides the first insight into a novel neutralization process using rare earth-bearing carbonatite from a waste rock dump that generates a marketable by-product, capable to defray the water treatment cost.

Mineralogical and geochemical analysis of the carbonatite, performed before and after the treatment, showed REE-enrichment in a specific section of the water treatment prototype, while the hydrochemical analysis of the water revealed effective neutralization and removal of pollutants.

Introduction

The environmental impact of acid drainages in South Africa affects ground- and surface water in a country already stricken by the extreme scarcity of water resources. Ba-Phalaborwa municipality of Limpopo province is a clear example of this environmental impact. The Phalaborwa Industrial Complex (PIC) hosts manufacturing plants and mines, whose activities are closely monitored due to their proximity to the Kruger National Park (KNP) and human settlements (DEA 2009). The waste rock dumps (WRD) of this complex are composed mainly of carbonatite-material, with high concentrations of rare earth elements (REE) (Gómez-Arias et al. 2016).

Therefore, this alkaline material becomes an attractive solution to not only neutralize the acid drainage, but also to enrich them in REE. In fact, the REE from both the carbonatite and the drainage could be concentrated while treating the acid water (Gómez-Arias et al. 2016). A bench scale water treatment

was used to chemically and mineralogically characterize the removal of pollutants from the acid drainage, as well as the concentration the REE within the matrix of the reactor. The successful outcome is exciting since a) a reduction of the waste rocks deposited within the mining facility can be achieved, b) a reduction of the volume of acid water retained from the manufacturing plant can be achieved while improving the water quality and c) additional value will be generated from the wastes generated by the companies by yielding a marketable concentrated-rare-earth-product.

Methodology

Experiment set up

The bench-scale water treatment set-up consisted of two reactors made of PVC pipes (10 cm inner diameter, height 50 cm) connected in series, as well as two decanters. Each reactor had four sampling ports and an outlet port connected with perforated pipes inside



the reactors. The decanters were placed after each reactor to allow suspended solids to settle and to hold small particles that may be released from the reactors.

Each reactor contained a layer of quartz gravel (particle size: $\approx 5\text{--}8$ mm) at the bottom (2.5 cm) covering the outlet port. This layer was used as a drain and was covered with 40 cm of reactive material, which is a mixture of wood shavings and powdered alkaline material. Carbonatite powder collected from a WRD was used for the first reactor (reactor A) and BaCO_3 (Protea Chemicals Company, SA) was used in the second reactor (reactor B) as the alkaline material.

Acid water from manufacturing plant (50L) was collected from PIC's dam and pumped to the top of reactor A with a peristaltic pump. The water flowed gravitationally through the mixture and it was collected from the bottom of the reactor in a container that acted as a decanter (decanter A). Then the water was pumped to the top of reactor B and it was finally collected in decanter B. The flow rate was 1.1 mL/min with a residence time of 24 hours per reactor.

Hydrochemical characterization

Samples were collected daily for 30 days from each sampling-port as well as from the outlets, the inlet and both decanters. The physicochemical parameters of the samples were analysed immediately to avoid the dissolution effects of the CO_2 (g) and O_2 (g). Parameters such as dissolved oxygen (DO), temperature (T), pH, electrical conductivity (EC) and to-

tal dissolved solids (TDS) were measured in all samples with an ExStix®II multi-probe, while oxidation-reduction potential (ORP) was measured with an ExStix®II ORP (Pt and Ag/AgCl electrodes) probe. Then each sample was filtered with Teflon filters $0.45\text{ }\mu\text{m}$ and acidified with 10% HNO_3 . Total Element Concentration (TEC) was analysed by ICP-OES Teledyne Leeman-Prodigy XP, minor elements with ICP-MS PerkinElmer-Nex-Ion2000 and major anions (PO_4^{3-} , SO_4^{2-} and NO_3^-) with HPLC Shimadzu-Prominace.

Geochemical characterization

At the completion of the experiment, both reactors were drained, opened and 3 samples were collected at the top, middle and bottom of each reactor. The samples were freeze dried overnight and prepared for mineralogical and geochemical characterization. The mineralogical characterization of the final products was performed by X-ray diffraction (XRD, powder method) using a methodology described in Gomez-Arias et al. (2016).

Results and discussion

The hydrochemical characterization showed an improvement in the water quality after treatment. In order to facilitate a full and coherent interpretation of the results, the discussion of each step on the system will be done individually.

Reactor A:

An averaged increase of pH from 1.4 to 3.53, was achieved in reactor A (Fig. 2). At the be-

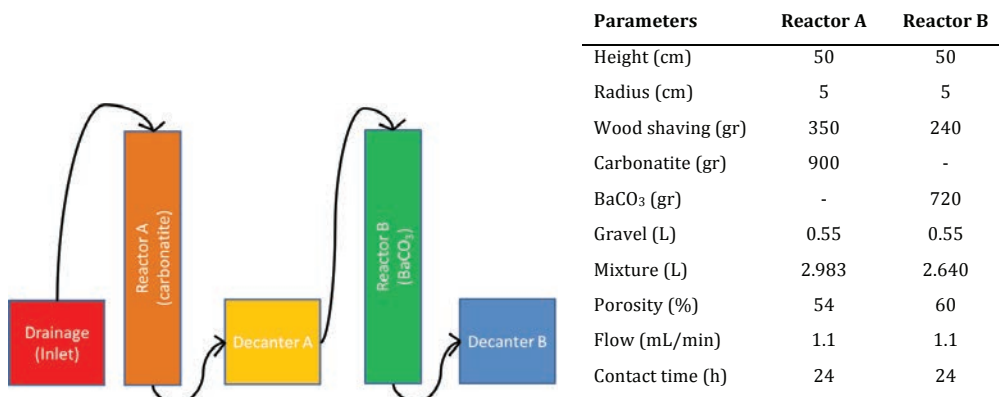


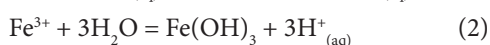
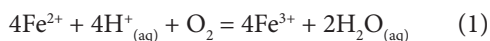
Figure 1 Bench-scale water treatment scheme (left) and specifications (right)



gining of the experiment the pH increased up to 4.48, however the efficiency decreased over time, due to the consumption of CaCO_3 present in the carbonatite and/or the passivation of the system, probably due to the precipitation of gypsum and Fe- oxyhydroxysulfates, as it was previously described by Soler et al. 2008.

An average decrease in EC and TDS of 56.1%, was measured (Fig. 2), mainly due to the removal of sulfate and phosphate. At the beginning of the experiment both parameters decreased about 73%, but their decreasing rate declined between 40 and 66.7% thereafter, which was probably related to the passivation of the calcite, as mentioned above.

DO decreased from the top to the bottom of the reactor and it decreased over time up to 85% (Fig. 2). This correlates with the ORP measurements that showed an evolution of the redox conditions, which alter from an oxidizing to a reducing environment. This was partially due to the precipitation of Fe, which is an oxygen consuming reaction (Eq 1 - 2), but probably enhanced by the usage of wood shavings in the reactive material, which could serve as a carbon source for sulfate reducing bacteria (SRB), known precursor of the reducing environment (Caraballo et al. 2011).



The concentration of sulfate decreased by 46.5%, on average, which means that more than 4000 mg of sulfate was precipitated as neoformed minerals per litre of water treated (Fig. 2). The sulfate removal observed in this experiment is higher than previous batch experiments where the same water was treated with a carbonatite sample (Gómez-Arias et al. 2016). This might be due to the possible presence of SRB, previously described.

On average, the concentration of phosphate decreased by 66.6% (Fig. 2). As described by Liu et al. (2012), the presence of calcite and the increase of pH are directly related to the precipitation of phosphate. However, Liu et al. (2012) also described the influence of the ratio / at low pH; with ratios of between 1.5-3 phosphate, removal will be enhanced, while higher ratios will inhibit phosphate removal. The ratio of the drainage was 4 before treatment, but as sulfate was removed through the reactor, this ratio kept oscillating. This could explain the oscillation of the phosphate concentration, not only in reactor A, but along the entire water treatment system.

The analyses by ICP-OES showed high concentrations of trivalent (523.7 mg/L of Al, 165.0 mg/L of Fe and 7.7 mg/L of Cr) and divalent metals (1102.8 mg/L of Mg, 774.53 mg/L of Ca, 21.9 mg/L of Cu, 43.4 mg/L of Mn, 0.94 mg/L of U, among others) in the inlet. The neutralization process produced by the disso-

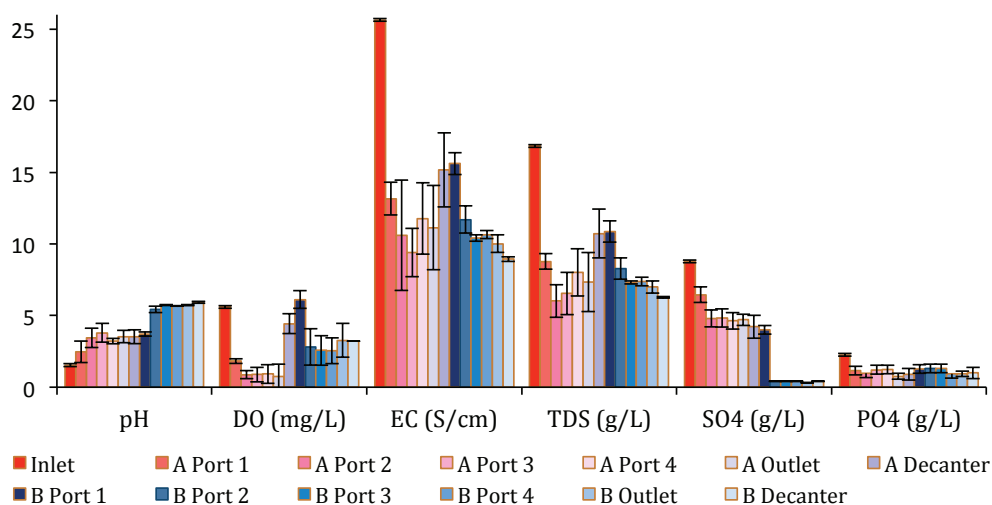


Figure 2 Evolution of physicochemical parameters throughout the entire water treatment, showing the average of each section (columns) and their standard deviations (lines).



lution of the calcite promoted the precipitation of Al (92.0%), Fe (81.2%), Cr (90.4%), Cu (68.8%), Pb (61.4%) and U (63.7%), among others. However, there was an increase in the concentrations of Ca and Mg, due to the dissolution of the carbonatite, which contained these elements in the form of carbonates (Gómez-Arias et al. 2017). While their concentrations increased from port 1, it was in port 2 where the maximum concentration was achieved (1515.1 mg/L of Mg and 1575 mg/L of Ca), decreasing thereafter.

The ICP-MS analysis detected high concentrations of REE (Fig. 3), especially light lanthanides (Ce>La>Nd>Y>Gd>Sm>Pr>Dy>Sc>Er>Eu>Yb>Ho>Lu>Tm), with a sum of 419.1 µg/L in the water used as inlet. The concentration of REE in solution increased at the first port (up to 1236.12 µg/L, in total), due to the dissolution of the carbonatite that hosts high concentrations of REE (Gómez-Arias, et al. 2017). Thereafter, REE decreased drastically in port 2, and from port 3 to the outlet most REE were below detection limit (4.5 µg/L), except for Sc and Y (8.4 and 5.2 µg/L, respectively).

Decanter A

The characteristics of the water that reached the decanter from reactor A changed over

time. The small turbulence produced by the water dropping from reactor A to the decanter promoted the introduction of oxygen in water. This enhanced the precipitation of Iron oxy-hydroxides (Taylor et al. 1984; Banks et al. 1997) as it was shown by the decrease in Fe concentration between the inlet and the outlet of the decanter (from 41.8 to 6.7 mg/L, on average), as well as the acidification of the water due to the Hydroxyl-group consumption (Eq. 1-2). Some particles released from reactor A were probably re-dissolved within decanter A due to this acidification (pH decreased from 4.03 to 3.05). This process probably contributed to the increase of EC, TDS, SO_4^{2-} and PO_4^{3-} (14534 to 17760 mS/cm, 10.048 to 12.405 g/L 4.7 to 6.4 g/L and 0.74 to 1.27 g/L, respectively). However, all the elements analysed by ICP decreased; Al, Cu, Fe, Pb and U were removed by more than 80%, while the rest were removed between 12 and 51%.

Reactor B

The dissolution of the BaCO_3 produced an increase in the pH (eq. 3 to 5) (Gómez-Arias et al., 2015) from 3 to 5.78, on average. The maximum pH achieved at the outlet of column B was 6.08. The TDS and EC decreased between 44 and 47% (from 12.42 to 6.99 g/L

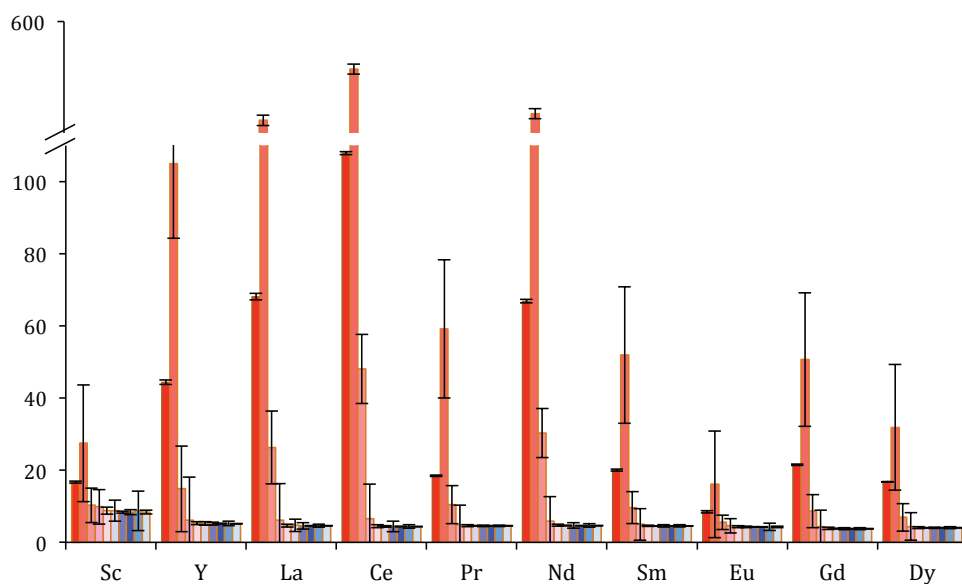
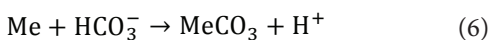
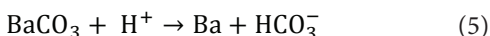
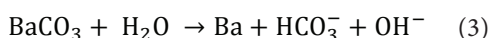


Figure 3 Evolution of main REE, including Y and Sc, throughout the entire water treatment, showing the average of each section (columns) and their standard deviations (lines) colour coded as figure 2.



and from 17740 to 1000 mS/cm, on average). The dissolved sulfate was precipitated as barite (BaSO_4) decreasing the concentration of it in solution down to 0.67 g/L (eq. 4). While Ca and Mg were mainly precipitated as Ca-MgCO_3 (eq. 6), dropping their concentration in solution from 0.86 to 0.03 g/L of Ca and from 1.24 to 0.48 g/L of Mg. At the outlet of column B, the concentration of the other metals analysed were below 0.001 g/L, except for Ba that oscillated between 0.9 and 3.2. At the inlet of Reactor B the concentration of U was already depleted to 0.02 mg/L, which was completely depleted in the top section of the reactor, since no trace of U was detected from port 2 downwards.



Decanter B

The main function of decanter B was the settling of suspended solids that could come from reactor B, as well as to promote the stabilization of the water characteristics. The pH increased slightly to 5.94, while the TDS and EC decreased by approximately 4%.

The comparison between the characteristics of the water before treatment (inlet) and at the end of the treatment (Decanter B) demonstrates the improvement on the water quality achieved throughout the water treatment system (Fig. 2); pH increased from 1.5 to 5.94, while TDS, EC, sulfate and phosphate decreased from 16.8 g/L, 25.63 mS/cm, 7.3 g/L and 2.3 g/L to 6.28 g/L, 8.94 mS/cm, 0.4 g/L and 1 g/L, respectively. All the metals analysed were removed by more than 95%, including Al (99.8%), Cr (94.4%), Cu (97.5%), Fe (98.9%), Mn (99.3%), Pb (95.9%) and Se (99.9%). Only Ca removal was slightly lower (92.6%) and Mg was removed by 56.6%. There were no REE nor U detected at the end of the treatment.

XRD results

The mineralogy characterization by XRD analysis to the starting alkaline material (carbonatite) used in reactor A, showed calcite

(CaCO_3) as the principal compound, followed by dolomite (Ca-MgCO_3) and apatite (REE-bearing $\text{Ca}_5(\text{PO}_4)_3$). However, the matrix of carbonatite used for water treatment showed lower concentration of calcite after treatment. This was expected since the dissolution of the calcite by the acid drainage is well documented and commonly used as remediation of acid mine drainages (AMD) (e.g. Caraballo 2015). The main neoformed mineral phases at the top and middle sections of reactor A were gypsum, hydrotalcite and anhydrite. According to literature (Birjega et al., 2005 and Baumer et al., 1996), those neoformed minerals can accommodate REE in their structure. In contrast, the bottom showed calcite as predominant mineralogy. Consequently, scarce neoformed minerals were detected in this section of reactor A.

The analysis of the witherite (barium carbonate) used as the reagent in reactor B, showed the following neoformed minerals: barite (BaSO_4), brushite ($\text{CaHPO}_4 \cdot 2\text{H}_2\text{O}$) and gypsum ($\text{CaSO}_4 \cdot 2\text{H}_2\text{O}$), which act as a sink for divalent elements. The dissolution of witherite during the water treatment was demonstrated by the decrease in its concentration. However, the total consumption of this reagent was not achieved at the end of the experiment.

Conclusions

This study has demonstrated: a) that the bench scale successfully remediated acid water with high concentration of salts and metals, b) that commercial calcite, commonly used in any DAS system can be replaced by carbonatite (mining by-product) which will decrease costs dramatically, c) that the high concentrations of REE, commonly found in acid water from mines and industries, can be precipitated within the carbonatite matrix, and finally d) that REE-bearing minerals of the carbonatite can be dissolved by acid water to re-precipitate together with acid-water-REE. Further studies need to be performed in order to characterize the REE-enriched material and its feasibility as a marketable product.

Acknowledgements

This project was funded by ERAMIN-PCIN2015-242-256 project and supported by the Technology and Innovation Agency



(TIA) through the SAENSE platform of the University of the Free State.

References

- Banks D, Younger PL, Arnesen RT, Iversen ER, Banks SB. (1997). Mine-water chemistry: the good, the bad and the ugly. *Environ Geol* 32: 157—4.
- Caraballo, M., Macías, F., Nieto, J., et al. (2015). Hydrochemical performance and mineralogical evolution of a dispersed alkaline substrate (DAS) remediating the highly polluted acid mine drainage in the full-scale passive treatment of Mina Esperanza (SW Spain). *American Mineralogist*, 96(8-9), pp. 1270—1277. Retrieved 8 May. 2018, from doi:10.2138/am.2011.3752
- Gomez-Arias A, Castillo J, Posthumus J, van Heerden E (2015) Evidences of Effective Treatment of Alkaline Mine Drainage with BaCO₃. – In: Agreeing on solutions for more sustainable mine water management – Proceedings of the 10th ICARD & IMWA Annual Conference. – electronic document (paper 303); Santiago, Chile (GECAMIN).
- Gomez-Arias A, Castillo J, van Heerden E, Vermeulen D (2016) Use of alkaline mine waste as treatment for acid drainage. – In: Drebenstedt, C. & Paul, M.: IMWA 2016 – Mining Meets Water – Conflicts and Solutions. – p. 931 – 936; Freiberg/Germany (TU Bergakademie Freiberg).
- Gomez-Arias A, Castillo J, Welman-Purchase M, Maleke M, van Heerden E (2017) Novel Strategy To Concentrate Rare Earth Elements By Neutralization Of Acid Drainage From Phosphogypsum Stacks Using Carbonatites. – In: The second conference on European Rare Earth RE-Sources – Proceeding of ERES2017. – electronic document (paper 16); Santorini, Greece.
- Liu, Y., Sheng, X., Dong, Y., & Ma, Y. (2012). Removal of high-concentration phosphate by calcite: effect of sulfate and pH. *Desalination*, 28:, 66—71.
- SABS Standards Division (2015). SOUTH AFRICAN NATIONAL STANDARD- SANS 242-2:2015 Drinking water. Part 1: Microbiological, physical, aesthetic and chemical determinands, Edition 2. ISBN 978-0-626-29841-8. Pretoria, South Africa, 17 pp.
- Soler, J. M., Boi, M., Mogollón, J. L., Cama, J., Ayo-ra, C., Nico, P. S., ... & Kunz, M. (2008). The passivation of calcite by acid mine water. Column experiments with ferric sulfate and ferric chloride solutions at pH 2. *Applied Geochemistry*, 23(12), 3579—3588.
- Taylor BE, Wheeler MC, Nordstrom DK. (1984) Stable isotope geochemistry of acid mine drainage: Experimental oxidation of pyrite. *Geochim Cosmochim Ac* 48:2669—2678. Singer PC, Stumm W. Acidic mine.





Utilization of iron ochre – making auxiliary water treatment materials from mine water treatment waste

Tim Aubel¹, Franz Glombitza¹, Eberhard Janneck¹, Petra Schönherr², Wolfram Palitzsch², Arvid Killenberg², Volker Schubert³, Lutz Weber⁴

¹G.E.O.S. Ingenieurgesellschaft mbH, Freiberg, Germany, t.aubel@geosfreiberg.de

²LOSER Chemie GmbH, Zwickau, Germany

³WätaS Wärmetauscher Sachsen GmbH, Olbernhau, Germany

⁴Lausitzer und Mitteldeutsche Bergbau-Verwaltungsgesellschaft mbH, Senftenberg/Leipzig, Germany

Abstract

In the Lusatian lignite mining area huge amounts of iron and sulphate enter the receiving water bodies caused by groundwater rise after closure of many opencast lignite mines in the 1990th. Water treatment actions mainly for iron removal prepared and accomplished by the mining rehabilitation company LMBV and ochre sedimentation in still unprotected water bodies result in huge iron sludge accumulations, which have to be removed/ disposed. This paper presents a novel approach on significantly decreasing the iron sludge amount through utilization. It involves mechanical and thermal dewatering/drying and subsequent production of auxiliary water treatment chemicals. The produced chemicals had comparable treatment properties as commercial products. The proposed utilization will lead to a significant decrease of the ecological and economical foot print.

Keywords: lignite mine closure, iron ochre, iron hydroxide sludge, groundwater rise, auxiliary water treatment chemicals

Introduction

In the Lusatian lignite mining area the regional water balance is heavily changed by the past and present mining industry. Caused by the groundwater rise significant amounts of iron and sulphate enter the receiving water bodies. The mining rehabilitation company LMBV (Lausitzer und Mitteldeutsche Bergbau-Verwaltungsgesellschaft mbH) prepared and accomplished various water treatment actions in particular for the removal of the iron load. Both the LMBV water treatment measures and the ochre sedimentation in water bodies not protected so far lead to a large amount of iron sludge.

About 70.000 t iron ochre is accumulated every year which has to be removed and disposed. The LMBV classified 5 different types of iron sludge with regard to their origin:

1. Sludge from water site clearance (dredgings)
2. Sludge from pristine or nearly-naturally designed sedimentation ponds
3. Sludge from river water treatment

4. Sludge from ground water treatment
5. Sludge from in lake treatment measures

These types vary greatly in terms of their dry mass, iron content and impurities. Therefore it is clear, that utilization of the total sludge amount is almost impossible. Considering its sludge strategy “prevention before utilization before flushing before landfilling” the mining rehabilitation company LMVB has identified two main options for dealing with the huge sludge amounts: a) liquefying by mixing with water and flushing in a specifically prepared pit lake and b) deposit in an industrial mono-landfill. But both of these options are extremely expensive and every ton which does not have to be dumped or flushed will save costs.

Many attempts for the utilization of iron ochre from abandoned mines have already been undertaken, e.g. application as pigments (Hedin, 2002), production of sorbents (Simon, 2016; Kießig, 2004) and bricks, application for phosphor removal from wastewaters.



Recently, a new idea arose being worth enough to start further investigations. It involved the utilization of iron ochre for the production of auxiliary water treatment chemicals such as solutions of FeCl_3 , Fe_2SO_4 or FeClSO_4 which are widely used as flocculants.

Project idea and scope of work

Flocculants based on iron salts are usually produced from pickling solutions from the steel industry as raw material with the disadvantage of a difficult and expansive oxidation step from ferrous to ferric iron. Excavated iron ochre from drainage ditches and iron hydroxide sludge from water treatment plants contains the iron already in the trivalent status. Therefore oxidation is not needed and a simple dissolution of the iron ochre in acid (HCl , H_2SO_4) should be appropriate to produce flocculant solutions being utilizable as auxiliary water treatment reagents.

The main project idea is the production of auxiliary water treatment chemicals (FeCl_3 , Fe_2SO_4 or FeClSO_4) from the iron ochre sludge, using the iron ochre sludge as cheap raw material.

Cost saving can be expected in the areas of raw material, energy, auxiliary materials and finally lower disposal costs due to mass reduction of iron ochre sludge for flushing or landfilling.

To check the feasibility of this idea a two stage project was established funded by LMBV. The first stage was carried out on lab scale and had the aims a) to identify suitable sludge qualities, b) to prove the basic technical feasibility and c) to evaluate the quality of the produced flocculants. In the second stage which is now in preparation a pilot test on industrial scale is planned to prove economic feasibility.

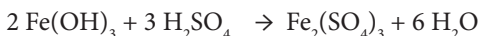
Types of sludge

For the first stage the following sludge types were selected and tested for conversion after sampling

- Lime rich iron ochre sludge (water treatment plant Borna-West)
- Iron ochre sludge with a pH around neutral (“Eichower Fließ”)
- Acidic iron ochre sludge with a fraction of Schwertmannite (“Meuroer Graben”)

Before carrying out the experimental work on dewatering/drying and chemical conversion all sludges were chemically analysed and soil parameters were determined as shown in Table 1.

The chemical conversion was accomplished with hydrochloric or sulphuric acid according to the following main reactions:



Because of minor components in the iron ochre sludge several side reactions are possible, for example

- $\text{CaCO}_3 + 2 \text{HCl} \rightarrow \text{CaCl}_2 + \text{CO}_2 + \text{H}_2\text{O}$
- $\text{CaMg}(\text{CO}_3)_2 + 4 \text{HCl} \rightarrow \text{CaCl}_2 + \text{MgCl}_2 + 2 \text{CO}_2 + 2 \text{H}_2\text{O}$
- $\text{CaCO}_3 + \text{H}_2\text{SO}_4 \rightarrow \text{CaSO}_4 + \text{CO}_2 + \text{H}_2\text{O}$
- $\text{CaMg}(\text{CO}_3)_2 + 2 \text{H}_2\text{SO}_4 \rightarrow \text{CaSO}_4 + \text{MgSO}_4 + 2 \text{CO}_2 + 2 \text{H}_2\text{O}$

Preliminary considerations included the acid amount and concentration as well as the iron content in the raw material required for the conversion.

Commercially available Iron(III)-chloride solutions contain 40% FeCl_3 (13.8% iron as active substance), marketable Iron(III)-sulphate solutions contain 12.5% iron as active substance.

Table 1 Characterization of test sludges

Sludge	Clay	Silt	Sand	Gravel	DMC	Iron	Sulphate	Calcium	TOC
Borna	*	95%	5%	0%	41%	12%	2.5%	14.8%	1.3%
Eichow	18%	23%	56%	3%	54%	22%	0.8%	1.0%	7.4%
Meuro	39%	41%	20%	0%	38%	14%	3.3%	0.3%	10%

*analytical problems due to high lime content

DMC= dry mass content

elemental and TOC contents are given in percent by weight in dry mass



To achieve comparable iron contents the following aspects had to be considered:

- Iron content in the raw material
- Dry mass content in the raw material
- Concentration of the used acid

The iron content in the raw material is dependent on the dry mass content. Lower concentrated acids used for chemical conversion and sludges with a lower dry mass content introduce more water into the product solution. Both aspects lead to a diluted product solution.

To raise the iron content in the raw material an energy efficient dewatering and drying procedure is necessary.

Dewatering/Drying experiments

Lab tests were performed to determine energetic key figures for the technical design of a dryer as well as characteristics of the bulk material (incrustation, caking, dust formation) in the dryer.

One priority of the experiments was the development of suitable drying/conveyor belts.

These belts were a decisive control parameter to influence the drying result for different raw materials (grain size, dry mass content).

The combination of materials (special woven plastics), perforation and operation mode was identified as crucial parameter for the drying result. However, the influence of the sludge's chemical composition was found to be not very significant.

The tested pilot drying system had a capacity of 2.8 kg sludge per minute and achieved a mechanical dewatering grade up to 49% DMC. It can be predicted to achieve a DMC of 55% at a larger scale with solely mechanical dewatering.

Thermal drying would enable a DMC of up to 100%. However, the targeted DMC is dependent from the subsequent chemical conversion and the needed dry mass content there.

The use of mechanical dewatering as much as possible before thermal drying is very important because the effort for mechanical dewatering is only 50% in comparison to thermal drying for each percent of dry mass content.

Therefore the combination of mechanical dewatering and thermal drying is the most appropriate solution concerning both technological and energetic efficiency.

Chemical Conversion

The basic principle of the intended chemical conversion is the dissolution or leaching of the sludge with hydrochloric acid or sulphuric acid.

Different parameter fields were tested:

- Dry mass content of the raw material
- Acid concentration
- Reaction temperature (room temperature, reflux)
- Pressure

The performed tests allowed the following statements:

- Using raw material with a higher DMC and using higher acid solutions lead to higher iron concentrations in the product solution
- Very high DMC and acid solution require the addition of water to provide a homogeneous and stirrable solution
- Product solutions include a proportion of Fe(II). The concentration of Fe(II) raises with a conversion at higher temperatures
- Some product solutions tend to gel at prolonged standing time
- Active iron concentration in the product solution varies between 40 and 80 g/kg product solution
- Amount of residuals varies between 7% and 76% referring to DMC of the raw material

Challenges of the chemical conversion

Some product solutions tend to gel at prolonged standing time. This gelation effect is likely the result of a condensation reaction of silica. Further experiments are currently in progress to solve this challenge. First results are promising and investigations will be continued in the second project phase.

In addition a large scale test of technical solar drying is in preparation in that phase.

Chemical conversions applying higher temperatures or increased pressure led to likewise increased Fe(II) contents in the



product solutions. Different tests were performed concerning the removal of organic components from the raw material by washing. It can be clearly stated that most of the Fe(II) in the product solution is a result of Fe(III) reduction by organic material in the iron ochre, preferably at higher temperatures or pressures.

The product solutions have to be compared with standard market solutions for which the product has to meet specific quality criteria. One quality criterion is the heavy metal concentration in the product solution.

The guideline values for the different heavy metals are specified in the leaflet DWA-A 202 of the DWA (German Association for Water, Wastewater and Waste) and are given as relation of heavy metal concentration to active substance (iron) in mg/mol.

A theoretical calculation was conducted, assuming that all iron and all heavy metals dissolve and can subsequently be detected in the product solution.

The theoretically calculated values exceeded the guideline values only in single cases (Cr at “Meuro”, Ni/Zn at “Borna”) and were confirmed at the test stage.

In conclusion, it is possible to identify and exclude non usable sludges with excessive heavy metal levels or to find compositions of different sludge types to avoid an exceeding.

Application tests

The produced solutions of $\text{Fe}(\text{Cl})_3$ and $\text{Fe}_2(\text{SO}_4)_3$ were tested and compared with regular market products on a broad base:

- Testing effectiveness of the products by using synthetic waters
- Transfer of the results to original waters
- Evaluation of the achieved water qualities
- Comparison with regular market products
- Evaluation of the resulting sludges (sedimentation properties)

An example of an application test is given in Table 2. The test was accomplished with water from a sewage treatment plant after the mechanical treatment step which had the following parameters:

- pH 7.02
- turbidity (TE/F) 100
- total P [mg/L] 2.63
- total PO_4^{3-} [mg/L] 8.05
- COD [mg/L] 166

The results clearly show that the produced treatment chemicals had a comparable product quality regarding phosphor elimination and COD reduction although the amount of active substance in the product solution was lower.

Table 2: Application test results

Product	Product solution			After treatment		
	DMC	Acid	Fe [g/kg]	Total P [mg/L]	Total PO_4^{3-} [mg/L]	COD [mg/L]
Fe ₂ (SO ₄) ₃ standard product			138	< 0.5	< 1.5	66.1
Westrandgraben	20.4 %	55% H ₂ SO ₄	62.08	< 0.5	< 1.5	47.5
Westrandgraben	100%	55% H ₂ SO ₄	72.52	< 0.5	< 1.5	64.2
Westrandgraben	70.8 %	55% H ₂ SO ₄	64.07	< 0.5	< 1.5	49.6
Eichow	47 %	55% H ₂ SO ₄	76.43	< 0.5	< 1.5	63.1
FeCl ₃ standard product			125	< 0.5	< 1.5	63.0
Westrandgraben	20.4 %	31% HCl	45.64	< 0.5	< 1.5	55.8
Westrandgraben	100%	31% HCl	90.86	< 0.5	< 1.5	65.1
Westrandgraben	70.8 %	31% HCl	67.20	< 0.5	< 1.5	71.8
Eichow	47 %	31% HCl	62.06	< 0.5	< 1.5	63.6



So, products from iron ochre revealed an equivalent treatment success compared to commercially available products.

Residues

The residues from chemical conversion can be separated by solid-liquid separation after the conversion process. Solids were analysed and compared with the German soil classification regulations (LAGA codes) for soil emplacement and backfilling with the following conclusions:

- Most of the iron content is in the liquid
- Zinc and arsenic remain in the residue and are concentrated
- Soil emplacement classes Z1.2 or Z2 for the residues are suitable, meaning that a restricted open soil emplacement (class Z1.2) or a soil emplacement with technical safety measures (class Z2) are possible

Cost estimation

Cost estimations can be performed after realisation of the second stage of the pilot project. Because of the predicted cost increases for landfilling and/or iron ochre flushing the economic feasibility of the proposed utilization route is very likely.

Conclusions

The following conclusions can be drawn:

- Utilization of iron ochre by chemical conversion with acid is possible
- Products have comparable treatment properties as commercial products
- Residue amount can be significantly decreased
- Production of auxiliary water treatment materials from mine water treatment waste is most likely economically feasible
- Key figures for the commercial-scale use will be investigated in the next project phase

Acknowledgements

We would like to thank Lausitzer und Mitteldeutsche Bergbau-Verwaltungsgesellschaft mbH (LMBV) for financing this pilot and demonstration project and for all their support and input to this project.

References

- Hedin RH (2002) Recovery of marketable iron oxide from mine drainage. National Meeting of the American Society of Mining and Reclamation, Lexington KY, June 9-13, 2002. Published by ASMR, 3134 Montavesta Rd., Lexington, KY 40502.
- Uhlmann W, Theiss S, Totsche O, Ben-thaus FC (2015a) Bergbauverursachte Fließgewässerverockerung im Einzugsgebiet der Spree – Teil 1: Ursachen und aktuelle Belastung (Mining caused ochre formation in the catchment of river Spree, part 1: causes and current load). Freiberg Online Geoscience Vol 40(2015) p 45-56
- Uhlmann W, Theiss S, Totsche O, Ben-thaus FC (2015b) Bergbauverursachte Fließgewässerverockerung im Einzugsgebiet der Spree - Teil 2: Gegenmaßnahmen (Mining caused ochre formation in the catchment of river Spree, part 2: countermeasures). Freiberg Online Geoscience Vol 40(2015) p 57-64
- Simon E, Burghardt D, Richter J, Reichel S, Jan-neck E (2016) Removal of Oxoanions From Water: Comparison of a Novel Schwertmannite Adsorbent and an Iron Hydroxide Adsorbent. Proceedings IMWA 2016, Leipzig/Germany p 1004-1007
- Kießig G, Kunze C, Küchler A, Zellmer A, Meyer J, Kalin M (2004) Kostengünstige passive Nachsorgelösung mit einem Constructed Wetland, Proceedings 55. Berg- und Hüttenmännischer Tag, Treatment Technologies for Mining Impacted Water, Freiberg, 18.06.2004



Treatment of copper leachate for the recovery of valuable products

J.P. Maree^{1,2}, T. Mtombeni², P. Ramothole² and L. Letjiane²

¹Division of Water and Sanitation, University of Limpopo, Private Bag X1106, Sovenga, 0727, South Africa

²ROC Water Technologies, P O Box 70075, Die Wilgers, 0041, Pretoria, South Africa, maree.jannie@roc-water.co.za

Abstract

Copper leachate containing 13 500 mg/L Al^{3+} , 8 500 mg/L Mg^{2+} and 109 000 mg/L SO_4^{2-} requires to be treated. The purpose of this investigation was to identify a process configuration for the recovery of clean water and saleable products such as $\text{Al}_2(\text{SO}_4)_3$, $\text{Al}(\text{OH})_3$ and MgSO_4 from copper leachate. It was predicted from OLI software that: 40% of the water can be recovered before $\text{Al}_2(\text{SO}_4)_3$ -crystallization will occur and 80% before MgSO_4 -crystallization will commence. Pilot studies showed that the TDS can be reduced from 119 000 mg/L to 2 100 mg/L. The total cost, including capital redemption cost, was estimated at R207.32/m³. The value of the products were estimated at R550.37/m³.

Key words: Aluminium sulphate, Freeze crystallization, Leachate treatment, Magnesium sulphate, Mine water, ROC process

Introduction

The *Waste Act, 2008* and *National Water Act, 1998* of South Africa were enacted to promote cleaner production, waste minimization, water reuse, recycling and waste treatment, with disposal seen as a last resort (IWMSA, 2000). The Act stipulates that acids should be neutralized to have a pH between 6 and 12 before discharge onto a landfill site. The TDS content of brine or waste with a high salt content should not exceed 50 000 mg/L and the TDS from leachables should not exceed 100 000 mg/L (Gazette, 2008). Copper leachate is an example of such a waste stream and has a pH of 3.2 and contains 8 520 mg/L Mg^{2+} , 510 mg/L Ca^{2+} , 86.6 mg/L Cu^{2+} , 509.5 mg/L Fe^{2+} , 509.2 mg/L Fe^{3+} , 13 538 mg/L Al^{3+} and 109 408 mg/L SO_4^{2-} . Current methods of water treatment remove the adverse impacts, providing clean water for discharge, but leaves behind a concentrated waste that requires further treatment or disposal as a hazardous waste. Freeze desalination can be used for treatment of such highly saline solutions to: (i) produce water of a good enough quality and (ii) enable product recovery from a concentrated brine stream.

The potential of freeze desalination of sea water to produce drinking water was derived

from the natural phenomenon of pure ice formation from frozen sea water (Nebbia & Menozzi, 1968). This led to the realization of the possibility of using freezing to produce fresh water from brackish water, industrial brines and a range of other saline water streams (Schroeder, 1980; Khawaji, et al., 2008). The major benefit of freeze crystallization, over current brine treatment technologies e.g. distillation and evaporation ponds, derives from the much lower heat of fusion of ice (333 kJ/kg) compared to the heat of evaporation of water (2500 kJ/kg). The **ROC (Reverse Osmosis/Cooling) process** was developed for the treatment of brines from desalination processes, such as reverse osmosis (**Figure 1**) (Mtombeni & Maree, 2014; Mtombeni, et al., 2016). In the ROC process, brine is treated with chemicals such as Na_2CO_3 and/or NaOH in the pre-treatment stage to allow selective precipitation of metals (CaCO_3 , MnO_2 and $\text{Mg}(\text{OH})_2$). After pre-treatment, the sodium- and magnesium-rich water is passed through a membrane stage to produce drinking water and brine. The brine has a Na_2SO_4 -concentration which is high enough to allow Na_2SO_4 crystallization upon cooling/freeze desalination.

The purpose of this investigation was to validate a process configuration as shown in



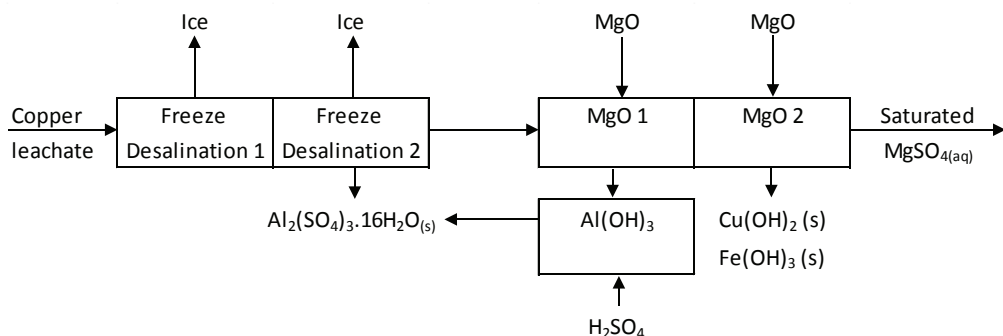


Figure 1 Process configuration for treatment of copper leachate

Figure 1 for the recovery of clean water and saleable products such as $\text{Al}_2(\text{SO}_4)_3$, $\text{Al}(\text{OH})_3$ and MgSO_4 from copper leachate.

Methods

Modelling

The *OLI ESP* software program was used to predict the water quality after treatment with (i) alkalis such as Na_2CO_3 and NaOH (OLI, 2015) for removal of metals, (ii) freeze crystallization to further concentrate the brine to the level where $\text{Na}_2\text{SO}_4 \cdot 10\text{H}_2\text{O}$ crystallizes. *OLI* is an aqueous equilibrium chemistry estimator with an interactive and self-instructive interface for clarifying reactions, having the ability to work with all kinds of common equilibrium reactions, with a strong solution algorithm, possessing expressive and easily understandable displays for results, and the ability to produce results in multiple formats according to different uses. The *Stream Analyzer* of *OLI* was used to perform single point equilibrium calculations, multiple point survey calculations for calculating a complete trend analysis for characteristics such as temperature, pressure, pH and composition effects, and simple mix and separation capability. The calculations provide liquid- and solid-phase separations for a specialized model.

The *OLI Analyser 9.0 System* was used to simulate the reactions by running a simulated AMD sample with assumed values of temperature, pressure, and pH. The base titrants used were NaOH , Na_2CO_3 and MgO . The temperature was assumed to be 25°C , the pressure, 1 atm and the pH was varied as desired with the different alkalis. Once the in-

put values were run in the *OLI Systems Chem Analyzer*, a calculated summary of the simulated results would appear. This could be used to predict the actual reactions to use in the treatment methods according to the specific characteristics. Thus it was used to optimize a neutralisation-precipitation-desalination process for AMD.

Feedstock

Copper leachate containing 8 520 mg Mg^{2+} , 510 mg Ca^{2+} , 86.6 mg Cu^{2+} , 509.5 mg Fe^{2+} , 509.2 mg Fe^{3+} , 13 538 mg Al^{3+} and 109 408 mg SO_4^{2-} per L of water, was prepared artificially.

Equipment and Procedure

A Tecumseh 971 W (input power) reciprocating compressor (Model: AJE2444ZHZ [CAJ2464Z]) with a refrigeration capacity of 727 W, was used to cool the primary refrigerant, R-404A. The primary refrigerant was recycled through a heat exchanger in the water bath to cool the secondary refrigerant (30% methanol/water mixture) to -10°C or as required. Leachate was cooled to freezing point by passing it through a second heat exchanger, submerged in the water bath containing the secondary refrigerant. The ice/brine mixture was passed through a static brine/ice separator. The separation was based on the density difference between water and ice. The separator consisted of an ice column (110 mm diam; 1.2 m height) and a drain pipe (50 mm diam.) inside the ice column. Ice/brine slurry was pumped upwards through the ice column under low pressure using a peristaltic pump. The drain pipe was perforated, to allow brine to flow by gravity to a sump directly under-



neath the drain pipe. The lower section of the drain pipe had 12 mm holes covered with a 1 mm mesh wire gauze. Due to continuous deposition of ice crystals at the base of the column, the ice column moved to the top where a portion was harvested as product. The feed line to the ice column was provided with a pressure gauge to monitor pressure. Pressure build-up was an indication of excessive ice accumulation in the separator instead of normal upward ice movement in the ice column.

Analytical

Samples were collected at various stages in the treatment process, filtered (Whatman No. 1) and analysed for pH, conductivity, acidity, Mg^{2+} , $Al(III)$ and SO_4^{2-} using standard procedures (American Public Health Association, 2012). A calibrated Knick Stratos Eco 2505 meter was used to measure electrical conductivity. Ice content was determined by mixing

250 mL ice slurry (mass m_i ; temperature T_1) with 200 mL (m_2) warm water (T_2). The mass of ice (m_i) was determined from m_1 , T_1 , m_2 , T_2 and the temperature (T_3) was measured after the ice had melted. Microsoft Excel *Goal Seek* was used to calculate m_i using the following equation:

$$4.18(m_1 - m_i)(T_1 - T_3) + 330m_i + 4.18m_2(T_2 - T_3) = 0 \quad (1)$$

Results and discussion

Process configuration

OLI software was used to predict the behaviour of copper leachate (1 000 000 mg H_2O = 1L H_2O), containing 8 520 mg Mg^{2+} , 510 mg Ca^{2+} , 86.6 mg Cu^{2+} , 509.5 mg Fe^{2+} , 509.2 mg Fe^{3+} , 13 538 mg Al^{3+} and 109 408 mg SO_4^{2-} . This was treated by freeze crystallization and MgO. Table 1 shows the chemical composition of the feed water and after treatment for,

Table 1 Chemical composition of copper leachate before and after treatment by freeze crystallization and MgO dosing (predicted by OLI software)

Parameter	Water quality (mg)					
	Copper leachate	Freeze Des 1	Freeze Des 2	MgO dosing 1	MgO dosing 2	Sludge separation
<i>Chemical dosing</i>						
MgO				14 406.9	435.8	
<i>Solution</i>						
pH	3.4	3.3	3.0	4.5	8.9	9.0
H_2O (mg)	1 000 000	600 000	200 000	200 000	200 000	200 000
Al^{3+} (mg)	13 523	13 523	6 190	1.0	0	0
Ca^{2+} (mg)	469	266	49	49	49	49
Cu^{2+} (mg)	121	121	121	121	0	0
Fe^{2+} (mg)	510	510	510	510	16	16
Fe^{3+} (mg)	509	509	509	0.5	0	0
Mg^{2+} (mg)	8 522	8 522	8 522	17 209	17 472	17 472
SO_4^{2-} (mg)	109 600	109 113	69 326	69 326	69 326	69 326
TDS (mg)	133 254	132 564	85 227	87 217	86 863	86 863
TDS (mg/L solution)	120 092	186 943	316 445	323 833	322 519	322 519
Mass (mg solution)	1 133 254	732 564	285 227	287 217	286 863	286 863
Cations (meq)	2 277	2 267	1 441	1 441	1 441	1 441
Anions (meq)	2 283	2 273	1 444	1 444	1 444	1 444
<i>Solution</i>						
$MgSO_4$ (mg)				86 535	86 798	86 798
$MgSO_4$ (mg/L)				432 675	433 989	433 989
<i>Solids</i>						
Ice (mg)		399 779	360 474	0		
$Al_2(SO_4)_3 \cdot 16H_2O$ (mg)			85 554			
$Al(OH)_3$ (mg)				17 879		
$CaSO_4 \cdot 2H_2O$ (mg)		1 058	1 987			
$Cu(OH)_2$ (mg)					186	
$Fe(OH)_2$ (mg)					795	
$Fe(OH)_3$ (mg)					1.0	
Suspended solids (mg/L)		1 763	437 703	89 397	4 907	



(i) removal of water via freeze crystallization for recovery of water and $\text{Al}_2\text{SO}_4 \cdot 16\text{H}_2\text{O}$ and (ii) chemical treatment with MgO for removal of impurities (Cu^{2+} , Fe^{2+}) and recovery of a saturated MgSO_4 solution. The chemical composition was expressed in mg in solution and not the conventional mg/L. The reason was because water was removed in addition to chemical compounds. It was shown in Step 1 (Freeze Des 1) that 40% water was removed with no removal of Al^{3+} and Mg^{2+} . The low mass of 469 mg Ca^{2+} in the 1 000 000 mg water was reduced to 266 mg in the remaining 600 000 mg water. This was due to the limited solubility of gypsum. In Step 2 (Freeze Des 2) a further 40% of the water was removed. This resulted in removal of Al^{3+} as the solubility of $\text{Al}_2\text{SO}_4 \cdot 16\text{H}_2\text{O}$ at -1°C was exceeded. Al^{3+} mass in solution was reduced from 13 523 mg to 6 190 mg to produce 85 554 mg $\text{Al}_2\text{SO}_4 \cdot 16\text{H}_2\text{O}$. Ca^{2+} mass was further reduced from 266 mg to 49 mg due to gypsum crystallization.

In Step 3 a dosage of 14 410 mg MgO was applied to precipitate the remaining Al^{3+} as $\text{Al}(\text{OH})_3$ at pH4.5. This step offered the benefit that Al^{3+} was completely removed. $\text{Al}_2(\text{SO}_4)_3$ is used as a coagulant in water treatment. $\text{Mg}(\text{OH})_2$ can also be converted to MgSO_4 by dissolving it in H_2SO_4 . MgSO_4 is a valuable product used in fertilizer manufacturing.

In Step 4, the predominant MgSO_4 solution was purified by precipitating Fe^{2+} and

Cu^{2+} as hydroxides by dosing 435.8 mg MgO . The remaining solution contained 86 798 mg MgSO_4 . The original 1 L (1 000 000 mg) of water in the 1 133 254 mg copper leachate was reduced to 0.2 L (200 000 mg) of water, representing a MgSO_4 concentration of 433 989 mg/L, which is at saturation level. This solution can be sold as is for fertilizer manufacturing.

Freeze crystallization

Freezing point and water quality

Figure 2 shows the time needed to reduce the temperature of 64.6 g of water from room temperature (15°C) to 0°C and to freezing point and ice formation. In the case of the pipe (20 mm diam. 1.5 mm wall thickness) a time of 7.1 min was needed to lower the temperature from 15°C to 0°C . A further 12 min was needed to decrease the temperature from 0°C to -7°C , where after freezing commenced and continued over a period of 23 min. These calculations explained why water is rapidly cooled from room temperature to 0°C compared to the time needed for freezing the water. The energy usage to freeze the 64.6 g water amounted to 21 576 J.

Ice production

Ice slurry was produced by passing copper leachate through a PVC pipe, submerged in a water bath at -8°C and passed through an ice separation system as shown in Photo 1. Ice production on a continuous basis can be seen

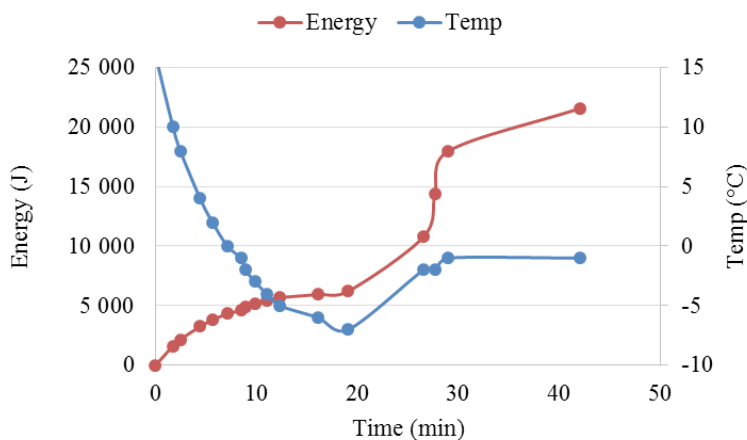


Figure 2 Temperature and energy behaviour during cooling of copper leachate to freezing point



Photo 1 Ice separation



in the following link: <https://www.dropbox.com/s/bm9olu58r02qalo/Copper%20Leachate.AVI?dl=0>

A filter inside the ice separation system allowed brine to be returned by gravity to the recycle stream while ice was forced to move up the column to be harvested. Over a period of 5 hours operation the conductivity of the melted ice decreased gradually from 27 to 7 mS/m. After harvesting and by allowing the ice to mature further by recirculation, the conductivity decreased to 2 mS/m. The purity of the ice is dependent on crystal growth and recrystallization. By running the plant for a longer period, it is expected that the ice purity will improve further. Table 2 shows that clean ice can be produced. In the copper leachate the TDS content had been reduced from 119 138 mg/L to 2 102 mg/L.

Feasibility

A cost-effective process configuration was proposed for treatment of copper leachate by using the following approach: (i) Use freeze crystallization for recovery of water from a highly saline stream, (ii) Precipitate $\text{Al}_2(\text{SO}_4)_3 \cdot 16\text{H}_2\text{O}$ directly with freeze crystallization for as long as MgSO_4 remains in solution, (ii) Use MgO to precipitate the last fraction of Al^{3+} in solution (as $\text{Al}(\text{OH})_3$) at the stage just before MgSO_4 starts to precipitate, (iii) Convert the $\text{Mg}(\text{OH})_2$ with H_2SO_4 to MgSO_4 , and (iv) Use the saturated MgSO_4 solution as a final product.

The feasibility of processing copper leachate is calculated in and demonstrated by the results in Tables 3 - 6. Electricity cost amounted to R50.07/m³ (Table 3); capital cost to R27.3million for a 68.1 m³/h plant

Table 2 Water quality of Feed, melted ice and brine

Parameter	Chemical composition		
	Feed	Ice	Brine
Cond. (mS/cm)	44.0	2.5	62.0
pH	3.4	3.3	3.2
Al^{3+}	13 500	244	20 195
Mg^{2+}	6 439	95	9 700
Fe^{2+}	471	19	650
Cu^{2+}	2.5	0.0	3.7
Ca^{2+}	21	7	21
SO_4^{2-}	98 706	1 742	147 000
Cations (meq/L)	2 056	36	3 078
Anions (meq/L)	2 056	36	3 063
TDS (mg/L)	119 138	2 107	177 570

Table 3 Energy cost

Parameter	Value
Plant capacity (kg/s)	18.92
Electricity usage (80% ice recovery; COP = 1.5; 80% efficiency) (kW)	4 871.36
Electricity usage (kWh/m ³)	71.53
Electricity price (R/kWh)	0.70
Electricity cost (R/m ³)	50.07

Table 4 Capital cost

Cost items	Value
Plant capacity (m ³ /h)	68.10
Plant capacity (gal/min)	300.00
Chiller capacity (MW)	4.87
Capital cost: Chiller (R/MW)	2 800 000
Capital cost: Chiller (R)	13 639 803
Capital cost: Other (R)	13 639 803
Total Capital cost (R)	27 279 607



Table 5 Cost of raw materials and value of products

Chemical	Usage kg/m ³	Price R/t	Cost/Value R/m ³
<i>Raw materials</i>			
MgO	13.10	4 000	-52.39
H ₂ SO ₄	29.73	3 000	-89.20
Total cost			-141.59
<i>Products</i>			
Al ₂ (SO ₄) ₃ ·16H ₂ O	139.21	2 000	278.42
MgSO ₄ ·7H ₂ O	156.81	1 700	266.58
Water	670.86	8	5.37
Total value			550.37

Table 6 Feasibility

Cost item	Value
Capital redemption cost (R/m ³) (1%/month; 120 month)	-7.88
Electricity cost (R/m ³)	-50.07
Labour (R/m ³) (10 operators; R7000/Month)	-1.41
Maintenance (R/m ³) (3% of Capital cost)	-1.37
Other (R/m ³)	-5.00
Chemical cost (R/m ³)	-141.59
Total cost (R/m ³)	-207.32
Value of products (R/m ³)	550.37
Profit (R/m ³)	343.05

(Table 4); chemical cost to R141.59/m³ (Table 5); capital redemption cost to R7.88/m³ (Table 6), and the value of water and products (Al₂(SO₄)₃·16H₂O and MgSO₄) to R550.37/m³ (Table 5). The combined value of products clearly exceeds the costs by R343.05/m³ (Table 6).

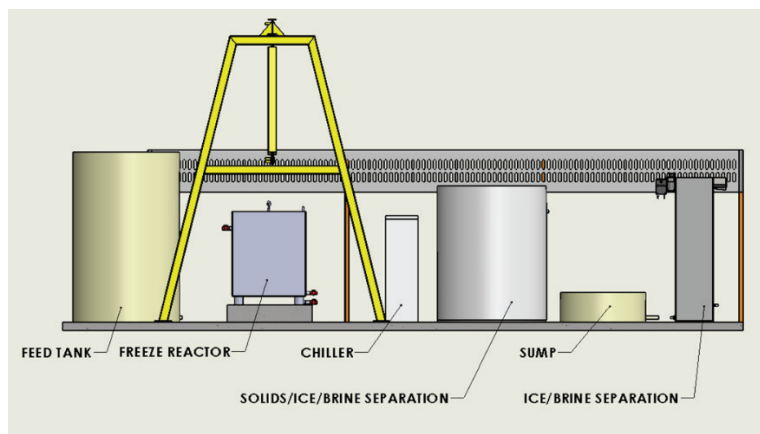
A pilot-plant with a capacity of 300 L/h (Figure 3) has been designed and is under construction which will be used to demonstrate that brine can be concentrated in two stages: (i) where 40% of the water is removed through ice formation with no removal of Al³⁺ and Mg²⁺ and (ii) where a further 40% of the water is removed together with a portion of the Al³⁺ as Al₂(SO₄)₃.

Beaker studies will be carried out on the remaining brine for removal of Al³⁺, Fe²⁺ and Cu²⁺ with MgO. The following items are shown in Figure 3: Feed tank, Chiller, Freezing reactor, Ice/brine/solids separation reactor and Ice/brine separation reactor.

Conclusions

The following conclusions were drawn from the results of this study:

1. With OLI software it was predicted that from 1 113 254 mg copper leachate (1 000 000 mg H₂O + 133 254 mg salt) the following can be recovered: (i) 399 799 mg ice in Step 1 (Freeze Crystallization 1), (ii) 360 474 mg ice, 85 554 mg

**Figure 3** Schematic diagram of a 300 L/h copper leachate pilot-plant

- $\text{Al}_2(\text{SO}_4)_3 \cdot 16\text{H}_2\text{O}$ and 1 987 mg gypsum in Step 2 (Freeze Crystallization 2), (iii) 17 879 mg $\text{Al}(\text{OH})_3$ in Step 3 (MgO dosing 1), (iv) 186 mg $\text{Cu}(\text{OH})_2$ and 795 mg $\text{Fe}(\text{OH})_2$ in Step 4 (MgO dosing 2) and (v) 86 798 mg MgSO_4 (200 mL of a 43% MgSO_4 solution) in Step 5 (Final brine).
2. Pure ice with a TDS of 2 107 mg/L was recovered in a laboratory freeze crystallization unit from copper leachate with a TDS of 119 135 mg/L. The TDS of the brine increased to 177 570 mg/L.
 3. The total combined running and capital redemption costs were estimated at R207.32/m³.
 4. The total value of water and products ($\text{Al}_2(\text{SO}_4)_3 \cdot 16\text{H}_2\text{O}$ and MgSO_4) were estimated at R550.37/m³.
 5. This technology is an improvement on existing desalination technology for the following reasons: (i) It decreases brine volumes by crystallization of dissolved species enabling further water recovery, and (ii) It reduces sludge formation by enabling the selective production of saleable products.

Recommendation

Copper leachate and other brine streams need to be treated on pilot-scale with the focus on recovery of water, $\text{Al}_2(\text{SO}_4)_3 \cdot 16\text{H}_2\text{O}$, $\text{Al}(\text{OH})_3$ and a saturated MgSO_4 solution or other saleable products.

Acknowledgements

The authors express their gratitude to Tshwane University of Technology for providing laboratory facilities to conduct this study.

References

- American Public Health Association (APHA) (2012). *Standard methods for the examination of water and wastewater*. 22nd ed. Washington: American Water Works Association, Water Environment Federation.
- Gazette (2008) Landfill, National norms and standards for disposal of waste to landfill. National Environmental Management: Waste Act 59 of 2008 (Govt. Gazette No. 32000, Notice No. 278. Commencement date: 1 July 2009 – save for sections 28(7)(a), sections 35 to 41 and section 46 [Proc. No. 34, Gazette No. 32189])
- IWMSA, I. o. W. M. S. A., (2000) *Waste Management*. [Online]
- Available at: http://www.enviroopaedia.com/topic/default.php?topic_id=239
- [Accessed 18 December 2015]
- Khawaji AD, Kutubkhanah IK, Wie JM (2008) Advances in seawater desalination technologies. *Desalination*, 221(1), 47-69
- Mtombeni T, Maree, JP (2014) Treatment of water – ROC process. South Africa Provisional Application (26 June), Patent No. 2014/04734
- Mtombeni T, Maree JP, Zikalala NS, Fourie CJ (2016) Desalination with a combined membrane filtration/freeze desalination process. WISA Biennial Conference, Durban, South Africa.
- Nebbia G, Menozzi GN (1968) Early experiments on water desalination by freezing. *Desalination*, 5, 49-54.
- OLI, (2015) OLI. [Online]
- Available at: <http://www.olisystems.com/>
- [Accessed 23 11 2015]
- Schroeder PJ (1980) Freezing processes. *Desalination*, 33, 299-310.



Recovery and Synthesis of Al³⁺/Fe³⁺ Polycationic-Nanocomposites from Acid Mine Drainage Treatment Process and their Respective Application in the Removal of Arsenic and Chromium Ions from Polluted Water Resources

Khathutshelo L. Muedi¹; Hendrik G. Brink¹; Vhahangwele Masindi^{2,3}; Jannie P. Maree⁴

¹University of Pretoria, Department of Chemical Engineering, School of Engineering, Faculty of Engineering, Built Environment and Information Technology, Private Bag X20, Hatfield, 0028, South Africa
Email: khathumuedi@gmail.com

²Council for Scientific and Industrial Research (CSIR), Built Environment (BE), Hydraulic Infrastructure Engineering (HIE), P.O Box 395, Pretoria, 0001, South Africa

³University of South Africa (UNISA), Department of Environmental Sciences, School of Agriculture and Environmental Sciences, P. O. Box 392, Florida, 1710, South Africa

⁴ROC Water Technologies, P O Box 70075, Die Wilgers, 0041, Pretoria, South Africa

Abstract

As the quest for effective and affordable techniques for the treatment of wastewater continues, this study was therefore designed with the aim of recovering and synthesizing Al/Fe polycationic-nanocomposite from authentic acid mine drainage (AMD) and explore its efficacy in the removal arsenic and chromium ions from an aqueous system. Batch experiments were used to fulfil the goals of this study. The Fe/Al matrix was recovered from coal mine drainage and was then used to synthesize a polycationic-nanocomposite through calcination and vibratory ball-milling. Obtained results revealed > 95 and 99 % removal efficiency for chromium and arsenic ions, respectively. In that regard, preliminary assays from this novel, double-edged and innovative study proved that valorisation of mine water by acceptable treatment and extraction of valuable minerals that has myriads of industrial applications such as contaminated water depollution is achievable.

Keywords: Acid mine drainage, Al/Fe nanocomposite, recovery, adsorption, arsenic ions, chromium ions

Introduction

In recent decades, industries have been discharging water that is rich in potentially toxic and hazardous pollutants such as arsenic and chromium to the environment. This has significantly impaired the quality of the environment and its ability to render endowed intrinsic values (El-Zeiny and El-Kafrawy 2017; Masindi and Gitari 2016). Although arsenic and chromium are important in the society for various uses, they can cause detrimental impacts to the human health, ecosystems, soil and the environment if discharged at high levels since the environment can tolerate a certain range of this pollutants as specified in a number of environmental and toxicological guidelines and standards (Edelstein and Ben-Hur 2018). This is may be attributed to the

fact that these ions can be taken up by plants, consumed by animals and humans via a number of routes and escalate in food chains, thus degrading the environment, and its ability to foster life (Singh and Kalamdhad 2011).

The high carcinogenicity and toxicity nature of As(V) and Cr(VI) have led to a continuous search for amicable and effective depollution technologies. This was further dictated by tight environmental regulations that require industries to clean their water to acceptable standards before they could discharge their effluents to the environment. These technologies include different mechanisms such as adsorption, filtrations, precipitations, ion-exchange, bio-sorption and phytoremediation (Masindi et al. 2014). Amongst these techniques, adsorption has



received paramount attention (Masindi and Gitari 2016). This is attributed to the fact that they rely heavily on locally available materials, cheap and easy to operate and high efficacy. A number of materials have been used for adsorption and they include: carbon nanotubes, aluminium oxide, magnesite-bentonite clay, ceria nanoparticles, and zirconium nanoparticles (Masindi and Gitari 2015). However, there's still a challenge with operational cost and waste disposal which lead to secondary pollution. In light of that, the present study aims at the removal of pollutants from wastewater, and utilizes them to remove other pollutants from contaminated water. This has a binary approach since it is solving an industrial problem by treating AMD and attains materials that can be used to treat another environmental problem that involves the removal of arsenic and chromium.

Materials and Methods

Sampling, feedstock acquisition and preparation

Raw acid mine drainage (AMD) was collected from a Coal mine in Mpumalanga Province, South Africa. Sodium arsenate dibasic heptahydrate ($\text{Na}_2\text{HAsO}_4 \cdot 7\text{H}_2\text{O}$) and Potassium dichromate salt ($\text{K}_2\text{Cr}_2\text{O}_7$) salts were purchased from Sigma-Aldrich and stored until utilisation for stock solution preparation. Caustic soda (NaOH), Sulphuric acid (98.5% H_2SO_4) and Hydrochloric acid (37% HCl) were purchased from Merck. All chemicals were used as obtained without processing. Aqueous solutions were prepared using ultra-pure water (18.2 $\text{M}\Omega\text{-cm}$). Experimental vessels (glassware) were carefully and thoroughly cleaned before and after every use to avoid contamination.

Recovery and synthesis of the nanocomposite

Al^{3+} and Fe^{3+} rich acid mine drainage was used for fractional precipitation of those chemical species using Na-salts as seeding materials. The species were then calcined at 100°C to encourage dehydration and promote reactivity. The dry samples were then milled in a vibratory ball mill to homogenise the samples and ensure efficacy of arsenic and chromium adsorption.

Adsorption studies

To determine the adsorption of arsenic and chromium from an aqueous system, a number of operational parameters that include time, dosage, temperature and pH were evaluated. The results were used to determine the optimum conditions that are suitable to remove arsenic and chromium.

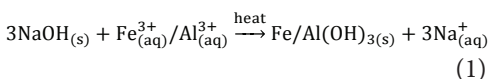
Characterisation

Metal ions in aqueous samples and solutions were analysed using AAS and ICP-MS. Surface area, pore volume and pore size of Al/Fe nanocomposite and resultant residues were determined using a Brunauer-Emmet-Teller (BET) equipment equipped with micromeritics VacPrep 061 degassing system (Micromeritics Tri-Star II 3020, Surface area and porosity, Poretech CC, USA). For quality control/assurance (QC/QA), all the experiments were carried out in triplicates and the data was reported as mean value as reported in the EPA guidelines.

Results and discussions

Recovery, synthesis and adsorption studies

Caustic soda was added to authentic AMD to elevate the pH for the recovery of Al/Fe nanocomposite via selective precipitation. The interaction of NaOH with Fe^{3+} and Al^{3+} in AMD is shown in equation 1.



The synthesis was done at room temperature. Agglomeration of the particles occurred during heating which was done after precipitation. Synthesis and optimisation parameters are shown in Figure 1 (A – F).

As shown in Figure 1A, it is clear that molecules and particles in AMD slowly gain kinetic energy between 20°C and 75°C . This can be attributed to an exponential growth in the time trend graphs with temperature. After 80°C , collision of molecules and particles increases. As particles continue absorbing heat with time, they start moving faster and kinetic energy increases, hence temperature increases, as the reaction is endothermic. The rate at which particles collide increased and led to coagulation of small particles which



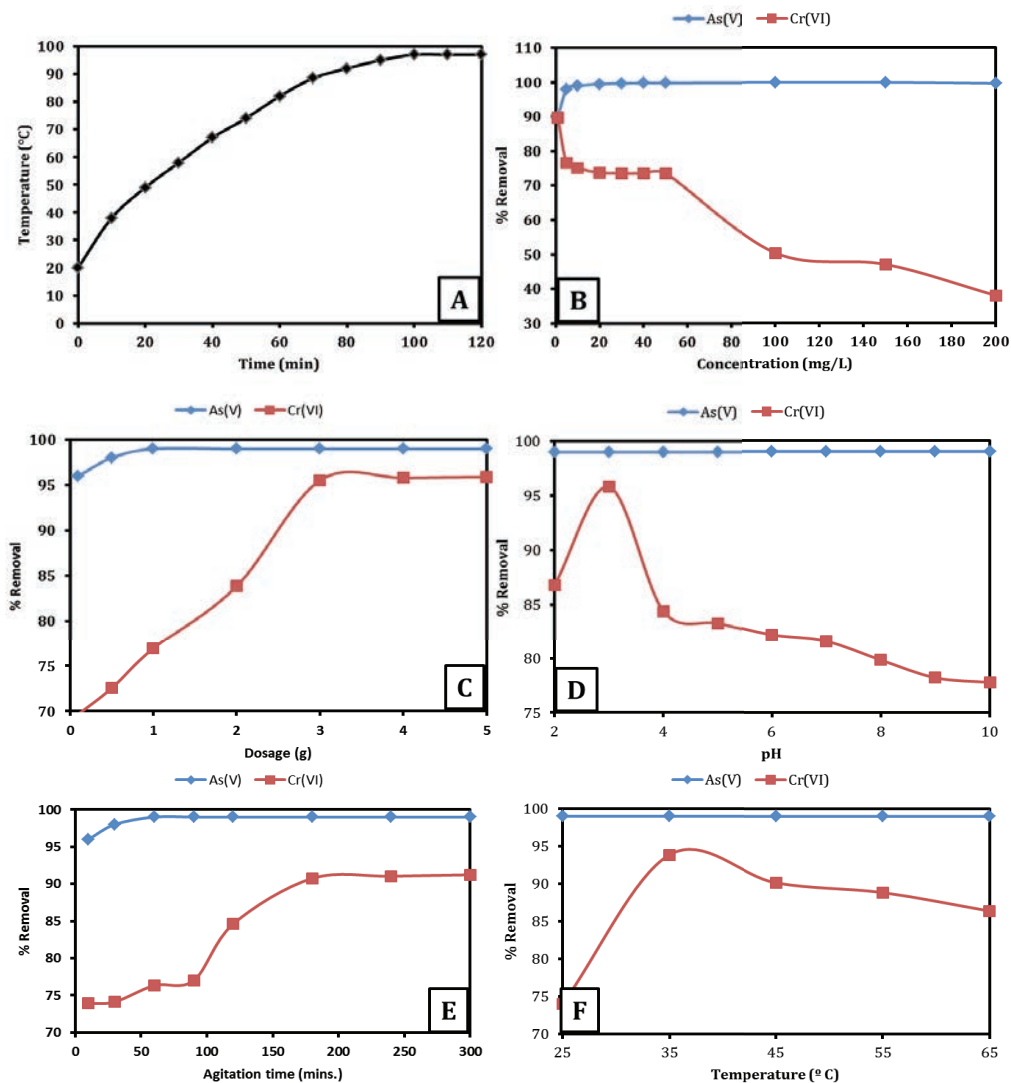


Figure 1: Synthesis of Al/Fe nanocomposite (Figure 1A) and Variation of parameters for the adsorption of As(V) and Cr(VI) onto Al/Fe nanocomposite in a 250 mL aq solution (Figures 1B – 1F)

formed agglomerates of Al/Fe nanocomposites with high surface area and pore volume. This was due to the precipitation of metal cations during neutralisation of AMD. This behaviour is also in agreement with the Le Chatelier's Principle and Collision theory because the reaction favoured the formation of products.

Effect of initial concentration

As shown in Figure 1B, the removal of arsenic from aqueous solution using the synthesized nanocomposite was observed to increase

with an increase in concentration. This justifies that the adsorbent was enough for the removal of arsenic whereas for Cr(VI), the removal efficacy was observed to decrease with an increase in Cr concentration. This is an indication that the adsorption sites were saturated with the Cr ions from aqueous solution. Moreover, this study further proved that As has high affinity for Al/Fe nanocomposite as compared to Cr. Although a decrease in the percentage removal of As(V) was observed between 150 mg/L and 200 mg/L, it was, however, insignificant. Further variation on



As(V) would clearly indicate a clear decrease on the graph. From this results, 150 mg/L and 50 mg/L are optimum initial concentrations for As(V) and Cr(VI), respectively, and they were taken as the optimum and they will be used in subsequent experiments.

Effect of adsorbent dosage

As shown in Figure 1C, the removal of arsenic was observed to increase with an increase in adsorbent dosage. Similar trend was observed for chromium. For As(V), it can be noted that more than 1 g of the adsorbent leads to over-saturation of the system. The % removal of As(V) from water remains constant between 1 g – 5 g, which means that, 1 g is enough for the removal of 10 mg/L As(V) ions from 250 mL of aqueous solution. This stability of the curve tells that the surface of the adsorbent can accommodate more of As (V) onto its interlayers and matrices. For Cr(VI), an even increase in percentage removal of Cr (VI) is observed from 0.1 – 3 g of Al/Fe nanocomposite dosage. After 3 g, the graph took a gentle slope. This could indicate saturation of the adsorbent; hence it could not take any more of Cr (VI) ions. Therefore, 3 g was adequate for the removal of chromium from aqueous solution. The challenge is the affinity and ionic strength of these toxic elements.

Effect of initial pH

In colloidal science, the adsorption of pollutants is firmly dependent on the supernatant pH. pH governs the state of chemical components in aqueous solution and dictate the charge and elements that are going to be adsorbed in aqueous solution. As shown in Figure 1D, there was no effect on the behaviour of initial pH of As (V) solution on the adsorption of As(V) by Al/Fe polycationic-nanocomposite. This could be attributed to: [1] As (V) salt is dibasic and makes its solution alkaline; [2] Sodium arsenate dibasic heptahydrate ($(\text{Na}_2\text{HAsO}_4 \cdot 7\text{H}_2\text{O})$ salt is a conjugate base of arsenic acid, which is why the pH of its aqueous solution is within 7 – 9; [3] Al/Fe nanocomposite was precipitated using NaOH which is a strong base, hence the pH does not have much effect as the adsorption process is accommodated within a wide pH range; [4] As(V) ions are more dominant between

pH of 2 – 11, according to arsenic Pourbaix diagram, where the probability of removing them from water is high. This is when they are in solution as dihydrogen arsenate (H_2AsO_4^-) and hydrogen arsenate (HAsO_4^{2-}). This zone accommodates the adsorption of As(V) onto Al/Fe nanocomposite as the adsorbent was also synthesised within that pH range. Ferric iron also plays an important role in anionic exchange within this pH range. On the other hand, for the removal of Cr (VI), the highest removal occurred at a pH of 3. This could better be explained by the value of point of zero charge of the adsorbent which was found to be $\text{pH}_{\text{PZC}} = 3.02$. A pH_{PZC} indicates that at pH below the PZC the adsorbent will adsorb anions and above the PZC, the adsorbent will adsorb cations.

Effect of agitation time

As shown in Figure 1E, the % removal of species under study was observed to increase with an increase in contact time. There was a rapid increase in the removal efficiency. After 1 hour (60 minutes) and 3 hours (180 minutes) of agitation, the graphs take a gentle slope for As(V) and Cr(VI), respectively, thus showing that those are the optimum times of agitation for the removal of those heavy metals from water using Al/Fe nanocomposite. The optimum time was observed to be 180 minutes for all the species under study. As such 180 mins will be used for all the subsequent experiments.

Effect of temperature

As shown in Figure 1F, the removal of As was independent of temperature. Furthermore, Cr was observed to be firmly dependent on temperature. From the Cr(VI) graph, it can be noted that the percentage removal increases as temperature increases, but within a range 25 – 40 °C. Temperatures higher than 40 make Cr (VI) go back into solution, hence making 40°C optimum for this study.

Surface area and porosity

The synthesised PTFE/Al nanocomposite has surface area and pore size of 25 m²/g and 8.6 nm, respectively, which serve as basis that the material is a mesoporous nanocomposite material as its pore size falls within the range of 2



– 50 nm (Thommes et al. 2015). After adsorbing As and Cr, the surface area was observed to have decreased, this is an indication that the material adsorption sites are getting saturated with the pollutants that is being scavenged from the solution.

Conclusions and recommendations

From the preliminary studies, it was observed that polycationic ($\text{Al}^{3+}/\text{Fe}^{3+}$) nanocomposite can be successfully recovered and synthesised from natural acid mine drainage (AMD). The recovered and synthesised product can be beneficiated by using them in the removal of pollutants from water. In this study, polycationic composites were used for the removal of arsenic and chromium ions from aqueous solution and they showed great potential and high efficiency. The removal efficacy were observed to be >99% and >95% for arsenic and chromium ions. This can be attributed to high surface area, porous nature and composition of the adsorbents. Al/Fe nanocomposite has a high adsorption capacity of $q_e=37.48$ mg/g and 4.17 mg/g which made it effective in removing 150 mg/L As (V) and 50 mg/L Cr(VI), respectively. Researchers should adopt technologies which use natural pollutants to treat wastewater in place of synthetic adsorbents. Future work involves modelling the adsorption of these pollutants from aqueous solution using a number of mathematical models and to test it against authentic water that is rich in arsenic and chromium ions.

Acknowledgements

The authors wish to convey profound gratitude to the National Research Foundation (NRF) for providing financial support for this study. Furthermore, sincere appreciation goes to the University of Pretoria (UP) and Council for Scientific and Industrial Research

(CSIR) for the necessary infrastructure and facilities for the execution of this research study.

References

- Edelstein M, Ben-Hur M (2018) Heavy metals and metalloids: Sources, risks and strategies to reduce their accumulation in horticultural crops. *Scientia Horticulturae*, doi:<https://doi.org/10.1016/j.scienta.2017.12.039>
- El-Zeiny A, El-Kafrawy S (2017) Assessment of water pollution induced by human activities in Burullus Lake using Landsat 8 operational land imager and GIS. *The Egyptian Journal of Remote Sensing and Space Science* 20:S49-S56, doi:<https://doi.org/10.1016/j.ejrs.2016.10.002>
- Masindi V, Gitari MW, Tutu H, De Beer M (2014) Application of magnesite-bentonite clay composite as an alternative technology for removal of arsenic from industrial effluents. *Toxicological & Environmental Chemistry* 96:1435-1451
- Masindi V, Gitari W (2015) Simultaneous removal of metal species from acidic aqueous solutions using cryptocrystalline magnesite/bentonite clay composite: an experimental and modelling approach. *Journal of Cleaner Production*
- Masindi V, Gitari WM (2016) Removal of arsenic from wastewaters by cryptocrystalline magnesite: complimenting experimental results with modelling. *Journal of Cleaner Production* 113:318-324, doi:[10.1016/j.jclepro.2015.11.043](https://doi.org/10.1016/j.jclepro.2015.11.043)
- Singh DJ, Kalamdhad A (2011) Effects of Heavy Metals on Soil, Plants, Human Health and Aquatic Life vol 1.
- Thommes M, Kaneko K, Neimark AV, Olivier JP, Rodriguez-Reinoso F, Rouquerol J, Sing KSW (2015) Physisorption of gases, with special reference to the evaluation of surface area and pore size distribution (IUPAC Technical Report). 87:1051-1069, doi:[10.1515/pac-2014-1117](https://doi.org/10.1515/pac-2014-1117)



Can Phosphate Be Used To Improve The Hazardous Status Of High Density Sludge And Transform It Into An Agricultural Product?

B.H. Sukati, P.C. De Jager, J.G. Annandale, P.D. Tanner

Department of Plant and Soil Sciences, University of Pretoria, X20, Hatfield 0028, South Africa

chris.dejager@up.ac.za

Abstract

High Density Sludge (HDS) is often classified as hazardous due to metal solubility. The objective was to investigate if phosphate (PO_4) treatment can stabilize HDS. HDS with high soluble Mn (Hi-sol Mn) and another with low soluble Mn (Lo-sol Mn) were treated with 50 mg/L P and 4000 mg/L P solutions. Lo-sol Mn showed low metal solubility before and after treatment. Soluble Ni in Hi-sol Mn was reduced from 2.9 to 0.07 mg/L after 4000 mg/L P treatment and Pb remained at <0.1 mg/L before and after treatment. This improved both materials towards a better plant nutrient source.

Keywords: High Density Sludge, TCLP, AMD

Introduction

High density sludge (HDS) is generated during acid mine drainage (AMD) treatment by a mixture of recycled sludge and a combination of limestone (CaCO_3) and lime (Ca(OH)_2) (Aubé and Zinck 1999). Depending on the chemical used to treat AMD, HDS can be alkaline regardless of the process and contains varying concentration of various transition metals (e.g. Ni, Pb, Hg, Co, Cr, Cd, Zn, Cu). These metals can be traced back to the chemistry of AMD treated and the liming material (Johnson and Hallber 2005, Kalin et al. 2006). Based on composition and solubility of metals, HDS is often classified as a hazardous waste. The potential environmental risk is a function of the solubility of these metals.

From an agricultural point of view, it contains various elements essential for plant growth. As a result of the treatment, it is particularly high in Ca and S, as SO_4 , residing in gypsum ($\text{CaSO}_4 \cdot 2\text{H}_2\text{O}$). Other essential elements are Mg, an element often deficient in highly leached soils, and trace elements like Zn and Cu. The material also contains 10 – 30 % residual lime depending on the process (Maree et al. 2004 and Zinck 2006) that can increase the pH of acid soils. Using phosphate (PO_4) to chemically stabilize waste by decreasing the solubility of metals in it, is a well-established practice. Metal stabilization

by PO_4 was demonstrated; in bottom ash of municipal solid wastes (Crannell et al. 2000), in polymineralic mine wastes (Harris and Lottermoser 2006), and in soils (Kumpiene et al. 2006). Phosphate facilitates surface sorption and precipitation of especially transition metals reducing their solubility. Crannell et al. (2000) results indicated that Pb was precipitated by PO_4 into a sparingly soluble mineral, lead hydroxypyromorphite ($\text{Pb}_5(\text{PO}_4)_3\text{OH}$). According to Barthel and Edwards (2004), Kumpiene et al. (2008) metal-phosphate precipitates have low solubility due to their low K_{sp} (solubility potential) values. Stabilization of other metals (e.g. Zn, Cu, Cd) also occurs on the surfaces of $\text{Ca}_5(\text{PO}_4)_3\text{OH}$ through sorption processes or by isomorphous substituting for Ca in the $\text{Ca}_5(\text{PO}_4)_3\text{OH}$ structure (Eighmy et al. 1997 and Crannell et al. 2000). Not investigated in these studies were the potential redox stabilisation introduced by phosphate. HDS contains a fair amount of iron oxides, hence the objective of this study, was to investigate the effectiveness of phosphate (PO_4) as a form of environmental stabilisation of metals in HDS. That is if phosphating decreases the susceptibility of HDS to reduction and if this decreases the solubility of the constituents of HDS, for example metals, such as Ni and Pb.



Methods

Types of HDS used and their sources

Two HDS sludges from Mpumalanga Coalfields in South Africa, sampled in 2016, were considered. One HDS was sourced from an AMD treatment plant that uses CaCO_3 alone (Hi-Sol Mn HDS). The other was from a plant that uses a combination of CaCO_3 and Ca(OH)_2 (Lo-Sol Mn HDS).

Determination of mineralogy

Mineralogy of HDS was determined with X-ray Diffraction (XRD) before and after phosphating. PANalytical X'Pert Pro Powder Diffractometer. The procedure described by Loubser and Verryn (2008) was followed.

Alkalinity and pH determination

The pH was determined before and after phosphating as described by Thomas (1996) in *Methods of Soil Analysis Part 3 Chemical Methods* (1996) in both HDS types.

Phosphating of HDS and solubility assessment

The two types of HDS were treated with solutions spanning a wide phosphate concentration range: 0, 50, 100, 250, 500, 1000, 2000, 4000 and 6000 mg P l⁻¹. In each case, one gram of material was reacted with 25 ml of solution prepared from KH_2PO_4 . Equilibration was allowed to occur for two days at constant temperature (25 °C). During this time the stoppered tubes were shaken end to end at 180 oscillations per minute for 2 hours per day. After 48 hours the samples were centrifuged at 300 revolutions per minute for 10 minutes and filtered through Whatman No. 42 filter paper and 0.45 µm EconoClear membrane filters. Standard P solutions; 0, 5, 10, 50, 100 lnd 250 mg l⁻¹ were prepared and read through ICP-OES before the determination of P in the filtered solutions. This data as used separately to asses P sorption of HDS. The phosphated material was then oven-dried at 30 °C until attained a constant mass. To assess metal solubility before and after phosphating the Toxicity Characteristic Leaching Procedure (TCLP 1311): from the Solid Waste Manual 846 (SW-846) by the US Environmental Protection Agency (EPA) (1992) was used.

Determination of total elemental content before and after phosphating

Microwave assisted acid digestion, EPA method 3052 (EPA SW-846 2014) was followed. After digestion, elements were determined by Inductively Coupled Plasma Optical Emission Spectrometry (ICP-OES). X-ray Fluorescence (XRF) which uses ARL 9400XP+ Wavelength dispersive XRF Spectrometer was also used to determine total elemental content following the procedure described by Loubser and Verryn (2008).

Redox stability assessments

Susceptibility to reductive dissolution was investigated by using reductants to extract Fe, Mn, Al, Pb and Ni. As discussed by Courchesne and Turmel (2007), dithionite-citrate, was used to determine amorphous inorganic forms of Al, Fe and Mn. Similarly, acid ammonium oxalate and acid hydroxylamine were also used to estimate the same elements and forms as with dithionite-citrate, but to a lesser extent crystalline form.

Determination of Total Electron Demand (TED) and Manganese Electron Demand (MED) before and after phosphating

Total Electron Demand and MED were determined by following procedures described by Bartlett and James (1995).

Results and discussion

Mineralogy and basic chemical properties of non-phosphate HDS

The pH of Hi-Sol Mn HDS was 5.5 with an alkalinity of 13 while Lo-Sol Mn HDS had a pH of 8.2 with an alkalinity of 16 as CaCO_3 (Table 1). The acidic pH in Hi-Sol Mn HDS was due to the use of CaCO_3 alone which has slow reaction kinetics and there was possibility of particles being coated by Fe precipitates making it unable to achieve a higher pH (Lottermoser 2007). While the alkaline pH 8.2 of Lo-Sol Mn HDS resulted from using the combination of $\text{CaCO}_3/\text{Ca(OH)}_2$. Limestone effectively increases the solution pH to 4.5 and from this point Ca(OH)_2 is used to increase the pH to desired levels precipitating most metals (Wilmoth 1977 and Lottermoser 2007).



Table 1: Mineralogy and basic chemical properties of HDS

Parameter	Hi-Sol Mn HDS	Lo-Sol Mn HDS	Units
Process	Limestone	Lime/Limestone	
pH _{H2O}	5.5	8.2	
Total Alkalinity as CaCO ₃	13	16	mg kg ⁻¹
Mineralogy ^a	Gypsum (72 – 77 %), 22 % ferric hydroxide (Fe(OH) ₃), 4 % ankerite (Ca(Fe,Mg,Mn)(CO ₃) ₂)	Gypsum (> 95 %)	
As	0.1	0.5	mg kg ⁻¹
B	379.7	329	mg kg ⁻¹
Ba	465	118	mg kg ⁻¹
Cd	< 1	<0.1	mg kg ⁻¹
Ca	182961	235849	mg kg ⁻¹
Co	73	149	mg kg ⁻¹
Cu	80	15.5	mg kg ⁻¹
Cr	68	134	mg kg ⁻¹
Fe	146319	114570	mg kg ⁻¹
Hg	N.A.	<0.1	mg kg ⁻¹
Mg	6513	46015	mg kg ⁻¹
Mn	7590	7847	mg kg ⁻¹
Mo	3.3	2.8	mg kg ⁻¹
Ni	108	167	mg kg ⁻¹
Pb	<1	143	mg kg ⁻¹
Sb	N.A.	N.A.	mg kg ⁻¹
Se	25	21	mg kg ⁻¹
V	56	4	mg kg ⁻¹
Zn	285	611	mg kg ⁻¹

^a Determined by XRD, ^b Determined by XRF

Hi-Sol Mn HDS was approximately 72 – 77 % crystalline phase of CaSO₄·2H₂O (Table 1). According to Zinck et al. (1997), Aubé and Lee (2015) the only mineral often identified in fresh HDS are CaSO₄·2H₂O and CaCO₃. Gypsum precipitation in sludge was facilitated by high concentrations of Ca from the limestone and S from AMD. In addition XRD further showed 4 % of a carbonate mineral – ankerite (Ca(Fe,Mg,Mn)(CO₃)₂). Ankerite formation was facilitated by the lower pH (5.5) of HDS and the increased concentrations of Fe, Mg, Mn and Ca (Hendry et al. 2000 and Lollar et al. 2005). Amorphous Fe(OH)₃ formed 22 % of the non-phosphated Hi-Sol Mn HDS mineral composition. XRD technique showed > 95 % crystalline phase of CaSO₄·2H₂O as the only mineral that was dominating the non-phosphated Lo-Sol Mn HDS (Table 1).

Phosphate effect on the reduction of Hi-Sol Mn and Lo-Sol Mn HDS

The main environmental concern was the solubility of metals requiring chemical stabilization, especially Pb and Ni in HDS (Table 2). The solubility of these metals is controlled by pH and the addition of PO₄ at 4000 mg P l⁻¹ slightly reduced the pH by 0.6 down to 4.9 for the Hi-Sol Mn HDS. Phosphating effectively prevented the reduction of Hi-Sol Mn HDS which further reduced Ni solubility. Soluble Ni (2.9 mg l⁻¹) in the non-phosphated material was reduced by a maximum of 97.6 %. The reduction in soluble Ni substantially improved the environmental hazardous status of Hi-Sol Mn HDS. Solubilities of other metals including Pb were extremely low even before the addition of PO₄, that is, in the non-phosphated Hi-Sol Mn HDS. To further explain



Table 2: total and leachable concentrations of constituents for both HDS

Constituents	Hi-Sol Mn HDS						Lo-Sol Mn HDS					
	Non-phosphated		Phosphated at 50 mg P kg ⁻¹		Phosphated at 4000 mg P kg ⁻¹		Non-phosphated		Phosphated at 50 mg P kg ⁻¹		Phosphated at 4000 mg P kg ⁻¹	
	TC (mg kg ⁻¹)	TCLP (mg l ⁻¹)	TC (mg kg ⁻¹)	TCLP (mg l ⁻¹)	TC (mg kg ⁻¹)	TCLP (mg l ⁻¹)	TC (mg kg ⁻¹)	TCLP (mg l ⁻¹)	TC (mg kg ⁻¹)	TCLP (mg l ⁻¹)	TC (mg kg ⁻¹)	TCLP (mg l ⁻¹)
Fe	146319	<0.01	149158	1.9	142353	0.02	114570	<0.4	114940	0.14	94947	<0.01
Mn	7590	259	6016	4.8	5207	1.16	7847	<0.04	7772	2.9	6867	1.03
Ni	108	2.9	107.5	0.26	104.7	0.07	167.3	<0.04	159.5	0.26	128.6	<0.01
Pb	<1	<0.1	<1	<0.1	<1	<0.1	143	<0.1	<0.1	<0.1	<0.1	<0.1

Note: TC = Total Concentration; TCLP = Toxicity Characteristic Leaching Procedure, N.A. = Not analysed, N.R. = Not Reported

elemental speciation and mineral phases formed, Phreeqc Interactive version 3.3.12-12704 was used.

Phosphate stabilized Ni in Hi-Sol HDS by forming $\text{Ni}_3(\text{PO}_4)_2(\text{s})$ phase but was under saturated. No phases were formed between PO_4 and Pb. Most of the PO_4 was precipitated with respect to hydroxyapatite ($\text{Ca}_5(\text{PO}_4)_3\text{OH}$) with a Saturation Index (SI) of 6.8. Other mineral phases that were saturated but not involving PO_4 included; Anhydrite (CaSO_4), Gypsum ($\text{CaSO}_4 \cdot 2\text{H}_2\text{O}$) and Alunite ($\text{KAl}_3(\text{SO}_4)_2(\text{OH})_6$) with SI that ranged from 0.1 to 1.0. Therefore, the added PO_4 stabilized mostly Ca. The substantial reduction in the solubility of Ni, Pb and other metals of concern was mainly a contribution of adsorption on the reactive surfaces of saturated phases (Eighmy et al. 1997, Crannell et al. 2000 and Karna et al. 2017) since there were no substitutions identified.

Using a combination of CaCO_3 and $\text{Ca}(\text{OH})_2$ to treat AMD generated Lo-Sol Mn HDS that showed minimal solubility of metals making it a less risk to the environment. Phosphating this material with PO_4 , substantially decreased the solubility of metals reducing further its environmental risk. The addition of PO_4 at 4000 mg P l⁻¹ slightly reduced the pH by 0.4 down to 7.9. There was a complete immobilization of both Ni and Pb. The added PO_4 improved the chemical stability of Ni by forming $\text{Ni}_3(\text{PO}_4)_2(\text{s})$ phase although it was undersaturated. Mostly the solution was saturated with respect to $\text{Ca}_5(\text{PO}_4)_3\text{OH}$ that had an SI of 19. Other mineral phases that precipitated but excluded PO_4 were $\text{Al}(\text{OH})_3$, CaSO_4 , Boehmite ($\gamma\text{-AlO}(\text{OH})$), CoSe, Dia-

spore ($\alpha\text{-AlO}(\text{OH})$), Gibbsite ($\text{Al}(\text{OH})_3$) and $\text{CaSO}_4 \cdot 2\text{H}_2\text{O}$ with SI ranging from 0.02 to 1.0. There were no phases that were formed between PO_4 and Pb. There is possibility that this element, some of the Ni and other metals were adsorbed on the surfaces of saturated phases (Eighmy et al. 1997, Crannell et al. 2000 and Karna et al. 2017)

In summary, the solubility of metals especially Ni in Hi-Sol Mn and Pb in Lo-Sol Mn HDS were chemically stabilized successfully by the addition of PO_4 as demonstrated in Table 2. Therefore, both materials can be of low risk to the environment after phosphating. The sequestration of plant nutrients Mn, Fe, P, Ca, Mg and K could be a disadvantage in the short term but can be slowly released through dissolution of e.g. $\text{CaSO}_4 \cdot 2\text{H}_2\text{O}$ and $\text{Ca}(\text{Fe,Mg,Mn})(\text{CO}_3)_2$ for the benefit of plants.

Does phosphating HDS make it more stable against reduction?

Manganese electron demand directly determined the oxidation capacity of Mn oxides in HDS, whereas TED estimated the oxidation capacity of both Mn and Fe (Van Bodegom et al. 2002 and Sparks 1993). Amorphous ferrihydrite remained as the predominant Fe source in HDS. As determined by TED, the addition of PO_4 from 50 to 6000 mg P l⁻¹ significantly decreased reducible Fe in Hi-Sol Mn HDS from 28 to 0.9 mmol e⁻ (Fig. 1 a). This showed that PO_4 prevented the reduction of HDS hence reduced the concentration of Fe^{2+} determined by TED. The added PO_4 was adsorbed and formed sparingly soluble complexes with ferrihydrite preventing the



reduction of HDS (Cornell and Schwertmann 2003). The addition of PO_4 in Lo-Sol Mn HDS from 50 to 6000 mg P l^{-1} facilitated the reduction of this material significantly increasing Fe release from 2.6 to 7 mmol e^- . This indicated that phosphating increased TED. A significant increase in the MED from 0.2 to 1.7 mmol e^- in Lo-Sol Mn HDS was achieved by increasing the application rate of PO_4 from 50 to 6000 mg P l^{-1} as determined by MED (Fig. 1 a). But in Hi-Sol Mn HDS adding any rate of PO_4 could not increase the oxidation capacity of Mn. The reason was that Mn was already oxidised to Mn(III) or Mn(IV). The reason why TED increased is because it seemed that phosphate actually facilitated the oxidation of Mn(II).

Reductive promoted dissolution of HDS before and after phosphating

Generally, the addition of PO_4 at 50 and 6000 mg P l^{-1} to both materials significantly reduced the extractability of Fe, Mn and Al (Fig. 1 b) for all extractants. Fe was the most extracted by all extractants in all sludges (before and after phosphating) followed by Al, Mn, Ni and Pb being the least. Ni extracted by all extractants in both HDS before and after treatment was less than 0.014 %, while Pb was 0 %. Mn was extracted mostly from Lo-Sol Mn HDS by dithionite and hydroxylamine. The high concentration of Mn extracted from Lo-Sol Mn HDS was due to the reduction conditions and the existence of PZC of Mn oxides at $\text{pH} > 7$ that prohibited complexation with

PO_4 (Graham et al. 1988) since the material had a pH of 8.2. Acid ammonium oxalate was not only able to extract most of this Mn oxide from the 6000 mg P l^{-1} phosphated Lo-Sol Mn HDS. The reason was that acid ammonium oxalate enhanced the reduction and dissolution of the highly phosphated HDS releasing both Fe and Mn oxides. Hi-Sol Mn HDS (both phosphated and non-phosphated) had a pH of 5.5, which falls within a pH range 2 – 7 where Mn had a high affinity for PO_4 hence the extracted quantities by all extractants were lower (Graham et al. 1988). Fe and Al oxides were significantly extracted mostly from Hi-Sol Mn HDS (both phosphated and non-phosphated) by all extractants.

Conclusions and recommendations

Phosphating Hi-Sol Mn and Lo-Sol Mn HDS at 4000 mg P l^{-1} substantially reduced the solubility of Mn, Ni, Pb and other metals through adsorption on reactive surfaces of amorphous $\text{Fe}(\text{OH})_3$ and precipitation into mineral phases. After PO_4 addition, Fe proved to be the most soluble when both HDS were subjected to different reducing extractants, followed by Al, Mn, Ni and Pb being the least. Adding PO_4 at 50 and 6000 mg P l^{-1} reduced TED in Hi-Sol Mn HDS, but increased it in Lo-Sol Mn HDS. The addition of PO_4 did not change MED for Hi-Sol Mn HDS but increased that of Lo-Sol Mn HDS phosphate at 6000 mg P l^{-1} . Phosphating reduced metal solubility and improved both materials towards better plant nutrient sources.

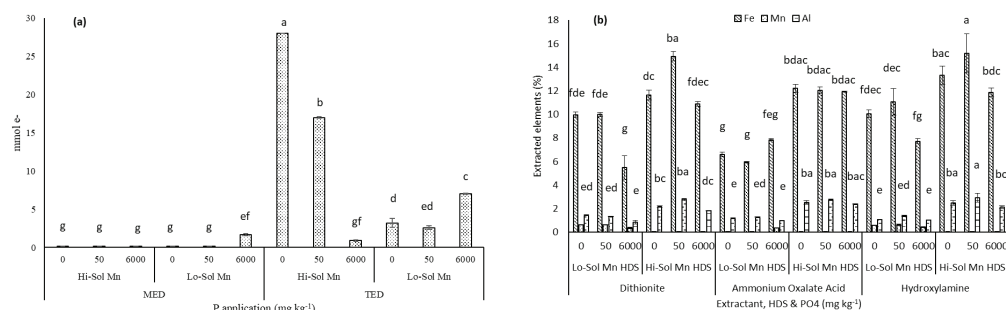


Fig. 1: a) Mn electron demand and Total electron demand for HDS, b) Fe, Mn and Al extraction by Dithionite, Acid ammonium oxalate and Hydroxylamine in HDS



Acknowledgements

The Authors would like to acknowledge the Water Research Commission of South Africa for supporting the study through financial assistance.

References

- Aubé B, Zinck JM (1999) Comparison of AMD treatment processes and their impact on sludge characteristics. Noranda Inco. Technology Centre, 240 Hymus, Blvd Pointe-Claire, Quebec, H9R 1 G5, Canada. Proceedings; 1
- Barthel J, Edwards S. (2004) Chemical stabilization of heavy metals. *Met. Treat. Technol.* MT2 3, 151e162
- Bartlett RJ, James BR 1995. System for categorizing soil redox status by chemical field testing. *Geoderma*, 68: 211-218.
- Cornell RM, Schwertmann U (2003) Formation In: *The Iron Oxides, Structure, Properties, Reactions, Occurrences and Uses*. Second Completely Revised and Extended Addition. Wiley-VCH Verlag GmbH & Co KGaA, Weinheim. pp 345-407
- Courchesne F, Turmel MC (2007) Extractable Al, Fe, Mn, Si, In: Carter RM and Gregory EG (Ed). *Soil sampling and methods of analysis*, 2nd Ed. Canadian Society of Soil Science. Florida: CRC Press, pp 309-311
- Crannell BS, Eighmy TT, Krzanowski JE, Eusden Jr. JD., Shaw EL, Francis (2000) Heavy metal stabilization in municipal solid waste combustion bottom ash using soluble phosphate *Waste Management* 20: 135-148.
- Eighmy TT, Crannell BS, Butler LG, Cartledge FK, Emery EF, Oblas D, Krzanowski JE, Eusden, Jr. JD, Shaw EL, Francis CA (1997) Heavy Metal Stabilization in Municipal Solid Waste Combustion Dry Scrubber Residue Using Soluble Phosphate. *Environ. Sci. Technol.* 31:3330-3338
- Graham RD, Hannam RJ, Uren NC (1988) Inorganic Reactions of Manganese in Soils, In: *Manganese in Soils and Plants*. Kluwer Academic Publishers, Netherlands. pp 37 - 50
- Harris DL, Lottermoser BG (2006) Evaluation of phosphate fertilizers for ameliorating acid mine waste. *Applied Geochemistry* 21:1216–1225. doi:10.1016/j.apgeochem.2006.03.009
- Johnson DB, Hallberg KB (2005) Acid mine drainage remediation options: a review. *Science of the Total Environment* 338:3-14
- Kalin M, Fyson A, Wheeler WN (2006). The chemistry of conventional and alternative treatment systems for the neutralization of acid mine drainage. *Science of the Total Environment* 366:395–408
- Karna RR, Luxton T, Bronstein KE, Redmon JH, Scheckel KG (2017) State of the science review: Potential for beneficial use of waste by-products for in situ remediation of metal-contaminated soil and sediment, *Critical Reviews in Environmental Science and Technology*, 47:2, 65-129, DOI: 10.1080/10643389.2016.1275417
- Kumpiene J, Lagerkvist A, Maurice C (2007) Stabilization of As, Cr, Cu, Pb and Zn in soil using amendments – A review. *Waste Management* 28:215–225
- Loubser G, Verryn S (2008) Combining XRF and XRD analyses and sample preparation to solve mineralogical problems. *South African Journal of Geology*.111:229-238
- Lottermoser BG (2007) Mine water, In: *Mine Wastes, Characterization, treatment, environmental impacts*, 2nd Ed. Springer-Verlag Berlin Heidelberg, pp 139-140
- Loubser G, Verryn S (2008) Combining XRF and XRD analyses and sample preparation to solve mineralogical problems. *South African Journal of Geology*.111:229-238
- Maree JP, Strydom WF, Adlem CJL, De Beer M, Van Tonder GJ, Van Dijk BJ (2004) Neutralization of Acid Mine Water and Sludge Disposal. Division of Water, Environment and Forestry Technology CSIR. WRC Report No 1057/1/04
- Method 3051A, Revision V (2014) Final Update II to the Third Edition of the Test Methods for Evaluating Solid Waste, Physical/Chemical Methods, EPA publication SW-846.
- Thomas GW (1996) Soil pH and Soil Acidity. In: *Methods of Soil Analysis, Part 3 – Chemical methods*. SSSA Book Series No. 5, pp 475
- United States Environmental Protection Agency (EPA) (1992) SW-846 Test Method 1311: Toxicity Characteristic Leaching Procedure (TCLP). <https://www.epa.gov/hw-sw846/sw-846-test-method-1311-toxicity-characteristic-leaching-procedure>. Accessed 9 March 2017
- Van Bodegom PM, Van Reeve J, Van Der Gon HACD (2003) Prediction of reducible soil iron content from iron extraction data. *Biogeochemistry* 64:231-245.



- Wilmoth RC (1977) Limestone and lime neutralization of ferrous iron acid mine drainage. Environmental Protection Technology Series. EPA-600/2-77-101
- Zinck JM (2006) Disposal, reprocessing and reuse options for acidic drainage treatment sludge. American Society of Mining and Reclamation (ASMR), 3134 Montavesta Road, Lexington, KY 40502
- Zinck JM, Wilson LJ, Chen TT, Griffith W, Mikhail S, Turcotte AM (1997) Characterization and Stability of Acid Mine Drainage Treatment Sludges. Mining and Mineral Sciences Laboratories Report MMSL 96-079 (CR). MEND Project 3.42.2a, Job No. 51144, Canada. <http://mend-nedem.org/wp-content/uploads/2013/01/3.42.2a.pdf>. Accessed 28 April 2016





Adsorption and Desorption of Metals onto Reusable Adsorbent

Esther Marina Takaluoma^{1,2}, Tuomo Pikkarainen¹, Kimmo Kempainen²

¹*Aquaminerals Finland Oy, Kajaanintie 29 A, 88300 Paltamo, Finland, esther.takaluoma@aquaminerals.fi*

²*Kajaanin Ammattikorkeakoulu, Ketunpolku 2, Mining engineering, 8700 Kajaani, Finland*

Abstract

This paper discusses the adsorption of metals and metalloids on modified natural material. In case of an economically valuable contaminant, such as copper or cobalt, recovering the metal provides value to the water treatment. For copper, a method is demonstrated in which the adsorbent can be recovered by the formation of a complex, leading to the regeneration of the adsorbent and recovery of the metal. After this, the metal can be hydrometallurgically recovered. The adsorbent can be used over twenty times without loss of efficiency.

Metal oxide adsorbents are an economic and easy way to lower the metal content in mine effluent. Utilizing reusable adsorbents, in case of copper, the value of the recovered metal offsets the cost of water treatment. This approach presents a win/win solution for the mining company and environment.

Keywords: adsorbent, contaminant removal, copper recovery, adsorbent recycling

Introduction

Even when operating within the concentration limits of environmental permits, small amounts of contaminants may be released into the environment or are discharged into the tailings pond or the surrounding aquifer. Large streams of mine effluents or process water result in discharging hundreds of kilograms of contaminants into the receiving water streams or ground water. For example, a 5 mg/L copper solution with a discharge of 500 m³/h releases annually 21 900 kg of copper. With a copper price of 6,822 USD/t, the lost revenues might be up to 149,411 USD (Infomine 2018). Currently, the rising price of copper and the decreasing ore grades make the recovery of metals from secondary streams economically feasible.

The adverse effects of copper for aquatic life is dominated by the bioavailability of the copper complex (Langmuir 1997). Potentially negative effects of copper in soil are currently under scrutiny of environmental agencies, because copper is toxic for bacteria and therefore reduces the microbial activity in soil (Marques et al. 2018). This in turn leads to a poor nutrient status in the soil and to reduced yields on farmland (Adrees et al. 2015). Furthermore, copper in high concentrations is toxic to plants.

Reducing the copper emissions, therefore, has an immediate positive effect on the social acceptance of the mine by surrounding farmers. In addition, the potential revenue of copper sales assists to offset the water treatment costs.

Recovery of copper from secondary sources or and from tailings is of ecological and economical interest and has sparked research interest in this area, for which the term “precision mining” has been coined (Crane 2018). Zero valent iron on inert support has been used to selectively obtain copper from waste sources. A variety of adsorbents has been tested for metal and especially copper removal, ranging from nanotubes (Ihsanullah et al. 2016), natural and modified minerals (Uddin 2017), immobilized organic compounds (Moscatello et al. 2018) to biobased waste products, such as chitin (Anastopoulos et al. 2017). The high costs of many possible adsorbents prevent the use in an industrial application.

Among the cheaper options for treatment of mine or waste water is a natural modified mineral adsorbent commercialized as Aquaminerals PalPower M10. According to the manufacturer's specification, this magnesium and iron oxides based adsorbent can be used to remove Ni, Co, Pb, Cr, Cd, Zn, Al, Cu, Fe,



Mn, P, U and As contaminants from water. In this paper, we present the use of Aquaminerals Palpower M10 to remove copper from water and its subsequent recovery as CuS after hydrometallurgical treatment.

Methods

Metal and metalloid analysis was performed by an accredited laboratory (Ahma Ympäristö Oy, Oulu) using ICP-OES. Additionally, copper was analysed in house by UV-VIS spectrometry on a Specord 50 plus by AnalytikJena at 600 nm wavelength. Solid-state characterizations have been performed on a PANalytical XPert Pro diffractometer with a Copper X-ray anode and X'Celerator detector. All resulting data was handled with the Highscore plus software package. XRF spectroscopy was conducted with a PANalytical Minipal 4 RoHS WEEE utilizing the OMNIAN function.

Laboratory scale tests were performed as batch tests in 250 mL PTEE bottles, which were agitated in an end-over-end tumbler at 20 rpm (rotations per minute). Desorption tests were performed as batch tests in an end-over-end tumbler. Filtering of occurring sludge was performed by vacuum suction, and a glass fibre filter was used for separating the copper amine complex.

Materials

A commercially available adsorbent (Aquaminerals PalPower M10) was obtained and used as is. Synthetic water solutions were prepared by dissolution of the respective salts in deionized water. Copper(II)chloride dihydrate ($\text{CuCl}_2 \cdot 2\text{H}_2\text{O}$, technical, VWR chemicals), Manganese sulfate monohydrate ($\text{MnSO}_4 \cdot \text{H}_2\text{O}$, p.A., Merck), Sodium aluminate anhydrous (NaAlO_2 , technical, Sigma

Aldrich), Ammonia (25% aqueous solution, technical, VWR chemicals) and sodium sulfate anhydrous (Na_2SO_4 , >99 %, VWR chemicals) were used as received. Iron(III)sulfate ($\text{Fe}_2(\text{SO}_4)_3$, technical, Kemira) granules were grinded in a ring mill to facilitate dissolution in water.

Results and Discussion

Adsorption experiments

Copper is conveniently adsorbed on to the PalPower M10 modified mineral adsorbent. According to the XRF characterization (Table 2), the adsorbent consists of mainly MgO (58 %), SiO_2 (22 %), and Fe_2O_3 (14 %). The required contact time of M10 depends on the initial copper concentration and adsorbent dosage, between 5 minutes and 2 hours.

Two spiked copper solutions with a concentration of 100 mg/L and 5 mg/L were prepared to imitate a range of concentrations in common mining effluents. The M10 adsorbent was added as a dosage of 2 g/L and 0.3 g/L and stirred for 30 min (Table 1). After 30 min, the 100 mg/L copper solution shows a reduction of 67% at a dosage of 2 g/L. Higher dosages of the adsorbent resulted in lower copper concentrations in the solution. For a 5 mg/L copper solution, dosage was varied from 1 to 5 g/L, a 2 g/L dosage results in quantitative removal of copper of initial concentration of 5 mg/L. PalPower M10 has an adsorption capacity for copper of 33 mg/g (33 kg/t), and therefore M10 ranks among the highest copper (II) adsorbing materials known (Ahmed 2016).

Five samples of 5 mg/L solution were prepared and analyzed to alleviate the larger margins of error for small concentrations. All five samples resulted in a reduction of 99 % copper, leaving the initial 5 mg/L copper so-

Table 1 Results of ICP-OES results of the initial solution and after adsorption to M10.

#	initial Cu mg/L	Cu after, mg/L	removal rate, %	adsorbent dose, mg/L
1	99.5	32.9	66.9	2000
2	4.85	0.022	99.55	300
3	4.96	0.010	99.80	300
4	4.87	0.033	99.32	300
5	4.83	0.032	99.34	300
6	4.65	0.015	99.68	300



Table 2 Fresh adsorbent, used adsorbent and extraction test results.

	M10 new	Cu adsorbed	NH ₃ 12.5%	NH ₃ 6.25%	NH ₃ 3%	NH ₃ 1.5%
MgO	58.81	47.76	51.97	52.78	51.85	46.65
SiO ₂	21.70	15.01	16.00	16.44	16.20	14.48
SO ₃	1.28	0.96	0.64	0.68	0.73	0.77
Cl	--	1.42	0.06	0.12	0.16	0.18
K ₂ O	0.12	0.05	0.06	0.06	0.05	0.06
CaO	1.11	0.90	0.96	0.93	0.88	0.88
Cr	0.25	0.25	0.25	0.26	0.26	0.25
Mn	0.15	0.15	0.16	0.16	0.16	0.16
Fe ₂ O ₃	13.58	14.36	15.13	15.00	14.93	15.03
Ni	0.16	0.19	0.18	0.19	0.19	0.20
Cu	--	5.73	1.46	1.94	2.73	3.81
Ag	0.17	0.16	0.17	0.17	0.16	0.17
Eu	0.06	0.13	0.12	0.12	0.12	0.11

Table 3 ICP-OES results of leachate of some eluents from copper loaded M10 (20.00 g adsorbent, 5.00 g/LCu).

	Leached with H ₂ SO ₄	Leached with NH ₃ (aq)	Leached with H ₂ O
Cu mg/L	4690	3390	0.58

Table 4 Copper concentrations of leachate from 20.00 M10 loaded with 5.00 g/L Cu at different ammonia concentrations.

	NH ₃ (aq) 12.5 %	NH ₃ (aq) 6.25 %	NH ₃ (aq) 3 %	NH ₃ (aq) 1.5%
Cu mg/L	3520	3080	2480	1790

lution to a concentration under 0.035 mg/L copper (WHO guideline is 2 mg/L; Table 1).

The XRF results of adsorbed copper on adsorbent (1 g/L onto 20 g) in comparison to fresh PalPower M10 show that the adsorption of 1.00 g/L Cu to 20 g/L adsorbent is quantitative (Table 2). The remaining copper concentration in water is below the detection limit of the ICP-OES, and the behaviour is reflected in the 5.7 % Cu adsorbed according to XRF (Table 2).

Copper recovery

The adsorption of copper to the adsorbent PalPower M10 is a combination of surface precipitation from local lowering of the pH and adsorption onto the solid material. Copper from slags and spent adsorbents can be recovered by acid washing. 1 M HCl does not appear to be extracting copper in substantial amounts. Treatment of M10 with 2 M H₂SO₄

releases the copper, but dissolves the adsorbent M10, which can be observed by the mass loss of about 75 % and the loss of MgO in XRF. A comparison of the leaching of 2 M H₂SO₄, 12.5 % NH₃ (aq.) and H₂O gave the extraction of 4690 mg/L, 3390 mg/L, and 0.58 mg/L (Table 3; 200 mL eluent used).

Leaching of M10 with 12.5 % NH₃ (aq) mobilizes copper in form of the deep blue tetraamminecopper(II)-complex [Cu(NH₃)₄]²⁺ in reasonable quantities of 3.4 g/L. In the next step the concentration of ammonia solution required was investigated.

An aqueous solution of ammonia in concentrations from 1.5 % to 12.5 % was used to extract the copper as an tetraamminecopper(II)-complex. The extracted adsorbent was characterized by XRF (Table 2) and the leachate analysed by ICP-OES (Table 4).



Table 5: Loop of adsorbent used, copper extracted and recovered CuS. Experimental setup: M10: 20.00 g; Cu: 1.00 g.

used M10, g	CuS prec., g	recovered M10, g	Yield of Cu recovered, %	comments
20.6888	1.1829	19.0628	71.9	
19.6445	1.1105	17.7348	67.5	
20.6886	0.862	18.8410	52.4	
20.7486	0.388	19.3977	23.6	
20.4808	2.0802	17.0370	126.4	fresh ammonia
20.4972	1.2011	18.8475	73.0	
20.7520	1.3116	19.4793	79.7	25 % ammonia
overall	8.1363		494.3	70,6 % average yield

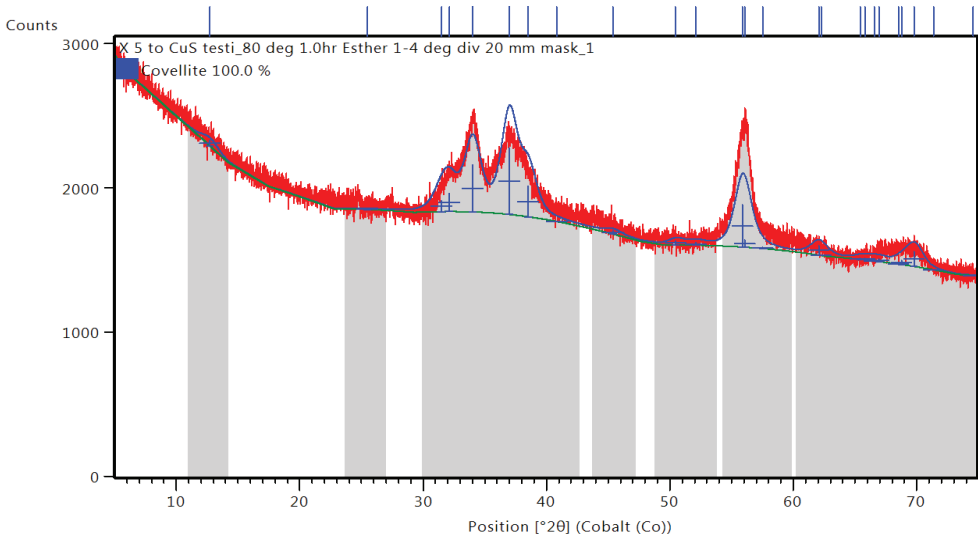


Figure 1 X-ray diffractogram of recovered CuS.

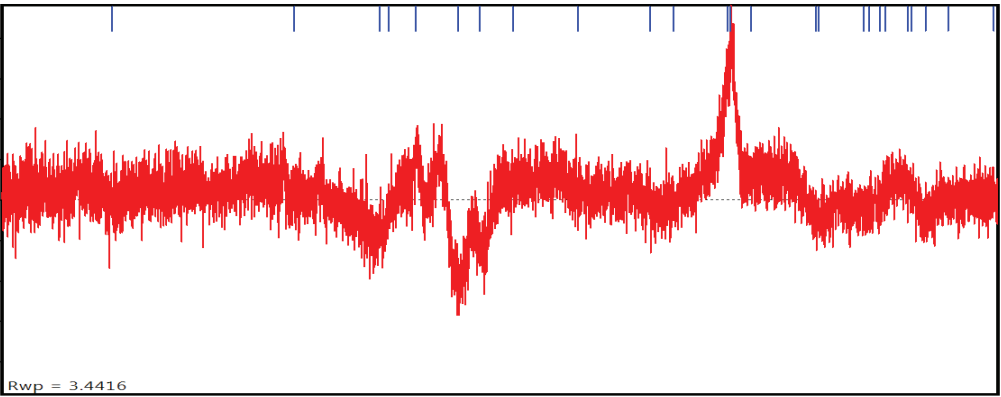


Figure 2 Rietveld refinement of the recovered CuS.



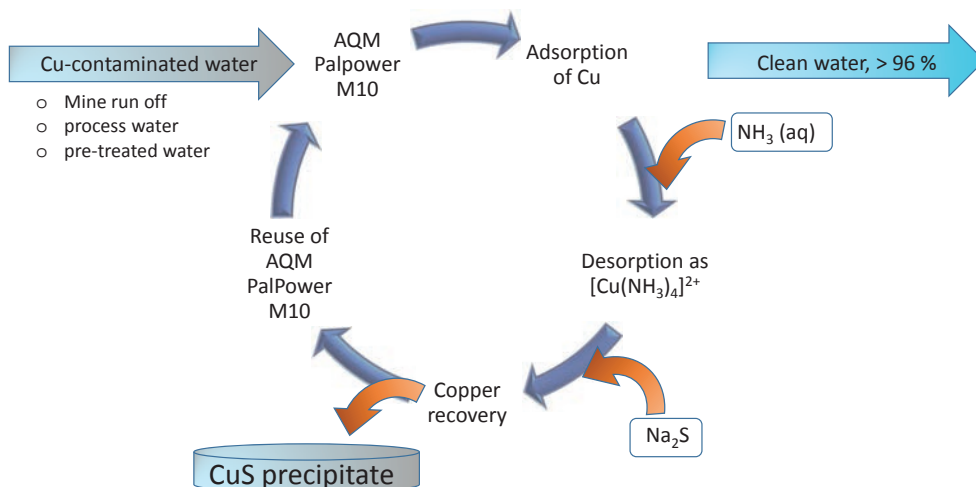


Figure 3 Loop of copper recovery from the adsorbent.

As can be seen, the remaining copper percentage in the extracted material correlates with the decreased extraction power of lower amine concentration. While 25 % ammonia solution has shown higher yields in copper removal, it is technically impractical to be used in large scale operations (1.3116 g, Table 5).

A loop with 20 g M10, adsorbing 1 g/L Cu from 1 L of water and subsequent recovery by ammonia and precipitation as CuS was run for 7 times (Table 3, Figure 4). About 1/20 of the M10 adsorbent was lost during handling and possible partial dissolution in water, and ammonia and was replaced by fresh M10 until 20 g initial weight was achieved. The resulting CuS was characterized by XRD (Figure 2 and Figure 3). Copper sulfide was the only phase, for which Rietveld refinement resulted in a good wRp of 3.4 %. The 12.5 % ammonia solution was recycled. A decrease in copper recovery is noticed after leaching, with simultaneous increase in copper remaining in the leached adsorbent (XRF). Using fresh ammonia leaches earlier accumulated copper. Cursive data in Table 3 indicates the use of 25 % ammonia. As expected, the percent of leached copper (80 %) is higher than for the 12.5 % ammonia solution. However, the corrosive properties and volatile characteristics of 25 % ammonia solution may make the use for industrial applications difficult. It is noteworthy, that in all cases, XRF of leached PalPower M10 showed the presence of fur-

ther copper. As this did not inhibit the adsorption of further copper in the next cycle, the saturated point of the adsorbent was not reached yet, though not all Cu was recovered by leaching, no copper was lost in the process. Occasional higher concentrations of leachate could dissolve the adsorbed copper. Over time, an equilibrium of adsorbed copper and leached copper will build up.

Finally, the selectivity of the loop was verified by artificial mine water containing 1 g Cu²⁺ and 5 g Fe³⁺ as well as 100 mg Al³⁺, 100 mg Mn²⁺ and 0.1 M Na₂SO₄. The copper and iron were adsorbed by 20.00 g M10 adsorbent. Pure CuS (XRD) was recovered with a 63.4 % yield.

Currently piloting of the copper recovery is in planning at a suitable copper containing process water.

Conclusions

The use of PalPower M10 as adsorbent for copper and subsequent desorption via the coppertetraamine complex and copper sulfide precipitation has been demonstrated. Due to the easiness of upscale, this procedure shows economic interest for application in mine effluent or mine water. Treatment of water even with low concentrations of copper may result into better social acceptance of the mine, due to decreased contamination of soil, while revenue of recovered copper may be used to off-set parts of water treatment costs.



Acknowledgements

The authors thank Kajaani University of Applied Science for laboratory space and Mrs Marjukka Hyyriäinen and Mr Kai Tiihonen for help with laboratory work.

References

- Adrees M, Shafaqat A, Rizwan M, Ibrahim M, Abbas F, Farid M, Zia-ur-Rehman M, Irshad MK, Bharwana SA (2015) The effect of excess copper on growth and physiology of important food crops: a review, *Environmental Science and Pollution Research*, 22: 8148–8162. doi:10.1007/s11356-015-4496-5.
- Ahmed M, Ahmaruzzaman M (2016): A review on potential usage of industrial waste materials for binding heavy metal ions from aqueous solutions, *Journal of Water Process Engineering*, 10: 39–47. doi:10.1016/j.jwpe.2016.01.014
- Anastopoulos I, Bhatnagar A, Bikiaris DN, Kyzas GZ (2017): Chitin Adsorbents for Toxic Metals: A Review, *International Journal of Molecular Sciences*, 18: 114–125. doi:10.3390/ijms18010114
- Crane RA, Sapsford DJ, (2018) Towards “Precision Mining” of wastewater: Selective recovery of Cu from acid mine drainage onto diatomite supported nanoscale zerovalent iron particles, *Chemosphere*, 202: 339–348. And articles cited herein. doi:10.1016/j.chemosphere.2018.03.042
- Ihsanullah AA, Al-Amer AM, Laoui T, Al-Marri MJ, Nasser MS, Khraisheh M, Atieh MA (2016): Heavy metal removal from aqueous solution by advanced carbon nanotubes: Critical review of adsorption applications, *Separation and Purification Technology*, 157: 141–161. doi: 10.1016/j.seppur.2015.11.039
- Infomine (2018) Copper Metal Price: <http://www.infomine.com/investment/metal-prices/copper> Accessed 17.5.2018.
- Langmuir, D. (1997): *Aqueous Environmental Geochemistry*. – 602 p., Upper Sadle River (Prentice Hall).
- Moscatelloa N, Swayambhua G, Jones CH, Xu J, Dai N, Pfeifer BA (2018): Continuous removal of copper, magnesium, and nickel from industrial wastewater utilizing the natural product yersiniabactin immobilized within a packed-bed column, *Chemical Engineering Journal*, 343: 173–179. doi:10.1016/j.cej.2018.02.093
- Uddin M (2017): A review on the adsorption of heavy metals by clay minerals, with special focus on the past decade, *Chemical Engineering Journals*, 308:438–462. doi:10.1016/j.cej.2016.09.029





Water reuse in the mining industry – a resource, financial and socio-economic imperative ©

J.J. van der Walt, H.A. van der Merwe

PO Box 29, The Innovation Hub, Pretoria, 0087
mias.vanderwalt@bigengroup.com, hayley.vandermerwe@bigengroup.com

Abstract

In the mining industry water was historically seen as one of many services and not a lot of focus was given to ensure its reliable and sustainable use. Not only is the efficient use of water a commercial and environmental imperative, but also of strategic importance. The cost of water in the larger scheme of mining cost is relatively small, but if the water supply is not available or not reliable the cost of mining suddenly increases as a result of production inefficiencies. Water security on a mine is therefore of cardinal importance and the case study presented will demonstrate how water security was improved significantly through a number of logical steps.

As part of developing a sustainable solution it was necessary to develop an integrated water balance for all water circuits on the mine. After analysing various water demand centres, water circuits, water volumes and water quality requirements for each type of water, for the current and future water footprint, water inefficiencies and potential water reuse interventions were identified.

A central component of the reuse interventions was a water reuse treatment plant to treat the eutrophic, mildly acidic and brackish water from the return water dam. As a result of various unknowns in terms of the water balance, water demands and plant size, scenarios were developed to test the sensitivity of certain assumptions on the water treatment works capital and operating cost.

The water reuse facility has been in operation for more than 12 months and based on actual water savings and operating cost savings the capital invested is projected to be paid back in less than 4 years. What is even more remarkable is the fact that the potable water use was reduced by 50%. Some of this water will be used for future production expansion and it could also be used for expanding potable water supply to neighbouring communities.

The case study demonstrates that with a proper understanding of mine water circuits many water reuse opportunities exist and that water reuse is not only an imperative from a water resource perspective, but also from a financial and socio-economic perspective. Ultimately the water security of the mine has improved significantly and with associated benefits in lower water input costs as well as lower probability of production stops due to water shortages.

Keywords: Dissolved air flotation, mine water, mine water balance, water treatment, water reuse.

Introduction

The Bafokeng Rasimone Platinum Mine (BRPM) is a Joint Venture between Anglo Platinum and Bafokeng Platinum Resources located on the Western Limb of the Bushveld Igneous Complex approximately 30 km from the town of Rustenburg in the North

West Province and immediately south of the Pilanesberg Complex. BRPM has been in operation since 1999 and comprises a number of shafts, a concentrator facility and a central logistics area.

The water supply to BRPM originates from the Magalies Water Vaalkop System.



Since the development of BRPM numerous new mining developments have taken place along the Pilanesburg which have increased the water demand from the area placing more strain on the already stressed water supply system.

The constrained water supply system severely impacted the mining industry in Rustenburg with limited supply to BRPM and increased potable water cost. In order to mitigate the risk of limited water supply BRPM decided to embark on a process to become less dependent on potable water as its primary water supply source and explore the feasibility of re-using local water sources.

In South Africa water reclamation is not only a legal requirement, but also provides strategic and in some cases even financial benefits. Since around 2004 BRPM has been in a water surplus scenario in the sense that not all water discharged to the return water dams could be reclaimed. Since the end of 2009 this situation was aggravated by the fact that the mine's filtration plant could not cope with the quality of the return water dam. BRPM was in the fortunate position that they have the facility to store surplus water in open cast pits, but this was only a temporary arrangement for a number of reasons. Firstly the water storage is not authorised in terms of DWS legislation, secondly there is evidence that the water in the pits could potentially pollute the ground water and finally the open cast pits can overflow and also pollute the surface water sources. It was therefore essential that the open cast pits be emptied and retained in that condition.

BRPM commissioned Bigen Africa to investigate the current problems experienced with the water reclamation circuit and present a solution.

Methodology

Water Balance

As part of developing a sustainable solution it was necessary to develop an integrated water balance for mining, minerals processing, the tailings return water facility and the sewage treatment plant. A number of water demand zones were identified and the inflow and outflow streams from these demand zones were identified. The streams were categorised ac-

cording to the three different water quality supplies available:

- A potable water stream feeding offices and ablution facilities, reagent make up water, underground drinking water system and cooling water system
- A clear water stream feeding gland seal water system, washing and spraying systems
- A process water stream feeding crushing and milling processes and mining processes

In order to quantify the flow into and from each of the zones flow meters on each of the streams feeding into and from each zone were identified. A detailed analysis of the demand zones and meters revealed that an accurate water balance could not be set up for the entire demand zone as not all the flows were metered. In the case where a meter was installed the average consumption was calculated based on the historic consumption. In some cases inferences had to be made as a result of insufficient flow data.

Water Reclamation Potential

After analysing various water demand centres (Zones), water circuits, water volumes and water quality requirements for each type of water, for the current and future water footprint it was concluded that the current average water reclamation potential from local water sources was 3 900 m³/d. The current pipeline system could transfer a theoretical maximum of 9 800 m³/d. The reclamation was constrained as a result of the current WTW not being able to treat the return water dam water to a suitable quality.

The current return water dam reclamation potential is largely dependent on the amount of tailings deposited as well as the evaporation losses. As the tailings return flows were not measured two scenarios were considered, one in which the evaporation losses are linked to the wetted area and the average evaporation rate for the area and another for a much larger area with an average evaporation rate. In the case of a low SG tailings pumped to the tailings dams the current return water dam reclamation potential was estimated at between 8 500 m³/d and 9 700 m³/d for high and low evaporation rates.



Based on production data it appeared that more water entered the return water dam than predicted. Using an average tailings SG (produced over 11 consecutive months) of 1.6 a water reclamation potential of 6 229 m³/d was indicated by the water balance. However, of this 3 980 m³/d was used for the Ultraseps. If the water demand for gland service water of 2 100 m³/d is deducted from this, 149 m³/d is not recovered from the return water dam and will overflow into the open cast pits. The evaporation loss in the open cast pits will be more than 149 m³/d. In fact the evaporation is estimated at about 900 m³/d. It was, however, known that the open cast pits have been filling up since 2004. It was therefore evident that more than 900 m³/d was required in order to fill the open cast pits. The under-prediction of the return water dam reclamation potential was attributed to errors in the tailings SG measurements, over-prediction of the evaporation losses and under-prediction of the water recovered from underground sources. After making some informed corrections the water reclamation potential was estimated therefore closer to 7 500 m³/d.

The future reclamation potential would therefore more than double if the production capacity is increased as planned. In order to optimise the potable water use in the largest potable water use zone it was decided to focus the water reclamation efforts in the Concentrator area. Another practical reason for this decision was that the return water pipes already fed to the Concentrator area and will therefore require the least amount of modifications in order to utilise the existing return water pipeline and pumping station.

Concentrator water quality and quantity requirements

The current Concentrator water treatment system is unable to utilize the return water dam quality and a large portion of the clear water requirements were being supplemented from the potable water system. The various quality streams that could potentially be supplied from the reclamation plant included the reagent makeup water, gland service water, fire water, water for sprays, screens, milling and Ultraseps and drinking water.

Water Source Characterisation

The return water dam was identified as the largest source of process water for reclamation and required the characterisation of the water quality. Based on the water quality measurements, the return water dam water was classified as mildly acidic and brackish, while the salinity levels are primarily due to the high levels of Sulphates (600 mg/L), Chlorides (180 mg/L), Nitrates (147 mg/L), calcium (223 mg/L), magnesium (129 mg/L) and Sodium (204 mg/L). The Nitrate level was not only attributed to the treated wastewater, but to the nature of the ore processed as well as the explosives used underground. The nutrient load into the return water dam was more than sufficient for algae to proliferate and also support other fauna. Chlorophyll-a counts were in the order of 60 µg/L. As a result the water was highly coloured (48 Pt Co units) with a medium turbidity of about 6 NTU. (Dissolved organic carbon, chemical oxygen demand and high faecal coliform counts indicate that the return water dam is not fit for human consumption.) Metal levels were low with only Mn and Ni exceeding 0.04 mg/L. The silicon concentrations were quite high at 10 mg/L. Laboratory work confirmed that silicon could not be removed by means of coagulation and flocculation.

Water Reclamation Plant Conceptual Design

The most practical location for the water reclamation plant (WRP) was as close as possible to the largest demand centre, i.e. the concentrator and an area where technical support is close by. The initially conceptualised treatment train would be able to treat water for a number of water quality and quantity streams that have been identified. It was realised at the time that all the water may not have to be treated to the highest standard and that the implementation of the UF and downstream processes need to be implemented at a later stage. The full treatment train comprised the following unit process:

- Abstraction, raw water pumping and transfer
- Mixing and aeration
- Coagulation and flocculation



- Dissolved Air Flotation
- Ultrafiltration (UF)
- Reverse Osmosis (RO)
- Gas stripping and Stabilisation
- Disinfection
- Storage
- Sludge and brine disposal

As a result of various unknowns in terms of the water balance, water demands and plant size scenarios were developed to test the sensitivity of certain assumptions on the water treatment works capital and operating cost. **Water balance scenarios** were used to determine the water reclamation potential with changing evaporation rate and tailings specific gravity. **Treatment plant scenarios** were used to determine to what extent the water available in the return water dam could be optimally utilised. The scenarios were developed for various degrees of potable water use, cooling water use, reagent makeup water use and gland service water use. Plant scenario 1 developed a water treatment works treating only for gland service water needs. Plant scenario 2 developed a plant for gland service water needs, reagent makeup water needs and cooling water needs. Plant scenario 3 developed a plant that can meet all of the above

plus potable water supply to the concentrator area. The capital and operating cost for the various plant scenarios were determined for the production rate at increased capacity, high SG and high evaporation loss (adjusted) water balance option. In order to maximise the water reclamation potential plant scenario 3 was selected and the outcome was in order to maximise the return water yield a water treatment plant with a capacity of 4 000 m³/d is required. In this case a DAF unit process with a capacity of 4 000 m³/d and UF and RO unit process with a capacity of 1 000 m³/d will be required. All the unit processes can be sized for 4 modules per unit process.

Results and discussion

It was eventually decided to implement the WRP in two phases, only Phase 1, i.e. the industrial water quality stream. This stream replaces potable water to the gland service water system at the concentrator. Construction of Phase 1 of the WRP has been completed and was implemented using the FIDIC Plant and Design-Build (Yellow Book) form of Contract. The first phase was completed within budget and is currently in operation producing about 3 Ml/d producing DAF clarified water of < 1 NTU.



Figure 1 – Dissolved air flotation units inside the WRP



From a **water resource perspective** many benefits can be listed such as reduced water footprint, reduced unintended infiltration of mine water into surrounding aquifers, reduced demand on regional water resources and infrastructure. Reduced water use also opens up opportunities for other water users to access water that would not have been available in the project was not implemented.

The **financial perspective** also present a win-win solution. The BRPM water reuse facility has at the time been in operation for nearly 24 months and based on actual water savings and operating cost savings the capital invested is projected to be paid back in less than 4 years. The savings will continue to accrue and will soon result in savings in multiples of the initial investment. The reduced top-up water required from Magalies Water and associated savings over the next 10 years assuming the current 2,64 ml/day reduced potable water usage from Magalies Water can result in a R100 million saving as indicated in the figure below.

Socio-economic benefits are not immediately evident, but many benefits can be listed. The plant required additional personnel to operate and contributed towards job creation. The negative impact of impacting local water resources has been significantly reduced which improves access to local pota-

ble water sources. Reduced consumption also improved access of communities to potable water from regional water sources.

Conclusion

The approach in addressing the mine water quality issues demonstrates that a water balance is not merely a legal requirement but a source of intelligence and presents current and future water re-use and reclamation opportunities. This Water Reclamation Plant was at the time the first dissolved air flotation reclamation system used on a platinum mine to reduce the potable water consumption for gland service water.

The BRPM case study demonstrates that with a proper understanding of mine water circuits many water reuse opportunities exist and that water reuse is not only an imperative from a water resource perspective, but also from a financial and socio-economic perspective. Not only did the water security of BRPM mine improved significantly, but it also has indirectly improved the water security of the neighbouring communities as well as the regional water supply security of the entire Magalies Water system.

Incremental improvement such as these will in future contribute to the triple bottom line of mining companies in Africa.



Colloids and their influence in the diagnosis of minewater quality

F.M. Vasconcelos¹; C.S. Zanetti¹; A. M. Soares²

¹Hidrogeo Engenharia e Gestão de Projetos, Rio Grande do Norte street, 1.164, room 501, Belo Horizonte, Brazil

²Nexa Resources S.A. LMG 706 s/n Km 65 CEP 38.780-000 Vazante MG, Brazil

Abstract

The Aroeira tailing dam of Nexa Resources SA is located at Vazante MG town in Brazil. This mine is the largest zinc producer in the country and has operating over 50 years. It has recently incorporated a new zinc deposit known as “Extremo Norte”, located couple kilometers northeast from Vazante Mine, and has featured a sporadically reddish color effluent. However, a numeric correlation of turbidity with the visual water color of the dam with a red color effluent was not verified. This water phenomena also had no correlation with the seasonality where rainiest period in tropical countries, like Brazil, typically increase parameters such as: turbidity, water color and total suspended solids.

The main goals of this study were to find out the causes for the change in water color and how to manage this issue. So, historical satellite image analysis of the dam, technical visits, and water sampling campaign at several points (in the effluent of the underground mine, inside the tailing reservoir and one in the receiving water) were performed. The parameters sampled were (trace and major metals, pH, temperature, electric conductivity, turbidity, color, total solids, total dissolved solids and suspended solids). The main cause of the reddish color is the addition of 30% of ore from the “Extremo Norte”, which has in average 10% of iron oxide in its chemical composition, according to results from ore chemical characterization.

Introduction

This zinc mine owned by Nexa Resources S.A is located at Vazante/MG in Brazil (Figure 1). This unit has recently incorporated a deposit

known as “Extremo Norte” and has featured a sporadically reddish color effluent in its tailing dam effluent.

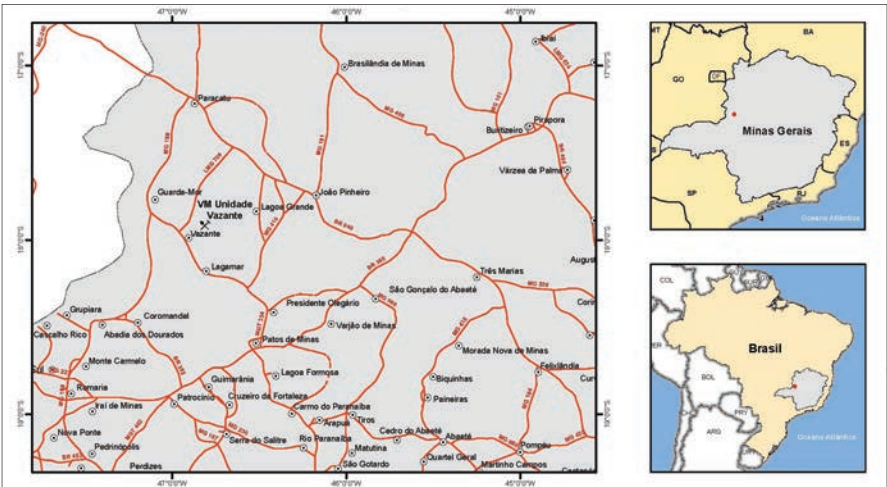


Figure 1: Location of Vazante Mine.



Technical Background

The cause of reddish water coloration in the dam water is associated with the processing of zinc ore from the “*Extremo Norte*” Mine that has a high content of hematite in its composition. Another possibility that was discarded, would be due to the change in atmospheric temperature that would “raise” the very fine particles from the bottom of the tailing dam.

The monitoring data of the dam and its effluent chemical parameters such as: color, dissolved iron and total iron, are not conclusive about the causes of the change in color in the water reservoir and what must be done to solve this phenomenon. Therefore, the objective of this study is to establish the causes of this phenomenon and to be able to present possible solutions. To achieve this, a water sampling campaign as well as analysis of historical images of this reservoir were performed.

The presence of colloids in solution: Colloids are particles of 1 μm (micrometer) to 1 nm (nanometer) in size and are composed of

mineral or organic material. These can significantly influence the characteristics of the water (Vasconcelos et al. 2009).

Based on the history of occurrence of apparent color in the Aroeira dam and the inclusion of “*Extremo Norte*” ore in January 2015, it is very probable that the reddish color of the dam is associated with the presence of colloids generated by the ore processing of this new mine, in a proportion that is above 30%. Generally, the proportion is 80% of ore from the Vazante mine and 20% of the “*Extremo Norte*”. In the sample collected on 12/14/2016 the percentage of ore from the Far North was 51% and the percentage of iron in this waste was about 15%.

When analyzing water samples like those collected on 12/14/2016, due to the size of these suspended particles, it is not possible to characterize higher turbidity, color, or total iron. However, the presence of these colloidal particles in the water is remarkable and for sure they are able to change the apparent color of it. The best strategies to deal with

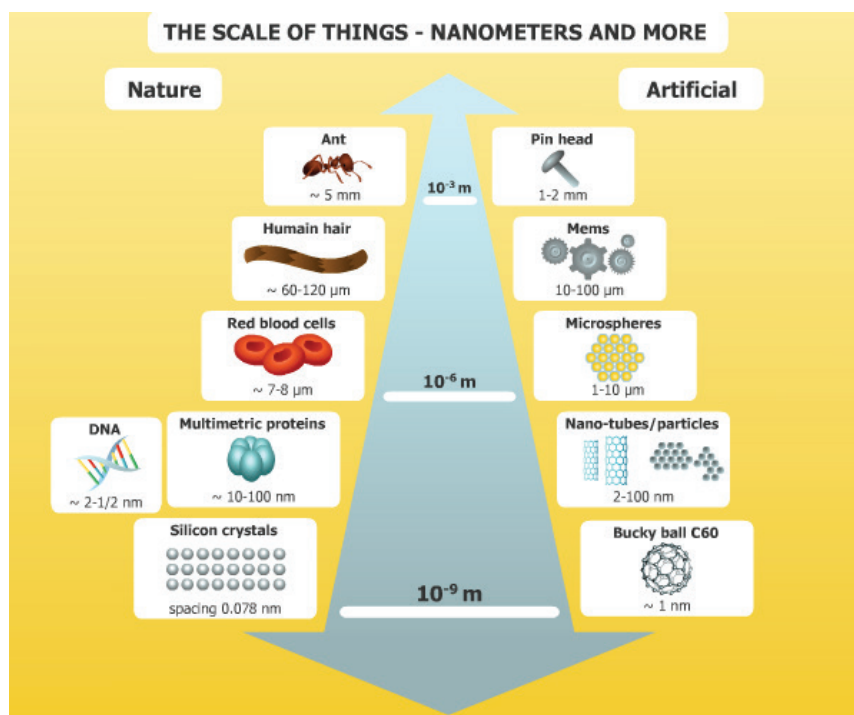


Figure 2: Solid particle size spectrum including the fraction of the colloids (source: www.prochimia.com (2016)).



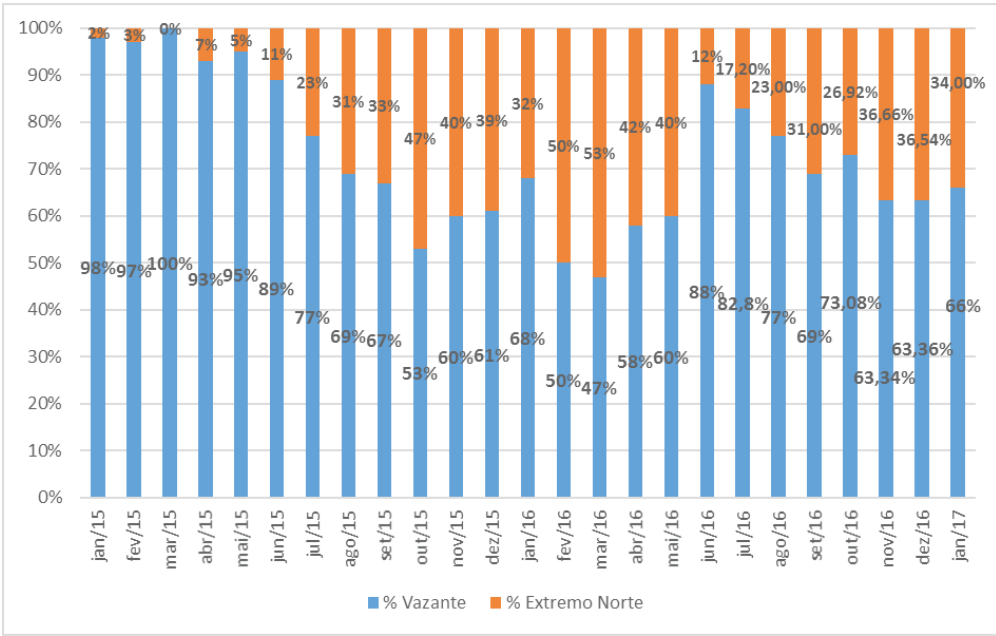


Figure 3: Contribution percentage of the northernmost ore in the USICON plant feed cell.

this problem would be: 1- Controlling the percentage of ore from the “*Extremo Norte*”, or 2- by treating the mill plant effluent, using chemical reagents.

The percentage of ore from the Far North deposit has been reported from January 2015 to January 2017. These data are presented in the following figure(Figure 3).

For the validation of the causal nexus of the inclusion of the *Extremo Norte* ore in the USICON mill plant and the appearance of the red coloration in the dam, a historical survey was made via satellite images obtained via Google Earth. In this survey we searched for

images available on the web in years before the plant received ore from the “*Extremo Norte*” Mine and in years after receiving this type of zinc ore. It is easy to observe the color change of the tailings located on the dam beach, as shown in the following image record. So, in the first two imagens there is no strong red color, but in the three imagens someone can notice the difference in red color. In addition, that the addition of zinc ore from “*Extremo Norte*” Mine, increased significantly after September 2015; therefore, the color in the tailing dam also changed.



Picture 1: Aroeira DAM in 11/06/2009.



Picture 2: Aroeira DAM in 07/21/2013.





Picture 3: Aroeira DAM in 07/10/2015.



Picture 4: Aroeira DAM in 04/10/2016.



Picture 3: Aroeira DAM in 07/10/2015.

Methodology

Sampling: Four water samples were collected, in December of 2016, and the percentage of “Extremo Norte” Mine ore in the whole process was 51%. The sampling points were the following: one of the effluent from the dam, the second from the underground mine, the third from the waste that was disposed in the dam and finally the waste from the underground mine. Sampling was carried out based on ABNT NBR 9897, and the methodologies of analysis of the water samples used are those recommended by the Standard Methods for the Examination of Water and Wastewater. Environmental Protection Agency (EPA) methodologies were also adopted. The samples were: sample 01 (tailing dam effluent), sample 02 (effluent from the underground mine), sample 03 (effluent from mill plant processing Vazante + Extremo Norte ore), sample 04 effluent from mill plant processing Vazante mine ore only).

Treatability Study: Treatability studies evaluating the possible chemical routes to reduce the presence of colloids in the USICON

effluent were carried out by a specialized laboratory. Samples 2 and 3 presented in the previous item, were submitted to the treatability study.

The Physical Chemical treatment was divided into four (4) alternatives:

1. System 01: Treatment with aluminum sulfate: For this treatability test, the simulation of a Chemical Physical system under agitation with the addition of 700 ppm of 10% lime was used to raise the pH to 9.5. After this blending 2,000 ppm of 50% Aluminum Sulfate Coagulant and then 6 ppm of Anionic Polymer Flocculant was added.
2. System 02: PAC treatment: For this treatability test, the simulation of a Chemical Physical system under agitation with the addition of 700 ppm of 10% lime was used to raise the pH to 9.5. After this blend was added 900 ppm of PAC flocculant and then 6 ppm of Anionic Polymer.
3. System 03: Treatment with Tanac (Tanfloc SL 10% solution): For this treatability test, a physical Chemical system simulation



was used under agitation with addition of 100 ppm Tanfloc SL 10% and 0.6 ppm anionic polymer.

4. System 04: Treatment with Tanac (10% Tanfloc SG solution): For this treatability test, a physical chemical system was simulated under agitation with addition of 200 ppm Tanfloc SL 10% and 0.6 ppm anionic polymer.

Analysis and Interpretation of results

Table 1 presents the results of the chemical analysis of the four water samples collected.

Results of Water Analyses: It is observed that the first two samples have similar characteristics, whereas the third and fourth samples had more total suspended solids and similar pH values. Between the last two samples collected from the mill plan the third one, that has ore from the “*Extremo Norte*” had higher values of total suspended solids.

According to the chemical analyzes of the samples 2, 3, and 4, concentrations of the total suspended solids, cadmium, total iron, lead and zinc concentrations were found to be above the limits established in Brazilian

regulation (CONAMA Resolution 430/11 and DN COPAM 01/08), which establish release parameters of effluents in the receiving body. Again, someone can notice that sample 3 has a very high concentration of iron and probably in the colloidal form.

Treatability Study: Four routes for treatment using basically three different reagents (Aluminum sulphate, aluminum polyclorate – PAC, and Tanac) were tried in laboratory in sample 3 collected from the mill plant. From the analysis of the results it was concluded that the system 03 is the best treatment option for both the underground mine effluent (sample 02) and the mill plant processing Vazante. + “*Extremo Norte*” mines (sample 03).

Conclusions

According to the history of the appearance of the phenomenon of increasing the water color of the dam and the disposal of effluent from the USICON plant, it is very probable that the increase of the ore percentage of the “*Extremo Norte*” mine is the cause of the increase of the water color of the tailing dam Aroeira;

Table 1: Results of chemical analyzes of water and effluent samples

Parameters	DN COPAM 01/08	Sample 01	Sample 02	Sample 03	Sample 04
pH	6.0 – 9.0	6.1	6.3	8.8	8.6
Total Suspended Solids mg/L	100	8.0	321	6,136	3,332
Total Lead (mg/L)	0.1	<0.02	0.13	2.75	1.05
Total Coper (mg/L)	1.0	<0.02	<0.02	<0.02	<0.02
Total iron (mg/L)	15	0.09	7.2	15	3.3
Cadmium (mg/L)	0.1	<0.02	<0.02	0.06	0.24
Dissolved iron (mg/L)	15	0.09	5.8	7.9	2.5
Total Zinc (mg/L)	5.0	0.04	0.93	26	10

Table 2: Results of treatability test of effluent samples

Treatment system	DN COPAM 01/08	Sample 01	Sample 02	Sample 03	Sample 04
01	TSS = 100 (mg/L)	23	19	53	172
02	Fe diss. (mg/L)	0.21	0.22	1.3	1.0
03	Pb total (mg/L)	0.02	0.06	< 0.02	0.33
04	Zn total (mg/L)	0.21	0.35	0.19	3.0



The causes of this change in water color are most likely related to the presence of hematite mineral colloids that are present in the “*Extremo Norte*” ore tailings at a concentration above 10%;

The field results have shown that the change of color of the dam was associated with the use of more than 30% of a new zinc ore from the “*Extremo Norte*” mine that had a higher percentage of iron oxide in relation to the Vazante mine. After processing of these two types of ore in the mill a significant amount of Hematite mineral colloids were formed. These colloids particles were at the surface of the dam and change its color; however, this does not modify the monitoring parameters in the water dam (e.g., total suspended solids and color).

The extremely reduced size of the material causes an extremely slow sedimentation. Therefore, a strategy to increase the water residence time in the dam to allow sedimentation will not work. So, the best way to reduce its presence, is either by reducing the percentage of “*Extremo Norte*” ore in the beneficia-

tion plant, or, by treating the effluent from the plant according to the results of this study.

References

- ABNT – NBR 9897 (1987). Planejamento de amostragem de efluentes líquido e corpos receptores. Rio de Janeiro RJ.
- ABNT – NBR 9898 (1987). Preservação e técnicas de amostragem efluentes líquidos e corpos receptores. Rio de Janeiro RJ.
- Deliberação Normativa Conjunta COPAM/CERH-MG nº 01, de 05 de maio de 2008. Dispõe sobre a classificação dos corpos de água e diretrizes ambientais para o seu enquadramento, bem como estabelece as condições e padrões de lançamento de efluentes, e dá outras providências, 2008.
- STANDART METHODS FOR THE EXAMINATION OF WATER AND WASTEWATER, 21ª edição, 2005 - determinação dos parâmetros físico-químicos das águas superficiais;
- VASCONCELOS, F.; TUNDISI, J. G. e TUNDISI, T. M. Avaliação da Qualidade de Água – Base Tecnológica para Gestão Ambiental. SMEA – 323 pp. Belo Horizonte MG – Brasil.



Microbial-mediated Ni and Co recovery from mine tailings

Denys Villa Gomez¹, Yun Liu¹, James Vaughan², Esteban Marcellin³, Valentina Wyman¹, Antonio Serrano¹, Gordon Southam⁴

¹*School of Civil Engineering, The University of Queensland, 4072 QLD, Australia*

²*School of Chemical Engineering, The University of Queensland, 4072 QLD, Australia*

³*Australian Institute for Bioengineering and Nanotechnology, The University of Queensland, 4072 QLD, Australia*

⁴*School of Earth and Environmental Sciences, The University of Queensland, 4072 QLD, Australia*

Abstract

This study shows the microbe-metal interactions that allow the fractionation of Ni and Co in sulphate reducing bioreactors. Ni and Co precipitation experiments with sulfate reducing bacteria (SRB) or with biogenic sulfide effluent were carried out. Lower NiS precipitation occurred in the presence of SRB as compared to the experiments with biogenic sulphide, even when both Ni and Co were added. This and the identified proteins expressed by SRB shows that Ni is complexed by extracellular proteins generated by SRB, which could allow selective recovery of Ni and Co from tailing streams in Australia.

Keywords: sulphate reducing bacteria, Nickel, Cobalt, recovery, proteins

Introduction

Mine tailings and waste streams are known as “the largest environmental liability of the mining industry” left over due to the historical mining activities in Australia (Thurtell et al. 2018). Some of these tailings came from the mining of Ni sulphidic ores (Nehdi and Tariq 2007; Sima et al. 2011), where Co is mostly present (Crundwell et al. 2011). Due to the low recovery efficiencies (70–85% Ni, 20–50% Co), tailing lagoons from this mine activity represents a potential pollutant threat, but also an opportunity to recover these metals for economic revenue (Simonot et al. 2018).

Up to date, conventional technologies for the treatment of metal-containing waste streams are based on the addition of chemicals for precipitation, thus creating high amounts of a secondary waste with no option of reprocessing. Selective recovery of Ni and Co in waste streams for reprocessing is a challenge due to their similar chemical behaviour. Therefore, the addition of reagents is a common practice for concentrated streams that allows selective separation through precipitation, ion exchange and solvent extraction

(Flett 2004). These options are not economic nor environmentally supportable.

Sulphide precipitation, on the other hand, is an excellent chemical to remove metals from waste streams because it allows the formation of highly insoluble salts, even at ppm and ppb concentrations, that can be directly reprocessed (Villa-Gomez and Lens 2017). In this sense, sulfide produced by biological sulphate reduction is a step forward, because it eliminates the costs associated with the acquisition of sulphide reagents, as it uses a pollutant already present in tailings (sulphate) and finally, it allows the production of sulphide on-site, thus avoiding transportation of a hazardous chemical (Villa-Gomez and Lens 2017). The process relies on the activity of sulphate reducing bacteria (SRB) that reduces sulphate (SO_4^{2-}) to sulphide (S^{2-}), which can be used to recover metals as sulphidic precipitates (Sánchez-Andrea et al. 2016; Villa-Gomez and Lens 2017). So far, biological sulphate reduction has been assessed at full-scale to treat acid mine drainage in passive systems and to recover metals such as copper, and zinc from wastewaters coming from metal associated processes in active systems



(bioreactors) (Sánchez-Andrea et al. 2016). While showing very successful results, this technology needs to be further developed to allow separation of metals such as Ni and Co for their recovery.

In bioreactors, the interactions between metals and the microbial environment can affect metal precipitation. This can be due by substances associated to microorganisms can enhance aggregation/settling or metal complexation (Hennebel et al. 2015). All these could open alternatives for metals recovery and separation. It has been demonstrated that SRB generate extracellular proteins that complex metals such as zinc and Ni, chromium, and molybdenum in natural environments (Beech and Cheung 1995; Fortin et al. 1994; Guibaud et al. 2005; Moreau et al. 2007a; Moreau et al. 2007b). This is a protection mechanism against metals and occurs by an alteration of their protein expression profiles (Gillan 2016; Moreau et al. 2007b; Schneider and Riedel 2010). While these defence mechanisms are reported, no one has looked at how these mechanisms complex metals and if there is a difference in complexation depending on the metal. Therefore, the aim of this study was to determine the metal-microbe interactions in sulphate reducing bioreactors as a way to foresee opportunities for selective metal recovery of Ni and Co. The affinity proteins produced by SRB due to the presence of Ni and Co were identified through metagenomics, proteomics and metaproteomics techniques were applied.

Methods

A first set of batch experiments with Co and Ni and centrifuged biogenic sulphide effluent (170 mg sulphide/L) from a sulphate reducing bioreactor were carried out to assess the differences in the characteristics of the Ni and Co sulphide precipitates. 100 or 500 ppm of Ni or Co as chlorides were added into 160ml of biogenic sulphide that contained 25 mM of sulphide. To determine which compound(s) can contribute to the difference of the metal precipitates formed in biogenic sulphide, acetate (0.4 g/L sodium acetate) and phosphate (1.86 g/L KH_2PO_4 and 1.1 g/L K_2HPO_4), mainly present in the VFA-S was added individually into chemically produced sulphide.

Each experiment was done in triplicate in serum bottles of 250 mL. Samples were collected after 20 minutes for particle size distribution (PSD) and 4 days for scanning electron microscopy (SEM) analysis.

A second set of experiments were carried out with SRB biomass from a Continuous Stirred-Tank Reactor (CSTR). The experiments were done in triplicate using serum bottles (120 mL) with a working volume of 100 mL at 120 rpm and 30 °C. In each system, biomass (0.2g VSS/L), nutrients (Alexander J. B. Zehnder 1980), carbon source (sodium lactate), sulphate (sodium sulphate) and metals (NiCl_2 and/or $\text{CoCl}_2 \cdot 6\text{H}_2\text{O}$) were added. Sulphide concentration was measured every day, while COD, sulphate, pH and metals were measured at the end of the experiments. The following metals concentrations were evaluated: 1) 0, 10, 50, 100, 200 and 500 mg Ni^{2+} /L; (2) 0, 10, 50, 100, 200 and 500 mg Co^{2+} /L; (3) a mixture of 100 mg Ni^{2+} /L with 10, 50 and 100 mg Co^{2+} /L.

Ni and Co concentrations were measured with Perkin Elmer AAnalyst 400 Atomic Absorption Spectrometry (AAS) in an air-acetylene flame. Dissolved sulfide was determined spectrophotometrically by the colorimetric method described by Cord-Ruwisch (Cord-Ruwisch 1985) using a UV-VIS-NIR spectrophotometer, while sulfate was quantified using Dionex™ ICS-1100 Ion Chromatography System (IC) equipped with a Dionex AS-DV Autosampler. Visual characterization and semi-quantitative analysis of the Ni and Co sulfides produced in VFA-S were carried out using JEOL JSM 6610 Scanning Electron Microscope coupled with Energy-dispersive X-ray spectroscopy (SEM-EDS). PSS Nicomp Accusizer 780 AD was used to analyze PSD of Ni and Co sulfides. 0.5 ml of the samples was diluted to 80ml of Milli-Q water to ensure minimal particles were present in the water.

Samples of the liquid phase from the batch experiments were taken for protein identification using a Q-Exactive HF-X available through Proteomics Australia after trypsin digestion. The analyses of microbial community structure will be carried out using the Illumina platform at the Australian Centre for Ecogenomics at UQ, this information will be used as data library on the protein analysis.



Results and discussion

Metal precipitation experiments with biogenic sulphide showed that Ni precipitates were larger than Co precipitates (Figure 1). Acetate and phosphate present in the bioreactor were mainly responsible for the presence of larger Ni precipitates ($7.80 \pm 0.52 \mu\text{m}$ and $12.28 \pm 0.75 \mu\text{m}$ of mean size), while these compounds did not affect Co precipitates ($3.70 \pm 0.27 \mu\text{m}$ and $6.18 \pm 0.79 \mu\text{m}$ of mean size). Both compounds have been previously reported to affect particle size of metals (Esposito et al. 2006; Villa-Gomez et al. 2012). By contrast, Co solids could showed aggregation in the matrix (Figure 1), thus demonstrating a different interaction with the substances present on the biogenic sulphide.

The experiments with SRB biomass showed that an increase in Co addition, in-

crease the sulphide production by SRB up to 277.8 mg/L (200 mg Co/L) due to Co sulphide precipitation (Figure 2), while at 500 mg/L , a significant decrease (129.8 mg/L) was observed, suggesting that the inhibitory concentration threshold was surpassed. By contrast, sulphide produced in Ni system decreased to 20.8 mg/L at 100 mg/L Ni supplementation, before increasing to 97.7 mg/L at 500 mg/L addition (Figure 2).

Co precipitation was high (90-95%) at $10\text{-}200 \text{ mg Co/L}$ added in the experiments with SRB biomass (Figure 3a), while low removal (42%) at 500 mg Co/L was observed, probably due to the lack of sulphide for precipitation (Figure 2). Ni removal was lower than 45% at the different Ni supplementation concentrations (Figure 3a), and even non-removal was detected at 100 mg Ni/L

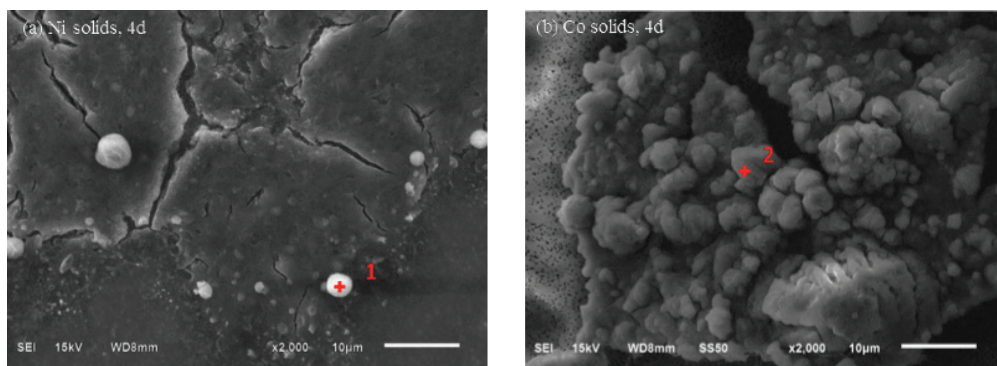


Figure 1 Secondary electron images and EDS of Ni and Co precipitates formed with biogenic sulphide.

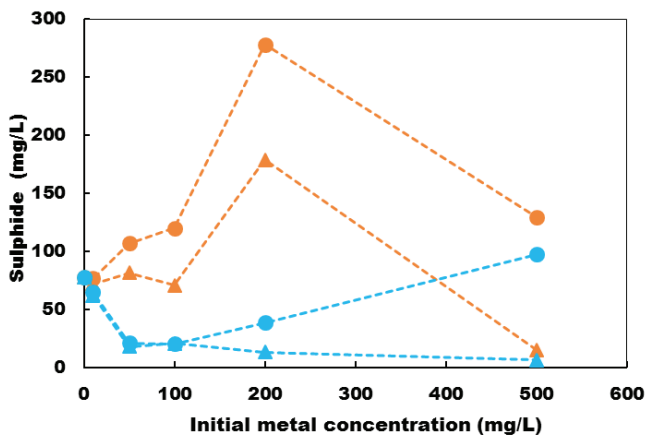


Figure 2 Remaining sulphide (Δ) and total sulphide (\circ) production (=remaining sulphide + sulphide in metal sulphide precipitates) in the experiments carried out with SRB biomass with Co addition (blue) and Ni addition (orange).



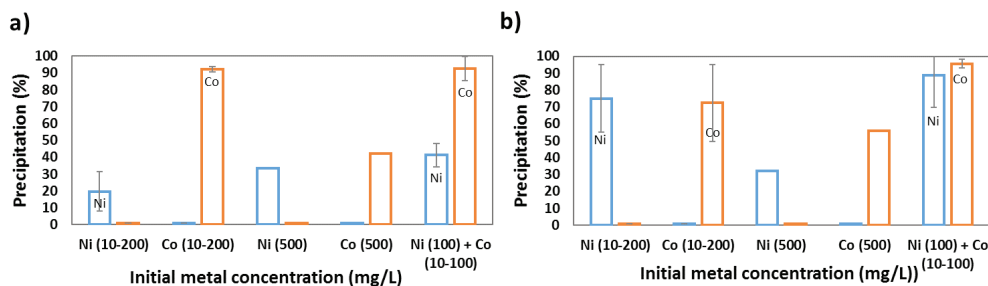


Figure 3 Ni (blue) and Co (orange) precipitation results in the experiments with a) SRB biomass and c) biogenic sulphide effluent.

(data not shown) despite the available sulphide for precipitation (Figure 2). Similar behaviour (low Ni precipitation and high Co precipitation) occurred when both metals were added together (Figure 2). These results suggest that in the presence of Ni, SRB generates extracellular proteins that selectively complex Ni, while Co does not generate this response. Unlike the experiments with SRB biomass, the experiments carried out with only biogenic effluent displayed 75% of Ni removal and 72% of Co removal for Ni and Co addition at 10-200 mg/L (Figure 3b). The decreased Ni and Co removal at 500 mg/L supplementation was a result of a lack of enough sulphide for metal precipitation (Figure 2). In these experiments, also both Ni and Co equally precipitated regardless being added together (Figure 3). Overall comparison among the experiments with SRB biomass and with only sulphide effluent allows to confirm that complexation of Ni is occurring in the system, that could be due to extracellular proteins generated by SRB in response to Ni stress. This has been previously observed by Fortin et al. (1994) on the SRB *Desulfotomaculum* sp., where in the presence of Ni with or without Fe, Ni remained mostly soluble at the cell surface, when cells were subjected to 100 mg/L of both metals, while with Fe only, large amounts of FeS (70% of the Fe) precipitated at the bacterial cell surface and extracellularly.

Microbial and protein analysis

This is the first study that shows the proteins involved in the complexation of Ni in sulphate reducing bioreactors. The high-throughput techniques used in this study have been scarcely used to understand the

effect of metals on protein and gene expression in engineered systems. Previous work has identified proteins in the complexation of metals in pure cultures and with non-specific protein identifiers (Fortin et al. 1994; Lenz et al. 2011; Moreau et al. 2007b). Such information is highly relevant to develop a *technology that maintains Ni complexation in continuous sulphate reducing bioreactors and thus, separates Ni from Co*. In total, over 200 proteins were isolated from the experiments with SRB biomass, but this study only considered the first 10 identified proteins as they had the maximum number of peptides to bind metals. Some of these proteins were exclusively encountered on Ni or Co experiments (Table 1), while others were shared in both experiments as well as in the control experiments with no metals added (data not shown). The high affinity proteins associated with Ni precipitation were involved in transfer of electrons (Rubredoxin-oxygen oxidoreductase), iron uptake (Bacterioferritin) and outer membrane. *Desulfovibrio desulfuricans* ND132 and *Desulfomicrobium baculatum* DSM 4028 were the main responsible for these proteins. The proteins encountered exclusively in the SRB biomass experiments with Co, were related to ATP, oxidoreductase, periplasmic and binding proteins. The same SRB organism was found to be responsible for the expression of these proteins but also *Pseudomonas* and *Marinobacterium*. [NiFe] hydrogenases were also detected in the experiments, which obviously harbor Ni (Ogata et al. 2016) and are widely predominant in SRB species with versatile respiratory electron transport chain system such as *Desulfovibrio* (Zhuang et al. 2015). However, they were not



Table 1 Dominant proteins and the associated organisms encountered in the SRB biomass experiments.

	Characteristic protein	Accession ID	Gene Organism Name
Ni exposure	Selenocysteine-containing peroxiredoxin PrxU	R4187_S62_R4188_S63_02620	<i>Desulfovibrio desulfuricans</i> ND132
	Outer membrane protein P6	R4187_S62_R4188_S63_02748	<i>Desulfomicrobium baculatum</i> DSM 4028
	Bacterioferritin	R4187_S62_R4188_S63_06127	<i>Desulfomicrobium baculatum</i> DSM 4028
	Outer membrane efflux protein BepC	R4187_S62_R4188_S63_07083	<i>Desulfomicrobium baculatum</i> DSM 4028
	Rubredoxin-oxygen oxidoreductase	R4187_S62_R4188_S63_10797	<i>Desulfomicrobium baculatum</i> DSM 4028
	Rubredoxin-oxygen oxidoreductase	R4187_S62_R4188_S63_95586	<i>Desulfomicrobium baculatum</i> DSM 4028
	Rubredoxin-oxygen oxidoreductase	R4187_S62_R4188_S63_84067	<i>Desulfomicrobium baculatum</i> DSM 4028
Co exposure	ATP synthase subunit beta	R4187_S62_R4188_S63_55496	<i>Pseudomonas simiae</i>
	ATP synthase subunit alpha	R4187_S62_R4188_S63_55499	<i>Pseudomonas veronii</i> 1YdBTEX2
	ATP synthase subunit beta	R4187_S62_R4188_S63_22536	<i>Marinobacterium</i> sp. ST58-10
	Transcription termination/antitermination protein NusG	R4187_S62_R4188_S63_74555	<i>Pseudomonas veronii</i> 1YdBTEX2
	Leucine-%2C isoleucine-%2C valine-%2C threonine-%2C and alanine-binding protein	R4187_S62_R4188_S63_03572	<i>Desulfomicrobium baculatum</i> DSM 4028
	putative FAD-linked oxidoreductase	R4187_S62_R4188_S63_56986	<i>Desulfomicrobium baculatum</i> DSM 4028
	putative FAD-linked oxidoreductase	R4187_S62_R4188_S63_09244	<i>Desulfomicrobium baculatum</i> DSM 4028
	Spermidine/putrescine-binding periplasmic protein	R4187_S62_R4188_S63_08733	<i>Desulfomicrobium baculatum</i> DSM 4028
	Spermidine/putrescine-binding periplasmic protein	R4187_S62_R4188_S63_55657	<i>Desulfomicrobium baculatum</i> DSM 4028

exclusively detected only on the presence of Ni. Contrary, in a previous study, expressed autolysis-inducible proteins and cell wall autolysis by-products that binds Ni where detected on a pure culture of *Desulfotomaculum* sp. (Fortin et al. 1994). Nevertheless, this study used a mixed culture unlike the aforementioned study, which shows that the Ni effect can be found in other SRB species and thus, it could allow the development of a more versatile and efficient sulphate reducing bioreactor system for Ni recovery.

Conclusions

The results presented in this study shows that in the presence of Ni, SRB generates extracellular proteins that selectively complex Ni, while Co does not generate this response and tends to precipitate with sulphide. The modification of the removal behaviour of Ni and Co through SRB culture is a sustainable solution to selectively recover both metals from mine drainages, thus providing an environmental and economic benefit.

Acknowledgements

The authors thank the laboratory staff of the Centre for Microscopy and Microanalysis (CMM) and Solid Waste Management at UQ for the analytical support. The authors also acknowledge the support on the bioinformatics analysis to Dr Robin Palfreyman from the Australian Institute for Bioengineering and Nanotechnology (AIBN) at UQ.

References

- Alexander J. B. Zehnder BAH, Thomas D. Brock, and Karl Wuhrmann (1980) Characterization of an Acetate-Decarboxylating, Non-Hydrogen-Oxidizing Methane Bacterium Arch Microbiol 124:1-11
- Beech IB, Cheung CWS (1995) Interactions of exopolymers produced by sulphate-reducing bacteria with metal ions Int Biodeterior Biodegrad 35:59-72 doi:10.1016/0964-8305(95)00082-G
- Cord-Ruwisch R (1985) A quick method for the determination of dissolved and precipitated sulfides in cultures of sulfate-reducing bacteria J Microbiol Methods 4:33-36
- Crundwell FK, Moats MS, Ramachandran V, Robinson TG, Davenport WG (2011) Cobalt – Occurrence, Production, Use and Price chapter 28:357-363 doi:10.1016/b978-0-08-096809-4.10028-0
- Esposito G, Veeken A, Weijma J, Lens PNL (2006) Use of biogenic sulfide for ZnS precipitation Sep Purif Technol 51:31-39 doi:10.1016/j.seppur.2005.12.021
- Flett DS (2004) Cobalt-Nickel Separation in Hydrometallurgy: a Review Chemistry for Sustainable Development 12:81-91
- Fortin D, Southam G, Beveridge TJ (1994) Nickel sulfide, iron-nickel sulfide and iron sulfide precipitation by a newly isolated *Desulfotomaculum* species and its relation to nickel resistance FEMS Microbiol Ecol 14:121-132 doi:10.1111/j.1574-6941.1994.tb00099.x



- Gillan DC (2016) Metal resistance systems in cultivated bacteria: are they found in complex communities? *Curr Opin Biotechnol* 38:123-130 doi:<https://doi.org/10.1016/j.copbio.2016.01.012>
- Guibaud G, Comte S, Bordas F, Dupuy S, Baudu M (2005) Comparison of the complexation potential of extracellular polymeric substances (EPS), extracted from activated sludges and produced by pure bacteria strains, for cadmium, lead and nickel *Chemosphere* 59:629-638 doi:<http://dx.doi.org/10.1016/j.chemosphere.2004.10.028>
- Hennebel T, Boon N, Maes S, Lenz M (2015) Biotechnologies for critical raw material recovery from primary and secondary sources: R&D priorities and future perspectives *New Biotechnology* 32:121-127 doi:<http://dx.doi.org/10.1016/j.nbt.2013.08.004>
- Lenz M, Kolvenbach B, Gyax B, Moes S, Corvini PFX (2011) Shedding Light on Selenium Biomineralization: Proteins Associated with Bionanominerals *Appl Environ Microbiol* 77:4676-4680 doi:10.1128/aem.01713-10
- Moreau J, Weber P, Martin M, Gilbert B, Hutcheon I, Banfield J (2007a) Extracellular Proteins Limit the Dispersal of Biogenic Nanoparticles *Science* (Washington) 316:1600-1603
- Moreau JW, Weber PK, Martin MC, Gilbert B, Hutcheon ID, Banfield JF (2007b) Extracellular Proteins Limit the Dispersal of Biogenic Nanoparticles *Science* 316:1600-1603 doi:10.1126/science.1141064
- Nehdi M, Tariq A (2007) Stabilization of sulphidic mine tailings for prevention of metal release and acid drainage using cementitious materials: a review *Journal of Environmental Engineering and Science* 6:423-436 doi:10.1139/s06-060
- Ogata H, Lubitz W, Higuchi Y (2016) Structure and function of [NiFe] hydrogenases *J Biochem* 160:251-258 doi:10.1093/jb/mvw048
- Sánchez-Andrea I, Stams AJM, Weijma J, Gonzalez Contreras P, Dijkman H, Rozendal RA, Johnson DB (2016) A case in support of implementing innovative bio-processes in the metal mining industry *FEMS Microbiol Lett* 363 doi:10.1093/femsle/fnw106
- Schneider T, Riedel K (2010) Environmental proteomics: Analysis of structure and function of microbial communities *Proteomics* 10:785-798 doi:10.1002/pmic.200900450
- Sima M, Dold B, Frei L, Senila M, Balteanu D, Zobrist J (2011) Sulfide oxidation and acid mine drainage formation within two active tailings impoundments in the Golden Quadrangle of the Apuseni Mountains, Romania *Journal of hazardous materials* 189:624-639 doi:10.1016/j.jhazmat.2011.01.069
- Simonnot M-O, Vaughan J, Laubie B (2018) Processing of Bio-ore to Products. In: Van der Ent A, Echevarria G, Baker AJM, Morel JL (eds) *Agromining: Farming for Metals: Extracting Unconventional Resources Using Plants*. Springer International Publishing, Cham, pp 39-51. doi:10.1007/978-3-319-61899-9_3
- Thurtell D, Gibbons M, Philalay M, Drahos N, Martin K, Moloney J, Nguyen T (2018) Resources and Energy Quarterly March 2018. Australian Government, Office of the Chief Economist
- Villa-Gomez DK, Lens PNL (2017) Metal recovery from industrial and mining wastewaters using sulphate-reducing bioreactors. In: Rene ER, Sahinkaya E, Lewis A, Lens P (eds) *Sustainable Heavy Metal Remediation: Volume 2: Case studies*, vol 9. Springer Cham, Switzerland. doi:10.1007/978-3-319-61146-4_3
- Villa-Gomez DK, Papirio S, van Hullebusch ED, Farges F, Nikitenko S, Kramer H, Lens PN (2012) Influence of sulfide concentration and macronutrients on the characteristics of metal precipitates relevant to metal recovery in bioreactors *Bioresource technology* 110:26-34 doi:10.1016/j.biortech.2012.01.041
- Zhuang W-Q, Fitts JP, Ajo-Franklin CM, Maes S, Alvarez-Cohen L, Hennebel T (2015) Recovery of critical metals using biometallurgy *Curr Opin Biotechnol* 33:327-335 doi:<http://dx.doi.org/10.1016/j.copbio.2015.03.019>





A decorative background pattern consisting of stylized, overlapping shapes that resemble hands or figures reaching out, arranged in a diagonal flow from the top left towards the bottom right. The pattern is rendered in a light gray color.

13

**BEST PRACTICE
GUIDELINES**



Dissection of the NAG pH Test: Tracking Efficacy Through Examining Reaction Products

Anita Parbhakar-Fox¹, Nathan Fox², Tony Ferguson³, Roger Hill³, Ben Maynard³

¹*Transforming the Mining Value Chain, ARC Industrial Transformation Hub, University of Tasmania, Private Bag 79, Hobart, TAS, 7001. Australia*

²*CRC ORE, University of Tasmania, Private Bag 79, Hobart, TAS, 7001. Australia*

³*Grange Resources Tasmania, 34A Alexander St, Burnie, TAS, 7320. Australia*

Abstract

In this study we sought to better understand the mechanics of the NAG pH test and determine the influence each variable has in controlling the resulting NAG pH, a value which is commonly used by the mining industry for waste classification. Three bulk samples (20 kg) representative of waste types A (alkaline), B (weakly-NAF) and D (PAF) were obtained from the Savage River mine, Tasmania. Variables tested included initial reaction time, heating temperature, heating length, post reaction cooling time and hydrogen peroxide (H_2O_2) strength ($n=126$). Our observations showed that for this suite, a multi-addition NAG pH test facilitated efficient sulphide oxidation for low sulphide-sulphur samples (i.e., < 0.3 wt. %) with an initial reaction time of at least 480 minutes given per 15% H_2O_2 addition, heating to 80 to 90 °C for 2.5 hours, and then cooling of the reaction solution overnight with the NAG pH reading taken the following morning. This study demonstrated that using the recommended standard conditions given in Smart et al. (2002) is not appropriate for general use. Rather a suite of representative waste samples should initially be selected and the optimal conditions to facilitate sulphide oxidation determined on a site-per-site basis.

Keywords: Static testing| Waste classification| Prediction | NAG testing

Introduction

Improving waste classification predictions is an ongoing area of research (e.g., Chopard et al., 2017; Dold, 2017) but despite several researchers suggesting that such classifications should be based on mineralogical data, the industry remains reliant on static geochemical data. Therefore, it is imperative to ensure that classifications made using these data are as robust as possible. One such screening tool is the net acid generation (NAG) pH test. Whilst it is typically screened against net acid producing potential (NAPP) values (Smart et al., 2002) it is now being increasingly used against other values including total-sulphur, paste pH, and acid rock drainage index (ARDI) values as a lower cost means of allowing waste classification (Weber et al., 2006; Parbhakar-Fox et al., 2011). Given the growing importance placed on this test, its reproducibility is critical, however, in confi-

dential inter-laboratory comparisons, values measured for duplicate samples across three laboratories were vastly different resulting in conflicting waste classifications. This is likely a manifestation of procedural interpretation errors of the most widely cited NAG procedure given in the AMIRA P387A Handbook (Smart et al., 2002). For example, the test is stated as suitable for samples containing $<1.5\%$ S and with low concentrations of Cu, but for samples undergoing geoenvironmental characterisation, these values may yet be unknown. Further, the procedure states that after the reaction, the beaker should be placed on a hot plate and gently heated until effervescence stops (i.e., minimum of 2 hours), but no clear recommendation of which temperature to heat to is given. Finally, on completion, the sample is to cool to room temperature with no exact length of time given as to when to take the final NAG pH measurement. Obser-



variations of procedural errors have been noted most recently by Charles et al. (2015) who stated that for carbonate-bearing samples, the pre-boil time length is critical in controlling the final pH. However, discrepancies could arise for samples with differing mineralogy (i.e., silicate or sulphide rich) with the controlling variables on these NAG results yet to be documented. Whilst dissecting the NAG test may help develop improved laboratory protocols, the industry remains plagued by one fundamental error, there is an absence of a (global) standard to use during NAG pH testing. Whilst several exist for acid base accounting tests (e.g., KZK-1, NBM-1; Canmet) commercial laboratories rarely report on the use of a similar standard for NAG pH testing, thus, how can confidence be given in resulting values if QA/QC measures cannot be demonstrated for a given analytical suite? This paper presents a snapshot of the overall study which aimed to demonstrate the importance of using site-specific NAG pH protocols with an example from the Savage River mine, Tasmania, Australia given.

Methods

Three bulk samples representative of wastes types A (alkaline), B (weakly non-acid forming; NAF) and D (potentially acid forming; PAF) were obtained from the Savage River mine, Western Tasmania. The samples were dried and prepared to <75 µm, split into four portions (1 to 4) using a riffle splitter with two parts selected (blindly) for use. The in-use portions were placed in zip-lock plastic bags and stored in a cool and dry place to limit opportunities for oxidation between experiments. The workflow adopted during

this investigation is shown in Figure 1 with all analyses performed at the University of Tasmania. X-ray diffractometry (XRD) measurements were performed using a Bruker D2 Phaser (Co-X-ray source) with data processed using Topas V4 software. A Hitachi SU-70 field emission scanning electron microscope (FE-SEM) was used to examine the reaction feed and products, with samples mounted on double-sided carbon tape placed on a 10 mm metal stub and carbon coated prior to analysis. All other analytical procedures are as given in Parbhakar-Fox et al. (2011).

Results and Discussion

The bulk mineralogy of all tested parent samples (n=6) is dominated by magnesiohornblende, chlorite, quartz and albite. D-Type is the most pyrite bearing (6.6-7.7 wt. %) with 5.1-5.7 wt. % calcite + dolomite, B-Type contains moderate pyrite (0.9-1.3 wt. %) and 2.8-3 wt. % dolomite+ trace calcite, and A-Type contains the least pyrite (< 0.5 wt. %) with 5 to 5.5 wt. % calcite + dolomite. D-Type is potentially acid forming (PAF), A-Type is non-acid forming (NAF; likely an effective neutraliser), whilst B-Type fall proximal to the ANC/PAF cut-off when simple mineralogical classifications are performed (Parbhakar-Fox et al. 2011). Trace elements measured in the parent samples include Cu (65 to 443 ppm), As (11 to 29 ppm), Ni (44 to 217 ppm) and Zn (174 to 305 ppm) with the highest quantities reported for D-Type. Total sulphur values confirm mineralogical observations that D-type is the most acid forming (range: 5.94 to 6.55 %) with a predicted MPA of 182 to 200 kg H₂SO₄/t. B-Type had a calculated MPA range of 11 to 35 kg H₂SO₄/t and for A-Type

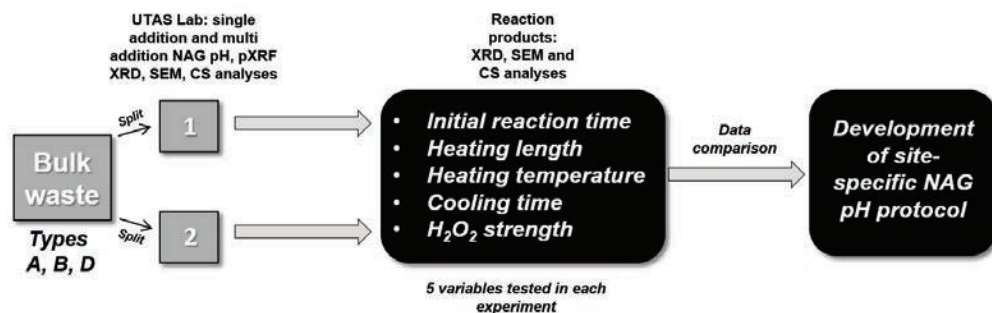


Figure 1. Experimental program followed in this study.



it was $< 10.5 \text{ kg H}_2\text{SO}_4/\text{t}$. In these experiments, a baseline by which to benchmark results against was required, so multi-addition NAG values (performed at 15 % H_2O_2) were used (A-Type: pH 9.12 and 9.28; B-Type: pH 9.13 and 9.21; D-Type: pH 8.06 and 8.09). This test was used in preference over sequential NAG to mimic what a commercial laboratory might do when considering logistical constraints (i.e., fixed time length per experiment known reagent consumption quantity). The results for each tested variable are summarised in the next sections *NB. The reader is encouraged to download the associated presentation to view the supporting figures.*

Initial reaction time

The procedure recommends that the initial reaction evolves until ‘boiling’ or effervescence ceases, and may recommend a sample to be left overnight. In this study, six experiments were performed (10, 30, 60, 120, 240 and 480 minutes). A-Type is carbonate bearing (5 to 5.5 wt. %) which typically requires a long initial reaction time. Our observations showed that after 10 minutes, only mild effervescence was seen along the liquid meniscus (NAG pH: 8.49-9.42) and after 120 minutes, this had become more apparent (NAG pH: 9-9.8). Samples were allowed to continue to react until 480 minutes with effervescence only gradually decreasing (NAG pH 8.98). The 240 minute samples both best approximated the multi-addition baseline values (A-Type: pH 9.12 and 9.28), with the 480 minute experiment the only to drop below. The relative proportion of dolomite decreased with increasing time length, conversely calcite appeared to relatively increase, with discernable change observed for pyrite (though it was present in trace quantities hard to resolve by XRD). B-Type material was more reactive than A-Type with all experiments immediately showing a higher degree of effervescence with larger bubbles forming. This likely corresponds to its higher pyrite content with a contribution too from the reactive carbonates (up to 3 wt. %). Considering this, terminating the experiment at 10 minutes certainly did not allow for total reaction (pH: 9.41-9.85), indeed, the effervescence only appeared to significantly reduce again after 480 minutes, as seen for both splits (NAG pH: 8.53-8.6). Pyrite content decreased

with increased reaction time, with $< 0.3 \text{ wt. \%}$ difference measured for dolomite, with a net decrease over time only observed for B-Type sample 3. D-Type material was the most exothermic and reactive of all waste types with vigorous effervescence and very large bubbles frequently produced after H_2O_2 addition and a constant ‘scum’ forming on the surface. This reaction appeared to abate after 240 minutes; but no discoloration of the solution occurred (i.e., changing from black to orange/brick red, which can occur for high-sulphide bearing samples). NAG pH values measured after 480 minutes (pH 8.53-8.6) were closest to the multi-addition baseline data. Pyrite decreased in D-Type sample 2 from 6.6 to 5 wt. % however it did not significantly vary for D-Type sample 1 (except at 240 minutes where it dropped to 1.8 wt. %). When evaluating the rate of pyrite dissolution, these results suggest that extending the reaction time beyond 480 minutes will still not oxidise even 50% of the pyrite contained in this waste material.

Heating length

This part of the procedure is designed to i) break down residual H_2O_2 in the sample and ii) encourage carbonate dissolution allowing for an assessment of neutralising potential. In the previous experiment, lower pH values were measured prior to heating, confirming that alkalinity is realised on heating. The heating length times used in these experiments were 30, 60, 90, 120 and 150 minutes. The initial reaction time used in this experiment was 480 minutes (as informed by the previous experiment) with a heating temperature of 80 to 90 °C with NAG pH readings taken after 1-hour cooling time. For A-Type sample 2, the NAG pH slightly dropped with increased heating length (pH 11.8 to 11.3) with similar values measured for A-Type sample 3. However, NAG pH values for both samples were higher than their respective baseline values by at least 2 pH units. These highly basic values support observations given in Charles et al. (2015) and suggest that the maximum length of time allowed may still be too short, with bulk-mineralogical analysis on post-reaction residues from the 150 minutes samples still reporting calcite (3- 3.4 wt. %) but only trace dolomite ($< 0.4 \text{ wt. \%}$). For Type-B, basic NAG pH values were again



measured in each experiment ranging from pH 10.1 to 11 for Type-B sample 1, and pH 10.6 to 11.3 for Type-B sample 3. In general, results were lower after 150 minutes than 10 minutes with classifications remaining NAF but were still approximately 1 unit above the multi-addition baseline value. Whilst pyrite decreased over time, dolomite content varied by only 0.2 wt. %. The NAG pH values for D-Type samples were notably lower than those measured for A- and B-Type (D-Type sample 1: pH 8.1– 8.61, baseline pH: 8.06; D-Type sample 2: pH 8.17 to 8.41; baseline pH 8.09), with a much smaller range recorded due to the increased pyrite oxidising (as confirmed by bulk mineralogical measurements on the reacted residues) and overshadowing the alkalinity generated by carbonate dissolution. At the end of the reaction, between 5–6 wt. % pyrite remained, indicating that up to 12% only had reacted. Similarly only 30% of carbonates had reacted after 150 minutes. These results suggest that for these samples, a minimum heating length of 150 minutes should be used.

Heating temperature

The original procedure states that after the reaction, the beaker should be placed on a hot plate and gently heated, however the temperature at which this ‘gentle’ heating is performed at is not clearly stated. Weber et al. (2005) stated their heating as 80–90 °C therefore this was the temperature used in the previous two experiments, but, this is considerably higher than a gentle heating. Experiments were conducted at room temperature (≈25°C), 60, 80 and 90 °C. Two pH measurements were made, soon after cooling (i.e., 1 hour) and after overnight cooling (approximately 10 hours) with an initial reaction time of 480 minutes used, and heating length of 120 minutes (NB. These experiments were performed in parallel to the previous, thus the recommended minimum of 150 minutes was not used). For both A-Type samples, the NAG pH values increased considerably with heating temperature, with the lowest values measured at 25°C (pH 7.2), both of which were lower than the benchmark values (pH 9.12 and 9.28), suggesting these are too acidic. The on-cooling NAG pH values for 60 to 90 °C showed remarkable consistency with

increased temperature, with a slight overall increase in NAG pH noted for A-Type sample 2 (pH 11.2 to 11.3) and pH 11.3 consistently measured for A-Type sample 3. These values are two units about the baseline value, suggesting they are too basic. However, the overnight cooling values better show the effect of heating temperature, with a net-decrease in pH clearly noted for A-Type sample 2 (pH 10.2 to 8.8), but for A-Type sample 3 this peaked at 80 °C (pH 10.4) and decreased at 90 °C, with a value approximating the baseline achieved (i.e., pH 9.1). This suggests, if a higher temperature is used, then the NAG pH should be taken after leaving the sample overnight, otherwise a temperature of 40–45 °C is optimal. Bulk contents of pyrite and dolomite measured in post reaction residues confirmed it to decrease with temperature. Results from B-Type are similar, with carbonates measured in post reaction residues showing a general decrease for calcite (less so for dolomite) though pyrite showed no linear trends with a range of 0.4 wt. %. However, for D-Type, it appeared that heating temperature had little effect on the final NAG pH when measured after overnight cooling with a range of 7.8 to 8.2 for D-Type sample 1 (baseline: pH 8) and pH 7.9 to 8.1 for D-Type sample 2 (baseline: pH 8.1). If measured after 1 hour of cooling, an increase in pH was noted as temperature increased (7.5 to 9.3: Type D sample 1; 7.56 to 9.1: Type D sample 2), thus, an optimal reaction temperature of 55 °C identified. Despite this recommendation, pyrite remained between 4 to 5 wt. % in all D-Type samples.

Cooling length

The cooling length time can considerably impact the final NAG pH reading as indicated in the previous section. The original procedure stipulates that the sample should be allowed to cool to room temperature. However, the amount of time this may take is not quoted and therefore could be as quick as 30 minutes (or less if a cold water bath is used) or could be left overnight to react (particularly if experiments were performed over several working hours in a commercial laboratory). In this experiment, NAG pH measurements were taken after 10, 30, 60, 120, 240 and 720 minutes cooling, with these samples also left overnight and additional pH reading tak-



en. For both A-Type samples, the NAG pH maxima were measured after 240 minutes (pH 11.2 and 11.7) and minima at 60 minutes (pH 9 to 9.3). This trend was mimicked again after overnight cooling for all samples, however the pH values had all uniformly dropped with several values (10, 30 minutes and overnight) similar to the benchmark values for both splits (i.e., pH 9.28 and 9.12). For B-Type, the NAG pH values ranged from pH 10.6 (10 minutes) to 8.4 (240 minutes). The lowest values were measured after cooling overnight, with a small range measured (0.3 to 0.6 pH units) and readings very close to the benchmark values for B-Type sample1 (pH 9.13). However, when measured again after being left overnight, all readings were near-identical to the benchmark pH. For B-Type sample 3 it was also very close, with the 10 and 240 min samples the closest to the baseline (pH 9.21). For D-Type samples, NAG pH values on cooling were reasonably similar to the benchmark values ranging from pH 7.8 to 8.7. The maximum value for D-Type sample 1 was measured at the start with a mild progressive decline observed over time. In contrast, values appeared to increase with cooling time length for D-Type sample 2. The overnight pH for both samples were closest to the mNAG benchmark values. These observations show that measuring the pH of the NAG solution after an overnight rest period is most likely to yield a more accurate pH measurement.

Hydrogen peroxide strength

All experiments up to this point focused on changing variables in the experimental procedure. It is evident from B-Type and D-Type materials that changing or fine-tuning these variables does not result in total pyrite oxidation, or indeed, full consumption of effective carbonate neutralisers. Considering this, our final experiment focussed on changing the strength of the H₂O₂, with 7.5 %, 15% and 30 % tested following a single-addition methodology (480 minutes initial reaction time, 120 minutes on hot plate at 80-90 °C, with the final pH taken after overnight cooling). Lower pH readings were consistently measured for all samples when using 7.5 % strength relative to 15% H₂O₂, with values for all waste types around pH 8. It is likely that carbonates

are mildly reacting with only very minor pyrite oxidation (if at all) allowed as the H₂O₂ strength is simply too weak. At 15% H₂O₂, the highest results were measured for A-Type and B-Type samples suggesting, that sufficient oxidative capacity is present to attack pyrite generating acidity causing carbonate dissolution and elucidating alkalinity. Bulk mineralogical measurements provided no evidence of intermediate reaction products (i.e., calcium or magnesium hydroxides) influencing the final pH. At 30 %, lower pH values are reported for all samples showing pyrite oxidation is now the dominant reaction with mineralogical classifications approximated, particularly for D-Type, with both samples classified as PAF (pH 2.16 and 2.75). These data show that this is the most important factor controlling NAG pH values. These results show that the standard single NAG pH test is not appropriate for samples containing > 0.3 % sulphide-sulphur, which is much less than that stated by Smart et al. (2002) and yet, it is widely performed. As a final piece of supporting evidence, SEM investigations on NAG residues showed that even at 30% strength, unreacted sulphides remained in a single addition test. Therefore, adopting a multi-addition approach should be mandatory and supersede the single-addition test entirely. Whilst it will add time (and costs) to the overall experimental run, it will improve NAG testing accuracy.

Standard development

These investigations have highlighted the difficulty in performing consistent analyses when undertaking the NAG pH test and clearly show that the first step to overcoming this is to develop a specific NAG pH standard which can be analysed as part of a sample suite when sent to a laboratory for analysis. Thus, the final part of this study sought to initiate the develop of such standards using TASBAS and TASDOL which are routinely used in whole rock geochemical analyses performed in Tasmanian laboratories (and present in abundant quantities). TASDOL contains more sulphur but less carbon than TASBAS with both contain less than 0.1 and 0.05% respectively suggesting an absence/trace presence of sulphide and carbonate phases (thus negligible variability is likely



during NAG pH testing). TASBAS is dominated by augite, forsterite, analcime and sanadine, whilst TASDOL is anorthite, augite, quartz and sanadine dominated. For both, Si, Al, Fe, Mg, Ca and Sr (higher in TASBAS) are measured in both with F also measured in TASDOL. Trace elements include Zr, Ba, Cr, V, Ni and Zn. Ten split samples of these materials were individually prepared and tested using a standard single addition NAG test (2 hours reaction time, 2 hours heating at 80-90 °C with the final NAG pH measured after 2 hours cooling time). For the TASBAS, NAG pH values ranged from pH 6.7 to 6.8 (standard deviation: 0.03). For TASDOL, NAG pH values were consistently lower ranging from pH 5.9 to 6.4 with an average of pH 6.19, and a higher standard deviation (0.17). The post reaction residues of four of these samples were analysed by XRD to help indicate which silicates may have reacted (i.e., imparting a mild neutralising potential), as relative to the standard pH of both H₂O₂ and H₂O (pH 5- 5.5), these values are slightly alkaline. TASBAS values show that after NAG testing, phillipsite (3Al₆Si₁₀O₃₂·12H₂O) appears to have reacted with a minor net proportion decrease, along with laumontite (Ca(AlSi₂O₆)₂·4H₂O) both of which belong in the zeolite group. Similar net-changes were not observed in the TASDOL NAG residues suggesting this is a more inert. Further standard development using these materials is ongoing with additional test work focussing on testing a larger number of samples and exploring how the NAG pH values change with different parameters (as performed in this study).

Conclusions

The single-addition net acid generation (NAG) test is used to forecast the acid generating properties of mine wastes with results used to assist in mine waste management. In recent times, the industry-trend has been to only perform the test to the stage whereby pH measurements are made and a waste classification assigned (i.e., no back-titration to quantify maximum potential acidity). However, discrepancies between laboratory results have been reported when testing splits of the same samples resulting in vastly different, and occasionally, erroneous waste classifications. In this study, the influence of several

experimental variables on the final NAG pH value was explored using three waste types obtained from the Savage River mine, Tasmania. For these materials a multi-addition NAG should be used for low sulphide-sulphur (i.e., < 0.3 wt. %), carbonate-bearing samples with an initial reaction time of at 480 minutes given per 15% H₂O₂ addition, heating to 80 to 90 °C for 2.5 hours and then cooling of the reaction solution overnight with the NAG pH reading taken the following morning. For high sulphide-sulphur materials (i.e., > 0.3 wt.%) 30% H₂O₂ should be used instead, as XRD and SEM studies performed on powder residues revealed that 15% H₂O₂ does not cause substantial sulphide oxidation (even when experimental variables are changed), thus the final waste classification may be incorrect (i.e., underestimating acid forming potential). Where commercial laboratory discrepancies are reported, it may be due to poor preparation of 15% H₂O₂ and erroneously high values are most likely due to reading pH when sample has not reacted for long enough during the heating step and the reading is taken too quickly after cooling (confirming observations given in Charles et al. 2015). This study highlights i) the importance of understanding a sample's mineralogy prior to commencing static testing; ii) the necessity for developing a site-specific NAG testing protocol prior to starting work on a new waste classification project to optimise experimental efficiency; and iii) the importance of developing and using a standard reference material during NAG testing to ensure waste classifications are based on robust values.

Acknowledgements

This research was conducted through the Australian Research Councils Industrial Research Hub for Transforming the Mining Value Chain (project number IH130200004). Acknowledgments are given to Grange Resources for providing research funding for this study.

References

- Charles, J., Barnes, A., Declerq, J., Warrender, R., Brough, C., & Howell, R. 2015. Difficulties of interpretation of NAG test results on net-neutralising mine wastes: initial observations of elevated



- conditions and theory of CO₂ disequilibrium. Proceedings of the 10th International Conference on Acid Rock Drainage and IMWA annual conference, pp.1-10.
- Chopard, A., Benzaazoua, M., Bouzazah, H., Plante, B., Marion, P. 2017. A contribution to improve the calculation of the acid generating potential of mining wastes. *Chemosphere*, 175: 95-107.
- Dold, B. 2017. Acid rock drainage prediction: a critical review. *Journal of Geochemical Exploration* 172: 120–132.
- Parbhakar-Fox, A., Edraki, M., Walters, S., Bradshaw, D. 2011. Development of a textural index for the prediction of acid rock drainage. *Minerals Engineering*, 24: 1277-1287.
- Smart, R., Skinner, W.M., Levay, G., Gerson, A.R., Thomas, J.E., Sobieraj, H., Schumann, R., Weisener, C.G., Weber, P.A., Miller, S.D., Stewart, W.A., 2002. ARD test handbook: Project P387A, A prediction and kinetic control of acid mine drainage, Melbourne, Australia: AMIRA, International Ltd, Ian Wark Research Institute.
- Weber, P.A., Hughes, J.B., Conner, L.B., Lindsay, P., Smart, R.St.C., 2006. Short-term acid rock drainage characteristics determined by paste pH and kinetic NAG testing: Cypress prospect, New Zealand, Paper presented at the 7th International Conference on Acid Rock Drainage (ICARD).



Solution collection system for a ROM leach dump: Design criteria to meet best available control techniques rules

Jorge Puell^{1,2}, Paloma Lazaro^{1,3}, Víctor Tenorio¹

¹Mining and Geological Engineering Department, University of Arizona, 1235 James E. Rogers Way, Tucson, AZ 85719, United States; jpuell@email.arizona.edu

²Freeport-McMoran Copper & Gold, 4521 US-191, Morenci, AZ 85540, United States

³Rio Tinto Borates, 14486 Borax Road, Boron, CA 92342, United States

Abstract

Low grade ore dumps subject to leaching operations typically report the pregnant leach solution (PLS) to a downstream collection point, which is subsequently pumped out and processed for copper recovery. Proper design and operation of leaching collection facilities are critical to prevent the run-of-mine (ROM) dump from seepage and unpermitted discharge of these solutions into the environment. Structures making up for the solution collection system may include PLS impoundments, storm water diversions, check dams, lined pre-stacking material, collection channels, ponds and other facilities. This paper outlines the criteria to determine the specific engineering design of such facilities by meeting the use of the best available control techniques to minimize environmental releases and comply with government regulations. Techniques and calculations should be performed to estimate: i) limit-equilibrium slope stability; ii) runoff and storages evaluation under historical storm event scenarios; iii) peak discharge values and reductions, and iv) facilities size optimization. Finally, an application example in support of a copper leaching dump exposed to extreme climate conditions in a surface mine illustrates the proposed design criteria, methods, assumptions and outcomes.

Keywords: Solution collection system, leach dump, best available control techniques

Introduction

In the mining industry, leaching is a hydro-metallurgical process that separates valuable minerals from ore by dissolving the mineral with a dilute cyanide solution in the case of gold, or a sulfuric acid to dissolve copper (Hearn RL & Hoyer R 1998). Dump leaching is a technique where run-of-mine low grade material is stacked on prepared sites (pads) and wetted with lixiviant chemicals under atmospheric conditions. The metal content is then recovered from the rich 'pregnant leach solution' through mineral processing (Zanbak C 2012). The main environmental concern in permitting dump leaching facilities is that of the pregnant leach solution and its containments, and thus it is absolutely imperative that no leakage takes place from the solution collection systems (Van Zyl D et al. 1998). Other ways of leaking solution can result from dump sliding, broken pipes, dam

failure, and the occurrence of overflows due to severe storm events.

Economic and sustainable management of dump leaching operations implies that the mining company should proactively adopt the best available practices in the design, construction, operation, maintenance, closure and post-closure of every component of these facilities. Modern environmental legislation has introduced the concept of 'best available technology', 'best available control techniques' or 'best available demonstrated control technique' which would ensure the elimination or the greatest degree of discharge reduction of pollutants in order to prevent groundwater contamination (Singh MM 2010). While the directives given by environmental authorities must follow a defined general pattern, the applications of the best available practices at particular mines will depend on several site-specific factors, such as the meteorology,



Table 1 General guidance/requirements for leach dump facilities

Criteria	General Guidance
Site characterization	Appropriate when topography, soil properties, vadose zone, surface and subsurface hydrology may influence the dump design
Surface water control	Identify all surface waters locations around the facility (lakes, springs, etc.). Information on 100-year floodplains in the area. Control of runoff and run-on.
Geological Hazards	Identify actual and potential geologic hazards (soil collapse, landslides, subsidence and settlement, liquefaction)
Solution/Waste/Tailings characterization	Identify chemical and physical characteristics of solution, waste and tailings
Pad construction	Site preparation for pad construction. Grubbing, grading and sub-grading the area.
Liner specifications	Design and installation of pad components. Appropriate specifications for non-storm water ponds, PLS impoundments, leaching dumps, tailings impoundments.
Stability design	Provide stability under static and seismic loading conditions. Shear strength evaluation. Recommended minimum factor of safety 1.3 (Non-storm water ponds, PLS Impoundments) and 1.5 static factor of safety for tailings impoundments. For leach dumps and engineered heap leach dumps, the recommended FOS for static analysis is 1.5 (if geosynthetic components are not used), and 1.3 otherwise
Closure /Post-Closure	Present a Closure/Post-closure plan to prevent/control releases

hydrogeology, topography, geology, and magnitude of the mining operation (Hearn RL & Hoye R 1998). A brief description of the general guidance to engineering criteria and best available practices is shown in Table 1.

Although all significant components in a leach dump systems should be evaluated, the present work will only focus on measure operation flow rates, retention check dams, and leach dump slope stability.

Case Study: ROM Leach dump

Final dump design can accommodate the placement and leaching of approximately 212-Million tonnes of ROM material (Figure 1) located in the Western US. This paper

evaluates the design and construction of the leach dump and associated leach collection facilities directed to satisfy the long-range mine plans and to meet environmental and civil design requirements. Items within the design criteria include regional design factors (design storm events and flow rates), leaching solution properties, application rate and design process flow rates. The base surface area will be compacted and graded to conduct pregnant leaching solution to the collection area located in the Southeast side of the leach dump. The dump design criterion has been developed to meet the requirements for liner systems, piping layout, and slope stability.

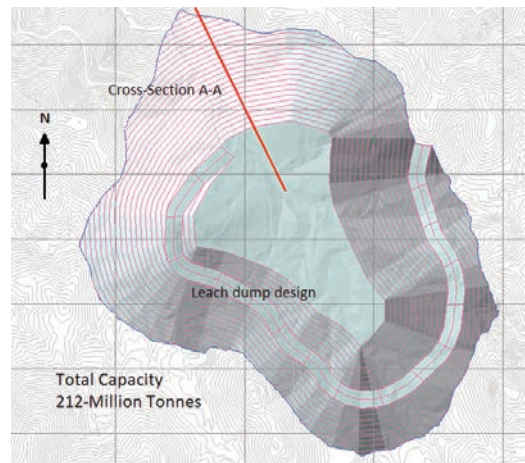


Figure 1 Leach dump design for a total capacity of 212-Million tonnes



Table 2 Summary of hydrology calculation results

Area (sq. miles)	Area (m ²)	Depth 100- yr, 24-hr (m)	Volume (m ³)	Leach dump Flow Rate (m ³ /s)
0.2559	662,896	0.0940	62,299	54.0

Operational flow rates

Surface water hydrology analysis around the proposed Leach Dump has been performed to determine the approximate peak stormwater runoff volume for the 100-year, 24-hour storm event. Sub-basin areas are calculated from the projection of the leach dump design to the topography. It is assumed that all rainfall will percolate through the leach dump and eventually will report to a contingency pond for capacity considerations, and the solution collection pipelines will discharge into the pregnant leach solution pond, with overflows reporting to the contingency pond in case of upset conditions. Rainfall depth is 0.094 m and the process solution flows were calculated assuming nominal solution application rate of 0.00489 m/h (Table 2)

Retention check dams

Check dams are structures installed perpendicular to water channels and are aimed to control wash off, trap sediments from run-

off and prevent discharge of pollutants to groundwater (ADEQ 2005). Small check dams can be used to reinforce the surface water control systems in conjunction with major dams or reservoirs. Check dams should be sized to retain the maximum volume of runoff attainable in considerations of site limitations and access and will protect the work during construction of the lined areas of the leach dump infrastructure. Runoff is calculated by amount of precipitation in the catchment area and by infiltration properties of the soil type and moisture (U.S. Depart, of Agriculture 1986). Check dams are placed within the dump limits in locations where high volume precipitation flow could negatively impact the leach dump foundation liners system during construction and prior to leach dump operation. The number of check dams, material quantities and storage capacities are estimated based upon storage requirements for a 100-year, 24-hour design storm event so that the impact on the dump foundation construction activities and downstream system due to precipitation are minimal (Figure 2)

Runoff depths for the 100-year, 24-hours storm for each watershed have been calculated using the TR-55 method (U.S. Depart, of Agriculture 1986). Total estimated runoff depth, then, is the starting point to design the check dams, so that the storage capacity created by check dams can exceed or be equal to

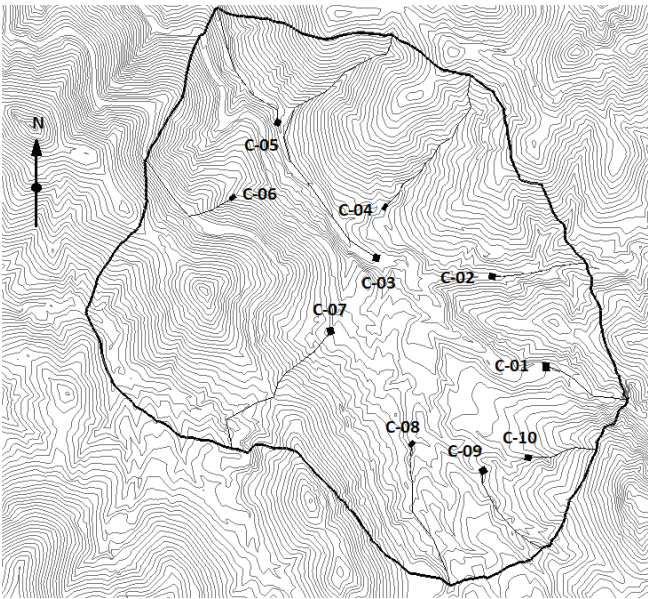


Figure 2 Check dam watershed site plan



Table 3 Check dam analysis

P = Rainfall 100-yr (m)	Curve number CN (m)	S=1000/CN - 10 (m)	$Q=(P-0.255)2/(P+0.85)$ (m)	Overexcavation depth (m)
0.094	2.210	0.038	0.060	1.5

Table 4 Check dam storage volume for the Optimized check dam model (10 total locations)

Check Dam #	Area Upstream of Dam (m ²)	Estimated Runoff (m ³)	Dam Height (m)	Dam Length (m)	Storage Volume Available (m ³)
C-01	19,974	1,199	1.5	167.6	2,370
C-02	38,090	2,286	4.6	174.3	8,104
C-03	65,961	3,959	4.6	576.1	26,759
C-04	56,950	3,418	4.6	306.3	14,297
C-05	42,364	2,543	3.0	249.3	6,957
C-06	100,335	6,022	7.6	216.4	21,178
C-07	82,962	4,979	3.0	319.4	8,945
C-08	45,151	2,710	1.5	278.0	3,899
C-09	23,133	1,388	1.5	188.1	2,676
C-10	15,979	959	1.5	134.4	1,911

the estimated runoff volume. The optimized model is subject to successive iterations by strategically placing each check dam to maximize its ability to retain stormwater. The optimization was performed iteratively using 5' contours to estimate storage capacity for each check dam at an upstream and downstream check dam slope of 2H: 1V.

The results for the optimized stormwater check dam placement are shown in Table 3-4 below. Note that P is rainfall in inches (NOAA 2018); CN is the curve number, S is the potential maximum retention after runoff begins (inches), and Q is runoff. Values for S and Q are calculated based on the TR-55 method (U.S. Depart, of Agriculture 1986).

In order to reduce the risk of damage to the dump foundation, construction of check dams is completed upstream of construction activities. Once the leach dump has been established and ready to receive run-of-mine material from the mine, checks dams will be covered. Because of the its temporary nature, check dams are exempt from freeboard and spillway construction

Leach dump slope stability

Leach dumps usually become these large mining structures for which slope stability studies must be considered in their designs.

Appropriate procedures for stability analysis of leach dumps are determined by the type of rock the dump is composed, whether it is classified as hard or soft rock, and other dump design considerations that include: maximum height, volume, slope angle, foundation material and conditions, and berms at the edges of lifts (Marcus 1997). Leach dumps built with hard, durable broken rock will be stable under static conditions and will only require evaluating slope stability if failure can occur through potentially weak foundation. On the other hand, for dumps built with soft rock, static and seismic stability analysis should be performed. The factor of safety (FOS) is the minimum ratio of available shear strength to the shear stress required for equilibrium. The recommended FOS is 1.3 for leach dumps where site specific testing and geosynthetic material have been used, otherwise the recommended FOS is 1.5 (ADEQ 2005).

A limit-equilibrium analysis was performed to assess the global stability of the leach dump for the ultimate design. The slope stability method calculates the minimum shear stress to maintain the slope stable. The maximum shear resistance is calculated for the corresponding shear surface using rock strength properties and pore water pressures. One cross-section has been analysed that best



Table 5 Material Properties

Material name	Unit Weight (kN/m3)	Effective Cohesion (KPa)	Friction angle (degrees)
Foundation	22	900	35
Low Grade ROM	21	0	37
Oxide ROM	21	0	37

represent the most adverse slope conditions using a two-dimensional, limit equilibrium modelling software Geo Studio Slope/W (GeoSlope 2012). Morgenstern-Price method of analysis was used to evaluate every cross-section, considering both static and seismic conditions. An effective friction angle of 37degrees (angle of repose) that corresponds with a slope of approximately 1.3H: 1V sustains slope inclination of the ROM leach dump. Prior to ROM material deliveries, dump footprint will be covered by a liner protection system (liners and geomembranes). Afterwards and during the entire dumping operation, a consistent leaching solution flow, runoff and rain water should be maintained through the leach dump and collection channels.

Based on the mine plans, the dump consists of three main components: a liner system at the dump foundation, low grade ROM ma-

terial until a horizontal level is established to place Oxide ROM material on top. The slope geometries of the cross sections used in the analysis is provided in Figure 3. Stratigraphy and material properties used in slope stability are summarized in Table 5. In addition, the hydrostatic head in the proposed dump design is assumed to be 1 m.

Conclusions

Environmental quality standards may be violated around active leach dump facilities by leachates discharges that can seep into the groundwater. Therefore, the applications of efficient water management practices in mining are mandatory for permitting approval and renewal. Modern environmental regulations that adopt the concept of ‘best available technology’ work dynamically and are open to using state-of-the-art technology that has proven to be the best available in the industry.

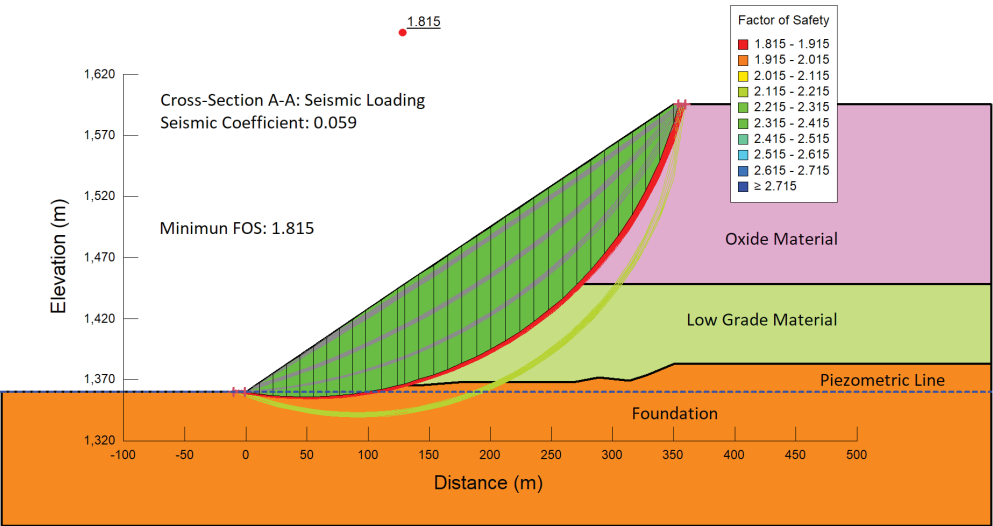


Figure 3 Slope Stability Analysis. Cross-Section A-A



References

- Arizona Department of Environmental Quality ADEQ (2004) *Arizona Mining Guidance Manual BADCT, Aquifer Protection Program*. Publication TB 04-01
- Hearn RL, Hoyer R (1998) Copper Dump Leaching and Management Practices that minimize the potential for environmental releases. Hazardous Waste Engineering Research Laboratory. Office of Research and Development. U.S. Environmental Protection Agency. Ohio
- GeoSlope International (2012) *Modelling with SLOPE/W Manual*
- Marcus JJ (1997) *Mining environmental handbook: effects of mining on the environment and American environmental controls on mining*. United Kingdom: Imperial College Press
- NOAA Atlas 14, National Oceanic and Atmospheric Administration (2013) Point Precipitation Frequency Estimates. <http://hdsc.nws.noaa.gov/hdsc/pfds>
- U.S. Department of Agriculture, Soil Conservation Service, Engineering Division. (1986), *Urban Hydrology for Small Watersheds*. Technical Release 55, 2nd ed
- Van Zyl D, Hutchison IPG & Kiel JE (1988) *Introduction to evaluation, design, and operation of precious metal heap leaching projects*. Littleton, Colo, Society of Mining Engineers.
- Singh MM (2010) *Water Consumption at Copper Mines in Arizona*. State of Arizona. Department of Mines & Mineral Resources. Special Report.
- Zanbak, C. (2012) *Heap Leaching techniques in Mining, within the context of best available techniques (BAT)*. Euromines – The European association of mining industries, metal ores & industrial minerals.





International Network for Acid Prevention (INAP)

Gilles Tremblay¹, Bruce Kelley²

¹INAP Technical Manager, Ottawa, Ontario, Canada

²INAP Senior Advisor, Melbourne, Australia.

Abstract

Acid rock drainage (ARD) or acid and metalliferous drainage (AMD). is one of the most severe and potentially enduring environmental problems of the mining and minerals industry. High liability costs carried by many mining companies to cover potential costs of ARD/AMD are a clear indication of the magnitude of the problem. Unmitigated, ARD/AMD can result in water quality impacts that could well be the industry's most significant financial and credibility risk. Effectively preventing acidic drainage is a daunting challenge that requires all of a mining company's technical and managerial resources. Successful ARD/AMD prevention also entails engaging industry stakeholders throughout the entire life-cycle of a mine.

The International Network for Acid Prevention (INAP) is an international network of mining companies dedicated to the prevention and mitigation of acid rock, saline and neutral drainage and metal leaching to support sustainable mining. INAP is committed to assist in building capacity of all stakeholders whether they be large or small operators, regulators or communities through relevant research, information transfer and continuous improvement of operational and remedial practice. INAP has grown into a proactive, global leader in the field. INAP is in turn supported by the Global Alliance, which pulls together technical expertise and knowledge from across the world.

The key element in INAP's sustainable mining program is the development and maintenance of globally-recognized, authoritative technical guides, such as Global Acid Rock Drainage (GARD) Guide and the Global Cover System Guidance Document, both international best practice guides to address issues for the prevention of acid-rock, neutral and saline drainage.

In this presentation, examples of best practices and how mining companies can obtain value from the technical guidance documents will be given along with an update on future projects, including how INAP is working to make the GARD Guide more effective and useful to all stakeholders worldwide. Lastly, a few words on the Global Alliance, and how INAP works closely with these groups that have significant technical and regional expertise on ARD/AMD to offer.

Keywords: INAP, acid rock drainage, GARD Guide

Introduction

Acid rock drainage (ARD) or acid and metalliferous drainage (AMD). is one of the most severe and potentially enduring environmental problems of the global mining and minerals industry. The potential for acidic drainage to form from mining has been known since at least 1556 and ARD was observed as early as 1698 associated with coal mining in Pennsylvania (BC Acid Mine Drainage Task Force, 1989). Research into the process of ARD/AMD formation and methods to minimize its impact has been ongoing for over 50 years.

At first, successful revegetation of tailings sites was thought to be a sustainable solution but it was soon realized that this major environmental issue persisted and could require in perpetuity treatment if poorly managed. There was a need to better understand the processes involved, and for new remedial technologies to be developed and demonstrated. Much progress has been made in the last 25 years through a number of research organizations and consortiums resulting in a considerable body of scientific and engineering guidance available on ARD/AMD.



Who is INAP?

INAP is a global industry led group of mining companies focused on the adoption of site-specific best practices to prevent acid rock drainage (ARD) or acid and metalliferous drainage (AMD). Responsible management of these materials, some reactive, through to beyond closure is critical. INAP provides an international focus on this issue to mobilize information, experience and resources to prevent ARD/AMD. The network was created in 1998. Present members are: Anglo American, Barrick Gold Corp, BHP, Kinross Gold, Newcrest Mining, Newmont Mining, Rio Tinto Ltd, Teck Resources, Detour Gold and Lundin Mining. INAP is operated as a company, registered in Australia. The Technical Manager is Gilles Tremblay. INAP has an operating committee made up of member company representatives, and its activities are overseen by the INAP Board.

Benefits of INAP membership are primarily associated with its support for best practice and the development and transfer of knowledge. These benefits include:

1. INAP initiates and supports site-based projects which return significant benefits to its members. These benefits can provide immediate financial benefit, as demonstrated by the Diavik scale-up project that resulted in a \$40 M CDN bond reduction, as well as reduced closure costs by avoiding or minimizing the need for long-term water management. INAP provides leveraged seed money to promising research projects helping attract funding from government, academic and industry sources.
2. INAP facilitates the development and maintenance of globally-recognized, authoritative technical guides, such as the GARD and Global Covers guides, that serve to:
 - a. Promote proven ARD/AMD management strategies
 - b. Lend credibility to broad adoption of pragmatic strategies aiding industry in regulatory engagement and permitting
 - c. Reduce environmental risks and financial liabilities across the industry.

3. INAP provides a forum for industry experts and managers to meet and candidly discuss common challenges, opportunities and solutions.
4. INAP facilitates knowledge transfer and collaboration across the mining, academic, consulting and regulatory communities through the International Conference on Acid Rock Drainage (ICARD), workshops on recent advances in the field, newsletters and its Global Alliance network. It galvanises global expertise on ARD/AMD prevention and management.

INAP has also successfully coordinated an international network of AMD/ARD practitioners which includes key regional ARD/AMD organizations. The Global Alliance (GA) partnership was launched in 2003 and is an international model of interaction among organizations involved in acidic drainage research. The GA brings numerous benefits to the partners, including minimizing research duplication, maximizing research dollars, worldwide links, and enhanced technology transfer capabilities. Members of the Global Alliance include:

- The Sustainable Minerals Institute (SMI) in Australia,
- The Acid Drainage Technology Initiative (ADTI) in the USA,
- The Mine Environment Neutral Drainage (MEND) program in Canada,
- The International Mine Water Association in Europe
- The Water Research Commission (WRC) in South Africa
- The South American Network for Acid Prevention (SANAP)
- The Indonesian Network for Acid Drainage (INAD).

INAP continues to drive the expansion of ARD/AMD efforts across the globe. In 2016, INAP focussed its effort on Australia to encourage an ongoing interaction among the ARD/AMD community, including INAP companies, ARD/AMD consultants, regulators and other stakeholders. Dr Bruce Kelley, one the founding members of INAP, continues to spearhead these efforts that have resulted in an Australian network that is more active. Annual meetings are being held which



include INAP company member business followed by a more general INAP/AMD meeting. The overarching focus of the meetings are to gain a better understanding of ARD/AMD issues, expertise, capacity and capability across Australia, with a number of presentations scheduled, but also covers other aspect such as project development, the Australian AMD Workshop and ICARD conference. The success of the Australian model, using a very experienced ARD/AMD practitioner to provide support and coordination through INAP is an option that could be pursued on a limited basis in other regions.

INAP’s achievements and current activities

One of INAP’s major achievements has been the development, publication and promotion of the GARD Guide, a global practical, reference document on “how to” prevent, minimize and control ARD/AMD under all climatic conditions. This guide brings together the best technical and management practices to enhance the capabilities of global ARD/AMD practitioners. It is free for use by all mining industry stakeholders and can be downloaded from www.gardguide.com. It references and makes ample use of numerous guidance documents including those published by the Australian Department of Industry Tourism and Resources, MEND (Canada), WRC (South Africa) and US Environmental Protection Agency (US EPA). While this guidance document is not prescriptive, increasingly regulatory agencies are recommending its use by proponents, operators and land managers. Examples where it is referenced include the US EPA, the Interstate Technology and Regulatory Council (ITRC) web pages and in mining guidance documents prepared by International Finance Corporation (IFC).

Since its roll-out in 2009, the GARD Guide has been updated three times and plans are in place for a fourth update. The original version of the GARD Guide was compiled by an international team of consultants and academics lead by Golder. Since that first version, numerous organizations and consulting firms have participated in additions and upgrades to the GARD Guide. A review of all

chapters was conducted in 2017 by numerous experts and their recommendations will be used to select chapters for upgrades starting in 2018. Feedback received to date has been largely positive. INAP continues to look for ways to improve the Guide, including making the guide more accessible by providing summaries with key messages for the non-technical users at the beginning of each chapter and providing guidance to the user on which option is most appropriate in the circumstances at a specific site.

Early in 2018 INAP released the Global Cover System Design – Guidance Document. This document, like the GARD Guide, is intended as a best practice summary to assist mine operators, designers, and regulators to address issues where cover systems can be employed. It builds on previous technical guidance documents on cover system design, construction, and performance monitoring. The Global Cover System Guidance Document will be of interest to individuals who are seeking more detailed information than what is outlined in Section 6.6.6 of the GARD Guide – Engineered Barriers.

A holistic framework, at both high and conceptual levels is presented for management of reactive materials during operations and at closure. Application of this framework is achieved through the use of a cover system design tool that walks users through relevant climatic factors to optimize cover system design alternatives for a desired performance design criteria (e.g. control of net percolation or oxygen ingress). This allows users to understand more realistic objectives when developing cover system design alternatives based on site-specific climate conditions.

The information provided within the tool is not a replacement for site-specific classification and engineering required for cover system design. However, the tool is a means of beginning early conceptualization to help focus further investigation at a site level and to begin to form realistic expectations for cover system performance at an early stage of a project. The Global Cover System Design document is available from the INAP website.

INAP also participates in collaborative research investigations. Typically, these efforts concentrate on large-scale projects that re-



quire large collaborative efforts or large-scale demonstration. An example of this is a mine waste scale-up project in Northern Canada, which sought to correlate small scale test work with large scale reality. The project concept was conceived by INAP member companies. Sponsors for this university-led project included the mine operator, MEND, the Natural Sciences and Engineering Research Council of Canada, and INAP. The waste management data from this 10-year project helped support a \$40 million CND reduction in closure bonding associated with the site's mine waste storage strategy. A secondary benefit of this project was the successful development of many highly qualified students that have since or will soon join the mining and minerals industry.

Recently, INAP agreed to participate in the Toward Environmentally Responsible Resource Extraction Network (TERRE-NET), a multi-institutional and multi- and trans-disciplinary research Network comprised of 15 co-investigators from 7 universities across Canada, with the overarching goal of ensuring the “environmentally responsible, socially acceptable extraction of mineral and energy resources using cutting-edge approaches and technologies”. This five-year initiative is supported by numerous partner organizations, as well as Canadian and international research collaborators.

INAP needs to continue its position of promoting ARD/AMD prevention best practice and excellence in mine closure industry-wide to all stakeholders. In recognition and international acknowledgement for mine sites for their work, INAP is sponsoring an international award for the implementation of best practice in the identification, planning and management of potentially reactive geologic materials at a mining site. The awards will be presented at ICARD, which are held every 3 years.

The first recipients of INAP's international ARD Best Practice Award were recently announced and are Kinross Brazil for their operation of their Paracatu site in Brazil and Rio Tinto's Iron Ore Pilbara operations at the corporate level. Both operations were found to exemplify global best practice and deserve international recognition. These awards will

be formally presented to Kinross Brazil and Rio Tinto Iron Ore at the 11th International Conference on Acid Rock Drainage (ICARD) in Pretoria, South Africa in September 2018.

INAP also sponsors and is the home of ICARD, the International Conference for Acid Rock Drainage, which is held every 3 years. The 10th ICARD took place in Santiago, Chile in April of 2015, where over 400 delegates from 22 countries attended 186 technical presentations. The 11th ICARD will be held in Pretoria, South Africa in September 2018 and hosted by the International Mine Water Association (IMWA). Previous ICARDs have been held in Norway (1988), Canada (1991, 1997 and 2012), United States (1994, 2000 and 2006), Australia (2003), and Sweden (2009).

Technology transfer is an important element of collaborative partnerships, especially with partners scattered throughout the globe. Examples of INAP's technology transfer or capacity building program include specialty workshops and short courses as well as GARD Guide short courses. Funding is also provided to sponsor GA workshops such as the Annual British Columbia / MEND Workshop in Vancouver and INAP members are asked frequently to provide presentations at various national and international events. Newsletters are produced up to three times a year and are a great way to enhance communications and a new INAP website was developed (www.inap.com.au)

Recent Activities of the Global Alliance

INAP's profile continues to grow internationally. The Global Alliance (GA) is an important part of this growth and GA members are invited to participate in the semi-annual INAP meetings with member companies to network and update the group on their regional activities. The INAP Newsletter is also used as a vehicle to publish key GA activities.

INAP also seeks to recognize recent relevant reports that have been published by Global Alliance members. In 2017, MEND published a report that examines and compares alternatives to conventional slurry for the management of tailings. This report presents a snapshot of the current state-of-



practice in the mining industry in Canada, and other countries with similar climatic conditions. It looks at the technologies used to dewater tailings, how tailings are placed and managed, and evaluates their relative efficacy in addressing physical and geochemical risks. The report titled Study of Tailings Management Technologies MEND 2.50.1, can be downloaded from the MEND website at <http://www.mend-nedem.org>.

The Water Research Commission (WRC) actively contributes to South Africa's water knowledge base by funding fundamental water research, growing scientific capacity and disseminating knowledge to a broad range of stakeholders through focused workshops and relevant guidance documents. One excellent example of the type of information available is the launching of a national mine water atlas for South Africa (<http://www.wrc.org.za/Pages/MineWaterAtlas.aspx>). It shows the critical interplay between mining and water resources and is the most extensive set of documents of its kind. More articles and reports are available from the WRC website at (www.wrc.org.za).

The major effort of Acid Drainage Technical Initiative (ADTI) has been the preparation, editing and publication of a set of 6 workbooks in the Management Technologies for Metal Mining Influenced Water series. The sixth volume, Geochemical Modelling for Mine Site Characterization and Remediation is now available. This handbook describes the important components of hydrogeochemical modelling for mine environments, primarily those mines where sulphide minerals are present – metal mines and coal mines. Copies of the six handbooks from this series can be purchased from the SME online bookstore at <http://www.sme.org/books/>.

The transfer of information on developed technologies to partners and the public has always been an important element for GA members. Workshops are a very effective way of bringing ARD/AMD practitioners together. The annual BC-MEND ARD/ML Workshop in Vancouver, the biannual Australian AMD Workshop and the annual International Mine Water Association (IMWA) Congress are examples put on by regional organizations that bring together technical presentations from leading global practitioners.

Future Development Opportunities

INAP is continually looking for new ways to improve ARD/AMD management. In particular it is focused on an industry wide and global approach. Some of the ideas currently under consideration include:

- Can the successful scale up project in Canada at Diavik be extended to include other geographies, climates and different mineralogy? Could similar projects be run in Australia, South America or Africa?
- Poor management of waste rock is the major contributor to the ARD/AMD problem globally. How can waste rock piles/dumps be constructed in a way that reduces the risk of ARD generation?
- Improving our understanding of the global extent of pit lakes and voids, including their locations, chemistries, liabilities and opportunities that they might offer? Are there better ways to obtain data on these to inform closure considerations?
- Effective mine planning is one of the keys to improving ARD/AMD management. How can mine planners be more effectively engaged? This might include specific, less technical sections in the GARD guide, input into mine planning workshops and webinars providing a better understanding in hydrogeochemistry, and changes to mine operating practices.
- Development of a powerful business case around ARD/AMD management. This would enable more effective engagement of company senior management.
- Understanding treatment options that are currently operating as a black box. How can mine operators have more confidence and understanding of the numbers from suppliers?
- Develop and share more effective tools to evaluate risks for ARD/AMD, neutral drainage and salinity, across the industry.
- Develop a suite of powerful case studies. Learning from failures is very important. A financial case study highlighting the benefits of effective mine planning could also be of value.
- Harnessing the power of major workshops and conferences to better identify major, industry wide ARD/AMD best practices and new opportunities.



INAP will be focusing on these and other issues as part of its on-going strategy and project implementation plan.

Conclusion

INAP evolved through an urgent need to combat a global environmental issue. It remains a powerful example of how companies can work collaboratively and collectively when faced with major challenges. INAP has also brought ARD practitioners together through its Global Alliance, enabling far better connectivity between industry issues and those with the skills to address them. Over the past number of years, many sites have successfully demonstrated that these issues can be successfully managed to avoid legacy environmental impacts. Importantly INAP

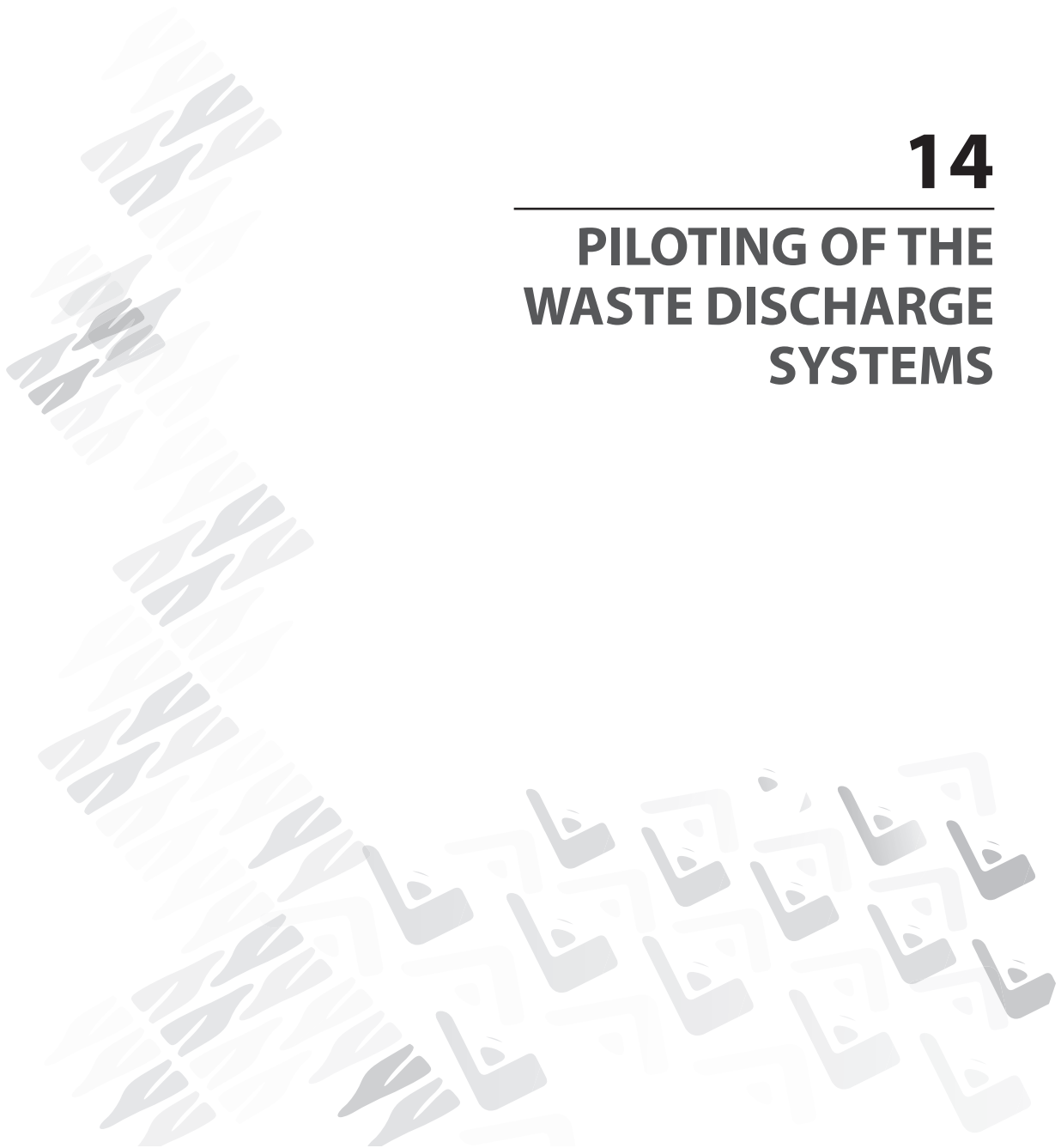
is industry led and its member companies continue to drive for leadership in addressing one of the most significant environmental issues facing the industry.

References

- BC Acid Mine Drainage Task Force 1989. Draft Acid Rock Drainage Technical Guide – Volume I, BC AMD Task Force, Vancouver.
- International Network for Acid Prevention (INAP), 2014. The Global Acid Rock Drainage Guide. (www.gardguide.com)
- International Network for Acid Prevention (INAP), 2017. Global Cover System Design – Guidance Document (www.inap.com.au).
- MEND 2.50.1 (2017) Study of Tailings Management Technologies. (<http://www.mend-nedem.org>).



**PILOTING OF THE
WASTE DISCHARGE
SYSTEMS**





A Pilot Optimisation of Sulphate Precipitation in the High-Density Sludge Process

Bernard Aubé¹, Moacir Lamares², Stéphan Lone Sang³

¹*Envirobay Inc., Sainte-Anne-de-Bellevue, Québec, Canada*

²*Sociedade Mineira de Neves-Corvo, S.A., Portugal*

³*Wood Environment & Infrastructure Solutions, Montréal, Québec, Canada*

Abstract

High sulphate concentrations can cause issues both in a mine's process water recycle and for effluent discharge. This is the case for the Neves-Corvo mine in Portugal. A large study looked at control of sulphate and the part presented here details the optimisation of sulphate removal in the high-density sludge (HDS) process. The HDS process was operated at different pH setpoints, varying sludge recycle rates, and several different reactor retention times for three different water sources. An added step in the process was the addition of carbon dioxide to precipitate calcium carbonate and further minimise the gypsum saturation level. The tests defined optimal HDS conditions to provide improved feed conditions for nanofiltration or for non-scaling process water.

Keywords: Sulphate removal, HDS process, gypsum precipitation, calcium carbonate, nanofiltration, reverse osmosis

Introduction

The Neves-Corvo Mine is located in Baixo (Lower) Alentejo, on the south edge of the Iberian Pyrite Belt. The nearest town is Castro Verde, Portugal. It is operated by Sominco (Sociedade Mineira de Neves Corvo SA), a subsidiary of Lundin Mining. Neves-Corvo is the biggest copper and zinc mine in the European Union and has been in operation since 1988.

Prior to 2014, the mine had experienced problems with site water quality, both internally and in their final effluent. A project was initiated to evaluate commercially available options which could be applied to meet the water needs, both for effluent discharge to the environment and for internal use and consumption as a process water recycle. Within this project, a pilot plant study was completed to evaluate the most economic and efficient process to oxidise thiosalts, precipitate metals, and to reduce sulphate concentrations. The base process of the pilot campaign was the conventional HDS process.

In addition to the HDS process, the pilot test plan included thiosalt oxidation and various sulphate removal techniques such as barium hydroxide precipitation and membrane

filtration (both nanofiltration and reverse osmosis). These other tests are discussed in a separate paper (Aubé et al, 2018).

This paper presents the new and extensive tests reviewing all aspects of the HDS process to decrease total dissolved solids in the treated effluent. The HDS process was operated at different pH setpoints, varying sludge recycle rates, and several different reactor retention times. This was done for three different water sources: 1) acid water, 2) process water including thiosalts, and 3) nanofiltration concentrate. The results are detailed in the next sections for these three types of feed waters.

The results of the pilot test were used to design the full-scale treatment plant with confidence. The process setpoints developed in these tests could be applicable to other mine sites around the world for improved HDS treatment and minimisation of the gypsum saturation level and total dissolved solids concentration.

Materials and Methods

The pilot plant was operated on-site at the Neves-Corvo Mine continuously from October to December 2015. As shown in Figure 1, the pilot plant was built inside a 40-foot-





Figure 1: Pilot plant used for the study

long maritime container. The pilot plant was provided by Wood (formerly Amec Foster Wheeler). The two pools near the plant were used to prepare different feed water qualities expected under future mine operating conditions.

The pilot plant consisted of a series of engineered PVC reactors equipped with baffles and risers. Agitation was provided using radial impellers when the reactor was also aerated or axial impellers when there was no gas sparging. The design flowrate of the plant was 2 L/min, but it was sometimes operated at 1 L/min for certain tests. A 150-cm high and 50-cm diameter clarifier with a conical bottom and a rake system was used for solid/liquid separation. The pilot plant was also equipped with a membrane filtration skid for nanofiltration or reverse osmosis.

A programmable logic controller (PLC)

system allowed the pilot plant to run unattended for short periods of time and to log key parameters. Reagents, including lime slurry, hydrogen peroxide, ferric sulphate as catalyst, an anionic flocculant, barium hydroxide and carbon dioxide, were fed from reagent storage tanks. Lime feed was controlled by pH and other reagent addition rates were controlled by flow. Air was sparged into reactors when ferrous oxidation was required, and carbon dioxide was used for calcium carbonate precipitation.

Physico-chemical parameters and reagent storage tanks levels were recorded several times per day. The solids content of the different reactor slurries and of the clarifier sludge were measured regularly. Filtered samples were taken twice daily from all reactors to monitor the dissolved concentrations of key elements.

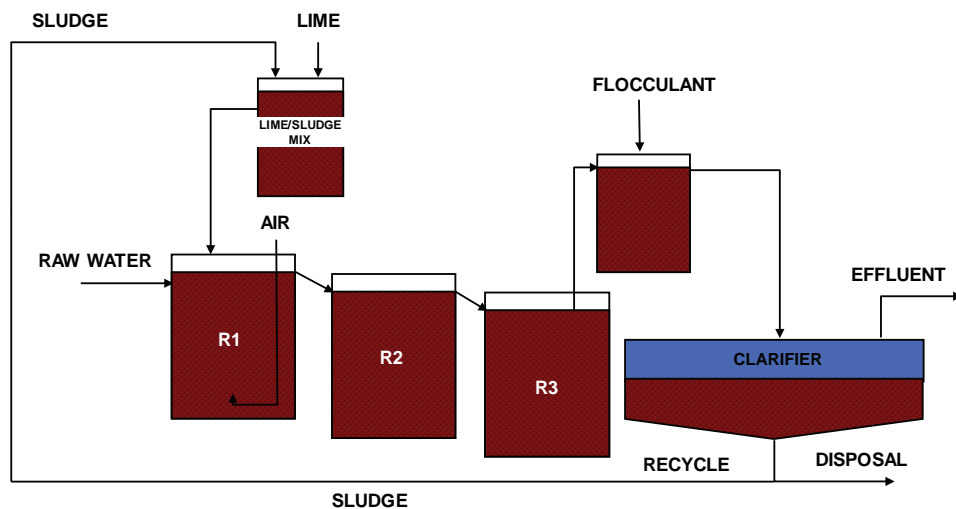


Figure 2: HDS process



Description of Processes

The central component of the pilot plant was an HDS system that allowed enough flexibility to evaluate different retention times, pH setpoints, and sludge recycle flowrates (Figure 2). The HDS process is well-known and described in detail elsewhere (Aubé and Lee, 2015). As a summary description of the HDS process applied here, high-sulphate water was contacted with a mixture of recycled sludge and lime slurry in a reactor. The quantity of lime slurry added in the Lime/Sludge Mix Tank was controlled to maintain the pH of the overflow in the first reactor. Neutralisation reactors were added as needed to provide additional retention time. This formed a slurry consisting of treated water with fresh precipitates combined with recycle sludge solids. This was then flocculated and fed to a clarifier for solid-liquid separation.

To meet the site water objectives, additional process options were evaluated. Notably, a thiosalt oxidation reactor using Fenton's reagent was installed upstream of the HDS for some of the tests. A barium hydroxide reactor was also introduced in the HDS process to precipitate sulphate as barium sulphate for two of the tests. Nanofiltration and reverse osmosis membranes were tested on the feed water upstream of the HDS process and on the HDS effluent. Those distinct process arrangements resulted in different water qualities being evaluated in the HDS section of the process.

Fenton's reagent is a combination of peroxide and iron (Rolia, 1984). These tests, as well as the barium precipitation and membrane filtration tests, are discussed in Aubé et al, 2018.

Acid Water Tests

The first water tested was an acid water source from the tailings area named Cerro do Lobo (CdL). This acid mine drainage (AMD) contains tailings runoff and residual process water from the paste tailings disposal. It is characterised by a low pH near 2.6 and high Fe content averaging 213 mg/L (total). The total sulphate content averaged 4,577 mg/L. This water also contained high Na (983 mg/L), Ca (627 mg/L), and Cl (565 mg/L). The sodium chloride content is mostly from the ore. This salinity significantly affects the equilibrium saturation level of gypsum in the HDS process as the activity (or effective concentration) is decreased for the calcium and sulphate.

CdL water was fed to the HDS process for treatment at pH 10.0 with reactor retention times varying from 0.5 to 4.0 hours. The sludge densification was very efficient, with the minimum target of 20% solids attained within 2.5 days of operation. The highest sludge density attained was 35% solids, without any pumping or viscosity problems. The sludge recycle rate was controlled to maintain a target reactor solids content between 30 and 40 g/L. As gypsum tends to form more readily onto existing gypsum precipitates, higher reactor solid contents serve to offer more precipitation sites onto which the dissolved sulphate and calcium can precipitate. However, the amount of solids to be maintained in the reactor is limited by the flocculation efficiency. If the reactor solids content is too high, the flocculant will not attach to a sufficient fraction of the particles and the clarifier overflow will contain a high total suspended solids (TSS) content. Despite this theory, even at reactor solid contents as high as 45 g/L, the clarifier overflow turbidity and total

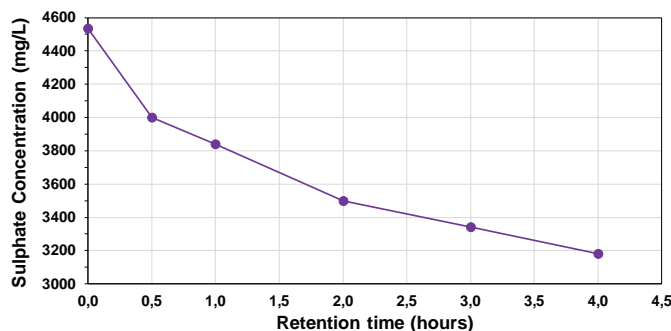


Figure 3 Sulphate concentration versus retention time for CdL waters



suspended solids content were low, averaging of 4.2 NTU and 10.7 mg/L TSS. In the best conditions, the TSS was maintained below 4 mg/L.

Figure 3 shows that increasing the retention time up to 4 hours incrementally increased gypsum precipitation and sulphate removal. It is clear that the higher retention time improved sulphate removal as even between 3 and 4 hours retention time, there was an added sulphate removal of 160 mg/L.

The final sulphate concentration attained at Neves Corvo (3200 mg/L) is high in comparison to what is achievable with HDS treatment at other mine sites. This is due to the very high sodium and chloride concentrations of the Neves Corvo waters. This high salinity increases the solubility of all other elements in solution. Despite this comparatively high final concentration, the data clearly indicate that sulphate precipitation as calcium sulphate (gypsum) is improved with increased retention time.

Process Water Tests

A synthetic water was generated on site to simulate future operating conditions. The mixture was composed of 50% CdL water, 30% overflow from the paste tailings thickeners, and 20% mine water. This process water was blended in two 55 m³ pools and fed to the pilot plant. The water is characterised by a pH that ranged from 2.7 to 3.3, Fe content averaging 94 mg/L and sulphate averaging 3692 mg/L. Thiosalt concentrations averaged

467 mg/L. Ca, Na and Cl concentrations are respectively 702, 906 and 505 mg/L.

Fenton's oxidation (hydrogen peroxide catalysed with ferric sulphate) in the first reactor was used to oxidise thiosalts prior to treatment by the HDS process in subsequent reactors for metals and gypsum precipitation. This process is detailed in Aubé et al, 2018. Essentially, oxidation with Fenton's reagent converts the thiosalts (thiosulphates and other polythionates) to sulphate.

In the HDS portion, three pH setpoints (10.5, 11.0 and 11.5) were tested to evaluate the effect on sulphate removal. Filtered samples from each reactor were analysed to evaluate the progression of gypsum precipitation (Figure 4). This figure shows an increase in sulphate concentration in the Fenton Reactor, despite some gypsum precipitation occurring simultaneously in this reactor. Complete thiosalt oxidation alone would have produced in the order of 800 mg/L of sulphate and the increase in Fenton's Reactor was in the order of 200 mg/L.

Figure 4 shows two important conclusions from the trials: an increased retention time up to 5 hours clearly shows improved gypsum precipitation, and a pH setpoint of 11 improves sulphate removal over pH 10.5 or 11.5. There appears to be only a slight improvement of sulphate removal beyond the 5-hour retention mark, but this is unclear.

During this test, the sludge density generally varied between 20 to 30% solids. The reactor solid contents often exceeded the maxi-

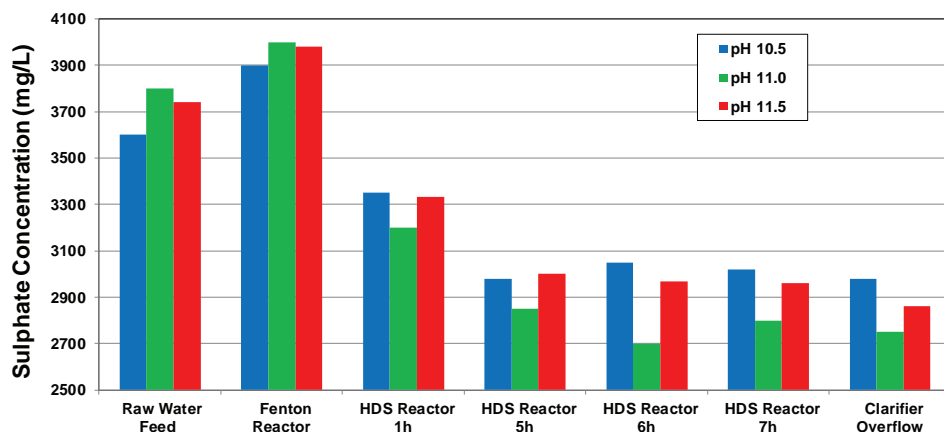


Figure 4 Sulphate concentrations throughout the Fenton-HDS process



mum target of 40 g/L, even going beyond 60 g/L at times. Despite this, the clarifier overflow remained clear and the TSS was maintained well below the target with an average of 8.4 mg/L.

Nanofiltration Concentrate Tests

Nanofiltration tests were conducted to remove sulphate to low levels, meeting strict guidelines of 250 mg/L for discharge (Aubé et al, 2018). The results presented here are from a test where the sulphate-rich concentrate issuing from membrane filtration was treated using HDS. Prior to nanofiltration (using an NF270 membrane), the process water had been treated via Fenton-HDS, as per the previous section, removing metals and thiosalts. Therefore, the concentrate treatment in this 5-hour HDS test was focused specifically on sulphate removal.

The nanofiltration concentrate fed to the HDS process had an average pH of 4.7 with sulphate at 4500 mg/L, Ca at 856 mg/L, Na at 1000 mg/L and Cl at 462 mg/L. As the water fed to the nanofiltration membrane had previously been treated by the Fenton-HDS process, the thiosalts and Fe contents were low (37 and 1 mg/L, respectively). A key factor to consider is that an anti-scalant (SpectraGuard 250) had been added during the nanofiltration tests. As an anti-scalant is designed to inhibit precipitation, it could affect gypsum formation in the HDS process.

The sludge produced from this process

was white and consisted almost entirely of gypsum. It had reached 20% solids content after only 3 days. Two pH setpoints were operated during this test and it appeared that the final sulphate concentration was approximately 100 mg/L lower when operating at pH 11.5 over pH 11.0. It is unclear if the anti-scalant had a significant impact, as the final concentrations attained, though higher than for other tests, are also affected by the higher salinity of the concentrate. A clear and consistent increase in sulphate removal was shown for increased retention times up to 3 hours, beyond which only a marginal increase was measured (67 mg/L).

Reducing Calcium Concentration

Gypsum precipitation, the source of scaling problems, is a function of both sulphate and calcium concentrations. In order to provide an improved water quality for either a membrane feed or for re-use at the mine, decreasing calcium would be a significant benefit. Also, the optimum pH setpoint in the HDS process was defined as pH 11.0, which is above the maximum water quality objective of 10.0. Trials were conducted using carbon dioxide sparging in a final reactor with a 30-minute retention time, prior to the clarifier and solid/liquid separation, to see if both pH reduction and some calcium removal could be simultaneously attained.

The target pH for calcite precipitation requires a balance between the amount of car-

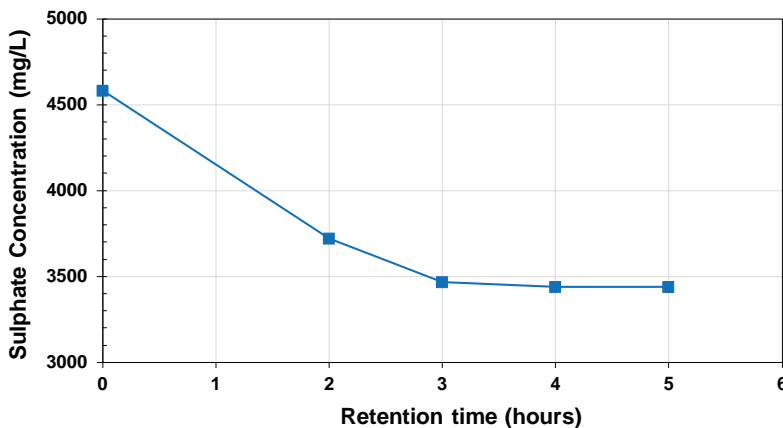


Figure 5 Treatment of nanofiltration concentrate with respect to retention time



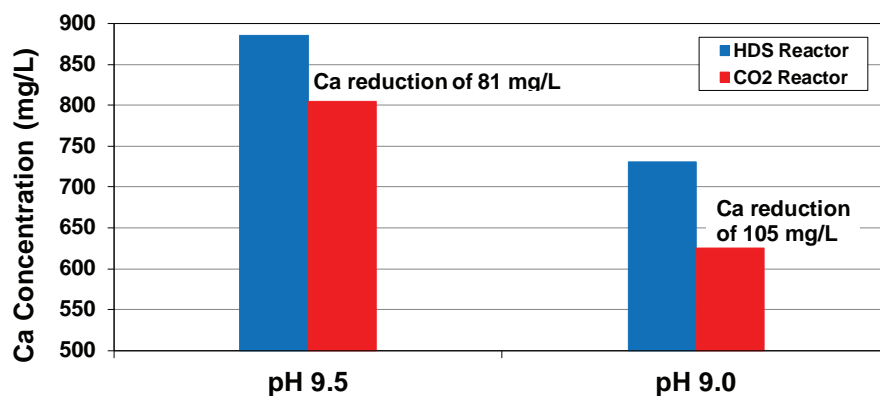


Figure 6: Calcium removal with carbon dioxide sparging

bon dioxide added and the form in which it is present. Precipitation only occurs with the CO_3^{2-} form, which is predominant at high pH values. At a pH of 9.0, less than 5% of the total inorganic carbon is in CO_3^{2-} form while at pH 9.5, almost 10% is in the desired form. The results shown in Figure 6 indicate that both these pH setpoints decreased Ca concentrations significantly, with pH of 9.0 showing a slightly better removal with a 105 mg/L difference.

Conclusions

Results of this pilot campaign clearly showed that sulphate removal through gypsum precipitation improves with retention time. Significant added precipitation was shown in all cases for the first 3 hours and marginal improvement beyond 4 hours and up to 7 hours retention.

For treatment of acidic water, a setpoint pH of 11 performed best for sulphate removal. When treating a nanofiltration concentrate, pH 11.5 was slightly better over a setpoint of 11.0.

The pilot results clearly indicated that higher concentrations of gypsum solids in the

reactors improved sulphate removal. The tests showed increased sulphate precipitation and a clear effluent with reactor solid contents of up to 60 g/L.

Sparging carbon dioxide in the process as a final step before the clarifier serves to both decrease the final effluent pH and reduce the final calcium concentration, thus producing a treated effluent with lower scaling potential. A setpoint pH of 9.0 showed better results than pH 9.5.

References

- Aubé, B., Lamares, M, Lone Sang, S., 2018 “A Pilot Comparison of Sulphate Removal Technologies at Neves Corvo”. Paper presented at the 11th ICARD | IMWA | MWD 2018, Pretoria, South Africa.
- Aubé, B., Lee, D.H., 2015. “The High Density Sludge (HDS) Process and Sulphate Control”, Paper presented at ICARD-IMWA 10th International Conference on Acid Rock Drainage and International Mine Water Association Annual Conference, April 21-24, 2015, Santiago, Chile.
- Rolia E., 1984. “Oxidation of Thiosalts with Hydrogen Peroxide”, Report CANMET Canada Centre for Mineral and Energy Technology”.



Estimation of nanofiltration solute rejection in reverse osmosis concentrate treatment processes

Sebastian Franzsen¹, Ricky Bonner¹, Jivesh Naidu¹
Craig Sheridan², Geoffrey S. Simate²

¹Miwatek, P/Bag X29, Gallo Manor, 2052, Johannesburg, South Africa, sebastianf@miwatek.co.za

²School of Chemical and Mechanical Engineering, University of Witwatersrand, Johannesburg, P/Bag 3,

Abstract

A nanofiltration (NF) model was built in the programming language Python and interfaced with geochemical calculation software PHREEQC COM v3 for the prediction of NF rejection performance in the treatment of reverse osmosis (RO) concentrate. The built NF model is considered to have three industrial applications – (1) tracking in service element degradation in terms of increasing pore radius, decreasing effective active layer thickness and decreasing feed-membrane $\Delta\phi_{D,m}$, (2) element selection in the design of RO concentrate treatment processes and (3) estimation of unknown solute permeability values by considering the likely ion-pairs and dominant ions that characterises a given aqueous solution.

Keywords: Mine water treatment, brine treatment, nanofiltration modelling

Introduction

Research studies have shown that intermediate chemical demineralisation (CD) of primary reverse osmosis (RO) concentrate followed by secondary RO desalination can substantially improve the volumetric recovery of brackish feed waters (Gabelich et al. 2007, Rahardianto et al. 2007, McCool et al. 2013, Rahardianto et al. 2010, Greenlee et al. 2011).

Different NF elements show substantial performance variation for systems with only slight variation (Artuğ 2007). Phenomenological models and the typical application of single salt (e.g. NaCl, Na₂SO₄, CaSO₄, MgSO₄ etc.) rejection data are considered inappropriate for NF modelling or NF element selection due to the complexity of the solute transport mechanism.

The DSPM&DE model considers the membrane as having effective pore radius, effective active layer thickness, effective membrane charge density and membrane dielectric constant and is capable of describing the asymptotic concentration gradient at the membrane-solution interfaces (Artuğ 2007, Galdes and Brites Alves 2008).

The Pitzer aqueous speciation model (pitzer.dat) supplied with PHREEQC can ac-

curately predict thermodynamic properties at high ionic strength for solutions with compositions substantially different from that of seawater (Appelo 2015, Harvie et al. 1984, Pitzer 1981).

The intent of this paper is to present an alternative DSPM & DE model in which (1) the Pitzer activity and osmotic coefficients are determined by incorporating the PHREEQC COM module in the solution algorithm, (2) the aqueous solution is expressed as cation-anion ion pairs with a selected dominant ion for transport and partitioning modelling, and (3) the inclusion of the uncharged specie SiO₂ provides regression in the absence of electrostatic effects. The model was fitted to data from a pilot scale high recovery RO-CD-NF with recycle to CD process (RO-CD-NF-RCY) and a full-scale RO-NF-CD process. The former process was piloted and the later currently in operation at the Newmont Ahafo mine water treatment plant in Ghana.

Methods

The model domain comprises ten nodes j along the element string feed channel and three distinct regions of solute mass transport at each node presented in Figure 1. The solute transport path and mechanisms through



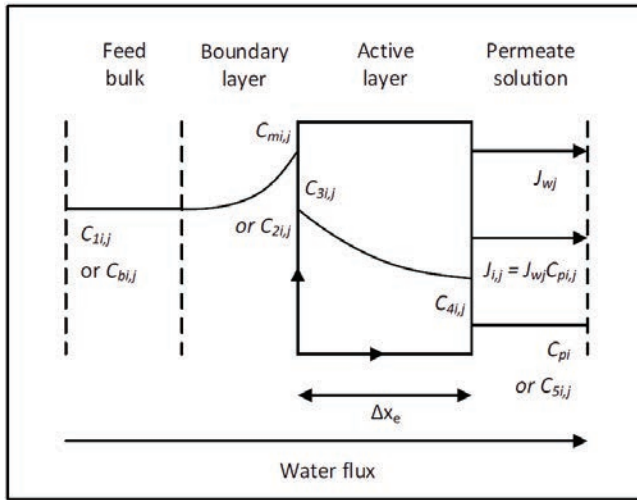


Figure 1 Schematic diagram of the solute concentration profile for each node j

the membrane includes (1) development of a concentration polarisation boundary layer approaching the feed-membrane interface, (2) feed-membrane interface partitioning occurs through steric, Donnan potential and dielectric exclusion, (3) active layer transport and (4) membrane-permeate interface partitioning occurs through steric, Donnan potential and dielectric exclusion.

The aqueous system included H-Na-K-Ca-Mg-OH-HCO₃-Cl-SO₄-SiO₂-CO₂ and was arranged into Na₂SO₄, NaCl, NaHCO₃, NaOH, K₂SO₄, KCl, KHCO₃, KOH, CaCl₂, CaSO₄, Ca(HCO₃)₂, Ca(OH)₂, MgCl₂, MgSO₄, Mg(HCO₃)₂, Mg(OH)₂, HCl, H₂SO₄, CO₂ and SiO₂ ion pairs and molecules.

Equation 1 is the combination of the Mariñas and Urama mass transfer correlation and a correction factor ϵ for the suction effect generated by permeation through the membrane (Geraldes and Brites Alves 2008, Crittenden et al. 2012). ϵ is described by semi empirical correlation shown in Equation 2 (Geraldes and Brites Alves 2008).

$$k_{cpi,j} = k_{ij}\epsilon_{ij} = \kappa \frac{D_i}{d_H} (Re_j)^{0.5} (Sc_{ij})^{0.33} \cdot \epsilon_{ij} \quad \text{Equation 1}$$

$$\epsilon = \phi_i + (1 + 0.26\phi_i^{1.4})^{-1.7} \quad \text{where } \phi_i = \frac{J_{w,j}}{k_{c,i}} \quad \text{Equation 2}$$

The partitioning at the feed-membrane and membrane-permeate interface is described in Equation 3 as a function of three transport resistances – (1) Steric partitioning,

(2) Donnan potential effect and (3) dielectric exclusion (Artuğ 2007). Steric partitioning θ_i expressed in Equation 4, refers to the transport hindrance as a function of solute radii and pore-radii within well-defined cylindrical pores (Labban et al. 2017). The effect of the Donnan potential promotes the transport of counter-ions and hinders the transport of co-ions (Peeters et al. 1998). Dielectric exclusion refers to the reduction in solvation capacity of the pore fluid due to the hydraulics in the confined space of the pores. This barrier to ionic species entering the active layer is referred to as the Born solvation energy barrier $\Delta W_{i,Born}$ and is shown in Equation 5 (Bowen and Welfoot 2002).

$$\frac{\gamma_{si}C_{si}}{\gamma_{2i}C_{2i}} = \theta_i \cdot \exp\left(-\frac{z_i F}{R_g T} \Delta \phi_D\right) \cdot \exp\left(-\frac{\Delta W_{i,Born}}{k_B T}\right) \quad \text{Equation 3}$$

$$\theta_i = \left(1 - \frac{r_{si}}{r_p}\right)^2 = (1 - \lambda_i)^2 \quad \text{Equation 4}$$

$$\Delta W_{i,Born} = \frac{z_i^2 e^2}{8\pi\epsilon_0 r_{si}} \left(\frac{1}{\epsilon_p} - \frac{1}{\epsilon_b}\right) \quad \text{Equation 5}$$

Equation 6 represents the solute flux through the membrane using the ENP equation which includes terms for diffusion, electromigration and convection transport (Artuğ 2007, Peeters et al. 1998). Hindrance factors K_{id} and K_{ic} must be applied to the diffusion and convection terms respectively for transport in the active layer (Artuğ 2007).

$$J_{i,j}^{ENP} = -K_{id}D_i \frac{dc_i}{dx} - \frac{z_i c_{i,j} D_{pi}}{R_g T} F \frac{d\phi}{dx} + K_{ic} c_{i,j} V \quad \text{Equation 6}$$



In this study the active layer transport is reduced to the linear transport between the two inside membrane interfacial concentrations c_3 and c_4 – refer to Figure 1. To evaluate the $d\phi/dx$ term, the cation-anion ion pairs were speciated out to individual ions using PHREEQC. Initial estimates of the concentration polarisation layer and permeate concentrations, c_2 and c_5 respectively, are determined through Equations 7 to 11.

Solution algorithm for NF model

Step 1 is to separate the feed solution into cation-anion ion pairs, specify the element properties, model parameters, process inputs and regression parameters. The parameters specific to each of the ion pairs and the individual ions are calculated – stokes radius, stokes radius to membrane pore radius, convection hindrance factor, diffusion hindrance factor and Born solvation energy barrier. Table 1 lists the input parameters for the calibration cases of the RO-NF-CD and RO-CD-NF-RCY processes.

Step 2 is to estimate the hydraulic parameters, water flux, solute flux and outside membrane concentrations (c_1 , c_2 and c_5) to enable the evaluation of the ENP and partitioning equations (Equations 3 and 6 respectively). Equation 7 is the solute flux as each stage j expressed in terms of a phenomenological constant that is generalised for each of the cation-anion ion pairs. Equation 8 is the membrane water flux equation with the

membrane specific water permeability constant A .

$$J_{i,j} = B_i(\beta_{i,j}c_{bi,j} - c_{pi,j}) \quad \text{Equation 7}$$

$$J_{w,j} = A[(P_{b,j} - P_p) - (\pi_{m,j} - \pi_{p,j})] \quad \text{Equation 8}$$

The concentration polarisation at each node, expressed in terms of water flux, mass transfer coefficient and rejection and generalised for each specie, is shown in Equation 9 (Crittenden et al. 2012). Equation 10 is the definition of the solute flux generalised for each specie and the permeate concentration substituted with the equivalent in terms of solute rejection and feed bulk concentration (Crittenden et al. 2012).

$$\beta_{i,j} = e^{J_{w,j}/k_{cpi,j}} r_{i,j} + (1 - r_{i,j}) \quad \text{Equation 9}$$

$$J_{i,j} = J_{w,j}c_{pi,j} = J_{w,j}(1 - r_{i,j})c_{bi,j} \quad \text{Equation 10}$$

Setting Equation 10 equal to Equation 7 and substituting Equation 9 leads to an equation that relates the solute rejection, solute permeability constant, concentration polarisation mass transfer coefficient and the water flux – Equation 11:

$$r_{i,j} = [B_i e^{J_{w,j}/k_{cpi,j}} + J_{w,j}]^{-1} \cdot J_{w,j} \quad \text{Equation 11}$$

The solver iterates through the nodes several times and utilises the Newton method from the *Scipy.Optimize* package to solve for the water flux at each node that satisfies the solute rejections from Equation 11 at the

Table 1. Model input parameters for calibration case

Model input parameters	Unit	RO-NF-CD	RO-CD-NF-RCY
Element		MDS NF 8040	MDS NF 4040T
Design volumetric recovery	%	50	50
Membrane surface area	m ²	33.1	7.3
Feed pressure	kPag	1065	1750
Operating temperature	°C	30	30
Feed flow rate	m ³ /h	5.1	1.9
Elements per string		5	8
Nodes per element string		10	10
Feed spacer thickness	Mil	31	31



specified feed pressure. This iterative strategy, as opposed to a simultaneous solution algorithm, was used to incorporate the PHREEQC COM module.

Step 3 is to evaluate the c_3 and c_4 using Equation 3. The $d\phi/dx$ term must be determined to calculate the solute flux according to the ENP Equation 6. The ratio of the solute flux determined by the ENP Equation 9 and the solute permeability constant in Equation 7 are used to adjust the solute permeability constant of each cation-anion ion pair. The solute permeability constant for the next solver iteration is determined by using Equation 12

Step 4 checks the convergence criteria and returns the solver to step 2 until convergence is achieved. The final cation-anion ion pairs are speciated out in PHREEQC and the overall rejection of individual ions reported.

Results and Discussion

The results of the regression of key parameters to operational data are shown in Table 2 and the comparison of rejection performance between the model and the analytical results are shown in Table 3. The regression of the pore radius and effective active layer thickness was constrained to yield close agreement with rejection of uncharged species SiO_2 . This technique is useful as the rejection of SiO_2 is not subject to the electrostatic effects at the system pH.

The dominant ions were assigned for a negative feed-membrane Donnan potential, since (1) ion pairs with divalent anion has the anion as dominant as the repulsion from

the feed-membrane interface appeared dominant, (2) ion pairs with monovalent anion and cation has the cation as dominant as the attraction to the feed-membrane interface appeared dominant, (3) pairs with divalent cation and monovalent anion had the divalent cation as dominant as the attraction to the feed-membrane interface appeared dominant and (4) pairs with divalent cation and divalent anion had the divalent anion as dominant as the repulsion from the feed-membrane interface appeared dominant.

$$B_{ij} = J_{ij}^{\text{ENP}} \cdot [\beta_{ij} c_{bi,j} - c_{pi,j}]^{-1} \text{ and } B_i = \bar{B}_{i,j} \quad \text{Equation 12}$$

The effect of membrane pore dielectric constant ϵ_{pore} and feed-membrane Donnan potentials $\Delta\phi_{\text{D,m}}$ on rejection performance of the MDS NF 8040 elements in the RO-NF-CD process are shown in Figures 2 and 3. Reducing ϵ_{pore} increases the Born solvation energy barrier ΔW_i at the feed-membrane interface and hence the rejection performance of all charged species is improved.

The uncharged specie SiO_2 is not affected by changes in $\Delta\phi_{\text{D,m}}$ or ϵ_{pore} . Increasing the negative $\Delta\phi_{\text{D,m}}$ increases the repulsion of co-ions and the attraction of counter-ions. For higher negative $\Delta\phi_{\text{D,m}}$, SO_4 rejection increases due to co-ion repulsion, Ca and Mg rejection decreases due to counter-ion attraction, HCO_3 and Cl rejection decreases due to counter-ion attraction (dominant ions are cations for monovalent anions).

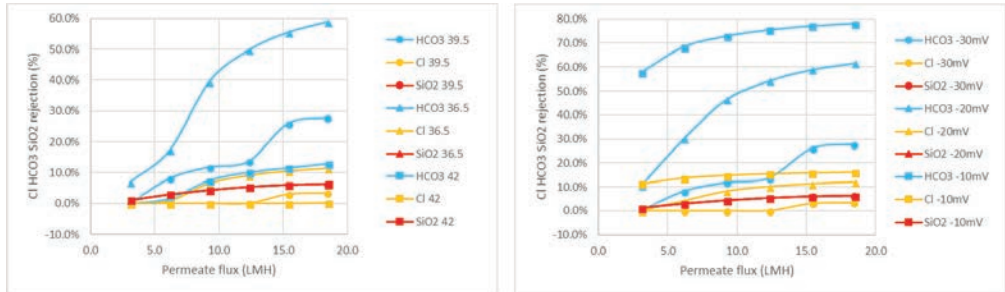
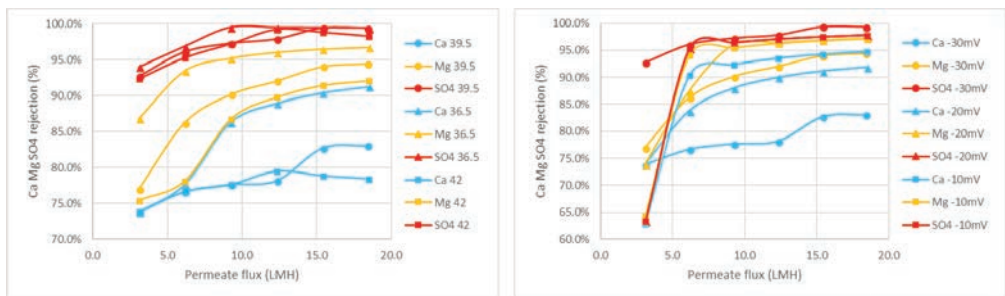
Table 2. Regression results for RO-NF-CD full scale and RO-CD-NF-RCY pilot processes

Calibration case regression results		Unit	RO-NF-CD FULL SCALE	RO-CD-NF w/ recycle PILOT
Element	r_{pore}		MDS NF 8040	MDS NF 4040T
Pore radius	Δx_e	nm	0.57	0.535
Active layer thickness	ϵ_{pore}	μm	0.3	0.3
Membrane dielectric constant	A		39.5	39.5
Water permeability constant	$\Delta\phi_{\text{D,m}}$	$\text{ms}^{-1}\text{bar}^{-1}$	5.28E-07	7.5E-07
Feed-membrane potential	$\Delta\phi_{\text{D,p}}$	mV	- 30	- 4.5
Membrane-permeate potential		mV	+ 20	+ 0.5
Permeate pH [model / (analytical)]			7.6 / (7.7)	5.7 / (5.7)
Feed pH [model / (analytical)]			7.7 / (7.9)	5.9 / (5.9)



Table 3. Comparison of ion rejections determined by the model and the analytical results from SGS

Date	Data	Na rej %	K rej %	SO ₄ rej %	Ca rej %	Mg rej %	HCO ₃ rej %	Cl rej %	SiO ₂ rej %
RO-NF-CD	Model	25.1	25.1	99.4	82.7	94.1	26.0	3.1	6.1
FULL SCALE	SGS	21.0	23.5	99.6	86.7	94.4		0.3	5.9
RO-CD-NF-RCY	Model	96.4	96.4	99.2	99.2	99.3	20.5	0.0	11.7
PILOT	SGS	96.4	96.8	99.1	99.6	99.1		< 0	13.5

**Figure 2** The effect of membrane pore dielectric constant and feed-membrane Donnan potentials on the HCO₃, Cl and SiO₂ rejection performance of the MDS NF 8040 elements in the RO-NF-CD process**Figure 3** The effect of membrane pore dielectric constant and feed-membrane Donnan potentials on the Ca, Mg and SO₄ rejection performance of the MDS NF 8040 elements in the RO-NF-CD process

Conclusions

The fundamental differences between this work and other ENP and DSPM & DE studies are (1) the arrangement of the ions into cation-anion ion pairs with a representative dominant ion, (2) the assignment of $\Delta\phi_{D,m}$ and $\Delta\phi_{D,p}$ as input values, and (3) the omission of the charge offset $-C_x$. The built NF model can match the rejection performance of the MDS elements in the RO-NF-CD and RO-CD-NF-RCY processes with resulting $\Delta\phi_{D,m}$ and $\Delta\phi_{D,p}$ values and membrane pore dielectric constant (39.5 for both NF elements) that are within the expected ranges for Polyamide membrane active layers. It is recommended that the NF model is fitted to

additional operational data and the fitted parameters, $\Delta\phi_{D,m}$, $\Delta\phi_{D,p}$ and ϵ_{pore} , compared to fitted parameters of a conventional ENP and DSPM & DE model to better understand the limitations and advantages of the ion pairing with dominant ion feature of the built NF model.

The built NF model is considered to have three industrial applications – (1) tracking in service element degradation in terms of increasing pore radius, decreasing effective active layer thickness and decreasing feed-membrane $\Delta\phi_{D,m}$, (2) element selection in the design of RO-NF-CD and RO-NF-CD-RCY processes and (3) estimation of unknown solute B values by considering the likely ion-



pairs and dominant ions that it may form for a given solution type. The interface with the PHREEQC COM module for the calculation of Pitzer activity and osmotic coefficients is considered an advantage for fitting of high ionic strength applications.

Acknowledgements

The authors gratefully acknowledge Miwatek for their financial support and project opportunity through which this work was made possible. Further, the authors gratefully acknowledge the Water Research Commission of South Africa for their financial and scientific support for the continuation of this work into a public demonstration scale project (contract no. K5/2483//3).

References

- Gabelich, C.J., Williams, M.D., Rahardianto, A., Franklin, J.C. and Cohen, Y. (2007) High-recovery reverse osmosis desalination using intermediate chemical demineralization. *Journal of Membrane Science* 301(1–2), 131–141.
- Rahardianto, A., Gao, J., Gabelich, C.J., Williams, M.D. and Cohen, Y. (2007) High recovery membrane desalting of low-salinity brackish water: Integration of accelerated precipitation softening with membrane RO. *Journal of Membrane Science* 289(1–2), 123–137.
- McCool, B.C., Rahardianto, A., Faria, J.I. and Cohen, Y. (2013) Evaluation of chemically-enhanced seeded precipitation of RO concentrate for high recovery desalting of high salinity brackish water. *Desalination* 317, 116–126.
- Rahardianto, A., McCool, B.C. and Cohen, Y. (2010) Accelerated desupersaturation of reverse osmosis concentrate by chemically-enhanced seeded precipitation. *Desalination* 264(3), 256–267.
- Greenlee, L.F., Testa, F., Lawler, D.F., Freeman, B.D. and Moulin, P. (2011) Effect of antiscalant degradation on salt precipitation and solid/liquid separation of RO concentrate. *Journal of Membrane Science* 366(1–2), 48–61.
- Artuğ, G. (2007) Modelling and Simulation of Nanofiltration Membranes, Cuvillier.
- Geraldes, V. and Brites Alves, A.M. (2008) Computer program for simulation of mass transport in nanofiltration membranes. *Journal of Membrane Science* 321(2), 172–182.
- Appelo, C.A.J. (2015) Principles, caveats and improvements in databases for calculating hydro-geochemical reactions in saline waters from 0 to 200°C and 1 to 1000atm. *Applied Geochemistry* 55, 62–71.
- Harvie, C.E., Møller, N. and Weare, J.H. (1984) The prediction of mineral solubilities in natural waters: The Na-K-Mg-Ca-H-Cl-SO₄-OH-HCO₃-CO₃-CO₂-H₂O system to high ionic strengths at 25°C. *Geochimica et Cosmochimica Acta* 48(4), 723–751.
- Pitzer, K.S. (1981) Characteristics of very concentrated aqueous solutions. *Physics and Chemistry of the Earth* 13–14, 249–272.
- Crittenden, J.C., Harza, M.W., Trussell, R.R. and Hand, D.W. (2012) *MWH's Water Treatment: Principles and Design*, Wiley.
- Labban, O., Liu, C., Chong, T.H. and Lienhard, J.H. (2017) Fundamentals of low-pressure nanofiltration: Membrane characterization, modeling, and understanding the multi-ionic interactions in water softening. *Journal of Membrane Science* 521, 18–32.
- Peeters, J.M.M., Boom, J.P., Mulder, M.H.V. and Strathmann, H. (1998) Retention measurements of nanofiltration membranes with electrolyte solutions. *Journal of Membrane Science* 145(2), 199–209.
- Bowen, W.R. and Welfoot, J.S. (2002) Modelling the performance of membrane nanofiltration—critical assessment and model development. *Chemical Engineering Science* 57, 1121–1137.





A Pilot Comparison of Sulphate Removal Technologies at Neves Corvo

Bernard Aubé¹, Moacir Lamares², Stéphan Lone Sang³

¹*Envirobay Inc., Sainte-Anne-de-Bellevue, Québec, Canada*

²*Sociedade Mineira de Neves-Corvo, S.A., Portugal*

³*Wood Environment & Infrastructure Solutions, Montréal, Québec, Canada*

Abstract

The process water at Neves Corvo mine contains high sulphate and thiosalt concentrations, as by-products from the milling and flotation process. The pilot study described in this paper established the most cost effective options for treating thiosalts and sulphates at this site. A prefeasibility study was previously completed to compare existing and proposed sulphate treatment technologies. Only the most promising technologies were studied in the pilot test. Membrane nanofiltration and reverse osmosis were tested extensively, in conjunction with the high-density sludge (HDS) process for pre-treatment and for treatment of the membrane concentrate. Barium sulphate precipitation tests were also completed in conjunction with the HDS process. Thiosalts were successfully oxidised using Fenton's Reagent.

Keywords: Sulphate removal, HDS process, nanofiltration, reverse osmosis, barium hydroxide

Introduction

The Neves-Corvo Mine is located in Baixo (Lower) Alentejo, on the south edge of the Iberian Pyrite Belt in Portugal. The nearest town is Castro Verde. It is operated by Sominor (Sociedade Mineira de Neves Corvo SA), a subsidiary of Lundin Mining. Neves-Corvo is the biggest copper and zinc mine in the European Union and has been in operation since 1988.

Prior to 2014, the mine had experienced problems with site water quality, both internally and in their final effluent. A project was initiated to evaluate commercially available options which could be applied to meet the water needs, both for effluent discharge to the environment and for internal use and consumption as a process water recycle. Internal quality requirements were identified as a need for non-scaling water with a pH within the range of 7.0 to 10.0, and non-hazardous.

The Neves Corvo discharge is regulated both by final effluent concentration limits and stricter environmental guidelines to be met in the Oeiras River. The most critical parameters of concern include sulphate (SO_4^{2-}), chloride (Cl^-), and thiosalts for toxicity. The

sulphate effluent discharge limit is 2000 mg/L and the more stringent receiver guideline that could apply during dry periods is 250 mg/L. Chloride is an issue only during these dry periods, with a guideline of 250 mg/L. In this paper, the term thiosalts is used to represent thiosulphate $\text{S}_2\text{O}_3^{2-}$ and other polythionates ($\text{S}_x\text{O}_6^{2-}$ where $3 \leq x \leq 10$). Concentrations of thiosalts were reported as thiosulphate and a target of 10 mg/L was established to ensure that pH depression in the receiver was prevented.

Within this project, a pilot plant study was completed to evaluate the most economic and efficient processes to oxidise thiosalts, precipitate metals, and to reduce sulphate concentrations.

Raw Water Qualities

In order to design a system that would meet the needs in coming years, two synthetic water qualities called "CdL Sim" and "CdM Sim" were tested during the pilot plant study (Table 1). These synthetic waters were generated on site from existing available water sources. The simulated water was created using tailings water, overflow from the paste tailings



thickeners and mine water (underground de-watering). The proportion of each was determined based on projected future water conditions as predicted by a site water reticulation model.

Table 1 Raw water qualities

Average Concentration (mg/L)	CdL Sim	CdM Sim
Sulphate	3537	2800
Thiosalt	501	1180
pH	2.7 – 3.3	5.2 – 6.1
Fe	98	0.62
Ca	677	766
Na	885	805
Cl	511	555

Pre-Feasibility Study

The first phase of the study included a pre-feasibility study (PFS) of different sulphate treatment technologies. Five different technologies were considered as potential components of the required treatment complex. These were the high density sludge (HDS) system, Fenton’s oxidation process, barium precipitation, an ettringite process, and membrane treatment. Various combinations and permutations of these treatment technologies were then considered as individual reticulation scenarios, and two levels of flowrates were considered for each. A total of 22 scenarios were thus considered. Each was engineered to a pre-feasibility level in order to develop the Process Flow Diagrams, preliminary Process and Instrumentation Diagrams, preliminary General Arrangements, equipment lists, and associated capital and operation costs.

Detailed water and mass balance modelling suggested that to meet all the site requirements for water, it was necessary to oxidise the thiosalts, treat acidity via HDS and apply one of the three retained sulphate removal technologies. Using the PFS-level cost esti-

mates developed for all 22 scenarios, three specific treatment trains were retained for cost comparison in Table 2. These are:

- Fenton’s oxidation, HDS process, followed by ettringite precipitation;
- Fenton’s oxidation, HDS process, followed by barium sulphate precipitation;
- Fenton’s oxidation, HDS process, followed by membrane treatment.

The costing was completed by obtaining actual quotes for all major equipment, then adding factors for installation (when missing), civil (including concrete, structural, buildings), electrical, automation, and process piping. Engineering and construction management costs were estimated, and a 30% contingency was added to the total. Table 2 shows the results of capital, operating, and net present value costs (CAPEX, OPEX and NPV) of the three treatment trains retained.

The ettringite process costs were estimated in cooperation with a process supplier of good reputation in the mining industry. This process was found to have the highest capital costs and also a very high operating cost, due to the numerous reagents required and the management of large volumes of sludge. For this reason, it was eliminated and not tested at the pilot scale.

Barium sulphate precipitation was very expensive for operation, simply due to the high cost of the barium hydroxide reagent and its limited availability. The capital cost of using barium precipitation, on the other hand, was low as the process step could be integrated in an HDS plant, which was needed regardless of the approach. It was therefore considered worth testing in order to properly define best operating conditions and dosages as a back-up option or on a temporary basis.

Membrane filtration following Fenton and HDS showed the lowest net present value costs. It was determined that membrane filtration would be a viable sulphate removal

Table 2 Estimated cost of different treatment options (flowrate of 400 m³/h)

Proposed Treatment	Total CAPEX (€)	OPEX (€/year)	NPV ^{8%,20years} (M€)
Fenton + HDS + Barium	≈ 11 000 000	≈ 6 980 000	≈ 80
Fenton + HDS + Membrane	≈ 18 800 000	≈ 3 440 000	≈ 50
Fenton + HDS + Ettringite	≈ 48 800 000	≈ 6 030 000	≈ 108



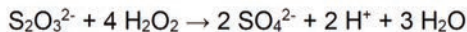
technology to meet the needs at Neves Corvo. Tests were planned with different nanofiltration and reverse osmosis membranes.

Equipment and Methods

The pilot plant was operated on-site at the Neves-Corvo Mine continuously from October to December 2015. A detailed description of the metal hydroxide and gypsum precipitation section of the plant is available in Aubé et al, 2018. In this paper, the specific processes other than HDS are described.

Thiosalt Oxidation

Prior to the pilot plant trials, thiosalt oxidation testing using the Fenton reaction was completed at the bench level and also in another smaller pilot trial at a very low flow-rate. This reaction uses hydrogen peroxide (H_2O_2) as an oxidizing agent. A metal catalyst in slightly acidic conditions (pH 4.0) such as iron can improve efficiency and reduce reaction times. Thiosalts are oxidized to sulphuric acid. In this trial, ferric sulphate was added as a catalyst when needed. The thiosalt oxidation formula is the following:



The thiosalt oxidation tests were integrated as part of the HDS treatment in the first reactor, as shown in Figure 1. Due to acid formation during the oxidation process, alkalinity had to be added during the oxidation

stage. In most tests, pH control was achieved by recycling the clarifier underflow sludge from the HDS neutralisation to this first reactor (R1). The speed of the pump feeding sludge to R1 was controlled on a pH setpoint of 4.0. This meant that no lime was required to control pH in this reactor and the sludge also served to provide seed particles for precipitation. This served to increase particle size, sludge density, and prevented scaling in this reactor. This recycle can also serve to assist in catalysing the reaction as the sludge already contains iron. The remainder of the recycled sludge was directed to the Lime/Sludge Mix Tank to be combined with lime prior to controlling the pH of the HDS process reactor to setpoints ranging from 10 to 11.5.

The thiosalt oxidation part of the process is important in this discussion on sulphate removal as the product of oxidation is sulphate, specifically sulphuric acid. This means that one process step required for water treatment at Neves Corvo includes the formation of additional sulphate, while others are focused on its removal.

Membrane Filtration Tests

The pilot plant was equipped with a membrane filtration skid including a 100-mm diameter (4") stainless steel vessel of 1013 mm (40") in length for operating at a maximum pressure of 2050 kPa (300 psi) and a nominal flowrate of 50 L/min. The raw water was pumped through a pre-filter using a centrifugal

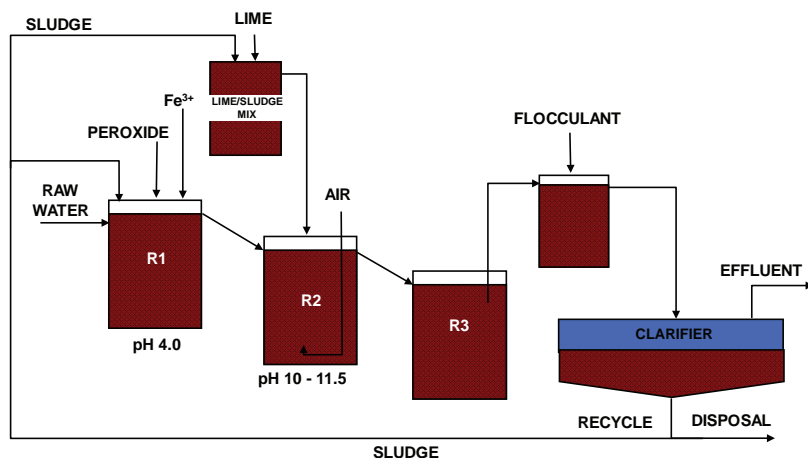


Figure 1 Flowsheet for Fenton's Reagent combined with HDS



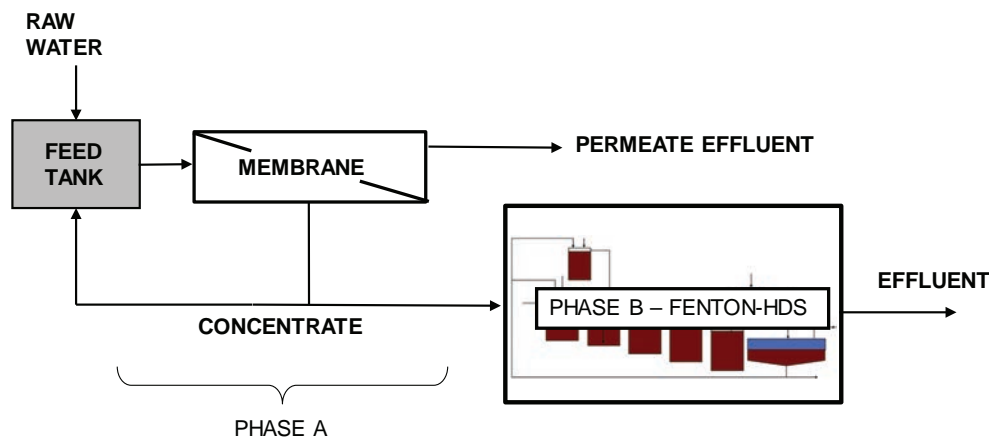


Figure 2 First continuous membrane test configuration

gal pump, prior to the booster pump feeding the membranes. The resulting pressures, flows, and conductivities were monitored continuously. A 100-L reservoir was used for Clean-In-Place (CIP).

Both batch tests and continuous tests were completed using this skid. For the batch membrane testing, two 1000-L totes were required; one was filled with 1000 L of raw water and the second tote served for permeate collection. An initial one-time dosage of an antiscalant was added (at 3.7 mg/L) to the feed tank in order to minimise the potential for membrane fouling from scale formation. Permeate was routed to the graduated permeate storage tank and the concentrate was recirculated to the feed tank. Four different membranes were tested in the batch tests, including two reverse osmosis membranes, BME-4040 and ESPA2-LD-4040 and two nanofiltration membranes: NF90-4040 and NF270-4040.

The objectives of the first continuous test were to confirm the constant permeate water quality for continuous operation of the membrane and to evaluate membrane fouling over time, as well as define the needs for concentrate treatment. The process was configured as shown in Figure 2, with CdM Sim as the membrane feed water. The continuous operation of the membrane was set to represent only 50% recovery rate to minimise fouling of the membrane due to gypsum precipitation. As that recovery rate cannot be achieved in a single pass with the filtration skid used,

partial recirculation of the concentrate was applied. The pilot membrane system was fed at a rate of 20 L/min with 2.5 L/min in permeate production. Therefore, to operate at a 50% recovery rate, 5.0 L/min of raw water was fed and the concentrate bleed was also set to 2.5 L/min. Most of the concentrate (15 L/min) was returned to the feed tank to be mixed with the raw water. The concentrate bleed was then sent to Fenton-HDS treatment, as discussed in Aubé et al, 2018.

The nanofiltration membrane used for this test was the NF90-4040. The membrane pressure was adjusted to maintain the permeate flowrate at 2.5 L/min. Over time, the fouling of the membrane required higher pressures. Once the high pressure setpoint of 1250 kPa (180 psi) was reached, the membrane system underwent a Clean In Place (CIP) sequence. Following the cleaning, the membrane was restarted at a lower pressure, typically around 1050 kPa (150 psi).

The second continuous membrane test had a similar configuration, but with a different feed water and with pre-treatment, as shown in Figure 3. The feed water for the membrane section was the effluent from a Fenton-HDS treatment with 3.5 hours of retention time in the HDS reactors, and calcium carbonate precipitation using carbon dioxide in the final reactor. The pre-treated water was allowed to age for a minimum of 2 days prior to being fed to the membrane skid, simulating a pond between the process steps.

Apart from the tests carried out by Wood,



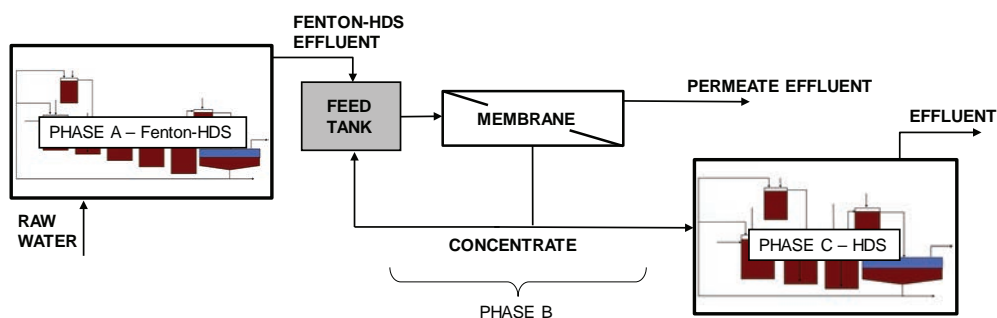
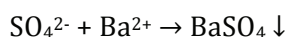


Figure 3 Membrane treatment of pre-treated water through Fenton-HDS, with concentrate treatment

a membrane supplier was also on-site for extensive testing of both nanofiltration and reverse osmosis membranes. A summary of the results from all the continuous tests are described under the “Results and Discussion” section.

Barium Sulphate Precipitation

Sulphate is known to precipitate readily with barium as per the equation below. This reaction was completed using barium hydroxide monohydrate as the reagent. The amount of barium hydroxide added was calculated based on a targeted residual sulphate concentration of 1900 mg/L in the final effluent. While barium chloride is less expensive than barium hydroxide, it was not chosen for use in this project because Neves Corvo also have constraints for chloride concentrations in the effluent.



A barium hydroxide slurry was used for dosing with two different process configurations being tested. Configuration #1, as shown in Figure 4, combined the Fenton’s oxidation, HDS, and the barium treatment steps simply by adding a reactor where both the barium hydroxide slurry and carbon dioxide were dosed. This configuration used a single clarifier, which means that a single sludge from the HDS and barium precipitation reactions was produced in the clarifier and was recirculated back to the front end of the process.

In Configuration #2, as shown in Figure 5, an independent Fenton-HDS process was operated and the clarifier overflow was conveyed to the barium treatment process. With each process having its own dedicated reactors and clarifiers, two different types of sludge were produced. Sludge from each clarifier was recirculated back into the respective process.

In both configurations, a barium hydrox-

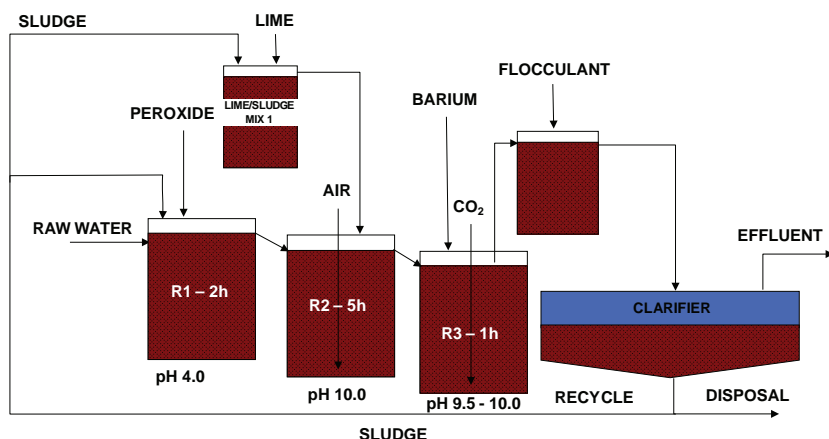


Figure 4 Barium sulphate precipitation: Configuration #1, with a single clarifier



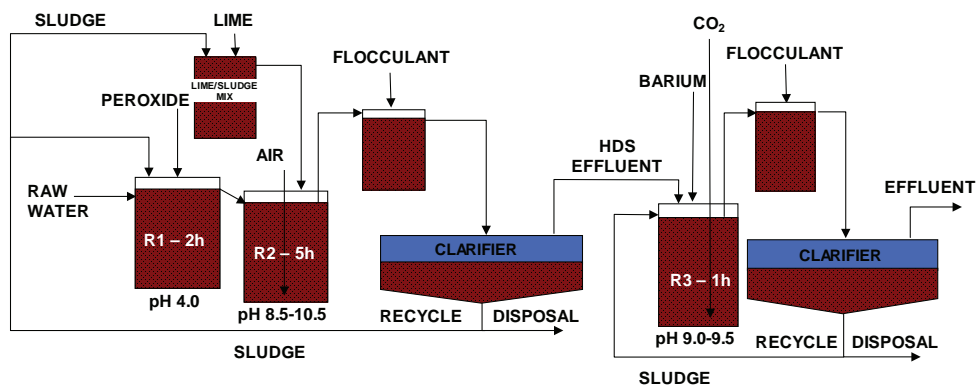


Figure 5 Barium sulphate precipitation: Configuration #2, with two clarifiers

ide monohydrate slurry was added in a reactor with a 1-hour retention time, in which carbon dioxide was also added to control pH to a range of 9.0 to 10.0. The slurry was then pumped to a flocculant tank before flowing to a clarifier.

Results and Discussion

Although many of the tests combined different processes, for simplicity, the results are presented one technology at a time.

Thiosalt Oxidation

Thiosalt oxidation with hydrogen peroxide catalysed with ferric sulphate was successful. Residual thiosalt concentrations below 25 mg/L were achieved at 90% stoichiometric hydrogen peroxide addition. Residual thiosalt concentrations as low as 10 mg/L were achieved in the pilot test at stoichiometric addition of hydrogen peroxide (100%). It was found that pH control to 4.0 is an important operational parameter in order to maintain process efficiency. When pH increases above 4.0, the Fenton reaction kinetics are greatly reduced. Below pH 2.5, the risk of hydrogen sulphide generation increases; it is a hazardous gas that needs to be carefully monitored and controlled.

The preferred operating conditions were a retention time of 2 hours, a pH setpoint of 4.0, and a stoichiometric addition rate of peroxide to thiosalts concentration. Recycling the sludge is beneficial to the process: it prevents scaling since new gypsum precipitates will form on existing sludge particles; it can be used to maintain the pH in the reactors;

it provides more catalyst when there is Fe in the sludge; and it maintains the Fenton reaction. One test without sludge and only lime addition showed major scaling in the reactor, while it was negligible with a sludge recycle.

Membrane Filtration Tests

Batch membrane tests were completed using two reverse osmosis membranes (BME-4040 and ESPA2-LD-4040) and two nanofiltration membranes (NF90-4040 and NF270-4040). Test results showed that the target sulphate concentration of 250 mg/L could be met with the NF membranes at lower feed pressures. For the continuous tests completed by Wood, these two NF membranes were used.

As mentioned, a supplier also completed some testing on site using one nanofiltration (HL4040FM) and one reverse osmosis (AK-4040FM) membranes.

These membranes were selected as they were expected to ensure that local discharge limits were respected. Table 3 presents the concentration of the feed and permeate from each membrane. The metal concentrations in the permeate for NF90 were all below the discharge limits. Thiosalts were also rejected by the NF90 with a residual concentration of 17 mg/L for a 98.6% rejection. To prevent acidification in the environment, a thiosalts concentration of less than 10 mg/L could be necessary, depending on the alkalinity of the effluent and the receiver.

The NF270 was less efficient with sulphate treatment (210 mg/L in the permeate). Chloride concentrations in the permeate were shown to be higher than in the concentrate.



Table 3 Summary of membrane test results

Membrane	NF90-4040		NF270-4040		HL4040FM		AK4040FM	
Average Conc. (mg/L)	Feed	Permeate	Feed	Permeate	Feed	Permeate	Feed	Permeate
Sulphate	2800	39	3167	210	2700	31	2782	<10
Thiosalts	1180	17	23	4.2	1144	94	1179	3.3
Ca	815	8.0	703	42	799	23	818	1.3
Na	883	36	877	333	908	408	896	14
Cl	555	49	510	529	518	610	538	37

This phenomenon is called the “Donnan effect” which is the consequence of the movement of monovalent ions in the membrane to maintain the ionic balance in the solution – essentially, the permeating sodium pulled the chloride through the membrane. Similar results were obtained with HL4040FM, which is a nanofiltration membrane from the previously mentioned supplier.

As expected, the RO membrane (AK-4040FM) produced the best permeate quality and met all the discharge limits. However, it required higher pressures and showed a greater fouling potential, requiring more frequent cleaning.

As two of the NF membranes increased the chloride concentrations in the permeate, these were discounted for potential full-scale application. Overall, the results obtained from these tests suggest that NF90 could be a potential option for a full-scale system as the concentrations met all the required criteria for discharge at lower pressures than any RO membranes. If a thiosalt removal rate of 98.6% was found to be insufficient, some oxidation could also be provided either upstream or downstream of the nanofiltration.

Barium Sulphate Precipitation

As described previously, two different configurations of barium addition were tested: one combining the HDS and the barium treatment steps using a single clarifier (Configuration #1, Figure 4) and the other maintaining separate HDS and barium treatment processes, each with its own dedicated reactors and clarifiers (Configuration #2, Figure 5). In both cases, the barium consumption rate was stoichiometric to the amount of sulphate removed. The final sulphate concentration could be controlled as required, to a target of less than 2000 mg/L (note that these tests

focused on attaining the higher of the two sulphate limits as it is proposed to be applied only during the wet season).

The difference between the tests lies in the sulphate concentration prior to barium dosing. In Configuration #1, with a single clarifier, the sulphate concentration in the reactor prior to barium addition averaged 3600 mg/L. With a separate complete HDS treatment prior to barium addition, the sulphate concentration was 3250 mg/L and could be optimised to a lower level.

In the optimised HDS treatment (Aubé et al, 2018), sulphate concentrations of less than 3000 mg/L were achieved. This could not be done in Configuration #1 as the recycled sludge contained a significant fraction of barium sulphate. For the HDS process to remove sulphate as calcium sulphate, the recycled sludge must consist mostly of gypsum to provide precipitation sites. This means that Configuration #2, with two clarifiers, could meet the same target concentration of sulphate (<2000 mg/L), with 40% lower consumption of barium than for Configuration #1.

This process is most readily applicable to higher sulphate concentration targets, as a high barium dosage could result in residual barium concentrations in the treated effluent. That said, the results from both tests indicated that dissolved barium concentration in the effluent was less than 0.15 mg/L. Total Ba concentrations in Configuration #1 and #2 averaged 1.4 mg/L and 0.84 mg/L, respectively. These results indicate that most of the residual Ba was in the suspended solids and a polishing step such as a settling pond or a filter could decrease the residual concentrations further.

The barium precipitation process was also shown to produce very high sludge densities as both configurations attained sludge solids



contents exceeding 40% solids. Despite these very high densities, the sludge rheology was such that conveying the sludge did not pose any viscosity problems.

Since it is proven that Barium hydroxide can stoichiometrically reduce sulphate concentrations, it could be used as a back-up option, but operating costs remain much higher than with membrane filtration due to reagent costs.

Conclusion

The tests described in this paper include thio-salt oxidation by Fenton's Reagent, barium sulphate precipitation and membrane filtration for sulphate removal. All tests were successful.

Thiosalt oxidation was most efficient at a pH of 4.0, in a reactor with a two-hour retention time and recycled HDS sludge used for pH control. Under these conditions, the peroxide consumption was slightly less than the stoichiometric requirement to meet the treatment target.

Barium sulphate precipitation was stoichiometric to meet the sulphate target of 2000 mg/L. It is best to dose the barium in a separate process after a complete HDS process to minimise the sulphate concentration prior to barium dosage, thereby minimising barium reagent consumption.

Nanofiltration membranes could be used to meet the target of 250 mg/L sulphate. Due to chloride limits and the Donnan effect, the preferred membrane was the NF90. Although reverse osmosis membranes produced a better permeate, higher feed pressures were required and more frequent cleaning was needed.

Overall, the most effective treatment train for controlling thiosalts and high sulphate concentrations at Neves Corvo was shown to be Fenton's oxidation combined with the HDS process, followed by nanofiltration.

References

- Aubé, B., Lamares, M, Lone Sang, S., 2018 “A Pilot Optimisation of Sulphate Precipitation in the High-Density Sludge Process”. Paper presented at the 11th ICARD | IMWA | MWD 2018, Pretoria, South Africa.
- Aubé, B., Lee, D.H., 2015. “The High Density Sludge (HDS) Process and Sulphate Control”, Paper presented at ICARD-IMWA 10th International Conference on Acid Rock Drainage and International Mine Water Association Annual Conference, April 21-24, 2015, Santiago, Chile.
- Rolia E., 1984. “Oxidation of Thiosalts with Hydrogen Peroxide”, Report CANMET Canada Centre for Mineral and Energy Technology”.





15

**FUNDING MODELS
FOR MINE WATER**



Regional Mine Water Treatment Plants: Tolloed treatment financial analysis and viability

Ashton Drummond

Aveng Water, Ashton.drummond@avenggroup.com

Abstract

The Upper Olifants River Catchment area located in Mpumalanga is the centre of South Africa's coal mining industry. Coal mining operations in this area generally have a positive water balance, and this Mine Impacted Water (MIW) to be released into the environment has serious detrimental effect on the environment, specifically the catchment streams of the Olifants River.

The capital requirements for a MIW Plant can often delay the execution of a project when funded solely by the mines. A technical and financial analysis has been performed, which investigates what pricing structure would be required for mines serviced by a regional MIW Treatment Plant. The model is based on a capital structure that is comprised of a mix of debt and equity, thus considering an acceptable return on investment for private investors.

Keywords: Mine Impacted Water, Mine Water Treatment, Regional MIW Treatment Plant, Tolloed Treatment, Capital funding

Introduction

Aveng Water, together with the Industrial Development Corporation (IDC) are considering the potential opportunity to invest in a regional Mine Impacted Water Treatment Plant in the Upper Olifants River catchment area in Mpumalanga.

The Upper Olifants River Catchment area located in Mpumalanga is the centre of South Africa's coal mining industry. Coal mining operations in this area generally have a positive water balance which needs to be released to the environment. This Mine Impacted Water (MIW) runoff into the catchment streams of the Olifants River can have a serious detrimental effect on the environment.

The construction and operation of a regional MIW plant will bring benefits to the local economy through various avenues:

- Employment created for the construction of the plant and surrounding infrastructure
- Employment created to operate the plant
- Distribution of potable water to water scarce regions
- Sale of gypsum for building material – possible employment opportunity

- Potential recovery of other valuable minerals dissolved in the water
- Enforcement and improvement of environmental management plans for mines in the targeted region

Coal mining activities in the Upper Olifants River catchment area has created a need to treat approximately 200 - 250 ML/day of Mine Impacted Water. This water is found both in currently operating mines, where there is a requirement for water to be pumped out to maintain mining capacity, as well as in defunct mining areas, where rainfall percolates through old mining areas, slowly filling the empty voids with highly saline water which eventually finds the lowest point to decant from. A COALTECH report from 2000 (Maree et al., 2000) estimated that there was 44ML/d of MIW decanting into the river systems of the Upper Olifants river catchment, which amounted to 4.54% of the total water usage (volume), but accounted for 78.4% of the sulphate load in the system. It was estimated in the same report that by the year 2020, the volumes decanting into the river system would be closer to 131 ML/d.



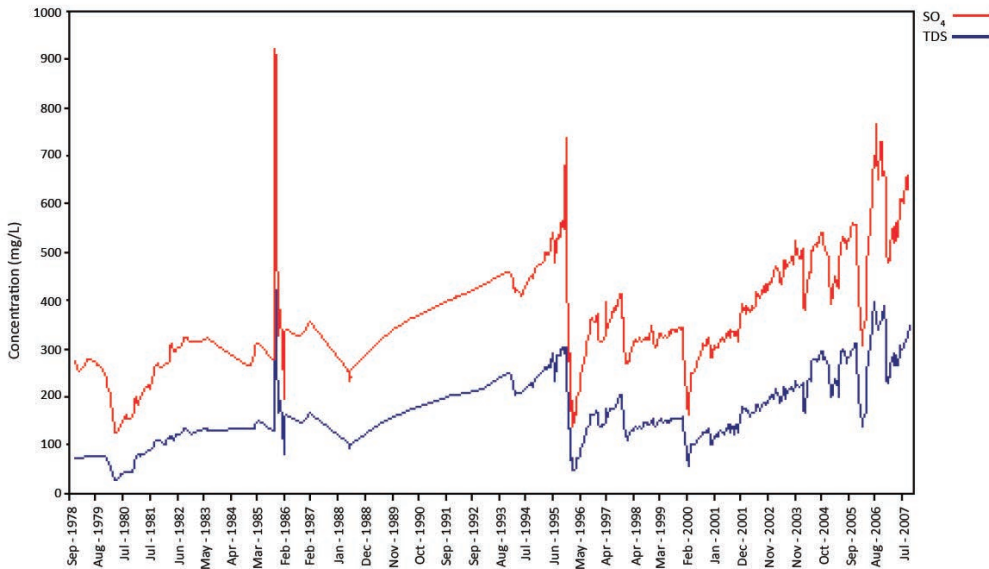


Figure 1 Concentration of sulphates and total dissolved solids from September 1978 to July 2007 in the Middelburg Dam (Source: Department of Water Affairs)

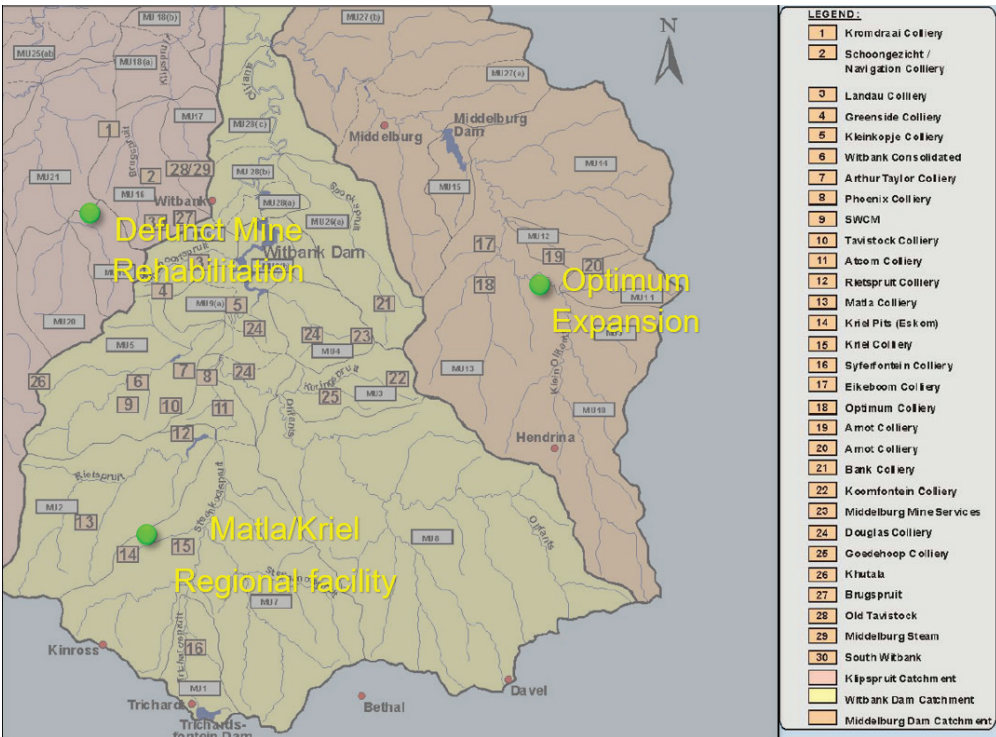


Figure 2 Potential Locations for a Regional MIW Treatment Plant



Figure 1 above is an indication of the effect that coal mining has had on the holding dams in the region. The increased salinity is exacerbated in dry periods, and diluted with good rains, but the general trend is undoubtedly upwards for both salinity and sulphate levels.

Current and Future Mining

Plans showing the mining and prospective areas in the upper catchments of the Vaal, Olifants, Komati and Mfolozi-Pangola-Usutu rivers in Mpumalanga (McCarthy, T.S) indicate the potential to increase the mining footprint up to 40% (from the current 14%) of the provincial surface area. This would suggest that the dewatering, and water treatment requirements would be compounded as old mines close down, and new mining areas are explored.

It is worth noting that future mining projects in the region will have difficulty receiving water allocation from the DWEA, due to the current deficit of water in the entire catchment (Cogho, V.E, 2012). This again indicates the potential value in effectively utilising MIW to help the mining economy.

Potential Locations for a Regional Treatment Plant

Figure 2 above indicated three potential locations for a regional plant. The first option for placing a regional plant would be to approach stakeholders in projects which have already been conceptualised and offer to take over responsibility for the capital expenditure and project development. The second would be to identify a new region where there is an obvious need for water treatment, and begin discussions with the mines in the area to get letters of intent from potential MIW suppliers.

The first option could potentially circumvent the EIA and mine negotiation phase, which could fast track a project, and this should be the preferred route for a regional installation.

Optimum Expansion

Mines in the region of the OWRP need extra MIW treatment requirements in the region of 15ML/d. This water would come from;

Optimus, Zevenfontein, Pullenshope, Boschmanspoort, Kwagga, Schoonoordt and Eikeboom.

The Arnot Colliery is another potential supplier of MIW in the Optimum region. From the COALTECH 2020 report published in 2000, it was estimated that Arnot colliery had an average decanting rate of 4.43ML/d. The COALTECH 2020 report seemed to underestimate many of the decanting volumes that are well known today. Some examples are below:

1. Kromdraai estimated at 1.26ML/d – reality today is 8ML/d
2. Optimum Colliery estimated at 9.5ML/d – reality today is 15ML/d, needing a further expansion
3. Middelburg Mine estimated at 1.32ML/d – reality today is 20ML/d

It is therefore estimated that there is a considerably higher decant volume to be treated at Arnot Colliery.

Arnot Colliery has used various pits to store MIW, and this volume of water should be treated in the long term to avoid further contamination of ground water, and amounts to approximately 285.7 million m³, which is over and above the decant flow rate. If this is to be treated over 20 years, this amounts to an extra flow rate of 39ML/d, and gives a sense of how much MIW is available in the region to treat.

From the above mentioned water sources, it is evident that there is at least 35ML/d available to treat in the long term:

- Optimum Colliery and surrounds – 15ML/d
- Arnot – 20ML/d (could be higher as a result of dewatering pit requirements)

Matla/Kriel Regional Treatment Facility

It was mentioned in the Matla tender documentation that the Matla plant would be in operation for approximately 5 years before tying in to the 40ML/d Eskom-led Matla/Kriel Regional Scheme Water Treatment Facility as planned to be commissioned in July 2016. This is a potential opportunity, as it does not seem as if this project has received the go-ahead yet, and there may be a chance to provide the capital and project execution.



Defunct Mine Rehabilitation west of Witbank

The WRC Report No. 1628/1/11 (2011) by Coleman et al. explains that there is a high concentration of defunct and abandoned mines in the Klipspruit Catchment. These mines started in the early 1900's, and the responsibility has since been handed over to the Department of Minerals and Energy. There is an opportunity to construct a regional plant to treat the historical environmental concerns in the region. More investigation would be needed regarding the volumes available to treat, and whether the financial model can be sustained by an array of defunct mines with limited financial backing.

Potential Off takers

Water resources in the Upper Olifants River Catchment area are stressed in terms of usage, which presents many opportunities for potential off-takers of product water emanating from a MIW treatment facility

Irrigation

Irrigation is the largest water user in the Olifants River catchment, with an estimated supply of 508 million m³/a (Beumer et al., 2011), while the requirement is closer to 708 million m³/a.

A few research papers (Coleman et al., 2011 for example), have discussed studies regarding using gypsiferous mine water for irrigation. Indications are that neutralized MIW could be used for irrigation, after a 3 year trial at Kleinkopje Colliery. Salinity in the soil increased over the duration of the trial due to high concentrations of Ca²⁺, SO₄²⁻ and Mg²⁺ in the irrigation water, but was never at levels

too high for yields of most crops. Further research is still required to confirm these findings over a longer period, as well as investigate the local environmental impacts of this practice.

Power Plants

The estimated supply of water to power stations located in the Upper Olifants River catchment in 2010 was 228 million m³/a (625ML/d), and due to the poor quality of water in the Olifants catchment, all of this water is supplied from either the upper Komati or the Vaal Systems (Beumer et al., 2011). This adds strain on other crucial water systems, and supplemented water from the Olifants catchment in terms of treated MIW could remove a portion of this import requirement.

The MIW treatment plant could be tailor designed to send a high quality (low TDS) water specification to the power plants, so that extra treatment on their premises would not be necessary.

Municipalities

Emalahleni, as with most municipalities in South Africa, has the growing challenge of scattered informal communities within its area of jurisdiction, in some cases illegally (Coleman et al., 2011). In terms of the Water Services Act, 1997, the municipality is responsible for providing these communities with basic services, and these are currently served by means of water tankers. Witbank town is currently growing rapidly with residential developments covering the range from low- to high-income markets. The future growth of the town will be severely constrained without an additional source of water (Coleman et al., 2011).

Town/Community	Water Requirements (ML/day)			
	2007	2030	2050	Water Source
Witbank (Potable)*	81.4	160.6	195.9	Witbank Dam
Phola/Ogies (Potable)*	6.2	12.2	14.9	Witbank Dam
Highveld Steel (Raw)	22.0	22.0	22.0	Witbank Dam
Total from Witbank Dam	109.6	194.8	232.8	
Rietspruit**	3.0	3.8	4.6	Rietspruit Dam
Kriel/Thubelihle***	3.9	6.1	9.1	Usutu GWS
TOTAL	116.5	204.7	246.5	

Note: *based on 3% population growth rate; ** 1% growth rate; ***2% (national average)

Figure 3 Projected water requirements for the eMalahleni local municipality (Coleman et al., 2011)



Figure 3 above gives an indication of how the water demands are expected to grow. It should be noted that the requirements of Highveld Steel are now no more. If the current housing backlog is completed and supplied with full services, this demand water demand could increase by 25ML/d (Coleman et al., 2011), and would remove the current water freed up by the Highveld Steel closure.

Current estimates show that by 2030 there will be a shortfall of 83.3ML/d in the Witbank area (Coleman et al., 2011). There is a huge opportunity to make up some of this shortfall with water reclaimed from MIW decanting and storage areas.

Business Case

The initial feasibility investigation has taken the most recent build price for the Middelburg Water Reclamation Plant, and added inflationary effects, together with logarithmic six-tenths-factor rule relationships (Peters & Timmerhaus, 1980) to account for the up-scaling of the potential facility to get an estimated capital price for a 35ML/d plant; which includes brine treatment, surrounding infrastructure and solid waste disposal facilities. This amounts to an estimated R 2.9 billion for the project.

Operational costs have been developed to account for chemicals, power, brine treatment, product distribution pumping and membrane replacements, as well as the fixed costs associated with the plant operation. These costs have been developed by using historical data from similar operational MIW treatment plants.

The business model will need to ensure that mines supplying water to the plant pay for the operational costs, as well as finance costs associated with the capital payback.

There is the added income that comes from sale of potable water (assumed to be at R7.00 per m³), as well as the sale of high

quality gypsum that the plant will produce, at R100/ton. With feed water similar to what is found in the Optimum region, this amounts to an income of R0.10/m³.

The financial modeling involved looking into the requirements for capital spending over and above the plant construction, and includes; interest during construction, senior debt upfront fees, project development costs & success fees, and the working capital injection requirements which increases the total capex spend to just over R3.25 billion.

Outputs from the model show that mines in the region of the plant would be able to send mine water for treatment at an approximate rate of R36.50 per m³ (depending on water quality from the individual mine), and this would account for the operational expenses as well as capital payback, while servicing the debt and providing a reasonable return on equity for investors.

The analysis is based on a 70:30 debt to equity split for the financing, and results in a 10.5 year equity payback, linked to a 12% ROE over the 20 year project life. Modeling ensured that debt repayment sculpting created debt service coverage ratios that show minimal risk associated with leverage.

Conclusions

This opportunity is hinged on the willingness and ability of the mines to send water to the regional plant. It will be required to meet with the stakeholders in the various mines to discuss this opportunity, with the aim of getting letters of intent signed for sending water to a MIW treatment facility. The interest shown in specific regions will help with the direction that the opportunity needs to be directed.

The costs associated with sending the water to a regional plant can be reasonably well defined, thus it will be crucial to discuss these costs with the potential MIW suppliers to get

Table 1. Operational cost relating to 35ML/d facility

Cost Component	Cost Per m ³	Cost per annum
Fixed Cost	R1.67	R 21 395 892
Variable Costs	R12.74	R 162 805 740
TOTAL	R14.42	R 184 201 632



letters of intent based on these costs. The investigation will then need to understand the optimal placement between various mines to ensure that pumping and pipeline costs incurred by the mine does not make the overall scheme unaffordable.

The financial model could always be tweaked to improve return on equity resulting from elevated risks associated with projects of this nature that require exceptional technical knowledge to consistently operate for 20 years. However, from an economic point of view, the return on equity should not as much of a concern due to the positive impact that a project such as this would give the local economy. These include the ability for mines to expand and operate in a more sustainable manner; farmers having access to larger quantities of higher quality water; and communities having access to high quality drinking water.

These project impacts, which encompass the financial, environmental and social benefits, can be delivered to ensure the triple bottom line approach to sustainable business is fulfilled.

Businesses that are designed to be ‘future fit’ cannot take a one-dimensional view of financial profits as the final decision factor. Projects such as this can ensure that financial profits are improved through social and environmental initiatives that create various spillovers into other industries, with the longer terms view of growing the economy, thus

providing a more sustainable business ecosystem in which to operate.

Acknowledgements

The authors thank the IDC for all the assistance with guiding the financial modelling of the project

References

- McCarthy TS. The impact of acid mine drainage in South Africa. *S Afr J Sci.* 107(5/6), Art. #712, 7 pages. doi:10.4102/sajs.v107i5/6.712
- Maree JP, van Tonder GJ, van Niekerk AM, Naidoo C. The collection, treatment and utilization of water accumulated in the coal mines located in the Upper Olifants River catchment. Coaltech 2020, 2000.
- Cogho VE. Optimum Coal Mine: striving towards a ‘zero effluent’ mine, *Journal of the Southern African Institute of Mining and Metallurgy*, 2012.
- Coleman T.J., Usher B, Vermeulen D, Lorentz S, Scholtz N. Prediction of how different management options will affect drainage water quality and quantity in the Mpumalanga coal mines up to 2080. WRC Research Report No. 1628/1/11, 2011.
- Beumer J, Van Veelen M, Mallory S, Timm D. Development of a reconciliation strategy for the Olifants River water supply system: Preliminary Reconciliation Strategy report, 2011
- Peters MS, Timmerhaus KD. *Plant Design and Economics for Chemical Engineers.* McGraw-Hill, Third Edition. 1980





16

**MINE WATER
HYDRAULICS**

Occurrence of coal seam as main aquifer

Haibo Bai, Hao Li, Dan Ma, Bin Du

State Key Laboratory for geomechanics and deep underground engineering, China University of Mining and Technology, Xuzhou, Jiangsu, 221116 China; hbbai@126.com, 153145839@qq.com, Madan518@126.com, 1016717942@qq.com

Abstract

Hydrogeologically coal seam is always viewed as aquifuge. However, the upper mineable coal seams of the Ordos Jurassic Coal Basin were actually disclosed as the main flooding aquifer of the coal mines. To investigate the occurrence of the coal seams as the main aquifer, a comprehensive method is adopted, which includes geological analysis, coal seam fractures survey, underground stress measurement, rock constituent analysis, and mechanical tests of the roof and floor rock. The results show that (1) the neo-tectonic survey indicated an overall shift of stress field, where the maximum principal stress changed from the E-W to the N-S direction and the minimum principal stress shifted from the N-S to the E-W direction; (2) the underground stress tests proved that the in-situ measured maximum and minimum principal stress was $200 \sim 206^\circ \angle 7^\circ$ and $111 \sim 117^\circ \angle 7^\circ$ in strike respectively, which were agree with the regional tectonic movement; (3) water in the coal seams was observed releasing from and flowing along two groups of water-conducting fractures with the strike of $10 \sim 20^\circ$ and $285 \sim 295^\circ$, which were consistent with the regional neo-tectonic movement and stress field; (4) the sandstone of the roof and floor formations is mainly composed of grains of feldspar and lithic and clay fillings, which makes the fractures in the roof and floor strata almost closed and the whole roof and floor even serve as aquifuge; and (5) the unusually high strength, hardness and brittleness of coal seams makes it generate a large amount of open fractures. The effective water control measures involved pre-water-availability exploring and dewatering of the coal seam aquifer and the coal mines had kept safe mining so far.

Keywords: Coal seam, main aquifer, cause, neo-tectonic movement

Introduction

Hydrogeologically coal seam is always viewed as aquifuge. However, the upper mineable coal seams of the Ordos Jurassic Coal Basin were actually disclosed as the main flooding aquifer of the coal mines. To investigate the occurrence of the coal seams as the main aquifer, a comprehensive method is adopted, which includes geological analysis, coal seam fractures survey, underground stress measurement, rock constituent analysis, and mechanical tests of the roof and floor rock.

Proofs of the coal seam as an aquifer

It was convinced that the water violently bursting into the central intake and venting shafts under construction was running out from the No. 2 coal seam at X coal mine. When digging the central intake and vent

shafts and just approaching the No. 2 coal seam, one routine explosion accidentally induced such a big water inrush of $82 \text{ m}^3/\text{h}$ with high water pressure of 2MPa that the shafts being digging were flooded then.

Further exploratory drilling revealed that the No. 2 coal seam was functioning as a typical aquifer. In order to salvage the flooded shafts, the ingates of the shafts had to be elevated by 23 m and then a series of hydrogeological exploratory boreholes were drilled. From October of 2011 to December of 2012, seven boreholes were drilled at the main-gate towards the underlying No.2 coal seam. It showed that (Table 1) the inrush of water into the boreholes occurred when drilling reached 0.7-6.7m above the coal seam, then violently increased to the its peak flow after drilling 0.2-1.7m into the coal seam, and fi-



nally didn't go up any more even till the borehole fully penetrating the coal seam. Hence it indicated that the coal seam here is a typical and main aquifer, especially its medium and bottom section, to flood the coal mine. Based on the following underground pumping tests, the coal seam was assessed as a medium water-bearing aquifer with a specific capacity of $0.52 \approx 0.82 \text{ L/(m}\cdot\text{s)}$.

The afterwards occurrence of water inrush as excavating the roadways, maingates, tailgates, etc. fully proved that the No.2 coal seam was functioning as the main flooding aquifer. In April 6, 2012, when the return return roadway came across the No. 2 coal seam, coal seam water burst into at an initial rate of $90\text{m}^3/\text{h}$ and the inrush still increased with the further disclosing the coal seam. On Aril 26, 2012, the peak inrush went up to

$540\text{m}^3/\text{h}$. As shown in Figure 1, high dip fractures with a common strike of North-South, where the water was running out, widely and intensively occurred in the No.2 coal seam, which further proved that the coal seam itself was the main flooding aquifer instead of other overlying or underlying weak aquifer.

Geoetic analysis

The neo-tectonic survey indicated an overall shift of stress field, where the maximum principal stress changed from the E-W to the N-S direction and the minimum principal stress shifted from the N-S to the E-W direction. Two in situ stress test were conducted via (Table 2), the results showed (Table 3) that the underground stress tests proved that the in-situ measured maximum and minimum principal stress was $200\approx 206^\circ \angle 7^\circ$ and

Table 1. Comparison table of construction results of water probe hole constructing

Boreholes	1#	2#	3#	4#	5#	6#	7#
Level of drill floor (m)	914.1	914.6	913.2	901.9	897.3	907.7	907.5
Initial water level (m)		896.8	897.5	893.4	891.8	899.6	896.2
Level of inrush obviously increasing (m)	894.9	895.9	894.3	892.3	891.4	894.5	895.7
Level of coal seam roof (m)	891.0	892.4	891.9	891.1	891.1	892.2	894.9
Level of inrush re-abruptly increasing (m)	890.2	891.9	891.6	890.3	890.9	890.6	894.7
Level of coal seam floor (m)	not yet seen	891.5	not yet seen	889.4	not yet	889.8	894.4
End of the boreholes (m)	889.7	888.5	890.9	889.3	seen	889.78	894.1
Flow rate(m^3/h)	>40	20	>93	29.4	890.6	45	flooded
water pressure (MPa)	2.6	2.5	2.6	2.4	>60		

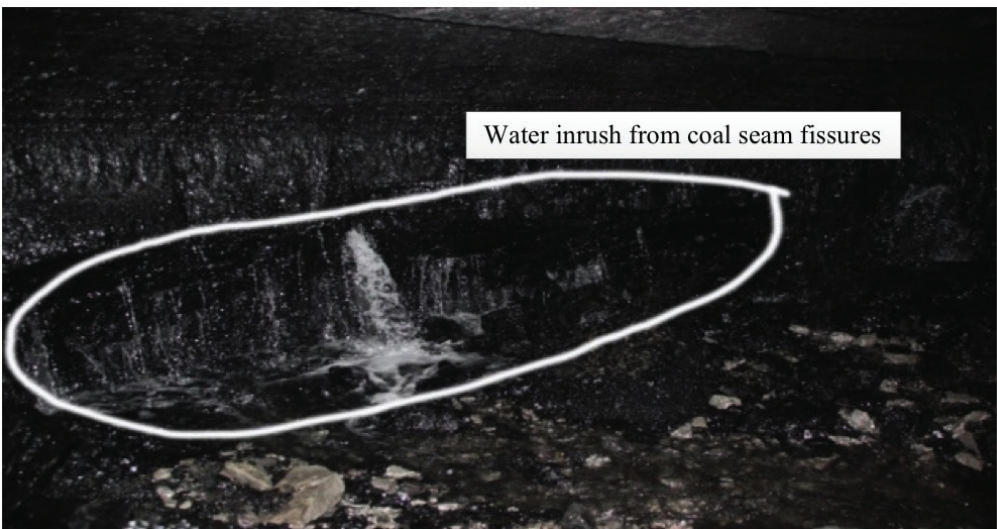


Figure 1 N-S to fractured water in the alley gang coal seam of the return ventilation roadway

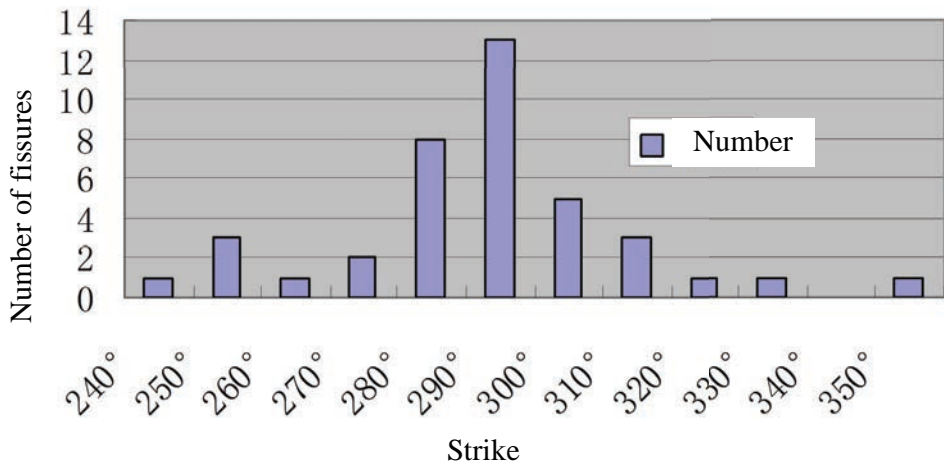


Table 2. Drilling of in situ stress measurement at the X coal mine

Measuring sites	Depth (m)	Location	borehole		
			length (m)	Azimuth (°)	Dip (°)
Point 1#	327	Right side of central air intake shaft	9.6	1	3
Point 2#	325	Left side of central air intake shaft	8.4	55	4

Table 3. Test results of in-situ stress in X coal mine

Measuring sites	Principal stress				Vertical stress (MPa)
	Principal stress	Value (MPa)	Azimuth (°)	Dip (°)	
Point 1#	σ_1	10.74	200.55	6.69	8.97
	σ_2	8.95	58.98	81.48	
	σ_3	7.96	111.17	-5.25	
Point 2#	σ_1	11.25	206.06	-10.65	9.19
	σ_2	9.12	60.82	-77.11	
	σ_3	8.93	117.41	7.18	

*Figure 2 Observation statistics of effluent cracks in 11203 return airway*

111 \approx 117° \angle 7° in strike respectively, which were agree with the regional tectonic movement;

The fracture observation and statistics along the tailgates of Face 11203, as shown in Figure 2, indicated that inrush released from and flowed along two groups of water-conducting fractures with the strike of 10 \approx 20° and 285 \approx 295°, which were consistent with the regional neo-tectonic movement and stress field.

The sandstone of the roof and floor formations is mainly composed of grains of feldspar and lithic and clay fillings, which makes the fractures in the roof and floor strata almost closed and the whole roof and floor even serve as aquifuge (Figure 3). However, the unusually high strength, hardness and brittleness of coal seams makes it generate a large amount of open fractures.



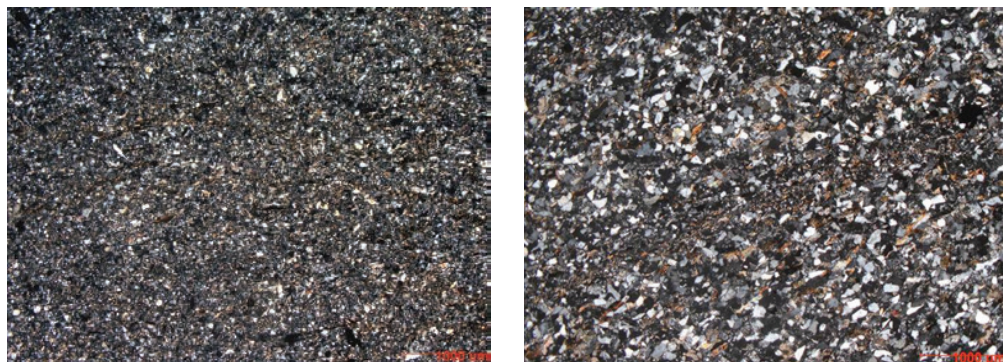


Fig. 3 Overlying clayey siltstone (left) and fine-grained lithic feldspar sandstone (right)

Conclusions

Methods of geological analysis, coal seam fractures survey, underground stress measurement, rock constituent analysis, and mechanical tests of the roof and floor rock were adopted to investigate the occurrence of the coal seams as the main aquifer. Coal seam aquifer mainly contained water in its popular N-S direction fractures, which were consistent with the regional neo-tectonic movement and stress field in the Ordos basin.

The features of unusually high strength, hardness and brittleness of coal seams makes it an aquifer. The effective water control measures involved hydrogeologically exploring and dewatering of the coal seam aquifer.

Acknowledgements

The study presented in this paper was supported by the grant of the National Basic Research Program of China (Grant No 2013CB227900).





Groundwater Modelling in Support of Post-Closure Acid Mine Drainage and Treatment Planning - Case Study

R. Gebrekristos, G. Trusler

*Digby Wells Environmental, Johannesburg, South Africa, +27 11 789 9495, robel@digbywells.com
graham.trusler@digbywells.com*

Abstract

As coal mines close and active dewatering ceases it is likely that most of them will decant over time. This is a major concern in South Africa as the post-closure decant water is often at a low pH and of poor quality. These older coal mines often thus pollute aquifers and rivers with little chance of dilution in the relatively dry interior of the country.

Groundwater modelling was conducted by Digby Wells Environmental on a defunct coal mine that operated between mid 1950's and early 1990's. Mining had been conducted using open pit and underground methods. The mine has been decanting since 2004. The objective of the groundwater modelling was to assess the current groundwater status and predict future acid mine drainage (AMD) decant rates and qualities to be able to properly plan for post closure management and treatment at least cost. The mine is currently decanting at 3.2 ML/d but the prediction is that this could range between 1 and 6 ML/d depending on rainfall conditions and possible subsidence. The decant quality is also variable based on the volume of the flooded mine void as well as the interconnectivity between the open pits and the underground void. The pH of the flooded mine void is neutral as long as more than 95% is under water. The pH is lowered to 3.4 if the water seeps through the pits via interconnecting tunnels. The ideal abstraction point for the AMD treatment was one which was accessible, allowed for least flow of water through the workings, allowed for maximum flooding of the workings whilst still allowing for a buffer in case of heavy water ingress and one which allowed the best quality water to be abstracted. The depth of the pump was determined considering the chemical stratification of the borehole water.

The groundwater modelling was effective in predicting if and where new decants could occur and the expected AMD quality. Passive treatment using constructed wetlands would help mitigate the AMD but will not be sufficient due to the decant volume and site geomorphological setting. Active treatment, such as a reverse osmosis, will be required to ensure that the in-stream water quality objectives are met. Further optimisation of the system to provide water to regional large scale consumers is possible. The use of vegetation to reduce groundwater ingress in some areas seemed to be an effective way of reducing contaminated water volumes.

Keywords: Decant, AMD, groundwater, coal mine

Introduction

Coal is the main energy resource of South Africa contributing to 77% of the energy needs (Department of Energy 2018) and is considerably higher than the 36% average internationally. In addition to its extensive use in the domestic economy, about 28% of the production is exported, making South Africa

the fourth-largest coal exporting country in the world.

Coal is found in 19 coalfields in the country. The pertinent geological features controlling the occurrence and quality of the coal is site specific. A number of the coalfields are found in topographic highs, along watersheds. The seams in low-lying areas have been eroded by rivers and streams (Figure 1).



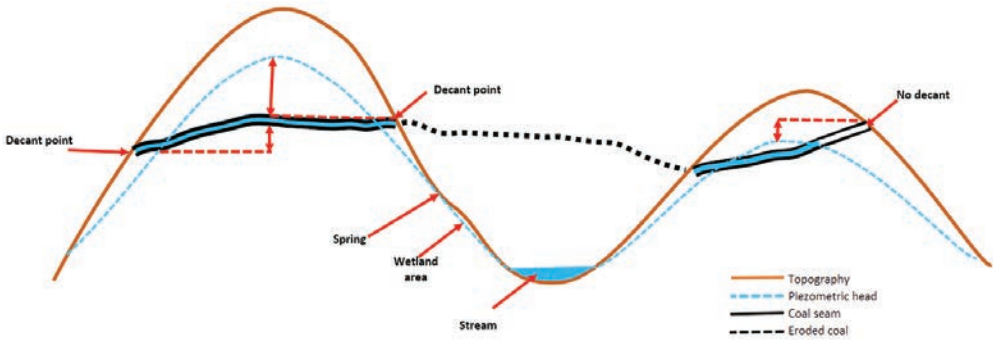


Figure 1: A conceptual model illustrating a coal seam and potential decant points

The steady state hydraulic head is often above the coal seam elevation. Due to this setting, these mines are likely to decant after closure. The decant takes place through shafts, boreholes, geological structures and/or weathered zones connecting the mine void with the topographic surface at an elevation that is lower than the hydraulic head. The decant is a serious environmental concern as it is often of poor quality and low in pH.

This paper looks into a decant investigation conducted at a coal mine in the KwaZulu-Natal. The mine was in operation between 1954 and 1992, and started decanting to the surface water streams in 2004. The objective of the study was therefore to assess the hydro-geochemical status quo and predict future trends in decant rates and qualities with the use of a conceptual and analytical models. The investigation outcome was then used to plan for post closure decant management and treatment at least cost.

The objective was also to define an optimum abstraction point and level to which the water in the working should be maintained to keep long term costs to a minimum and to prevent uncontrolled discharge.

Methods

The investigation was conducted following the review of existing reports, site visit, hydrocensus as well as conceptual and analytical modelling.

The colliery was an underground mine (Figure 2 and Figure 3) with a bord-and-pillar extraction method. Opencast mining was also performed to extend the life of the mine where the depth to the coal seam was less than 20 m below surface. A total of 12 boreholes were drilled for aquifer characterisation and groundwater monitoring. However, only three boreholes (BH1, BH2 and BH3) are included in this paper as they are deemed to be representative.

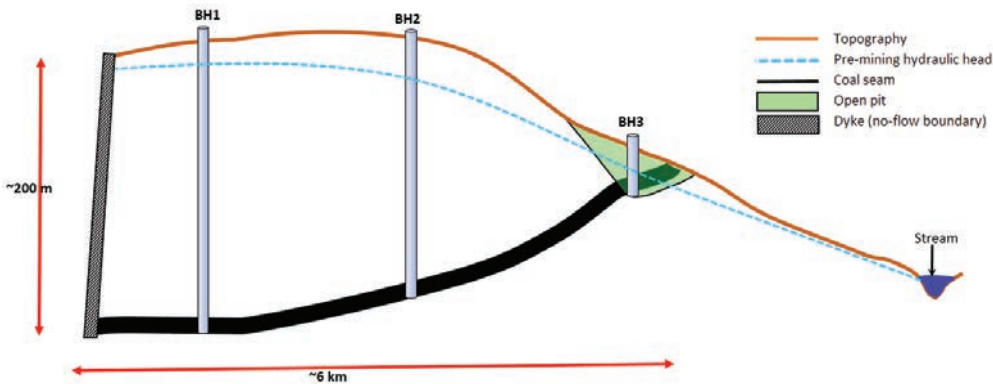


Figure 2: A simplified hydrogeological profile of the project site



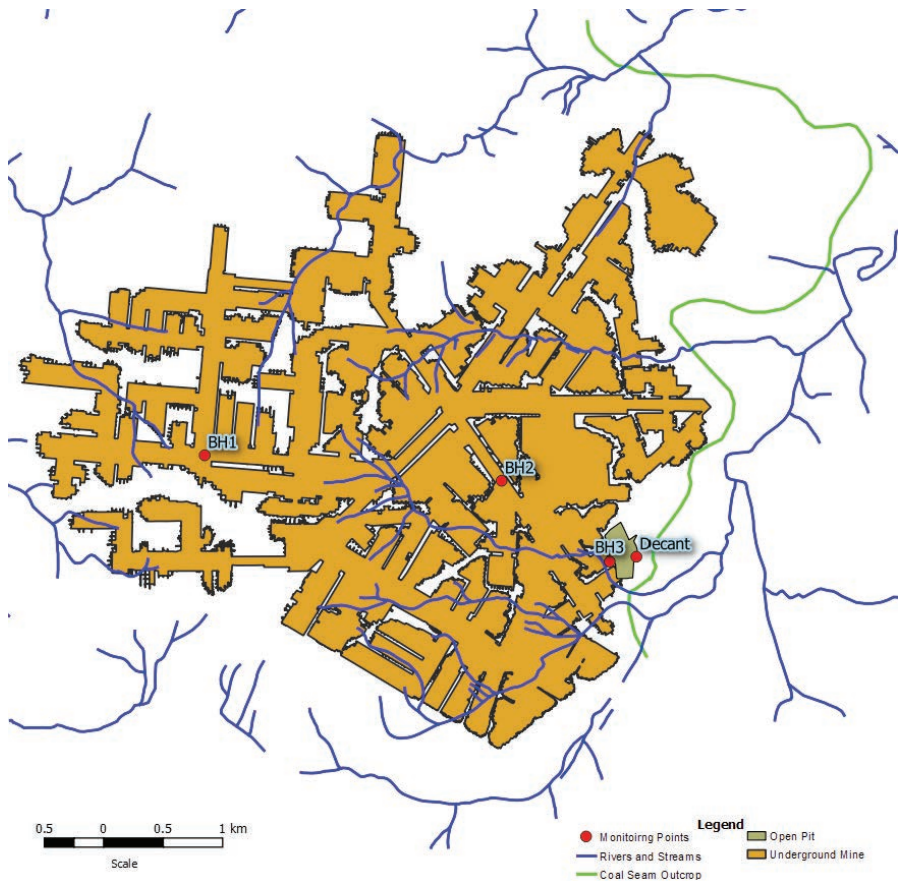


Figure 3: Site layout map

A stage curve (showing the capacity of the void to hold water at different elevations) was obtained from Hodgson (2006) and available mine plans. The maximum storage capacity of the mine void is $43.6 \times 10^6 \text{ m}^3$, found at an elevation of 1194 meters above mean sea level (m amsl).

Discussion

Time-series water level of the monitoring boreholes is shown in Figure 5. By the time the mine closed in 1992, the water level was at 1160 m amsl. This elevation corresponds to a mine volume of $8.8 \times 10^6 \text{ m}^3$ (Figure 4) and indicates that 20% of the void was already flooded. The water level rose steadily and reached to a maximum of 1190 m in 2004 where after decant started to take place from the open pit (Hodgson 2006, Vermeulen et al. 2011).

The decant is taking place at the intersec-

tion of the open pit and underground workings (Figure 5). Currently the water level in all of the boreholes intersecting the coal seam are at the same elevation (approximately 1190 m amsl), meaning that the voids are hydraulically connected.

Considering the amount of water that already existed in 1992, it took 12 years for the mine to flood. This translates into an average recharge rate of $4000 \text{ m}^3/\text{d}$, a conclusion also reached by Hodgson (2006). However, this is an average recharge and the influx into the mine void is seasonally controlled. The total amount could be as little as 1 ML/d in winter and as much as 6 ML/d after heavy rainfall periods. An average yearly value of approximately $3200 \text{ m}^3/\text{d}$ is proposed for the mine.

The water quality can be classified into two distinct water types: those with pH around 7 (all boreholes intersecting the mine void including BH1 and BH2) and those with



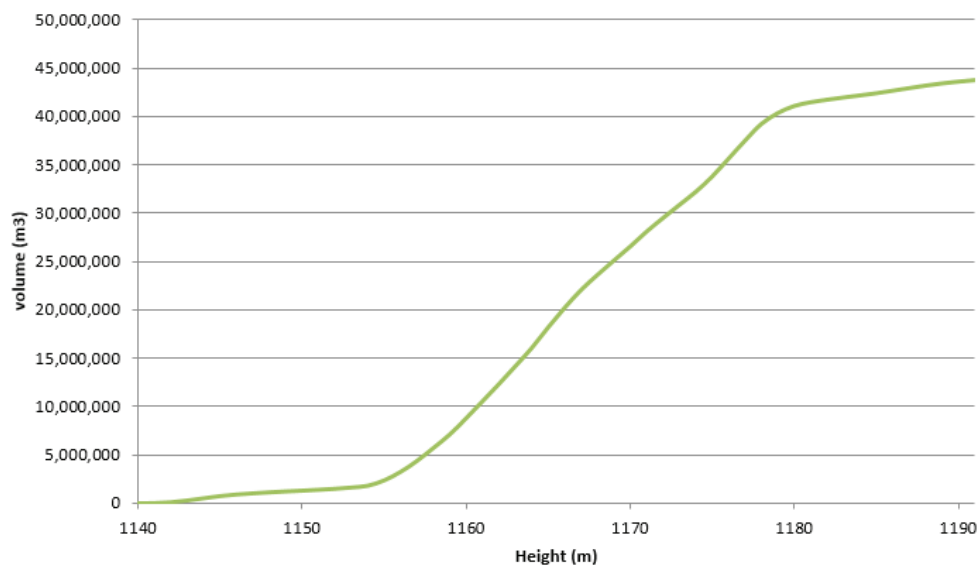


Figure 4: Stage curve of the underground workings

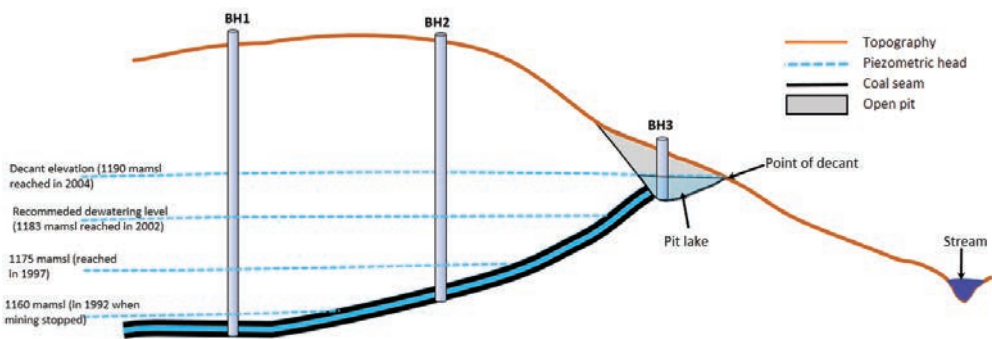


Figure 5: Mine-void flooding history and current decant elevation

Table 1: Mine water quality

Monitoring point	pH	EC	TDS	Cl	Alkalinity	SO4	Ca	Mg	Na	K	Fe	Mn	Al
BH1	7.8	44.3	267	8.8	243	0.92	32	18.3	53.7	2.6	0	0	0
BH2	7.4	50.4	323	22	202	54.2	49.4	15.4	41	15.9	0	0.05	0
BH3	3.5	548	4950	116	<2.48	3574	483	137	586	53.5	325	84.2	26.2
Decant	3.4	551	4912	120	<2.48	3561	453	138	584	53.1	317	81.6	25.9

Units are in mg/L, except for EC where it is in mS/m



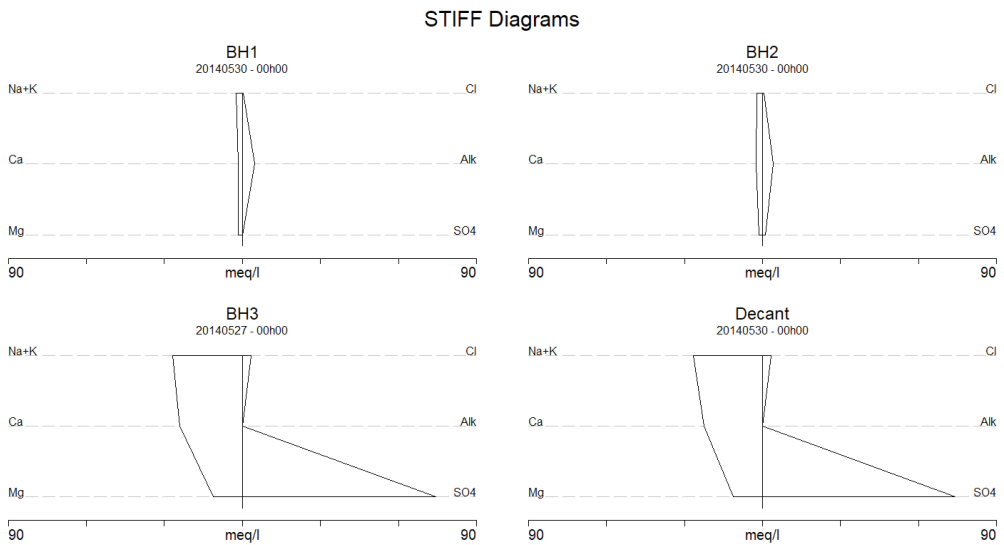


Figure 6: Stiff diagram of the mine water

a value of about 3.5 (borehole BH3 and the decant). The water chemistry is given in Table 1 and displayed in Figure 6.

The fact that the mine pH is around 6.5 indicates that calcium carbonate in the flooded mine voids buffers water from becoming acid. The flooding also minimises pyrite oxidation and hence acid generation.

Borehole BH3 is drilled in the backfilled pit where sufficient oxygen and water exists to generate acid. This borehole has very high sulphate values, together with a number of other elements such as Ca, Mg, Na, K, Al, Fe and Mn. Although the decant is originating from the mine void, it drains through the backfilled pit where the water is exposed to oxygen and the pyrite is oxidised. This results in the lowering of the decant pH, to the same level to the water in the backfilled pit.

Conclusion

Remediation through natural attenuation is not an option. Although the pyrite may eventually be completely oxidised, this is likely to take hundreds of years, if not more. However, there are many active and passive remediation techniques that could be applied based on the final quality objectives and the AMD geochemistry.

Sealing of the decanting point is another option to be considered. The hydrostatic

pressure exerted by the decanting water is proportional to the hydraulic head above the decant point. The sealant applied should be able to withstand the hydrostatic pressure to form a reliable seal. However, the blocking of a decanting hole could force the water to daylight in areas that were not decanting previously and could possibly result in multiple decant zones.

In order to be discharged into the surface water regime and to meet the catchment management objectives, the preferred AMD management was pump and treat. Dewatering for the plant treatment is recommended to be directly from the underground workings to benefit from the alkaline nature of the groundwater. Passive treatment using constructed wetlands would help mitigate the AMD but will not be sufficient due to the decant volume, high proportion of monovalent ions and site geomorphological setting. Active treatment, such as a reverse osmosis, will be required to ensure that the in-stream water quality objectives are met. Further optimisation of the system to provide water to regional large scale consumers is possible. The use of vegetation to reduce groundwater ingress in some areas seemed to be an effective way of reducing contaminated water volumes.

Hodgson (2006) identified that a water elevation of 1188 m amsl has been insuffi-



cient to contain recharge during the rainfall seasons. Considering the average rainfall, lowering of the water level to approximately 1183 m amsl should be sufficient to buffer sudden increase of the decant rate that may be handled by the treatment plant. This elevation should provide for up to 2 years of water storage under average inflow conditions. At this elevation the mine will be flooded to 96% that will limit the space available for potential oxygenation and acid generation.

The volume of the mine void at 1183 m is approximately $41.9 \times 10^6 \text{ m}^3$ (Figure 4). Considering the maximum void of $43.6 \times 10^6 \text{ m}^3$, the amount of water that needs to be pumped is $1.6 \times 10^6 \text{ m}^3$. This is on top of the rainfall inflow of $3200 \text{ m}^3/\text{d}$ into the underground void. If the water level is to be lowered to the buffer elevation of 1183 m within a year, the pumping rate should be $7700 \text{ m}^3/\text{d}$. Thereafter, the rate could be reduced to the decant rate of $3200 \text{ m}^3/\text{d}$.

The ideal abstraction point for the AMD treatment was one which was accessible, allowed for least flow of water through the workings, allowed for maximum flooding of

the working whilst still allowing for a buffer in case of heavy water ingress and one which allowed the best quality water to be abstracted. Treating better quality water at this site would save money due to reduced treatment costs and is possible to maintain this as the working get filled over a large area and not mainly from the outcrop area. Water flow is thus from the deeper levels to the shallow areas.

The mine water quality is stratified. The quality of the upper section of the boreholes intersecting the mine void is cleaner than the bottom section of the boreholes. The depth of the pump was determined considering the chemical stratification of the borehole water.

References

- Department of Energy (2018), http://www.energy.gov.za/files/coal_frame.html
- Hodgson FDI (2006) The Colliery: Update of the water balance for the mine, University of the Orange Free State Bloemfontein 9300.
- Vermeulen D, and van Zyl N (2011), Groundwater investigation at the mine, Draft Report. Report number: 2011/28/PDV.



Furthering the Conceptual Groundwater Model for Sarcheshmeh Copper Pit, Iran

Ismail Mahomed¹, Colleen Kessopersadh¹, Mahmood Shams Alipour²

¹SRK Consulting, 265 Oxford Road, Johannesburg. IMahomed@srk.co.za

²National Iranian Copper Industries (NICICO), 1019 Valy-e-Asr. Avenue, Tehran, Iran

Abstract

A conceptual hydrogeological model is an essential tool for the interpretation of available data and its linkages to understanding the relationships between components of the groundwater system, and other variables in a given problem. The climate, structural geology, dyke emplacement and hydrothermal alteration in the vicinity of the Sarcheshmeh Copper Porphyry play important roles in determining the hydrogeological conditions at the Sarcheshmeh open pit mine. Inflows into the pit and pore pressure distribution around the pit will be dictated by these and other factors. Understanding these factors will help the mine operator's deal with its groundwater issues and optimise water management plans.

Keywords: Conceptual Hydrogeological Model, Sarcheshmeh Mine, Hydraulic Properties

Introduction

The Sarcheshmeh Copper Mine (SCM) is located in the central Zagros mountain range in Iran. The area is characterised by incised watercourses and sparse vegetation of grasses and shrubs. Precipitation occurs as both rainfall and snow and varies with altitude (Figure 1). Rainfall averages between 120 mm to 400 mm per annum with snowfall usually occurring between November and February, but rarely exceeding 50 mm per season.

Mining operations at SCM began circa 1973. The pit floor as at the end 2015 was at approximately 2,337 mamsl, [approximately

200m deep], with the final pit planned to reach 1,852 mamsl, and hence establish a 700 m deep pit. The western highwall, which was developed into the adjacent mountain, is at present over 500 m high and will be approximately 1,000 m high at the end of the life of mine in 2043. Mine waste rock dumps are located across catchment valleys, damming up some of the tributaries.

A detailed conceptual hydrogeological model was developed in order to inform the groundwater management strategies for the planned pit expansion.

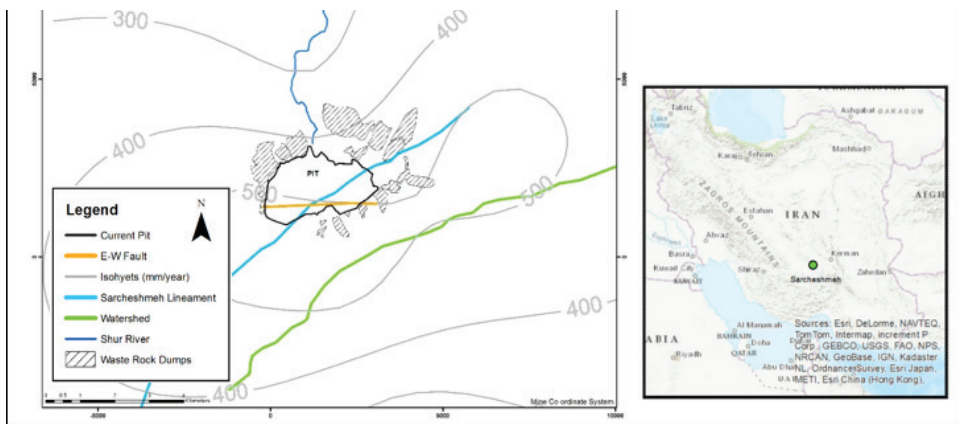


Figure 1: Locality and Isohyets Map



Geology

The SCM is located near the centre of the Zagros mountain belt that is bordered to the south-west by a major thrust zone. The mountains are a complex of folded, faulted and metamorphosed rocks. The mine geology can be summarised as follows:

- The Sarcheshmeh Porphyry and the Late Fine Porphyry are the main intrusions which date from the late Tertiary; these units intruded the early Tertiary andesite host rocks (Figure 2);
- The andesite is flanked to the north by the granodiorite and the quartz-eye granite;
- Metamorphism generated by both porphyry intrusions can be divided into three main alteration zones at SCM; by decreasing intensity these alteration zones are as follows:
 - o High alteration: silicic zone and potassic zone, biotite zone, phillite-sericite-quartz or quartz-sericite zone ;
 - o Moderate alteration: quartz-sericite zone, porphyritic medium-strong and,
 - o Weak alteration: porphyritic weak.
- Three different vertical dyke generations intruded the Sarcheshmeh Porphyry with a general north-north-west to south-

south-east orientation. The thickness is variable but can reach up to 200 m. There are a number of dykes intersected by the open pit and they may represent at least a third of the volume of the pit;

- The strike-slip faults and dykes dip steeply, mostly between 60 and 80 degrees. The faults often have slickensides, are mineralised and altered (SRK, 2015).
- The fault geometry could in part be related to regional north-south directed transpressional right lateral orogeny. This has produced dominant north-west trending right lateral strike slip faults with conjugate north to north-north-east trending, left lateral shears (SRK, 2015).

Hydrogeological units

Groundwater is associated with joints, fractures and faults within the various lithological units. Alteration and weathering has enhanced the hydraulic conductivity of some lithological units. The dykes typically impede flow and are believed to be the cause of the artesian conditions encountered in some of the coreholes drilled in the western portion of the pit. An east-west fault is also presumed

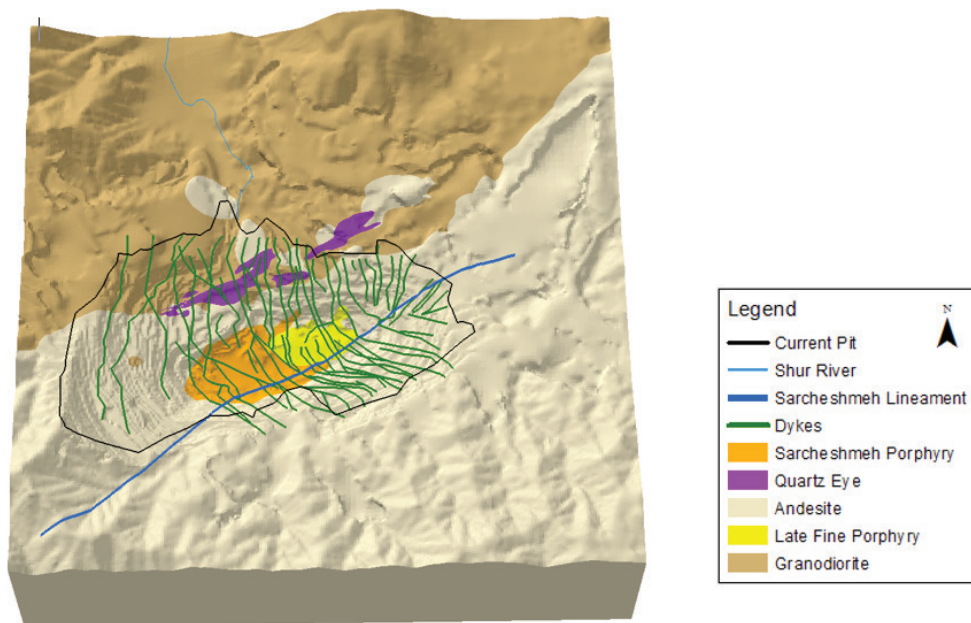


Figure 2: Geological Map



Table 1: Summary of Hydraulic Test Results

Rock type	Hydraulic Conductivity (K) in m/d			No. of tests
	Geometric mean	Minimum	Maximum	
Andesite	0.12	0.03	0.68	7
Granodiorite	0.11	0.02	1.04	16
Hornblende dyke	0.06	0.01	0.23	6
Quartz Eye	0.01	0.01	0.01	1
Sarcheshmeh Porphyry	1.65	1.60	1.70	2
Sarcheshmeh Lineament	3.64	1.07	12.35	2

to impede groundwater flow due to the steep water-level gradient measured across the fault. However the Sarcheshmeh Lineament which is orientated north-east to south-west was found to be a preferential groundwater conduit.

The granodiorite stock and possibly dyke intrusions into the andesite has caused some fracturing and weakening of the rock mass, potentially creating more permeable zones. The contact of the porphyry with country rock is not well understood, but field testing indicates that the porphyry itself is more permeable than the andesite and granodiorite.

The hydraulic conductivity, particularly of the granodiorite, is expected to decrease with depth and to be anisotropic; with preferential flow parallel to the dykes in a north-south direction rather than laterally across the dykes in the east-west direction.

The hydraulic conductivity values range over several orders of magnitude, from 6×10^{-3} m/d to 12 m/d (Table 1). The higher values (those greater than 1 m/d) are associated with the Sarcheshmeh Lineament and Porphyry. There is no distinct hydraulic conductivity amongst the various igneous and metamorphic lithologies; however, values on the upper end of the scale represent the fractures within the rock, whilst values on the lower end represent the weakly jointed, less-fractured rock mass.

Environmental Isotopes

Isotope data indicates that the groundwater originates as precipitation (rainfall and snowmelt) with some evaporation occurring prior to recharge (Figure 3 [includes data from Parizi and Samani, 2014]). The presence of Tritium (^3H) in the shallow groundwater

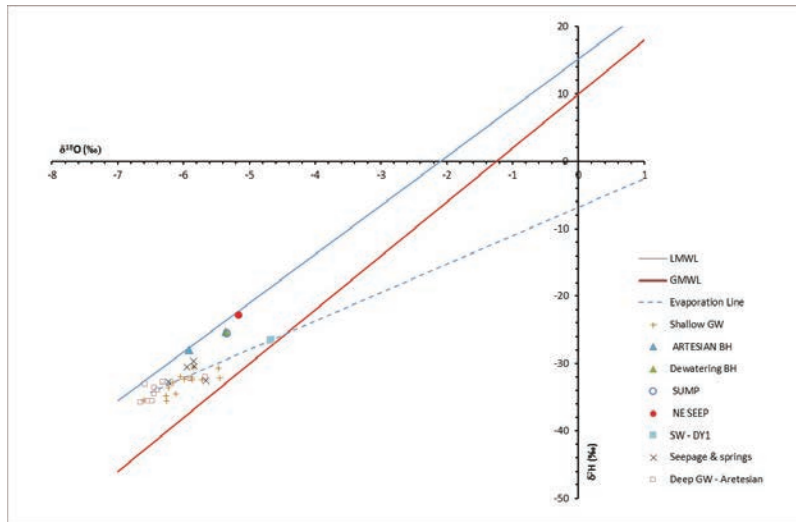


Figure 3: Plot of $\delta^2\text{H}$ (Deuterium) vs $\delta^{18}\text{O}$ (Oxygen-18) (Parizi & Samani, 2014)



samples suggests that shallower groundwater has a residence time of less than two decades whilst the deeper groundwater, although also of meteoric origin, has a longer residence time of two or more decades (Parizi and Samani, 2014).

Recharge and discharge zones

Recharge is expected to vary in accordance with precipitation; however five percent of mean annual precipitation (MAP) was used as a recharge rate in a previous groundwater model developed by HATCH (HATCH, 2003). The NICICO numerical groundwater model estimated the recharge rate to be 20% of MAP using a mass balance approach. Stable isotope data indicates that most of the groundwater recharge in the mine occurs at elevations between 2,730 and 2,970 mamsl (Parizi and Samani, 2014).

Outside the mine pit, groundwater discharges into various drainage lines where it daylights as springs and then flows along defined drainage lines. Many of the drainage lines do not flow throughout the year, and it is likely that the groundwater seeps into the alluvial material and is not evident as surface flow.

Groundwater levels

Water levels around SCM are relatively deep (>100 mbgl). The groundwater level conditions can be described as follows:

- The regional groundwater divide is located south of the Zagros Mountain range. Under natural conditions it would be expected that the groundwater divide would be located at the Zagros Mountain range and would be coincident with the surface watershed. It is possible that the divide has moved to the south due to the expanding zone of drawdown around the pit (Figure 4);
- There is a steep groundwater gradient to the south of the pit area and also along the south-western wall; this gradient appears to be structurally and lithologically controlled and does not appear to be only controlled by the mountainous terrain;
- Seepage faces of between 100 m and 200 m in height are present along the eastern and western highwalls respectively (Figure 4), and this is probably due to reduced pumping capacity; and
- The dykes, particularly on the western side of the pit, act as barriers to flow and cause the groundwater gradients to steepen.

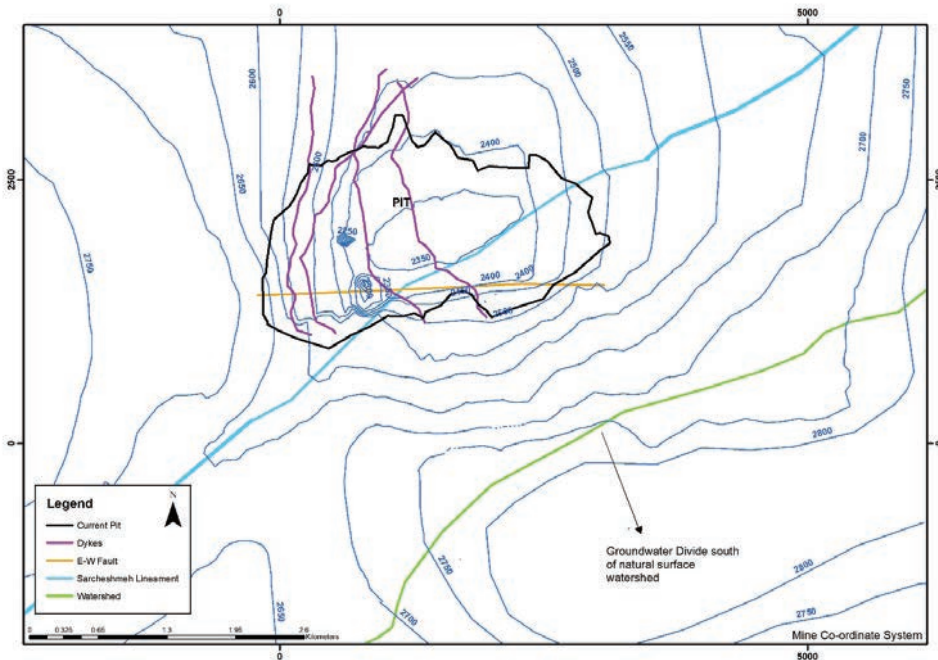


Figure 4: Piezometric Surface (2016-2017)



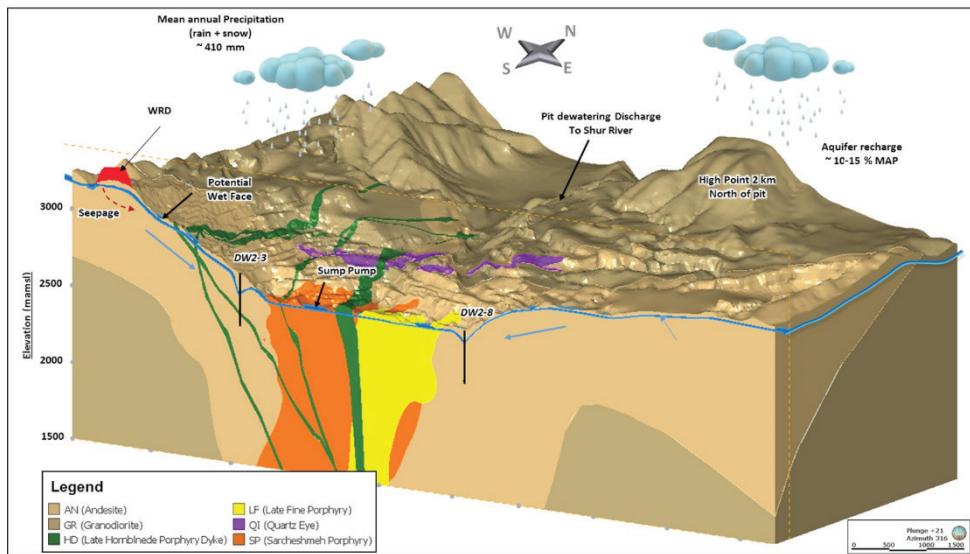


Figure 5 Conceptual groundwater model for the mine site

Conceptual model

At SCM, the granodiorite porphyry stock intruded into an andesite country rock, leading to a hydrothermal alteration of the andesite. The granodiorite stock and possibly the network of dyke intrusions into the andesite has caused fracturing and weakening of the rock mass, potentially creating zones with a higher permeability. The structural geometry in the pit is dominated by steeply-dipping faults and a complex network of dykes. Groundwater is associated with joints, fractures and faults within the various lithological units. In particular, the Sarcheshmeh Lineament which is orientated north-east to south west is permeable and conveys groundwater into the pit. The dykes are typically barriers to groundwater flow, and this is particularly noticeable in the western part of the pit, where some coreholes are artesian on the floor of the pit. Similarly, some structural features such as the east-west fault system to the south of the pit appear to be barriers to flow. The Sarcheshmeh Porphyry itself is generally more permeable than the surrounding andesite host rocks. There is a sharp increase in rainfall from the plain to the mountain peaks, and recharge to groundwater increases with increasing elevation.

The conceptual groundwater model for the mine site is depicted in Figure 5 and

is a synthesis of current information. The groundwater controls are complex and have been simplified in the conceptual model. The key features of the conceptual groundwater model are:

- The Sarcheshmeh pit is located close to the surface watershed and is in the region of highest precipitation; hence it experiences higher recharge rates compared to surrounding areas.
- Groundwater recharge is from rainfall and snowmelt. Groundwater discharges directly into the Shur River, but in addition also to its tributaries, and to springs.
- The dykes, faults and Sarcheshmeh Lineament surrounding and within the pit control the flow of groundwater.
- The Sarcheshmeh Lineament will have to be actively dewatered in order to control inflows into the pit.
- The compartmentalisation of the groundwater indicates that dewatering infrastructure will need to be placed in an arrangement that ensures that zones in front of and behind the dykes are dewatered and depressurised.

Conclusions

SCM is located in a complex geological region, with the complexity effecting the occurrence and flow of groundwater. Many other



mines in Iran are also located in complex geological settings. This case study emphasizes the need for a comprehensive conceptual model founded on good data, for effective mine water management. It also illustrates the need for multiple data sets from multiple disciplines.

Acknowledgements

The authors thank NICICO for granting permission to use their data. The authors thank colleagues for proof reading this paper.

References

- Hatch (2003). Sarcheshmeh Hydrogeological Studies – Phase 3. Conceptual Pit Dewatering Design. Hydrogeological Model of Mine Area. Report No. H/022106
- Mahmoud Alipour (2011). Groundwater modeling and dewatering system design (Abbreviated translation of original Farsi document)
- Parizi, H.S. and Samani, N. (2012). Geochemical evolution and quality assessment of water resources in the Sarcheshmeh copper mine area (Iran) using multivariate statistical techniques. *Environmental Earth Science*. Vol 69. Pages 1699-1718.
- Parizi, H.S. and Samani, N. (2014). Environmental Isotope Investigation of Groundwater in the Sarcheshmeh Copper Mine Area, Iran. *Mine Water Environ*. Vol 33. Pages 97-109.
- SRK 2015. Sarcheshmeh Structural Geology Report. Report No. 452422/7.3.11





The anatomy and circulation of mine water in carbonatite mines with specific reference to kimberlite pipes. ©

Kym L Morton

KLM Consulting Services, Johannesburg, South Africa, kmorton@klmcs.co.za

Abstract

Ground water occurrence and movement around and in Carbonatite mines, specifically diamond pipes, are dominated by three types of structures; first is the weak zone which allowed the carbonatite to be emplaced; second are the structures that opened when the emplacement occurred and third are the relaxation structures created by mining the ore body and country rock. The latter is described as a Zone of Relaxation (ZOR). They are all significant because they control the mechanism allowing the country rock water to enter the mine workings and are important components of the conceptual hydrogeological model. Knowledge and measurement of the three structural domains enable more accurate interception and control of the dewatering over life of mine. Generic domains are discussed, and examples are given from Finsch diamond mine, South Africa.

Keywords: Dewatering, inflows, kimberlite, Zone of Relaxation, ZOR, conceptual modelling, fracture flow

Introduction

Thirty-six years' experience and research has been consolidated into understanding the anatomy of the flow paths of water into deep and shallow mines over their life and closure. Often the ore body is a carbonatite that has been extruded into very old and hard rocks. The hydrogeology of fractured rocks (predominantly metasediments) is different to the hydrogeology described in most European and North American text books, which emphasize primary permeability in sedimentary aquifers.

Some of the main findings are the hydrogeological parameters of the country rock changes as the mine void allows relaxation of the country rock. This creates zones of relaxation and preferred pathways for ground water flow. This necessitates bespoke monitoring designs to ensure accurate and relevant measurement of hydraulic head.

In general, the mine hydrogeology changes over time and depth, and there are specific zones of relaxation with ground water flow along tensional structures, which require targeted dewatering techniques and detailed monitoring for effective and accurate mine water control.

The main applications of this research are in cost effective mine dewatering design

for block cave mines and other deep mines; as well as in more intelligent monitoring of high walls and open pit development. Case studies are used to illustrate the testing and measurement of ground water movement in highwalls, pit bottom and at the contact between the ore body and country rock.

Big Data techniques are used to design, install and implement automated multi probe monitoring systems, often linked to geotechnical monitoring systems. These assist the distinct levels of mine management including production, engineering as well as board level control and allow financial accountability.

Explanation

Understanding of the conduits for ground water flow into a mine has been developed through years of observation as mines developed from open pit to underground. Hypotheses were developed and tested using infiltration tests and packer testing. Results of specific tests are reported in Morton 2008.

The structure of the country rock initially determines the position of the emplacement of the carbonatite or ore body with the ore injection exploiting zones of weakness. For example, during kimberlite emplacement, the country rock is affected by the implosion of the pipe. During mining, the blasting of the



excavation and the relaxation of the rocks into the mining void also alter the original country rock competence and therefore affect the hydrogeology. For hydrothermal emplaced ore bodies, the structural detail can be very fine with openings associated with each branch of stock work.

There are therefore three main structural sets of relevance when interpreting the hydrogeological regime of a mine:

The three types of structures are

1. The pre- emplacement crustal structure and concomitant regional lineaments

2. Structures created during emplacement. This includes the carbonatite-country rock unbonded contact, radial structures and intra-ore body structures between each intrusion
3. Structures created or opened during mining.

Figure 1 illustrates the three types of structures that control ingress of water

The pre-emplacement crustal structure can be determined from regional geological maps of the area and from aerial photo interpretation. Figure 2 shows the pre-cursors as-

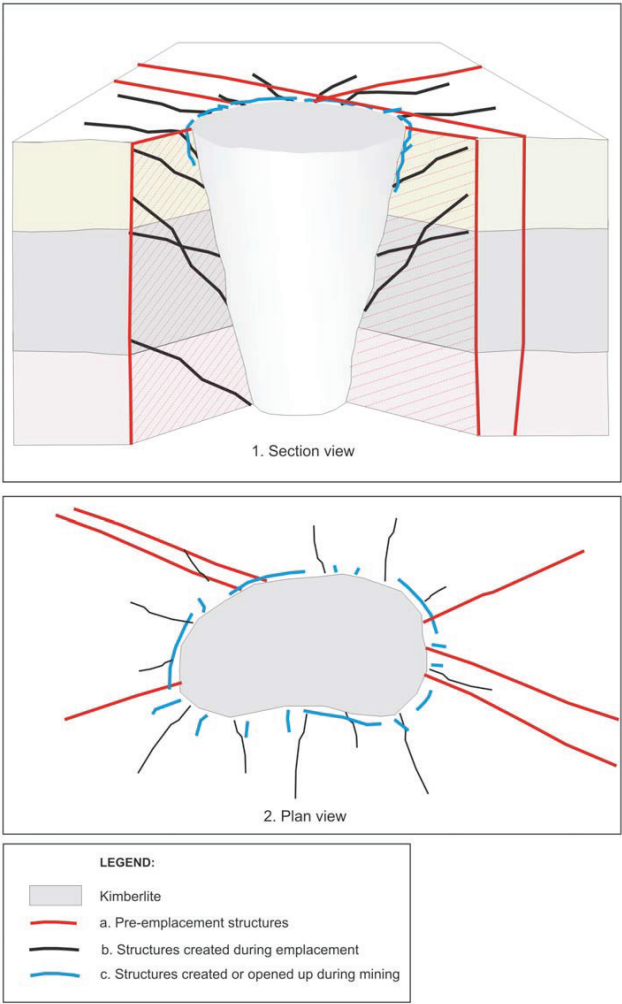


Figure 1 Three types of geological structures associated with carbonatite ore body mines.



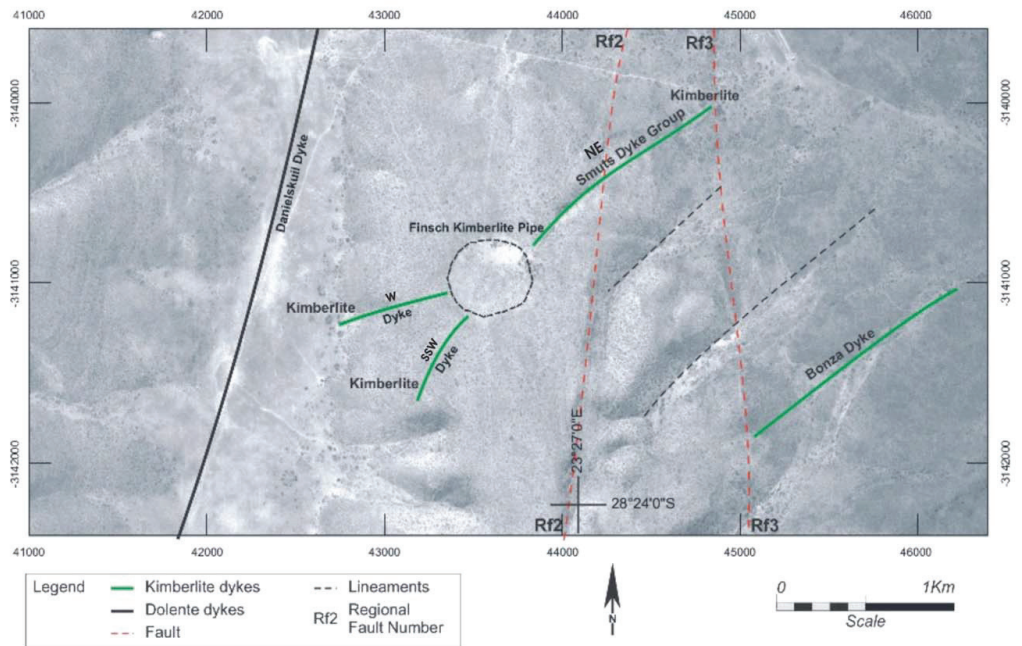


Figure 2 Aerial photograph of Finsch kimberlite pipe and kimberlite dykes (pre-cursors) pre- mining 1959

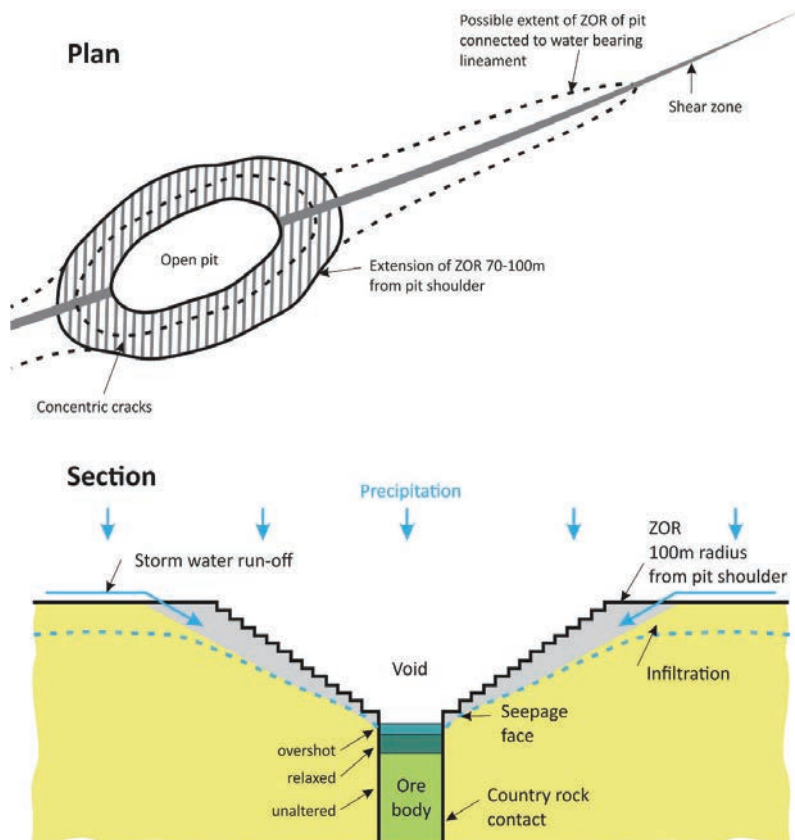


Figure 3 Diagram of the concept of the Zone Of Relaxation (plan and section)



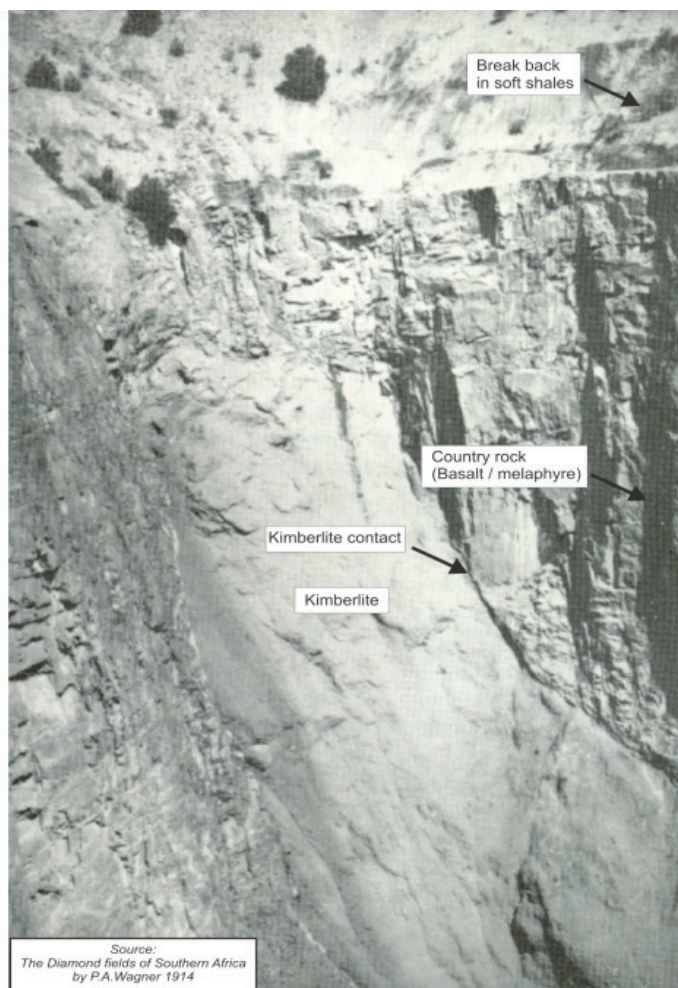


Figure 4 Kimberlite pipe showing clear contact between pipe and country rock (Kimberley Mine) Wagner 1914

sociated with the emplacement of the Finsch kimberlite pipe. Each precursor, when intercepted underground created a conduit for water inflow to the underground workings to 650m depth and below.

Once mining starts the rocks around the pit relax into the void, creating a circular wedge of transmissive rock. Figure 3 illustrates the Zone of Relaxation (ZOR) in plan and section.

Kimberlites have an unbonded contact with the country rock that when relaxed allows rapid movement of ground water.

The floor of an open pit is also connected to the ZOR and shows three layers of differing hydraulic conductivity;

1. The higher K overshoot zone created by blasting, typically 3m – 5m thick
2. The relaxed rock beneath the pit floor, created by pressure release following the removal of the overlying weight of rock, typically 10m – 20m thick but dependent on internal structure and age of pit
3. The unaltered rock below

They are also illustrated in Figure 3. Packer and airlift tests done at Venetia Mine (Morton and Muller 2003) gave K values of the overshoot zone that were 20 times higher than the unaltered ore body.

Figure 4 shows the unbonded kimberlite /country rock contact at Kimberley mine. South Africa.



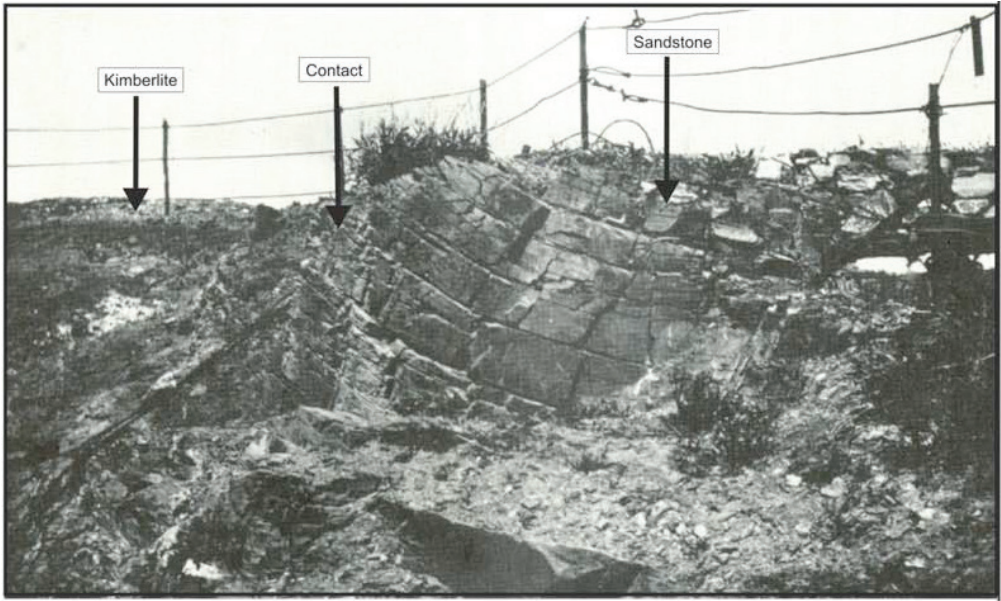


Figure 5 Upturned sandstone at Jagersfontein (Source P.A. Wagner (1914))

Figure 5 shows the upturned sandstone at Jagersfontein mine, South Africa created during emplacement. Figure 6 shows the wet contact at Jwaneng Mine, Botswana created by ground water movement along the open contact.

Figure 7 is the zone of relaxation observed in Finsch Mine open pit.

Packer testing done from underground at Finsch mine in horizontal core holes both inbound and outbound of the ring tunnels on 43 Level (430 mbgl), 59 Level (590 mbgl) and 65 Level (650 mbgl) showed decreasing hydraulic conductivity with depth (Morton 2008). This supported the hypothesis that the ZOR pinches with depth. Figure 8 shows the



Figure 6 Jwaneng Mine Zone of Relaxation and wet kimberlite contact (crater)



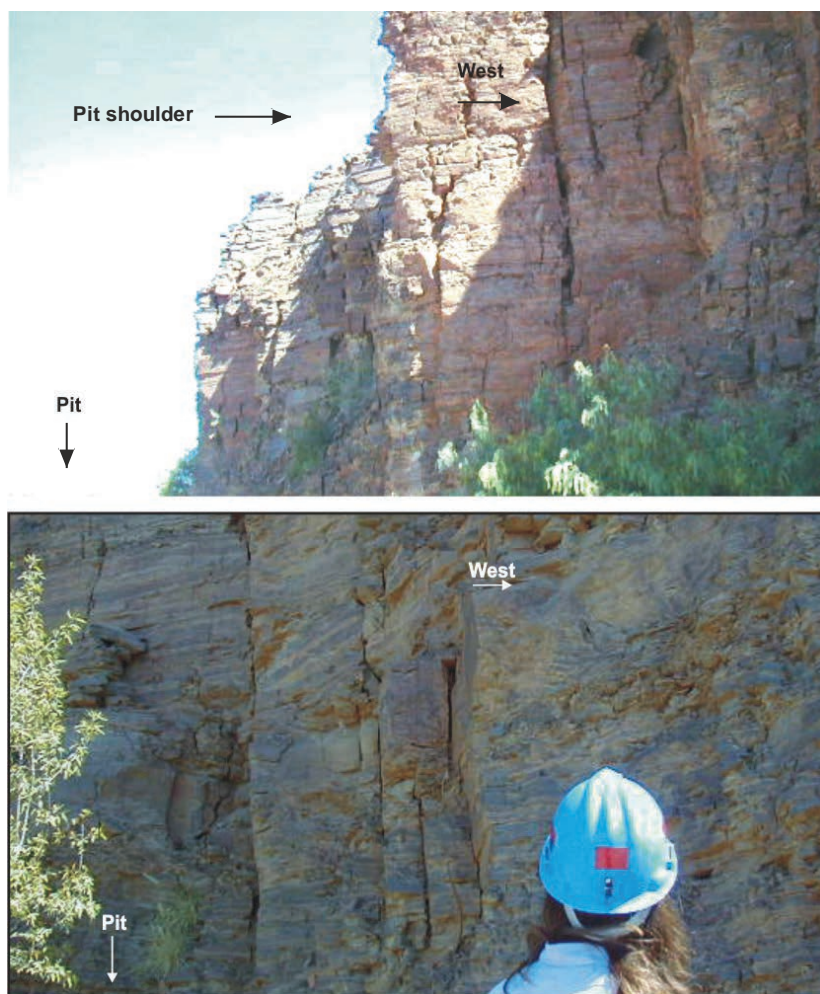


Figure 7 Observation of the Zone of Relaxation (ZOR) in Finsch pit 2002

location of the tested core holes underground in plan view.

Figure 9 gives the hydraulic conductivities and geology in section plotted from the tests conducted on 59 Level.

Knowledge of the three types of structures are useful for understanding then predicting inflows to a mine in a fractured aquifer, as it enables interception of the inflows, management of the water and accurate placement of monitoring devices. The monitoring devices can then be linked to dashboards to illustrate and quantify the effectiveness of dewatering, as well as link expenditure to success.

Conclusions

Experience in watching and monitoring the movement in mines over 35 years of their lives has shown the importance of understanding the flow paths that ground water (and surface water) follows into the workings. Three sets of structures have been observed at carbonatite mines; the weak crustal structures that facilitate the emplacement of the ore body, the structures created during emplacement and the relaxation structures created during mining. All three are important to plot, monitor and manage.



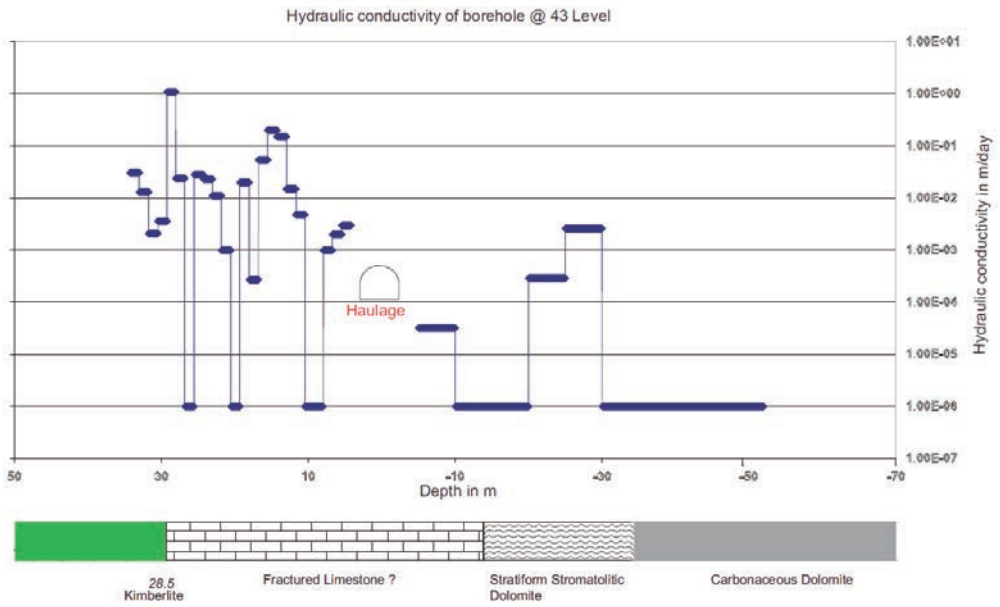


Figure 9 ZOR core hole testing results for 43 level in section

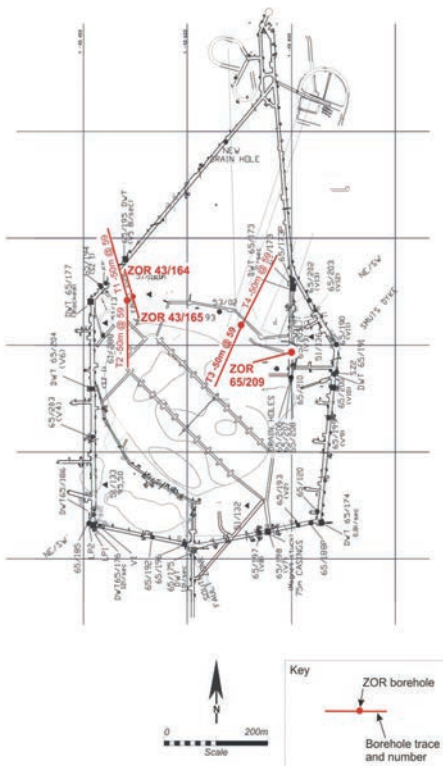


Figure 8 Overlay of the horizontal packer tested core holes on 43, 59 and 65 Levels.

Acknowledgements

The author thanks De Beers' Consolidated Mines for the permission to publish the work and the kind guidance of A R Guest.

References

- Morton KL (2008) The Hydrogeology of Kimberlite Mines in Southern Africa with specific reference to Finsch Mine. PhD thesis, Imperial College, London University 439pp
- Wagner PA 1914 (3rd Edition reprint) The diamond Fields of Southern Africa Struik Cape Town 355pp
- Morton KL and Muller S (2003) The hydrogeology of Venetia Diamond Mine, South Africa, in South African Journal of Geology 106 Number 2/3 September 2003 pp193 – 204



Flow measurement using the salt dilution method at the mine water influenced Tweelopiespruit, Witwatersrand, South Africa

Christian Wolkersdorfer^{1,2}, Elke von Hünefeld-Mugova³

¹*Lappeenranta University of Technology, Laboratory of Green Chemistry, Sammonkatu 12, 50130 Mikkeli, Finland, christian@wolkersdorfer.info*

²*South African Research Chair for Acid Mine Drainage Treatment, Tshwane University of Technology (TUT), Private Bag X680, Pretoria 0001, South Africa*

³*Technische Hochschule Georg Agricola (THGA), Research Institute of Post-Mining, Herner Straße 45, 44787 Bochum, Germany*

Abstract

Out of the different flow measurement methods available, the salt dilution method is highly accurate for measurement under turbulent flow conditions. Not well known in South Africa, the main purpose of this article is to introduce the technique at the Tweelopiespruit, Witwatersrand, South Africa. At five different sites along the stream, measurements in June and October 2014 were conducted. Different from previous investigations it could be shown that the general flow increases during the course of the rivulet and that only minor localized discharge losses can be observed.

Keywords: Flow measurement, discharge, salt dilution method, tracer, Witwatersrand/ South Africa

Introduction

In the past few years, there has been a growing interest in the mine water discharging in the Western Basin of the Witwatersrand, South Africa. After flooding of the abandoned gold mines, first mine water discharges occurred in late August 2002 (Coetzee 2011). The Tweelopiespruit, a stream predominantly recharged by mine water and treated mine water, is highly influenced by its sources (Hobbs & Cobbing 2007). This paper describes the “sudden injection (‘gulp’) method” by using diluted salt as a tracer substance (“salt dilution method”) (Wolkersdorfer 2008) and investigates potential stream loss into the underlying dolomitic aquifer in the reach of the Krugersdorp game reserve. Background of this investigation is the hypothesis that the caves of the world heritage site “Fossil Hominid Sites of South Africa” (vulgo “Cradle of Humankind”) might be negatively effected by the mine drainage form the Western Pool of the Witwatersrand Gold Fields.

Methods

Originating at Robinson Lake, the Tweelopiespruit flows over a distance of approximately 10 km west of Krugersdorp, which is

located 30 km WNW of Johannesburg. Eventually, it flows from south to north through the Krugersdorp Game Reserve and the dolomitic outcrops there.

Underlying the Krugersdorp Game reserve is dolomitic strata, an outlier within the Black Reef Formation quartzite, belongs to the Malmani Subgroup and is characterised by its very porous composition. Mainly, the stream is fed by treated mine water, discharging at various locations along the stream. Additionally, the Tweelopiespruit is assumed to be fed by dolomitic groundwater.

To measure the discharge at six locations in the Tweelopiespruit, the salt dilution method was used, which is discussed in detail by Moore (2005). A high accuracy of the procedure and the possibility to measure under turbulent flow conditions are characteristic for this method. Yet, thorough mixing between the injection and measuring site must be guaranteed. Sodium chloride was chosen as the tracer substance and used for on site measurements of the electrical conductivity change during the course of the study. At each site, 1000 to 2500 g of carefully weighted sodium chloride were dissolved in a 10 L bucket of stream water.



Injecting the tracer into the stream water took place as quick as possible with carefully rinsing the bucket to ensure all tracer was injected. This is referred to as “sudden injection (gulp)” or “slug method” (Wolkersdorfer 2008, Moore 2005). Simultaneously, recording of the electrical conductivity started.

Breakthrough curves represent the relationship between electrical conductivity and measuring time (t). By using the calibration coefficient, the integral for the concentration over time can be calculated, resulting from the linear relationship between electrical conductivity and the dissolved salt content. The discharge (Q) is the quotient of injected salt mass (M) divided by the concentration-time-integral (c_t) (Eq. 1).

$$Q = \frac{M}{\int_{t_0}^{\infty} c_t \times dt} \quad (1)$$

Results and Discussion

An increase in the flow in the course of the Tweelopiespruit can be observed. After the inflow into the game reserve, the flow is increasing. A first peak is reached at measuring point TFS, where after the flow is decreasing again. The increase in flow before TFS is in the same range as the decrease at this measurement point. This is clearly evident in the June 2014 measurement. After measuring point ALS, the following values from June and October 2014 differ substantially. In June 2014 the flow increased by more than 660 L s⁻¹. Then it decreased, with high discharge values over 1000 L s⁻¹. The same trends can be seen in the October measurement with flows being substantially lower.

Flow changes before and after location TFS by approximately the same discharge might be explained by the fact that around this point a larger flow in the gravel bed is occurring. Large infiltration of stream water into the ground is not to be expected.

At measuring point DAD and N14 the discharge for June and October 2014 is substantially different. In June 2014, the measurement was carried out at the beginning of the dry winter season, and little feeder streams above point DAD may have been water bearing. During and after rain events a strong flow

increase in Tweelopiespruit by these sources is to assume. The measurement in October 2014 was conducted towards the end of winter, after a long season with no precipitation. The small rivulet upstream point DAD has dried up, hence no increase in discharge can be observed. This lack of precipitation is also responsible for the low mean discharge during the October measurements.

Conclusions

One of the purposes of this paper was to introduce the salt dilution method for flow measurements in South Africa. The method is an effective way for precise flow measurement under turbulent flow conditions, as in the case of the Tweelopiespruit. Sodium chloride as a tracer substance is cost effective and easy to handle.

A strong increase of the flow rate in June 2014 from point DAD can be explained by an additional inflow near the north-western entrance to the lion's camp. However, the degree of inflow needs more detailed investigation. Supplementary measurements with the salt dilution method in the Tweelopiespruit are therefore necessary to verify the findings. Recommended are the establishment of additional measuring points and the implementation in different seasons. Summing up the results of the flow measurement in the Tweelopiespruit, it can be concluded that the flow increases over the measuring distance. Loss of stream water into the underlying karst, and therefore a potential negative influence of the world heritage caves, is not a predominant process.

Acknowledgements

The authors express their thanks for financial support to Tshwane University of Technology, South African Research Chair for Mine Water Management, Freunde und Förderer der Technischen Universität Bergakademie Freiberg e.V. and Förderkreis Freiburger Geowissenschaften e.V. Furthermore, we want to acknowledge S. Du Toit from Mogale City Municipality for his kind support and providing us access to the Krugersdorp Game Reserve. Dr Henk Coetzee thanks for supporting us.

Parts of this paper have already been published in: Hünefeld, E. v. & Wolkersdorfer,



C. (2015): Flow Measurement Using the Salt Dilution Method at Tweelopiespruit, Witwatersrand, South Africa. Paper presented at the Geoecology and Rational Surveillance: from Science to Practice, Belgorod, 6–10 April 2015. – p. 138–141, 1 Abb.; Belgorod (Polyterra).

References

- Coetzee, H. (2011): A flooding and pumping model for the Western Basin of the Witwatersrand Gold Fields, based on empirical data. Council for Geoscience Report No. 2011-0176. Edited by Council for Geoscience.
- Day, T.J. 1976. On the precision of salt dilution gauging. *Journal of Hydrology* 31, pp. 293–306.
- Department of Water Affairs South Africa (2013): Feasibility Study for a Long-Term Solution to address the Acid Mine Drainage associated with the East, Central and West Rand underground mining b. Assessment of the Water Quantity and Quality of the Witwatersrand Mine Voids. Study Report No.5.2. Edition 1.
- Digby Wells & Associates (Pty) Ltd. Co. (2012): Draft Scoping Report for the Immediate and Short Term Interventions for the Treatment of Acid Mine Drainage (AMD) in the Western, Central and Eastern Basins of the Witwatersrand Gold Fields. Digby Wells & Associates (Pty) Ltd. Co. Randburg (12/1220/2403).
- Hobbs, Philip J. (2011): Situation assessment of the surface water and groundwater resource Cradle of Humankind world heritage site. With assistance of Council for Scientific and Industrial Research, Council for Geoscience, Wits School of Geoscience, iThemba LABS, A. Jamison, D. Hardwick. Edited by Management Authority Cradle of Humankind World Heritage Site & Dinokeng, Department of Economic Development, Gauteng Provincial Government.
- Hobbs, Philip J.; Cobbing, Jude E. (2007): A Hydrogeological Assessment of Acid Mine Drainage Impacts in the West Rand Basin, Gauteng Province. Council for Scientific and Industrial Research Natural Resources & the Environment. Pretoria (CSIR/NRE/WR/ER/2007/0097/C).
- Moore, R. Dan (2005): Introduction to Salt Dilution Gauging for Streamflow Measurement Part III: Slug Injection Using Salt in Solution. In *Streamline Watershed Management Bulletin* 8 (2).
- Wolkersdorfer, Christian (2008): Water Management at Abandoned Flooded Underground Mines – Fundamentals, Tracer Tests, Modelling, Water Treatment. Heidelberg: Springer.





17

NEW TECHNOLOGIES



Passive Metal Mining and Mine Water Treatment Using Crushed Concrete

Adrian Brown

*Adrian Brown Consultants Inc., 130 West Fourth Avenue, Denver, Colorado 80223 USA
abrown@abch2o.com*

Abstract

Metal mining and mine water treatment using crushed concrete is passive, simple, long-term, cheap, and sustainable. It can remove >99% of dissolved “trace” metals (including cadmium, copper, iron, mercury, manganese, nickel, lead, and zinc) from water by slowly passing it through a large bed of crushed concrete particles. The water dissolves alkalinity from the concrete and the metals precipitate as hydroxides into the concrete bed. The treated filtered water discharges under gravity. When the alkalinity in the concrete bed is exhausted, the charge is excavated, the metals beneficially recovered, remaining sand and gravel recycled, and the crushed concrete is replaced.

Keywords: Hydrometallurgical mining, mine water treatment, passive treatment, concrete particles, metal impurities, sustainable water treatment

Introduction

There are over 18,000 abandoned metal mines in the Rocky Mountain cordillera in Colorado, USA (Colorado Geological Survey 2018). The majority are small, underground mines, abandoned long ago before there was any requirement for environmentally protective closure. In general the mines were operated by organizations that are long defunct, so there is no financially viable entity remaining to fund cleanup and closure now. Many of these mines have seepage coming from portals and ponds, in general metal-bearing, and frequently acidic. This seepage discharges into the pristine montane streams which form the headwaters of the major river systems of the United States, the Colorado system flowing west, the Rio Grande flowing south, and the Mississippi/Missouri system flowing east. These surface waters constitute a sensitive aquatic ecosystem that supports and contains the economically important sport fishery of the mountain west, an important source of drinking water for most of the cities of the mountain and western US, and a substantial proportion of the water used by agriculture, industry, and mining in the arid west.

There has been a continuing need for a method of dealing with the mine discharge water that is capable of being deployed and

operated in the rugged terrain of the Rockies. Such a method has to meet a demanding specification: 1) be passive enough to allow unattended operation over particularly the winter months, when most of the mine sites are inaccessible; 2) inexpensive enough to be funded by the small municipalities and non-profit entities who are affected by the contamination; 3) simple enough to be installed and operated by the volunteers who form the bulk of the committed stakeholder group who are determined to solve this problem; 4) acceptable to regulatory agencies for deployment in these mountain sites without prohibitive site-specific testing and demonstration; and 5) generate no waste.

This paper describes a system that has the ability to meet that specification, and produce usable metal from it to generate revenue. Applied across the abandoned mines in the Rocky Mountains, such a system would result in substantial metal production, as well as perform an important water quality cleanup for the nation's river systems.

Metal removal from water using crushed concrete

When water containing metal impurities (in particular Al, Cd, Cu, Fe, Hg, Mn, Ni, or Zn) is brought into contact with crushed



concrete and is allowed to approach chemical equilibrium, the metal impurities are removed (Schreiter et al. 1994; Johnson et al. 2000). The typical quality of the water that the author’s testing has shown results from this process is largely independent of the pH and the input concentration of the trace metals in the water being processed (Tab. 1). In addition, the concrete does not add any substantial concentration of metal impurities to the flow. This behaviour provides the basis for a method to remove trace metals from water and concentrate them in the solid phase.

Metal Removal Process

The metal removal process using crushed concrete involves these six steps: 1) Water containing trace metals contacts the crushed concrete, 2) Cementitious constituents in the concrete slowly dissolve, 3) The alkalinity of the treatment water is raised, to pH in the order of 12, 4) Metal impurities in the influent water form hydroxides and precipitate, 5) The precipitates are filtered out of the water flow and retained in the concrete granular mass and 6) Water substantially free of trace metals

flows out of the crushed concrete treatment bed for discharge.

Metal Recovery Process

When the cementitious material is exhausted, it is excavated and the metals are recovered by a four-step-process: 1) Metal hydroxides are removed from the sand and gravel host material by mechanical separation (trommel washing and gravity separation), chemical leaching (acid wash), and/or chelation (EDTA or ammonia leach), 2) Hydroxides are dissolved in acid to create high concentration pregnant liquor, 3) Metals are recovered from the pregnant liquor by electrolytic means and 4) The acid is regenerated from the barren liquor and recycled.

The solid residue from this process is barren sand and gravel, which is recycled, in general as the silicate portion of new concrete.

Metal Removal Facility Specification

The facility for removal of metal from water using crushed concrete has only two essential requirements: it must contain the crushed concrete charge, and it must allow long-term

Table 1 Typical metal impurity removal using crushed concrete; all units in mg/L, pH without unit

Parameter	Influent	Effluent
pH	7	11
Calcium	376	563
Magnesium	121	30
Potassium	4	11
Sodium	73	76
Silica	22	1
Chloride	3	5
Sulfate	1941	1638
Aluminum	0.12	<0.01
Cadmium	0.065	<0.005
Copper	<0.01	<0.005
Iron	94	<0.01
Lead	0.11	<0.005
Manganese	50	<0.01
Mercury	<0.001	<0.001
Nickel	0.12	<0.01
Zinc	125	<0.01



contact between the concrete charge and the water from which the metals are to be removed.

Facilities that accommodate these requirements include the following:

- **Axial Trench:** Concrete is placed in a sloping trench, lined or unlined; metal-containing water is introduced at one end of the trench; the metals are removed in transit; and clean water is discharged at the other end (well suited to stream beds in steep valleys).
- **Upflow Trench:** A perforated delivery pipe is placed in a horizontal trench, lined or unlined, the trench is filled with concrete particles, and water flows upward through the concrete, the metals removed in transit, and clean water is discharged at the top of the concrete charge (well suited to locations where space is limited, such as narrow creek valleys).
- **Side-flow Trench:** Concrete is placed in a horizontal trench, unlined, dug on contour across shallow metal-containing water flow; the water passes through the trench where the metals are removed; and clean water discharges on the downhill side (well suited to treatment of superficial groundwater flow in shallow hillside alluvium).
- **Underground Mine Stope/Drift:** Concrete is packed into or introduced through a borehole into an underground stope or drift which is in the flow pathway for metal-containing water in the mine; the metals are removed and deposited in the placed concrete; and clean water discharges from the mine (well suited to abandoned underground mines in terrain where surface facilities are difficult to locate).
- **Heap:** Concrete is piled on a lined area; the metal-containing water is sprinkled at slow rate onto the concrete; metals are removed in the concrete mass; and clean water is collected from the base of the heap (well suited for a fine-grained concrete charge).
- **Vat:** Concrete is loaded into an impervious containment vessel, the treatment water is passed slowly through the concrete charge, either upflow or downflow, metal

is removed in the concrete, and clean water exits the vat (well suited to low flow, high concentration treatment water, and valuable metals like silver and gold).

Metal-containing Water Specification

The specification of the water from which metals can be removed from the influent water and concentrated in the concrete particulate bed by this method is as follows:

1. Contains dissolved metals at any concentration so far tested (for metal production, the more concentrated the better the result).
2. Is acidic through alkaline (but the system works most efficiently with acidic water).
3. Contains essentially no sediments (to avoid plugging at the influent ports of the treatment system).
4. Is substantially free of dissolved organics, including petroleum hydrocarbons and organic ligands (to avoid metals chelation, which reduces the capture of metals, and increases the concentration of metals in the discharge water, which risks not meeting relevant and applicable discharge standards).

The method works best if influent water is reduced, to minimize precipitation of (particularly) trivalent iron as hydrated ferric oxide (HFO), which may have the potential to coat or partially plug the concrete particles.

Concrete Particle Specification

The specification of concrete particles that can be effectively used in this method is as follows:

1. May be of any grainsize, although grain-sizes in the 5 – 10 mm range are optimal for most systems. Granular concrete may be produced by crushing and screening recycled or new concrete, or by manufacture of agglomerated or formed concrete pellets from sand, gravel, cement and water.
2. Should be clean, that is substantially free of non-concrete materials, including bitumen, soil, vegetative matter, putrescible wastes, solvents, hydrocarbons, pesticides, poisons, pharmaceuticals, and chemicals.



3. May be made using any kind of portland cement, including Type I - General purpose; Type II - Moderate sulfate resistance; Type III - High early strength; Type IV - Low heat of hydration; Type V - High sulfate resistance; waterproof; air entraining cement; high alumina cement; and expansive cement. Other concrete materials cemented with pozzolans may also be effective, but require testing. Metal removal and water treatment time depends on cement type.

Filtration Specification

The crushed concrete particles in the facility bed filter the metal hydroxide precipitates from the treated water, resulting in the discharge being particle free. No additional filtration is required prior to discharge. This may seem surprising, as the mean particle size of the crushed concrete bed is in the order of 1 cm, which is larger than typical filtration beds. The reason the crushed concrete works as a filter is that the retention time is so long and the water velocity so slow that the metal hydroxide particles have time to settle into the interstices of the filter material and be trapped in the laminar flow regime close to the particles.

The precipitate volume is similar to the volume of cementitious material that is dissolved to create the alkalinity that drives the precipitation, with the result that there is no substantial plugging of the granular concrete metal removal medium during the process. If plugging occurs, this indicates that there has been substantial metal recovery, and the concrete particle bed is ready for metal harvesting and replacement.

Bed filtration results in the metal precipitates being captured in the treatment bed, which results in accumulation of metals in the treatment material, a form of supergene enrichment. The crushed concrete treatment bed is transformed by this process into an orebody, which is available for metal extraction when exhausted.

Effluent Water Specification

The specification of the effluent water resulting from treating metal-containing water with concrete is as follows:

1. Quality. The equilibrium quality of the effluent water (Tab. 1) is generally independent of influent water quality, except for major ions like sodium, chloride, sulfur as sulfate, and nitrogen (usually as nitrate), which pass through largely unchanged. In general, calcium is elevated by the treatment. Contact time shorter than that required to approach equilibrium results in less-complete metal production and higher concentrations of metals in the process effluent.
2. Alkalinity and pH. The effluent water is highly alkaline at equilibrium, and emerges from the treatment facility at pH of 10 to 13. Discharge of this water to most aquatic systems is beneficial, as most streams are acidic, and fish do better in hard, alkaline water due to improved gill function. However if discharge water is required to be at a lower pH, the pH can be adjusted by mixing with stream water, by contact with a vegetative bed, or by addition of acid (preferably hydrochloric acid), or by carbon dioxide treatment. The author of this paper is strongly opposed to acid treatment because it wastes resources, adds TDS (chloride or sulfate) to the environment, removes environmentally beneficial alkalinity, makes the treatment active rather than passive, and involves the handling and control of a hazardous material (concentrated hydrochloric or sulfuric acid).
3. Total Dissolved Solids. TDS is slightly reduced by the treatment, due to the increased calcium concentration being more than balanced by the removal of metals and the precipitation of magnesium carbonate (magnesite). Alkalinity increases, but does not add to TDS as it is generally hydroxide alkalinity (cement contains no carbonate, although some concrete aggregate does).
4. Sulfate. Sulfate is not present in noteworthy quantities in concrete, and as a result sulfate is not increased by the treatment. Due apparently to the elevation of the concentrations of calcium and magnesium dissolved from the cement in the concrete, sulfate is in general somewhat reduced in concentration by the treatment.



5. **Toxicity.** The raw effluent water has a Whole Effluent Toxicity (WET) test survival rate for both *Ceriodaphnia dubia* (freshwater flea) and *Pimephales promelas* (fathead minnow) of about 50%. After dilution with approximately equal parts of stream water, survival rates increase to about 100% (Brown 2013).

Post-Treatment Reclamation

Following complete passive metal removal to exhaustion, the concrete particulate medium will contain approximately 23 % w/w Metal Hydroxides, 47% w/w Coarse aggregate and 30% w/w Fine aggregate. It turns out that the metal hydroxides precipitated are approximately the same mass (and volume) as the hydrated cementitious materials dissolved. The exhausted crushed concrete bed can be reclaimed by closure in place. To achieve this, the supply of treatment water is turned off, and the facility is revegetated if necessary. The metals in the closed facility are not mobile, so there is no risk to the environment greater than the risk posed by any other concrete located in the environment.

However, in most applications there will be a permanent water stream requiring continuing treatment. This represents a sustainable opportunity: the spent concrete charge can be dug out and hauled to the concrete source; a new concrete charge can be back-hauled from the concrete source and placed in the treatment facility; at the concrete facility the metals can be extracted from the exhausted concrete, produced, and sold; and the remaining sand and gravel can be recycled to make new concrete.

In this way the treatment cycle is closed, with recycled material as the reagent, and treated water, metals, and concrete sand and gravel as the products. And the produced metal value will offset – or in some cases exceed – the cost of the concrete needed to replace the treatment charge, thus beneficially solving a water quality challenge by reduction of toxicity (conversion of metal from dissolved to elemental form), reduction of mobility (removal of metal from the mobile water stream to the immobile solid phase), and reduction of volume (removal of metals from the environment).

Treatment Time

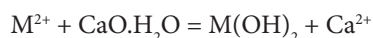
Concrete is almost insoluble, so the contact time that it takes for sufficient concrete to dissolve from the crushed particles to remove metal impurities needs to be in the order of 24 h for most mine waters. This time depends primarily on two factors:

1. **The surface area of the concrete treatment medium.** The larger the specific surface area of the concrete, the more rapid the dissolution of the alkaline constituents in the concrete. Fine-grained crushed concrete (1-10 mm) has a large specific surface area, and treats most metal-containing water in the order of an hour. Coarser-grained crushed concrete (10-25 mm) has a smaller specific surface area, and treatment takes in the order of a day. Larger grainsizes require impractically long treatment times.
2. **The concentration of metal impurities in the water.** The more metal constituents that are precipitated, the more dissolution of concrete is required, and the longer it takes. While the relationship is weak, a guideline is that the treatment time doubles by the time the total metal impurity concentration in the input water reaches 1 g/L, and quadruples by the time the total metal impurity concentration reaches 10 g/L.

The contact time required for metal removal is determined experimentally, by filling a 20 L (5 US gal) HDPE bucket with clean (acid etched) concrete particles of the maximum size expected to be used in the treatment facility, filling the bucket with the test water, and sampling periodically. The contact time is the time taken for the pH of the sampled water to reach 12 (or for the dissolved metal concentrations to reach required regulatory levels for discharge).

Metal Removal Capacity

The metals (M) that are removed by contact with concrete particles (Al, Cd, Cu, Fe, Hg, Mn, Ni, and Zn) are mostly divalent, and the main alkaline component of concrete is portlandite ($\text{CaO} \cdot \text{H}_2\text{O}$), so the metal removal process can be generalized by the following characteristic equation:



As the most abundant metals (Fe, Mn, Zn, Cu) that are removed have molecular weights averaging around 60 g/mol, and portlandite has a molecular weight of 74 g/mol, it follows that dissolution of 1 t of alkaline concrete components will remove about 0.8 tonnes of metal from solution. Typical concrete is made by mixing 8% w/w Water, 15% w/w Cement (dry), 47% w/w Coarse aggregate and 30% w/w Fine aggregate.

Accordingly, concrete typically contains about 23% by weight of hydrated cementitious materials, like portlandite. Based on this, dissolution of the hydrated cementitious components in 1 tonne of concrete can remove up to 0.19 t of metal from water. Put another way, concrete can remove as much as 19% of its weight in metal from the water. Not all of the hydrated cementitious materials in concrete may be sufficiently soluble to participate in metal removal, even in the long term, so a good rule of thumb is that concrete can remove up to 10% of its weight in metals from the water. For most practical mine water metal extraction systems, this results in the facility requiring several thousand tonnes of crushed concrete. Testing by the author referenced above indicates that IRM has a similar metal-removal capacity (Brown 2013).

Metal Removal Facility Design

The metal removal facility must be sized to provide sufficient retention time to allow dissolution of alkaline constituents from the concrete, but may also be sized to contain more concrete if necessary to remove metals from the influent water for a specified life.

Retention time sizing

Sizing for retention time is achieved as follows:

1. Compute the volume of water that must be retained to achieve the required metal removal: $\text{Wastewater retention volume} = \text{flow rate} \times \text{retention time}$
2. Compute volume of crushed concrete necessary to have a pore volume equal to the retention volume: $\text{Concrete Retention Volume} = \text{wastewater retention volume} / \text{crushed concrete porosity} (\approx 40\%)$

3. Compute the mass of concrete that has the concrete retention volume: $\text{Concrete retention mass} = \text{concrete retention volume} / \text{particle density of concrete}$

Facility lifetime sizing

The expected operational lifetime of a single charge of crushed concrete in a metal removal facility designed to hold the above retention volume is computed as follows:

1. Compute the mass of metal that is available for removal from the waste water by the concrete charge: $\text{Metal removal} = \text{mass of crushed concrete} \times \text{metal removal capacity of crushed concrete} (\approx 10\%)$
2. Compute the rate of metal removal from the waste water: $\text{Rate of metal removal} = \text{total mass concentration of metal} \times \text{treatment flow rate}$
3. Compute lifetime of concrete in facility containing the concrete retention mass: $\text{Life of concrete retention mass} = \text{Available metal removal} / \text{Rate of metal removal}$

If a greater life is required, then the concrete particle mass should be increased by the desired multiple.

How it works

As noted above, the hydrated cement that bonds concrete comprises approximately 28% by weight of the total concrete. X-ray diffraction (XRD) identified the two principal alkaline minerals in the hydrated cement in the concrete to be 6% - 12% Portlandite [$\text{CaO} \cdot \text{H}_2\text{O}$] and 3% - 5% Ettringite [$\text{Ca}_6\text{Al}_2(\text{SO}_4)_3(\text{OH})_{12} \cdot 26\text{H}_2\text{O}$]. There is also very likely tricarboaluminate [$\text{Ca}_6\text{Al}_2(\text{CO}_3)_3(\text{OH})_{12} \cdot 26\text{H}_2\text{O}$] and an assortment of calcium aluminum silicates such as Strätlingite [$2\text{Ca}_2\text{Al}_2\text{SiO}_2(\text{OH})_{10} \cdot 3\text{H}_2\text{O}$] making up the balance of the 23% of the hydrated cementitious materials (Matschei 2007). Yet, these are not identifiable by XRD methods, as they appear to be amorphous. Both of the main identified minerals dissolve to release hydroxyl ions as shown by their dissolution reactions, but neither is very soluble as shown by the equilibrium constants of $\log_{10}K = -22.675$ for Portlandite and $\log_{10}K = -44.90$ for Ettringite (Allison et al. 1990; Matschei 2007).



However, at high pH the metals in the influent water form low solubility hydroxides, and they precipitate, removing the hydroxyl ions from the water, resulting in a continuing dissolution of the alkaline materials to replenish the hydroxyl ions in the solution until the metals are removed.

Conclusion

Trace metals (including cadmium, copper, iron, mercury, manganese, nickel, lead, and zinc) can be removed from metal-bearing water by passing it slowly through a large bed of crushed concrete, turning the concrete into an orebody, and reducing the trace metal concentration in the water stream to levels that allow discharge to surface or groundwater resources. The process is sustainable, as the crushed concrete metal-removal substrate is a readily available recycled material, the removed metals are filtered out of the water by the bed material, and the removed metals are recovered from the material when the treatment medium is exhausted or replaced. This metal recovery and water treatment method can be implemented by a relatively unskilled workforce at low cost at almost any location in the world.

References

- Allison JD, Brown DS, Novo-Gradac KJ (1990). MINTEQA2/PRODEFA2 – A geochemical assessment model for environmental systems – Version 3.0 user's manual. Environmental Research Laboratory, Office of Research and Development, U.S. Environmental Protection Agency, Athens, Georgia, 106 p.
- Brown A (2013). Low-cost Long-term Passive Treatment of Metal-Bearing and ARD Water using Iron Rich Material. Reliable Mine Water Technology, Proceedings of the International Mine Water Association Annual Conference, Golden, Colorado, pp 21-27, August 2013.
- Brown A (2017). Process for Removing Metal Impurities from Water. Provisional Patent Application U.S. Serial No. 62/551,911 filed on August 30, 2017. Non-Provisional Patent Application filed April 20, 2018.
- Colorado Geological Survey (2018). U.S. Forest Service Abandoned Mine Land Inventory Project, <http://coloradogeologicalsurvey.org/water/abandoned-mine-land/united-states-forest-hazard-abandoned-mine-land-inventory-project/>, Colorado Geological Survey, referenced 20-July-2018.
- Gao YM (1995). Sorption enhancement of heavy metals onto a modified iron-rich material. Doctor of Philosophy in Civil (Environmental) Engineering Thesis, Lehigh University, Bethlehem PA.
- Johnson DC, Coleman NJ, Lane J, Hills CD, Poole AB (2000). A preliminary investigation of the removal of heavy metal species from aqueous media using crushed concrete fines, Waste Materials in Construction, Woolley GR, Goumans JJM, Wainwright PJ (Editors), Elsevier Science Ltd, 2000.
- Matschei T (2007). Thermodynamics of Cement Hydration. A Thesis presented for the degree of Doctor of Philosophy at the University of Aberdeen, Department of Chemistry, December 2007.
- Schreiter M, Neudert A, Hitzig D, Weigelt H, Priesster J, Dullies F (1994). Process for the precipitation of heavy metals, uranium and toxic metals in the remediation of mining equipment, in particular contaminated water. Patent DE 43 07 468 A1, Deutsches Patentamt, Bundesrepublik Deutschland, 15 September 1994.



Experiences with Autonomous Sampling of Pit Lakes in North America using Drone Aircraft and Drone Boats

Devin Castendyk¹, Bryce Hill², Pierre Filiatreault³, Brian Straight¹, Abdulla Alangari², Patrick Cote², William Leishman²

¹*Golder Associates, Denver, Colorado, United States, Devin_Castendyk@golder.com*

²*Department of Electrical Engineering, Montana Tech, Butte, Montana, United States*

³*BBA, Sudbury, Ontario, Canada*

Abstract

Autonomous drones have created opportunities for pit lake monitoring. This paper reviews two water sampling programs conducted on pit lakes in North America since 2017 using unmanned aircraft and boats. The Canadian-based engineering firm Hatch connected an off-the-shelf unmanned aerial vehicle (UAV) to a commercial sample bottle and collected samples as deep as 80 m from seven pit lakes. Montana Tech used a custom-built drone boat to measure physiochemical profiles and sample the Berkeley Pit. These examples highlight the potential for drones to collect high-frequency, vertically-distributed data from pit lakes, minimize human health risks, and improve pit lake management.

Keywords: pit lakes, UAV, UAS, ASV, drones, sampling, geochemistry, water quality

Introduction

On a global scale, 70% of the properties owned by the six largest mining companies exist in water stressed regions (Beck, 2018). Open pit mining in these regions will often result in the formation of mine pit lakes following mine closure (Castendyk and Early, 2009). Given the present value of water in these regions, post-closure pit lake water quality is highly scrutinized by companies, regulators, and the public. Management of pit lake water quality requires frequent water sampling at multiple depths to assess the accuracy of predictive models, maximize post-mining re-use, mitigate poor water quality, comply with regulatory requirements, and ideally, receive bond return and release from liability. To facilitate best management practices, regulators in the State of Nevada, USA, require pit lakes with maximum depths greater than 8 m deep to be routinely sampled at multiple depths.

However, pit lakes present high health and safety risks for human water samplers. Fatal risks include drowning, hypothermia, rock falls, landslides, tsunami, fall from heights, and asphyxiation from water degassing. These risks are compounded by limited communication, remoteness of sites, and minimal access for emergency response crews. In some

cases, these risks combined with the expense of risk mitigation have been used to justify an indefinite postponement of sampling. The resulting data gaps limit stakeholder knowledge on the state of the pit lake, the ability to verify numerical predictions, and ability to pro-actively manage water quality.

Recent technological advances have made it financially feasible to obtain an off-the-shelf unmanned aerial vehicle (UAV, or drone aircraft) with an advanced flight controller and suitable payload capacity capable of performing routine water sampling at mine sites, and thereby, significantly reduce the risks and costs of pit lake sampling. Since 2013, researchers have used UAV's to collect surface water samples from ponds and lakes (Ore et al. 2015). Castendyk et al. (2017a) collected deep water samples and measured *in situ* physiochemical profiles from a pit lake and a drinking water reservoir using a drone aircraft. This was the first published application of a UAV completing pit lake water sampling at depth.

Elsewhere, advances in communications technology have led to autonomous surface vehicles (ASV; or drone boats) capable of measuring water quality properties (Dunbabin et al. 2009). Duime et al. (2018) report



on a custom-built drone boat which has repeatedly collected samples and measured *in situ* physiochemical profiles from the Berkeley Pit in Butte, Montana, USA.

This paper synthesizes the works of Castendyk et al. (2017a) and Duaime et al. (2018) plus experience from recent sampling events, in order to assess the state-of-the-art of drone water sampling of pit lakes in North America. We identify the successes and challenges facing both programs and define the steps needed for industry-wide adoption of drone sampling techniques. We anticipate that the adoption of drone sampling programs will improve safety, lower costs, produce more data, and ultimately, improve pit lake management.

The Hatch Drone Aircraft

Design and Operations: In 2016, the Chinese UAV manufacturer DJI released the *Matrice 600* hexacopter for \$4,500 USD. With the ability to lift a payload of 6 kg, this drone aircraft made it possible to transport items other than cameras for a considerably lower cost than existing commercial UAV's with equivalent lift capacity. Researchers at Hatch Associates Consultants in Denver, Colorado developed an attachment for the *Matrice 600* which connected the UAV to a 1.2-L Niskin water bottle sold by General Oceanographics in Florida, USA (Castendyk et al. 2017b). This patent-pending attachment enabled the drone to transport the sample bottle at the end of a 100-m static tether (Figure 1). In operation, the drone would lower the sample bottle to the desired sample depth, an independent remote-control would release a 0.9 kg messenger suspended below the drone, the messenger would travel down the tether and close the sample bottle, and the drone would rise and return to the staging area.

Prior to water sampling, the tether was connected to a YSI *CastAway* conductivity, temperature, depth probe (CTD). This lightweight sonde was lowered through the full extent of the water column and measured *in situ* temperature, electrical conductivity and water density as a function of depth at 5 times per second during both the decent and ascent. Upon retrieval, these data profiles were immediately uploaded to a laptop computer via Bluetooth connection. These data served

two important purposes: (1) sounding the lake to find the surface location corresponding to the deepest point in the lake, and (2) defining the depths of internal layers and boundaries (e.g. epilimnion, thermocline, hypolimnion, chemocline, monimolimnion) from which sample depths were targeted.

Two independent methods were used to measure the depth of a water sample. During flights, the drone pilot positioned the Niskin bottle on the water surface and noted the drone's elevation, called the “baseline.” The target sample depth was subtracted from baseline to determine the sample elevation. The drone was lowered to the sample elevation and the sample was collected. The *Matrice 600* has an altitude error of ± 50 cm which became the initial depth error. In addition, a small pressure transducer (Van Essen, *Micro-Diver, DI610*) with a depth error of ± 10 cm at 100 m of water pressure was connected to the mid-point of the sample bottle which allowed the actual depth of the bottle to be verified during post-flight processing. This approach potentially yields greater depth certainty than traditional boat-based methods which typically do not use a pressure transducer.

Achievements: To date, the Hatch drone aircraft has sampled two pit lakes in Ontario, Canada, and five pit lakes in Nevada, USA (Table 1). The system has measured multiple *in situ* profiles of temperature, electrical conductivity and water density from each pit lake, and has collected water samples from multiple depths with a maximum record of 80 m deep in the Pamour Pit at the Porcupine Gold Mines in Timmins, Ontario. To the best of our knowledge, this is the deepest water sample ever collected with a UAV. These flights demonstrated the ability of the system to consistently collect water samples at depth from pit lakes lacking safe shoreline access. The Nevada Department of Environmental Protection (NDEP) observed the system in operation in August 2017 and reported “The methodology is acceptable for regulatory purposes and allows for multiple samples to be collected while maintaining human and environmental safety” (Newman et al., 2017).

Limitations and Challenges: Limitations of the Hatch drone aircraft include the following: (1) The maximum sampling and profil-





Figure 1 The Hatch drone aircraft sampling Pamour Pit, Ontario, Canada, June 2017

Table 1 North American pit lakes sampled by the Hatch drone aircraft

Name	Location	Owner	Depths (m)	Date
Pamour	Ontario, CAN	Goldcorp	3, 15, 80	6 June 2017
Owl Creek	Ontario, CAN	Goldcorp	0, 8, 18	6 June 2017
Boss	Nevada, USA	BLM*	0	30 July 2017
Manhattan West	Nevada, USA	Kinross	0, 12	31 July 2017
Clipper	Nevada, USA	BLM*	0, 7, 30	1 August 2017
Big Ledge	Nevada, USA	NOV	0, 10, 13	2 August 2017
Dexter	Nevada, USA	BLM*	0, 7, 15	3 August 2017

*US Bureau of Land Management, Nevada

ing depth is ≈ 100 m because the maximum height for commercial drone operations in the USA and Canada is 122 m (without special permission); (2) The tether can become snagged on trees or powerlines; (3) The sampling bottle can pendulum below the drone making landing the payload difficult; (4) The weight of the payload limits flight duration to < 15 minutes which negates the use of multiparameter sondes that need ≈ 2 minutes to stabilize readings at each depth; and (6) Moderate winds and light rain can delay or cancel drone operations.

The Montana Tech Drone Boat

Background: The world-famous Berkeley Pit in Butte, Montana, USA, is another example

a hazardous environment for water sampling (Tucci and Gammons, 2015). The circular lake is over 1.6 km in diameter, approximately 370 m deep, and stores about 180 billion litres of water. The US Environmental Protection Agency (EPA) and Montana Department of Environmental Quality (MDEQ) have required semi-annual profiling and sampling of the Berkeley Pit as part of monitoring for the Butte Mine Flooding Operable Unit of the Silver Bow Creek Superfund Site. This sampling was performed manually with a field crew using a boat and traditional sampling methods. By 2013, the pH of the pit lake ranged from 2.5 to 3.0 (PitWatch, 2013). In 1998, a significant slope failure occurred on the south east rim that caused 15 m waves to propagate



across the lake. More recently (2012-2013), a number of smaller wall-rock failures made pit managers concerned that a wave could capsize the sample boat and slam the occupants into the pit walls, resulting in drowning or hypothermia. Due to these health and safety risks, sampling and profiling operations temporarily ceased in 2013.

Design: In 2015, Montana Tech of the University of Montana in Butte, Montana, USA, was commissioned by Montana Resources and the Atlantic Richfield Company (a subsidiary of British Petroleum) to develop a remotely operated, semi-autonomous, drone boat to profile and sample the upper 200 m of the Berkeley Pit. The design had to consider the caustic nature of the water, telecommunication over a large water body, and management of hoses and reels.

The physical platform was built around a 4-m-long, flat-bottomed, drift boat (Duaiame et al., 2018). Two electric trolling motors were mounted in fixed orientation on opposite sides of the boat. Each motor was controlled independently for skid-steer navigation. The boat itself was made of fiberglass and very resistant to the caustic water within the Berkeley Pit. The fiberglass body made an ideal platform for mounting hardware and transporting necessary equipment (Figure 2).

Central control of the boat was built around a Raspberry *Pi* computer. The Raspberry *Pi* controlled several custom printed circuit boards with their accompanying microcontroller to control the data reel, the hose reel, the sampling mechanism, the pumping and various other systems. The two primary tasks were profiling and sampling, but also of interest were auto-pilot and communication.

Profiling the water was performed using a Hydrolab *MS5* data sonde. The data sonde was able to measure depth, temperature, pH, electrical conductivity, dissolved oxygen, and turbidity. The sonde comes with a manually-reeled data cable of 200 m length which had to be motorized to be operated remotely. The reel was also modified to have a bump-stop to sense when the sonde had reeled all the way in, click counters to determine the approximate depth, and a linear stage to raster the cable evenly across the reel. The data from the sonde was able to be logged directly to the Raspberry *Pi* computer during descent and as-

cent through the water column. As with the CTD used in the Hatch system, sonde data aided the targeting sample depths.

Sampling the water was performed using a 228-m-long vinyl hose on a motorized reel. The reel was further modified to have a traveller to raster the hose evenly across the reel. Like the data sonde reel, the hose reel used a click counter and bump stop to manage the length of the hose in the water. It also had a mechanized outrigger to hold the hose below the level of the electric props during sampling and to raise the hose above the level of the water for navigation purposes. To prevent the weight of the hose alone from unravelling the hose, a brake was added to the reel.

An ISCO 3700 sampler was used to pump water from the lake and to store samples in twenty four, 1-L polypropylene bottles. The ISCO 3700 sampler was reverse engineered to be remotely controlled. An additional pump was used to prime the hose to ensure that no air pockets existed within the hose and to purge the volume of the hose between samples. Due to the negative pressure pumping and length of the hose, a single purge volume of the hose took 20 minutes.

Communications were achieved using two different pathways: a 2.4 GHz wifi link using high-gain antennas, and a standard radio control utilizing 433 MHz. The wifi link was able to flawlessly achieve high bandwidth communications at over 4.8 km on water. This allowed for control of the many systems, video and audio feedback, and direct data feedback from the instruments. The 433 MHz radio had to have a modified base station antenna to eliminate picket fence interference (i.e. constructive interference) due to the proximity of the boat's receiver to water. This radio controlled the autopilot as well as the locomotion of the boat.

Video feedback was relayed through the wifi link. These provided feedback with relatively high latency of 500-1500 ms as well as the ability to pan and tilt the cameras. The accompanying audio was an important feedback mechanism for the operator helping to determine when motors were working and whether a command had been completed. A lower latency camera (130 ms) was added for ease of navigation though it was on a fixed view.





Figure 2 The Montana Tech drone boat prior to deployment in the Berkeley Pit, Butte, Montana, USA

Achievements: Between its first deployment in May 2017 and May 2018, the drone boat had completed six successful profiling and sampling trips. A comparison of physiochemical profiles collected between May 2017, October 2017, November 2017, and May 2018 show that average pH rose from 3.7 to 4.2, and that the lake was oxygenated and fully mixed to a depth of 200 m (Montana Bureau of Mines and Geology, unpublished data). Not only has the drone boat allowed data collection to safely resume, the results dramatically reshaped the geochemical conceptual model of the Berkeley Pit, demonstrated the potential to improve the water quality of very acidic pit lakes, and underscored the importance of high-frequency profiling and sampling in pit lakes. The drone boat was actively being used to collect data at the time of writing.

Limitations and Challenges: The principle limitations of the Montana Tech drone boat are: (1) the need to maintain a stable, obstacle-free, access road leading to the pit lake shoreline; (2) the need for humans to drive inside the pit perimeter and manually deploy the boat; (3) the maximum profiling and sampling depth of the boat is 200 m whereas the maximum depth of the Berkeley Pit is close to 370 m, meaning the lower 170 m of the lake is not studied by the system; and (4) with a price tag of close to \$80,000 USD, re-

production of the drone boat for use at other pit lakes may be cost prohibitive. Several challenges, such as picket fence interference and hose line management, created initial difficulties which were surmounted over the course of the project.

Comparison of Methods

The examples presented herein demonstrate the potential for drone water sampling methods to replace traditional water sampling methods in pit lakes. This shift is likely to improve safety, reduce costs, increase data collection, and improve pit lake management. Both systems initially collect profiles of physiochemical parameters throughout the water column, and use these profiles to select appropriate sample depths.

The main advantages of the Hatch drone aircraft are the transportability from pit lake to pit lake and the ability to sample pit lakes that lack any safe access to the water surface. The disadvantages are the short flight times (< 15 minutes), the limited sample depth (< 100 m), and potential air space restrictions. In contrast, the main advantages of the Montana Tech drone boat are the considerable depth of sampling (> 200 m), the profiling of additional physiochemical parameters, and the ability to collect two dozen water samples in a single voyage. The disadvantages include the need for a safe, stable access road and for



humans to drive the drone boat to the lake shoreline, plus the high cost. Both systems operate best under calm winds, flat water, and no rain.

Both drones fill sampling niches and are likely to be utilized in the future. Mining companies that anticipate developing low-water-quality, deep pit lakes that will require routine sampling long into the future may consider building a dedicated drone boat. This will ensure frequent water sampling provided there is continuous access to the shoreline. Mining companies looking to survey existing pit lakes on their properties may wish to initially employ a drone aircraft.

Steps Needed for the Adoption of Drone Water Sampling

The following non-technical issues need to be investigated before the mining industry widely embraces drone water sampling: (1) Mining companies need to quantify the costs and safety risks associated with boat-based sampling and compare these against drone sampling; (2) Regulators need to accept water samples collected by drones for compliance monitoring; (3) Mining companies need to review insurance and liability requirements for drone pilots to ensure that the level of required financial assurance is consistent with the degree of risk; (4) Government agencies overseeing commercial drone activities need to clarify requirements for commercial drone pilots and advance beyond line-of-site operations; (5) Consultancies need to train commercial drone pilots consistent with local government regulations; and (6) Mining companies need to sign non-disclosure agreements to protect the intellectual property rights of drone innovators.

Acknowledgements

The authors wish to thank Hatch Associates Consultants, Mississauga, the University of Colorado, Boulder, Montana Tech, Montana Resources, and Atlantic Ridgefield for their support of this research. We especially thank Connor Newman at NDEP for his willingness to observe water sampling and to evaluate our methods. We also thank Denver Water, Goldcorp Porcupine Mines, Kinross Round Mountain Mine, NOV Big Ledge Mine, the

US Bureau of Land Management, and Montana Resources for permission to collect water samples.

References

- Beck, C. (2018) Keynote Presentation, Annual Meeting, Soc. Mining, Metallurgy, and Exploration. Minneapolis, MN
- Castendyk D, Eary LE (eds.) (2009) Mine Pit Lakes; Characteristics, Predictive Modelling, and Sustainability. Soc. Mining, Metallurgy and Exploration, Littleton, CO, 304 pp
- Castendyk D, Straight B, Filiatreault P (2017b) Apparatus connecting a water sample bottle to an unmanned aerial vehicle (UAV) in order to collect water samples from below the surface of a water body. US Patent Office Application US20170328814A1: patents.google.com/patent/US20170328814A1/en
- Castendyk D, Straight B, Filiatreault P, Thibeault S, Cameron L (2017a) Aerial drones used to sample pit lake water quality reduce costs and improve safety. *Mining Engineering* 69(7): 20-28
- Duaime TA, Icopini GA, Hill BE, Cote P, Leishman W, Alangari A, Erickson M, Holliday T, Ellertson C, Fricks T (2018) Unmanned Partially Autonomous Boat for Profiling and Sampling the Berkeley Pit. *Proc. 11th Int. Conf. Remediation of Chlorinated and Recalcitrant Compounds*, Battelle, Palm Springs, CA
- Dunbabin M, Grinham A, Udy J (2009) An autonomous surface vehicle for water quality monitoring. *Proc. Australasian Conf. Robotics and Automation*, vol. 13, Sydney, NSW
- Newman CP, Castendyk D, Straight B, Filiatreault P, Pino A (2018) Remote water-quality sampling of Nevada pit lakes using unmanned aircraft systems. *Geological Society of America, Abstracts with Programs* 50(5), doi: 10.1130/abs/2018RM-313820
- Ore JP, Elbaum S, Burgin A, Detweiler C (2015) Autonomous aerial water sampling. *J Field Robotics* 32(8): 1095-1113, doi:10.1002/rob.21591
- PitWatch (2013) What's in the Berkeley Pit water? Berkeley Pit Public Education Committee, Butte, MT, July 6: www.pitwatch.org/whats-in-the-berkeley-pit-water
- Tucci NJ, Gammons CH (2015) Influence of copper recovery on the water quality of the acidic Berkeley Pit lake, Montana, USA. *Environmental Science and Technology* 49(7): 4081-4088



Desulphurisation of fine coal waste tailings using algal lipids

Kudzai Chiodza¹, Susan TL Harrison¹, Marijke A Fagan-Endres¹

¹Centre for Bioprocessing Engineering Research (CeBER), Department of Chemical Engineering, University of Cape Town, South Lane, Upper Campus, Rondebosch, Cape Town, 7700.

CHDGOD002@myuct.ac.za, sue.harrison@uct.ac.za, marijke.fagan-endres@uct.ac.za

Abstract

Flotation desulphurisation experiments were performed using algal lipids (raw algal lipids (RALs) and their derivatives, fatty acid methyl esters (FAMES)) as biocollectors for recovering saleable clean coal from waste. The results from batch flotation experiments on a coal sample from a site in the Waterberg region in South Africa were evaluated in terms of overall yield, recoveries (combustibles, ash and sulphur) and product quality (ash and sulphur content). The product yield using the lipids was between 34 and 35%, with a combustible matter recovery between 40 and 50%. The lipids reduced the ash content of the discards from 49% to less than 27%, and the sulphur content from 5.7% to less than 2.8%. These results were comparable to those obtained using oleic acid under similar conditions.

Keywords: Algal lipids, fatty acid methyl esters (FAMES), oleic acid, coal, bioflotation

Introduction

The amount of coal waste generated annually in South Africa is estimated to be around 60 million tonnes (Chamber of Mines Of South Africa 2018, Department of Energy South Africa 2018). This has resulted in over a billion tonnes of coal waste accumulated in mine dumps in South Africa to date. Apart from its land footprint, the coal waste contains pyritic sulphur which, when oxidised, results in the formation of acid mine drainage (AMD) (Kazadi Mbamba et al. 2012). AMD, once started, has been known to persist for decades, resulting in the contamination of surface and ground water.

Various methods have been developed to prevent AMD forming. One such technique is the two-stage coal flotation for desulphurisation, developed at the University of Cape Town (Harrison et al. 2010, Kazadi Mbamba 2011). The first separation stage recovers clean coal using oleic acid as the collector, and the second stage recovers pyrite using the potassium amyl xanthate (PAX) collector. Applying the two-stage flotation process to coal cleaning showed that it was technically feasible to recover valuable coal from waste tailings (Iroala 2014, Kazadi Mbamba et al. 2012). An economic evaluation of the overall process (Jera 2013) showed greatest sensitiv-

ity to operating costs, primarily the reagent costs, including the oleic acid reagent used in the first stage of the process. The aim of this work was to investigate alternative reagents that will enhance the process economics, while being environmentally benign.

Algal lipids, raw or modified into methyl esters, have physical and chemical properties that are similar to commonly used coal collectors. They have the carboxyl group (-COOH), for the raw algal lipids (RALs) are triglycerides containing three long chain fatty acids (C12 – C22) linked by ester bonds to glycerol. The fatty acid methyl esters (FAMES) are comprised of the single fatty acid chain linked to an alcohol via the ester bond. Both have polar heads and hydrophobic hydrocarbon tails of C12 to C22. These functional groups that make algal lipids of interest in coal cleaning by froth flotation.

Materials and methods

The algal lipids used in this evaluation were extracted from *Scenedesmus* sp. The algae was subcultured in 500 mL aerated and illuminated Erlenmeyer flasks before inoculating into 3.2 L batch photobioreactors. The reactor design, inoculation and cultivation procedure were carried out according to Langley et al. (2012). The algae culture in the airlift



reactors was carried out for at least 25 days to maximise lipid production, based on a recommendation by Mandal and Mallick (2009). The algal suspension was harvested on day 30 of each batch and dewatered using high speed centrifugation (Beckman Coulter Avanti® J-E with JA-10 rotors) at $10\,000 \times g$ for 15 minutes. Raw algal lipids (RALs) were extracted using the Axelsson and Gentili (2014) method. A portion of the dewatered algae was used to produce fatty acid methyl esters (FAMES), which are products of transesterification, using the protocol detailed by Griffiths et al. (2010). The RALs and FAMES were recovered from the solvent phase using a rotary evaporator (Heidolph Hei-VAP Value) and stored in absolute ethanol. Ethanol was used as the carrier solvent for the lipids since it does not interfere with the flotation process, i.e. it does not have any collecting or frothing properties (Klassen and Vlasova 1967).

Fine coal waste from the Waterberg area, South Africa, was used for the coal recovered by batch flotation as the first stage of the two-stage desulphurisation process. Samples were prepared by representative sampling and size reduction as outlined by Kazadi Mbamba et al. (2012). The freshly milled coal had a particle size distribution of 11.8% +212 μm , 31.6% +150 μm to -212 μm , 19.0% +106 μm to -150 μm , 11.4% +75 to -106 μm , 20.8% +25 to -75 μm and 5.5% -25 μm . About 56% of the particles passed through the 150 μm sieve. The sample comprised 49.0% ash and 5.71% sulphur.

In each batch flotation experiment, 34 g milled fine coal waste was added to water at a pH of 2.7 (the natural pH of the coal waste sample) in a 500 mL Leeds-type flotation cell

to produce 6% solids loading. The aeration rate and impeller speed were set at 5 L/min (10 vvm) and 170 rpm, respectively, for all experiments. All experiments used a methyl isobutyl carbinol (MIBC) frother at a dosage of 0.28 kg/t. For the control experiments, oleic acid was used as the collector at a dosage of 2.79 kg/t, based on the results of Kazadi Mbamba et al. (2013). Collector and frother conditioning times were 5 min and 1 min, respectively.

For each batch flotation experiment, the following samples were taken: 2 mL feed slurry; concentrate samples after 0.5 min, 1 min, 2 min and 5 min operation and the residual tails at the end of experiment. These samples were filtered and dried at 80 °C to constant mass (for at least 24 hours), weighed and analysed for ash and sulphur content. Ash analysis was performed according to the South African National Standard SANS 131:2011 and sulphur analysis was done using the LECO S632 (LECO Corporation 2010).

The results obtained were used to determine the following performance indicators: yield – the total mass recovery to the concentrate, combustibles recovery – the amount of combustibles material in the concentrate expressed as a percentage of the combustibles material in the feed, ash recovery – the percentage of ash in the feed that is recovered in the concentrate, sulphur recovery – the percentage of sulphur in the feed that is recovered in the concentrate, and flotation efficiency index – the ability of a collector to effect separation between combustible material and ash. The determination of these is detailed in Equations 1 to 4:

$$\text{Yield:} \quad Y = \frac{M_C}{M_F} \times 100\% = \frac{(T_A - F_A)}{(T_A - C_A)} \times 100\% \quad (\text{eqn. 1})$$

$$\text{Combustibles recovery:} \quad R_C = Y \times \frac{(100 - C_A)}{(100 - F_A)} \quad (\text{eqn. 2})$$

$$\text{Ash recovery:} \quad R_A = Y \times \frac{(C_A)}{(F_A)} \quad (\text{eqn. 3})$$

$$\text{Sulphur recovery:} \quad R_S = Y \times \frac{(C_S)}{(F_S)} \quad (\text{eqn. 4})$$

$$\text{Flotation efficiency index:} \quad FEI = \frac{(1 - R_A)}{(100 - F_A)} \quad (\text{eqn. 5})$$



where Y is the yield (%), R_C is combustibles recovery (%), R_A is the ash recovery (%), R_S is sulphur recovery (%), M_C is the mass of concentrate (g), M_F is the mass of the feed (g), T_A is tails ash composition (%), F_A is feed ash composition (%), C_A is concentrate ash composition (%), C_S is concentrate sulphur (%), and F_S is feed sulphur (%).

Results and discussion

Table 1 summarises the results obtained using RALs, FAMEs and oleic acid on the coal waste from the Waterberg area. Under the

conditions of investigation, the summary shows that there was no statistically significant difference in performance of the two bioflotation reagents in comparison to oleic acid.

In terms of flotation yield and recovery, both RALs and FAMEs gave similar results as oleic acid at the same dosage of 2.79 kg/t (Figure 1). Both reagents recovered about 34% of the waste coal with an increase in combustible material from 52% to 74% and 76% for RALs and FAMEs, respectively, compared to 77% for oleic acid.

Table 1 Collector performance for flotation of sample from the Waterberg area at a collector and MIBC dose of 2.79 and 0.28 kg/t, respectively. Feed had 49.0% ash, 5.71% sulphur.

Collector	Yield (%)	Recovery (%)	Ash (%)		Sulphur (%)	
			Product	Tails	Product	Tails
FAMEs	35.3 ± 0.65	50.1 ± 1.48	24.4 ± 0.18	60.8 ± 1.04	2.76 ± 0.26	5.13 ± 0.17
RALs	34.1 ± 1.18	47.1 ± 1.65	26.1 ± 0.30	59.8 ± 0.20	2.56 ± 0.33	4.68 ± 0.08
Oleic acid	34.3 ± 0.58	50.6 ± 1.15	23.5 ± 0.72	58.6 ± 2.28	2.41 ± 0.20	4.75 ± 0.14

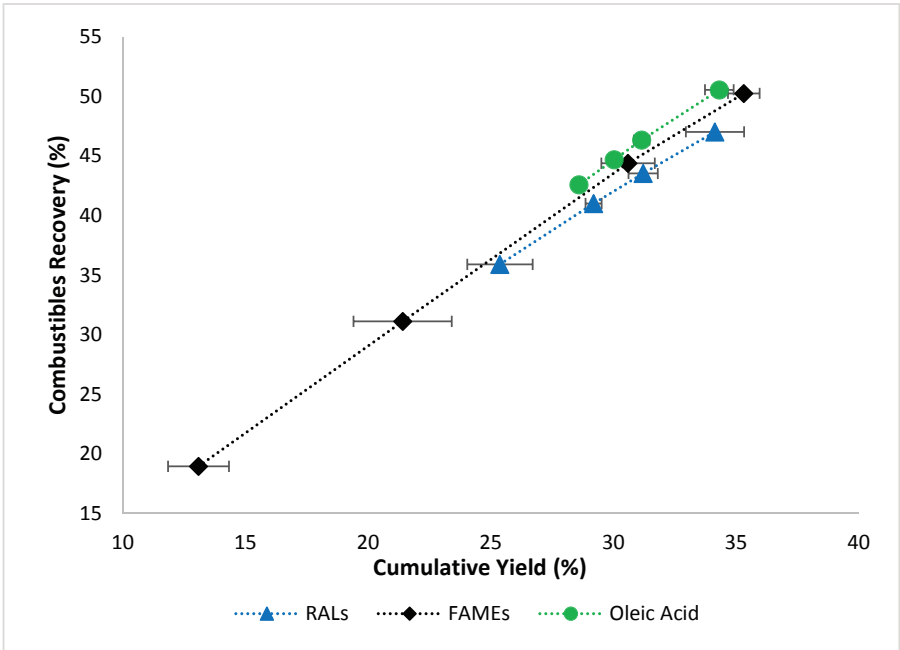


Figure 1 Cumulative yield vs combustibles recovery to the concentrate for flotation of Waterberg discards at a collector dosage of 2.79 kg/t and MIBC dosage at 0.28 kg/t. All points are an average of three experiments. The lowest yield point for each reagent is for concentrate recovered after 0.5 min, subsequently increasing for concentrate recovered at 1 min, 2 min and finally 5 min.



The similarities in performance between the algal lipids and the oleic acid is attributable to the similarities in the chemical structure of the three reagents. As shown in Figure 2, all three reagents have a polar head and a hydrocarbon tail that is hydrophobic.

Figure 3 shows that the selectivity of both bioflotation reagents towards sulphur is similar under the conditions tested. When compared to the algal lipids, the oleic acid showed better sulphur rejection, despite having a higher ash recovery than the two bioreagents. This difference in selectivity is attributable to the chemical composition of the reagents. RALs and FAMEs contain a mixture of molecules, in different proportions, with carbon chain lengths ranging from 12 carbon atoms to 22, compared to oleic acid which is a pure reagent. The molecules with a lower number of carbon atoms are less hydrophobic and easily attach to hydrophilic pyrite particles. This is supported by Han (1983) who pointed out that lower molecular weight collectors are less specific than larger molecular weights.

Figure 4 shows the results of flotation experiments that were carried out at varying

biocollector dosages. The flotation efficiency index (FEI), which is the difference between combustibles and ash recovery, gives an indication of how efficient a reagent is at separating wanted material from unwanted material. It was observed that increasing the biocollector dosage increased the FEI. This is because increasing the concentration of the biocollector in solution increases the chances of hydrophobic interactions between the biocollector and the coal particles. This is supported by the collision theory presented by Demirbas and Balat (2004) where they described the flotation rate as a probability function of collector concentration, aeration rate and other parameters.

It was, however, noted that the increase in FEI with increase in collector dosage was coupled with a decrease in selectivity, with respect to sulphur recovery. For example, at a dosage of 1.20 kg RALs/t, there was about 24% combustibles recovery, 9.3% ash recovery and 12% sulphur recovery, while at a dosage of 3.70 kg RALs/t the coal recovered had a combustibles recovery of 53%, ash recovery of 25% and 34% sulphur recovery.

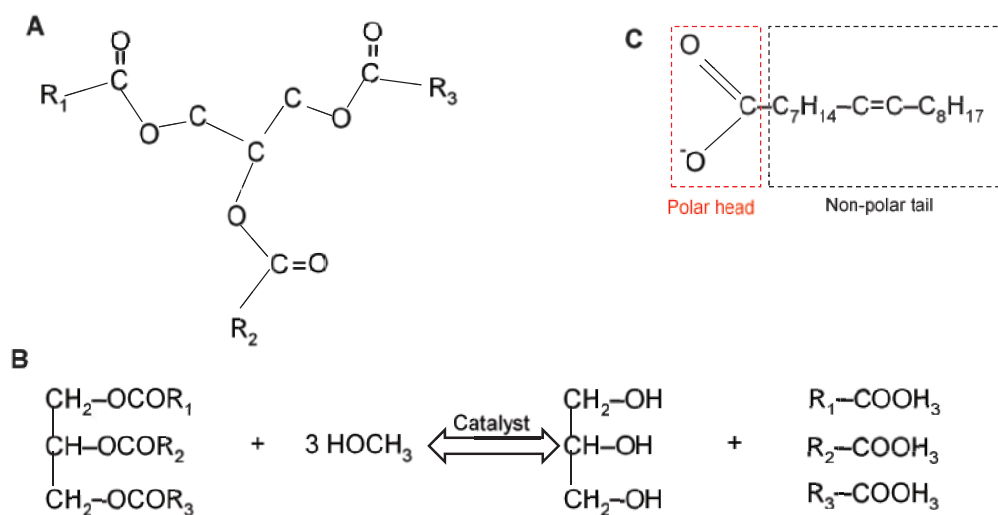


Figure 2 A - a triglyceride representing RALs, B - transesterification of a triglyceride to form a fatty acid methyl esters (FAMEs), C - An oleate ion, formed from the ionisation of oleic acid. The non-polar portions of RALs and FAMEs are represented by R_x where x is 1, 2 or 3. The R_x group can be either saturated (no double bonds in the chain length) or saturated.



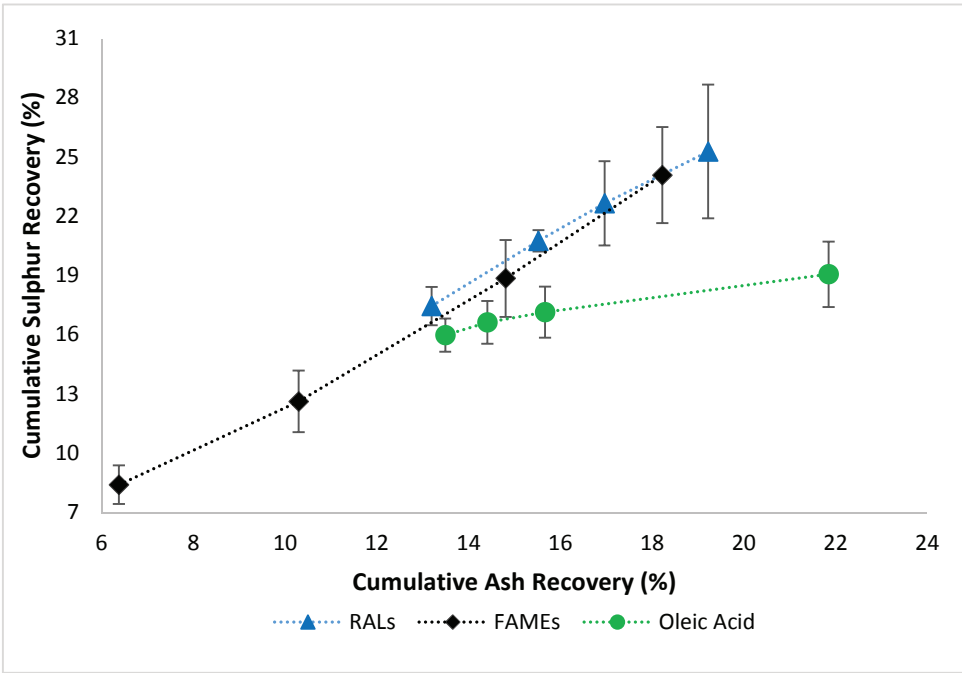


Figure 3 Ash recovery vs sulphur recovery to the concentrate for Waterberg discards flotation at a collector dosage of 2.79 kg/t and MIBC dosage of 0.28 kg/t.

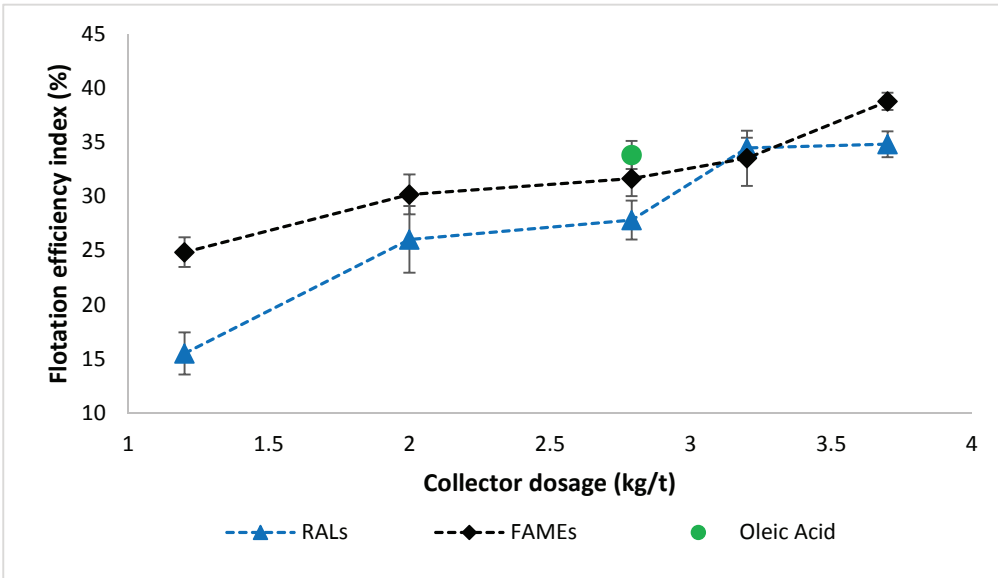


Figure 4 Flotation efficiency index results as a function of biocollector dosage for discards from the Waterberg area. RALs had a low FEI at low collector dosage (1.2 kg/t) compared to FAMEs.



Conclusions

The results proved that biologically derived products have the potential to replace chemically derived collectors for the desulphurisation of fine coal waste by froth flotation. The two bioflotation reagents successfully recovered a combustible coal fraction with reduced ash and sulphur content. The ash content was reduced by about 22.6%, from 49% in the feed to 26.4% in the product coal concentrate, and sulphur was reduced from 5.7% to below 3% in the product coal concentrate. The ash and sulphur were concentrated in the mineral tailings which would enter a second flotation stage for desulphurisation. Despite having the same coal recoveries as oleic acid, the two bioflotation reagents were not as selective as oleic acid with regards to sulphur. However, with further optimisation, the process may be improved to give even better yields, recoveries and selectivity.

A key benefit of biological reagents such as algal lipids is their environmental sustainability, whereas most of the collectors currently used have environmental risks associated with them. A preliminary economic evaluation on the production of the two bioreagents (not presented here) showed that they were about 20% cheaper to produce compared to oleic acid purchase (in 2011 costs), which makes them an economically viable option at the prevailing low coal prices.

Acknowledgements

The authors extend their gratitude to following for their generous financial support: the Water Research Commission (WRC) or their support of WRC K5/2389, Council for Scientific Industrial Research (CSIR) for postgraduate scholarship funding of KC and the Department of Science and Technology (DST) and National Research Foundation (NRF), South Africa for their support of the national SARChI research chair in bioprocess engineering (UID 64788). Further we are grateful to the Centre for Minerals Research (CMR), UCT for use of their laboratory and equipment and to Shireen Govender and Juarez Amaral Filho for technical advice.

References

- Axelsson, Martin, and Francesco Gentili. 2014. “A Single-Step Method for Rapid Extraction of Total Lipids from Green Microalgae.” *PLoS ONE* 9 (2):6. doi: doi:10.1371/journal.pone.0089643.
- Chamber of Mines Of South Africa. 2018. “Coal.” accessed 25 January. <http://www.chamberofmines.org.za/sa-mining/coal>.
- Demirbas, Ayhan, and Mustafa Balat. 2004. “Coal Desulfurization via Different Methods.” *Energy Sources* 26 (6):10. doi: 10.1080/00908310490429669.
- Department of Energy South Africa. 2018. “Coal Resources: Discards.” accessed 25 January. http://www.energy.gov.za/files/esources/coal/coal_discards.html.
- Griffiths, Melinda J., Robert P. van Hille, and Susan T. L. Harrison. 2010. “Selection of Direct Transesterification as the Preferred Method for Assay of Fatty Acid Content of Microalgae.” *Lipids* 45 (11):8. doi: 10.1007/s11745-010-3468-2.
- Han, Choon. 1983. “Coal Cleaning by Froth Flotation.” PhD, Chemical Engineering, Iowa State University (8476).
- Harrison, S. T. L., J. L. Broadhurst, R. P. van Hille, O. O. Oyekola, C. Bryan, A. Hesketh, and A. Opitz. 2010. A Systematic Approach to Sulphidic Waste Rock and Tailings Management to Minimise ARD Formation.
- Iroala, Onyinye Judith. 2014. “Combining Froth Flotation With Reflux Classification to Mitigate ARD Generating Potential of the Waterberg and Witbank Coal Ultrafines Via Sulfide Removal.” Master of Science in Engineering (Chemical Engineering), Chemical Engineering, University of Cape Town.
- Jera, Melody Kudzai. 2013. “An Economic Analysis Of Coal Desulphurisation By Froth Flotation To Prevent Acid Rock Drainage (ARD) And An Economic Review Of Capping Covers And Ard Treatment Processes.” Master of Science in Engineering (Chemical Engineering), Chemical Engineering, University of Cape Town.
- Kazadi Mbamba, Christian. 2011. “Using Froth Flotation To Mitigate Acid Rock Drainage Risks While Recovering Valuable Coal From Ultrafine Colliery Wastes.” Master of Science in Engineering (Chemical Engineering), Chemical Engineering, University of Cape Town.



- Kazadi Mbamba, Christian, J.-P. Franzidis, S.T.L. Harrison, and J.L. Broadhurst. 2013. “Flotation of Coal and Sulphur from South African ultra-fine colliery wastes.” *The Journal of the Southern African Institute of Mining and Metallurgy* 113 (2013):8.
- Kazadi Mbamba, Christian, S.T.L. Harrison, J.P. Franzidis, and J.L. Broadhurst. 2012. “Mitigating Acid Rock Drainage Risks While Recovering Low-sulfur Coal From Ultrafine Colliery Wastes Using Froth Flotation.” *Minerals Engineering* 29 (2012):9. doi: 10.1016/j.mineng.2012.02.001.
- Klassen, V. I., and N. S. Vlasova. 1967. “The Effect of Reagents in Coal Flotation.” *Fiziko-Tekhnicheskie Problemy Razrabotki Poleznykh Iskopaemykh* 1 (5):7.
- Langley, N, S. T. L. Harrison, and R. P van Hille. 2012. “The Effect of CO₂ Availability on the Growth of *Chlorella Vulgaris*.” *Biochemical Engineering Journal* 68:6.
- LECO Corporation. 2010. “Sulfur and Carbon in Coal, Coke, and Graphite.” Last Modified October 2010, accessed 2 May. http://www.leco.co.za/wp-content/uploads/2012/02/SC632_S-C_COAL_COKE_GRAPHITE_203-821-304.pdf.
- Mandal, Shovon, and Nirupama Mallick. 2009. “Microalga *Scenedesmus Obliquus* as a Potential Source for Biodiesel Production.” *Applied Microbiology and Biotechnology* 84 (2):11. doi: 10.1007/s00253-009-1935-6.



New sensing system based on electromagnetic waves and functionalised EM sensors for continuous monitoring of Zn in freshwater

Ilaria Frau¹, Steve Wylie¹, Patrick Byrne², Jeff Cullen¹, Olga Korostynska¹, Alex Mason³

¹*Built Environment and Sustainable Technologies (BEST) Research Institute, Department of Civil Engineering, Faculty of Engineering and Technology, Liverpool John Moores University, Liverpool, L3 3AF, UK*

²*School of Natural Sciences and Psychology, Faculty of Science, Liverpool John Moores University, Liverpool, L3 3AF, UK*

³*Animalia AS, Norwegian Meat and Poultry Research Centre, PO Box Økern, 0513 Oslo, Norway*

Abstract

Toxic metals are a significant cause for concern, considering freshwater the major route of their transport even far from point and diffuse sources. This paper presents a novel combined method using electrical measurements and microwave spectroscopy based on functionalised electromagnetic (f-EM) sensors. Thick films based on β - Bi_2O_3 were screen-printed on planar sensors for monitoring continuously Zn concentrations in water. Results demonstrate the capability of this novel sensing system to measure in real-time Zn concentrations, especially in the range 0-1 mg/L and consequently the possibility to detect an unexpected pollution event, which can generate an increase of Zn in water.

Keywords: Zinc, online monitoring, microwave spectroscopy, f-EM sensor, water pollution

Introduction

Metal pollution from both active and abandoned mines is a global environmental problem, with leaching from waste heaps and the groundwater which ascends after pumping stops, being a particular concern (Environment Agency 2008). The combination of point and diffuse sources and freshwater largely determines the dispersion of toxic metals (Cd, Pb, Cu, Zn, Ni, Fe, etc) into the environment. Surface waters are the major dispersion vehicle of pollution of these contaminants.

Zinc (Zn) is an essential element having a role in many biological functions (e.g. cellular metabolism, catalytic activity of enzymes, protein synthesis, and so forth) in living organisms. However, at high concentrations and with long-term exposure, Zn can have toxic effects on humans and other living organisms, that can include respiratory and neuronal disorder (Kashin and Ivanov 2010). Accordingly, several environmental quality standards (EQS) exist for Zn in water; these are summarised in tab. 1 (Edokpayi et al. 2016; UK Technical Advisory Group on

Table 1 Summary of the EQS established for Zinc (in mg/L) by worldwide organisations.

EQS	UK TAG UK Technical Advisory Group on the EU Water Framework Directive	US EPA US Environmental protection agency	WHO World Health Organisation	US EPA US Environmental protection agency	DWAF South African Department of Water Affairs and Forestry	DWAF South African Department of Water Affairs and Forestry
	Surface water	Surface water	Drinking water	Drinking water	Domestic water use	Protection of aquatic life
Zinc (mg/L)	0.008-0.125 ^a	0.059-0.210 ^a	3	5	3	0.002



the Water Framework Directive 2008). Zn concentrations in mine water typically range from 0.1 to 10 mg/L but can be as high as 500 mg/L (Byrne et al. 2012).

There are many examples where the waste from mining has posed a risk to water resources and to animal and human health. For example, high-flow conditions lead to an increase in Zn concentrations, due to the erosion and weathering of the waste materials and the dissolution of efflorescent salts (Cidu et al. 2011). However, this is not a general rule: at many sites the metal concentrations decrease because of the dilution (Wolkersdorfer 2008). Therefore, proper impact assessment by continuous monitoring of toxic metals in water is essential for the optimal environmental management, understanding better metal dynamics and for planning effective water remediation.

Currently, no method can guarantee in-situ continuous monitoring of water resources. Traditional methods require labour intensive field sampling and costly off-line laboratory-based methods of analysis, limiting the ability to manage remote sites, and the detection of

the immediate effects of accidental contamination events. Consequently, it is necessary to develop advanced sensor technologies for adequate in-situ and real-time water properties monitoring.

Accordingly, a developing sensing system able to monitor Zn ions in mine water continuously is an electromagnetic (EM) wave sensor system, operating at microwave frequencies (Korostynska et al. 2013). This method is able to give an immediate and continuous response at specific frequencies when a water sample with diverse pollutant concentration is placed in vicinity of the EM field. With the purpose to produce a more specific spectral response for measuring a single contaminant at low concentration in water, the synergy with chemical materials is providing interesting advantages (Azmi et al. 2017).

This work reports the preliminary findings of an investigation into the use of microwave, electric techniques and interdigitated (IDE) sensors functionalised with β -Bi₂O₃ based coatings for continuously detecting changes in the concentration of Zn in the range 0-10 mg/L in water.

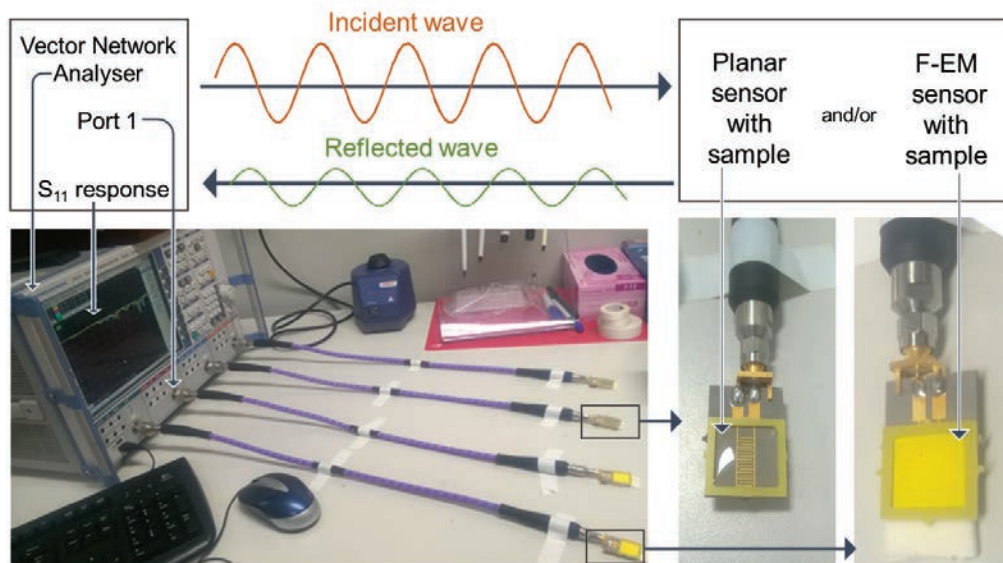


Figure 1 Scheme which explains the microwave interaction with a water sample placed on uncoated planar sensors and f-EM sensors: the incident waves, originated from a Vector Network Analyser (VNA), interact in a unique manner with the sample under test and generate a reflected signal (S_{11}) at specific EM frequencies.



Materials and methods

Microwave spectroscopy

The principle of microwave spectroscopy is based on the interaction between incident waves and the properties of the water sample presented to the sensing structure. This produces a reflected wave, with a spectral response at specific frequencies (Korostynska et al. 2013), as illustrated in fig. 1. The change in the reflection coefficient (S_{11}) can be linked to the composition and concentration of the measured solution, which depends on the variations in several parameters (such as conductivity, capacitance, resistance, and permittivity, as well as temperature, chemical structure, molecular composition, etc.). By specialising the sensor with some specific functional material (e.g. inorganic oxides, zeolites, organic polymers), it is possible to obtain a more specific signal, due to the physical or chemical interaction between the material and the analyte under test (Frau et al. 2017).

F-EM sensors

F-EM sensors are a novel alternative for improving the performance of the outgoing microwave spectroscopy and solve the lack of sensitivity and selectivity response for each metal, hence detecting lower concentrations than 1 mg/L and distinguishing between different metals. By combining functional materials and determining a consequent change in complex permittivity due to the singular interaction of the chemical material and the metal under test, it is possible to obtain a more specific EM spectrum response, with specific shifts in amplitude (in S_{11}) and/or in frequency (in Hz) at distinct frequencies.

Bismuth (Bi) has been used in the last two decades to detect Zn in water, mostly using electrochemical methods (Švancara et al. 2010). The nanoparticle form in particular has been shown to have superior sensing characteristics compared to the bulky Bi film electrode using electrochemical methods (Kadara et al. 2009). In addition, nanomaterials as inorganic oxide compositions are considered to be advantageous, owing to their strong adsorption (Sen Gupta and Bhattacharyya 2011).

In this work, planar Au eight-pair IDE sensors were functionalised with 60 μm of $\beta\text{-Bi}_2\text{O}_3$ based coatings as shown in fig. 2. $\beta\text{-Bi}_2\text{O}_3$ 90< Φ <210 nm particle size (Sigma-Aldrich 637017) (92.5 wt. %) was used as the principal chemical and was mixed with 7.5 wt. % of a binder (Butvar B98), and a suitable amount of ethylene glycol butyl ether (solvent). The paste mixture was printed with a semi-automatic screen-printer (Super Primex) for creating the thick film onto the planar sensors. Moreover, a set of Ag eight-pair IDE was screen-printed using a silver paste (Heraeus LCT3410) and functionalised with the same paste mixture based on $\beta\text{-Bi}_2\text{O}_3$ (fig. 3c, d).

The thickness of the thick film was increased by multiple screen-printing, with curing between each layer at 170°C. The final thickness (60 μm) was measured with a surface profiler (Taylor Hobson – Form Taly-surf 120).

Sample preparation

Water samples with various Zn concentrations (0, 0.1, 0.5, 1, 5, 10 mg/L) were prepared

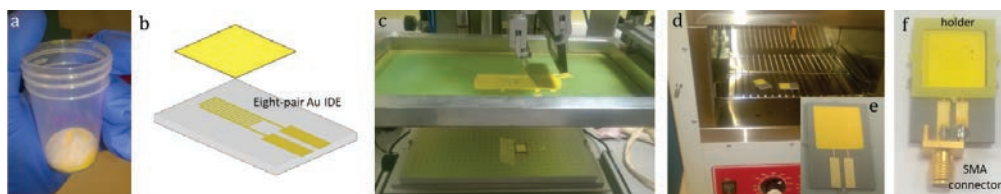


Figure 2 Manufacturing of the f-EM sensors: the mixture in powder form (a) was mixed with a binder and a solvent for reaching the right viscosity to be printed onto a planar sensor (b) using a screen-printer (c). The f-EM sensors were then put in an oven at 170°C (d); thus, the f-EM sensor (e) was welded with a SMA connector and a sample holder was settled onto it (f).

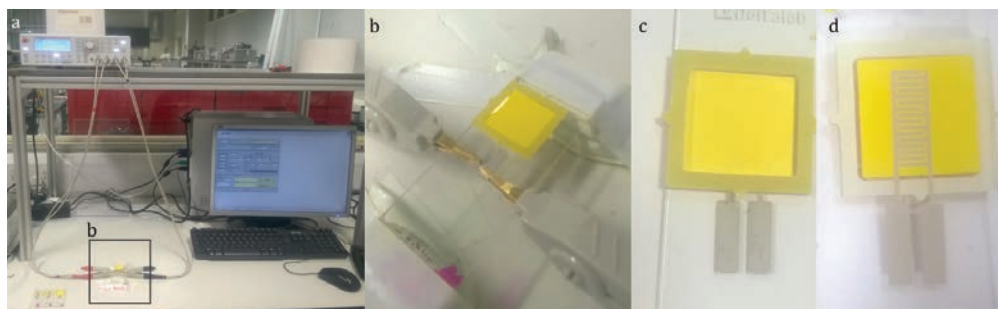


Figure 3 Set up of the impedance measurement using a LCR bridge connected to the screen-printed microscope slide with a Ag-IDE with β - Bi_2O_3 based coating (a-b); (c) front and (d) back of the functionalised Ag-IDE.

by spiking a precise volume of Zn 1,000 ppm ICP standard solution (Sigma-Aldrich 18562) in deionised water.

Experimental setup

In this experimental work, the microwave (reflected coefficient, S_{11} , dB) and electrical (capacitance, C_p , F, and resistance, R_p , Ω) properties were measured using f-EM sensors based on β - Bi_2O_3 and their interaction with the Zn samples at various concentrations:

- S_{11} was measured with a one-port configuration by connecting both uncoated and f-EM sensors to a Rohde and Schwarz ZVA 2.4 VNA through coaxial cables in the 100 MHz-8 GHz frequency range (as shown in fig. 1). For each measurement ($n=5$), 400 μL of Zn samples were allocated on the holder placed onto the sensor using a pipette;
- C_p and R_p were measured using a programmable LCR bridge HAMEG 8118 measured at low frequency (30 Hz-20 kHz) (fig. 3a): 400 μL of Zn samples

were placed on a coated Ag-IDE screen-printed on a microscope slide (fig. 3b, c, d) connected with the LCR bridge through a Rohde and Schwarz HZ184 Kelvin measurable cable.

Results and discussion

This work demonstrates the ability of this novel, electric and microwave sensing system combined with functional materials, to recognise and quantify Zn in water. Specifically, S_{11} measured with f-EM sensors with β - Bi_2O_3 based coating in the frequency range 1-4 GHz, as shown in fig. 4a, shows two pronounced amplitude shifts which are dependent on the Zn content. The peak at 1.57-1.68 GHz (magnified in fig. 4b) shows improved performance for detecting smaller changes in Zn concentrations, compared with the uncoated sensors (fig. 4c), where the concentration 0-1 mg/L of Zn are not separated (at 1.26 GHz).

This peak is set at a diverse frequency because there is an overall shift toward higher frequencies ($\Delta f_{\beta\text{-Bi}_2\text{O}_3 + \text{Zn samples}} = 300\text{-}400 \text{ MHz}$)

Table 2 Summary of statistical features obtained for electrical and microwave measurements of Zn water samples (0-10 mg/L).

Properties and sensing structure	Frequency	R^2	Sensitivity ^a	RSD (%)
C_p - coated IDE on microscope slide (60 μm)	150 Hz	0.998	0.79 nF	0.1 %
R_p - coated IDE on microscope slide (60 μm)	150 Hz	0.978 ^b	34 k Ω	2 %
S_{11} - uncoated EM sensor	1.26 GHz	0.983	0.0039 dB	0.9 %
S_{11} - f-EM sensor (60 μm)	1.57-1.68	0.960	0.0064 dB	1.5 %

^afor each 0.1 mg/L change of Zn concentration; ^blogarithmic correlation;



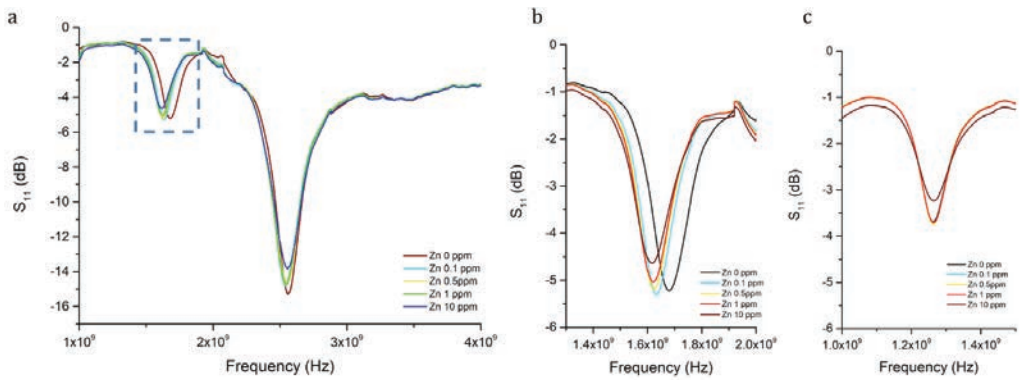


Figure 4 Microwave response for spiked-water with Zn at diverse concentrations at the frequency 1-4 GHz (a); the highlight area, where Zn concentrations < 1mg/L were better distinguished, is expanded in (b) and compared with the response obtained with the uncoated sensors (c) where the Zn content is not differentiated, demonstrating the increased performed produced by the f-EM sensor.

due to the thickness of the coating with a consequent change in dielectric properties (Patil and Puri 2010).

Overall results, obtained measuring Zn solutions at the range 0-10 mg/L using electrical and microwave techniques with coated and uncoated sensors are summarised in tab. 2, with R^2 , the sensitivity (as change of each parameter for 0.1 mg/L of Zn concentration) and RSD (relative standard deviation, as % of SD/mean). The signals were dependent on the type and concentration of Zn with $R^2 = 0.998$ and $R^2 = 0.978$, respectively for Cp and Rp (fig. 5a, b): Rp is related with Zn concentration and with the Cp with logarithmic correlation. Thereby, as the Cp and Zn con-

centration increase, the Rp decreases logarithmically.

Figures 5c and d show the linear correlations between Zn concentration and S_{11} , respectively $R^2 = 0.96$ and $R^2 = 0.98$ for the reflected coefficient measured with f-EM and uncoated sensors. Although the R^2 is slightly smaller with the f-EM sensor, it improves the capability of detecting changes of Zn especially at concentrations between 0-1 mg/L. Consequently, f-EM sensors were able to detect Zn concentrations in water with higher sensitivity than the uncoated sensors, especially to distinguish Zn concentrations both above and below the EQS established for surface water (0.1-0.2 mg/L).

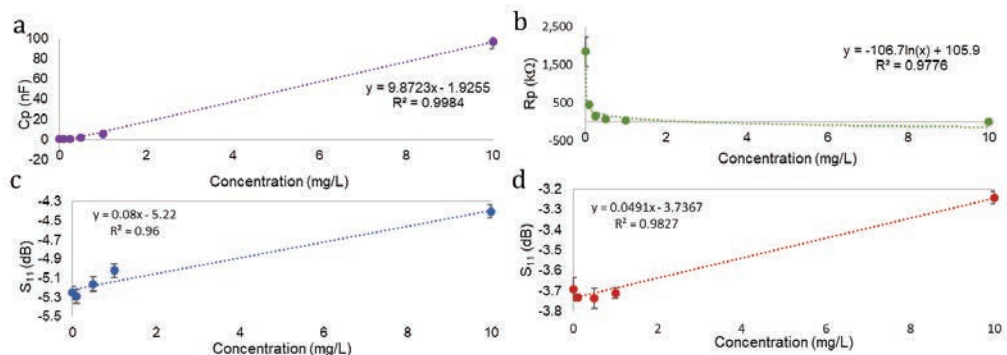


Figure 5 Correlation using functionalised Ag-IDE for Cp and Rp and Zn samples at 150 Hz, respectively linear (a) and logarithmic (b); Linear correlation between S_{11} coefficient and Zn samples (0-10 mg/L) using f-EM sensors (at 1.57-1.68) (c) and uncoated sensor (at 1.26 GHz) (d).



These effects are probably due to the effect of the permittivity variation of the sensitive chemical layer (Bernou et al. 2000). The overall propagation will depend on the permittivity of the substrate and its thickness, and on the sensitive material permittivity, which will change with the adsorption of the Zn ions in the sensitive layer. Whenever the Zn water samples were removed and the sensor was rinsed and allowed to dry, the sensor output returned to its baseline level (air spectra). This indicates that planar EM sensors are reusable, probably due to the weak solubility of metal oxides (Chu et al. 2017) and the reversible interaction between Zn and β -Bi₂O₃ based coating.

Conclusions

This work communicates the feasibility of using a novel EM sensing approach combined with f-EM sensors based on β -Bi₂O₃ for detecting Zn concentrations in water. Exposure of f-EM sensors to Zn-spiked-laboratory samples demonstrate the ability to detect continuous changes in Zn concentration with higher sensitivity than uncoated sensors, especially for concentrations in the range 0-1 mg/L. This level of sensitivity is significant as it enables the sensor to be used to monitor adherence to EQS. This method potentially offers a viable alternative to costly and labour intensive field sampling and laboratory-based methods of analysis.

Ongoing work is investigating new sensing materials to increase sensitivity and sensitivity for simultaneous analysis of multi-metal solutions and to move on the field to guarantee in situ and real-time monitoring.

Acknowledgements

The authors gratefully acknowledge the support of Liverpool John Moores University, the Faculty of Engineering and Technology PhD Scholarship Programme, which allowed this research to be undertaken. Special thanks go to Prof Rafid Al Khaddar, Head of the Department of Civil Engineering, for funding this Conference.

References

- Azmi A, Azman AA, Kaman KK, Ibrahim S, Mukhopadhyay SC, Nawawi SW, Yunus MAM (2017) Performance of Coating Materials on Planar Electromagnetic Sensing Array to Detect Water Contamination. *IEEE Sensors Journal* 17 (16):5244-5251. doi:10.1109/JSEN.2017.2720701
- Bernou C, Rebière D, Pistré J (2000) Microwave sensors: a new sensing principle. Application to humidity detection. *Sensors and Actuators B: Chemical* 68 (1):88-93. doi:10.1016/S0925-4005(00)00466-4
- Byrne P, Wood PJ, Reid I (2012) The Impairment of River Systems by Metal Mine Contamination: A Review Including Remediation Options. *Critical Reviews in Environmental Science and Technology* 42 (19):2017-2077. doi:10.1080/10643389.2011.574103
- Chu Z, Peng J, Jin W (2017) Advanced nanomaterial inks for screen-printed chemical sensors. *Sensors and Actuators B: Chemical* 243:919-926. doi:10.1016/j.snb.2016.12.022
- Cidu R, Frau F, Da Pelo S (2011) Drainage at Abandoned Mine Sites: Natural Attenuation of Contaminants in Different Seasons. *Mine Water and the Environment* 30 (2):113-126. doi:10.1007/s10230-011-0146-4
- Edokpayi J, Odiyo J, Popoola O, Msagati T (2016) Assessment of Trace Metals Contamination of Surface Water and Sediment: A Case Study of Mvudi River, South Africa. *Sustainability* 8 (2). doi:10.3390/su8020135
- Environment Agency (2008) Abandoned mines and the water environment. Science project SC030136.
- Frau I, Korostynska O, Byrne P, Mason A Continuous monitoring of Zn in water with bismuth oxide thick-film using microwave and electric techniques. In: 2017 Eleventh International Conference on Sensing Technology (ICST), 4-6 Dec. 2017. pp 1-6. doi:10.1109/IC-SensT.2017.8304479
- Kadara RO, Jenkinson N, Banks CE (2009) Disposable Bismuth Oxide Screen Printed Electrodes for the High Throughput Screening of Heavy Metals. *Electroanalysis* 21 (22):2410-2414. doi:10.1002/elan.200900266



- Kashin VK, Ivanov GM (2010) Zinc in natural waters in the Selenga River basin. *Water Resources* 37 (4):481-487. doi:10.1134/S009780781004007X
- Korostynska O, Mason A, Al-Shamma'a AI (2013) Flexible microwave sensors for real-time analysis of water contaminants. *Journal of Electromagnetic Waves and Applications* 27 (16):2075-2089. doi:10.1080/09205071.2013.832393
- Patil S, Puri V (2010) Effect of bismuth oxide thick film overlay on microstrip patch antenna. *Microelectronics International* 27 (2):79-83. doi:10.1108/13565361011034759
- Sen Gupta S, Bhattacharyya KG (2011) Kinetics of adsorption of metal ions on inorganic materials: A review. *Advances in Colloid and Interface Science* 162 (1-2):39-58. doi:10.1016/j.cis.2010.12.004
- Švancara I, Prior C, Hočevar SB, Wang J (2010) A Decade with Bismuth-Based Electrodes in Electroanalysis. *Electroanalysis* 22 (13):1405-1420. doi:10.1002/elan.200970017
- UK Technical Advisory Group on the Water Framework Directive (2008) UK environmental standards and conditions (phase 1 - SR1-2006).
- Wolkersdorfer C (2008) *Water Management at Abandoned Flooded Underground Mines — Fundamentals, Tracer Tests, Modelling, Water Treatment*. Springer, Heidelberg
- Kashin VK, Ivanov GM (2010) Zinc in natural waters in the Selenga River basin. *Water Resources* 37 (4):481-487. doi:10.1134/S009780781004007X
- Korostynska O, Mason A, Al-Shamma'a AI (2013) Flexible microwave sensors for real-time analysis of water contaminants. *Journal of Electromagnetic Waves and Applications* 27 (16):2075-2089. doi:10.1080/09205071.2013.832393
- Patil S, Puri V (2010) Effect of bismuth oxide thick film overlay on microstrip patch antenna. *Microelectronics International* 27 (2):79-83. doi:10.1108/13565361011034759
- Sen Gupta S, Bhattacharyya KG (2011) Kinetics of adsorption of metal ions on inorganic materials: A review. *Advances in Colloid and Interface Science* 162 (1-2):39-58. doi:10.1016/j.cis.2010.12.004
- Švancara I, Prior C, Hočevar SB, Wang J (2010) A Decade with Bismuth-Based Electrodes in Electroanalysis. *Electroanalysis* 22 (13):1405-1420. doi:10.1002/elan.200970017
- UK Technical Advisory Group on the Water Framework Directive (2008) UK environmental standards and conditions (phase 1 - SR1-2006).
- Wolkersdorfer C (2008) *Water Management at Abandoned Flooded Underground Mines — Fundamentals, Tracer Tests, Modelling, Water Treatment*. Springer, Heidelberg





Reuse of Treated Mine-Impacted Water as a Potential Resource for Accelerated Carbon Sequestration

Tamsyn Grewar

Mintek, South Africa, TamsynG@mintek.co.za

Abstract

Mine impacted water (MIW) can refer to any water impacted by a mining process including AMD and brines all of which pose a major environmental threat. The vast quantities of MIW present in South Africa has created serious problems in the water cycle. However this has also provided opportunities where these waste streams could be considered resources under the right conditions. South Africa is not only water scarce but also one of the top 20 CO₂ polluters, world-wide. Average global monthly temperatures are now cresting at 1 °C above pre-industrial levels while atmospheric CO₂ levels seem to have permanently breached 400 µmol/mol. These levels are projected to increase to over 800 µmol/mol by the end of the century if no action is taken. The work presented here provides a potential CO₂ sequestration mechanism using MIW.

Carbon sequestration is defined as a natural/artificial process by which CO₂ is removed from the atmosphere and held in solid/liquid form. Carbon mineralisation for carbon sequestration involves the leaching of Ca-Mg-Fe cations from silicate minerals which are then reacted with CO₂ to form inert carbonate minerals, sustainably trapping CO₂. However, due to the slow kinetics of the initial dissolution step the research focus has shifted to speeding up the dissolution of the target minerals, and identifying more reactive mineral resources. Alternatively, we investigated through batch tests under varying conditions of pH and temperature, the potential of a variety of Ca-Mg-Fe-rich MIWs to function as resources for carbon sequestration where the costly, rate-limiting mineral dissolution step was bypassed altogether. In addition, we investigated the water treatment potential of the carbonation reaction, to co-precipitate and encapsulate other elements present in the MIW into the stable carbonate products, to lead to cleaner effluents.

The work conducted was designed to answer questions relating to; a) how to cost-effectively maintain the alkaline pH required for carbonation, b) the effect of other MIW components on the carbonation reaction, c) how this in turn affected the final carbonate product and d) the effect of elemental encapsulation on MIW quality.

New regulations being imposed worldwide aiming to mitigate the risks of global warming necessitates the R&D of new technologies for carbon sequestration. Linking these technologies to the use of the vast MIW resources present in South Africa that could themselves be treated in the process provides an attractive opportunity on two fronts.

Keywords: Mine-Impacted Water, Carbon Sequestration, Treatment, Encapsulation



Reutilization of mine water as a heat storage medium in abandoned mines

Florian Hahn¹, Gregor Bussmann¹, Felix Jagert¹, Roman Ignacy¹,
Rolf Bracke¹, Torsten Seidel²

¹Bochum University of Applied Sciences, International Geothermal Centre (GZB), Lennershofstr. 140,
44801, Bochum, Germany, florian.hahn@hs-bochum.de

²delta h Engineering GmbH, Parkweg 67, 58453, Witten, Germany

Abstract

The development of innovative storage technologies as well as the use of sustainable low grade heat and cold sources are essential to expand the use of renewable energy sources. The utilization of mine water as a geothermal resource and/or as a thermal energy storage has the potential to play a key role to reach the ambitious climate goals set by the COP21. Flooded mines represent major low temperature geothermal reservoirs, which also provide large-scale seasonal thermal storage capacities. These characteristics enable the development and dissemination of renewable energy systems and the improvement in energy efficiency of conventional systems.

Keywords: mine, thermal, energy, storage

Introduction

At the end of 2018, the last operative hard coal mine in Northrhine-Westphalia (Germany), Prosper-Haniel, is going to be closed down, plugged and abandoned. Large amounts of subsurface infrastructure, resembled mainly by open parts of former galleries and mining faces are going to be flooded after the mine is abandoned and therefore have the potential of becoming an enormous geothermal reservoir for seasonal heat storage. At the moment a seasonal heat storage within an abandoned hard coal mine has not yet been realized in Germany. Therefore the HT-MTES (High Temperature-Mine Thermal Energy Storage)

project (feasibility study) of the International Geothermal Centre (in cooperation with RAG AG and delta h Ingenieurgesellschaft mbH) would lead the way within the sector of renewable energy storage systems. This R&D project is funded by the German Federal Ministries BMWi, BMU and the BMBF "Initiative Energy Storage" program. The aim of this project is to create a technically and economically feasible conceptual model of a HT-MTES for the energetic reuse of the hard coal mine Prosper-Haniel, which is situated in Bottrop (Germany).

The conceptual model (fig. 1) is based on the storage of seasonal unutilized heat during

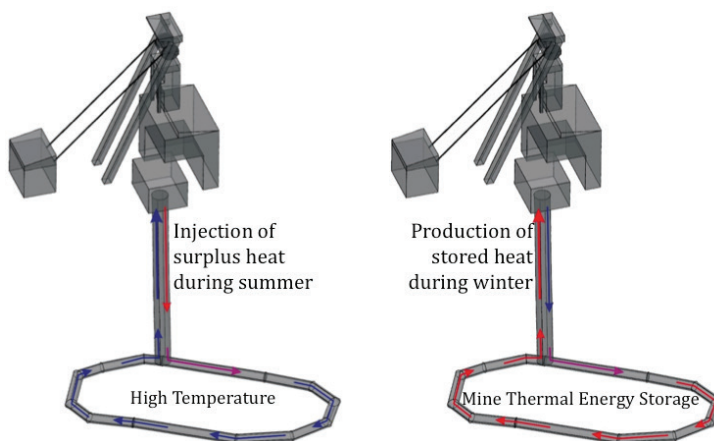


Figure 1 Conceptual model of a HT-MTES (GZB)



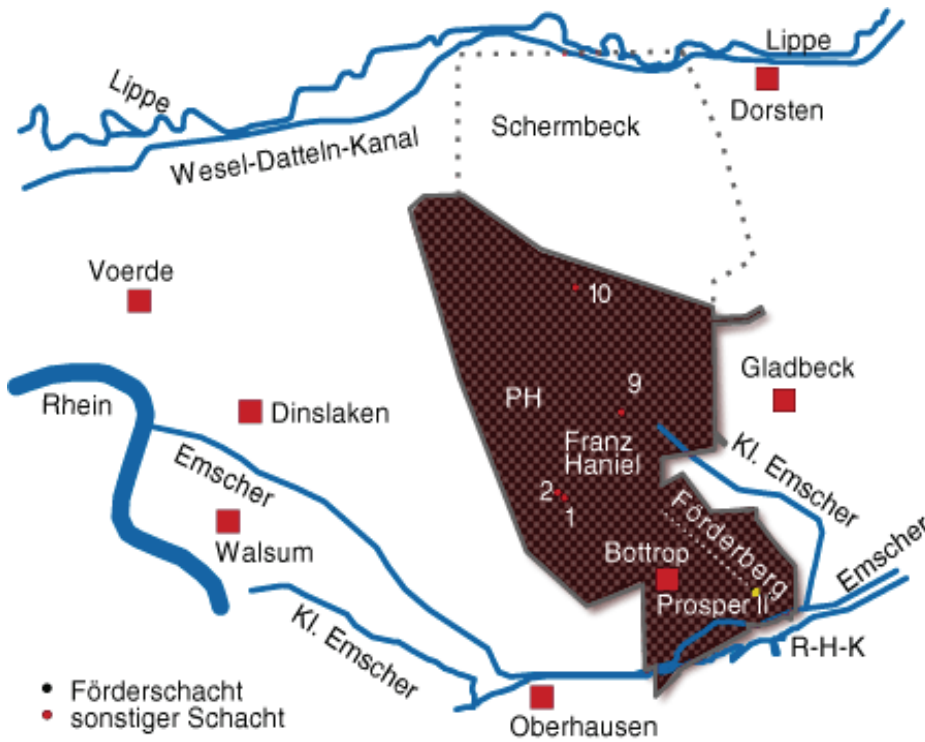


Figure 2 Location of Prosper-Haniel within the Ruhr area (RAG AG)

the summer from solar thermal power plants, industrial production processes or CHP plants within the mine layout and to utilize the stored heat e.g. through the distribution of a district heating grid during the winter, when there is a high heat demand.

For the implementation of such a HT-MTES within a former hard coal mine, the corresponding infrastructure measures and appropriate circulation applications have to be developed. Precondition for this development is the presence of a still active and fully open mine, which is resembled by the hard coal mine Proper-Haniel. As a foundation for the implementation of a mine thermal energy storage, the undisturbed rock temperatures range between 30°C and 50°C (Leonhardt 1983) within the galleries and mining faces that are going to be flooded, after the mine is abandonment. The total mining area consists of 165 km² (see brown area fig. 2) and the

subsurface galleries have a total length of 141 km, at a maximum depth of –1159 m NHN.

A HT-MTES needs to have a large mine water volume, in order to store vast amounts of heat. At the same time, it has to be reliable, cost efficient and should be integrated into existing urban frameworks. In order to meet economical requirements, a HT-MTES needs to be operative in the range of 40 to 50 years. Depending on the utilized heat source and its application, different heat capacities, mass flows and temperature levels would be encountered within the mine thermal energy storage. All affected components need to be suitable for the intended operations and their possible resulting stresses. If the seasonal heat storage is operated by several different heat sources, a careful coordination of the specific heat amounts and loading cycles of the relative source needs to be taken into consideration.



Current state of technology

The idea of obtaining thermal energy from an inoperative colliery has already been pursued for a long time, although to a comparatively limited extent. Up to this point a pilot plant has not been established, in which the possibility of thermal energy storage in a former colliery has been considered. Well-known executed projects concerning the utilization of mine water include:

- The Mijnwater-project in Heerlen (Netherlands), whereby an already completely flooded and no longer accessible mine layout was accessed through directional drilling technology.
- The building of the School of Design at the Zeche Zollverein in Essen (Germany), which is heated by 28°C warm mine water, originating from the mine drainage of the RAG AG.
- The utilization of mine water of the former Robert Müser colliery in Bochum (Germany) as an energy source for the heat supply of two schools and the main fire station in Bochum. Within this pilot plant the 20°C warm mine water, which originates from the mine drainage of the RAG AG from a depth of -570 m NHN, is being used.
- Seven operational mine water utilization plants in Saxony (Germany), which can be categorized as shallow geothermal reservoirs. A deep mine water project is currently being implemented at the West Saxon University of Zwickau, where mine water from a depth of 625 m below ground with a temperature of 26°C is planned to be extracted.

The thermal utilization of the mine water from existing mine drainage stations, as they are realized in Essen or Bochum (Germany), show the highest economic efficiency, as no additional pumping costs are being generated. Due to the lack of suitable customers and a not yet existing final planning security concerning the future locations of mine drainage stations after the end of active coal mining (end of 2018) and the renaturation of the Emscher, a further expansion currently only

takes place to a limited extent. The “open” utilisation plan of the Mijnwater-project could be realized in the Netherlands, as the mine workings are already flooded after being closed down. In case of a mine water table < 80 m below ground, the proportion between the thermal energy obtained and the input energy (pumping energy) is to be assessed as positive, despite the low temperature of the mine water of about 28°C. Nevertheless, the mine water must be brought to a higher temperature level with the use of heat pumps. In contrast to the Mijnwater-project in the Netherlands, the mine water table in the majority of the central and northern Ruhr area, with a depth of approx. -600 m NHN below the surface (RAG AG 2015), is considerably deeper so that at water temperatures of up to 35°C, the energetic expense of the lifting is too high compared to the thermal energy obtained.

One way of increasing the efficiency is to increase the temperature of the mine water through the storage of seasonal heat in the mine layout, which has not been realized yet. Currently, merely a few medium-deep hydrothermal aquifer storages are in the planning stage or in operation in Germany. All of them are similar in regard of the temperature regime and the layer depth. Worth mentioning here are a project of the BMW Group at the plant Dingolfing (planning stage), the deep storage Neubrandenburg (in operation) and the energy concept Spreebogen (in operation).

Numerical modelling of the HT-MTES

Modelling hydraulic and thermal impacts on a regional scale for the HT-MTES project presented many challenges, including appropriate discretization of mine drifts as well as accurate modelling of layered aquifer systems. To accommodate the complex underground heat reservoir and its interaction with the surrounding aquifers and fault system, the finite element (FE) modelling code SPRING (König, 2014) was selected. SPRING includes a boundary condition specifically to describe mines or separate mining fields within a finite element mesh and to couple their hydraulic



and thermal behaviour to the surrounding rock mass (fig. 3) and aquifers. The software was first published in 1970 and has undergone a number of revisions. SPRING uses the finite-element approximation in solving the ground-water flow and transport equations. Different model layers with varying thicknesses, including the pinching out of a layer, are possible.

In order to predict the impacts of both historic mining operations and future thermal impacts, a detailed conceptual model of the aquifer systems and a three-dimensional model of the mine drifts were incorporated into a regional numerical heat and transport model. The model was used for dimensioning of the reservoir layout as well as for optimization of flow rates, dam positions and temperature profiles (fig. 4).

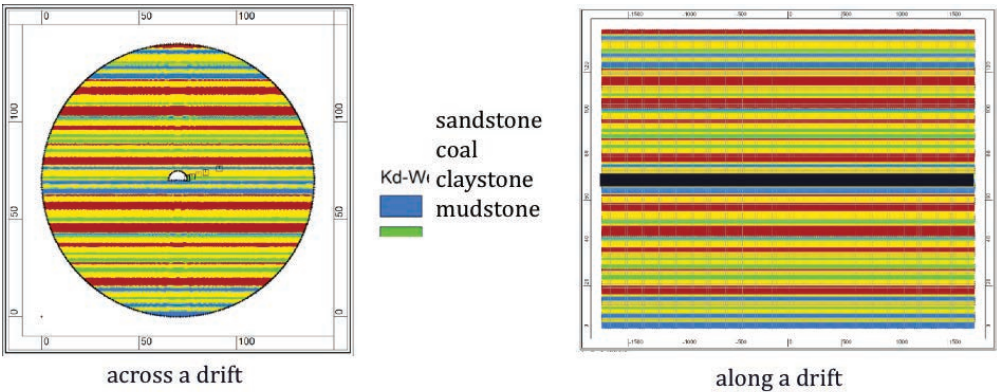


Figure 3 Vertical cross sections of a conceptual drift model (delta h)

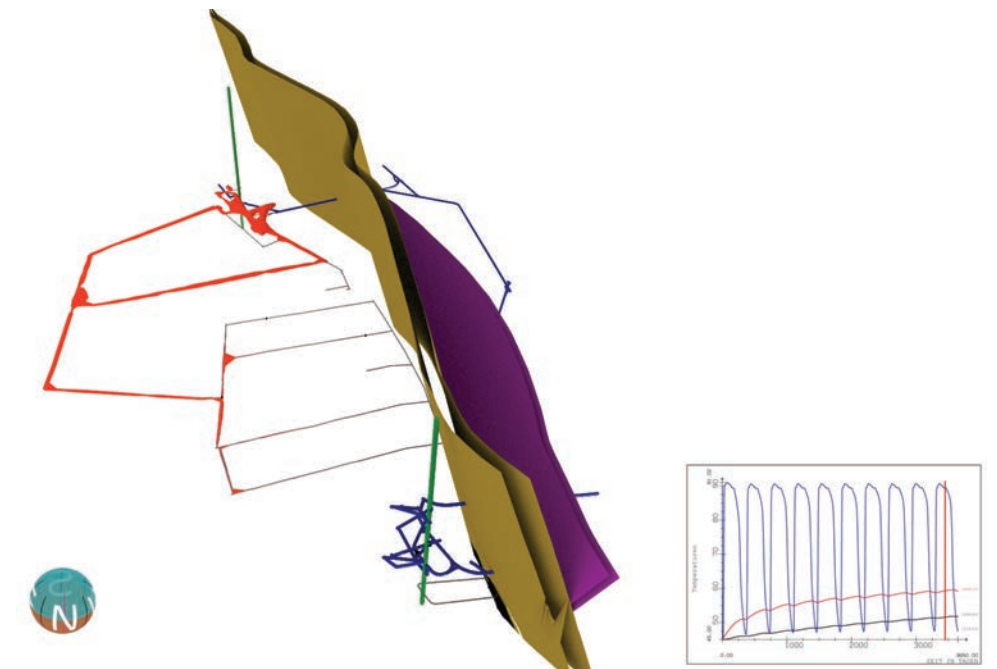


Figure 4 Calculated temperature field of the HT-MTES with temperatures coloured from red (high) to blue (low), regional fault system in yellow/violet (delta h)



HT-MTES - Prosper Nord

The fact that Prosper-Haniel is still an open and active hard coal mine facilitates numerous advantages for the development and exploitation of a mine thermal energy storage system:

- Increased hydraulic properties are encountered, due to the presence of former mining areas and galleries within the relatively dense carboniferous rock. This infrastructure substantially enhances the heat transport capability of the underground.
- Open shafts and drifts allow a comparatively easy accessibility and technical feasibility of a mine thermal energy storage during the closure phase.
- A positive customer structure is anticipated, due to the high population density within the vicinity of the mine.

The seasonally stored heat could be utilized to supply the surrounding residential and commercial areas, e.g. through a coupling with the Ruhr district heating grid or with the integration into the “InnovationCity Ruhr” process. Consecutively, the main conceptual model of the HT-MTES within the Prosper-

Haniel hard coal mine is illustrated below and described in further detail.

The following conceptual model consists of the HT-MTES within the mining area “Prosper Nord” between shaft 9 (Prosper IV) and 10 (Prosper V) (see fig. 2). Based on the mine water drainage concept of the RAG AG, the hard coal mine Prosper-Haniel will be completely flooded up to –687 m NHN by 2035 (RAG AG 2015). Out of this reason, the drifts on level 7 could be utilized as a mine thermal energy storage in the future. In this case, surplus heat would be injected into the storage via shaft 9 during the summer, stored within the drifts of level 7 and reproduced via shaft 9 during the winter. It must be ensured that the in fig. 5 (red) illustrated drifts are to the greatest possible extent hydraulically decoupled from the rest of the mine layout by dams, in order to increase the efficiency of the overall storage capacity. An interference with the planned mine drainage on level 6 should be avoided by all means, as this will be the main flow paths of the mine water through Prosper-Haniel towards the prospective central dewatering station Lohberg (Drobniewski 2016) in the future. Therefore, suitable dam positions (fig. 5; magenta) have been local-

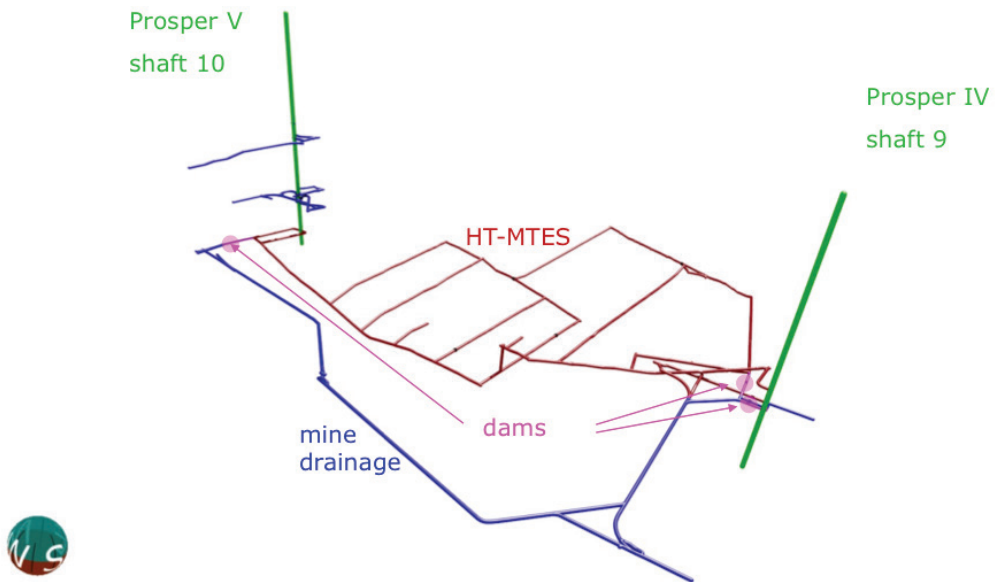


Figure 5 HT-MTES (red) within the mining area “Prosper Nord” (delta h)



ized and verified within the SPRING model of the HT-MTES. Based on the injection with a maximum temperature of 90°C (Jagert et al. 2018) for 6 months and a storage volume of 252.000 m³, the conceptual HT-MTES would have a storage capacity of 12.8 GWh/a. After ten years, the SPRING model revealed a storage efficiency of up to 84 % for the proposed HT-MTES.

Additionally, a surface line between shaft 9 (Prosper IV) and shaft 2 (Franz Haniel) would have to be installed, in order to couple the HT-MTES with the existing district heating grid. Since 2014, an extended mine gas utilization plant has been put into operation at shaft 2 (Franz Haniel), for which a 3.3 km long mine gas transportation line has been installed between shaft 9 (Prosper IV) and shaft 2 (Franz Haniel). This plant could act as a possible heat source for the HT-MTES, as the cooling water of the cogeneration unit produces temperatures in the range of approx. 90°C, which could be directly utilized for storage purposes.

Conclusion

The development of diversified storage capacities will have a great impact on the future promotion of renewable energy sources. Within the Ruhr area, unused mine structures in combination with available unutilized surplus heat from power plants and industrial processes, resemble a vast potential for large heat storage capacities. Out of this reason, fundamental research in the field of seasonal heat storage in abandoned mines has to be conducted for further technology development and establishment of large scale storage systems. The aim of this feasibility study is to

conceptualize a mine thermal energy storage system for the hard coal mine Prosper-Haniel. Until the end of 2018 Prosper-Haniel is still in operation, so that specific underground measures (dams, tubings, etc.) for a mine thermal energy storage are possible to be conducted. The HT-MTES could be prepared based on the results of the feasibility study during the three-year closure phase after 2018, when the production has ceased. Once the mine layout is fully flooded by 2035, the HT-MTES could be connected to the Ruhr district heating grid. In the case of a technical and economical implementation of the HT-MTES, the design and operation results of the seasonal heat storage within an abandoned hard coal mine, would be scalable to other locations in Germany and worldwide.

References

- Drobniewski M (2016) Die technische Ausgestaltung und der Stand des Grubenwasserkonzeptes
- Jagert F, Hahn F, Bussmann G, Ignacy R, Bracke R (2018) Mine Water Of Abandoned Coal Mines For Geothermal Heat Storage: Hydrogeochemical Modeling And Predictions. Proceedings from the 11th ICARD | IMWA | MWD 2018 Conference
- König, C. M. et. al. (2012) SPRING Manual, Vol. 4.1, ISBN 978-3-00-040369-9, delta h Ingenieurgesellschaft mbH, Witten
- Leonhardt J (1983) Die Gebirgstemperaturen im Ruhrrevier 90:218–230
- RAG AG (2015) Grubenwasserkonzept der RAG Aktiengesellschaft. http://www.energieagentur.nrw/content/anlagen/2015_03_12%20Grubenwasserkonzept%20der%20RAG%20Aktiengesellschaft.pdf. Accessed 19 November 2017





Influence of Probability Distribution Function Sampling Frequency on Stochastic Water Quality Model Predictions

Michael Herrell^{*1}, Kristina Skeries², Jerry Vandenberg², John Faithful², April Hayward³,
Lukas Novy³

¹*SRK Consulting (Canada) Ltd., Vancouver, British Columbia, Canada*

²*Golder Associates Ltd., Vancouver, British Columbia, Canada*

³*Dominion Diamond Ekati Corporation, Calgary, Alberta, Canada*

**Corresponding author: Michael K. Herrell, SRK Consulting (Canada) Inc., Senior Consultant (Geochemistry), Suite 2200 1066 West Hastings St., Vancouver, BC, Canada V6E3X2. Phone: +1 604-681-4196. mherrell@srk.com*

ABSTRACT

Stochastic water quality models provide a mechanism to estimate uncertainty in water quality model inputs. This approach requires fitting an input dataset to a statistical distribution, which is entered into the model as a Probability Distribution Function (PDF). The input PDFs are randomly sampled at user-defined intervals using the Monte Carlo method to generate a model input time series for the duration of the model run.

A stochastic water quality model was developed to support the Environmental Assessment and Water Licence Permit applications for the Jay Project, a new open pit development at the Ekati diamond mine, located in the Northwest Territories, Canada. Model input PDFs were developed using existing seepage monitoring data from a surrogate waste rock storage area at the mine selected to represent the drainage water quality for the Jay Waste Rock Storage Area (WRSA). The total drainage from the Jay WRSA is estimated to be small in comparison to other mine site flows (e.g., Jay Pit groundwater inflow); however, as part of the model sensitivity analysis, it was identified that the combined site discharge water quality results (including Jay WRSA drainage) were sensitive to the sampling frequency selected for the Jay WRSA input PDFs for some constituents. This paper presents a case study to highlight how stochastic model results can be sensitive to PDF sampling frequency and the implications to mine permit applications. An approach for selecting PDF sampling frequencies is also presented.

Additional Key Words: mine water quality prediction

Introduction

Dominion Diamond ULC (Dominion Diamond) is currently constructing the Jay Project at the Ekati Mine in the NWT, Canada (Figure 1). A stochastic site-wide water quality model was developed to predict the concentration of chemical constituents in discharge to Lac du Sauvage. Predicted concentrations were used as the basis for evaluating impacts to surface water quality as part of the Developer's Assessment Report (DAR) (Dominion Diamond 2014) and to evaluate if proposed effluent quality criteria (EQC) developed for discharge to the receiving environment in the Water Licence application (Golder 2016a) would be achievable.

Probability distribution functions (PDF), developed based on seepage monitoring data from the Misery WRSA, were used as an analogue for the proposed Jay WRSA seepage and runoff water quality. During the DAR (Dominion Diamond 2014), model input PDFs were sampled once per realization; however, when the DAR model was updated and used to evaluate if proposed EQC would be achievable as part of the Water Licence submission (Golder 2016b), it was identified that predicted upper percentile concentrations in Misery Pit discharge were sensitive to the PDF sampling frequency of the Jay WRSA for select parameters, even though the total drainage from the Jay WRSA represented a



small component of the total inflow to Misery Pit. To account for uncertainty in model inputs, a conservative assumption that is often applied is to select a percentile above 50 to bias the results away from underprediction. The risk with this approach is that it can indicate a need for costly mitigation, sometimes due to the conservatively selected percentile of input. Therefore, an additional examination of the PDF sampling frequency was warranted to determine if the predicted discharge concentrations were reasonable or were an artefact of the PDF sampling frequency.

This paper presents predicted Misery Pit discharge water quality for nitrate under three PDF sampling frequencies (once per realization, annually and monthly) over 200 realizations to illustrate how stochastic modelling results can be sensitive to PDF sampling frequencies for a fixed number of model realizations. Guidance on selecting sampling frequencies is also presented.

Project description

The Ekati mine is located approximately 300 kilometres (km) northeast of Yellowknife, NWT, Canada (Figure 1). The Jay kimberlite pipe will be mined using open pit methods.

Access to the Jay Pit requires partial dewatering of a small area of Lac du Sauvage, which will be separated from the main body of the lake through construction of a dyke (Figure 2).

Mining in Jay Pit will produce saline groundwater and contact catchment runoff that will need to be managed during operations. During mining of Jay Pit, saline groundwater and catchment runoff draining to Jay Pit will be pumped to the bottom of Misery Pit and subsequently discharged to Lac du Sauvage once the storage capacity of Misery Pit is exceeded. Water pumped from Jay Pit will mix with Jay Waste Rock Storage Area (WRSA) runoff, Misery Pit wall rock and catchment runoff.

Waste rock produced from mining of Jay Pit will be stored in the Jay WRSA (Figure 2). Approximately, 67% of the Jay WRSA seepage and runoff will drain to Misery Pit (Golder 2016b), where it will mix with water pumped from Jay Pit, Misery Pit wall rock and catchment runoff.

Methods

A stochastic site-wide water quality model was developed in GoldSim v.11 (GoldSim 2010). In GoldSim, each flow that could influ-



Figure 1 Location of the Jay Project



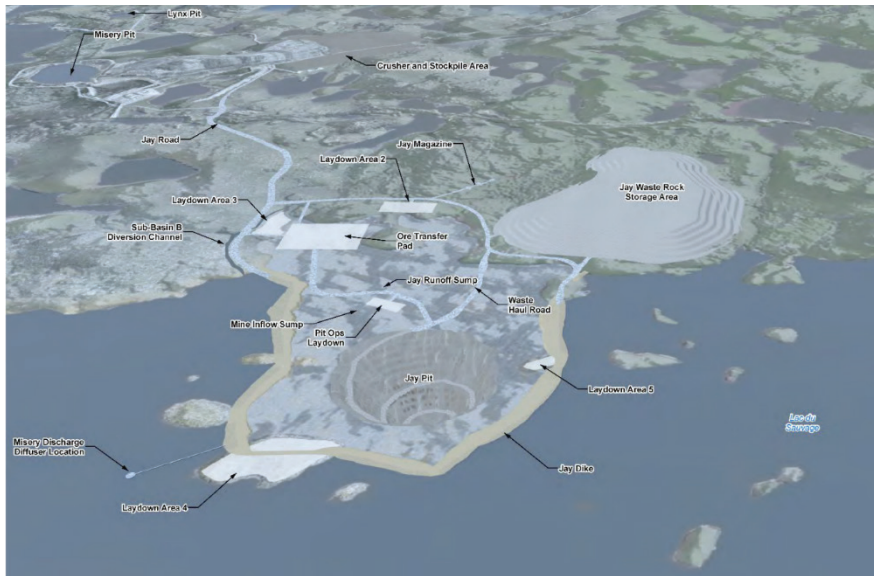


Figure 2 Proposed Jay Project Infrastructure

ence water quality was itemized and assigned a source term chemical profile based on geochemical test work of mine waste materials, mine site facility monitoring data, baseline surface and groundwater monitoring results or outputs from supporting models (e.g., hydrogeological model outputs).

PDFs were developed using seepage water quality monitoring results from the Misery WRSA and, based on the compositional similarity (Dominion Diamond 2014), were used to represent the quality of seepage and runoff from the Jay WRSA. PDFs were developed using the approach described in Vandenberg et. al. (2015). The model input PDFs were randomly sampled using the Monte Carlo approach for 200 model realizations at three different frequencies: once per realization, annually and monthly. The randomly generated input concentrations were used to represent the drainage quality from the Jay WRSA in the model.

Only model results for nitrate are presented in this paper. This constituent was selected since during the Jay Project Water Licence application process, it was identified that predicted nitrate concentrations were sensitive to PDF sampling frequency. The reader is referred to the following documents for a detailed description of the model setup, in-

puts and subsequent updates: Appendix 8E of Dominion Diamond (2014) and Golder (2015; 2016b).

Results

Predicted nitrate concentrations, accounting for all sources that can influence Misery Pit discharge water quality, are presented in Figure 3. Only predicted concentrations in the surface layer (from which discharge occurs) are presented in Figure 3. Therefore, concentrations are zero prior to water being stored in this layer in October 2026.

Predicted average nitrate concentrations show virtually no variability for the scenarios modelled, indicating the average model results are not sensitive to the Jay WRSA PDF sampling frequency. This occurs because the magnitude change in peak and trough nitrate concentrations in the stochastic time-series generated for Jay WRSA for annual and monthly sampling frequencies is small, and all sampled concentrations are similar to the average concentrations produced when the Jay WRSA PDF is sampled once per realization. In addition, Jay WRSA represents a small component of the overall flow to the Misery Pit on an annual basis. Therefore, the variation in average WRSA concentrations is not large enough to increase loadings to an

extent that influences Misery Pit discharge water quality.

The predicted 95th percentile nitrate concentrations decrease with increased sampling frequency. This trend occurs for the following reasons:

- When a single value is selected for an entire simulation, that value will be a driver of the long-term chemistry of the waterbody. With higher frequency sampling, all scenarios, even those at higher percentiles, will include a mixture of high and low values. Over time, these values will regress toward the mean, as illustrated by lower 95th percentiles for higher frequency sampling scenarios in Figure 3.
- Lower 95th percentile concentrations will be selected and used when Jay WRSA and wall rock runoff accounts for higher proportion of the inflow to the Jay Pit earlier in operations (e.g., prior to Misery Pit being flooded).
- Peak concentrations are not always coupled to peak flows (i.e., freshet) in the model loadings calculations for higher frequency sampling scenarios, resulting in lower cumulative loadings over the model duration (Figure 4).

Discussion

As part of the Water Licence application, the 95th percentile Misery Pit discharge nitrate concentrations were predicted to be greater than proposed EQC at different times during operations but the mean concentrations were predicted to be consistently lower than the proposed EQC. A detailed review of the model inputs revealed that elevated 95th percentile concentrations were occurring because there was a large degree of variability in the nitrate input data that was used to develop the Jay WRSA PDF.

Upon further examination of the dataset used to define the nitrate PDF, it was identified that the maximum concentration (326 mg-N/L) was much greater than the mean concentration (34 mg-N/L) and the lognormal nature of the distribution fitted to the data resulted in high concentrations, that have lower probabilities of occurrence, being carried forward into the model predictions. Concentrations rapidly decrease from

the maximum value with the 95th percentile concentration (185 mg-N/L) being approximately half of the maximum. Therefore, it is considered highly unlikely that drainage from the Jay WRSA would contain nitrate concentrations at the 95th percentile value for the duration of operations.

The maximum concentration was not screened out as an outlier using the statistical methods described above and therefore, it cannot be excluded from the dataset. However, only sampling the distribution once per realization assumes all drainage from the Jay WRSA will be equal to or higher than the 95th percentile concentrations in some model realizations, which is unlikely to occur in reality. To account for the upper percentile concentrations (e.g., maximum, 95th percentile, etc.), that are based on empirical data, the sampling frequency of the PDF was increased. This approach carries forward the upper percentile concentrations but for a shorter duration. This is considered to be a reasonable replication of what would occur in reality for a parameter such as nitrate, which is observed to be highly variable at mining operations.

Conclusion

The Jay Project water quality model indicates that the predicted Misery Pit discharge water quality is sensitive to the PDF sampling frequency for some constituents. If too long a frequency is selected, the model can produce overly conservative, and potentially unrealistic, predictions. This requires the modeller to develop an intimate understanding of the input data for each PDF and use professional judgement to determine if the loadings that are being produced are realistic, or an artefact of an anomalously high concentration being sustained as a result of an unreasonable PDF sampling frequency.

The appropriate PDF sampling frequency is partially dependent on the purpose of the water quality model. For example, sampling once per realization was determined to be appropriate for the DAR, where overly conservative model predictions did not change the outcomes of the study. From this perspective, the PDF sampling frequency was considered fit for purpose. As part of the Water Licence



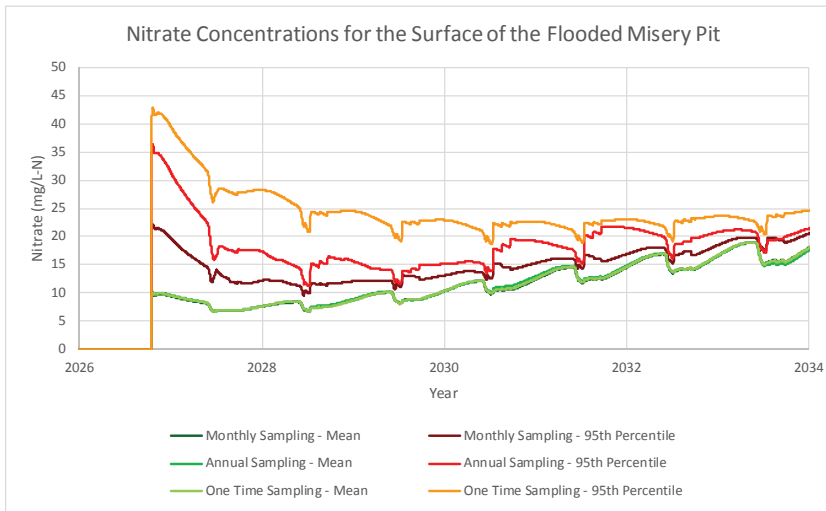


Figure 3 Modelled Nitrate Concentrations in Jay WRSA Drainage

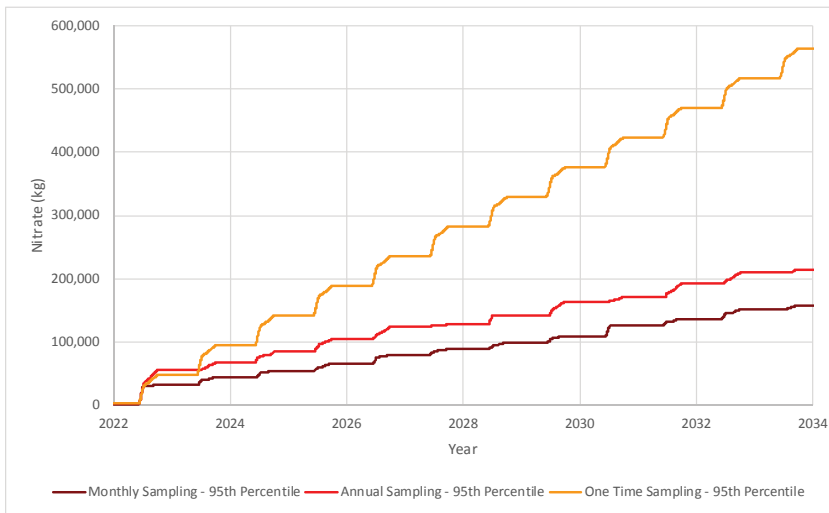


Figure 4 Cumulative Jay WRSA Runoff Nitrate Loadings

application, it was identified that model predictions based on sampling the PDF once per realization were overly conservative and adjustment of the sampling frequency was warranted.

Ideally it would be preferable to have sufficient data to develop PDF that are seasonal or linked directly to flow to better align predictions to different precipitation events. However, such datasets rarely exist at the planning stages of projects and it be-

comes incumbent on the modeller to select the most appropriate approach, balancing conservatism with realism. In such cases, the degree of autocorrelation observed in datasets from similar facilities at other sites may be a guide to setting the appropriate sampling frequency. Similarly, the residence time of the waterbody being modelled is an important consideration, with the waterbodies with shorter residence time being more sensitive to selection of sampling frequency.



References

- Dominion Diamond (Dominion Diamond Ekati Corporation) (2014) Developer's Assessment Report for the Jay Project. Prepared by Golder Associates Ltd., October 2014. Yellowknife, NWT, Canada.
- Golder (Golder Associates Ltd.) (2015) Compendium of Supplemental Water Quality Modelling – Jay Project. April 7, 2015.
- Golder (2016a) Effluent Quality Criteria for the Jay Project. June 2016.
- Golder (2016b) Jay Project – Water Licence Water Quality Model Updates. June 2016.
- GoldSim (GoldSim Technology Group) (2010) Users Guide for GoldSim Version 10.5 in a Probabilistic Simulation Environment.
- Vandenberg J, Herrell M, Faithful J, Snow A, Lacrampe J, Bieber C, Dayyani S, Chisholm V. Multiple Modeling Approach for the Aquatic Effects Assessment of a Proposed Northern Diamond Mine Development. Mine Water and the Environment. DOI 10.1007/s10230-015-0337-5. March 26, 2015.





The preferential localisation of SRB in an acetate supplemented up-flow anaerobic packed bed reactor

Tomas Hessler¹, Susan T.L. Harrison^{1,2} and Robert J. Huddy^{1,2}

¹Centre for Bioprocess Engineering Research, Department of Chemical Engineering,
University of Cape Town, South Africa

²The Future Water Institute, University of Cape Town, South Africa

Abstract

Biological sulphate reduction (BSR), catalysed by consortia of sulphate reducing bacteria (SRB) represents a low-cost and sustainable remediation strategy for low-flow acid mine drainage (AMD) effluents. This study investigates the performance and the microbial ecology throughout an acetate-supplemented up-flow anaerobic packed bed reactor (UAPBR). The reactor, operated at a four-day hydraulic retention time (HRT), achieved 78% sulphate removal in the first third of the reactor, and 97% removal in the effluent. Metagenomic 16S rRNA gene sequencing identified eight SRB operational taxonomic units (OTUs) which were preferentially located between the planktonic and biofilm communities as well as different zones along the reactor.

Keywords: Biological sulphate reduction (BSR), sulphate reducing bacteria (SRB), 16S rRNA metagenomics, biofilm.

Introduction

Acid mine drainage (AMD) is a serious form of pollution in countries with extensive mining operations, characterised by acidified water with high concentrations of sulphate and dissolved heavy metals (Johnson and Hallberg 2005). AMD originating from diffuse sources, such as abandoned mines and tailing impoundments often generate smaller volumes of AMD, but the number of these sites and longevity of the generation has created a problem requiring low-cost remediation strategies which can operate sustainably for decades to come.

Biological sulphate reduction (BSR) has been demonstrated at laboratory- and pilot-scale, as an effective low-cost strategy for the remediation of low-flow AMD (Kolmert and Johnson, 2001; Lens et al., 2002; Boshoff et al., 2004; Zagury and Neculita, 2007). This process uses mixed consortia of sulphate reducing bacteria (SRB), which use sulphate as a terminal electron acceptor in the oxidation of organic compounds, resulting in the formation of sulphide and carbonate (Muyzer and Stams 2008). The sulphide product can be used to precipitate contaminant heavy

metals, or be biologically oxidised to sulphur as a value-added product, and the carbonate aids in neutralisation of the acidic solution, making this process ideal for the treatment of AMD effluents.

Implemented BSR systems must overcome two major issues associated with this process: the low bacterial growth rates associated with SRB; and the provision of a suitable low-cost electron donor. The low growth rates of SRB can be overcome by decoupling the hydraulic and biomass retention times within BSR reactor systems. This has been achieved through granulation of SRB biomass in fluidized bed reactors (Alphenaar et al., 1993), or through providing a large surface for microbial attachment and biofilm formation within the reactor (Bachmann et al. 1985; Zhang and Wang 2016; Hessler et al. under review). Acetate is a low-cost and widely available electron donor with potential to be generated from waste streams such as anaerobic digestion. However, acetate supports considerably lower SRB growth rates than other more expensive electron donors such as ethanol and lactate (Thauer et al. 1977). Efficient sulphate removal using acetate therefore requires significant



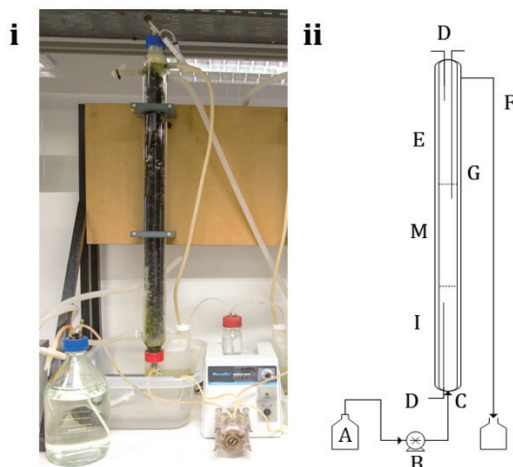


Figure 1 Photograph (i) and annotated schematic diagram (ii) of the UAPBR used in this study. The feed solution (A) was continuously supplied to the reactor via a peristaltic pump (B) via the inlet (C) at the base of the reactor. The reactor is demarcated into three sequential zones, namely the inlet (I), middle (M) and effluent zone (E). Sampling ports (D) at the base and top of the reactor are used to sample for solution chemistry leaving each zone. Effluent is discharged by gravity via an overflow tube (F). The reactor was maintained at 30°C by a circulating waterbath and glass heating jacket (G).

biomass accumulation (Harada 1994).

Previous BSR reactor studies have described the ecology of these systems but have typically characterised a single sample, assuming microbial homogeneity throughout the reactor. Differences in the speciation between planktonic cells and those associated with biofilms have been described in bioleaching (Wang et al. 2014) and marine environments (Rickard et al. 2003), but have not yet been investigated within BSR systems. This study looks to describe the reactor performance and the detailed ecology of an acetate-supplemented Up-flow anaerobic packed bed reactor (UAPBR), characterised by plug-flow fluid dynamics. The SRB ecology of the planktonic and biofilm communities, from multiple reactor zones, are analysed by 16S rRNA sequencing of extracted metagenomic DNA.

Methods

Reactor system and operation

This study was conducted using a 1 L glass up-flow anaerobic packed bed reactor with an internal diameter of 4 cm and height of 80 cm (fig. 1) as described in Hessler et al (under re-

view). The reactor was packed with open-pore polyurethane foam cubes of approximately 2 cm³. The reactor was inoculated with a composite culture drawn together from a number of long-term SRB stock reactors. The reactor was operated at a four-day HRT and fed sterile modified Postgate B media (Postgate 1984) containing 10.4 mM sulphate, supplemented with 11.2 mM sodium acetate at neutral pH.

Analytical methods

The bulk liquid leaving each of the three reactor zones was sampled for solution chemistry by drawing 2 ml via the reactor sampling ports (Fig.1). The residual sulphate and the produced sulphide concentrations were determined by the APHA 1975 turbimetric method (Greenberg and Eaton 1999) and DMPD method described by Cline (1969), respectively. The concentration of acetate was determined by high performance liquid chromatography (HPLC) using a Waters Breeze 2 system equipped with a Bio-Rad Organic Acids ROA column and UV (210 nm wavelength) detector. The system was operated with a 0.01M H₂SO₄ mobile phase, with a flow rate of 0.6 ml/min.



Steady-state biological sampling

Steady-state conditions were assumed to be established within the UAPBR when residual sulphate concentrations leaving each reactor zone varied by less than 10% over a minimum period of three hydraulic residence times. Each zone of the reactor was sampled a total of eight times for solution chemistry and once for biological material during the defined steady state period. The cells attached and weakly associated to the polyurethane foam matrix, present in the inlet and effluent zones, were isolated using a modified detachment protocol and together with the planktonic cells present in the bulk liquid of each of the three zones, quantified by direct cell counting (Hessler et al. 2017).

The planktonic community was harvested from the reactor by removing 15 ml of bulk liquid, via the respective sampling ports, followed by centrifugation (10 000 g for 10 min at room temperature) to recover the microbial cells. The genomic DNA was immediately extracted from the resulting cell pellets, as described below. Matrix attached and associated cells were recovered from the UAPBR by aseptically removing polyurethane foam pieces from the inlet and effluent regions. The matrix associated cells were removed from the foam by mild agitation in reactor media, followed by centrifugation (10 000 g for 10 min at room temperature). The total genomic DNA of the matrix attached communities were then extracted directly off the polyurethane foam. Scanning electron microscopy (SEM) was used as a visual conformation of the microbial colonisation of the polyurethane foam. Polyurethane foam was removed from the inlet zone and prepared for SEM as described in Hessler et al. (2017) and viewed using a FEI NOVA NANO SEM 230.

DNA extraction and Sequencing

Total genomic DNA was extracted and purified from the cell pellets and polyurethane foam, collected as described above, using a NucleoSpin® Soil Genomic DNA Extraction Kit (Machery-Nagel, Germany) according to the manufacturer's instructions. The purified genomic DNA was subsequently sent to Macrogen Korea for sample preparation,

Illumina® MiSeq® sequencing, read pre-processing, clustering and taxonomic assignment. Briefly, the bacterial V3-V4 region of the 16S rRNA gene was PCR amplified using dual-index barcoded primers FwOvAd_341F and ReOvAd_785R. Fast Length Adjustment of Short reads (FLASH; Magoč and Salzberg 2011) was used to merge the paired-end reads. Read trimming, filtering and OTU picking was performed using CD-HIT-OTU (Li et al. 2012). The taxonomy of the OTUs was then assigned against the RDP 16S rRNA classifier algorithm (Edgar 2010) using QI-ME, UCLUST (Langille et al. 2013).

Results

Reactor performance

The UAPBR showed effective sulphate conversions at a four-day HRT, with 78% removal within the inlet zone of the reactor (Fig. 2B), corresponding to a volumetric sulphate reduction rate (VSRR) of 0.26 mmol/L.h. The concentration of acetate leaving the inlet zone of 11.6 mM is greater than predicted based on the equimolar oxidation of acetate coupled to the reduction of sulphate. The excess acetate is likely the result of the oxidation of other Post-gate B media components, namely citrate and yeast extract. Subsequent sulphate scavenging was seen in the middle and effluent reactor zones, bringing the total sulphate removal to 97%, with an overall VSRR of 0.11 mmol/L.h. The 1.9 mM sulphate removed in the middle and effluent zones corresponded with an approximately 2-fold equimolar reduction in the acetate concentration, indicating that acetate oxidation, by SRB and non-sulphate reducing microorganisms, had taken place.

Biomass retention

The UAPBR successfully developed an attached biofilm community on the incorporated polyurethane foam (Fig 2D). Quantification of the attached cells within the inlet zone revealed that this community was two to three orders of magnitude more concentrated than the planktonic cells which remained constant throughout the three zones at approximately $2 \times 10^8 \pm 9.3 \times 10^7$ cells/ml (Fig. 2C). The concentration of attached cells within the effluent zone was lower, at $1.1 \times 10^8 \pm 2.1 \times 10^7$ cells/ml.



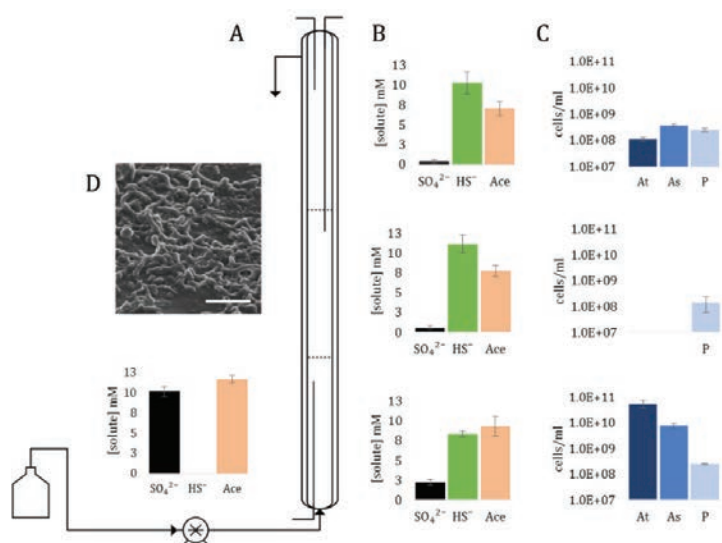


Figure 2 Schematic diagram of the UAPBR used in this study (A) showing the three sequential reactor zones. The sulphate, sulphide and acetate concentration in the feed and leaving each of these zones (B) is shown. The concentration of planktonic (P) cells, cells attached to (At) and weakly associated (As) with the polyurethane foam (C) were determined by detachment protocol and direct cell counting. The attached and associated cell concentration of the middle zone was not determined due inaccessibility to this zone. Error bars represent one standard deviation of the mean. SEM image (D) of colonised polyurethane foam from the inlet region of the UAPBR. Scale bar represents 4 μ m.

Bacterial community structure

The planktonic microbial communities from each of the three zones as well as attached and associated cells from the inlet and effluent zones were resolved using 16S rRNA gene metagenomic sequencing. The overall community structure at the phylum level was similar between all samples, and predominantly consisted of Proteobacteria and Bacteroidetes (Fig. 3A). A number of other bacterial phyla, including Firmicutes, Synergistetes, Thermotogae and Verrucomicrobia, made up the remaining 14 – 27% of these microbial communities. Thermotogae and Verrucomicrobia showed an inverse propensity for planktonic versus biofilm communities.

The OTUs that could be identified as SRB were classified within the Proteobacteria class of Deltaproteobacteria. These Eight SRB OTUs belong to six genera, namely *Desulfomicrobium*, *Desulfovibrio*, *Desulfobacter*, *Desulfarculus*, *Desulfatitalea* and *Desulfobulbus* (Fig. 3B). The absolute cell concentrations of these OTUs were calculated by multiplying their relative abundance by the determined total cell concentration of each com-

munity. These SRB OTUs showed significant distinctions between the planktonic and biofilm communities. A *Desulfomicrobium* and *Desulfovibrio* OTUs made up over 90% of the SRB OTUs present within the planktonic communities in each of the three reactor zones. However, these SRB made up less than 10% of the attached community within the same zones. The inlet attached and associated SRB community was dominated by *Desulfobulbus*, *Desulfarculus* and *Desulfobacter*. The attached community within the effluent zone contained very low numbers of the *Desulfomicrobium* and *Desulfovibrio* OTUs present in the planktonic community, instead made up predominantly the same *Desulfobulbus* OTU identified in the inlet zone. Two *Desulfatitalea* OTUs were found almost exclusively in the attached and associated communities in the inlet and effluent zones but made up a greater proportion of the community within the effluent zone. These three microorganisms, being present in this zone, are likely suited to sulphate and acetate scavenging and can tolerate high concentrations of sulphide.



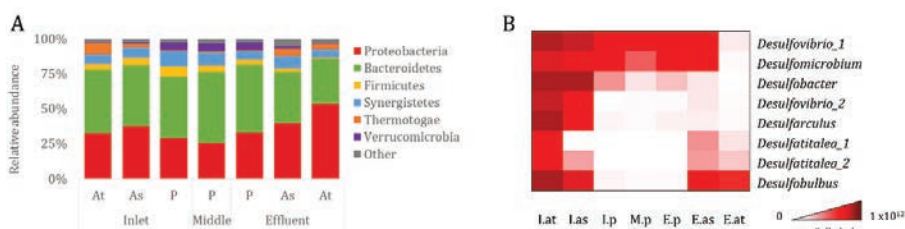


Figure 3 The bacterial community structure, at the phylum level (A), of the planktonic (P), associated (As) and attached (At) microbial communities from the inlet, middle and effluent zones of the UAPBR. The absolute cell concentrations of the eight identified SRB OTUs (B) present in the planktonic (p), associated (As) and attached (At) communities of the inlet (I), middle (M) and effluent (E) zones of the UAPBR are shown in a heatmap.

Conclusion

The acetate supplemented UAPBR showed effective sulphate conversion and VSRRs at a four-day HRT. Acetate represents one of the most viable electron donors for use in passive and semi-passive bioremediation of AMD, due to its low cost and wide availability. The incorporation of a biomass support matrix, polyurethane foam, into the UAPBR allowed for the decoupling of the biomass and hydraulic retention time, successfully addressing the low bacterial growth rates on acetate and enhancing biomass retention within the continuous reactor system. The SRB within the inlet's attached and associated communities are likely responsible for most of the sulphate reduction within the system.

Metagenomic 16S rRNA gene sequencing of the bacterial communities revealed differing prevalence of SRB OTUs between biofilm and planktonic communities as well as across the different zones of the reactor. *Desulfobulbus*, *Desulfarculus* and *Desulfobacter* were the dominant SRB attached and associated to the polyurethane foam within the inlet zone of the reactor. In contrast the SRB community within the planktonic phase throughout the reactor were dominated by *Desulfomicrobium* and *Desulfovibrio*. The attached and associated SRB community within the effluent zone of the reactor were colonised predominantly by a *Desulfobulbus* OTU, likely responsible for the sulphate scavenging in this zone. It is important to note the limitation of 16S rRNA gene metagenomic sequencing for the identification of microorganisms on the basis of their metabolic function. It is possible that

microorganisms other than those identified above may be contributing to sulphate reduction. This approach combined with further functional gene studies or whole genome sequencing will enable a more comprehensive description of the sulphate reducing potential of BSR reactor communities.

However, the differing SRB ecology identified between the inlet zone, responsible for rapid acetate oxidation and sulphate reduction, and the effluent zone, responsible for sulphate scavenging, provides support for a zoned BSR reactor configuration. The incorporation of polyurethane supports allows not only for biomass retention but the retention of several SRB genera found in low abundance in the planktonic communities. This confers the reactor with increased SRB diversity and potentially improved system robustness. The physiochemical conditions needed to stimulate attachment and biofilm formation of these SRB onto solid supports warrants further investigation.

Acknowledgements

Funding for this study has been provided by the Water Research Commission (K5-2393) and the DST/NRF of South Africa through the SARChI Chair in Bioprocess Engineering (STLH, UID 64778). Dr Huddy is funded through a DST/NRF Research Career Advancement Fellowship (UID 91465) and Competitive Support for Unrated Researchers (CSUR) Grant (UID 111713). Mr Hessler is funded through a NRF Scarce-skills MSc scholarship (UID 108052).



References

- Alphenaar, P.A., Visser, A. and Lettinga G (1993) The effect of liquid upward velocity and hydraulic retention time on granulation in UASB reactors treating wastewater with a high sulphate content. *Bioresour Technol* 43(3):249–258
- Bachmann A, Beard VL, McCarty PL (1985) Performance characteristics of the anaerobic baffled reactor. *Water Res* 19:99–106. doi: 10.1016/0043-1354(85)90330-6
- Boshoff G, Duncan J, Rose PD (2004) Tannery effluent as a carbon source for biological sulphate reduction. *Water Res* 38:2651–2658. doi: 10.1016/j.watres.2004.03.030
- Cline JD (1969) Spectrophotometric determination of hydrogen sulfide in natural waters. *Limnol Oceanogr* 14:454–458. doi: 10.4319/lo.1969.14.3.0454
- Edgar RC (2010) Search and clustering orders of magnitude faster than BLAST. *Bioinformatics* 26:2460–2461. doi: 10.1093/bioinformatics/btq461
- Greenberg AE, Eaton AD (eds) (1999) *Standard Methods for the Examination of Water and Wastewater*. APHA American Public Health Association
- Harada HUSMK (1994) Interaction Between Sulfate Reducing Bacteria and Methane Producing Bacteria In Uasb Reactors Fed With Low Strength Wastes Containing Different Levels Of Sulfate. *Water Res* 28:355–367. doi: 10.1016/0043-1354(94)90273-9
- Hessler T, Harrison S, Huddy R (under review) Stratification of microbial communities throughout a biological sulphate reducing up-flow anaerobic packed bed reactor, revealed through 16S metagenomics. *Res Microbiol*
- Hessler T, Marais T, Huddy RJ, et al (2017) Comparative Analysis of the Sulfate-Reducing Performance and Microbial Colonisation of Three Continuous Reactor Configurations with Varying Degrees of Biomass Retention. *Solid State Phenom* 262:638–642. doi: 10.4028/www.scientific.net/SSP.262.638
- Johnson DB, Hallberg KB (2005) Acid mine drainage remediation options: A review. *Sci Total Environ* 338:3–14. doi: 10.1016/j.scitotenv.2004.09.002
- Kolmert A, Johnson DB (2001) Remediation of acidic waste waters using immobilised, acidophilic sulfate-reducing bacteria. *J Chem Technol Biotechnol* 76:836–843. doi: 10.1002/jctb.453
- Langille MGI, Zaneveld J, Caporaso JG, et al (2013) Predictive functional profiling of microbial communities using 16S rRNA marker gene sequences. *Nat Biotechnol* 31:814–821. doi: 10.1038/nbt.2676
- Lens P, Vallero M, Esposito G, Zandvoort M (2002) Perspectives of sulfate reducing bioreactors in environmental biotechnology. *Rev Environ Sci Biotechnol* 1:311–325. doi: 10.1023/A:1023207921156
- Li W, Fu L, Niu B, et al (2012) Ultrafast clustering algorithms for metagenomic sequence analysis. *Brief Bioinform* 13:656–668. doi: 10.1093/bib/bbs035
- Magoč T, Salzberg SL (2011) FLASH: Fast length adjustment of short reads to improve genome assemblies. *Bioinformatics* 27:2957–2963. doi: 10.1093/bioinformatics/btr507
- Muyzer G, Stams AJM (2008) The ecology and biotechnology of sulphate-reducing bacteria. *Nat Rev - Microbiol* 6:441–454. doi: 10.1038/nrmicro1892
- Postgate JR (1984) *The Sulphate-Reducing Bacteria*. Second Edition., second. Cambridge University Press, UK.
- Rickard AH, McBain AJ, Ledder RG, et al (2003) Coaggregation between freshwater bacteria within biofilm and planktonic communities. *FEMS Microbiol Lett* 220:133–140. doi: 10.1016/S0378-1097(03)00094-6
- Thauer RK, Jungermann K, Decker K (1977) Energy conservation in chemotrophic anaerobic bacteria. *Bacteriol Rev* 41:100–180. doi: 10.1073/pnas.0803850105
- Wang Y, Zeng W, Chen Z, et al (2014) Bioleaching of chalcopyrite by a moderately thermophilic culture at different conditions and community dynamics of planktonic and attached populations. *Hydrometallurgy* 147–148:13–19. doi: 10.1016/j.hydromet.2014.04.013
- Zagury GJ, Neculita C (2007) *Passive Treatment of Acid Mine Drainage in Bioreactors: Short Review, Applications, and Research Needs*. 1439–1446
- Zhang M, Wang H (2016) Preparation of immobilized sulfate reducing bacteria (SRB) granules for effective bioremediation of acid mine drainage and bacterial community analysis. *Miner Eng* 92:63–71. doi: 10.1016/j.mineng.2016.02.008





Integrating hyperspectral analysis and mineral chemistry for geoenvironmental prediction

Laura Jackson¹, Anita Parbhakar-Fox¹, Nathan Fox², Sebastian Meffre¹,
David R Cooke¹, Anthony Harris³, Ekaterina Savinova⁴

¹*Transforming the Mining Value Chain, ARC Industrial Transformation Hub, University of Tasmania,
Private Bag 79, Hobart, TAS, 7001. Australia*

²*CRC ORE, University of Tasmania, Private Bag 79, Hobart, TAS, 7001. Australia*

³*Newcrest Mining Limited Level 8*

⁴*Corescan PTY LTD*

Abstract

Hyperspectral drill core scanning technology (e.g., CoreScan®), which uses visual near-infrared (VNIR), shortwave infrared (SWIR), and longwave infrared (LWIR) data, is being increasingly used for geological domaining of ore deposits. Advantageously, this technology can identify carbonate-group minerals that can effectively neutralise many mine wastes. The chemistry of neutralising minerals in drill core can also be routinely analysed by multiple techniques (e.g., portable X-ray fluorescence (pXRF), laser-ablation inductively coupled plasma mass spectrometry (LA-ICP-MS),) but hasn't been integrated with hyperspectral data for deposit-scale geoenvironmental characterisation.

In this study we integrate hyperspectral mineral data with a newly developed LA-ICP-MS line-scan method to characterise major and trace element chemistry of neutralising minerals in drill core. We demonstrate how this data can enable effective geoenvironmental domaining of ore deposits with examples from a porphyry Au-Cu deposit in Australia. We validate Corescan® data using X-ray diffractometry (XRD) and a series of acid-base accounting tests to define geological domains with high and low acid neutralising capacity (ANC). The distribution and abundance of trace elements are defined in these domains using by LA-ICP-MS. A new geoenvironmental domaining index (GDI) is developed using Corescan® data, which can assist with deposit-wide characterisation.

The rapid and cost-effectiveness of hyperspectral core scanning and LA-ICP-MS techniques makes them critical emerging technologies for routine geoenvironmental risk domaining using drill core. Here we emphasize that integrating these techniques potentially enables best practice ARD management at the beginning of the life-of-mine cycle by allowing early forecasting of the geoenvironmental properties of future wastes.

Keywords: Hyperspectral, mineralogy, geoenvironmental domaining, prediction, LA-ICP-MS

Introduction

Waste produced by the Mining Industry is one of the largest industrial waste streams on the planet with an estimated 4–15 Gt of broken waste rock and tailings produced annually (Lottermoser, 2010; Haas et al., 2015; Lèbre et al., 2017). The increased potential for acid and metalliferous drainage (AMD) from mining activities and mine waste poses a serious threat to the environment (e.g., Gurung et al., 2017; Anderson and Butler, 2017). Although Industry-wide geoenvironmental predictive codes (e.g., AMIRA, 2002; MEND 2009

guidelines; ASTM methods (e.g., D5744-13e1, D6234-13)) can discriminate between acid-forming and acid-neutralising mine wastes (Ashley et al., 2004), they are fraught with limitations and can easily be misused (Dold, 2016). Sampling protocols may also inadequately assess the acid-forming or acid-neutralising characteristics of an ore deposit. For example, Price (2009) suggests at least 3–5 representative samples should be tested for each key lithology or alteration type at the exploration stage of the mine life cycle. Following this suggestion, a newly discovered



ore deposit with 4 alteration types would require only 12–20 samples for geoenvironmental testing, which would be assumed to be representative of the thousands of tonnes of waste rock produced during the life of the mine. Successful geoenvironmental characterisation early in the life of mine can be more cost effective than rehabilitation upon mine closure.

Modern analytical techniques such as hyper-spectral core scanning, LA-ICP-MS, portable XRF, present an opportunity to optimise the use of waste material for mine rehabilitation. These techniques can identify neutral or acid-neutralising waste material during the early life of the mine, which can assist in minimising and treating AMD, avoiding the need to import costly neutralising materials. This study uses drill core from a porphyry Au-Cu mine to develop and test new hyperspectral protocols to enhance deposit-scale geoenvironmental domainning. The goal is to integrate key mineralogy and mineral chemistry data for early forecasting of geoenvironmental properties of waste materials, creating the opportunity to transform how waste materials are characterised and managed over the life of a mine.

Methods

Hyperspectral analysis was conducted using a Corescan® HCI-3 system operating across the VNIR and SWIR bands from 450 nm–2500 nm collecting continuous images of rough sawn half core (n=100) representing various alteration styles from 7 drill holes of a porphyry deposit. Specifics of the Corescan® instrument used were as follows: spectral resolution ≈ 4 nm; photography, 50 μm pixels; spectral imagery, 500 μm pixels; and profiler image, 200 μm . High quality optics focused spectral measurements to a 0.5 mm point on the core resulting in $\approx 150,000$ spectra per meter of scanned core. A spectrally calibrated RGB camera provided a high-resolution visual record of the core at 60 μm per pixel. Core surface features, texture, and shape was captured using a 3D laser profiler with a surface profile resolution of 20 μm . The data was used in geoenvironmental domainning index (GDI) calculations following Jackson et al. (2017), which considers the carbonate, and/or silicate abundance at each measured point

and multiplies this by relative reactivity and theoretical neutralising capacity values. High GDI values (>400) represent areas dominated by carbonate, which have the largest ANC potential. Low values (<100) represent areas with $< 10\%$ primary neutralisers, with lower ANC potential.

To validate Corescan® results, the bulk mineralogy of the same samples (n=100) were analysed using a benchtop Bruker D2 Phaser XRD instrument with a Co X-ray tube, at the University of Tasmania (UTas). Samples were crushed and milled, following by micronizing of 2 g of sample with a Retsch micronizing mill with zirconium oxide grinding elements for 10 minutes using ethanol and oven-dried overnight at 40°C. Individual XRD analyses were performed using a step size of 0.02 $^{\circ}2\theta$ with a dwell time of 0.4 seconds/step at an operating voltage of 30 kV and 10mA. Minerals were identified using the Bruker DIFFRAC.EVA software package with the PDF-2 (2012 release) powder diffraction file mineral database. Mineral abundances were semi-quantified by Rietveld refinement using TOPAS (Version 4.2) pattern analysis software.

The current alkalinity of each sample was assessed using ASTM D4972-13 (2013) paste pH method at UTas following Noble et al. (2015). Measurements of total sulfur (%) for the calculation of maximum potential acidity (MPA) and total carbon (%) were performed using a Thermo Finnigan EA 1112 Series Flash Elemental Analyser. Multi-addition net acid generation (mNAG) pH testing and ANC testing was conducted following the AMIRA P387A AMD Test Handbook methods (Smart et al., 2002) with NAPP values calculated accordingly.

Mineral chemistry was measured on unpolished drill core (n=7) using LA-ICP-MS following the method piloted by Meffre et al. (2017). Measurements were conducted on an Agilent 7900 quadrupole ICP-MS coupled to a Resonetics RESolution ablation cell and a 193 nm Coherent COMPex Pro ArF excimer laser. A total of 45 elements were analysed simultaneously using a 50 μm spot size pulsing at 20 Hz and moving along the core at 100–150 $\mu\text{m}\text{s}^{-1}$. Data was processed using in-house software that corrects for the different ablation rates of various minerals and mineral mixtures (Meffre et al., 2017).



To identify if data produced by μ XRF is useful in the context of producing textural maps showing mineral chemistry (to complement LA-ICP-MS), analyses on select samples ($n=7$) were performed at the CSIRO Advanced Characterisation Facility, Perth. Samples ($\approx 11 \times 5 \times 1$ cm) were mapped using a Bruker M4 Tornado using a Rh X-ray source (50 kV, 600 μ A) under vacuum using a 25 μ m spot size, a step size of 40 μ m and dwell time of 5s. A flat surface was the only sample preparation requirement. Qualitative element abundance maps with an atomic number greater than 12 (i.e., heavier than Mg) were output.

Results

Mineralogy of the analysed drill holes is dominated by quartz, feldspar, chlorite, and epidote. Calcite is the dominant carbonate (max 50.9 wt. %). Sulfides include pyrite (max 31.6 wt. %) and chalcopyrite (max 2.1 wt. %). Calcite abundance determined from Corescan[®] was compared against XRD and total carbon values (C_{TOTAL} % $\times 8.33$; Herrmann and Berry, 2002) to validate these results. A comparison

of calcite abundance using these three techniques is presented in Fig 1 and shows high R^2 values (range: 0.57–0.8) (Calcite_{Corescan} average: 2.8 wt. %, max: 34.4 wt. %; Calcite_{XRD} average: 8.9 wt. %, max: 50.9 wt. %; Calcite_{calculated} average: 7.1 wt. %, max: 48 wt. %). Comparisons imply that Corescan[®] data is sufficiently accurate for the purpose of domaining.

Using Corescan[®] data, GDI values were calculated for discrete samples, up to 30 cm length, from one drill hole (Fig. 2) with values shown alongside continuous alteration and static data (e.g., S %, mNAG, ANC, MPA). High GDI values (classified as extremely low risk; Jackson et al., 2017) strongly correlate with static data (e.g., 150 m: GDI 344; paste pH 8.3; mNAG pH 9.3; S_{TOTAL} 0.3%; MPA 10 kgH₂SO₄/t; ANC 1132 kg H₂SO₄/t). These results show that GDI values are able to independently define neutralising zones when compared to static data.

To demonstrate how hyperspectral and LA-ICP-MS data can be used for geoenvironmental domaining, we show the classified mineralogy, static testing, μ XRF, and LA-ICP-MS data for one drill core sample

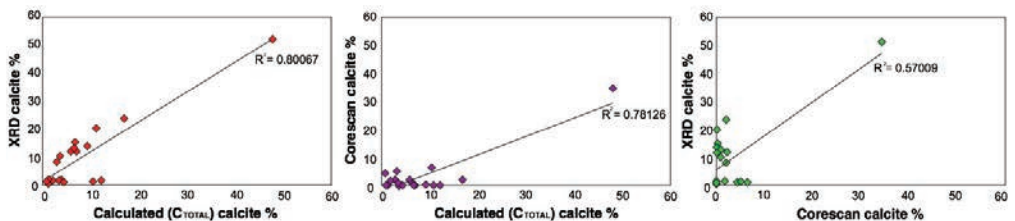


Figure 1 Comparison of calcite identification from XRD, Corescan[®] and calculated from total carbon values.

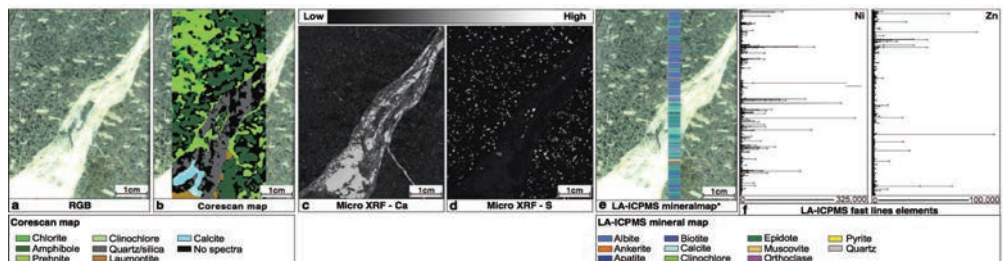


Figure 2 Drill core slab displaying mineralogy and trace element chemistry collected using different techniques; Corescan[®] classified mineral map, micro X-ray fluorescence (μ XRF), mineral liberation analysis (MLA), laser ablation inductively coupled plasma mass spectroscopy (LA-ICP-MS) collected as fast line scans elemental data and derived mineralogy. * LA-ICP-MS line not true line width to allow for visual representation.



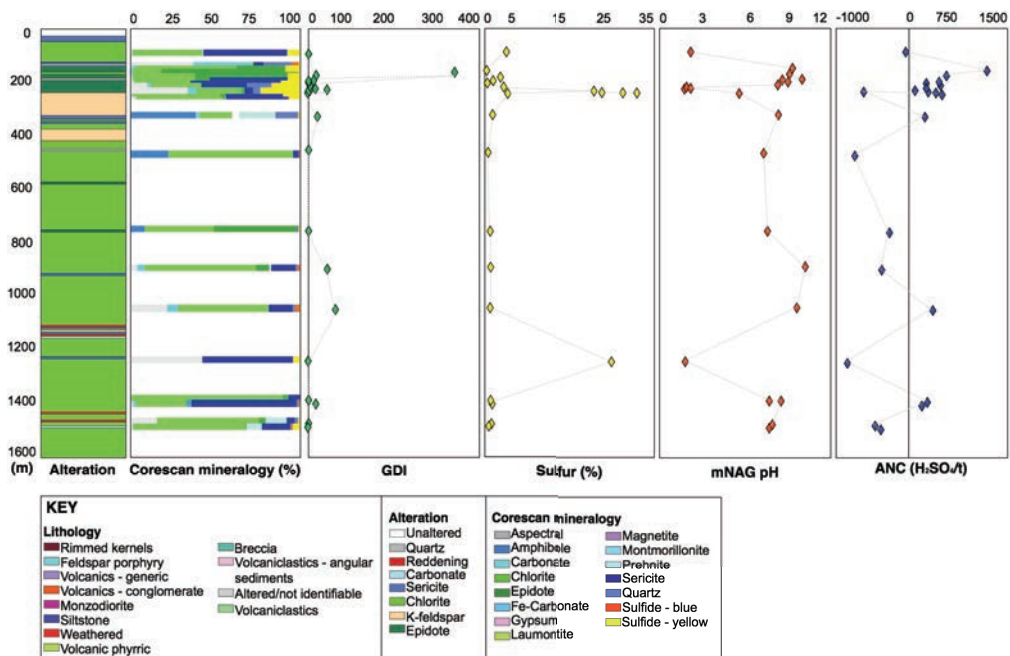


Figure 3 Down-hole log displaying lithology and alteration against Corescan® classified mineral map, geoenvironmental domain index (GDI), sulfur %, paste pH, multi addition net acid generation (NAG) pH, acid neutralising capacity (ANC) and maximum potential acidity (MPA) value.

(Fig 2). Static testing confirmed its high ANC (227 kgH₂SO₄/t) and negative NAPP (-185.6 kgH₂SO₄/t) with a calculated GDI of 21.57 (i.e., low risk). Fig 3d shows the μ XRF S map and highlights sulfide group minerals pyrite and chalcopyrite present in the sample's groundmass. Although the μ XRF images are not quantitative, the high resolution of this technique shows the distribution of sulfur, which can be used as a proxy for sulfides. As sulfides do not have a spectral signature in the IR region this can be used effectively with Corescan® data to resolve mineralogy of aspectral data.

Fig 3e shows calculated mineralogy based on 1,769 data points from a single LA-ICP-MS line across the drill core surface. This data correlates strongly to classified mineralogy (active in SWIR region) output by Corescan® (Fig. 2b). Examples of trace element distribution (Fig. 3f) along the LA-ICP-MS line indicate that calcite contains Zn (max: 1,235 ppm, average: 259 ppm) and Ni (max: 12,397 ppm; average: 269.1 ppm). Both Ni and Zn values are above ANZECC (2000) 90% species pro-

tection freshwater trigger values (0.013 ppm and 0.008 ppm respectively). Other trace elements above the ANZECC (2000) 90% species protection trigger values for freshwater include mean values Al: 8,139 ppm, As: 11.9 ppm, Cu: 337 ppm and Pb: 145 ppm.

Discussion

Mineralogy and texture are significant factors that influence contaminant release from waste rock materials but are not assessed by static tests. Thus, critical information regarding the onset and longevity of AMD can be misunderstood. Parbhakar-Fox and Lottermoser (2017) initially demonstrated how Hylogger™ hyperspectral data could be used to rapidly perform AMD risk assessment for drill core materials. Advantageously, Corescan® records high-resolution RGB images and textural data along with mineralogy. As Corescan® measures in the SWIR region only, mineralogical identification could be improved with hardware modifications to allow for spectral analysis in the LWIR region. This would enable for mineral speciation (e.g.,



carbonate group– calcite, dolomite, ankerite, siderite) therefore improving GDI calculations.

Some specific advantages of the GDI include: (1) Its ability to domain large volumes of drill core faster than visual logging; (2) Reduction of expenditure for mineralogical testing (i.e., Corescan® + C_{TOTAL} in place of XRD); (3) Reduction of cost for static testing (i.e., select representative samples identified from Corescan® for validation); (4) The preservation of the textural context of neutralising minerals and the ability to characterise these textures at high spatial resolution allows for liberation forecasting (i.e., coarse grained calcite would dissolve slower over time compared to disseminated calcite and therefore have a longer neutralising effect).

Characterising trace element chemistry of waste rock is an essential pre-requisite to assessing whether material is an effective neutraliser that will not compromise the downstream environment (Lottermoser, 2010). The LA-ICP-MS fast line method offers a new opportunity to quantify trace element chemistry in drill core or waste rock. This method delivers both classified mineralogy and mineral chemistry. Limited sample preparation requirements, cost efficiency, speed, low detection limits, and the ability to simultaneously analyse a large suite of elements is far advantageous over other methods (e.g., chemical leach sequential extractions; Fig. 3f). The limitations of LA-ICP-MS fast line scanning such as differing mineral ablation rates and mixing of spectra can mostly be overcome by post-analysis data processing (Meffre et al., 2017). Fig 2 demonstrates the potential of combining LA-ICP-MS line-scanning results with high spatial resolution μ XRF maps to effectively characterise the distribution of minerals hosting deleterious trace elements in texturally complex samples. This new method is limited to single line data, future development potentials include mapping functions to produce outputs similar to μ XRF but with advantages of both quantified element chemistry, mineralogy, and low detection limits.

Conclusions

Integrating quantitative mineralogy (Cores-

can®) with trace element chemistry (LA-ICP-MS) from drill core produces unprecedented recognition of low trace element content acid neutralising waste rock within an ore deposit. In this study Corescan® data was used to calculate GDI values drill core to identify samples with effective neutralising capacity. Trace element analyses using LA-ICP-MS line scan method identified the calcite as Zn and Ni rich, which should be considered when planning waste pile design. Modifications to Corescan® processing techniques are being investigated to resolve spectral fractions (e.g., Cracknell et al., 2017). Improved spectral identification will produce an enhanced sulfide recognition workflow. Amendments will produce an updated and comprehensive index more comparable to NAPP.

Acknowledgements

This research was conducted through the Australian Research Councils Industrial Research Hub for Transforming the Mining Value Chain (project number IH130200004). Acknowledgments go to all TMVC members for their contributions to this work and to Dr Mark Pearce at the CSIRO Advanced Characterisation Facility for his help in conducting μ XRF analysis.

References

- Anderson TR, Butler AR (2017) A standard for design life and durability for engineered mine wastes structures. *Journal of Cleaner Production*, 141: 67-74
- Ashley PM, Lottermoser BG, Collins AJ, Grant CD (2004) Environmental geochemistry of the derelict Webbs Consols mine, New South Wales, Australia. *Environmental Geology*, 46(5): 591-604
- Cracknell MJ, Jackson L, Parbhakar-Fox A, Savinova K (2017) Automated classification of Acid Rock Drainage potential from Corescan drill core imagery. In *December AGU Fall Meeting Abstracts*
- Dold B (2016) The biogeometallurgical approach – the information we need to increase the sustainability of mining. *Proceedings of the Third International AUSIMM Geometallurgy Conference*, 15-16 June 2016, Perth, WA, pp 169-171.
- Gurung SR, Wijesekara H, Seshadri B, Stewart RB (2017) Sources and Management of Acid Mine



- Drainage. *Spoil to Soil: Mine Site Rehabilitation and Revegetation*.
- Haas W, Krausmann F, Wiedenhofer D, Heinz M (2015) How circular is the global economy?: An assessment of material flows, waste production, and recycling in the European Union and the world in 2005. *Journal of Industrial Ecology* 19(5): 765-777
- Herrmann W, Berry RF (2002) MINSQ—a least squares spreadsheet method for calculating mineral proportions from whole rock major element analyses. *Geochemistry: Exploration, Environment, Analysis*, 2(4): 361-368
- Jackson L, Parbhakar-Fox A, Fox N, Cooke DR, Harris AC, Savinova E (2017) Intrinsic neutralisation potential from automated drillcore logging for improved geoenvironmental domaining, Proceedings of the 2017 Workshop on Acid and Metalliferous Drainage, 20-23 November, Burnie, Tasmania
- Lèbre É, Corder G, Golev A (2017) The role of the mining industry in a circular economy: A framework for resource management at the mine site level. *Journal of Industrial Ecology* 21(3): 662-672
- Lottermoser BG (2010) *Mine Wastes* (3rd Edition): Characterization, Treatment and Environmental Impacts. Characterization, Treatment and Environmental Impacts :1-400.
- Meffre S, Danyushevsky L, Harraden C, Berry R, Olin P, Fox N (2017) Scanning unpolished drill cores with laser ablation quadrupole ICPMS Goldschmidt Abstracts, 2017 2679
- Noble, TL, Lottermoser, BG, Parbhakar-Fox, A (2015) Evaluation of pH testing methods for sulfidic mine waste. *Mine Water Environment*.
- Parbhakar-Fox A, Lottermoser B (2017) Predictive waste classification using field-based and environmental geometallurgy indicators, Mount Lyell, Tasmania. In *Environmental Indicators in Metal Mining* :157-177
- Price WA (2009) Prediction manual for drainage chemistry from sulphidic geologic materials (CANMET Mining and Mineral Sciences Laboratories): 579
- Smart R, Skinner WM, Levay G, Gerson AR, Thomas JE, Sobieraj H, Schumann R, Weisener CG, Weber PA, Miller SD, Stewart WA (2002) ARD test handbook: Project P387, A prediction and kinetic control of acid mine drainage, Melbourne, Australia, AMIRA, International Ltd, 10 p.





Coupling PHREEQC with GoldSim for a More Dynamic Water Modeling Experience

Brent C. Johnson¹, Pamela Rohal¹, Ted Eary²

¹HydroGeoLogica, Inc., 414 Garden Glen Court, Golden, CO, USA 80403
bcjohnson@hydrogeologica.com

²Enchemica LLC, 2335 Buckingham Circle, Loveland, CO, USA 80538

Abstract

Mining operators strive to improve their tools for decision-making about water management to minimize risks and costs related to water quantity and quality issues. These issues are typically interrelated and complex such that interpretation and prediction of system dynamics requires implementation of innovative approaches that make use of observed data and fundamental hydrochemical concepts. We have developed an approach that couples the dynamic systems modelling framework of GoldSim with the geochemical reaction simulation capabilities of PHREEQC as described by Eary (2007). The approach utilizes a dynamic link library (DLL) code to handshake and transfer data between the two programs at every model timestep.

The coupled GoldSim-PHREEQC approach simulates mixing and reactions taking place at key mixing points along flow paths and at key water storage locations (e.g., ponds, tanks, pit lakes). Empirical factors affecting chemical loads can be calibrated to observed flows and chemistry at multiple locations and then used for predicting future water quality as operating and environmental conditions change.

Including geochemical reactions at each model time-step provides an efficient approach for applying a thermodynamic framework for understanding important geochemical processes that affect water chemistry. The approach also identifies the subset of reaction processes that may not be well explained by thermodynamic-based calculations and require empirical adjustment and time periods in response to events such as facility shut downs, climate events, and closure and remediation. The resulting calibrated model can be used to challenge our understanding of the reactions that are attenuating or not attenuating solutes at various site locations and to help understand, predict, and manage water quality going forward.

This modelling approach was applied to a proposed mine site in the northern Michigan (U.S.A.) to simulate various stages of operational and closure conditions to predict the quality of water that will require treatment. The model provided an efficient approach for making robust predictions of treatment requirements in terms of both water quality and quantity as a function of mine operations and closure.

Keywords: water balance, GoldSim, geochemical modelling, PHREEQC, water management, closure

Introduction

Effective mine water management and closure planning require a system-wide understanding of both the water balance and chemical balance. They also require modeling tools that can be used to answer specific questions important for planning, such as:

- How reliable is our water source (quality and quantity) and how much storage will we need?
- What treatment methods will be required to meet discharge standards?
- What is the most efficient way to reduce the water inventory when nearing closure?
- Will the pit lake require treatment and, if so, how can costs be minimized?
- Are there opportunities to blend or segregate waste streams to reduce operational and closure cost and risk?



The foremost requirement for answering these types of questions is an accurate water and solute conceptual model, upon which, predictive models can be constructed using representative hydrologic, geochemical, and water chemistry data.

Mine water flows and chemistry are strongly interdependent and while they can be managed separately, there are significant advantages to integrating flow and chemistry evaluations. Historically, the common approach has been to evaluate flow and reactive chemistry separately and then integrate the results through approximation of system dynamics. The most common simulation platform used for site-wide mine water and chemical balances with true temporal dynamics is GoldSim (GTG, 2017). Coupling GoldSim with more advanced, reactive chemistry has typically involved manually exporting output from the flow model, as input to the reactive chemistry model. This method necessarily required the user to extract a few timesteps over the life of the model period and set up the reactive chemistry model to simulate and predict the chemistry for these few timesteps. This method is effective at predicting the general trends and overall chemistry at selected locations; however, it is not effective at evaluating short term trends (e.g., climatic effects and kinetically controlled reactions) without the time-consuming effort of exporting high-resolution timesteps. In addition, simulating even shorter-duration trends or events, such as upset conditions, or particular storm events was not practical. Recent advances; however, have made it possible to couple these types of models using a linking program to simulate the reactive chemistry at every timestep, e.g., monthly, daily, or hourly, thereby facilitating the simulation of short-term trends and episodic events.

In this paper, we present a description of the approach for linking GoldSim to PHREEQC using a Dynamic Linking Library (DLL). This approach provides a seamless link between GoldSim and PHREEQC to allow programs to handshake and transfer flow and chemistry data between the two programs during each timestep. We also present a case study where this approach was used to predict the chemistry of various site sources and support water treatment plant design.

Methodology

A variety of water balance and geochemical modeling platforms can be run in batch environments and/or link to other programs to share data. The authors have successfully linked GoldSim with PHREEQC and with Geochemists Workbench (Bethke, 2018) in a variety of ways via an external dynamic link library (DLL) file.

The following methods have been utilized for integrating PHREEQC calculations with the GoldSim model:

Manual Method – This method involves exporting GoldSim mass/volume results to a spreadsheet for post-processing at selected GoldSim time steps into values that can be manually entered into the PHREEQC input file. This “hands-on” approach allows as much flexibility as needed to customize the PHREEQC model to suit the geochemical conditions. This approach also provides an opportunity for modelers to provide a “common sense” check on both the GoldSim and PHREEQC outputs for each simulation. Some automation of this process can be built into the post-processing spreadsheet to speed up the process for multiple, similar runs.

Pre-Modeling Method – This involves running a large number of PHREEQC models to create a database of various combinations of mixing waters of different types and different ratios. Results are compiled as a set of mixing/reaction “type curves” and are used in GoldSim as multi-dimensional Lookup Table elements. Programming can be written into GoldSim to select the appropriate water chemistry from the Lookup Table. This approach results in fast run-times for GoldSim (because it will not have to call PHREEQC during the model run) but is limiting because with more than one or two waters, the number of pre-modeling runs can be excessive. Also, if there are any changes in water chemistry or reaction conditions, pre-modeling would have to be re-done and re-submitted into the GoldSim Lookup Tables.

DLL (automated) Method – This method involves setting up GoldSim to communicate with PHREEQC via a DLL file. Figure 1 shows the overall concept. It involves setting up two approximately parallel models: one for the water balance and a second for the chemical balance. The water balance keeps



track of flows and storage. Flows are typically input as time series data. Storage is simulated through the use of reservoirs or pool modeling elements. In parallel, GoldSim tracks the chemical balance as masses of solute transferred in flows over time. Typically, water chemistry data are input as time series, which when multiplied by flow rates gives mass transfer rates. A modeling element called a cell pathway links the two parallel calculation sequences of the water balance and chemical

balance together to produce concentrations for the storage reservoir. This is not the only sequence of calculations that can occur but is perhaps the most common.

The bulk concentrations yielded by the cell pathway in GoldSim represent the result of conservative mixing, that is, no reactions are included. The purpose of the DLL is to account for the effects of reactions on the bulk concentrations. To achieve this purpose, the DLL performs the following functions: re-

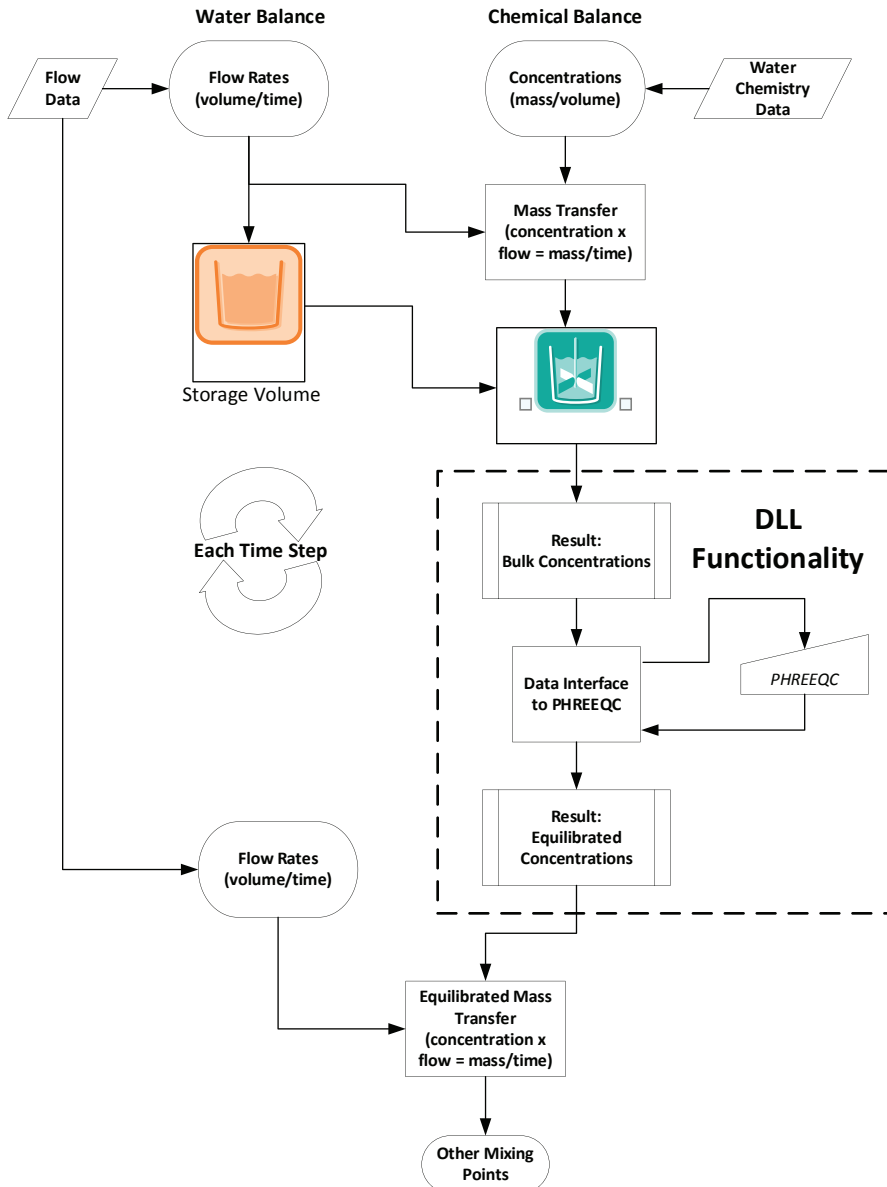


Figure 1 Conceptual depiction of the DLL operation



ceives the bulk concentrations via GoldSim’s DLL interface and formats them for input to PHREEQC, runs PHREEQC, reads the PHREEQC outputs, and returns the results to GoldSim (Figure 1). The returned concentrations represent the effects of chemical processes defined in the PHREEQC model on the bulk concentrations. The equilibrated concentrations can then be used in subsequent modeling calculations. The power of this approach is that these operations can be done at each time step of the model. The

negative aspect of this approach is that the run time can be very long, depending on the number of times PHREEQC is called for calculations, timestep, and simulation period.

Validation

One of the most common types of calculation needed in GoldSim models of water chemistry is mixing two or more waters with different chemical compositions. A typical scenario is an acidic water mixing with an alkaline water. Under these circumstances, conserva-

Table 1 Validation Model Input Chemistry and Equilibrium Phases

Species	Acidic Chemistry	Alkaline Chemistry	Species	Acidic Chemistry	Alkaline Chemistry	Equilibrium Phases	SI	Initial amount (mol)
Al	124.03	0.009	Mn	33.1	0.831	O ₂ (g)	-0.7	1
As	0.0103	0.0348	Mo	0.0186	0.009	CO ₂ (g)	-3.5	1
Ba	0.041	0.048	NO ₃ -N	0.827	2.02	Gypsum	0	0
Ca	616	722	Na	17.9	52	Fe(OH) ₃ (a)	0	0
Cd	0.01034	0.0002	Ni	0.041	0.0014	Al(OH) ₃ (a)	0	0
Cl	14.5	15.9	Pb	0.186	0.022			
Co	0.08243	0.00055	SO ₄	2512	1855			
Cu	0.454	0.0033	Sb	0.001	0.164			
HCO ₃	0	60.9	Si	0.0047	0.0019			
Fe	66.2	0.007	Sr	0.299	0.738			
K	10.6	85.471	Zn	7.97	0.58			
Mg	36	6.8	pH	3.68	8.86			

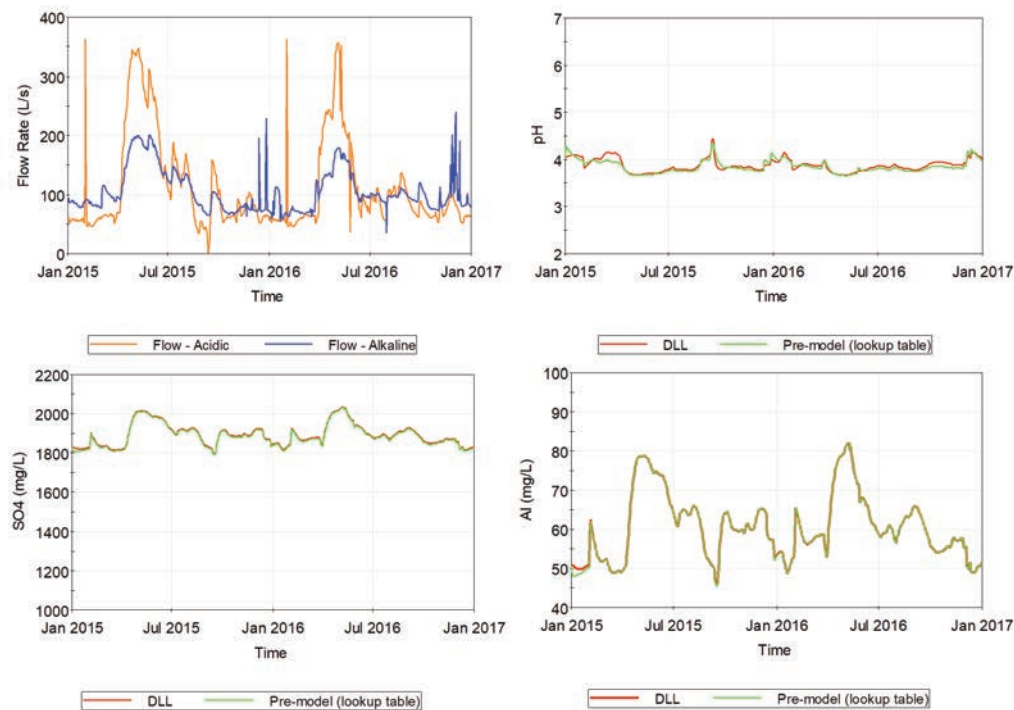


Figure 2 Comparison of the DLL (automated) method to the pre-modelling (lookup table) method



tive mixing calculations will not be representative of the final water chemistry because of the effects of aqueous speciation, mineral/gas solubility, and redox.

Mixing an acidic water with an alkaline water is used here as a test case to compare the DLL (automated) method directly to the pre-modeling method. In this comparison, the pre-modeling was done by mixing the solution chemistries in Table 1 in 1 percent increments to create a table of results representing 100 possible outcomes resulting from mixing. The mixing calculations assumed equilibrium with atmospheric $O_2(g)$ and $CO_2(g)$ and the solubilities of secondary solids of gypsum, ferrihydrite, and $Al(OH)_3(a)$ (Table 1). The results from the calculations were used to construct a lookup table where the index to the resulting water chemistries is the mixing proportion. The flows are dynamic, so the mixing proportions change over time. These calculations were implemented in a GoldSim model.

For comparison, the same solution chemistries were input to a second GoldSim model. In this second model, the DLL functionality was added to allow the calls to PHREEQC to be performed at each time step. The same set of equilibria as specified in Table 1 was also used in this model.

The results from the two approaches are shown in Figure 2. There are small differences at the start of the simulation, but after about 5 to 10 days, the results are very close. There are also small differences in pH at times when the flows are changing rapidly due to the sensitivities of the solubilities of ferrihydrite and $Al(OH)_3(a)$. These differences could be minimized by increase the number of mixing increments for the pre-modeling lookup table.

Case Study – Water Treatment Plant Design at a Proposed Mine in Northern Michigan

The Back Forty Project (Aquila Resources) is a gold-zinc sulfide mine project in the Upper Peninsula of Michigan in the northern United States. Aquila is evaluating future site water quality with respect to water treatment requirements in a strict regulatory environment with highly-sensitive ecological risk issues. The sulfidic ore and waste pose acid-

generation risk; however, the groundwater that will enter the pit sump during operations is predicted to carry significant alkalinity load which, based on the current mine plan, will mix with runoff/seepage from waste piles, stockpiles and tailings in engineered seepage collection systems and reservoirs. This design has raised questions about the need for, type, and scale of water treatment that will be required for managing site water quality prior to surface water discharge via a permitted outfall.

A predictive, GoldSim-PHREEQC coupled model was built based on the conceptual design of the site water circuit, presented in Figure 3. The model was enabled with a stochastic precipitation data set to support probabilistic simulation to generate stochastic/random precipitation events, when required. The model was developed for the pre-operations construction period of 12 months, the entire life of mine of 78 months, and pre-closure period of 3 months. Contact water and storm water flow rates, associated with each of the facilities, was represented in the water balance portion of the model based on the projected facility size, material characteristics, estimates of runoff coefficients, and unsaturated infiltration rates, as appropriate. Estimates of water chemistry, associated with each of the respective flow components, were derived from either site-specific water quality data, process water chemistry data, or were derived from a significant database of geochemical testing data from static and kinetic testing of site soil, waste rock, ore, and tailings materials. The proposed mine materials balance for the site was used to assign chemical source terms to pit wall runoff and waste rock piles containing a mixture of geologic rock types. As described above, solute mass loading calculations were tracked in GoldSim for 41 chemical constituents (pH, alkalinity, major ions, and dissolved metals and metalloids). The GoldSim model was linked via DLL coding to PHREEQC to apply geochemical speciation, redox, and mineral/gas solubility controls to predict the chemistry of water to be treated that is collected in the Contact Water Basin (CWB) (Figure 3). Results from PHREEQC were imported back into GoldSim at each timestep and used



in subsequent mixing calculations in the CWB. Flow and geochemical model predictions were produced at several locations and through time over the life-of-mine modeling period.

The final product from this phase of work was a user-friendly modeling tool that could be updated and refined for future calibration and predictions of flows and water chemistry at several points in the circuit. A major finding of this phase was the importance of the alkalinity loading for maintaining circum-neutral pH conditions in the inflow to the water treatment plant (Figure 3). Identifying this as a risk allowed Aquila Resources to direct efforts toward improving confidence in the pit groundwater inflow rates through advancement of their hydrogeologic modeling in combination with their site groundwater quality dataset. Upcoming work includes updating the water chemistry model with refined site engineering plans, additional water quality and geochemical data, and extending the model into the post-closure period.

Acknowledgements

We appreciate the use of site data and project information provided by Aquila Resources, Inc.

References

- Bethke, C.M., 2018. The Geochemist Workbench Release 12.0, Reaction Modeling Guide, a User's Guide to React and Gplot. Aqueous Solutions, LLC.
- Eary, T. (2007) Linking GoldSim with the PHREEQC Geochemical Model with a Dynamic Link Library. 2007 GoldSim User's Conference, San Francisco, CA.
- GTG. 2017. Dynamic Monte Carlo Simulation Software. GoldSim Technology Group, LLC (www.goldsim.com)
- Parkhurst DL, Appelo CAJ (2013). Description of Input and Examples for PHREEQC Version 3 – A Computer Program for Speciation, Batch-Reaction, One-Dimensional Transport, and Inverse Geochemical Calculations. US Geological Survey Techniques and Methods 6:1-497.

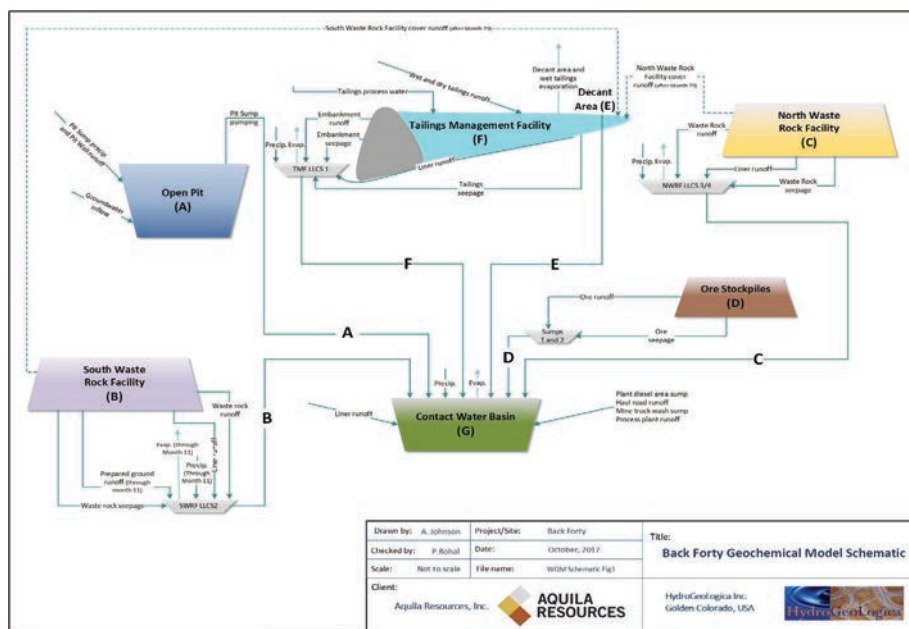


Figure 3 Back Forty Mine Site Water Conceptual Model





Recovery of Value from an Electronic Waste Stream using a Biological Matrix

Thabo Mabuka, Susan T. L. Harrison, Elaine Govender-Opitz

Centre for Bioprocess Engineering Research (CeBER), Department of Chemical Engineering, University of Cape Town, Rondebosch 7701, South Africa

Abstract

Increasing reserves of electronic waste highlight this as a valuable source of metals to re-enter the manufacturing circuit while minimising its environmental burden and realising a circular economy. Base metals may be extracted by bio-assisted ferric and acid prior to precious metal extraction. Recycling of the iron fraction intensifies this process; hence recovery of ferrous ions is important in the leaching of printed circuit boards (PCBs) by acidophiles. Chitin has shown high selectivity for iron in multi-metal solutions. In this study, chitin sourced from fly larvae (*Hermetia illucens*) was able to absorb ferrous ions up to an absorption capacity of 6.03 mg/g of chitin. The results of this study show the potential for chitin sourced from fly larvae to act as a sorbent for ferrous ion recovery from leachate solutions.

Keywords: E-waste, Waste electronic and electrical equipment (WEEE), bioleaching, iron, chitin, fly larvae

Introduction

In 2017, 47 million metric tonnes of Waste electronic and electrical equipment (WEEE) was produced globally, with South Africa producing 340 metric tonnes (Baldé et al., 2017). The need to recover value from waste metal streams and to reduce their environmental impact has motivated research into metal recovery from these waste streams. WEEE has been identified as a waste stream of high value, with about 40% of printed circuit boards (PCBs) containing base, precious and platinum group metals in greater amounts than found in mined ores (Yunus & Sengupta 2016). WEEE is also classified as hazardous, due to the high amounts of metal and other compounds such as polychlorinated biphenyl and halogenated flame retardants. Pyrometallurgy is the current conventional method of processing WEEE, however, bioleaching has been proposed to be a more environmentally friendly and less energy intensive route (Kavitha 2014). Biohydrometallurgy along with hydrometallurgical routes result in the production of metal-rich leachates.

Metal recovery from leachate solutions may include but not limited to several processes such as precipitation, cementation, solvent extraction, electrowinning, ion exchange

and biosorption. Cementation of copper and iron has several drawbacks, the most limiting being its poor selectivity in multi-metal ion solutions (Panão et al. 2006). Iron recovery by precipitation with limestone was found to be inefficient due to contamination with gypsum and slow settling time of the precipitated iron (Neale et al. 2011). Solvent extraction-electrowinning (SX-EW) process for copper recovery has been found to have a high environmental impact with respect to the climate change indicators (Ayres et al. 2002). Ion exchange resins, although efficient, may be too expensive for use in recovery of metals from waste streams. The various limitations in these processes has resulted in the consideration of bio sorbents for the selective recovery of metals from multi-metal solutions. Chitin and chitosan have been distinguished as more effective bio sorbents than bacteria, fungi, algae, proteins and tannin derivatives (Cui & Zhang 2008). Fly larvae shells are a large waste product in the biological treatment of industrial food wastes to produce protein rich feeds and have been shown to contain 40 % of their weight as chitin (Gyliene et al. 2003). Chitin is the second most abundant natural polymer after cellulose and chitosan is its deacetylated derivative (Zhou et al. 2004). Both



polymers have shown great potential for application as bio sorbents of metals in solutions (Dutta et al. 2004).

Metal absorption studies using chitin and chitosan have shown higher selectivity for iron and copper respectively, from multi-metal solutions (Gyliene et al. 2002; Rhazi et al. 2002; Zhou et al. 2004). However, the ability of these polymers to recover metals from leachate solutions has not been investigated in-depth, particularly in the application to metal-rich solutions from the acidic bio-leaching of electronic waste. Iron is a lixiviant in the mechanism for the bio-assisted ferric and acid leaching of PCBs by acidophiles (Choi et al. 2004) and recovery of ferrous ions after chemical leaching is important in a two-step bioleaching process in which Fe^{2+} is oxidised to the lixiviant Fe^{3+} microbially (Brandl et al. 2001). Although Gyliene et al. (2002) investigated the recovery of ferric ions by fly larvae shells of *Musca Domestica*, recovery of ferrous ions was not investigated. The objective of this paper is to investigate the recovery of ferrous ions from a model leachate solution using chitin sourced from fly larvae of *Hermetia illucens* and to investigate the cost of producing chitin from fly larvae as an adsorbent material for iron.

Methods

Preparation of Sorbent

Fly larvae (*Hermetia illucens*) are produced as a waste stream during the production of animal feed. The fly larvae, initially stored at -20°C , was used to produce chitin as described in Gyliene et al (2002), except for the use of room temperature conditions for the deproteinisation steps as described in Tetteh (1991). Furthermore, the decolorisation of the chitin was not performed. The major steps in the extraction of chitin involved removal of proteins and minerals in an acidic solution (demineralisation) and removal of the proteins from the fly larvae using alkali treatment (deproteinisation). In preparation, the fly larvae were first washed with water, then dried at room temperature for 24 hours and crushed to liberate the material inside the fly larvae. Demineralisation was performed using 2M HCl at ambient conditions, where 20 g crushed fly larvae were placed into 225

ml of 2M HCl for 2 hours. After the demineralisation process, the fly larvae were filtered and washed with de-ionized water until neutral pH, then dried at room temperature for 24 hours. The remaining dried demineralised fly larvae of 8 g was then crushed to sizes range between 0.150 mm and 2 mm. The dried demineralised fly larvae were then deproteinised in 200 ml of 4 % (w/v) NaOH at ambient conditions for 5 h. The small dark brown chitin particles produced were used in the ferrous iron absorption and desorption experiments.

Absorption experiments

Experiments to investigate the absorption of ferrous ion were performed under batch conditions in Erlenmeyer flasks at 31.5°C on a shaker at 120 rpm, in triplicate. Aliquots of 200 mL of the model stock solution was added to each Erlenmeyer flask. The model stock solution contained 176 mg/L Fe^{2+} to represent the average concentration in the leachate from acidic bioleaching of 1g of PCB with acidophiles (Brandl et al. 2001). Adsorption conditions were adapted from Zhou et al (2004) and the pH was set to 4 by addition of H_2SO_4 (96 %) and maintained by adjustment with NaOH or H_2SO_4 accordingly. A mass of 0.7 g chitin was loaded into the Erlenmeyer flasks. Solution samples were taken hourly until equilibrium was reached. Ferrous iron concentrations in solution were measured spectrophotometrically using the modified ferric chloride assay developed by Govender et al (2012).

Desorption experiments

The desorption experiments were carried out in 0.1 M HCl with magnetic stirring according to the method proposed in Vijayaraghavan et al (2005). The ferrous-loaded chitin was placed in 100 ml 0.1 M HCl. The metal concentration of ferrous iron eluted into solution was measured every 15 mins for the first hour and then every half an hour thereafter spectrophotometrically.

Results and discussion

Preparation of Sorbents

During the preparation of bio sorbents, it was observed that settling, decanting followed



Table 1: Yields and cost of chitin production in this study and the study by Glyliene et al. (2002)

Studies	Present study	(Glyliene et al 2002)
Chitin source	Fly larvae (<i>Hermetia illucens</i>)	Fly Larvae Shells (<i>Musca domestica</i>)
raw material used (g)	20	40
HCl used (kg)	0.0164	0.0602
NaOH used (kg)	0.008	0.024
Chitin produced (g)	2.2	24
Electricity used (kWh)	-	0.143
Yield (%)	11	60
Cost of chitin production (R/kg)	66	26

by filtration was the most efficient method of separating the fly larvae material from reagents. The settling time prior to decanting was less than 2 minutes. Crushing of the fly larvae directly after the initial washing step resulted in a mushy paste of fly larvae material and exposed the material covered by the fly larvae shells for liberation. Demineralization resulted in the liberation of material inside the fly larvae. Prolonged drying of fly larvae in an 80°C oven after washing resulted in a release of a foul odour. Therefore, drying at room temperature for 24 hours was adopted to successfully dry the fly larvae material. Table 1 shows the yield and cost of production based on operational costs only of chitin in this study in comparison to that by Glyliene et al. (2002). The yield obtained in the present study was 11%. However, the yield relative to the fly larvae shell component of the fly larvae is 46 %, estimated based on the compositions of fly larvae given in Glyliene et al. (2003) and Caruso et al. (2014). The yield in this study was low in comparison to the yield of 60% obtained by Glyliene et al. (2002), which is similar to those reported in Horowitz et al. (1957) and Tetteh (1991). In the deproteinization conditions in Glyliene et al. (2002), fly larvae shells were placed in 4 % (w/v) NaOH at 60 °C for 2 hours while in this study larvae were placed in the same concentration of NaOH at room temperature for 5 hours. The prolonged deproteinization in this study may have resulted in the loss of raw material, however the major factor for the difference in yield is the raw materials used. This study used fly

larvae from *Hermetia illucens* while Glyliene et al. (2002) used fly larvae shells from *Musca domestica*. Fly larvae has been shown to contain a large amount of protein and lipids of about 40 % to 60 % by dry mass (Caruso et al. 2014). Therefore, the large loss of material in this study may be attributed to the removal of the larger amounts lipids and proteins from the fly larvae.

Table 1 shows that the cost of production of chitin in this study was R 66 per kg of chitin while the cost of production in Glyliene et al. (2002) was R 26 per kg of chitin. The use of fly larvae shells in Glyliene et al. (2002) resulted in higher yields of chitin when compared to the use fly larvae in this study. This shows that regardless of larger amounts of reagents used and the use of electricity in heating the NaOH to 60°C in the deproteinization conditions in Glyliene et al. (2002), the higher yield due to the use of fly larvae shells compared to fly larvae resulted in 60 % less cost of production than obtained in this study. These results indicate that yield of chitin relative to the raw material is an important parameter in the cost of production of chitin. The amount of indirect CO₂ emission produced from the use of electricity in the deproteinization conditions in Glyliene et al. (2002) is 0.0061 kg of CO₂ per g chitin produced. This value is based on the emission factor of electricity in South Africa and indicates a higher environmental impact than the deproteinization at ambient conditions as done in this study.

The average market value of chitin is R 200 per kg of agriculture grade chitin (Alibaba,



2018). The cost of production of chitin in this study is 3 times less than that of the average market value of agriculture grade chitin. This indicates high value addition with regards to the fly larvae.

Sorption of free metal ion

Figure 1 shows the adsorption of ferrous ions from a solution of 176 mg/L of Fe^{2+} onto 0.7 g chitin. The sorption capacity obtained in this study was 6.03 mg Fe^{2+} /g chitin (0.108 mmol Fe^{2+} /g chitin), with 4.10 mg ferrous ions being absorbed in the first 220 minutes (3.67 hours). This was equivalent to 94.8 % of sorption capacity of the 0.7 g chitin used, indicating an average sorption rate of 0.0279 mg Fe^{2+} per g chitin per minute. Similar absorption times for ferric ions were observed in Gyliene et al. (2002), and Zhou et al. (2004). The sorption capacity obtained in this study for ferrous ions was 82 % less than the 0.6 mmol Fe^{3+} /g chitin obtained by Gyliene et al. (2002) for

ferric ions. The difference in sorption capacity might be due to the difference in the metal ions being adsorbed and possible difference in degree of acetylation of the chitin.

Table 2 shows the recovery cost of iron from solution using chitin as sorbent in this study relative to ion exchange resins as reported in the literature. The absorption capacity of chitin produced in this study is less than that of the ion exchange resins, shown in Table 2 and the cost of recovery of iron was 73 %, 85 %, 474 % more than that of the ion exchange resins Purolite S957, Na-Y zeolite, Lewatit TP 207 resin respectively used in Martins et al. (2017). These preliminary results show that there is a need to reduce the cost of production of chitin or to improve the absorption capacity of the chitin produced from fly larvae for it to be competitive with ion exchange resins in the recovery of ferrous ion from solution.

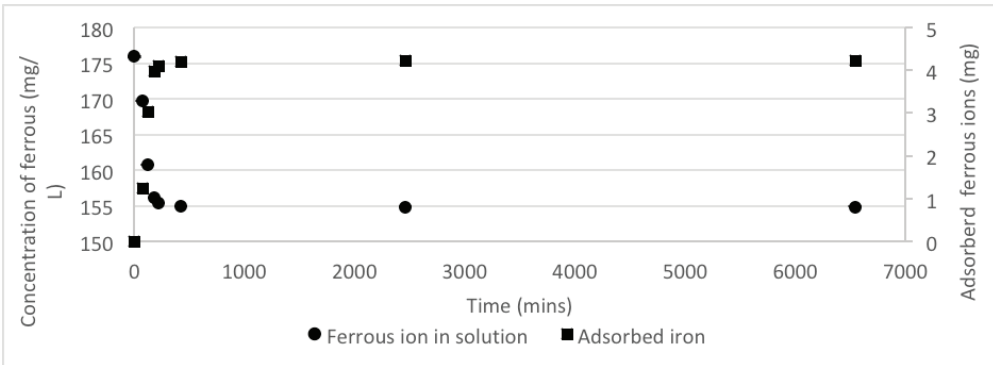


Figure 1: Adsorption of ferrous ions onto 0.7 g of chitin produced from Fly larvae (*Hermetia illucens*) from a solution of 176 mg/L ferrous ions

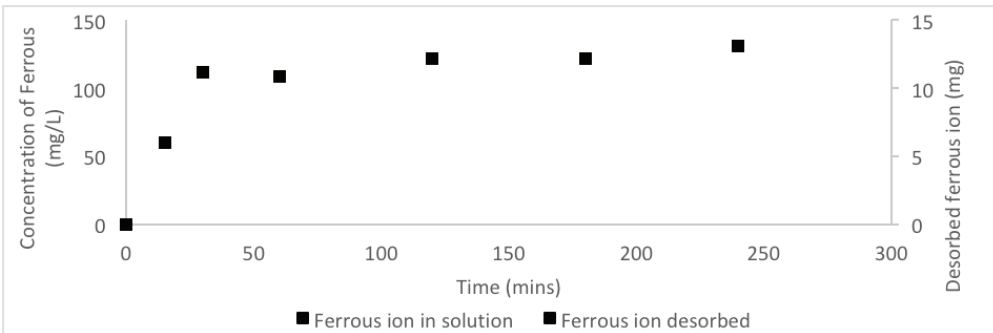


Figure 2: Desorption of ferrous ions from 2.1 g of chitin produced from Fly larvae (*Hermetia illucens*) in 0.1M HCl



Table 2: Comparison of the recovery costs of iron from solution using chitin in this study relative to ion exchange resins

Material	Cost (R/kg)	Absorption capacity (mg Iron/g)	Recovery costs (R/mg Iron)	Reference
Purolite S957	263	42.0	0.0063	(Izadi et al. 2017)
Na-Y zeolite	325	55.9	0.0059	(Kim & Keane 2002)
Chitin	66	6.03	0.0109	This study
Lewatit TP 207 resin	106	56.0	0.0019	(Martins et al., 2017)

Desorption of free metal ion

Figure 2 shows the desorption of ferrous ions from chitin. The average desorption was 6.21 mg Fe²⁺/ g chitin, compared to a loading of 6.03 mg / g chitin. In the first 30 minutes, 85.0 % of the ferrous ions adsorbed on the chitin was desorbed while the rest was desorbed after 2 hours. A desorption time of 2 h was also observed in Gyliene et al. (2002). This gives an average desorption rate of 0.0518 mg Fe²⁺ per gram of chitin per minute. The amount of ferrous ion desorbed relative to the amount adsorbed was 103 %. These results show that there was complete desorption of ferrous ions adsorbed and that desorption of ferrous ion on chitin occurs at a faster rate than adsorption.

Conclusions

This study demonstrated the preparation of chitin from the fly larvae (*Hermetia illucens*) and the ability to recovery ferrous iron using this bio sorbent. Settling, decanting followed by filtration is an efficient method of separating fly larvae from reagent solutions. Drying fly larvae after washing is an important pre-step before the crushing of fly larvae. Drying the fly larvae at room temperature is as effective as drying in the oven at 80°C. The initial crushing of the fly larvae results in the exposure of material in the fly larvae for liberation and demineralization resulted in liberation of some of the materials inside the fly larvae. The use of fly larvae as a raw material resulted in lower yields of chitin when compared to the use of fly larvae shells. The yield of chitin relative to the raw material used indicated to be an important parameter in the cost of production of chitin. The cost of production for chitin from fly larvae was three times less

than the market value of agriculture grade chitin. The chitin produced from fly larvae (*Hermetia illucens*) adsorbed ferrous ions to a loading capacity of 6.03 mg Fe²⁺/ g chitin. There is a need to reduce the cost of production of chitin or to improve the absorption capacity of the chitin produced from fly larvae (*Hermetia illucens*) to improve its ferrous ion recovery cost. This study showed that all adsorbed ferrous ions can be completely desorbed with HCl and that the desorption rate of ferrous ion from chitin is faster than the adsorption rate. This investigation shows that fly larvae (*Hermetia illucens*) has a potential to be a sorbent for ferrous ions in leachate solutions.

Acknowledgements

The authors would like to thank the Council for Scientific and Industrial Research (CSIR), the Centre for Bioprocess Engineering Research (CeBER) and AgriProtein Technologies for their contributions towards this work.

References

- Alibaba (2018) Chitin products. Available: https://www.alibaba.com/trade/search?fsb=y&IndexArea=product_en&CatId=&SearchText=chitin [2018, May 14].
- Ayres RU, Ayres LW, Rade I (2002) The Life Cycle of Copper, its Co-Products and By-Products. Journal of Industrial Ecology. (24). DOI: 10.1162/108819899569458.
- Baldé CP, Forti V, Kuehr R, Stegmann P (2017) The Global E-waste Monitor 2017: Quantities, Flows, and Resources. Bonn: UNU-VIE SCYCLE. DOI: ISBN 978-92-808-4556-3.
- Brandl H, Bosshard R, Wegmann M (2001) Computer-munching microbes: Metal leaching from electronic scrap by bacteria and fungi. Process



- Metallurgy. 9(C):569–576. DOI: 10.1016/S1572-4409(99)80146-1.
- Caruso, D, Devic E, Subamia IW, Talamond P, Baras E (2013) *Technical handbook of domestication and production of diptera Black Soldier Fly (BSF) *Hermetia illucens*, Stratiomyidae*. D. Nastiti Murti, Ed. PT Penerbit IPB Press. Available: <https://uved-formation-aquaculture.cirad.fr/content/download/4328/32130/version/3/file/BLACK+SOLDIER+Technical+Handbook.pdf>. Choi MS, Cho KS, Kim DJDS (2004) Microbial Recovery of Copper from Printed Circuit Boards of Waste Computer by *Acidithiobacillus ferrooxidans*. Journal of Environmental Science and Health, Part A- Toxic/Hazardous Substances & Environmental Engineering. A 39(11–12):2973–2982. DOI: 10.1081/lesa-200034763.
- Dutta PK, Dutta J, Tripathi VS (2004) Chitin and chitosan: Chemistry, properties and applications. Journal of Scientific & Industrial Research. 63(January):20–31.
- Govender E, Harrison STL, Bryan CG (2012) Modification of the ferric chloride assay for the spectrophotometric determination of ferric and total iron in acidic solutions containing high concentrations of copper. Minerals Engineering. 35:46–48. DOI: 10.1016/j.mineng.2012.05.006.
- Gyliene O, Rekertas R, Šalkauskas M (2002) Removal of free and complexed heavy-metal ions by sorbents produced from fly (*Musca domestica*) larva shells. Water Research. 36(16):4128–4136. DOI: 10.1016/S0043-1354(02)00105-7.
- Gyliene O, Razmūte I, Tarozaitė R, Nivinskienė O (2003) Chemical composition and sorption properties of chitosan produced from fly larva shells. Chemija (Vilnius). 14(3):121–127.
- Horowitz T, Roseman S, Blumenthal J (1957) The Preparation of Glucosamine Oligosaccharides. I. Separation. J. Am. Chem. Soc. 79:5046–5049.
- Izadi A, Mohebbi A, Amiri M, Izadi N (2017) Removal of iron ions from industrial copper raffinate and electrowinning electrolyte solutions by chemical precipitation and ion exchange. Minerals Engineering. 113(April):23–35. DOI: 10.1016/j.mineng.2017.07.018.
- Kavitha AV (2014) Extraction of precious metals from ores thereof. Journal of Chemical and Pharmaceutical Sciences. (3):147–149.
- Kim JS, Keane MA (2002) The removal of iron and cobalt from aqueous solutions by ion exchange with Na-Y zeolite: Batch, semi-batch and continuous operation. Journal of Chemical Technology and Biotechnology. 77(6):633–640. DOI: 10.1002/jctb.618.
- Lehohla P (2015) Environmental Economics Accounts Compendium. Pretoria.
- Martins PJM, Reis PM, Martins RC, Gando-Ferreira LM, Quinta-Ferreira RM (2017) Iron recovery from the Fenton's treatment of winery effluent using an ion-exchange resin. Journal of Molecular Liquids. 242:505–511. DOI: 10.1016/j.molliq.2017.07.041.
- Neale JW, Gericke M, Ramcharan K (2011) The application of bioleaching to base metal sulfides in Southern Africa: prospects and opportunities. The Southern African Institute of Mining and Metallurgy. 367–388.
- Panão ASI, Carvalho JMR De, Correia MJN (2006) Copper Removal from Sulphuric Leaching Solutions by Cementation. Technical University of Lisbon. Available: https://fenix.tecnico.ulisboa.pt/downloadFile/395137462214/Artigo_Cementacao.pdf.
- Rhazi M, Desbrières J, Tolaimate A, Rinaudo M, Vottero P, Alagui A, El Meray M (2002) Influence of the nature of the metal ions on the complexation with chitosan. Application to the treatment of liquid waste. European Polymer Journal. 38(8):1523–1530. DOI: 10.1016/S0014-3057(02)00026-5.
- Tetteh AY (1991) Optimization studies on chitin extraction from crustacean solid wastes. McGill University. Department of Food Science and Agricultural Chemistry. 15–80.
- Vijayaraghavan K, Jegan JR, Palanivelu K, Velan M (2005) Nickel recovery from aqueous solution using crab shell particles. Adsorption Science & Technology. 23(4):303–311. DOI: 10.1260/0263617054770002.
- Yunus PA, Sengupta B (2016) E-Waste Indian Perspective and Recovery of Valuable Metals From E-Waste-A Review. *International Refereed Journal of Engineering and Science (IRJES)*. 5(4):70–80.
- Zhou D, Zhang L, Zhou J, Guo S (2004) Cellulose/chitin beads for adsorption of heavy metals in aqueous solution. Water Research. 38(11):2643–2650. DOI: 10.1016/j.watres.2004.03.026.





A Cradle to Grave Treatment Solution for Mine Waters

Malcolm Man, Ben Sparrow, Megan Low

Saltworks Technologies Inc.

13800 Steveston Highway Richmond, British Columbia, Canada V6W 1A8

Abstract

The global mining industry is seeking economical tailings treatment options. The paper introduces two step change technologies for cradle-to-grave mine waters treatment and zero liquid discharge (ZLD). ZLD is defined as only two plant outputs: (1) treated water meeting specification; (2) all contaminants reduced to a solid for final disposal. The innovative technologies that will be presented are a salt splitting electrodialysis – reverse osmosis hybrid and a non-metallic, low temperature (<90°C) crystallizer. The presented treatment solutions are applicable to treating any mine waters, such as tailings, runoff, and acid mine drainage. It provides an end-to-end treatment process with recovery of freshwater and final landfill disposal of the residuals.

Keywords: water treatment, tailings, runoff, acid rock drainage, acid mine drainage, ARD, AMD, softening, reverse osmosis, RO, zero liquid discharge, ZLD, electrodialysis, ion exchange, evaporator, crystallizer, desalination.

Introduction

An innovative mine water treatment system is presented that achieves extreme recoveries and a 45% total cost of ownership savings over conventional lime - soda ash - reverse osmosis (RO) – evaporator - crystallizer systems. The system is based around reverse osmosis (RO) hybridized with electrodialysis. The novel process and modified electrodialysis system changes water chemistry from highly scaling to non-scaling by use of selective ion exchange membranes. The water chemistry is changed from, for example, scaling calcium sulfate into non-scaling calcium chloride and sodium sulfate. This eliminates the need for expensive soda ash softening and associated hassles of sludge management. The ion exchange membrane system also concentrates the RO brine to extreme levels previously only attainable by thermally driven processes ($\approx 200,000$ mg/L TDS). The result is both lower operating costs and reducing the brine volume by two thirds using a membrane system. Importantly, this results in smaller capacity downstream evaporators lowering project costs. A case study and economic analysis are presented whereby savings of up to 45% in total cost of ownership are achieved. These savings result from a 25% reduction in capital

and 37% reduction in operating costs relative to above referenced conventional treatment train.

Scaling Management

Mine waters vary widely but most contain the following types of scalants:

- Low solubility metals, such as iron, nickel, cobalt, and aluminum, can create scaling compounds but can be readily precipitated by raising pH via caustic or lime addition;
- Low solubility anions, such as fluoride, phosphate, and sulfate, can combine with calcium to create scale and are not readily removed to reliable levels through precipitation, thus requiring further management;
- Divalent cations responsible for high hardness, primarily calcium and magnesium, as well as barium and strontium. Elevating pH will precipitate magnesium but has little effect on calcium, barium or strontium unless carbonate is present.

Conventional Treatment Process

Although mine water chemistry varies between sites, there are common treatment systems that are employed (Table 1).



Table 1 Mine water Conventional Treatment Processes

Process	Description
Lime (calcium hydroxide) softening	Removes magnesium hardness and heavy metals. Some calcium is removed but only calcium that is “associated” with carbonate.
Soda ash (sodium carbonate) softening	Removes calcium hardness. The cost of soda ash can account for over 20% of the treatment total cost of ownership (capital plus operating cost).
Ion exchange	Employs resins to adsorb calcium, reducing calcium levels to less than 50 mg/L. However, the resins must be regenerated with acid, resulting in high operating costs and acidic chemical waste that requires disposal.
Reverse Osmosis (RO)	The most dominant and widely practiced desalination technology for removal of total dissolved solids (TDS). RO is low cost but requires notable chemical pre-treatment for reliable operation on mine waters. When operated on scaling ion chemistry, RO is susceptible to fouling and does not concentrate well past 60,000 mg/L. This results in low recoveries and high brine volumes (or very frequent chemical cleans). Any RO unit can be hybridized with the innovative treatment system presented in this article.
Thermal brine management (evaporator, crystallizer, SaltMaker)	Evaporators concentrate the final brine waste and crystallizers produce solids. These systems are required for brine management and ZLD – and are the most expensive process equipment in the treatment train in terms of both capital and energy cost. The required capacity and energy used by these systems can be reduced if the recovery of upstream membrane system is increased. Membrane systems are often 5-10 times lower cost per unit volume processed and therefore it makes sense to maximize their recovery.

Salt Splitter-RO: High Recovery Mine Water Treatment System

A mine water treatment solution was developed by Saltworks Technologies that builds on the past work of Toshikatsu Hamano (1993) and Thomas Davis (2008). Hamano’s original concept in 1993 was a desalination process comprising of two electrodialysis stages that permanently changed low-solubility calcium sulfate into highly soluble calcium chloride and sodium sulfate. Solubility of these ion pairs is shown in Figure 1 (low solubility means greater scaling risk). Davis worked on a similar process in 2008 when he developed an electrodialysis metathesis

(EDM) process for feed waters comprised solely of calcium sulfate.

Saltworks’ Salt Splitting system expands on this work with several proprietary innovations – monovalent selective ion exchange membranes process, and controls – that enable an industrially applicable treatment plant. The technology is built around hybridizing two common desalination technologies: electrodialysis (ED) and reverse osmosis (RO). The advanced salt splitting electrodialysis unit acts as a turbocharger for the RO. It removes scaling limits by permanently changing water chemistry: divalent scaling low solubility ion pairs such as calcium sulfate are “split” into non-scaling high solubility ion pairs such as sodium sulfate and calcium chloride. The RO unit operates on an electrochemically softened feed, at a greater reliability level and lower pressure than conventionally possible. The combined ED-RO hybrid produces two highly soluble output brines with a combined average brine concentration of $\approx 210,000$ mg/L TDS. These can be sent to separate downstream processing stages for volume reduction or solidification. A simplified electrodialysis stack arrangement dia-

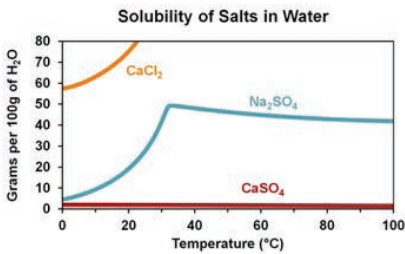


Figure 1 Solubility of CaSO_4 , Na_2SO_4 , and CaCl_2



gram, showing how the ions are selectively transferred into separate brine compartments to produce non-scaling Na_2SO_4 and CaCl_2 (Figure 2).

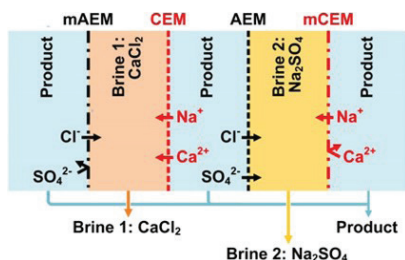


Figure 2 Salt Splitting Electrodialysis

The salt splitting ED-RO hybrid provides the following benefits:

- Recovery of the membrane system is three times that of chemically softened RO, while eliminating the need for expensive soda ash softening;
- Improved RO reliability and reduced operating costs from lower pressure requirements;
- The non-scaling, lower volume brines reduce the need for chemical softening of the evaporator inlet and allow downsizing of brine management assets;
- Less residual waste mass is produced since soda ash addition is eliminated and because useful by-products, such as sodium sulfate, can be recovered from the waste.

Shown below are modular salt splitting electrodialysis stack (Figure 3), containerized pi-

lot (Figure 4), RO (Figure 5), and Saltworks' proprietary highly selective membranes (Figure 6).

SaltMaker for Zero Liquid Discharge: Low Temperature Evaporator Crystallizer

The SaltMaker is a non-metallic, low temperature ($<90^\circ\text{C}$) crystallizer that achieves zero liquid discharge (ZLD) (Figure 4). It is a one-step treatment plant (no chemical softening) for a complete cradle-to-grave mine water treatment solution. The crystallizer enables ZLD through:

1. Multiple effect evaporation with low grade heat recycle reducing energy consumption. The SaltMaker can use a variety of thermal sources: steam, low grade waste heat, and gas or liquid fuel fired low pressure water heaters. It operates at atmospheric pressure and temperatures less than 90°C , employing humidification dehumidification air cycles that do not require a vacuum, pressure, or boiling water on any heat transfer surfaces.
2. Modular design based on engineered plastics and built-in redundancy. The SaltMaker is predominantly built from gel-coated, fibre-reinforced plastics – with low surface energy that provides resistance to corrosion and scale. The plant has redundant process sets for no single point of failure.
3. Advanced automation and self-cleaning. The plant's self-cleaning modes prevent irreversible scaling or fouling by regularly

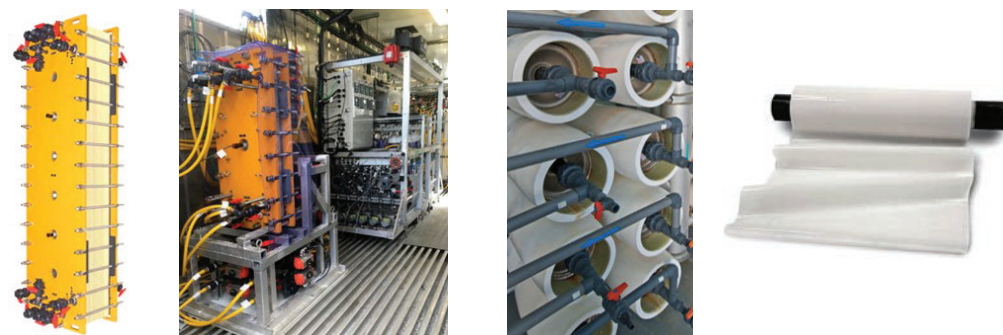


Figure 3 (left to right) Salt Splitting Stack, ED-RO pilot, RO elements, and salt splitting ion exchange membrane



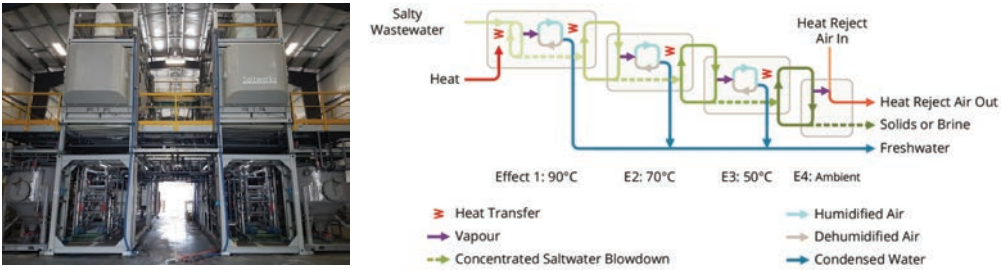


Figure 4 SaltMaker Crystallizer (left) and simplified process flow diagram (right)

- monitoring key performance metrics. It will then automatically trigger the appropriate level of cleaning, from ‘light rinse’ to ‘heavy scrub’. The SaltMaker uses distilled water as the cleaning fluid, which can be chemically augmented based on the type of scaling compounds and foulants in the brine. The wash solution is re-used multiple times before being fed back to the SaltMaker for treatment once it has been spent.; and
4. A simplified solids extraction and bagging process. A circulating slurry continuously forms and grows crystals in the SaltMaker. Solid salt is discharged to an automated bagging system which dewateres the solids to pass paint filter tests for landfill disposal.

Case Study

A fully automated salt splitting ED-RO pilot plant was operated on a coal plant wastewater, with the following objectives:

1. Confirm treated discharge water quality;
2. Confirm membrane system recovery, reliability, chemical and energy consumption; and

3. Develop economics for a full-scale system, including a downstream evaporator-crystallizer.

The treatment process is shown schematically in Figure 5 below. Pre-treatment for the reverse osmosis unit is required, such as multimedia filtration or ultrafiltration.

Detailed analytics for all streams are shown in Table 2 and compared to the discharge regulations.

The salt splitting ED-RO hybrid successfully treated the coal plant wastewater to meet the discharge regulations. The pilot plant operated continuously for 90 days. Freshwater recovery of 90% was achieved from the membrane system, with no soda ash softening. In comparison, chemically softened RO system projections showed a recovery of approximately 70%. Put another way, the ED-RO hybrid produced one third the brine reject volume or 67% less brine, requiring a 67% smaller evaporator system. The ED-RO hybrid generated non-scaling, high concentration, low volume brines. Most importantly, two non-scaling brines were produced in excess of 200,000 mg/L, which is brine con-

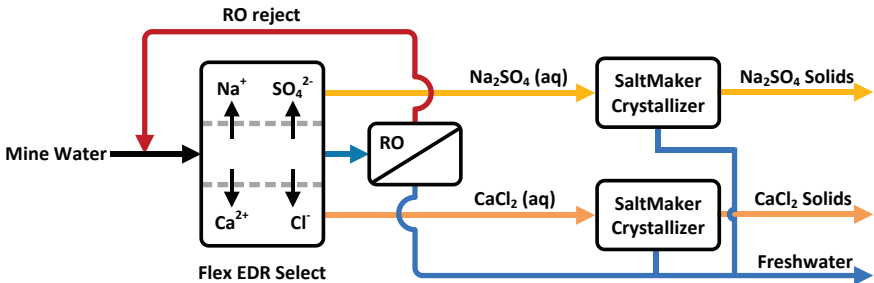


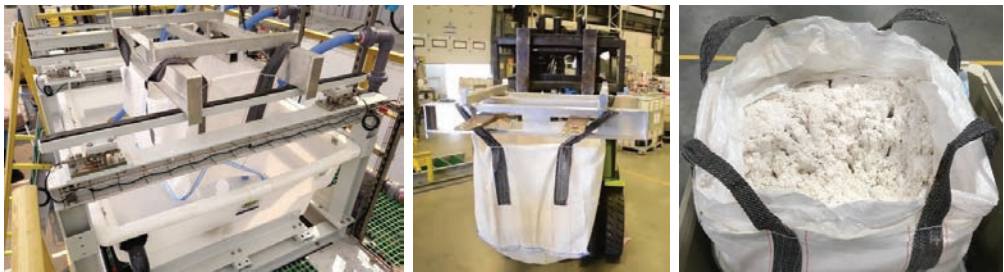
Figure 5 Salt splitting ED-RO-SaltMaker process



Table 2 Salt splitting ED-RO treatment of FGD wastewater: water chemistry results

Parameter (mg/L)	Coal Plant Wastewater	CaCl ₂ Brine	Na ₂ SO ₄ Brine	RO Permeate	Discharge Regulations
pH	7.02	6.98	6.70	6.52	6 - 9
TDS	19300	220700	209700	120	N/A
Aluminum	0.04	0.01	<0.01	<0.0001	0.05
Arsenic	0.45	3.06	0.85	<0.0001	0.005
Cadmium	0.11	0.02	<0.01	0.00010	0.000005
Calcium	3290	73230	768	6.0	N/A
Chloride	11050	140300	93100	23.2	150
Cobalt	0.00162	0.0187	0.0011	<0.00005	0.004
Fluoride	9.0	7.8	0.34	<0.05	0.4
Iron	0.11	0.02	<0.01	<0.01	0.35
Lead	<0.0002	<0.0002	<0.0002	<0.0002	0.003
Magnesium	1850	1580	17.4	2.20	N/A
Mercury	0.10	0.02	0.0002	<0.00001	0.00001
Selenium	0.28	0.10	4.90	<0.0005	0.002
Sodium	663	2400	77400	9.3	N/A
Sulfate	1945	352	36620	3.1	128
Zinc	1.52	0.26	<0.01	<0.0001	0.0075

ITALIC indicates meets Discharge Regulations. **BOLD** indicates does not meet Discharge Regulations.

**Figure 6** (left to right) automater bagging system, bag removed by forklift, and bag of solids

centration territory normally reserved for evaporators.

The high solubility, low volume salt splitting ED-RO brines can be treated with a low temperature crystallizer for additional freshwater and solids production. Figure 6 shows solids produced (10% moisture content that passes paint filter tests) by SaltMaker crystallizer for true ZLD.

Economics

The salt splitting ED-RO SaltMaker has an overall 45% total cost of ownership savings over a conventional chemical softening RO-evaporator-crystallizer treatment train for a 1090 m³/day plant. This is due to savings of 25% in capital cost on the process equip-

ment and savings of 37% by eliminating soda ash softening. An economic analysis is summarized in Table 3 based on the water chemistry shown in Table 2. It assumes that ZLD is required. Capital costs were based on US market prices for chemical softeners, industrial reverse osmosis, and evaporator-crystallizers. Only process equipment costs were accounted for in both options. Building and installation costs were not accounted for and assumed to be the same for both options. Capital costs were amortized over 10 years at an 8% discount rate. Plant availability was assumed to be 95%. Power costs were assumed to be USD\$0.065/kWh and thermal energy costs at USD\$3/MMBTU.



Table 3 Economic Analysis Summary

Performance Summary	Conventional: Soda-RO-Evap-Crys	Advanced: SS-RO-SaltMaker
Plant Inlet Capacity (m3/day)	1,090	1,090
Plant Inlet Capacity (tonnes/day)	1,123	1,123
Plant Inlet Total Dissolved Solids (TDS)	19,062	19,062
Membrane System Recovery	70%	90%
Size of Evaporation System (tonnes/day inlet)*	337	125
Size of Evaporation System (m3/day inlet)	327	104
Mass of Solids Produced (tonnes/day)	25	21
Performance Summary	Conventional: Soda-RO-Evap-Crys	Advanced: SS-RO-SaltMaker
Capital Costs		
Pre-Treatment & Membrane System	\$ 2,788,634	\$ 4,113,636
Evaporation-Crystallization System	\$ 6,200,000	\$ 2,650,000
Installation (assumed equal for both)	Not included	Not included
Sub-Total Capital Cost	\$ 8,988,634	\$ 6,763,636
Capital Cost (\$/m3)	\$ 3.68	\$ 2.67
Energy Consumption Analysis		
Power: Pre-Treat & Membrane System (kW_e)	178	429
Power: Thermal System(kW_e)	501	60.4
Power: Total	679	490
Thermal Power as Low Pressure Steam (MW_t)	0.3	0.8
Thermal Power as Low Pressure Steam (tonnes/day)**	11.7	27.0
Operating Costs		
Labor (assumed equal for both)	Not included	Not included
Soda Ash (\$/yr)	\$ 1,125,857	\$ -
Soda Ash (\$/m3 inlet)	\$ 2.98	\$ -
Sodium Chloride (\$/yr)	\$ -	\$ 14,740
Sodium Chloride (\$/m3 inlet)	\$ -	\$ 0.04
Chemicals: Other (\$/yr)	\$ 41,799	\$ 275,192
Chemicals: Other (\$/m3)	\$ 0.11	\$ 0.73
Energy: Electrical (\$/yr)	\$ 386,013	\$ 318,152
Energy: Electrical (\$/m3 inlet)	\$ 1.02	\$ 0.84
Energy: Thermal (\$/yr)	\$ 110,753	\$ 76,737
Energy: Thermal (\$/m3 inlet)	\$ 0.29	\$ 0.20
Sub-Total Operating Cost (\$/yr)	\$ 1,664,422	\$ 670,082
Sub-Total Operating Cost (\$/m3)	\$ 4.40	\$ 1.77
Total Cost (Less Install & Labor) (\$/m3)	\$ 8.09	\$ 4.44
Savings		
CapEx Savings From Increased Membrane System Recovery (%)		25%
OpEx Savings From Eliminating Soda Ash (%)		37%
Total Cost of Ownership Savings (%)		45%

*Density of the brine adjusted inlet volume. Salt Splitter ED-RO brines have high density with specific gravity of ~1.2

** Advanced option assumes a multiple effect thermally driven crystalizer driven with 95 deg C heat (SaltMaker)

Conclusion

Changing regulations are driving both innovation and the uptake of mine water treatment solutions. Treatment approaches vary widely depending on the mine site and its particular water chemistry, flow rate, and discharge regulations. However, to optimize treatment economics, there are steps a mine or water treatment plant designer can take that are consistent across all facilities:

- Eliminate soda ash softening; and
- Increase membrane system recovery to

reduce size of thermal evaporation technologies.

The case study and economic comparison presented demonstrate the salt splitting ED-RO hybrid's ability to achieve these objectives.

References

- Davis, T.A. (2008). U.S. Patent No. 7,459,088 B2. Alexandria, VA: U.S. Patent and Trademark Office.
- Hamano, T. (1993). U.S. Patent No. 5,376,250. Alexandria, VA: U.S. Patent and Trademark Office.



Reclamation, Recovery and the Synthesis of Valuable Minerals from Acid Mine Drainage Treatment Process

Vhahangwele Masindi^{1&2}, Rhulani Shingwenyana¹

¹*Council for Scientific and Industrial Research (CSIR), Built Environment (BE), Hydraulic Infrastructure Engineering (HIE), P.O Box 395, Pretoria, 0001, South Africa*

²*Department of Environmental Sciences, School of Agriculture and Environmental Sciences, University of South Africa (UNISA), P. O. Box 392, Florida, 1710, South Africa*

Abstract

In this pilot study, the treatment of acid mine drainage (AMD) using an integrated approach was evaluated. The developed approach uses an integration of pre-treated magnesite, lime, soda ash, and Reverse Osmosis (RO) system to produce valuable minerals. AMD and product water were mixed with magnesite, lime, soda at 0.7 g:100 mL, 0.7 g:100 mL and 0.5 g:100 mL S/L ratios respectively. The product water was determined to surpass the South African National Standards (SANS 241) water quality specifications for drinking water. Recovered minerals include Fe-based minerals, gypsum and limestone. The resultant minerals were drinking water, Fe-based minerals (75% purity), gypsum (75% purity) and calcium carbonate (100% purity). Selling of the recovered minerals will make this technology feasible and more economically viable since the returns will aid in off-set the running cost of the treatment process.

Keywords: Acid mine drainage, treatment, drinking water, minerals recovery, minerals synthesis

Introduction

Pollution of surface and subsurface water resources by Acid Mine Drainage (AMD) emanating from Coal and Gold mine activities has rendered the environment unfit to foster life and render its intrinsic values. This is attributed to the fact that AMD contains potentially toxic and hazardous chemical components that originate from the weathering of host rocks. The embedding seams and lithologies in coal and gold mining area contain sulphide bearing minerals that when they get into contact with water and oxygen lead to the formation of a very acidic and metals-rich drainage. The acidic nature of AMD further degrades the surrounding geology by leaching out heavy metals in the surrounding aqueous media. AMD mainly contain Fe, Al, Mn, S as sulphate and traces of other chemical components (Masindi et al. 2018).

In an attempt to protect the environment, governments and environmental activists are advocating for proper management of AMD prior discharge to different receiving environments. To date, progress has been made

but mining houses are still in a quest for effective, efficient and sustainable approaches in treating acid mine drainage (AMD) and attain value from the treatment process since most of the treatment technologies pose secondary pollution due to sludge generation (Masindi 2016). Active and passive treatment approaches have been widely used in the treatment of AMD. Those approaches use different chemical attenuating mechanisms and they include precipitation, adsorption, filtration, bio-sorption, ion-exchange, phytoremediation, desalination, or an integration approach (Simate and Ndlovu 2014).

The present study was therefore designed with the aim of treating acid mine drainage and attain valuable minerals that has commercial value. It involves the use of a number of treatment processes that relies on calcined magnesite, lime, soda ash, and RO in a stage-wise fashion. The first stage uses calcined magnesite to recover Fe-based minerals and partially sulphate as gypsum, the 2nd stage entails the use of lime to synthesize gypsum, and the 3rd stage entails the use of lime to remove



residual Ca and Mg to synthesize limestone. The product minerals have a number of industrial applications hence demonstration a room for products valorisation. The product water is soft due to removal of Ca and Mg and it is safer for RO system purification. The water will be purified and Na-rich brine will be taken to a number of emerging processes such as membrane distillation, eutectic freeze or cooling systems for further minerals acquisition.

Materials and Methods

Treatment of field AMD at optimized conditions

The schematic presentation of acid mine drainage treatment process is depicted in Figure 1.

As shown in Figure 1, calcined cryptocrystalline magnesite, lime and soda ash (MASRO process) were utilised to recover valuable minerals that have commercial value, and to produce water that is fit for myriads of defined uses such as drinking, irrigation, and industrial purposes. The minerals recovery, synthesis, and water reclamation process used authentic AMD from coal mining processes. In the first reactor, a sequential and fractional precipitation method was executed for precipitation of metals as hydroxides. Masindi et al. (2016) reported that the

interaction of magnesite with AMD lead to the precipitation of metals as hydroxides (solids). The formation of complexes, precipitates and other products was investigated in each stage of the process. Stage two focuses on gypsum synthesis from lime additions, stage three focuses on calcium carbonate synthesis from soda ash addition. The last stage is the RO system which further purifies the water to drinking standard.

Neutralization of AMD and the recovery of Fe-based minerals

Magnesite was calcined at 900°C. Calcined cryptocrystalline magnesite was used to treat authentic AMD samples at 60 minutes of equilibration, 0.7 g:100 mL S/L ratios, 650 rpm agitation speed and $\leq 32 \mu\text{m}$ particle size of calcined cryptocrystalline magnesite, as optimized.

Synthesis of gypsum

For synthesis of gypsum ($\text{CaSO}_4 \cdot 2\text{H}_2\text{O}$), an industrial grade lime was used, where alkaline reagent was added to magnesite-treated water which is rich in magnesium sulphate as a complex. 0.7 g:100 mL of lime per treated water was used as optimised. The mixture was then equilibrated at 650 rpm shaking speed for 120 mins using an overhead stirrer. The resultant residues and water were taken for analysis.

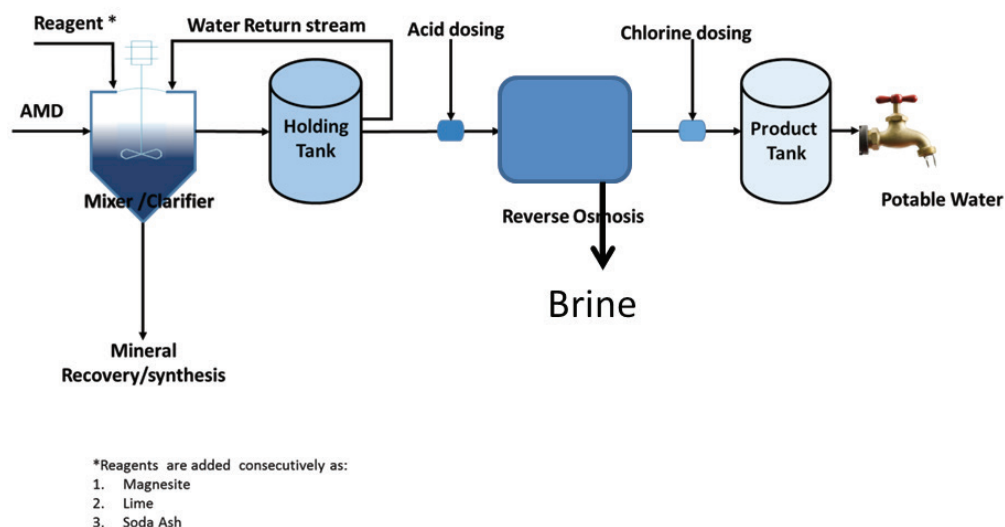


Figure 1: Schematic presentation of acid mine drainage treatment process.



Synthesis of calcium carbonate

Synthesis of calcium carbonate (CaCO_3) synthesis, an industrial grade soda ash was used, where the alkaline reagent was added into lime-treated water and then mixed for a specified time interval. 0.5 g:100 mL of soda ash per treated water was used as optimised. The mixture was then equilibrated at 650 rpm shaking speed for 30 mins using an overhead stirrer.

Reverse osmosis purification

In this study, FILMTEC BW30-4040 is the industry standard for reliable operation and production of the highest quality water membrane was used.

Characterisation of material

HANNA (HI 98194) portable pH/EC/DO multi-parameter probe was used to determine pH, Total Dissolved Solids (TDS) and Electrical Conductivity (EC). Inductively Coupled Plasma – Mass Spectrometry (ICP-MS) was used to analyse aqueous samples. The National Institute of Standards and

Technology (NIST) water standards were of use in monitoring the accuracy of analysis. X-ray Diffraction (XRD) was used to determine the mineralogy of synthesised materials. An Auriga Cobra FIB FESEM instrument high resolution scanning electron microscope (HR-SEM) with the precision milling and nanofabrication abilities of high resolution focused ion beam (FIB) at an accelerating voltage of 3 KeV was used to determine morphological properties (Model: Sigma VP FE-SEM with Oxford EDS Sputtering System Make: Carl Zeiss, Supplier: Carl Zeiss, USA).

Results and discussions

Morphology of synthesized materials

The morphology of Fe-based mineral, gypsum and calcium carbonate are shown in Figure 2.

As shown in Figure 2A, the recovered Fe-based mineral has spherical structures that are homogenous hence indicating that the recovered material is uniform. Figure 2B, shows the rod-like structures for the synthesized gypsum. This is consistent to what have been

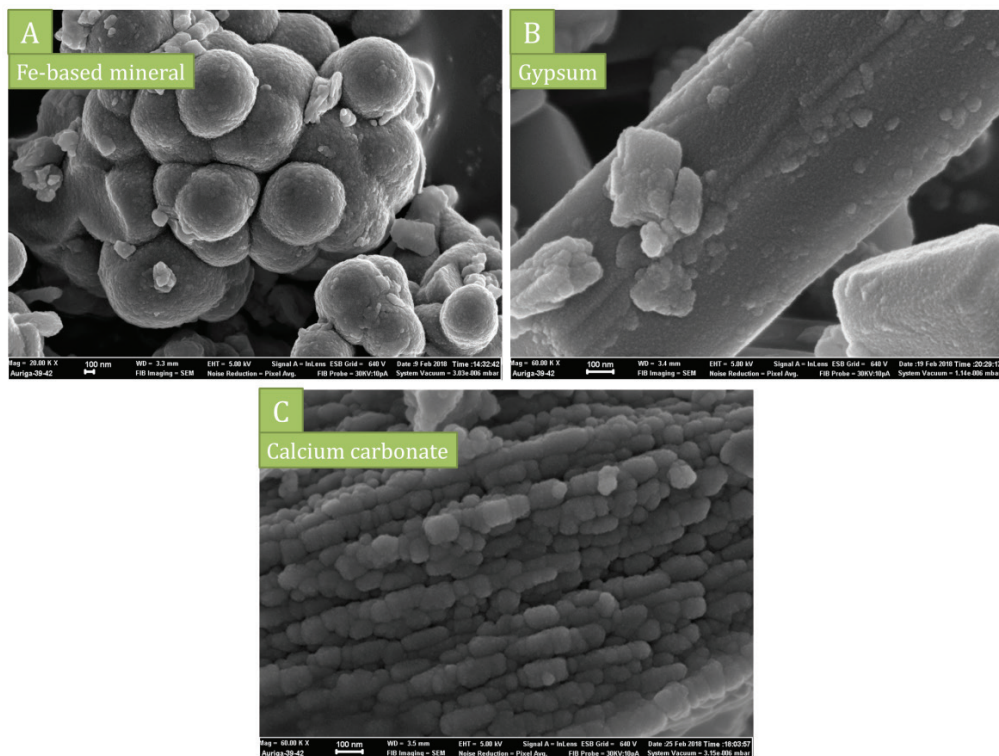


Figure 2: Morphology of Fe-based mineral (A), gypsum (B), and limestone (C)



reported in literature (Masindi et al. 2018). The synthesized calcium carbonate (Figure 2C) shows the presence of spherical and nodular linked structures that are consistent hence depicting that the synthesized material is uniform.

Mineralogical composition of synthesized materials

The mineralogical properties of Fe-based mineral, gypsum and calcium carbonate are shown in Figure 3.

As shown in Figure 3, Fe-based mineral was characterised of hematite, jarosite, magnetite, and hexahydrate. Quartz was observed as an impurity. Gypsum was observed to be characterised of bassanite, brucite and gypsum. Quartz and montmorillonite were also observed to be present. The presence of mag-

nesium is attributed to lime addition and an increase in pH. The limestone was observed to contain the calcite, brucite, quartz and hydro-magnesite. The obtained results are in agreement with the water quality results.

Water quality

The product water qualities of acid mine drainage treated using pre-treated magnesite, lime, soda ash, and reverse osmosis are shown in Table 1.

As shown in Table 1, the initial pH of acid mine drainage was observed to be 2.4 and it was observed to increase to 10, 11, 10 and 7 after contacting the pre-treated magnesite, lime, soda ash, and RO purification respectively. The major component of this mine water was observed to be Fe and Sulphate hence indicating that this mine water origi-

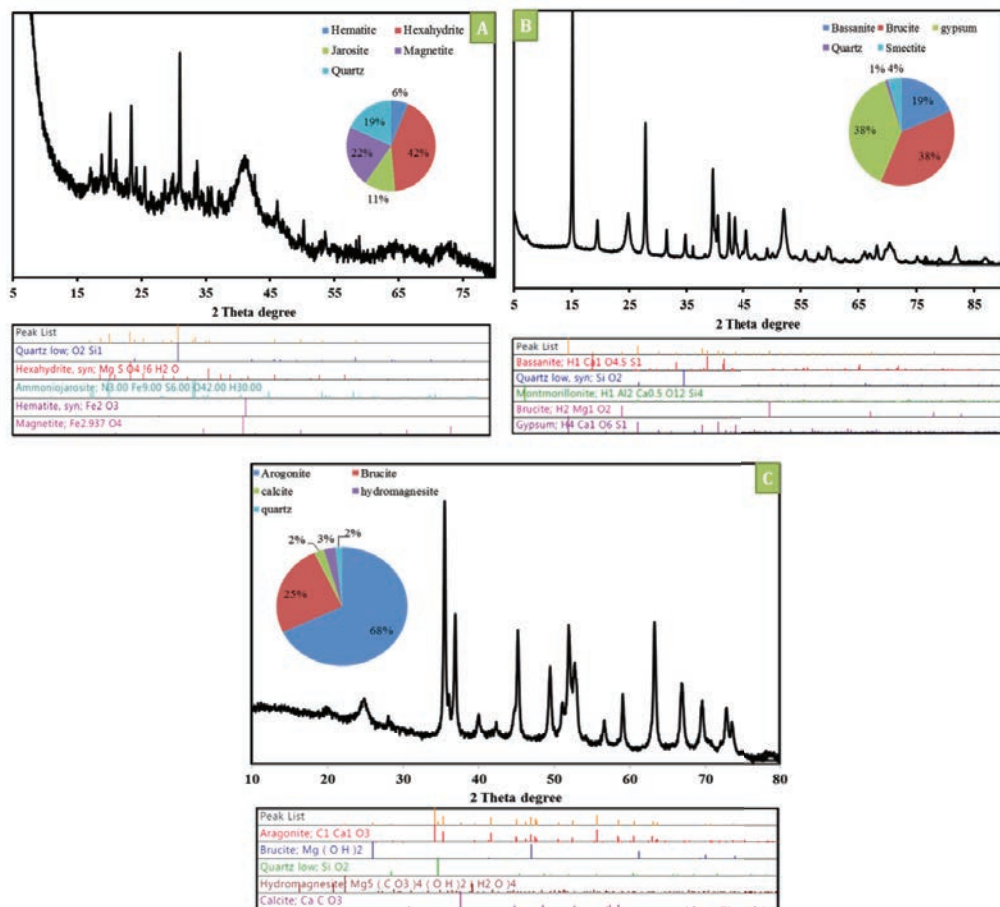


Figure 3: Mineralogical properties of Fe-based minerals (A), gypsum (B) and calcium carbonate (C).



Table 1: Chemical compositions of AMD before and after treatment

Parameters	Unit	SANS 241	Raw AMD	Magnesite	Lime	Soda ash	Permeate	Brine
Aluminium	mg/L	0.03	70	0.03	0.01	0	0	0
Ammonia	mg/L	1.5	7.7	8.2	6.3	6.5	0.8	12
Barium	mg/L	0.7	0.1	0.1	0.1	0.4	0.1	0.3
Cadmium	mg/L	0.03	0.04	0.02	0.02	0.02	0.02	0.02
Chloride	mg/L	300	3.8	2.1	6.3	6.3	32	28
Chlorine	mg/L	5	1.1	0.25	0.05	0.05	0.05	0.04
Chromium	mg/L	0.05	0.04	0.02	0.02	0.02	0.02	0.02
Colour	mg/L	15	600	5	7	<5.0	6	6
Copper	mg/L	2	0.5	0.04	0.04	0.04	0.04	0.04
EC	mS/cm	170	10	19	4	4	0.1	3
TDS	Mg/L	1200	5000	9900	2100	3900	300	3500
Iron	mg/L	2	1000	2	0.02	0.02	0.02	0.02
Lead	mg/L	0.01	0.02	0.01	0.01	0.01	0.01	0.01
Manganese	mg/L	0.4	30	0.5	0.5	0.2	0.01	0.2
Mercury	mg/L	0.06	0.2	0.02	0.02	0.02	0.02	0.02
Nickel	mg/L	0.07	1	0.04	0.04	0.04	0.04	0.04
pH	pH	5 - 9,5	2.38	10.5	11	10	7	7.5
Sodium	mg/L	<200	91	110	103	1624	100	2803
Sulphate	mg/L	<500	11681	11000	621	71	8	53
Turbidity	NTU	<5	43	66	110	75	0.62	0.88
Uranium	mg/L	0.03	0.01	0.008	0.08	0.80	0.08	0.80
Zinc as Zn	mg/L	5	2	0.05	0.05	0.05	0.05	0.05

nates from the weathering of FeS_2 . Notable components of Al and Mn were also observed to be presence hence showing that these are the associated minerals. Traces of other toxic chemical components were observed to be present in significant concentration in relation to their toxicity. After contacting the pre-treated magnesite the pH had increase and significant amount of metals were removed except for sulphate. Addition of lime led to an increased removal of residual sulphate and metals. The water was much cleaner and rich in Ca ions. Soda ash was added to remove the Ca and Mg hence forming the carbonates. The water was much softer and ready to pass through an RO. The water was purified with an RO system to SANS 241 water quality specifications. This is evident because the Na ions were observed to be present in the brine stream. The water is safe for human

consumption. Brine stream is going to be further treated using membrane distillation in order to attain a Zero-Liquid-Discharge (ZLD) system.

Conclusions

This pilot study successfully reclaimed drinking water and attained valuable minerals from acid mine drainage treatment process. A 3.5 KL clarifier with a return stream was used for the recovery of valuable minerals and the purification of drinking water. The plant managed to reclaim portable water that complies with SANS 241 water quality specifications. The recovered products showed good industrial quality. These materials have a number of industrial, agricultural and metallurgical applications. More so, this pilot study proved to be successful, effective and economically viable. Furthermore, it was also proven that



there is feasibility of AMD valorisation. This will aid in an endeavour to minimise the environmental footprints by protecting the environment and its precious resources. Future work involves detailed costing

Acknowledgements

The author would wish to express their sincere gratitude to the Council for Scientific and Industrial research (CSIR) for supporting this project.

References

- Masindi V (2016) A novel technology for neutralizing acidity and attenuating toxic chemical species from acid mine drainage using cryptocrystalline magnesite tailings. *Journal of Water Process Engineering* 10:67-77, doi:10.1016/j.jwpe.2016.02.002
- Masindi V, Gitari MW, Tutu H, De Beer M (2016) Fate of inorganic contaminants post treatment of acid mine drainage by cryptocrystalline magnesite: Complimenting experimental results with a geochemical model. *Journal of Environmental Chemical Engineering* 4:4846-4856, doi:10.1016/j.jece.2016.03.020
- Masindi V, Ndiritu JG, Maree JP (2018) Fractional and step-wise recovery of chemical species from acid mine drainage using calcined cryptocrystalline magnesite nano-sheets: An experimental and geochemical modelling approach. *Journal of Environmental Chemical Engineering* 6:1634-1650, doi:https://doi.org/10.1016/j.jece.2018.02.005
- Simate GS, Ndlovu S (2014) Acid mine drainage: Challenges and opportunities. *Journal of Environmental Chemical Engineering* 2:1785-1803, doi:http://doi.org/10.1016/j.jece.2014.07.021





High Resolution Estimates of Tailings Facility Evaporation Using Landsat Data

Jason Keller¹, Jan Hendrickx², Michael Milczarek³, Frederick Partey⁴, Michael Geddis⁵

¹*GeoSystems Analysis, Inc., Hood River, OR, USA*

²*SoilHydrology Associates, LLC*

³*GeoSystems Analysis, Inc., Tucson, AZ, USA*

⁴*Robinson Nevada Mining Company*

⁵*KGHM*

Abstract

A three-temperature (3T) energy balance model was developed to predict monthly distributed actual evaporation (AE) from a large TSF in Nevada, USA for the period of 1996 through 2015. The 3T energy balance model uses Landsat surface reflectance and temperature data to predict the AE as a relative fraction of local weather station estimated potential evaporation on 30 m centers (pixels). Additionally, Landsat reflectance data were used to develop a site specific algorithm to estimate the TSF footprint on six month time intervals. Estimated monthly AE ranged from over 150 mm/month during the summer months, to less than 20 mm/day during the winter months. Estimated TSF evaporation increased over time from an annual maximum of 60 l/s to greater than 350 l/s due to the increase in the evaporative surface of the TSF. Landsat based estimates of the TSF surface area were in agreement with storage curve tailings area estimates, and also provided a high resolution estimate of the tailings footprint over time.

Keywords: actual evaporation, Landsat, model, water balance

Introduction

Evaporation is often the largest unknown component of a tailings storage facility (TSF) water budget, which can result in significant errors about the rate and sources of tailings seepage and other losses. Potential evaporation (PE) can be estimated using weather station measurements; however, PE assumes a continuous water supply and cannot account for the variable nature of TSF operations. Actual evaporation (AE) rates depend on factors such as: climate; tailings moisture content, texture and water holding capacity; and solution salinity. Most TSFs have a large surface area which allows spatial and temporal estimates of AE using satellite data and an energy balance energy model. Specifically, biweekly Landsat datasets can be used to estimate AE from land surfaces with 30 × 30 m resolution. Satellite based energy balance models have been previously used to estimate evapotranspiration from irrigated agricultural and riparian habitat areas (i.e. METRIC and SEBAL, see Allen et al, 2011). However, these model applications are generally labor intensive and

costly. Landsat data also can be used to determine the growth of the TSF over time.

A three-temperature (3T) energy balance model was developed to predict monthly AE from a large TSF in Nevada, USA for the period of 1996 (start of operations) through 2015. The site is located in a semi-arid climate with an average December temperature (coldest month) of -4 °C and an average July temperature (warmest month) of 20 °C. The tailings embankment is constructed using centerline raise methods with cyclone underflow sand deposition. Cyclone deposition typically occurs during the summer (May to September) with whole tailings deposition from the perimeter of the facility from October to April.

The 3T energy balance model predicts the AE as a relative fraction of nearby weather station estimated PE, using Landsat surface reflectance and temperature data on 30 m centers (pixels). The local weather station calculated PE is then used to predict the daily changes in AE at each pixel during the periods between each Landsat data event. Additionally, Landsat reflectance data were used to



develop a site specific algorithm to estimate the TSF footprint every six months.

Methods

AE estimates were based on calculations using a 3T model based on the physics of the full energy balance (Qiu and Zhao, 2010) as determined from local weather and data from Landsat satellite imagery. A total of 157 images, evenly distributed over the period 1996-2015, were selected for processing and input into the 3T model. A summary of the methodology of the energy balance approach used is provided below.

At the TSF where tailings exist under dry and wet conditions, evaporation can be estimated by:

$$LE = R_n - G - H \quad (1)$$

where LE is the latent heat flux in watts per square meter (W/m^2), R_n is the net radiation (W/m^2), G is the soil heat flux (W/m^2), and H is the sensible heat flux (W/m^2).

The R_n at satellite overpass is the sum of the net short wave radiation (R_{ns}) and the net longwave radiation (R_{nl}).

$$R_n = R_{ns} + R_{nl} \quad (2)$$

$$R_{ns} = (1 - \alpha) R_s \quad (3)$$

where α is the albedo (unitless) that varies for most pixels from 0.18 to 0.30 and R_s is the incoming solar radiation (W/m^2). The net longwave radiation (R_{nl}) equals:

$$R_{nl} = R_{lin} - R_{lout} - (1 - e_o) R_{lout} \quad (4)$$

$$R_{lin} = e_a \sigma T_{swet}^4 = 0.85 (-\ln \tau_{sw})^{0.09} \sigma T_{swet}^4 \quad (5)$$

$$R_{lout} = e_o \sigma T_s^4 \quad (6)$$

where R_{lin} and R_{lout} are the incoming and outgoing longwave radiation, respectively (W/m^2), e_o is the broadband surface emissivity (unitless), e_a is the effective atmospheric emissivity (unitless), σ is the Stefan-Boltzmann constant ($5.67 \times 10^{-8} W/m^2/K^4$), τ_{sw} is the broadband atmospheric transmissivity for short-wave radiation (unitless), T_s is the surface temperature in Kelvin (K) as calculated from the thermal band, T_{swet} is the surface temperature of the coldest non-

ded pixels. Qiu and Zhao (2010) assume an average value of $e_o = 0.925$ and use the simple function $e_a = 0.92 \times 10^{-5} T_a^2$ for the estimation of the emissivity values.

The G (W/m^2) was estimated using an empirical equation for soils with no or little vegetation (leaf area index less than 0.5) (Allen et al., 2011).

$$G = R_n \times \left\{ 1.80 \frac{T_s - 273.15}{R_n} + 0.084 \right\} \quad (7)$$

where T_s is the surface temperature (K).

The H (W/m^2) was estimated from:

$$H = (R_{nd} - G_d) \frac{T_s - T_{swet}}{T_{sd} - T_{swet}} \quad (8)$$

where R_{nd} is the net radiation of a reference dry soil surface without evaporation (W/m^2), G_d is the soil heat flux in dry soil (W/m^2), T_{sd} is the temperature of a reference dry soil surface (K).

The instantaneous evaporation (E_{inst}) in millimeters per hour (mm/hr) at the time of the satellite overpass is calculated as:

$$E_{inst} = 3600 \frac{LE}{L} \quad (9)$$

where 3600 is the time conversion from seconds to hours, and L is the latent heat of vaporization (at $20^\circ C$ about 2.45×10^6 Joules per kilogram (J/kg)).

E_{inst} was extrapolated to daily evaporation values using the hourly standardized reference evapotranspiration for a short crop (ETo_{inst}) (ASCE-EWRI, 2005) to calculate the Reference ET Fraction ($EToF$), defined as:

$$EToF = \frac{E_{inst}}{ETo_{inst}} \quad (10)$$

$EToF$ was then applied to the daily reference evapotranspiration (ETo_{daily}) to calculate daily evaporation (E_{daily}):

$$E_{daily} = EToF \times ETo_{daily} \quad (11)$$

where ETo_{daily} is the daily reference ETo in millimeters per day (mm/day).

ETo_{daily} and ETo_{inst} were calculated from a series of consistent hourly meteorological measurements of air temperature, air relative humidity, wind speed, and incoming solar radiation available from a nearby weather



station. The weather station environment is similar to the TSF, located approximately 40 km southeast of the TSF and at a similar elevation.

The Landsat data processing using the 3T model produced 30 m by 30 m areal predictions of the actual monthly evaporation for the period from 1996-2015. The aerially distributed monthly evaporation rates were then summarized to yield monthly evaporation volumes from the TSF.

The boundary of the TSF between 1996 and 2015 was estimated on an approximate six month time interval using Landsat reflectance data and application of a site-specific processing algorithm. The boundary between the TSF embankment and impoundment area was based on the location of the cyclone header pipe visible in aerial photographs. Estimated TSF areas were validated against aerial photographs and area estimates from the TSF annual monitoring report.

Results

The estimated monthly average AE depths and rates from 1996 through 2015 are pro-

vided in Figure 1 and Figure 2, respectively. To delineate AE from the actively wetted embankment areas, predicted AE was separated into impoundment and embankment areas. Examples of the predicted growth of the TSF and the spatially distributed AE in the winter and summer of 2005 and 2015 are provided in Figure 3.

Mining operations were suspended between July 1999 and September 2004, resulting in decreased AE due to water no longer being directed onto the TSF surface as part of the tailings slurry (Figure 1 and 2). Tailings deposition resumed October 2004 with the restart of mining and estimated AE increased (Figure 1 and 2).

Estimated monthly impoundment AE rates were in excess of 150 mm/month during the summer months when solar energy and evaporative demand is at its peak, to less than 20 mm/month during the winter months when evaporative demand is at its minimum (Figure 1). Due to the increase in the evaporative surface of the TSF, estimated TSF impoundment AE volume rates increased over time from an annual maximum of 60 l/s in

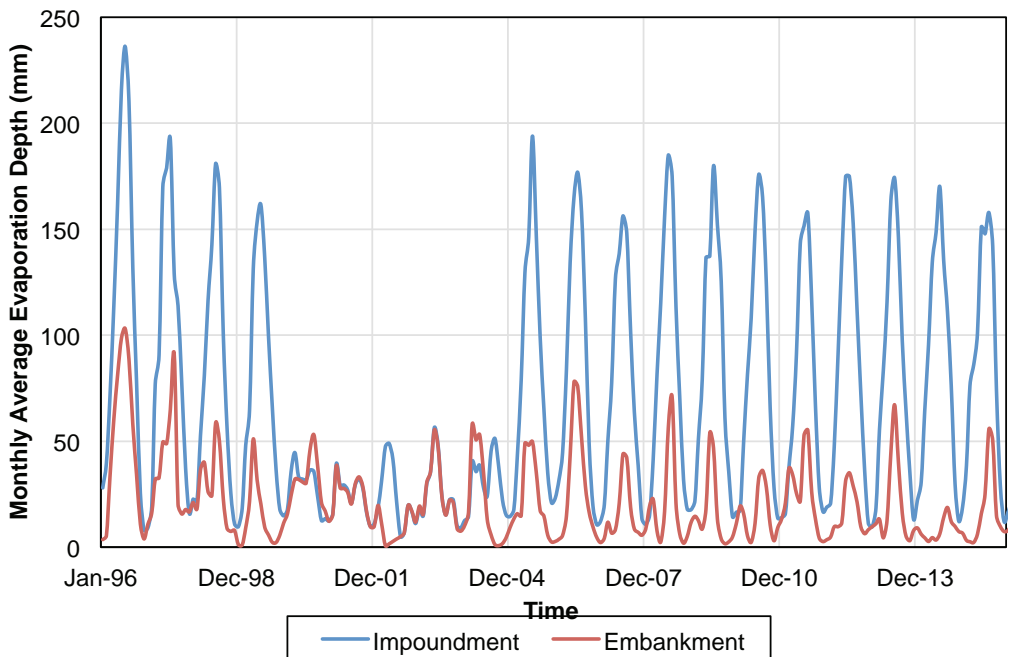


Figure 1 Estimated monthly evaporation depth



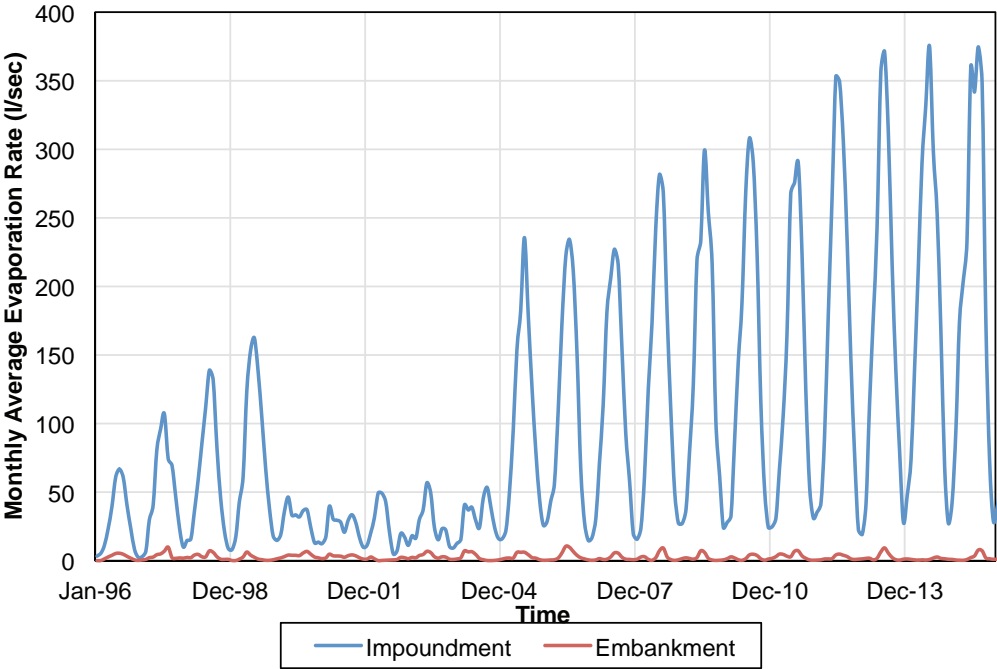


Figure 2 Estimated monthly evaporation rate

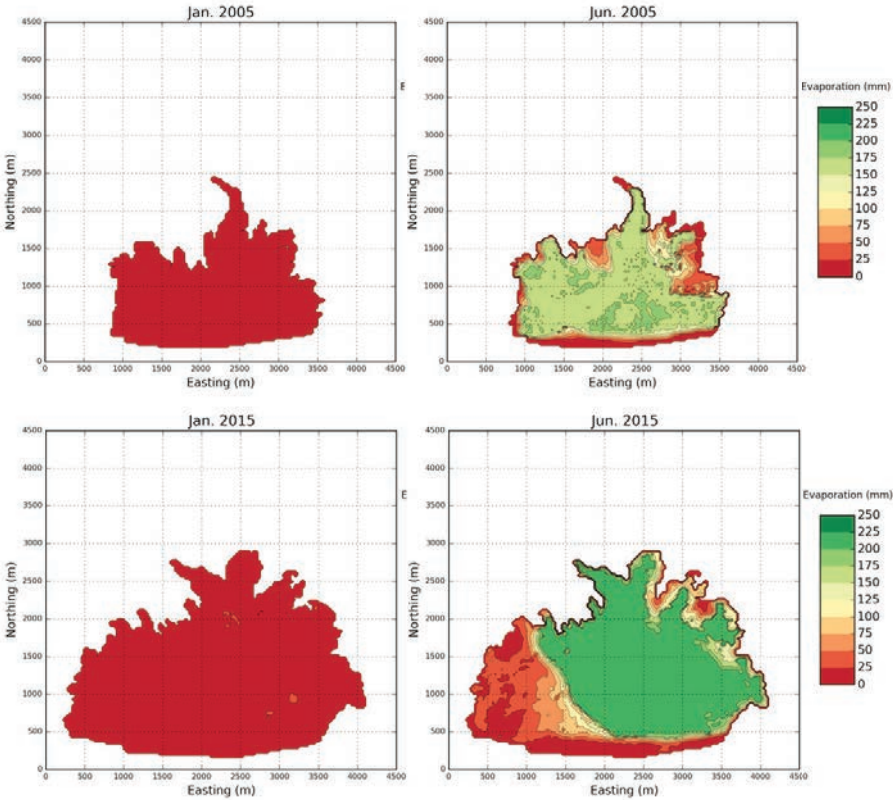


Figure 3 Example distributed evaporation from the TSF



1996 to 350 l/s or greater after 2012 (Figure 2, Figure 3).

Greater AE depths were estimated for the impoundment than the embankment due to the higher moisture retaining characteristics of the finer grained impoundment tailings and presence of wet/ponded conditions in the decant pond area (Figure 1 through 3). Additionally, water was added to the embankment only during the summer cyclone period. The greater impoundment AE depth and surface area compared to the embankment resulted in considerably greater estimated AE rates from the impoundment (Figure 2).

TSF areas estimated from Landsat reflectance data were also used to predict the tailings depth distribution (Figure 4). In ad-

dition, the biweekly AE data allowed us to understand the progression of the tailing placement, such that tailing material estimates (i.e. underflow, overflow, mixed and slime tailings) could be made. These data were then used to develop a distributed seepage model based on tailing material properties and a predicted water balance using site specific data and the AE model. To validate the Landsat TSF area estimates, they were compared to mine annual report storage curve estimates and showed good agreement (Figure 5). The TSF had a rapid growth progression early-on during operations between 1996 and 1999 as the embankment grew and the basin was filled in with tailings.

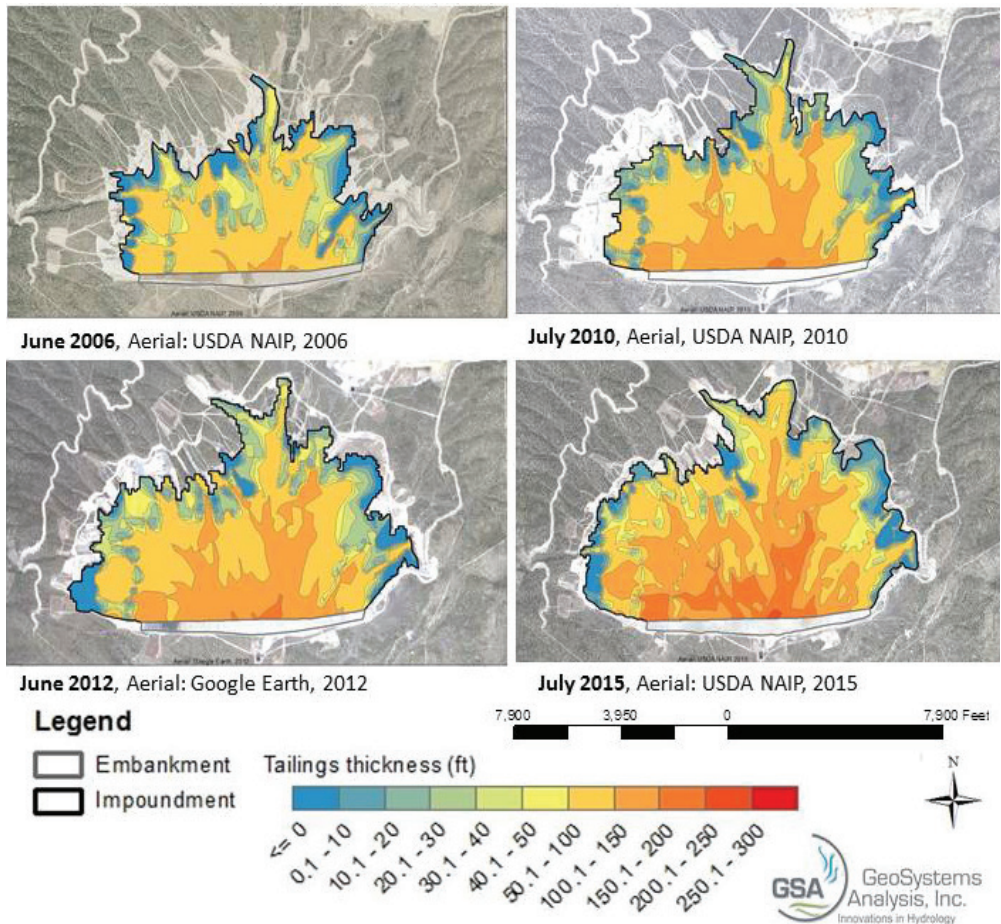


Figure 4 Estimated Tailings Depth Distribution



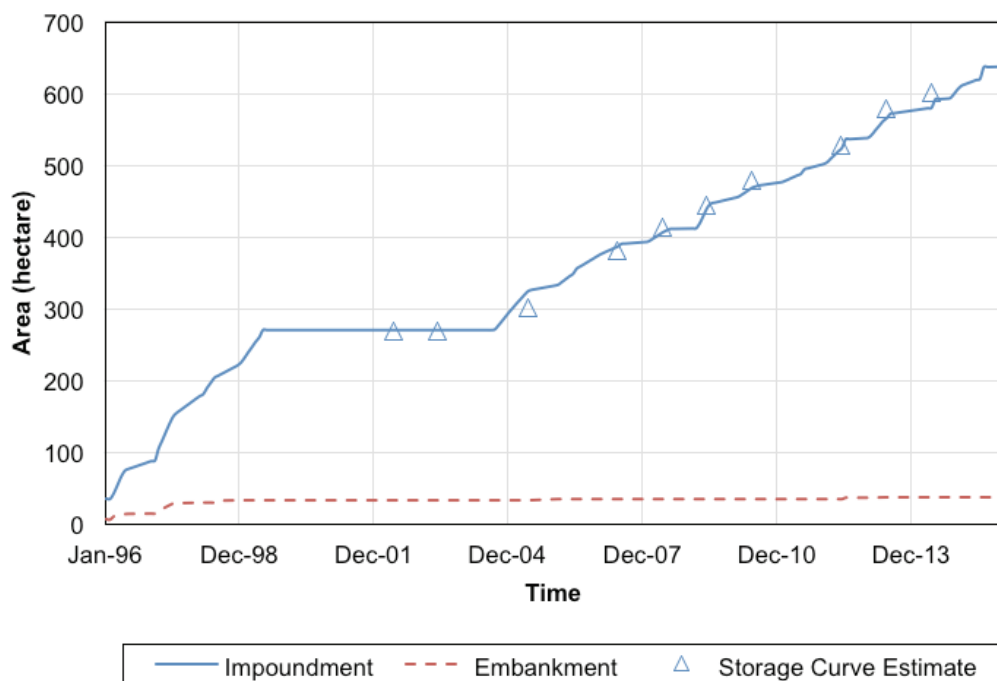


Figure 5 Estimated TSF embankment and impoundment areas

Conclusions

The 3T model provides a cost-effective and accurate method to calculate high resolution spatial and temporal estimates of TSF AE, and it also captures seasonal changes in AE and surface ponding. Estimated monthly AE ranged from over 150 mm/month during the summer months, to less than 20 mm/day during the winter months. Estimated TSF evaporation increased over time from an annual maximum of 60 l/s to greater than 350 l/s due to the increase in the evaporative surface of the TSF. Landsat based 3T model estimates of the TSF surface area were in good agreement with storage curve tailings area estimates, and also provided a high resolution estimate of the tailings footprint distribution over time. Additional benefits to the method include the ability to predict tailings depth and the progression of tailings placement over time which can then be used to prepare estimates of tailings material types and a distributed seepage model.

Acknowledgements

The authors thank Robinson Nevada Mining Company for granting permission to publish this work.

References

- Allen RG, Irmak A, Trezza R, Hendrickx JMH, Bastiaanssen WGM, Kjaersgaard J (2011) Satellite-based ET estimation in agriculture using SEBAL and METRIC, *Hydrologic Processes*, 25, 4011–4027.
- ASCE-EWRI (2005) *The ASCE standardized reference evapotranspiration equation.*, pp. 59 with six appendices, Environmental and Water Resources Institute, American Society of Civil Engineers, Reston, Virginia.
- Qiu GY, Zhao M (2010) Remotely monitoring evaporation rate and soil water status using thermal imaging and “three-temperatures model (3T Model)” under field-scale conditions, *Journal of Environmental Monitoring*, 12(3):716–723.





The recovery of Pt(IV) from aqueous solutions by APDEMS-functionalised zeolite ©

Alseno K. Mosai, Luke Chimuka, Ewa M. Cukrowska, Izak A. Kotzé and
Hlanganani Tutu

*Molecular Sciences Institute, School of Chemistry, University of the Witwatersrand, Private Bag X3, WITS,
2050, South Africa*

Abstract

The recovery of Pt(IV) from aqueous solutions by zeolite functionalised with 3-aminopropyl(diethoxy)methylsilane (APDEMS) was studied at various adsorbent dosage, pH, time, concentration and competing ions was studied. The adsorbent was highly efficient at pH 2 and the maximum adsorption was reached at 180 min. The adsorption of Pt(IV) was not affected by the presence of competing ions instead, other precious metals and trace elements were adsorbed. The strong Pt-adsorbent interaction concluded from kinetic and isotherms models makes the adsorbent suitable for the recovery of Pt(IV) and other metals from mining wastewater.

Keywords: Pt(IV), recovery, platinum group elements, APDEMS-functionalised zeolite

Introduction

Large amount of water is used during mineral processing and the resulting wastewater is discharged into the environment (Lottermoser 2003). The discharged water normally contains significant concentrations of metals. Studies have shown that platinum group metals (PGMs) are discharged along with wastewater as by-products of nickel and copper mining (Xiao and Laplante 2004). Moreover, PGMs mining plants lose significant amounts of PGMs during processing (Hunt et al. 2013). Thus, the accumulation of PGMs could be quite significant in the environment and their recovery could add value to the economy of many countries dependant on them. PGMs are widely used in jewellery, catalytic converters, laboratory equipment and medicine (Chassari et al 2005; Xiao and Laplante 2004). The production of PGMs has increased over the years due to their increasing demand and since only a few countries (South Africa, Canada and Russia) have large reserves, there is a danger of the scarcity of their minerals worldwide and thus a need for recovery from wastewater solutions (Alonso et al 2009).

Zeolites are aluminosilicate clay minerals which are among the cheapest naturally available adsorbents. They consist of SiO_4 and AlO_4

frameworks which are linked through oxygen atoms in a three-dimensional array. The overall charge of zeolite is negative due to the replacement of Si^{4+} with Al^{3+} and is balanced by cations such as Ca, Mg, Na and K in the cavities of the zeolite (Malamis and Katsou 2013). Zeolites have been found to be good adsorbents for trace metals due to their high cation exchange capacity and molecular sieve properties (Bakatula et al. 2015). Moreover, studies have shown that the adsorption capacities of zeolites can be improved by modification where the zeolite acts as a support (Ren et al. 2016). Platinum has been found to interact strongly with nitrogen and thus, the aim of the study to use zeolite functionalised with 3-aminopropyl(diethoxy)methylsilane (APDEMS) which has a primary amine group to recover Pt(IV) from aqueous solutions.

Materials and methods

Chemicals

The chemicals used in this study were of analytical reagent grade and were obtained from Sigma Aldrich, South Africa. The 10 mg L^{-1} platinum stock solution was prepared from Pt(IV) standard and deionised water in 1 L volumetric flask and was stored in the refrigerator (4°C) until required. Working solutions with specific concentrations were pre-



pared daily from the stock solution through serial dilutions. The pH of the solutions was controlled with 0.01 mol L⁻¹ NaOH and 0.01 mol L⁻¹ HCl. The stock solution of the mixed metals was prepared in the same way.

Functionalisation of zeolite and characterisation

The zeolite was purchased from Sigma Aldrich (Steinheim, Germany). The chemical functionalization was achieved by mixing 5g zeolite with 10 mL of 3-aminopropyl(diethoxy) methylsilane (bp: 85 – 88°C) in a glass vial and the contents were interacted at 180°C for 30 min in an automated Microwave-assisted Extraction monowave 450 (Anton Paar, South Africa). The contents were cooled to room temperature and filtered using 0.45µm cellulose natrete filtech filter paper using suction and rinsed with ethanol. The functionalised zeolite was then dried at 100°C for 24 h.

The natural and functionalised zeolite were characterised with fourier transform infrared (FTIR) spectroscopy in the range of 4000 – 400 cm⁻¹ for the determination of functional groups, the mineralogy was determined with powder X-ray diffraction (PXRD) D2 Phaser (Bruker, Germany), X-ray fluorescence (XRF) (PANalytical, Netherlands) was used to determine the chemical composition, varioELcube V4.0.13 (Elementar, Germany) was used for elemental analysis. Textural properties (surface area, pore size and pore volume) were analysed with Micromeritics Flow Prep 060 instrument (Aachen, Germany). The point of zero charge (PZC) was also determined using KCl for ionic strength, HNO³ and NaOH to control pH.

Batch adsorption studies

The study was carried out by placing the adsorbent and 10 mL Pt(IV) solution at various conditions in 50 mL polypropylene containers which were shaken at room temperature with an elliptical benchtop shaker (Labcon, USA) to attain equilibrium and the contents were filtered with 0.45 µm cellulose natrete Filtech filter paper and the filtrate was analysed with inductively coupled plasma optical emission spectroscopy (ICP-OES) (Spectro genesis, Germany).

Effect of adsorbent mass (50 – 500 mg) on the adsorption of Pt(IV) by APDEMS-functionalised zeolite was determined at pH 2 and room temperature (25°C). Effect of pH (2 – 9), concentration of Pt(IV) (0.5 – 5 mg L⁻¹) and contact time (0 – 540 min) on the adsorption of Pt(IV) was determined. Competing ions (Rh(III), Pd(II), Ir(III), Ru(III), Os(III), Fe(III), Ca(II), Mg(II), K(I), Co(II), Ni(II), Hf(IV), Zn(II) and Au(I)) were prepared with Pt(IV) and exposed to APDEMS-functionalised zeolite to determine their effect on adsorption or recovery of Pt(IV).

Data treatment

The adsorption capacity, q_e (mg g⁻¹) and the adsorption efficiency were calculated using equations 1 and 2, respectively.

$$q_e = \frac{(C_0 - C_e)V}{M} \quad (1)$$

$$\text{adsorption efficiency} = \frac{(C_0 - C_e)}{C_0} \times 100 \quad (2)$$

where C_0 and C_e are initial and equilibrium concentrations of metals (mg L⁻¹), V is the volume of the solution used (L) and M is the mass of the adsorbent (g).

Adsorption isotherms

The type of adsorption occurring between Pt(IV) and APDEMS-functionalised zeolite was determined with Langmuir, Freundlich and Dubinin Radushkevich (D-R) adsorption isotherms. The Langmuir isotherm describes the monolayer adsorption between adsorbents and substances (Mushtaq et al. 2016). The Freundlich isotherm describes the non-ideal and reversible adsorption of elements onto the heterogeneous surface (Chen 2015; Mushtaq et al. 2016). The Dubinin-Radushkevich (D-R) isotherm describes the adsorption mechanism with a Gaussian energy distribution onto a heterogeneous surface (Chen 2015). The Langmuir, Freundlich and Dubinin Radushkevich (D-R) adsorption can be expressed as, respectively:

$$\frac{C_e}{q_e} = \left(\frac{1}{q_m} \right) C_e + \left(\frac{1}{K_L q_m} \right) \quad (3)$$

$$q_e = K_f C_e^{\frac{1}{n}} \quad (4)$$

$$\ln q_e = \ln X_m - K_{ad} \varepsilon^2 \quad (5)$$



where q_e (mg g^{-1}) is the quantity of the adsorbate adsorbed per gram of adsorbent at equilibrium, q_m (mg g^{-1}) is the maximum monolayer coverage capacity and K_L is the Langmuir isotherm constant (L mol^{-1}), K_f ($(\text{mg g}^{-1})/(\text{mol L}^{-1})^{1/n}$) is the Freundlich isotherm constant and n is the adsorption intensity, K_{ad} ($\text{mol}^2 (\text{kJ}^2)^{-1}$) is the Dubinin-Radushkevich isotherm constant, X_m (mg g^{-1}) is theoretical isotherm saturation capacity and ε is the Polanyi constant.

Kinetic models

The adsorption process controlling mechanism between Pt(IV) and APDEMS-functionalised zeolite was determined with pseudo first- and second order kinetic models represented by equations 6 and 7, respectively (Bakatula et al 2015). The correlation coefficient (R^2) and the closeness of the experimental adsorption capacity, q_{exp} to the calculated, q_{cal} were used to determine the model that best describes the kinetic data.

$$\log(q_e - q_t) = \log q_e - \frac{k_1 t}{2.303} \quad (6)$$

$$\frac{t}{q_t} = \frac{1}{k_2 q_e^2} + \frac{1}{q_e} t \quad (7)$$

where q_t (mg g^{-1}) and q_e (mg g^{-1}) are the adsorption capacities at time t and equilibrium, respectively, k_1 (min^{-1}) and k_2 ($\text{g mg}^{-1} \text{min}^{-1}$) are the rate constants.

Results and discussion

Characterisation

The results from XRF showed that silica (SiO_2) (68.49%) and alumina (Al_2O_3) (11.48%) are main components of the zeolite. Other

chemical components are K_2O (3.79%), Na_2O (1.47%), CaO (1.22%), Fe_2O_3 (1.09%) and loss on ignition of 11.03%. The PXRD results are shown in Fig. 1. The zeolite was mainly composed of clinoptilolite, quartz and sanidine. From these results, it was clear that the natural zeolite can be classified as clinoptilolite. The FTIR spectra of the raw and functionalised zeolite are shown in Fig. 2. The peaks at 695 and 964 cm^{-1} which are present in both the raw and functionalised zeolite are due to the Si-O and Al-O-Si and Si-OH groups (Guaya et al. 2015). The success of functionalization was confirmed by the peaks at 790 and 765 cm^{-1} which are due to Si-O-Si bonds of the zeolite and APDEMS. The peak at 1644 cm^{-1} can be attributed to the deformation vibration of water. The peaks beyond 3300 cm^{-1} are due to the hydroxyl groups of the zeolite. The $-\text{CH}_2$ and $-\text{CH}$ stretching vibrations of APDEMS are represented by the peaks at 2925 and 2872 cm^{-1} . The peaks at 1182 and 1257 cm^{-1} on the functionalised zeolite can be attributed to Si- CH_2 and Si- CH_3 , respectively. The presence of the nitrogen groups is represented by the peaks at 1575 cm^{-1} ($-\text{NH}$ vibration) and 3366 cm^{-1} (primary amines). Moreover, the elemental analysis showed that the C and H percentages were high on the functionalised zeolite and that of N was observed on APDEMS-functionalised zeolite which was not present on the raw zeolite. These results show that the functionalization of raw zeolite was successful. The surface area of the raw zeolite decreased from 16.28 to 2.17 $\text{m}^2 \text{g}^{-1}$ due to functionalization with APDEMS and this also confirmed the success of the addition of

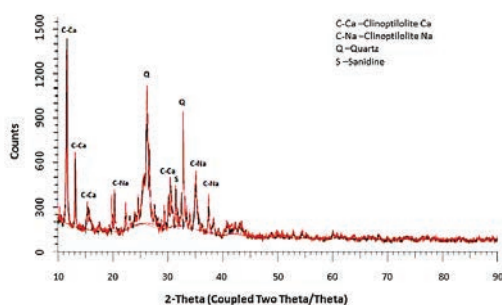


Fig. 1 PXRD pattern of zeolite

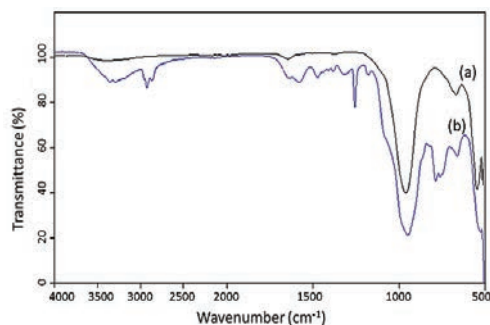


Fig. 2 FTIR spectra of raw zeolite (a) and functionalised zeolite (b)



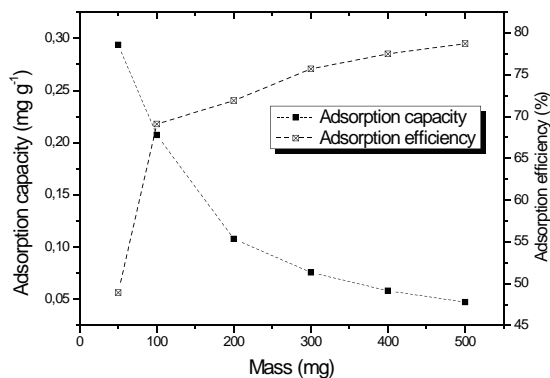


Fig. 3 Effect of mass on the adsorption of Pt(IV) by APDEMS-functionalised zeolite

the ligand on zeolite. This reduction can be attributed to the smothering of the pores by APDEMS as the pore size and pore volume also decreased from 12.97 to 4.50 nm and 0.052 to 0.0045 cm³, respectively.

Effect of adsorbent mass

The effect of adsorbent mass on the adsorption or recovery of Pt(IV) was studied and the results are shown in Fig. 3. The adsorption efficiency increased with increasing adsorbent mass but the adsorption capacity decreased. For subsequent experiments, 10 g L⁻¹ adsorbent mass was used as the adsorption capacity and the adsorption efficiency were significant.

Effect of pH

Studies have shown that pH can affect the behaviour and hence the adsorption efficiency of adsorbents (Bakatula et al. 2015; Ren et al. 2016). The adsorption capacity decreased with increasing solution pH and this could

be attributed to the speciation of Pt(IV) and the surface charge (Fig. 4). At acidic pH, the surface groups were protonated and thus, –NH³⁺ which had high affinity for the anionic Pt(IV) species (PtCl₆²⁻) resulted. The anionic chloride species were more prevalent at acidic pH due to the addition of HCl. During the processing of PGMs, concentrated acids are used for extraction and thus, the discharged water is highly acidic (Nguyen et al. 2016). Thus, the adsorbent will work well and significantly recover Pt(IV) from mining wastewaters which are highly acidic. PZC was found to be 5.3. The adsorption capacity decreased significantly beyond pH 2 and this can be attributed to the low amount of chloride species favourable for adsorption as well as electrostatic repulsion between the Pt species and the surface groups.

Effect of concentration

The adsorption of Pt(IV) at pH 2 was observed to increase with increasing Pt(IV)

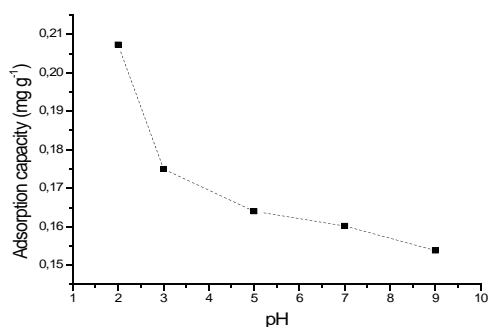


Fig. 4 Effect of pH on Pt(IV) adsorption

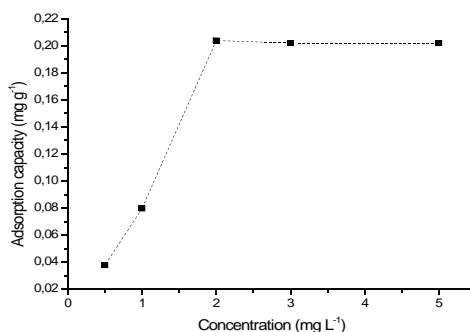


Fig. 5 Effect of concentration on Pt(IV) adsorption



Table 1 Adsorption isotherm constants

Langmuir			Freundlich			Dubinin-Radushkevich (D-R)		
q_m (mg g ⁻¹)	K_L (L mol ⁻¹)	R^2	K_f ((mg g ⁻¹)/(mol L ⁻¹) ^{1/n})	n	R^2	X_m (mg g ⁻¹)	E_s (kJ mol ⁻¹)	R^2
0.117	3.5x105	0.98	32.29	1.99	0.91	1.37	12.42	0.92

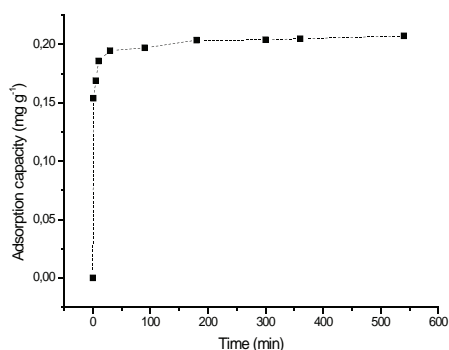
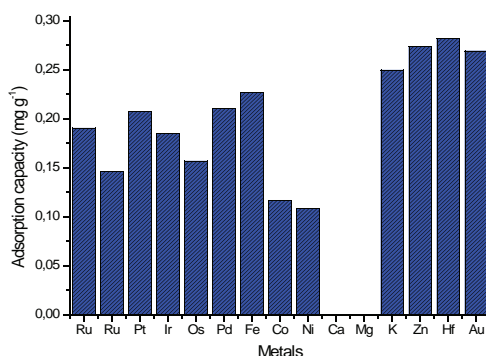
Table 2 Kinetic parameters for Pt(IV) adsorption by APDEMS-functionalised zeolite

Pseudo first-order			Pseudo second-order		
K_1 (min ⁻¹)	q_{exp} (mg g ⁻¹)	R^2	K_2 (g mg ⁻¹ min ⁻¹)	q_{exp} (mg g ⁻¹)	R^2
0.0088	0.0061	0.71	6.71	0.103	0.99

concentration from 0.5 to 2 mg L⁻¹ (Fig. 5). The increase in adsorption capacity can be attributed to the availability of binding sites (-NH₃⁺). The adsorption efficiencies were 75.6, 79.7, 78, 3, 57.7 and 40.4% at 0.5, 1, 2, 3 and 5 mg L⁻¹, respectively. The ability of the adsorbent to significantly adsorb very low concentrations of Pt(IV) makes it a suitable adsorbent for PGMs wastewater which contains very low concentrations of PGMs (Hunt and Clark 2013, Hunt et al 2015). This also means that there is a strong interaction between Pt(IV) and the adsorbent. Beyond 2 mg L⁻¹, no increase in adsorption was observed. The adsorption isotherm results (Table 1) indicated that the interaction of Pt(IV) onto APDEMS-functionalised zeolite is through monolayer adsorption since the experimental data was described better by Langmuir isotherm ($R^2 > 0.98$). The free energy change as determined from D-R isotherm was found to 12.42 kJ mol⁻¹ indicating that the adsorption process is through ion exchange (Bakatula et al. 2015).

Effect of contact time

The effect of contact time on the adsorption of Pt(IV) by APDEMS-functionalised zeolite was investigated and the results are shown in Fig. 6. A rapid increase in adsorption was observed between 0 and 30 min after which, a slow uptake was observed until 180 min. Equilibrium was reached at 180 min where the adsorption was controlled by diffusion. Thus, 180 min was chosen as the sufficient time for the recovery of Pt(IV) by the adsorbent. The kinetic data was best described by pseudo second-order indicating that chemisorption was the rate controlling mechanism ($R^2 > 0.99$) (Table 2). This was also supported by the calculated adsorption capacity (q_{cal}) (0.102 mg g⁻¹) which was very similar to the experimental adsorption capacity (0.103 mg g⁻¹). The experimental adsorption capacity determined with pseudo first-order was found to be 0.0061 mg g⁻¹ which is very different from the calculated capacity, further explaining that there is no good correlation with pseudo first-order.

**Fig. 6** Effect of time on Pt(IV) adsorption**Fig. 7** Effect of competing ions on Pt(IV) adsorption

Effect of competing ions

A mixture of 2 mg L⁻¹ Pt(IV) and other ions at pH 2 was exposed to APDEMS-functionalised zeolite to determine the efficiency of the adsorbent on the recovery of Pt(IV) in the presence of other ions. The adsorption capacity of Pt(IV) was not affected by the presence of other ions, some of which are PGMs (Fig. 7). Moreover, these PGMs and other cations except Ca and Mg were adsorbed by the adsorbent making APDEMS-functionalised zeolite a dual efficacy adsorbent. The ability to significantly adsorb Pt(IV) in the presence of other ions makes the APDEMS-functionalised zeolite a suitable adsorbent to be used in mining wastewater.

Conclusion

In this study, APDEMS-functionalised zeolite was synthesised and used to recover Pt(IV) from aqueous solutions. The characterisation results showed that the functionalization was successful. The experimental studies were carried out under the optimised conditions (100 mg adsorbent, pH 2, 2 mg L⁻¹ and 180 min) and indicated that 0.207 mg g⁻¹ of Pt(IV) was removed from aqueous solutions by APDEMS-functionalised zeolite. The adsorbent was significantly adsorbed Pt(IV) at highly acidic pH (pH 2) which makes the adsorbent very suitable for PGM mining wastewater which is highly acidic. The kinetic (pseudo second-order) and isotherm (Langmuir) models as well as the energy from D-R isotherm indicated that there was strong chemisorptive Pt-adsorbent interaction. The presence of competing ions did not affect the adsorption of Pt(IV). The adsorbent can be applied in retaining ponds into which processing solutions are discharged and fed to the processing units together with fresh ore after recovery.

Acknowledgements

The authors would like to thank the National Research Foundation (NRF), the University of the Witwatersrand and the Water Research Commission (WRC project no. K5/2589) for financial support.

References

- Alonso E, Field FR, Roth R, Kirchain RE (2009) Strategies to address risks of platinum scarcity for supply chain downstream firms. In Sustainable Systems and Technology, 2009. ISSST'09. IEEE International Symposium on (pp. 1-6). IEEE.
- Bakatula EN, Mosai AK, Tutu H (2015) Removal of Uranium from Aqueous Solutions using Ammonium-modified Zeolite, S Afr J Chem, 68:165–171
- Chassary P, Vincent T, Marciano JS, Macaskie LE, Guibal E (2005) Palladium and platinum recovery from bicomponent mixtures using chitosan derivatives, Hydrometallurgy 76(1-2):131-147
- Chen X (2015) Modeling of experimental adsorption isotherm data, Information 6(1):14-22.
- Guaya D, Valderrama C, Farran A, Armijos C, Cortina JL (2015) Simultaneous phosphate and ammonium removal from aqueous solution by a hydrated aluminum oxide modified natural zeolite, Chem Eng J 271:204-213
- Hunt AJ, Matharu AS, King AH, Clark JH (2015) The importance of elemental sustainability and critical element recovery, Green Chem, 17(4):1949-1950
- Lottermoser B (2003) Mine Water. In Mine wastes, Springer, Berlin, Heidelberg, pp. 83-141
- Malamis S, Katsou E (2013) A review on zinc and nickel adsorption on natural and modified zeolite, bentonite and vermiculite: Examination of process parameters, kinetics and isotherms, J Hazard Mater 252:428-461
- Mushtaq M, Bhatti HN, Iqbal M, Noreen S (2016) Eriobotrya japonica seed biocomposite efficiency for copper adsorption: isotherms, kinetics, thermodynamic and desorption studies, J Environ Manage 176:21-33
- Nguyen TH, Sonu CH, Lee MS (2016) Separation of Pt (IV), Pd (II), Rh (III) and Ir (IV) from concentrated hydrochloric acid solutions by solvent extraction. Hydrometallurgy, 164:71-77
- Ren H, Jiang J, Wu D, Gao Z, Sun Y, Luo C (2016) Selective adsorption of Pb (II) and Cr (VI) by surfactant-modified and unmodified natural zeolites: a comparative study on kinetics, equilibrium, and mechanism, Water Air Soil Pollut 227(4):101
- Xiao Z, Laplante AR (2004) Characterizing and recovering the platinum group minerals—a review. Miner Eng, 17(9-10):961-979





What Art Can Tell About Modified Environmental Systems ©

Grit Ruhland¹

¹*Bauhaus Universität Weimar, Faculty of Art and Design, Weimar, Germany
grit.ruhland@web.de*

Abstract

Mining is not just a technical, but a political, ecological, and social activity. Living space, in a cultural sense, has been described as “landscape” originating in a creative process – unlike wilderness, it does not simply arise, it is manmade, and thus aesthetic.

Sensory perception is seen as a basis for producing knowledge and understanding. Therefore, perception of art produces knowledge, and is capable of engaging with entities beyond the senses and imagination, such as long time-spans, complex systems and invisible phenomena. An open democratic discourse may be facilitated by artistic examinations of mining technologies and their impacts.

This paper introduces examples of artistic projects that are relevant, in various ways, to the topic of mine-water.

Keywords: landscape, artistic research, mine water, aesthetics, perception

The beginning of this paper covers several large territories rather cursory. The intention behind this approach is to point out the peaks of several discourses - “tips of icebergs” - that have taken place within the arts or regarding them. This broadness is necessary: as one can not expect to share the same understanding of terms and approaches in the various disciplines, a widespread introduction frames possible perspectives for a relation between the arts and (environmental) sciences. In the end, three artworks are discussed as examples for “best practice” regarding different issues of mine water which are relevant in a cultural sense.

Fig. 1 is not an actual illustration to the text, but attempts to draw a “map” of the complex territory that shows a selection of the most relevant disciplines and topics around the core problem and their interaction.

Landscape as living and cultural space

Mining, though at first glance focused mainly on inorganic matter, is actually a change in earth systems, occurring in living spaces. Many species, human and non-human alike, are impacted by removal and repositioning of materials and the influence this has on hydrological systems, both during a mining operation and after its closure.

Lucy R. Lippard points out in “Undermining” with the telling subtitle “a wild ride

through land use, politics, and art in the changing West” that there is a “romanticized notion” within the expression “landscape”, which is why she prefers the term “land use” instead (Lippard 2014, 4). Certainly, landscape is a hotly argued term in several disciplines, (especially in German-speaking geography), but also among different methodologies and languages (Kühne 2008, 43). But rather than avoiding it, I suggest an appreciation of the aesthetic emphasis, and focus on elaborating why an aesthetic regime is crucial to land use and its related practices, such as mining and mine water. I prefer to engage and explore the perception, understanding, and interpretation of landscape which is understood as the “archetype of normative projections, aesthetic experiences and sensory appropriation” (Kühne 2008, 43).

The German term “Landschaft (landscape)” can be traced back to „landscaf“ – describing most of all a political-topographic entity: a swath assigned to a social group, an administrative unit (Kirchhoff and Trepl 2009, 19). The root-meaning and usage are similar, though the dating of the term varies throughout the histories of the different Germanic languages and English – „lantschaft“ and „lantskepi“ are already documented as far back as the 8th century (Kluge and Seebold 2002, s.v. Landschaft). Consisting of two parts: „lant“ is associated with free or fallow



land, and „skepi“ with creation. So, from the very beginning, “landscape” has referred to cultivated territory as opposed to uncultivated wilderness or savage nature (Schama 1995). Simon Schama emphasizes in his standard work „Landscape and Memory“: “Before it can ever be the repose for the senses, landscape is the work of the mind. Its scenery is built up as much from strata of memory as from layers of rock.” (Schama 1995, 6–7).

Some authors state that landscape can not be understood as an object without an observer (Trepl 2012, 20). Socio-scientific landscape perspectives suggest models based on physical space which includes an appropriated physical level, a personal level, and a societal level (Kühne 2013). Parts of a landscape can consist not only of objects created and used in the present, but also objects created in the past and abandoned, or visible just in traces, or existing only in stories – even without certain proof (Kühne 2013, 71).

A brief summary on aesthetics as cognition, experience and world view

The question “what can art tell/do/provide ...” has been a fertile territory of arguments from early in the 20th Century until the present day. It is certainly on the agenda, and becomes especially relevant, when contextualized with eco-politics, changed environmental systems and living spaces — for instance those changed as a result of mining activities. The regime of politics in these terms is not merely understood as formalized procedures in parliament and elections, but as a “configuration of a specific space, the framing of a particular sphere of experience” — within this space “objects posited as common” are defined and discussed by “subjects recognized as capable of designing these objects and putting forward arguments about them.” (Rancière 2009b, 24). The regimes of aesthetics and politics, according to Rancière, are not generally “permanent, separate realities”, but share common ground in the “distribution of the sensible” (Rancière 2009b, 25). For instance the “the refusal to consider certain categories of people as political beings”, along with “a refusal to hear the words exiting their mouths as discourse” is one cogent example of this “distribution of the sensible”: an

alteration in processes which have been not physically, but politically invisible or unheard - “to render visible what had not been, and to make heard as speakers those who had been perceived as mere noisy animals” (Rancière 2009b, 24–25).

In “Le destin des images (The Future of the Image)” Rancière analyzed another relevant discourse in the production of knowledge by the arts, basing on aesthetics. He retraces the line of argument back to Plato, whose statements have partly led to a skepticism towards visual representation, having determined that it is a “simulacrum” possessing an overpowering presence which violates the severity of experience. Plato preferred the simple, direct report of a witness, since it is more authentic than a mimetic representation. Rancière points out that this is rather a ban, supported by an ethical argument, making its own paradigms invisible (Rancière 2009a).

Thus, skepticism against the credibility of images and even sensuous impressions in these terms has a tradition in western philosophy, and it is not until the 18th century when it is first made a subject of epistemology, by Francis Hutcheson and Alexander Gottlieb Baumgarten. While Hutcheson was mainly concerned with aesthetic judgment and saw the senses as having “no intellectual element, no reflection on principles and causes”, Baumgarten, (although also coming from a tradition of German enlightenment scholars that “dismissed the senses and the imagination as incapable of providing a genuine cognition of their objects”), was the first to attribute a cognitive function to the senses, aesthetics and the arts (Munro und Scruton 2017). Baumgarten’s treatise „Metaphysica“ published in 1737, lays the foundation for “Aesthetics as science of sensory and imaginative experience” (Baumgarten 1983, 79). Although this argumentation for aesthetic judgment is still seen as general motive behind this text, it only appears after a detailed description of perception, knowledge and interpretation. He was the first philosopher who opened the door for artists to join in the production of knowledge. Immanuel Kant agreed with this argumentation in “Kritik der Urteilskraft (The Critique of Judgment)” in 1790, and acknowledged “aesthetic experi-



ence as a distinct exercise of rational mentality” (Munro und Scruton 2017).

The article is in these traditions more concerned with the cognitive aspects, rather than aesthetic judgments of sensory experience and artistic expressions. Furthermore, western art history in the second half of the 20th century has mainly abandoned the discourse on defining general rules for aesthetic judgments and therefore it is no longer a general criterion.

In the 20th century, John Dewey, philosopher and early theorist and proponent of progressive education, published “Art as Experience” in 1934 - as the title suggests, his main focus is on interactive processes: coding and decoding, accessing and creating experiences through the arts. The term experience itself is not limited to humans, but is universal. Dewey aims to free the arts from isolation as a sublime classical subject in order to protect their power of being rooted in actual, complex experiences (Dewey 2005). Aesthetic understanding is not simply admiration and pleasurable, mindless enjoyment, but includes cognitive knowledge (i.e., in the case of a plant, knowledge of its living conditions in soil, air and light), which makes the aesthetic experience rich and full.

He regrets that the expression “aesthetic” is mainly seen as the passive process of a consumer, while “artistic” is the active, distinguished term in that sense (Dewey 2005, 47–48). Both are forms of aesthetic perception: experiencing and creating art require active and passive processes – they involve reception and exercise of energy. What once was condensed by an artist as aesthetic experience in an artwork needs to be remade as experience by the audience (Dewey 2005). This explains why experiencing art requires exercise and experience.

A misguided experiment on arts and mining – the art collection of Wismut

Having mentioned some already, there is still one important condition to add: freedom of the arts. The German constitution (Basic Law for the Federal Republic of Germany) in Article 5, “Freedom of speech”, reads “Arts and sciences, research and teaching shall be free.” (Basic Law, Art. 5 1949). This may seem so

fundamental, that it might be irritating to see it mentioned at all. But, the singular historical and political conditions of 20th century Germany have left their imprint in art history and discourse, and have had a more important and lingering effect than is often taken into account. The violation of this freedom of the arts was especially strong in the 3rd Reich, starting at the dawn of the 1930’s. Furthermore, this German urge to try to tame the arts did not end there. After the formation out of the Soviet occupation zone of the German Democratic Republic, freedom of arts and science was enshrined in its constitution as Article 34 with almost the same wording as in its West-German counterpart, even with the same reassurance of government protection and support (Constitution, Art. 34 1949). But through lack of application, according to some hypotheses, this legal guarantee of freedom for arts and sciences was erased in the revised version of this statute in 1968 – and in addition arts and science were divided into two different articles, Nr. 17 and Nr. 18. Though still nominally supported, within certain goals and guidelines, (especially for the arts) they were to be devoted to a close relation to the life-world of the nation/folk/people, to what is known as “Socialist Realism” (Constitution, Art. 18 1968).

Why do I mention all this? SDAG Wismut was one of the world’s largest producers of Uranium ore until 1990 - and acting under the guidelines of the GDR constitution has assembled a large collection of more than 4.000 artworks covering a period of several decades, including works of music and literature, (mainly commissioned), that are today owned by Wismut GmbH (Wismut GmbH 2011). One could consider this as a large experiment in the relation of arts to mining. Unfortunately, as I stated above, it was a rather poisonous one for the artworks. As in other GDR-companies which have bought or commissioned artworks, there have been guidelines applied, motifs selected, goals and uses defined – premises which have undermined the independence and reputation of artworks and artists (Spreitz 2011, 606).

As would be the case for biased science, it is almost impossible to reintegrate artworks which have been produced under partial,



purposive circumstance into a discourse, even though some aspects of the artworks may be intrinsically interesting. Although they have been preserved and still physically exist, they are cut off from the general artistic discourse. However there are a few exceptions, those that have defended their independence in some way and may have a potential to contribute their examinations to a broader audience.

My position is not one of an art critic, but of an artist, a practitioner – my main interest is not in judging artistic quality, but in the conditions under which artists made artworks. The examples aim to make this point: Any preset, forced goal or guideline concerning the premises, outcome, appearance or approach, will harm artworks, especially those that are in some way commissioned – this applies to any context, but especially to controversial issues such as mining or mine water. Of course, respectful debates and a fair exchange of views about those opinions will rather contribute to a vivid production process and are exempt from this warning.

What to do? The relation of aesthetics and ecology

Ben Valentine asked in “Hyperallergic”, a New York-based online art-magazine: “How Can Ecological Artists Move Beyond Aesthetic Gestures?” Facing serious environmental problems, he is unhappy with a majority of artworks that in his opinion are “aesthetic interventions forced onto the environment by artists with little to no deep understanding (e.g. geologic, ecologic, botanic) of the materials they are using”, representing mostly an “aesthetic, surface-level intervention, which documents well for exhibition” or another “art-world setting, be it via a gallery or a coffee table book” (Valentine 2017). Although not clearly expressed, it seems that Robert Smithson’s land artwork “Spiral Jetty” (1971) stands as a prototype for these “hollow aesthetic gestures” Valentine criticizes (Valentine 2017).

Along with Dewey and Rancière, one could argue that this critique concerns not only “ecological artists” as Valentine calls them, but all artworks. According to Rancière in the contemporary “relational aesthet-

ics” passive material is no longer devoted to active form, but new practices uniting both form and material come into being. Dewey’s request for what I would call an “informed aesthetics” would prevent such hollow superficiality, especially when dealing with environmental topics. Although I understand Valentine’s dissatisfaction, I do not agree with his assumption that a “clear, factual, historical, but compelling story for these environmental catastrophes” is needed. His last point in the article is most problematic, since he sets an emotional goal for these artworks, one which sounds more like a social campaign strategy than anything else: “it must be a story that disgusts, places correct blame, and, of course, elicits action.” It is not only manipulative to set this kind of goal, but also questionable as method: “the end justifies the means” – what is more, it would violate the freedom of art from the other side, so to speak. His subtitle to the whole article is: “If art is to be relevant to the environment, it needs to move beyond an art context to engage with the land itself.” What does “the land itself” mean? Presumably, he refers to the physical, material sphere of landscape – but as stated above, it has from the beginning been shaped by cultural practices. Therefore, I assume there is more than one appropriate strategy – even from within the very core of the art context, the art gallery. But in general the observation that there is a preference for dealing with art-specific or art-historical questions is shared by several authors (Rancière 2009b, Krolczyk and Emde 2013). Nevertheless, the question remains: what could be an appropriate approach for an artwork in an ecological context?

Art critic Tom Holert expressed hesitation about the claims being raised that art should solve environmental problems with its own resources – the resources available to art are rather politically and economically weak when compared to political and scientific institutions, he believes, are in control in the first place, plus the often requested assistance in illustration of scientific findings and scenarios is not the primary role of artists in the production of knowledge (von Borries, Hiller, and Renfordt 2011). In this sense, for Rancière it would not be in “the land itself” that art has its most valuable political contri-



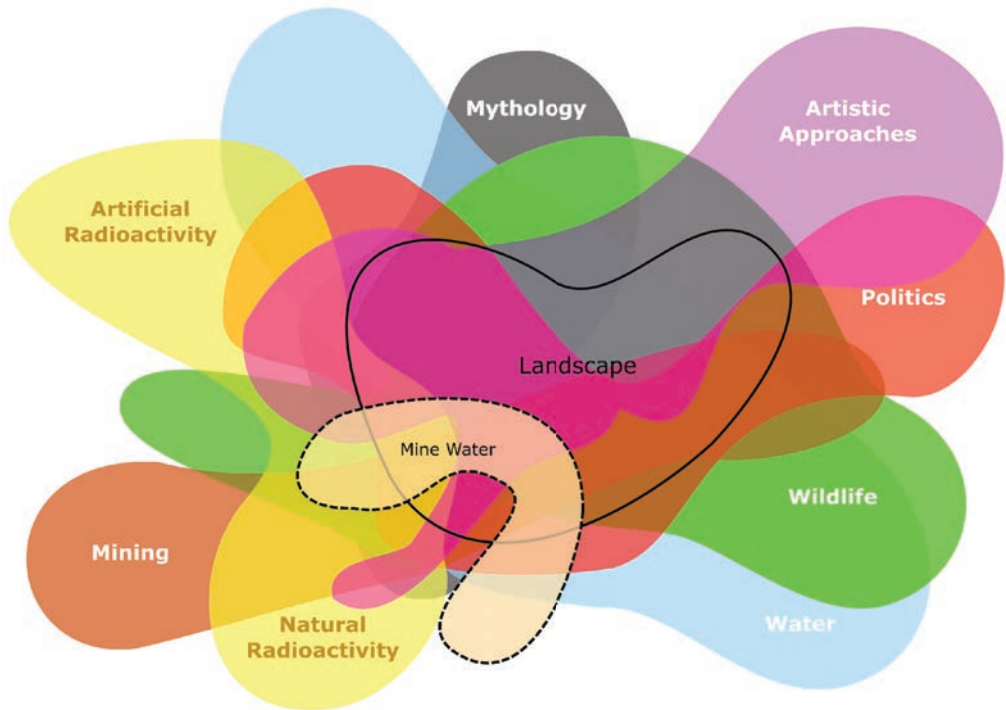


Figure 1 schematic diagram of subjects, topics and disciplines concerned with mine water – the representation aims to show interaction, intersection and overlap up to and beyond recognition, but is non-exhaustive

bution to make, but in the mode of “as if”, the alternative world-model, the micro-politics of neighborhood.

The following three artworks highlight examples dealing with issues related to mine water – as common artistic practice, the relation is rather associative than distinct. Each of the covers one or more subjects or topics shown in Figure 1.

Marc Böhlen – WaterBar (2012–13): WaterBar was realised as a public art installation in Singapore – a public well “designed for the post-sustainability age when clean water is simply not good enough” (Böhlen 2012). The first stage starts with cleaning municipal water: purifying the water via an anthracite filter – after that other filters are added to remineralize the water through geoengineering.

Among these additional filters are “quartz-rich granite from Inada by Fukushima, home of the latest devastating high-tech catastrophe; sandstone from La Verna, Italy, where St. Francis cared for the poor; marble from Thassos, Greece, source of art and architecture and the beginning and possible end

of democracy; limestone from Jerusalem/Hebron, Israel, a place of eternal conflict and shared hopes; and basalt from Mount Merapi, Indonesia, an unpredictable, active volcano.” (Böhlen 2012). An “internet-scanning, text-processing control system” (search-bot) checks online daily and mixes water in reaction to the news on water related issues, by circulating water through those filters releasing “trace elements of the minerals and rocks” according to the “catch of the day” (Böhlen 2012). The project highlights the fact that water not only has an origin, but also a story that goes along with it. The story of the places water has touched contributes to an intangible quality that can not be measured with an ICP. For Böhlen, most technologies focus on “risk minimization”, which is suitable for survival, but with WaterBar he wants to take a further step towards “a deep culture of resource management” (Böhlen 2012).

Christina Kubisch – Unter Grund (2014): The 26-channel sound installation has been the result of an invitation by Museum Zeche Zollverein Essen, Germany. It is an acous-

tic portrait of the mine water aquifers both below the building and farther. Mine water is a mostly invisible landscape element in the whole Ruhr area. Sound artist Christina Kubisch and her team have recorded above and below surface engine rooms, pumping stations, water plants, ponds, swamps, pit cages, drainages – mainly with contact microphones and hydrophones (Fabian Lasarzik und Gruenrekorder 2014). These sounds have been arranged into a 23:47 min composition of documentary water and engine sounds creating their own mine water world. Rhythmic sounds and deep noises are present, which left curator Lasarzik with the impression the subconscious of the post-mining landscape spirit and movement had become perceptible. Kubisch's work in general deals with invisible, mostly technically altered realities; she offers an alternative perspective on the world. In this case, she was mainly working on “the so called ‘eternity costs’ [...] The pumps have to run forever or the Ruhr area will become a jungle.” The sound art label “Gruenrekorder” released a CD, with a new composition made from the recorded material including a piece called “Vision”, which is “an ironic view into the future in case the pumps will stop” (Kubisch 2018). http://www.gruenrekorder.de/?page_id=14340

Mari Keto/Erich Berger – Inheritance Project (2016): Artist Erich Berger and jewelry artist Mari Keto have created a special heirloom intended to emphasize another approach to our nuclear heritage and its deep time effects. They have crafted a magnificent and delicate necklace made from gold and Thorianite from Myanmar, Thorite from Madagascar, and Uraninite from Congo. It is made to be considered a heritage which requires a special care, inscribed as a set of rules and rituals that represent basic measurements of radioactivity. One is not allowed to wear it, until the outcome of measurement rituals using special measuring tools show certain definite signs that the level of radioactivity is low enough. The jewelry and tools are stored in a stackable concrete container. The tools are a Fenjaan water clock, an electroscope and other “accessories to operate the

electroscope: spare gold leaves which are the indicator for the electrostatic charge, and an acrylic rod on a piece of rabbit fur to electrostatically charge the electroscope”. (Berger and Keto 2016) The electroscope was the first instrument devised to “register and measure the phenomena caused by radioactivity”, famously used by Marie and Pierre Curie in their laboratory (Berger and Keto 2016, Carpenter et al. 2016).

The “Inheritance Project” exercises and gives an impression of a possible experience regarding theories about long-term nuclear waste storage projects that aim at “Constructing Memory” such as the Nuclear Energy Agency. Though these storage projects usually focus on high-level radioactive waste, the necklace is made from low-level radioactive minerals. But, tailings ponds, in particular, are considered large, low-level radioactive waste facilities that will need special care or at least a restriction of use for a time beyond historical expertise. Experts such as Högberg and Holtorf who work on Archeology as Future studies, emphasize that these long-term communications will not work as a “transfer of knowledge” (Högberg and Holtorf 2018). <http://inheritance-project.net>

Preliminary conclusions and suggestions

Artworks will not replace the tasks of scientists or administration. Their strength is their narrative, cognitive and Utopian qualities, which require the guaranteed, full freedom of art. In order to be relevant within the context of changed environmental systems such as mine water, the following non-exhaustive enumeration of criteria will be useful for the production of these artworks:

- to work within informed aesthetic decisions on a “conceptual level”
- to not treat material as passive substance
- to reflect the artists own social, cultural and biologic position
- to make works both site-specific and appropriate to their subjects
- to open up a new cognitive layer in an issue



References

- Baumgarten AG (1983) *Texte zur Grundlegung der Ästhetik: Lateinisch – Deutsch*, Meiner, F, Hamburg
- Böhlen M (2012) WaterBar. <http://www.realtech-support.org/waterbar>. Accessed 13 May 2018
- Carpenter E, Wyck PCV, Schuppli S, Hecht G, Honda E, Morton T, Phalkey J, Gama V, Sawaragi N, Triscott N (2016) *The Nuclear Culture Source Book*. Black Dog Publishing, London
- Clements A (2013) Reconsidering John Dewey's Art as Experience. In: Hyperallergic. <https://hyperallergic.com/67081/reconsidering-john-dewey-art-as-experience>. Accessed 13 May 2018
- Dewey J (2005) *Art as Experience*. Penguin
- Högberg A, Holtorf C (2018) *Nuclear Waste as Cultural Heritage*. Nuclear Roundtable, Konstmuseum Malmö
- Kirchhoff T, Trepl L (2009) *Vieldeutige Natur: Landschaft, Wildnis und Ökosystem als kulturegeschichtliche Phänomene*. transcript, Bielefeld
- Keto M, Berger E (2016) *Inheritance Project*. <http://inheritance-project.net/index.php/page-2>. Accessed 13 May 2018
- Kluge F, Seebold E (2002) *Etymologisches Wörterbuch der deutschen Sprache*
- Kubisch C (2018) Re: “Unter Grund” in Artikel für IMWA. Letter to Grit Ruhland, May 15, 2018.
- Kühne O (2008) *Distinktion, Macht, Landschaft: zur sozialen Definition von Landschaft*, VS Verlag für Sozialwissenschaften, Wiesbaden
- Kühne O (2013) *Landschaftstheorie und Landschaftspraxis*. Springer, Wiesbaden
- Lasarzik F (2014) *Unter Grund* | Christina Kubisch & Eckehard Güther. In: Gruenrekorder. http://www.gruenrekorder.de/?page_id=14276. Accessed 23 Mar 2018
- Munro T, Scruton R (2017) *Aesthetics – Taste, criticism, and judgment*. Encyclopedia Britannica. <http://www.britannica.com/topic/aesthetics/Taste-criticism-and-judgment>. Accessed 13 May 2018
- Parliamentary Council (1949) *Basic Law for the Federal Republic of Germany*
- Rancière J (2009a) *The Future of the Image*. Verso
- Rancière J (2009b) *Aesthetics and Its Discontents*, Polity, Cambridge
- Schama S (1995) *Landscape and Memory*. Vintage Books
- Spreitz A (2011) *Vom Sinfonieorchester bis zum Laienzirkel*. In: Karlsch R, Boch R (eds) *Uranbergbau im Kalten Krieg: Die Wismut im sowjetischen Atomkomplex Band 1: Studien*. Ch. Links Verlag
- Valentine B (2017) *How Can Ecological Artists Move Beyond Aesthetic Gestures?* In: Hyperallergic. <https://hyperallergic.com/394849/how-can-ecological-artists-move-beyond-aesthetic-gestures>. Accessed 7 Oct 2017
- Wismut GmbH (2011) *Kunst im Bergbau*. Die Sammlung der Wismut GmbH
- Volkskammer der DDR (1949) *Die Verfassung der Deutschen Demokratischen Republik*, in: documentArchiv.de, URL: <http://www.documentArchiv.de/ddr/verfddr1949.html>, Accessed 12 May 2018
- Volkskammer der DDR (1968) *Die Verfassung der Deutschen Demokratischen Republik*, in: documentArchiv.de, URL: <http://www.documentArchiv.de/ddr/verfddr1968.html>, Accessed 12 May 2018



Remediation of historic waste rock by injection of green liquor dregs – results from a field scale trial, Gladhammar, Southern Sweden

Lotta Sartz^{1,2}, Stefan Sädbom², Mattias Bäckström^{1,2}

¹Man-Technology-Environment Research Centre, Örebro University, 701 82 Örebro, Sweden,

lotta.sartz@oru.se

²Bergskraft Bergslagen AB, Fordonsgränd 4, 692 71 Kumla, Sweden

Abstract

Mining in Gladhammar, southern Sweden started in the 15th century, generating waste rock containing copper, cobalt, and arsenic. During remediation (2011) some waste rock was preserved, due to its geoscientific value, and placed on a geomembrane surface. Eventually, it became apparent that it had a substantial environmental impact (pH 3.8, Cu 96 mg/L, Co 21 mg/L). In 2017, green liquor dregs was injected in order to increase pH and decrease trace element mobility. Ten months after injection pH was 8.3 and concentrations of copper and cobalt 1.3 mg/L and 1.1 mg/L, respectively. Evaluation will continue for at least five years.

Keywords: Mine waste, alkaline, cobalt, copper, arsenic, pH

Introduction

Gladhammar mine in southern Sweden was mined for copper and cobalt already in the 15th century and finished in 1892. Mining resulted in waste rock containing copper, cobalt, lead, and arsenic. Remediation was performed in 2011 and waste rock was mixed with lime and deposited under water in a nearby lake. Gladhammar mining area is type locality for the three minerals Gladite ($\text{PbCuBi}_3\text{S}_9$), Hammarite ($\text{Pb}_2\text{Cu}_2\text{Bi}_4\text{S}_9$) and Lindströmite ($\text{Pb}_3\text{Cu}_3\text{Bi}_7\text{S}_{15}$) and hence, authorities decided that some waste rock should be collected and preserved due to its high geoscientific value. Representative waste rock material was collected from eight areas representing the geology at the mine site. The material was then rearranged into eight piles on a geomembrane covered surface (1 000 m²) with a well collecting all leachates. Eventually, it became apparent that the piles had a large negative impact on the environment, with acidic pH and high concentrations of cationic trace elements like copper, cobalt, and nickel.

A non-invasive remediation of waste rock at Gladhammar was needed. Preferably it should allow for continued geoscientific research and the material being accessible for mineral hunters in the future. Injection of al-

kaline materials to pre-oxidized waste rock, as a way of increasing pH within acidic waste rock piles and decrease mobility of cationic trace elements, has been developed during more than 10 years (Bäckström et al. 2011). By using alkaline injection, waste rock/acidic leachate is treated and the visual appearance of the area is unchanged. Aim with this project was to verify injection of green liquor dregs, a by-product from the pulp and paper industry, in larger scale.

Methods

Characterisation of waste rock

The waste pile in Gladhammar consists of eight separate piles of varying size (fig. 1). Prior to injection, sampling of waste rock was performed for leaching studies (50 L) and for chemical analysis and mineralogical studies, in order to determine if some of the piles contributed to a significant portion of the load from the remaining waste rock. Leaching studies were performed at liquid to solid ratio (L/S) = 1 in 50 L plastic containers. Waste rock was flooded (barely covered) with deionized water for 3 weeks, where after the overlying water phase was sampled and analyzed for pH, acidity, sulfate and major and trace elements.



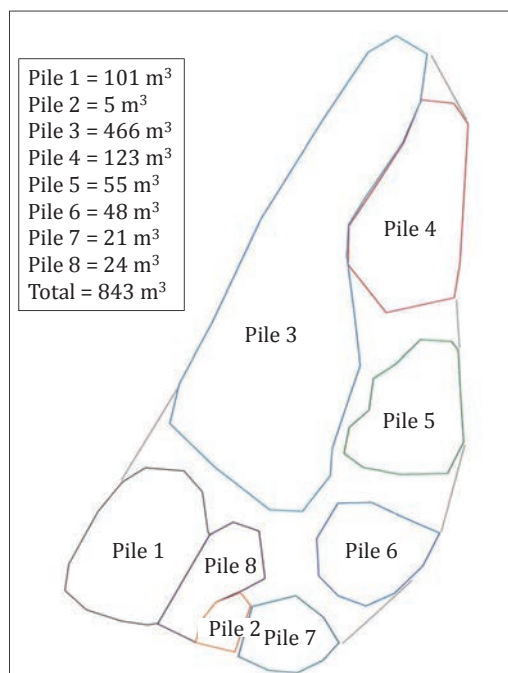


Figure 1 The waste pile consists of eight separate piles with varying size.

Analytical results are not available for the waste rock in the waste pile. Instead results from all mining waste prior to the reclamation has been used. Since the waste pile is composed of waste from the entire site this data is thought to be representative for the waste rock.

In table 1 below total concentrations are found for some selected elements in the waste rock. Results also indicate a low content of sulfur and a low buffering capacity (tab. 2).

Performed acid-base accounting indicate that a large portion of the original waste rock is acid generating (tab 2) with an average and

median NNP of -24.3 and -17.6 kg CaCO_3 /tonne, respectively.

Performed sequential extraction (Västervik municipality, 2005) also indicate that arsenic and lead is mainly associated with secondary iron phases within the weathered waste rock.

Injection

Injection was done at 99 points evenly spread over the area (fig. 2). Green liquor dreg was transported from Mönsterås pulp and paper facility and was tipped close to the waste pile. Slurry mixing was done using pan mixer

Table 1 Selection of problematic elements in waste rock at Gladhammar mining site (Västervik municipality, 2005). *Italic indicate half of the used detection limit for the analytical method used (MG-1).*

	CaO (%)	As (mg/kg dw)	Co (mg/kg dw)	Cu (mg/kg dw)	Pb (mg/kg dw)	S (mg/kg dw)
15:1	0.045	210	806	3 750	708	5 530
17:1	0.045	230	1 820	3 700	821	8 010
29:1	0.045	87.7	1 070	4 410	1 050	5 670
15:2	0.129	890	321	1 790	2 380	4 170
27:1	0.213	129	1 450	35 100	1 110	21 500
39:1	2.59	4.18	26.2	4 480	771	7 020



Table 2 Results from acid-base accounting of waste rock samples from the mining area prior to reclamation (Västervik municipality, 2005). NNP: net neutralising potential.

	pH	S (%)	NNP (kg CaCO ₃ /ton)
12:1	5.8	0.473	-12.3
15:1	6.1	0.553	-13.2
17:1	5.7	0.801	-24.4
21:1	4.9	0.845	-23.9
24:1	5.3	0.558	-14.9
26:1	5.3	2.15	-65.2
29:1	5.2	0.729	-20.3
36:1	5.4	0.252	-5.4



Figure 2 Part of the waste pile (parts of piles 3 and 4) and injection points marked.

and pumping was performed using a slurry pump. A total of 63 tonnes of dry green liquor dreg was injected.

Green liquor dreg

Green liquor dreg (GLD) is a by-product from the pulp and paper industry consisting of CaCO₃, Na₂CO₃, Na₂S and insoluble solids (Pöykiö et al. 2006; Martins et al. 2007; Nurmesniemi et al. 2005). Studies have shown

that GLD typically has low hydraulic conductivity (10⁻⁷-10⁻⁹ m/s) and is strongly alkaline (pH 11-13). Its properties suggest that GLD can be used to construct sealing layers that will prevent oxygen from entering un-oxidized mining waste. Due to its alkaline properties GLD is also a promising material to be used as neutralizer for already oxidized mining waste. GLD used in Gladhammar was transported from Södra Cell pulp and paper



Table 3 Total and leachable concentrations (mg/kg dry weight) in green liquor dreg from Södra Cell Mönsterås pulp and paper facility.

	Total	L/S 2	L/S 10
pH	12.7	10.0	10.2
Ca	190 000	NA	NA
As	<2.6	<0.040	<0.050
Co	<2.6	NA	NA
Cu	34	0.37	0.32
Pb	4.0	<0.020	<0.050
S	5 400	1 100	1 130

facility in Mönsterås. Total and leachable concentrations of the GLD are found in table 3.

Results

The piles varied significantly in size of individual pieces, mineralogical grain size, and the proportions between sulfide-, silicate-, carbonate- and secondary- minerals.

Leaching studies (50 L) implicated that one of the piles generated more acid and leached higher concentration of cobalt than the others (Pile 8, fig. 3). Pile 5 generated the highest copper concentrations, but apart from these, pH and leached concentrations of major and trace elements were fairly similar for the different piles.

During injection pH in the well draining the area increased from 3.5 to above 10, due to excess GLD being washed out. One to two months after injection pH was around 7.5 and concentrations of copper and cobalt were 38 mg/L and 4.9 mg/L, respectively.

Discussion

Follow-up measurements of leachates from the waste pile indicate a clear increase in pH (from 3.8 to 8.3), and with markedly decreased levels of cadmium (93 %), cobalt (94 %), copper (98 %), nickel (95 %), lead (99 %), and zinc (97 %). Increased concentrations have been noticed for iron and sulfate in particular, which probably has to do with acidic secondary minerals that were dissolved as pH increased. As iron started to precipitate again as oxidized iron these levels have decreased again. At the second and third sampling after injection there were significantly decreased levels of iron. To summarize, the remediation has worked very well and concentrations of the main problematic elements have decreased considerably.

Conclusions

As a whole the remediation was performed as planned and without any major technical

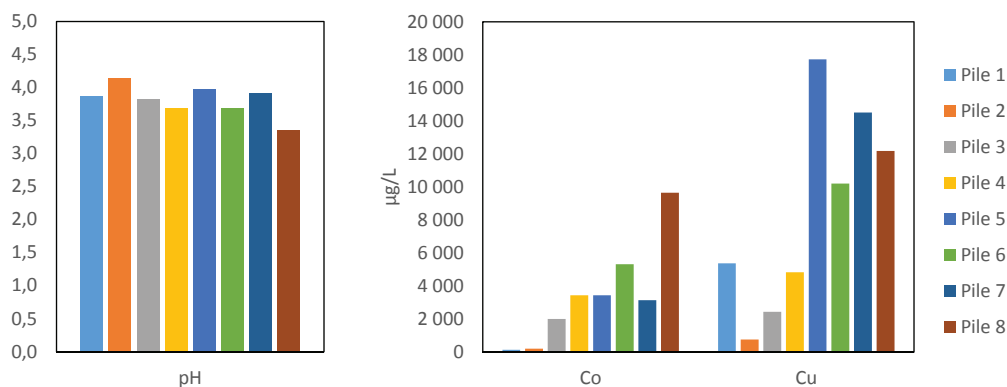


Figure 3 pH, cobalt and copper (µg/L) in leaching studies (L/S = 1) of waste rock from different parts of the waste pile (Piles 1-8).



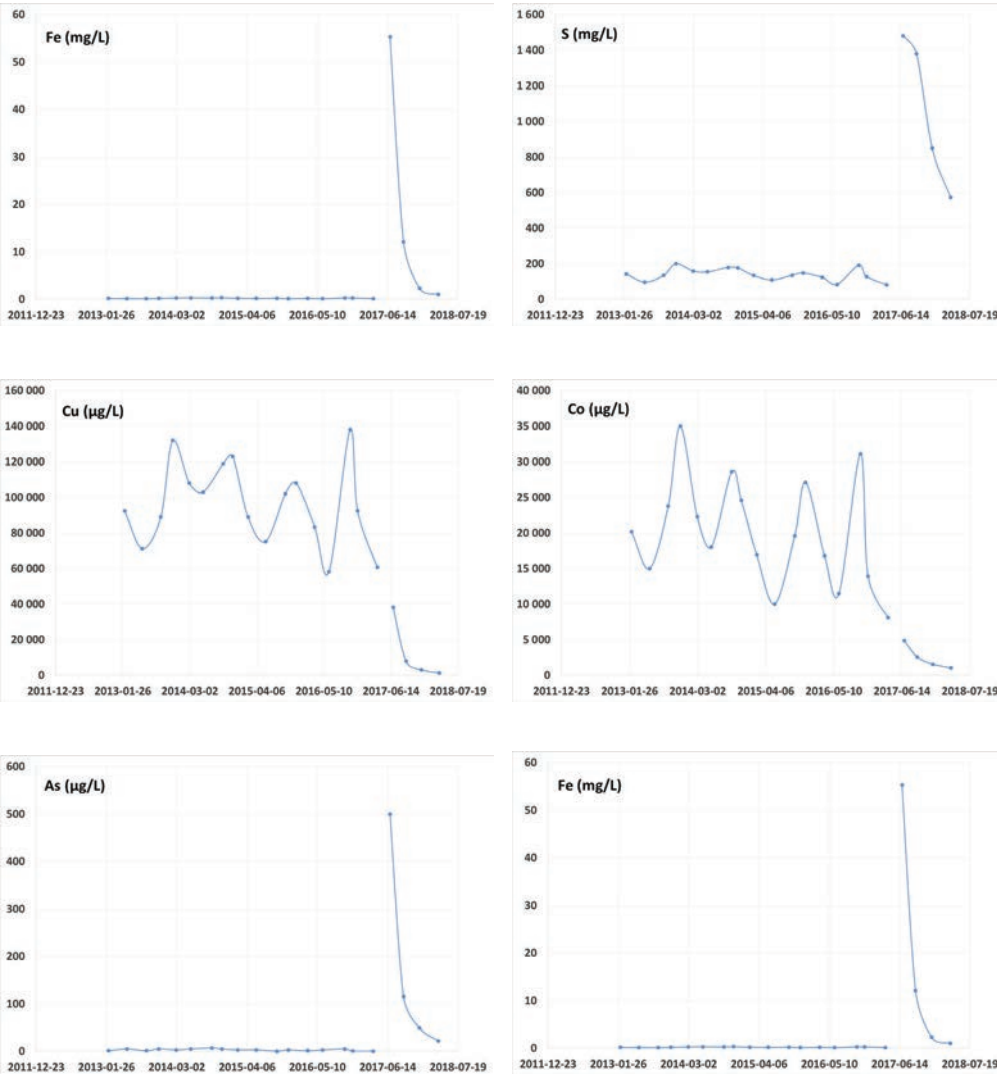


Figure 4 Selection of data from the monitoring program at the site from February 2013 to March 2018. a) pH, sulfur (mg/L), copper (µg/L), cobalt (µg/L), arsenic (µg/L) and iron (mg/L).

Table 4 Reduction or increase (%) in element concentrations for the months September, November and February/March. Comparison made between single measurements after reclamation and average concentrations (n 4 or 5) prior to the reclamation.

	September	November	February/March
Cu	-93	-97	-98
Co	-90	-94	-94
S	764	421	348
Fe	5 410	930	390
As	3 360	1 350	1 210



problems. Injection of green liquor dreg slurry increased pH in the leachates from around 3.8 to around 8.3. Concentrations of cobalt and copper were reduced with 94 and 98 %, respectively. The appearance of the waste rock did not change, which means that the waste pile is still accessible for mineral hunters and geoscientific research.

With alkaline injection, areas with cultural, historical and geological values can be treated with low visual impact and remnants can be left to all appearances intact. Evaluation of the remediation at Gladhammar will be performed by continuing measurements for at least five years. The pilot study indicates that GLD can be used for full scale applications and that it increases pH and decreases trace element concentrations.

Acknowledgements

The authors thank the Municipality of Väster-
vik (Christer Ramström and Christer Her-
mansson) for providing access to the field site
and data from the start. Sweden's Innovation
Agency (VINNOVA) is greatly acknowledged
for financial support.

References

- Bäckström M, Sartz L, Larsson E, Karlsson S (2011) Properties of alkaline materials for injection into weathered mine waste piles – methods and initial pilot trials. In: Råde RT, Freund A & Wolkersdorfer Ch; Mine Water – Managing the Challenges, p. 265–269; Aachen, Germany
- Martins FM, Martins JM, Ferracin LC, da Cunha CJ (2007) Mineral phases of green liquor dregs, slaker grits, lime mud and wood ash of a Kraft pulp and paper mill. *J Haz Mat* 147:610–617, doi:10.1016 / j.jhazmat.2007.01.057
- Nurmesniemi H, Pöykiö R, Perämäki P, Kuokkanen T (2005) The use of a sequential leaching procedure for heavy metal fractionation in green liquor dregs from a causticizing process at a pulp mill. *Chem* 61: 1475–1484, doi:10.1016 / j.chemosphere.2005.04.114
- Pöykiö R, Nurmesniemi H, Kuokkanen T, Perämäki P (2006) Green liquor dregs as an alternative neutralizing agent at a pulp mill. *Environ Chem Lett* 4:37–40, doi:10.1007/ s10311-005-0031-0
- Västervik municipality (2005) Inventering och karaktärisering av avfallen vid Gladhammars gruvor – Undersökning av utbredning, halter, vittringsbenägenhet och lakegenskaper. Projekt Gladhammars gruvor. Report 2004:03 (in Swedish)



Exploring an alternative approach to mine waste management in the South African gold sector of the article

Lesley Kudakwashe Sibanda, Jennifer Lee Broadhurst

Minerals to Metals, Department of Chemical Engineering, University of Cape Town, Private Bag X3, Rondebosch, Cape Town, South Africa, maikizie@gmail.com

Abstract

The large volumes of waste generated during gold beneficiation are a major pollution concern in South Africa. To remove these potential pollution risks in perpetuity, non-conventional approaches to mine waste management are required which avoid land disposal of “unwanted” material. This paper explores the opportunities, drivers and barriers for the re-purposing of gold waste in the South African context. The findings identify numerous opportunities for reusing gold mine tailings and tailings dumps, and highlight the interrelated factors that constrain their uptake.

Keywords: gold tailings, mine waste management, mine waste reuse

Introduction

Despite the gold industry's contribution to the national economy, the industry has been plagued by labour disputes and is widely criticized for its negative impacts on the surrounding environment and local communities (Antin 2013). Many of these impacts are associated with the land disposal of the large-volume wastes generated by the industry, which include overburden, waste rock and tailings (Bellenfant et al. 2013). In South Africa, defunct gold tailings dumps occupy large areas of land, with more than 270 mine dumps covering an area of 400km² having been identified (Oelofse et al. 2010). Many of these tailings dumps are situated in close proximity to human settlements, and typically contain reactive minerals and toxic metals, such as uranium, thus representing a significant, and often irreversible, risk to the surrounding environment and local communities (Franks et al. 2011). Of particular concern in the Witwatersrand gold basin of South Africa, is the prolonged generation of salt-laden and metal-rich acid rock drainage (ARD), formed through the exposure of sulfide minerals to air and water (Oelofse et al. 2010). These dumps are also a source of wind-blown dust, which affects the health and quality of life of surrounding communities.

To address the potential long-term risks associated with these dumps, alternate approaches to the non-conventional management of large-volume mine waste streams are required (Yellishetty et al. 2008). One alternative approach to the land disposal of large-volume mine waste entails the re-allocation of these wastes as feedstock for other uses. Such an approach is aimed at simultaneously minimising the waste burden and maximising the efficient use of mined materials, and is consistent with the principles of resource efficiency and the circular economy (Pajunen 2015). This paper presents the findings of a study to explore the opportunities, drivers and barriers for the re-purposing of gold tailings in the South African context.

Methodology

This study is based on a comprehensive review and analysis of information and data in the public domain, complimented by semi-structured interviews with nine experts and practitioners in the field of mine waste management. The findings of the research are presented below by first providing a review and analysis of the opportunities for re-purposing gold tailings material and mine dumps in South Africa, and subsequently assessing the key factors influencing the development and implementation of these opportunities.



Opportunities for gold waste utilization

From the review of literature and interviews with various experts, numerous applications for gold tailings were identified, including using tailings for making bricks, ceramics, cement, mine backfill, stone paper and as aggregate material for construction. The findings also indicated that the discarded tailings dump themselves can be used for recreation, tourism and other alternative land uses, such as for the generation of clean energy. Each of the opportunities identified is discussed briefly in the sub-sections below:

Bricks

Studies by Roy et al. (2007), Zhang and Ahmari (2014), and Kiventerä et al. (2016) have indicated that gold tailings are a viable alternate aggregate for brick making. However, all these studies have indicated that additives need to be including in the tailings brick mixture to improve the compressive strengths of the bricks, with cement resulting in the highest compressive strength and thus being the preferred additive across all studies. In South Africa, a study by (Malatse and Ndlovu 2015) evaluated the viability of using Witwatersrand gold mine tailings for brickmaking, with positive results. In addition, the interviews with experts and industry representatives indicated that the use of gold tailings for the production of bricks has been both investigated and applied on a commercial scale in South Africa. However, attempts to obtain further information from two local organisations reportedly making bricks from tailings were unsuccessful. One of the research participants (participant 2) had been involved in a project which confirmed the feasibility of using gold tailings to produce brick specimens. Participants 4 and 5 both raised concerns on the the potential radioactive nature of tailings material and stated that this would pose a significant challenge to using tailings.

Ceramics

Liu et al. (2015) assessed the technical viability of using gold mine tailings as a resource in place of clay in the production of ceramic products. The research findings showed that blending gold tailings and clay resulted in op-

timum mineral composition, particle gradation, and shaping property. Similarly, a study by Yassine et al. (2016) determined that gold tailings are a feasible alternative material for producing ceramic products. Two interviewees (participants 2 and 8) indicated that they were aware of cases of gold tailings being used to produce ceramic products in the United States. However, no evidence could be found of any attempts to produce ceramics from gold tailings in South Africa.

Cement additive

Globally, investigations on alternative binders and the production of blended cements using either industrial by-products and/or mineral additives have gained momentum (Sobolev 2003). Çelik et al. (2006) used different ratios of cement, tailings, fly ash and silica fumes for the production of Portland cement. The results revealed that gold tailings are a viable additive in the production of Portland cement, and that samples with up to 25% gold tailings within the clinker mix produced cement of the required standard in terms of comprehensive strength (Çelik et al. 2006). Although fly ash is commonly used as a cement additive within the South African construction sector, no evidence of the local use of gold tailings as a cement additive could be found.

Backfill

The use of backfill is common practice worldwide in mining operations. Research studies by Amaratunga and Yaschyshyn (1997), Benzaazoua et al. (2008) and Yilmaz (2011) have demonstrated the potential viability of using gold tailings as backfill, and the research findings suggest that tailings are a viable option. Whilst no such academic studies have been documented in South Africa, some mines make use backfill for structural stability and alleviating problems such as rock falls and rock bursts in mines (Squelch 1994). One such example of backfill operations is at the Gold Fields' South Deep Mine. The mine has a cemented tailings plant onsite and uses its own gold tailings produce backfill. This backfill is then used mainly to fill mining voids (Gold Fields 2012). Another example is at the Harmony's Target Mine which makes backfill



from a mix of cyclone tailings, cement and additives (Le Roux and du Plooy 2007).

Stone Paper

Stone paper, also referred to as mineral paper, is a novel paper type which is a blend of crushed stones and/or tailings as a substrate (80%), with polymers (20%) as a binding agent (Pauli 2012). An economic feasibility study conducted by the ZERI foundation indicated that the use of tailings is more cost-effective than crushed rock, whilst the capital costs of stone paper production are approximately 40% less than those for conventional pulp-based paper production (Pauli 2014). In South Africa, media reports suggest that the City of Johannesburg is exploring the establishment of a stone paper factory which will make use of gold railings and rubble from illegal dump sites for making stone paper (Knopjes 2015). Although participants 1 and 8 identified stone paper as a potential opportunity for gold tailings, no further information could be accessed on the development of this opportunity in the South African context.

Aggregate for road base and or construction material

The use of mining and metallurgical waste as aggregates for embankments of roadways, railways, rivers and dams has been on the rise over the past three decades (Yellishetty et al. 2008). According to Yellishetty et al. (2008), tailings as a replacement aggregate reduces the demand for natural aggregates and presents a practical solution to the environmental liabilities of tailing dams. Participants 1, 2 and 6 indicated that they were aware of cases where tailings have been used as a natural aggregate replacement in South Africa, but were unable to provide specific examples. In addition to using tailings as an aggregate for road base and construction materials, participants 2 and 6 mentioned that gold tailings are compatible for making plaster sand and paving material.

Alternative uses of defunct gold tailings dumps

Across the globe, mine sites have been repurposed for different uses such as manufacturing, industrial and residential redevelop-

ments, heritage attractions, and tourism (O'Neill 2015). Other uses that were identified include using the sites as wildlife habitats, educational, leisure and sport facilities (Pearman 2009). In South Africa, very few of these initiatives are documented, although four of the interviewees (participants 1, 4, 7 and 8) indicated that defunct tailings facilities were being used for a number of (mostly informal and unregulated) activities, including agriculture, educational tours, recreation (quad biking, skate-boarding, off-roading), as well as photo and music video shoots.

Mine waste dumps also provide large, flat areas without significant vegetation that can be used for clean energy generation. In the United States of America, a project titled “Re-Powering America’s Land” assessed the feasibility of generating wind power, solar, and hydroelectric systems on abandoned mines and contaminated land (Environmental Protection Agency 2013). As part of the project, renewable energy projects have been successfully implemented and are operating across the United States. The largest of these projects occurs in New Mexico, and generates 1 megawatt of electricity (peak output) from a total of 173 solar panels covering 21 acres. Numerous sites in Canada, Germany and the United States of America have used defunct mine land and dumps to generate clean energy (Choi and Song 2016). However, whilst participants 5 and 7 noted that generating renewable energy, specifically wind and solar energy, is a viable option and should be explored further, no energy generation on abandoned mines and tailings facility has been recorded in South Africa.

Drivers and Barriers to gold waste reuse

This section explores the key factors that both constrain and drive the uptake of the identified opportunities, namely material properties, technology, economics, corporate culture and values, and legislation.

Material properties

The physical and chemical properties of the tailings can determine its suitability as feedstock for different applications, and also give rise to specific health and environmental risks



during processing and/or utilization. In certain cases, pre-treatment to remove impurities, as well as crushing and re-sizing may be required to render the tailings suitable (Godfrey et al. 2007). According to all the participants interviewed, the major constraint to reusing gold tailings in South Africa is their potentially toxic and radioactive nature. Gold tailings typically contain potentially hazardous metals, particularly uranium, and chemicals, such as cyanide, which pose significant contamination challenges (Durand 2012; Nengovhela et al. 2006).

Technology

In South Africa, improved technology has resulted in the recovery of gold (and other minerals) from both low-grade ores and waste tailings (Gericke 2014). Whilst this provides an ideal opportunity to simultaneously re-purpose the bulk material, this has not been the case in practise and, with the exception of a few isolated cases, the gold-depleted re-processed tailings are being largely disposed of in engineered tailings dams. In line with this, participant 1 noted that whilst technological advancements have resulted in increased gold recovery from mine waste, the technology is not fully tried and tested in the case of most re-purposing options. Generally, new technology is characterized by a degree of uncertainty and there is a risk that unproven technology may not perform to the required standard and specifications, and/or be compatible to current technologies (Johnston 2012). Uncertainties and risks associated with unproven technology have been identified as a key technological barrier to mine waste utilization (Pajunen et al. 2012).

Economics

The findings of this study have revealed that economics is both an enabler and impediment to the uptake of reuse options. The escalating costs of complying with increasingly stringent legislation, particularly in terms of the land disposal of large-volume wastes, has the potential to provide financial incentives for companies to explore alternative uses (Godfrey et al. 2007). On the other hand, four participants (1, 6, 7 and 9) considered

economics as a barrier to the uptake of reuse options. This was due to the fact that reuse options are considered financially non-viable on the basis of conventional financial indicators such as IRR, due to both the high direct costs entailed and the relatively low value of the products generated. Two of the interviewees (participants 1 & 6) emphasised that the uptake of the reuse options would only occur if it is deemed to be financially viable. In addition, the participants highlighted the high costs associated with transporting tailings. This, combined with the low price of virgin aggregate currently in use, renders the reuse of tailings uneconomic and provides no further incentives to reuse tailings.

Corporate culture and values

Corporate culture, leadership and overall company strategy influence how companies are run, the way tailings are classified, the uptake of waste reuse options, and the adoption of new technologies within the organization (Pajunen 2015; Pauli 2012). According to participant 3, companies can classify tailings as either a liability or an asset, and this determines the approach to tailings management. Participant 3 argued that organizations who viewed tailings as an asset are more willing to exploring reuse options and drive innovative solutions for dealing with waste; whereas organizations that view tailings as a liability or waste are often averse to the different waste reuse opportunities and likely to opt for conventional tailings disposal. Viewing tailings as an asset requires mining companies to look beyond the core business of extracting minerals from the ground (Pauli 2012). This, according to participant 3, requires businesses to create entrepreneurial linkages and strategic partnerships with organizations that are likely to utilize the mine waste.

Legislation

An in-depth review of literature on the legislation governing mineral waste, indicates that South Africa has robust legislation, policies and strategies which are on par with international legislation. Despite the robust legislative framework, the legislation governing mine waste is fragmented across different pieces of



legislation and there is no unifying policy outlining exactly how mining waste issues need to be addressed (Adler et al. 2007). Two of the participants (1 and 7) concurred with this thinking and stated that because there no clear legislative guidelines on the procedure and requirements for reuse of mine waste in South Africa, it posed a barrier to reuse of mine waste and created confusion on the appropriate measures to be taken for reusing waste. Participant 1 also cited the inconsistency in the definition of mine waste across different pieces of legislation, and the frequent changes to legislation as barriers to mine waste reuse, as it adds more complexity and makes it difficult to know what to comply with.

Concluding remarks

A number of potential uses for gold tailings and gold tailings dumps have been identified. However, despite existing opportunities, the re-purposing of gold tailings as feedstock for other purposes is currently constrained in South Africa. Uses of defunct gold mine dumps for recreational purposes, and tailings material for brick-making, appears to be largely informal and uncontrolled. The lack of formalised application of gold tailings and dumps can be attributed to a number of inter-related factors, such as inadequate technology development, lack of an enabling legislative framework, high short-term and direct costs, potential environmental risks associated with hazardous components in the waste, as well as a traditional corporate culture which views waste as unwanted material and focuses on conventional disposal as a waste management strategy. Given these constraints, it is unlikely that there will be a significant uptake of reuse options without concerted collaborative effort between different stakeholders, underpinned by a sustained programme of Research & Development.

Acknowledgements

This work is based on research supported by the South African Water Research Commission (WRC). Any opinion, finding, conclusions or recommendation expressed in this material is that of the authors and the WRC does not accept any liability in this regard.

References

- Adler RA, Claassen M, Godfrey L, Turton AR (2007) Water, mining, and waste: an historical and economic perspective on conflict management in South Africa *The Economics of Peace and Security Journal*, 2:32-41
- Amaratunga LM, Yaschyshyn DN (1997) Development of a high fill using fine gold mill modulus tailings *Geotechnical and Geological Engineering*, 15:205-219
- Antin D (2013) *The South African Mining Sector: An Industry at a Crossroads*. Hanns Seidel Foundation,
- Bellenfant G, Guezennec AG, Bodenan F, D'Hugues P, Cassard D (2013) Reprocessing of mining waste: combining environmental management and metal recovery? Paper presented at the Mine Closure,
- Benzaazoua M, Bussiere B, Demers I, Aubertin M, Fried E, Blier A (2008) Integrated mine tailings management by combining environmental desulphurization and cemented paste backfill: Application to mine Doyon, Quebec, Canada *Minerals Engineering*
- Çelik Ö, Elbeyli IY, Piskin S (2006) Utilization of gold tailings as an additive in Portland cement Waste Management & Research 24:215–224 doi:10.1177/0734242X06064358
- Choi Y, Song J (2016) Sustainable Development of Abandoned Mine Areas Using Renewable Energy Systems: A Case Study of the Photovoltaic Potential Assessment at the Tailings Dam of Abandoned Sangdong Mine, Korea *Sustainability* 8:1320-1332
- Durand JF (2012) The impact of gold mining on the Witwatersrand on the rivers and karst system of Gauteng and North West Province, South Africa *Journal of African Earth Sciences* 68:24-33 doi:http://dx.doi.org/10.1016/j.jafrearsci.2012.03.013
- Environmental Protection Agency (2013) *New Energies: Utility-Scale Solar on a Tailing Disposal Facility Chevron Questa Mine Superfund Site in Questa, New Mexico*.
- Franks DM, Boger DV, Cote CM, Mulligan DR (2011) Sustainable development principles for the disposal of mining and mineral processing wastes *Resources Policy* 36:114–122
- Gericke M Trends and opportunities - mining and mineral waste In: DST Workshop, 2014.



- Godfrey L, Oelofse S, Phiri A, Nahman A, Hall J (2007) Mineral waste and the required governance environment to enable reuse. Council for Scientific and Industrial Research (CSIR), Pretoria
- Gold Fields (2012) South Deep Gold Mine Technical Short Form Report.
- Johnston OR (2012) Analysis of energy efficiency in South Africa's primary mineral industry: A focus on gold. University of Cape Town
- Kiventerä J, Golek L, Yliniemi J, Ferreira V, Deja J, Illikainen M (2016) Utilization of sulphidic tailings from gold mine as a raw material in geopolymerization International Journal of Mineral Processing 149:104-110
- Knopjes B (2015) Stone Paper from Rubble. Infrastructure news
- Le Roux P, du Plooy D Design Considerations for the Implementation of Tailings Based Wetcrete at Harmony's Target Mine. In: Potvin Y (ed) Proceedings of the 4th International Seminar on Deep and High Stress Mining, Perth, Australia, 7-9 November 2007. Australian Centre for Geomechanics,
- Liu R, Huang F, Du R, Chunming Zhao, Li Y, Yu H (2015) Recycling and utilisation of industrial solid waste: An explorative study on gold deposit tailings of ductile shear zone type in China Waste Management & Research 33:570-577 doi:10.1177/0734242X15584843
- Malatse M, Ndlovu S (2015) The viability of using the Witwatersrand gold mine tailings for brick-making The Journal of The Southern African Institute of Mining and Metallurgy 115:321-327
- Nengovhela A, Yibas B, Ogola J (2006) Characterisation of gold tailings dams of the Witwatersrand Basin with reference to their acid mine drainage potential, Johannesburg, South Africa Water SA 32:499 -506
- O'Neill K (2015) Bridging Mining-Scarred Landscapes and Nature- and Resource-Based Tourism and Recreation in Northern Ontario. University of Waterloo
- Oelofse S, Hobbs P, Rascher J, Cobbing J (2010) The pollution reality of gold mining waste on the Witwatersrand Resource 12:51-55
- Pajunen N (2015) Decision making towards sustainability in process industry – drivers, barriers and business opportunities. Aalto University, Finland
- Pajunen N, Watkins G, Wierink M, Heiskanen K (2012) Drivers and barriers of effective industrial material use Minerals Engineering 29 39-46
- Pauli G (2012) The Future of Manufacturing in Resource-rich Economies: How mining could generate jobs and competitiveness beyond extraction of ore Revista de Tecnología - Journal of Technology 12:8-19
- Pauli G (2014) A revolutionary production of water and tree free paper from stones and mining waste.
- Pearman G (2009) 101 Things To Do With A Hole In The Ground. Post-Mining Alliance in association with the Eden Project 2009,
- Roy S, Adhikari GR, Gupta RN (2007) Use of gold mill tailings in making bricks: a feasibility study Waste Management and Research 25:475 - 482
- Sobolev K (2003) Sustainable Development of the Cement Industry and Blended Cements to Meet Ecological Challenges The Scientific World Journal 3:308-318 doi:10.1100/tsw.2003.23
- Squelch AP (1994) The determination of the influence of backfill on rockfalls in South African gold mines. University of the Witwatersrand
- Yassine T, Benzaazoua M, Mansori M, Yvon J, Ndue Kanari, Hakkou R (2016) Manufacturing of ceramic products using calamine hydrometallurgical processing wastes Journal of Cleaner Production 127:500-510
- Yellishetty M, Karpeb V, Reddyb EH, Subhashb KN, Ranjitha PG (2008) Reuse of iron ore mineral wastes in civil engineering constructions: A case study Resources, Conservation and Recycling 52:1283-1289
- Yilmaz E (2011) Advances in reducing large volumes of environmentally harmful mine waste rocks and tailings.
- Zhang L, Ahmari S (2014) Production bricks from mine tailings through geopolymerization vol WO2014055558 A1.



Electrobiological reduction for low level selenium removal from mine water and reverse osmosis brine

Martin Williams¹, Eduardo Piñana², Ola Opara³, Jack Adams³,
Esther Fernández⁴

¹Piteau Associates, 25 Rudd Road, Illovo, Johannesburg, 2196 South Africa; mwilliams@piteau.com

²Piteau Associates, Francisco Silvela 21, 1^o, 2^a. CP 28028, Madrid, Spain; epinana@piteau.com

³INOTEC, 2712 S. 3600 W. Suite A, Salt Lake City, Utah, 84119, USA; www.inotec.us

⁴Orovalle Minerals, Planta El Valle-Boinas, 33836 Begega, Belmonte de Miranda, Asturias, Spain; efernandez@orvana.com

Abstract

Laboratory-scale assessment of an electro-biochemical reactor (EBR) system was performed to determine its potential ability to meet a 1 µg/L mine effluent threshold for selenium (Se) at the Boinás gold mine in Asturias, Spain. The EBR process is differentiated from conventional biologically-mediated reduction through the administration of a constant low µAmp-level current to overcome rate-limitations associated with electron demand. Trials performed using Boinás mine water and RO brine containing Se at 40 µg/L and >200 µg/L respectively yielded post-treatment concentrations of between 0.1 and 0.05 µg/L in mine water and <2 µg/L in RO brine. Based on these results, EBR may offer both improved performance and significant Opex savings relative to the existing reverse osmosis treatment system deployed at Boinás mine.

Keywords: Selenium, water treatment, Electro Biological Reactor (EBR), Spain.

Introduction

Las Boinás mine is located approximately 36 km west of Oviedo in Asturias, northern Spain. The mine lies in the Rio Narcea Gold Belt, in which several historical centres of gold production exist. Mineralization at Boinás is associated with acid-intermediate intrusions which were emplaced into a regional dolomite sedimentary sequence of Palaeozoic age between around 300 and 250 Ma. Two phases of mineralization are evident, the first associated with metasomatism and skarn formation along intrusive–dolomite contacts and the second with epithermal overprinting. As observed widely in the Rio Narcea Gold Belt, gold is accompanied by the metalloid elements arsenic (As) and selenium (Se), which occur both as discrete sulphides and as lattice substitutes in pyrite and copper sulphides.

The Las Boinás mine was initially developed in 1997 by Río Narcea Gold Mines (RNGM). The property was later acquired by Orovalle Minerals, who commenced production in 2011. Mining is undertaken exclusively by underground methods. Due to the

juxtaposition of the ore-zones against a high-yield dolomite aquifer, continuous dewatering of the mine is required at rates which typically exceed 100 L/s. This is achieved by a combination of dewatering wells completed in the dolomite and sumps within the underground workings.

Boinás mine water is of near-neutral pH and low (<1000 mg/L) total dissolved solids (TDS). However, levels of Se and As in water discharged from sumps in the ‘Boinás Este’ sector of the mine are commonly in the ranges 40 – 160 µg/L and 0.15 to 0.4 mg/L respectively. This precludes direct environmental without treatment as Orovalle is required to comply with criteria of 1 µg/L and 0.1 mg/L for Se and As respectively. While concerted effort is made by Orovalle to consume non-compliant mine water as process plant make-up, an excess of the order of 30 L/s must typically be treated and discharged to neutralize the overall mine water balance.

Orovalle currently operates a two-stage system for treatment water from the Boinas Este sector of the mine, plus contact water

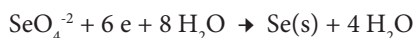


from two waste rock storage areas. The first stage consists of an ACTIFLO unit for sediment removal and clarification, with the second deploying reverse osmosis (RO). Two limitations are associated with the current treatment system. Firstly, its design capacity of 60 m³/h is insufficient to treat the flows discharged from the underground mine and waste rock facility source-terms. Secondly, RO brine is generated at an average volume equating to 21% of the RO feed. The discharge of brine to the Boinás tailings storage facility (TSF) produces a positive water balance and attendant build-up of solution inventory in the TSF.

In 2016, Orovalle initiated screening of technology alternatives which may be of utility to meet one or more of the following objectives: (i) supplementation of existing RO capacity, (ii) replacement of RO to avert the impact of RO brine disposal on the TSF water balance, and (iii) treatment of RO brine to a quality which would permit discharge in conjunction with RO permeate. An electro-biochemical reactor (EBR) system was identified as potentially applicable to the flow rate, feed chemistry and broader site characteristics of the Boinás setting. This paper describes the design, results and practical implications of bench-scale testing of EBR for the treatment of Boinás mine water and RO brine performed in 2017.

Principles of electro-biochemical reactor system

Biologically-mediated reduction and attendant immobilization of several metals and metalloids may occur in virtually any aqueous environment in which anaerobic conditions are established and residual organic carbon is available. In the decomposition of organic matter, consumption of O₂ is succeeded by reduction of NO₃⁻, SO₄²⁻ and metals/metalloids, including Se, which provide electron acceptors. In the case of Se, the reaction can be expressed as:



In the above reaction, six electrons are required to reduce one mole selenite to elemental Se. In conventional anaerobic treatment systems, the supply of electrons exerts

the critical rate-control. EBR overcomes this through the application of a low voltage (1 to 3V), micro-amp level current through the reactor cell. In addition to reducing the sensitivity of the system to its nutrient (principally glucose) balance, the application of a direct electron stream inhibits efficiency fluctuations associated with temperature and pH/Eh regime.

The mechanisms of removal of contaminants from solution in the EBR process are essentially the same as those operative in any anaerobic cell and involve the biochemical reduction of SO₄²⁻, metals and metalloids to low mobility metal sulphides, or to an insoluble elemental-state. The efficiency of reduction of any specific target element is, however, highly dependent on the redox potential at which the reactor cell is operated, the make-up of the microbial population present and the range of competing ‘reducible solutes’ in the influent water. This necessitates that any EBR system is judiciously optimized to meet the requirements of water to be treated on a site-specific basis.

Methods

Structure of laboratory investigation

Laboratory scale testing of the viability of EBR treatment for Boinás Mine water and RO brine was undertaken over the period May to November 2017 at the INOTEC laboratory in Utah, USA. The test program comprised two principal phases of investigation:

1. Assessment of the suitability of the mine water and brine solutions for treatment in an EBR cell, as dictated by multi-element chemistry, the presence of potential microbial toxins and competing ions.
2. Assessment of performance efficiency under variable conditions of EBR cell operation with respect to hydraulic residence time (HRT), temperature and nutrient dosing regimen.

Sample sources

For each of the two phases of laboratory assessment, stock solutions were collected from (a) the outflow from the ACTIFLO system at the Boinás water treatment plant, and (b) the reject stream of the second of the two-stage RO configuration operated at Boinás. Trans-



port of samples to INOTEC was undertaken prior to each of the two phases of investigation to avert any requirement for prolonged storage and associated risk of chemical or microbiological alteration. Sub-samples were subject to chemical analysis prior to shipment and on receipt by INOTEC. Variability between the Phase 1 and 2 sample consignments, and also between pre- and post-shipment analytical data, was found to be minimal (<5%) for all parameters with the exception of dissolved oxygen and ORP. Table 1 provides a summary of the composition of the Phase 1 stock solutions, as reported following analysis by INOTEC.

The mine water and brine Se concentrations shown in Table 1 are typical of those reporting to the RO stage of treatment and discharged in the reject stream in the existing Boinás plant. Concentrations of As shown for the mine water in Table 1 are, however, significantly lower than those in the mine dewatering stream. This reflects the collection of the mine water stock solution from the point of discharge of the ACTIFLO plant which feeds

the Boinás RO system. In conjunction with sediment removal, the addition of flocculant in the ACTIFLO circuit typically removes up to 90% of the As load from the influent water.

Treatability assessment and microbial screening

Water quality data shown in Table 1 were screened to assess the presence of solutes which may inhibit the establishment of a suitable microbial population in an EBR cell, or which may adversely impact the immobilization of Se through competitive consumption of nutrients and electrons. Typical microbial toxins in mine waters with respect to anaerobic treatment systems include cyanide species and chloride. These were confirmed to occur at concentrations of no practical significance.

Targeting of Se in anaerobic treatment systems, and in particular avoidance of competitive effects arising from SO_4^{2-} reduction, can be achieved through establishing a redox condition adequate to induce Se reduction without further progression through the sequence of electron acceptors which assume

Table 1 Chemical composition of Boinas mine water and RO brine used for EBR performance trials

Parameter	Mine water	RO brine
Dissolved oxygen (mg/L)	4.30	3.91
Electrical cond. ($\mu\text{S}/\text{cm}$)	851	6370
pH	8.02	7.74
CN total (mg/L)	<0.001	<0.001
Salinity (%)	0.43	3.18
$\text{NO}_3\text{-N}$ (mg/L)	1.13	11.31
$\text{NO}_2\text{-N}$ (mg/L)	<0.003	<1.5
Alkalinity (mg/L CaCO_3)	>300	>300
Cl^- (mg/L)	17.9	290
SO_4^{2-} (mg/L)	271	2680
Al (mg/L)	<0.005	<0.005
As (mg/L)	0.024	0.197
Ba (mg/L)	0.076	0.643
Cd (mg/L)	0.001	0.002
Ca (mg/L)	98	1061
Cu (mg/L)	0.008	0.10
Fe (mg/L)	<0.02	0.152
Mg (mg/L)	55.2	547
Mn (mg/L)	0.026	0.25
Ni (mg/L)	0.003	0.034
Pb (mg/L)	<0.005	0.007
Se ($\mu\text{g}/\text{L}$)	46	625
Na (mg/L)	9.3	48.6
Zn (mg/L)	0.026	0.49



dominance at lower Eh. This is not, however, possible with respect to NO_3^- , which constitutes the primary competing solute in most mine waters. The concentrations of NO_3^- recorded in Boinás mine water (1.13 mg/L) and RO brine (11.3 mg/L) are, however, well within the range demonstrated through independent EBR trials to permit uninhibited Se removal.

Microbial screening of the Boinás mine water and RO brine, performed to discriminate the production of elemental Se, indicated that the autochthonous microbial population in the waters possesses substantial capacity to mediate Se reduction. Selected microbes from both solutions were nonetheless used to cultivate biofilms for prospective EBR system inoculation if necessary.

Steady and transient-state treatment trials

Steady- and transient-state testing of the EBR process for removal of Se from Las Boinás mine water and RO brine was performed at INOTEC using identical sets of two in-sequence EBR cells. Each pair of cells was continuously supplied with mine water or RO brine using a peristaltic pump over a total test period of 115 days. A continuous current of approximately 3V was applied to each cell for the duration of the test period.

The overall period of testing was subdivided into three principal phases, as summarized in Table 2. The first, referred to as the ‘validation period’, was intended to define

the level of Se removal efficiency achievable under near-optimum conditions of nutrient dosing. Flow rates into the EBR cells were maintained throughout the validation period such that a total of 8 hours HRT could be accommodated in each of the two cells. Subsequent phases of the testing were dedicated to assessing EBR system performance sensitivity to transient conditions of nutrient dosing and HRT.

Throughout the test period, analysis of influent feed solution was performed at approximately weekly intervals to confirm consistency. Effluent analysis for each cell was performed at 2 to 3 day intervals for Se and at weekly to bi-weekly intervals for SO_4^{2-} plus a full suite of metals (by ICP-MS). Physico-chemical parameters (pH, temperature, ORP and EC) were recorded continuously.

Results

Selenium removal from mine water

Influent and effluent Se concentrations in the EBR cell pair deployed for treatment of Boinás mine water during the first 40 days of the test program are shown in Figure 2. Data for the first 7 days of the test were not compiled as the system is initially inherently unstable with respect redox condition and microbial productivity. By day 11, concentrations of Se in effluent were reduced from by more than a factor of 100 relative to the feed, with residual Se levels of around 0.3 $\mu\text{g/L}$. Such levels were sustained in effluent from cell throughout the

Table 2 Summary of EBR test protocol and operating variables during test duration

Test week	Test phase	Description	Conditions	Variable adjustment
1 to 4	Validation	Assessment of EBR removal efficiency for Se and other solutes under stable conditions	Iterative adjustment to produce optimum operating environment	No adjustment following initial optimization
5 to 9	Nutrient stress testing	Assessment of EBR performance sensitivity to changes of nutrient dosing regime.	Progressive reduction of nutrient dose rate until point of significant performance degradation reached	Nutrient concentration
10 – 16	HRT optimization	Assessment of sensitivity of treatment efficiency to hydraulic residence time	Progressive increase of treatment flow rate until significant degradation of performance efficiency observed.	Flow rate



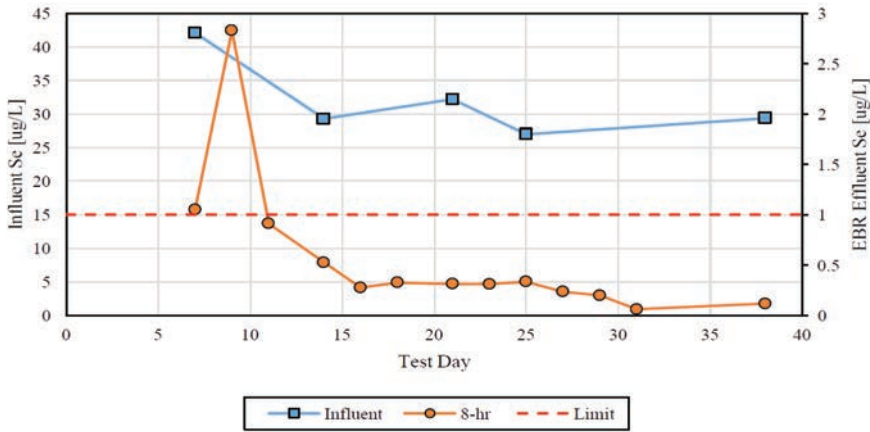


Figure 2 Inflow and effluent Se concentrations during the validation phase of EBR testing of treatment of Boinás mine water

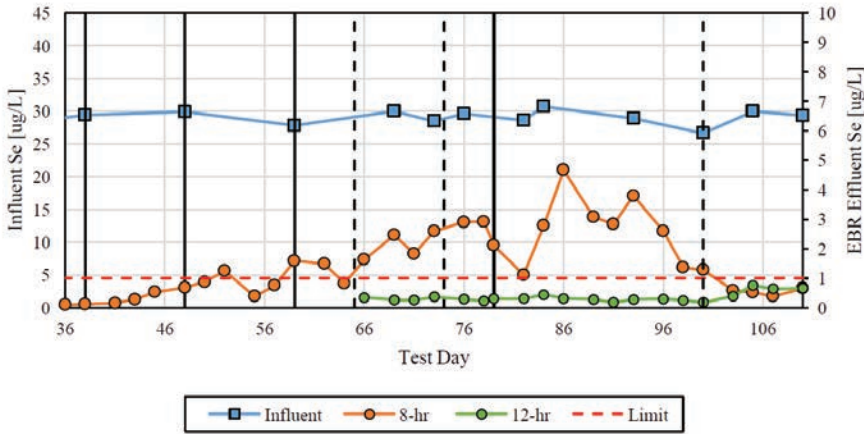


Figure 3 Inflow and effluent Se concentrations during the stress testing phase of EBR assessment for Boinás mine water. Solid vertical lines indicate points of step-wise reduction of nutrient dosing rates. Dashed vertical lines indicate points of step-wise reduction of HRT.

remainder of the validation period. The flow rate throughout this period was set such that cell 1 HRT was consistently 8 hours.

Results of EBR performance in the treatment of Boinás mine water under transient conditions of nutrient dosing regime and HRT, introduced with effect from day 38 of the test sequence, are shown in Figure 3. Nutrient dose reduction was undertaken in four steps. Following the second of these, involving a 50% reduction from an initial level of around 5 g/L molasses at day 58, effluent Se levels transgressed the 1 µg/L design requirement following 8 hours of EBR cell residence time. At 12 hours HRT, sensitivity to nutrient regimen remained low. Average 12 hour HRT

effluent concentrations of Se throughout the stress period were 0.29 µg/L across a molasses dosing range from >5 g/L to as little as 1.8 mg/L.

Selenium removal from RO brine

Results of EBR treatment of RO brine during the first 40 days of the test program are shown in Figure 4. Following initial stabilization, the effluent Se concentration at day 11 was 1 µg/L at 8 hours HRT. Over the remainder of the validation period, effluent Se concentrations remained below 3 µg/L at 8 hours HRT. At 16 hours HRT, concentrations in treated brine effluent remained systematically below 1 µg/L with effect from day 16.



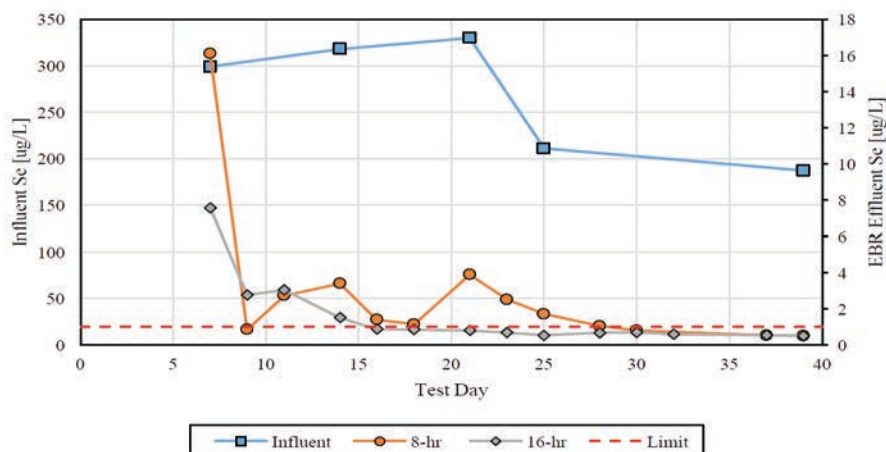


Figure 4 Inflow and effluent Se concentrations during the validation phase of EBR testing of treatment of Boinás RO brine

During the remainder of the 115 day test period, EBR sensitivity to nutrient dosing and HRT variations appeared closely analogous to that described for the treatment of mine water, with deterioration of performance associated with reduced nutrient supplementation at 8 hours HRT and minimal influence exerted at 15 hours HRT.

Removal of other solutes

Multi-element analysis of feed and effluent chemistry for the mine water and RO brine EBR cells confirmed excellent performance in the removal of a range of other solutes. These included NO_3^- , As, Cu, Ni and Zn for which average concentrations reductions of >60%, >90%, >90%, 50% and 75% respectively were observed in both the mine water and RO brine EBR cells at 16 hours HRT.

Conclusions

Results of laboratory testing of EBR for removal of Se from Boinás mine water confirm its capacity to meet the strict 1 µg/L compliance criterion applicable in discharge from the mine. Treatment of RO brine to a residual Se level apt for blending into treated RO permeate prior to environmental discharge is also indicated to be feasible. Using an 8 hour HRT design criterion, preliminary cost estimates for a full scale plant suggest that Capex would compare favourably with the provision of expanded RO capacity at Boinás, while Opex costs for water treatment using EBR would be around 50% of those associated with RO.

Acknowledgements

The authors thank Orovalle Minerals for permission to publish this paper.



Lagniappe





—A

Adam, Katerina	381
Adams, Jack	1136
Adeniyi, Amos	188
Adjie, Wisjnoe	611
Åhlgren, Kristina	782
Alakangas, Lena	351, 617, 723
Alangari, Abdullah	1036
Alipour, Mahmoud	1011
Amaral Filho, Juarez	417
Amos, Adeniyi	177
Amos, Richard T	458, 487
Annandale, John George	239, 916
Atanasova, Maria	171
Aubé, Bernard	971, 983
Aubel, Tim	83, 899

—B

Bäckström, Mattias	782, 1124
Badhuraḥman, Abie	611
Bai, Haibo	1001
Bain, Jeff	579
Baker, Andy	808
Balding, Barry	585
Baldwin, Susan	258
Banga, Chantal Mbala	859
Bannister, Alyson	84
Banuelos, Jaime	641
Barabash, Sarah	692
Barnard, Philip	476, 685
Barnes, Samantha	303
Becker, Megan	309, 345, 424
Bell, David	116
Bellenfant, Gaël	27
Ben Ali, Housseḡ Eddine	245
Benghiat, Phil	791
Benthaus, Friedrich-Carl	199
Berezina, Olga	406
BéruBé, Kelly	757
Bezuidenhout, Nico	660
Bilek, Felix	210
Billström, Kjell	723
Bird, Graham	611
Blanchette, Melanie Lise	34
Blowes, David	458, 487, 579
Boland, Martin Paul	791
Bonner, Ricky	977
Bowell, Rob	84, 91, 315, 321, 501, 757

Brabham, Peter	84
Bracke, Rolf	375, 1057
Bradshaw, Dee	309, 345, 424
Brink, Hendrik Gideon	911
Broadhurst, Jennifer	309, 345, 417, 424, 565, 820, 1130
Broemme, Katrin	97
Brömmme, Katrin	210
Brookes, Freddy	328
Brown, Adrian	1029
Bunting, Lindsey	641
Burgess, Jo	239
Burke, Jacqueline	797
Bush, Richard	629
Bussière, Bruno	559
Bussmann, Gregor	375, 1057
Byrne, Patrick	843, 1049

—C

Caldwell, Robert John	369
Campbell, Sam	629
Castendyk, Devin	1036
Castillo, Julio	893
Charikinya, Edson	309
Cheng, Hong	109
Chimhanda, Wadzanai	591
Chimuka, Luke	103, 1111
Chiodza, Godknows Kudzai	1042
Christenson, Hana	204, 430, 573
Clark, Cal	518
Coetzee, Henk	146, 171, 803, 838
Collins, Kevin	9
Cook, Diana	579
Cooke, David R	1075
Cote, Patrick	1036
Cotillas, Salvador	267
Cox, Nick	288
Craw, Dave	80, 573
Crozier, Trevor	579, 623, 666
Cui, Siyuan	738
Cukrowska, Ewa	103, 1111
Cullen, Jeff	1049

—D

Dagenais, Anne-Marie	559
Daley, Stuart	791
Danehy, Timothy	151
David, Katarina	808
Davies, Susan	288





Davis, Jane	826	Garrick, Hollie	339
De Los Hoyos, Camilo	321, 501	Gaspar, Christopher	579, 623, 666
de Wit, Maarten	553, 838	Gault, Andrew	121, 763
Declercq, Julien	321, 501	Gautama, Rudy Sayoga	604, 611
deJager, Pieter Christiaan	916	Gebrekrastos, Robel	1005
Demenev, Artem	406	Geddis, Michael	1105
Deng, Jinxun	109	Gericke, Mariekie	114, 164
Dent, Julia	3, 442	Germishuizen, Charne	977
Devoy, Cora Ann	9	Girard, Romain	339
Digges La Touche, Gareth	328, 339, 585	Glasson, Kate	17
Digges La Touche, Susan	585	Glombitza, Franz	899
Dingley, Karen	865	Gomes, Patrick Botsch Cellette	221
Do, Hao Hong	871	Gomez-Arias, Alba	893
Dold, Bernhard	723	Goodman, William Mario	507
Dong, Shuning	815	Gordon, Kerry	430
Draba, Bakary	3	Gossen, Jake	705
Drummond, Ashton	133, 182, 275, 993	Govender-Opitz, Elaine	1087
du Plessis, H Meiring	239	Govender-Ragubeer, Yageshni	215
du Preez, Kerri	114, 215	Greassidis, Sandra	97
Du, Bin	1001	Green, Ros	17
Durocher, Jennifer Lee	717	Grewar, Tamsyn	1056
Duthe, Diana Mary	591	Griffith, Ruth	321
		Grobler, Nico	507
		Guimarães, Sara	452
		Gumbo, Jabulani Ray	392
		Guseva, Olga	345

__E

Eary, L.E. {Ted}	1081
Evans, Lee	878

__F

Fagan-Endres, Marijke	399, 1042
Faithful, John	252, 1063
Ferguson, Tony	949
Fernandes, António	452
Ferreira, Diana	452
Ferreira, Juliene	481
Filiatreault, Pierre	1036
Fiúza, António	452
Forbes, Amanda	21
Forbes, Emma	116
Fosso-Kankeu, Elvis	332
Foster, Jennifer	518
Fourie, Johan	884
Fox, Nathan	949, 1075
Franzsen, Sebastian	977
Frau, Ilaria	1049
Frazier, William	629
Friesen, Vanessa	121
Frör, Oliver	871

__G

Gabora, Michael M.	41
Gałuszka, Agnieszka	598, 672
Gandy, Catherine	826
Gao, Shang	738

__H

Hahn, Florian	375, 1057
Häkkinen, Antti	267
Hällström, Lina	351
Hamai, Takaya	128
Hamberg, Roger	617
Hammond, Andrew Michael	133, 275, 993
Harck, Terry Richard	357
Harkin, Colm	34
Harley, Andrew	363
Harrington, Jim	121
Harris, Anthony	1075
Harrison, Sue	140, 309, 345, 399, 424, 541, 565, 820, 1042, 1069, 1087
Hatam, Ido	258
Hayashi, Kentaro	128
Hayes, Eoghan	339
Hayward, April	252, 1063
Heikkinen, Eero	654
Helsen, Jordi	579, 623, 666
Hendrickx, Jan	1105
Herrell, Michael Keith	252, 1063
Hessler, Tomas	1069
Hill, Bryce	1036
Hill, Roger	949
Hofmann, Harald	221
Holland, Martin	512





Huddy, Robert	140, 399, 1069	Komulainen, Jere Johannes	654
Hudson, Amy L	363	Korostynska, Olga	1049
Hudson, Carla	282	Kotsiopoulos, Athanasios	541
Hudson-Edwards, Karen A.	843	Kotze, Izak	1111
Hunt, Christopher	843	Kristina, Skeries	1063
		Kusuma, Ginting Jalu	604, 611
I		Kyllönen, Hanna	157
Ignacy, Roman	375, 1057		
Ingri, Johan	723	L	
Irwin, Robert	369	Labuschagne, Pieter	884
		Lacasa, Engracia	267
J		Lahdenperä, Esko	387
Jackson, Laura Marie	1075	Lamares, Moacir	971, 983
Jacob, Jérôme	27	Landers, Matt	21
Jagert, Felix	375, 1057	Langman, Jeff B.	487
Janneck, Eberhard	83, 899	Larsen, Morten Birch	529
Jarvis, Adam	826	Lattin, Daniel	641
Javani, Hossein	295	Laubrich, Jan	833
Jenk, Ulf	411	Lazaro, Paloma	956
Jensen, Soren Ross	518	Le Petit, Mark	481
Jewiss, Carrie Sara	80	Lee, Steven	17
Jia, Yu	529	Leishman, William	1036
Joensen, Sigga	529	Lemière, Bruno	27
Johns, Justin	573	Letjiane, Leny	904
Johnson, Brent C.	1081	Letourneau, Yanick	559
Johnson, Raymond H.	629	Li, Hao	1001
Johnstone, Andrew	647, 679	Li, Jianhua	109
Jones, Jason	21	Lima, Geraldo	481
Jones, Tim	84, 757	Liu, Jiawei	465
		Liu, Yun	940
K		Liu, Zaibin	815
Kaartinen, Tommi	157	Lone Sang, Stéphan	971, 983
Kangas, Petteri	157	Long, Chazanne	838
Kassahun, Andrea	635	Lorentz, Simon	471, 535
Kawali, Liisa	591	Lottreaux, Gareth	524
Keenan, Brian	585	Love, David	660
Keller, Jason	641, 1105	Low, Megan	1093
Kelly, Ben	231	Lucke, Beate	199
Kemppainen, Kimmo	923	Lund, Mark Andrew	34
Kennedy, Lizel	647	Lupankwa, Keretia	660
Kessopersadh, Colleen	1011	Lusambo, Victor	757
Khmurchik, Vadim	406	Lusunzi, Rudzani	392
Kiipula, Kaisa	157		
Killenberg, Arvid	899	M	
King, Karen Nicole	524	Ma, Dan	1001
Kleiber, Chris	17	Mabuka, Thabo	1087
Klingelhöfer, Heinz Eckart	859	Macniks, Jéssica	481
Kluza, Anna	878	Maddocks, Greg	21, 231
Kobayashi, Mikio	128	Maharajh, Dheepak	114
Kober, Eugen	83	Mahomed, Ismail	1011
Koiranen, Tuomas	387	Makaula, Didi Xhanti	399
Kojima, Kazuhiro	128	Maksimainen, Tomi	339
Kollias, Konstantinos	381	Maksimovich, Nikolai	406





Maleke, Maleke	893	Nairn, Robert W.	151, 849
Mamelkina, Maria A.	267	Nappa, Marja	157
Man, Malcolm	1093	Neale, John William	164
Mandaran, Kristian	21	Neculita, Carmen Mihaela	245
Mann, Vanessa	579, 623	Neely, Cody	151
Maqsoud, Abdelkadir	245	Nepomuceno, Alessandro	52
Maraïs, Tynan Steven	140	Newman, Nigel	573
Marcellin, Esteban	940	Nicholson, Ronald Vincent	692
Maree, Johannes Philippus	904, 911	Nigel, Newman	430
Marrero, Diego Alejandro	501	Nigéus, Susanne Pia Teresia	57
Martin, Alan J.	579, 623, 666	Nkansah-Boadu, Frank	258
Martin, Nicholas D.	41	Noel, Marie-Christine	518
Martindale, Richard	303	Novhe, Ntshengedzeni Obed	146, 171
Martinsson, Olof	351, 723	Novy, Lukas	252, 1063
Marton, Richard	447	Ntholi, Thakane	553
Masaki, Yusei	128	Ntlhabane, Sithembiso	309
Mashalane, Tlou Betty	146, 171	Nucifora, Candice	21
Masindi, Vhahangwele	911, 1099		
Mason, Alex	1049	— O	
Mason, Kathy	204	O’Kane, Michael	447
Masuda, Nobuyuki	128	Obed, Novhe	392
Mathur, Shilika	9	Ochieng, Levi	103, 699
Maurice, Christian	57, 617	Onnis, Patrizia	843
Maynard, Ben	949	Onyango, Maurice S.	177, 188
Mazaheri, Nader	295	Opara, Ola	1136
Mazzetti, Anne	204	Opitz, Alexander	345, 424
Mbaya, Richard	188	Orme, Patrick	826
McDonald, Grant	204	Osborne, Antony	507
McDonald, Johann	535	Oyewo, Opeyemi	177, 188
McGeeney, Dayna	808		
Mendoza, Carl	579, 623, 666	— P	
Metschies, Thomas	411	Pajarre, Risto	157
Migaszewski, Zdzisław Maksymilian	598, 672	Palitzsch, Wolfram	899
Milczarek, Michael	641, 1105	Pamplona, Jorge	751
Mjonono, Donald	541	Papassiopi, Nymphodora	381
Mokhahlane, Lehlohonolo	47	Papini, Gerry	705
Molson, John W.	245	Parbhakar-Fox, Anita	949, 1075
Moore, Oliver	611	Parent, Genevieve	579, 623, 666
Moore, Scott	641	Partey, Frederick	1105
Moorhouse, Arabella ML	769	Paszkowski, Dawn	579, 666
Morris, Sarah	629	Paul, Michael	411, 635
Morton, Kym Lesley	548, 1017	Perkins, William	611
Mosai, Alseno Kagiso	1111	Petschel, Brendan Emil	182
Moyo, Annah	417	Picken, Päivi	654
Mpetle, Matsatsi	679	Pierce, Ben	705
Mtombeni, Tabani	904	Pikkarainen, Tuomo	923
Muedi, Khathutshelo Lilith	911	Pinana, Eduardo	1136
Mühlbauer, Ritva	164	Pope, James	80, 116, 204, 430, 573
Mukwena, Tafadzwa	283	Potter, Hugh	826
Mylona, Evangelia	381	Pouliot, Sandra	559
		Pretorius, Freek	884
— N		Provost, Heather	579, 666
Naicker, Koovila	476, 685	Puell, Jorge	956
Naidoo, Roxanne	215	Puhalovich, Alan Anton	436, 711





Pujiantoro, Eko
Pyankov, Sergey

__R

Ramakuela, Mashudu
Ramothole, Phalakwane
Redelinghuys, Johannes
Reyes, Rene
Richardson, Doc
Robertson, Alan McLeod
Robertson, Cameron
Robertson, Lindsay Anne
Rodrigo, Manuel A.
Roetting, Tobias S
Rohal, Pamela A.
Rolle, Jessica
Rosemann, Robert
Ruhland, Grit
Russell, James

604
406

188
904
332
442
363
231
121
717
267
442
1081
83
833
1117
579, 623, 666

Smith, Leslie
Soares, Adriano Marcio
Sousa, Rayssa Garcia
Southam, Gordon
Sowanaka, Masahiro
Sparrow, Ben
Squire, Russel
Stander, Helene-Marie
Stastna, Marek
Steinepreis, Mark David
Stephen, Newman
Steyn, Jarmi
Stirling, Jim
Stolpe, Harro
Stott, Tim
Straight, Brian
Sui, Wanghua
Sukati, Bonokwakhe Hezekiel
Sun, Yajun
Szczepiński, Jacek

487
934
493
940
128
1093
204
565
458
458
21
884
692
97
843
1036
465
916
74, 738
744

__S

Sädbom, Stefan
Safari, Fatemeh
Sakata, Takeshi
Salifu, Musah
Salmon, David Anthony
Salmon, Ursula
Santos, Renata
Sapsford, Devin
Sartz, Lotta
Sato, Yuki
Satterley, Christopher James
Savinova, Ekaterina
Schabronath, Christoph Alexander
Schmidt, Roxane
Schönherr, Petra
Schubert, Volker
Sedinin, Alexey
Sego, David C.
Seidel, Torsten
Serrano, Antonio
Shaw, Sean
Shepherd, Nicholas L.
Sheppard, Ian
Shingwenyana, Rhulani
Sibanda, Lesley Kudakwashe
Sidenko, Nikolay V.
Sillanpää, Mika
Silva, Marco Antonio
Simair, Monique
Sitjá y Balbastro, Juan Martín
Sjöberg, Viktor
Skinner, Sarah Jane Wolfe
Slatter-Christie, Kerry

1124
295
128
723
64
447
452
315
1124
128
288
1075
193
884
899
899
406
487
1057
940
692
151, 849
231
1099
1130
729
267
493
121
501
782
733
820

Tafoya, Kara
Takaluoma, Esther
Tanner, Phil
Taylor, Jon
Terrusi, Lisa
Thorn, Peter
Tigar, Aaron
Timms, Wendy
Totsche, Oliver
Tremblay, Gilles
Trinh, Viet Quoc
Trumm, Dave
Trusler, Graham
Tutu, Hlanganani
Tuunila, Ritva

629
923
239, 916
258
17
288
629
808
199
962
97, 871
116, 204, 430, 573
1005
103, 1111
267

__T

__U

Ulbricht, Antje
Usher, Brent

210
717

__V

Vadapalli, Viswanath Ravi Kumar
Vaezihir, Abdorreza
Vaittinen, Tiina
Valente, Teresa Maria
Van Aardt, Joanne Michelle
van Berk†, Wolfgang
Van Der Merwe, Hayley
Van Der Walt, Jeremia Jesaja
Van der Walt, Mias
Van Dyk, Deon

171
295
654
751
757
411
929
283
929
507





van Heerden, Esta	893	Witthüser, Kai Thorsten	512
van Hille, Robert Paul	140	Wolkersdorfer, Christian	146, 171, 177, 859, 1024
Van Tol, Johan	471	Woloshyn, Kai Skyler	763
Van Zyl, Albert	476, 685	Wrong, Linda Ann	9
Vandenbergh, Jerry	252, 1063	Wyatt, Lee M	769
Vasconcelos, Flavio de Moraes	493, 934	Wylie, Steve	1049
Vaughan, James	940	Wyman, Valentina	940
Verger, Robert Paul	884		
Vermeulen, Danie	775, 893	__X	
Vila, Maria Cristina	452	Xenidis, Anthimos	381
Vilela, Fernando	481	Xu, Ying	109
Villa Gomez, Denys	221, 940	Xu, Zhimin	74, 738
Voigt, Marcelene	309		
von Hünefeld-Mugova, Elke	1024	__Y	
__W		Yang, Binbin	465
Wang, Changshen	70	Yibas, Bisrat	146, 171, 392
Watson, Ian A	769	Yohannes, Rezene	791
Watson, Kerry	204		
Weber, Lutz	899	__Z	
Welman-Purchase, Megan	893	Zagury, Gérald J.	245
White, Jamie	791	Zanetti, Caroline Sant'Ana	493, 934
Williams, David	221	Zhan, Guosheng	641
Williams, Martin	3, 1136	Zhang, Chenming	221
Wilson, David	487	Zhang, Chong	109
Wilson, Gordon Ward	458	Zhang, Mengfei	74
Wilson, Ward	21, 559	Zhou, Genmao	109
Wisnugroho, Pajar Hariadi	604	Zielke-Olivier, Josepha Simone Doris Renate	775





16S rRNA metagenomics

1069

A

accurate detection

815

acid and/or metalliferous drainage

447

Acid Base Accounting

47, 369, 392

acid drainages

893

acid forming

52

acid mine drainage

34, 84, 116, 171, 204, 215,

221, 381, 392, 541, 598, 911,

983, 1024, 1099, 1130

Acid mine water

406, 553

acid neutralization capacity

52

Acid rock drainage (ARD)

859

acid rock drainage

47, 52, 452, 692, 751,

763, 962

acid

188

acidic conditions

103

acidic mine water

611

acidity

430

acidophiles

332

Actual evaporation

1105

adit plug

763

adsorbent

923

adsorption

911, 923

aeration

151

aerobic cells

84

aesthetics

1117

agricultural waste

177

algal lipids

1042

alkaline

1124

Alum shale

782

AMD in coal mine

604

AMD

128, 231, 295, 332, 548

ammonia

729

Anaerobic and aerobic passive treatment systems

171

Anaerobic and Aerobic Units

146

anaerobic cells

84

anions

267

antiscalants

188

APDEMS-functionalised zeolite

1111

appetite

865

ARD Characterisation

424

ARD/ML

717

ARD

128, 1124

arsenic

27, 91, 573, 579, 666

arsenopyrite

660

artistic research

1117

assessment

711

Association

345

B

backfill hydrogeology

64

barium

971

batch adsorption

177

Beaver

849

bedrock characterisation

654

Bellvue Mine

116

beneficial end uses

34

beryllium

351

best available control guidelines

956

Biochemical passive reactor

245

biodiversity

9

biofilm

332, 1069

bioflotation

1042

biogeochemistry

635

Biokinetic test

399

Biological Fouling

275

Biological sulphate reduction (BSR)

1069

biological sulphate reduction

114, 140, 940

Biological treatment

121

biological

164

bioreactivity

757

bioremediation

258, 579

botany

328

brine treatment

182, 977

brine

904, 1093

Brines

321

C

cadmium

121

Calcined Magnesite

1099

Carbon Sequestration

1056

carbonatite

893

Case Studies

17

catchment

826

cause

1001

cemented paste backfill

617

ceramic membranes

83

characterisation

417

chitin

1087

chitosan

1087

Classification

916

Clean-up

548

climate

865

closure costs

52





closure planning	363	dissolution	188
Closure	559, 1005, 1036	diversion well	116
CO ₂ +O ₂ in situ leaching	109	doline	585
coal ash landfill	452	domaining	1075
coal discard	685	drainage	541
coal measures	430	drinking water	1099
coal mine in tropical environment	611	Drones	1036
Coal Mining	884		
coal seam	1001	— E	
coal tailings	565	East Rand	803
Coal wastes	417	economics	929
Coal	34, 258, 357, 1042	Ecosystem Engineers	849
Cobalt	579, 666, 940	ecosystem services	871
CoHKWHS	838	efficiencies	288
cold climate	245	efflorescent crusts	332
cold climates	339	effluent treatment	934
Collaboration	231	effluents	493
colloidal silica	103	electrobiological reduction	1136
colloids	934	Electrocoagulation	267
column tests	629	Electronic waste	1087
complex structures	591	element signatures	672
compliance	797	Encapsulation	1056
compressibility	541	engineered	9
COMSOL Multiphysics	458	environment	956
concept development	157	environmental impacts.	417
Conceptual	1011	evaporites	507
Conservative Tracer	849	Explosives	699
constraints	411		
Constructed	9	— F	
contaminated catchment	843	fatty acid methyl esters	1042
contamination	751	fault system	775
contingent valuation	871	FEFLOW	41
control of contaminant migration	52	f-EM sensor	1049
controllable grouting	815	ferrous iron	369
cost-benefit analysis	871	Field columns	3
Co-treatment	288	Field Kinetic Tests	699
Cover	21	fissures	507
Crop quality	239	fit-for-purpose water	820
Crop yield	239	flooded uranium mines	635
crushed concrete	1029	Flow measurement	654, 1024
		Flow-imagery	641
— D		fluorometer	623
decision making process	64	fly larvae shells	1087
decision making	565	fractures	507
Decision Support System	239	freeze desalination	904
Decision-making model	465	Funding Models	993
depressurisation	524, 1017	future	865
developing country	871		
dewatering	524, 585, 878, 1017	— G	
discard dump	775	GARD Guide	962
Discard facility	476	Gas transport	458
discard	357	GDEs	711
discharge	956, 1024		





geobotany	328	impacts	436
geochemical evaluation	315	in situ treatment	121
geochemical evolution	487	INAP	962
Geochemistry	447, 501, 629, 808, 1036	Industrial residue	57
Geo-engineering	553	Infiltration	641
geoenvironmental	1075	ingress	803
Geographic information system (GIS)	465	injection	507
Geothermal energy	553	In-Lake-Neutralization	199
geothermal	375	integrated water management	210
GIS-based technologies	406	integrated	309
GLUE	357	integration	52
goaf water	74	intergrated modelling	685
gold tailings	1130	intervention	283
Gold	660	Inundation	641
GoldSim	41, 1081	iron ochre	899
Green Engine	282	iron removal	84
Green Liquor Dregs	57	iron	579, 666
groundwater contamination	452	iron-rich	769
groundwater flow model	744	Irrigation water quality	239
Groundwater remediation	666	isotherm	911
Groundwater	585, 705, 733, 878, 1005	Isothermal microcalorimetry	399
grout	507	isotopes	591
guidelines	64		
Gypsum Precipitation	133	— K	
— H		Kimberlite	1017
Halong	97	kinetic test and prediction	481
HDS	916	kinetic testing	447
Heap leach pads	3	Kinetic tests	345
Heap Leach	231	kinetics	911
heat transport	458	Kvarntorp	782
Hexavalent chromium	3	— L	
high-density sludge process	971	Lab methods	481
horizontal boreholes	512	laboratory columns	717
humidity cell	685	Lake Kepwari	34
humidity cells	381	Lake	199
hydraulic connection	623	land deforestation	406
hydraulic containment	512	Landsat	1105
hydraulic plug	763	landscape	1117
hydraulic residence time	579	leach dump	956
hydraulic zone	775	leaching test	529
hydrochemistry	775, 838	leaching	782
hydroecology	328	Liberation	345
Hydrogeobotany	328	licence	797
hydrogeology	328, 654, 711	lignite mining	744, 899
hydrological variations	843	lime treatment	363
Hypopedology	471	Lime	199, 295, 1099
Hyperspectral	1075	limestone leaching bed	204
— I		Lithium	321
immobilization	617	loading	826
impact	711	long-term weathering	351
		low-tech remediation	529





__M

main aquifer	1001
Mali	524
management accounting techniques	859
Management Plans	17
Management	1011
managing	52
manganese	204, 751
marbles	591
material flow analysis	97
material recovery	899
mathematical modeling	493
mechanical milling	177
membrane distillation	83
membrane	971, 983
metagenomy	332
metal impurities	1029
metal leaching	692
metal mine waste	843
metal recovery	157, 940, 1087
metal-attenuation	705
metals	529, 826
Microbial colonisation	399
Microbial community	258
microbial sulphate reduction	121
microwave spectroscopy	1049
mine closure and reclamation strategies	692
mine closure	3, 70, 74, 282
mine design	518
mine drainage	74, 529, 738
mine flooding	411
mine landforms	436
mine material valorisation	559
mine planning	52
Mine reclamation	57
Mine Residue Deposits	699
Mine rock	692
mine thermal energy storage	1057
mine waste	57, 315, 1124, 1130
mine water control	815
Mine Water for Irrigation	282
mine water inflow	738
Mine water management	252, 1081
mine water quality prediction	1063
Mine Water Treatment	91, 133, 275, 769, 977, 993
mine water use	210
mine water	47, 80, 97, 157, 177, 193, 729, 871, 904, 1117
Mine-Impacted Water	1056
Mineral phases	171
mineralogy	309, 345, 424, 1075

mining waters	267
mining	1005
mitigation cover	559
mitigation	524, 541
MIW Effluent	182
mobility	351, 757
model	1011, 1105
Modeling	375, 573, 1081
modelling	309, 387, 711, 791, 878, 1005
Monitoring	27, 193, 221, 641, 751, 1036
moss	598
multi tracer approach	843

__N

NAG testing	949
nanocomposite	911
nanofiltration modelling	977
nanofiltration	83
natural flushing	629
neo-tectonic movement	1001
Net Acid Potential	392
Net Acid Producing Potential	392
neutral mine water	288
Neutralization	723
Nickel	940
nitrate	258, 518, 729, 733
Nitrates	699
nitrogen	729
NMD	351
North China	70
Numerical Modelling	321
numerical simulation	458

__O

online monitoring	1049
operational	309
orange peels	188
organic matters	109
Overburden Model	21
oxidation	151, 357, 381
oxygenation	151

__P

packing methods	541
Partial sulphide oxidation	140
passive constructed wetlands	84
passive treatment	128, 146, 171, 204, 245, 763
passive wetlands	9
passive	164, 1029
Paste rock	559
Pb-Zn tailings	501
perception	1117



Permo-Carboniferous	70	remediation options	501
phosphate reduction	288	remediation solutions	452
PHREEQC	321, 332, 375, 1081	remediation strategy	406
piloting	164	repurposing	1130
pit lake operations management	41	residuals	1093
pit lake water quality	252	resource management	791
Pit Lake	363, 884	reusable	923
Pit lakes	647, 679, 1036	Reuse	442, 929
pit wall stability	64	reverse osmosis	275, 904
Pitzer	321	rhodamine	623
planning	52	risk assessment	41
platinum group elements	1111	risk	865
Platinum	733	river pollution	406
plume persistence	629	river	826
pollutant mobilization and immobilization	635	rock geochemical characterization	604
pollution	548	runoff	27, 1093
Pore water equilibration method	808		
post-mining land use planning	210	— S	
PRB design	579	saline mine drainage	245
precipitation	157	saline water	252
prediction	315, 436, 476, 744, 949, 1005, 1075	saline	769
predictive modeling	363	salt dilution method	1024
Predictive Modelling	303	Sampling technique	193
pretreatment	188	Sand aquifers	465
probabilistic modelling	442	saprolite	524
Probabilistic simulation	339	savings	52
process simulation	157	scale-up	487
P-sorption	916	Scaling Control	275
Pt(IV)	1111	scaling factor	685
PTSA	623	scalings	375
pyrite	357, 381, 660, 672	Scheduling	21
— Q		scorodite	91
quality	283	Sealing layer	57
— R		seasonal variability	611
radial jet drilling	815	secondary mineral precipitates	717
RAPS	146	secondary source	820
Rare Earth Elements	598, 893	Seepage impact	476
reactive transport modelling	411	Seepage plume	512
reactive transport	487	Seepage	436, 641
recharge	591	segregation	52
recovery	1111	selective handling	660
recycling and reuse	97	Selenium	258, 518, 1136
reduction	164	Semi-passive process	140
REE minerals	672	semi-passive treatment	116
Regional MIW Treatment Plant	993	sensitivity analysis	387
rehabilitation	21, 64, 231, 548	sensors	221
Relaxation	1017	sequential extraction	573
Release Rates	699	siderite correction	369
Relinquishment	34	silica coating	381
		Silicates	723
		simulation	70
		sinkhole	585
		snowmelt	738





Soda ash	1099	tracer	1024
sodium carbonate	904	treatment	295, 826, 929, 983, 1056, 1136
sodium sulphate	904	tungsten	351
Soil cover design	476		
Soil quality	239	— U	
solar	151	ultrafiltration	109
solute transport modelling	705	uncertainty analysis	41
Solution collection system	956	uncertainty	865
Source-pathway-receptor	471	Underground coal gasification	47
South Africa	647, 1024	underground mine	808
South African collieries	417	Underground mining	465
spatial variability	604	underground runoff	738
speciation	103	underground	729
stable isotopes	808	UNESCO World Heritage Site	1024
stable sulfur isotopes	672	UNESCO.	838
Static & Biokinetic tests	424	Unsettled Solids	303
static testing	949	uranine	623
steady state simulation	387	uranium mine	757
steel slag leaching bed	204	uranium	629, 782, 833
strategies	283	utilization	899
Strontium isotopes	723		
Sulfate reducing bacteria	128, 553	— V	
sulfate removal	215	valuable minerals	1099
sulfate	267	vanadium	177, 782
sulfide oxidation	458	vascular plants	598
sulfidic wastes	381	vermiculite cover	535
sulphate reducing bacteria (SRB)	1069	Vietnam	210
Sulphate removal	971, 983		
sulphate	164	— W	
sulphide inhibition	114	Wall wash	430
sulphide	940	waste classification	949
sulphides	52	waste impacts	471
sulphidic	1124	waste reprocessing	565
Sungun mine	295	waste rock dumps	447
Suspended matter	193	waste rock lysimeters	535
sustainability management accounting	859	waste rock	399, 487, 529
sustainability	9, 283, 791, 929	waste water balance	535
swamps	808	waste water treatment	387
		waste water	288
— T		Waste	231
Tailings Deposition	303	water balance modelling	339
tailings pond	833	water balance	303, 647, 679, 1081, 1105
tailings	21, 27, 221, 392, 573, 717, 723, 733, 1093	water color in dam	934
target metals	757	water demand	283
TCLP	916	water integration	820
technical concept	210	water level monitoring	74
Texture	345	water level recovery	74
thiosalts oxidation	971, 983	water management	518, 769
Tolled Treatment	993	water pollution	1049
trace elements	598	Water Quality Monitoring	303
trace metals	617, 843	water quality prediction	493, 763
tracer substances	635	water quality.	647





water quality	9, 692	wind-remobilised	501
Water Supply	751, 884	WIN-WIN	548
Water Treatment Boats	199	Witwatersrand gold mines	553
Water Treatment Plant	199	Witwatersrand	803, 838, 1024
water treatment technologies	215		
water treatment	193, 442, 518, 833,	—Z	
	893, 1029		
Water	929, 1011	Zeolite	295
Weathering	723	Zero Liquid Discharge	182
West Africa	660	Zinc	121, 1049
West Rand	838	ZLD	1093
wind	151	ZOR	1017





**11th International Conference on Acid Rock Drainage
International Mine Water Association
WISA Mine Water Division (MWD)**

**Pretoria, South Africa
September 10 – 14, 2018**

Mine water, and especially acid rock drainage (ARD) or acid and metalliferous drainage (AMD) is considered one of the most serious threats to the environment in a mining context. Yet, researchers, practitioners and regulators as well as mining companies constantly aim to prevent damage to the environment and receiving water. The 11th ICARD | IMWA | WISA MWD 2018 conference in Pretoria, South Africa, brings together nearly 350 experts from around the world. It provides an invaluable opportunity for sharing information on current good practice, emerging technologies, on-going research, and developments in regulation. The conference also helps to highlight advances in our knowledge as well as gaps and challenges.

187 peer reviewed papers, which can all be freely downloaded from the IMWA web site (www.IMWA.info), are collected in this proceedings volume. Seventeen topics, covering an extensive range of mine water related subjects are included – mitigation and geochemistry having attracted the largest interest. This proceedings volume represents the most current developments in the field and cover different experiences from around the world and can be considered the state-of-the-art in mine water management and mitigation.



ISBN 978-0-620-80650-3

